AD_____

Award Number: W81XWH-04-1-0142

TITLE: VITAL: VANGUARD INVESTIGATIONS OF THERAPEUTIC APPROACHES TO LUNG CANCER

PRINCIPAL INVESTIGATOR: Waun Ki Hong, M.D.
Reuben Lotan, Ph.D.
David Stewart, M.D.

CONTRACTING ORGANIZATION: The University of Texas M.D. Anderson Cancer Center
Houston, TX 77030

REPORT DATE: July 2011

TYPE OF REPORT: Addendum to Final

PREPARED FOR: U.S. Army Medical Research and Materiel Command
Fort Detrick, Maryland 21702-5012

REPORT DOCUMENTATION PAGE

Form Approved
OMB No. 0704-0188

1. REPORT DATE	2. REPORT TYPE	3. DATES COVERED
July 2011	Addendum to Final	15 December 2010 – 15 June 2011

4. TITLE AND SUBTITLE

VITAL: VANGUARD INVESTIGATIONS OF THERAPEUTIC APPROACHES TO LUNG CANCER

5a. CONTRACT NUMBER

5b. GRANT NUMBER
W81XWH-04-1-0142

5c. PROGRAM ELEMENT NUMBER

6. AUTHOR(S)

Waun Ki Hong, M.D.
Edward Kim, M.D.
Ignacio Wistuba, M.D., J. Jack Lee, Ph.D.
E-Mail: whong@mdanderson.org

5d. PROJECT NUMBER

5e. TASK NUMBER

5f. WORK UNIT NUMBER

7. PERFORMING ORGANIZATION NAME(S) AND ADDRESS(ES)

The University of Texas M.D. Anderson Cancer Center
Houston, TX 77030

8. PERFORMING ORGANIZATION REPORT NUMBER

9. SPONSORING / MONITORING AGENCY NAME(S) AND ADDRESS(ES)
U.S. Army Medical Research and Materiel Command
Fort Detrick, Maryland 21702-5012

10. SPONSOR/MONITOR'S ACRONYM(S)

11. SPONSOR/MONITOR'S REPORT NUMBER(S)

12. DISTRIBUTION / AVAILABILITY STATEMENT
Approved for Public Release; Distribution Unlimited

13. SUPPLEMENTARY NOTES

14. ABSTRACT

The VITAL Research Program will provide a better understanding of the cellular and molecular processes that drive lung tumorigenesis so that an accurate risk model for recurrence and/or the development of the secondary primary tumor can be developed, and the biologic agents most effective in reducing these events in the group of high-risk patients can be identified. We will be incorporating retrospective clinical trial specimens to develop our risk model and validating it with specimens collected from our Vanguard study. The research projects are proceeding well as proposed, producing valuable findings with cell lines, and will validate these results using the clinical samples obtained from the VITAL trials in the coming years.

15. SUBJECT TERMS
Lung cancer, risk model, cancer recurrence, clinical trials

16. SECURITY CLASSIFICATION OF:			17. LIMITATION OF ABSTRACT	18. NUMBER OF PAGES	19a. NAME OF RESPONSIBLE PERSON
a. REPORT	b. ABSTRACT	c. THIS PAGE			USAMRMC
U	U	U	UU	619	19b. TELEPHONE NUMBER *(include area code)*

TABLE OF CONTENTS

INTRODUCTION

The program VITAL (Vanguard Trial of Investigational Therapeutics in Adjuvant Treatment of Lung Cancer) initiated in 2003 was developed to gain a better understanding of the molecular events underlying the progression of NSCLC in order to develop a risk model for cancer recurrence and development of smoking-related SPT in the high-risk population, and to identify effective preventive agents for this group of patients. Specifically, our objectives are:

- To identify biologically-based treatments for prevention of cancer recurrence and development of second primary tumors in high-risk patients;
- To understand molecular events in premalignant tissues that contribute to progression or malignancy;
- To develop a risk prediction model for disease recurrence and development of second primary tumors in high-risk patients by combining clinical treatment outcomes with molecular and imaging data.

Three clinical trials were proposed, in part, to acquire the necessary correlative samples to develop this risk model, which will significantly improve decision-making for patients and physicians in the management of this challenging disease. Histologic assessment was planned to determine whether malignant changes would occur during this time period. Despite substantial efforts, our patient accrual was significantly lower than expected due to a number of factors; thus, a ReVITALization plan was proposed (see revised Aims below) and implemented after receiving DoD approval. Implementation of the alternative ReVITALization strategy over the past three years was based on the revised project aims that were developed to accomplish our goal of the development of the risk model. An overview of the changes is provided below with additional details in each relevant project.

ReVITALization Aims:

1. **Circumvent low accruals using surgical specimens in our tissue bank.** These specimens (about 500 samples) of resected lung cancer will be utilized for biomarker assessment and will serve as the foundation for a biomarker-based risk assessment model.

2. **Continue enrolling patients in our Vanguard trial to accrue 50-60 patients.** This cohort will provide sufficient biospecimens for the aims proposed in the other projects of the VITAL program. Additionally, the clinical data obtained from these patients will be used to test the biomarker-based risk assessment model and the follow-up bronchoscopy specimens will provide important information for biomarker changes in the bronchial epithelium.

3. **Close the celecoxib and erlotinib trials to focus resources on specimen analyses to develop the biomarker risk model.**

4. **Perform two additional discovery projects related to increased risk that are only now possible due to continued progress in VITAL.**
   - **a.** Identify gene expression signatures in bronchial brush specimens using high-throughput genomics approach.
   - **b.** Identify genes expression signatures in epithelial cells detected by LIFE bronchoscopy that determine aggressiveness.

The final report summarizes work conducted over the entire research period, highlights key research accomplishments and reportable outcomes with the bibliography of all publications and meeting abstracts derived from **VITAL,** and includes a list of personnel receiving pay from the research effort.

PROGRESS REPORT

Project 1: Biologic Approaches for Adjuvant Treatment of Aerodigestive Tract Cancer

(PI and co-PIs: Drs. Waun Ki Hong, Edward S. Kim, Rodolfo C. Morice, David J. Stewart)

Aim 1 Assess the smoking-related disease-free survival in patients who are current or former smokers with a prior definitively-treated stage I/II lung or head and neck cancer.

The main objective for this project was to open the Vanguard study at MDACC as well as the 2 other participating sites. Enrollment was planned for a total of 300 patients with definitively treated stage I/II lung or head and neck cancer and at least a 20-pack-year smoking history. Patients undergo baseline testing including chest x-ray, CT scan, labs, bronchoscopy, and other specimen collections (i.e., sputum, saliva, serologies). Bronchoscopies and specimen collection are performed at baseline and at months 12, 24, and 36. White-light alone or white-light and autofluorescence modalities are used. Abnormal areas detected by bronchoscopy are biopsied. Histologic assessment is performed to determine whether malignant changes will occur during the time period. If severe dysplasia, carcinoma *in situ,* or carcinoma is discovered, patients follow the plans outlined in the clinical protocol. Once patients have completed 3 years of testing, they are followed until the study is completed. As per the revised ReVITALization aims, the study will be closed when a total of 54 patients were accrued; all patients will be followed as outlined above.

Findings: A total of 54 patients were enrolled to the Vanguard trial, and our number of evaluable patients (having completed both the baseline and 12-month bronchoscopy) is 38. The study was closed to new patients in March 2009. The median age is 61 years (range, 53-81 years), and 26 of the 54 patients (53%) were male. A total of 44 patients had NSCLC, with 36 patients having stage I (82%), 7 stage II (16%) and 1 IIIA (2%) disease. At the time of this report, a total of 38 pts (70%) have completed bronchoscopy at 12 months, 29 pts (54%) at 24 months, and 18 pts (33%) at 36 months. To date, a total of 9 pts (18%) have recurred and 3 pts (6%) have had second primary tumors (SPTs) recorded. Four additional bronchoscopies at 36 months are scheduled to be completed by March 2012. Our plan is to continue to collect clinical data from these patients outside the scope of this grant. Further follow-up for these last patients will be supported through other funding sources (e.g., institutional, philanthropy).

Dr. Ignacio Wistuba and his lab (Core C) analyzed the bronchial epithelium and have completed the assessment of possible molecular markers. Planned biomarker analyses for Projects 2-5 have been supplemented using retrospectively collected specimens through the ReVITALization effort to maximize data acquisition while minimizing the time required to develop the proposed risk model (See Aim 3 below and Core B and C reports). The ReVITALization effort collected over 500 specimens and has completed the database with both pathological and clinical data.

Aim 2 Evaluate effects of biologic agents as adjuvant therapy on the modulation of histology and specific biomarkers in this high-risk population.

Our plan was to open several biologic adjuvant clinical trials with novel agents such as celecoxib, erlotinib, lonafarnib, and possibly others; however, poor accrual due to changes in the standard of care for lung cancer patients prohibited successful completion of the proposed trials and, thus, the trials were deferred as previously described. Our revised aim is now focused on the timely development of the risk model (see Aim 3 / Revised Task 3). The retrospective specimens will be used for the proposed analyses and correlated with the available clinical data.

Findings: As noted previously, the celecoxib trial was closed, and the proposed erlotinib trial was deferred. We focued our efforts on the productive analysis of acquired samples from the clinical trial and from our tissue bank to allow us to develop our lung cancer risk model described in Core B.

Aim 3 Develop a lung cancer risk model to help predict the likelihood of development of relapse or new smoking related primary tumors

Patients with a history of smoking and a prior surgically resected stage I/II head and neck or lung cancer are at high risk for cancer recurrence or SPTs. These patients are deemed "cured" but there are no standard interventions that have been proven to help reduce the risk of cancer reccurrence. Patients enrolled in the Vanguard trial had aggressive post-treatment follow-up with frequent analysis including serologies, bronchoscopy with bronchial specimens and CT scanning. Utilizing this unique collection of biospecimens, multiple biomarkers were analyzed and used for the development of a predictive risk model. Establishing a predictive risk model will potentially help identify patients who may be at higher risk for subsequent lung cancer development and promote opportunities for earlier preventive interventions and/or more aggressive follow-up strategies.

Findings: VITAL project investigators, in close collaboration with Cores B and C, identified 542 potential patients in our Thoracic Tissue Database. Specimens from 370 patients with early stage (I 63%, II 20%, or IIIA 17%) NSCLC resected at MDACC between 2002 and 2005 were selected for this analysis based on clinical characteristics and tissue adequacy. Project investigators proposed a total of 21 biomarkers for potential inclusion in the risk model development based on promising preclinical data including IGF1R, IGFBP3, Insulin Receptor, pAKT, pIGF1R, pSRC, pmTOR, pAMPK, pEGFR, pS6, FEN1, MCM2, MCM6, SFN, TPX2, UBE2C,CASK, CD51, CXCR2, EpCAM, and SPP1 (see Appendix for report). The resected tissue specimens were collected and processed per the standard operating procedures of our research laboratory. We have thus established a unique cohort of early stage non-small cell lung cancer patients from our institution that includes carefully annotated, prospectively collected medical-demographic, treatment, and follow-up information as well as tissue specimens available to begin development of a biologic risk model. This patient population includes 186 (50.3%) male, 330 (89%) white, 162 (44%) current smokers, 170 (46%) former smokers, and 38 (10%) never smokers, 227 (61%) adenocarcinomas and 126 (34%) squamous cell carcinomas. One hundred and sixty patients (45%) received chemotherapy (adjuvant or neoadjuvant) or radiation treatment in addition to surgery. In collaboration with our laboratory investigators, we have identified and analyzed the 21 pre-specified markers relevant to early pathogenesis of lung cancer, including pathways related to apoptosis, metabolism, and growth factors. Potential covariates in risk models included both pertinent biomarkers and patient clinical characteristics. The median follow-up in this cohort was 5.3 years (among patients that are still alive as of the last follow-up). The median overall survival (OS) was 6.4 years. A total of 209 cases with recurrence and/or death were observed. The median recurrence-free survival

(RFS) was 4.1 years and 1-, 3-, and 5-year recurrence rates were 80%, 59%, and 45%, respectively. These values are similar to other historical reports of early stage lung cancer patients. When adjusted for clinical factors (age and stage), important risk predictors (hazard ratio, p-value) for RFS include positive cytoplasmic pAMPK (0.65, p=0.004), positive membrane insulin receptor (1.44, p=0.01), positive cytoplasmic EpCAM (0.71, p=0.02), high (defined as > or = median) cytoplasmic CXCR2 (1.36, p=0.04), membrane CASK (0.996, p=0.049), cytoplasmic IGF1R (1.004, p=0.04), and positive cytoplasmic pmTOR (0.70, p=0.03). It is important to note that this is a preliminary risk model and further mechanistic studies and larger sample sizes will be needed to validate these findings and to develop a more informed risk model. We note that the relative risk of each individual marker may also be informative. For example, in this model, when including age and stage, a patient with a positive cytoplasmic pAMPK will have a reduced risk of recurrence or death by 35% when compared to a patient with negative cytoplasmic pAMPK, while other covariates remain the same. On the other hand, a patient with positive membrane insulin receptor will have an increased risk of recurrence or death of 44% compared to a patient with negative membrane insulin receptor (again while other covariates remain the same). We utilized the C-index to measure the predictive accuracy of this model; the C-index for RFS is 0.68 with a 95% confidence interval of (0.60, 0.75), which indicates that our preliminary model has moderate predictive accuracy.

In terms of overall survival (OS), the significant risk predictors were positive cytoplasmic pAMPK (0.67, p=0.02), positive cytoplasmic pmTOR (0.66, p=0.03), positive cytoplasmic EpCAM (0.65, p=0.01), high cytoplasmic CXCR2 (1.47, p=0.007) and high nuclear FEN1 (1.42, p=0.04). The C-index for OS is 0.68 with a 95% confidence interval of (0.59, 0.76). In addition, we also applied the resampling (bootstrap) method to provide an internal validation of the predictive accuracies of these models. The resampling C-indices were 0.66 for both RFS and OS, adjusted for overfitting. Again, the bootstrap C-indices shows that the models have moderate prediction accuracy.

To provide an independent validation, we tested the effect of the risk model covariates in *normal* bronchoscopy specimens obtained from our prospective Vanguard study that included 45 evaluable patients with available biomarker data and recurrence/survival endpoints (noting that *tumor* tissue specimens were evaluated in the ReVITALization cohort). pAMPK, CXCR2, EpCAM, and pmTOR were analyzed in the Vanguard patients' serial bronchoscopic biopsy tissues. While not statistically significant, both our Kaplan-Meier and Cox model analyses show a trend for patients with higher pAMPK having a longer RFS. This observed trend is consistent with the results of our retrospective database patient cohort as presented earlier. Forthcoming clinical trials under development in high-risk patients with aerodigestive cancer will incorporate some of these promising biomarkers.

These results represent the use of a unique cohort of patients, as well as prospectively collected and archived clinical tissue, and the related clinically annotated data to create a risk model for lung cancer development. The unique biospecimens collected from these populations of patients (Vanguard trial and ReVITALization retrospective cohorts) have allowed us for the first time to interrogate the underlying mechanisms of cancer development in the airways of patients at high risk for developing lung cancer. Given on the limited progress in the field of lung cancer prevention to date, we believe that similar small studies focused on biospecimen enrichment (i.e., prospective collection of tissue, blood, sputum, etc.) may help uncover findings that may advance the field more rapidly. Further studies are needed to test this approach and these and other novel biomarkers in expanded prospective cohorts to leverage our initial findings. Through these biomarker-enriched clinical studies in at-risk patients, we hope to achieve our goal of establishing a validated predictive risk model for lung cancer.

Project 2: Identification of Biomarkers of Response to Chemoprevention Agents in Lung Epithelium

(PI and co-PIs: Ignacio Wistuba, M.D., Reuben Lotan, Ph.D., John Minna, M.D.)

We hypothesized that immortalized, transformed, and tumorigenic human bronchial epithelial cell (HBEC) line models will have similar abnormalities in gene expression profiles as premalignant and malignant tissues *in vivo*. Therefore, such cell models will be useful to identify markers of early disease.

We proposed to use genomic and proteomic analyses to identify changes in gene expression (including mRNA and miRNAs) and proteins that correlate/associate with cancer risk in the carcinogen damaged aerodigestive tract field, and also use these signatures to monitor the response of this field to chemoprevention. We developed a model HBEC system to study the effect of specific oncogenic changes and also the response of these manipulated HBECs to various carcinogenic and chemoprevention agents. Thus, we will determine modifications of these changes by chemopreventive agents in premalignant cells *in vitro* and to use probes for the modified genes and proteins to analyze tissue specimens from individuals participating in the chemoprevention clinical trials.

Aim 1 Develop immortalized human bronchial epithelial cell cultures using a subset of patient tissue specimens collected in Project 1 and characterize the expression profiles of these cells using oligonucleotide based microarrays.

The main goal of this aim of this project was to establish these cultures from lung cancer patients and persons without lung cancer, including those patients entered onto the clinical trial described in Project 1, and to characterize their gene expression profiles.

Findings: We generated HBECS from over 50 different individuals and we immortalized 15 peripheral small airway epithelial cells (HSAECs). We compared the HBECs and HSAECs with each other and with NSCLCs by genome-wide array mRNA expression profiling. We found the HBECs and HSAECs expression mRNA signatures to be distinct (but closely related to) from each other and separate from those for NSCLCs. New methods and media for airway epithelial cell differentiation were developed to study their stem cell-like properties, and we discovered that the HBECs and HSAECs are immortalized cells that express many properties of pulmonary stem cells and have the capacity to differentiate along several lineages.

Aim 2 Characterize effects of the chemo preventive agents used in Project 1 on cell proliferation and apoptosis in the immortalized human bronchial epithelial cell cultures developed in Specific Aim 1.

We aimed to determine the potential role of different chemopreventive agents [e.g., celecoxib, N-[4-hydroxyphenyl]retinamide (4-HPR), Iressa (gefitinib), and SCH63663] alone or in combination with one another for their effects on cell proliferation and apoptosis in cell cultures established in Aim 1. We also aimed to determine the relative sensitivity among the various cell cultures to each of the agents by determining the 50% growth inhibitory concentration (IC_{50}).

Findings: We analyzed the effects of several agents (gefinitib, 4HPR, celecoxib and SCH66336) on the growth of premalignant HBECs, most of which were developed in Aim 1. The responses of the different cell lines varied by as much as several fold with respect to the IC_{50} concentration.

Further studies were performed using the EGFR inhibitor erlotinib demonstrated that this agent was as effective in inhibiting the tumorigenic 1170-I cells as it was in inhibiting the less progressed cell lines of the BEAS-2B family, including the immortalized 1799 and the transformed 1198. The results of inhibition of the HBEC series indicate that whereas erlotinib inhibited all cell lines, the degree of inhibition was lowest for the KT53 cell line (no more than 45% inhibition at any dose compared to 60-80% for some others).

Aim 3 Identify gene expression and protein "signatures" which reflect lung tumorigenesis and sensitivity or resistance to chemo preventive regimens proposed in Project 1, and to validate the signatures and to determine their biological importance in precancer cell models of lung cancer.

Findings: We studied DNA copy number changes in lung cancers and preneoplastic tissues, identified the key genes within these amplicons, and performed functional studies to identify which are the most important in the pathogenesis of lung cancer. Comparing 104 cancer lines representing diverse tissue origins to identify genes residing in amplification 'hotspots,' we discovered an unexpected frequency of genes activated by this amplification. The amplification regions were correlated with microarray data and the overexpressed genes in each of the regions were identified. The 135 hotspots identified contain 538 unique genes and are enriched for proliferation, apoptosis and linage-dependency genes, reflecting functions advantageous to tumor growth. Our findings suggest that amplification is far more common a mechanism of oncogene activation than previously believed, and that specific regions of the genome are hotspots of amplification.

Aim 4 Develop techniques to assess these molecular signatures in tissue specimens and serum obtained in Project 1, and assess the relevance of these molecular signatures as *in vivo* biomarkers using baseline and post-treatment specimens.

Findings: We identified the overexpression of *BRF2* (chromosome region 8p), a RNA polymerase III (Pol III) transcription initiation factor, as the result of increased gene dosage in the squamous cell lineage leading to lung squamous cell carcinoma (SqCC). We found that *BRF2* was amplified and overexpressed in preneoplastic carcinoma in situ (CIS) lesions in the airway epithelium of lung cancer patients. Our data suggests that genetic alteration of BRF2 represents a novel mechanism of lung tumorigenesis through the increase of Pol III-mediated transcription in cancer.

Aim 5. Identify gene expression signatures that characterize progression from immortalized to transformed to tumorigenic human bronchial epithelial cells based on already available high-throughput gene expression microarray data and validate these signatures using tissue microarrays (TMAs) containing normal bronchial epithelium, hyperplasia, squamous metaplasia, dysplasias, squamous cell carcinomas, atypical adenomatous hyperplasia, and adenocarcinomas (Years 4-5).

Findings: We produced data depicting the derivation of a five-gene signature (FILM, five-gene *in vitro* lung carcinogenesis model) that was effective in predicting the survival of lung adenocarcinoma patients upon analysis of publicly available NSCLC microarray datasets. The signature is comprised of genes (UBE2C, MCM2, MCM6, TPX2, and FEN1) that we had previously shown to be differentially expressed and functionally modulated between the components of an *in vitro* lung carcinogenesis model encompassing normal, immortalized, transformed, and tumorigenic lung epithelial cells. We assessed the immunohistochemical (IHC) expression of the protein products in NSCLC TMAs of formalin-fixed and paraffin-embedded

(FFPE) tissues and found that the prognostic efficacy of the protein signature was superior in comparison to that of each IHC protein marker alone. Further independent studies are warranted to externally validate the potential clinical use of this five-gene/protein signature.

Aim 6. Identify gene expression signatures in bronchial brush specimens from the 50-60 patients enrolled in the Vanguard study using high-throughput genomics approach (Years 4-5).

Findings: In our previous report, we selected 19 patients from the prospective Vanguard study with definitively treated ES (I/II) NSCLC and were current or former smokers for our initial analysis to study the potential associations between field of cancerization expression profiles and lung cancer relapse. Patients had bronchoscopies with brushings obtained from the main carina (MC), airways adjacent (ADJ) to the previously resected tumor and from airways distant from the tumor in the ipsilateral (NON-ADJ) and contralateral (CONTRA) lung at baseline, 12, 24 and 36 months following resective surgery (Figure 1).

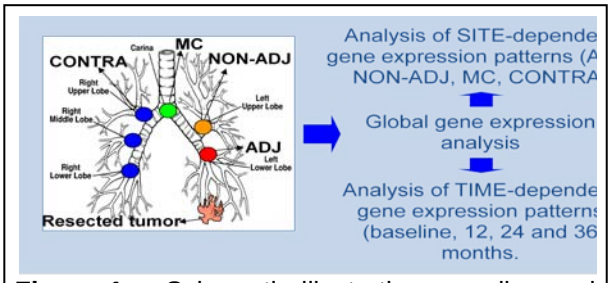

Figure 1. Schematic illustrating sampling and collection of bronchial brushes from different airway sites at different time points following respective surgery from early stage smoker NSCLC patients enrolled in the phase II cancer surveillance Vanguard study.

These nineteen patients were selected for the study based on airway sampling of at least five different regions per time point and continuously up to 24 or 36 months (391 airway samples from nineteen patients). Total RNA was isolated from brushings using the RNeasy Mini kit (Qiagen). Due to the paucity of the material, we employed the Nugen WT-Ovation system for RNA amplification (Nugen technologies, San Carlos, California). Synthesis of single-stranded DNA, fragmentation and biotin labeling was performed using the WT-Ovation Pico RNA amplification system, WT-Ovation Exon-Module and Encore™ Biotin Module (NuGEN technologies), respectively, according to the manufacturer's instructions. 2-2.5 micrograms of biotin-labeled DNA was then hybridized to Affymetrix Human Gene 1.0 ST arrays from Affymetrix. Analysis began by construction of a mixed-effects model that incorporated information on the site and time (continuous) the bronchial brushing was obtained as fixed effects. Characteristics of fixed effects and their interaction, in terms of number of genes differentially affected by the effect, were examined by fitting beta-uniform-models (BUMs) based on p-value distributions of all genes according to the fixed-effect (Figure 2). Histograms of p-value distribution of fixed effects (Figures 2A, 2B and 2C) and a smoothened scatter plot of transformed p-values of both site and time fixed effects (Figure 2D) demonstrate

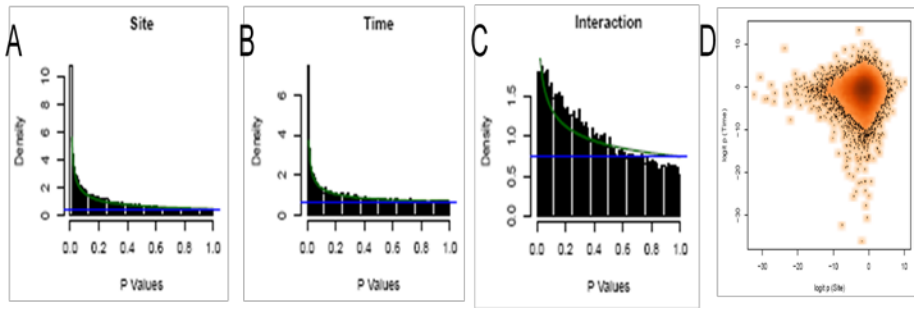

Figure 2. Histograms demonstrating p-value distributions for site (A), time (B) and interaction between both after fitting beta-uniform-mixture (BUM) models (3). D. Smoothed scatter plot of transformed p-values from site and time.

that there is little evidence for any interaction between site and time. These findings suggest that, although the airway brushings were collected at different sites and at time points following respective surgery from each patient, all airway samples (n=391) can be utilized independently to study genes differentially expressed in two ways - by site from original resected tumor and by time following removal of the same tumor in all patients. Subsequently, time and site-dependent differential expression profiles representing a field of cancerization were identified based on a false discovery rate (FDR) cut-off of 5% and 1% based on p-value distributions, respectively, studied by hierarchical clustering and functionally analyzed using network analysis. A total of 1395 genes were determined to be differentially expressed over time in the cancerization fields. Hierarchical clustering analysis using these genes demonstrated that samples (n=391) were divided into two clusters or branches that were significantly unbalanced, with respect to time, with the majority of the baseline and 36 months samples well separated ($p<0.001$ of the Fisher's Exact test) (Figure 3A). Moreover, functional analysis of these genes showed that a nuclear factor-κB (NF-κB)-mediated gene-network was most significantly elevated ($p<0.001$) with time (Figure 3B).

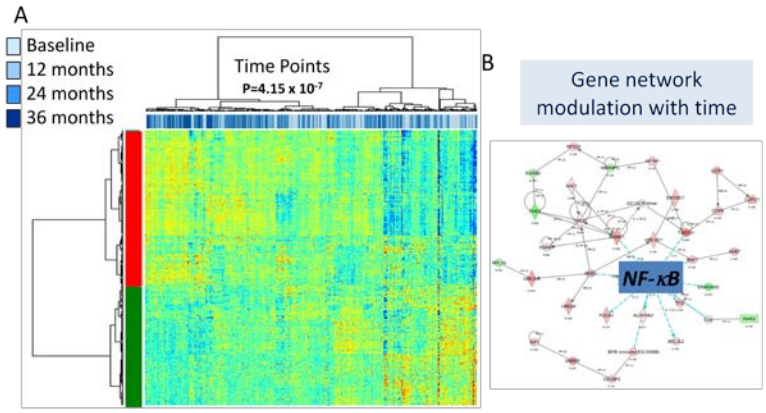

Figure3. Gene expression profiles are different in a time-dependent manner in the field of cancerization. Hierarchical clustering (A) and functional gene-interaction network analysis (B) of genes (n=1395) differentially expressed continuously with time.

A total of 1165 gene features were differentially expressed by site. Two-dimensional clustering of these genes and samples showed distinct classes of differential expression and revealed two main sample clusters with significant separation of ADJ samples from MCs and non-adjacent CONTRA airway samples ($p=0.003$) (Figure 4A). Similar results were obtained when main carinas were excluded from analysis of genes differentially expressed by site in relation to the original resected tumor (Figure 4B). Using both site-dependent analyses, genes were identified that exhibited highest

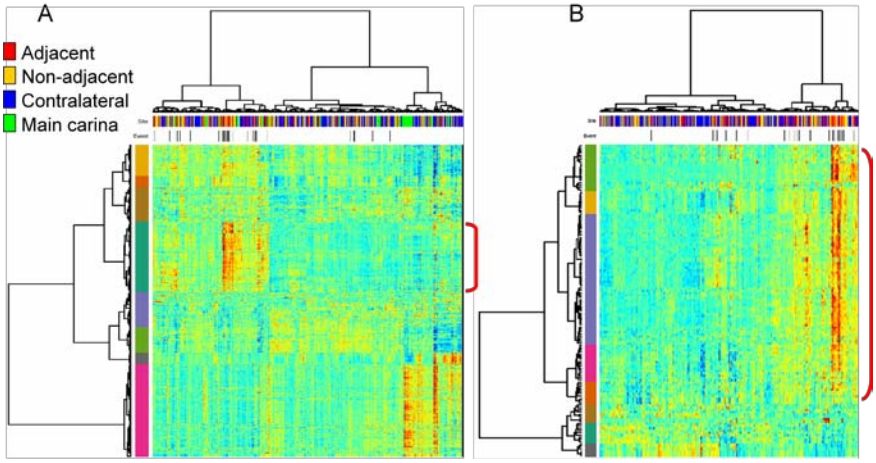

Figure 4. Hierarchical clustering of all samples (A) or excluding main carinas (B) using genes differentially expressed by site. Recurrences (black) and suspicions (grey) are labeled based on adjacent airways. Genes with highest expression in adjacent airways are indicated by the red bars.

average expression in airways adjacent to tumors (cluster of genes highlighted by red bars) (Figures 4A and 4B). It is worthwhile to mention that, following two-dimensional clustering of the site-dependent differentially expressed genes and airway samples, adjacent airways isolated from patients with recurrence or suspicion of recurrence, (black, recurrence; grey, suspicion of recurrence), exhibited on average elevated expression of the highest-in-adjacent airway gene cluster compared to adjacent airways isolated from patients with no events in recurrence (Figures 4A and 4B). These findings suggest that differential gene expression patterns in fields of cancerization, by site of the original tumors, in early stage patients may be associated with recurrence or second primary tumor development.

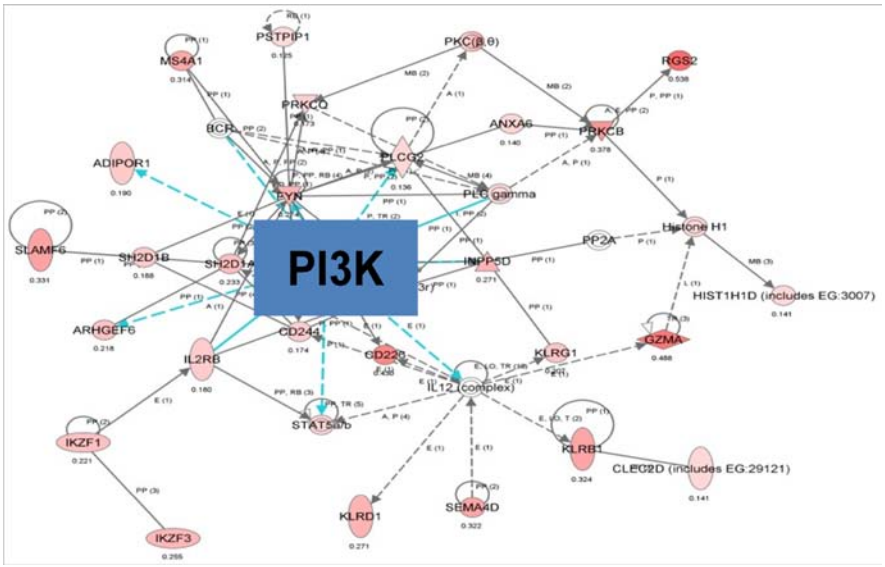

Figure 5. Network analysis of cluster of genes depicted in **Figure 4** with highest average expression in airways adjacent to original resected tumors. PI3K-mediated network is shown as most significantly up-regulated in adjacent airways. red, up-regulated in adjacent airways relative to non-adjacent or contralateral airways.

To further understand the relevance of this gene cluster with highest expression in adjacent airways and in those isolated from patients with recurrence, we performed functional pathways analysis of the genes using the knowledge-dependent analysis, Ingenuity Pathways analysis (IPA). Functional analysis of the highest expression of genes-in-adjacent airways revealed that gene-networks mediated by PI3K, NF-κB, and ERK1/2 were more significantly elevated ($p<0.001$) in function in ADJ airway samples, with a gene-interaction network mediated by PI3K being most significantly elevated in function, as predicted by the IPA software, based on number of genes differentially expressed within the network and topological interactions among the same genes (Figure 5). These findings suggest that the aforementioned canonical cell

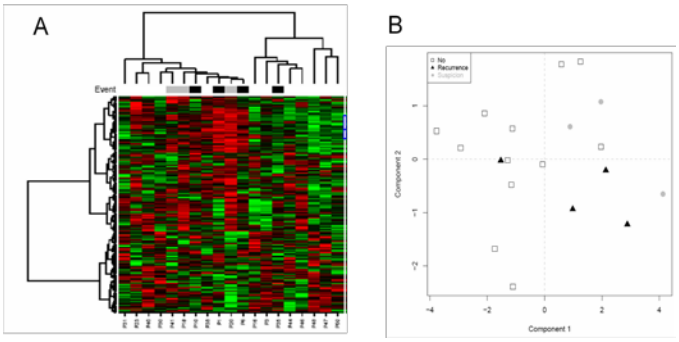

Figure 6. Field of cancerization molecular profiles are associated with patterns of recurrence. Genes with significant expression differences between adjacent and non-adjacent airways (ADJ/NON-ADJ) were used to analyze the 19 pts by clustering (A) and principal component analysis (B). Black, recurrence; grey suspicion of recurrence.

signaling pathways, in particular the PI3K survival pathway, may be highly relevant to biologically to the molecular pathogenesis of NSCLC, and clinically to prediction of recurrence or second primary tumor development in early stage patients definitively cured by respective surgery.

We further identified genes differentially expressed by site using different statistical methods, including paired t-test analysis of the 19 NSCLC patients based on differences in expression between adjacent and non-adjacent/contralateral airways. An average adjacent (ADJ) expression score and average non-adjacent/contralateral (NON-ADJ) score was measured for each gene based on all available airway samples per patient. Hierarchical clustering (Figure 6A) and principal component (Figure 6B) analysis of patients (n=19) based on differences of expression (ADJ/NON-ADJ) of genes significantly differentially expressed by paired t-tests between ADJ and NON-ADJ samples revealed two main clusters with three of four relapses located in one sub-cluster suggesting potential associations between field of cancerization expression profiles and lung cancer relapse. These initial studies will be expanded in additional analysis of other avaioable specimens outside the scope of this application, and demonstrate the potential for the utility of this approach in identifying predictors of risk of recurrence or SPT in definitively treated early stage lung cancer patients.

Project 3: Premalignant Bronchial Epithelia: Molecular and Cellular Characterization of Lung Tumorigenesis

(PI and co-PIs: Walter Hittelman, Ph.D., Ja Seok Koo, Ph.D., Rodolfo C. Morice, M.D.)

Aim 1 Identify and characterize differentially expressed genes in the LIFE bronchoscopy-identified abnormal areas of the bronchial epithelia of enrolled subjects in VITAL trials.

Previous studies have shown that bronchial regions that appear abnormal by light-induced fluorescence endoscopy (LIFE) bronchoscopy show increased genetic changes when compared to normal-appearing sites, even if there are no differences in histological appearance. Since LIFE-positive lesions are at increased risk for cancer development, especially when they contain particular genetic alterations, we hypothesized that these LIFE-positive sites represent lesions at an early stage of tumorigenesis and may differentially express genes important for driving tumorigenesis. Thus, comparative gene expression analyses between LIFE-positive and LIFE-negative sites within the same individual may provide a filter for identifying genes whose levels of expression are important for driving tumorigenesis.

Findings: We used paired bronchial brush samples from the normal and abnormal areas of each individual to perform microarray analysis. We examined the commonly regulated genes using the expression level of all the sample sets, and we analyzed the potential key signal pathways that are involved with a Kegg pathway analysis program. The pathway analysis revealed that the cytokine-cytokine receptor pathway is the top signal pathway involved, followed by other tumorigenesis pathways, such as cell migration and adhesion. Whole genome expression microarray analysis provided tremendous information about the molecular differences between abnormal and normal tissues. By distinguishing the subsets of the sample population, we identified the consistently regulated genes and the signaling pathway that are critical for tumorigenesis.

Aim 2 Establish an organotypic model system that mimics *in vivo* interactions between normal, premalignant, and malignant bronchial epithelial cells in the lung using cells derived from bronchial biopsies and immortalized bronchial cells.

To better understand the molecular basis of preferential outgrowth of more advanced bronchial epithelial clones, we proposed to utilize a cell culture model whereby normal and abnormal bronchial epithelial cells are grown on collagen or stromal cell-coated, suspended filters and exposed to an air-liquid interface. This organotypic culture environment mimics lung stratified epithelium, complete with basal cells, ciliated columnar cells, and mucus-producing goblet cells. Our group has extended this model system by tagging cell populations with fluorescent probes (e.g., green fluorescence protein, or GFP) that allows us to carry out live cell imaging of mixed clonal populations. This model system permits characterization of the ability of more advanced bronchial epithelial cell populations to expand on the growth surface at the expense of less advanced bronchial epithelial cell populations.

Findings: We developed a color-coding methodology to distinguish subpopulations of cells within heterogeneous lung tumors and immortalized human bronchial epithelial cell populations. We also utilized the "Brainbow" vector to permit the visualization of clonogenic cell expansion in lung tumor xenografts and to determine differential radiation sensitivity and metastatic capability of clonal subpopulations within heterogeneous lung tumors. This new approach will allow us to identify and selectively isolate more aggressive subpopulations that exist within heterogeneous cell populations and characterize the specific genetic and expression changes associated with their more aggressive behavior.

Aim 3 Determine the mechanisms of genetic instability and elucidate the signaling pathways associated with clonal outgrowth of premalignant and malignant bronchial epithelial cells using the organotypic model system.

Our working hypothesis was that years of tobacco exposure induces a chronic damage and wound-healing cycle that results both in the accumulation of genetic alterations in the epithelial cells that influences both chromosome stability mechanisms (e.g., loss of cell cycle checkpoint and cell loss mechanisms through loss of p16 expression, p53 mutations, Cyclin D1 overexpression, etc) and creates a poor growth environment (e.g., altered stromal signals). The goal of this specific aim was to utilize the lung organotypic model to address this hypothesis *in vitro* utilizing bronchial epithelial cells derived from LIFE bronchoscopically identified "abnormal" and "normal" regions of the lung of current and former smokers participating in the clinical trial of Project 1.

Findings: We noted that the levels of genetic instability increased when cells proliferate away from the basal layer, suggesting dysregulation of cell cycle control when cells try to proliferate in inappropriate spatial regions. We also showed that mitotic instability was associated with increased expression of stress-response proteins, including phosphorylated histone H2AX. We quantitatively analyzed images of the three-dimensional cultures to determine the relationship between changes in mitotic orientation relative to the basal layer plane and the frequencies of mitotic errors, and we found that as the cultures fashioned toward the tumor phenotype, they more frequently exhibited mitoses away from the basal layer and the orientation angle of the mitotic spindle (and degree of mitotic error) increased with distance from the basal layer. This result supports the hypothesis that mitotic directionality and fidelity depend on cell-cell and cell-substrate interactions. This organotypic culture model might be useful in the detection of potential chemopreventive agents that can reregulate the spatial patterns of mitotic events in the bronchial epithelium.

Aim 4 Characterize the impact of chemopreventive and/or chemotherapeutic agents on early lung tumorigenesis events in reconstructed bronchial epithelium and in the bronchial biopsies of subjects entered onto the clinical trials in Project 1.

The goals of the first three specific aims of this project are essentially to develop and utilize the lung organotypic culture model to identify the factors that control ongoing clonal expansion and genetic instability in the lungs of current and former smokers. The idea behind this fourth specific aim is to integrate the information garnered from the first three specific aims to identify targeted strategies to slow preferential outgrowth of more advanced bronchial epithelial cells and to decrease the levels of ongoing genetic instability. We also proposed to determine whether treatment of these organotypic cultures with the chemopreventive agents used in the clinical trial of Project 1 would slow these aberrant properties *in vitro* and whether results obtained in the organotypic culture model reflected that seen in the lungs of the participants in the clinical trial.

Findings: We generated lentiviral vectors for inducing living color probes in primary bronchial epithelial cells to examine clonal outgrowths. We also generated lentiviral vectors for color-marked histone H2B that will permit us to directly monitor mitotic fidelity in real time in organotypic cultures of bronchial epithelial cells, and have developed lentiviral vectors containing either color-marked Cyclin D1a or Cyclin D1b that allowed us to determine the relative impact of Cyclin D1 isoform overexpression on genetic instability. Parallel studies in immortalized oral epithelial cells have demonstrated that *Cyclin D1* overexpression induces various types of mitotic instability including increased frequencies of chromosome bridges and lagging chromosome fragments and generation of binucleate cells associated with incomplete cell separation at the end of mitosis.

Aim 5. Identify gene expression signatures in epithelial cells detected by LIFE bronchoscopy that determine aggressiveness.

This new aim under the ReVITALization plan was performed in conjunction with Dr. Wistuba, Core C Director. Our preliminary results from our research in VITAL have shown that epithelial cells isolated from bronchial biopsies of LIFE-abnormal mucosa can be characterized as more aggressive (invasive and migratory) than those of LIFE-normal mucosa. Microarray analysis suggested that several CXCL-chemokine signaling pathways are mainly deregulated in LIFE-abnormal cells. Moreover, we identified that pro-angiogenic ELR+ (glutamic acid, lysine and arginine motif) chemokines were strongly upregulated by inflammatory cytokines in lung cancer cells.

Findings: We demonstrated that targeting EGFR and its signaling pathway can be a useful method for chemoprevention as shown by the successful blockage of hyperplasia and metaplasia in bronchial epithelium using MEK or EGFR inhibitor. We used pharmacological inhibitors to selectively inhibit components of the PI3K/Akt and Erk pathways to determine which pathway impacts the proliferation capacity in NHTBE cells; results suggest that the Erk signal pathway is critical for EGF-induced hyperplasia of NHTBE cells. Data demonstrated that normal bronchial epithelial cells grown in a 3-dimensional organotypic method reconstitute bronchial hyperplasia/dysplasia if elevated concentrations of ErbB1 ligands.

CXCR2 expression was determined using IHC and microarray with a large set (n=458) of NSCLC tissues. The association between cytoplasmic CXCR2 (cCXCR2) expression in tumor cells and clinico-pathological factors as well as survival was analyzed. High cCXCR2 was

associated with overall survival [Hazard ratio (HR) 1.5696; confidence interval (CI)=1.176-2.096, p-value=0.002] and recurrence-free survival (HR 1.321; CI=1.027-1.698, p-value=0.030) in a univariate Cox proportional hazards (CPH) model. These findings strongly suggest that cCXCR2 expression in NSCLC tumor cells is frequent and associated with an adverse outcome. The CXCR2/CXCR2 ligands biological axis may be associated with activation of the KRAS and NFKB signaling pathways, and poor prognosis, in lung adenocarcinomas.

Project 4: Modulation of Death Receptor-Mediated Apoptosis for Chemoprevention

(Project Leader and co-leaders: Shi-Yong Sun, Ph.D.; Taofeek Owonikoko, M.D., Ph.D.)

The objective of Project 4 is to understand the role of death receptor (DR)-mediated apoptotic pathways in lung carcinogenesis, cancer prevention, and therapy in order to develop mechanism-driven combination regimens by modulating DR-mediated apoptosis for chemoprevention and therapy of lung cancer.

Aim 1: To determine whether decoy receptor (DcR) and tumor necrosis factor-related apoptosis-inducing ligand (TRAIL) expression are reduced or lost while DR remains largely expressed and whether procaspase-8 and FLIP expression and Akt activity are increased during lung carcinogenesis.

Findings: We constructed lentiviral-inducible expression systems for the following genes, whose products are key components in the extrinsic apoptotic pathway: DR4, DR5, DcR1, DcR2 and caspase-8. In addition, we also constructed and validated lentiviral vial expression constructs for wild-type FADD, dominant-negative FADD and FADD-S194A (phosphorylation-resistant mutant). These valuable resources will be very useful for our future studies in this direction to understand and dissect this pathway in regulation of cancer development and in mediation of cancer therapy.

Aim 2: To establish TRAIL-resistant cell lines from a TRAIL-sensitive lung cancer cell line and determine whether levels of DcRs, DRs, procaspase-8, TRAIL and FLIPs and Akt activity are altered and are associated with cell resistance to TRAIL and DR-inducing agents.

Findings: We were not able to demonstrate that the TRAIL-resistant lung cancer cell lines exhibited cross-resistance to some DR-inducing agents. We focused on addressing the question of whether these agents modulate the DR-mediated apoptotic pathway and, if so, how they modulate the DR-mediated apoptotic pathway and whether the modulations impact apoptosis by these DR-inducing agents. Using celecoxib as a DR5 inducer, we revealed a novel ERK/RSK-dependent mechanism that regulates DR5 expression. Both CHOP and Elk1 are required for celecoxib-induced DR5 expression based on promoter deletion and mutation analysis and siRNA-mediated gene silencing results. Further studies revealed that oncogenic Ras and B-Raf increase DR5 expression involving co-activation of ERK/RSK and JNK signaling via enhancing CHOP, Elk1, and c-Jun-dependent transcription. **T**his study has demonstrated that the oncogenic Ras induces DR5 expression through activation of both ERK/RSK and JNK signaling pathways and subsequent CHOP, Elk1, and c-Jun-mediated gene transactivation. Cancers with Ras mutation may suitable for TRAIL-based cancer therapy.

Aim 3: To determine whether suppression of PI3K/Akt activity sensitizes premalignant and/or malignant airway epithelial cells to apoptosis induced by DR-induced agents via enhancement of TRAIL/DR-mediated mechanism.

Findings: We studied the effects of the novel Akt inhibitor API-1 on c-FLIP expression and TRAIL-induced apoptosis, and we found that API-1 potently reduced the levels of c-FLIP enhanced TRAIL's cell killing effect in both lung and head and neck cancer cells. The ongoing works will be conducted outside the scope of this grant: 1) further demonstrate the cooperative effect of API-1 and TRAIL combination on induction of apoptosis; 2) understand the mechanism(s) by which API-1 induces c-FLIP downregulation; and 3) study the relationship between Akt inhibition and c-FLIP reduction.

We tested the novel PI3K inhibitor BKM120 (Novartis) for its effect on TRAIL-mediated cell killing effect in human lung cancer cells. We found that BKM120 in combination with TRAIL exhibited enhanced killing effects in the tested cell lines. Further research to reveal the mechanism by which BMK120 enhances TRAIL-induced apoptosis will be conducted outside the scope of this grant.

Aim 4: To determine whether DRs, DcRs, c-FLIP, and procaspase-8 serve as biomarkers for lung cancer chemoprevention and therapy.

We deferred analysis of these markers in the limited clinical specimens due to the lack of compelling data, when reviewed in collaboration with the project investigators, statisticians and molecular pathologist, to justify such work at this time.

Project 5: Molecular Strategies Targeting the AKT Signaling Pathway for Lung Cancer Chemoprevention and Therapy

(PI and co-PI: Ho-Young Lee, Ph.D., Edward S. Kim, M.D.)

Our goal was to find novel chemopreventive/therapeutic agents that can prevent lung carcinogenesis effectively. Results from our work and others' have demonstrated that Akt, which has a clear role in cellular survival and transformation, is constitutively active in premalignant and malignant HBECs and in NSCLC cell lines. These findings suggest an importance of PI3K/Akt signaling pathway in lung carcinogenesis. The purpose of our studies is to determine whether activation of Akt induces malignant transformation of HBE cells and to develop novel agents inhibiting Akt activity as a strategy to prevent lung carcinogenesis.

Aim 1 Develop a retroviral vector expressing constitutively active Akt and characterize the *in vitro* and *in vivo* effects of Akt activation on the malignant transformation of HBE cells.

Findings: We constructed retroviral vectors expressing constitutively active or dominant negative Akt1, 2, or 3. The Akt constructs were confirmed by sequencing and Western blot analysis. Viral titers have been determined by the colony formation analysis. To analyze roles of Akt 1, 2 or 3 in the survival of HBE cells, BEAS2B cells were stably transfected with retroviral vectors expressing constitutively active Akt 1, 2, 3. We analyzed the survival of the cells in the presence of H2O2, and found that Akt1, 2, and 3 protected HBE cells from cell death.

Aim 2 Evaluate the ability of chemopreventive agents used in VITAL trials (gefitinib, erlotinib, SCH66336, and celecoxib, alone and in combination) to inhibit Akt activity and induce apoptosis in transformed HBE and NSCLC cell lines.

Findings: We analyzed the chemopreventive and/or therapeutic activities of agents used in the VITAL trials, including inhibitors of EGFR signaling and their downstream effectors. We found that gefitinib, erlotinib, and SCH66336 in combination with IGF-1R inhibitors effectively inhibited Akt activity and induced apoptosis in transformed HBE and NSCLC cell lines.

Aim 3 Determine whether Akt is activated in bronchial specimens from enrolled patients in VITAL trials and whether treatment with chemopreventive agents suppresses Akt level or activity in these patients.

Findings: We described the expression patterns of IGF-1R, IGFBP-3, IR, pAKT, pIGF-1R, pSrc, pmTOR, pAMPK, pEGFR, and pS6 and their correlation with clinicopathologic characteristics in a large tissue microarray. We found that: 1) this TMA approach is highly effective in identifying the expression patterns of possible biomarkers and could be useful to identify subsets of NSCLC patients who might be candidates for further clinical trials incorporating inhibitors of IGF-1R, EGFR, or Src signaling components; 2) IGF-1R and Src signaling are highly activated in patients with NSCLC and should be investigated as therapeutic targets in NSCLC patients; and 3) Src activity may counteract the antitumor action of molecularly targeted agents against IGF-1R, providing the rationale to integrate Src-targeted agents in treatment regimens with IGF-1R inhibitors for patients with NSCLC.

Core A: Administrative Core

(Core Director: Waun Ki Hong, M.D.)

Core Goals: The Administrative Core will have a dynamic, functional role in support of the individual projects, including their integration into the program as a whole. The Administrative Core will have overall fiscal, administrative and scientific responsibility for the research projects, including employment of key personnel to guarantee effective financial administration of the projects and timely, accurate compliance with reporting requirements. Such administrative control of fiscal and administrative matters will ensure that careful and appropriate direction is given to all components of the projects and that goals are met within realistic time and budget constraints.

Findings: The Administrative Core supported the research conducted in the VITAL program, and worked with the individual projects to ensure full integration into the program, fiscal accountability, and to provide organization and direction to guarantee the timely completion of the proposed research. Activities conducted include:

- Coordination of monthly and ad hoc meetings of Principal Investigators and clinical/laboratory research teams
- Administrative updates of the VITAL program at the DoD Executive Committee Meetings held every other month
- Monthly reviews of program budgets and expenditures
- Monthly reviews of personnel supported by VITAL funds
- Ensuring annual regulatory reviews of and submission of related documentation for VITAL clinical trial protocols to maintain federal, state, and institutional compliance

- Ensuring annual reviews of and submission of related documentation for animal research protocols to maintain federal, state, and institutional compliance
- Prarpation and submission of annual reports to the DoD
- Coordination of Scientific Advisory Board meetings to monitor program performance

A detailed listing of all personnel supported by VITAL funding is included in Appendix 3.

Core B: Biostatistics & Data Management Core

(Core Director: J. Jack Lee, Ph.D.)

Core Goals:

1. To provide statistical design, sample size/power calculations, and integrated, comprehensive analysis for each basic science, pre-clinical, and clinical study.
2. To develop a data management system that provides tracking, quality control, and integration of clinical, pathological, and basic science data. New database modules will be developed and integrated to the existing VITAL web-based database and with the clinical database from the Department of Thoracic/Head and Neck Medical Oncology.
3. To provide statistical and data management support for genomic and imaging studies including microarray, proteomics, protein antibody array, and spiral CT.
4. To develop and adapt innovative statistical methods pertinent to biomarker-integrated translational lung cancer studies.
5. To generate statistical reports for all projects.
6. To collaborate and assist all project investigators in the publication of scientific results.

Findings: The Biostatistics and Data Management Core worked actively with all the VITAL Projects in their research efforts in the areas of biostatistical support and consulted in the clinical trial design, implementation, conduct, and analysis of experimental results.

Two databases were created to facilitate the work performed for the VITAL Projects: the VITAL database is a web-enabled database system to facilitate the conduct of the Vanguard Trial, and the ReVITALization database was designed to integrate the retrospectively collected data with the prospectively conducted clinical trial data. We generated the statistical report for ReVITALization data incorporating the important patients' clinicopathological characteristics, treatment, and 21 biomarkers located in the histological analysis.

Core C: Pathology and Specimen Procurement Core

(Core Director: Ignacio Wistuba, M.D.)

Aim 1. Develop and maintain a repository of tissue and other biologic specimens from patients enrolled on the clinical trials in Project 1.

Findings: As of June 2011, 131 bronchoscopies have been performed at baseline, 12-, 24- and 36-month periods. From these patients, Core C has acquired, processed, and banked a total of 1,840 specimens obtained during these bronchoscopies (Table 1).

Table 1. Summary of specimens collected and banked in the Pathology Core

Type of Specimen	Number
Sputum	122
Buccal Brush	122
Bronchial Brush	737
Bronchial Wash	123
Tissue Specimens	736
Total	**1,840**

In collaboration with Project 2, mRNA was extracted from 320 bronchial epithelial samples for mRNA Affymetrix profiling, including RNA quality control and RNA amplification.

Aim 2. Maintain a comprehensive database of tissue and specimen characteristics from patients enrolled in the clinical trials of Project 1, including pathologic characteristics of each specimen, inventory and distribution.

Findings: The Biostatistics Core (Dr. J.J. Lee) has developed a Web-based database that has been used by the Pathology Core members to catalogue all the specimens obtained and banked in the Core C and to report pathology diagnosis. From the Vanguard patients, 1,104 cytological specimens and 736 bronchial biopsies have been tracked and inventoried using the Web-based database.

Aim 3. Provide comprehensive pathologic characterization of all tissues and other biologic specimens and assist in preparation and evaluation of studies involving these tissues.

Findings: Core C processed and performed histopathological diagnosis of 1,608 histology sections from patient bronchoscopies (Table 2). We examined two H&E-stained tissue sections per bronchial biopsy.

Table 2. Summary of the histopathology diagnoses made in 1,608 histology sections from bronchial biopsies obtained from Vanguard clinical trial (Project 1).

Diagnosis	N	%
No Tissue/Denuded Epithelium	45	2.8%
Normal Epithelium	1,102	68.5%
Goblet Cell Metaplasia (GCM)	94	5.8%
Basal Cell Hyperplasia (BCH)	292	18.2%
Combined GCM/BCH	386	24.0%
Squamous Metaplasia	57	3.5%
Angiogenic Squamous Dysplasia (ASD)	2	0.1%
Mild Dysplasia	8	0.5%
Moderate Dysplasia	8	0.5%

Aim 4. Provide centralized immunohistochemistry and laser capture microdissection services, nucleic acid extractions and assistance with construction and evaluation of tissue arrays.

Findings: Core C performed the analysis of molecular markers using lung cancer and respiratory epithelium tissue specimens. We discovered that twenty-nine markers had a significant association with *EGFR* mutation in tumors in the multivariate analysis adjusting by patients' sex, smoking status, and tumor stage. Additionally, 47 markers showed significant differences in the level of expression comparing patients' smoking status, including current, former, and never-smokers. Our findings indicated that there are multiple molecular differences between lung adenocarcinomas arising in never- and ever-smokers, suggesting that they are different entities. These findings have implications for the selection of molecular targets for developing novel therapy in patients with lung adenocarcinoma based on their smoking history.

Aim 5. Identify ~600 surgically resected tissue specimens from stages I/II NSCLC (tumor, normal and abnormal adjacent bronchial epithelium specimens) and their complete clinical and pathologic information.

Findings: We identified tumor and adjacent normal epithelium and preneoplastic lesions from more than 500 NSCLCs as part of the TMA set II. We completed the construction of the TMA set in 2008, and we used it for the analysis of molecular markers by IHC. Nineteen TMAs were constructed using triplicate tissue cores (1 mm diameter) from 598 NSCLCs obtained from 558 patients. In addition, in collaboration with Project 1 (Dr. E. Kim) and Biostatistics Core (Dr. JJ Lee), detailed demographic and clinical information was obtained in all the cases, including follow-up information for adjuvant therapy, secondary tumor development, recurrence, metastasis pattern, and survival. All the pathological and clinical data was entered in database modules developed by the Biostatistic Core.

Aim 6. Examine over 40 biomarkers in those specimens by immunohistochemical (IHC) and tissue microarrays (TMAs).

Findings: Our initial aim was to study over 40 markers by IHC using TMA methodology. However, as part of the ReVITALization project, we studied 25 IHC markers in total as requested by the research projects: Project 2 (J. Minna, L. Mao, and R. Lotan), six markers; Project 3 (P. Koo and W. Hittelman), five markers; Project 4 (F. Khuri), four markers; Project 5 (H-Y Lee), ten markers. Based in the tissue and data available from the research projects, 21 markers were examined and reported. The data generated by Core C were reported to the Biostatistics Core (Core B) for analysis. We also have TMA histology sections for future IHC analysis, including those generated by the analysis of the data obtained during the mRNA profiling of the Vanguard bronchoscopy biopsies.

DRP - 1: Enhanced Oral/Head and Neck Examination Protocol

(PI and co-PIs: Waun Ki Hong, M.D., Jack Martin, D.D.S., Captain Larry Williams)

This project was discontinued.

DRP - 2: Biomarkers for Aggressive Lung Carcinomas in African American Men

(PI: Sharon Lobert, Ph.D., University of Mississippi, Jackson, MS)

We hypothesized that 1) β class III tubulin levels are higher in NSCLCs from African American men compared to white men; 2) The expression of proteins that alter microtubule dynamics is

increased in NSCLCs from African American men compared to white men. Higher levels of these proteins would reduce the effectiveness of antimitotic agents such as paclitaxel or vinorelbine used in the treatment of NSCLC that stabilize or destabilize mitotic spindles.

Findings: 64 NSCLCs (Stages IA, IB and IV) and 12 normal lung tissue specimens were obtained from the NCI Cooperative Human Tissue Network and quantitative real-time RT-PCR was used to measure tubulin isotype, stathmin and MAP4 mRNA levels. Our goal was to determine whether β-tubulin mRNA levels could be useful as biomarkers. Using quantitative real-time RT-PCR, we measured the levels of seven classes of β-tubulin isotypes, stathmin, and MAP4 in 64 NSCLC and 12 normal lung tissue specimens. We found significantly higher fractions of β-tubulin classes II and V mRNA compared to other isotypes in all tumor samples ($p < 0.05$). In addition, the ratio of β-tubulin classes II/V mRNA was significantly higher in NSCLCs compared to normal tissues ($p < 0.001$). The data suggest that the ratio of β-tubulin classes II and V mRNA could be useful as a biomarker for NSCLCs, tumor differentiation and/or aggressiveness. Furthermore, the ratio of MAP4 to stathmin mRNA was found to be higher in diseased tissues compared to normal lung tissues suggesting this ratio might also be used as a clinically relevant biomarker. These changes are likely due to dysregulation of microtubule dynamics in the disease state, essential for cell division and proliferation, but these mechanisms need to be further explored.

KEY RESEARCH ACCOMPLISHMENTS (IN SUMMARY)

Project 1: Biologic Approaches for Adjuvant Treatment of Aerodigestive Tract Cancer

- Enrolled a total of 54 patients to the Vanguard trial, and with 38 evaluable patients (having completed both the baseline and 12-month bronchoscopy).
- Performed statistical analyses on data from 542 patients (including 19 from the Vanguard trial) whose tumor specimens were analyzed for 21 markers.
- Completed tissue identification and clinical data collection of over 500 archived tissue specimens from the pathology database for the ReVITALization plan.

Project 2: Identification of Biomarkers of Response to Chemoprevention Agents in Lung Epithelium

- Generated HBECS from over 50 different individuals and immortalized 15 peripheral small airway epithelial cells (HSAECs).
- Discovered that the HBECs and HSAECs are immortalized cells that express many properties of pulmonary stem cells and have the capacity to differentiate along several lineages.
- Demonstrated that amplification is far more common a mechanism of oncogene activation than previously believed and that specific regions of the genome are hotspots of amplification.
- Produced data to illustrate that genetic alteration of BRF2 represents a novel mechanism of lung tumorigenesis through the increase of Pol III-mediated transcription in cancer.
- Derived a five-gene signature, comprised of genes UBE2C, MCM2, MCM6, TPX2, and FEN1, that was effective in predicting the survival of lung adenocarcinoma patients upon analysis of publicly available NSCLC microarray datasets.
- Analyzed genes differentially expressed among airways sampled at different anatomical locations of the lung and at various distances from the original resected tumors and identified site-dependent differentially expressed genes and pathways in the field of cancerization that have potential value in predicting recurrence or second primary tumor development.

Project 3: Premalignant Bronchial Epithelia: Molecular and Cellular Characterization of Lung Tumorigenesis

- Identified the consistently regulated genes and the signaling pathway that is critical for tumorigenesis.
- Developed a color-coding methodology to distinguish subpopulations of cells within heterogeneous lung tumor and immortalized human bronchial epithelial cell populations.
- Demonstrated that mitotic instability was associated with increased expression of stress-response proteins.
- Illustrated that mitotic directionality and fidelity depend on cell-cell and cell-substrate interactions.
- Generated lentiviral vectors for inducing living color probes in primary bronchial epithelial cells to examine clonal outgrowths.
- Demonstrated that chemokine receptor CXCR2 expression in tumor cells is associated with a poor prognosis in NSCLC.
- Demonstrated that CREB and NF-kB-regulated CXC chemokine gene expression in lung carcinogenesis.
- Used pharmacological inhibitors to selectively inhibit components of the PI3K/Akt and Erk pathways to determine which pathway impacts the proliferation capacity in NHTBE cells.
- Demonstrated growth suppression of lung cancer cells by targeting CREB.

Project 4: Modulation of Death Receptor-Mediated Apoptosis for Chemoprevention

- Constructed lentiviral-inducible expression systems for the following genes, whose products are key components in the extrinsic apoptotic pathway: DR4, DR5, DcR1, DcR2 and caspase-8.
- Constructed and validated lentiviral vial expression constructs for wild-type FADD, dominant-negative FADD and FADD-S194A.
- Demonstrated ERK/RSK-dependent regulation of DR5 expression through co-activation of CHOP and ElK1 transcriptional factors.
- Conducted the first detailed experiment to demonstrate the mechanism by which the oncogenic Ras induces DR5 expression. This finding provides a scientific rationale for targeting tumors with Ras or B-Raf mutation with TRAIL- or DR5 agonistic antibody-based therapies.
- Demonstrated that the Akt inhibitor API-1 downregulates c-FLIP and enhances TRAIL-induced apoptosis.
- Demonstrated that the PI3K inhibitor BKM120 sensitizes lung cancer cells to TRAIL-induced apoptosis.

Project 5: Molecular Strategies Targeting the AKT Signaling Pathway for Lung Cancer Chemoprevention and Therapy

- Constructed retroviral vectors expressing constitutively active or dominant negative Akt1, 2, or 3.
- Demonstrated that that Akt1, 2, and 3 protected HBE cells from cell death.
- Tested gefitinib, erlotinib, and SCH66336 in combination with IGF-1R inhibitors and inhibited Akt activity and induced apoptosis in transformed HBE and NSCLC cell lines.
- Described the expression patterns of IGF-1R, IGFBP-3, IR, pAKT, pIGF-1R, pSrc, pmTOR, pAMPK, pEGFR, and pS6 in a large tissue microarray.
- Discovered that IGF-1R and Src signaling are highly activated in patients with NSCLC.
- Found that Src activity may counteract the antitumor action of molecularly targeted agents against IGF-1R.

Core B: Biostatistics & Data Management Core

- Created two databases to store and analyze patient data: the VITAL database to facilitate the conduct of the Vanguard Trial, and the ReVITALization database to integrate the retrospectively collected data with the prospectively conducted clinical trial data
- Analyzed data for Project investigators to predict patient outcome.
- Completed the statistical analysis on the ReVITALization data to build a risk model.

Core C: Pathology and Specimen Procurement Core

- Acquired, processed, and banked a total of 1,840 specimens obtained during the 131 bronchoscopies from patients enrolled in the Vanguard trial (Project 1).
- Identified tumor and adjacent normal epithelium and preneoplastic lesions from more than 500 NSCLCs.
- Analyzed molecular markers using lung cancer and respiratory epithelium tissue specimens.
- Discovered that twenty-nine markers had a significant association with *EGFR* mutation in tumors in the multivariate analysis adjusting by patients' sex, smoking status, and tumor stage.
- Identified multiple molecular differences between lung adenocarcinomas arising in never- and ever-smokers, suggesting that they are different entities.

- Obtained detailed demographic and clinical information from 558 patients, including follow-up information for adjuvant therapy, secondary tumor development, recurrence, metastasis pattern, and survival.
- Studied 21 markers by IHC using TMA methodology.

Developmental Research Project (DRP) 2: Biomarkers for Aggressive Lung Carcinomas in African American Men

- Determined that the ratio of β-tubulin classes II/V mRNA was significantly higher in NSCLCs compared to normal and correlated with level of differentiation.
- Determined that ratio of MAP4 to stathmin mRNA was also found to be higher in tumor than normal lung tissue.

REPORTABLE OUTCOMES

Publications

Aggarwal S, Kim SW, Ryu SH, Chung WC, Koo JS. Growth Suppression of Lung Cancer Cells by Targeting Cyclic AMP Response Element-Binding Protein. *Cancer Research.* 2008; Feb 15;68(4):981-8. PMCID: PMC2921320.

Behrens C, Feng L, Kadara H, Kim HJ, Lee JJ, Mehran R, Hong WK, Lotan R, Wistuba I. Expression of Interleukin-1 Receptor-Associated Kinase-1 in Non-Small Cell Lung Carcinoma and Preneoplastic Lesions. *Clinical Cancer Research*. 2010 Jan 1;16(1):34-44. PMCID: PMC2811365.

Chen S, Fu L, Raja SM, Yue P, Khuri FR, Sun SY. Dissecting the roles of DR4, DR5 and c-FLIP in the regulation of geranylgeranyltransferase I inhibition-mediated augmentation of TRAIL-induced apoptosis. *Molecular Cancer.* 2010 Jan 29;9:23. PMCID: PMC2824632.

Chen S, Liu XG, Yue P, Schonthal AH, Khuri FR, Sun S-Y. CCAAT/enhancer binding protein homologous protein-dependent death receptor 5 induction and ubiquitin/proteasome-mediated cellular FLICE-inhibitory protein downregulation contribute to enhancement of tumor necrosis factor-related apoptosis-inducing ligand-induced apoptosis by dimethyl-celecoxib in human non small-cell lung cancer cells. *Molecular Pharmacology.* 72:1269-79, 2007. PMID: 17684158.

Cucciarelli V, Hiser L, Smith H, Frankfurter A, Spano A, Correia JJ, Lobert S. b-Tubulin isotype classes II and V expression patterns in nonsmall cell lung carcinomas. *Cell Motility and the Cytoskeleton*. 2008; Aug;65(8):675-85. PMID: 18613117.

Elrod HA, Lin Y-D, Yue P, Wang X, Lonail S, Khuri FR, Sun S-Y. The alkylphospholipid perifosine induces apoptosis of human lung cancer cells requiring inhibition of Akt and activation of the extrinsic apoptotic pathway. *Molecular Cancer Therapeutics* 6:2029-38, 2007. PMID: 17604333.

Elrod HA, Sun S-Y. Modulation of death receptors by cancer therapeutic agents. *Cancer Biology & Therapy.* 2008 Feb;7(2):163-73. PMID: 18059181.

Elrod HA, Sun SY. PPARgamma and Apoptosis in Cancer. *PPAR Research.* 2008:704165. PMCID: PMC2442903.

Elrod HA, Yue P, Khuri FR, Sun S-Y. Celecoxib antagonizes perifosine's anticancer activity involving a cyclooxygenase-2-dependent mechanism. *Molecular Cancer Therapeutics*. 2009 Sep;8(9):2575-85. PMCID: PMC2755226.

Fan S, Li Y, Yue P, Khuri FR, Sun SY. The eIF4E/eIF4G interaction inhibitor 4EGI-1 augments TRAIL-induced apoptosis through DR5 induction and c-FLIP downregulation independent of inhibition of cap-dependent protein translation. *Neoplasia*. 2010 Apr;12(4):346-56. PMCID: PMC2847742.

Gazdar AF,Minna JD. Deregulated EGFR signaling during lung cancer Progression: Mutations, amplicons and autocrine loops. *Cancer Prevention Research.* 2008 Aug;1(3):156-60. PMCID: PMC2849648.

Guha U, Chaerkady R, Marimuthu A, Patterson AS, Kashyap MK, Harsha HC, Sato M, Bader JS, Lash AE, Minna JD, Pandey A, Varmus HE. Comparisons of tyrosine phosphorylated proteins in cells expressing lung cancer-specific alleles of EGFR and KRAS. *Proceedings of the National Academy of Sciences U S A.* 2008; Sep 16;105(37):14112-7. PMCID: PMC2531065.

Han J-Y, Liu DD, Lee JJ, Kurie JM, Lotan R, Hong WK, Lee H-Y. 9-*cis*-retinoic acid treatment increases serum concentrations of α-tocopherol in former smokers. *Clinical Cancer Research.* 11:2305-11, 2005. PMID: 15788681.

Hiser L, Aggarwal, Young R, Spano A, Frankfurter A, Correia JJ, Lobert S. Comparison of beta-tubulin mRNA and protein levels in twelve human cancer cell lines. *Cell Motility and the Cytoskeleton.* 2006 Jan;63(1):41-52. PMID: 16362954.

Ivanova MM, Mazhawidza W, Dougherty SM, Minna JD, Klinge CM. Activity and intracellular location of estrogen receptors alpha and beta in human bronchial epithelial cells. *Molecular and Cellular Endocrinology.* 2009 Jun 16;305(1-2):12-21. PMCID: PMC2767333.

Jeong Y, Xie Y, Xiao G, Behrens C, Girard L, Wistuba II, Minna JD, Mangelsdorf DJ. Nuclear receptor expression defines a set of prognostic biomarkers for lung cancer. *PLoS Medicine.* 2010 Dec 14;7(12):e1000378. PMCID: PMC3001894.

Jin Q, Menter DG, Mao, L, Hong WK, Lee HY. Survivin expression in normal human brochial epithelial cells: an early and critical step in tumorigenesis induced by tobacco exposure. *Carcinogenesis.* 2008; Aug;29(8):1614-22. PMCID: PMC2516487.

Kadara H, Behrens C, Yuan P, Solis LM, Liu D, Gu X, Minna JD, Lee JJ, Kim ES, Hong WK, Wistuba II, Lotan R. A five-gene and corresponding-protein signature for stage-I lung adenocarcinoma prognosis. *Clinical Cancer Research.* 2011 Mar 15;17(6):1490-501. PMCID: PMC3079395.

Kadara H, Lacroix L, Behrens C, Solis L, Gu X, Lee JJ, Tahara E, Lotan D, Hong WK, Wistuba II, Lotan R. Identification of gene signatures and molecular markers for human lung cancer prognosis using an in vitro lung carcinogenesis system. *Cancer Prevention Research.* 2009 2(8):702-11. PMID: 19638491.

Kim ES, Hong WK, Lee JJ, Mao L, Morice RC, Liu DD, Jimenez CA, Eapen GA, Lotan R, Tang X, Newman RA, Wistuba II, Kurie JM. Biological activity of celecoxib in the bronchial epithelium of current and former smokers. *Cancer Prevention Research.* 2010 Feb;3(2):148-59. PMID: 20103722.

Kim WY, Jin Q, Oh SH, Kim ES, Yang YJ, Lee DH, Feng L, Behrens C, Prudkin L, Miller YE, Lee JJ, Lippman SM, Hong WK, Wistuba II, Lee HY. Elevated epithelial insulin-like growth factor expression is a risk factor for lung cancer development. *Cancer Research*. 2009 Sep 15;69(18):7439-48. PMCID: PMC2745504.

Kim WY, Kim MJ, Moon H, Yuan P, Kim JS, Woo JK, Zhang G, Suh YA, Feng L, Behrens C, Van Pelt CS, Kang H, Lee JJ, Hong WK, Wistuba II, Lee HY. Differential impacts of insulin-like growth factor-binding protein-3 (IGFBP-3) in epithelial IGF-induced lung cancer development. *Endocrinology*. 2011 Jun;152(6):2164-73. PMCID: PMC3100627.

Kim YH, Kwei KA, Girard L, Salari K, Kao J, Pacyna-Gengelbach M, Wang P, Hernandez-Boussard T, Gazdar AF, Petersen I, Minna JD, Pollack JR. Genomic and functional analysis identifies CRKL as an oncogene amplified in lung cancer. *Oncogene.* 2009 Dec 7. [Epub ahead of print]. PMID: 19966867.

Kong M, Lee JJ. A generalized response surface model with varying relative potency for assessing drug interaction. *Biometrics* 62:986-95, 2006. PMID: 17156272.

Kong M, Lee JJ. A semiparametric response surface model for assessing drug interaction. *Biometrics*. 2008; Jun;64(2):396-405. PMID: 17900314.

Kwei KA, Kim YH, Girard L, Kao J, Pacyna-Gengelbach M, Salari K, Lee J, Choi YL, Sato M, Wang P, Hernandez-Boussard T, Gazdar AF, Petersen I, Minna JD, Pollack JR. Genomic profiling identifies TITF1 as a lineage-specific oncogene amplified in lung cancer. *Oncogene.* 2008; Jun 5;27(25):3635-40. PMCID: PMC2903002.

Larsen JE, Spinola M, Gazdar AF, Minna JD. An overview of the molecular biology of lung cancer. *In:* H. I. Pass, D. P. Carbone, D. H. Johnson, J. D. Minna, A. T. Turrisi III, and G. V. Scagliotti (eds.), *Lung Cancer: Principles and Practice*, 4th edition. Philadelphia: Lippincott Williams & Wilkins, 2009.

Lee H-Y. Molecular mechanisms of deguelin-induced apoptosis in transformed human bronchial epithelial cells. *Biochemical Pharmacology.* 2004 Sep 15;68(6):1119-24. PMID: 15313408.

Lee H-Y, Chang YS, Han J-Y, Liu D, Lee JJ, Lotan R, Hong WK. Effects of 9-*cis*-retinoic acid on the insulin-like growth factor axis in former smokers. *Journal of Clinical Oncology.* 2005 Jul 1;23(19):4439-49. PMID: 15994153.

Lee H-Y, Oh SH, Woo J-K, Price R, Cody D, Tran H, Hong WK. Chemopreventive effects of deguelin, a novel Akt inhibitor, on tobacco-induced lung tumorigenesis*. Journal of the National Cancer Institute*. 2005 Nov 16;97(22):1695-9. PMID: 16288123.

Lee J, Ryu SH, Kang SM, Chung WC, Gold KA, Kim ES, Hittelman WN, Hong WK, Koo JS. Prevention of Bronchial Hyperplasia by EGFR Pathway Inhibitors in an Organotypic Culture Model. *Cancer Prevention Research*. 2011 Jul 12. [Epub ahead of print]. PMID: 21505178.

Lee JJ, Kong M. Confidence Interval of Interaction Index for Assessing Multiple Drug Interaction. *Statistics in Biopharmaceutical Research*. 2009 Feb 1;1(1):4-17. PMCID: PMC2796809.

Lee JJ, Kong M, Ayers GD, Lotan R. Interaction index and different methods for determining drug interaction in combination therapy. *Journal of Biopharmaceutical Statistics.* 17:461-80, 2007. PMID: 17479394.

Li C, Chen S, Yue P, Lonial S, Khuri FR, Sun SY. The proteasome inhibitor PS-341 (Bortezomib) induces calpain-dependent IκBα degradation. *Journal of Biological Chemistry.* 2010 May 21;285(21):16096-104. PMCID: PMC2871478.

Lin YD, Chen S, Yue P, Zou W, Bendrook DM, Liu S, Le TC, Berlin KD, Khuri FR, Sun SY. CAAT/enhancer binding protein homologous protein-dependent end death receptor 5 induction is a major component of SHetA2-induced apoptosis in lung cancer cells. *Cancer Research*.

2008; Jul 1;68(13):5335-44. PMID: 18593935.

Lin Y, Liu X, Yue P, Benbrook DM, Berlin KD, Khuri FR, Sun SY. Involvement of c-FLIP and survivin down-regulation in flexible heteroarotinoid-induced apoptosis and enhancement of TRAIL-initiated apoptosis in lung cancer cells. *Molecular Cancer Therapeutics.* 2008; Nov 7(11):3556-65. PMID: 19001438.

Liu P, Vikis HG, Wang D, Lu Y, Wang Y, Schwartz AG, Pinney SM, Yang P, de Andrade M, Petersen GM, Wiest JS, Fain PR, Gazdar A, Gaba C, Rothschild H, Mandal D, Coons T, Lee J, Kupert E, Seminara D, Minna J, Bailey-Wilson JE, Wu X, Spitz MR, Eisen T, Houlston RS, Amos CI, Anderson MW, You M. Familial Aggregation of Common Sequence Variants on 15q24-25.1 in Lung Cancer. *Journal of the National Cancer Institute.* 2008; Sep 17;100(18):1326-30. PMCID: PMC2538550.

Liu X, Yue P, Khuri FR, Sun S-Y. Decoy receptor 2 (DcR2) is a p53 target gene and regulates chemosensitivity. *Cancer Research*. 2005 Oct 15;65(20):9169-75. PMID: 16230375.

Liu XG, Yue P, Chen S, Hu L, Lonial S, Fadlo FR, Sun S-Y. The proteasome inhibitor PS-341 upregulates death receptor 5 expression leading to induction of apoptosis and enhancement of TRAIL-induced apoptosis despite upregulation of c-FLIP and survivin in human lung cancer cells. *Cancer Research.* 67:4981-8, 2007. PMID: 17510429.

Liu XG, Yue P, Schonthal AH, Khuri FR, Sun S-Y. Cellular FLICE-Inhibitory Protein Down-regulation Contributes to Celecoxib-Induced Apoptosis in Human Lung Cancer Cells. *Cancer Research.* 2006 Dec 1;66(23):11115-9. PMID: 17145853.

Liu X, Yue P, Zhou Z, Khuri FR, Sun S-Y. Death receptor upregulation and celecoxib-induced apoptosis in human lung cancer cells. *Journal of the National Cancer Institute.* 2004 Dec 1;96(23):1769-80. PMID: 15572759.

Lockwood WW, Chari R, Coe BP, Girard L, Macaulay C, Lam S, Gazdar AF, Minna JD, Lam WL. DNA amplification is a ubiquitous mechanism of oncogene activation in lung and other cancers. *Oncogene.* 2008;27:4615-24. PMCID: PMC2849646.

McMahon KA, Zajicek H, Li WP, Peyton MJ, Minna JD, Hernandez VJ, Luby-Phelps K, Anderson RG. SRBC/Cavin-3 Is A Caveolin Adapter Protein That Regulates Caveolae Function. *EMBO Journal.* 2009 Apr 22;28(8):1001-15. PMCID: PMC2683698.

Morgillo F, Kim W-Y, Kim ES, Ciardiello F, Hong WK, Lee HY. Implication of the insulin-like growth factor-IR pathway in the resistance of non-small cell lung cancer cells to treatment with gefitinib. *Cancer Research* and *Clinical Cancer Research* 13(9):2795-2803, 2007. PMID: 17473213.

Morgillo F, Woo JK, Kim ES, Hong WK, Lee H-Y. Heterodimerization of IGFR/EGFR and Induction of Survivin Expression Counteracts the Antitumor Action of Erlotinib. *Cancer Research.* 2006 Oct 15;66(20):10100-11. PMID: 17047074.

Oh SH, Kim W-Y, Woo J-K, Kim J-H, Younes MN, Myers JN, Hong WK, Lee H-Y. Identification of insulin-like growth factor binding protein-3 as a farnesyltransferase inhibitor SCH66336-induced negative regulator of angiogenesis in head and neck squamous cell carcinoma. *Clinical Cancer Research.* 2006 Jan 15;12(2):653-61. PMID: 16428512.

Oh YT, Liu X, Yue P, Kang S, Chen J, Taunton J, Khuri FR, Sun SY. ERK/RSK signaling positively regulates death receptor 5 expression through co-activation of CHOP and Elk1. *Journal of Biological Chemistry.* 2010 Dec 31;285(53):41310-9. PMCID: PMC3009856.

Prudkin L, Behrens C, Liu DD, Zhou X, Ozburn NC, Bekele BN, Minna JD, Moran C, Roth JA, Ji L, Wistuba II. Loss and reduction of Fus1 protein expression is a frequent phenomenon in the pathogenesis of lung cancer. *Clinical Cancer Research.* 2008; Jan 1;14(1):41-7. PMCID: PMC2833352.

Prudkin L, Liu DD, Ozburn NC, Sun M, Behrens C, Tang X, Brown KC, Bekele BN, Moran C, Wistuba II. Epithelial-to-mesenchymal transition in the development and progression of adenocarcinoma and squamous cell carcinoma of the lung. *Modern Pathology.* 2009 May;22(5):668-78. PMCID: PMC2675657.

Prudkin L, Tang X, Wistuba II. Germ-line and somatic presentations of the EGFR T790M mutation in lung cancer. *Journal of Thoracic Oncology*. 2009 Jan; 4:139-4. PMID: 19096324.

Qiu Y, Liu X, Yue P, Lonial S, Khuri FR, Sun S-Y. The farnesyltransferase inhibitor R115777 upregulates DR5 expression and enhances TRAIL-induced apoptosis in human lung cancer cells. *Cancer Research.* 67:4973-80, 2007. PMID: 17510428.

Raja SM, Chen S, Yue P, Acker TM, Lefkove B, Arbiser J, Khuri FR, Sun SY. The natural product honokiol preferentially inhibits c-FLIP and augments death receptor-induced apoptosis. *Molecular Cancer Therapeutics.* 2008; Jul;7(7):2212-23. PMCID: PMC2756752.

Raso MG, Behrens C, Herynk MH, Liu S, Prudkin L, Ozburn NC, Woods DM, Tang X, Mehran RJ, Moran C, Lee JJ, Wistuba II. Immunohistochemical expression of estrogen and progesterone receptors identifies a subset of NSCLCs and correlates with EGFR mutation. *Clinical Cancer Research*. 2009 Sep 1;15(17):5359-68. PMCID: PMC2893045.

Sato M, Vaughan MB, Girard L, Peyton M, Lee W, Shames DS, Ramirez RD, Sunaga N, Gazdar AF, Shay JW, Minna JD. Multiple oncogenic changes (K-RASV12, p53 knockdown, mutant EGFRs, p16 bypass, telomerase) are not sufficient to confer a full malignant phenotype on human bronchial epithelial cells. *Cancer Research*. 2006 Feb 15;66(4):2116-28. PMID: 16489012.

Seo HS, Liu DD, Bekele BN, Kim MK, Pisters K, Lippman SM, Wistuba II, Koo JS. Cyclic AMP response element-binding protein overexpression: a feature associated with negative prognosis in never smokers with non-small cell lung cancer. *Cancer Research.* 2008 Aug 1;68(15):6065-73. PMCID: PMC3058903.

Shivapurkar N, Stastny V, Xie Y, Prinsen C, Frenkel E, Czerniak B, Thunnissen FB, Minna JD, Gazdar AF. Differential methylation of a short CpG-rich sequence within exon 1 of TCF21 gene: a promising cancer biomarker assay. *Cancer Epidemiology Biomarkers Prevention.* 2008 Apr;17(4):995-1000. PMCID: PMC2762937.

Solis LM, Raso MG, Kalhor N, Behrens C, Wistuba I, Moran CA. Primary oncocytic adenocarcinomas of the lung: a clinicopathologic, immunohistochemical, and molecular biologic analysis of 16 cases. *American Journal of Clinical Pathology*. 2010 Jan;133(1):133-40. PMID: 20023269.

Sun HX, Chung WC, Ryu SH, Ju ZL, Tran HT, Kim ES, Kurie JM, Koo JS. CREB- and NF-κB-Regulated CXC Chemokine Gene Expression in Lung Carcinogenesis. *Cancer Prevention Research.* 1(5):316-328, 2008. PMCID: PMC2768131.

Sun S-Y. Chemopreventive agent-induced modulation of death receptors. *Apoptosis*. 2005 Dec;10(6):1203-10. PMID: 16215675.

Sun S-Y. N-acetylcysteine, reactive oxygen species and beyond. (Commentary) *Cancer Biology & Therapy*, 2010 Jan 10;9(2). PMCID: PMC2854288.

Sun S-Y, Liu X, Yue P, Zhou Z, Zou W, Marcus AI, Khuri FR. The farnesyltransferase inhibitor lonafarnib induces CCAAT/enhancer-binding protein homologous protein-dependent expression of death receptor 5, leading to induction of apoptosis in human cancer cells. *Journal of Biological Chemistry.* 282:18800-9, 2007. PMID: 17493934.

Tang X, Kadara H, Behrens C, Liu DD, Xiao Y, Rice D, Gazdar AF, Fujimoto J, Moran C, Varella-Garcia M, Lee JJ, Hong WK, Wistuba II. Abnormalities of the TITF-1 lineage-specific oncogene in NSCLC: implications in lung cancer pathogenesis and prognosis. *Clinical Cancer Research.* 2011 Apr 15;17(8):2434-43. PMCID: PMC3078948.

Tang X, Shigematsu H, Bekele B N, Roth JA, Minna J D, Hong WK, Gazdar A F, Wistuba I. EGFR tyrosine kinase domain mutations are detected in histologically normal respiratory epithelium in lung cancer patients. *Cancer Research*. 65:7568-7572, 2005. PMID: 16140919.

Tang X, Varella-Garcia M, Xavier AC, Massarelli E, Ozburn N, Moran C, Wistuba I. Epidermal growth factor receptor abnormalities in the pathogenesis and progression of lung adenocarcinomas. *Cancer Prevention Research.* 2008; 1: 192-200. PMID: 19138956.

Tsao AS, Tang X, Sabloff B, Xiao L, Shigematsu H, Roth J, Spitz M, Hong WK, Gazdar A, Wistuba I. Clinical-pathological characteristics of the EGFR gene mutation in non-small cell lung cancer. *Journal of Thoracic Oncology*. 2006 Mar;1(3):231-9. PMID: 17409862.

Vaughan MB, Ramirez RD, Wright WE, Minna JD, Shay JW. A three-dimensional model of differentiation of immortalized human bronchial epithelial cells. *Differentiation*. 2006 Apr;74(4):141-8. PMID: 16683984.

Vikis H, Sato M, James M, Wang D, Wang Y, Wang M, Jia D, Liu Y, Bailey-Wilson JE, Amos CI, Pinney SM, Petersen GM, de Andrade M, Yang P, Wiest JS, Fain PR, Schwartz AG, Gazdar A, Gaba C, Rothschild H, Mandal D, Kupert E, Seminara D, Viswanathan A, Govindan R, Minna J, Anderson MW, You M. EGFR-T790M Is a Rare Lung Cancer Susceptibility Allele with Enhanced Kinase Activity. *Cancer Research.* 2007;67:4665-70. PMID: 17510392.

Weerasinghe P, Garcia GE, Zhu Q, Yuan P, Feng L, Mao L, Jing N. Inhibition of Stat3 activation and tumor growth suppression of non-small cell lung cancer by G-quartet oligonucleotides. *International Journal of Oncology.* 31(1):129-36, 2007. PMID: 17549413.

Weir BA, Woo MS, Getz G, Perner S, Ding L, Beroukhim R, Lin WM, Province MA, Kraja A, Johnson LA, Shah K, Sato M, Thomas RK, Barletta JA, Borecki IB, Broderick S, Chang AC, Chiang DY, Chirieac LR, Cho J, Fujii Y, Gazdar AF, Giordano T, Greulich H, Hanna M, Johnson BE, Kris MG, Lash A, Lin L, Lindeman N, Mardis ER, McPherson JD, Minna JD, Morgan MB,

Nadel M, Orringer MB, Osborne JR, Ozenberger B, Ramos AH, Robinson J, Roth JA, Rusch V, Sasaki H, Shepherd F, Sougnez C, Spitz MR, Tsao MS, Twomey D, Verhaak RG, Weinstock GM, Wheeler DA, Winckler W, Yoshizawa A, Yu S, Zakowski MF, Zhang Q, Beer DG, Wistuba II, Watson MA, Garraway LA, Ladanyi M, Travis WD, Pao W, Rubin MA, Gabriel SB, Gibbs RA, Varmus HE, Wilson RK, Lander ES, Meyerson M. Characterizing the cancer genome in lung adenocarcinoma. *Nature.* 450(7171):893-8, 2007. PMCID: PMC2538683.

William WN, Kim JS, Liu DD, Solis L, Behrens C, Lee JJ, Lippman SM, Kim ES, Hong WK, Wistuba II, Lee HY. The impact of phosphorylated AMP-activated protein kinase expression on lung cancer survival. *Annals of Oncology.* 2011 Mar 23. PMID: 21430184.

Wistuba I. Genetics of preneoplasia: lessons from lung cancer. *Current Molecular Medicine.* 7(1):3-14, 2007. PMID: 17311529.

Wistuba I, Gazdar AF. Lung cancer preneoplasia. *Annual Review of Pathology: Mechanisms of Disease*. 2006;1:331-48. PMID: 18039118.

Wistuba I, Meyerson M. Chromosomal Deletions and Progression of Premalignant Lesions. *Cancer Prevention Research.* 2008; 1;404-408. PMID: 19138986.

You M, Wang D, Liu P, Vikis H, James M, Lu Y, Wang Y, Wang M, Chen Q, Jia D, Liu Y, Wen W, Yang P, Sun Z, Pinney SM, Zheng W, Shu XO, Long J, Gao YT, Xiang YB, Chow WH, Rothman N, Petersen GM, de Andrade M, Wu Y, Cunningham JM, Wiest JS, Fain PR, Schwartz AG, Girard L, Gazdar A, Gaba C, Rothschild H, Mandal D, Coons T, Lee J, Kupert E, Seminara D, Minna J, Bailey-Wilson JE, Amos CI, Anderson MW. Fine mapping of chromosome 6q23-25 region in familial lung cancer families reveals RGS17 as a likely candidate gene. *Clinical Cancer Research.* 2009 Apr 15;15(8):2666-74. PMCID: PMC2746091.

Zhang L, Lee JJ, Tang H, Fan HT, Xiao L, Ren H, Kurie J, Morice RC, Hong WK, Mao L. Impact of smoking cessation on global gene expression in the bronchial epithelium of chronic smokers. *Cancer Prevention Research.* 2008; 1:112-118. PMID: 19138944.

Zou W, Chen S, Liu XG, Yue P, Sporn MB, Khuri FR, Sun S-Y. c-FLIP downregulation contributes to induction of apoptosis and enhancement of TRAIL-induced apoptosis by the novel synthetic triterpenoid methyl-2-cyano-3, 12-dioxooleana-1, 9-dien-28-oate (CDDO-Me) in human lung cancer cells. *Cancer Biology & Therapy.* 2007 Oct;6(10):1614-20. PMID: 18253090.

Zou W, Liu X, Yue P, Khuri FR, Sun SY. PPARγ ligands enhance TRAIL-induced apoptosis through DR5 upregulation and c-FLIP downregulation in human lung cancer cells. *Cancer Biology & Therapy.* 2007 Jan;6(1):99-106. PMID: 17172826.

Zou W, Yue P, Khuri FR, Sun SY. Coupling of endoplasmic reticulum stress to CDDO-Me-induced up-regulation of death receptor 5 via a CHOP-dependent mechanism involving JNK activation. *Cancer Research.* 2008 Sep 15;68(18):7484-92. PMCID: PMC2597446.

Abstracts

Behrens C, Lin H, Nunez M, Yuan P, Solis LM, Raso MG, Prudkin L, Sun M, Li X, Tang X, Roth JA, Minna JD, Stewart D, Hong WK, Lee JJ, Wistuba II. Differences in protein expression patterns in lung adenocarcinomas arising in never versus ever smokers. Proceedings of the 101st Annual Meeting of the American Association for Cancer Research; 2010 Apr 17-21; Washington, DC. Philadelphia (PA): AACR; 2010. Abstract #787.

Behrens C, Wistuba II, Feng L, Lee JJ, Hong WK, Lotan R**.** Immunohistochemical validation of differentially expressed protein markers in the sequential pathogenesis of non-small cell lung cancer using premalignant and malignant lung tissue microarrays. *Proceedings of AACR* 46: 2005. Abstract #765

Behrens C, Yuan P, Solis L, Saintigny P, Kadara H, Fujimoto J, Moran C, Swisher SG, Heymach JV, Wistuba II. EZH2 expression is an early event in the pathogenesis of non-small cell lung cancer (NSCLC) and correlates with tumor progression. Proceedings of the 102nd Annual Meeting of the American Association for Cancer Research; 2011 Apr 2-6; Orlando, Florida. Philadelphia (PA): AACR; 2011. Abstract #3196.

Chen S, Fu L, Raja SM, Yue P, Peterson YK, Khuri FR, Sun S-Y. Differential roles of DR4, DR5 and c-FLIP in regulation of geranylgeranyltransferase I inhibitor-induced augmentation of tumor necrosis factor-related apoptosis-inducing ligand-induced apoptosis. 100th AACR Annual Meeting-- Apr 18-22, 2009; Denver, CO. Abstract #2041.

Chen S, Liu X, Yue P, Schönthal AH, Khuri RK, Sun S-Y. Dimethyl-celecoxib, a derivative of the COX-2 inhibitor celecoxib that lacks COX-2 inhibitory activity, sensitizes human lung cancer cells to tumor necrosis factor-related apoptosis-inducing ligand (TRAIL) through induction of DR5 and downregulation of c-FLIP. 98th AACR Annual Meeting- Apr 14-18, 2007; Los Angeles, CA. Abstract #3598.

Fan S, Li Y, Yue P, Khuri FR, Sun S-Y. The eIF4E/eIF4G interaction inhibitor 4EGI-1 augments TRAIL-induced apoptosis through DR5 induction and c-FLIP downregulation independent of inhibition of cap-dependent protein translation. 100th AACR Annual Meeting-- Apr 18-22, 2009; Denver, CO. Abstract #5132.

Fujimoto J, Kadara H, Behrens C, Liu D, Lee JJ, Solis LM, Kim ES, Shalafkhane A, Wistuba II, Lotan R. · Implication of GPRC5A loss in lung carcinogenesis in patients with and without chronic obstructive pulmonary disease. Proceedings of the 102nd Annual Meeting of the American Association for Cancer Research; 2011 Apr 2-6; Orlando, Florida. Philadelphia (PA): AACR; 2011. Abstract #2203.

Hong WH, Kim ES, Lee JJ, Wistuba I, Lippman S. The landscape of cancer prevention: Personalized approach in lung cancer. Proceedings of the 102nd Annual Meeting of the American Association for Cancer Research. Abstract PL01-03.

Kadara H, Hong WK, Wistuba II, Lotan R. A five-gene signature predictive of survival in lung adenocarcinoma but not in squamous cell carcinoma. Proceedings of the 101st Annual Meeting of the American Association for Cancer Research; 2010 Apr 17-21; Washington, DC. Philadelphia (PA): AACR; 2010. Abstract 4817.

Kadara H, Saintigny P, Fan Y, Chow CW, Chu ZM, Lang W, Behrens C, Gold K, Liu D, Lee JJ, Mao L, Kim ES, Hong WK, Wistuba II. Gene expression analysis of field of cancerization in early stage NSCLC patients towards development of biomarkers for personalized prevention. Proceedings of the 102nd Annual Meeting of the American Association for Cancer Research; 2011 Apr 2-6; Orlando, Florida. Philadelphia (PA): AACR; 2011. Abstract #3674.

Kawaguchi H, Ren H, Lang W, Chu Z, Fan Y-H, Mao L. Detecting low-abundant proteins in human plasma proteome by using multi-lectin affinity chromatography and two-dimensional gel electrophoresis. *Proceedings of AACR* 47: 2006. Abstract #2864.

Kim W-Y, Jin Q, Oh S-H, Kim E, Yang Y-J, Feng L, Behrens C, Prudkin L, Miller YE, Lee JJ, Lippman S, Hong WK, Wistuba I, Lee H-Y. Elevated Epithelial Insulin-Like Growth Factor Expression is a Risk Factor for Lung Cancer Development. 100th AACR Annual Meeting- Apr 18-22, 2009; Denver, CO. Abstract #793.

Kim WY, Jin Q, Prudkin L, Kim JS, Morgillo F, Feng L, Kim ES, Hennessy B, Lee JS, Mills M, Lee J, Glisson B, Lippman SM, Wistuba II, Lee HY. *EGFR and K-Ras* mutations and resistance of lung cancer to the IGF-1R tyrosine kinase inhibitors. Proceedings of the 101st Annual Meeting of the American Association for Cancer Research; 2010 Apr 17-21; Washington, DC. Philadelphia (PA): AACR; 2010. Abstract #4127.

Kong M, Lee JJ. A response surface model for drug combinations. The Spring ENAR Meeting, March 2005.

Lacroix L, Tahara E, Behrens C, Kadara H, Lotan D, Wistuba II, Lotan R. Identification of biomarkers for human lung carcinogenesis by analysis of transcriptomes of cell lines representing different stages of lung carcinogenesis. 98th AACR Annual Meeting-Apr 14-18, 2007; Los Angeles, CA. Abstract # 2956.

Li X, Tang X, Behrens C, Dong W, Ozburn N, Woods DM, Yin G, Hong WK, Moran C, Wistuba I. STAT1 protein frequently overexpressed in non-small cell lung carcinoma. AACR Annual Meeting 2008. San Diego, California, April 2008. Abstract #2166.

Lee JS, Ryu SH, Chung WC, Kang SM, and Koo JS. The Mechanism of EGF-Induced Hyperplasia in Normal Bronchial Epithelial Cells. 100th AACR Annual Meeting-- Apr 18-22, 2009; Denver, CO. Abstract #5055.

Liu X, Yue P, Chen S, Hu L, Lonial S, Khuri F, Sun SY. The proteasome inhibitor PS-341 (Bortezomib) upregulates death receptor 5 expression leading to induction of apoptosis and enhancement of TRAIL-induced apoptosis despite increase of c-FLIP and survivin in human lung cancer cells. 98th AACR Annual Meeting-- Apr 14-18, 2007; Los Angeles, CA. Abstract #2406.

Liu X, Yue P, Khuri FR, Sun SY. FLIP downregulation and its impact on celecoxib-induced apoptosis in human lung cancer cells. *Proceedings of AACR* 47: 2006. Abstract #752.

Lu T, Wistuba II, Hittelman W. Existence of clonal and subclonal outgrowths in premalignant and stromal cells in the upper aerodigestive tract of current smokers. *Proceedings of AACR* 47: 2006. Abstract #462.

Raso MG, Behrens C, Liu S, Prudkin L, Woods DM, Ozburn N, Moran C, Lee JJ, Wistuba I.

Immunohistochemical expression of estrogen and progesterone receptors identifies a subset of non-small cell lung cancers and correlates with EGFR Mutations. 99th AACR Annual Meeting- Apr 12-16, 2008; San Diego, CA. Abstract #2165.

Raso MG, Xie Y, Behrens C, Woods D, Jeong Y, Mehran R, Mangelsdorf D, Moran C, Minna J, Wistuba II. Immunohistochemical expression of nuclear receptors PPARγ, LXR-β and LRH-1 in NSCLC and correlation with clinicopathologic features. 13th World Lung Cancer Conference, IASLC, San Francisco, California, July-August, 2009.

Ren H, Hawke D, Chu Z, Mao L. Protein profiles of lung tumorigenesis using immmobilized metal ion adsorption chromatography. *Proceedings of AACR* 47: 2006. Abstract #3582.

Saintigny P, Liu J, Lee JJ, Ping Y, Behrens C, Solis Soto LM, Heymach JV, Kim ES, Hong WK, Kurie JM, Wistuba II, Koo JS. CXCR2 expression in tumor cells is associated with an adverse outcome in a large set of non-small-cell lung cancer (NSCLC). Proceedings of the 102nd Annual Meeting of the American Association for Cancer Research; 2011 Apr 2-6; Orlando, Florida. Philadelphia (PA): AACR; 2011. Abstract #392.

Saintigny P, Ren H, Zhou X, Mao L. microRNA (miRNA) species differentially expressed between immortalized normal bronchial epithelial cells and non-small cell lung cancer (NSCLC) cells. 99th AACR Annual Meeting- Apr 12-16, 2008; San Diego, CA. Abstract #5046.

Sato M, Girard L, Peyton M, Ramirez RD, Sunaga N, Gazdar AF, Shay JW, Minna JD. Genetic manipulation of immortalized normal human bronchial epithelial cells. *Proceedings of AACR* 46: 2005. Abstract #3896.

Sato M, Lee W, Girard L, Ramirez RD, Shames DS, Gazdar AF, Shay JW, Minna J D. Oncogenic manipulation and biologic selection for complete tumorigenic transformation of immortalized normal human bronchial epithelial cells. *Proceedings of AACR* 47*:* 2006. Abstract #2849.

Spencer ML, Tang X, Ozburn N, Kakarala L, Bekele BN, Vaporciyan A, Roth JA, Minna JD Wistuba II. Caveolin-1 abnormal expression is a frequent and early event in the pathogenesis of lung cancer. *Proceedings of AACR* 46: 2005. Abstract #3630.

Tahara E, Kadara H, Lacroix L, Lotan D, Lotan R. Inhibition of lung cancer cell growth by the putative tumor suppressor gene KLF6 through activation of PKC αpathway and inhibition of PI3Kinase pathway 98th AACR Annual Meeting- Apr 14-18, 2007; Los Angeles, CA. Abstract #3677.

Tang X, Bi X, Ozburn N, Hong WK, Wistuba II**.** "Field" defect abnormalities in lung adenocarcinoma: KRAS vs. EGFR mutant tumors. *Proceedings of AACR* 47: 2006. Abstract #5683.

Tang X, Liu D, Behrens C, He D, Sun M, Rice D, Lee JJ, Hong W, Wistuba I. *TITF-1* and *EGFR* gene copy variations are associated with prognosis for the patients with non-small cell lung cancer. 100th AACR Annual Meeting- Apr 18-22, 2009; Denver, CO. Abstract #3841.

Tang X, Ozburn N, Wistuba I. Caveolin-1 gene methylation is a field effect phenomenon in lung cancer patients. 98th AACR Annual Meeting, Apr 14-18, 2007; Los Angeles, CA. Abstract #2869.

Tang X, Shigematsu H, Roth JA, Minna JD, Hong WK, Gazdar AF, Wistuba II. EGFR tyrosine kinase domain mutations are also found in histologically normal lung epithelium of patients containing lung adenocarinomas with EGFR mutations indicating a field effect *Proceedings of AACR* 46: 2005. Abstract #4308.

Tang X, Sun M, Behrens C, Prudkin L, Ozburn N, Gazdar A, Moran C, Varella-Garcia M, Wistuba I**.** *TITF-1* gene amplification and protein expression pattern identify adenocarcinoma of lung with worse prognosis. 99th AACR Annual Meeting-- Apr 12-16, 2008; San Diego, CA. Abstract #4952.

Tang X, Varella-Garcia M, Xavier AC, Bi XQ, Ozburn N, Hong WK, Wistuba II. Analysis of EGFR abnormalities in the sequential pathogenesis and progression of lung adenocarcinoma. *Proceedings of AACR* 47: 2006. Abstract #69.

Tang X, Yang F, Huang J, Woods D, Corvalan C, Hong WK, Wistuba II. TITF-1 protein expression associates with gene methylation and gene copy gain in Non-Small Cell Lung Carcinoma. 13th World Lung Cancer Conference, IASLC, San Francisco, California, July-August, 2009.

Yuan P, Behrens C, Huang J, Spinola M, Prudkin L, Dong W, Yin G, Moran C, Kim E, Zhou BB, Minna J, Wistuba II. Expression of stem cell markers in non-small cell lung carcinoma (NSCLC) and correlation with clinico-pathologic features. 13th World Lung Cancer Conference, IASLC, San Francisco, California, July-August, 2009.

Yuan P, Kadara H, Behrens C, Tang X, Woods D, Solis LM, Huang J, Spinola M, Dong W, Yin G, Fujimoto J, Kim E, Xie Y, Girard L, Moran C, Hong WK, Minna JD, Wistuba II. Sex determining region Y-box 2 is a potential cell-lineage gene highly expressed in the pathogenesis of squamous cell carcinomas of the lung. Proceedings of the 101st Annual Meeting of the American Association for Cancer Research; 2010 Apr 17-21; Washington, DC. Philadelphia (PA): AACR; 2010. Abstract #5166.

Zou W, Liu X, Yue P, Khuri FR, Sun SY. PPARγ ligands induce death receptor 5 (DR5) expression and redistribution in lipid rafts and enhance TRAIL-induced apoptosis in human lung cancer cells. *Proceedings of AACR* 47: 2006. Abstract #759.

Grants/programs awarded

NIH/NCI **"**Role of CREB in Lung Cancer Development" (1R01CA126801 PI; Ja Seok Koo).

DoD Lung Cancer Research Program collaborative Award (W81XWH-10-1-1007, PI: Ignacio I. Wistuba).

Scientific Products

Developed immortalized HBEC lines that were deposited in the American Type Culture Collection (ATCC) for worldwide distribution. The HBEC lines are a valuable tool for studying the pathogenesis of lung cancer and developing new reagents to test for chemoprevention and chemotherapeutic drugs. The isogenically manipulated HBEC system is also a powerful approach to assess the contribution of individual genetic alterations to tumorigenesis of lung cancer. (PIs: Li Mao, John Minna).

APPENDICES

0026-895X/07/7205-1269–1279$20.00
MOLECULAR PHARMACOLOGY

Mol Pharmacol 72:1269–1279, 2007

Vol. 72, No. 5
37465/3264850
Printed in U.S.A.

CCAAT/Enhancer Binding Protein Homologous Protein-Dependent Death Receptor 5 Induction and Ubiquitin/Proteasome-Mediated Cellular FLICE-Inhibitory Protein Down-Regulation Contribute to Enhancement of Tumor Necrosis Factor-Related Apoptosis-Inducing Ligand-Induced Apoptosis by Dimethyl-Celecoxib in Human Non–Small-Cell Lung Cancer Cells[S]

Shuzhen Chen, Xiangguo Liu, Ping Yue, Axel H. Schönthal, Fadlo R. Khuri, and Shi-Yong Sun

Winship Cancer Institute, Emory University School of Medicine, Atlanta, Georgia (S.C., X.L., P.Y., F.R.K., S.Y.S.); and University of Southern California, Los Angeles, California (A.H.S.)

Received April 25, 2007; accepted August 7, 2007

ABSTRACT

2,5-Dimethyl-celecoxib (DMC) is a derivative of celecoxib, a cyclooxygenase-2 (COX-2) inhibitor with anticancer activity in both preclinical studies and clinical practice, and lacks COX-2-inhibitory activity. Several preclinical studies have demonstrated that DMC has better apoptosis-inducing activity than celecoxib, albeit with undefined mechanisms, and exhibits anticancer activity in animal models. In this study, we primarily investigated DMC's cooperative effect with tumor necrosis factor-related apoptosis-inducing ligand (TRAIL) on the induction of apoptosis and the underlying mechanisms in human non–small-cell lung cancer (NSCLC) cells. We found that DMC was more potent than celecoxib in decreasing the survival and inducing apoptosis of NSCLC cells. When combined with TRAIL, DMC exerted enhanced or synergistic effects on the induction of apoptosis, indicating that DMC cooperates with TRAIL to augment the induction of apoptosis. To determine the underlying mechanism of the synergy between DMC and TRAIL, we have demonstrated that DMC induces a CCAAT/enhancer binding protein homologous protein-dependent expression of DR5, a major TRAIL receptor, and reduces the levels of cellular FLICE-inhibitory protein (c-FLIP) (both the long and short forms), key inhibitors of death receptor-mediated apoptosis, by facilitating c-FLIP degradation through a ubiquitin/proteasome-dependent mechanism. It is noteworthy that enforced expression of c-FLIP or silencing of DR5 expression using DR5 small interfering RNA abrogated the enhanced effects on induction of apoptosis by the combination of DMC and TRAIL, indicating that both DR5 up-regulation and c-FLIP reduction contribute to cooperative induction of apoptosis by the combination of DMC and TRAIL. Together, we conclude that DMC sensitizes human NSCLC cells to TRAIL-induced apoptosis via induction of DR5 and down-regulation of c-FLIP.

This study was supported by Georgia Cancer Coalition Distinguished Cancer Scholar award (to S.-Y.S.) and Department of Defense VITAL grant W81XWH-04-1-0142 (to S.-Y.S. for Project 4). F.R.K. and S.-Y.S. are Georgia Cancer Coalition Distinguished Cancer Scholars.

Article, publication date, and citation information can be found at http://molpharm.aspetjournals.org.

doi:10.1124/mol.107.037465.

[S] The online version of this article (available at http://molpharm.aspetjournals.org) contains supplemental material.

Celecoxib (Celebrex, Pfizer Inc., New York, NY) is an approved drug for adjuvant treatment of patients with familial adenomatous polyposis. In addition, celecoxib is being tested in various clinical trials for its chemopreventive and therapeutic efficacy against a broad spectrum of epithelial malignancies, including lung cancers, either as a single agent or in combination with other agents (Koki and Masferrer, 2002;

ABBREVIATIONS: COX-2, cyclooxygenase-2; DMC, 2,5-dimethyl-celecoxib; TRAIL, tumor necrosis factor-related apoptosis-inducing ligand; NSCLC, non–small-cell lung cancer; c-FLIP, cellular FLICE-inhibitory protein; c-FLIP$_L$, long form of cellular FLICE-inhibitory protein; c-FLIP$_S$, short form of cellular FLICE-inhibitory protein; DR, death receptor; CHOP, CCAAT/enhancer binding protein homologous protein; siRNA, small interfering RNA; JNK, c-Jun N-terminal kinase; p-c-Jun, phospho-c-Jun; ER, endoplasmic reticulum; DMSO, dimethyl sulfoxide; PARP, poly(ADP-ribose) polymerase; HA, hemagglutinin; ChIP, chromatin immunoprecipitation; SRB, sulforhodamine B; SP600125, anthra(1,9-*cd*)pyrazol-6(2*H*)-one 1,9-pyrazoloanthrone; MG132, *N*-benzoyloxycarbonyl (*Z*)-Leu-Leu-leucinal.

Grösch et al., 2006). Although celecoxib is a cyclooxygenase 2 (COX-2) inhibitor, it also exerts antitumor activity in tumor cells and tissues that lack the COX-2 enzyme (Grösch et al., 2006). Therefore, celecoxib seems to be able to inhibit tumor growth independently of its COX-2-inhibitory activity.

The major concern for celecoxib as a cancer therapeutic agent is that it induces apoptosis only at high concentrations (>50 μM) in cell culture systems, which exceed clinically achievable plasma levels (<10 μM) (Davies et al., 2000). In addition, a more practical issue is the potential cardiovascular side effects of celecoxib, which probably are associated with its COX-2-inhibitory activity (Dogné et al., 2006; Marwali and Mehta, 2006). Given that celecoxib has been developed and marketed mainly for the treatment of arthritis and pain but not primarily for anticancer purposes, it is conceivable that this drug might be suboptimal for inclusion in the treatment of advanced cancers, such as non–small-cell lung cancer (NSCLC). To this end, efforts have been made recently to synthesize celecoxib derivatives optimized for anticancer applications, and novel non-COX-2 inhibitory celecoxib derivatives have been identified that show better activity than celecoxib in inducing apoptosis and inhibiting the growth of tumors (Zhu et al., 2002, 2004; Kardosh et al., 2005; Pyrko et al., 2006).

Among these derivatives, 2,5-dimethyl-celecoxib (DMC) mimicked celecoxib's numerous antitumor effects, including the induction of apoptosis, the reduction of neovascularization, and the inhibition of experimental tumor growth in some in vivo tumor models with increased efficacy (Schönthal, 2006). Thus, this compound exhibits cancer therapeutic potential in the absence of COX-2 inhibitory activity. Recently, it has been shown that DMC down-regulates survivin expression in human cancer cells; this effect seems to correlate with DMC's ability to induce apoptosis (Pyrko et al., 2006).

There are two major apoptotic signaling pathways: the intrinsic mitochondria-mediated pathway, and the extrinsic death receptor-induced pathway, and cross-talk between these pathways is mediated by the truncation of the proapoptotic protein Bid (Hengartner, 2000). It is well known that the extrinsic apoptotic pathway is negatively regulated by the cellular FLICE-inhibitory protein (c-FLIP), including both long ($FLIP_L$) and short ($FLIP_S$) forms, through inhibition of caspase-8 activation (Krueger et al., 2001). The tumor necrosis factor-related apoptosis-inducing ligand (TRAIL) binds to its receptors: death receptor 4 (DR4, also called TRAIL-R1), and death receptor 5 (DR5, also named Apo2, TRAIL-R2, or Killer/DR5) to activate the extrinsic apoptotic pathway (Kelley and Ashkenazi, 2004). Recently, TRAIL has received much attention because it preferentially induces apoptosis in transformed or malignant cells, demonstrating potential as a tumor-selective apoptosis-inducing cytokine for cancer treatment (Kelley and Ashkenazi, 2004). Currently, TRAIL is being tested in phase I clinical trials. It is noteworthy that certain cancer therapeutic agents including celecoxib sensitize various types of cancer cells to TRAIL-induced apoptosis (Wang and El-Deiry, 2003; Kelley and Ashkenazi, 2004; Liu et al., 2004b). Thus, these agents are useful in combination with TRAIL to overcome TRAIL resistance as demonstrated in some types of cancer cells (Wang and El-Deiry, 2003).

We have shown previously that celecoxib increases DR5 expression, down-regulates c-FLIP levels, and hence enhances TRAIL-induced apoptosis in human NSCLC cells (Liu et al., 2004b, 2006). The present study determined whether DMC exerted similar effects on induction of apoptosis, modulation of DR5 and c-FLIP, and sensitization of TRAIL-induced apoptosis in human NSCLC cells. We show that DMC potently stimulates the expression of DR5, which is dependent on the transcription factor CCAAT/enhancer binding protein homologous protein (CHOP)/growth arrest and DNA damage gene 153. Furthermore, the drug stimulates ubiquitin/proteasome-mediated degradation of c-FLIP, and both of these events contribute to DMC-mediated enhancement of TRAIL-induced apoptosis.

Materials and Methods

Reagents. DMC was synthesized as described previously (Kardosh et al., 2005). Celecoxib was purchased from LKT Laboratories (St. Paul, MN). Both drugs were dissolved in DMSO at the concentration of 100 mM, and aliquots were stored at −80°C. Stock solutions were diluted to the appropriate concentrations with growth medium immediately before use. The soluble recombinant human TRAIL was purchased from PeproTech, Inc. (Rocky Hill, NJ). The specific JNK inhibitor SP600125 was purchased from BIOMOL Research Laboratories (Plymouth Meeting, PA). The proteasome inhibitor MG132 was purchased from Sigma Chemical Co. (St. Louis, MO). Rabbit polyclonal anti-DR5 antibody was purchased from ProSci Inc. (Poway, CA). Mouse monoclonal anti-DR4 antibody (B-N28) was purchased from Diaclone (Stamford, CT). Mouse monoclonal anti-FLIP antibody (NF6) was purchased from Alexis Biochemicals (San Diego, CA). Mouse monoclonal anti-CHOP antibody (B-3) was purchased from Santa Cruz Biotechnology (Santa Cruz, CA). Mouse monoclonal anticaspase-3 antibody was purchased from Imgenex (San Diego, CA). Rabbit polyclonal anticaspase-8, anticaspase-9, and anti-PARP antibodies were purchased from Cell Signaling Technology, Inc. (Danvers, MA). Rabbit polyclonal anti-β-actin antibody was purchased from Sigma Chemical Co.

Cell Lines and Cell Culture. Human NSCLC cell lines used in this study were purchased from the American Type Culture Collection (Manassas, VA). The stable H157-$FLIP_L$-5 and H157-$FLIP_L$-21 transfectants that express ectopic $FLIP_L$, and H157-$FLIP_L$-16 transfectant that were infected with lentiviral $FLIP_L$ but did not express ectopic $FLIP_L$, were established as described previously (Liu et al., 2006). Both H157-lac Z-5 (Liu et al., 2006) and H157-$FLIP_L$-16 transfectants were used as control cell lines. These cell lines were cultured in RPMI 1640 medium containing 5% fetal bovine serum at 37°C in a humidified atmosphere of 5% CO_2/95% air.

Cell Survival Assay. Cells were seeded in 96-well cell culture plates and were treated the next day with the agents indicated. The viable cell number was determined using the sulforhodamine B assay as described previously (Sun et al., 1997).

Detection of Apoptosis. Apoptosis was evaluated by Annexin V staining using Annexin V-PE apoptosis detection kit purchased from BD Biosciences (San Jose, CA) following the manufacturer's instructions. We also detected caspase activation by Western blotting (as described below) as an additional indicator of apoptosis.

Western Blot Analysis. Whole-cell protein lysates were prepared and analyzed by Western blotting as described previously (Sun et al., 1999; Liu et al., 2004b).

Immunoprecipitation for Detection of Ubiquitinated c-FLIP. H157-$FLIP_L$-21 cells, which stably express $FLIP_L$, were transfected with HA-ubiquitin plasmid using the FuGENE 6 transfection reagent (Roche Diagnostics, Indianapolis, IN) following the manufacturer's instructions. After 24 h, the cells were treated with DMC or MG132 plus DMC for 4 h and then were lysed for immunoprecipitation of Flag-$FLIP_L$ using Flag M2 monoclonal antibody

(Sigma) as described previously (Chen et al., 2005) followed by the detection of ubiquitinated $FLIP_L$ with Western blotting using anti-HA antibody (Abgent, San Diego, CA).

Silencing of DR5 Expression Using Small Interfering RNA. The nonsilencing control small interfering RNA (siRNA) and DR5 siRNA duplexes were described previously (Liu et al., 2004b). Transfection of these siRNA duplexes was conducted in six-well plates using the HiPerFect transfection reagent (QIAGEN, Valencia, CA) following the manufacturer's manual. Gene-silencing effect was evaluated by Western blot analysis.

Transient Transfection and Luciferase Activity Assay. pGL3-DR5(−552) containing a wild-type CHOP binding site and pGL3-DR5(−552)CHOPm, in which the CHOP binding site was mutated, were generously provided by H. G. Wang (University of South Florida College of Medicine, Tampa, FL) (Yamaguchi and Wang, 2004). To examine the effects of DMC on DR5 promoter activity, cells were cotransfected with 0.35 μg of reporter plasmids and 0.25 μg of β-galactosidase expression plasmid (Pharmacia Biotech, Piscataway, NJ) using FuGENE 6 transfection reagent (Roche Molecular Biochemicals, Indianapolis, IN) following the manufacturer's protocol. Twenty-four hours later, the cells were treated with DMC. After 12 h, the cells were lysed and subjected to luciferase activity assay using Luciferase Assay System (Promega, Madison, WI) in a luminometer. Relative luciferase activity was normalized to β-galactosidase activity, which was measured as described previously (Pfahl et al., 1990).

Chromatin Immunoprecipitation Assay. Chromatin immunoprecipitation (ChIP) assay was conducted using the ChIP assay kit purchased from Upstate Biotechnology (Charlottesville, VA) following the manufacturer's instruction and was described previously (Liu et al., 2004a). CHOP antibody for immunoprecipitation in this assay was the same used in the Western blot analysis. Mouse IgG_{2a} isotype antibody was purchased from EMD Bioscience, Inc. (La Jolla, CA). Polymerase chain reaction amplification of a 111-bp fragment of DR5 promoter containing a CHOP binding site on immunoprecipitated chromatin was conducted using the primers 5′-AGGTTAGTTCCGGTCCCTTC-3′ (forward) and 5′-CAACTGCAAATTCCACCACA-3′ (reverse) as described previously (Abdelrahim et al., 2006).

Results

DMC Was More Potent than Celecoxib in Inhibiting the Growth and Inducing Apoptosis of Human NSCLC Cells. We first compared the effects of DMC with celecoxib on the growth of a panel of human NSCLC cell lines. In this experiment, six NSCLC cell lines including H157, H460, H1792, A549, Calu-1, and H226 were treated with increasing concentrations of DMC or celecoxib for 3 days, and then cell growth inhibition was determined. As presented in Fig. 1, A and B, both compounds inhibited the growth of the tested cell lines in a dose-dependent manner. DMC inhibited cell growth with IC_{50} values ranging from 10 to 20 μM, whereas celecoxib did so with IC_{50} values ranging between 20 and 35 μM, indicating that DMC is more effective than celecoxib in inhibiting the growth of NSCLC cells. Second, we examined the effects of DMC and celecoxib on the induction of apoptosis in four NSCLC cell lines. At the concentration of 50 μM, DMC induced more than 60% apoptosis in all of the cell lines tested, whereas celecoxib caused only up to 35% apoptosis (Fig. 1C). Together, these results indicate that DMC is more potent than celecoxib in inhibiting cell growth and inducing apoptosis in human NSCLC cells.

DMC Cooperated with TRAIL to Augment the Induction of Apoptosis in Human NSCLC Cells. Our previous work has shown that celecoxib enhances TRAIL-induced apoptosis in NSCLC cells (Liu et al., 2004b). Therefore, we determined whether DMC also augmented TRAIL-induced apoptosis in human NSCLC cells. To this end, we treated four NSCLC cell lines (i.e., H157, Calu-1, H460, and A549) with TRAIL alone, DMC alone, or both drugs combined and then assessed cell survival and apoptosis. As presented in Fig. 2A, the combination of DMC at concentrations of 10 to 30 μM with either dose of TRAIL (10 or 20 nM) was much more effective in decreasing tumor cell survival than either single agent alone. For example, in Calu-1 cells, DMC alone at 20

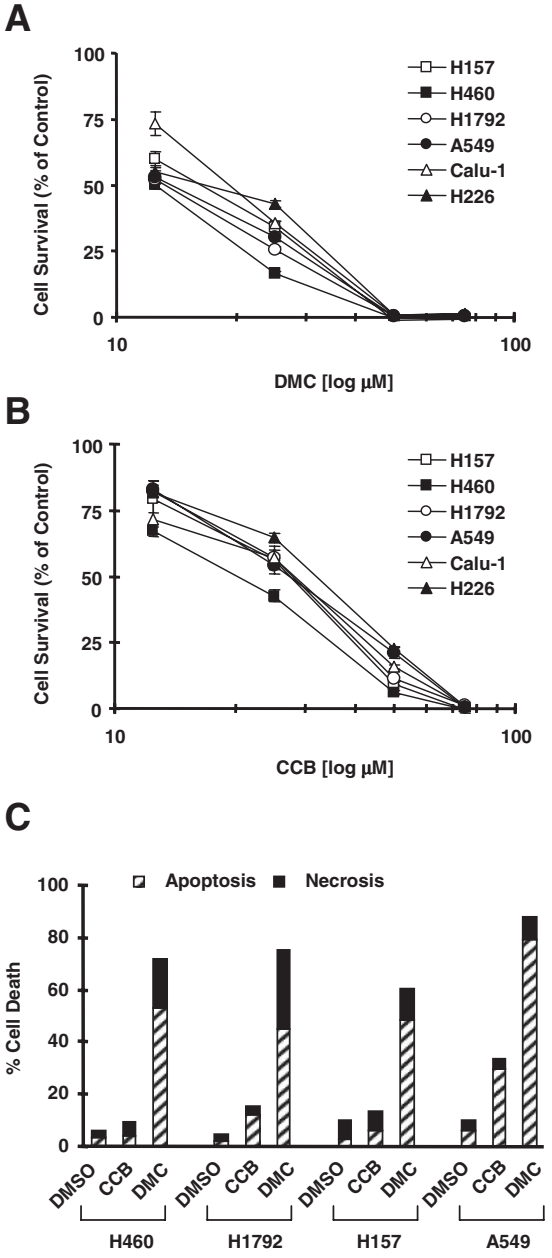

Fig. 1. DMC exhibits more potent efficacy than celecoxib in decreasing the survival (A and B) and inducing apoptosis (C) of human NSCLC cells. A and B, the indicated NSCLC cell lines were seeded in 96-well cell culture plates and were treated the next day with the given concentrations of DMC (A) or celecoxib (CCB) (B). After 3 days, cell number was estimated using the SRB assay. Cell survival was expressed as the percentage of control (DMSO-treated) cells. Data are the means of four replicate determinations; bars, ± S.D. C, the indicated NSCLC cell lines were treated with DMSO, 50 μM DMC, or 50 μM celecoxib for 24 h. Cell death, including apoptosis and necrosis from these cell lines, was then determined by Annexin V staining.

μM decreased cell survival by 33%, and TRAIL (10 ng/ml) alone decreased cell survival by 10%, but the combination of the two agents reduced cell survival by almost 70%, which is greater than the sum of the effects of each agent alone. Moreover, we detected apoptosis in two NSCLC cell lines (H157 and H460) exposed to the combination of DMC and TRAIL. During a 24-h treatment, DMC at 25 μM did not increase apoptosis in either cell line, and 10 ng/ml TRAIL alone induced only 24 (H460) and 15% (H157) apoptosis. However, the combination of DMC and TRAIL caused 63 and 30% of cells to undergo apoptosis (Fig. 2B). In addition, the combination of DMC and TRAIL was much more potent than each single agent alone in inducing cleavage of caspase-8, caspase-9, caspase-3, and PARP (Fig. 2C). Together, these results clearly indicate that DMC cooperates with TRAIL to augment the induction of apoptosis in human NSCLC cells.

DMC Induced CHOP-Dependent DR5 Expression. DR5 induction is one mechanism accounting for the sensiti-

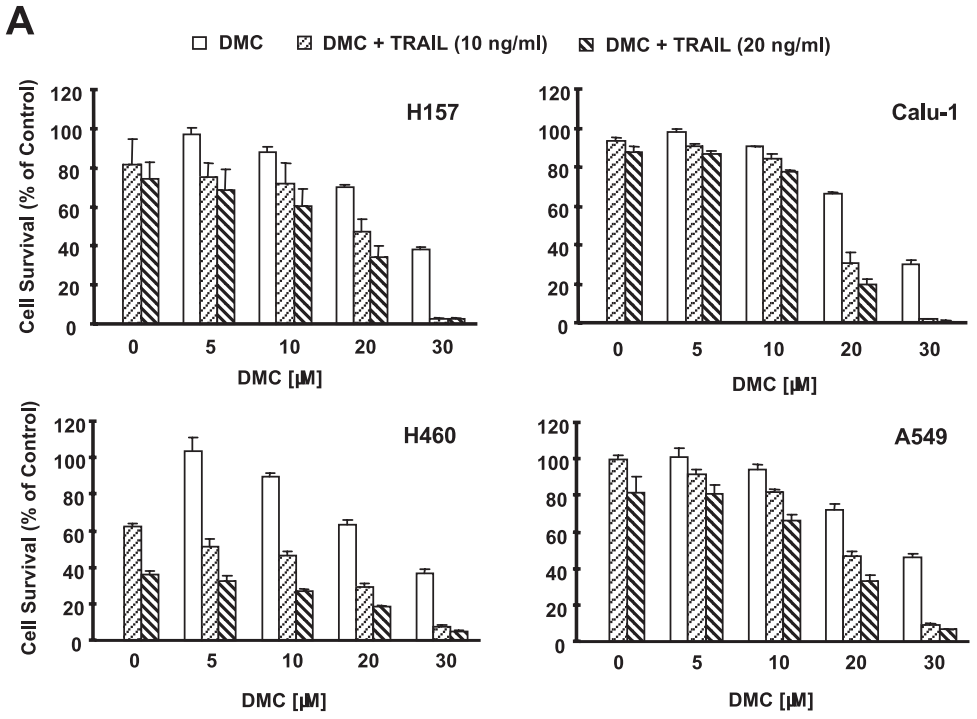

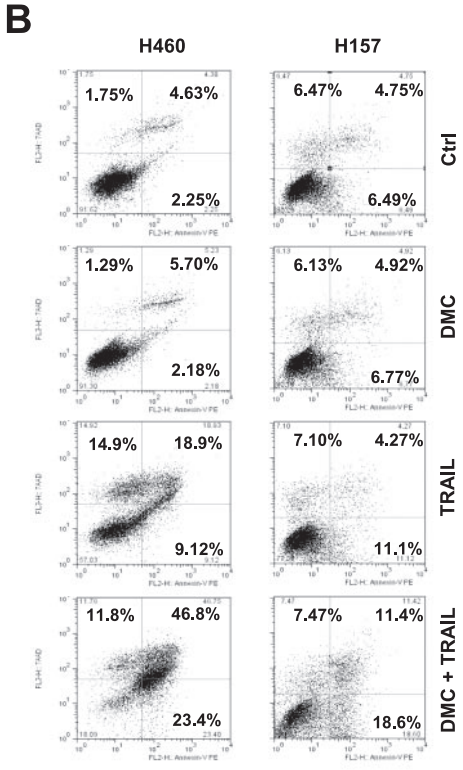

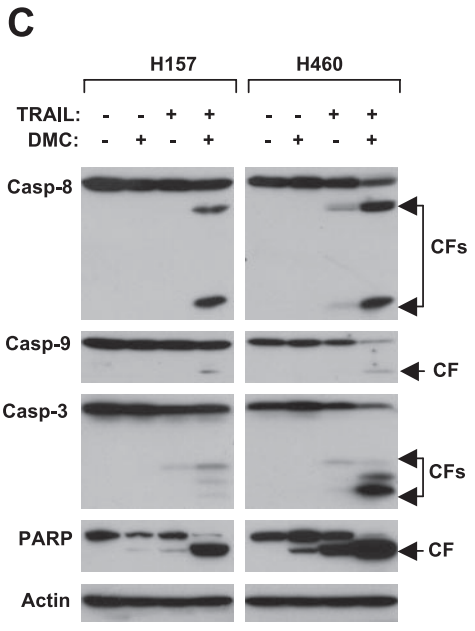

Fig. 2. DMC enhances TRAIL's effects on decreasing cell survival (A), inducing apoptosis (B), and activating caspases (C) in human NSCLC cells. A, the indicated cell lines were treated with the given concentrations of TRAIL alone, DMC alone, and their combination as indicated. After 24 h, cell number was estimated using SRB assay for the calculation of cell survival. Data are the means of four replicate determinations. Bars, S.D. B, the indicated cell lines were treated with 10 ng/ml TRAIL alone, 25 μM DMC alone, and their respective combination as indicated. After 24 h, the cells were subjected to measurement of apoptosis using Annexin V staining. The percentage of positive cells in the upper right and lower right quadrants were added to yield the total of apoptotic cells. C, the indicated cell lines were treated with 25 μM DMC alone, 10 ng/ml TRAIL alone, and their combination. After 8 h, the cells were harvested for the preparation of whole-cell protein lysates and subsequent Western blot analysis for detecting cleavage of caspases and their substrates. Casp, caspase; CF, cleaved fragment.

zation of TRAIL-induced apoptosis by some small-molecule drugs, including celecoxib (Liu et al., 2004b; Sun, 2005). Thus, we next determined whether DMC modulated DR5 expression in human NSCLC cells. By Western blot analysis, we detected a time-dependent induction of DR5 expression in both H157 and H460 cell lines exposed to DMC, which occurred early at 4 h and was sustained for at least 16 h (Fig. 3A). In addition, we found that DMC at a concentration as low as 10 μM was able to increase DR5 expression in both H157 and H460 cell lines (data not shown). Because DR4 is another TRAIL death receptor, we also examined DR4 expression in cells exposed to DMC and found that DMC increased DR4 levels in H157 cells but not in H460 cells (Fig. 3A). Thus, we focused on DR5 in the subsequent studies.

To understand the mechanism by which DMC induces DR5 expression, we analyzed the expression of CHOP, a transcriptional factor that is known to regulate DR5 expression via binding to its promoter region (Yamaguchi and Wang, 2004; Yoshida et al., 2005; Abdelrahim et al., 2006). As shown in Fig. 3A, DMC increased CHOP levels in both H157 and H460 cell lines, and the kinetics of induction were similar to those of DR5. To determine whether CHOP mediates DMC-induced DR5 expression, we compared the effects of DMC on transactivation of DR5 promoters with and without the wild-type CHOP binding site. As shown in Fig. 3B, DMC significantly increased the luciferase activity in cells transfected with pGL3-DR5(−552) carrying the wild-type promoter, but this effect was completely inhibited in cells transfected with the mutant construct pGL3-DR5(−552)CHOPm, in which the CHOP binding site was inactivated. Moreover, DMC facilitated CHOP binding to DR5 promoter evaluated by ChIP assay (Fig. 3C). Together, these results indicate that the CHOP binding site is essential for DMC-mediated transactivation of the DR5 promoter. To firmly prove that DMC-induced DR5 expression is CHOP-dependent, we knocked down CHOP expression using CHOP siRNA and then examined its impact on DMC-induced DR5 expression. As presented in Fig. 3D, DMC increased levels of CHOP in control siRNA-transfected H460 cells but not in CHOP siRNA-transfected cells, indicating the successful blockage of CHOP induction by DMC. Therefore, DMC failed to increase DR5 expression in cells transfected with CHOP siRNA compared with cells transfected with control siRNA, indicating that DR5 induction by DMC is CHOP-dependent. Together, we

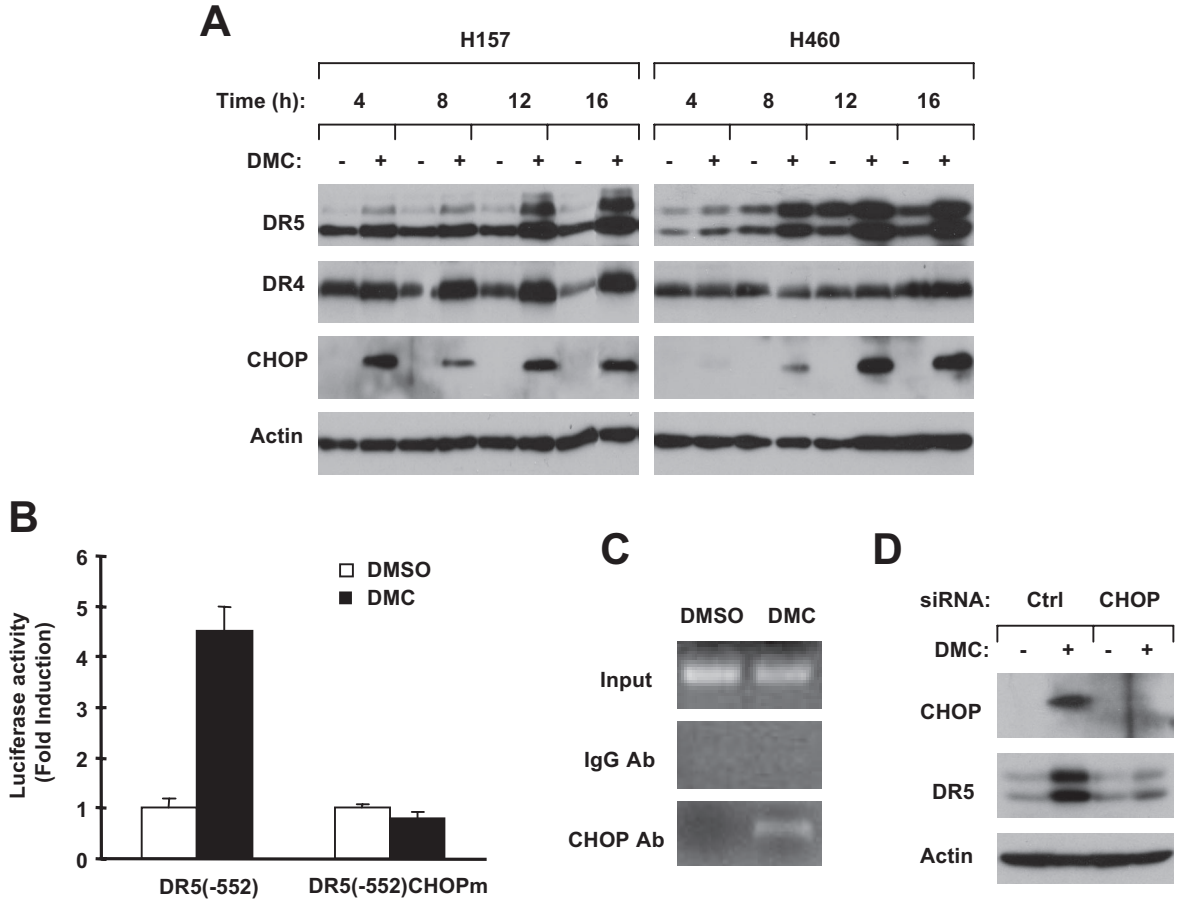

Fig. 3. DMC induces DR5 expression (A) through a CHOP-mediated mechanism (B–D). A, time-dependent modulatory effects of DMC on the expression of DR5, DR4, and CHOP. The given cell lines were treated with 25 μM DMC for various times from 4 to 16 h as indicated and then subjected to the preparation of whole-cell protein lysates and subsequent Western blot analysis for the given proteins. B, effects of DMC on the transactivation of DR5 promoters with and without wild-type CHOP binding sites. The given reporter constructs were cotransfected with pCH110 plasmid into H460 cells. After 24 h, the cells were treated with DMSO or 25 μM DMC for 12 h and then subjected to luciferase assay. Data are means of triplicate determinations. Bars, ± S.D. C, DMC facilitates CHOP binding to DR5 promoter. H460 cells were treated with 25 μM DMC for 8 h and then subjected to ChIP assay for detecting CHOP binding in the DR5 promoter. The amplified DNA fragment by polymerase chain reaction was 111 bp. Ab, antibody. D, effect of CHOP knockdown on DMC-induced DR5 expression. H460 cells were transfected with control (Ctrl) or CHOP siRNA. After 48 h, the cells were treated with 25 μM DMC for 12 h and then subjected to the preparation of whole-cell protein lysates and subsequent Western blot analysis.

conclude that DMC induces CHOP-dependent DR5 expression in human NSCLC cells.

DMC Down-Regulated c-FLIP Levels through Ubiquitin/Proteasome-Mediated Degradation. In addition to DR5 induction, c-FLIP down-regulation is another important mechanism underlying enhancement of TRAIL-induced apoptosis by some anticancer drugs, including celecoxib (Liu et al., 2006; Zou et al., 2007). Therefore, we further determined whether DMC also down-regulates c-FLIP levels. DMC decreased the levels of both $FLIP_L$ and $FLIP_S$ in H157 and H460 cells at 4 h after treatment. It is interesting that prolonged treatment with DMC generated cell line-dependent results on c-FLIP modulation. The decrease of c-FLIP ($FLIP_L$ and $FLIP_S$) by DMC was maintained for up to 16 h in H157 cells. However, $FLIP_L$ was actually increased by DMC at late times (e.g., 12 and 16 h) in H460 cells, although $FLIP_S$ was still decreased at up to 16 h (Fig. 4A). For a fixed 16-h treatment experiment, we found that DMC at concentrations ranging from 10 to 30 μM decreased levels of $FLIP_L$ and $FLIP_S$ in H157 cells; however, it increased levels of $FLIP_L$ while still reducing the levels of $FLIP_S$ in H460 cells (Fig. 3B).

Because c-FLIP proteins are known to be regulated by ubiquitin/proteasome-mediated degradation (Kim et al., 2002; Chang et al., 2006), we investigated whether the observed down-regulation of c-FLIP by DMC would be mediated via this process. To this end, we found that DMC-induced down-regulation of c-FLIP was abrogated by the presence of the proteasome inhibitor MG132 (Fig. 4C), indicating that DMC-induced c-FLIP reduction is proteasome-dependent. By immunoprecipitation/Western blotting, we detected the highest levels of ubiquitinated $FLIP_L$ in cells treated with DMC plus MG132 compared with cells exposed to DMC alone or MG132 alone (Fig. 4D), indicating that DMC increases c-FLIP ubiquitination. Taken together, we conclude that DMC facilitates ubiquitin/proteasome-mediated c-FLIP degradation, leading to down-regulation of c-FLIP in human NSCLC cells.

DMC Exerted Minimal Modulatory Effects on the Expression of Bax, Bcl-X_L, Bcl-2, Bad, and Survivin. Bcl-2 family members such as Bax, Bcl-2, and Bcl-X_L and inhibitor of apoptosis proteins such as survivin are know to be involved in the regulation of the intrinsic apoptotic pathway (Hengartner, 2000; Harada and Grant, 2003). To further understand the molecular mechanism underlying DMC enhancement of TRAIL-induced apoptosis, we also analyzed the modulatory effects of DMC on Bax, Bcl-X_L, Bcl-2, Bad, and survivin in H157 and H460 NSCLC cell lines. Our results

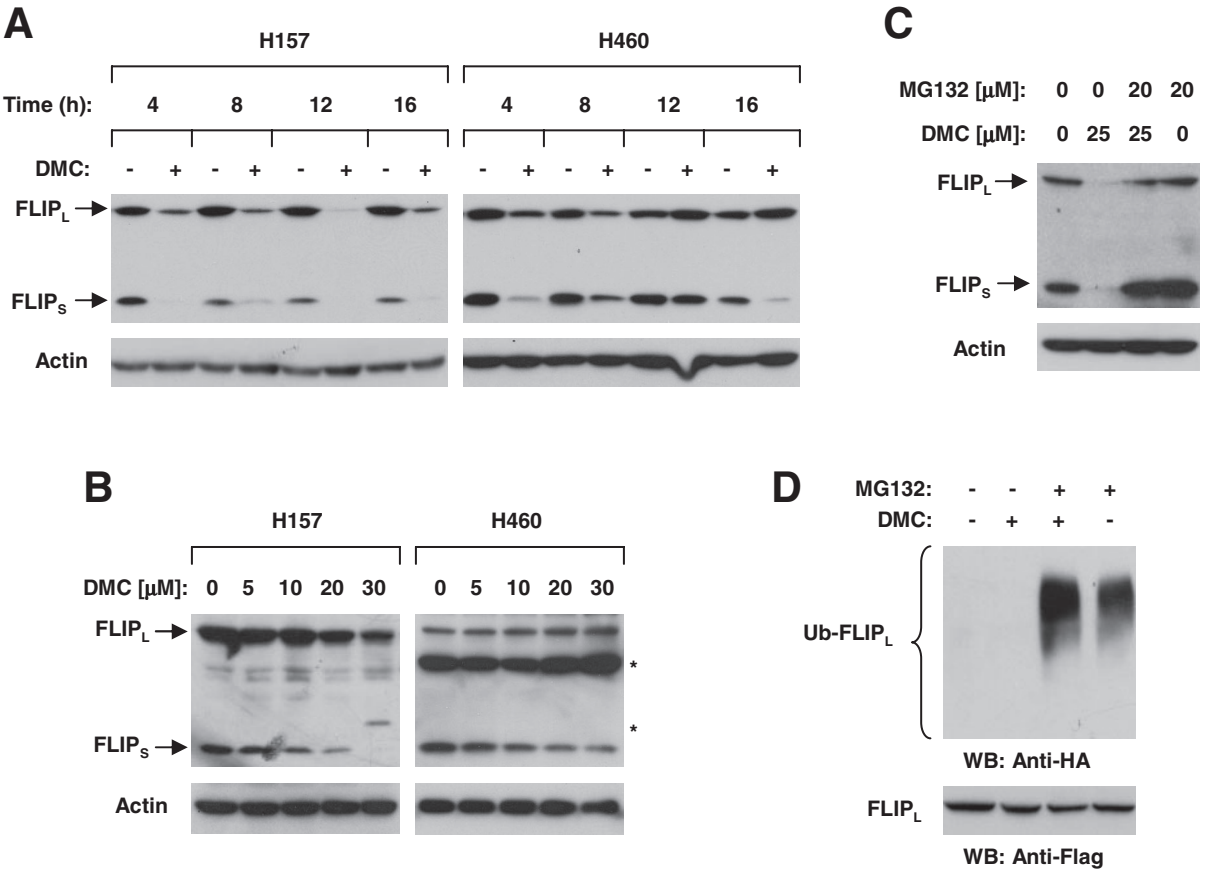

Fig. 4. DMC down-regulates c-FLIP levels (A and B) through ubiquitin/proteasome-mediated protein degradation (C and D). A and B, the given cell lines were treated with 25 μM DMC for the indicated times (A) or with the indicated concentrations of DMC for 16 h (B). The cell lines were then subjected to preparation of whole-cell protein lysates and subsequent Western blot analysis. C, H157 cells were pretreated with 20 μM MG132 for 30 min and then cotreated with 25 μM DMC for another 8 h. The cells were then harvested for preparation of whole-cell protein lysates and subsequent Western blot analysis. D, H157-$FLIP_L$-21 cells that stably express ectopic flag-$FLIP_L$ were transfected with HA-ubiquitin plasmid using FuGENE 6 transfection reagent for 24 h. The cells were then pretreated with 20 μM MG132 for 30 min and then cotreated with 25 μM DMC for 4 h. Whole-cell protein lysates were then prepared for immunoprecipitation using anti-Flag antibody followed by Western blotting (WB) using anti-HA antibody for the detection of ubiquitinated $FLIP_L$ (Ub-$FLIP_L$) and anti-Flag antibody for the detection of ectopic $FLIP_L$.

showed that DMC only decreased the levels of survivin but had minimal effects on the expression of Bax, Bcl-X_L, Bcl-2, and Bad (see Supplemental Fig. S1). The down-regulation of survivin by DMC in human NSCLC cells is in agreement with the finding by Pyrko et al. (2006) in other types of cancer cell lines. However, we found that DMC reduced the levels of survivin in H460 cells only starting at 8 h, indicating that survivin modulation is not as early an event as the modulation of DR5 and c-FLIP in DMC-treated cells.

DMC Modulated DR5 Expression and c-FLIP Levels Independently of JNK Activation. Several studies have demonstrated that JNK activation regulates DR5 expression (Higuchi et al., 2004; Zou et al., 2004). Recently, JNK has also been demonstrated to be responsible for tumor necrosis factor-induced, ubiquitin/proteasome-mediated $FLIP_L$ degradation (Chang et al., 2006). Therefore, we wanted to determine whether DMC induces JNK activation in human NSCLC cells and, if so, whether JNK activation is responsible for DR5 induction and c-FLIP down-regulation by DMC. By Western blot analysis, we detected that DMC increased levels of phosphorylated c-Jun (p-c-Jun), a well known substrate and indicator of JNK activation, in a time- and dose-dependent manner in H157 cells. In parallel, a comparatively smaller and later increase of total c-Jun protein levels was noted as well. However, such an increase in p-c-Jun and c-Jun was not detected in H460 cells (Fig. 5, A and B), primarily because of the absence of basal level c-Jun expression. The stimulation of c-Jun phosphorylation in H157 cells occurred early at 2 h and was sustained for up to 16 h after DMC treatment (Fig. 5A). Moreover, p-c-Jun levels were increased even by 5 μM DMC (Fig. 5B).

To further address the involvement of JNK activation in the modulation of DR5 and c-FLIP by DMC, we examined the effects of DMC on DR5 and c-FLIP expression in the presence of the JNK-specific inhibitor SP600125 in H157 cells. SP600125 at the concentrations of 10 to 20 μM inhibited the phosphorylation of c-Jun (Fig. 5C), confirming that SP600125 worked as expected in our cell system. However, SP600125 did not block DMC-induced DR5 up-regulation and did not prevent the down-regulation of c-FLIP by DMC (Fig. 5C). Together, our results suggest that JNK does not play a significant role in DMC-mediated modulation of either DR5 or c-FLIP in human NSCLC cells.

DMC Enhanced TRAIL-Induced Apoptosis through DR5 Induction and c-FLIP Down-Regulation. It is well known that both DR5 and c-FLIP are key components in the TRAIL/death receptor-mediated apoptotic pathway (Wang and El-Deiry, 2003; Kelley and Ashkenazi, 2004). We wanted to know whether DR5 induction and c-FLIP down-regulation were required for DMC-mediated enhancement of TRAIL-induced apoptosis. To demonstrate the involvement of DR5 induction in cooperative augmentation of apoptosis by the combination of DMC and TRAIL, we used DR5 siRNA to block DMC-induced DR5 up-regulation and then examined its impact on the induction of apoptosis by the combination of DMC and TRAIL. In control siRNA-transfected H460 cells, we detected basal levels of DR5, which were increased by DMC treatment as expected. In contrast, in DR5 siRNA-

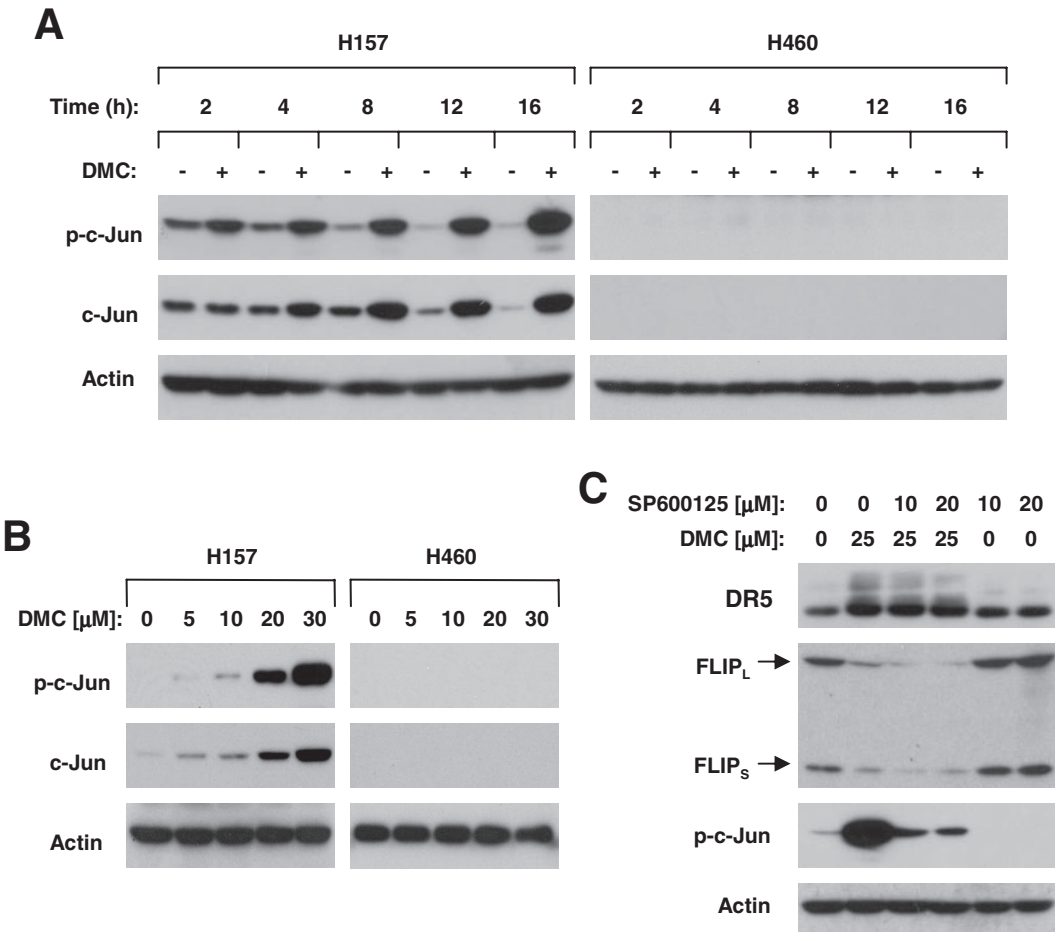

Fig. 5. Effects of DMC on JNK activation (A and B) by DMC in human NSCLC cells and the impact of JNK activation on DMC-induced DR5 expression and c-FLIP down-regulation (C). A and B, the indicated cell lines were treated with 25 μM DMC for the given times (A) or the indicated concentrations of DMC for 16 h (B). C, H157 cells were treated with 25 μM DMC alone, DMC plus the indicated concentrations of SP600125, and SP600125 alone for 8 h (B). Whole-cell protein lysates were then prepared from the aforementioned treatments for detection of the indicated proteins by Western blot analysis.

transfected cells, the basal levels of DR5 were substantially reduced and were not induced upon treatment with DMC (Fig. 6A). These results clearly indicate the successful knockdown of DR5 expression and blockade of DR5 induction. As a result, we detected cooperative induction of apoptosis by the combination of DMC and TRAIL in control siRNA-transfected cells but not in DR5 siRNA-transfected cells (Fig. 6B), indicating that DR5 up-regulation is required for the enhancement of TRAIL-induced apoptosis by DMC.

To determine the involvement of c-FLIP down-regulation in the induction of apoptosis by the DMC and TRAIL combination, we used a lentiviral expression system to enforce c-FLIP overexpression in NSCLC cells and then analyzed its effect on induction of apoptosis by the DMC and TRAIL combination. Taking advantage of a lentiviral expression system that achieves stable gene expression, we established H157 cell lines that stably expressed high levels of ectopic $FLIP_L$ (i.e., H157-$FLIP_L$-5 and H157-$FLIP_L$-21). As controls, we also used H157-Lac Z-5, which expressed irrelevant Lac Z protein and H157-$FLIP_L$-16, which did not express ectopic $FLIP_L$ albeit being infected with lentiviral $FLIP_L$ (Fig. 7A). Treatment of H157-Lac Z-5 and H157-$FLIP_L$-16 with TRAIL, a death ligand known to activate the extrinsic death receptor-mediated apoptotic pathway, induced substantial cleavage of caspase-8, caspase-3, and PARP; however, these effects were only minimally observed in H157-$FLIP_L$-5 and H157-$FLIP_L$-21 cells (Fig. 7A). Thus, enforced expression of ectopic $FLIP_L$ indeed confers cell resistance to TRAIL-induced apoptosis.

By measuring cell survival, we found that the combination of DMC and TRAIL very effectively decreased cell survival in H157-Lac Z-5 and H157-$FLIP_L$-16 cell lines but had only a weak effect in H157-$FLIP_L$-5 and H157-$FLIP_L$-21 cells (Fig. 7B), indicating that enforced overexpression of ectopic $FLIP_L$ confers cell resistance to the combination of DMC and TRAIL. By directly measuring apoptosis using annexin V staining after combination drug treatment, we detected much less apoptotic cell death in H157-$FLIP_L$-5 or H157-$FLIP_L$-21 cell lines than in H157-Lac Z-5 and H157-$FLIP_L$-16 control cell lines. Specifically, the combination of DMC and TRAIL caused 50% apoptosis in H157-Lac Z-5 cells and 97% apoptosis in H157-$FLIP_L$-16 control cells but only 34% apoptosis in H157-$FLIP_L$-5 and 11% apoptosis in H157-$FLIP_L$-21 cells (Fig. 7C). Thus, these results collectively show that down-regulation of c-FLIP contributes to DMC-mediated enhancement of TRAIL-induced apoptosis.

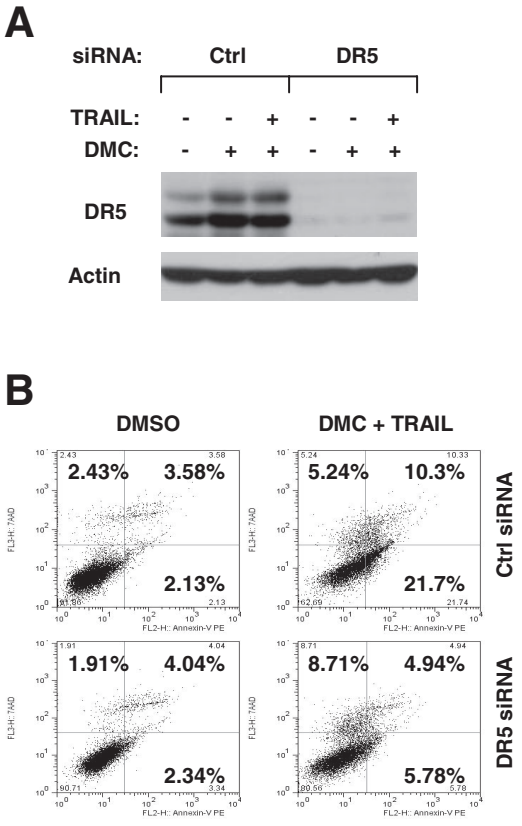

Fig. 6. Blockage of DR5 induction (A) attenuates the induction of apoptosis by DMC and TRAIL combination (B). H460 cells were cultured in a six-well plate and the next day were transfected with control (Ctrl) or DR5 siRNA. Forty-eight hours after transfection, cells were treated with 25 μM DMC alone or DMC plus 10 ng/ml for 8 h and then subjected to preparation of whole-cell lysates for Western blot analysis (A) or harvested for detection of apoptosis by Annexin V staining (B). In Annexin V assay, the percentage of positive cells in the upper right and lower right quadrants were added to yield the total of apoptotic cells.

Discussion

In the present study, we demonstrated that DMC is more active than its parental compound celecoxib in decreasing the survival and inducing apoptosis of human NSCLC cells and that DMC sensitizes human NSCLC cells to TRAIL-induced apoptosis. Given that TRAIL is a potential cancer therapeutic protein and is being tested in phase I clinical trials, our finding on the enhancement of TRAIL-induced apoptosis by DMC is of clinical significance in terms of its potential application in combination with TRAIL in cancer treatment. Our previous work has shown that celecoxib enhances TRAIL-induced apoptosis in human NSCLC cells (Liu et al., 2004b). Thus, our current finding implies that DMC, which lacks COX-2 inhibitory activity, retains celecoxib's ability to enhance TRAIL-induced apoptosis and thereby indicates that the inhibition of COX-2 is not involved in these processes.

It is generally recognized that both the death receptor-mediated extrinsic and the mitochondrial intrinsic apoptotic pathways, respectively, are regulated by multiple proteins; the former involves proteins like DR5, DR4, and c-FLIP, and the latter includes Bcl-2 family members such as Bax, Bcl-2, Bcl-X_L, and inhibitor of apoptosis proteins such as survivin (Hengartner, 2000; Harada and Grant, 2003). Our results showed that DMC only decreased the levels of survivin but had minimal effect on the expression of Bax, Bcl-X_L, Bcl-2, and Bad (Supplemental Fig. S1). We noted that DMC also induced DR4 expression; however, this effect is cell line-dependent because DMC induced DR4 in H157 cells but not in H460 cells. Given the important roles of DR5 and c-FLIP in the regulation of the TRAIL-mediated extrinsic apoptotic pathway, and considering that both proteins are quickly and strongly modulated by DMC in all tested NSCLC cell lines, we believe that DR5 induction and c-FLIP down-regulation are two major key events that mediate cooperative induction of apoptosis by the combination of DMC and TRAIL. This view is further supported by our findings that blockade of DR5 induction by knocking down DR5 expression using DR5 siRNA or enforced overexpression of ectopic c-FLIP confers cell resistance to induction of apoptosis by the combination of

DMC and TRAIL. In this study, we do not exclude the possibility that DR4 and survivin modulation also contribute to DMC-mediated enhancement of TRAIL-induced apoptosis in certain cell lines (e.g., H157).

Our study further demonstrates that DMC down-regulates c-FLIP levels by facilitating ubiquitin/proteasome-mediated degradation of c-FLIP. This is evidenced by the prevention of DMC-induced c-FLIP reduction using the proteasome inhibitor MG132 and by increased levels of ubiquitinated c-FLIP, which are detected in cells cotreated with MG132 and DMC using immunoprecipitation/Western blotting (Fig. 4). This mechanism is consistent with the one by which celecoxib decreases c-FLIP levels, as we have demonstrated previously (Liu et al., 2006), furthering the notion that DMC retains

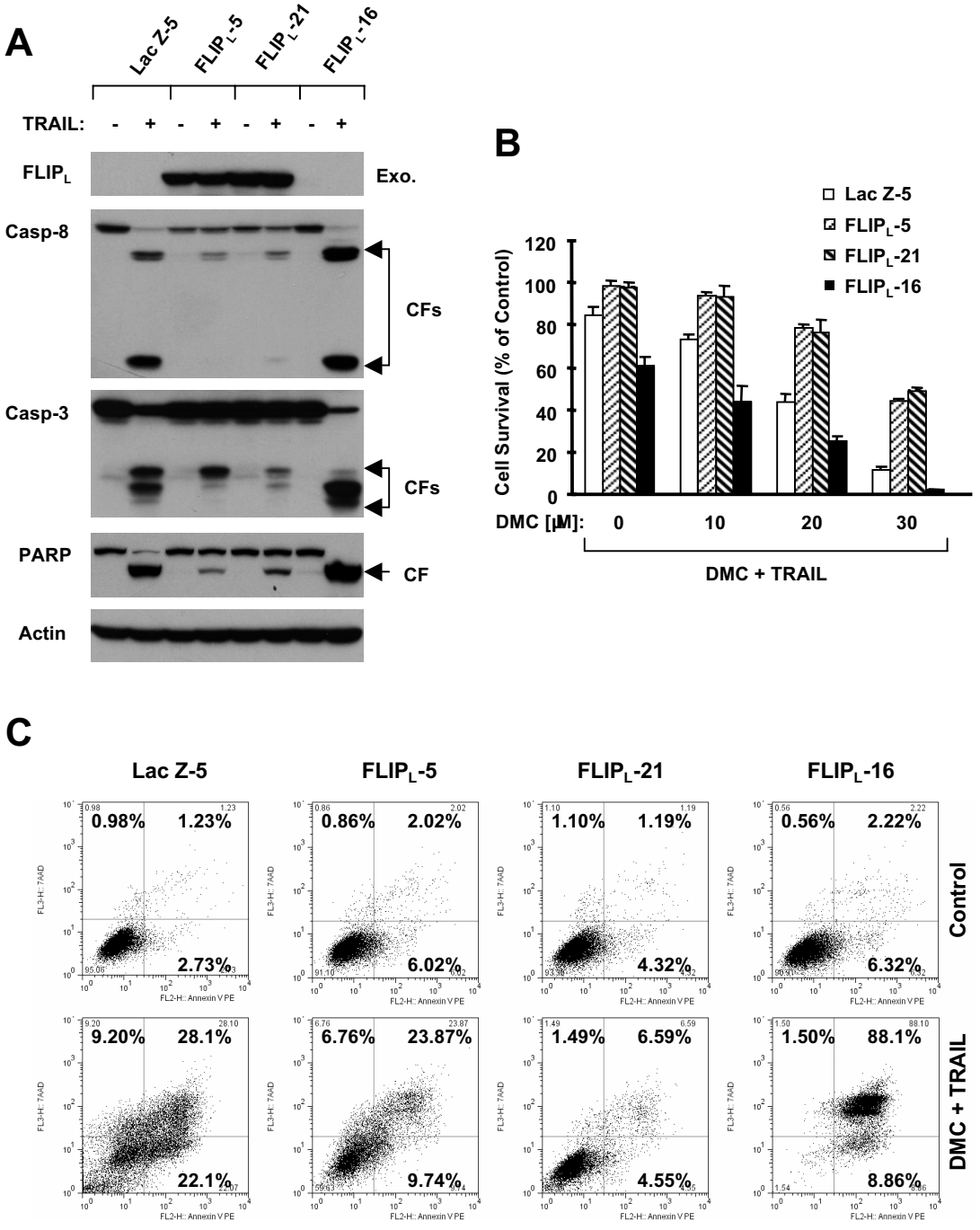

Fig. 7. Enforced expression of ectopic FLIP$_L$ confers resistance to induction of apoptosis by TRAIL (A) or the combination of DMC and TRAIL (B and C). A, the indicated transfectants were exposed to 20 ng/ml TRAIL. After 4 h, the cells were harvested and subjected to preparation of whole-cell lysates for the detection of exogenous (Exo.) FLIP$_L$ and caspase cleavage by Western blot analysis. B, the indicated transfectants were seeded in 96-well plates and treated with the indicated concentrations of DMC combined with 10 ng/ml TRAIL. After 24 h, the cells were subjected to the SRB assay for measurement of cell survival. Data are means of four replicate determinations. Bars, ± S.D. C, the indicated transfectants were treated with DMSO and 25 μM DMC plus 10 ng/ml TRAIL for 24 h and then subjected to detection of apoptosis by Annexin V staining. In Annexin V assay, the percentage of positive cells in the upper right and lower right quadrants were added to yield the total of apoptotic cells.

some major biological activities similar to celecoxib, even at molecular levels. A recent study has shown that JNK activation is involved in regulating ubiquitin/proteasome-dependent degradation of $FLIP_L$ (Chang et al., 2006). In our study, however, we did not detect a role of JNK in mediating DMC-induced c-FLIP degradation, and this conclusion is based on the following observations. First, DMC decreases both forms of c-FLIP (i.e., $FLIP_L$ and $FLIP_S$), whereas JNK regulates the degradation of only $FLIP_L$ (Chang et al., 2006). Second, DMC increases JNK activation in one cell line (i.e., H157) but not in another cell line (i.e., H460), in which c-FLIP was still down-regulated. Third, the JNK inhibitor SP600125 inhibited DMC-induced JNK activation but at the same time failed to prevent DMC-induced down-regulation of c-FLIP. It therefore seems that JNK does not play a major role in these DMC-induced processes.

We noted that $FLIP_L$ levels were decreased by DMC at early times (e.g., 4 and 8 h) and then increased after prolonged treatment (e.g., 12 and 16 h), whereas $FLIP_S$ levels were still reduced in H460 cells (Fig. 4A). The mechanism and biological significance of DMC-induced later increase in $FLIP_L$ are currently unclear. It is possible that the later increase in $FLIP_L$ may represent a survival mechanism for cells trying to escape DMC-induced cell death. Although DR5 can be induced through a JNK-dependent mechanism, as demonstrated in some studies (Higuchi et al., 2004; Zou et al., 2004), our results demonstrate that DMC induces DR5 expression in NSCLC cells independently of JNK activation because DMC did not induce JNK activation in H460 cells in which DR5 was induced and DMC could still induce DR5 expression in the presence of the JNK inhibitor SP600125 in H157 cells in which JNK was activated (Fig. 5).

DR5 is known to be regulated by p53 (Wu et al., 1997), nuclear factor-κB (Shetty et al., 2005), and CHOP (Yamaguchi and Wang, 2004; Yoshida et al., 2005). Because DMC induced DR5 expression in H157 cells carrying mutant p53, it is likely that DMC induced a p53-independent DR5 expression. In an effort to reveal the mechanism by which DMC induces DR5 expression, we found that CHOP was induced by DMC and accompanied with DR5 up-regulation. By analyzing the DR5 promoter, we found that the presence of the CHOP binding site is required for transactivation of the DR5 promoter by DMC. ChIP assay demonstrated that DMC also enhanced the binding of CHOP to DR5 promoter. Moreover, blockade of CHOP induction by silencing CHOP expression with CHOP siRNA abolished DMC's ability to induce DR5 expression. Thus, we conclude that DMC induces a CHOP-dependent DR5 up-regulation. Because CHOP is a typical protein associated with endoplasmic reticulum (ER) stress-induced apoptosis (Oyadomari and Mori, 2004), it is possible that DMC-induced up-regulation of CHOP and DR5 is caused by ER stress. Indeed, a recent study has demonstrated that DMC indeed induces ER stress of cancer cells in both cell culture and xenograft models in vivo, including CHOP up-regulation (Pyrko et al., 2007). Future studies need to demonstrate how DMC increases CHOP expression and whether nuclear factor-κB is activated and involved in DMC-induced DR5 expression.

It has been documented in the literature that activation of the TRAIL apoptotic pathway such as up-regulation of DR5 contributes to the induction of apoptosis by certain anticancer agents, including celecoxib (Huang et al., 2001; LaVallee et al., 2003; Wagner et al., 2003; Liu et al., 2004b; Kabore et al., 2006). The current work does not address whether DR5 up-regulation participated in the induction of apoptosis by DMC only, although we assume that it may contribute to DMC-induced apoptosis because celecoxib induces apoptosis requiring DR5 up-regulation. The ongoing work is to test whether DR5 induction is indeed involved in DMC-induced apoptosis.

In summary, the present study has shown for the first time that DMC, a celecoxib derivative lacking COX-2 inhibitory activity, induces CHOP-mediated DR5 up-regulation and ubiquitin/proteasome-mediated down-regulation of c-FLIP, leading to the enhancement of TRAIL-induced apoptosis in human NSCLC cells. Our results clearly indicate that DMC possesses more potent anticancer activity than celecoxib, although the underlying mechanisms seem to be quite similar. Given the concern over cardiovascular side effects of celecoxib, which is associated with its anti-COX-2 activity and is also noted with other COX-2 inhibitors (Dogné et al., 2006; Marwali and Mehta, 2006), DMC might be a better candidate or alternative to celecoxib for cancer chemoprevention and therapy.

Acknowledgments

We are grateful to H.-G. Wang (University of South Florida College of Medicine, Tampa, FL) for providing DR5 reporter constructs with a wild-type and mutant CHOP binding site, respectively, and H. A. Elrod in our lab for editing of the manuscript.

References

Abdelrahim M, Newman K, Vanderlaag K, Samudio I, and Safe S (2006) 3,3′-Diindolylmethane (DIM) and its derivatives induce apoptosis in pancreatic cancer cells through endoplasmic reticulum stress-dependent upregulation of DR5. *Carcinogenesis* **27:**717–728.

Chang L, Kamata H, Solinas G, Luo JL, Maeda S, Venuprasad K, Liu YC, and Karin M (2006) The E3 ubiquitin ligase itch couples JNK activation to TNFalpha-induced cell death by inducing c-FLIP(L) turnover. *Cell* **124:**601–613.

Chen C, Sun X, Ran Q, Wilkinson KD, Murphy TJ, Simons JW, and Dong JT (2005) Ubiquitin-proteasome degradation of KLF5 transcription factor in cancer and untransformed epithelial cells. *Oncogene* **24:**3319–3327.

Davies NM, McLachlan AJ, Day RO, and Williams KM (2000) Clinical pharmacokinetics and pharmacodynamics of celecoxib: a selective cyclo-oxygenase-2 inhibitor. *Clin Pharmacokinet* **38:**225–242.

Dogné JM, Hanson J, Supuran C, and Pratico D (2006) Coxibs and cardiovascular side-effects: from light to shadow. *Curr Pharm Des* **12:**971–975.

Grösch S, Maier TJ, Schiffmann S, and Geisslinger G (2006) Cyclooxygenase-2 (COX-2)-independent anticarcinogenic effects of selective COX-2 inhibitors. *J Natl Cancer Inst* **98:**736–747.

Harada H and Grant S (2003) Apoptosis regulators. *Rev Clin Exp Hematol* **7:**117–138.

Hengartner MO (2000) The biochemistry of apoptosis. *Nature* **407:**770–776.

Higuchi H, Grambihler A, Canbay A, Bronk SF, and Gores GJ (2004) Bile acids up-regulate death receptor 5/TRAIL-receptor 2 expression via a c-Jun N-terminal kinase-dependent pathway involving Sp1. *J Biol Chem* **279:**51–60.

Huang Y, He Q, Hillman MJ, Rong R, and Sheikh MS (2001) Sulindac sulfide-induced apoptosis involves death receptor 5 and the caspase 8-dependent pathway in human colon and prostate cancer cells. *Cancer Res* **61:**6918–6924.

Kabore AF, Sun J, Hu X, McCrea K, Johnston JB, and Gibson SB (2006) The TRAIL apoptotic pathway mediates proteasome inhibitor induced apoptosis in primary chronic lymphocytic leukemia cells. *Apoptosis* **11:**1175–1193.

Kardosh A, Wang W, Uddin J, Petasis NA, Hofman FM, Chen TC, and Schönthal AH (2005) Dimethyl-celecoxib (DMC), a derivative of celecoxib that lacks cyclooxygenase-2-inhibitory function, potently mimics the anti-tumor effects of celecoxib on Burkitt's lymphoma in vitro and in vivo. *Cancer Biol Ther* **4:**571–582.

Kelley SK and Ashkenazi A (2004) Targeting death receptors in cancer with Apo2L/TRAIL. *Curr Opin Pharmacol* **4:**333–339.

Kim Y, Suh N, Sporn M, and Reed JC (2002) An inducible pathway for degradation of FLIP protein sensitizes tumor cells to TRAIL-induced apoptosis. *J Biol Chem* **277:**22320–22329.

Koki AT and Masferrer JL (2002) Celecoxib: a specific COX-2 inhibitor with anticancer properties. *Cancer Control* **9 (2 Suppl):**28–35.

Krueger A, Baumann S, Krammer PH, and Kirchhoff S (2001) FLICE-inhibitory proteins: regulators of death receptor-mediated apoptosis. *Mol Cell Biol* **21:**8247–8254.

LaVallee TM, Zhan XH, Johnson MS, Herbstritt CJ, Swartz G, Williams MS, Hembrough WA, Green SJ, and Pribluda VS (2003) 2-Methoxyestradiol up-regulates

death receptor 5 and induces apoptosis through activation of the extrinsic pathway. *Cancer Res* **63:**468–475.
Liu X, Yue P, Khuri FR, and Sun SY (2004a) p53 upregulates death receptor 4 expression through an intronic p53 binding site. *Cancer Res* **64:**5078–5083.
Liu X, Yue P, Schönthal AH, Khuri FR, and Sun SY (2006) Cellular FLICE-inhibitory protein down-regulation contributes to celecoxib-induced apoptosis in human lung cancer cells. *Cancer Res* **66:**11115–11119.
Liu X, Yue P, Zhou Z, Khuri FR, and Sun SY (2004b) Death receptor regulation and celecoxib-induced apoptosis in human lung cancer cells. *J Natl Cancer Inst* **96:** 1769–1780.
Marwali MR and Mehta JL (2006) COX-2 inhibitors and cardiovascular risk. Inferences based on biology and clinical studies. *Thromb Haemost* **96:**401–406.
Oyadomari S and Mori M (2004) Roles of CHOP/GADD153 in endoplasmic reticulum stress. *Cell Death Differ* **11:**381–389.
Pfahl M, Tzukerman M, Zhang XK, Lehmann JM, Hermann T, Wills KN, and Graupner G (1990) Nuclear retinoic acid receptors: cloning, analysis, and function. *Methods Enzymol* **189:**256–270.
Pyrko P, Kardosh A, Liu YT, Soriano N, Xiong W, Chow RH, Uddin J, Petasis NA, Mircheff AK, Farley RA, et al. (2007) Calcium-activated endoplasmic reticulum stress as a major component of tumor cell death induced by 2,5-dimethyl-celecoxib, a non-coxib analogue of celecoxib. *Mol Cancer Ther* **6:**1262–1275.
Pyrko P, Soriano N, Kardosh A, Liu YT, Uddin J, Petasis NA, Hofman FM, Chen CS, Chen TC, and Schönthal AH (2006) Downregulation of survivin expression and concomitant induction of apoptosis by celecoxib and its non-cyclooxygenase-2-inhibitory analog, dimethyl-celecoxib (DMC), in tumor cells in vitro and in vivo. *Mol Cancer* **5:**19.
Schönthal AH (2006) Antitumor properties of dimethyl-celecoxib, a derivative of celecoxib that does not inhibit cyclooxygenase-2: implications for glioma therapy. *Neurosurg Focus* **20:**E21.
Shetty S, Graham BA, Brown JG, Hu X, Vegh-Yarema N, Harding G, Paul JT, and Gibson SB (2005) Transcription factor NF-kappaB differentially regulates death receptor 5 expression involving histone deacetylase 1. *Mol Cell Biol* **25:**5404–5416.
Sun SY (2005) Chemopreventive agent-induced modulation of death receptors. *Apoptosis* **10:**1203–1210.
Sun SY, Yue P, Dawson MI, Shroot B, Michel S, Lamph WW, Heyman RA, Teng M, Chandraratna RA, Shudo K, et al. (1997) Differential effects of synthetic nuclear retinoid receptor-selective retinoids on the growth of human non-small cell lung carcinoma cells. *Cancer Res* **57:**4931–4939.
Sun SY, Yue P, Wu GS, El-Deiry WS, Shroot B, Hong WK, and Lotan R (1999) Mechanisms of apoptosis induced by the synthetic retinoid CD437 in human non-small cell lung carcinoma cells. *Oncogene* **18:**2357–2365.
Wagner KW, King F, Nomoto K, Knee DA, Hampton G, Nasoff M, and Deveraux QL (2003) Activation and suppression of the TRAIL death-receptor pathway in chemotherapy sensitive and resistant follicular lymphoma cells. *Cancer Biol Ther* **2:**534–540.
Wang S and El-Deiry WS (2003) TRAIL and apoptosis induction by TNF-family death receptors. *Oncogene* **22:**8628–8633.
Wu GS, Burns TF, McDonald ER 3rd, Jiang W, Meng R, Krantz ID, Kao G, Gan DD, Zhou JY, Muschel R, et al. (1997) KILLER/DR5 is a DNA damage-inducible p53-regulated death receptor gene. *Nat Genet* **17:**141–143.
Yamaguchi H and Wang HG (2004) CHOP is involved in endoplasmic reticulum stress-induced apoptosis by enhancing DR5 expression in human carcinoma cells. *J Biol Chem* **279:**45495–45502.
Yoshida T, Shiraishi T, Nakata S, Horinaka M, Wakada M, Mizutani Y, Miki T, and Sakai T (2005) Proteasome inhibitor MG132 induces death receptor 5 through CCAAT/enhancer-binding protein homologous protein. *Cancer Res* **65:**5662–5667.
Zhu J, Huang JW, Tseng PH, Yang YT, Fowble J, Shiau CW, Shaw YJ, Kulp SK, and Chen CS (2004) From the cyclooxygenase-2 inhibitor celecoxib to a novel class of 3-phosphoinositide-dependent protein kinase-1 inhibitors. *Cancer Res* **64:**4309–4318.
Zhu J, Song X, Lin HP, Young DC, Yan S, Marquez VE, and Chen CS (2002) Using cyclooxygenase-2 inhibitors as molecular platforms to develop a new class of apoptosis-inducing agents. *J Natl Cancer Inst* **94:**1745–1757.
Zou W, Liu X, Yue P, Khuri FR, and Sun SY (2007) PPARgamma ligands enhance TRAIL-induced apoptosis through DR5 upregulation and c-FLIP down-regulation in human lung cancer cells. *Cancer Biol Ther* **6:**99–106.
Zou W, Liu X, Yue P, Zhou Z, Sporn MB, Lotan R, Khuri FR, and Sun SY (2004) c-Jun NH2-terminal kinase-mediated up-regulation of death receptor 5 contributes to induction of apoptosis by the novel synthetic triterpenoid methyl-2-cyano-3,12-dioxooleana-1, 9-dien-28-oate in human lung cancer cells. *Cancer Res* **64:**7570–7578.

Address correspondence to: Dr. Shi-Yong Sun, Winship Cancer Institute, Emory University School of Medicine, 1365-C Clifton Road, Clinical Building C, Suite C3088, Atlanta, GA 30322. E-mail: shi-yong.sun@emoryhealthcare.org

Cell Motility and the Cytoskeleton 65: 675–685 (2008)

β-Tubulin Isotype Classes II and V Expression Patterns in Nonsmall Cell Lung Carcinomas

Valeria Cucchiarelli,[1] Laree Hiser,[2] Hilda Smith,[2] Anthony Frankfurter,[3] Anthony Spano,[3] John J. Correia,[1] and Sharon Lobert[1,2]*

[1]*The University of Mississippi Medical Center, Department of Biochemistry, Jackson, Mississippi*
[2]*The University of Mississippi Medical Center, School of Nursing, Jackson, Mississippi*
[3]*University of Virginia, Department of Biology, Charlottesville, Virginia*

Previous studies suggest that β-tubulin isotype protein levels could be useful as indicators of nonsmall cell lung cancer (NSCLC) aggressiveness. However, measurement of protein amounts in tissue samples by staining techniques is semiquantitative at best. Since technologies for measuring mRNA levels have become more efficient and quantitative, we wanted to determine whether β-tubulin message levels may be useful as biomarkers. Quantitative real-time RT-PCR was used to measure the seven classes of β-tubulin isotypes, stathmin and MAP4 mRNA levels in 64 NSCLC and 12 normal lung tissue samples. We found significantly higher fractions of β-tubulin classes II and V mRNA compared to the other isotypes in all lung tumor samples ($P < 0.05$). In addition, the ratio of β-tubulin classes II/V mRNA was significantly higher in NSCLCs compared to normal lung tissues ($P < 0.001$). The data suggest that the ratio of β-tubulin classes II and V mRNA could be useful as a biomarker for NSCLC tumor differentiation and/or NSCLC aggressiveness. Furthermore, the ratio of MAP4 to stathmin mRNA was found to be higher in diseased lung tissues compared to normal lung tissues, suggesting this ratio might also be used as a clinically relevant biomarker for NSCLCs. Cell Motil. Cytoskeleton 65: 675–685, 2008.

Key words: tubulin isotypes; nonsmall cell lung cancer; beta II tubulin; beta V tubulin; microtubules

INTRODUCTION

Lung cancer is the leading cause of cancer deaths in the United States [Seer Incidence and US Mortality Statistics, 1975–2004 http://seer.cancer.gov/canques]. Lung tumor heterogeneity hinders efforts to determine prognosis and select appropriate treatment regimens. Unfortunately, there are currently no consistently reliable biomarkers that can be used as prognostic indicators [Brundage et al., 2002]. Typically, lung tumors are classified into two major categories based on morphology and behavior: small cell lung cancer (SCLC) and nonsmall cell lung cancer (NSCLC). Small cell lung cancers (SCLCs) are generally more aggressive than NSCLCs and often display a neuroendocrine phenotype [Zochbauer-Muller et al., 2002]. The NSCLCs are a

Contract grant sponsor: Department of Defense (V.I.T.A.L. project); Contract grant number: W81XWH-04-1-0142-03.

*Correspondence to: Sharon Lobert, The University of Mississippi Medical Center, School of Nursing, 2500 North State Street, Jackson, MS 39216, USA. E-mail: slobert@son.umsmed.edu

Abbreviations used: MAP, microtubule associated protein; MES, 2-[*N*-morpholino]-ethane sulfonic acid; NSCLCs, nonsmall cell lung carcinomas; qRT-PCR, quantitative real-time reverse transcriptase polymerase chain reaction.

Received 19 February 2008; Accepted 21 May 2008

Published online 8 July 2008 in Wiley InterScience (www.interscience.wiley.com).
DOI: 10.1002/cm.20297

diverse class of tumors (squamous cell, adenocarcinomas and large cell undifferentiated) with some aggressive subsets characterized by neuroendocrine features. Neuroendocrine features can be identified by tissue staining using specific markers such as neuron-specific enolase, chromogranin A, synaptophysin and neurofilament protein. Although these markers are used to identify potentially aggressive tumors, they can not discriminate between high and low grade neuroendocrine tumors. In addition for NSCLCs there are no specific and reliable markers for more aggressive and poorly differentiated squamous cell carcinomas or adenocarcinomas that lack the neuroendocrine phenotype. Thus, biomarkers for aggressive tumors are clearly needed.

In a study of 88 primary and metastatic lung tumors using immunohistochemical staining, β-tubulin class III protein was identified as a biomarker for high grade aggressive tumors (small cell lung carcinomas, adenocarcinomas and neuroendocrine type large cell carcinomas) [Katsetos et al., 2000]. This tubulin isotype was not found in non-neoplastic lung biopsies, pneumonectomy, lobectomy or transbronchial biopsy specimens. It also was absent from airway mucosa, submucosal glands, myoepithelial cells, alveolar pneumocytes and macrophages, hyaline cartilage, fibroblasts, endothelial cells, smooth muscle cells, pericytes and lymphoid cells. In contrast, high levels of β-tubulin class III staining were found in all the small cell lung carcinomas (SCLCs) examined and in large cell neuroendocrine lung tumors. Lower levels of β-tubulin class III were found in NSCLC adenocarcinomas and staining was absent from squamous cell lung carcinomas (SQCC), suggesting that this biomarker might be useful for distinguishing SCLC and SQCC. This work suggested that β-tubulin class III may be a biomarker for aggressive NSCLCs; although other tubulin isotype distributions were not measured. The TUJ1 monoclonal antibody for β-tubulin class III used by Katsetos et al. [2000] is one of the most stable and specific tubulin antibodies commercially available. There are no commercially available monoclonal antibodies for β-tubulin classes V and VI or that differentiate β-tubulin classes IVa from IVb. Therefore studies comparing all of the β-tubulin isotypes found in normal lung tissue or lung tumors by immunostaining are not currently feasible.

A more recent clinical investigation of biomarkers, including tubulin isotypes, distinguished those that predict prognosis for patients with NSCLCs from those that predict drug response. In a study of 91 NSCLCs, low levels of β-tubulin class III protein measured by immunostaining correlated with a better response to paclitaxel, an antimitotic agent often used to treat advanced stage NSCLCs [Seve et al., 2005]. Only β-tubulin classes I, II and III were evaluated. In contrast to Katsetos et al. [2000], the β-tubulin class III protein level was not found to be a prognostic indicator for patients who had not received paclitaxel.

In addition to β-tubulin isotype amounts, altered levels of proteins that interact with tubulin or microtubules, such as stathmin or MAP4, could affect tumor response to antimitotics such as paclitaxel. Stathmin belongs to a family of proteins that destabilize microtubules in mitotic spindles. During interphase, stathmin regulates microtubule depolymerization. High levels of stathmin have been found in many tumors, and it has been proposed that the effect of stathmin is to increase the proliferative activity of tissues [Mistry and Atweh, 2002]. MAP4 is a microtubule-associated protein expressed constitutively and known to stabilize microtubules. Decreased levels of MAP4 are associated with decreased sensitivity to paclitaxel and increased sensitivity to other antimitotics such as vinblastine [Wahl et al, 1996; Zhang et al., 1999]. Measurement of the expression of mRNA for proteins that interact with tubulin and microtubules (e.g., stathmin and MAP4) could lead to the identification of biomarker patterns useful as indicators of tumor response to chemotherapy.

The study presented here is the first quantitiative comparison of mRNA levels for all seven β-tubulin isotypes, stathmin and MAP4 in NSCLCs. This work included 64 NSCLC samples and 12 normal lung samples in an attempt to describe patterns of mRNA β-tubulin isotypes or microtubule-associated proteins that might serve as biomarkers for tumor differentiation and/or aggressiveness.

MATERIALS AND METHODS

Collection of Lung Tissues

Lung tissue samples and pathology reports for each tissue were obtained from the Cooperative Human Tissue Network (CHTN, National Cancer Institute). Sixty-four (64) primary nonsmall cell lung tumor samples and 12 "normal" lung tissue samples were collected prior to drug treatment and quick-frozen in liquid nitrogen within 1 h of surgical removal. Normal tissues were collected from a section of the lung at a distance from the primary tumor at the same time as surgical resection of the primary tumor. The absence of tumor cells in these normal samples was verified by histopathological examination. The normal lung tissues were from a subset of the 64 patients with primary tumors. Table I describes the samples included in this study as well as the manner in which these samples were subdivided for analysis.

Sample Preparation

Tissues were homogenized in a dounce homogenizer on ice in 1 ml of lysis buffer (25 mM MES, 1 mM

TABLE I. NSCLC and Normal Lung Tissue Samples

	Race	
	[a]BM	WM
NSCLC samples		
Number of samples	20	44
Age range	43–79	40–85
Tissue differentiation		
Poorly differentiated	9	19
Moderately differentiated	4	15
Well differentiated	3	4
Not determined	5	5
Histological classification		
Squamous cell carcinoma	8	18
Adenocarcinoma	6	10
Large cell carcinoma with neuroendocrine features	1	3
Various	5	13
Normal lung tissues		
Number of samples	2	10
Age range	75–76	40–82

[a]BM, African American males; WM, White males.

TABLE II. Primers for qRT-PCR (MAP4 and Stathmin)

Human stathmin
Forward primer: 5′ - GGT GGC GGC AGG ACT TTC CTT ATC CCA GTT GAT T - 3′ (34 bp)
Reverse primer: 5′ - TTC TCG TGC TCT CGT TTC TCA GCC AGC TGC TTC – 3′ (33 bp)
Human MAP4
Forward primer: 5′ - CCC TTT CTG AGG TAG CAG TGC CTT GTG GAG GT – 3′ (32 bp)
Reverse primer: 5′ - CTG GCT CCC TCA TGT TCT TGG CAC AGC AGA - 3′ (30 bp)

$MgSO_4$, 2 mM EGTA, 0.1 mM GTP, 0.1% Triton X-100 with a protease inhibitor cocktail [Complete Protease Inhibitor Tablets, Roche, Indianapolis, IN]). 100 μl of tissue homogenate were processed for total RNA extraction using the TRIzol reagent (Invitrogen, Carlsbad, CA) and the RNeasy kit (Qiagen, Valencia, CA) to obtain total RNA for qRT-PCR experiments. After DNase treatment of the total RNA, poly dT was used in reverse treanscription reactions to generate cDNA. The concentration of total RNA for each sample was determined by A_{260} measurements. The remainder of the tissue homogenate was made 1:1 with SDS sample buffer and frozen for Western blotting.

Quantitative Real Time Reverse Transcriptase Polymerase Chain Reaction (qRT-PCR)

Primers were designed for each β-tubulin isotype (classes I, II, III, IVa, IVb, V and VI) [Dozier et al., 2003; Hiser et al, 2006] and for MAP4 and stathmin (Table II). Although β-tubulin isotype class II is considered a single isotype class based upon the carboxyl terminal protein sequence, there are two genes for this isotype (NIH Genbank map elements: TUBB2A; NM_001069 and TUBB2B; NM_178012.3). The primers used in this study recognize the gene product for TUBB2B. Two-step qRT-PCR was used to measure the amount of mRNA for each β-tubulin isotype using protocols described previously [Dozier et al., 2003; Hiser et al., 2006]. To obtain the control cDNA template of a known quantity for the generation of standard curves, product from PCR reactions was isolated from agarose gels with the CONCERT™ Rapid Gel Extraction kit (Marligen Biosciences, Inc., Ijamsville, MD). The use of a standard curve eliminates the need to correct for primer efficiencies. The concentration of purified cDNA was determined by analyzing serial dilutions using a bioanalyzer (Agilent Technologies, Inc., Santa Clara, CA). For the standard curve, 10-fold serial dilutions are done to obtain a minimum of five samples and these are plated in triplicate. Each experiment included unknown samples in triplicate run together with the standard curve and a quality control sample. We used SYBR Green I (Invitrogen, Carlsbad, CA) as the detection method. Experiments were repeated at least twice. The data were normalized as the β-tubulin isotype mRNA copy number in the unknown sample to 1 μg of total RNA. The percentage of each β-tubulin isotype was determined by totaling the mRNA copy number/μg of total RNA for all isotypes in a sample and then dividing the copy number/μg total RNA for each isotype by the total. The ratios of copy mumbers/μg of total RNA or ratios of percentages therefore are identical.

Western Blotting

Western blots were used to evaluate the presence of β-tubulin isotype classes II, III and V proteins. The antibodies used in this study were mouse monoclonal 7B9 anti-β-tubulin class II, monoclonal TUJ1 anti-β-tubulin class III and rabbit polyclonal anti-β-tubulin class V. TUJ1 and 7B9 antibodies have been previously characterized [Lee et al., 1990; Lobert et al., 1998]. The anti-β-tubulin class V polyclonal antibody was characterized in this study using maltose binding protein (MBP) β-tubulin fusion proteins as described in Hiser et al. [2006]. Fusion proteins and dot blots were used to determine the specificity and optimal solution conditions for the anti-β-tubulin class V antibody. Tissue samples expressing high and low mRNA levels of β-tubulin classes II and V were chosen for Western blotting. Immunoblotting with anti-actin mouse monoclonal antibody (Chemicon International, Inc., Temecula, CA) was

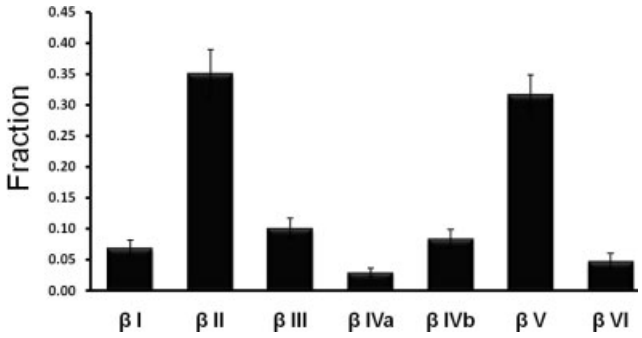

Fig. 1. Fraction of β-tubulin isotypes in NSCLC tissues. The average β-tubulin isotype fractions from all 64 NSCLC samples are shown. The sum of the values for all seven β-tubulin isotype classes was considered as the total tubulin for the mRNA percentage (fraction) calculations. Each bar of the graph represent the average of the percentage of each isotype. Error bars represents the standard error of the mean. β-Tubulin classes II and V differ significantly from β-tubulin classes I, III, IVa, IVb and VI at $P < 0.05$.

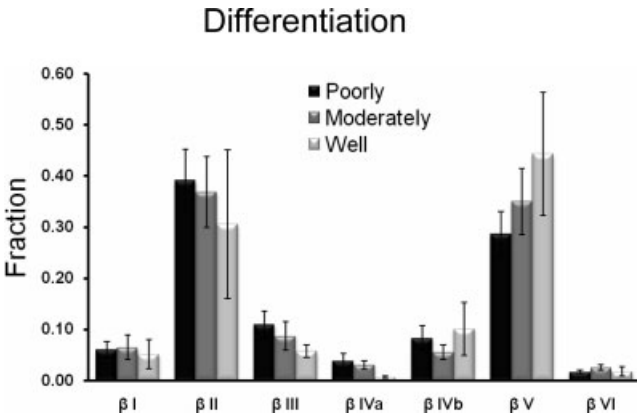

Fig. 2. Fraction of β-tubulin isotypes in NSCLCs grouped by level of differentiation. The bar graphs represent the averages and error bars represent the standard error of the mean. The numbers of samples in each group were: poorly differentiated $n = 28$, moderately differentiated $n = 19$ and well differentiated $n = 7$.

used to establish that the total protein loaded in each lane was comparable.

Statistical Analysis

For statistical comparisons of mRNA amounts in tissue samples, Student's *t* test or one-way ANOVA with Tukey's Multiple Comparison post test was performed using GraphPad Prism version 5.00 for Windows (GraphPad Software, San Diego, CA).

RESULTS

β-Tubulin Classes II and V mRNA Predominate in NSCLC Tissues

The amounts of β-tubulin isotype mRNA classes I, II, III, IVa, IVb, V, and VI were measured by qRT-PCR. This is the first quantitative comparison of mRNA for all seven β-tubulin isotypes in NSCLCs. The sum of the mRNA amounts for all seven isotypes was considered to be the total tubulin for each sample, and the percentage (fraction) of each isotype was calculated (Fig. 1). Data analysis by one-way ANOVA demonstrated that the fractions of β-tubulin classes II and V were significantly higher than the other β-tubulin isotypes in diseased tissues at $P < 0.05$. Together they comprise over 65% of all β-tubulin mRNA in NSCLC tissues. When these data were compared with β-tubulin isotype fractions in a small sample of normal lung tissues ($n = 12$), interesting differences were noted. We found that normal lung tissues had on average about 3-fold fewer copies of total β-tubulin mRNA/μg of total RNA compared to diseased lung tissue. For paired normal and tumor lung tissues, we found the mean copies of β-tubulin mRNA/μg of total RNA for normal samples was $3.0\ (\pm 2.3) \times 10^5$ and for tumors from the same patient $1.0\ (\pm 0.003) \times 10^6$ [all tumors $3.3\ (\pm 0.05) \times 10^6$]. The β-tubulin isotype class distribution in normal lung tissues was as follows: βI 6% ± 0.4% βII 2.5% ± 0.2%, βIII 36% ± 2%, βIVb 8% ± 0.8%, βV 13% ± 1%, βVI 34.5% ± 2%. The normal lung tissues did not have measurable amounts of β-tubulin class IVa mRNA. Data analysis by one-way ANOVA demonstrated that the predominant isotypes in this small sample of normal lung tissues, β-tubulin classes III and VI, were present in significantly larger amounts than the other β-tubulin isotypes ($P < 0.001$). There was no statistically significant difference in β-tubulin isotype classes I, II, IVb or V. Student's *t* test demonstrated that the fractions of β-tubulin isotype classes II and V were significantly smaller in normal lung tissues compared to NSCLCs ($P < 0.05$).

β-Tubulin Classes II and V mRNA Fractions Follow Similar Trends by Level of Differentiation and Histopathology in NSCLCs

NSCLC samples were grouped according to tissue differentiation as determined in the pathology report: poorly-differentiated ($n = 28$), moderately differentiated ($n = 19$) and well-differentiated ($n = 7$). Only data from samples that were classified as one of these three types ($n = 54$) were used in this analysis. We observed a trend in the average mRNA fraction of β-tubulin class II mRNA: well-differentiated < moderately-differentiated or poorly-differentiated; in contrast, the mRNA fraction of β-tubulin class V mRNA followed the reverse pattern: well-differentiated > moderately-differentiated > poorly-differentiated (Fig. 2). Statistical analysis did not demonstrate significance, possibly due to the small n for each

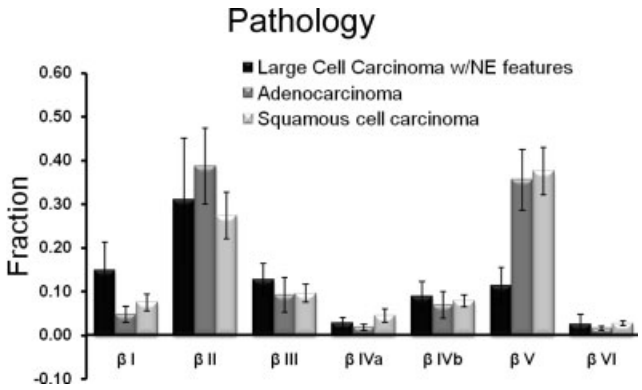

Fig. 3. Fraction of β-tubulin isotypes in NSCLCs grouped by histopathology. The bar graphs represent the averages and error bars represent the standard error of the mean. The numbers of samples in each group were: large cell carcinoma with neuroendocrine (NE) features $n = 4$, adenocarcinoma $n = 16$, and squamous cell carcinoma $n = 28$.

group or the uncertainty in the criteria used for histopathological determinations.

Samples were divided into histopathological groups: squamous cell carcinoma ($n = 28$), adenocarcinoma ($n = 16$) and large cell carcinoma with neuroendocrine features ($n = 4$). Only data from samples that had these designations on the pathology reports were utilized in this analysis ($n = 48$). The results show β-tubulin class II mRNA fractions ranged as follows: squamous cell < adenocarcinomas or large cell carcinomas with neuroendocrine features. In contrast, we found that β-tubulin class V mRNA fractions followed the reverse trend: large cell carcinomas with neuroendocrine features < adenocarcinomas or squamous cell carcinomas (Fig. 3). Statistical analysis did not demonstrate significance, possibly due to the small n for each group or the uncertainty in the criteria used for histopathological determinations.

Significant Differences are Present in β-Tubulin Class II to V mRNA Copy Number Ratios in Normal Lung Tissues and NSCLCs

Because β-tubulin isotype mRNA classes II and V were found to be the predominant isotypes in NSCLCs and they have reverse patterns of expression when comparing well-differentiated and poorly-differentiated tissues, the ratios of the copy numbers of these two isotypes were analyzed. The ratio of the copy numbers of β-tubulin isotype classes II to V in normal lung tissues ($n = 12$) was also included in this analysis. The ratio of β-tubulin isotype classes II to V in NSCLCs was significantly higher than in normal lung tissues (unpaired Student's t test, $P < 0.001$) (Fig. 4A). This was true also for paired comparison of normal and tumor lung tissues from the same patient: $P < 0.0001$, Student's t test (data not shown). When the β-tubulin II/V ratio data were grouped by level of differentiation a trend was found: the value decreased from poorly- to moderately- to well-differentiated tissues and the ratio in well-differentiated tissues approaches that of the normal lung tissues (ANOVA, $P = 0.17$) (Fig. 4B). When the data were grouped by histopathology, we found that the trend for the ratio of β-tubulin classes II/V approached statistical significance at $P < 0.05$: large cell carcinomas with neuroendocrine features > adenocarcinomas > squamous cell carcinoma > normal lung tissues (ANOVA, $P = 0.06$) (Fig. 4C). The fact that these ratios are determined for each patient before averaging must contribute to the increased statistical significance of these data compared to the aggregate data for each isotype alone, suggesting potential utility of the β-tubulin class II/V ratio as a biomarker for aggressive lung tumors.

β-Tubulin Classes II and V Proteins are Present in NSCLCs

The presence of protein for β-tubulin isotype classes II and V was evaluated by Western blotting of three samples that showed high and low mRNA levels for β-tubulin classes II and V. The specificity of anti-β-tubulin class II antibody, 7B9, has been previously characterized [Lobert et al., 1998]. In this study we used a newly developed polyclonal antibody raised against the carboxy-terminal peptide for β-tubulin class V. Dot blots with maltose binding protein (MBP) β-tubulin isotype fusion proteins representing peptides from the carboxyl terminus of all seven β-tubulin isotype classes were used to characterize the specificity of this antibody and to establish the optimal working dilution. The use of MBP tubulin isotype fusion proteins in Western blotting is described in our previous work [Hiser et al., 2006]. The optimal dilution was found to be 1:30,000 (~0.1 μg/ml) (Fig. 5A). Both β-tubulin isotype classes II and V proteins were found in the three tissue samples that were examined. There was no apparent difference in protein expression of β-tubulin isotype class II, but the different levels of β-tubulin isotype class V protein were consistent with the different levels of mRNA (Fig. 5B). The findings for β-tubulin isotype class II protein were not surprising since primers used in our qRT-PCR measurements for this class recognized the mRNA product of the TUBB2B gene only, while the antibody recognizes the products of TUBB2A and TUBB2B. Tubulin class V protein has not previously been measured in lung tumor tissues. Note that we divided our total tissue lysate into fractions to use for total RNA extraction and for semiquantitative protein measurements by Western blotting. Tissue samples are inherently heterogeneous and we wanted to

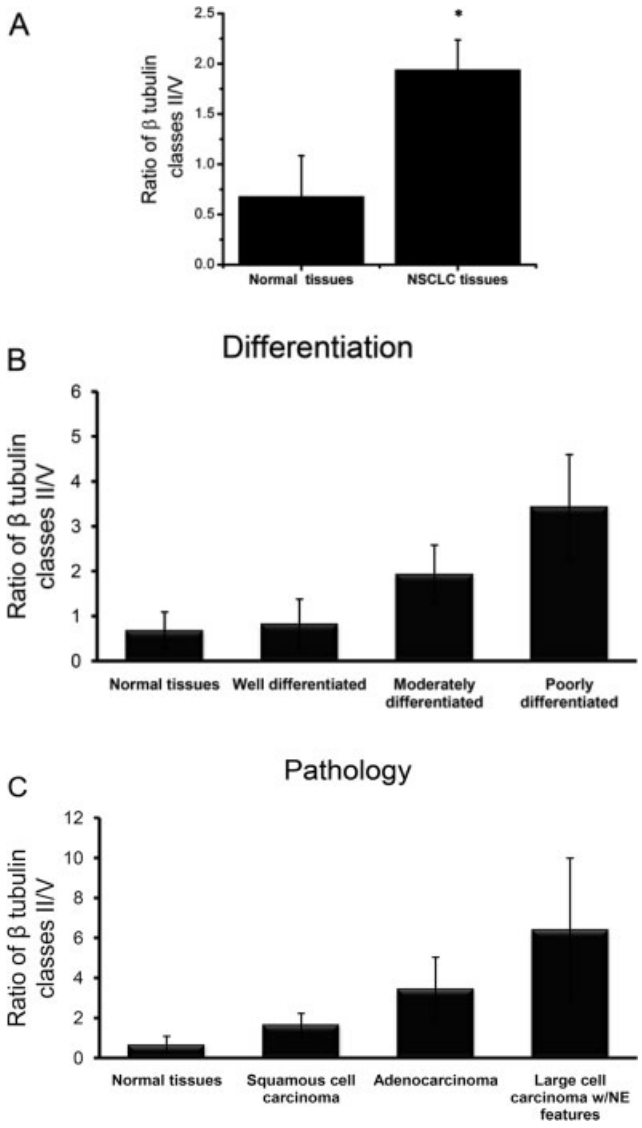

Fig. 4. Ratio of β-tubulin classes II to V. **Panel A:** Comparison of normal lung tissues ($n = 12$) and NSCLCs ($n = 64$). * Indicates a significant difference by unpaired Student's t test, $P < 0.001$. **Panel B:** Data are grouped by differentiation (ANOVA, $P = 0.17$). **Panel C:** Data are grouped by histological classification (ANOVA, $P = 0.06$). The numbers of samples used to calculate the averages are shown for each grouping in Figures 2 and 3. Error bars represent the standard error of the mean.

minimize differences in mRNA and protein quantities that might be due to different cell types within a section of a sample. Therefore the semiquantitative Westerns show a reasonable estimate of the protein in the sample used for mRNA quantitation.

MAP4 to Stathmin Ratio is Significantly Higher in NSCLCs Compared to Normal Lung Tissues

Stathmin and MAP4 are microtubule associated proteins important in cell division and proliferation [Andersen, 2000], and therefore changes in these proteins may have implications for tumorigenesis. In addition, alterations in levels of stathmin and MAP4 can change the sensitivity of cells to antimitotic drugs commonly used in chemotherapy protocols for NSCLC [Zhang et al., 1999; Alli et al., 2002]. MAP4 and stathmin have opposing effects on microtubules; MAP4 stabilizes and stathmin destabilizes polymer formation. qRT-PCR was used to measure the copy number of MAP4 and stathmin mRNA in normal lung tissue ($n = 12$) and NSCLCs ($n = 64$). Analagous to the results that we found with tubulin message, we found significantly more MAP4 and stathmin in NSCLCs compared to normal lung tissues (Student's t-test, $P < 0.0001$). The mean mRNA copy number/μg total RNA of MAP4 in normal lung tissues was 7.2 (± 2.8) $\times$ 10^4 and in NSCLCs it was 8.8 (± 1.3) $\times$ 10^5; for stathmin in normal lung tissues, it was 2.8 (± 0.4) $\times$ 10^5 and in NSCLCs 9.4 (± 1.6) $\times$ 10^5. In addition, when the ratios of MAP4 to stathmin mRNA copies/μg of total RNA for each patient sample were averaged, we found the ratio was significantly higher in NSCLCs than in normal lung tissues (Fig. 6). This reflects a trend toward increasing microtubule stabilizing factors in NSCLCs compared to normal lung tissues.

DISCUSSION

β-Tubulin Isotypes in Tumor Cells and Tissues: Association with Tumor Formation and Aggressiveness

This study describing β-tubulin, MAP4 and stathmin mRNA in NSCLC tissues was undertaken to search for biomarker patterns useful for determining prognosis. Specific and reliable markers to distinguish NSCLCs are needed, as are reliable predictors of response to chemotherapy that could reduce the morbidity associated with ineffective chemotherapy. This is the first study of NSCLCs comparing all seven β-tubulin isotype mRNA fractions. Thus the findings regarding β-tubulin classes II and V levels are novel and further exploration of these isotypes as prognostic biomarkers is warranted.

Recent work suggested a role for β-tubulin class III protein as a biomarker for NSCLC aggressiveness and patient prognosis, indicating a dysregulated, poorly-differentiated tumor type [Katsetos et al., 2000]. This was in contrast to normal lung tissues that did not have measurable β-tubulin class III protein. However, the only β-tubulin isotype evaluated in that study was β-tubulin class III. Since β-tubulin class III is a member of the family of β-tubulins, comprised of at least seven gene products that are grouped into classes based upon their carboxy-terminal amino acid sequences, a compari-

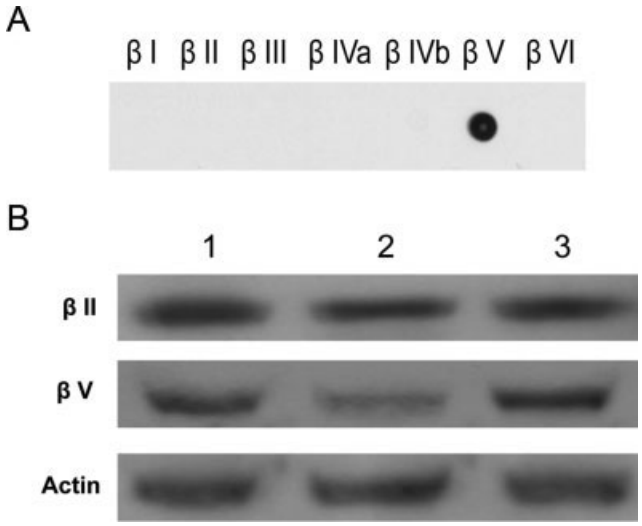

Fig. 5. **A**: Dot blot showing the specificity of anti-β-tubulin class V polyclonal antibody. Using maltose binding fusion proteins for the seven tubulin isotype classes, the concentration of antibody that reacts specifically with β-tubulin class V was determined to be 1:30,000. This dilution was used for Western blotting. **B:** Western blots showing the protein expression of β-tubulin isotype classes II and V in NSCLC tissues. Tissues with low and high levels of β-tubulin isotype classes II and V mRNA were used. Immunoblotting with anti-actin monoclonal antibody was used to establish that the total protein loaded in each lane was comparable. Lane 1: whole cell lysate from a sample with high β-tubulin isotype classes II and V mRNA. Lane 2: whole cell lysate from a sample with low β-tubulin isotype classes II and V mRNA; and Lane 3: whole cell lysate from a sample with high β-tubulin isotype classes II and V mRNA. For comparison, the message levels (mRNA copies/μg total RNA) for each sample were as follows: Top panel: β-tubulin isotype class II -lane (1) 4570, lane (2) 134, lane (3) 58,400; Middle panel: β-tubulin isotype class V- lane (1) 6010, lane (2) 52, lane (3) 43,900; Lower panel: samples reacted with anti-actin monoclonal antibody to establish that equal amounts of total protein were loaded in each lane.

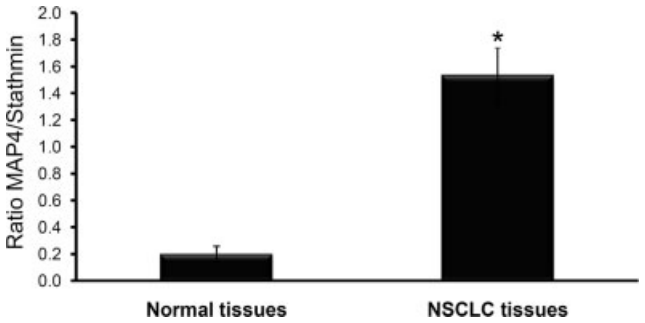

Fig. 6. Ratio of MAP4 to stathmin mRNA in NSCLCs and normal lung tissues. Each bar of the graph represents the average of the ratio from each patient sample of MAP4 to stathmin in normal or diseased tissues. Error bars represent the standard error of the mean. The ratio of MAP4 to stathmin is significantly higher in NSCLCs compared to normal lung tissues at $P < 0.05$ (Student's t test).

son of the amounts of β-tubulin isotypes in tissues should provide additional data for understanding tubulin dysregulation in tumors. The levels of specific β-tubulin isotypes vary in different mammalian tissues [Sullivan, 1988; Luduena, 1993]; however, the functional role for the variability in tubulin polypeptides is uncertain [Luduena, 1993; Raff, 1994]. β-Tubulin classes I, II and IVb are reported to be constitutively expressed in many vertebrate tissues (mouse, rat, chicken) [Lewis et al., 1985; Sullivan and Cleveland, 1986]. Classes III and IVa are primarily found in neurons; in fact, β-tubulin class III is often used as a marker for neuronal tissues. β-Tubulin class V has been less well studied because a specific and stable antibody for this isotype has not been widely available. It has been thought to be present in small amounts in many cell types, but not in neurons [Sullivan, 1988]. Class VI was found in the avian and mammalian blood cells (specifically the marginal band of avian erythocytes and mammalian nucleated immature erythrocytes and platelets), as well as in hematopoietic tissues (in mouse spleen and liver) [Murphy and Wallis, 1983; Wang et al., 1986]. In that work it was noted that lung tissue of young mice also expressed β-tubulin class VI [Wang et al., 1986].

Increased levels of β-tubulin class III protein could affect the tumor response to chemotherapy. The properties of β-tubulin classes III, V and VI are reported to render microtubules more dynamic than β-tubulin classes I, II, IVa and IVb [Luduena, 1993; Cabral, 2008]. Some investigators have speculated that alterations in microtubule dynamics due to varying levels of β-tubulin isotypes may contribute to differential responses to antimitotic agents that interact with tubulin heterodimers or microtubules [Hari et al., 2003; Bhattacharya and Cabral, 2004]. This should affect patient outcomes. Recent work indicates that changes in the abundance of β-tubulin isotypes confer differential drug responses perhaps as a result of changes in drug binding affinity and/or microtubule dynamics [Yang and Cabral, 2007]. For example, in a recent study of the effect of increased levels of β-tubulin class IVa in CHO cells on the response to paclitaxel, small increases of this isotype enhanced drug sensitivity and high levels produced drug resistance [Yang and Cabral, 2007]. Note that in the work of Cabral and colleagues, the amount of only one isotype is changed and therefore, may not reflect global intracellular changes in real physiological systems. Two recent studies identified β-tubulin class III protein as a predictor of NSCLC response to antimitotic drugs [Dumontet et al., 2005; Seve et al., 2005]; although, it may not be a general prognostic indicator [Seve et al., 2005]. Note that in both studies, only β-tubulin isotype classes I, II and III protein were evaluated. While all three isotypes were identi-

fied in these NSCLC samples they were not quantitatively compared.

We quantitatively measured β-tubulin isotype mRNA levels in 76 lung tissue samples (64 NSCLCs and 12 normal lung tissues). Normal lung tissues were obtained from a subset of the 64 patients diagnosed with NSCLC and the pathology reports identified the tissues as exhibiting normal histological characteristics. The β-tubulin isotype pattern was clearly different when normal and NSCLCs were compared; β-tubulin classes II and V mRNA predominate in NSCLCs and β-tubulin classes III and VI mRNA predominate in normal lung tissues. This finding was unexpected since Katsetos, et al. [2000] did not find appreciable amounts of β-tubulin class III protein in normal lung tissues. However, they did not attempt to compare β-tubulin class III levels with other isotype levels. It is important to note that these data are presented as fractions of each isotype, rather than as copy number. We found that normal lung tissues tend to have on average about 3-fold fewer copies of β-tubulin mRNA/μg of total RNA compared to diseased tissue. More specifically, we found 3.5-fold fewer copies of β-tubulin class III mRNA in normal tissues compared to NSCLCs [normal 8.0 ($\pm$1.4) $\times$ 10^4 and NSCLCs 2.8 ($\pm$0.6) $\times$ 10^5 mRNA copies/ μg total RNA]. Although we found relatively high levels of β-tubulin class III mRNA in normal tissues when analyzed as a percentage of the total tubulin mRNA, the amounts were small compared to the β-tubulin class II mRNA copy number in NSCLCs [2.0 ($\pm$1.3) $\times$ 10^6 mRNA copies/μg of total RNA]. Immunostaining for protein is dependent upon the sensitivity of the antibody and the amount of protein present. In the study by Katsetos, et al. [2000], the β-tubulin class III protein in normal lung tissues was clearly below the level of detection, but this result does not necessarily contradict our qRT-PCR data. The fraction of β-tubulin class III may be highest in normal lung tissues but the protein signal may not be detectable by immunostaining. Because of the high amounts of β-tubulin class III mRNA in our normal lung tissue samples, we used Western blotting to determine whether β-tubulin class III protein was present in selected normal and tumor tissues and found detectable amounts in these samples (data not shown). We also found measurable amounts of β-tubulin classes II and V protein in NSCLC tissues by selective Western blotting (Fig. 5B); however it was not feasible to do these measurements for all 76 tissue samples.

β-Tubulin class VI has been reported to be present in significant amounts in blood cells and hematopoietic cells [Murphy and Wallis, 1983; Wang et al., 1986]. The elevated mRNA levels for β-tubulin class VI in our small sample of normal lung tissues could be due to relatively higher amounts of blood cells in these heterogeneous tissues. We also note that although tumors can be highly vascular, there are sections of tumors that are not penetrated by the developing blood vessels. We measured β-tubulin isotype mRNA levels in whole blood (β-tubulin isotypes I, II, III, V and VI) and found that β-tubulin isotypes I, II and VI predominated [mean copies mRNA/μg total RNA: 3.3 ($\pm$1.9) $\times$ 10^6; 2.5 ($\pm$0.4) $\times$ 10^6; 1.0 ($\pm$0.4) $\times$ 10^6, respectively]. Class V was in the lowest abundance [mean copies mRNA/μg total RNA: 2.4 ($\pm$0.4) $\times$ 10^4]. Class III was on average: 2.4 ($\pm$0.3) $\times$ 10^5 copies mRNA/μg total RNA. Thus it is not clear that the presence of whole blood is the reason for our findings in normal lung tissue. This observation warrants further exploration; however, there is no commercially available antibody to confirm the presence of β-tubulin class VI protein in these tissues.

In a recent study of twelve human cancer cell lines [Hiser et al., 2006], we found that β-tubulin class I mRNA predominated and, in several cell lines, significant amounts of β-tubulin class V mRNA were also found. High levels of β-tubulin class I have been found in many immortalized cell lines and for that reason this class has been presumed to predominate in all tissues. However, there are few quantitative reports comparing all β-tubulin isotype classes in human tissues [Dozier et al., 2003] and this is the first comparison in NSCLCs. In our previous study of human cancer cell lines [Hiser et al., 2006], high fractions of β-tubulin classes I and V mRNA were measured in two NSCLC lung cancer cell lines (A549 and HOP 18). In that study, we also measured protein levels for β-tubulin classes I, II, III, and IVa plus IVb by quantitative Western blotting. For β-tubulin isotype classes I and III there was good agreement between the isotype mRNA fractions and protein fractions. For β-tubulin isotype classes IVa + IVb, there was consistently more protein than mRNA. Thus when quantitative measurements of both mRNA and protein are done, we expect that β-tubulin mRNA and protein isotype fractions are likely to show reasonable agreement. As noted above, immunostaining of tissues does not yield quantitative data and therefore it is difficult to compare the results of the current qRT-PCR study with previous studies that utilized immunohistochemical staining. Thus, because of the quantitative limitations of immunostaining for proteins and the difficulty of isolating sufficient protein from tissue samples for quantitative Western blotting, the measurements of mRNA levels in the work presented here were done to establish whether β-tubulin mRNA levels might be more useful as biomarkers for NSCLC aggressiveness and/or level of differentiation.

The Ratio of β-Tubulin Class II to Class V as a Biomarker for NSCLCs

The trends in the β-tubulin class II to V mRNA copy number ratios suggest that β-tubulin isotype patterns should be further explored as biomarkers of NSCLC aggressiveness and/or level of differentiation. We found that this ratio is significantly higher in NSCLCs compared to normal lung tissues (unpaired Student's t test, $P < 0.001$). We also found the ratio was higher in poorly-differentiated NSCLCs compared to normal lung tissues. A trend was found showing that the ratio for moderately-differentiated tumors tends to fall in between that of normal and poorly-differentiated tissues (ANOVA, $P = 0.17$). Similarly, the β-tubulin class II to V ratio in samples grouped by pathology is highest in large cell carcinomas with neuroendocrine features and lowest in both squamous cell carcinomas and normal lung tissues (ANOVA, $P = 0.06$). These results suggest an exciting possibility for the use of the ratio of β-tubulin class II to V mRNA as a marker for tumor aggressiveness and/or level of differentiation. In fact, analysis of qRT-PCR data from a previous report from our laboratory measuring β-tubulin isotypes in normal and tumor breast tissues [Dozier et al., 2003], shows the same trend for a higher ratio of β-tubulin class II to V mRNA in tumor tissue compared to normal breast tissue (normal, $n = 6$, 0.14 ± 0.07; tumor, $n = 7$, 1.13 ± 0.74; Student's t test, $P = 0.10$). This biomarker would be a valuable resource for tissues that cannot be easily classified using common histopathological microscopic or staining criteria.

The mechanistic reasons for the differences in the higher fractions of β-tubulin classes II and V in tumor tissues compared to normal lung tissues remain to be explored. It is possible that an increase in the amount of one isotype in these tissues must be compensated by an increase in another. Since β-tubulin classes II and V have contrasting properties, where β-tubulin class V is more dynamic than β-tubulin class II [Cabral, 2008], it is compelling to speculate that the dysregulation of tumor cells that causes an increase in one isotype (e.g. β-tubulin class II or V), leads to an increase in another with complementary properties to meet the intracellular requirement for microtubule dynamics. Thus our measurements of high fractions of β-tubulin classes II and V may be evidence of intracellular changes needed to maintain cell viability. The higher ratios of β-tubulin classes II to V in the poorly-differentiated or large cell (with neuroendocrine features) NSCLCs suggests that these compensatory changes are associated with dysregulation of microtubule dynamics in the disease state. Alternatively, these patterns may also reflect alterations in genomic stability that cause overexpression of many proteins in an unregulated manner [Soucek et al., 2006]. Regardless of the mechanism, our study suggests that ratios of β-tubulin class II to V mRNA may be a biomarker for aggressive NSCLCs.

Altered Expression of MAP4 and Stathmin in Normal Lung Tissue and NSCLCs

In this study we also found a statistically significant difference in the ratio of MAP4 to stathmin when normal and diseased lung tissues were compared. In diseased tissues, the copy number of MAP4 mRNA was nearly equal to that of stathmin mRNA; however normal lung tissues showed significantly higher copy numbers of stathmin compared to MAP4 mRNA. MAP4 and stathmin play important roles in the regulation of microtubule dynamics, essential for cell division and tissue proliferation; MAP4 stabilizes microtubules and stathmin induces depolymerization [Andersen, 2000]. Some studies suggest that MAP4 and/or stathmin may be good targets for combination chemotherapy to improve patient outcomes when treated with antimitotic agents aimed at disrupting microtubule dynamics [Bhat and Setaluri, 2007]. The implications of the different ratios of MAP4 to stathmin for tumor development and/or aggressiveness are unclear. In breast carcinomas, high levels of stathmin were associated with a subset of cancers classified as grade III with a high proliferative index, suggesting these were aggressive tumors [Curmi et al., 2000]. In contrast, in another study of peripheral blood samples from 51 patients with NSCLC, lower MAP4/stathmin ratios were associated with response to the antimitotic vinorelbine that destabilizes microtubules [Galan et al., 2007]. In the NSCLCs examined in our study, there was no trend observed for the MAP4/stathmin ratio within either of the groupings (pathological description or level of differentiation) and therefore, no clear association with prognosis. However, as suggested by the study by Galan et al. [2007], a subset of NSCLCs with low MAP4/stathmin ratios may respond more readily to antimitotic therapy with vinorelbine. Decreased levels of MAP4 in another study were implicated in decreased sensitivity to paclitaxel [Zhang et al., 1999], an antimitotic that stabilizes microtubules and is commonly used to treat advanced-stage NSCLCs. Our data showing that normal lung tissues have relatively lower amounts of MAP4 mRNA compared to diseased tissues suggest that normal lung tissues may be less sensitive to paclitaxel. Differential sensitivity to paclitaxel of NSCLCs compared to normal lung tissues may, in part, be explained by a difference in the MAP4/stathmin ratio. It should be noted that stathmin and MAP4 activities are regulated by phosphorylation [Vandre et al., 1991; Curmi et al, 1999]. Thus, to better understand the role of the MAP4/stathmin ratio, the phosphorylation status of stathmin and/or MAP4 in

NSCLCs, as well as levels of kinase or phosphatase activity need to be evaluated. Nonetheless, the observed difference between diseased and normal lung tissues suggests that the MAP4/stathmin mRNA ratio may have potential as a biomarker for aggressive NSCLCs.

Properties of microtubules that are critical for cell division, cell movement and response to antimitotic chemotherapy agents are thought to be regulated by the tubulin isotype composition and microtubule interacting proteins (MIPs). The work presented here demonstrates the utility of methods to quantitatively measure tubulin and MIP mRNA amounts in human tissue samples. We designed highly specific primers and were able to quantify message from all seven β-tubulin genes, as well as mRNA for the gene products known to regulate microtubule dynamics and stability, MAP4 and stathmin. Inherent in analysis of data from whole tissue samples is the problem of heterogeneity of cell types, including contamination of samples with whole blood components. This can lead to bias in the data collected and result in unwarranted conclusions. While it is clear that no single biomarker can point conclusively to a prognosis, it is possible that patterns of biomarkers such as those presented here can together be used as reliable indicators of potential outcomes or help in the selection of appropriate treatments.

REFERENCES

Alli E, Bash-Babula J, Yang J-M, Hait W. 2002. Effect of stathmin on the sensitivity to antimicrotubule drugs in human breast cancer. Cancer Res 62:6864–6869.

Andersen SSL. 2000. Spindle assembly and the art of regulating microtubule dynamics by MAPs and Stathmin/Op18. Trends Cell Biol 10:261–267.

Bhat KMR, Setaluri V. 2007. Microtubule-associated proteins as targets in cancer chemotherapy. Clin Cancer Res 13:2849–2854.

Bhattacharya R, Cabral F. 2004. A ubiquitous β-tubulin disrupts microtubule assembly and inhibits cell proliferation. Mol Biol Cell 15:3123–3131.

Brundage MD, Davies D, Mackillop WJ. 2002. Prognostic factors in non-small cell lung cancer: a decade of progress. Chest 122: 1037–1057.

Cabral F. 2008. Mechanisms of resistance to drugs that interfere with microtubule assembly. In: Fojo T, editor. Microtubules in Health and Disease. Humana Press, in press.

Curmi PA, Gavet O, Charbaut E, Ozon S, Lachkar-Colmerauer S, Manceau V, Slavoshian S, Maucuer A, Sobel A. 1999. Stathmin and its phosphoprotein family: general properties, biochemical and functional interaction with tubulin. Cell Struct Funct 24:345–357.

Curmi PA, Nogues C, Lachkar S, Carelle N, Gonthier M-P, Sobel A, Lidereau R, Bieche I. 2000. Overexpression of stathmin in breast carcinomas points out highly proliferative tumours. Brit J Cancer 82:142–150.

Dozier J, Hiser L, Davis JA, Thomas ND, Tucci M, Benghuzzi HA, Frankfurter A, Correia JJ, Lobert S. 2003. β class II tubulin predominates in normal and tumor breast tissue. Breast Cancer Res 5:R157–R169.

Dumontet C, Isaac S, Souquet P-J, Bejui-Thivolet F, Pacheca Y, Peloux N, Frankfurter A, Luduena R, Perol M. 2005. Expression of class III β-tubulin in non-small cell lung cancer is correlated with resistance to taxane chemotherapy. Bull Cancer 92:E25–E30.

Galan G, del Barco S, Mendez M, Esquerdo G, Huarriz MG, Bandres E, Gil MC, Paules AB, Gayo J, Garcia-Foncillas J. 2007. MAP4/Op18 mRNA expression predicts progression in patients treated with vinorelbine plus carboplatin in advance lung cancer patient in a multicenter trial. J Clin Oncol 25 (18S):14088, Abstract.

Hari M, Zeng C, Yang H, Canizales M, Cabral F. 2003. Expression of class III β-tubulin in CHO cells reduces microtubule stability and confers resistance to paclitaxel. Cell Motil Cytoskeleton 56:45–56.

Hiser L, Aggarwal A, Young R, Spano A, Frankfurter A, Correia JJ, Lobert S. 2006. Comparison of beta-tubulin mRNA and protein levels in twelve human cancer cell lines. Cell Motil Cytoskeleton 63:41–52.

Katsetos CD, Kontogeorgos G, Geddes JF, Herman MM, Tsimara-Papastamatiou H, Yu Y, Sakkas LI, Tsokos M, Patchefsky AS, Ehya H, Cooper H, Provencio J, Spano AJ, Frankfurter A. 2000. Differential distribution of the neuron-associated class III β-tubulin in neuroendocrine lung tumors. Arch Pathol Lab Med 124:535–544.

Lee MK, Tuttle JB, Rebhun LI, Cleveland DW, Frandfurter A. 1990. The expression and posttranslational modification of a neuron-specific β tubulin isotype during chick embryogenesis. Cell Motil Cytokseleton 17:118–132.

Lewis SA, Gwo-Shu Lee M, Cowan N. 1985. Five mouse tubulin isotypes and their regulated expression during development. J Cell Biol 101:852–861.

Lobert S, Frankfurter A, Correia JJ. 1998. Energetics of vinca alkaloid interactions with tubulin isotypes: implications for drug efficacy and toxicity. Cell Motil Cytoskeleton 39: 107–121.

Luduena RF. 1993. Are tubulin isotypes functionally significant? Mol Biol Cell 4:45–457.

Mistry SJ, Atweh GF. 2002. Role of stathmin in the regulation of the mitotic spindle: potential applications in cancer therapy. Mt Sinai J Med 69:299–304.

Murphy DB, Wallis KT. 1983. Brain and erythrocyte microtubules from chicken contain different β-tubulin polypeptides. J Biol Chem 258:7870–7875.

Raff EC. 1994. The role of multiple tubulin isoforms in cellular microtubule function. In: Hyams JS, Lloyd C, editors. Microtubules. New York: Wiley-Liss. pp 85–109.

Seer Incidence and US Mortality Statistics. 1975–2004. Available at http://seer.cancer.gov/canques.

Seve P, Mackey J, Isaac S, Tredan O, Souquet P-J, Perol M, Lai R, Voloch A, Dumontet C. 2005. Class III β- tubulin expression in tumor cells predicts response and outcome in patients with non-small cell lung cancer receiving paclitaxel. Mol Cancer Ther 4:2001–2007.

Soucek K, Kamain A, Phung AD, Kubala L, Bulinski JC, Harper RW, Eiserich JP. 2006. Normal and prostate cancer cells display distinct molecular profiles of α-tubulin posttranslational modifications. Prostate 66:954–965.

Sullivan KF. 1988. Structure and utilization of tubulin isotypes. Ann Rev Cell Biol 4:687–716.

Sullivan KF, Cleveland DW. 1986. Identification of conserved isotype-defining variable region sequences for four vertebrate β-tubulin polypeptide classes. Proc Natl Acad Sci USA 83:4327–4331.

Vandre DD, Centonze VE, Peloquin J, Tombes RM, Borisy GG. 1991. Proteins of the mammalian mitotic spindle: phosphorylation/dephosphorylation of MAP4 during mitosis. J Cell Sci 98:577–588.

Wahl AF, Donaldson KL, Fairchild C, Lee FYF, Foster SA, Demers GW, Galloway DA. 1996. Loss of normal p53 function confers sensitization to Taxol by increasing G2/M arrest and apoptosis. Nat Med 2:72–79.

Wang D, Villasante A, Lewis SA, Cowan NJ. 1986. The mammalian β-tubulin repertoire hematopoietic expression of a novel, heterologous β-tubulin isotype. J Cell Biol 103:1903–1910.

Yang H, Cabral C. 2007. Heightened sensitivity to paclitaxel in class IVa β-tubulin transfected cells is lost as expression increases. J Biol Chem 282:27058–27066.

Zhang CC, Yang J-M, Bash-Babula J, White E, Murphy M, Levine AJ, Hait WN. 1999. DNA damage increases sensitivity to vinca alkaloids and decreases sensitivity to taxanes through p53-dependent repression of microtubule-associated protein 4. Cancer Res 59:3663–3670.

Zochbauer-Muller S, Gazdar AF, Minna JD. 2002. Molecular pathogenesis of lung cancer. Annu Rev Physiol 64:681–708.

Published OnlineFirst June 29, 2007; DOI:10.1158/1535-7163.MCT-07-0004

Molecular Cancer Therapeutics

The alkylphospholipid perifosine induces apoptosis of human lung cancer cells requiring inhibition of Akt and activation of the extrinsic apoptotic pathway

Heath A. Elrod, Yi-Dan Lin, Ping Yue, et al.

Mol Cancer Ther 2007;6:2029-2038. Published OnlineFirst June 29, 2007.

Published OnlineFirst June 29, 2007; DOI:10.1158/1535-7163.MCT-07-0004

The alkylphospholipid perifosine induces apoptosis of human lung cancer cells requiring inhibition of Akt and activation of the extrinsic apoptotic pathway

Heath A. Elrod, Yi-Dan Lin, Ping Yue, Xuerong Wang, Sagar Lonial, Fadlo R. Khuri, and Shi-Yong Sun

Department of Hematology and Oncology, Winship Cancer Institute, Emory University School of Medicine, Atlanta, Georgia

Abstract

The Akt inhibitor, perifosine, is an alkylphospholipid exhibiting antitumor properties and is currently in phase II clinical trials for various types of cancer. The mechanisms by which perifosine exerts its antitumor effects, including the induction of apoptosis, are not well understood. The current study focused on the effects of perifosine on the induction of apoptosis and its underlying mechanisms in human non–small cell lung cancer (NSCLC) cells. Perifosine, at clinically achievable concentration ranges of 10 to 15 μmol/L, effectively inhibited the growth and induced apoptosis of NSCLC cells. Perifosine inhibited Akt phosphorylation and reduced the levels of total Akt. Importantly, enforced activation of Akt attenuated perifosine-induced apoptosis. These results indicate that Akt inhibition is necessary for perifosine-induced apoptosis. Despite the activation of both caspase-8 and caspase-9, perifosine strikingly induced the expression of the tumor necrosis factor–related apoptosis-inducing ligand (TRAIL) receptor, death receptor 5, and down-regulated cellular FLICE-inhibitory protein (c-FLIP), an endogenous inhibitor of the extrinsic apoptotic pathway, with limited modulatory effects on the expression of other genes including Bcl-2, Bcl-X_L, PUMA, and survivin. Silencing of either caspase-8 or death receptor 5 attenuated perifosine-induced apoptosis. Consistently, further down-regulation of c-FLIP expression with c-FLIP small interfering RNA sensitized cells to perifosine-induced apoptosis, whereas enforced overexpression of ectopic c-FLIP conferred resistance to perifosine. Collectively, these data indicate that activation of the extrinsic apoptotic pathway plays a critical role in perifosine-induced apoptosis. Moreover, perifosine cooperates with TRAIL to enhance the induction of apoptosis in human NSCLC cells, thus warranting future *in vivo* and clinical evaluation of perifosine in combination with TRAIL in the treatment of NSCLC. [Mol Cancer Ther 2007;6(7):2029–38]

Introduction

Alkylphospholipids are a class of antitumor agents which target the cell membrane and induce apoptosis (1, 2). Perifosine, the first orally bioavailable alkylphospholipid, has shown antitumor activity in preclinical models and is currently in phase II clinical trials (1, 3). The mechanisms by which perifosine exerts its antitumor effect remain unclear, although it seems to inhibit Akt (2, 4) and mitogen-activated protein kinase activation (5), whereas inducing c-Jun-NH_2-kinase (JNK) activation (5). Perifosine has also been shown to induce p21 expression leading to cell cycle arrest (6). In addition, perifosine, in combination with other antitumor agents such as the PDK1 inhibitor, UCN-01 (7), histone deacetylase inhibitors (8), and the chemotherapeutic agent etoposide (9), show synergistic antitumor effects.

It is well known that there are two major apoptotic pathways used by mammalian cells to undergo apoptosis. One pathway involves signals transduced through death receptors known as the extrinsic apoptotic pathway; the second pathway relies on signals from the mitochondria called the intrinsic apoptotic pathway. Both pathways involve the activation of a set of caspases, which in turn, cleave cellular substrates and result in the characteristic morphologic and biochemical changes constituting the process of apoptosis (10, 11). The extrinsic pathway is characterized by the oligomerization of cell surface death receptors and activation of caspase-8, whereas the intrinsic pathway involves in the disruption of mitochondrial membranes, the release of cytochrome *c*, and the activation of caspase-9. Through caspase-8–mediated cleavage or truncation of Bid, the extrinsic death receptor apoptotic pathway is linked to the intrinsic mitochondrial apoptotic pathway (10, 11).

Molecules that can block the extrinsic apoptotic pathway include cellular FLICE-inhibitory protein (c-FLIP). c-FLIP prevents caspase-8 activation by death receptors. There are two major isoforms of c-FLIP: $FLIP_L$ consists of two

Received 1/4/07; revised 5/2/07; accepted 5/25/07.

Grant support: The Georgia Cancer Coalition Distinguished Cancer Scholar award (S-Y. Sun), Department of Defense grants W81XWH-04-1-0142-VITAL (S-Y. Sun for Project 4), DAMD17-01-1-0689-BESCT (F.R. Khuri), and an American Cancer Society Fellowship award (H.A. Elrod).

The costs of publication of this article were defrayed in part by the payment of page charges. This article must therefore be hereby marked *advertisement* in accordance with 18 U.S.C. Section 1734 solely to indicate this fact.

Note: H.A. Elrod and Y-D. Lin contributed equally to this work and share equal first authorship. F.R. Khuri and S-Y. Sun are Georgia Cancer Coalition Distinguished Cancer Scholars. H.A. Elrod is a recipient of an American Cancer Society Fellowship.

Requests for reprints: Shi-Yong Sun, Winship Cancer Institute, Emory University School of Medicine, 1365-C Clifton Road Northeast, C3088, Atlanta, GA 30322. Phone: 404-778-2170; Fax: 404-778-5520. E-mail: shi-yong.sun@emoryhealthcare.org

doi:10.1158/1535-7163.MCT-07-0004

Published OnlineFirst June 29, 2007; DOI:10.1158/1535-7163.MCT-07-0004

NH_2-terminal death effector domains and a COOH-terminal caspase homology domain devoid of enzymatic activity, whereas $FLIP_S$ is only composed of the NH_2-terminal death effector domains and a short COOH-terminal stretch of amino acids not found in $FLIP_L$. It has been shown that c-FLIP expression correlates with resistance against death receptor–induced apoptosis in a variety of cancer cells, and c-FLIP–transfected tumor cell lines develop more aggressive tumors *in vivo* (12, 13). In addition, many studies have shown that down-regulation of c-FLIP is sufficient to confer sensitivity against death receptor–induced apoptosis, whereas c-FLIP expression is associated with chemoresistance and down-regulation of c-FLIP using antisense oligonucleotides or small interfering RNAs (siRNA) sensitizes cells to chemotherapeutic agent–induced apoptosis (12–14).

Akt is known to be critical for tumor cell survival. One of the ways that Akt promotes cell survival is to inhibit apoptosis through its ability to phosphorylate several proapoptotic proteins such as Bad, which are involved in the regulation of the intrinsic apoptotic pathway (15). Moreover, Akt also inhibits the extrinsic death receptor–mediated apoptotic pathway through up-regulation of c-FLIP expression (16, 17). Thus, Akt negatively regulates apoptosis by suppressing both the mitochondria- and death receptor–mediated pathways.

The induction of apoptosis by perifosine has been observed in several cancer cell lines (3, 8, 9, 18). However, this effect has not been determined in non–small cell lung cancer (NSCLC) cells. Moreover, the mechanisms by which perifosine induces apoptosis is generally unknown. In this study, we examined the effects of perifosine on apoptosis in human NSCLC cells and its modulation on different apoptotic molecules in an attempt to understand its mechanisms of action. Our data show that perifosine induces apoptosis, inhibits Akt activation, up-regulates death receptor 5 (DR5) expression, and reduces c-FLIP levels in NSCLC cells. In addition, perifosine in combination with tumor necrosis factor–related apoptosis-inducing ligand (TRAIL) augments the induction of apoptosis.

Materials and Methods

Reagents

Perifosine was supplied by Keryx Biopharmaceuticals, Inc. This agent was dissolved in PBS and stored at −20°C. Stock solution was diluted to the appropriate concentrations with growth medium immediately before use. Human recombinant TRAIL was purchased from PeproTech, Inc.

Cell Lines and Cell Culture

The human NSCLC cell lines used in this study were described previously (19). H157 cell lines that stably express ectopic Lac Z (Lac Z-5) and $FLIP_L$ ($FLIP_L$-6), respectively, and A549 cell lines that stably express ectopic Lac Z (Lac Z-9) and $FLIP_L$ ($FLIP_L$-2), respectively, were described previously (20, 21). These cell lines were grown in a monolayer culture in RPMI 1640 supplemented with glutamine and 5% fetal bovine serum at 37°C in a humidified atmosphere consisting of 5% CO_2 and 95% air.

Cell Growth Assay

Cells were cultured in 96-well cell culture plates and treated the next day with the agents indicated. Viable cell number was estimated using the sulforhodamine B assay, as previously described (19).

Western Blot Analysis

Preparation of whole cell protein lysates and Western blot analysis were described previously (22, 23). Mouse anti–caspase-3 monoclonal antibody was purchased from Imgenex. Rabbit polyclonal antibodies against PTEN, Akt, phospho (p)-Akt (Ser^{473}), phospho (p)-FKHR (Ser^{256}), phospho (p)-GSK3β (Ser^{9}), c-Jun, phospho (p)-c-Jun (Ser^{63}), p44/42, phospho (p)-p44/42 (Thr^{202}/Tyr^{204}), survivin, caspase-8, caspase-9, poly(ADP-ribose) polymerase (PARP) were purchased from Cell Signaling Technology. Rabbit polyclonal anti-DR5 antibody was purchased from ProSci, Inc. Mouse monoclonal anti-FLIP antibody (NF6) was purchased from Alexis Biochemicals. Rabbit anti-G3PDH polyclonal antibody and mouse anti-Bax monoclonal antibody were purchased from Trevigen. Rabbit anti-Puma polyclonal antibody was purchased from EMD Biosciences, Inc. Mouse anti–Bcl-2 and rabbit anti–Bcl-X_L antibodies were purchased from Santa Cruz Biotechnology, Inc. Rabbit anti–β-actin polyclonal antibody was purchased from Sigma Chemicals. Secondary antibodies, goat anti-mouse and goat anti-rabbit horseradish peroxidase conjugates, were purchased from Bio-Rad.

Adenoviral Infection

Adenovirus harboring an empty vector (Ad-CMV) or a constitutively activated form of Akt (myristoylated Akt; Ad-myr-Akt) were provided by Lily Yang (Department of Surgery, Emory University School of Medicine, Atlanta, GA). The procedure for adenoviral infection of cancer cells was described previously (24).

Gene Silencing Using siRNA

Silencing of caspase-8, DR5, c-FLIP, and PTEN were achieved by transfecting siRNA using RNAifect transfection reagent (Qiagen) following the instructions of the manufacturer. Control, caspase-8, and DR5 siRNAs were described previously (22). These siRNAs and c-FLIP siRNA targeting the sequence 5′-AATTCTCCGAACGTGTCACGT-3′ (14) were all synthesized from Qiagen. PTEN siRNA was purchased from Cell Signaling. Cells were plated in 6- or 24-well cell culture plates and transfected with the given siRNAs the next day. After 24 h, the cells were trypsinized and replated in new plates, and on the second day, treated with perifosine as indicated. Gene silencing effects were evaluated by Western blot as described above after the indicated times of treatment.

Apoptosis Assays

Apoptosis was detected either by analysis of caspase activation using Western blot analysis as described above or by Annexin V staining using Annexin V-PE apoptosis detection kit (BD Bioscience) following the instructions of the manufacturer, and analyzed by flow cytometry using FACScan (Becton Dickinson). In addition, we measured

Published OnlineFirst June 29, 2007; DOI:10.1158/1535-7163.MCT-07-0004

the amounts of cytoplasmic histone-associated DNA fragments (mononucleosome and oligonucleosomes) formed during apoptosis using a Cell Death Detection ELISA^{Plus} kit (Roche Molecular Biochemicals) according to the instructions of the manufacturer.

Results

Effects of Perifosine on Cell Survival and Apoptosis in NSCLC Cells

The effects of perifosine on cell survival were examined in a panel of NSCLC cell lines (Fig. 1A). For the majority of the cell lines tested, there was a dose-dependent decrease in cell survival. The H460 cell line was the most sensitive to perifosine, showing an IC_{50} value of ~1 μmol/L. The H226 cell line was the most resistant to perifosine, in which perifosine at 20 μmol/L decreased cell survival by <20%. Most of the tested cell lines exhibited moderate response to perifosine with IC_{50}s ranging from 8 to 15 μmol/L (Fig. 1A), which are within the clinically achievable and safe peak plasma concentrations of 12 to 15 μmol/L (25, 26). The *p53* and *PTEN* mutation status in the NSCLC cell lines tested did not correlate with sensitivity to perifosine, suggesting that perifosine inhibits cell growth independently of *p53* and *PTEN* mutation status (Fig. 1A). In addition, we examined the protein expression levels of PTEN, total Akt, and p-Akt in the cell lines tested. It seemed that those cell lines (e.g., H460 and H358) with low levels of p-Akt and high levels of PTEN were the most sensitive to perifosine (Fig. 1B).

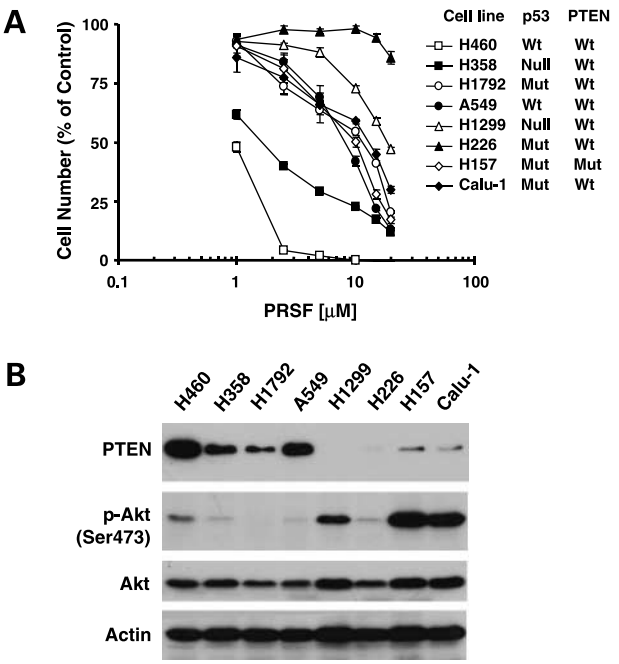

Figure 1. Effects of perifosine on the survival of NSCLC cells (**A**) and their association with basal levels of p-Akt (**B**). **A,** cell lines treated with different concentrations of perifosine (*PRFS*) ranging from 1 to 20 μmol/L. After 3 d, the cells were subjected to sulforhodamine B assay for estimating the viable cells. In addition, the *p53* status and *PTEN* status of the cell lines were also indicated. *Points,* means of four replicate determinations; *bars,* SD. **B,** cell lines with similar cell densities were harvested for the preparation of whole cell protein lysates. The indicated proteins were analyzed by Western blot analysis.

We further examined the effects of perifosine on apoptosis in NSCLC cell lines. As shown in Fig. 2A, perifosine induced apoptosis in H460 and A459 cells as indicated by Annexin V–positive staining. At concentrations of 10 μmol/L, perifosine induced cell death in ~50% of H460 cells, whereas apoptosis was induced in 23% and 33% of the A549 cells after treatment with 10 and 15 μmol/L of perifosine, respectively, suggesting that the H460 cells were more sensitive to perifosine-induced apoptosis. The H157 cells were the least sensitive to perifosine-induced apoptosis with only 10% of H157 cells undergoing apoptosis after treatment with 15 μmol/L of perifosine. We found that perifosine at concentrations ranging from 2.5 to 10 μmol/L induced cleavage of caspase-8, caspase-9, caspase-3, and PARP in H460 cells, whereas it induced partial cleavage of the caspases and PARP only at 10 μmol/L in A549 cells (Fig. 2B). In H157 cells treated with perifosine (up to 10 μmol/L), we failed to detect cleaved bands of the caspases and PARP (Fig. 2B). Because perifosine is effective in decreasing cell number in H157 cells (Fig. 1), we further examined cell cycle alteration in H157 cells after exposure to perifosine and detected 17.9%, 35.8%, and 42.4% G_2-M cells in cells treated with PBS, 10 μmol/L of perifosine, and 15 μmol/L of perifosine, respectively, after a 48 h treatment, indicating that perifosine primarily decreases cell numbers in H157 cells via induction of cell cycle arrest. In the following studies, we focused on revealing the mechanisms underlying perifosine-induced apoptosis.

Effects of Perifosine on the Phosphorylation of Akt, JNK, and ERK

Perifosine has been shown to modulate Akt as well as other signaling pathways (6, 18, 27). We therefore examined whether perifosine modulated similar signal transduction pathways in human NSCLC cells. In examining Akt phosphorylation, we observed that both H460 and A549 cells have very low basal levels of p-Akt, whereas H157 cells have much higher basal levels of p-Akt. When comparing the apoptosis results presented in Fig. 2A, it seems that low basal levels of p-Akt correlated with high sensitivity to perifosine-induced apoptosis. These cell lines exhibited a concentration-dependent decrease in p-Akt levels when exposed to perifosine (p-Akt levels were only detectable in H460 cells after a very long exposure). Interestingly, perifosine also decreased the levels of total Akt in the tested cell lines (Fig. 3A) and the degree of Akt down-regulation also seemed to correlate with cell sensitivity to perifosine-induced apoptosis. In H460 cells, decreases in both Akt and p-Akt levels occurred at 3 h after treatment with perifosine (Fig. 3B), indicating that Akt down-regulation is an early event. In H157 cells, Akt levels were only slightly decreased, whereas p-Akt levels were substantially (by 2.5 μmol/L of perifosine) and rapidly (3 h posttreatment) reduced upon perifosine treatment

Published OnlineFirst June 29, 2007; DOI:10.1158/1535-7163.MCT-07-0004

(Fig. 3A and B). These results suggest that the perifosine-mediated decrease in p-Akt levels could be due to either Akt protein down-regulation or upstream signaling suppression, depending on the cell lines used. To our knowledge, this is the first demonstration that perifosine down-regulates the levels of total Akt in human cancer cells. We also detected a decrease in the levels of p-FKHR and p-GSK3β, two well-known substrates of Akt (Fig. 3B), furthering the notion that perifosine inhibits Akt signaling in NSCLC cells.

In examining other signal transduction pathways, we observed the basal levels of p-c-Jun were very low in the tested NSCLC cells and were only slightly increased by perifosine in H157 cells, indicating that perifosine-induced JNK activation was a cell line–dependent event. Perifosine did not alter the levels of p42/44, but did decrease the levels of p-p42/44 in all three cell lines tested (Fig. 3A). These data indicate that perifosine down-regulates the ERK (or p42/44) signaling pathway in NSCLC cells.

Enforced Akt Activation Attenuates Perifosine-Induced Apoptosis

To decipher the role of Akt inhibition in perifosine-induced apoptosis, we artificially activated Akt in H460 cells by infecting the cells with adenoviruses carrying a *myr-Akt* gene that codes a constitutively activated form of Akt, and then examined the response of these cells to perifosine treatment. Using Western blot analysis, we detected high levels of myr-Akt, p-Akt, and p-GSK3β in cells infected with Ad-myr-Akt (Fig. 3C). In addition, infection of cells with Ad-myr-Akt also elevated the levels of c-FLIP, which has been shown to be regulated by Akt. (refs. 16, 17; Fig. 3C). In Ad-CMV–infected control cells, treatment with perifosine caused 37% apoptotic cell death (9% in PBS-treated cells) plus 15.2% necrotic cell death. However, we detected only 16% apoptosis (~12% in PBS-treated cells) and <2% necrosis in cells infected with Ad-myr-Akt after treatment with perifosine (Fig. 3D). These results clearly show that enforced Akt activation restores cell resistance to perifosine-induced apoptosis, thus indicating that Akt inhibition is necessary in mediating perifosine-induced apoptosis.

Given that there is an inverse relationship between PTEN expression and p-Akt levels (Fig. 1B), we further determined whether down-regulation of PTEN affects p-Akt levels and cell sensitivity to perifosine. Knockdown of PTEN using PTEN siRNA in H460 cells, which is the most sensitive cell line to perifosine and have the highest levels of PTEN (Fig. 1), increased basal levels of p-Akt. However,

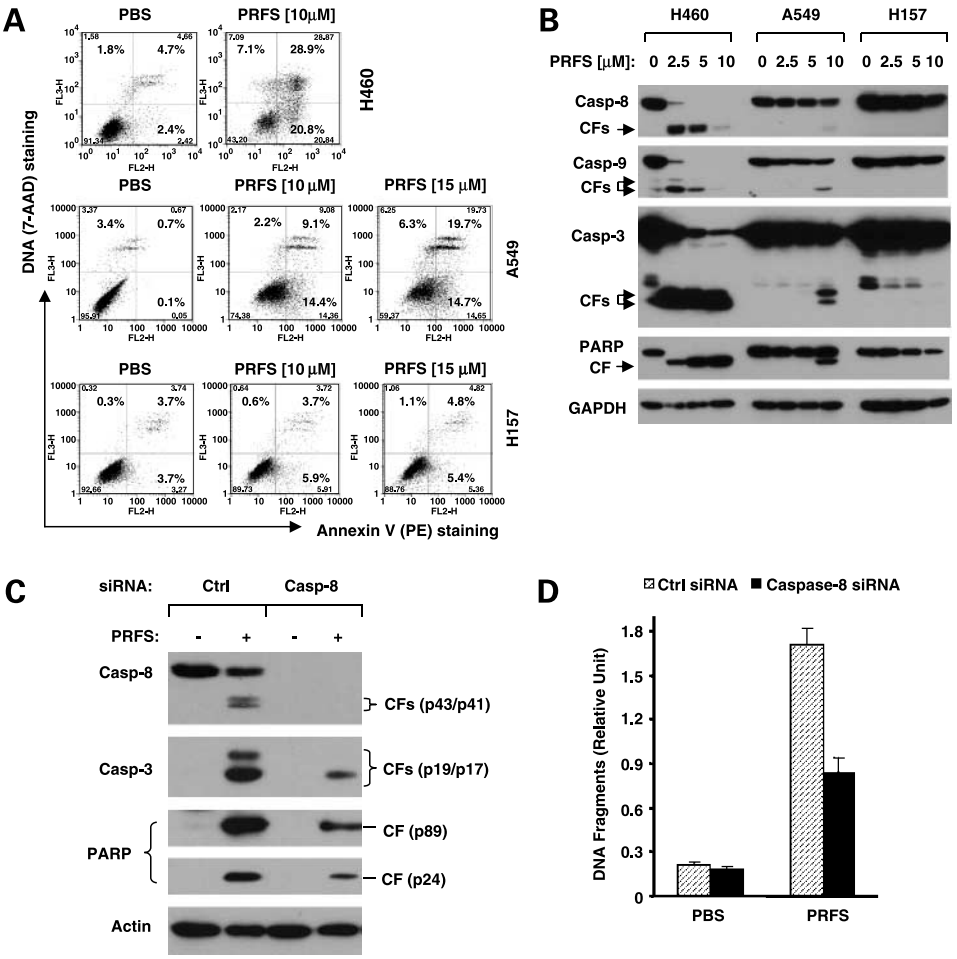

Figure 2. Effects of perifosine on apoptosis induction (**A**) and caspase activation (**B**), and involvement of caspase-8 activation in perifosine-induced apoptosis (**C** and **D**) in NSCLC cells. **A,** cell lines treated with the given concentrations of perifosine (*PRFS*) for 24 h and harvested for the estimation of apoptosis by Annexin V staining. Early apoptotic (*bottom right*), late apoptotic (*top right*), and necrotic (*top left*) cells. **B,** the indicated cell lines were treated with the given concentrations of perifosine for 16 h and harvested for the detection of caspase cleavage by Western analysis. **C** and **D,** H460 cells were seeded in 24-well plates and transfected with control (*Ctrl*) or caspase-8 siRNA the next day. After ~24 h, the cells were trypsinized and replated in new 6-well (**C**) or 96-well (**D**) plates. On the second day, the cells were treated with PBS or 5 μmol/L of perifosine. After 16 h, the cells were subjected to Western blot analysis for the indicated proteins (**C**) or ELISA for measurement of DNA fragments (**D**). *CF,* cleaved form. *Columns,* means of triplicate determinations; *bars,* SD.

Published OnlineFirst June 29, 2007; DOI:10.1158/1535-7163.MCT-07-0004

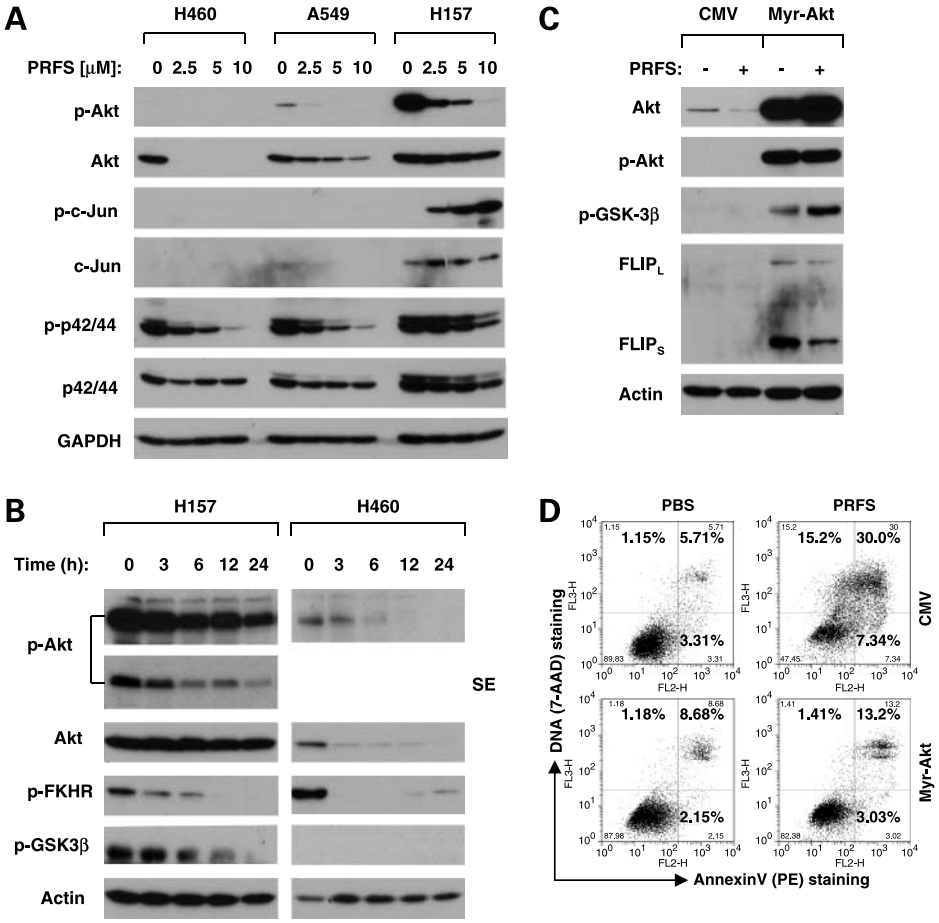

Figure 3. Modulation of Akt, JNK, and ERK signaling pathways by perifosine (**A** and **B**), and involvement of Akt inhibition in perifosine-induced apoptosis (**C** and **D**) in human NSCLC cells. **A** and **B,** NSCLC cell lines treated with the given concentrations of perifosine (*PRFS*) for 16 h (**A**) or with 10 μmol/L (H157) or 5 μmol/L (H460) of perifosine for the indicated times (**B**). The cells were then subjected to a preparation of whole cell protein lysates and subsequent detection of the indicated proteins using Western blot analysis. **C** and **D,** H460 cells were infected with a multiplicity of infection of 200 Ad-CMV or Ad-myr-Akt. Twenty-four hours later, the cells were exposed to 10 μmol/L of perifosine. After 24 h, the cells were harvested for analysis of the given proteins by Western blotting (**C**) and for the detection of apoptosis by Annexin V staining (**D**). *SE,* short exposure.

the p-Akt increase caused by PTEN knockdown could be abrogated by perifosine treatment. Surprisingly, perifosine decreased PTEN levels, which itself did not result in an increase of p-Akt levels, probably because perifosine also inhibits Akt phosphorylation (see Supplemental Fig. S1A).[1] As a result, down-regulation of PTEN by siRNA did not alter cell sensitivity to perifosine as shown by measuring cell number change (Supplemental Fig. S1B),[1] caspase activation (Supplemental Fig. S1A),[1] and apoptotic cells (Supplemental Fig. S1C).[1]

Effects of Perifosine on the Expression of Key Molecules Involved in the Regulation of Apoptosis

To further explore how perifosine induces apoptosis, we next examined the effects of perifosine on the expression of several key genes involved in either the extrinsic apoptotic pathway (e.g., DR5 and c-FLIP) or the intrinsic apoptotic pathway (e.g., Bax, Bcl-2, Bcl-X_L, PUMA, and survivin). Perifosine increased the levels of DR5, particularly in H460 cells (Fig. 4). It seems that DR5 induction is associated with increased sensitivity of cell lines to perifosine. c-FLIP is another key protein that inhibits the extrinsic apoptotic pathway by blocking caspase-8 activation (12). The H460 cells, which are the most sensitive to perifosine, had very low basal levels of c-FLIP, particularly FLIP$_L$, which were further down-regulated by perifosine, whereas the less sensitive A549 and H157 cells have high basal levels of c-FLIP, particularly FLIP$_L$, which were only weakly decreased by perifosine. Perifosine also decreased FLIP$_S$ levels in these cell lines (Fig. 4). It seems that low levels of c-FLIP and their further down-regulation by perifosine were associated with high sensitivity to perifosine-induced apoptosis. Collectively, these results suggest that activation of the DR5-mediated extrinsic apoptotic pathway is important in perifosine-induced apoptosis.

In examining the signaling molecules involved in the intrinsic apoptotic pathway, we found that perifosine did not significantly alter the levels of Bcl-2 in NSCLC cells (Fig. 4). Surprisingly, perifosine decreased Bax levels in all the tested NSCLC cell lines. Perifosine decreased Bcl-X_L levels in H460 cells that were very sensitive to perifosine, but not in A549 and H157 cells that were less sensitive to perifosine (Fig. 4). These data suggest that Bcl-X_L down-regulation may affect cell sensitivity to undergo perifosine-induced apoptosis. H460 cells had low basal levels of survivin, which were further decreased by perifosine,

[1] Supplementary material for this article is available at Molecular Cancer Therapeutics Online (http://mct.aacrjournals.org/).

Published OnlineFirst June 29, 2007; DOI:10.1158/1535-7163.MCT-07-0004

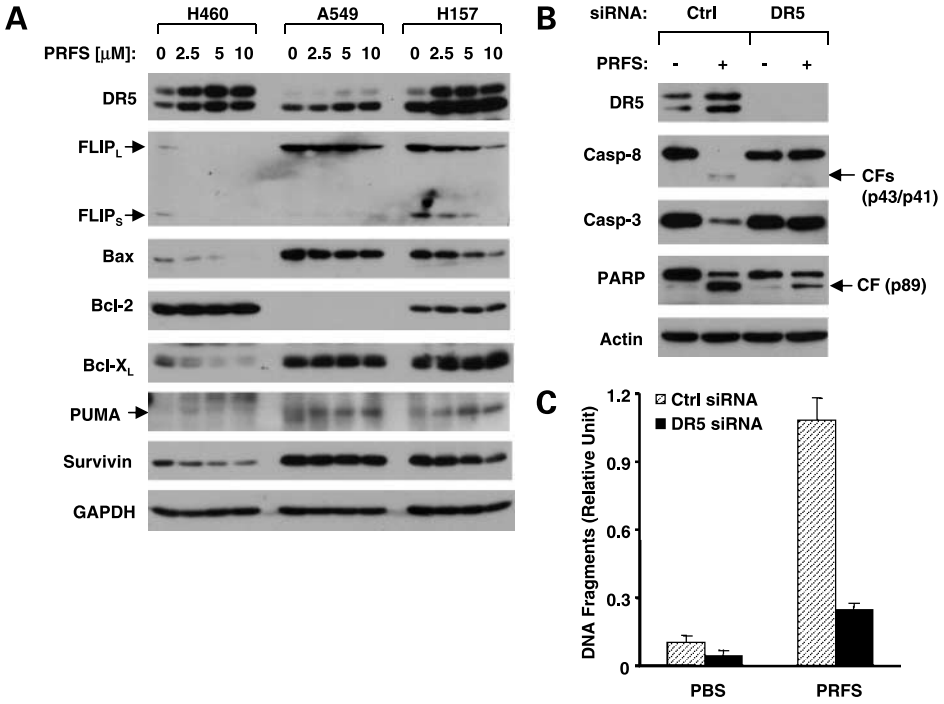

Figure 4. Modulation of apoptosis-related gene expression by perifosine (**A**) and demonstration of the role of DR5 induction in perifosine-induced apoptosis (**B** and **C**) in human NSCLC cells. **A,** NSCLC cell lines treated with the given concentrations of perifosine (*PRFS*) for 16 h. The cells were then subjected to a preparation of whole cell protein lysates and subsequent detection of the indicated proteins using Western blot analysis. **B** and **C,** H460 cells were seeded in six-well plates and transfected with control (*Ctrl*) or DR5 siRNA the next day. After ~20 h, the cells were trypsinized and replated in new 6-well (**B**) or 96-well (**C**) plates. On the second day, the cells were treated with PBS or 7.5 μmol/L of perifosine. After 16 h, the cells were subjected to Western blot analysis for the detection of the indicated proteins (**B**) or ELISA for the measurement of DNA fragments (**C**). *Columns,* means of triplicate determinations; *bars,* SD; *CF,* cleaved form.

whereas H157 and A549 cells had high levels of survivin, which were apparently not altered by perifosine (Fig. 4). Thus, it seems that low basal levels of survivin and its further down-regulation with perifosine are also associated with increased cell sensitivity to perifosine-induced apoptosis. PUMA was slightly increased in A549 and H157 cells, but not in H460 cells, suggesting that PUMA was not important in perifosine-induced apoptosis.

Perifosine Cooperates with TRAIL to Enhance the Induction of Apoptosis

Because perifosine induces DR5 expression and down-regulates c-FLIP levels, we hypothesized that perifosine would cooperate with TRAIL, a DR5 ligand, to enhance the induction of apoptosis. Thus, we examined the effects of perifosine in combination with TRAIL on apoptosis induction in NSCLC cells. As shown in Fig. 5A, perifosine in combination with TRAIL induced higher levels of DNA fragments than did each single agent alone. Moreover, increased amounts of cleaved caspase-8, caspase-9, caspase-3, and PARP were detected in cells treated with the perifosine and TRAIL combination, but were only minimally detected in cells treated with either perifosine or TRAIL alone (Fig. 5B). Thus, we conclude that perifosine cooperates with TRAIL to enhance the induction of apoptosis.

Perifosine Induces Apoptosis Requiring Caspase-8 Activation and DR5 Up-regulation

The data presented above strongly suggest a role for the activation of the extrinsic apoptotic pathway in perifosine-induced apoptosis. Thus, we determined whether perifosine induces apoptosis requiring activation of caspase-8 and up-regulation of DR5. To this end, we silenced the expression of caspase-8 and DR5 using caspase-8 and DR5 siRNAs, respectively, and then examined cell sensitivity to perifosine. By Western blotting, we detected substantially reduced levels of caspase-8 levels including cleaved forms in H460 cells transfected with caspase-8 siRNA compared with those in control siRNA-transfected cells (Fig. 2C), indicating successful caspase-8 knockdown or inhibition of caspase-8 activation. Accordingly, cleavage of caspase-3 and PARP and an increase in DNA fragmentation were also attenuated in caspase-8 siRNA-transfected cells in comparison with control siRNA–transfected cells (Fig. 2C and D). These results indicate that perifosine induces a caspase-8–dependent apoptosis. Similarly, silencing of DR5 expression using DR5 siRNA abrogated DR5 induction (Fig. 4B) and impaired the ability of perifosine to induce cleavage of caspase-8, caspase-3, and PARP (Fig. 4B). In addition, an increase in DNA fragmentation in DR5 siRNA-transfected cells was also reduced compared with control siRNA-transfected cells (Fig. 4C). These data show that DR5 up-regulation is also involved in perifosine-induced apoptosis.

Manipulation of c-FLIP Levels Regulates Cell Sensitivity to Perifosine-Induced Apoptosis and Enhancement of TRAIL-Induced Apoptosis

To further show that the activation of the extrinsic apoptotic pathway participates in perifosine-induced apoptosis, we examined the sensitivity of cell lines that express ectopic FLIP$_L$ to perifosine-induced apoptosis. As presented in Fig. 6A, perifosine increased DNA fragmentation in a dose-dependent fashion in H157-Lac Z-5 cells, but only minimally in H157-FLIP$_L$-6 cells. As a positive control treatment, TRAIL-induced increase in DNA fragmentation

Published OnlineFirst June 29, 2007; DOI:10.1158/1535-7163.MCT-07-0004

was abolished in H157-FLIP$_L$-6 cells. Similarly, perifosine-induced increase in DNA fragmentation was also abrogated in A549-FLIP$_L$-2 cells in comparison with A549-Lac Z-9 cells (Fig. 6B). Together, these results clearly show that overexpression of ectopic c-FLIP protects cells from perifosine-induced apoptosis.

Because c-FLIP down-regulation was often associated with the enhancement of TRAIL-induced apoptosis (20, 21, 28), we further compared apoptosis induction by the combination of perifosine and TRAIL between A549-Lac Z-9 and A549-FLIP$_L$-2 cell lines. In agreement with the results presented in Fig. 5, the combination of perifosine and TRAIL was much more potent than either perifosine or TRAIL alone in increasing DNA fragmentation in A549-Lac Z-9 cells. However, not only perifosine and TRAIL alone but also their combination exhibited minimal effects on increasing DNA fragmentation in A549-FLIP$_L$-2 cells (Fig. 6B). These results clearly show that overexpression of ectopic c-FLIP confers cell resistance to the combination of perifosine and TRAIL, indicating that c-FLIP down-regulation contributes to perifosine-mediated enhancement of TRAIL-induced apoptosis.

Because the cell lines, A549 and H157, with high basal levels of c-FLIP were relatively less sensitive than H460 cells which have low basal levels of c-FLIP to perifosine-induced apoptosis, we wanted to determine whether down-regulation of c-FLIP sensitized cells to perifosine-induced apoptosis. To this end, we silenced the expression of c-FLIP (both FLIP$_L$ and FLIP$_S$) using siRNA in A549 cells, and then examined their response to perifosine-induced apoptosis. As presented in Fig. 6C, transfection of c-FLIP siRNA reduced the levels of both FLIP$_L$ and FLIP$_S$, which were further reduced after treatment with perifosine. Those cells whose expression of c-FLIP had been reduced with siRNA were more sensitive to caspase-8, caspase-3, and PARP cleavage after perifosine treatment compared with control cells, indicating that c-FLIP levels indeed affect cell sensitivity to perifosine-induced apoptosis.

Discussion

In this study, we have shown that perifosine exerts its growth-inhibitory effects in a panel of NSCLC cell lines, primarily through the induction of apoptosis and/or cell cycle arrest. Importantly, perifosine inhibited the growth of most of the tested NSCLC cell lines with IC$_{50}$s ranging between 8 and 15 μmol/L (Fig. 1A), which are within the

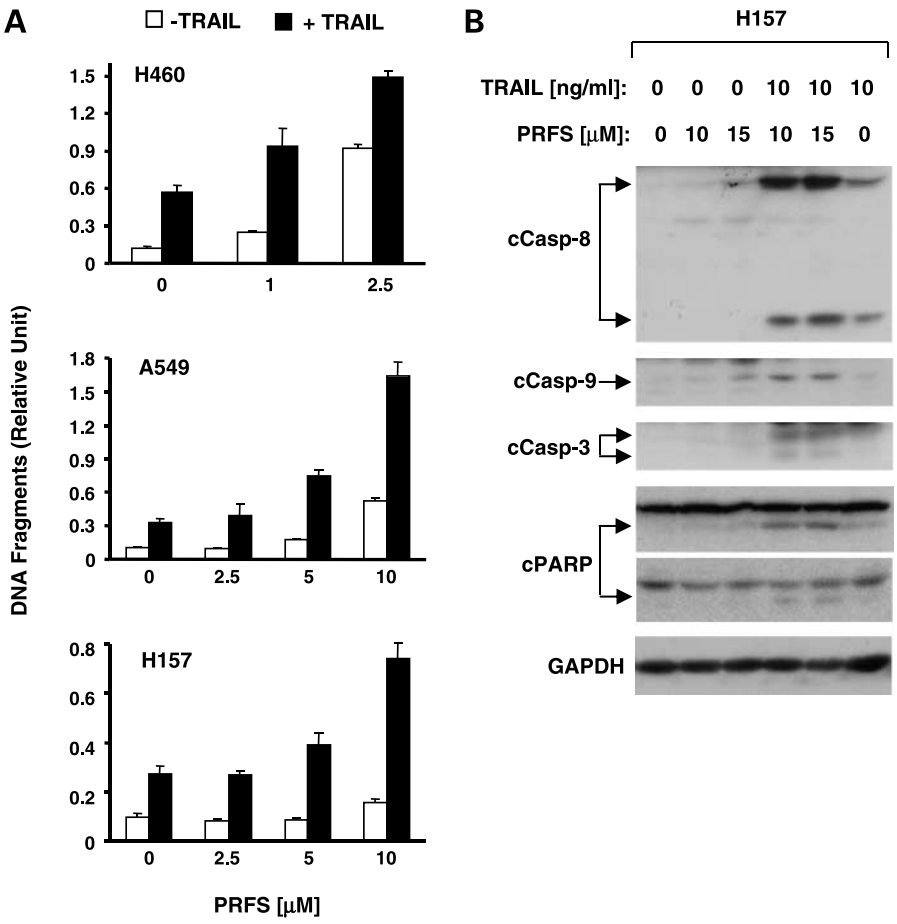

Figure 5. Perifosine cooperates with TRAIL to enhance DNA fragmentation (**A**) and caspase activation (**B**) in human NSCLC cells. **A,** cell lines plated in 96-well plates and treated with the given doses of perifosine (*PRFS*) alone, 20 ng/mL TRAIL alone, or TRAIL plus perifosine on the second day. After 24 h, the cells were subjected to DNA fragmentation using the Cell Death Detection ELISA kit. *Columns,* means of triplicate determinations; *bars,* SD. **B,** H157 cells were treated with perifosine alone, TRAIL alone, and their combinations. After 16 h, the cells were subjected to a preparation of whole cell protein lysates and subsequent detection of the indicated proteins by Western blot analysis. *c,* cleaved.

Published OnlineFirst June 29, 2007; DOI:10.1158/1535-7163.MCT-07-0004

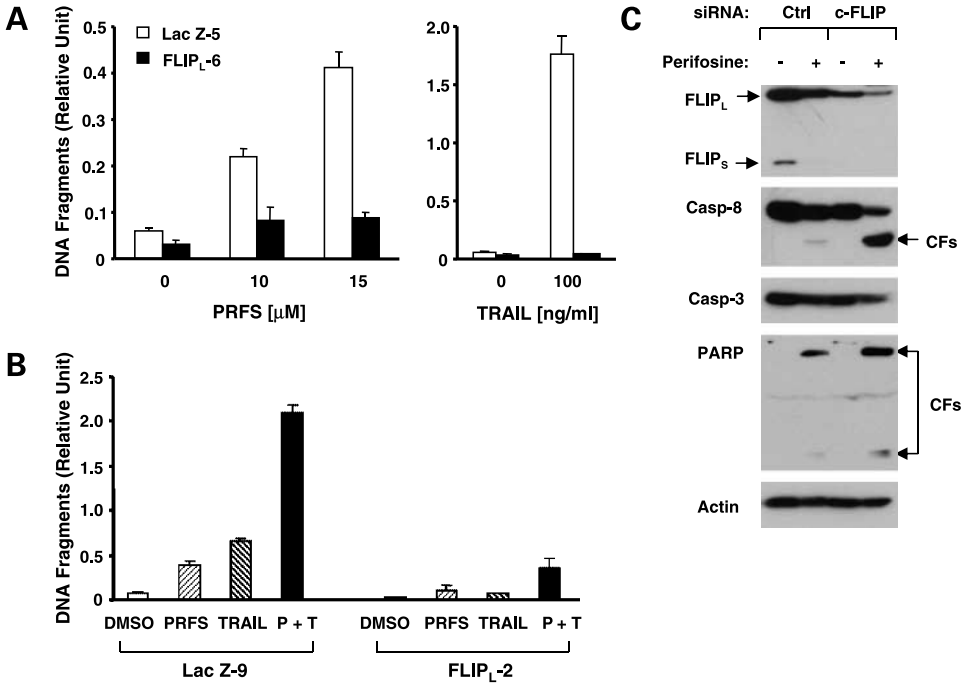

Figure 6. Overexpression of ectopic c-FLIP (**A** and **B**) and silencing of c-FLIP expression (**C**) modulate cell sensitivity to perifosine-induced apoptosis. **A,** H157 cell lines that stably express Lac Z and FLIP$_L$, respectively, were treated with the indicated concentrations of perifosine (*PRFS*) or TRAIL. **B,** A549 cell lines that stably express Lac Z and FLIP$_L$, respectively, were exposed to 10 μmol/L of perifosine, 20 ng/mL of TRAIL, and the combination of perifosine and TRAIL (*P + T*). Twenty-four hours later, after the aforementioned treatment, the cells were subjected to estimation of DNA fragmentation using the Cell Death Detection ELISA kit. *Columns,* mean of triplicate determinations; *bars,* SD. **C,** A549 cells plated in 24-well plates were transfected with control (*Ctrl*) or c-FLIP siRNA. Twenty-four hours later, the cells were exposed to 10 μmol/L of perifosine (*PRFS*). After 24 h, the cells were subjected to a preparation of whole cell protein lysates and subsequent detection of the indicated proteins using Western blot analysis. *CFs,* cleaved fragments.

clinically achievable and safe peak plasma concentration ranges (i.e., 10–15 μmol/L; refs. 25, 26), suggesting the potential of perifosine in the treatment of NSCLCs.

Modulation of Akt, JNK, and ERK signaling pathways and their involvement in perifosine-induced apoptosis has been studied in other types of cancer cells (4, 18, 27). Despite the proapoptotic role of JNK activation in perifosine-induced apoptosis in multiple myeloma (18), we found that perifosine increased p-c-Jun only in one (i.e., H157 cells) of three cell lines tested (Fig. 3A). Given that H157 cells were relatively insensitive to perifosine-induced apoptosis (Fig. 2), we suggest that JNK activation is unlikely to account for the perifosine-induced apoptosis in human NSCLC cells. Perifosine was reported to either decrease or increase ERK phosphorylation depending on cancer cell type (5, 18, 27). In our study, perifosine decreased ERK phosphorylation in all of the three tested cell lines tested, regardless of cell sensitivity to TRAIL-induced apoptosis. Thus, we suggest that ERK inhibition is also unlikely to be critical for perifosine-induced apoptosis in human NSCLC cells.

Although perifosine inhibits Akt activation in different types of cancer cells including the NSCLC cells shown in the current study, enforced activation of Akt through overexpression of the constitutively activated form of Akt, myr-Akt, protects cells from perifosine-induced cell death in one type of cancer cell line (e.g., PC-3 prostate cancer cells; ref. 4) but not in another type of cancer cell (e.g., MM.1S multiple myeloma cells; ref. 18). In our study, we found that the low basal levels of p-Akt (e.g., H460 < A549 < H157) and its further down-regulation were associated with high sensitivity to perifosine-induced apoptosis (H460 > A549 > H157; Figs. 1 and 2). Moreover, overexpression of myr-Akt in H460 cells led to increased levels of p-Akt and resistance to perifosine-induced apoptosis (Fig. 3). Collectively, we conclude that Akt inhibition plays an important role in mediating perifosine-induced apoptosis in human lung cancer cells. We noted that perifosine decreased the levels of total Akt in some NSCLC cells (e.g., H460 and A549), the potency of which is associated with cell sensitivity to perifosine-induced apoptosis, in addition to decreasing Akt phosphorylation. To the best of our knowledge, this is the first demonstration that perifosine decreases the total levels of Akt. Given that Akt reduction is an early event, which occurred at 3 h post–perifosine treatment (Fig. 3B), it is unlikely that Akt reduction occurs secondary to perifosine-induced apoptosis (e.g., cleavage by caspase activation). Nevertheless, ongoing studies are attempting to reveal how perifosine decreases the levels of total Akt.

Perifosine activated both caspase-8 and caspase-9 in human NSCLC cells (Fig. 2B), suggesting that perifosine can induce apoptosis through the extrinsic and/or intrinsic apoptotic pathways. In examining several key proteins involved in the regulation of the extrinsic or intrinsic apoptotic pathways, we found that perifosine strikingly induced DR5 expression and decreased the levels of c-FLIP in all the cells lines tested, whereas having limited or no modulatory effects on the levels of Bcl-2, Bcl-X$_L$, PUMA, and survivin (Fig. 4A). Importantly, the low basal levels of c-FLIP (e.g., FLIP$_L$) and its further down-regulation are associated with increased sensitivity to undergo perifosine-induced apoptosis (e.g., H460 cells). We noted that Bax

Published OnlineFirst June 29, 2007; DOI:10.1158/1535-7163.MCT-07-0004

levels were lower and Bcl-2 levels were higher in the sensitive H460 cells than in less sensitive A549 and H157 cells (Fig. 4A). Moreover, we found that Bax levels were actually decreased in cells treated with perifosine, although the underlying mechanisms and its effects on perifosine-induced apoptosis are unclear. In fact, our preliminary data show that Bax or PUMA deficiency does not alter cell sensitivity to perifosine-induced apoptosis.[2] Together, we suggest that the activation of the extrinsic apoptotic pathway is important in mediating perifosine-induced apoptosis. This observation is supported by our findings that silencing of caspase-8 or DR5, or overexpression of ectopic c-FLIP protects cells from perifosine-induced apoptosis (Figs. 2, 4, and 6), whereas down-regulation of endogenous c-FLIP using c-FLIP siRNA sensitizes cells to perifosine-induced apoptosis (Fig. 6). In agreement with our findings, a recent study has shown that perifosine induces apoptosis through activation of the Fas-mediated extrinsic apoptotic pathway in human leukemia cells (29). To the best of our knowledge, this is the first study showing that perifosine modulates the expression of DR5 and c-FLIP in human cancer cells.

Some studies have shown that Akt also inhibits the extrinsic apoptotic pathway through the up-regulation of c-FLIP expression (16, 17). In this study, we have shown that perifosine inhibits Akt and reduces c-FLIP levels, both of which are involved in perifosine-induced apoptosis. Indeed, we detected increased levels of c-FLIP in cells infected with Ad-myr-Akt (Fig. 3C), suggesting that Akt activation indeed increases c-FLIP levels in the tested cells. Thus, it is possible that Akt exerts its inhibitory effect on perifosine-induced apoptosis through the up-regulation of c-FLIP. On other hand, perifosine may down-regulate c-FLIP levels through inhibition of Akt; this needs to be investigated in detail in the future.

It is known that TRAIL functions as the DR5 ligand and rapidly induces apoptosis in a wide variety of transformed cells but is not cytotoxic in normal cells *in vitro* and *in vivo* (10, 16, 17). Therefore, TRAIL is considered to be a tumor-selective, apoptosis-inducing cytokine with promising potential for cancer treatment and is currently being tested in phase I clinical trials. In our study, we showed that the combination of perifosine and TRAIL exhibited augmented induction of apoptosis in human NSCLC cells (Fig. 5), which is likely due to the ability of perifosine to induce DR5 expression and down-regulate c-FLIP levels. This finding warrants future *in vivo* animal studies and clinical evaluation of the efficacy of perifosine in combination with TRAIL for the treatment of NSCLC.

Acknowledgments

We are grateful to Zhongmei Zhou for her excellent technical assistance, Dr. Xiangguo Liu for establishment of stable cell lines that overexpress c-FLIP, and Dr. Lily Yang for providing us with Ad-CMV and Ad-myr-Akt.

[2] Unpublished data.

References

1. Hilgard P, Klenner T, Stekar J, et al. D-21266, a new heterocyclic alkylphospholipid with antitumour activity. Eur J Cancer 1997;33:442 – 6.

2. Ruiter GA, Verheij M, Zerp SF, van Blitterswijk WJ. Alkyl-lysophospholipids as anticancer agents and enhancers of radiation-induced apoptosis. Int J Radiat Oncol Biol Phys 2001;49:415 – 9.

3. Vink SR, Schellens JH, van Blitterswijk WJ, Verheij M. Tumor and normal tissue pharmacokinetics of perifosine, an oral anti-cancer alkylphospholipid. Invest New Drugs 2005;23:279 – 86.

4. Kondapaka SB, Singh SS, Dasmahapatra GP, Sausville EA, Roy KK. Perifosine, a novel alkylphospholipid, inhibits protein kinase B activation. Mol Cancer Ther 2003;2:1093 – 103.

5. Li X, Luwor R, Lu Y, Liang K, Fan Z. Enhancement of antitumor activity of the anti-EGF receptor monoclonal antibody cetuximab/C225 by perifosine in PTEN-deficient cancer cells. Oncogene 2006;25:525 – 35.

6. Patel V, Lahusen T, Sy T, et al. Perifosine, a novel alkylphospholipid, induces p21(WAF1) expression in squamous carcinoma cells through a p53-independent pathway, leading to loss in cyclin-dependent kinase activity and cell cycle arrest. Cancer Res 2002;62:1401 – 9.

7. Dasmahapatra GP, Didolkar P, Alley MC, et al. *In vitro* combination treatment with perifosine and UCN-01 demonstrates synergism against prostate (PC-3) and lung (A549) epithelial adenocarcinoma cell lines. Clin Cancer Res 2004;10:5242 – 52.

8. Rahmani M, Reese E, Dai Y, et al. Coadministration of histone deacetylase inhibitors and perifosine synergistically induces apoptosis in human leukemia cells through Akt and ERK1/2 inactivation and the generation of ceramide and reactive oxygen species. Cancer Res 2005;65:2422 – 32.

9. Nyakern M, Cappellini A, Mantovani I, Martelli AM. Synergistic induction of apoptosis in human leukemia T cells by the Akt inhibitor perifosine and etoposide through activation of intrinsic and Fas-mediated extrinsic cell death pathways. Mol Cancer Ther 2006;5:1559 – 70.

10. Ashkenazi A, Dixit VM. Death receptors: signaling and modulation. Science 1998;281:1305 – 8.

11. Hengartner MO. The biochemistry of apoptosis. Nature 2000;407:770 – 6.

12. Kataoka T. The caspase-8 modulator c-FLIP. Crit Rev Immunol 2005;25:31 – 58.

13. Wajant H. Targeting the FLICE inhibitory protein (FLIP) in cancer therapy. Mol Interv 2003;3:124 – 7.

14. Longley DB, Wilson TR, McEwan M, et al. c-FLIP inhibits chemotherapy-induced colorectal cancer cell death. Oncogene 2006;25:838 – 48.

15. Cheng JQ, Lindsley CW, Cheng GZ, Yang H, Nicosia SV. The Akt/PKB pathway: molecular target for cancer drug discovery. Oncogene 2005;24:7482 – 92.

16. Panka DJ, Mano T, Suhara T, Walsh K, Mier JW. Phosphatidylinositol 3-kinase/Akt activity regulates c-FLIP expression in tumor cells. J Biol Chem 2001;276:6893 – 6.

17. Nam SY, Jung GA, Hur GC, et al. Upregulation of FLIP(S) by Akt, a possible inhibition mechanism of TRAIL-induced apoptosis in human gastric cancers. Cancer Sci 2003;94:1066 – 73.

18. Richardson PG, Mitsiades C, Hideshima T, Anderson KC. Bortezomib: proteasome inhibition as an effective anticancer therapy. Annu Rev Med 2006;57:33 – 47.

19. Sun SY, Yue P, Dawson MI, et al. Differential effects of synthetic nuclear retinoid receptor-selective retinoids on the growth of human non-small cell lung carcinoma cells. Cancer Res 1997;57:4931 – 9.

20. Liu X, Yue P, Schonthal AH, Khuri FR, Sun SY. Cellular FLICE-inhibitory protein down-regulation contributes to celecoxib-induced apoptosis in human lung cancer cells. Cancer Res 2006;66:11115 – 9.

21. Zou W, Liu X, Yue P, Khuri FR, Sun SY. PPARγ ligands enhance TRAIL-induced apoptosis through DR5 upregulation and c-FLIP down-regulation in human lung cancer cells. Cancer Biol Ther 2007;6:99 – 106.

22. Liu X, Yue P, Zhou Z, Khuri FR, Sun SY. Death receptor regulation and celecoxib-induced apoptosis in human lung cancer cells. J Natl Cancer Inst 2004;96:1769 – 80.

23. Sun SY, Yue P, Wu GS, et al. Mechanisms of apoptosis induced by the synthetic retinoid CD437 in human non-small cell lung carcinoma cells. Oncogene 1999;18:2357 – 65.

Published OnlineFirst June 29, 2007; DOI:10.1158/1535-7163.MCT-07-0004

24. Jin F, Liu X, Zhou Z, et al. Activation of nuclear factor-κB contributes to induction of death receptors and apoptosis by the synthetic retinoid CD437 in DU145 human prostate cancer cells. Cancer Res 2005;65:6354 – 63.

25. Crul M, Rosing H, de Klerk GJ, et al. Phase I and pharmacological study of daily oral administration of perifosine (D-21266) in patients with advanced solid tumours. Eur J Cancer 2002;38:1615 – 21.

26. Van Ummersen L, Binger K, Volkman J, et al. A phase I trial of perifosine (NSC 639966) on a loading dose/maintenance dose schedule in patients with advanced cancer. Clin Cancer Res 2004;10:7450 – 6.

27. Momota H, Nerio E, Holland EC. Perifosine inhibits multiple signaling pathways in glial progenitors and cooperates with temozolomide to arrest cell proliferation in gliomas *in vivo*. Cancer Res 2005;65:7429 – 35.

28. Zhang S, Shen HM, Ong CN. Down-regulation of c-FLIP contributes to the sensitization effect of 3,3′-diindolylmethane on TRAIL-induced apoptosis in cancer cells. Mol Cancer Ther 2005;4:1972 – 81.

29. Gajate C, Mollinedo F. Edelfosine and perifosine induce selective apoptosis in multiple myeloma by recruitment of death receptors and downstream signaling molecules into lipid rafts. Blood 2007;109:711 – 9.

[Cancer Biology & Therapy 7:2, 163-173; February 2008]; ©2008 Landes Bioscience

Review

Modulation of death receptors by cancer therapeutic agents

Heath A. Elrod and Shi-Yong Sun*

Department of Hematology and Oncology; Winship Cancer Institute; Emory University School of Medicine; Atlanta, Georgia USA

Key words: death receptors, apoptosis, cancer therapy

Death receptors are important modulators of the extrinsic apoptotic pathway. Activating certain death receptors such as death receptors for tumor necrosis factor-related apoptosis-inducing ligand (TRAIL) (i.e., DR4 and DR5) selectively kills cancer cells via induction of apoptosis while sparing normal cells. Thus, soluble recombinant TRAIL and agonistic antibodies to DR4 or DR5 have progressed to phase I and phase II clinical trials. Many cancer therapeutic drugs including chemotherapeutic agents have been shown to induce the expression or redistribution at the cell surface of death receptors including TRAIL death receptors. In addition, chemotherapeutic agents have also been shown to enhance induction of apoptosis by TRAIL or agonistic antibodies or overcome cell resistance to TRAIL or agonistic antibodies. Targeted induction of apoptosis by activation of the death receptor-mediated extrinsic apoptotic pathway should be an ideal therapeutic strategy to eliminate cancer cells. Therefore, death receptors, particularly TRAIL death receptors, have emerged as an important cancer therapeutic target. This article will focus on reviewing and discussing the modulation of death receptors by cancer therapeutic agents and its implications in cancer therapy.

Introduction

Apoptosis or programmed cell death is a tightly controlled process essential for embryonic development as well as normal tissue homeostasis and the regulation of cell number after an immune response. Apoptosis is regulated by signals such as growth factors, cell damage and hormones.[1] Aberrant regulation of apoptosis can lead to cancer. Tumor cells often acquire resistance to normal apoptotic signals allowing for uncontrolled cell growth. The process of targeting the apoptotic pathway in tumor cells while sparing normal cells is of interest in cancer therapy. Such targeted therapy to induce apoptosis in cancer cells has emerged as a strategy to more effectively treat cancer patients and reduce toxicity.

Death receptors are key components in the extrinsic apoptotic pathway.[2] Their activation due to ligand binding or receptor clustering and aggregation triggers an extrinsic apoptotic signaling pathway leading to apoptosis. Therefore, the death receptor ligands or agonistic antibodies against the death receptors are potent inducers of apoptosis and thereby have therapeutic potential in the treatment of cancer. One example is tumor necrosis factor (TNF)-related apoptosis-inducing ligand (TRAIL), which is the ligand for death receptor 4 (DR4) and death receptor 5 (DR5) and induces apoptosis upon ligation with DR4 or DR5. TRAIL has attracted attention recently because it preferentially induces apoptosis of transformed or malignant cells, when administered systemically, with limited inflammatory response and liver damage, which are major side effects or toxicity of other death receptor ligands such as the cytokines TNFα and Fas.[2] Therefore, TRAIL is considered to be a tumor-selective apoptosis-inducing cytokine and a promising new candidate for cancer treatment.[3] There is a concern about TRAIL's potential hepatotoxicity,[4] but this can be avoided by appropriate preparation of recombinant human TRAIL.[5,6] Currently, TRAIL is being tested in phase I clinical trials.[7] In addition to TRAIL ligand, agonistic antibodies against DR4 and DR5, respectively, have also been developed. These antibodies mimic TRAIL's function to activate death receptor-mediated apoptosis with potential as cancer therapeutic agents and have progressed to phase I or phase II trials in treatment of multiple types of cancers.[7]

The expression of death receptors is induced by many small molecules including some cancer therapeutic drugs. Conventional chemotherapy or radiotherapy damages proliferating cells and induces cell death usually by engaging the intrinsic mitochondrial apoptotic pathway through p53 activation.[8] Recent studies have shown that certain small molecules can also induce apoptosis by engaging the extrinsic apoptotic pathway through the activation of death receptors. Therefore, death receptors have emerged as an important cancer therapeutic target.[9,10]

There are many elegant review articles on cancer therapeutic potentials of the death ligands such as TRAIL and agonistic antibodies to death receptors such as DR4 and DR5.[7,10-12] This article will primarily review the recent studies on the modulation and activation of death receptors by small molecules with cancer therapeutic activity and discuss possible underlying mechanisms and their clinical implications.

Death Receptor-Mediated Extrinsic Apoptotic Pathway

Apoptosis can occur through two distinct pathways: the intrinsic apoptotic pathway and the extrinsic apoptotic pathway. The intrinsic pathway results in signals from the mitochondria whereas the extrinsic pathway is characterized by activation of death receptors.[13] Both pathways engage a family of cysteine proteases, the caspases,

*Correspondence to: Shi-Yong Sun; Winship Cancer Institute, Emory University School of Medicine; 1365-C Clifton Road, C3088; Atlanta, Georgia 30322 USA; Tel.: 404.778.2170; Fax: 404.778.5520; Email: shi-yong.sun@emoryhealthcare.org

Submitted: 11/14/07; Accepted: 11/21/07

Previously published online as a *Cancer Biology & Therapy* E-publication: www.landesbioscience.com/journals/cbt/article/5335

whose cleavage of cellular substrates leads to apoptosis. The death receptors involved in the extrinsic apoptotic pathway belong to the TNF receptor superfamily that include Fas (CD95 or Apo1), TNFR1, DR3, DR4 (TRAIL-R1), DR5 (TRAIL-R2) and DR6.[2] These receptors are characterized by a cysteine-rich cytoplasmic domain and an intracellular death domain. The death domain enables transmission of death signals after ligand binding or trimerization.[2] There are also decoy receptors (e.g., DcR1 and DcR2) that contain no death domain or a truncated death domain and can bind ligand but cannot signal.[14] Therefore, these decoy receptors function as antagonists to inhibit death ligand/death receptor-induced apoptosis.

The death receptors, Fas, DR4 or DR5, bind to their respective ligands (i.e., FasL or TRAIL) and trimerization of the receptor occurs at the cell surface inducing apoptosis though the recruitment of adaptor proteins such as the Fas-associated death domain (FADD). The recruitment of FADD forms the death inducing signaling complex (DISC), which results in the recruitment of pro-caspase-8 to the DISC. This results in activation of caspase-8, which leads to the activation of effector caspases such as caspase-3. Death receptors can also indirectly activate effector caspases by caspase-8 cleaving Bid, which leads to activation of Bax resulting in pore formation in the mitochondrial membrane and release of cytochrome c leading to activation of caspase-9 (Fig. 1).[2,15] Therefore, death receptors activate the intrinsic mitochondrial apoptotic pathway in certain types of cells as well.

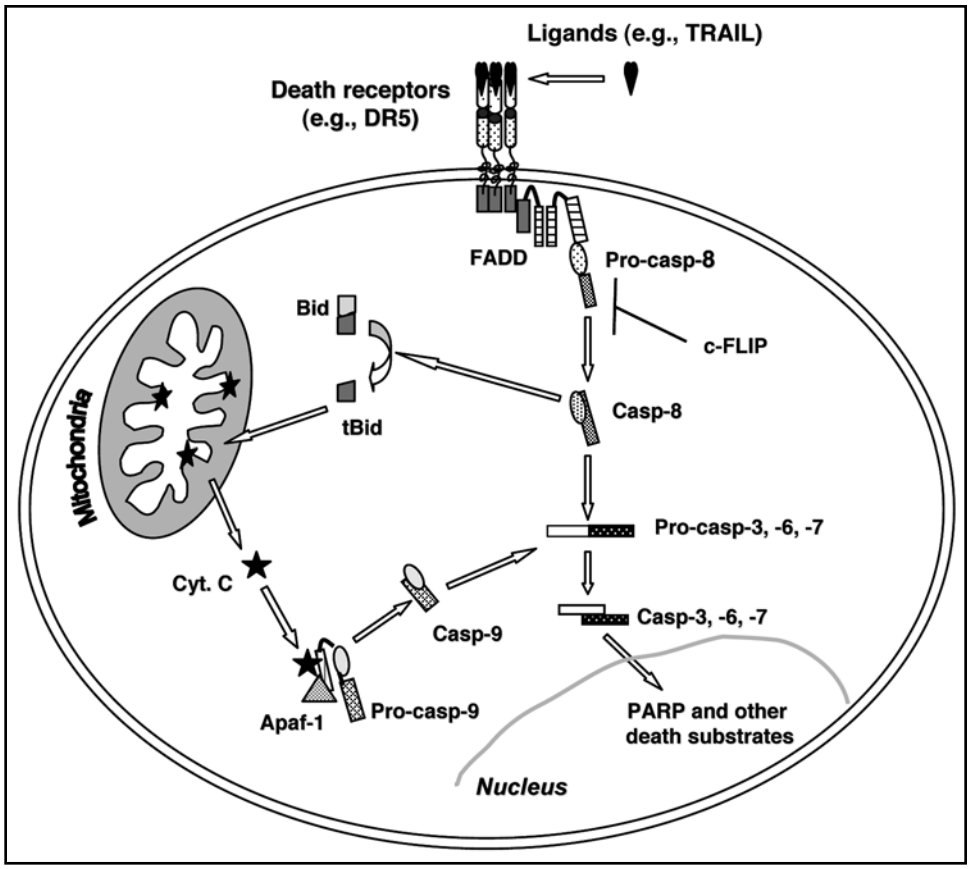

Figure 1. Schema for extrinsic death receptor-mediated apoptotic signaling pathway. Ligation of death ligands (e.g., TRAIL) with their receptors (e.g., DR4 and DR5) results in activation of caspase-8 (Casp-8) through a death adaptor protein FADD in the death-inducing signaling complex (DISC). Activated caspase-8 can directly activate downstream caspase-3 (Casp-3), caspase-6 (Casp-6) and caspase-7 (Casp-7) leading to cleavage of their target proteins such as PARP, DFF45 and lamins. Moreover, activated caspase-8 can cleave Bid, generating truncated Bid (tBid), which can facilitate insertion of BAX into the mitochondrial membrane leading to cytochrome C (Cyt. C) release. Thus, caspase-8 can also activate the intrinsic mitochondria-mediated apoptotic pathway, which involves cytochrome C (Cyt. C) release from mitochondria into cytosol and subsequent caspase-9 (Casp-9) activation.

In contrast to Fas, DR4 and DR5, the biological function of TNF receptor 1 (TNFR1) is more complex. This complexity is reflected in the increased variety of proteins that are present in the TNFR1 complex. TNFR1 first recruits another adaptor protein, TNF-associated death domain (TRADD), which in turn not only recruits FADD, but also recruits TNFR-associated factor 2 (TRAF2) and the kinase receptor-interacting protein (RIP). TRAF2 is essential for c-Jun N-terminal kinase (JNK) activation, whereas RIP is instrumental for the activation of the NFκB pathway. TNF-mediated JNK activation favors its apoptosis-inducing activity, whereas NFκB activation by TNFα signals inflammation and cell survival by inhibiting TNFα-induced apoptosis.[2,16]

Death Receptors and Cancer

Fas, DR4 and DR5 are generally expressed in both normal and malignant cells. However, the abnormal modulation of death receptors has been observed in several different cancers possibly as a mechanism for tumor cells to escape immunosurveillance. The Fas gene has been shown to be mutated in both hematopoietic malignancies (0–65%) and solid tumors (0–28%).[17] Among the hematopoietic malignancies, high frequencies of Fas mutations occur in thyroid lymphoma (65.4%), cutaneous T-cell lymphoma (59%), and nasal NK/T cell lymphoma (50%). Among solid tumors, Fas mutations occur frequently in bladder transitional cell carcinoma (28%) and burn scar-related squamous cell carcinoma (14.3%).[17] Compared to Fas, the frequencies of DR4 and DR5 mutations detected in cancers including lung, head and neck, breast, bladder, gastric and hepatocellular carcinomas, non-Hodgkin's lymphoma and chronic myelogenous leukemia are very low (0–10.6%).[18-20]

Downregulation of expression of death receptors has also been observed in cancer. In cervical cancer, the expression of Fas decreases with more progressive cervical intraepithelial neoplasia (CIN).[21] In urothelial cancer, decreased Fas expression was significantly associated with a higher pathological grade, a more advanced stage and poorer prognosis.[22] In ovarian cancer, loss or downregulation of DR4 expression was observed in 10.3% and 8.8% of patients, respectively, which was associated with methylation of the DR4 gene promoter.[23] As well, in small cell lung cancer a 40% reduction in Fas and DR4

expression was observed as a result of DNA methylation.[24] A study in acute myelogenous leukemia (AML) has shown that relapse-free survival was significantly prolonged in patients with CD95-positive AML cells compared with patients with CD95-negative AML cells.[25] However, in nonsmall cell lung cancer, poorly differentiated tumors showed increased expression of DR4, DR5 and TRAIL and the expression of DR5 was associated with increased risk of death.[26] Similarly, in colon cancer, the expression of DR4 and DR5 is stronger in neoplastic tissues than in normal tissues and is accompanied by a higher degree of apoptosis.[27] Another study in stage III colon cancer patients treated with adjuvant chemotherapy has shown that the majority of tumors showed high expression of TRAIL (83%), DR4 (92%), and DR5 (87%) and high DR4 expression was associated with worse disease-free and overall survival in these patients.[28] Although both DR4 and DR5 were detected in the majority of colorectal tumors, a recent study failed to demonstrate that they are associated with survival; instead, overexpression of $FLIP_L$, a major inhibitor of death receptor-mediated apoptosis, provides stage-independent prognostic information.[29] In breast cancer, DR5 expression is stronger in malignant specimens than in normal breast epithelium, and expression correlated strongly with lymph node involvement, and was independently associated with decreased survival; however, DR4 expression was not associated with survival.[30] These data indicate that the expression of death receptors and the correlation with tumor progression seem to be tumor type specific.

Fas-associated death domain (FADD) is the main adaptor for transmitting death signal from activation of death receptors. It has been shown that low or absent expression of the FADD protein in leukemic cells at diagnosis is a poor independent prognostic factor that can predict worse clinical outcome even for patients with standard- or good-risk AML.[31] However, in lung adenocarcinomas, increased FADD expression is detected in aggressive tumors and is significantly associated with poor survival.[32] It seems that the impact of FADD expression on cancer patient survival is also tumor-type specific.

The abnormal expression of the decoy receptors has also been observed in cancer; however, the expression of the decoy receptors and DR4 or DR5 does not always correlate with sensitivity to apoptosis.[33] Tumor cells can overexpress decoy receptors, which can compete with death receptors for ligand binding. The gene coding for DcR3, a secreted protein that binds FasL, is amplified in about 50% of lung and colon cancers.[34] Frequent gene amplification and overexpression of DcR3 were also observed in glioblastoma.[35] In addition, DcR3 is overexpressed in carcinomas of the stomach, esophagus, rectum and liver independently of gene amplification.[36,37] Cells that overexpress DcR3 presumably have a survival advantage because of their ability to resist FasL-mediated attack by cytotoxic lymphocytes, although the role of DcR3 in tumorigenesis remains unclarified. In contrast to DcR3, DcR1 and DcR2 are generally downregulated in many types of cancer, largely due to gene methylation.[38,39] It is possible that DcR overexpressing tumors may gain a selective growth advantage by escaping from death ligand/death receptor-induced apoptosis. Given the frequent downregulation or loss of DcR1 and DcR2 expression in multiple cancers, which still express DR4 and/or DR5 or exhibit increased DR4 and DR5 expression, there may be an opportunity to treat these cancers with TRAIL or agonistic DR4 or DR5 antibodies via targeted induction of TRAIL/death receptor-mediated apoptosis of cancer cells.

General Mechanisms Underlying Modulation of Death Receptors

The expression of death receptors appears to be induced by some anticancer agents. In general, modulation of death receptors involves p53-dependent and p53-independent mechanisms.

The tumor suppressor gene p53 plays a critical role in regulating apoptosis and cell cycle arrest after cells undergo cellular stress such as induction of DNA damage or hypoxia.[40] p53 is one of the most common genes mutated in cancer and can regulate many downstream target genes including death receptors. Activation of p53 can contribute to increased surface expression of Fas and apoptosis.[41] Fas is the first death receptor demonstrated to be directly regulated by p53 through a p53-responsive element in the first intron of the Fas gene and putative elements in the promoter.[42] Subsequently, DR5 was demonstrated to be induced by DNA-damaging agents in a p53-dependent fashion[43] and its transcription is directly transactivated by p53 through an intronic sequence-specific p53 DNA-binding site.[44] We recently have shown that DR4 expression can also be induced by DNA damaging agents in a p53-dependent manner[45] and p53 directly regulates the transcription of DR4 through a p53 binding site located in the first intron of the DR4 gene, in a similar fashion as demonstrated in the DR5 gene.[46]

Death receptors can also be regulated by p53 independent mechanisms. The Fas gene contains consensus sequences for AP-1, Sp-1, NFκB and NFAT in its promoter[47] and Fas transcription has been shown to be directly regulated by NFκB.[48] Moreover, transcriptional regulation of Fas expression by AP-1 was also reported.[49] There have been only a few studies dealing with p53-independent regulation of DR4 or DR5. Sheikh et al.[50] reported that TNFα, a NFκB activator, induced DR5 expression in a number of cancer cell lines independently of p53. Ravi et al.[51] reported that NFκB induced expression of DR4 and DR5. Shetty et al.[52] recently demonstrate that a putative NFκB binding site in the first intron of the DR5 gene in cooperation with the p53 binding site in this region is responsible for DR5 upregulation by etoposide or histone deacetylase (HDAC) inhibitors. We found that phorbol 12-myristate 13-acetate (TPA), a potent AP-1 activator, increased AP-1 binding to the DR4 promoter and induced DR4 expression in cancer cell lines with mutant p53,[53] suggesting a possible role for AP-1 in DR4 regulation. We have demonstrated that this effect is mediated by an AP-1 site in the 5'-flanking region of the DR4 gene.[53] Recently, it has been shown that DR5 can be regulated by CCAAT/enhancer-binding protein homologous (CHOP) protein through the CHOP-binding site in the 5'-flanking region of the DR5 gene.[54,55] In addition to these positive regulations, DR5 can also be negatively regulated through a putative binding site for the transcription repressor Yin Yang 1 (YY1) in the DR5 promoter region.[56,57]

Modulation of Death Receptor Expression by Cancer Therapeutic Agents

It is generally thought that small molecules such as chemotherapeutic agents induce apoptosis through the intrinsic apoptotic pathway. However, many small molecules with anticancer activity including chemopreventive agents modulate the expression and/or activation of death receptors, which plays a critical role in mediating drug-induced apoptosis. The modulation of death receptor

expression by chemopreventive agents was discussed by us previously in reference 58. The current review will focus on modulation of death receptors by cancer therapeutic agents and possible underlying mechanisms.

DNA damaging agents. Many studies have shown that DNA damaging chemotherapeutic agents can modulate death receptor expression and render cells more sensitive to death receptor-induced apoptosis. Cisplatin (CDDP), mitomycin, methotrexate, mitoxantrone, doxorubicin, and bleomycin induced Fas expression in human cancer cells, primarily through a p53-dependent mechanism.[42] Similarly, DR5 was demonstrated to be a DNA damaging-inducible and p53-regulated gene.[43,44] Following these findings, we demonstrated that DR4 is also a DNA damaging-inducible and p53-regulated gene.[45,46] In the literature, doxorubicin, etoposide, Ara-C, cisplatin and camptosar (CPT-11) were shown to induce the expression of both DR4 and DR5 or only DR5 expression, through either p53-dependent, or p53-independent mechanisms.[43,45,50,59-62] For example, etoposide increased the expression of both DR4 and DR5 and enhanced TRAIL-induced apoptosis in breast cancer[59] and osteogenic sarcoma cells.[62] Etoposide was also shown to induce DR5 expression in glioma cells,[60] human acute leukemia cells,[61] and breast cancer cells.[63] Our work showed that etoposide increased DR4 expression in lung cancer cells.[45]

Currently, it is not clear whether upregulation of death receptors plays any role in DNA damaging agent-induced apoptosis. It was shown that addition of a soluble DR4 fusion protein (DR4:Fc) to cell cultures reduced the amount of etoposide-induced apoptosis in a dose-dependent manner.[59] In colon cancer cells, it was recently shown that chemotherapy downregulated FLIP expression, whereas overexpression of $FLIP_L$ potently inhibited apoptosis induced by chemotherapy.[64] Of note, a recent clinical study has shown that absence or low expression of fas-associated with death domain (FADD) in acute myeloid leukemia cells predicts resistance to chemotherapy and poor outcome.[31] These results suggest that the activation of the extrinsic death receptor-mediated apoptotic pathway may play a role in chemotherapy-induced apoptosis.

HDAC inhibitors. HDAC inhibitors represent a group of novel cancer therapeutic agents.[65] These agents induce apoptosis and enhance TRAIL-induced apoptosis in a variety of cancer cells. Suberoylanilide hydroxamic acid (SAHA) and trichostatin A (TSA) were shown to increase the levels of cell surface DR4 and DR5 in human multiple myeloma cell lines.[66] LAQ824 (a cinnamic acid hydroxamate), SAHA, MS-275, m-carboxycinnamic acid bishydroxamide (CBHA), and TSA increased the expression of DR5 and/or DR4, reduced the levels of c-FLIP, and enhanced TRAIL-induced apoptosis in human acute leukemia cells.[67-70] One study showed that blockage of DR5 activation using DR5 siRNA in the breast cancer cell line MCF-7 decreased HDAC inhibitor-induced apoptosis,[52] suggesting an important role of DR5 activation in apoptosis induced by HDAC inhibitors. Two recent elegant studies have shown that HDAC inhibitors upregulate not only DR5 and Fas expression but also the expression of their ligands TRAIL and FasL in leukemic cells. Importantly, such findings were not observed in normal hematopoietic progenitors. Moreover, they further demonstrated that HDAC inhibitors induce apoptosis of leukemia cells through activation of a specific death pathway (i.e., TRAIL/DR5).[71,72]

Currently, it is not clear how HDAC inhibitors upregulate the expression of death receptors. One study has suggested that HDAC inhibitors upregulate DR5 expression through cooperative activation of NFκB and p53.[52] Another study has demonstrated that sodium butyrate-induced expression of DR5 involves the putative Sp1 site within the DR5 promoter region (located at -195 bp relative to the transcription start site).[73]

Proteasome inhibitors. Inhibition of the proteasome has been considered to be an effective strategy for cancer therapy. Thereby, novel anticancer drugs with proteasome-inhibitory activity have been developed.[74] The proteasome inhibitor MG132 upregulated DR5 expression and effectively cooperated with Apo2L/TRAIL to induce apoptosis in human colon cancer cells.[75] A similar finding was also demonstrated in human prostate cancer cells and primary chronic lymphocytic leukemia (CLL) cells.[55,76] It has been demonstrated that MG132 induces DR5 at the transcriptional level involving upregulation of CHOP protein.[55] Another clinically-used proteasome inhibitor, PS-341, does not affect the levels of Bax, Bak, caspase-3 and -8, c-FLIP or FADD, but elevates levels of DR4 and DR5 in human prostate and bladder cancer cells. This increase in receptor protein levels is associated with the ubiquitination of the DR5 protein.[77] We also showed that PS-341 increases DR5 expression and cell surface levels and enhances TRAIL-induced apoptosis in human lung cancer cells.[78] Interestingly, MG-132 also increases apoptosis and DR5 expression in normal B-cells. However, when it is combined with TRAIL or TRAIL receptor activating antibodies the amount of apoptosis is increased in CLL cells but not in normal B cells.[76]

Cyclooxygenase-2 (COX-2) inhibitors. Since COX-2 is overexpressed in malignant tissues, the COX-2 mediated signaling pathway has been recognized as a potential target for therapeutic intervention of cancer.[79] Sulindac sulfide, a COX-2 inhibitor, is one of the major metabolites of sulindac that is believed to mediate its antitumorigenic effects by inducing apoptosis. Sulindac sulfide specifically upregulates DR5 and activates caspase-8 in various colon and prostate cancer cell lines. Overexpression of a dominant-negative FADD (FADD-DN) suppresses sulindac sulfide-induced apoptosis and combination of sulindac sulfide with TRAIL exhibits an enhanced apoptosis-inducing effect, suggesting the involvement of DR5 in sulindac sulfide-induced apoptosis.[80] Induction of DR5 by sulindac sulfide in gastric cancer cells has also been reported. In this study, DR4 expression was also induced by sulindac sulfide.[81] Moreover, we found that celecoxib increased the expression of DR4 and particularly DR5 at both mRNA and protein levels in human lung cancer cells. Both overexpression of FADD-DN and silencing of DR5 expression using siRNA attenuated celecoxib-induced apoptosis. Moreover, celecoxib cooperated with TRAIL to augment the induction of apoptosis. These results indicate that the expression of death receptors, particularly DR5, contributes to celecoxib-induced apoptosis.[82] Similarly, we further showed that the celecoxib analog, dimethyl-celecoxib, which lacks COX-2-inhibitory activity, exerts similar effects on upregulation of DR5 and enhancement of TRAIL-induced apoptosis.[83] Thus, it appears that celecoxib regulates DR5 expression independent of its COX-2 inhibitory activity. Both celecoxib and dimethyl-celecoxib induce DR5 expression through a CHOP-dependent mechanism.[84]

Retinoid-related molecules. Retinoids, which include both synthetic and naturally occurring Vitamin A (retinal) metabolites and analogs, have long been considered to have cancer chemopreventive and therapeutic potential.[85] Some novel synthetic retinoids potently

induce apoptosis in cancer cells independent of retinoic acid receptors (RARs) and thus are named retinoid-related molecules (RRMs).[86] One such compound called 6-[3-(1-adamantyl-4-hydroxyphenyl]-2-naphthalene carboxylic acid (CD437 or AHPC) can induce Fas, DR4 and DR5 expression in lung cancer cells in a p53-dependent manner.[87-89] Importantly, CD437 does not induce the expression of Fas, DR4 and DR5, or induce apoptosis in normal human bronchial epithelial cells and small airway epithelial cells.[90] CD437 can also induce the expression of these death receptors independent of p53 in human prostate and head and neck cancer cells.[91,92] The CD437 analogue Cl-(1-adamantyl)-4-hydroxyphenyl]-3-chlorocinnamic acid (3-Cl-AHPC) also induces the expression of Fas, DR4 and DR5 in human prostate and breast cancer cells as well.[93] Another RRM, ST1926, in cooperation with epidermal growth factor receptor inhibitor ZD1839 also upregulates DR5 levels.[94] We and others have demonstrated that CD437 and 3-Cl-AHPC activate NFκB, which contributes to upregulation of DR4 and DR5 by CD437 or 3-Cl-AHPC in prostate cancer cells.[93,95]

N-(4-hydroxyphenyl) retinamide (4HPR) is another synthetic retinoid wildly tested in many cancer clinical trials. It was shown to enhance TRAIL-mediated apoptosis through enhancement of a mitochondrial-dependent amplification loop in ovarian cancer cell lines.[96] However, a recent study has shown that 4-HPR upregulates DR5 expression via the induction of the transcription factor CHOP, which sensitizes colon cancer cells to TRAIL-induced apoptosis.[97] Several studies have shown that 4HPR and its analog induce CHOP expression in different types of cancer cells, which plays a role in 4HPR-induced apoptosis.[98-103] Therefore, these data suggest that 4HPR induces CHOP-dependent DR5 expression.

Triterpenoids. Triterpenoids are another group of natural and synthetic compounds with cancer therapeutic potential. The natural triterpenoids betulinic acid (Fig. 2) and boswellic acid were reported to induce DR5 expression in melanoma, glioblastoma, and leukemia cells.[104,105] Our recent study has shown that the synthetic triterpenoid methyl-2-cyano-3,12-dioxooleana-1,9-dien-28-oate (CDDO-Me) increased the expression of DR4 and particularly DR5, and enhanced TRAIL-induced apoptosis in human lung cancer cells. Silencing of DR5 expression using siRNA inhibited both CDDO-Me-induced apoptosis and CDDO-Me-mediated enhancement of TRAIL-induced apoptosis, indicating the involvement of DR5 in both activities.[106] Upregulation of cell surface DR4 and DR5 by CDDO-Me analogues CDDO and CDDO-Im in breast cancer cells was also reported.[107] In addition, it has been shown that induction of DR5 by betulinic acid and CDDO-Me is independent of p53.[104,106] We found that CDDO-Me rapidly activated c-Jun NH_2-terminal kinase (JNK) before DR5 upregulation. Moreover, application of the JNK-specific inhibitor SP600125 blocked CDDO-Me-induced DR5 upregulation. These results indicate that CDDO-Me induces a JNK-dependent DR5 upregulation.[106]

Cytokines. Certain cytokines including interferons have anticancer activity. TNFα is the first cytokine demonstrated to induce the expression of DR5 in a number of cancer cell lines. The induction of DR5 by TNFα occurs at transcriptional levels irrespective of p53 status.[50] Subsequently, interferon-γ was shown to induce DR5 expression in cancer cell lines independent of p53.[104] Interferon-α was also reported to increase DR5 expression in human hepatoma cells; this increased expression is associated with its ability to enhance TRAIL-induced apoptosis.[108] In addition to regulation of death receptors, interferons regulate the expression of death ligands. For example, interferon γ increases TRAIL expression in colon cancer cells, which mediates interferon γ-induced apoptosis.[109] Moreover, interferon α increased expression of TRAIL, DR4 and DR5, which were involved in interferon α-induced apoptosis in Daudi B lymphoma cells.[110] Interestingly, TRAIL itself increases the expression of DR5 in human embryonic kidney (HEK) 293, MCF-7 and MDA-MB-231 epithelial cell lines while DR4 expression remains unchanged. This effect is mediated by NFκB activation.[63]

Natural products. Natural products have been the most significant source of drugs and drug leads in history. Their dominant role in cancer chemotherapeutics is clear with about 74% of anticancer compounds being either natural products, or natural product-derived.[111] Curcumin (Fig. 2), a plant product containing the phenolic phytochemical with apoptosis-inducing activity, has been demonstrated to increase Fas expression and induce Fas clustering in human melanoma cells, leading to the induction of apoptosis.[112] Curcumin also increased cell surface DR4 or DR5 and augmented TRAIL-induced apoptosis in prostate cancer[113] and renal cancer cells.[114] Although curcumin induced the expression of CHOP, suppression of CHOP expression by siRNA did not abrogate DR5 induction by curcumin and cell death induced by curcumin plus TRAIL, demonstrating that CHOP is not involved in curcumin-induced DR5 upregulation.[115] Sulforaphane (Fig. 2) is a naturally occurring isothiocyanate with potent anticancer activity. This agent has been demonstrated to upregulate DR5 expression and subsequently to enhance TRAIL-induced apoptosis in hepatoma[116] and osteosarcoma[117] cells. Importantly, sulforaphane neither induces DR5 protein expression nor enhances TRAIL-induced apoptosis in normal human peripheral blood mononuclear cells.[117] Luteolin (Fig. 2), a naturally occurring flavonoid, induces apoptosis in various cancer cells. A recent study has shown that luteolin upregulates DR5 expression in human cancer cell lines.[118] Suppression of DR5 expression with siRNA efficiently reduced luteolin-induced caspase activation and apoptosis. Human recombinant DR5/Fc also inhibited luteolin-induced apoptosis.[118] These results suggest that DR5 induced by luteolin plays a role in luteolin-induced apoptosis. Dihydroflavonol BB-1 (Fig. 2), an extract of the natural plant Blumea balsamifera, increases DR5 gene promoter activity and surface DR5 expression in a p53-independent manner in leukemia cells.[119] Silibinin (Fig. 2), a flavonoid isolated from Silybum marianum, can sensitize glioma cells to TRAIL-induced apoptosis, partially due to CHOP-dependent upregulation of DR5.[120]

Others. The synthetic glucocorticoid dexamethasone elevated DR5 expression and induced apoptosis in several types of cancer cell lines including glioblastoma, ovarian cancer, and colon cancer cell lines with mutant p53, and this induction was inhibited by the transcriptional inhibitor actinomycin D.[104] 2-methoxyestradiol (2ME Fig. 2), a natural metabolite of estradiol, is a potent antitumor and antiangiogenic agent and is currently being tested in several Phase I and Phase II clinical trials under the name Panzem. It has been recently shown that 2ME results in up-regulation of DR5 protein expression in several cancer cell lines including breast cancer cells in vitro and in vivo and renders cells more sensitive to TRAIL-induced apoptosis. Blockage of death receptor signaling by expression of dominant-negative FADD severely attenuates the ability of 2ME to

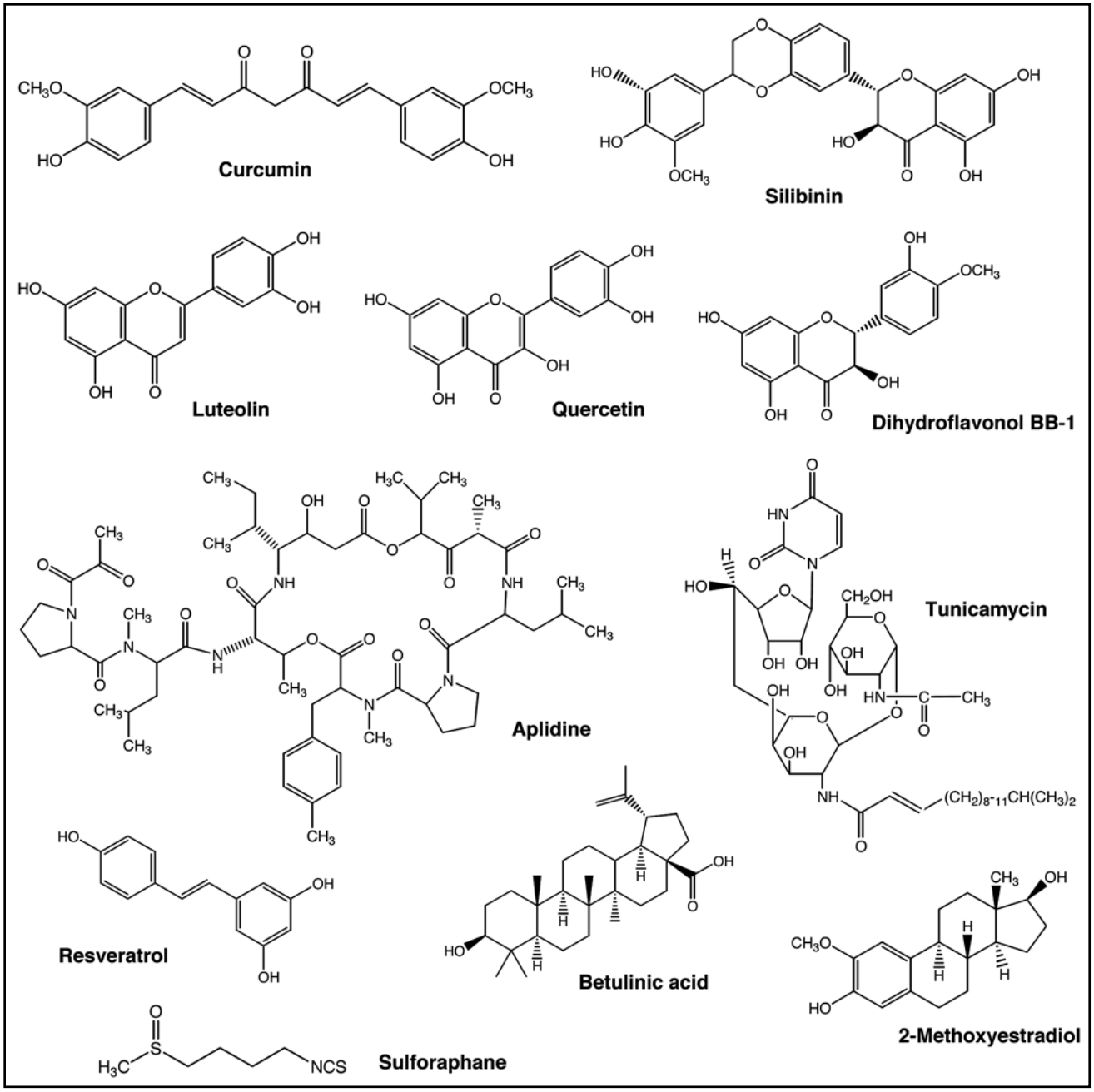

Figure 2. Chemical structures of natural products with death receptor-modulating activity.

induce apoptosis, suggesting that 2ME induces apoptosis through activation of the DR5-mediated extrinsic pathway.[121] However, another study failed to demonstrate upregulation of DR5 by 2ME and synergism between 2ME and TRAIL in glioma cells.[122] Induction of DR5 by 2ME was also not demonstrated in another CAL51 breast cancer cell line although 2ME synergized with TRAIL to induce apoptosis.[123] Thapsigargin (TG), an agent known to cause endoplasmic reticulum (ER) stress due to perturbations in intracellular Ca^{2+} homeostasis and induce apoptosis, upregulates DR5 expression as well as TRAIL expression.[54,124,125] The induction of DR5 occurs as a consequence of TG-induced ER Ca^{2+} pool depletion[124] involving CHOP-mediated transactivation of the DR5 gene.[54] Tunicamycin (Fig. 2), a naturally occurring antibiotic, upregulates DR5 expression through a CHOP-dependent mechanism and enhances TRAIL-induced apoptosis in human prostate cancer cells.[126] Of note, tunicamycin-mediated induction of CHOP and DR5 protein expression was not observed in normal human peripheral blood mononuclear cells.[126] Arsenic trioxide, a drug for treatment of leukemia, increases cell surface expression of DR5 and sensitizes leukaemic cells to TRAIL-induced apoptosis.[127] The semi-synthetic analogue of vitamin E, *a*-tocopheryl succinate, increases the expression of both DR4 and DR5 in human malignant mesothelioma cells in a p53-dependent manner; this increased expression is associated with its ability to enhance TRAIL-induced apoptosis.[128,129] As well, the alkylphospholipid perifosine increases DR5 expression in human lung cancer cells as we recently demonstrated.[130]

Induction of Death Receptor Redistribution and Clustering by Anticancer Agents

The majority of anticancer therapeutic agents upregulate the expression of death receptors. However, some agents are able to activate the death receptors in a ligand-dependent (autocrine) or -independent way, leading to activation of the extrinsic apoptotic pathway without apparently altering the expression levels of the death receptors. Since receptor trimerization is an essential step for activation of death receptor-mediated extrinsic apoptosis, induction of death receptor aggregation or clustering, even in the absence of a specific death ligand, should be sufficient to trigger apoptosis. Current studies have shown that several cancer therapeutic agents activate the death receptor-mediated apoptotic pathway through lipid raft-mediated death receptor aggregation or clustering, which concentrates and activates death receptors. Induction of death receptor redistribution and clustering in lipid rafts is also an important mechanism for certain agents to sensitize cancer cells to TRAIL-induced apoptosis.

Lipid rafts are microdomains of plasma membranes enriched in sphingolipids and cholesterol.[131] Recently, lipid rafts have been demonstrated to be involved in control of apoptosis, particularly death receptor-mediated apoptosis.[132,133] Aplidine (Fig. 2) is a promising antitumor agent derived from the Mediterranean tunicate Aplidium albicans. This agent induces apoptosis of leukemia cells involving activation of the Fas-mediated extrinsic apoptotic pathway.[134] It has been shown that Fas, TNFR1, and DR5 are clustered into lipid rafts in leukemic Jurkat cells following aplidin treatment.[135] Aplidine is rapidly incorporated into membrane rafts and induces Fas clustering and apoptosis, whereas disruption of lipid rafts inhibits uptake of aplidine and prevents Fas clustering. Thus, Aplidine-induced apoptosis involves Fas activation in both a FasL-independent manner and an autocrine manner through the concentration of Fas, membrane-bound FasL, and signaling molecules in membrane rafts.[135] The anticancer drug ET-18-OCH(3) (Edelfosine) does not promote the expression of Fas or FasL. However, it induces Fas-dependent apoptosis in leukemia cells independent of FasL.[136] Further study has shown that ET-18-OCH(3) similar to aplidin induces apoptosis by inducing formation of lipid rafts in tumor cells, followed by its coaggregation with Fas and recruitment of apoptotic molecules into Fas-enriched rafts.[137,138] A similar mechanism was also observed in multiple myeloma cells undergoing edelfosine- or perifosine-induced apoptosis.[139]

Cisplatin, a known DNA-damaging agent, also induces clustering of Fas at the surface of human colon cancer cells. It has been demonstrated that cisplatin activates acid sphingomyelinase (aSMase) and induces ceramide production, which triggers the redistribution of Fas into the plasma membrane rafts. Such redistribution contributes to cisplatin-induced cell death and sensitizes tumor cells to Fas-mediated apoptosis.[142]

Resveratrol (Fig. 2), a polyphenol found in grape skin and various other food products, exhibits both cancer chemopreventive and therapeutic activity. In contrast to other agents, studies in human colon cancer cells have shown that resveratrol does not modulate the expression of Fas, DR4, and DR5 at the surface of cancer cells; However, resveratrol induces the clustering of these death receptors and their redistribution in cholesterol and lipid rafts together with FADD and procaspase-8. These redistributions are associated with the formation of a DISC and contribute to the induction of apoptosis and sensitization of cells to death ligand- or death receptor activation-mediated apoptosis.[140,141] Similarly, the flavonoid quercetin (Fig. 2) enhances TRAIL-induced apoptosis by causing the redistribution of DR4 and DR5 into lipid rafts in colon cancer cells.[143]

The COX-2 inhibitor DuP-697 does not modulate the levels of DR5 and DR4 although it enhances TRAIL-induced apoptosis in cancer cells. Instead, it sensitizes cells to TRAIL-induced apoptosis by inducing clustering of DR5 at the cell surface and the redistribution of the death-inducing signaling complex components (DR5, FADD, and procaspase-8) into lipid rafts.[144] Similarly, the HDAC inhibitor depsipeptide (FR901228) also increases levels of DR4 and DR5 in membrane lipid rafts, leading to enhancement of TRAIL-induced apoptosis.[145]

Implications of Death Receptor Modulation in Cancer Therapy

Activation of death receptors with either ligand binding or receptor aggregation triggers the extrinsic apoptotic pathway. Therefore, the death ligands (e.g., TRAIL) or agonistic death receptor antibodies (e.g., antibody against DR4 or DR5) induce apoptosis of cancer cells with cancer therapeutic potential. Currently, both TRAIL and agonistic DR4 and DR5 antibodies are being tested in clinical trials for their anticancer activities.[7] The drugs that upregulate the expression of DR4 and/or DR5, or induce redistribution of DR4 and/or DR5 at the cell surface, preferentially in malignant cancer cells, are assumed to sensitize cancer cells to treatment with either TRAIL or agonistic DR4 or DR5 antibodies. This sensitization has been documented in many preclinical studies both in vitro and in vivo.[7] The good news is that many clinically used cancer therapeutic agents including chemotherapeutic drugs upregulate the expression of DR4 and/or DR5. Therefore, it should be easy to test the combination therapy of these drugs with TRAIL or agonistic antibodies in the clinic to enhance cancer therapy.

Some agents have been demonstrated to induce the expression of death ligands such as TRAIL. Examples of these agents are retinoic acid,[146,147] interferons,[147,148] and PI3 kinase inhibitors.[149] Therefore, it is plausible to speculate that the combination of a death receptor-inducing drug with a death ligand-inducing agent may enhance the killing or elimination of malignant cancer cells via death ligand/death receptor-mediated apoptosis. Studying the effect of this kind of combination may develop an effective combination regimen for cancer therapy.

Apoptosis induced by the interaction between death ligand (from NK cells or T cells) and death receptors (from target cells) is the primary mechanism underlying tumor immunosurveillance.[10,150,151] In death ligand-expressing cancer cells, the binding of death ligands such as Fas ligand (FasL) and TRAIL to an increased number of death receptors due to treatment with cancer therapeutic agents may trigger the apoptotic signal leading to the death of cancer cells (autocrine mechanism). Moreover, upregulation of death receptors in cancer cells may cause these cells to become more susceptible targets for immune cells (i.e., NK and T cells) that express and secrete death ligands such as TRAIL. Therefore, cancer therapeutic agents with death receptor-inducing activity can sensitize cancer cells to death receptor-mediated immune clearance or surveillance. Similarly these agents can also enhance death receptor-based cancer

immunotherapy.[152-154]

Summary and Perspectives

Extensive studies have shown that many cancer therapeutic agents increase the expression of death receptors or activate death receptors. The question is whether modulation of death receptors plays any role in drug-induced apoptosis because it is generally thought that small molecules induce apoptosis through activation of the intrinsic apoptotic pathway. Some studies indeed suggest that certain drugs induce apoptosis via ligand-dependent or -independent activation of the death receptor-mediated extrinsic apoptotic pathway. To robustly demonstrate the role of death receptor activation in drug-induced apoptosis, establishment of cancer cell lines deficient with one (e.g., DR5), two (e.g., DR4 and DR5), or even three (e.g., DR4, DR5 and Fas) death receptors will be very helpful. These cell lines would also be valuable for screening cancer therapeutic agents that induce apoptosis through the death receptor-mediated extrinsic apoptotic pathway. The current technology of homologous recombination[155] makes possible such kind of studies.

Given that TRAIL and agonistic antibodies to DR4 and DR5 exhibit cancer therapeutic potential and their efficacies can be enhanced by small molecules, it will be important to develop small molecules that upregulate the expression of DR4 and/or DR5 and potentiate TRAIL-induced apoptosis, preferentially in human cancer cells independent of p53. To this end, DR4 or DR5 should be a good target for discovery of anticancer drugs. Some clinically-used drugs such as sulindac and celecoxib, which potently increase the expression of TRAIL death receptors and enhance TRAIL-induced apoptosis, have simple chemical structures and could be considered as lead compounds for further modification. In addition, an important step is to develop assays for screening agents that upregulate TRAIL death receptors. To do so, we need a better understanding of general mechanisms by which TRAIL death receptors are induced.

Certain cancer therapeutic agents themselves are weak inducers of apoptosis in cell culture, but potently upregulate the expression of death receptors and cooperative with exogenous TRAIL to induce apoptosis. Therefore, it is important to consider the in vivo situation where stromal cells may impact the growth of tumors and the response of tumor cells to therapeutic drugs. We may speculate that these death receptor-inducing agents can effectively inhibit the growth of tumors by inducing apoptosis through promotion of the interaction between death receptors (in tumor cells) and endogenous death ligands (from stromal cells or immune cells) in vivo. If this is true, these agents should not be very effective to treat tumors (i.e., murine tumors) developed from death ligand (e.g., TRAIL)-null animals. Therefore, it is important to demonstrate this issue in vivo. Currently TRAIL-null[156] and or FasL-null[157] mice are available and thus make these studies possible.

In the field of death receptor research, some discrepancies in the literature among different studies may be caused by antibodies from different sources, some of which are not specific (e.g., DR4) based on our experience. Therefore, it is important to carefully characterize some antibodies (e.g., through siRNA and recombinant proteins), particularly those for immunohistochemical detection of clinical specimens. In this way, we will avoid or minimize artifacts or confusion.

In conclusion, as we further our understanding of the modulation of death receptors by cancer therapeutic agents, we will be able to more effectively and selectively target cancer cells sensitive to death receptor-mediated apoptosis.

Acknowledgments

Works in author's laboratory were supported by the Georgia Cancer Coalition Distinguished Cancer Scholar award, the Department of Defense VITAL grant W81XWH-04-1-0142 (Project 4 to S.-Y. Sun), and the National Cancer Center head and neck cancer SPORE grant P50 CA128613-01 (Project 2 to S-Y Sun). S.-Y. Sun is a Georgia Cancer Coalition Distinguished Cancer Scholar. H.A. Elrod is a recipient of a fellowship from the American Cancer Society.

References

1. Schulze-Bergkamen H, Krammer PH. Apoptosis in cancer—Implications for therapy. Semin Oncol 2004; 31:90-119.
2. Ashkenazi A, Dixit VM. Death receptors: Signaling and modulation. Science 1998; 281:1305-8.
3. Almasan A, Ashkenazi A. Apo2L/TRAIL: Apoptosis signaling, biology, and potential for cancer therapy. Cytokine Growth Factor Rev 2003; 14:337-48.
4. Jo M, Kim TH, Seol DW, Esplen JE, Dorko K, Billiar TR, Strom SC. Apoptosis induced in normal human hepatocytes by tumor necrosis factor-related apoptosis-inducing ligand. Nat Med 2000; 6:564-7.
5. Lawrence D, Shahrokh Z, Marsters S, Achilles K, Shih D, Mounho B, Hillan K, Totpal K, DeForge L, Schow P, Hooley J, Sherwood S, Pai R, Leung S, Khan L, Gliniak B, Bussiere J, Smith CA, Strom SS, Kelley S, Fox JA, Thomas D, Ashkenazi A. Differential hepatocyte toxicity of recombinant Apo2L/TRAIL versions. Nat Med 2001; 7:383-5.
6. Ashkenazi A. Targeting death and decoy receptors of the tumour-necrosis factor superfamily. Nat Rev Cancer 2002; 2:420-30.
7. Rowinsky EK. Targeted induction of apoptosis in cancer management: The emerging role of tumor necrosis factor-related apoptosis-inducing ligand receptor activating agents. J Clin Oncol 2005; 23:9394-407.
8. Petak I, Houghton JA. Shared pathways: Death receptors and cytotoxic drugs in cancer therapy. Pathol Oncol Res 2001; 7:95-106.
9. Sheikh MS, Huang Y. Death receptors as targets of cancer therapeutics. Curr Cancer Drug Targets 2004; 4:97-104.
10. Yagita H, Takeda K, Hayakawa Y, Smyth MJ, Okumura K. TRAIL and its receptors as targets for cancer therapy. Cancer Sci 2004; 95:777-83.
11. Fesik SW. Promoting apoptosis as a strategy for cancer drug discovery. Nat Rev Cancer 2005; 5:876-85.
12. Wajant H, Gerspach J, Pfizenmaier K. Tumor therapeutics by design: Targeting and activation of death receptors. Cytokine Growth Factor Rev 2005; 16:55-76.
13. Zimmermann KC, Green DR. How cells die: Apoptosis pathways. J Allergy Clin Immunol 2001; 108:S99-103.
14. Ashkenazi A, Dixit VM. Apoptosis control by death and decoy receptors. Curr Opin Cell Biol 1999; 11:255-60.
15. Lavrik I, Golks A, Krammer PH. Death receptor signaling. J Cell Sci 2005; 118:265-7.
16. Wajant H. Death receptors. Essays Biochem 2003; 39:53-71.
17. Timmer T, de Vries EG, de Jong S. Fas receptor-mediated apoptosis: A clinical application? J Pathol 2002; 196:125-34.
18. Ozoren N, El-Deiry WS. Cell surface death receptor signaling in normal and cancer cells. Semin Cancer Biol 2003; 13:135-47.
19. Liu LG, Tanaka H, Ito K, Ito T, Sultana TA, Kyo T, Kimura A. Absence of gene mutation in TRAIL receptor 1 (TRAIL-R1) and TRAIL receptor 2 (TRAIL-R2) in chronic myelogenous leukemia and myelodysplastic syndrome, and analysis of mRNA Expressions of TRAIL and TRAIL-related genes in chronic myelogenous leukemia. Acta Haematol 2005; 113:113-23.
20. Adams J, Cuthbert-Heavens D, Bass S, Knowles MA. Infrequent mutation of TRAIL receptor 2 (TRAIL-R2/DR5) in transitional cell carcinoma of the bladder with 8p21 loss of heterozygosity. Cancer Lett 2005; 220:137-44.
21. Reesink-Peters N, Hougardy BM, van den Heuvel FA, Ten Hoor KA, Hollema H, Boezen HM, de Vries EG, de Jong S, van der Zee AG. Death receptors and ligands in cervical carcinogenesis: An immunohistochemical study. Gynecol Oncol 2005; 96:705-13.
22. Yamana K, Bilim V, Hara N, Kasahara T, Itoi T, Maruyama R, Nishiyama T, Takahashi K, Tomita Y. Prognostic impact of FAS/CD95/APO-1 in urothelial cancers: Decreased expression of Fas is associated with disease progression. Br J Cancer 2005; 93:544-51.
23. Horak P, Pils D, Haller G, Pribill I, Roessler M, Tomek S, Horvat R, Zeillinger R, Zielinski C, Krainer M. Contribution of epigenetic silencing of tumor necrosis factor-related apoptosis inducing ligand receptor 1 (DR4) to TRAIL resistance and ovarian cancer. Mol Cancer Res 2005; 3:335-43.
24. Hopkins-Donaldson S, Ziegler A, Kurtz S, Bigosch C, Kandioler D, Ludwig C, Zangemeister-Wittke U, Stahel R. Silencing of death receptor and caspase-8 expression in small cell lung carcinoma cell lines and tumors by DNA methylation. Cell Death Differ 2003; 10:356-64.

25. Min YJ, Lee JH, Choi SJ, Chi HS, Lee JS, Kim WK, Lee KH. Prognostic significance of Fas (CD95) and TRAIL receptors (DR4/DR5) expression in acute myelogenous leukemia. Leukemia research 2004; 28:359-65.
26. Spierings DC, de Vries EG, Timens W, Groen HJ, Boezen HM, de Jong S. Expression of TRAIL and TRAIL death receptors in stage III nonsmall cell lung cancer tumors. Clin Cancer Res 2003; 9:3397-405.
27. Koornstra JJ, Kleibeuker JH, van Geelen CM, Rijcken FE, Hollema H, de Vries EG, de Jong S. Expression of TRAIL (TNF-related apoptosis-inducing ligand) and its receptors in normal colonic mucosa, adenomas, and carcinomas. J Pathol 2003; 200:327-35.
28. van Geelen CM, Westra JL, de Vries EG, Boersma-van Ek W, Zwart N, Hollema H, Boezen HM, Mulder NH, Plukker JT, de Jong S, Kleibeuker JH, Koornstra JJ. Prognostic significance of tumor necrosis factor-related apoptosis-inducing ligand and its receptors in adjuvantly treated stage III colon cancer patients. J Clin Oncol 2006; 24:4998-5004.
29. Ullenhag GJ, Mukherjee A, Watson NF, Al-Attar AH, Scholefield JH, Durrant LG. Overexpression of FLIPL is an independent marker of poor prognosis in colorectal cancer patients. Clin Cancer Res 2007; 13:5070-5.
30. McCarthy MM, Sznol M, DiVito KA, Camp RL, Rimm DL, Kluger HM. Evaluating the expression and prognostic value of TRAIL-R1 and TRAIL-R2 in breast cancer. Clin Cancer Res 2005; 11:5188-94.
31. Tourneur L, Delluc S, Levy V, Valensi F, Radford-Weiss I, Legrand O, Vargaftig J, Boix C, Macintyre EA, Varet B, Chiocchia G, Buzyn A. Absence or low expression of fas-associated protein with death domain in acute myeloid leukemia cells predicts resistance to chemotherapy and poor outcome. Cancer Res 2004; 64:8101-8.
32. Chen G, Bhojani MS, Heaford AC, Chang DC, Laxman B, Thomas DG, Griffin LB, Yu J, Coppola JM, Giordano TJ, Lin L, Adams D, Orringer MB, Ross BD, Beer DG, Rehemtulla A. Phosphorylated FADD induces NF-kappaB, perturbs cell cycle, and is associated with poor outcome in lung adenocarcinomas. Proc Natl Acad Sci USA 2005; 102:12507-12.
33. Debatin KM, Krammer PH. Death receptors in chemotherapy and cancer. Oncogene 2004; 23:2950-66.
34. Pitti RM, Marsters SA, Lawrence DA, Roy M, Kischkel FC, Dowd P, Huang A, Donahue CJ, Sherwood SW, Baldwin DT, Godowski PJ, Wood WI, Gurney AL, Hillan KJ, Cohen RL, Goddard AD, Botstein D, Ashkenazi A. Genomic amplification of a decoy receptor for Fas ligand in lung and colon cancer. Nature 1998; 396:699-703.
35. Arakawa Y, Tachibana O, Hasegawa M, Miyamori T, Yamashita J, Hayashi Y. Frequent gene amplification and overexpression of decoy receptor 3 in glioblastoma. Acta Neuropathol (Berl) 2005; 109:294-8.
36. Shen HW, Gao SL, Wu YL, Peng SY. Overexpression of decoy receptor 3 in hepatocellular carcinoma and its association with resistance to Fas ligand-mediated apoptosis. World J Gastroenterol 2005; 11:5926-30.
37. Li H, Zhang L, Lou H, Ding I, Kim S, Wang L, Huang J, Di Sant'Agnese PA, Lei JY. Overexpression of decoy receptor 3 in precancerous lesions and adenocarcinoma of the esophagus. Am J Clin Pathol 2005; 124:282-7.
38. van Noesel MM, van Bezouw S, Salomons GS, Voute PA, Pieters R, Baylin SB, Herman JG, Versteeg R. Tumor-specific down-regulation of the tumor necrosis factor-related apoptosis-inducing ligand decoy receptors DcR1 and DcR2 is associated with dense promoter hypermethylation. Cancer Res 2002; 62:2157-61.
39. Shivapurkar N, Toyooka S, Toyooka KO, Reddy J, Miyajima K, Suzuki M, Shigematsu H, Takahashi T, Parikh G, Pass HI, Chaudhary PM, Gazdar AF. Aberrant methylation of trail decoy receptor genes is frequent in multiple tumor types. Int J Cancer 2004; 109:786-92.
40. Levine AJ. p53, the cellular gatekeeper for growth and division. Cell 1997; 88:323-31.
41. Bennett M, Macdonald K, Chan SW, Luzio JP, Simari R, Weissberg P. Cell surface trafficking of Fas: A rapid mechanism of p53-mediated apoptosis. Science 1998; 282:290-3.
42. Muller M, Wilder S, Bannasch D, Israeli D, Lehlbach K, Li-Weber M, Friedman SL, Galle PR, Stremmel W, Oren M, Krammer PH. p53 activates the CD95 (APO-1/Fas) gene in response to DNA damage by anticancer drugs. J Exp Med 1998; 188:2033-45.
43. Wu GS, Burns TF, McDonald IIIrd ER, Jiang W, Meng R, Krantz ID, Kao G, Gan DD, Zhou JY, Muschel R, Hamilton SR, Spinner NB, Markowitz S, Wu G, el-Deiry WS. KILLER/DR5 is a DNA damage-inducible p53-regulated death receptor gene. Nat Genet 1997; 17:141-3.
44. Takimoto R, El-Deiry WS. Wild-type p53 transactivates the KILLER/DR5 gene through an intronic sequence-specific DNA-binding site. Oncogene 2000; 19:1735-43.
45. Guan B, Yue P, Clayman GL, Sun SY. Evidence that the death receptor DR4 is a DNA damage-inducible, p53-regulated gene. J Cell Physiol 2001; 188:98-105.
46. Liu X, Yue P, Khuri FR, Sun SY. p53 upregulates death receptor 4 expression through an intronic p53 binding site. Cancer Res 2004; 64:5078-83.
47. Cheng J, Liu C, Koopman WJ, Mountz JD. Characterization of human Fas gene: Exon/intron organization and promoter region. J Immunol 1995; 154:1239-45.
48. Chan H, Bartos DP, Owen-Schaub LB. Activation-dependent transcriptional regulation of the human Fas promoter requires NF-kappaB p50-p65 recruitment. Mol Cell Biol 1999; 19:2098-108.
49. Li XR, Chong AS, Wu J, Roebuck KA, Kumar A, Parrillo JE, Rapp UR, Kimberly RP, Williams JW, Xu X. Transcriptional regulation of Fas gene expression by GA-binding protein and AP-1 in T cell antigen receptor.CD3 complex-stimulated T cells. J Biol Chem 1999; 274:35203-10.
50. Sheikh MS, Burns TF, Huang Y, Wu GS, Amundson S, Brooks KS, Fornace Jr AJ, el-Deiry WS. p53-dependent and -independent regulation of the death receptor KILLER/DR5 gene expression in response to genotoxic stress and tumor necrosis factor alpha. Cancer Res 1998; 58:1593-8.
51. Ravi R, Bedi GC, Engstrom LW, Zeng Q, Mookerjee B, Gelinas C, Fuchs EJ, Bedi A. Regulation of death receptor expression and TRAIL/Apo2L-induced apoptosis by NF-kappaB. Nat Cell Biol 2001; 3:409-16.
52. Shetty S, Graham BA, Brown JG, Hu X, Vegh-Yarema N, Harding G, Paul JT, Gibson SB. Transcription factor NF-kappaB differentially regulates death receptor 5 expression involving histone deacetylase 1. Mol Cell Biol 2005; 25:5404-16.
53. Guan B, Yue P, Lotan R, Sun SY. Evidence that the human death receptor 4 is regulated by activator protein 1. Oncogene 2002; 21:3121-9.
54. Yamaguchi H, Wang HG. CHOP is involved in endoplasmic reticulum stress-induced apoptosis by enhancing DR5 expression in human carcinoma cells. J Biol Chem 2004; 279:45495-502.
55. Yoshida T, Shiraishi T, Nakata S, Horinaka M, Wakada M, Mizutani Y, Miki T, Sakai T. Proteasome inhibitor MG132 induces death receptor 5 through CCAAT/enhancer-binding protein homologous protein. Cancer Res 2005; 65:5662-7.
56. Baritaki S, Katsman A, Chatterjee D, Yeung KC, Spandidos DA, Bonavida B. Regulation of tumor cell sensitivity to TRAIL-induced apoptosis by the metastatic suppressor Raf kinase inhibitor protein via Yin Yang 1 inhibition and death receptor 5 up-regulation. J Immunol 2007; 179:5441-53.
57. Baritaki S, Huerta-Yepez S, Sakai T, Spandidos DA, Bonavida B. Chemotherapeutic drugs sensitize cancer cells to TRAIL-mediated apoptosis: Up-regulation of DR5 and inhibition of Yin Yang 1. Mol Cancer Ther 2007; 6:1387-99.
58. Sun SY. Chemopreventive agent-induced modulation of death receptors. Apoptosis 2005; 10:1203-10.
59. Gibson SB, Oyer R, Spalding AC, Anderson SM, Johnson GL. Increased expression of death receptors 4 and 5 synergizes the apoptosis response to combined treatment with etoposide and TRAIL. Mol Cell Biol 2000; 20:205-12.
60. Nagane M, Pan G, Weddle JJ, Dixit VM, Cavenee WK, Huang HJ. Increased death receptor 5 expression by chemotherapeutic agents in human gliomas causes synergistic cytotoxicity with tumor necrosis factor-related apoptosis-inducing ligand in vitro and in vivo. Cancer Res 2000; 60:847-53.
61. Wen J, Ramadevi N, Nguyen D, Perkins C, Worthington E, Bhalla K. Antileukemic drugs increase death receptor 5 levels and enhance Apo-2L-induced apoptosis of human acute leukemia cells. Blood 2000; 96:3900-6.
62. Evdokiou A, Bouralexis S, Atkins GJ, Chai F, Hay S, Clayer M, Findlay DM. Chemotherapeutic agents sensitize osteogenic sarcoma cells, but not normal human bone cells, to Apo2L/TRAIL-induced apoptosis. Int J Cancer 2002; 99:491-504.
63. Shetty S, Gladden JB, Henson ES, Hu X, Villanueva J, Haney N, Gibson SB. Tumor necrosis factor-related apoptosis inducing ligand (TRAIL) up-regulates death receptor 5 (DR5) mediated by NFkappaB activation in epithelial derived cell lines. Apoptosis 2002; 7:413-20.
64. Longley DB, Wilson TR, McEwan M, Allen WL, McDermott U, Galligan L, Johnston PG. c-FLIP inhibits chemotherapy-induced colorectal cancer cell death. Oncogene 2006; 25:838-48.
65. Kristeleit R, Fong P, Aherne GW, de Bono J. Histone deacetylase inhibitors: Emerging anticancer therapeutic agents? Clin Lung Cancer 2005; 7(Suppl 1):S19-30.
66. Fandy TE, Shankar S, Ross DD, Sausville E, Srivastava RK. Interactive effects of HDAC inhibitors and TRAIL on apoptosis are associated with changes in mitochondrial functions and expressions of cell cycle regulatory genes in multiple myeloma. Neoplasia 2005; 7:646-57.
67. Guo F, Sigua C, Tao J, Bali P, George P, Li Y, Wittmann S, Moscinski L, Atadja P, Bhalla K. Cotreatment with histone deacetylase inhibitor LAQ824 enhances Apo-2L/tumor necrosis factor-related apoptosis inducing ligand-induced death inducing signaling complex activity and apoptosis of human acute leukemia cells. Cancer Res 2004; 64:2580-9.
68. Shankar S, Singh TR, Fandy TE, Luetrakul T, Ross DD, Srivastava RK. Interactive effects of histone deacetylase inhibitors and TRAIL on apoptosis in human leukemia cells: Involvement of both death receptor and mitochondrial pathways. Int J Mol Med 2005; 16:1125-38.
69. Nakata S, Yoshida T, Horinaka M, Shiraishi T, Wakada M, Sakai T. Histone deacetylase inhibitors upregulate death receptor 5/TRAIL-R2 and sensitize apoptosis induced by TRAIL/APO2-L in human malignant tumor cells. Oncogene 2004; 23:6261-71.
70. Butler LM, Liapis V, Bouralexis S, Welldon K, Hay S, Thai le M, Labrinidis A, Tilley WD, Findlay DM, Evdokiou A. The histone deacetylase inhibitor, suberoylanilide hydroxamic acid, overcomes resistance of human breast cancer cells to Apo2L/TRAIL. Int J Cancer 2006; 119:944-54.
71. Insinga A, Monestiroli S, Ronzoni S, Gelmetti V, Marchesi F, Viale A, Altucci L, Nervi C, Minucci S, Pelicci PG. Inhibitors of histone deacetylases induce tumor-selective apoptosis through activation of the death receptor pathway. Nat Med 2005; 11:71-6.
72. Nebbioso A, Clarke N, Voltz E, Germain E, Ambrosino C, Bontempo P, Alvarez R, Schiavone EM, Ferrara F, Bresciani F, Weisz A, de Lera AR, Gronemeyer H, Altucci L. Tumor-selective action of HDAC inhibitors involves TRAIL induction in acute myeloid leukemia cells. Nat Med 2005; 11:77-84.
73. Kim YH, Park JW, Lee JY, Kwon TK. Sodium butyrate sensitizes TRAIL-mediated apoptosis by induction of transcription from the DR5 gene promoter through Sp1 sites in colon cancer cells. Carcinogenesis 2004; 25:1813-20.
74. Rajkumar SV, Richardson PG, Hideshima T, Anderson KC. Proteasome inhibition as a novel therapeutic target in human cancer. J Clin Oncol 2005; 23:630-9.

75. He Q, Huang Y, Sheikh MS. Proteasome inhibitor MG132 upregulates death receptor 5 and cooperates with Apo2L/TRAIL to induce apoptosis in Bax-proficient and -deficient cells. Oncogene 2004; 23:2554-8.
76. Kabore AF, Sun J, Hu X, McCrea K, Johnston JB, Gibson SB. The TRAIL apoptotic pathway mediates proteasome inhibitor induced apoptosis in primary chronic lymphocytic leukemia cells. Apoptosis 2006.
77. Johnson TR, Stone K, Nikrad M, Yeh T, Zong WX, Thompson CB, Nesterov A, Kraft AS. The proteasome inhibitor PS-341 overcomes TRAIL resistance in Bax and caspase 9-negative or Bcl-xL overexpressing cells. Oncogene 2003; 22:4953-63.
78. Liu X, Yue P, Chen S, Hu L, Lonial S, Khuri FR, Sun SY. The proteasome inhibitor PS-341 (bortezomib) up-regulates DR5 expression leading to induction of apoptosis and enhancement of TRAIL-induced apoptosis despite up-regulation of c-FLIP and survivin expression in human NSCLC cells. Cancer Res 2007; 67:4981-8.
79. Meric JB, Rottey S, Olaussen K, Soria JC, Khayat D, Rixe O, Spano JP. Cyclooxygenase-2 as a target for anticancer drug development. Crit Rev Oncol Hematol 2006.
80. Huang Y, He Q, Hillman MJ, Rong R, Sheikh MS. Sulindac sulfide-induced apoptosis involves death receptor 5 and the caspase 8-dependent pathway in human colon and prostate cancer cells. Cancer Res 2001; 61:6918-24.
81. Jang TJ, Kang HJ, Kim JR, Yang CH. Nonsteroidal anti-inflammatory drug activated gene (NAG-1) expression is closely related to death receptor-4 and -5 induction, which may explain sulindac sulfide induced gastric cancer cell apoptosis. Carcinogenesis 2004; 25:1853-8.
82. Liu X, Yue P, Zhou Z, Khuri FR, Sun SY. Death receptor regulation and celecoxib-induced apoptosis in human lung cancer cells. J Natl Cancer Inst 2004; 96:1769-80.
83. Chen S, Liu X, Yue P, Schonthal AH, Khuri FR, Sun SY. CHOP-dependent DR5 induction and ubiquitin/proteasome-mediated c-FLIP downregulation contribute to enhancement of TRAIL-induced apoptosis by dimethyl-celecoxib in human nonsmall cell lung cancer cells. Mol Pharmacol 2007; 72:1269-79.
84. He Q, Luo X, Jin W, Huang Y, Reddy MV, Reddy EP, Sheikh MS. Celecoxib and a novel COX-2 inhibitor ON09310 upregulate death receptor 5 expression via GADD153/CHOP. Oncogene 2007.
85. Sun SY, Lotan R. Retinoids and their receptors in cancer development and chemoprevention. Crit Rev Oncol Hematol 2002; 41:41-55.
86. Garattini E, Gianni M, Terao M. Retinoid related molecules an emerging class of apoptotic agents with promising therapeutic potential in oncology: Pharmacological activity and mechanisms of action. Curr Pharm Des 2004; 10:433-48.
87. Sun SY, Yue P, Wu GS, El-Deiry WS, Shroot B, Hong WK, Lotan R. Mechanisms of apoptosis induced by the synthetic retinoid CD437 in human nonsmall cell lung carcinoma cells. Oncogene 1999; 18:2357-65.
88. Sun SY, Yue P, Wu GS, El-Deiry WS, Shroot B, Hong WK, Lotan R. Implication of p53 in growth arrest and apoptosis induced by the synthetic retinoid CD437 in human lung cancer cells. Cancer Res 1999; 59:2829-33.
89. Sun SY, Yue P, Hong WK, Lotan R. Induction of Fas expression and augmentation of Fas/Fas ligand-mediated apoptosis by the synthetic retinoid CD437 in human lung cancer cells. Cancer Res 2000; 60:6537-43.
90. Sun SY, Yue P, Chen X, Hong WK, Lotan R. The synthetic retinoid CD437 selectively induces apoptosis in human lung cancer cells while sparing normal human lung epithelial cells. Cancer Res 2002; 62:2430-6.
91. Sun SY, Yue P, Lotan R. Implication of multiple mechanisms in apoptosis induced by the synthetic retinoid CD437 in human prostate carcinoma cells. Oncogene 2000; 19:4513-22.
92. Sun SY, Yue P, Mao L, Dawson MI, Shroot B, Lamph WW, Heyman RA, Chandraratna RA, Shudo K, Hong WK, Lotan R. Identification of receptor-selective retinoids that are potent inhibitors of the growth of human head and neck squamous cell carcinoma cells. Clin Cancer Res 2000; 6:1563-73.
93. Farhana L, Dawson MI, Fontana JA. Apoptosis induction by a novel retinoid-related molecule requires nuclear factor-kappaB activation. Cancer Res 2005; 65:4909-17.
94. Zanchi C, Zuco V, Lanzi C, Supino R, Zunino F. Modulation of survival signaling pathways and persistence of the genotoxic stress as a basis for the synergistic interaction between the atypical retinoid ST1926 and the epidermal growth factor receptor inhibitor ZD1839. Cancer Res 2005; 65:2364-72.
95. Jin F, Liu X, Zhou Z, Yue P, Lotan R, Khuri FR, Chung LW, Sun SY. Activation of nuclear factor-kappaB contributes to induction of death receptors and apoptosis by the synthetic retinoid CD437 in DU145 human prostate cancer cells. Cancer Res 2005; 65:6354-63.
96. Cuello M, Coats AO, Darko I, Ettenberg SA, Gardner GJ, Nau MM, Liu JR, Birrer MJ, Lipkowitz S. N-(4-hydroxyphenyl) retinamide (4HPR) enhances TRAIL-mediated apoptosis through enhancement of a mitochondrial-dependent amplification loop in ovarian cancer cell lines. Cell Death Differ 2004; 11:527-41.
97. Kouhara J, Yoshida T, Nakata S, Horinaka M, Wakada M, Ueda Y, Yamagishi H, Sakai T. Fenretinide up-regulates DR5/TRAIL-R2 expression via the induction of the transcription factor CHOP and combined treatment with fenretinide and TRAIL induces synergistic apoptosis in colon cancer cell lines. Int J Oncol 2007; 30:679-87.
98. Xia Y, Wong NS, Fong WF, Tideman H. Upregulation of GADD153 expression in the apoptotic signaling of N-(4-hydroxyphenyl)retinamide (4HPR). Int J Cancer 2002; 102:7-14.
99. Kim DG, You KR, Liu MJ, Choi YK, Won YS. GADD153-mediated anticancer effects of N-(4-hydroxyphenyl)retinamide on human hepatoma cells. J Biol Chem 2002; 277:38930-8.
100. Samuel W, Kutty RK, Nagineni S, Vijayasarathy C, Chandraratna RA, Wiggert B. N-(4-hydroxyphenyl)retinamide induces apoptosis in human retinal pigment epithelial cells: Retinoic acid receptors regulate apoptosis, reactive oxygen species generation, and the expression of heme oxygenase-1 and Gadd153. J Cell Physiol 2006; 209:854-65.
101. Lovat PE, Oliverio S, Ranalli M, Corazzari M, Rodolfo C, Bernassola F, Aughton K, Maccarrone M, Hewson QD, Pearson AD, Melino G, Piacentini M, Redfern CP. GADD153 and 12-lipoxygenase mediate fenretinide-induced apoptosis of neuroblastoma. Cancer Res 2002; 62:5158-67.
102. Corazzari M, Lovat PE, Oliverio S, Pearson AD, Piacentini M, Redfern CP. Growth and DNA damage-inducible transcription factor 153 mediates apoptosis in response to fenretinide but not synergy between fenretinide and chemotherapeutic drugs in neuroblastoma. Mol Pharmacol 2003; 64:1370-8.
103. Anding AL, Chapman JS, Barnett DW, Curley Jr RW, Clagett-Dame M. The unhydrolyzable fenretinide analogue 4-hydroxybenzylretinone induces the proapoptotic genes *GADD153* (CHOP) and *Bcl-2*-binding component 3 (PUMA) and apoptosis that is caspase- dependent and independent of the retinoic acid receptor. Cancer Res 2007; 67:6270-7.
104. Meng RD, El-Deiry WS. p53-independent upregulation of KILLER/DR5 TRAIL receptor expression by glucocorticoids and interferon-gamma. Exp Cell Res 2001; 262:154-69.
105. Xia L, Chen D, Han R, Fang Q, Waxman S, Jing Y. Boswellic acid acetate induces apoptosis through caspase-mediated pathways in myeloid leukemia cells. Mol Cancer Ther 2005; 4:381-8.
106. Zou W, Liu X, Yue P, Zhou Z, Sporn MB, Lotan R, Khuri FR, Sun SY. c-Jun NH2-terminal kinase-mediated up-regulation of death receptor 5 contributes to induction of apoptosis by the novel synthetic triterpenoid methyl-2-cyano-3,12-dioxooleana-1, 9-dien-28-oate in human lung cancer cells. Cancer Res 2004; 64:7570-8.
107. Hyer ML, Croxton R, Krajewska M, Krajewski S, Kress CL, Lu M, Suh N, Sporn MB, Cryns VL, Zapata JM, Reed JC. Synthetic triterpenoids cooperate with tumor necrosis factor-related apoptosis-inducing ligand to induce apoptosis of breast cancer cells. Cancer Res 2005; 65:4799-808.
108. Shigeno M, Nakao K, Ichikawa T, Suzuki K, Kawakami A, Abiru S, Miyazoe S, Nakagawa Y, Ishikawa H, Hamasaki K, Nakata K, Ishii N, Eguchi K. Interferon-alpha sensitizes human hepatoma cells to TRAIL-induced apoptosis through DR5 upregulation and NF-kappa B inactivation. Oncogene 2003; 22:1653-62.
109. van Geelen CM, de Vries EG, Le TK, van Weeghel RP, de Jong S. Differential modulation of the TRAIL receptors and the CD95 receptor in colon carcinoma cell lines. Br J Cancer 2003; 89:363-73.
110. Oshima K, Yanase N, Ibukiyama C, Yamashina A, Kayagaki N, Yagita H, Mizuguchi J. Involvement of TRAIL/TRAIL-R interaction in IFN-alpha-induced apoptosis of Daudi B lymphoma cells. Cytokine 2001; 14:193-201.
111. Tan G, Gyllenhaal C, Soejarto DD. Biodiversity as a source of anticancer drugs. Curr Drug Targets 2006; 7:265-77.
112. Bush JA, Cheung Jr KJ, Li G. Curcumin induces apoptosis in human melanoma cells through a Fas receptor/caspase-8 pathway independent of p53. Exp Cell Res 2001; 271:305-14.
113. Deeb D, Jiang H, Gao X, Hafner MS, Wong H, Divine G, Chapman RA, Dulchavsky SA, Gautam SC. Curcumin sensitizes prostate cancer cells to tumor necrosis factor-related apoptosis-inducing ligand/Apo2L by inhibiting nuclear factor-kappaB through suppression of IkappaBalpha phosphorylation. Mol Cancer Ther 2004; 3:803-12.
114. Jung EM, Lim JH, Lee TJ, Park JW, Choi KS, Kwon TK. Curcumin sensitizes tumor necrosis factor-related apoptosis-inducing ligand (TRAIL)-induced apoptosis through reactive oxygen species-mediated upregulation of death receptor 5 (DR5). Carcinogenesis 2005; 26:1905-13.
115. Jung EM, Park JW, Choi KS, Lee HI, Lee KS, Kwon TK. Curcumin sensitizes tumor necrosis factor-related apoptosis-inducing ligand (TRAIL)-mediated apoptosis through CHOP-independent DR5 upregulation. Carcinogenesis 2006.
116. Kim H, Kim EH, Eom YW, Kim WH, Kwon TK, Lee SJ, Choi KS. Sulforaphane sensitizes tumor necrosis factor-related apoptosis-inducing ligand (TRAIL)-resistant hepatoma cells to TRAIL-induced apoptosis through reactive oxygen species-mediated up-regulation of DR5. Cancer Res 2006; 66:1740-50.
117. Matsui TA, Sowa Y, Yoshida T, Murata H, Horinaka M, Wakada M, Nakanishi R, Sakabe T, Kubo T, Sakai T. Sulforaphane enhances TRAIL-induced apoptosis through the induction of DR5 expression in human osteosarcoma cells. Carcinogenesis 2006.
118. Horinaka M, Yoshida T, Shiraishi T, Nakata S, Wakada M, Nakanishi R, Nishino H, Matsui H, Sakai T. Luteolin induces apoptosis via death receptor 5 upregulation in human malignant tumor cells. Oncogene 2005; 24:7180-9.
119. Hasegawa H, Yamada Y, Komiyama K, Hayashi M, Ishibashi M, Yoshida T, Sakai T, Koyano T, Kam TS, Murata K, Sugahara K, Tsuruda K, Akamatsu N, Tsukasaki K, Masuda M, Takasu N, Kamihira S. Dihydroflavonol BB-1, an extract of natural plant Blumea balsamifera, abrogates TRAIL resistance in leukemia cells. Blood 2006; 107:679-88.
120. Son YG, Kim EH, Kim JY, Kim SU, Kwon TK, Yoon AR, Yun CO, Choi KS. Silibinin sensitizes human glioma cells to TRAIL-mediated apoptosis via DR5 up-regulation and down-regulation of c-FLIP and survivin. Cancer Res 2007; 67:8274-84.
121. LaVallee TM, Zhan XH, Johnson MS, Herbstritt CJ, Swartz G, Williams MS, Hembrough WA, Green SJ, Pribluda VS. 2-methoxyestradiol up-regulates death receptor 5 and induces apoptosis through activation of the extrinsic pathway. Cancer Res 2003; 63:468-75.

122. Braeuninger S, Chamaon K, Kropf S, Mawrin C, Wiedemann FR, Hartig R, Schoeler S, Dietzmann K, Kirches E. Short incubation with 2-methoxyestradiol kills malignant glioma cells independent of death receptor 5 upregulation. Clin Neuropathol 2005; 24:175-83.
123. Wood L, Leese MP, Mouzakiti A, Purohit A, Potter BV, Reed MJ, Packham G. 2-MeOE2bisMATE induces caspase-dependent apoptosis in CAL51 breast cancer cells and overcomes resistance to TRAIL via cooperative activation of caspases. Apoptosis 2004; 9:323-32.
124. He Q, Lee DI, Rong R, Yu M, Luo X, Klein M, El-Deiry WS, Huang Y, Hussain A, Sheikh MS. Endoplasmic reticulum calcium pool depletion-induced apoptosis is coupled with activation of the death receptor 5 pathway. Oncogene 2002; 21:2623-33.
125. Huang L, Xu J, Li K, Zheng MH, Kumta SM. Thapsigargin potentiates TRAIL-induced apoptosis in giant cell tumor of bone. Bone 2004; 34:971-81.
126. Shiraishi T, Yoshida T, Nakata S, Horinaka M, Wakada M, Mizutani Y, Miki T, Sakai T. Tunicamycin enhances tumor necrosis factor-related apoptosis-inducing ligand-induced apoptosis in human prostate cancer cells. Cancer Res 2005; 65:6364-70.
127. Szegezdi E, Cahill S, Meyer M, O'Dwyer M, Samali A. TRAIL sensitisation by arsenic trioxide is caspase-8 dependent and involves modulation of death receptor components and Akt. Br J Cancer 2006; 94:398-406.
128. Tomasetti M, Andera L, Alleva R, Borghi B, Neuzil J, Procopio A. Alpha-tocopheryl succinate induces DR4 and DR5 expression by a p53-dependent route: Implication for sensitisation of resistant cancer cells to TRAIL apoptosis. FEBS Lett 2006; 580:1925-31.
129. Tomasetti M, Rippo MR, Alleva R, Moretti S, Andera L, Neuzil J, Procopio A. Alpha-tocopheryl succinate and TRAIL selectively synergise in induction of apoptosis in human malignant mesothelioma cells. Br J Cancer 2004; 90:1644-53.
130. Elrod HA, Lin YD, Yue P, Wang X, Lonial S, Khuri FR, Sun SY. The alkylphospholipid perifosine induces apoptosis of human lung cancer cells requiring inhibition of Akt and activation of the extrinsic apoptotic pathway. Mol Cancer Ther 2007; 6:2029-38.
131. Rajendran L, Simons K. Lipid rafts and membrane dynamics. J Cell Sci 2005; 118:1099-102.
132. Garcia A, Cayla X, Fleischer A, Guergnon J, Alvarez-Franco Canas F, Rebollo MP, Roncal F, Rebollo A. Rafts: A simple way to control apoptosis by subcellular redistribution. Biochimie 2003; 85:727-31.
133. Dimanche-Boitrel MT, Meurette O, Rebillard A, Lacour S. Role of early plasma membrane events in chemotherapy-induced cell death. Drug Resist Updat 2005; 8:5-14.
134. Gajate C, An F, Mollinedo F. Rapid and selective apoptosis in human leukemic cells induced by Aplidine through a Fas/CD95- and mitochondrial-mediated mechanism. Clin Cancer Res 2003; 9:1535-45.
135. Gajate C, Mollinedo F. Cytoskeleton-mediated death receptor and ligand concentration in lipid rafts forms apoptosis-promoting clusters in cancer chemotherapy. J Biol Chem 2005; 280:11641-7.
136. Gajate C, Fonteriz RI, Cabaner C, Alvarez-Noves G, Alvarez-Rodriguez Y, Modolell M, Mollinedo F. Intracellular triggering of Fas, independently of FasL, as a new mechanism of antitumor ether lipid-induced apoptosis. Int J Cancer 2000; 85:674-82.
137. Gajate C, Mollinedo F. The antitumor ether lipid ET-18-OCH(3) induces apoptosis through translocation and capping of Fas/CD95 into membrane rafts in human leukemic cells. Blood 2001; 98:3860-3.
138. Gajate C, Del Canto-Janez E, Acuna AU, Amat-Guerri F, Geijo E, Santos-Beneit AM, Veldman RJ, Mollinedo F. Intracellular triggering of Fas aggregation and recruitment of apoptotic molecules into Fas-enriched rafts in selective tumor cell apoptosis. J Exp Med 2004; 200:353-65.
139. Gajate C, Mollinedo F. Edelfosine and perifosine induce selective apoptosis in multiple myeloma by recruitment of death receptors and downstream signaling molecules into lipid rafts. Blood 2007; 109:711-9.
140. Delmas D, Rebe C, Lacour S, Filomenko R, Athias A, Gambert P, Cherkaoui-Malki M, Jannin B, Dubrez-Daloz L, Latruffe N, Solary E. Resveratrol-induced apoptosis is associated with Fas redistribution in the rafts and the formation of a death-inducing signaling complex in colon cancer cells. J Biol Chem 2003; 278:41482-90.
141. Delmas D, Rebe C, Micheau O, Athias A, Gambert P, Grazide S, Laurent G, Latruffe N, Solary E. Redistribution of CD95, DR4 and DR5 in rafts accounts for the synergistic toxicity of resveratrol and death receptor ligands in colon carcinoma cells. Oncogene 2004; 23:8979-86.
142. Lacour S, Hammann A, Grazide S, Lagadic-Gossmann D, Athias A, Sergent O, Laurent G, Gambert P, Solary E, Dimanche-Boitrel MT. Cisplatin-induced CD95 redistribution into membrane lipid rafts of HT29 human colon cancer cells. Cancer Res 2004; 64:3593-8.
143. Psahoulia FH, Drosopoulos KG, Doubravska L, Andera L, Pintzas A. Quercetin enhances TRAIL-mediated apoptosis in colon cancer cells by inducing the accumulation of death receptors in lipid rafts. Mol Cancer Ther 2007; 6:2591-9.
144. Martin S, Phillips DC, Szekely-Szucs K, Elghazi L, Desmots F, Houghton JA. Cyclooxygenase-2 inhibition sensitizes human colon carcinoma cells to TRAIL-induced apoptosis through clustering of DR5 and concentrating death-inducing signaling complex components into ceramide-enriched caveolae. Cancer Res 2005; 65:11447-58.
145. Vanoosten RL, Moore JM, Ludwig AT, Griffith TS. Depsipeptide (FR901228) enhances the cytotoxic activity of TRAIL by redistributing TRAIL receptor to membrane lipid rafts. Mol Ther 2005; 11:542-52.
146. Altucci L, Rossin A, Raffelsberger W, Reitmair A, Chomienne C, Gronemeyer H. Retinoic acid-induced apoptosis in leukemia cells is mediated by paracrine action of tumor-selective death ligand TRAIL. Nat Med 2001; 7:680-6.
147. Clarke N, Jimenez-Lara AM, Voltz E, Gronemeyer H. Tumor suppressor IRF-1 mediates retinoid and interferon anticancer signaling to death ligand TRAIL. Embo J 2004; 23:3051-60.
148. Wang Q, Ji Y, Wang X, Evers BM. Isolation and molecular characterization of the 5'-upstream region of the human TRAIL gene. Biochem Biophys Res Commun 2000; 276:466-71.
149. Wang Q, Wang X, Hernandez A, Hellmich MR, Gatalica Z, Evers BM. Regulation of TRAIL expression by the phosphatidylinositol 3-kinase/Akt/GSK-3 pathway in human colon cancer cells. J Biol Chem 2002; 277:36602-10.
150. Wajant H, Pfizenmaier K, Scheurich P. TNF-related apoptosis inducing ligand (TRAIL) and its receptors in tumor surveillance and cancer therapy. Apoptosis 2002; 7:449-59.
151. Wajant H. CD95L/FasL and TRAIL in tumour surveillance and cancer therapy. Cancer Treat Res 2006; 130:141-65.
152. Takeda K, Stagg J, Yagita H, Okumura K, Smyth MJ. Targeting death-inducing receptors in cancer therapy. Oncogene 2007; 26:3745-57.
153. Simons MP, Nauseef WM, Griffith TS. Neutrophils and TRAIL: Insights into BCG immunotherapy for bladder cancer. Immunologic research 2007; 39:79-93.
154. Shanker A, Sayers T. Sensitizing tumor cells to immune-mediated cytotoxicity. Adv Exp Med Biol 2007; 601:163-71.
155. Bunz F. Human cell knockouts. Curr Opin Oncol 2002; 14:73-8.
156. Cretney E, Takeda K, Yagita H, Glaccum M, Peschon JJ, Smyth MJ. Increased susceptibility to tumor initiation and metastasis in TNF-related apoptosis-inducing ligand-deficient mice. J Immunol 2002; 168:1356-61.
157. Embree-Ku M, Boekelheide K. FasL deficiency enhances the development of tumors in p53+/- mice. Toxicol Pathol 2002; 30:705-13.

9-*cis*-Retinoic Acid Treatment Increases Serum Concentrations of α-Tocopherol in Former Smokers

Ji-Youn Han,[1] Diane D. Liu,[2] J. Jack Lee,[2] Jonathan Kurie,[1] Reuben Lotan,[1] Waun K. Hong,[1] and Ho-Young Lee[1]

Departments of [1]Thoracic/Head and Neck Medical Oncology and [2]Biostatistics and Applied Mathematics, University of Texas M.D. Anderson Cancer Center, Houston, Texas

ABSTRACT

Purpose: **Low serum concentrations of antioxidants may be associated with an increased risk of cancer. Based on the accumulated evidence, we hypothesized that retinoids would elevate serum α-tocopherol. This study was designed to determine whether 9-*cis*-retinoic acid (9-*cis*-RA), the most common chemopreventive agent, could alter serum α-tocopherol in former smokers. Because hyperlipidemia is a known side effect of retinoids, we also evaluated the association between serum α-tocopherol and lipids in the same population.**

Experimental Design: **Subjects who had stopped smoking at least 12 months before the study were randomly assigned to receive oral 9-*cis*-RA or placebo daily for 3 months. Clinical information and blood samples were obtained monthly; serum α-tocopherol concentrations were measured by high-performance liquid chromatography and lipid levels by enzymatic assays before treatment and every month during the treatment.**

Results: **Of the 149 subjects in the study, 113 completed 3 months of treatment and provided samples for evaluation of serum α-tocopherol. Serum α-tocopherol levels in the 9-*cis*-RA group ($n = 52$) were higher after treatment ($r = 0.445$, $P < 0.01$) than before. The incidences of grade ≥2 hypertriglyceridemia and hypercholesterolemia were higher in the 9-*cis*-RA group than in the placebo group ($P = 0.0005$ and $P = 0.01$, respectively), but there were no serious complications related to hyperlipidemia.**

Conclusions**: Treatment of former smokers with 9-*cis*-RA significantly increased their serum α-tocopherol levels, and this could be a benefit. In addition, serum α-tocopherol could serve as a biomarker for 9-*cis*-RA treatment.**

Received 10/11/04; revised 11/24/04; accepted 12/20/04.

Grant support: NIH grants U19 CA68437 (W. Hong) and 1R01 CA100816-01A1 (H.-Y. Lee), American Cancer Society grant RSG-04-082-01-TBE (H.-Y. Lee) and Department of Defense grants DAMD17-01-1-0689 and W81XWH-04-1-0142-01-VITAL (W. Hong). The costs of publication of this article were defrayed in part by the payment of page charges. This article must therefore be hereby marked *advertisement* in accordance with 18 U.S.C. Section 1734 solely to indicate this fact.

Requests for reprints: Ho-Young Lee, Department of Thoracic/Head and Neck Medical Oncology, Unit 432, University of Texas M.D. Anderson Cancer Center, 1515 Holcombe Boulevard, Houston, TX 77030. Phone: 713-792-3782; Fax: 713-796-8655; E-mail: hlee@mdanderson.org.

INTRODUCTION

Because lung cancer is the leading cause of cancer-related death worldwide (1, 2), chemoprevention has become an increasingly important priority in the effort to reduce its incidence (3). Thus far, the most often used chemopreventive agents for aerodigestive tract cancers have been retinoids (4), which bind and transactivate retinoic acid (RA) receptors (RAR) and retinoid X receptors (RXR), both of which belong to the superfamily of steroid nuclear receptors. Among the retinoids, all-*trans*-RA is selective for RARs, and 9-*cis*-RA binds both RARs and RXRs (5). In contrast, 13-*cis*-RA binds to neither receptor type but is thought to bind to the retinoid receptors after intracellular stereoisomerization to all-*trans*-RA or 9-*cis*-RA (6).

Several findings have shown the potential of retinoids as cancer chemopreventive agents (7–12). First, 9-*cis*-RA has shown antiproliferative activity against a broad range of neoplastic cells, including those from prostate cancer (7), breast cancer (8, 9), leukemia and lymphoma (10), lung cancer (11), and head and neck cancer (12). Second, 9-*cis*-RA had substantial *in vivo* anticarcinogenic activity in rat mammary glands (13, 14) and rat colons (15). Finally, in patients with a history of cancer of the head and neck region, 13-*cis*-RA treatment reduced the incidence of second primary tumors and reversed leukoplakia (i.e., premalignant oral lesions; refs. 16, 17).

Despite these promising findings, enthusiasm for the use of retinoids as chemopreventive agents for lung cancer waned after two large randomized clinical trials ended with disappointing results. The Alpha-Tocopherol, Beta Carotene Cancer Prevention Study, which tested the efficacy of the antioxidant dietary supplements α-tocopherol and β-carotene, actually showed that β-carotene significantly increased lung cancer incidence and mortality over the levels observed in participants not taking it (18). The detrimental effects of β-carotene were confirmed by the Beta-Carotene and Retinol Efficacy Trial, which revealed a 28% higher rate of lung cancer and 17% higher overall death rate in participants taking β-carotene than in those not taking the supplement (19). However, further analyses showed that the adverse effects of β-carotene were restricted to active smokers in both trials (20). In addition, there was some evidence of a benefit from retinoid treatment in nonsmokers and former smokers (21), suggesting that the response to retinoids differs in current and former smokers. Supporting these findings, 13-*cis*-RA treatment of current smokers had no effect on bronchial squamous metaplasia, a histologic abnormality associated with smoking, whereas 13-*cis*-RA treatment inhibited bronchial squamous metaplasia in former smokers (22). Wang et al. (23) reported that cigarette smoke and high doses of β-carotene induced a decrease in RA concentrations and RAR-β expression and an increase in cell proliferation and the expression of activating protein 1 family members (c-Jun and c-Fos) and cyclin D1 in the lung tissue of ferrets. Liu et al. (24) showed that the oxidative metabolites of β-carotene generated by smoke-induced production of cytochrome *P*450, which interferes with RA metabolism

by down-regulating RAR signaling and suppressing RAR-β expression. We recently showed in a chemopreventive trial that 9-*cis*-RA could benefit former smokers (25) by increasing RAR-β expression and decreasing metaplasia relative to the findings in the control group. These findings suggest that current and former smokers had different responses to retinoids and that retinoids, especially 9-*cis*-RA, have potential as chemopreventive agents in former smokers. Based on this notion, we sought to identify other benefits of 9-*cis*-RA for former smokers.

Antioxidants also have potential as chemopreventive agents (26–28), and low serum levels of antioxidants are associated with an increased risk of cancer (29–31). Because a correlation has been observed between serum levels of retinoids and the antioxidant α-tocopherol (32), we hypothesized that serum levels of α-tocopherol would be elevated in people who had been treated with retinoids. To test our hypothesis, we retrospectively analyzed data from a previously published three-arm, randomized, double-blinded, placebo-controlled trial comparing 9-*cis*-RA, 13-*cis*-RA plus α-tocopherol, and placebo daily for 3 months (25). Because hyperlipidemia is a common side effect of retinoid treatment (33, 34), we also evaluated possible associations between serum α-tocopherol and lipid levels in the same subjects.

MATERIALS AND METHODS

Subjects. The original trial design, the method of determining compliance with the trial protocol and the monitoring of toxic effects of the drugs have been previously described (25). That study was a three-arm, randomized, double-blinded, placebo-controlled trial comparing 9-*cis*-RA (100 mg), 13-*cis*-RA (1 mg/kg) plus α-tocopherol (1,200 IU), and placebo daily for 3 months (25). RAR-β was detected in 69.7% of all baseline biopsy samples, and metaplasia was evident in 6.9% of all baseline samples from 240 subjects enrolled between November 1995 and May 2001. RAR-β expression was restored and metaplasia was reduced after treatment in the 9-*cis*-RA group. After adjustment for years of smoking, packs per day smoked, and metaplasia, treatment with 9-*cis*-RA but not with 13-*cis*-RA plus α-tocopherol led to a statistically significant increase in RAR-β expression compared with placebo. All subjects were former smokers, defined as people with a smoking history of at least 20 pack-years who had stopped smoking at least 1 year before entering the study. To be eligible, subjects had to have adequate renal, hematologic, and hepatic function and must not have taken more than 25,000 IU of vitamin A or other retinoids per day within 3 months of study entry. Subjects with a prior smoking-related cancer were eligible if they had been tumor-free for 6 months before enrollment. Subjects were required to abstain from consuming vitamin supplements during the study. Before being randomly assigned to a treatment group, all eligible subjects provided written informed consent. This study was approved by the institutional review board at the University of Texas M.D. Anderson Cancer Center and by the U.S. Department of Health and Human Services. Subjects were seen monthly and evaluated for compliance with the trial protocol and for drug-related toxic effects. Serum cotinine levels were determined at baseline and at 3 and 6 months after treatment initiation to document compliance with smoking abstinence during the trial. The treatment duration of 3 months was chosen on the basis of toxicity data from prior phase I trials that involved 9-*cis*-RA treatment (35, 36). In the current analysis, we did not include the group treated with 13-*cis*-RA plus α-tocopherol to avoid possible confounding effects from oral supplementary α-tocopherol.

Specimen Collection. To analyze changes in α-tocopherol levels and toxicity, blood specimens (10 mL) were drawn from each participant at the beginning of the study and then monthly during treatment. Blood was collected in heparinized tubes and transported immediately to the laboratory, where the specimens were separated and processed. Serum was collected after centrifugation of the blood at 1,500 rpm for 10 minutes at room temperature and was stored at −80°C until it was needed for testing.

High-Performance Liquid Chromatography Analysis for α-Tocopherol. Methods for extracting analytes from serum, quality control variables and the high-performance liquid chromatography (HPLC) methods for analyzing α-tocopherol in serum have been published previously (29). Briefly, a hexane extract of 0.4 mL of serum was injected onto a 3-μm C-18 Spherisorb ODS-2 HPLC column (1050 HPLC system; Hewlett-Packard, Avondale, PA) and eluted with an isocratic solvent consisting of 73% acetonitrile, 12% tetrahydrofuran, 8% methanol, 7% water, 0.025% ammonium acetate, and 0.05% diethylamine (v/v) at 1.2 mL/min. α-Tocopherol was detected at 292 nm. The HPLC system was fully automated and equipped with quaternary pumps, an electronic degasser, insulated column housing, an automatic sampler diode array detector, and software to run the system and perform data management. The coefficient of variation for the pooled quality control samples for all of the analytes was ≤10%.

Biochemical Assays. Serum levels of triglycerides and cholesterol were measured with routine enzymatic methods on a random access clinical chemistry system (Dimension, Dade Behring International, Inc., Newark, NJ).

Statistical Analyses. The Wilcoxon rank sum test and Kruskal-Wallis test were used to test the equal medians of continuous variables between two treatment groups. Either the χ^2 test or Fisher's exact test was used to test the association between two categorical variables. Because the distributions of α-tocopherol were skewed, the differences in α-tocopherol levels between treatment groups were tested with the Wilcoxon rank sum test. Changes in serum α-tocopherol levels from baseline levels were tested separately at each subsequent patient visit (i.e., at 1-, 2-, 3-, and 6-month visits) and in each group by using the Wilcoxon rank sum test. All statistical tests were two-sided, with a 5% type I error rate. Statistical analysis was done with standard statistical software, including SAS Release 8.1 (SAS Institute, Cary, NC) and S-Plus 2000 (Mathsoft, Inc., Seattle, WA).

RESULTS

Characteristics of Subjects. The characteristics of the eligible subjects have been described in detail previously (25). Two hundred forty subjects were entered into the original clinical trial, of whom 226 were eligible to be randomly assigned into one of the three treatment groups (9-*cis*-RA, 13-*cis*-RA plus α-tocopherol, or placebo); 149 of these participants

Table 1 Baseline characteristics of subjects according to treatment group

	Placebo (n = 61)	9-*cis*-RA (n = 52)	P*
Gender (%)			
Male	37 (60.7)	27 (51.9)	0.35
Female	24 (39.3)	25 (48.1)	
Race (%)			
White	52 (85.3)	49 (94.2)	0.35
African	6 (9.8)	2 (3.9)	
Hispanic	3 (4.9)	1 (1.9)	
Oriental	0	0	
Smoking-related cancer (%)			
No	54 (88.5)	48 (92.3)	0.54
Yes	7 (11.5)	4 (7.7)	
Age			
Mean ± SD	58.1 ± 8.9	55.7 ± 9.2	0.12
Median (range)	58.8 (34.9-73.6)	54.9 (35.9-74.5)	
Body mass index			
Mean ± SD	27.8 ± 4.1	28.1 ± 5.38	0.92
Median (range)	27.1 (20.6-39.4)	27.3 (19.4-44.4)	
Smoking years			
Mean ± SD	29.1 ± 9.8	27.3 ± 9.5	0.39
Median (range)	30 (15-50)	26 (10-50)	
Packs per day			
Mean ± SD	1.7 ± 0.7	1.9 ± 0.8	0.23
Median (range)	1.5 (1-4)	2 (0.8-4)	
Pack-years			
Mean ± SD	50.2 ± 27.2	52.6 ± 30.5	0.94
Median (range)	42.5 (20-135)	42 (20-136)	
Smoking quit years			
Mean ± SD	10.4 ± 8.8	11.0 ± 8.7	0.56
Median (range)	10.1 (1.1-35.2)	7.8 (1.0-38.2)	
Cholesterol			
Mean ± SD	205.8 ± 37.5	206.9 ± 31.9	0.74
Median (range)	198 (141-292)	205 (151-283)	
Triglyceride			
Mean ± SD	142.4 ± 65.9	152.2 ± 60.4	0.39
Median (range)	132 (43-309)	136 (58-282)	

*The Wilcoxon rank sum test was performed to test of continuous variables between two treatment groups. The χ^2 test (for sex) and Fisher's exact test (for race and smoking-related cancer) were performed to test the association between two categorical variables.

(the subjects of the current analysis) had been randomly assigned to either the placebo or the 9-*cis*-RA groups, and 113 of them completed 3 months of treatment. The characteristics of the evaluable subjects are summarized in Table 1. Each treatment group was well balanced for age, sex, race, history of smoking-related cancer, number of pack-years, number of years since stopping smoking, body mass index, and serum levels of cholesterol and triglycerides. Serum cotinine levels drawn at registration, at 3 and 6 months showed that >95% of the participants had serum levels in the range of nonsmokers (<1.0 ng/mL) or passive smokers (1-20 ng/mL) at all three measurement times.

Effects of 9-*cis*-RA Treatment on Serum α-Tocopherol Level. We investigated whether 9-*cis*-RA treatment affected the serum α-tocopherol level. We found that baseline serum α-tocopherol level of the placebo group was not different from that of 9-*cis*-RA treatment group (Table 2). Serum α-tocopherol concentrations significantly increased over time in the 9-*cis*-RA group but not in the placebo group, peaking 1 month after the start of treatment and maintaining this level throughout treatment. This finding indicates that 9-*cis*-RA can increase serum α-tocopherol concentrations in former smokers.

Table 2 α-Tocopherol level at baseline and during treatment of 9-*cis*-RA

	α-Tocopherol level, median (range, μg/dl)		
	Placebo (n = 61)	9-*cis*-RA (n = 52)	P
Baseline	13,017 (2,241-45,620)	14,002 (6,162-33,779)	0.37*
1st month	11,818 (1,311-22,306)	16,456 (7,883-48,877)	0.005†
2nd month	11,454 (5,770-26,506)	15,847 (7,607-46,132)	0.003†
3rd month	12,354 (6,788-23,150)	15,381 (8,461-49,383)	0.01†

*P was obtained from the Wilcoxon rank sum test.
†P was obtained from repeated-measures analysis using a mixed model.

To determine whether subject characteristics may have affected their baseline serum α-tocopherol level, we evaluated possible associations between the characteristics listed in Table 1 and baseline serum α-tocopherol levels. Gender, race, body mass index, number of pack-years, number of years since stopping smoking, and levels of cholesterol were not associated with the baseline serum α-tocopherol level (Table 3). However, the baseline serum triglyceride level and age were significantly associated with higher baseline serum α-tocopherol levels. When adjusted for body mass index, the effects of both age (P = 0.02) and baseline serum triglyceride level (P = 0.008) on the baseline serum α-tocopherol concentration were found to be significant by regression analysis.

Effects of 9-*cis*-RA Treatment on Serum Concentrations of Triglycerides and Cholesterol. We tested the serum levels of lipids, including triglycerides and cholesterol, in all participants. During treatment, serum levels of lipids were significantly increased in 9-*cis*-RA group and decreased when treatment with 9-*cis*-RA was stopped (Fig 1). In testing the

Table 3 Association between baseline α-tocopherol level and demographic characteristics

Characteristics	α-Tocopherol level, mean ± SD (range, ng/mL)	P*
Gender		
Male	15,090 ± 6,967.4 (7,086-45,620)	0.96
Female	14,399 ± 5,993.7 (2,241-33,779)	
Race		
White	15,097 ± 6,701.4 (2,241-45,620)	0.24
African	12,796 ± 5,252.6 (7,086-21,245)	
Hispanic	11,047 ± 2,203.1 (8,484-13,792)	
Age (y)		
<60	13,885 ± 6,287.0 (5,575-45,620)	0.02
≥60	16,380 ± 6,758.4 (2,241-33,586)	
Body mass index		
Nonobese (<28)	14,040 ± 5,036.2 (5,575-29,889)	0.47
Obese (≥28)	15,531 ± 6,844.1 (6,162-33,779)	
Pack-years		
<40	14,357 ± 6,742.6 (5,575-45,620)	0.47
≥40	15,135 ± 6,415.0 (2,241-33,779)	
Smoking quit years		
<10	13,827 ± 5,515.5 (2,241-30,742)	0.15
≥10	15,921 ± 7,472.0 (5,575-45,620)	
Cholesterol (mg/dl)		
<200	14,060 ± 5,560.5 (5,575-33,586)	0.32
≥200	15,419 ± 6,992.6 (2,241-45,620)	
Triglyceride (mg/dl)		
≤135	12,562 ± 4,550.0 (2,241-25,603)	0.008
>135	16,440 ± 7,146.4 (7,681-45,620)	

*P was obtained from the Wilcoxon rank sum test.

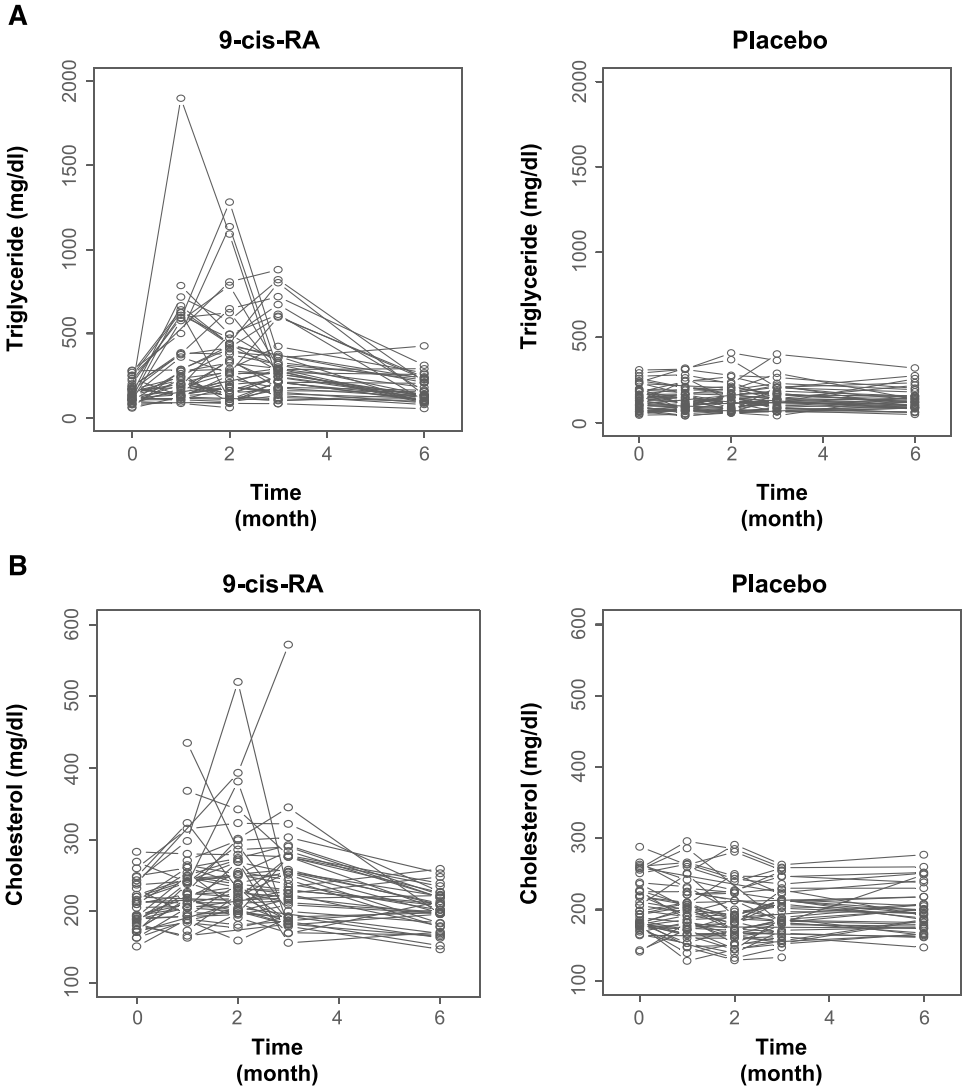

Fig. 1 Effect of 9-*cis*-RA on the serum levels of (*A*) triglycerides and (*B*) cholesterol after 3 months of treatment.

serum levels of lipids, including triglycerides and cholesterol, in all participants, we found no significant difference in the incidence of grade 1 hyperlipidemia between the 9-*cis*-RA group and the placebo group during treatment (Table 4). However, 9-*cis*-RA group showed significantly more subjects of grade ≥2 hypertriglyceridemia and hypercholesterolemia than the placebo group ($P < 0.0001$). Of 52 evaluable subjects in the 9-*cis*-RA group, 22 (42%, $P = 0.0001$) and 12 (23%, $P = 0.0001$) developed grade >2 hypertriglyceridemia and hypercholesterolemia, respectively. One of the participants in the 9-*cis*-RA group experienced grade 4 hypertriglyceridemia and discontinued treatment. However, no serious complications related to hypertriglyceridemia or hypercholesterolemia, such as cardiovascular events, pancreatitis, or death, were experienced in either group, and the hyperlipidemia disappeared after discontinuation of 9-*cis*-RA treatment. Finally, we evaluated whether the modulation of serum lipid levels was associated with modulation of serum α-tocopherol levels during 3 months of 9-*cis*-RA treatment. The modulation of serum α-tocopherol levels in the 9-*cis*-RA treatment group was significantly associated with the changes in serum levels of triglyceride (Fig. 2*A*) and cholesterol (Fig. 2*B*).

DISCUSSION

To our knowledge, this is the first report showing that 9-*cis*-RA affects serum α-tocopherol levels and that serum α-tocopherol levels correlated with serum lipid levels in the setting of a chemoprevention trial. Specifically, daily doses of 9-*cis*-RA increased serum concentrations of α-tocopherol, a well-known antioxidant, in former smokers who had not smoked for at least 1 year.

It has been suggested that an imbalance between oxidants and antioxidants results in a chronic state of oxidative stress that could contribute to various human diseases, including cancer (37). In fact, reactive oxygen species are constantly generated by ionizing and UV radiation, activation of chemical carcinogens, and the presence of heavy metal carcinogens, and these reactive oxygen species can damage DNA and thus cause mutations that can lead to cancers (38). Antioxidants protect cells from DNA damage by directly removing these

Table 4 The incidence of hypertriglyceridemia or hypercholesterolemia according to treatment group

National Cancer Institute Common Toxicity Criteria	Placebo (n = 61)	9-*cis*-RA (n = 52)	P*
Hypertriglyceridemia			
Grade 1 (>2.5 × ULN)	28	23	<0.0001
Grade 2 (>2.5-5.0 × ULN)	2	15	
Grade 3 (>5.0-10 × ULN)	0	6	
Grade 4 (>10 × ULN)	0	1	
Hypercholesterolemia			
Grade 1 (>ULN-300 mg/dl)	22	24	<0.0001
Grade 2 (>300-400 mg/dl)	0	8	
Grade 3 (>400-500 mg/dl)	0	2	
Grade 4 (>500 mg/dl)	0	2	

Abbreviation: ULN, upper limit of normal range.
*P value was obtained from the Fisher's exact test.

reactive oxygen species thus reducing DNA damage and potentially decreasing tumorigenesis. Indeed, several studies have already shown the cancer chemopreventive properties of antioxidants (39). For example, dietary supplementation with α-tocopherol has been shown to prevent exercise-induced DNA damage (40), and results from a randomized phase II chemoprevention trial showed that α-tocopherol decreased oxidative DNA damage (41). The use of α-tocopherol to prevent human cancer has been evaluated for lung cancer, oral leukoplakia, colorectal polyps, and prostate cancer (30, 39, 41, 42). In a separate study, vitamin C, vitamin E, and β-carotene supplementation also significantly reduced endogenous oxidative DNA damage in lymphocytes and increased resistance to oxidative damage induced by hydrogen peroxide (43). Taken together, these findings suggest that 9-*cis*-RA can induce potential cancer chemopreventive activities in former smokers by increasing α-tocopherol levels.

We found age to be significantly associated with higher baseline serum α-tocopherol levels, an observation also found in other cohort studies (30, 44, 45). The positive association between α-tocopherol levels and age can be explained by age-related changes in the metabolism and transport of α-tocopherol; for example, the activity of lipoprotein lipase, an enzyme that releases α-tocopherol from chylomicrons and transfers it to tissues, has been shown to decrease with age (30). We also noted a positive relationship between baseline triglyceride and α-tocopherol levels. Because α-tocopherol is preferentially bound by the hepatic tocopherol binding protein, which is incorporated into both low- and high-density lipoproteins (44, 46), increases in serum triglyceride levels could be expected in association with increased serum α-tocopherol levels. Baseline serum cholesterol levels also seemed associated with baseline serum α-tocopherol levels, but this apparent relationship was not statistically significant, perhaps because baseline serum cholesterol levels were distributed over a narrow range. Because hyperlipidemia, especially hypertriglyceridemia, is a well-known effect of the clinical use of retinoids, we evaluated serum lipid concentrations and found that hypertriglyceridemia and hypercholesterolemia developed in 42% and 23% of patients, all former smokers, treated with 9-*cis*-RA, respectively, proportions that are consistent with previous findings (47, 48). Moreover, elevation of serum α-tocopherol concentrations was significantly

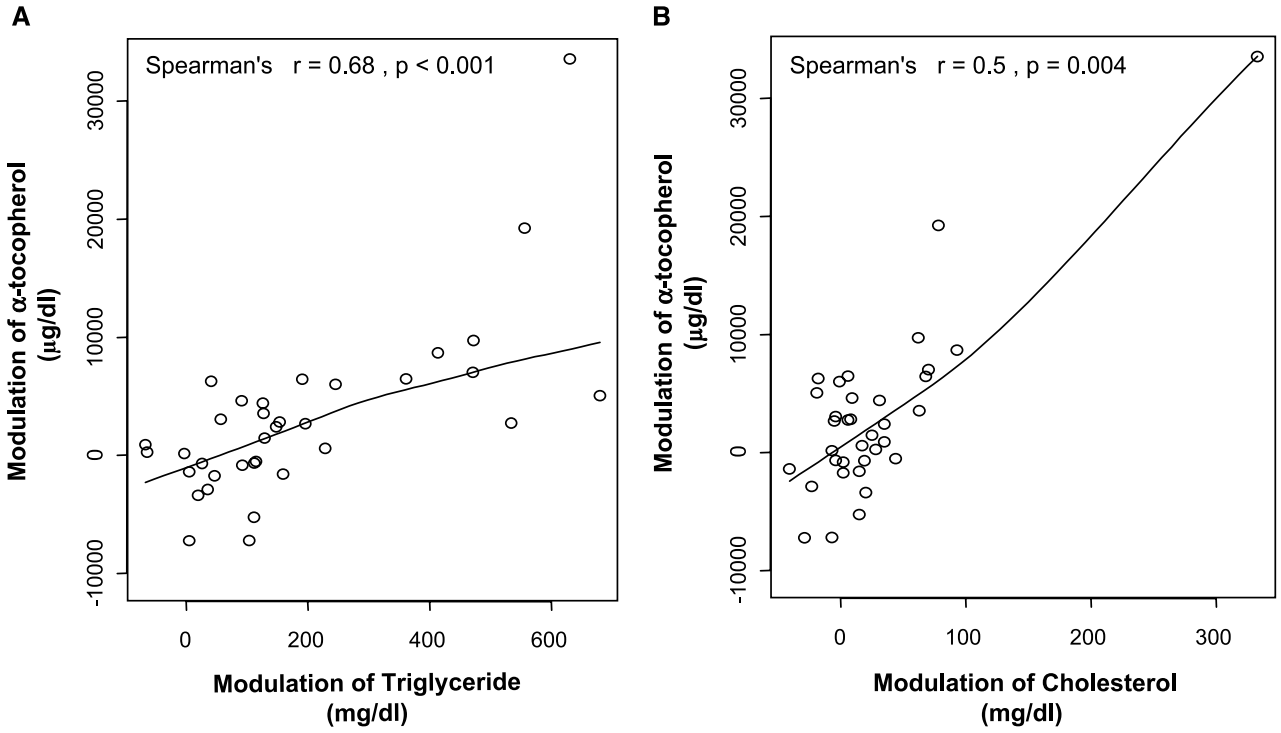

Fig. 2 The correlation between changes in serum levels of lipids and changes in serum levels of α-tocopherol level in the 9-*cis*-RA and placebo treatment groups. Wilcoxon rank sum test was performed to-tocopherol level (3-month value minus baseline value) compared with the changes in the median (*A*) triglyceride (3-month value minus baseline value) (r = 0.68, P < 0.001) and (*B*) cholesterol (3-month value minus baseline value) (r = 0.5, P = 0.004) levels.

associated with elevated levels of lipids in this group. A plausible explanation for this finding is the unique binding characteristics of 9-*cis*-RA to retinoid receptors that have transcription activities. Several studies have provided evidence that retinoids induce hyperlipidemia by activating RAR, RXR, or both (49–51). In one study, the simultaneous activation of RAR and RXR by panagonists induced 2- to 3-fold higher levels of serum triglycerides than did activation of RAR alone (51). Vu-Dac et al. (52) reported that RXR activation increased the expression of apo C-III, a key player in plasma triglyceride metabolism. Furthermore, 9-*cis*-RA induces the expression of the ATP-binding cassette transporter A1, a major regulator of peripheral cholesterol efflux and plasma high-density lipoprotein metabolism and increases apo A-I-mediated cholesterol efflux, thereby increasing the cholesterol concentration in the blood (53, 54). These data indicate that RAR and RXR ligands can act synergistically to induce high serum concentrations of lipids, suggesting that hyperlipidemia may be a greater issue for 9-*cis*-RA, an RAR/RXR panagonist, than for other RAs (6).

The risk of hyperlipidemia resulting from retinoid treatment in our chemoprevention trial was not clear. More small dense low-density lipoprotein particles are present in the blood in hyperlipidemia, and these particles are more susceptible to oxidation and are associated with enhanced peroxidation products (55). A high serum level of α-tocopherol, which breaks the chain reaction of lipid peroxidation by donating a hydrogen atom to the reactive oxygen species, could result in the formation of a relatively stable α-tocopherol radical that is thought to be recycled by ascorbate and ubiquinol (56, 57), suggesting that the ability of 9-*cis*-RA to modulate serum α-tocopherol concentrations may protect cells from increased concentrations of lipid peroxidants. Indeed, no serious complications related to hypertriglyceridemia or hypercholesterolemia, such as cardiovascular problems, pancreatitis, or death, were experienced in the subjects treated with 9-*cis*-RA in our study. Only one patient with grade 4 hypertriglyceridemia stopped 9-*cis*-RA treatment, and even that patient had no hyperlipidemia-associated complications. Furthermore, measurements of serum lipid levels after treatment was discontinued showed normalization of lipid levels in all subjects. However, considering recent findings that the risk of lung cancer is higher in recent former smokers than in current smokers (58), the inclusion of subjects (albeit few) with prior cancers and recent smoking cessation might have clouded our data. Therefore, cognizance of the potential cardiovascular risk should be well advised when oral supplementation of agents that increase serum α-tocopherol levels is considered for chemoprevention trial in a group of former smokers. Close monitoring of symptoms and signs of hyperlipidemia and the use of lipid- and cholesterol-lowering agents would be recommended for subjects taking 9-*cis*-RA for long periods. In addition, further study is needed to clarify the relationship between hyperlipidemia and retinoid treatment and to define the adequate duration of retinoid treatment in a chemoprevention trial.

In summary, to our knowledge, our results show for the first time that 9-*cis*-RA treatment increased serum α-tocopherol levels in former smokers. From the perspective of directing future public health initiatives, our current findings are important because increasing serum levels of the antioxidant may inhibit cell proliferation and angiogenesis and stimulate apoptosis and immune function (59–61). Additional work is warranted to determine whether other antioxidants, such as vitamin C, vitamin A, and β-carotene, are regulated by 9-*cis*-RA treatment in former smokers and whether the changes in α-tocopherol levels induced by 9-*cis*-RA correlate with their ability to reduce the risk of lung cancer in former smokers.

REFERENCES

1. Stewart AK, Bland KI, McGinnis LS Jr, et al. Clinical highlights from the National Cancer Data Base, 2000. CA Cancer J Clin 2000;50:171–83.

2. Parkin DM, Pisani P, Ferlay J. Estimates of the worldwide incidence of 25 major cancers in 1990. Int J Cancer 1999;80:827–41.

3. Tsao AS, Kim ES, Hong WK. Chemoprevention of cancer. CA Cancer J Clin 2004;54:150–80.

4. Lippman SM, Lee JJ, Karp DD, et al. Randomized phase III intergroup trial of isotretinoin to prevent second primary tumors in stage I non-small-cell lung cancer. J Natl Cancer Inst 2001;93:605–18.

5. Sun SY, Lotan R. Retinoids and their receptors in cancer development and chemoprevention. Crit Rev Oncol Hematol 2002;41:41–55.

6. Marchetti MN, Sampol E, Bun H, et al. *In vitro* metabolism of three major isomers of retinoic acid in rats. Intersex and interstrain comparison. Drug Metab Dispos 1997;25:637–46.

7. Blutt SE, Allegretto EA, Pike JW, et al. 1,25-Dihydroxyvitamin D3 and 9-*cis*-retinoic acid act synergistically to inhibit the growth of LNCaP prostate cells and cause accumulation of cells in G_1. Endocrinology 1997;138:1491–7.

8. Rubin M, Fenig E, Rosenauer A, et al. 9-*cis*-Retinoic acid inhibits growth of breast cancer cells and down-regulates estrogen receptor RNA and protein. Cancer Res 1994;54:6549–56.

9. Gottardis MM, Lamph WW, Shalinsky DR, et al. The efficacy of 9-*cis*-retinoic acid in experimental models of cancer. Breast Cancer Res Treat 1996;38:85–96.

10. Lutzky J, Vujicic M, Yamanishi DT, et al. Antiproliferative effects of all-*trans*-retinoic acid (tRA) and 9-*cis*-retinoic acid (9-cisRA) on human lymphoid cell lines [abstract]. Proceedings of the American Association for Cancer Res 1993;34:292.

11. Guzey M, Demirpence E, Criss W, et al. Effects of retinoic acid (all-*trans* and 9-*cis*) on tumor progression in small-cell lung carcinoma. Biochem Biophys Res Commun 1998;242:369–75.

12. Giannini F, Maestro R, Vukosavljevic T, et al. All-*trans*, 13-*cis*, and 9-*cis* retinoic acids induce a fully reversible growth inhibition in HNSCC cell lines: implications for *in vivo* retinoic acid use. Int J Cancer 1997;70:194–200.

13. Anzano MA, Byers SW, Smith JM, et al. Prevention of breast cancer in the rat with 9-*cis*-retinoic acid as a single agent and in combination with tamoxifen. Cancer Res 1994;54:4614–7.

14. Anzano MA, Peer CW, Smith JM, et al. Chemoprevention of mammary carcinogenesis in the rat: combined use of raloxifene and 9-*cis*-retinoic acid. J Natl Cancer Inst 1996;88:123–5.

15. Zheng Y, Kramer PM, Olson G, et al. Prevention by retinoids of azoxymethane-induced tumors and aberrant crypt foci and their modulation of cell proliferation in the colon of rats. Carcinogenesis 1997;18:2119–25.

16. Hong WK, Sporn MB. Recent advances in chemoprevention of cancer. Science 1997;278:1073–7.

17. Hong WK, Endicott J, Itri LM, et al. 13-cis-retinoic acid in the treatment of oral leukoplakia. N Eng J Med 1986;315:1501-5.

18. The Alpha-Tocopherol, Beta Carotene Cancer Prevention Study Group. The effect of vitamin E and β carotene on the incidence of lung cancer and other cancers in male smokers. N Engl J Med 1994;330:1029–35.

19. Omenn GS, Goodman GE, Thornquist MD, et al. Effects of a combination of β carotene and vitamin A on lung cancer and cardiovascular disease. N Engl J Med 1996;334:1150–5.

20. Albanes D, Heinonen OP, Taylor PR, et al. α-tocopherol and β-carotene supplements and lung cancer incidence in the Alpha-Tocopherol, Beta-Carotene Cancer Prevention Study: effects of base-line characteristics and study compliance. J Natl Cancer Inst 1996;88:1560–70.

21. Lippman SM, Lee JJ, Karp DD, et al. Randomized phase III intergroup trial of isotretinoin to prevent second primary tumors in stage I non-small-cell lung cancer. J Natl Cancer Inst 2001;93:605–18.

22. Lee JS, Lippman SM, Benner SE, et al. Randomized placebo-controlled trial of isotretinoin in chemoprevention of bronchial squamous metaplasia. J Clin Oncol 1994;12:937–45.

23. Wang XD, Liu C, Bronson RT, et al. Retinoid signaling and activator protein-1 expression in ferrets given β-carotene supplements and exposed to tobacco smoke. J Natl Cancer Inst 1999;91:60–6.

24. Liu C, Russell RM, Wang XD. Exposing ferrets to cigarette smoke and a pharmacological dose of β-carotene supplementation enhance *in vitro* retinoic acid catabolism in lungs via induction of cytochrome *P*450 enzymes. J Nutr 2003;133:173–9.

25. Kurie JM, Lotan R, Lee JJ, et al. Treatment of former smokers with 9-*cis*-retinoic acid reverses loss of retinoic acid receptor-β expression in the bronchial epithelium: results from a randomized placebo-controlled trial. J Natl Cancer Inst 2003;95:206–14.

26. Sawant SS, Kandarkar SV. Role of vitamins C and E as chemopreventive agents in the hamster cheek pouch treated with the oral carcinogen-DMBA. Oral Dis 2000;6:241–7.

27. Trickler D, Shklar G. Prevention by vitamin E of experimental oral carcinogenesis. J Natl Cancer Inst 1987;78:165–9.

28. Ross D, Moldeus P. Antioxidant defense system and oxidative stress. In: Vigo-Pelfrey C, editors. Membrane lipid oxidation. Boca Raton (FL): CRC Press; 1990. p. 151–70.

29. Goodman GE, Schaffer S, Omenn GS, Chen C, King I. The association between lung and prostate cancer risk, and serum micronutrients: results and lessons learned from β-carotene and retinol efficacy trial. Cancer Epidemiol Biomarkers Prev 2003;12:518–26.

30. Woodson K, Tangrea JA, Barrett MJ, Virtamo J, Taylor PR, Albanes D. Serum α-tocopherol and subsequent risk of lung cancer among male smokers. J Natl Cancer Inst 1999;91:1738–43.

31. Taylor PR, Qiao YL, Abnet CC. Prospective study of serum vitamin E levels and esophageal and gastric cancers. J Natl Cancer Inst 2003 Sep 17;95:1414–6.

32. Basile G, Gangemi S, Lo Balbo C, et al. Correlation between serum retinol and α-tocopherol levels in centenarians. J Nutr Sci Vitaminol (Tokyo) 2003;49:287–8.

33. Bershad S, Rubinstein A, Paterniti JR, et al. Changes in plasma lipids and lipoproteins during isotretinoin therapy for acne. N Engl J Med 1985;313:981–5.

34. Lowe NJ, David M. New retinoids for dermatologic diseases. Uses and toxicity. Dermatol Clin 1988;6:539–52.

35. Kurie JM, Lee JS, Griffin T, et al. Phase I trial of 9-*cis* retinoic acid in adults with solid tumors. Clin Cancer Res 1996;2:287–93.

36. Miller VA, Rigas JR, Benedetti FM, et al. Initial clinical trial of the retinoid receptor pan agonist 9-*cis* retinoic acid. Clin Cancer Res 1996;2:471–5.

37. Hu JJ, Chi CX, Frenkel K, et al. α-tocopherol dietary supplement decreases titers of antibody against 5-hydroxymethyl-2′-deoxyuridine (HMdU). Cancer Epidemiol Biomarkers Prev 1999;8:693–8.

38. Frenkel K. Role of active oxygen species in carcinogenesis. In: Bertino JR, editor. Encyclopedia of cancer. San Diego (CA): Academic Press; 1997. p. 233–45.

39. Benner SE, Wargovich MJ, Lippman SM, et al. Reduction in oral mucosa micronuclei frequency following α-tocopherol treatment of oral leukoplakia. Cancer Epidemiol Biomarkers Prev 1994;3:73–6.

40. Hartmann A, Niess AM, Grunert-Fuchs M, et al. Vitamin E prevents exercise-induced DNA damage. Mutat Res 1995;346:195–202.

41. McKeown-Eyssen G, Holloway C, Jazmaji V, et al. A randomized trial of vitamins C and E in the prevention of recurrence of colorectal polyps. Cancer Res 1988;48:4701–5.

42. Heinonen O, Albanes D, Virtamo J, et al. Prostate cancer and supplementation with α-tocopherol and β-carotene: incidence and mortality in a controlled trial. J Natl Cancer Inst 1998;90:440–6.

43. Duthie SJ, Ma A, Ross MA, Collins A. Antioxidant supplementation decreases oxidative DNA damage in human lymphocytes. Cancer Res 1996;56:1291–5.

44. White E, Kristal AR, Shikany JM, et al. Correlates of serum α- and γ-tocopherol in the Women's Health Initiative. Ann Epidemiol 2001;11:136–44.

45. Papas A, Stacewicz-Sapuntzakis M, Lagiou P, Bamia C, Chloptsios Y, Trichopoulou A. Plasma retinol and tocopherol levels in relation to demographic, lifestyle and nutritional factors of plant origin in Greece. Br J Nutr 2003;89:83–7.

46. Traber MG, Sies H. Vitamin E in humans: demand and delivery. Annu Rev Nutr 1996;16:321–47.

47. Bershad S, Rubinstein A, Paterniti JR, et al. Changes in plasma lipids and lipoproteins during isotretinoin therapy for acne. N Engl J Med 1985;313:981–5.

48. Lowe NJ, David M. New retinoids for dermatologic diseases. Uses and toxicity. Dermatol Clin 1988;6:539–52.

49. Standeven AM, Beard RL, Johnson AT, et al. Retinoid-induced hypertriglyceridemia in rats is mediated by retinoic acid receptors. Fundam Appl Toxicol 1996;33:264–71.

50. Rigas JR, Miller VA, Levine DM, et al. Lipoprotein alterations in patients treated with novel retinoids [abstract]. Proceedings of the American Association of Cancer Research 1995;36.

51. Standeven AM, Thacher SM, Yuan YD, et al. Retinoid X receptor agonist elevation of serum triglycerides in rats by potentiation of retinoic acid receptor agonist induction or by action as single agents. Biochem Pharmacol 2001;62:1501–9.

52. Vu-Dac N, Gervois P, Torra IP, et al. Retinoids increase human apo C-III expression at the transcriptional level via the retinoid X receptor: contribution to the hypertriglyceridemic action of retinoids. J Clin Invest 1998;102:625–32.

53. Koldamova RP, Lefterov IM, Ikonomovic MD, et al. 22*R*-Hydroxycholesterol and 9-*cis*-retinoic acid induce ATP-binding cassette transporter A1 expression and cholesterol efflux in brain cells and decrease amyloid β secretion. J Biol Chem 2003;278:13244–56.

54. Mascrez B, Ghyselinck NB, Watanabe M, et al. Ligand-dependent contribution of RXRβ to cholesterol homeostasis in Sertoli cells. EMBO Rep 2004;5:285–90.

55. de Graaf J, Hak-Lemmers HL, Hectors MP, et al. Enhanced susceptibility to *in vitro* oxidation of the dense low density lipoprotein subfraction in healthy subjects. Arterioscler Thromb 1991;11:298–306.

56. Oostenbrug GS, Mensink RP, Al MD, et al. Maternal and neonatal plasma antioxidant levels in normal pregnancy, and the relationship with fatty acid unsaturation. Br J Nutr 1998;80:67–73.

57. De Vriese SR, Dhont M, Christophe AB. Oxidative stability of low density lipoproteins and vitamin E levels increase in maternal blood during normal pregnancy. Lipids 2001;36:361–6.

58. Ebbert JO, Yang P, Vachon CM, et al. Lung cancer risk reduction after smoking cessation: observations from a prospective cohort of women. J Clin Oncol 2003;921–6.

59. Sigounas G, Anagnostou A, Steiner M. DL-α-Tocopherol induces apoptosis in erythroleukemia, prostate, and breast cancer cells. Nutr Cancer 1997;28:30–5.

60. Shklar G, Schwartz JL. Vitamin E inhibits experimental carcinogenesis and tumour angiogenesis. Eur J Cancer B Oral Oncol 1996;32B:114–9.

61. Meydani SN, Beharka AA. Recent developments in vitamin E and immune response. Nutr Rev 1996;56:S49–58.

Cell Motility and the Cytoskeleton 63:41–52 (2006)

Comparison of β-Tubulin mRNA and Protein Levels in 12 Human Cancer Cell Lines

Laree Hiser,[1] Ashish Aggarwal,[2] Rebekah Young,[1] Anthony Frankfurter,[3] Anthony Spano,[3] John J. Correia,[2] and Sharon Lobert[1,2]*

[1]*School of Nursing, University of Mississippi Medical Center, Jackson, Mississippi*
[2]*Department of Biochemistry, University of Mississippi Medical Center, Jackson, Mississippi*
[3]*Department of Biology, University of Virginia, Charlottesville, Virginia*

Antimitotic drugs are chemotherapeutic agents that bind tubulin and microtubules. Resistance to these drugs is a major clinical problem. One hypothesis is that the cellular composition of tubulin isotypes may predict the sensitivity of a tumor to antimitotics. Reliable and sensitive methods for measuring tubulin isotype levels in cells and tissues are needed to address this hypothesis. Quantitative measurements of tubulin isotypes have frequently relied upon inferring protein amounts from mRNA levels. To determine whether this approach is justified, protein and mRNA levels of β-tubulin isotypes from 12 human cancer cell lines were measured. This work focused on only β-tubulin isotypes because we had readily available monoclonal antibodies for quantitative immunoblots. The percentage of β-tubulin isotype classes I, II, III, and IVa + IVb mRNA and protein were compared. For β-tubulin class I that comprises >50% of the β-tubulin protein in 10 of the 12 cell lines, there was good agreement between mRNA and protein percentages. Agreement between mRNA and protein was also found for β-tubulin class III. For β-tubulin classes IVa + IVb, we observed higher protein levels compared to mRNA levels. β-Tubulin class II protein was found in only four cell lines and in very low abundance. We conclude that quantitative Western blotting is a reliable method for measuring tubulin isotype levels in human cancer cell lines. Inferring protein amounts from mRNA levels should be done with caution, since the correspondence is not one-to-one for all tubulin isotypes. Cell Motil. Cytoskeleton 63:41–52, 2006.

Key words: tubulin isotypes; microtubules; tubulin; β-tubulin

INTRODUCTION

Quantitative measurement of drug target proteins is essential for developing chemotherapeutic agents and understanding mechanisms that underlie drug resistance. Quantitative (real-time) reverse transcription polymerase chain reaction (qRT-PCR) is an established method for reliably measuring mRNA levels and may be useful for describing alterations in drug targets if protein levels can be inferred from mRNA levels. However, for many proteins, this is not a valid approach [Gygi et al., 1999; Nicoletti et al., 2001]. To study changes in drug target levels that may be associated with drug resistance to anti-

Abbreviations used: MBP, maltose binding protein; MDR, multidrug resistance; NCI, National Cancer Institute.

L. Hiser and A. Aggarwal contributed equally to this manuscript.

*Correspondence to: Sharon Lobert, School of Nursing, University of Mississippi Medical Center, 2500 N. State St., Jackson, MS 39216, USA. E-mail: slobert@son.umsmed.edu

Received 17 August 2005; accepted 17 November 2005

Published online 16 December 2005 in Wiley InterScience (www.interscience.wiley.com).
DOI: 10.1002/cm.20109

mitotic drugs, we wanted to determine whether mRNA levels could be used to accurately predict protein levels.

The ability of anticancer agents to destroy tumors is severely hampered by drug resistance that occurs initially or develops after prolonged or repeated exposure of cells and tissues to these drugs. In advanced-stage metastatic cancers, where treatment options are few, this problem is devastating. Important drugs used to treat solid and hematological tumors are antimitotic agents: taxanes (paclitaxel or docetaxel) and vinca alkaloids (vinblastine, vincristine, vinorelbine or vinflunine). Antimitotic drugs bind tubulin, a major protein in microtubules, and halt cell division at metaphase. Their effectiveness is thought to result from alterations of microtubule dynamics in mitotic spindles, thus preventing spindle assembly or interrupting the movement of sister chromatids toward the spindle poles [Dhamodharan et al., 1995; Yvon et al., 1999].

The drug receptor of antimitotic agents, tubulin, is a structurally heterogeneous 100,000 dalton αβ heterodimer. Six or seven genes encode α-tubulin isotypes, and seven genes encode β-tubulin isotypes [Sullivan and Cleveland, 1986; Sullivan, 1988]. Antimitotics interact with β-tubulin, which consists of seven isotype classes distinguished by the last 15–20 amino acids at the carboxyl termini [reviewed in Correia and Lobert, 2001].

We present here a quantitative comparison of β-tubulin isotype mRNA and protein levels (β-tubulin classes I, II, III, and IVa + IVb) in 12 human cancer cell lines. qRT-PCR was used to measure mRNA levels of all seven classes of β-tubulin isotypes. Quantitative immunoblotting was done to measure β-tubulin isotype protein levels. β-Tubulin classes I and IVa + IVb proteins were the most abundant. The mRNA and protein levels of β-tubulin class I were found to be in good agreement. β-Tubulin classes IVa + IVb made up a larger fraction of the total protein than of the total mRNA for 11 of the 12 cell lines. β-Tubulin class III protein was found at low levels that corresponded to mRNA levels, although the relationship was not one-to-one.

MATERIALS AND METHODS

Cell Culture

Twelve cell lines were selected on the basis of their relative sensitivities to vinblastine and paclitaxel, as reported by the National Cancer Institute (NCI) Developmental Therapeutics Program Human Tumor Cell Line Screen (http://dtp.nci.nih.gov/docs/cancer/cancer_data.html). Pairs or groups of cells with reported drug sensitivities that differed significantly were selected. Only one (HCT-15) is reported to have relatively high levels of *p*-glycoprotein/MDR1, a membrane-bound pump known to extrude drugs such as paclitaxel and vinblastine from cells [Alvarez et al., 1995; http://dtp.nci.nih.gov/docs/compare/cellmdr.html]. Cell lines were purchased from American Type Culture Collection (Manassas, VA), except for HOP 18, which was kindly provided by NCI-Frederick Cancer Division of Cancer Treatment and Diagnosis Tumor/Cell Line Repository (Frederick, MD). Cells were cultured according to the suppliers' recommendations, with the exception of MDA-MB-231 and Malme-3M, which were grown in RPMI-1640 rather than Leibovitz's L-15 medium.

Determination of IC_{50} Values

We determined IC_{50} values (concentration at which cell proliferation is reduced by 50%) for each cell line using two independent methods: cell counting and an assay for mitochondrial respiration. Duplicate 12-well plates (5000 cells/well) were set up for each cell counting experiment, and two to four independent experiments were done for each drug (vinblastine or paclitaxel) and cell line. Cells were incubated for 24 h to permit adherence and then exposed to serial dilutions (between one log unit above and below the predicted IC_{50} value) of vinblastine or paclitaxel for 48 h, released using trypsin, and counted in a hemocytometer using trypan blue to exclude nonviable cells. For control wells, an appropriate amount of PBS or dimethyl sulfoxide for vinblastine and paclitaxel, respectively, was added. Data were plotted using Origin 7.0 (OriginLab, Northampton, MA) as cell number vs. drug concentration. Data were fit to first-order exponential decay, and IC_{50} values were calculated.

The cell line sensitivities to vinblastine and paclitaxel were also determined using an assay for mitochondrial respiration. Cells were plated in 96-well microtiter plates at 8000 cells/well (10,000 cells/well for Malme-3M). Duplicate plates constituted each experiment; and two to four independent experiments were done for each drug (vinblastine or paclitaxel) and cell line. Cells were incubated for 24 h, and then the medium was replaced with fresh medium containing appropriate concentrations of drug or solvent. After 72 h, the medium was removed from the wells and 100 μl of CellTiter 96® AQ_{ueous} One solution (Promega, Madison, WI) diluted 1:5 with medium was added. This solution utilizes 3-(4,5-dimethylthiazol-2-yl)-5-(3-carboxymethoxyphenyl)-2-(4-sulfophenyl)-2H-tetrazolium (MTS, inner salt) in a colorometric reaction that is a linear measure of mitochondrial respiration. The plates were incubated 2 h, and absorbance at 490 nm was read using a microplate reader. Absorbance values were corrected by subtracting baseline values obtained from wells with no cells. IC_{50} values were determined as described for the cell counting assay.

Quantitative Reverse Transcription Polymerase Chain Reaction

Two-step qRT-PCR was used to determine the amount of mRNA present for each β-tubulin isotype (classes I, II, III, IVa, IVb, V, and VI) in all 12 cell lines. Cells were cultured as described earlier, total RNA was extracted, and qRT-PCR experiments were carried out using primers and protocols described previously [Dozier et al., 2003]. Briefly, qRT-PCR was performed on triplicate samples from at least two independent cell preps using SYBR® Green I (Invitrogen, Carlsbad, CA) as the detection method. The amount of β-tubulin isotype mRNA in a known amount of total RNA, determined by A_{260} measurements, was calculated using standard curves.

Quantitative Immunoblots

We developed a quantitative immunoblot assay for tubulin that is sensitive and highly reproducible. Cell lysates were prepared from 10–20 million cells by douncing on ice in 1 ml PBS with a protease inhibitor cocktail (Complete Protease Inhibitor Cocktail Tablets, Roche, Indianapolis, IN). Lysates were spun briefly in a microcentrifuge to remove membranes and mixed 1:1 with SDS sample buffer prior to electrophoresis. After electrophoresis, proteins were transferred to polyvinylidene difluoride (PVDF) membranes, incubated with primary antibody (1–2 mg/ml) at 1:2,500–1:10,000 dilutions overnight at 4°C, and developed using a horseradish peroxidase-conjugated secondary antibody. We used monoclonal antibodies that recognize individual tubulin isotypes: SAP4G5, anti-β-tubulin class I (Sigma-Aldrich, St. Louis, MO); 7B9, anti-β-tubulin class II; TUJ1, anti-β-tubulin class III; and 10A2, anti-β-tubulin classes IVa + IVb. The reactivity and specificity of SAP4G5, 7B9, and TUJ1 have been previously described [Lee et al., 1990; Lobert et al., 1995, 1998; Roach et al., 1998]. The monoclonal antibody 10A2 was raised against the carboxyl terminal peptide of β-tubulin class IVa. It was found to be specific for both β-tubulin classes IVa and IVb (Fig. 1). Blots were reacted with chemiluminescent reagents (SuperSignal® West Femto Maximum Sensitivity Substrate, Pierce, Rockford, IL) and exposed to X-ray film. Densities for the known and unknown sample bands on the films were obtained using a Molecular Dynamics densitometer with ImageQuant Software (Amersham, Piscataway, NJ).

Known amounts of pig brain tubulin were used as standards on all blots. Prior work demonstrated that microtubule associated protein-free phosphocellulose-purified tubulin preps from pig brain is 3% β-tubulin class I, 55% β-tubulin class II, 29% β-tubulin class III, and 13% β-tubulin class IV [Banerjee et al., 1988; Dozier et al., 2003]. The quantities of tubulin isotypes in unknown samples were calculated from linear fits of standard curves from each Western blot done in triplicate and for at least two lysates prepared from independently grown cell cultures. It was critical to establish the linearity of response for each antibody and to determine that unknown samples were within the linear range. Extrapolation to values outside the standard curve can result in significant error.

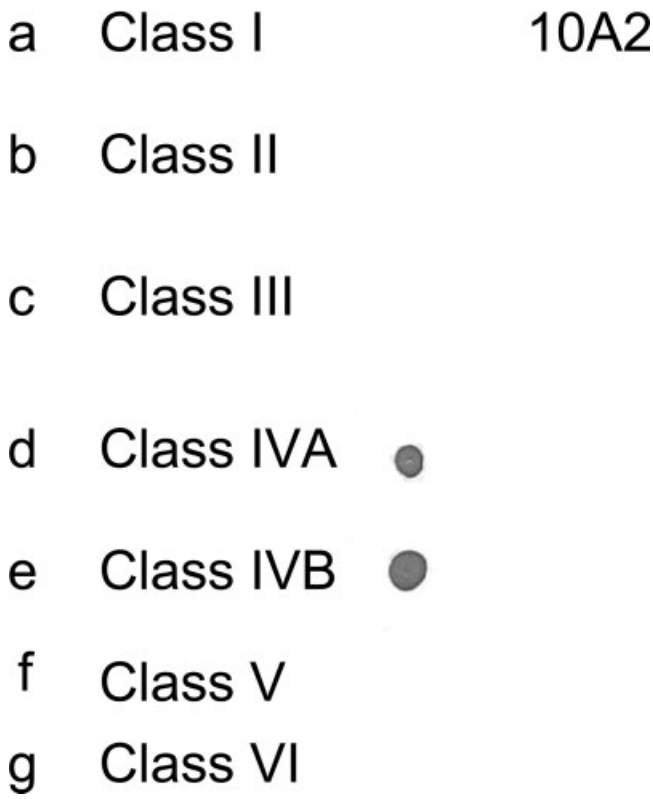

Fig. 1. Dot blots of β-tubulin isotype fusion proteins. β-Tubulin fusion proteins were transferred to PVDF filters and reacted with anti-β-tubulin class IVa + IVb monoclonal antibody 10A2. Fusion protein reactions shown are for β-tubulin class I (Panel a), class II (Panel b), class III (Panel c), class IVa (Panel d), class IVb (Panel e), class V (Panel f), and class VI (Panel g). Only β-tubulin fusion proteins constructed with class IVa or IVb carboxyl terminal peptides were found to react.

Calibration of Antibody Reactivity With β-Tubulin Fusion Proteins

The tubulin protein measurements in the work presented here were done on lysates from human cell lines. Because human and pig brain tubulins may interact differentially with mouse monoclonal antibodies, we constructed fusion proteins with human β-tubulin isotype peptides to compare and calibrate the antibody reactivity. Maltose binding protein (MBP) β-tubulin fusion proteins were constructed for each of the seven human β-

TABLE I. Oligonucleotide Primers and β-Tubulin Carboxyl Terminal Sequences for β-Tubulin Fusion Proteins

Class	Forward primer sequence 5′–3′	Reverse primer sequence 5′–3′	Fragment (bp)	Cloned as	Carboxyl terminal sequences
I	aaa gaa ttc gat gcc acc gca gaa gag gag gag gat ttc	aaa aag ctt cta ccc act acc ttc tac cat t	485	EcoRI/HindIII	DATAEEEEDFGEEAEEEA
II	aaa gaa ttc gac gcc acg gcc gac gaa caa ggg	aaa agc tta caa acg ttt atg tga ttt tag	325	EcoRI/HindIII	DATADEQGEFEEEEGEDEA
III	aaa gaa ttc gac gcc acg gcc gag gaa gag g	aaa aag ctt aag ggt atc tga cag caa tag a	388	EcoRI/HindIII	DATAEEEGEMYEDDEEESEAQGPK
IVa	aaa gaa ttc gac gcc acg gcc gag gag g	aaa aag ctt ggg tta aag ata aat tag gg	279	EcoRI/HindIII	DATAEEGEFEEEAEEEVA
IVb	aaa gaa ttc gat gcc aca gcc gag gag ga	aaa tct aga atg aaa atg ctt taa tgg	225	EcoRI/Xba I	DATAEEEGEFEEEAEEEVA
V	aaa gaa ttc gat gcc acc gcc aat gac g	aaa tct aga gaa gac aca cgt tta gta tt	519	EcoRI/Xba I	DATANDGEEAFEDEEEEIDG
VI	aaa gaa ttc gat gcc aaa gca gtt cta ga	aaa aag ctt ggc aaa cac ttt gaa aca aag gga g	388	EcoRI/HindIII	DAKAVLEEDEEVTEEAMEPEDKGH

tubulin isotypes (Table I). DNA fragments corresponding to the coding region of the extreme C-terminus of all seven human β-tubulin isotypes were obtained by PCR amplification from either cDNA or genomic DNA, using the primer sets indicated in Table I. The fragments were cloned in-frame (sites indicated in Table I) into a modified version of the pMBP-His-Parallel vector [Sheffield et al., 1999] (a gift from O. Karginova, Department of Biology and Z. Derewenda, Department of Physiology and Biophysics, University of Virginia), resulting in the generation of fusion proteins whose N-terminus was the MBP, and whose C-terminus was the tubulin isotype indicated, separated by a 6X His tag. Nucleotide sequences across the relevant portions of the tubulin coding regions were verified using the Big Dye method on an ABI 310 DNA sequencer. The fusion proteins were expressed in an *Escherichia coli* DH5α background with induction by 0.5 mM isopropyl-β-D-thiogalactopyranoside, and subsequently purified by metal chelate chromatography on nickel nitrilotriacetic resin (Qiagen). Purity was assessed by SDS-PAGE.

The fusion proteins were loaded in known amounts onto SDS-PAGE along with known quantities of pig brain tubulin. The fusion protein concentrations were determined from the optical density at 278 nm, using extinction coefficients calculated from the amino acid sequence: fusion-β-tubulin class I, $\varepsilon_{278} = 1.493$ l/g cm; fusion-β-tubulin class II, $\varepsilon_{278} = 1.489$ l/g cm; fusion-β-tubulin class III, $\varepsilon_{278} = 1.500$ l/g cm; fusion-β-tubulin class IVa, $\varepsilon_{278} = 1.493$ l/g cm; fusion-β-tubulin class IVb, $\varepsilon_{278} = 1.489$ l/g cm. The concentration of pig brain tubulin was also determined spectrophotometrically ($\varepsilon_{278} = 1.2$ l/g cm) [Detrich III and Williams Jr., 1978]. Gels were transferred to PVDF membranes for immunoblotting and the reactivity of the fusion proteins and pig brain were compared using densitometry. Correction factors and standard errors were calculated for each antibody (Table II) from triplicate Western blots by dividing the known amount of β-tubulin fusion protein loaded on

TABLE II. Corrections for β-Tubulin Isotype Data Determined Using Pig Brain Standards

β- Tubulin class	Correction factor ± SE[a]
I	0.64 ± 0.12
II	0.61 ± 0.17
III	0.27 ± 0.047
IVa + IVb	1.31 ± 0.31

[a]These correction factors were used to calculate the actual amount of β-tubulin in human cell lines: $\beta\text{-tubulin}_{human}$ = correction factor × $\beta\text{-tubulin}_{pig\ brain}$. Correction factors were calculated as the actual amount (μg) of β-tubulin fusion protein loaded on the gel for Western blotting divided by the amount of β-tubulin predicted using pig brain tubulin for the standard curve. The standard error (SE) from triplicate blots is indicated.

TABLE III. β-Tubulin Isotype Protein and mRNA Levels

Cell line	βI	βII	βIII	βIVa	βIVb	βV
Percentage tubulin isotype mRNA						
Colon cancer						
COLO 205	85.7	0.6	2.6	0	11.1	0
HCT-15	65.0	0.8	3.4	0	5.1	25.8
Breast cancer						
BT-549	74.9	0.1	16.0	0	2.3	6.7
T-47D	76.2	0.7	0.7	0.1	6.4	16.4
MCF-7	78.1	0.2	14.1	0.1	4.3	3.2
MDA-MB-231	78.3	0.2	2.4	0	15.8	13.2
Lung cancer						
A549	57.8	2.3	6.7	0.5	4.2	28.5
HOP 18	38.9	6.6	14.8	0	9.7	30.0
Melanoma						
Malme-3M	57.7	13.5	8.0	4.1	1.6	15.2
SK-MEL-2	51.2	1.1	3.5	0.9	3.1	40.2
Ovarian cancer						
OVCAR-3	42.6	5.2	5.2	0.7	9.4	36.8
SK-OV-3	55.9	0	1.6	0.1	4.3	38.1

Cell line	βI	βII	βIII	βIVa + βIVb
Percentage tubulin isotype protein				
Colon cancer				
COLO 205	36.0	0	0	64.0
HCT-15	61.8	0	0.2	38.0
Breast cancer				
BT-549	65.9	0.6	6.4	27.1
T-47D	85.7	0	0	14.3
MCF-7	39.1	0	2.5	58.4
MDA-MB-231	76.1	0	0	23.9
Lung cancer				
A549	71.9	0	1.6	26.5
HOP 18	63.2	1.5	5.0	30.3
Melanoma				
Malme-3M	84.4	3.8	5.1	7.0
SK-MEL-2	73.1	1.4	1.5	24.0
Ovarian cancer				
OVCAR-3	97.0	0	0	3.1
SK-OV-3	85.6	0	0.8	13.6

the gel by the amount of β-tubulin isotype estimated from the pig brain standard curve. These factors were used to correct the data obtained using pig brain standard curves on the Western blots. The percentages of tubulin isotype proteins shown in Table III and Fig. 3b were corrected using the correction factors in Table II.

RESULTS

β-Tubulin mRNA Expression

We used qRT-PCR to measure the amounts of β-tubulin isotype mRNA classes I, II, III, IVa, IVb, V, and VI for each of the 12 cell lines (Fig. 2). The mRNA levels for each isotype, with the exception of class I, differed by more than 10-fold between the 12 cell lines; however, the total tubulin mRNA levels were found to be fairly constant, differing by less than 10-fold across all 12 cell lines. This is consistent with the previous suggestion that total tubulin expression levels are regulated to fulfill the function of the cytoskeleton [Cabral and Barlow, 1991; Wang and Cabral, 2005].

Figure 3a and Table III present the isotype mRNA data as percentages of total β-tubulin mRNA for each cell line. As reported for other cell lines [Nicoletti et al., 2001], it is clear that β-tubulin class I mRNA comprises more than 50% of the β-tubulin mRNA for all but two of the cell lines examined. As expected, the hematopoietic-specific β-tubulin class VI mRNA was either absent or 4–6 orders of magnitude less prevalent (Fig. 2) than β-tubulin class I. The neuron-specific isotype, β-tubulin class III, was expressed at relatively high levels (>10% of total mRNA) in 3 of the 12 cell lines, including 2 of the 4 breast cancer cell lines. In fact, β-tubulin class III mRNA constituted more than 1% of the tubulin message in all of the cell lines except T-47D, a surprising result considering that β-tubulin class III is neuron specific. In addition, several cell lines expressed very low but measurable levels of the ''neuron-specific'' β-tubulin class IVa. Relatively high levels of β-tubulin class V mRNA (>25% of the total β-tubulin mRNA) were detected in half of the cell lines. This raises the intriguing possibility that β-tubulin class V is highly expressed in human cells, something that has not been measurable until recently due to the absence of a commercially available β-tubulin class V antibody. Overall, the mRNA levels of β-tubulin class IVb were comparable to those of β-tubulin class III, although one or the other was significantly more abundant in some cell lines. In general, β-tubulin class II mRNA was less abundant than β-tubulin classes I, III, IVb, and V messages.

Because alterations in tubulin isotype levels have been implicated in resistance to antimitotic agents [Kavallaris et al., 1997, 1999; Ranganathan et al., 1998; Banerjee, 2002], we measured IC_{50} levels for all 12 cell lines used in this study (Table IV). No correlations between IC_{50} values and tubulin isotype mRNA levels were found (data not shown). However, these cell lines represent several tumor types and the contribution of tubulin isotypes to drug sensitivity could be masked by many factors.

β-Tubulin Protein Levels

Mouse monoclonal antibodies specific for β-tubulin classes I, II, III, and IVa + IVb were utilized in quantitative Western blotting of whole cell lysates from 12 human cell lines. We found that pig brain tubulin is a plentiful and reliable source of tubulin for standard curves on Western blots. However, because pig brain tubulin and human cell lysates may react differently with the monoclonal antibodies, we constructed fusion proteins with the human tubulin carboxyl terminal peptides and compared

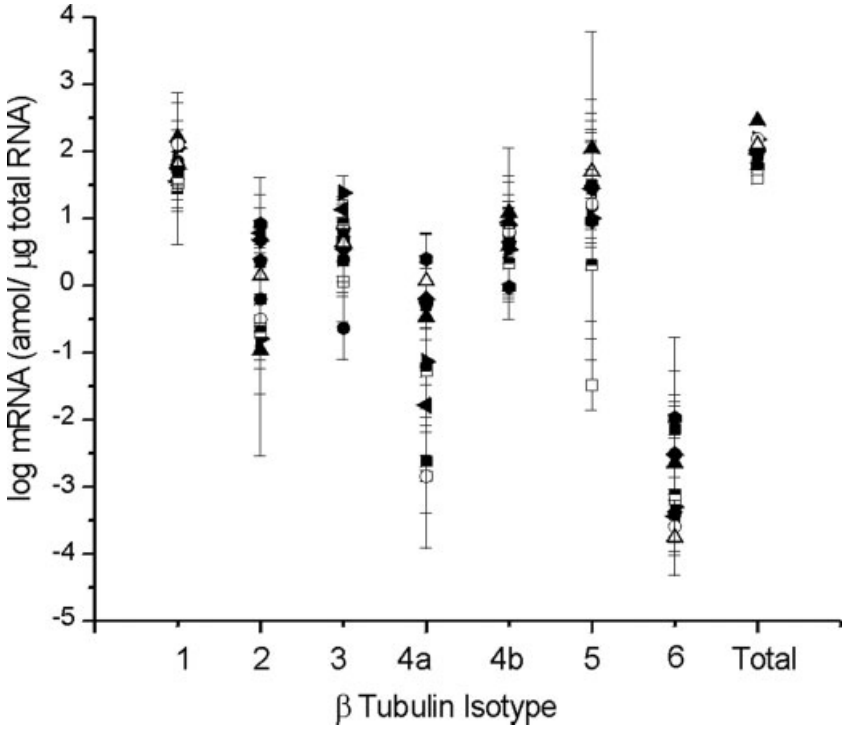

Fig. 2. β-Tubulin isotype mRNA for twelve cell lines. Mean data from qRT-PCR of two or more cell preps are shown. Data from β-tubulin isotype classes I (1), II (2), III (3), IVa (4a), IVb (4b), V (5), and VI (6) were summed to calculate the total β-tubulin mRNA in each cell line.

their reactivities on Western blots with that of pig brain tubulin. The largest difference in reactivity was found for β-tubulin class III (Table II). The reaction of TUJ1 monoclonal antibody with pig brain standard overestimates the actual amount of human β-tubulin class III fusion protein by 3.7 (±0.6)-fold. β-Tubulin classes I and II are overestimated by about 1.6 (±0.4)-fold using the pig brain standards, and β-tubulin classes IVa + IVb are underestimated by about 0.8 (±0.2)-fold. We adjusted all tubulin measurements, using the correction factors in Table II, to estimate actual tubulin protein levels in human cell lines. An alternate method of standardization is to construct standard curves with the β-tubulin fusion proteins. The advantage of the quantitative immunoblot method presented here is that it can be used as a rigorous tool for studying tubulin levels in whole cell or tissue lysates without requiring fusion protein standards.

We used quantitative Western blotting of whole cell lysates to measure β-tubulin isotype protein levels for classes I, II, III, and IVa + IVb (Fig. 3b and Table III). Significant levels of β-tubulin classes I and IVa + IVb were found in all 12 cell lines, ranging from 36.0–97.0% for β-tubulin class I and from 3.1–64.0% for β-tubulin classes IVa + IVb. β-Tubulin class I comprised >50% of the total β-tubulin measured in 10 of the 12 cell lines. β-Tubulin classes IVa + IVb comprised >50% of the total β-tubulin in breast cancer (MCF-7) and colon cancer (COLO 205) cells. β-Tubulin class III comprised more than 1% of the total β-tubulin protein (1.5–6.4%) in breast cancer cell lines, BT-549 and MCF-7; lung cancer cells, A549 and HOP 18; and melanoma cells, Malme-3M and SK-MEL-2. β-Tubulin class II was found at low but measurable levels (0.6–3.8%) in only four cell lines—breast cancer (BT-549), lung cancer (HOP 18) and melanoma (SK-MEL-2 and Malme-3M) cell lines.

Comparison of mRNA and Protein

β-Tubulin mRNA and protein levels for isotype classes I, II, III, and IVa + IVb are compared in Fig. 4. β-Tubulin classes V and VI mRNA data were not included in this analysis because we did not have corresponding protein data. Thus, the percentages of β-tubulin isotype mRNA in Fig. 4 were calculated assuming that the total tubulin was comprised of only β-tubulin isotype classes I, II, III, and IVa + IVb. β-Tubulin classes I and IVa + IVb are present in greatest abundance for both mRNA and protein. Only β-tubulin class I data suggest a near one-to-one correspondence for mRNA and protein. For β-tubulin class I, 10 of the 12 cell lines have both mRNA and protein levels >50%. For β-tubulin class IVa + IVb, there is consistently more protein than mRNA in 10 of the 12 cell lines. β-Tubulin class II protein is found in only four cell lines; therefore, no general conclusions regarding the relationship between mRNA and protein levels can be made. β-Tubulin class III protein is found in eight cell lines. The mRNA and protein amounts for β-tubulin class III correspond (Fig.

4, Panel c insert), although there is consistently more mRNA than protein.

DISCUSSION

The role of β-tubulin isotype levels in determining cellular responses to antimitotic agents has been controversial for more than a decade. Most studies have relied upon measurements of intracellular tubulin mRNA levels to infer protein levels. However, mRNA and protein levels are not correlated for many human and yeast proteins, especially those that are regulated by posttranscriptional processes [Anderson and Seilhamer, 1997; Gygi et al., 1999]. Thus, it is important to establish whether there is a correlation between tubulin mRNA and protein levels so as to better understand mechanisms that may underlie drug resistance.

We present here a reliable method for quantifying β-tubulin protein levels in whole cell lysates. We demonstrated that tubulin isotype fusion proteins or pig brain tubulin calibrated with the fusion proteins can be used to create a standard curve on Western blots. We find this to be an acceptable method for protein quantification for the following reasons: (1) The monoclonal antibodies used in this work are highly specific as demonstrated by blots with either purified tubulin isotypes or tubulin isotype fusion proteins [Lee et al., 1990; Lobert et al., 1995, 1998; Roach et al., 1998] (Fig. 1). (2) The data are highly reproducible. We present here data collected from independent cell protein extractions and at least three Western blots for each whole cell lysate. The standard error for each measurement was propagated from the biological (individual protein preparations) and technical (individual Western blots) replicates and is represented as the error bars in Fig. 3b. For the two most abundant isotypes measured, β-tubulin classes I and IVa + IVb, the average error was 14.6% and 23.3%, respectively. (3) There is good agreement between the mRNA and protein levels for β-tubulin isotype classes I and III (although for β-tubulin class III the correspondence is not one-to-one). The agreement in isotype percentages by two independent methods supports the findings and the method used for protein quantification.

The higher β-tubulin class IVa + IVb protein levels compared to mRNA levels suggest possible differential regulatory mechanisms for this isotype compared to β-tubulin classes I and III. Fine tuning of tubulin levels during the cell cycle occurs via autoregulation. This process alters mRNA stability and requires both an essential sequence on polysomal β-tubulin mRNA and an aminoterminal Met-Arg-Glu-Ile on the nascent tubulin polypeptide [Pachter et al., 1987; Cleveland, 1988; Yen et al., 1988]. Furthermore, α-tubulin mRNA levels remain high even when protein synthesis is repressed [Gonzalez-Garay and Cabral, 1996]. In fact, α-tubulin synthesis in Chinese hamster ovary (CHO) cells appears to play a role in regulating β-tubulin protein levels. This phenomenon of tubulin posttranscriptional autoregulation was demonstrated in a wide variety of vertebrate and invertebrate cell types. Intracellular tubulin levels are also transcriptionally regulated [Cleveland, 1989]. It is possible that individual isotypes may be differentially regulated while maintaining free tubulin subunits at levels necessary for different phases of the cell cycle. Our data demonstrate relatively constant amounts of total tubulin message in spite of variations in individual isotype mRNA levels (Fig. 2). Because of the relatively low levels of β-tubulin classes IVa + IVb mRNA compared to protein, our data suggest that differential methods for regulating β-tubulin classes (I or III vs. IVa + IVb) are likely. Alternatively, pairing of specific α- and β-tubulins may lead to differential stability of β-tubulins [Hoyle et al., 2001].

β-Tubulin class III has been studied extensively for its potential role in resistance to antimitotic agents. For example, paclitaxel-resistant lung cancer cells and ovarian tumors were shown to have increased levels of tubulin isotypes, particularly β-tubulin classes III and IVa mRNA levels [Kavallaris et al., 1997]. Furthermore, when paclitaxel-resistant lung cancer cells were treated with antisense oligonucleotides for β-tubulin class III, the drug resistance was partially reversed, coincident with reduced protein levels of β-tubulin class III [Kavallaris et al., 1999]. In other work, β-tubulin classes III and IVa transcripts were shown to increase in paclitaxel-resistant prostate cancer cells [Ranganathan et al., 1998]. Combined isoelectric focusing and mass spectrometry were used to measure tubulin isotypes in four cell lines [Verdier-Pinard et al., 2003]. This report demonstrated an increase in β-tubulin class III and associated this with paclitaxel resistance in lung cancer cells. In the most convincing study, when cells were transfected with β-tubulin class III, weak resistance to paclitaxel was found and this resistance was associated with decreased microtubule stability [Hari et al., 2002]. Thus, there is considerable interest in determining whether functional β-tubulin class III protein is involved in mechanisms that cause resistance to antimitotic agents. Because qRT-PCR is a commonly used reliable method for quantitation of mRNA levels, it is potentially an important method for better understanding the role of β-tubulin isotypes in drug resistance. To draw conclusions from mRNA measurements, it is essential to know whether transcript levels correlate with protein levels. In the work described here, β-tubulin class III mRNA and protein levels are correlated but do not demonstrate one-to-one correspondence. β-Tubulin class III mRNA may be useful for comparing relative amounts of this isotype across cell and tissue samples; however, quantitatively inferring β-tubulin protein

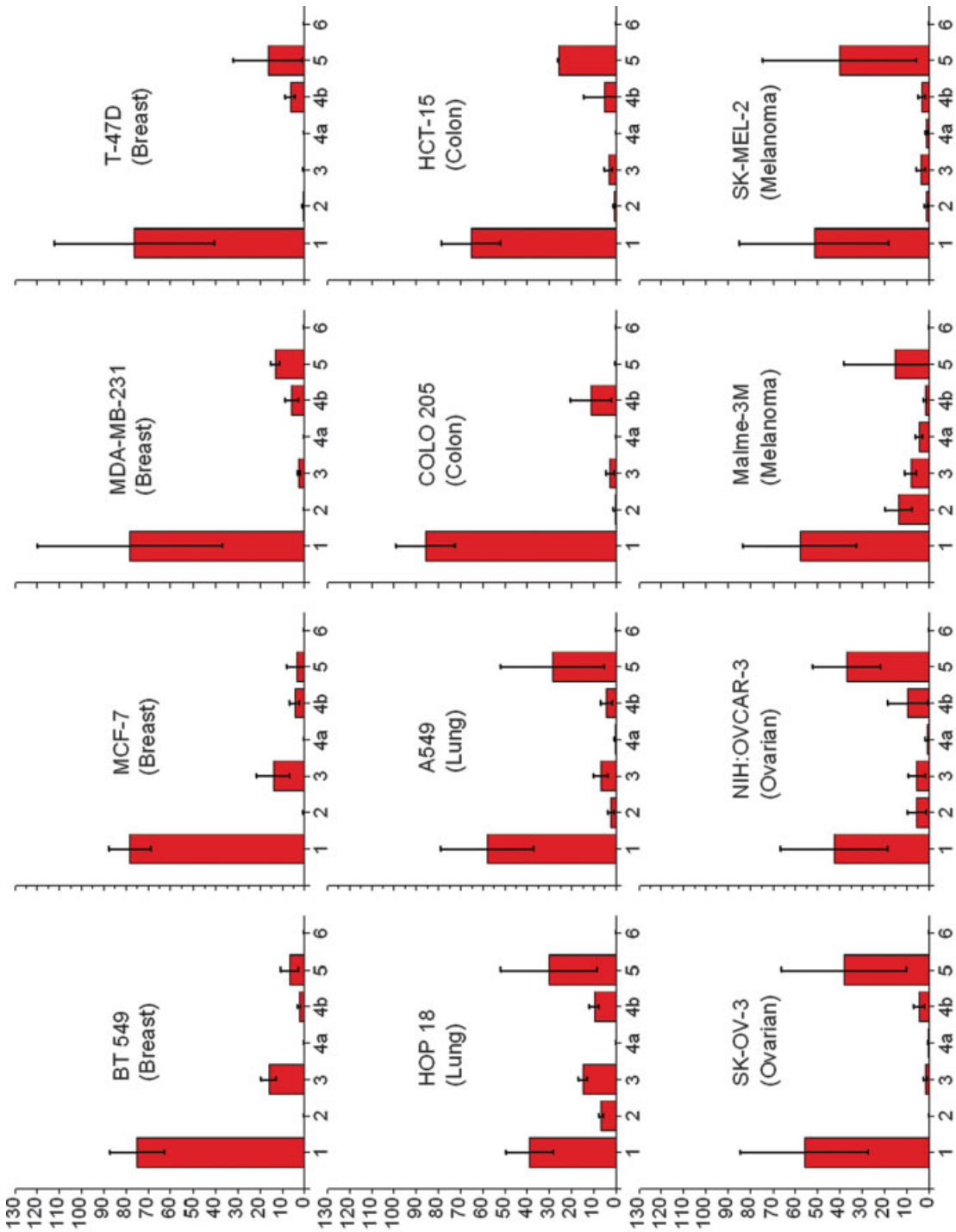

Fig. 3. β-Tubulin isotype profiles for 12 cell lines. The data in Table III are plotted as bars representing the percent contribution of each β-tubulin isotype mRNA (**a**) or protein (**b**) to the total tubulin in each cell line. The sum of the values for all six β-tubulin isotype classes was considered as the total tubulin for the mRNA percentage calculations. The sum of the β-tubulin isotype classes I, II, III, and IVa + IVb was considered to be the total tubulin for the protein analysis. Error bars represent standard deviation from multiple experiments, as described in the Materials and Methods.

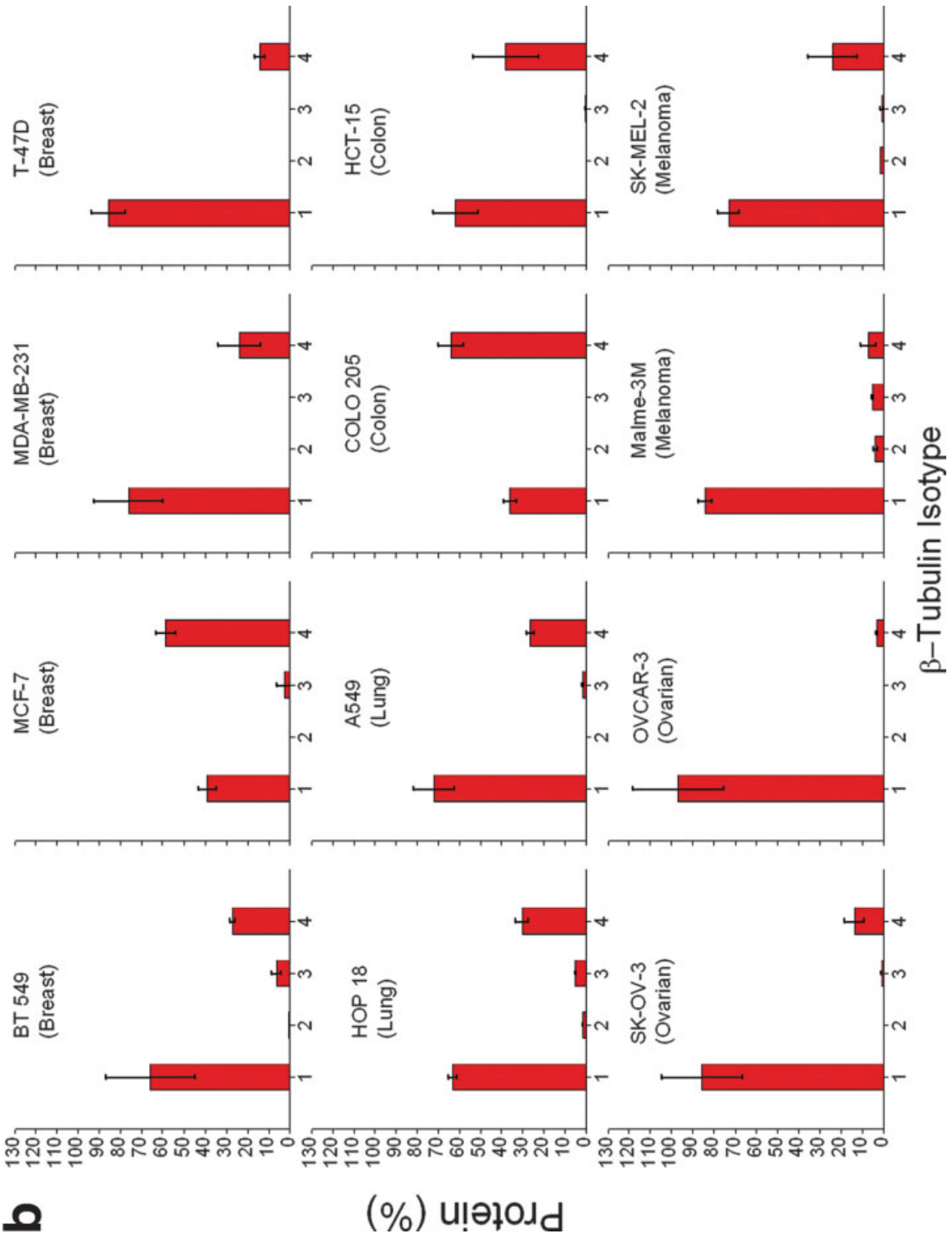

Figure 3. (Continued)

TABLE IV. Drug Sensitivities of Human Cancer Cell Lines to Paclitaxel and Vinblastine as Measured by Two Different Assays

Cancer cell line	Drug	IC_{50} (nM)		IC_{50} (nM) Mean	Fold difference[b]
		Cell count	MTS assay[a]		
Colon					
COLO-205	Paclitaxel	29.2	26.1	27.7	6.0
HCT-15	Paclitaxel	6.4	2.8	4.6	
COLO-205	Vinblastine	0.6	0.7	0.7	
HCT-15	Vinblastine	31.1	24.9	28.0	40
Breast					
BT-549	Paclitaxel	4.3	5.5	4.9	4.9 (MCF7), 12.3 (MDA), 3.3 (T-47D)
MCF-7	Paclitaxel	1.0	1.0	1.0	2.5 (MDA)
MDA-MB-231	Paclitaxel	0.3	0.5	0.4	
T-47D	Paclitaxel	0.8	2.3	1.5	1.5 (MCF7), 3.8 (MDA)
BT-549	Vinblastine	0.9	1.3	1.1	2.8 (MCF7)
MCF-7	Vinblastine	0.4	0.4	0.4	
MDA-MB-231	Vinblastine	2.2	0.9	1.6	1.5 (BT549), 4.0 (MCF7)
T-47D	Vinblastine	5.3	13.5	9.3	8.5 (BT549), 23.3 (MCF7), 5.8 (MDA)
Lung					
A-549	Paclitaxel	2.9	2.5	2.7	3.9
HOP-18	Paclitaxel	0.6	0.8	0.7	
A-549	Vinblastine	2.1	1.2	1.7	3.4
HOP-18	Vinblastine	0.7	0.4	0.5	
Melanoma					
Malme-3M	Paclitaxel	4.2	4.6	4.4	1.1
SK-MEL-2	Paclitaxel	3.7	4.1	3.9	
Malme-3M	Vinblastine	0.3	1.1	0.7	
SK-MEL-2	Vinblastine	0.6	1.3	0.9	1.3
Ovarian					
OVCAR-3	Paclitaxel	2.1	0.8	1.5	
SK-OV-3	Paclitaxel	2.0	4.6	3.3	2.2
OVCAR-3	Vinblastine	3.7	1.3	2.5	1.6
SK-OV-3	Vinblastine	2.3	0.9	1.6	

[a]MTS is 3-(4,5-dimethylthiazol-2-yl)-5-(3-carboxymethoxyphenyl)-2-(4-sulfophenyl)-2H-tetrazolium, inner salt, a component of CellTiter 96® AQ_{ueous} One Solution Cell Proliferation Assay.
[b]Determined by dividing the larger mean IC_{50} by the smaller for each pair of cell lines. For the breast cancer cells, the cell line compared is given in parentheses.

levels from mRNA levels within a cell or tissue type should be done with caution.

The work of Bhattacharya and Cabral [2004] suggests a minimum threshold level for β-tubulin class V that alters mitotic spindle function. They found that modest increases in β-tubulin class V, to levels of 15% or more of the total β-tubulin, may increase microtubule dynamics and decrease microtubule polymer levels. This was shown to be associated with weak resistance to paclitaxel. We found threshold levels of β-tubulin class V mRNA (>15%) in several cell lines: colon cancer, HCT-15; breast cancer, T-47D; lung cancer, A549 and HOP-18; melanoma, Malme-3M and SK-MEL-2; ovarian, OVCAR-3 and SK-OV-3. We found no correlation between IC_{50} values for paclitaxel or vinblastine and percentage β-tubulin class V mRNA (data not shown). While the relationship between mRNA and protein levels for this isotype remains to be determined, one difference between the work reported here and that of Bhattacharya and Cabral [2004] is that they carefully established that only one variable is altered in the β-tubulin class V overexpressing CHO cells. In our work, many variables differ among the 12 cell lines and some of them may compensate for changes in β-tubulin class V levels. Preliminary examination of one of the breast cancer cell lines, BT-549, by mass spectrometry revealed the presence of β-tubulin class V (data not shown). Therefore, we expect to find β-tubulin class V protein in some or all of the twelve cell lines. We have recently developed a monoclonal antibody to β-tubulin class V, which should permit quantitative measurement of protein levels and provide data regarding the contribution of β-tubulin class V to drug resistance.

CONCLUSIONS

From our comparison of β-tubulin isotype mRNA and protein levels on 12 human cancer cell lines, we conclude that quantitative Western blotting, utilizing human

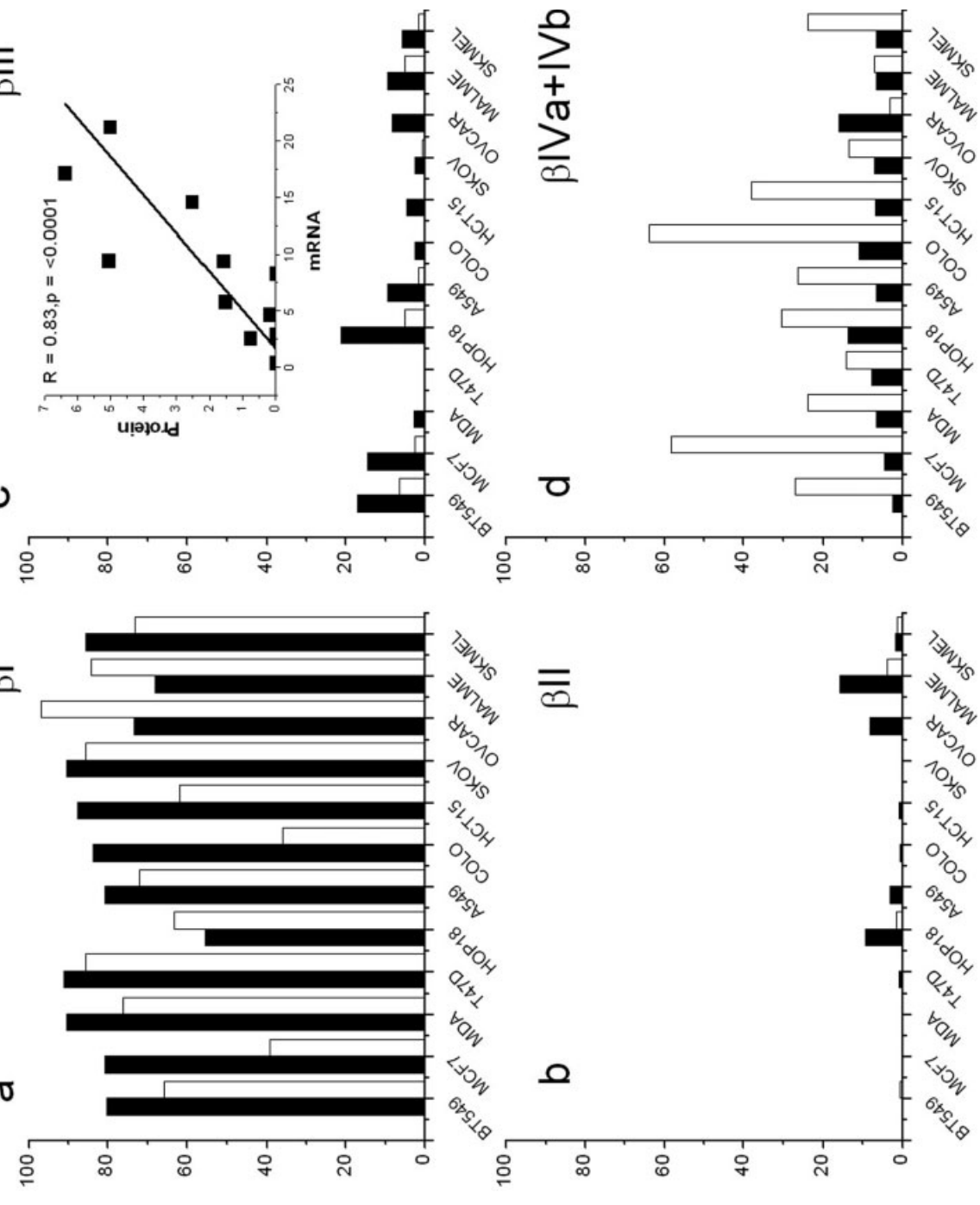

Fig. 4. Comparison of β-tubulin isotype protein levels with mRNA levels. Only β-tubulin isotype classes I (βI), II (βII), III (βIII), and IV (βIVa + IVb) were considered when calculating the total mRNA and protein levels. Solid bars represent mean mRNA and open bars represent mean protein values. Panel a: βI, Panel b: βII, Panel c: βIII, and Panel d: βIVa + IVb. Insert in Panel c shows a plot of mRNA vs. protein data for β-tubulin class III fit by linear regression. The straight line represents the best fit of the data. The correlation coefficient, R (Pearson's product-moment) for the fit and the P-value relative to a horizontal line (no correlation) are shown.

β-tubulin fusion proteins or pig brain tubulin with appropriate correction factors, is a reliable method for quantifying β-tubulin isotypes in human cancer cell lines. We found a good correspondence between β-tubulin mRNA and protein levels for classes I and III. For β-tubulin classes IVa + IVb, the higher levels of protein compared to mRNA suggest potential differential regulatory mechanisms for β-tubulin isotypes.

REFERENCES

Alvarez M, Paull K, Monks A, Hose A, Lee JS, Weinstein J, Grever M, Bates S, Fojo T. 1995. Generation of a drug resistance profile by quantitation of mdr-1/P-glycoprotein in the cell lines of the National Cancer Institute Anticancer Drug Screen. J Clin Invest 95:2205–2214.

Anderson L, Seilhamer J. 1997. A comparison of selected mRNA and protein abundances in human liver. Electrophoresis 18:533–537.

Banerjee A. 2002. Increased levels of tyrosinated α-, β(III)-, and β(IV)-tubulin isotypes in paclitaxel-resistant MCF-7 breast cancer cells. Biochem Biophys Res Commun 293:598–601.

Banerjee A, Roach MC, Wall KA, Lopata MA, Cleveland DW, Luduena RF. 1988. A monoclonal antibody against the type II isotype of β-tubulin. Preparation of isotypically altered tubulin. J Biol Chem 263:3029–3034.

Bhattacharya R, Cabral F. 2004. A ubiquitous β-tubulin disrupts microtubule assembly and inhibits cell proliferation. Mol Biol Cell 15:3123–3131.

Cabral F, Barlow SB. 1991. Resistance to antimitotic agents as genetic probes of microtubule structure and function. Pharmacol Ther 52:159–171.

Cleveland D. 1988. Autoregulated instability of tubulin mRNAs: a novel eukaryotic regulatory mechanism. TIBS: Trends in Biochemical Sciences 13:339–343.

Cleveland DW. 1989. Autoregulated control of tubulin synthesis in animal cells. Curr Opin Cell Biol 1(1):10–14.

Correia JJ, Lobert S. 2001. Physiochemical aspects of tubulin-interacting antimitotic drugs. Curr Pharm Des 7:1213–1228.

Detrich HW, III, Williams RC, Jr. 1978. Reversible dissociation of the αβ dimer of tubulin from bovine brain. Biochemistry 17:3900–3907.

Dhamodharan R, Jordan MA, Thrower D, Wilson L, Wadsworth P. 1995. Vinblastine suppresses dynamics of individual microtubules in living interphase cells. Mol Biol Cell 6:1215–1229.

Dozier JH, Hiser L, Davis JA, Thomas NS, Tucci MA, Benghuzzi HA, Frankfurter A, Correia JJ, Lobert S. 2003. β Class II tubulin predominates in normal and tumor breast tissues. Breast Cancer Res 5:R157–R169.

Gonzalez-Garay ML, Cabral F. 1996. α-Tubulin limits its own synthesis: evidence for a mechanism involving translational repression. J Cell Biol 135:1525–1534.

Gygi SP, Rochon Y, Franza R, Aebersold R. 1999. Correlation between protein and mRNA abundance in yeast. Mol Cell Biol 19:1720–1730.

Hari M, Yang H, Canizales M, Zeng C, Cabral F. 2002. Expression of class III [beta]-tubulin in CHO cells reduces microtubule stability and confers resistance to paclitaxel. Proc Am Assoc Cancer Res 43:LB139.

Hoyle HD, Turner FR, Brunick L, Raff EC. 2001. Tubulin sorting during dimerization in vivo. Mol Biol Cell 12:2185–2194.

Kavallaris M, Kuo DY, Burkhart CA, Regl DL, Norris MD, Haber M, Horwitz SB. 1997. Taxol-resistant epithelial ovarian tumors are associated with altered expression of specific β-tubulin isotypes. J Clin Invest 100:1282–1293.

Kavallaris M, Burkhart CA, Horwitz SB. 1999. Antisense oligonucleotides to class III β-tubulin sensitize drug-resistant cells to Taxol. Br J Cancer 80:1020–1025.

Lee MK, Tuttle JB, Rebhun LI, Cleveland DW, Frankfurter A. 1990. The expression and posttranslational modification of a neuron-specific β-tubulin isotype during chick embryogenesis. Cell Motil Cytoskeleton 17:118–132.

Lobert S, Frankfurter A, Correia JJ. 1995. Binding of vinblastine to phosphocellulose-purified and αβ-class III tubulin: the role of nucleotides and β-tubulin isotypes. Biochemistry 34:8050–8060.

Lobert S, Frankfurter A, Correia JJ. 1998. Energetics of vinca alkaloid interactions with tubulin isotypes: implications for drug efficacy and toxicity. Cell Motil Cytoskeleton 39:107–121.

Nicoletti MI, Valoti G, Giannakakou P, Zahn Z, Kim JH, Lucchini V, Landoni F, Mayo JG, Giavezzi R, Fojo T. 2001. Expression of β-tubulin isotypes in human ovarian carcinoma xenografts and in a sub-panel of human cancer cell lines from the NCI-Anticancer Drug Screen: correlation with sensitivity to microtubule active agents. Clin Cancer Res 7:2912–2922.

Pachter JS, Yen TJ, Cleveland DW. 1987. Autoregulation of tubulin expression is achieved through specific degradation of polysomal tubulin mRNAs. Cell 51:283–292.

Ranganathan S, Benetatos CA, Colarusso PJ, Dexter DW, Hudes GR. 1998. Altered β-tubulin isotype expression in paclitaxel-resistant human prostate carcinoma cells. Br J Cancer 77:562–566.

Roach MC, Boucher VL, Walss C, Ravdin PM, Luduena RF. 1998. Preparation of a monoclonal antibody specific for the class I isotype of β-tubulin: the β isotypes of tubulin differ in their cellular distribution within human tissues. Cell Motil Cytoskeleton 39:273–286.

Sheffield P, Garrard S, Derewenda Z. 1999. Overcoming expression and purification problems of RhoGDI using a family of ''parallel'' expression vectors. Protein Expr Purif 15:34–39.

Sullivan KF. 1988. Structure and utilization of tubulin isotypes. Annu Rev Cell Biol 4:687–716.

Sullivan KF, Cleveland DW. 1986. Identification of conserved isotype-defining variable region sequences for four vertebrate β-tubulin polypeptide classes. Proc Natl Acad Sci USA 83:4327–4331.

Verdier-Pinard P, Wand R, Martello L, Burd B, Orr GA, Horwitz SB. 2003. Analysis of tuublin isotypes and mutation from taxol-resistant cells by combined isoelectricfocusing and mass spectrometry. Biochemistry 42:5349–5357.

Wang Y, Cabral F. 2005. Paclitaxel resistance in cells with reduced β-tubulin. Biochim Biophys Acta 1744:245–255.

Yen TJ, Machlin PS, Cleveland DW. 1988. Autoregulated instability of β-tubulin mRNAs by recognition of the nascent amino terminus of β-tubulin. Nature 334:580–585.

Yvon AM, Wadsworth P, Jordan MA. 1999. Taxol suppresses dynamics of individual microtubules in living human tumor cells. Mol Biol Cell 10:947–959.

Published OnlineFirst July 28, 2009; DOI:10.1158/1940-6207.CAPR-09-0084

Cancer Prevention Research

Identification of Gene Signatures and Molecular Markers for Human Lung Cancer Prognosis using an *In vitro* Lung Carcinogenesis System

Humam Kadara, Ludovic Lacroix, Carmen Behrens, et al.

Cancer Prev Res 2009;2:702-711. Published OnlineFirst July 28, 2009.

Published OnlineFirst July 28, 2009; DOI:10.1158/1940-6207.CAPR-09-0084

Identification of Gene Signatures and Molecular Markers for Human Lung Cancer Prognosis using an *In vitro* Lung Carcinogenesis System

Humam Kadara,[1] Ludovic Lacroix,[1] Carmen Behrens,[1,2] Luisa Solis,[1,2] Xuemin Gu,[3] J. Jack Lee,[3] Eiji Tahara,[1] Dafna Lotan,[1] Waun Ki Hong,[1] Ignacio I. Wistuba[1,2] and Reuben Lotan[1]

Abstract Lung cancer continues to be a major deadly malignancy. The mortality of this disease could be reduced by improving the ability to predict cancer patients' survival. We hypothesized that genes differentially expressed among cells constituting an *in vitro* human lung carcinogenesis model consisting of normal, immortalized, transformed, and tumorigenic bronchial epithelial cells are relevant to the clinical outcome of non–small cell lung cancer (NSCLC). Multidimensional scaling, microarray, and functional pathways analyses of the transcriptomes of the above cells were done and combined with integrative genomics to incorporate the microarray data with published NSCLC data sets. Up-regulated (n = 301) and down-regulated genes (n = 358) displayed expression level variation across the *in vitro* model with progressive changes in cancer-related molecular functions. A subset of these genes (n = 584) separated lung adenocarcinoma clinical samples (n = 361) into two clusters with significant survival differences. Six genes, *UBE2C, TPX2, MCM2, MCM6, FEN1,* and *SFN,* selected by functional array analysis, were also effective in prognosis. The mRNA and protein levels of one these genes—UBE2C—were significantly up-regulated in NSCLC tissue relative to normal lung and increased progressively in lung lesions. Moreover, stage I NSCLC patients with positive UBE2C expression exhibited significantly poorer overall and progression-free survival than patients with negative expression. Our studies with this *in vitro* model have lead to the identification of a robust six-gene signature, which may be valuable for predicting the survival of lung adenocarcinoma patients. Moreover, one of those genes, UBE2C, seems to be a powerful biomarker for NSCLC survival prediction.

In 2008, 215,020 new cases, and 161,840 deaths due to lung cancer were expected in the United States, accounting for 31% of all cancer deaths (1). Lung cancer mortality is high because most cancers are diagnosed after regional or distant spread of the disease had already occurred (2, 3). It is noteworthy that even the 5-year survival rate of stage I lung cancer is among the worst for early-stage disease of all other malignancies (1, 4). It is plausible to assume that the mortality of patients will decrease if progress is made in identification of effective prognostic molecular biomarkers.

Lung carcinogenesis involves the accumulation of genetic and epigenetic alterations that occur over a long course due to chronic exposure to carcinogens such as tobacco smoke or to genetic susceptibility factors (2). Several early changes that occur during lung carcinogenesis have been identified including mutations of *TP53* and *KRAS* (5, 6), silencing of retinoic acid receptor β (7), inactivation of the cyclin-dependent kinase inhibitor p16/*CDKN2A* (8), epidermal growth factor receptor amplification and mutations in adenocarcinomas, and amplification and mutations of the tyrosine kinase receptors, *HER2* and *MET* (2, 3). However, all of the abovementioned changes account for <60% of human lung cancers. Moreover, compared with substantial knowledge about the malignant stage, our understanding of the molecular changes occurring early in lung carcinogenesis is still lacking.

One well-characterized system for studying changes that occur at different stages of lung carcinogenesis consists of normal human bronchial epithelial (NHBE) cells, NHBE cells

Authors' Affiliations: [1]Departments of Thoracic/Head and Neck Medical Oncology, [2]Pathology, and [3]Biostatistics, University of Texas M. D. Anderson Cancer Center, Houston, Texas

Received 4/1/09; revised 4/29/09; accepted 5/18/09; published OnlineFirst 7/28/09.

Grant support: Department of Defense grant W81XWH-04-1-0142, and by National Cancer Institute grants UO1 CA86390 (Early Detection Research Network), P50 CA70907 (Specialized Programs of Research Excellence program in lung cancer), and the Cancer Center Support grant P30 CA 16672 (Affymetrix Core).

Note: Supplementary data for this article are available at Cancer Prevention Research Online (http://cancerprevres.aacrjournals.org/).

H. Kadara and L. Lacroix contributed equally to this work and should be considered as first authors.

Current address for L. Lacroix: Department of Biopathology, Gustave-Roussy Institute, 94805 Villejuif, France.

Current address for E. Tahara: Wakunaga Pharmaceutical, Co. Ltd., 1624 Shimokotachi, Koda-Cho, Akitakata-Shi, Hiroshima, 739-1195, Japan.

Requests for reprints: Reuben Lotan, M. D. Anderson Cancer Center, 1515 Holcombe Boulevard, Houston, TX 77030. Phone: 713-792-8467; Fax: 713-796-8655; E-mail: rlotan@mdanderson.org.

doi:10.1158/1940-6207.CAPR-09-0084

Published OnlineFirst July 28, 2009; DOI:10.1158/1940-6207.CAPR-09-0084

immortalized with SV40 T/Adeno12 virus (BEAS-2B), and three cell lines derived from BEAS-2B after s.c. growth as xenotransplants in nude mice; immortalized (1799), transformed (1198), and tumorigenic (1170-I). The latter two were isolated after exposure of BEAS-2B transplants to cigarette smoke condensate *in vivo* (9). The study of this *in vitro* human lung carcinogenesis model offers opportunities to identify different progressive molecular changes that are relevant to human lung cancer development.

In this study, we identified genes that are expressed differentially and progressively among the cells that constitute the *in vitro* model that helped us identify a six-gene signature that is capable of predicting the survival of lung adenocarcinoma. Furthermore, we showed the sequential increase of ubiquitin-conjugating enzyme E2C (UBE2C) protein levels in lung lesions of various stages as well as its up-regulation in non–small cell lung cancer (NSCLC) tissue specimens and potential as a powerful molecular marker of early stage NSCLC prognosis.

Materials and Methods

Cell culture and tissue specimens

NHBE cells and normal small airway epithelial cells (SAEC) were purchased from Cambrex/Clonetics and used at the second passage in our laboratory. The *in vitro* lung carcinogenesis model that includes SV40 large T-immortalized NHBE cells (BEAS-2B and 1799), transformed (1198), and tumorigenic (1170-I) cells derived from BEAS-2B by exposure to cigarette smoke condensate during *in vivo* growth as xenotransplants (9) were obtained from Dr. Klein-Szanto (Fox Chase Cancer Center, Philadelphia, PA). All of the above cells were grown in Keratinocyte Serum-Free Medium (Life Technologies, Inc.) containing epidermal growth factor and bovine pituitary extract at 37°C in a humidified atmosphere of 95% air and 5% CO_2.

RNA extraction

Total RNA was purified from cultured cells or frozen tissues using the RNeasy Mini kit according to the manufacturer's instruction (QIAGEN, Inc.). RNA was treated with DNase provided by the manufacturer for elimination of genomic DNA. Extracted total RNA was quantified using the Nanodrop ND-1000 spectrophotometer (Thermo Fisher Scientific). RNA quality, based on the 28S/18S rRNAs ratio, was assessed using the Experion automated electrophoresis system (Bio-Rad Laboratories) according to the manufacturer's instructions. A total of 1 μg of RNA was reverse-transcribed using the Quantitect Reverse Transcription kit (QIAGEN, Inc.) for first-strand cDNA synthesis with random primers according to the manufacturer's instructions and diluted in nuclease-free water.

Microarray sample preparation, hybridization, scanning, and analysis

All steps leading to generation of raw microarray data were processed at the University of Texas MD Anderson Murine Microarray and Affymetrix Facility. After synthesis and cleanup of cRNA from double-stranded cDNA, fragmented cRNAs (15 μg) were hybridized to 12 (six cell lines in duplicate) GeneChip Human Genome U133A arrays (Affymetrix), according to the manufacturer's instructions and as previously described (10). The arrays were scanned with a GeneChip Scanner 3000 from Affymetrix and raw image files were converted to probe set data (*.CEL files), using the Affymetrix GeneChip Operating Software. Microarray analysis is detailed in the supplementary material accompanying this manuscript. Expression data were deposited into the Gene Expression Omnibus (GSE accession #17073).

Immunohistochemistry analysis

Immunohistochemistry was done on histology sections of formalin-fixed paraffin-embedded tissue samples, using the purified primary rabbit polyclonal anti-human UBE2C/UBCH10 antibody (A-650; Boston Biochem.) at a dilution of 1:500. The sections were deparaffinized, hydrated, subjected to antigen retrieval by heating in a steamer for 20 min with 10 mmol/L sodium citrate (pH 6.0), and then incubated in peroxidase blocking reagent (DAKO). Sections were then washed with Tris-containing buffer and incubated overnight at 4°C with the primary anti-UBE2C antibody. Subsequently, the sections were washed and incubated with the secondary antibody (goat anti-rabbit) using the Evision plus labeled polymer kit (DAKO) for 30 min followed by incubation with avidin-biotin-peroxidase complex (DAKO) and development with diaminobenzidine chromogen for 5 min. Finally, the sections were rinsed in distilled water, counterstained with hematoxylin (DAKO), and mounted on glass slides before evaluation under the microscope. Formalin-fixed and paraffin-embedded pellets from lung cancer cell lines displaying UBE2C expression by Western blot analysis were used as a positive control, whereas samples processed similarly, except for the omission of the primary antibody were used as negative controls. A lung cancer pathologist examined the UBE2C immunostaining using light microscopy. Only nuclear UBE2C expression was evaluated because most of the UBE2C immunoreactivity was detected in the nucleus. Nuclear UBE2C immunostaining was quantified using a range of 0 to 100 according to the percentage of positive nuclei present among all tumor or epithelium cells present in the tissue microarray (TMA) cores.

Statistical analyses

The data were summarized using standard descriptive statistics. The rank-based nonparametric Wilcoxon rank-sum test was used to assess the significance of the differences in nuclear UBE2C score among all normal, preneoplastic, and malignant lung tissue histologic sections. The association between nuclear UBE2C expression and NSCLC patients' smoking status was also assessed using the Wilcoxon rank-sum test. The association between nuclear UBE2C expression and patient survival was analyzed as previously described (11). Continuous UBE2C nuclear scores were dichotomized into two categories (UBE2C negative and UBE2C positive) using the Classification and Regression Tree algorithm for both the overall and progression-free survival of patients, which were compared by the Kaplan-Meier method for estimation of survival probability using the R 2.6.0 statistical package.[4]

Results

Identification of differential gene expression in normal, immortalized, transformed, and tumorigenic lung epithelial cells

Multidimensional scaling analysis of the transcriptome of the *in vitro* lung carcinogenesis cell constituents revealed that normal (NHBE and SAEC), immortalized (BEAS-2B and derived 1799), transformed (1198), and tumorigenic (1170-I) cells were positioned in different coordinates within the planes, with the normal and tumorigenic cells being the farthest apart (Fig. 1A). The two normal cell strains (NHBE and SAEC) were almost super-imposable, with the 1799 cells resembling more closely the transformed and tumorigenic cells, which were in close proximity to each other.

The initial analysis of the Affymetrix U133A chips gene expression data identified 1221 gene features that were differentially expressed by at least 1.65-fold in any of the indicated cells compared with the NHBE cells (Fig. 1B). SOM analysis and unsupervised clustering by Pearson correlation and average

[4] www.r-project.org

Published OnlineFirst July 28, 2009; DOI:10.1158/1940-6207.CAPR-09-0084

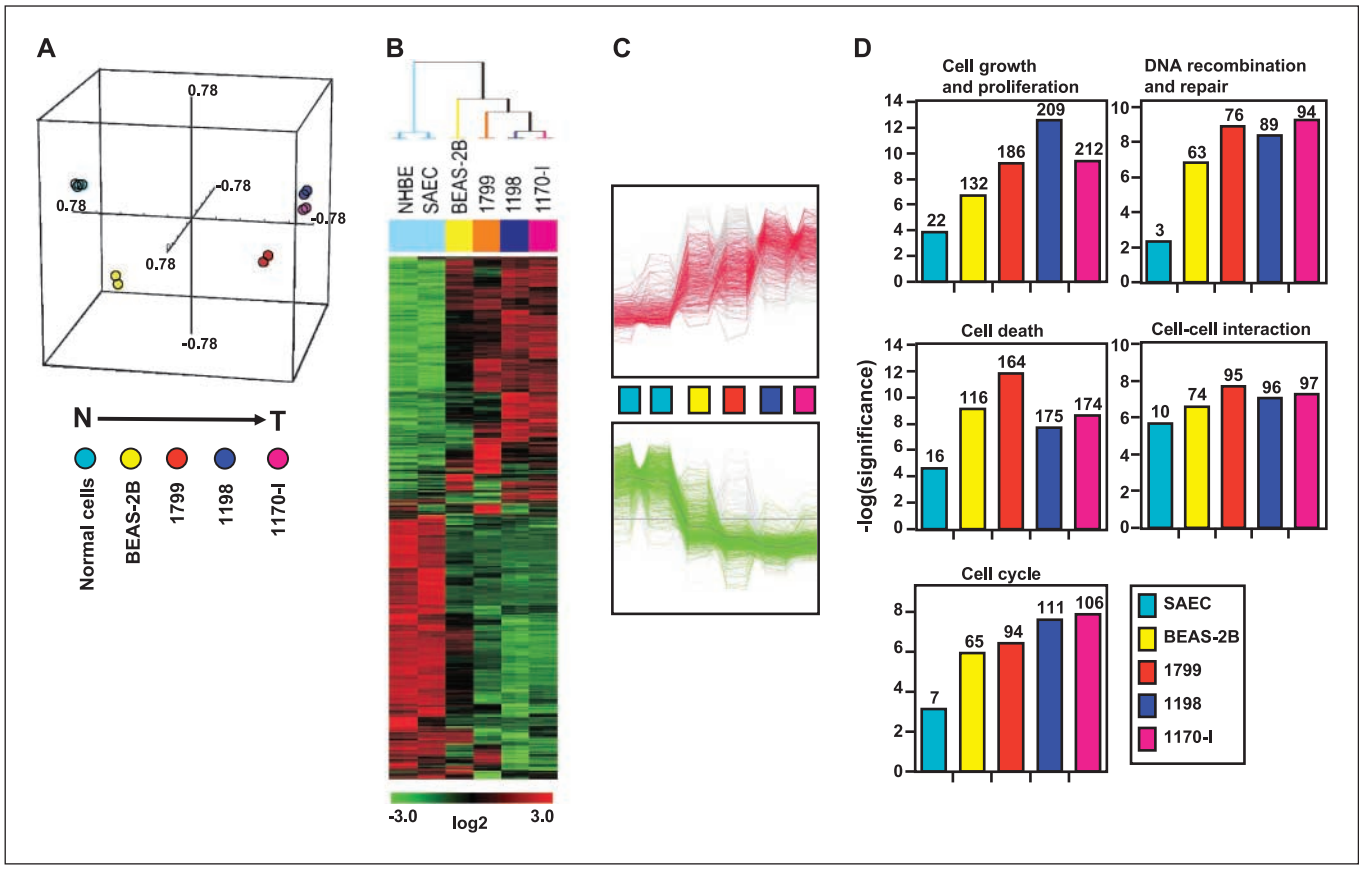

Fig. 1. Differentially expressed genes and cancer-related molecular functions between normal, immortalized, transformed, and tumorigenic lung epithelial cells. *A*, multidimensional scaling analysis by centered correlation and average linkage of the transcriptome of the indicated lung epithelial cells. *B*, unsupervised cluster analysis by Pearson correlation and average linkage of 1221 gene features found to be differentially expressed in the cells by at least 1.65-fold compared with NHBE cells. Data are represented in a matrix format in which individual rows represent single gene features and columns represent experiments. High (*red*) or low (*green*) gene expression levels are indicated, respectively, as indicated by the log2 transformed scale bar. *C*, SOM analysis of variation of the differentially expressed gene features. Genes with progressive up-regulation (*red*) or down-regulation (*green*) are highlighted, respectively, in the graphs. *D*, functional pathways analysis of genes differentially expressed in cells by at least 2-fold relative to the NHBE cells using global functional categories from IPA. The value of -log(significance) represents the inverse log of the *P* values of the modulation of the depicted functional categories between the different cells. The number of genes displaying >2-fold change is indicated above each bar.

linkage identified 659 genes (301 up-regulated and 358 down-regulated; red and green, respectively) displaying progressive variation from the NHBE to the 1170-I cells (Fig. 1C). Genes with progressive variation by at least 2-fold across cells of the *in vitro* human lung carcinogenesis model were further functionally analyzed using Ingenuity Pathways Analysis (IPA)®. Cell growth and proliferation, cell death, cell cycle, DNA recombination and repair, and cell to cell interaction gene sets were estimated by IPA® to be altered in function significantly (measured as -log of the *P* value) and progressively across cells of the *in vitro* model (Fig. 1D). In addition, the number of genes differentially expressed relative to NHBE cells and in four molecular gene sets (indicated above the bars) was highest in the 1170-I tumorigenic cells and lowest in the normal SAEC (Fig. 1D).

Significant modulation of high-interaction gene networks in the tumorigenic 1170-I cells relative to the NHBE cells

We next tried to identify genes predicted to be important in the progression of the *in vitro* human lung carcinogenesis model through both their modulation in expression and molecular interactions. Gene interaction network analysis of the 1221 gene features differentially expressed between the NHBE cells and tumorigenic 1170-I lung epithelial cells by IPA® revealed the significant (score; -log of the *P* value) modulation of functional networks related to DNA recombination and repair, cell cycle, cell death, cellular assembly and organization, and cell-to-cell signaling and interaction (Fig. 2A). The expression of Minichromosome maintenance (*MCM*) 2 and *6*, Stratifin (*SFN*), Flap structure-specific endonuclease 1 (*FEN1*), Targeting protein for Xklp2 (*TPX2*), and *UBE2C* is depicted in a representative gene network in the 1799, 1198, and 1170-I cells compared with NHBE cells (Fig. 2B). The expression levels of *UBE2C, TPX2, MCM2, MCM6*, as well as *FEN1* were increased (indicated by the red color) in the premalignant and tumorigenic cells relative to the NHBE cells, whereas the expression level of *SFN* was decreased (indicated by the green color).

Integrative genomics analysis of the association of differentially and progressively expressed genes within the human *in vitro* lung carcinogenesis model with NSCLC gene expression patterns and clinical outcome

To explore the relevance of this *in vitro* model to NSCLC, we developed a gene signature composed of 584 genes based

Published OnlineFirst July 28, 2009; DOI:10.1158/1940-6207.CAPR-09-0084

on a differential expression of at least 2-fold between the 1170-I tumorigenic and the NHBE cells and with a statistical significance of P value of <0.001 of an applied univariate t test with permutation, as well as displaying progressive variation across all cells of the *in vitro* model. The expression of these genes was then analyzed in 361 adenocarcinomas from the study by Shedden et al. (12) as described in the Supplementary Materials and Methods and integrated with their expression in the NHBE and 1170-I cells to create a composite gene expression data set depicted in Fig. 3A. Hierarchical cluster analysis of the integrated data revealed that the 361 patients could be divided into two groups or clusters comprising either the NHBE cells (NHBE cluster, highlighted in blue) or the 1170-I tumorigenic lung cells (1170-I cluster, highlighted in red; Fig. 3B). In addition, Kaplan-Meier plots and log-rank survival statistics showed that the lung adenocarcinoma patients from the 1170-I expression cluster displayed significantly poorer overall survival ($P = 0.0009$) and progression-free survival ($P = 0.03$) than patients from the NHBE expression subgroup (Fig. 3C). These findings show that the gene expression patterns of cells of the human *in vitro* lung carcinogenesis model used in this study are highly evident in NSCLC clinical samples and associated with lung adenocarcinoma prognosis.

Analysis of the prognostic potential of the six selected genes in lung adenocarcinoma patients

The functional pathways analysis of the transcriptome of the human *in vitro* lung carcinogenesis model enabled us to select six differentially expressed genes prominent in high gene interactions (*UBE2C*, *MCM2*, *MCM6*, *TPX2*, *FEN1*, and *SFN*). We next assessed the expression of these genes in published microarray data sets of lung adenocarcinoma cohorts. Hierarchical cluster analysis revealed that lung adenocarcinoma patients in each of the three cohorts (Shedden et al., Bhattacharjee et al., and Bild et al.; refs. 12–14) were each divided into two subgroups or clusters based on the expression of the selected genes alone (Fig. 4A, B, and C). In addition, Kaplan-Meier plots and log-rank statistics showed that the two divided lung adenocarcinoma patient clusters of the analyzed cohort published by Shedden et al. ($n = 361$; ref. 12) exhibited significant differences in overall survival ($P = 0.004$) and progression-free survival ($P = 0.04$; Fig. 4A). Consistently, the identified clusters in each of both the Bhattacharjee et al. (13) and Bild et al. (14) lung adenocarcinoma data sets exhibited significant differences in overall survival ($P = 0.004$ and $P = 0.02$, respectively; Fig. 4B and C). These findings show that the human *in vitro* lung carcinogenesis model is powerful for generation of gene classifiers associated with prognosis of lung adenocarcinoma.

Differential expression of UBE2C mRNA in NSCLC compared with adjacent normal lung tissues as revealed by *in silico* and quantitative real-time PCR analyses

Using Oncomine, a publicly available microarray analysis tool and platform (15), we found that the mRNA one of the six selected genes, *UBE2C*, was significantly elevated in human lung adenocarcinomas relative to adjacent normal lung tissue in four microarray databases and cohorts (all $P < 0.05$; Supplementary Fig. S1A). Moreover, *in silico* analysis of gene expression data from the Garber et al. cohort (16) also revealed the significant up-regulation of *UBE2C* in squamous cell carcinomas (SCC) relative to adjacent normal lung tissues ($P < 0.001$; Supplementary Fig. S1A). We also analyzed the mRNA levels of *UBE2C* in a set of frozen human lung adenocarcinomas tissues ($n = 26$) and adjacent normal lung tissues ($n = 24$) and found that they were significantly higher in the lung adenocarcinomas relative to adjacent normal lung ($P < 0.001$; Supplementary Fig. S1B).

Analysis of UBE2C protein expression by immunohistochemistry in normal, preneoplastic, and malignant lung tissue specimens and assessment of its value in lung cancer prognosis

We analyzed UBE2C expression at the protein level by immunohistochemistry using histologic tissue sections that included normal bronchial epithelia, preneoplastic lesions, SCCs ($n = 98$), and adenocarcinomas ($n = 141$). UBE2C protein was localized to the cell nucleus in most cases and its nuclear expression was very low in normal bronchial epithelia but was higher in preneoplastic and malignant lung lesions (Fig. 5A and B). In addition, UBE2C expression was statistically significantly different in SCCs ($n = 98$), or adenocarcinomas ($n = 141$), when compared with normal bronchial epithelia ($n = 62$; *, $P < 0.001$) or hyperplasias ($n = 61$; **, $P < 0.001$; Fig. 6A). In addition, squamous metaplasias ($n = 15$), dysplasias ($n = 9$), and carcinoma *in situ* ($n = 26$) exhibited significantly higher levels of nuclear UBE2C when compared with normal bronchial epithelia (*, $P < 0.001$) or hyperplasias (**, $P < 0.001$). Moreover, nuclear UBE2C levels were statistically significantly higher in hyperplasias relative to the levels in normal bronchial epithelia ($P < 0.001$; Fig. 6A).

Our analyses also showed that nuclear UBE2C protein expression was statistically different between SCCs and lung adenocarcinomas ($P < 0.001$; Fig. 6A). We also analyzed the correlation of nuclear UBE2C expression with clinicopathologic variables examined for all NSCLC histologic tissue specimens. There were no statistically significant correlations between nuclear UBE2C expression and age, gender, or disease stage in all NSCLC tissues or when adenocarcinomas or SCCs were analyzed alone (data not shown). However, nuclear UBE2C levels were significantly higher in NSCLC tissue resected from smokers ($n = 205$) relative to those resected from nonsmokers ($n = 34$; $P < 0.001$; Fig. 6B).

We next assessed the clinical relevance of nuclear UBE2C expression in early-stage lung cancer. Log-rank statistics and Kaplan Meier plots revealed that stage I NSCLC patients with positive UBE2C expression ($n = 118$) exhibited significantly poorer overall survival and progression-free survival than patients with negative nuclear UBE2C expression ($n = 53$; Fig. 6C and D). Moreover, multivariate Cox proportional hazard regression analyses revealed that nuclear UBE2C expression was an independent predictor of progression-free survival ($P = 0.05$) but not overall survival (data not shown). These results show the potential role of aberrant nuclear UBE2C expression in early-stage NSCLC progression and clinical outcome.

Discussion

Lung cancer is the leading cause of cancer deaths in the United States with the overall 5-year survival rate of <15%

Published OnlineFirst July 28, 2009; DOI:10.1158/1940-6207.CAPR-09-0084

A

Top categories	No. focus genes	Score	Genes in the network (modulated in 1170-I compared to NHBE)
DNA Replication, recombination, Repair, Cell Cycle, Cellular assembly and organization	35	47	↓ANXA4*, ↑AURKA*, ↑CCNA2, ↑CCNB1, ↑CCNB2, ↑CDC2*, ↑CDC6*, ↑CDC7, ↑CDC20, ↑CDC25B, ↑CDC25C, ↑CDC45L, ↑CDT1, ↑CKS1B, ↓CSTA, ↓FOS, ↑FOXM1, ↑GMNN, ↑HMMR*, ↓LAMP2*, ↓LTBP2, ↑MCM2, ↑MCM3, ↑MCM4*, ↑MCM5, ↑MCM6, ↑MCM7*, ↓MMP10, ↑PTTG1, ↓RBP1, ↑RUVBL2, ↓SERPINB7, ↓TGFBI, ↑TPX2, ↑UBE2C
Cancer, Cell-To-Cell Signaling and Interaction, Cellular Compromise	35	47	↑BUB1*, ↑BUB1B, ↓CD44*, ↑CENPE, ↑CENPF, ↑CSE1L*, ↓CSPG2*, ↓CTSB*, ↑DKK1, ↑EIF5A*, ↓F3, ↑FBLN1*, ↓FLNB, ↑FLOT1*, ↓FN1*, ↓GJB3*, ↓ITGB6, ↑KPNA2, ↑KPNB1*, ↓LTBP1, ↑NXF1, ↑PLEKHC1, ↓PTHLH*, ↑RAE1, ↑RANBP1, ↑RCC1 (includes EG:1104), ↓S100A10, ↓S100A11*, ↑TFPI, ↓TGM1, ↓THBS1*, ↑THY1*, ↓TNC, ↓TXNIP*, ↑XPO1
DNA Replication, Recombination, and Repair, Cell Death	35	47	↓APLP2*, ↓APOE, ↓APP, ↑ATAD2, ↓BIK, ↑CCT2*, ↑CCT5, ↓CD59*, ↑CDKN2A*, ↑DHFR*, ↑DONSON, ↓FABP5, ↑FEN1*, ↑G1P2, ↓GLUL*, ↑HLA-C, ↓IER3, ↓IFI16, ↑IFITM2, ↓ITM2B, ↑KIAA0101, ↑MAP1B, ↓MCL1*, ↑MELK, ↑MSH6, ↑PCNA, ↓RAB38, ↑RFC4, ↓S100A7, ↓SNCA, ↑TCP1, ↑TMEM97*, ↓TNFAIP3*, ↓TNFSF10*, ↑UCHL1
Cell cycle, and cellular assembly organization	26	27	↑AURKB, ↑BIRC5*, ↑BRRN1, CDCA8, ↑CENPA*, ↑CNAP1, DES, ↑DNAJA1*, ↓FSCN1, ↑HCAP-D3, ↑HCAP-G, ↑HCAP-H2, ↑HSP90AA1, ↑HSPA8*, INCENP, ↑KIF23, ↑KIF4A, ↓LIMA1, ↑LMNB1, ↑LUZP5, ↑NASP*, ↑PRC1, ↓PRNP, PTGES3, RACGAP1, SMC2L1, ↑SMC4L1*, ↑SOD1, ↑STIP1*, ↑TLN1, ↑TOP2A*, ↑TWIST1, ↓UPP1, ↑VIM, ↓YWHAZ*

B

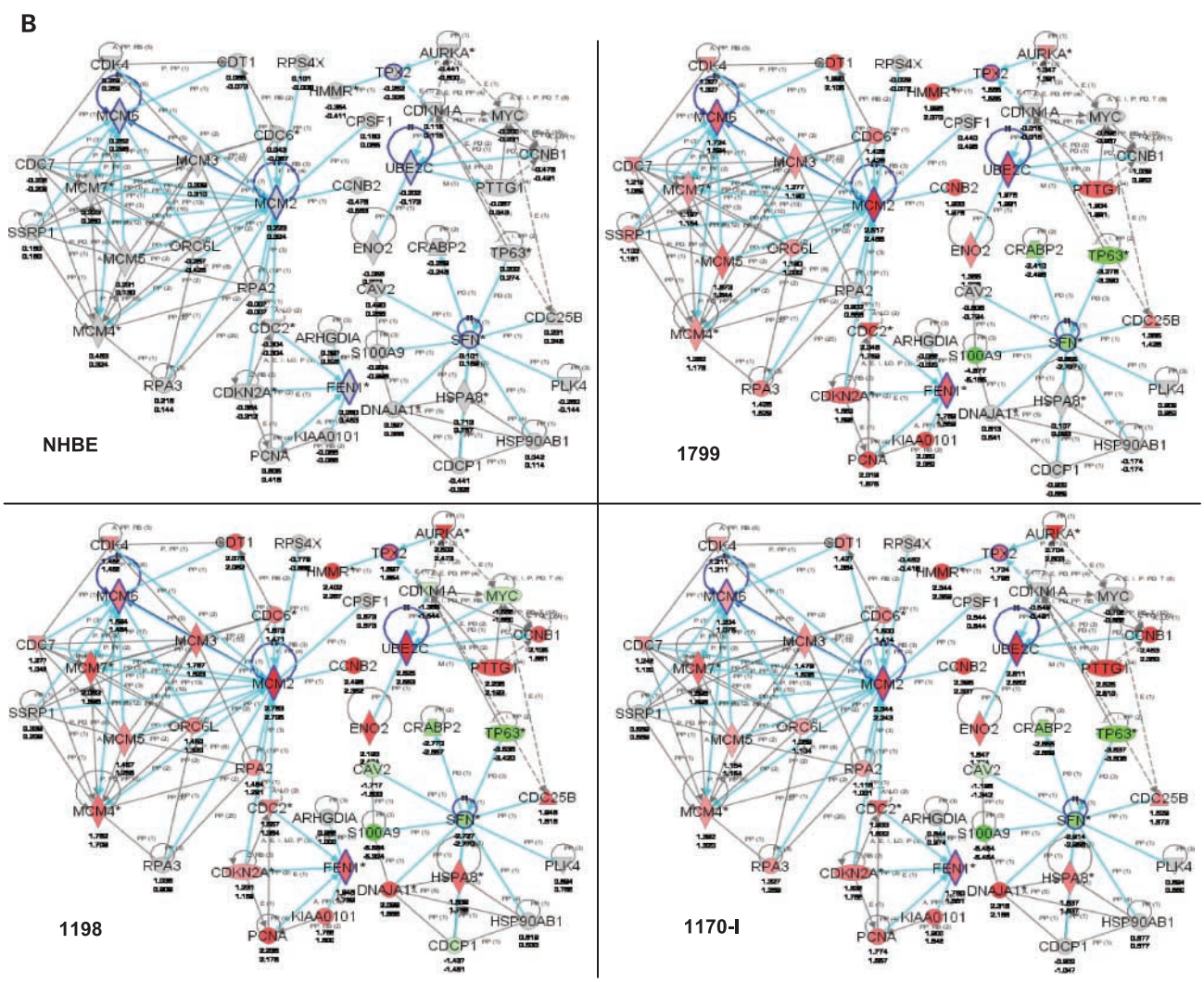

Published OnlineFirst July 28, 2009; DOI:10.1158/1940-6207.CAPR-09-0084

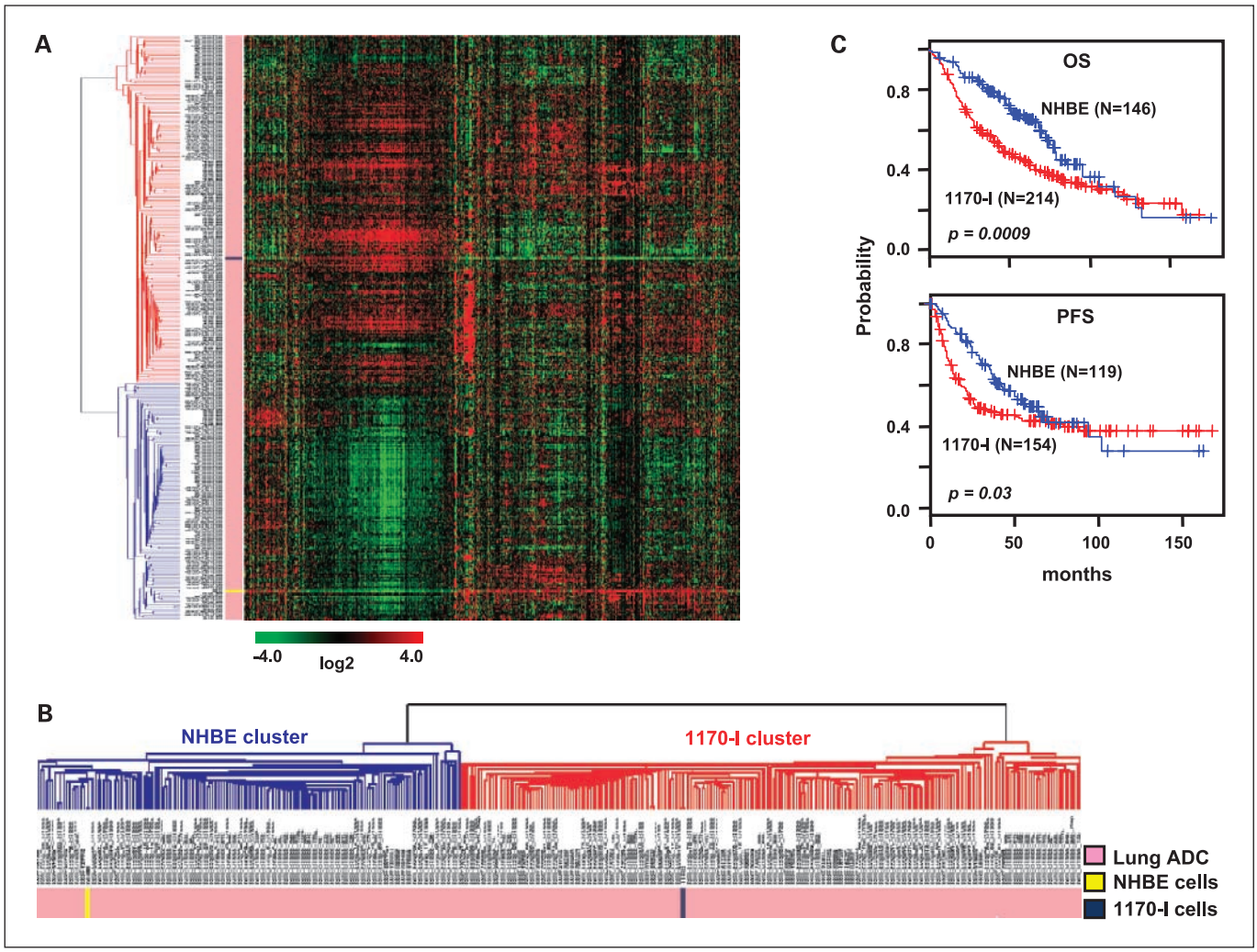

Fig. 3. The association of genes differentially expressed in the *in vitro* model of lung carcinogenesis with lung adenocarcinoma gene expression patterns and prognosis. *A* and *B*, the 584 genes were selected as described in the Supplementary Materials and Methods. The genes were median centered independently in the lung epithelial cells and adenocarcinomas (n = 361) before integration, further filtered to include those with modulation in expression of at least 2-fold in at least eight observations and then analyzed by hierarchical cluster analysis with average linkage. Data are represented in a matrix format in which individual columns represent single gene features and rows represent experiments. High (*red*) or low (*green*) gene expression levels are indicated, respectively, as indicated by the log2 transformed scale bar. *C*, Kaplan-Meier plots for the overall survival (*OS*) and progression-free survival (*PFS*) of lung adenocarcinoma patients separated according to clustering patterns (*blue*, NHBE cluster; *red*, 1170-I cluster). The number of analyzed samples of each cluster in both plots is indicated as N next to the plotted arms. *P* values were obtained by the log-rank test.

(1). However, the survival of stage I or early stage NSCLC patients is significantly higher than that of patients with advanced lung cancers (2, 3). Therefore, a considerable effort has been mounted over the last few years to apply the progress in various high throughput methods for the identification of potential molecular markers for diagnosis and prognosis (2, 17). Most of these studies were based on comparisons of gene expression in tumors relative to normal appearing tissue and almost no studies addressed changes in premalignant tissue, most likely due to the paucity of material available for high throughput analysis. Previously, several *in vitro* approaches have been applied to address the shortage of premalignant tissue. For example, ectocervical keratinocytes and mammary epithelial cells have been immortalized using human papillomavirus (18, 19), and normal bronchial epithelial cells were immortalized using telomerase plus CDK4 (20).

NSCLC develops by a multistep process that involves the accumulation of many genetic aberrations over a long period of time. Interestingly, most of these genetic changes (such as p53 loss or mutation or epidermal growth factor receptor

Fig. 2. Gene interaction network analysis of genes differentially expressed in the human *in vitro* lung carcinogenesis model. *A*, top four gene networks generated from IPA and significantly modulated between the 1170-I tumorigenic and NHBE cells. Gene symbols (*blue*) are presented; arrows, variation of their gene expression in the 1170-I tumorigenic cells relative to NHBE cells. The network score was calculated by the inverse log of the *P* value and indicates the likelihood of focus genes in a network being found together than due to chance. The number of focus genes (in bold) refers to the genes differentially regulated and within an IPA network composed of a maximum number of 35 genes. *B*, functional pathway analysis by IPA of selected genes and their interaction nodes in 1799, 1198, and 1170-I cells relative to NHBE cells. The selected genes (MCM2, MCM6, SFN, TPX2, UBE2C, and FEN1) are highlighted by a blue border. Gene expression variation by at least 2-fold is depicted by color (red, up-regulated; green, down-regulated; gray, no significant change).

Published OnlineFirst July 28, 2009; DOI:10.1158/1940-6207.CAPR-09-0084

mutation and amplification) occur very early in the premalignant stages and persist during the carcinogenesis process (2). Our study was aimed to gain information on genetic changes that occur at different early stages of lung carcinogenesis and can be relevant to the clinical outcome of the disease. Towards this, we used an *in vitro* lung carcinogenesis cell model composed of normal, immortalized, transformed, and tumorigenic lung epithelial cells, the latter two developed *in vivo* in mice that had the immortalized BEAS-2B transplanted and exposed to cigarette smoke condensate (9). We did global gene expression analysis on the transcriptome of these cells and showed the gradual modulation of genes and their associated cancer-related molecular functions and gene interaction networks. Using integrative gene expression analysis methodologies, we showed the relevance of genes differentially expressed within the *in vitro* model to lung adenocarcinoma gene expression patterns and clinical outcome. In addition and specifically, we showed the progressive increase in UBE2C protein expression in lung lesions and lastly unraveled an association between its expression and poor NSCLC prognosis.

Functional pathways and topological gene interaction network analyses helped us select genes with both differential expression as well as predicted deregulated signaling function. Our six gene signature includes two genes (*MCM2* and *TPX2*) that had been previously implicated independently in NSCLC progression and prognosis (21–23). We also found that the *FEN1* endonuclease was progressively differentially expressed in the premalignant lung cells. Interestingly, transgenic mice harboring mutant *FEN1* exhibit substantial pulmonary hypoplasia (24). The 14-3-3 protein family member, *SFN* (14-3-3 σ), was also found in our analyses to be differentially expressed in the premalignant lung cells. It is worthy to note that CpG hypermethylation of *SFN* promoter has been implicated in many cancers including bladder, breast, lymphoid, and lung tumors (25–28). Our findings suggest that epigenetic silencing of *SFN* may occur very early in lung cancer development.

Previous gene expression profiling of cultured cells have led to the discovery of individual genes or a group of genes for the study of distinct breast cancer subclasses (29), and predicting

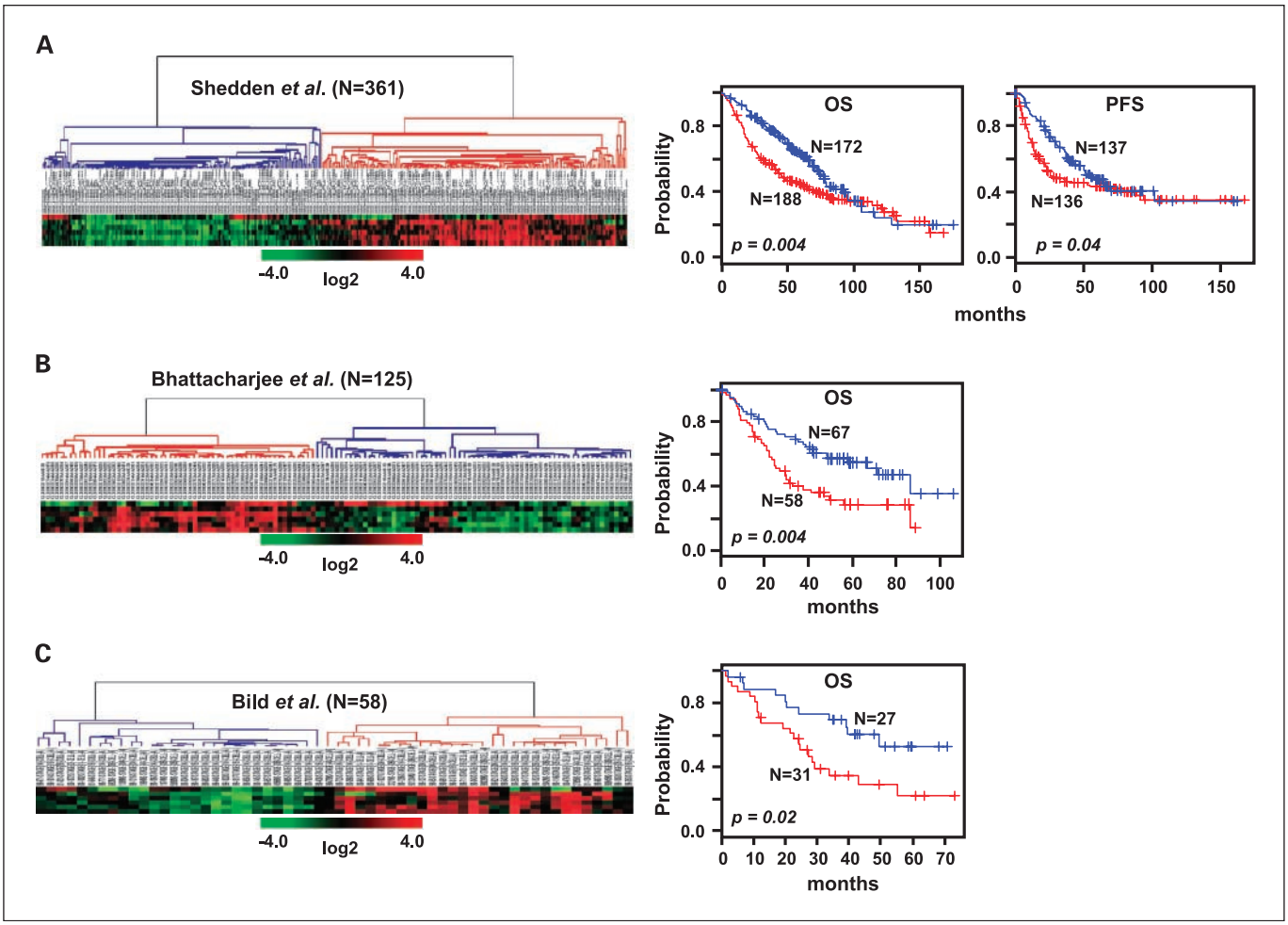

Fig. 4. An identified six gene classifier associated with lung adenocarcinoma prognosis. Hierarchical cluster analysis with average linkage of the expression of *UBE2C, MCM2, MCM6, TPX2, FEN-1,* and *SFN* in three published lung adenocarcinoma cohorts by Shedden et al. (*A*), Bhattacharjee et al. (*B*), and Bild et al. (*C*). Data are represented in matrix formats in which individual rows represent single gene features and columns represent experiments. High or low gene expression levels are indicated by red or green color, respectively as indicated by the log2 transformed scale bars. Overall and progression-free survival (OS and PFS) differences in the identified adenocarcinoma patient clusters were assessed by the Kaplan-Meier method of survival probability and *P*-values were obtained by the log-rank test.

Published OnlineFirst July 28, 2009; DOI:10.1158/1940-6207.CAPR-09-0084

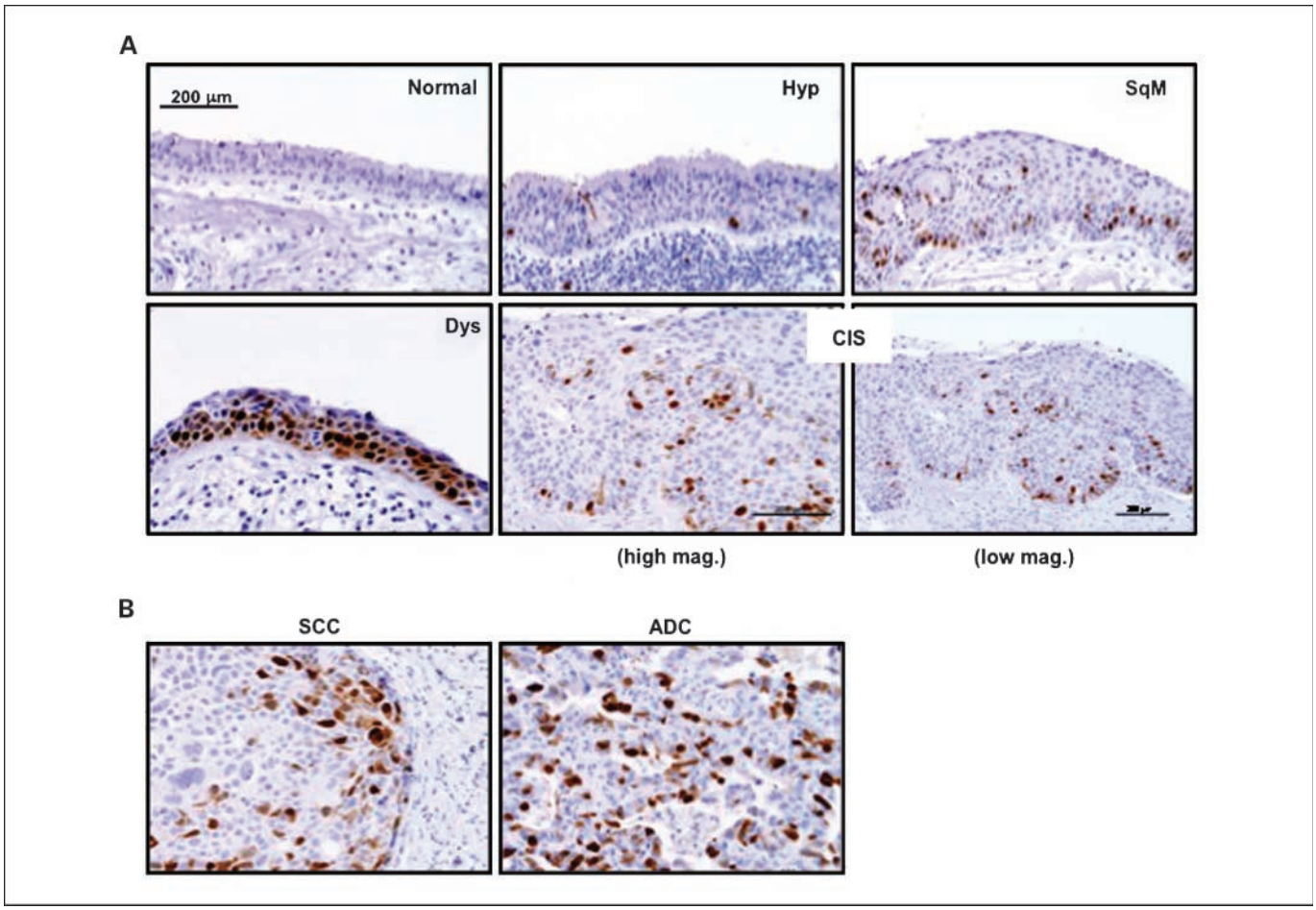

Fig. 5. Immunohistochemical analysis of UBE2C protein expression in normal bronchial epithelial, preneoplastic lung lesions, and NSCLC tissue samples. *A*, representative photomicrographs displaying the immunohistochemical expression of UBE2C in histologic tissue sections of normal bronchial epithelia (*normal*), and preneoplastic lung lesions (*hyp*, hyperplasia; *sqM*, squamous metaplasia; *dys*, dysplasia; *CIS*, carcinoma *in situ*). *B*, representative photomicrographs of UBE2C expression in lung SCC and adenocarcinoma.

survival of cancer patients, namely ovarian and breast cancers (17, 30). For example, a series of human mammary epithelial cells expressing different transfected and activated oncogenes were used to develop gene pathway signatures that distinguished between human cancer subtypes based on distinct oncogenic pathways and predicted clinical outcome in several cancer patient subsets (14). Interestingly, our list of 584 differentially expressed genes included 112 genes that were present in two gene classifier lists capable of predicting clinical outcome without the incorporation of clinical covariables and compiled in the multiblinded microarray validation study by Shedden et al. (12), which provides the largest available set of microarray data with extensive pathologic and clinical annotation for lung adenocarcinomas (supporting material). Our findings show that by analyzing the transcriptomes of normal, premalignant, and tumorigenic lung epithelial cells in culture, we were able to highlight genes prominent in NSCLC clinical samples and capable of predicting clinical outcome. Interestingly, six of these genes, selected after IPA® analysis, were also associated with lung adenocarcinomas of poor prognosis, which was reproducible in more independent cohorts than the total 584 genes. It is worthwhile to note that our study also incorporates one of the largest *in silico* validations of the prognostic potential of an identified gene expression signature.

It is worthy to note that both the 584-gene and the 6-gene signatures were specific for adenocarcinoma because, when analyzed in data sets of lung SCCs, they were not significantly associated with poor prognosis. The specificity of the signatures for adenocarcinomas may reflect the distinct molecular and biological profiles of lung adenocarcinomas and SCCs (2). Although restricted to adenocarcinomas, these findings are of value as there has been a major global trend with a sharp increase in adenocarcinoma and a decrease in SCC (31, 32). In addition and in the past five decades, adenocarcinoma has become the predominant type of lung cancer cell in smokers (33). The selective association of the signatures with adenocarcinoma survival seemed to be unexpected given that the *in vitro* cell system was derived from bronchial epithelial cells that are considered to harbor precursors of SCC. However, if one considers the finding of Klein-Szanto et al. (9) that the 1170-I lung tumorigenic cells derived from the bronchial BEAS-2B cells formed invasive lung adenocarcinomas rather than SCCs in xenotransplanted mice, then the specificity for adenocarcinoma survival is not counterintuitive.

To our knowledge, this is the first demonstration of the potential in predicting NSCLC prognosis of an *in vitro* system emulating the various lung carcinogenesis phases. The immortalization of the human bronchial epithelial cells that served as

Published OnlineFirst July 28, 2009; DOI:10.1158/1940-6207.CAPR-09-0084

the basis for this model was accomplished by infection with an adenovirus 12-SV40 hybrid virus (34). The molecular basis for the immortalization is most likely due to the inactivation of p53 and retinoblastoma tumor suppressor genes by the SV40 large tumor antigen (35). These molecular abnormalities led to changes in gene expression that seem to be shared by many NSCLC tumors because concurrent abnormalities in both p53 and retinoblastoma pathways have been identified in between 28% (36) and 37% (37) of NSCLC and the majority of the rest had an abnormality in at least one of the two pathways. It is also noteworthy that a previously identified SV40 T/t-Antigen cancer gene signature, developed and integrated from mouse models, was highly evident in the gene expression patterns of clinical samples of human breast, prostate, and lung cancers and was significantly associated with poor prognosis in these tumors (38). Moreover, we have previously validated aberrant gene expression within *the vitro* system we used at the mRNA level in 11 established NSCLC cell lines and at the protein level in clinical NSCLC samples (39, 40). In this much more comprehensive study using more advanced technology, we further established that this particular cell system provides a powerful tool to predict outcomes of NSCLC cancers and aids in the exploration of the molecular mechanisms of lung carcinogenesis that could be translated into both chemoprevention and treatment of lung cancer.

Our network analysis showed that the E2 ubiquitin-conjugating enzyme, *UBE2C*, was part of the most significantly activated gene interaction network. UBE2C up-regulation and marked nuclear expression is associated with esophageal adenocarcinoma progression (41). More recently, *UBE2C* was shown to be crucial for activation of the anaphase promoting complex for subsequent ubiquitination and deactivation of spindle checkpoint substrates (42, 43). Despite intriguing observations that *UBE2C* mRNA levels were higher in a variety of primary tumors compared with corresponding normal tissues (44), its expression in premalignant stages nor its potential as a prognostic marker for lung cancer has been investigated. We have shown that

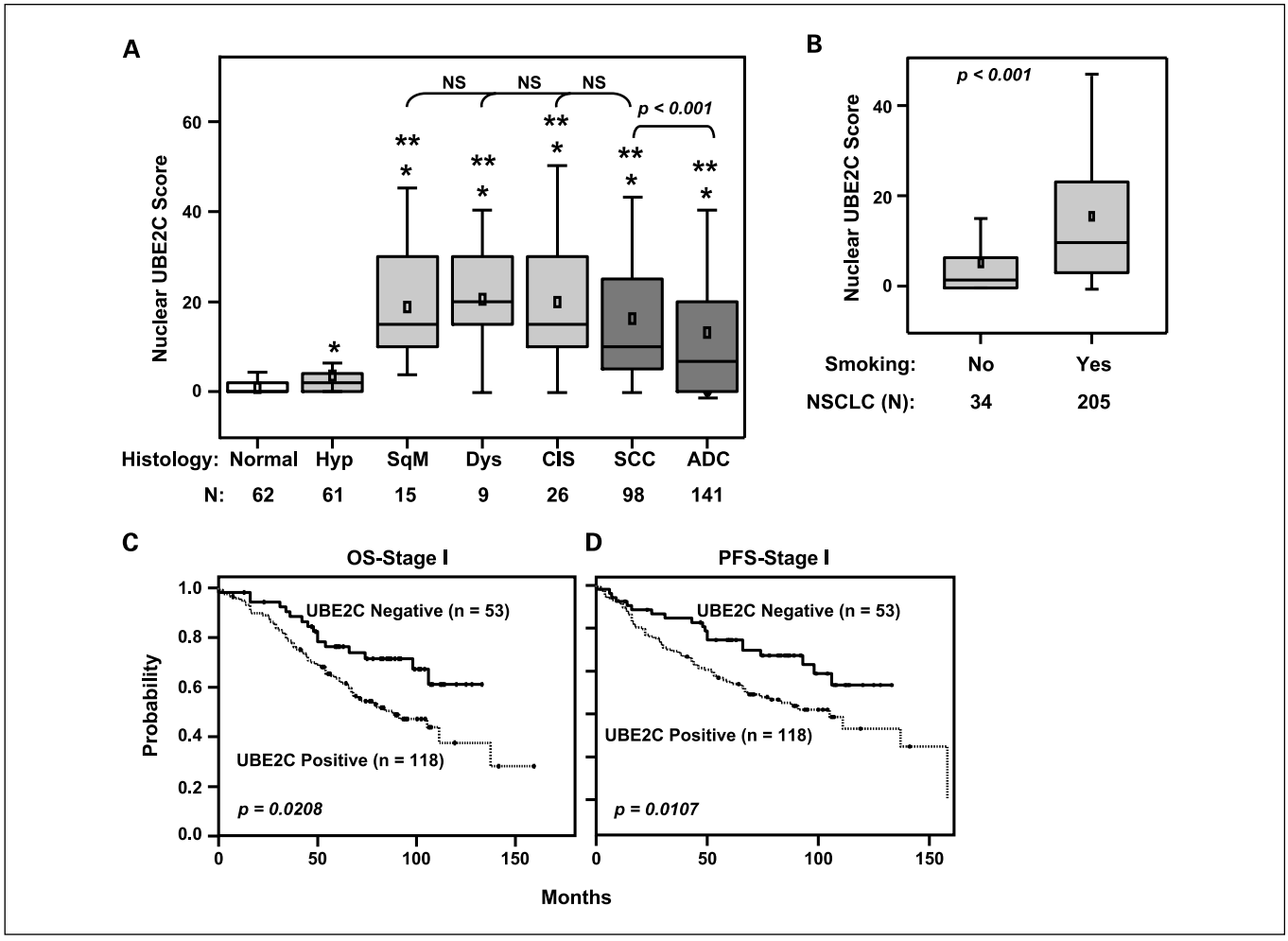

Fig. 6. Association of UBE2C expression with NSCLC progression and clinical outcome. *A*, box-plot depicting statistical analysis by the Wilcoxon-rank test of nuclear UBE2C score in normal bronchial epithelia (*white box*), preneoplastic lesions (*light gray boxes*), as well as lung SCC and adenocarcinoma (*dark gray boxes*). *P* values representing significance of pair-wise comparison between different lung lesions when compared with normal bronchial epithelia (*) or hyperplasias (**) are marked, respectively. Significance of other pair-wise comparisons is also indicated on the figure (*NS*, not significant). *B*, box-plot representing pair-wise comparison between NSCLC nonsmokers (*no*) and smokers (*yes*) for nuclear UBE2C score. Kaplan-Meier plots for the overall survival (*OS*; *C*) and progression-free survival (*PFS*; *D*) of stage I NSCLC patients stratified according to positive (n = 118) or negative (n = 53) nuclear UBE2C immunoreactivity. *P* values were obtained by the log-rank test.

Published OnlineFirst July 28, 2009; DOI:10.1158/1940-6207.CAPR-09-0084

UBE2C protein expression is up-regulated in preneoplastic lung lesions and NSCLC samples, its expression was significantly associated with smoking status and that stage I NSCLC patients who expressed nuclear UBE2C exhibited significantly poorer survival than patients who did not express it. It is possible that NSCLC patients with higher UBE2C expression are more resistant to Taxol-based chemotherapies because cells overexpressing UBE2C exhibit compromised mitotic arrest induced by the microtubule disrupting and spindle checkpoint activating Taxol (42).

In conclusion, our study using the human *in vitro* lung carcinogenesis model identified novel gene signatures that are effective in the prognostic evaluation of lung cancers. Moreover, we unravel a potential novel role for *UBE2C* expression in NSCLC pathogenesis and prognosis.

Disclosure of Potential Conflicts of Interest

No potential conflicts of interest were disclosed.

References

1. Jemal A, Siegel R, Ward E, et al. Cancer statistics, 2008. CA Cancer J Clin 2008;58:71–96.
2. Herbst RS, Heymach JV, Lippman SM. Lung cancer. N Engl J Med 2008;359:1367–80.
3. Sun S, Schiller JH, Spinola M, Minna JD. New molecularly targeted therapies for lung cancer. J Clin Invest 2007;117:2740–50.
4. Mountain CF. The international system for staging lung cancer. Semin Surg Oncol 2000;18:106–15.
5. Ponticiello A, Barra E, Giani U, Bocchino M, Sanduzzi A. P53 immunohistochemistry can identify bronchial dysplastic lesions proceeding to lung cancer: a prospective study. Eur Respir J 2000; 15:547–52.
6. Westra WH, Baas IO, Hruban RH, et al. K-ras oncogene activation in atypical alveolar hyperplasias of the human lung. Cancer Res 1996;56:2224–8.
7. Xu XC, Lee JS, Lee JJ, et al. Nuclear retinoid acid receptor β in bronchial epithelium of smokers before and during chemoprevention. J Natl Cancer Inst 1999;91:1317–21.
8. Belinsky SA, Nikula KJ, Palmisano WA, et al. Aberrant methylation of p16(INK4a) is an early event in lung cancer and a potential biomarker for early diagnosis. Proc Natl Acad Sci U S A 1998;95: 11891–6.
9. Klein-Szanto AJ, Iizasa T, Momiki S, et al. A tobacco-specific N-nitrosamine or cigarette smoke condensate causes neoplastic transformation of xenotransplanted human bronchial epithelial cells. Proc Natl Acad Sci U S A 1992;89:6693–7.
10. Hu J, Kapoor M, Zhang W, Hamilton SR, Coombes KR. Analysis of dose-response effects on gene expression data with comparison of two microarray platforms. Bioinformatics 2005;21:3524–9.
11. Behrens C, Lin HY, Lee JJ, et al. Immunohistochemical expression of basic fibroblast growth factor and fibroblast growth factor receptors 1 and 2 in the pathogenesis of lung cancer. Clin Cancer Res 2008;14:6014–22.
12. Shedden K, Taylor JM, Enkemann SA, et al. Gene expression-based survival prediction in lung adenocarcinoma: a multi-site, blinded validation study. Nat Med 2008;14:822–7.
13. Bhattacharjee A, Richards WG, Staunton J, et al. Classification of human lung carcinomas by mRNA expression profiling reveals distinct adenocarcinoma subclasses. Proc Natl Acad Sci U S A 2001;98: 13790–5.
14. Bild AH, Yao G, Chang JT, et al. Oncogenic pathway signatures in human cancers as a guide to targeted therapies. Nature 2006;439:353–7.
15. Rhodes DR, Yu J, Shanker K, et al. ONCOMINE: a cancer microarray database and integrated datamining platform. Neoplasia 2004;6:1–6.
16. Garber ME, Troyanskaya OG, Schluens K, et al. Diversity of gene expression in adenocarcinoma of the lung. Proc Natl Acad Sci U S A 2001;98:13784–9.
17. van't Veer LJ, Bernards R. Enabling personalized cancer medicine through analysis of gene-expression patterns. Nature 2008;452:564–70.
18. Dimri G, Band H, Band V. Mammary epithelial cell transformation: insights from cell culture and mouse models. Breast Cancer Res 2005;7:171–9.
19. Wan F, Miao X, Quraishi I, Kennedy V, Creek KE, Pirisi L. Gene expression changes during HPV-mediated carcinogenesis: a comparison between an *in vitro* cell model and cervical cancer. Int J Cancer 2008;123:32–40.
20. Ramirez RD, Sheridan S, Girard L, et al. Immortalization of human bronchial epithelial cells in the absence of viral oncoproteins. Cancer Res 2004; 64:9027–34.
21. Ma Y, Lin D, Sun W, et al. Expression of targeting protein for xklp2 associated with both malignant transformation of respiratory epithelium and progression of squamous cell lung cancer. Clin Cancer Res 2006;12:1121–7.
22. Ramnath N, Hernandez FJ, Tan DF, et al. MCM2 is an independent predictor of survival in patients with non-small-cell lung cancer. J Clin Oncol 2001;19:4259–66.
23. Tan DF, Huberman JA, Hyland A, et al. MCM2-a promising marker for premalignant lesions of the lung: a cohort study. BMC Cancer 2001;1:6.
24. Zheng L, Dai H, Qiu J, Huang Q, Shen B. Disruption of the FEN-1/PCNA interaction results in DNA replication defects, pulmonary hypoplasia, pancytopenia, and newborn lethality in mice. Mol Cell Biol 2007;27:3176–86.
25. Bhatia K, Siraj AK, Hussain A, Bu R, Gutierrez MI. The tumor suppressor gene 14-3-3 σ is commonly methylated in normal and malignant lymphoid cells. Cancer Epidemiol Biomarkers Prev 2003;12:165–9.
26. Lodygin D, Hermeking H. Epigenetic silencing of 14-3-3σ in cancer. Semin Cancer Biol 2006;16: 214–24.
27. Negraes PD, Favaro FP, Camargo JL, et al. DNA methylation patterns in bladder cancer and washing cell sediments: a perspective for tumor recurrence detection. BMC Cancer 2008;8:238.
28. Umbricht CB, Evron E, Gabrielson E, Ferguson A, Marks J, Sukumar S. Hypermethylation of 14-3-3 σ (stratifin) is an early event in breast cancer. Oncogene 2001;20:3348–53.
29. Neve RM, Chin K, Fridlyand J, et al. A collection of breast cancer cell lines for the study of functionally distinct cancer subtypes. Cancer Cell 2006;10:515–27.
30. Nevins JR, Potti A. Mining gene expression profiles: expression signatures as cancer phenotypes. Nat Rev Genet 2007;8:601–9.
31. Gabrielson E. Worldwide trends in lung cancer pathology. Respirology 2006;11:533–8.
32. Sun S, Schiller JH, Gazdar AF. Lung cancer in never smokers-a different disease. Nat Rev Cancer 2007;7:778–90.
33. Thun MJ, Lally CA, Flannery JT, Calle EE, Flanders WD, Heath CW, Jr. Cigarette smoking and changes in the histopathology of lung cancer. J Natl Cancer Inst 1997;89:1580–6.
34. Reddel RR, Ke Y, Gerwin BI, et al. Transformation of human bronchial epithelial cells by infection with SV40 or adenovirus-12 SV40 hybrid virus, or transfection via strontium phosphate coprecipitation with a plasmid containing SV40 early region genes. Cancer Res 1988;48: 1904–9.
35. Ahuja D, Saenz-Robles MT, Pipas JM. SV40 large T antigen targets multiple cellular pathways to elicit cellular transformation. Oncogene 2005; 24:7729–45.
36. Geradts J, Fong KM, Zimmerman PV, Maynard R, Minna JD. Correlation of abnormal RB, p16ink4a, and p53 expression with 3p loss of heterozygosity, other genetic abnormalities, and clinical features in 103 primary non-small cell lung cancers. Clin Cancer Res 1999;5: 791–800.
37. Burke L, Flieder DB, Guinee DG, et al. Prognostic implications of molecular and immunohistochemical profiles of the Rb and p53 cell cycle regulatory pathways in primary non-small cell lung carcinoma. Clin Cancer Res 2005;11:232–41.
38. Deeb KK, Michalowska AM, Yoon CY, et al. Identification of an integrated SV40 T/t-antigen cancer signature in aggressive human breast, prostate, and lung carcinomas with poor prognosis. Cancer Res 2007;67:8065–80.
39. Lacroix L, Feng G, Lotan R. Identification of genes expressed differentially in an *in vitro* human lung carcinogenesis model. Cancer Biol Ther 2006; 5:665–73.
40. Shen J, Behrens C, Wistuba II, et al. Identification and validation of differences in protein levels in normal, premalignant, and malignant lung cells and tissues using high-throughput Western Array and immunohistochemistry. Cancer Res 2006;66: 11194–206.
41. Lin J, Raoof DA, Wang Z, et al. Expression and effect of inhibition of the ubiquitin-conjugating enzyme E2C on esophageal adenocarcinoma. Neoplasia 2006;8:1062–71.
42. Reddy SK, Rape M, Margansky WA, Kirschner MW. Ubiquitination by the anaphase-promoting complex drives spindle checkpoint inactivation. Nature 2007;446:921–5.
43. Stegmeier F, Rape M, Draviam VM, et al. Anaphase initiation is regulated by antagonistic ubiquitination and deubiquitination activities. Nature 2007;446:876–81.
44. Okamoto Y, Ozaki T, Miyazaki K, Aoyama M, Miyazaki M, Nakagawara A. UbcH10 is the cancer-related E2 ubiquitin-conjugating enzyme. Cancer Res 2003;63:4167–73.

Cancer Prevention Research

Biological Activity of Celecoxib in the Bronchial Epithelium of Current and Former Smokers

Edward S. Kim, Waun K. Hong, J. Jack Lee, et al.

Cancer Prev Res 2010;3:148-159. Published OnlineFirst January 26, 2010.

Published OnlineFirst January 26, 2010; DOI:10.1158/1940-6207.CAPR-09-0233

Research Article

Cancer Prevention Research

Biological Activity of Celecoxib in the Bronchial Epithelium of Current and Former Smokers

Edward S. Kim[1], Waun K. Hong[1], J. Jack Lee[2], Li Mao[1], Rodolfo C. Morice[3], Diane D. Liu[2], Carlos A. Jimenez[3], Georgie A. Eapen[3], Reuben Lotan[1], Ximing Tang[1], Robert A. Newman[4], Ignacio I. Wistuba[1], and Jonathan M. Kurie[1]

Abstract

Non–small cell lung cancer is the primary cause of cancer-related death in Western countries. One important approach taken to address this problem is the development of effective chemoprevention strategies. In this study, we examined whether the cyclooxygenase-2 inhibitor celecoxib, as evidenced by decreased cell proliferation, is biologically active in the bronchial epithelium of current and former smokers. Current or former smokers with at least a 20 pack-year (pack-year = number of packs of cigarettes per day times number of years smoked) smoking history were randomized into one of four treatment arms (3-month intervals of celecoxib then placebo, celecoxib then celecoxib, placebo then celecoxib, or placebo then placebo) and underwent bronchoscopies with biopsies at baseline, 3 months, and 6 months. The 204 patients were primarily (79.4%) current smokers: 81 received either low-dose celecoxib or placebo and 123 received either high-dose celecoxib or placebo. Celecoxib was originally administered orally at 200 mg twice daily and the protocol subsequently increased the dose to 400 mg twice daily. The primary end point was change in Ki-67 labeling (from baseline to 3 months) in bronchial epithelium. No cardiac toxicities were observed in the participants. Although the effect of low-dose treatment was not significant, high-dose celecoxib decreased Ki-67 labeling by 3.85% in former smokers and by 1.10% in current smokers—a significantly greater reduction ($P = 0.02$) than that seen with placebo after adjusting for metaplasia and smoking status. A 3- to 6-month celecoxib regimen proved safe to administer. Celecoxib (400 mg twice daily) was biologically active in the bronchial epithelium of current and former smokers; additional studies on the efficacy of celecoxib in non–small cell lung cancer chemoprevention may be warranted. *Cancer Prev Res; 3(2); 148–59. ©2010 AACR.*

Introduction

Non–small cell lung cancer (NSCLC) is the leading cause of death from cancer among both men and women in the United States, accounting for ~28% of such deaths. Indeed, an estimated 160,000 Americans died of NSCLC in 2007. In recent years, the incidence of NSCLC has begun to decline among men (1). However, smoking-related NSCLC has continued to increase among women, surpassing even breast cancer as the leading cause of cancer death in this group (2). Despite aggressive treatment strategies, the 5-year survival rate for NSCLC remains only ~15% (1). These grim facts underscore the urgent need for a change in our approach to NSCLC.

Authors' Affiliations: Departments of [1]Thoracic/Head and Neck Medical Oncology, [2]Biostatistics, [3]Pulmonary Medicine, and [4]Pharmacology, The University of Texas M.D. Anderson Cancer Center, Houston, Texas

Corresponding Author: Jonathan M. Kurie, Department of Thoracic/Head and Neck Medical Oncology, The University of Texas M.D. Anderson Cancer Center, Box 432, 1515 Holcombe Boulevard, Houston, TX 77030. Phone: 713-792-6363; Fax: 713-792-1220; E-mail: jkurie@mdanderson.org.

doi: 10.1158/1940-6207.CAPR-09-0233

Smoking prevention and cessation have been emphasized as ways to reduce deaths from cancer. Despite the reduction in NSCLC risk observed with smoking cessation, however, several studies have shown that former smokers still have a higher NSCLC risk than nonsmokers have (3–7) and consequently account for a large proportion of NSCLC patients in this country. Chemoprevention strategies, especially for high-risk populations such as former smokers, are appropriate in NSCLC. However, large-scale NSCLC chemoprevention trials, including the Alpha-Tocopherol Beta-Carotene trial, Beta-Carotene and Retinol Efficacy Trial, and Lung Intergroup Trial, have yet to show that any agent can reduce lung cancer risk (8–11).

One of the changes identified in premalignant bronchial tissues that has potential therapeutic significance is an increase in expression of cyclooxygenase-2 (COX-2). COX-2 converts arachidonic acid to prostaglandin H_2, a precursor of prostaglandin E_2 that has been implicated in a variety of biochemical processes, required for cell proliferation and survival, and whose expression increases in response to growth factors, oncogenes, and carcinogens (12–18). COX-2 has been extensively studied in epithelial tumors, including colorectal cancer and NSCLC (19–22). COX-2 overexpression has prognostic value, predicting a worse

Published OnlineFirst January 26, 2010; DOI:10.1158/1940-6207.CAPR-09-0233

outcome in NSCLC patients with stage I disease whose tumors have been surgically resected (23, 24) and thus suggesting that COX-2 is an important biological determinant in NSCLC. Tellingly, COX-2 expression is higher in bronchial premalignant lesions than in adjacent normal lung tissue (22, 25), raising the possibility that COX-2 promotes malignant progression in the lung. Moreover, COX-2 inhibitors have shown efficacy as NSCLC chemopreventive agents in preclinical studies, reducing the size and number of carcinogen-induced NSCLC tumors in mice (26). These findings provide a compelling rationale to investigate the activity of COX-2 inhibitors as chemopreventive agents for lung cancer.

In this study, our goal was to determine whether a 6-month treatment with celecoxib, a COX-2 inhibitor, would be safe and have biological activity in the lungs of current and former smokers. We did a randomized, placebo-controlled study to examine the toxicity and efficacy of celecoxib; bronchial epithelial cell proliferation, as measured by the Ki-67 labeling index after 3 months, was the primary end point. We chose this primary end point on the basis of evidence that bronchial premalignant lesions increase epithelial cellular proliferation and that COX-2 promotes cellular proliferation and survival (27–29).

Materials and Methods

For the present study, we recruited current smokers (those actively smoking or those who had quit within the previous 12 mo) and former smokers (those who had quit at least 12 mo before study entry) who had at least a 20 pack-year history of smoking (pack-year = number of packs of cigarettes per day times number of years smoked). Patients could have had prior stage I NSCLC or stage I or II laryngeal cancer but had to have been free of disease for at least 6 mo before study entry. Other exclusion criteria included the chronic use of steroids, the use of H_2 blockers for active ulcers, the use of nonsteroidal anti-inflammatory drugs other than low-dose aspirin of ≤81 mg/d, and a history of stroke, uncontrolled hypertension, and/or angina pectoris. Patients were recruited through local community groups, health fairs, and advertisements distributed to referring practitioners and patients at The University of Texas M.D. Anderson Cancer Center. The study was approved by the Institutional Review Board and by the U.S. Department of Health and Human Services. All patients provided written informed consent before entering the study.

Trial design and treatment

The clinical study design was a four-arm, double-blind, placebo-controlled, randomized study to evaluate the biological effects of celecoxib as a chemopreventive agent in current and former smokers. The primary end point was modulation of Ki-67 in the bronchial epithelium after a 3-mo period of treatment. Patients were treated for up to 6 mo and were randomized onto one of four treatment arms: celecoxib daily for 3 mo, then placebo daily for 3 mo (CCX + PCB); celecoxib daily for 3 mo, then celecoxib daily for 3 mo (CCX + CCX); placebo daily for 3 mo, then celecoxib daily for 3 mo (PCB + CCX); and placebo daily for 3 mo, then placebo daily for 3 mo (PCB + PCB). The research pharmacy randomly assigned each patient to one of the four treatment arms and recorded this assignment by using a computer-generated treatment code that was available only to the pharmacist. Pfizer Corp. provided the 200-mg celecoxib capsules and the matching placebo capsules.

After a bronchoscopy at 3 mo, patients received treatment for an additional 3 mo. A bronchoscopy was then done at the 6-mo time point.

On completing informed consent and enrollment, patients were screened with a chest X-ray and bronchoscopy, which included bronchial washings, brushings, and biopsies from six predetermined sites (carina, right lower, middle, and upper lobes and left lower and upper lobe regions) as well as from any abnormal sites suspicious for cancer. Metaplasia indices (MI) were calculated from the biopsies done at the predetermined sites. The presence of dysplasia was confirmed by histologic evaluation of all biopsy samples. Patients with severe dysplasia at initial or subsequent bronchoscopy were strongly encouraged to undergo additional bronchoscopies at 6 mo.

Patients were stratified for randomization according to smoking history (current versus former), prior cancer (prior versus no prior), and MI (<15% versus ≥15% and/or dysplasia). Toxicity was monitored using the National Cancer Institute Common Toxicity Criteria 2.0, and patients who experienced grade 2 or higher toxicity had their dose reduced. Clinic visits occurred before treatment and during treatment at 1-mo intervals. A complete physical examination, which included asking about the patient's relevant medical history and history of tobacco and alcohol exposure, was done at each clinic visit. Patients were referred to smoking cessation programs on request.

Celecoxib dose

In the original study design, celecoxib was to be administered at 200 mg twice daily. At a scheduled External Advisory Board meeting, the committee raised the concern that in a recently completed colon polyp prevention study (20), a 100-mg dose of celecoxib did not differ from placebo in terms of polyp reduction. On the basis of this updated data, the External Advisory Board recommended a higher dose of celecoxib (400 mg). Therefore, the starting dose level, effective December 2003 (after 81 patients had been enrolled at the low-dose celecoxib level), was set at 400 mg for new patients randomized to receive celecoxib. The first subject was randomized using the new schedule on January 23, 2004.

On December 17, 2004, reports of cardiovascular toxicity in other COX-2 inhibitor trials were released (30–35). At that point, a total of 150 patients had been registered on the current study and 143 had been randomized to treatment. New subject entry and celecoxib treatment were put on hold by the principal investigator of the study and

Published OnlineFirst January 26, 2010; DOI:10.1158/1940-6207.CAPR-09-0233

The M.D. Anderson Cancer Center Institutional Review Board. During the subsequent months, efforts were made to follow-up with participants, audit clinical data and the laboratory specimen inventories, modify the eligibility criteria to exclude patients with preexisting cardiovascular conditions, and include additional procedures to screen and monitor for cardiovascular toxicities. The protocol was amended to address cardiovascular safety issues to ensure the safety of study patients. The M.D. Anderson Institutional Review Board approved the amended protocol, the study was reactivated in April 2005, and we began registering new patients; seven of the patients whose treatment was put on hold reentered the trial. We stopped patient accrual for this trial as of January 2007.

Biopsy specimens

Per the protocol, patients underwent bronchoscopies at the time of enrollment before randomization. All evaluable study patients then had repeat bronchoscopies with biopsies, brushings, and washes at the completion of the first stage of treatment (3 mo) and again at 6 mo. Biopsy, brushing, and wash samples were obtained from the same predetermined sites sampled in the initial bronchoscopy. As noted, these biopsy specimens were taken at six predetermined sites in the bronchial tree: the main carina, the bifurcation of the right upper lobe and the main stem bronchus, the bifurcation of the right middle lobe and right lower lobe, the bifurcation of the left upper lobe and lingula, the medial bronchus of the right lower lobe, and the anterior bronchus of the left lower lobe. We fixed the biopsy specimens in 10% buffered formalin, embedded them in paraffin, and sectioned them. The first two 4-μm tissue sections from each biopsy site were stained with H&E and evaluated for the presence of squamous metaplasia and dysplasia. We did histologic assessments to determine whether the MI had changed during the 3-mo period. The MI was calculated as the percentage of biopsy sections exhibiting squamous metaplasia out of the total number of sections examined. A single pathologist (X.T.) who was blinded to the study treatment served as the reference pathologist.

We cytologically analyzed sputum samples acquired by sputum induction from all patients before treatment and after 3 and 6 mo of treatment. Additionally, we did buccal brushings on all patients before treatment and after 3 and 6 mo of treatment to look for evidence of tobacco-induced histologic and genetic alterations.

Immunohistochemical analysis of Ki-67

We calculated the fraction of Ki-67–positive cells in the bronchial epithelium, including the basal, parabasal, and superficial layers of the biopsy specimens. Ki-67 labeling indices were expressed as the percentage of cells with positive nuclear staining, as detailed in our prior reports (27, 28). Slides that lacked evaluable epithelium were excluded from the analyses. Ki-67 labeling indices were analyzed on a per-biopsy-site basis and on a per-subject basis (the average of all biopsy sites that could be evaluated from a participant at a particular time point).

The immunohistochemical analysis was done as follows: one 4-μm tissue section was deparaffinized in xylene and rehydrated through a series of alcohols. Peroxide blocking was done by immersing the section in 3% hydrogen peroxide in methanol for 15 min. Antigen retrieval was accomplished by placing slides in a steamer for 10 min with 10 mmol/L sodium citrate (pH 6.0) and washing them in Tris buffer. The slides were then blocked in 10% fetal bovine serum for 35 min. The Ki-67 antibody used was MIB-1 (DAKO), and incubation occurred at room temperature at 1:200 dilution for 65 min. Secondary antibody was provided and detection was done using the Envision Link+ kit (DAKO) for 30 min. Diaminobenzidine chromogen was applied for 5 min. The slides were then counterstained with hematoxylin and topped with a coverslip. We used NSCLC cell line pallet sections that had been formalin fixed and paraffin embedded and that evidenced confirmed antigen expressions as the control cell lines.

Statistical design and analysis

This study was designed as a randomized, double-blinded, placebo-controlled trial to evaluate the efficacy and toxicity of celecoxib as a chemopreventive agent in current and former smokers. The planned duration of treatment was a total of 6 mo. The primary end point of the study was modulation of Ki-67, measured after a 3-mo treatment intervention. The secondary end point of the study was the change in Ki-67 labeling at 6 mo. The stratified Z test was applied for comparing the reduction of Ki-67 from baseline to 3 mo between the treatment and placebo groups. The target number of randomized and evaluable patients was 182, which would require a total of 216 randomized patients, allowing for a 15% dropout rate. The study design had at least 80% power to detect a 1.2% difference in the reduction of Ki-67 between the COX-2 inhibitor and placebo, with a two-sided 5% level of significance.

Summary statistics, including frequency, tabulation, mean (and SD), and median (and range), were used to characterize the distribution of Ki-67 labeling indices in the basal layer, parabasal layer, and all layers. The mean Ki-67 index across all six potential biopsy sites was computed with the patient used as the analysis unit. The Wilcoxon rank sum test was used to compare continuous variables between two groups. The Kruskal-Wallis test was used to compare continuous variables among three groups. The χ^2 test or the Fisher's exact test was used to test the statistical significance of the association between two categorical variables. The Wilcoxon signed-rank test was used to test changes in Ki-67 labeling indices by patient before and after treatment within each treatment group. To increase the efficiency of the statistical analysis, we also used the biopsy site as a unit of analysis under the assumption that the site was nested within the patient.

Published OnlineFirst January 26, 2010; DOI:10.1158/1940-6207.CAPR-09-0233

For these analyses, we used a mixed-effect model to test the effect of treatment with celecoxib against placebo on Ki-67 labeling indices, adjusting for covariates that affect Ki-67 levels, such as number of years since smoking cessation (in categories), squamous metaplasia (presence or absence), treatment arm, and time point (0 or 3 mo). When the mixed-effect model was used, a logarithmic transformation was applied to Ki-67 labeling indices to satisfy the Gaussian distribution assumption. All statistical tests were two-sided, with a 5% type I error rate. Statistical analysis was done using standard statistical software, including SAS release 9.1 (SAS Institute) and S-Plus version 7 (Insightful, Inc.).

Results

Patient characteristics

From November 2001 to September 2006, a total of 212 patients registered onto the study, with 204 patients randomized to treatment with either agent or placebo. Eight patients were not randomized to treatment arms: two patients because they declined bronchoscopies, two patients because they had concurrent medical conditions, and four patients because of the temporary protocol suspension on December 17, 2004.

Of the 204 patients randomized to study sections, 127 patients (61 receiving low-dose celecoxib and 66 receiving high-dose celecoxib) received baseline and 3-month bronchoscopies and thus had data evaluable for the primary end point analysis (Fig. 1). There were 104 patients who received all three (the baseline, 3-month, and 6-month) bronchoscopies. The characteristics of the patients who were randomized to study sections are listed in Table 1. Although the treatment groups generally had similar characteristics, there were fewer women in the arm treated with PCB + CCX ($P = 0.52$), no Hispanic patients in the CCX + PCB arm ($P = 0.06$), and less dysplasia at baseline in the CCX + PCB and PCB + CCX arms ($P = 0.10$).

More patients than expected dropped out of the study because of the temporary protocol suspension, which may explain why the accrual goal of 182 patients with evaluable data was not reached. Common reasons for study dropout in the low-dose celecoxib (200 mg) group included personal reasons (10 patients), being lost to follow-up (8 patients), and concurrent medical conditions (5 patients).

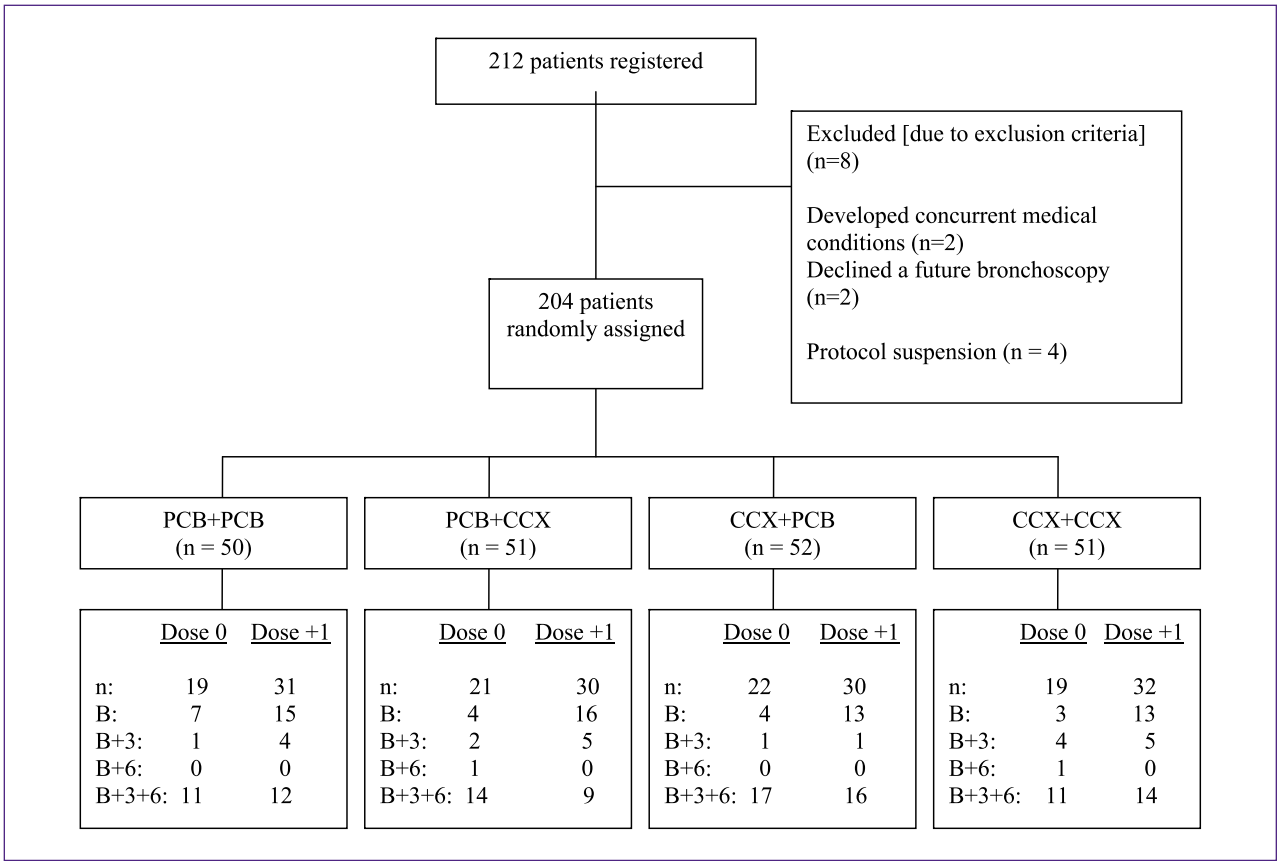

Fig. 1. CONSORT flow diagram of subject accrual into the trial. Patients were randomized to receive the following daily for 3-mo intervals: placebo then placebo (PCB + PCB), placebo then celecoxib (PCB + CCX), celecoxib then placebo (CCX + PCB), or celecoxib then celecoxib (CCX + CCX). Number of patients (*n*) who completed baseline (B), 3-mo (B+3), and 6-mo (B+6) evaluations are listed. Reasons for leaving the study are also listed.

Published OnlineFirst January 26, 2010; DOI:10.1158/1940-6207.CAPR-09-0233

Table 1. Characteristics of randomized patients by treatment arm

Characteristic	PCB + PCB	PCB + CCX	CCX + PCB	CCX + CCX	Total
Total patients treated	50	51	52	51	204
Age (y)					
Mean ± SD	53.6 ± 7.9	52.5 ± 9.0	54.3 ± 8.4	53.0 ± 9.5	53.4 ± 8.7
Median (range)	52.8 (39.6-70.4)	52.4 (32.9-73.2)	54.9 (39.9-73.6)	52.4 (32.0-71.8)	53.3 (32.0-73.6)
Gender					
Female	25 (50.0%)	20 (39.2%)	26 (50.0%)	27 (52.9%)	98 (48.0%)
Male	25 (50.0%)	31 (60.8%)	26 (50.0%)	24 (47.1%)	106 (52.0%)
Race					
Black	4 (8.9%)	3 (5.9%)	4 (7.7%)	6 (11.8%)	17 (8.3%)
Hispanic	1 (2.0%)	3 (5.9%)	0	5 (9.8%)	9 (4.4%)
White	45 (90.0%)	44 (86.3%)	46 (88.5%)	40 (78.4%)	175 (85.8%)
Other	0	1 (2.0%)	2 (3.8%)	0	3 (1.5%)
Cancer history					
No	46 (92.0%)	45 (88.2%)	43 (82.7%)	48 (94.1%)	182 (89.2%)
Yes	4 (8.0%)	6 (11.8%)	9 (17.3%)	3 (5.9%)	22 (10.8%)
Smoking-related cancer					
No	49 (98.0%)	49 (96.1%)	51 (98.1%)	51 (100%)	200 (98.0%)
Yes	1 (2.0%)	2 (3.9%)	1 (1.9%)	0	4 (2.0%)
Smoking status					
Former smokers	8 (16.0%)	13 (25.5%)	11 (21.2%)	10 (19.6%)	42 (20.6%)
Current smokers	42 (84.0%)	38 (74.5%)	41 (78.8%)	41 (80.4%)	162 (79.4%)
Pack-years, mean ± SD (range)					
Former smokers	46 ± 24.4 (21.3-85.2)	39.8 ± 13.7 (20.6-61.5)	39.8 ± 18.7 (20.4-73.9)	43.6 ± 24.2 (20.0-92.6)	41.9 ± 19.4 (19.9-92.6)
Current smokers	44.0 ± 14.7 (19.7-81.5)	38.4 ± 18.2 (20.8-85.6)	47.2 ± 17.7 (20.0-87.9)	45.0 ± 22.3 (21.3-132.8)	43.8 ± 18.5 (19.7-132.8)
Smoking quit-years, mean ± SD (range)	9.5 ± 7.2 (1.5-18.1)	7.2 ± 10.0 (1.0-33.4)	9.9 ± 9.6 (1.2-35.3)	9.0 ± 7.9 (1.3-23.8)	8.8 ± 8.7 (1.0-35.3)
MI, mean ± SD (range)					
Former smokers	6.3 ± 12.4 (0-33.3)	2.6 ± 6.3 (0-16.7)	4.5 ± 7.8 (0-16.7)	10.0 ± 14.1 (0-33.3)	5.6 ± 10.2 (0-33.3)
Current smokers	17.0 ± 24.3 (0-83.3)	14.9 ± 18.9 (0-66.7)	14.8 ± 19.3 (0-66.7)	14.0 ± 18.5 (0-60.0)	15.2 ± 20.3 (0-83.3)
Dysplasia					
No	46 (92.0%)	50 (98.0%)	51 (98.1%)	45 (88.2%)	192 (94.1%)
Yes	4 (8.0%)	1 (2.0%)	1 (1.9%)	6 (11.8%)	12 (5.9%)

Abbreviations: PCB, placebo; CCX, celecoxib.

During the protocol suspension, treatment was suspended for 29 patients, all of whom subsequently left the study. Four patients were randomized but never started the study drug because of safety concerns.

Common reasons for dropout in the high-dose celecoxib group (400 mg) included nonadherence as judged by pill counts (12 participants), having or developing concurrent medical conditions (10 participants), and personal reasons (5 participants).

Patients were stratified into statistical groups according to smoking status (current or former smokers). To monitor smoking status, patients were asked at each visit whether they were actively smoking, and serum cotinine levels were measured. In general, serum cotinine values agreed with the patient reports, but Fig. 2 shows two patients who reported having stopped smoking but had cotinine levels >20 ng/mL at baseline. An additional two former smokers admitted to resuming smoking during the study.

Adherence to treatment

Pill counts were done on a monthly basis to measure treatment adherence, which was excellent. Based on pill counts over the first 3 months of treatment, participants enrolled in the PCB, CCX0, and CCX1 arms took 93.7% (±15.2), 92.1% (±11.78), and 94.5% (±15.3) of the prescribed doses, respectively. Comparable results were

Published OnlineFirst January 26, 2010; DOI:10.1158/1940-6207.CAPR-09-0233

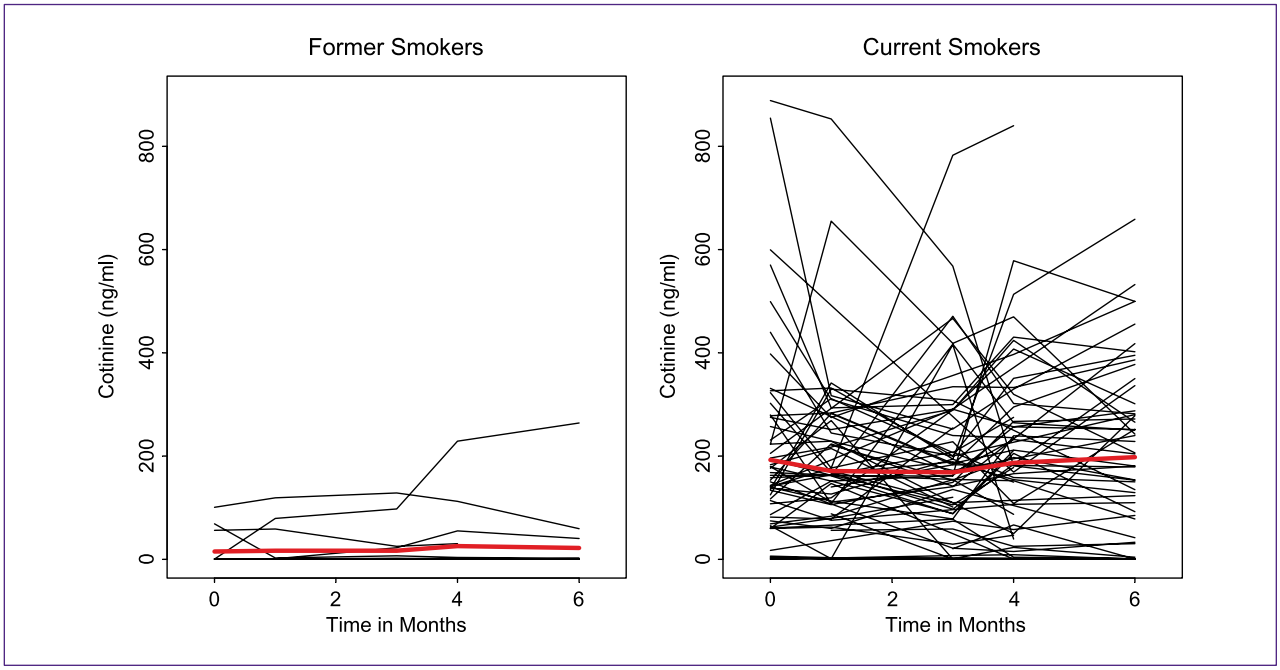

Fig. 2. Cotinine levels by smoking status over time in both former smokers and current smokers. Each black line represents one participant's data. The red line represents the average. The *Y* axis is the measured cotinine level.

observed at 6 months of follow-up (data not shown). There were no differences in adherence levels between the treatment groups.

Treatment-related toxicity

Of the 204 patients who were randomized to study sections, 92 experienced at least one toxic effect, and a total of 196 toxicity episodes were reported. Fifty-eight patients experienced grade 1 toxicities, 28 patients experienced grade 2 toxicities, and 6 patients reported grade 3 to 4 toxicities (confusion, thrombosis, hyperglycemia, allergic reaction, hypertension, and nausea/abdominal pain), but only hyperglycemia, hypertension, and nausea/abdominal pain were considered to be possibly treatment related (Table 2).

Table 2. Toxic effects of protocol treatment over time period

Treatment group	Time period	No. patients experiencing each grade of toxicity			
		1	2	3	4
PCB + PCB (*n* = 50)	All	17	7	1	0
PCB + CCX					
Dose 0 (*n* = 21)	1st 3 mo	6	0	0	0
	2nd 3 mo	4	1	0	0
Dose +1 (*n* = 30)	1st 3 mo	10	2	1	0
	2nd 3 mo	1	3	2	0
CCX + PCB					
Dose 0 (*n* = 22)	1st 3 mo	2	0	0	0
	2nd 3 mo	7	1	0	0
Dose +1 (*n* = 30)	1st 3 mo	5	6	0	0
	2nd 3 mo	2	4	0	0
CCX + CCX					
Dose 0 (*n* = 19)	All	4	0	0	1
Dose +1 (*n* = 32)	All	5	4	1	0

Abbreviations: PCB, placebo; CCX, celecoxib; Dose 0, low-dose; Dose +1, high-dose.

Published OnlineFirst January 26, 2010; DOI:10.1158/1940-6207.CAPR-09-0233

Table 3. Celecoxib levels at 3 months by smoking status

Smoking status	Celecoxib levels						
	Treatment	*n* observed	Mean (μmol/L)	SD	Minimum	Median	Maximum
Current	CCX: 0	23	2.11	3.40	0.00	1.26	16.53
	CCX: +1	17	2.71	1.34	0.00	2.43	5.16
Former	CCX: 0	7	2.86	0.79	1.92	2.62	3.98
	CCX: +1	4	3.23	3.08	0.64	2.38	7.50

NOTE: $P = 0.78$ and $P = 0.004$, Wilcoxon rank sum test, comparing celecoxib levels between dose levels in former (2.86 ± 0.79 versus 3.23 ± 3.08) and current (2.11 ± 3.40 versus 2.71 ± 1.34) smoker groups, respectively. $P = 0.008$ and $P = 0.89$, Wilcoxon rank sum test, comparing celecoxib levels between smoking status for dose 0 (2.11 ± 3.40 versus 2.86 ± 0.79) and +1 (2.71 ± 1.34 versus 3.23 ± 3.08) levels, respectively.
Abbreviations: CCX: 0, low-dose celecoxib; CCX: +1, high-dose celecoxib.

No cardiac toxicities were observed in the study. According to protocol guidelines, patients who experienced toxicities of grade 2 or greater had their dose levels reduced to the −1 dose level (100 mg).

Serum celecoxib levels

Serum celecoxib levels were collected via blood draw and measured at baseline and at defined treatment time points (1, 3, 4, and 6 months) before the patient taking the morning dose. At 3 months, mean celecoxib levels were generally in the low micromolar range (Table 3). Serum celecoxib levels were dose dependent in current smokers (2.71 ± 1.34 with high dose versus 2.11 ± 3.40 with low dose; $P = 0.004$, Wilcoxon rank sum test) but not in former smokers (Table 3). On the basis of findings from an *in vitro* study (29), low-micromolar celecoxib levels would be sufficient to have biological effects on NSCLC cells.

Squamous metaplasia and dysplasia in the bronchial epithelium

A total of 212 patients underwent at least one bronchoscopic procedure each, adding up to a sum of 443 bronchoscopic procedures generating 2,658 biopsy samples. Among them, 1,272 biopsy samples were done at baseline, 762 at 3 months of time, and 624 at 6 months of time. Eighteen baseline biopsy samples were inadequate for histologic interpretation. Of the remaining 1,254 baseline samples, 1,086 (86.6%) had normal histology, 152 (12.1%) had squamous metaplasia, and 16 (1.3%) had dysplasia. Squamous metaplasia or dysplasia was detected in 15.5% (148 of 958) of the samples obtained from current smokers and in 5.7% (14 of 248) of the samples obtained from former smokers. The corresponding MI was higher in current smokers [15.2 (±20.3), $n = 162$] than in former smokers [5.6 (±10.2), $n = 42$; $P = 0.004$, Wilcoxon

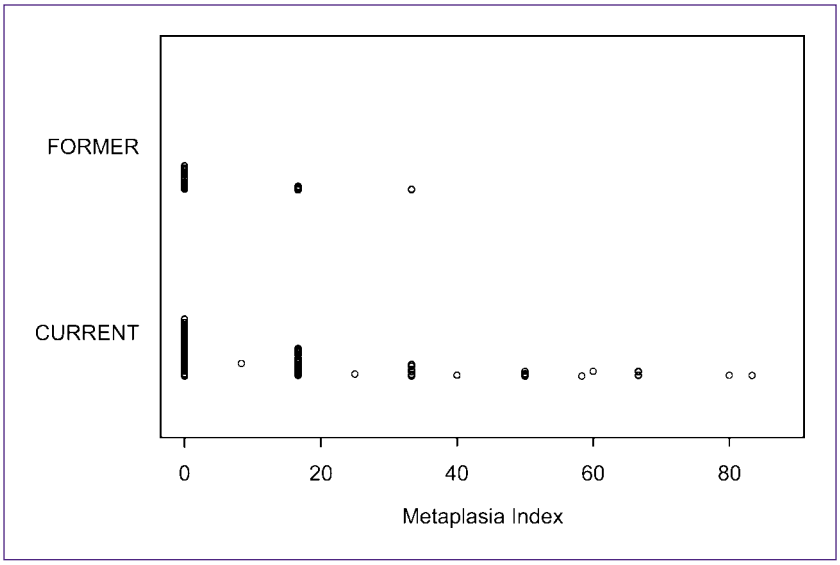

Fig. 3. Baseline squamous metaplasia. Current smokers had a higher percentage of squamous metaplasia than former smokers. Each dot represents one participant's information in relation to MI.

Published OnlineFirst January 26, 2010; DOI:10.1158/1940-6207.CAPR-09-0233

Table 4. Modulation of MI from baseline to 3 mo by treatment arm at each dose level, by smoking status

Smoking status	Treatment	Variable	*n*	Mean	SD	Minimum	Median	Maximum
Former	CCX, dose 0	MI_0	8	6.25	8.63	0.00	0.00	16.67
		MI_3	8	6.25	12.40	0.00	0.00	33.33
		MI_{30}	8	0.00	12.60	−16.67	0.00	16.67
	CCX, dose +1	MI_0	7	4.76	8.13	0.00	0.00	16.67
		MI_3	7	0.00	0.00	0.00	0.00	0.00
		MI_{30}	7	−4.76	8.13	−16.67	0.00	0.00
	Placebo	MI_0	13	5.13	10.51	0.00	0.00	33.33
		MI_3	13	1.28	4.62	0.00	0.00	16.67
		MI_{30}	13	−3.85	12.08	−33.33	0.00	16.67
Current	CCX, dose 0	MI_0	25	15.00	21.97	0.00	0.00	66.67
		MI_3	25	16.13	18.95	0.00	16.67	66.67
		MI_{30}	25	1.13	14.87	−33.33	0.00	33.33
	CCX, dose +1	MI_0	29	12.87	14.93	0.00	16.67	50.00
		MI_3	29	15.92	17.88	0.00	16.67	66.67
		MI_{30}	29	3.05	18.44	−33.33	0.00	33.33
	Placebo	MI_0	44	15.45	23.18	0.00	0.00	83.33
		MI_3	44	16.06	22.45	0.00	8.33	100.00
		MI_{30}	44	0.61	22.43	−50.00	0.00	66.67

NOTE: One patient did not have a 3-mo MI reading from the biopsy.
Abbreviations: CCX, dose 0, low-dose celecoxib; CCX, dose +1, high-dose celecoxib; MI_0, MI baseline; MI_3, MI at 3 mo; MI_{30}, MI difference ($MI_3 - MI_0$).

rank sum test; Fig. 3]. There were no differences in MI values among the treatment groups (Table 4).

Effect of treatment on Ki-67 labeling index

The primary end point of the study was modulation of the Ki-67 index from the baseline level after 3 months of treatment. Ki-67 values were measurable in 2,202 biopsy samples (1,069 at baseline, 627 at 3 months of time, and 506 at 6 months of time) obtained from 200 patients randomized to one of the four study groups (Table 5). Wilcoxon rank sum test shows that baseline Ki-67 expression was significantly higher in current than in former smokers among all epithelial layers (6.15 ± 6.01% versus 3.86 ± 5.56%; $P = 0.002$), the basal layer (6.07 ± 6.77% versus 3.49 ± 4.69%; $P = 0.003$), and the parabasal layer (9.23 ± 10.42% versus 6.31 ± 12.43%; $P = 0.009$). Other variables that affected Ki-67 labeling were the presence of squamous metaplasia ($P < 0.0001$) and the number of quit-years (1 to <5, $P = 0.0004$; >5, $P < 0.0001$). We first examined the effect of celecoxib treatment on Ki-67 labeling in all epithelial layers, which was the primary study end point, by combining the low- and high-dose treatment cohorts. Mixed-model analysis revealed that Ki-67 labeling was not significantly different between the celecoxib and placebo groups ($P = 0.12$). However, although the effect of low-dose treatment was not significant ($P = 0.79$), 3 months of high-dose treatment decreased Ki-67 labeling in all epithelial layers in both former smokers (3.85% decrease) and current smokers (1.10% decrease), which was a significantly greater reduction in both groups ($P = 0.02$, mixed-model analysis) than that in the placebo group after adjusting for metaplasia and smoking status (Table 6; Fig. 4A). This treatment effect persisted at the 6-month time point (Fig. 4B), which further supports the idea that there was a biological effect resulting from high-dose treatment. Additional analysis was then done to examine the effect of high-dose treatment on specific epithelial layers. Although changes in the parabasal layer did not reach significance, Ki-67 labeling decreased in the basal layer by 4.14% in former smokers and 1.41% in current smokers, which was a significantly greater reduction than that observed in the placebo arm ($P = 0.008$, mixed-model analysis).

Discussion

In this first-ever randomized clinical trial of a 6-month celecoxib regimen in current and former smokers, we found that celecoxib is safe to administer and biologically active in the bronchial epithelium. The effects of treatment on the primary end point, bronchial epithelial proliferation after 3 months of time, are noteworthy given that the participant accrual goal was not reached. Moreover, the biological activity and safety of celecoxib in this cohort warrant additional studies on the efficacy of celecoxib in NSCLC chemoprevention.

Problems encountered during the conduct of this trial highlight several important feasibility issues in planning lung chemoprevention studies. The unanticipated cardiac toxicities reported in large trials examining the efficacy of

Published OnlineFirst January 26, 2010; DOI:10.1158/1940-6207.CAPR-09-0233

Table 5. Distribution of Ki-67 index (all layers) in patients by smoking status and treatment at baseline, 3 mo, and difference from baseline to 3 mo (n = 200)

Smoking status	Treatment	Variable	*n*	Mean	SD	Minimum	Median	Maximum	*P**
Former	CCX, dose 0	Baseline	11	2.90	2.36	0.50	2.69	8.63	0.55
		3 mo	8	3.85	4.57	0.17	1.31	11.06	
		Difference	8	1.04	5.43	–8.19	0.55	9.88	
	CCX, dose +1	Baseline	10	4.89	7.68	0.93	1.87	26.24	0.38
		3 mo	7	2.47	2.75	0.10	1.62	8.18	
		Difference	7	–3.85	10.13	–25.6	–1.79	6.32	
	Placebo	Baseline	18	3.88	5.77	0.08	1.50	23.81	0.95
		3 mo	13	2.80	2.38	0.14	2.23	7.45	
		Difference	13	–1.23	6.16	–20.1	0.03	6.89	
Current	CCX, dose 0	Baseline	30	6.62	7.37	0.38	4.16	30.89	0.97
		3 mo	25	6.48	4.89	0.25	5.46	16.23	
		Difference	25	0.06	5.22	–11.5	–0.68	12.97	
	CCX, dose +1	Baseline	50	6.03	4.84	0.35	4.59	23.66	0.27
		3 mo	29	6.76	5.88	0.00	5.43	19.82	
		Difference	28	–1.10	6.91	–13.5	–1.71	14.12	
	Placebo	Baseline	80	6.05	6.18	0.00	4.65	32.13	0.89
		3 mo	44	7.66	7.10	0.00	6.15	38.10	
		Difference	44	0.15	8.58	–26.4	–0.15	34.42	

NOTE: One patient did not have a baseline Ki-67 reading due to inadequate tissue.
*Wilcoxon signed-rank test comparing modulation of Ki-67 index within each subgroup.

celecoxib and other nonsteroidal anti-inflammatory drugs in colon cancer chemoprevention (30–35) negatively affected the conduct of this study in several respects. First, participant accrual was interrupted for 6 months. Second, data from patients who had been actively receiving treatment at the time of protocol suspension were deemed inevaluable due to early treatment cessation. Third, patient accrual after the trial reopened proceeded at a slower rate than it had before trial suspension, which suggests that the negative publicity associated with the cardiac toxicity reports adversely affected patient accrual. In fact, we did not observe any cardiovascular toxicity in this cohort. This may have been related to the short duration of celecoxib treatment in this study relative to that of the trials reporting these toxicities, which required treatments of more than 12 months of duration (20, 30, 36–38).

The findings reported here on Ki-67 labeling in the bronchial epithelium are noteworthy for several reasons. First, Ki-67 labeling decreased in participants treated with high-dose but not low-dose celecoxib. Similarly, celecoxib

Table 6. Mixed-model analysis on the effects of Ki-67 (n = 200)

Covariates	Estimate	SE	*P*
SQM (+ vs –)	0.62	0.05	<0.0001
Quit-years			
1 to <5 y vs current smokers	–0.21	0.06	0.0004
≥5 y vs current smokers	–0.37	0.06	<0.0001
Treatment			
CCX (dose 0 vs placebo)	0.09	0.05	0.12
CCX (dose +1 vs placebo)	0.10	0.05	0.03
Time (3 mo vs baseline)	0.09	0.05	0.049
Treatment time			
CCX (dose 0 vs placebo at 3 mo)	–0.02	0.08	0.79
CCX (dose +1 vs placebo at 3 mo)	–0.17	0.07	0.02

Abbreviation: SQM, any squamous metaplasia.

Published OnlineFirst January 26, 2010; DOI:10.1158/1940-6207.CAPR-09-0233

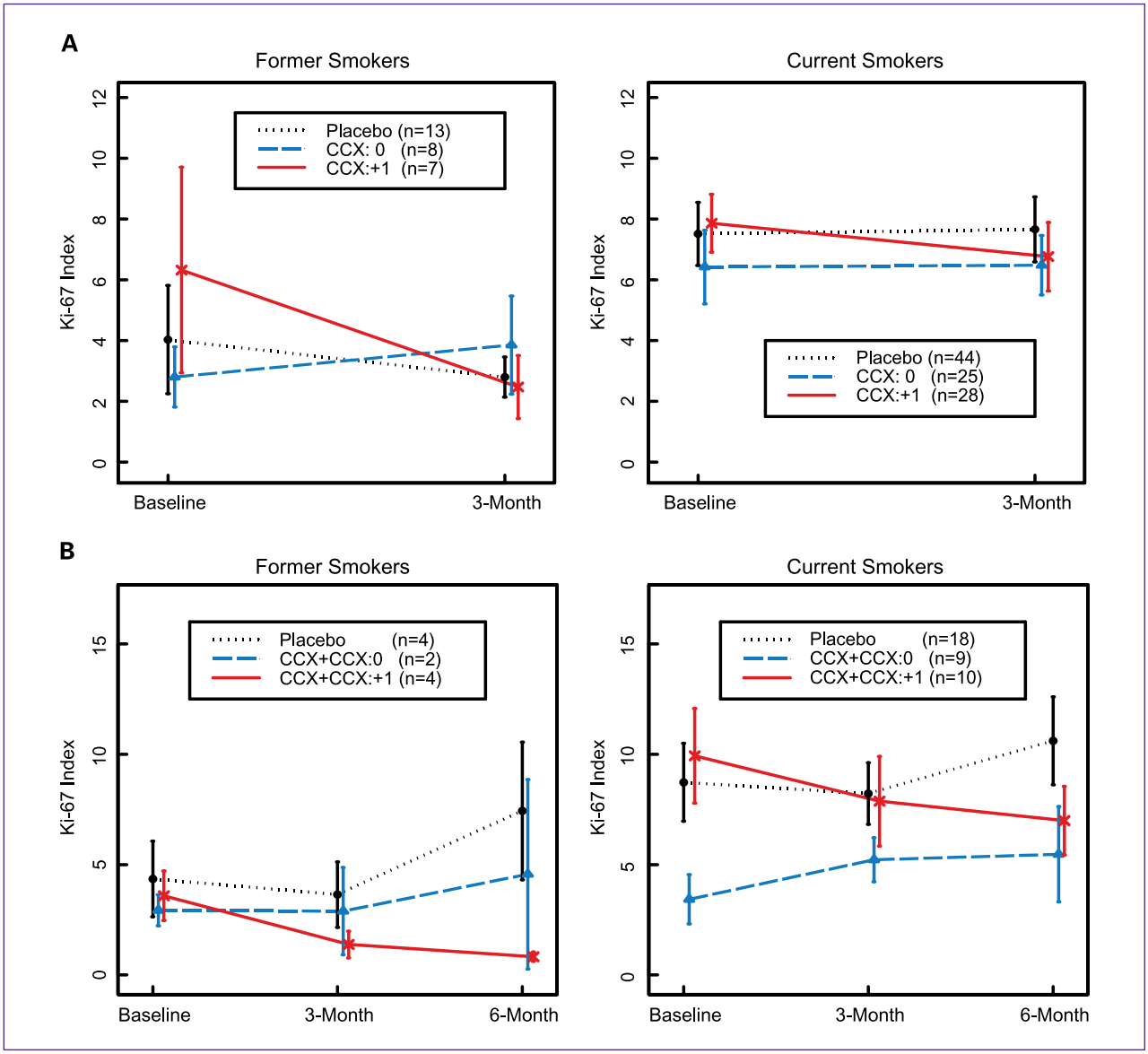

Fig. 4. Mean Ki-67 over time in all layers. A, baseline and 3-mo time points show decreasing expression of Ki-67 with high-dose celecoxib over time in both current and former smokers who had both baseline and 3-mo Ki-67 measurements. Total evaluable patients are 28 in former smoker group and 97 in current smoker group. *Y* axis, Ki-67 index. B, baseline, 3-mo, and 6-mo time periods show a similar trend for Ki-67 expression with high-dose celecoxib in both current and former smokers who had baseline, 3-mo, and 6-mo Ki-67 measurements. Total evaluable patients are 10 in former smoker group and 37 in current smoker group. Placebo and low-dose celecoxib follow similar patterns, especially in current smokers. *Y* axis, Ki-67 index.

is more efficacious in colon cancer chemoprevention when administered at 400 mg twice daily than at 200 mg twice daily (20, 30, 38). These findings suggest that, although it may have less treatment-related toxicity, low-dose (200 mg) celecoxib has no efficacy in NSCLC chemoprevention and argue against such a trial design.

Second, Ki-67 levels decreased more prominently in former smokers than in current smokers, especially in those patients who completed baseline and 3-month bronchoscopies (Fig. 4A). This effect was also observed in patients who completed baseline, 3-month, and 6-month bronchoscopies (Fig. 4B) and received high-dose celecoxib. It is important to note that these are subset analyses and the number of patients is low, especially in the former smokers. Serum celecoxib levels did not differ in current versus former smokers treated with high-dose celecoxib (data not shown), but detailed pharmacokinetic studies were not done, so we cannot exclude the possibility that the pharmacokinetics of celecoxib contributed to this outcome. Current and former smokers may differ with respect to the role that COX-2 plays in maintaining bronchial epithelial proliferation. In fact, other studies have reported

Published OnlineFirst January 26, 2010; DOI:10.1158/1940-6207.CAPR-09-0233

differences between these two groups with respect to bronchial epithelial biology (28, 39, 40).

Third, the reduction in Ki-67 labeling was not accompanied by a decrease in MI, and the effect of celecoxib on Ki-67 did not vary on the basis of histology, indicating that the decrease in Ki-67 was not due to a reduction in bronchial metaplasia, which has been reported to increase Ki-67 labeling (28, 41–43). Dysplasia was uncommon in this cohort, so no conclusions can be made about the effect of celecoxib on this histologic abnormality.

Fourth, Ki-67 decreased more prominently in the basal layer than it did in the parabasal layer, a strikingly different finding from those reported in chemoprevention studies using retinoids, which reduce bronchial metaplasia and are active primarily in the parabasal layer of the bronchial epithelium (27, 28, 44). Collectively, these findings suggest that the basal and parabasal compartments of the bronchial epithelium are biologically distinct, which is consistent with evidence that cells in the basal layer have a low proliferation rate, express progenitor cell markers, and have multipotent differentiation potential (45), whereas cells in the parabasal layer have a higher proliferation rate and have undergone differentiation into mucous-secreting and other epithelial cell types.

Progress in the field of NSCLC chemoprevention research will require the ability to identify individuals at high risk for the development of NSCLC, a way to isolate premalignant bronchial epithelial cells in danger of malignant progression, and a method to elucidate the mechanisms by which these premalignant cells maintain their proliferation and survival. With respect to the latter, findings presented here and elsewhere (46) raise the possibility that COX-2 is one mediator of bronchial epithelial proliferation in current and former smokers. Additional studies are warranted to examine the importance of COX-2 in NSCLC development and explore NSCLC prevention with COX-2 inhibitors.

Disclosure of Potential Conflicts of Interest

No potential conflicts of interest were disclosed.

Grant Support

National Cancer Institute grants CA 091844 and CA 16672 (J.M. Kurie), Department of Defense grant W81XWH-04-0142 (W.K. Hong), and Pfizer Pharmaceuticals.

Received 10/28/09; accepted 11/3/09; published OnlineFirst 1/26/10.

References

1. Jemal A, Siegel R, Ward E, et al. Cancer statistics, 2008. CA Cancer J Clin 2008;58:71–96.
2. U.S. Department of Health and Human Services. The health benefits of smoking cessation: a report of the Surgeon General. Atlanta (GA): U.S. Department of Health and Human Services, Public Health Service, Centers for Disease Control, Center for Chronic Disease Prevention and Health Promotion, Office on Smoking and Health; 1990, DHHS Publication No. (CDC) 90-8416.
3. Halpern MT, Gillespie BW, Warner KE. Patterns of absolute risk of NSCLC mortality in former smokers. J Natl Cancer Inst 1993;85:457–64.
4. Burns DM. Primary prevention, smoking, and smoking cessation: implications for future trends in NSCLC prevention. Cancer 2000;89:2506–9.
5. Godtfredsen NS, Prescott E, Osler M. Effect of smoking reduction on NSCLC risk. JAMA 2005;294:1505–10.
6. Lubin JH, Blot WJ. NSCLC and smoking cessation: patterns of risk. J Natl Cancer Inst 1993;85:422–3.
7. Tong L, Spitz MR, Fueger JJ, Amos CA. Lung carcinoma in former smokers. Cancer 1996;78:1004–10.
8. Kim ES, Hong WK, Khuri FR. Chemoprevention of aerodigestive tract cancers. Annu Rev Med 2002;53:223–43.
9. The α-Tocopherol, β-Carotene Cancer Prevention Study Group. The effect of vitamin E and β carotene on the incidence of NSCLC and other cancers in male smokers. N Engl J Med 1994;330:1029–35.
10. Omenn GS, Goodman GE, Thornquist MD, et al. Effects of a combination of β carotene and vitamin A on NSCLC and cardiovascular disease. N Engl J Med 1996;334:1150–5.
11. Lippman SM, Lee JJ, Karp DD, et al. Randomized phase III intergroup trial of isotretinoin to prevent second primary tumors in stage I NSCLC. J Natl Cancer Inst 2001;93:605–18.
12. Herschman HR. Prostaglandin synthase 2. Biochim Biophys Acta 1996;1299:125–40.
13. Subbaramiah K, Telang N, Ramonetti JT, et al. Transcription of cyclooxygenase 2 is enhanced in transformed mammary epithelial cells. Cancer Res 1996;56:4424–9.
14. Kelly DJ, Mestre JR, Subbaramaiah K, et al. Benzo[a]pyrene upregulates cyclooxygenase-2 gene expression in oral epithelial cells. Carcinogenesis 1997;18:795–9.
15. Kutchera W, Jones DA, Matsunami N, et al. Prostaglandin H synthase-2 is expressed abnormally in human colon cancer: evidence for a transcriptional effect. Proc Natl Acad Sci U S A 1996;93:4816–20.
16. Ebert CE, Coffey RJ, Radhika A, Giardiello FM, Ferrenbach S, DuBois RN. Up-regulation of cyclooxygenase 2 expression in human colorectal adenomas and adenocarcinomas. Gastroenterology 1994;107:1183–8.
17. Ristimaki A, Honkanen N, Jankala H, Sipponen P, Harkonen M. Expression of cyclooxygenase-2 in human gastric carcinoma. Cancer Res 1997;57:1276–80.
18. Hida T, Yatabe Y, Achiwa H, et al. Increased expression of cyclooxygenase 2 occurs frequently in human NSCLCs, specifically in adenocarcinomas. Cancer Res 1998;58:3761–4.
19. Oshima M, Dinchuk SL, Kargman H, et al. Suppression of intestinal polyposis in $Apc^{\Delta 176}$ knockout mice by inhibition of cyclooxygenase 2 (COX-2). Cell 1996;87:803–9.
20. Steinbach G, Lynch PM, Phillips RK, et al. The effect of celecoxib, a cyclooxygenase-2 inhibitor, in familial adenomatous polyposis. N Engl J Med 2000;342:1946–52.
21. Wolff H, Saukkonen K, Anttila S, Karjalainen A, Vainio H, Ristimaki A. Expression of cyclooxygenase-2 in human lung carcinoma. Cancer Res 1998;58:4997–5001.
22. Koki AT, Khan NK, Woerner BM, et al. Characterization of cyclooxygenase-2 (COX-2) during tumorigenesis in human epithelial cancers: evidence for potential clinical utility of COX-2 inhibitors in epithelial cancers. Prostaglandins Leukot Essent Fatty Acids 2002;66:13–8.
23. Lu C, Soria JC, Tang X, et al. Prognostic factors in resected stage I non-small-cell NSCLC: a multivariate analysis of six molecular markers. J Clin Oncol 2004;22:4575–83.

Published OnlineFirst January 26, 2010; DOI:10.1158/1940-6207.CAPR-09-0233

24. Khuri FR, Wu H, Lee JJ, et al. Cyclooxygenase-2 overexpression is a marker of poor prognosis in stage I non-small cell NSCLC. Clin Cancer Res 2001;7:861–7.
25. Hosomi Y, Yokose T, Hirose Y, et al. Increased cyclooxygenase 2 (COX-2) expression occurs frequently in precursor lesions of human adenocarcinoma of the lung. Lung Cancer 2000;30:73–81.
26. Rioux N, Castonguay A. Prevention of NNK-induced lung tumorigenesis in A/J mice by acetylsalicylic acid and NS-398. Cancer Res 1998;58:5354–60.
27. Hittelman WN, Liu DD, Kurie JM, et al. Proliferative changes in the bronchial epithelium of former smokers treated with retinoids. J Natl Cancer Inst 2007;99:1603–12.
28. Lee JJ, Liu D, Lee JS, et al. Long-term impact of smoking on lung epithelial proliferation in current and former smokers. J Natl Cancer Inst 2001;93:1081–8.
29. Hida T, Kozaki K, Muramatsu H, et al. Cyclooxygenase-2 inhibitor induces apoptosis and enhances cytotoxicity of various anticancer agents in non-small cell NSCLC cell lines. Clin Cancer Res 2000;6: 2006–11.
30. Bertagnolli MM, Eagle CJ, Zauber AG, et al. APC Study Investigators. Celecoxib for the prevention of sporadic colorectal adenomas. N Engl J Med 2006;355:873–84.
31. Solomon SD, McMurray JV, Pfeffer MA, et al. Cardiovascular risk associated with celecoxib in a clinical trial for colorectal adenoma prevention. N Engl J Med 2005;352:1071–80.
32. Bresalier RS, Sandler RS, Quan H, et al. Cardiovascular events associated with rofecoxib in a colorectal adenoma chemoprevention trial. N Engl J Med 2005;352:1092–102.
33. Nussmeier NA, Whelton AA, Brown MT, et al. Complications of the COX-2 inhibitors parecoxib and valdecoxib after cardiac surgery. N Engl J Med 2005;352:1081–91.
34. Fitzgerald GA. Coxibs and cardiovascular disease. N Engl J Med 2004;351:1709–11.
35. Solomon SD, Wittes J, Finn PV, et al. Cross Trial Safety Assessment Group. Cardiovascular risk of celecoxib in 6 randomized placebo-controlled trials: the cross trial safety analysis. Circulation 2008; 117:2104–13.
36. Arber N, Eagle CJ, Spicak J, et al. Celecoxib for the prevention of colorectal adenomatous polyps. N Engl J Med 2006;355:885–95.
37. Baron JA, Sandler RS, Bresalier RS, et al. A randomized trial of rofecoxib for the chemoprevention of colorectal adenomas. Gastroenterology 2006;131:1674–82.
38. Bertagnolli MM, Zauber AG, Hawk ET. The Adenoma Prevention with Celecoxib (APC) trial: five-year efficacy and safety results [abstract LB-141]. Proceedings of the 99th Annual Meeting of the American Association for Cancer Research. 2008.
39. Spira A, Beane J, Shah V, et al. Effects of cigarette smoke on the human airway epithelial cell transcriptome. Proc Natl Acad Sci U S A 2004;101:10143–8.
40. Zhang L, Lee JJ, Tang H, et al. Impact of smoking cessation on global gene expression in the bronchial epithelium of chronic smokers. Cancer Prev Res 2008;1:112–8.
41. Martin B, Paesmans M, Mascaux C, et al. Ki-67 expression and patients' survival in NSCLC: systematic review of the literature with meta-analysis. Br J Cancer 2004;91:2018–25.
42. Miller YE, Blatchford P, Hyun DS, et al. Bronchial epithelial Ki-67 index is related to histology, smoking, and gender, but not NSCLC or chronic obstructive pulmonary disease. Cancer Epidemiol Biomarkers Prev 2007;16:2425–31.
43. Szabo E. Lung epithelial proliferation: a biomarker for chemoprevention trials? J Natl Cancer Inst 2001;93:1042–43.
44. Kurie JM, Lotan R, Lee JJ, et al. Treatment of former smokers with 9-*cis*-retinoic acid reverses loss of retinoic acid receptor-β expression in the bronchial epithelium: results from a randomized placebo-controlled trial. J Natl Cancer Inst 2003;95:206–14.
45. Vaughan MB, Ramirez RD, Wright WE, et al. A three-dimensional model of differentiation of immortalized human bronchial epithelial cells. Differentiation 2006;74:141–8.
46. Mao JT, Fishbein MC, Adams B, et al. Celecoxib decreases Ki-67 proliferative index in active smokers. Clin Cancer Res 2006;12:314–20.

Oncogene (2010) 29, 1421–1430

www.nature.com/onc

ORIGINAL ARTICLE

Genomic and functional analysis identifies *CRKL* as an oncogene amplified in lung cancer

YH Kim[1,7], KA Kwei[1,7], L Girard[2], K Salari[1,3], J Kao[1], M Pacyna-Gengelbach[4], P Wang[5], T Hernandez-Boussard[3], AF Gazdar[2], I Petersen[6], JD Minna[2] and JR Pollack[1]

[1]*Department of Pathology, Stanford University, Stanford, CA, USA;* [2]*Hamon Center for Therapeutic Oncology Research, University of Texas Southwestern Medical Center, Dallas, TX, USA;* [3]*Department of Genetics, Stanford University, Stanford, CA, USA;* [4]*Institute of Pathology, University Hospital Charité, Berlin, Germany;* [5]*Division of Public Health Sciences, Fred Hutchinson Cancer Research Center, Seattle, WA, USA and* [6]*Institute of Pathology, Universitätsklinikum Jena, Jena, Germany*

DNA amplifications, leading to the overexpression of oncogenes, are a cardinal feature of lung cancer and directly contribute to its pathogenesis. To uncover such novel alterations, we performed an array-based comparative genomic hybridization survey of 128 non-small-cell lung cancer cell lines and tumors. Prominent among our findings, we identified recurrent high-level amplification at cytoband 22q11.21 in 3% of lung cancer specimens, with another 11% of specimens exhibiting low-level gain spanning that locus. The 22q11.21 amplicon core contained eight named genes, only four of which were overexpressed (by transcript profiling) when amplified. Among these, *CRKL* encodes an adapter protein functioning in signal transduction, best known as a substrate of the BCR-ABL kinase in chronic myelogenous leukemia. RNA-interference-mediated knockdown of CRKL in lung cancer cell lines with (but not without) amplification led to significantly decreased cell proliferation, cell-cycle progression, cell survival, and cell motility and invasion. In addition, overexpression of CRKL in immortalized human bronchial epithelial cells led to enhanced growth factor-independent cell growth. Our findings indicate that amplification and resultant overexpression of *CRKL* contribute to diverse oncogenic phenotypes in lung cancer, with implications for targeted therapy, and highlight a role of adapter proteins as primary genetic drivers of tumorigenesis.
Oncogene (2010) **29,** 1421–1430; doi:10.1038/onc.2009.437; published online 7 December 2009

Keywords: CRKL; lung cancer; DNA amplification; genomic profiling; adapter protein

Introduction

Lung cancer is the leading cause of cancer death in the United States, accounting for almost 30% of all cancer-related mortality (Jemal *et al*., 2008). Nearly 80% of lung cancers diagnosed are non-small-cell lung cancers (NSCLCs), which are classified into three main histological subtypes: adenocarcinoma, squamous cell carcinoma and large cell carcinoma. Despite the advancement of surgical, cytotoxic and radiological treatment options over the years, lung cancer therapy remains largely ineffective from a clinical standpoint, as evidenced by a low 5-year survival rate (<15%), and underscores the aggressive nature of the disease.

Much effort has been directed toward elucidating the pathogenetic alterations underlying the initiation and progression of NSCLC, with the hope of developing novel therapeutics to selectively target those alterations *in vivo*. Indeed, recent application of epidermal growth factor receptor (EGFR) tyrosine kinase inhibitors has been moderately successful in the treatment of NSCLCs harboring activating point mutations of EGFR (Lynch *et al*., 2004; Paez *et al*., 2004). It is likely that other genetic alterations in NSCLC await discovery, and once characterized might provide useful targets for therapy.

Genomic DNA amplifications are a frequent class of aberrations in NSCLC, where increased gene dosage leads to overexpression of key cancer genes. Genomic profiling studies of NSCLC, using cDNA (Tonon *et al*., 2005; Kwei *et al*., 2008), BAC (Garnis *et al*., 2006), oligonucleotide (Tonon *et al*., 2005; Kendall *et al*., 2007) and single nucleotide polymorphism (Zhao *et al*., 2005; Weir *et al*., 2007) arrays have revealed focal amplicons harboring known oncogenes, such as *KRAS* (12p12.1), *EGFR* (7p12.2), *ERBB2* (17q12), *MET* (7q31.2), *MYC* (8q24.1), *CDK4* (12q14.1) and *CCND1* (11q13.2), and have led to the recent discovery of *TITF1* (14q13) as a lineage-dependent oncogenic transcription factor amplified in lung cancer (Kendall *et al*., 2007; Weir *et al*., 2007; Kwei *et al*., 2008). For other recurrent amplicons, the driver oncogene(s) have not yet been identified, and mapping such loci provides a starting point for cancer gene discovery and characterization. Here, from a cDNA microarray-based genomic profiling analysis of 128 lung cancer specimens, we identify amplification of *CRKL* (22q11) as a recurrent genetic event promoting cell proliferation, survival and invasion in lung cancer.

Correspondence: Dr JR Pollack, Department of Pathology, Stanford University, CCSR Building, Room 3245A, 269 Campus Drive, Stanford, CA 94305-5176, USA.
E-mail: pollack1@stanford.edu
[7]These authors contributed equally to this work.
Received 17 February 2009; revised 4 September 2009; accepted 2 November 2009; published online 7 December 2009

Results

Recurrent 22q11 amplicon in NSCLC spans CRKL

To identify recurrent DNA amplifications pinpointing novel oncogenes in NSCLC, we analyzed cDNA array comparative genomic hybridization (CGH) data generated on 52 NSCLC cell lines and 76 NSCLC tumors, the latter comprising 36 adenocarcinomas (including 2 metastases) and 40 squamous cell carcinomas (with 1 metastasis), totaling 128 samples. One of the most frequently amplified loci not associated with a known oncogene occurred at cytoband 22q11.21 (Figure 1a), where high-level amplification (fluorescence ratios >3, corresponding to >5-fold amplification; Pollack *et al*., 1999) was found in 4 of 128 samples analyzed (3%), with low-level gain spanning 22q11.21 present in an additional 14 of 128 samples (11%). There was no significant difference in the frequency of 22q11.21 gain/amplification between adenocarcinoma and other histologies (both for cell lines and for tumors), nor in the NSCLC

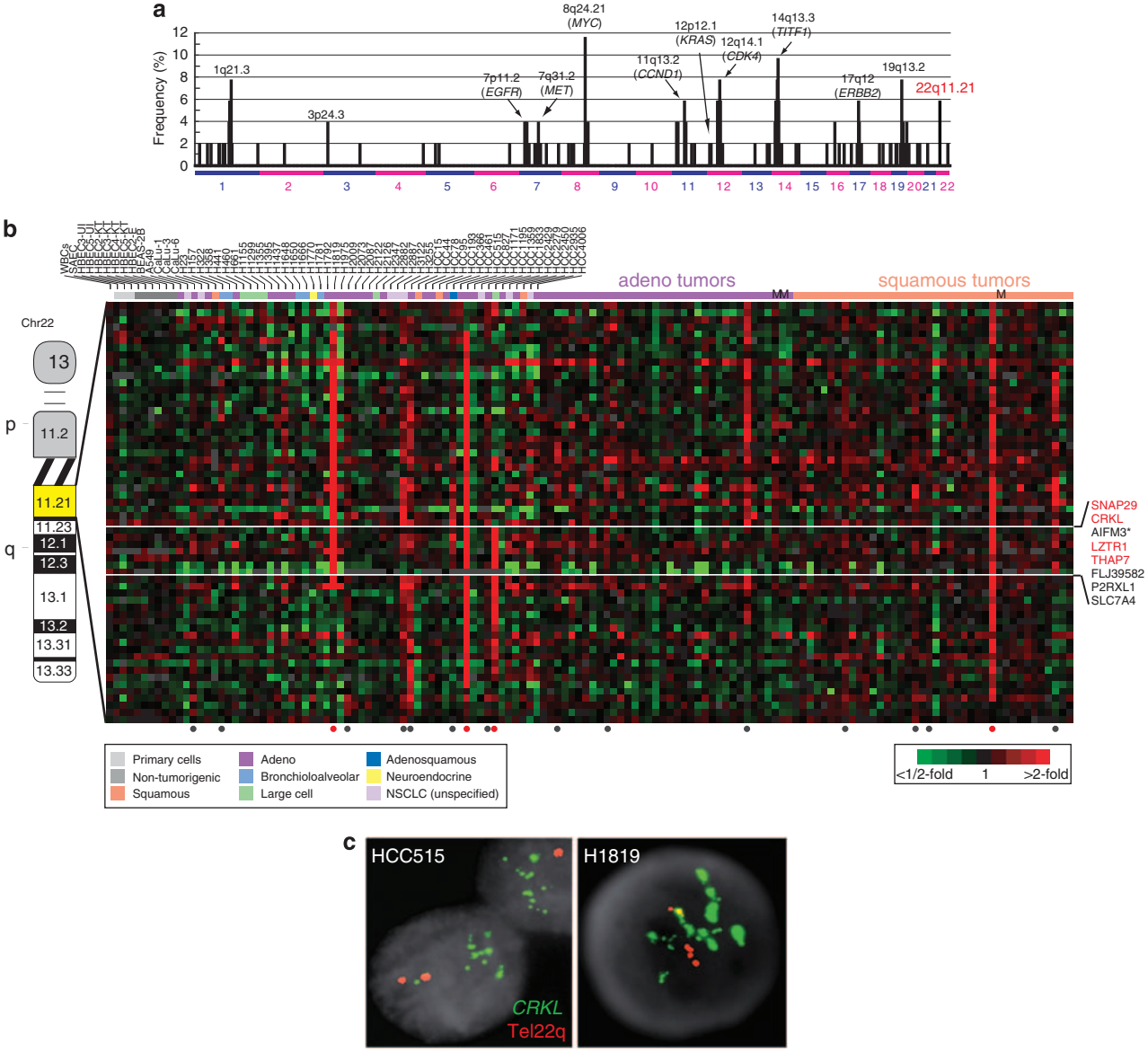

Figure 1 Recurrent 22q11 amplicon in non-small-cell lung cancer (NSCLC) spans CRKL. (**a**) Frequency plot of cytobands harboring high-level DNA amplification in NSCLC cell lines. Cytobands consisting known oncogenes in lung cancer are indicated, with 22q11.21 highlighted in red. (**b**) Heat map representation of array comparative genomic hybridization (CGH) profiles of NSCLC cell lines and tumors representing a segment of 22q11.21. Each column represents a different sample (histologies indicated, M = metastasis) and each row represents a different gene ordered by chromosome position. Red indicates positive tumor/normal array CGH ratios (scale shown), and samples called gained (by cghFLasso) or highly amplified at 22q11.21 are marked below by closed black or red circles. Genes residing within the smallest common region of gain (amplicon core) are indicated; those with increased expression when amplified (see Figure 2a) are highlighted in red. AIFM3 (asterisked) was not present on the array but resides where shown. (**c**) fluorescence *in situ* hybridization (FISH) validation of CRKL amplification in NSCLC cell lines HCC515 and H1819. DNA amplification is indicated by increased CRKL (green) to telomere-22q (red) signals or signal clusters.

lines was there a significant association between 22q11.21 gain/amplification and mutation of *KRAS*, *EGFR* or *TP53* (data not shown). Conversely, we observed significant (false discovery rate <0.01) association of 22q11.21 gain with concomitant gains elsewhere in the genome, namely at 9q34.3, 11q13.2–q13.3 (*CCND1*), 15q24.1 and 21q22.3 (Supplementary Table 2), suggesting possible cooperative interactions.

The smallest region of recurrent amplification (or amplicon core) (Figure 1b), spanned approximately 170 kb within 22q11.21, and contained eight known RefSeq genes, which included *SNAP29* (synaptosomal-associated protein 29), *CRKL* (v-crk avian sarcoma virus CT10 oncogene homologue-like), *AIFM3* (apoptosis-inducing factor, mitochondrion-associated 3), *LZTR1* (leucine-zipper-like transcriptional regulator 1), *THAP7* (THAP domain-containing protein 7), *FLJ39582* (hypothetical protein LOC439931), *P2RXL1* (purinergic receptor P2X-like 1, orphan receptor) and *SLC7A4* (solute carrier family 7 (cationic amino-acid transporter, y+ system), member 4). Expression profiling, performed in parallel with array CGH, revealed that only four genes (*SNAP29*, *CRKL*, *LZTR1* and *THAP7*) were overexpressed when amplified ($P<0.05$, Student's *t*-test) (Figure 2a), thus effectively narrowing the list of candidate 'driver' oncogenes. One of these genes, *CRKL*, encodes an Src homology 2 and 3 (SH2/SH3) domain-containing adapter protein that shares homology with the *CRK* proto-oncogene (ten Hoeve *et al*., 1993). Best known as a substrate of the BCR-ABL oncogenic kinase in chronic myelogenous leukemia (Sattler and Salgia, 1998), a role of CRKL in other cancer types remains largely unexplored. We therefore sought to characterize a possible role of *CRKL* amplification in lung cancer.

CRKL amplification promotes cell proliferation and survival

To assess the functional significance of *CRKL* amplification and overexpression in NSCLC, we used small-interfering RNAs (siRNAs) directed against *CRKL* in two cell lines, HCC515 and H1819, for which *CRKL* amplification had been validated by fluorescence *in situ* hybridization (Figure 1c), and with increased levels of total and phosphorylated (activated) CRKL protein (Figure 2b). Transfection of two different siRNAs targeting distinct sequences within CRKL each led to decreased levels of total and p-CRKL proteins (Figure 3a), and significantly decreased cell proliferation (measured using the WST-1 assay) compared with a negative control siRNA targeting an irrelevant gene, green fluorescent protein (*GFP*; Figure 3b). In contrast, knockdown of CRKL in H157, a lung cancer cell line without *CRKL* amplification and with comparatively

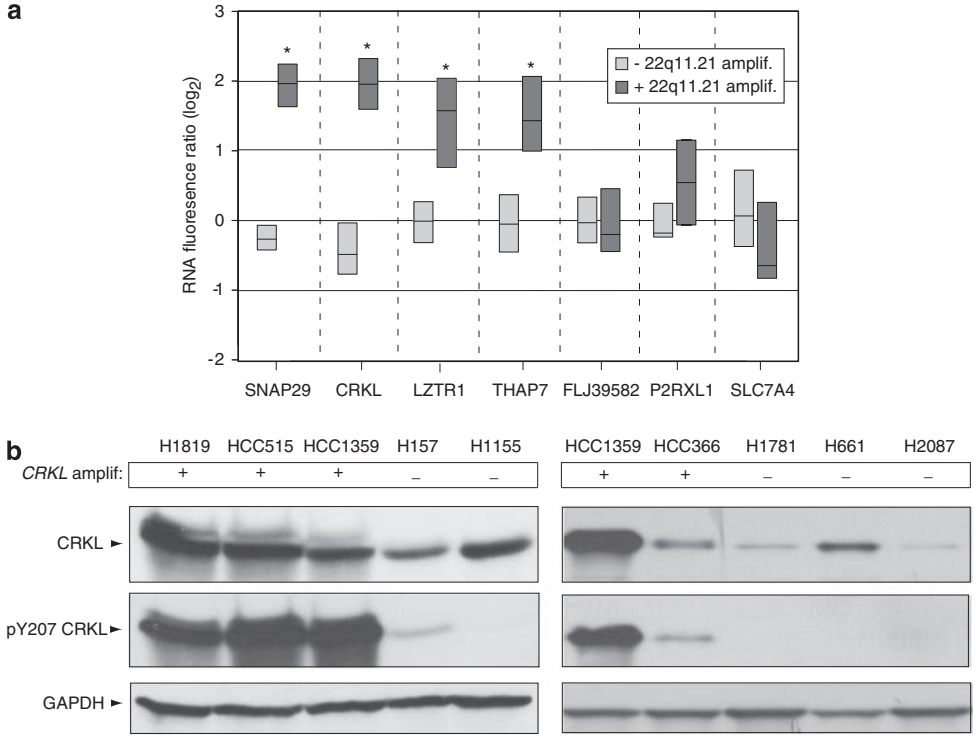

Figure 2 *CRKL* is overexpressed when amplified. (**a**) mRNA transcript levels (centered $\log_2$ ratios, measured by microarray) of genes residing within the 22q11.21 amplicon core, plotted separately for specimens with and without 22q11.21 amplification. Box plots show 25th, 50th (median) and 75th percentiles of expression for samples; genes whose expression is significantly (Student's *t*-test, $P<0.05$) elevated with DNA amplification are indicated (*). (**b**) Western blot analysis of CRKL protein in representative non-small-cell lung cancer (NSCLC) cell lines confirming overexpression in NSCLC cell lines with (compared to without) 22q11.21 amplification. Total and phosphorylated (active) CRKL (pY207) levels are shown. Glyceraldehyde-3-phosphate dehydrogenase (GAPDH) serves as a loading control. Note, *CRKL* amplification appears better correlated with p-CRKL than total CRKL (see Discussion section).

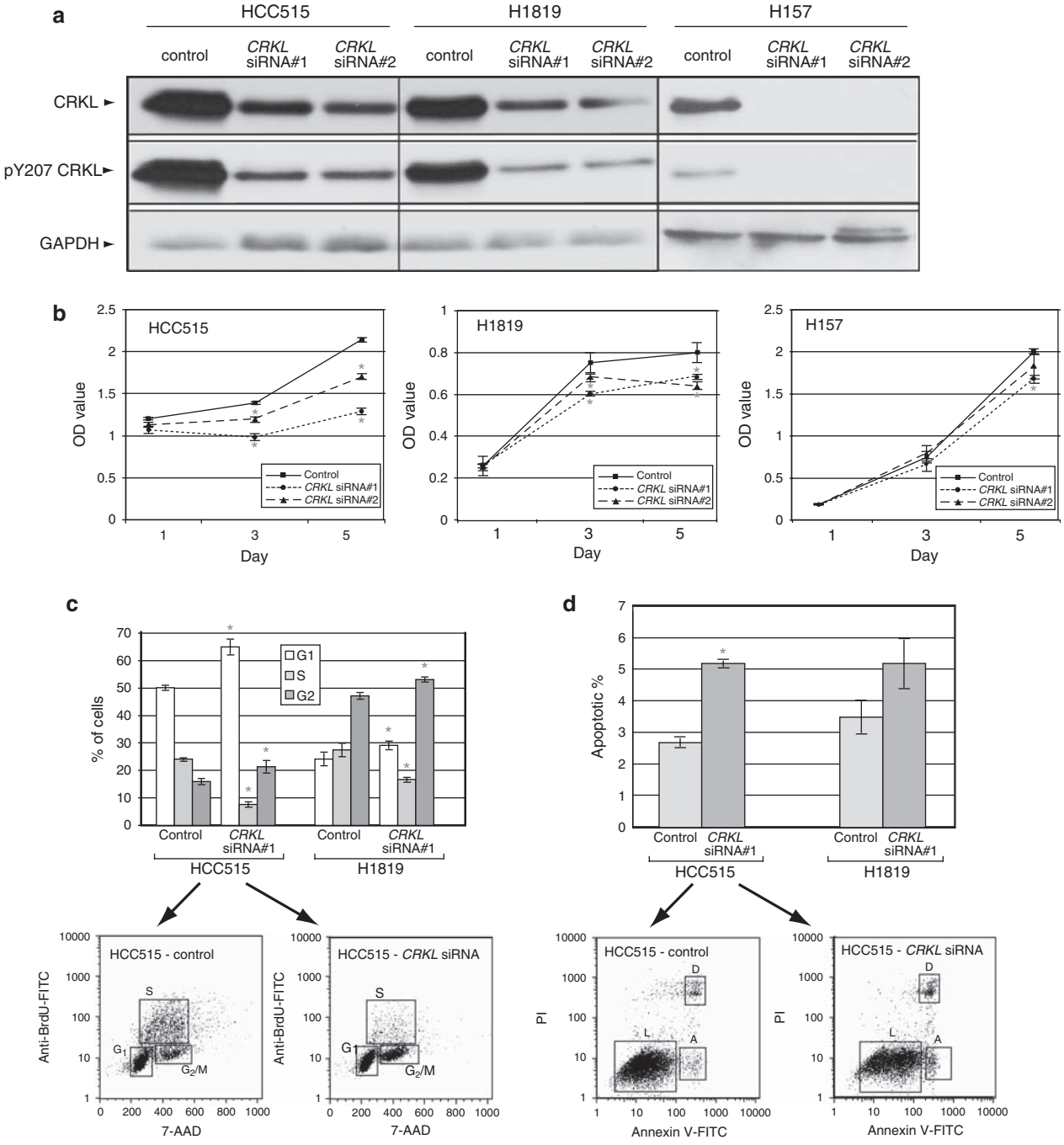

Figure 3 *CRKL* amplification contributes to cell proliferation and survival. (**a**) Confirmation of siRNA-mediated knockdown of CRKL protein by western blot analysis. Two different siRNA constructs targeting CRKL reduce total and phosphorylated protein levels in *CRKL*-amplified cell lines (HCC515 and H1819) and a cell line without amplification (H157), compared with a negative control siRNA targeting an irrelevant gene, green fluorescent protein (*GFP*). Glyceraldehyde-3-phosphate dehydrogenase (GAPDH) serves as a loading control. (**b**) siRNA-mediated knockdown of CRKL results in decreased cell proliferation, compared to control siRNA, as measured by WST-1 assay in *CRKL*-amplified cells (HCC515 and H1819), with less pronounced effects in a nonamplified line (H157) expressing lower levels of CRKL (*$P<0.05$, Student's *t*-test, CRKL siRNA compared to control). (**c**) Knockdown of CRKL reduces cell-cycle progression as measured 72 h after transfection by 5-bromo-2-deoxyuridine (BrdU) incorporation, indicated by a decrease in S-phase fraction with G_1 block compared to control siRNA (*$P<0.05$, Student's *t*-test). Representative flow cytometry plots are also shown. (**d**) Knockdown of CRKL leads to increased apoptosis levels 72 h after transfection, as quantified by flow cytometry-based Annexin V staining, compared to control siRNA (*$P<0.05$, Student's *t*-test). Representative flow cytometry plots are also shown; L, live; A, apoptotic; D, dead.

less expression of CRKL, led to a more subtle effect on cell proliferation, supporting the specificity of *CRKL* targeting.

The observed decrease in cell proliferation might be attributable to decreased cell-cycle progression, increased apoptosis or both. To distinguish these possibilities, we

assayed cell-cycle progression by measuring 5-bromo-2-deoxyuridine (BrdU) incorporation, and apoptosis by Annexin V staining. Targeted knockdown of CRKL in the amplified lines HCC515 and H1819 resulted in decreased cell-cycle progression, as evidenced by a significant decrease in S-phase fraction with G_1 block (Figure 3c) compared with control siRNA. CRKL knockdown in amplified cell lines also led to increased apoptosis, evidenced by the higher fraction of Annexin V-positive cells with siRNA targeting CRKL versus control (though reaching significance only for HCC515) (Figure 3d).

CRKL amplification promotes cell migration and invasion

Earlier studies have implicated a role for CRKL in epithelial cell migration and invasion, with relevance to metastatic potential (Feller, 2001). We therefore sought to evaluate a possible role of *CRKL* amplification in cell migration/invasion in lung cancer. Targeted knockdown of CRKL in amplified NSCLC cell lines HCC515 and H1819 led to a significant inhibition of both cell migration (Figure 4a) and invasion (Figure 4b), compared with control siRNA. Furthermore, no such effect was observed in the lung cancer cell line H157 without amplification (Figures 4a and b), revealing a specific connection between *CRKL* amplification and cell migration and invasion. Co-transfection of a siRNA-resistant CRKL cDNA (containing silent mutations in the siRNA target site) largely rescued CRKL/p-CRKL levels and invasiveness of H1819 cells (Figure 4c), further confirming siRNA targeting specificity.

CRKL overexpression promotes growth factor independence

To complement the RNAi knockdown studies, we sought to determine whether CRKL overexpression might promote oncogenic phenotypes in nontumorigenic lung epithelial cells. HBEC3 (Ramirez *et al*., 2004) is a human bronchial epithelial cell line immortalized by hTERT and Cdk4 (the latter bypassing p16-associated growth arrest), and provides a useful model for assessing the contribution of lung cancer genes (Sato *et al*., 2006). By retroviral transduction, we engineered HBEC3 cells stably overexpressing CRKL, though CRKL levels did not approach those observed in *CRKL*-amplified NSCLC lines (Figure 5a). Nonetheless, overexpression of CRKL in HBEC3 cells significantly enhanced growth factor (EGF)-independent cell growth (Figures 5b and c). However, CRKL overexpression in HBEC3 was not sufficient to promote cell invasion or anchorage-independent soft agar colony growth (data not shown).

Discussion

By genomic profiling, we have identified a focal and recurrent amplicon at cytoband 22q11.21 in NSCLC cell

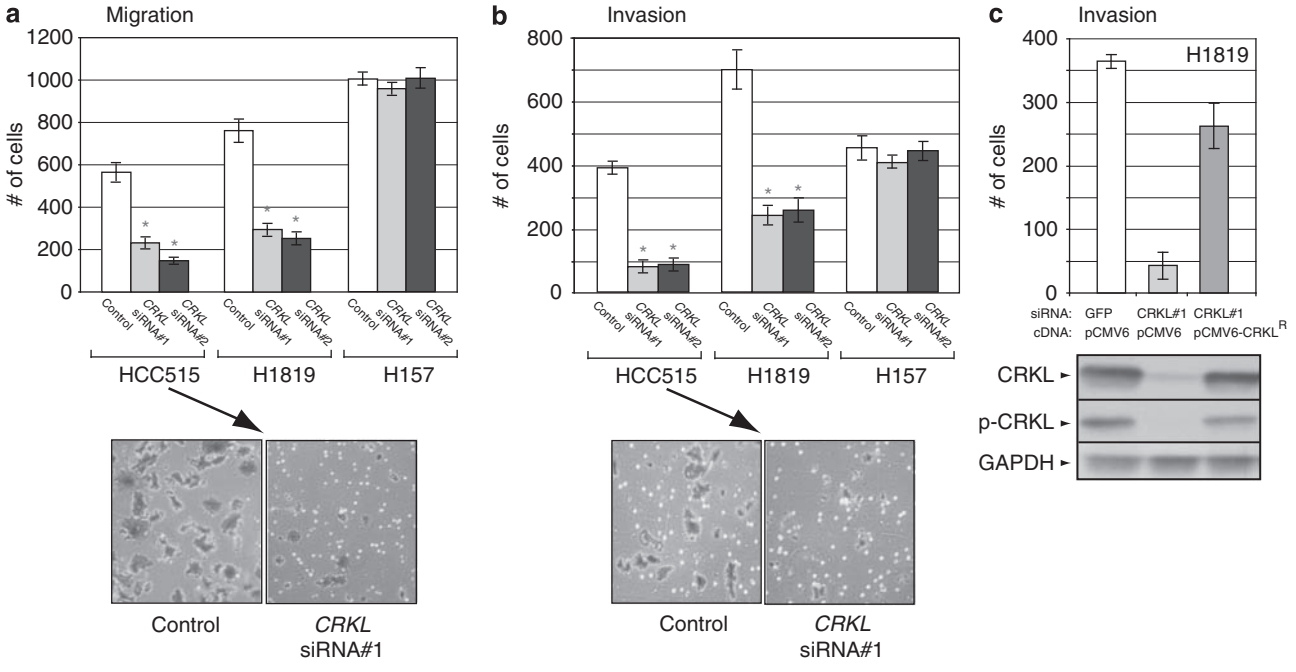

Figure 4 *CRKL* amplification potentiates cell motility and invasion. siRNA-mediated knockdown of CRKL, compared to control siRNA, results in significantly decreased cell counts for (**a**) migration and (**b**) invasion in cell lines with *CRKL* amplification (HCC515 and H1819) (*$P<0.05$, Student's *t*-test). No significant effects are seen in H157, a cell line without *CRKL* amplification. Representative microphotographs depicting cell migration and invasion (CRKL siRNA compared to control) are shown. (**c**) Rescue of siRNA knockdown confirms targeting specificity. H1819 cells were co-transfected with siRNAs and cDNA expression vectors as indicated, and invasion was assayed. pCMV6-CRKL^R contains silent mutations within the siRNA#1 target site, creating an siRNA-resistant transcript (see Materials and methods section). Western blot (Figure) confirms knockdown and rescue of CRKL and p-CRKL levels; glyceraldehyde-3-phosphate dehydrogenase (GAPDH) serves as loading control.

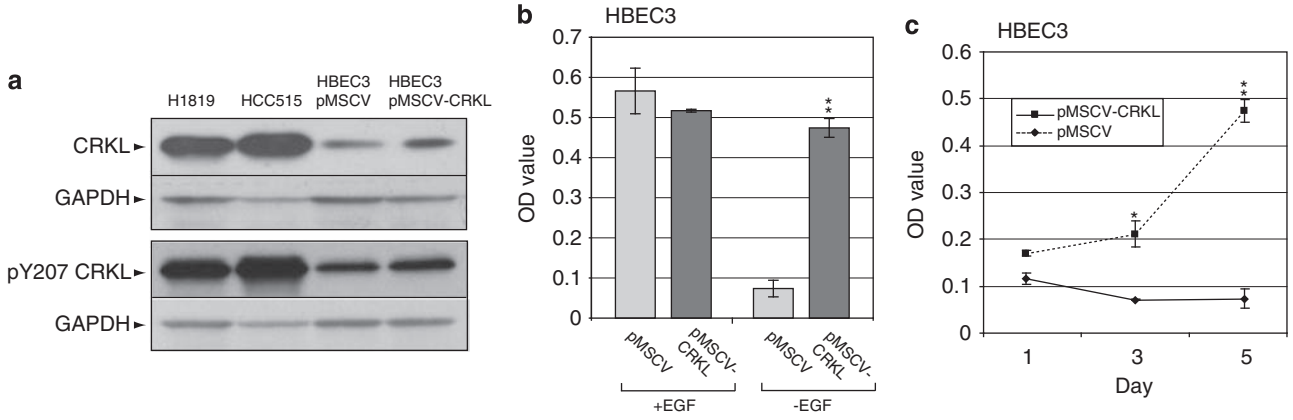

Figure 5 CRKL overexpression promotes growth-factor-independent proliferation. (**a**) Western blot confirmation of CRKL and p-CRKL overexpression in stably transduced HBEC3 cells. H1819 and HCC515 lines provide a comparison for *CRKL*-amplified levels. Glyceraldehyde-3-phosphate dehydrogenase (GAPDH) serves as a loading control. (**b**) CRKL overexpression leads to enhanced growth factor (EGF)-independent cell growth, measured by WST assay. (**c**) Time course confirmation of CRKL-promoted EGF-independent cell growth (*$P<0.05$; **$P<0.01$, Student's *t*-test; pMSCV-CRKL compared to pMSCV control).

lines and tumor samples. Within the amplicon core, *CRKL* is one of only four genes that are overexpressed when amplified. Interestingly, amplification appears even better correlated with p-CRKL levels than with total CRKL protein (Figure 2b), suggesting that amplification occurs within a genetic or cellular context appropriate for CRKL signaling. RNA interference studies in NSCLC cell lines with 22q11.21 amplification show a role and functional dependency on CRKL amplification for tumor cell proliferation, survival and motility/invasion. Overexpression studies in nontumorigenic HBEC3 cells also reveal a function of CRKL in growth-factor-independent proliferation, a classic oncogenic phenotype and, similar to that previously reported for K-RAS^{V12} expression and p53 knockdown (Sato *et al*., 2006). However, in contrast to p53 (knockdown) and K-RAS^{V12} (Sato *et al*., 2006), CRKL alone (at least at the expression levels achieved) appears insufficient to enhance anchorage-independent growth of HBEC3 cells. Further studies may reveal possible cooperative effects with other lung cancer genes.

Other recently published genomic profiling studies using various microarray platforms have also reported amplifications spanning 22q11.21 in NSCLC. Using submegabase resolution tiling BAC arrays, Garnis *et al*. (2006) identified high-level amplification at 22q11.21 in 2 of 28 NSCLC cell lines analyzed, both of which were verified in our study. Using 115K single nucleotide polymorphism arrays, Zhao *et al*. (2005) described 22q11.21 amplification in a panel of lung cancer cell lines (including HCC515, HCC1359 and H1819) and primary lung tumors. They were able to localize the amplicon to a 1 Mb region in 22q11.21, and suggested *CRKL* and *PIK4CA* (catalytic subunit of phosphatidylinositol 4-kinase-α) (centromeric to *CRKL*, and in our data set mapping outside the amplicon core), as possible driver genes. Interestingly, they went on to exclude *CRKL* as the likely driver because its protein levels were not increased in cell lines with amplification (their data not shown), a finding clearly discordant with ours. Most recently, Weir *et al*. (2007) used 250K single nucleotide polymorphism arrays to survey 371 lung adenocarcinomas, reporting high-level amplification at 22q11.21 in 2.4% of tumors, a frequency consistent with our findings. However, from the specimens surveyed they were only able to narrow down the amplicon to an ~1 Mb interval consisting about 15 genes. Our own studies define an ~140 Kb amplicon core, including four genes that are overexpressed when amplified. Though our functional studies implicate *CRKL* as the driver, we cannot exclude the possibility that one or more of the other three genes (*SNAP29*, *LZTR1* and *THAP7*) contributes, though we note that their known functions do not relate in obvious ways to carcinogenesis. Of interest, very recently, Luo *et al*. (2008) identified *CRKL* through a short-hairpin RNA screen as essential for cell proliferation in a subset of NSCLC cell lines studied.

Our findings define a role of *CRKL* amplification in NSCLC pathogenesis. CRKL (Crk-Like) (ten Hoeve *et al*., 1993) is a member of the human Crk adapter protein family, which also includes two alternatively spliced isoforms (CRKI/II) of *CRK*, the cellular homologue of the avian retroviral v-crk oncogene (Feller, 2001). CRKL contains SH2 and SH3 domains that mediate protein–protein interactions connecting tyrosine-phosphorylated upstream signaling components (for example, p130CAS, paxillin, CBL, GAB1) to downstream effectors (for example, C3G, DOCK180), regulating diverse cellular processes like cell adhesion, migration and immune cell responses (Feller, 2001). Early studies identified CRKL as a key substrate and effector of the BCR-ABL oncogenic tyrosine kinase in chronic myelogenous leukemia (ten Hoeve *et al*., 1994; Senechal *et al*., 1996; Hemmeryckx *et al*., 2001). CRKL overexpression was also shown to activate Ras and JUN kinase (JNK) signaling pathways, and to

transform Rat-1 (Senechal *et al*., 1996), though not NIH-3T3 (de Jong *et al*., 1997), rodent fibroblasts.

In epithelial cells, CRKL has been shown to potentiate hepatocyte growth factor (scatter factor)-induced cell motility through protein complexes connecting the MET receptor tyrosine kinase to downstream activation of effector proteins like Rap1 and Rac (Furge *et al*., 2000; Feller, 2001). The connection to MET is particularly intriguing given that MET is activated by mutation or amplification in some lung cancers (Ma *et al*., 2003; Zhao *et al*., 2005). In our NSCLC cell line panel, amplification of *MET* and *CRKL* was mutually exclusive (data not shown), consistent with their function in the same pathway (with CRKL downstream of MET). However, in preliminary studies, whereas knockdown of CRKL in an NSCLC cell line with *MET* amplification (H1648) reduced cell proliferation and survival, knockdown of MET in that same cell line reduced proliferation/survival (consistent with a recent report (Lutterbach *et al*., 2007)) but not phospho-CRKL levels (unpublished findings). Further studies are required to clarify the connection between MET and CRKL in NSCLCs with *MET* amplification.

Although we report here the amplification of *CRKL* in lung cancer, CRKL may have a pathogenic role in other epithelial cancers as well. Recently, Singer *et al*. (2006) described overexpression of phospho-CRKL, measured by immunohistochemistry, in breast, ovarian and colon cancer, as well as lung cancer, in comparison with the corresponding normal tissues. Our own array CGH studies have identified amplifications spanning 22q11.21 in breast and pancreatic cancers (Bashyam *et al*., 2005; Bergamaschi *et al*., 2006). Further studies are needed to establish a functional role of *CRKL* amplification/overexpression in these cancers. We also note that the related adapter *CRK* (at 17p13.3), although occasionally found within broad low-level gains in lung cancer, is not focally amplified as we have found *CRKL*.

A finding of particular interest from our study is that the amplification of an adapter protein, functioning solely to assemble other proteins, promotes strong and pleiotropic oncogenic phenotypes. Prototypic oncogenic amplifications include tyrosine kinases (*ERBB2*, *EGFR*, *MET*), ras proteins (*KRAS*), cell-cycle modulators (*CCND1*, *CDK4*) and transcription factors (*MYC*). Although overexpression of SH2/SH3 adapter proteins such as GRB2 (Daly *et al*., 1994), GRB7 (Stein *et al*., 1994) and GAB2 (Daly *et al*., 2002) has been implicated in oncogenesis, and v-Crk itself was discovered as an avian oncogene, our findings now place amplification of an adapter protein gene (*CRKL*) as a primary genetic event driving human cancer.

Our findings also underscore the potential of novel therapeutics targeting adapter protein interactions, and targeting CRKL in lung cancer in particular. Indeed, a small molecule inhibitor disrupting interactions of the GRB2 SH2 domain has been described (Gay *et al*., 1999), and more recently a peptide inhibitor selectively targeting the CRKL SH3 domain, disrupting its interaction with BCR-ABL (Kardinal *et al*., 2000). In summary, our combined genomic and functional analysis defines a novel role of *CRKL* amplification in lung carcinogenesis, potentiating cell proliferation, growth-factor independence, survival and migration/invasion, highlighting the oncogenic role of adapter proteins and suggesting a new point for therapeutic intervention.

Materials and methods

Lung cancer cell lines and tumors

'NCI-H' series NSCLC cell lines, established at the National Cancer Institute, and 'HCC' series cell lines, established at the Hamon Center for Therapeutic Oncology Research, UT Southwestern Medical Center (Dallas, TX, USA), together totaling 52 cell lines, were obtained from the latter's tissue culture repository (most lines are currently available through the American Type Culture Collection, Manassas, VA, USA). For functional studies, we cultured cells in RPMI 1640 (Invitrogen, Carlsbad, CA, USA) with 10% fetal bovine serum (FBS, Hyclone; Fisher Scientific, Pittsburgh, PA, USA). HBEC3 cells (Ramirez *et al*., 2004), obtained from the same repository, were grown in K-SFM medium (Invitrogen) containing 50 μg/ml bovine pituitary extract (Invitrogen) with 5 ng/ml EGF (Invitrogen). A total of 76 freshly frozen lung tumors were banked at the University Hospital Charité, Berlin, Germany, with institutional review board approval. Specimens were verified by hematoxylin and eosin staining to contain at least 70% tumor cells.

Genomic and gene expression profiling

cDNA microarray-based genomic profiling by CGH, and mRNA transcript profiling, of 128 lung cancer cell lines and tumors was described in a preliminary report of our study, focused on the identification of *TITF1* amplification (Kwei *et al*., 2008). cDNA microarrays contained 39 632 human cDNAs, representing 22 279 mapped human genes and 4230 additional mapped expressed sequence tags. The complete microarray data sets are available at Stanford Microarray Database (http://smd.stanford.edu) and at the Gene Expression Omnibus (accession GSE9995).

Microarray data analysis

Background-subtracted fluorescence ratios were normalized by mean-centering genes for each array. For array CGH analysis, we selected only those genes whose Cy3 reference-channel fluorescence signal intensity was at least 40% above background in at least 50% of samples. Map positions for arrayed cDNA clones were assigned using the NCBI genome assembly (Build 36), accessed through the UCSC genome database (Kent *et al*., 2002). We used the method cghFLasso (R package) to identify DNA gains and losses (Tibshirani and Wang, 2008). High-level DNA amplifications were defined as contiguous regions called by cghFLasso where at least 50% of genes show fluorescence ratios $\geqslant 3$. To detect associations between DNA copy number alterations at distinct loci, we computed a Pearson's correlation between the mean copy number of a given cytoband and that of all other cytobands. Statistically significant correlations were determined by randomly permuting cytoband labels and recalculating correlations 100 times; a false discovery rate of 1% was used to establish a significance threshold. For expression profiling, fluorescence ratios were normalized for each array, and then well-measured genes (fluorescence intensities for the Cy5

or Cy3 channel at least 50% above background) were subsequently mean-centered (that is, reported for each gene relative to the mean ratio across all samples).

Fluorescence in situ *hybridization*
Probe labeling and fluorescence *in situ* hybridization were performed using Vysis (Downers Grove, IL, USA; now Abott Molecular) reagents according to the manufacturer's protocols. A locus-specific BAC probe targeting *CRKL* at 22q11.21 (RP11-1058B20) (BACPAC Resources Center, Oakland, CA, USA) was labeled with Spectrum green-dUTP, and co-hybridized with Spectrum orange-dUTP-labeled chromosome 22 telomeric probe (TelVysion 22q; Vysis). Chromosomal locations of labeled BAC probes were validated on metaphase slides prepared from normal donors. Slides were counterstained with 46-diamidino-2-phenyl indole, and imaged using an Olympus BX51 fluorescence microscope with Applied Imaging (San Jose, CA, USA) CytoVision 3.0 software.

siRNA transfections
Two different siRNAs targeting *CRKL*, along with a negative control siRNA targeting an irrelevant gene, *GFP*, were obtained from Qiagen, Valencia, CA, USA. Complete siRNA sequences are provided (Supplementary Table 1). Cell lines were maintained at 37 °C in complete media of RPMI 1640 with 10% FBS before transfection. For transfection, 80 000–175 000 cells were seeded per six-well plate, and transfected using Lipofectamine 2000 reagent (Invitrogen) according to the manufacturer's protocol. Cells were transfected with a final concentration of 50 nM siRNA for 6 h, and subsequently replaced with complete growth media.

Plasmid constructs
A full-length human CRKL cDNA expression vector, pCMV6/XL4-CRKL, and the parent vector, pCMV6/XL4, were purchased from OriGene (Rockville, MD, USA). A CRKL siRNA#1-resistant CRKL cDNA was engineered using the QuikChange XL II Site-Directed Mutagenesis Kit (Stratagene, La Jolla, CA, USA), with the following mutational primers: 5′-GGTTGGTGACATCGTGAA**G**GT**G**AC**C**CGGATGAA**C**AT**T**AATGGCCAGTGGGAAG-3′ (degenerate, mutated bases denoted by bold) and 5′-CTTCCCACT GGCCATTAATGTTCATCCGGGTCACCTTCACGATG TCACCAACC-3′. To generate HBEC3 cells stably overexpressing CRKL, we created a retroviral expression vector by PCR-amplifying full-length CRKL cDNA and subcloning the product into the *Hpa*I and *Xho*I restriction sites of the vector pMSCV-Hyg (Clontech, Mountain View, CA, USA).

Viral transduction and stable selection
293T cells were transfected with either pMSCV-Hyg or pMSCV-Hyg-CRKL together with pVpack-VSVG and pVpack-GP vectors (Stratagene) to generate replication-defective retrovirus. Viral supernatants were collected 48 h after transfection, and used to infect HBEC3 cells, which were subsequently treated with 10 μg/ml hygromycin B (Invitrogen) for 14 days for stable selection.

Western blot analysis
Cells were lysed in 1 × RIPA Lysis buffer (Upstate/Chemicon, San Francisco, CA, USA) supplemented with 1 × Complete Protease Inhibitor (Roche, Indianapolis, IN, USA), 0.1 mM sodium orthovanadate, 1 mM sodium fluoride and 1 mM phenylmethylsulfonyl fluoride, and protein was quantified using the BCA assay (Pierce, Rockford, IL, USA). For western blot analysis, 20–30 μg of protein lysate was electrophoresed on a 4–15% Criterion Tris–HCl polyacrylamide gradient gel (Bio-Rad, Hercules, CA, USA) and transferred overnight to a PVDF membrane (Bio-Rad). After blocking in TBS-T buffer (20 mM Tris–HCl (pH 7.4), 0.15 M NaCl, 0.1% Tween 20) with 5% dry milk for 45 min, blots were incubated with primary antibody overnight (for phospho specificity) at 4 °C or 90 min (for native) at room temperature. After sequential washing steps, blots were incubated with horseradish-peroxidase-conjugated secondary antibody for 45 min at room temperature in TBS-T buffer. The following antibodies were used: phospho-CRKL Y207 (1:500; catalogue no. 3181; Cell Signaling, Danvers, MA, USA), anti-CRKL rabbit polyclonal antibody (1:1000; catalogue no. sc-319; Santa Cruz Biotechnology, Santa Cruz, CA, USA), glyceraldehyde-3-phosphate dehydrogenase (GAPDH, 1:5000, for loading control; Santa Cruz Biotechnology) and horseradish-peroxidase-conjugated anti-rabbit IgG (1:20 000; Pierce).

Proliferation assay
Cell proliferation was quantified by WST-1 assay (Roche), a colorimetric assay based on the metabolic cleavage of the tetrazolium salt WST-1 in viable cells, according to the manufacturer's protocol. WST-1 reagent (100 μl) was added to 1 ml of culture volume in six-well plates and incubated at 37 °C for 30 min. Absorbance was then measured at 450 nm with reference to 650 nm using a SpectraMax 190 plate reader (Molecular Devices, Sunnyvale, CA, USA). Transfections were performed in triplicate and average (±1 s.d.) OD reported.

Cell-cycle analysis
Cell-cycle distribution analysis was performed by flow cytometry using the BrdU-FITC Flow kit (BD Biosciences, San Jose, CA, USA) per the manufacturer's instructions. Cells were incubated with 10 μM BrdU at 37 °C for 5 h, then fixed and permeabilized with Cytofix/Cytoperm buffer (BD Biosciences). Cellular DNA was treated with DNase at 37 °C for 1 h to expose incorporated BrdU, then cells were stained with anti-BrdU fluorescein isothiocyanate antibody to quantify incorporated BrdU and 7-aminoactinomycin D to quantify total DNA content. A total of 15 000 events were scored by FACSCalibur (BD Biosciences) flow cytometer and analyzed using CellQuest software (BD Biosciences). Transfections were performed in triplicate and average (±1 s.d.) cell-cycle fractions were reported.

Apoptosis assay
Apoptosis levels were assayed by Annexin V staining, quantified by flow cytometry using the Vybrant Apoptosis Assay kit 2 (Invitrogen) per the manufacturer's recommendations. Briefly, floating and trypsinized adherent cells were pooled and resuspended in 200 μl 1 × Annexin binding buffer. One microliter Alexa Fluor 488 Annexin V and 1 μl of 100 μg/ml propidium iodide solution were added and cells were incubated for 15 min at room temperature. Cells were then resuspended in equal volume of 1 × Annexin binding buffer and analyzed immediately by flow cytometry. A total of 15 000 events were scored by FACSCalibur and analyzed using CellQuest software. Transfections were performed in triplicate, and average (±1 s.d.) percent apoptosis was reported.

Invasion and migration assays
Invasion and migration assays were carried out using BD Biocoat (BD Biosciences) modified Boyden chambers and

control inserts with polyethylene membrane, respectively. For invasion assays, precoated filters (8 μm pore size, Matrigel 100 μg/cm^2) were rehydrated with 500 μl of complete growth media (RPMI 1640, 10% FBS), then 1 to 5×10^4 cells resuspended in RPMI 1640 media with 2% FBS were seeded into the upper chamber. Following incubation for 16–72 h at 37 °C, cells were fixed in 10% buffered formalin and then stained with crystal violet. Migration assays were performed similarly to invasion assays, with the exception of using control inserts (with/without Matrigel coating) and using fewer cells (1 to 2.5×10^4 cells) and shorter time points (16–48 h). Noninvaded (or migrated) cells in the upper membrane were removed by swabbing, and the amount of invasion (or migration) was quantified by counting stained cells on the underside of the membrane. Assays were performed in triplicate and the average (± 1 s.d.) cell count was reported.

Conflict of interest

The authors declare no conflict of interest.

Acknowledgements

We thank the SFGF for fabrication of microarrays and the SMD for database support. We thank Eon Rios for assistance with flow cytometry analysis. We also thank the members of the Pollack lab for helpful discussion. This work was supported in part by grants from the NIH: R01 CA97139 (JRP), SPORE P50CA70907 (JDM), EDRN U01CA084971 (AFG); DOD VITAL (JDM); Longenbaugh Foundations (JDM); TRDRP (17FT-0062; KAK) and the Deutsche Krebshilfe: 108003 (IP). KS was supported by the Medical Scientist Training Program and is a Paul & Daisy Soros fellow.

References

Bashyam MD, Bair R, Kim YH, Wang P, Hernandez-Boussard T, Karikari CA *et al*. (2005). Array-based comparative genomic hybridization identifies localized DNA amplifications and homozygous deletions in pancreatic cancer. *Neoplasia* **7**: 556–562.

Bergamaschi A, Kim YH, Wang P, Sorlie T, Hernandez-Boussard T, Lonning PE *et al*. (2006). Distinct patterns of DNA copy number alteration are associated with different clinicopathological features and gene-expression subtypes of breast cancer. *Genes Chromosomes Cancer* **45**: 1033–1040.

Daly RJ, Binder MD, Sutherland RL. (1994). Overexpression of the Grb2 gene in human breast cancer cell lines. *Oncogene* **9**: 2723–2727.

Daly RJ, Gu H, Parmar J, Malaney S, Lyons RJ, Kairouz R *et al*. (2002). The docking protein Gab2 is overexpressed and estrogen regulated in human breast cancer. *Oncogene* **21**: 5175–5181.

de Jong R, ten Hoeve J, Heisterkamp N, Groffen J. (1997). Tyrosine 207 in CRKL is the BCR/ABL phosphorylation site. *Oncogene* **14**: 507–513.

Feller SM. (2001). Crk family adaptors-signalling complex formation and biological roles. *Oncogene* **20**: 6348–6371.

Furge KA, Zhang YW, Vande Woude GF. (2000). Met receptor tyrosine kinase: enhanced signaling through adapter proteins. *Oncogene* **19**: 5582–5589.

Garnis C, Lockwood WW, Vucic E, Ge Y, Girard L, Minna JD *et al*. (2006). High resolution analysis of non-small cell lung cancer cell lines by whole genome tiling path array CGH. *Int J Cancer* **118**: 1556–1564.

Gay B, Suarez S, Caravatti G, Furet P, Meyer T, Schoepfer J. (1999). Selective GRB2 SH2 inhibitors as anti-ras therapy. *Int J Cancer* **83**: 235–241.

Hemmeryckx B, van Wijk A, Reichert A, Kaartinen V, de Jong R, Pattengale PK *et al*. (2001). Crkl enhances leukemogenesis in BCR/ABL P190 transgenic mice. *Cancer Res* **61**: 1398–1405.

Jemal A, Siegel R, Ward E, Hao Y, Xu J, Murray T *et al*. (2008). Cancer statistics, 2008. *CA Cancer J Clin* **58**: 71–96.

Kardinal C, Konkol B, Schulz A, Posern G, Lin H, Adermann K *et al*. (2000). Cell-penetrating SH3 domain blocker peptides inhibit proliferation of primary blast cells from CML patients. *FASEB J* **14**: 1529–1538.

Kendall J, Liu Q, Bakleh A, Krasnitz A, Nguyen KC, Lakshmi B *et al*. (2007). Oncogenic cooperation and coamplification of developmental transcription factor genes in lung cancer. *Proc Natl Acad Sci USA* **104**: 16663–16668.

Kent WJ, Sugnet CW, Furey TS, Roskin KM, Pringle TH, Zahler AM *et al*. (2002). The human genome browser at UCSC. *Genome Res* **12**: 996–1006.

Kwei KA, Kim YH, Girard L, Kao J, Pacyna-Gengelbach M, Salari K *et al*. (2008). Genomic profiling identifies TITF1 as a lineage-specific oncogene amplified in lung cancer. *Oncogene* **27**: 3635–3640.

Luo B, Cheung HW, Subramanian A, Sharifnia T, Okamoto M, Yang X *et al*. (2008). Highly parallel identification of essential genes in cancer cells. *Proc Natl Acad Sci USA* **105**: 20380–20385.

Lutterbach B, Zeng Q, Davis LJ, Hatch H, Hang G, Kohl NE *et al*. (2007). Lung cancer cell lines harboring MET gene amplification are dependent on Met for growth and survival. *Cancer Res* **67**: 2081–2088.

Lynch TJ, Bell DW, Sordella R, Gurubhagavatula S, Okimoto RA, Brannigan BW *et al*. (2004). Activating mutations in the epidermal growth factor receptor underlying responsiveness of non-small-cell lung cancer to gefitinib. *N Engl J Med* **350**: 2129–2139.

Ma PC, Kijima T, Maulik G, Fox EA, Sattler M, Griffin JD *et al*. (2003). c-MET mutational analysis in small cell lung cancer: novel juxtamembrane domain mutations regulating cytoskeletal functions. *Cancer Res* **63**: 6272–6281.

Paez JG, Janne PA, Lee JC, Tracy S, Greulich H, Gabriel S *et al*. (2004). EGFR mutations in lung cancer: correlation with clinical response to gefitinib therapy. *Science* **304**: 1497–1500.

Pollack JR, Perou CM, Alizadeh AA, Eisen MB, Pergamenschikov A, Williams CF *et al*. (1999). Genome-wide analysis of DNA copy-number changes using cDNA microarrays. *Nat Genet* **23**: 41–46.

Ramirez RD, Sheridan S, Girard L, Sato M, Kim Y, Pollack J *et al*. (2004). Immortalization of human bronchial epithelial cells in the absence of viral oncoproteins. *Cancer Res* **64**: 9027–9034.

Sato M, Vaughan MB, Girard L, Peyton M, Lee W, Shames DS *et al*. (2006). Multiple oncogenic changes (K-RAS(V12), p53 knockdown, mutant EGFRs, p16 bypass, telomerase) are not sufficient to confer a full malignant phenotype on human bronchial epithelial cells. *Cancer Res* **66**: 2116–2128.

Sattler M, Salgia R. (1998). Role of the adapter protein CRKL in signal transduction of normal hematopoietic and BCR/ABL-transformed cells. *Leukemia* **12**: 637–644.

Senechal K, Halpern J, Sawyers CL. (1996). The CRKL adaptor protein transforms fibroblasts and functions in transformation by the BCR-ABL oncogene. *J Biol Chem* **271**: 23255–23261.

Singer CF, Hudelist G, Lamm W, Mueller R, Handl C, Kubista E *et al*. (2006). Active (p)CrkL is overexpressed in human malignancies: potential role as a surrogate parameter for therapeutic tyrosine kinase inhibition. *Oncol Rep* **15**: 353–359.

Stein D, Wu J, Fuqua SA, Roonprapunt C, Yajnik V, D'Eustachio P *et al*. (1994). The SH2 domain protein GRB-7 is co-amplified, overexpressed and in a tight complex with HER2 in breast cancer. *EMBO J* **13**: 1331–1340.

ten Hoeve J, Kaartinen V, Fioretos T, Haataja L, Voncken JW, Heisterkamp N *et al*. (1994). Cellular interactions of CRKL, and SH2-SH3 adaptor protein. *Cancer Res* **54**: 2563–2567.

ten Hoeve J, Morris C, Heisterkamp N, Groffen J. (1993). Isolation and chromosomal localization of CRKL, a human crk-like gene. *Oncogene* **8**: 2469–2474.

Tibshirani R, Wang P. (2008). Spatial smoothing and hot spot detection for CGH data using the fused lasso. *Biostatistics* **9**: 18–29.

Tonon G, Wong KK, Maulik G, Brennan C, Feng B, Zhang Y *et al*. (2005). High-resolution genomic profiles of human lung cancer. *Proc Natl Acad Sci USA* **102**: 9625–9630.

Weir BA, Woo MS, Getz G, Perner S, Ding L, Beroukhim R *et al*. (2007). Characterizing the cancer genome in lung adenocarcinoma. *Nature* **450**: 893–898.

Zhao X, Weir BA, LaFramboise T, Lin M, Beroukhim R, Garraway L *et al*. (2005). Homozygous deletions and chromosome amplifications in human lung carcinomas revealed by single nucleotide polymorphism array analysis. *Cancer Res* **65**: 5561–5570.

Supplementary Information accompanies the paper on the Oncogene website (http://www.nature.com/onc)

Biometrics 62, 986–995
December 2006

DOI: 10.1111/j.1541-0420.2006.00579.x

A Generalized Response Surface Model with Varying Relative Potency for Assessing Drug Interaction

Maiying Kong and J. Jack Lee*

Department of Biostatistics and Applied Mathematics, University of Texas, M. D. Anderson Cancer Center, Unit 447, 1515 Holcombe Boulevard, Houston, Texas 77030, U.S.A.
**email:* jjlee@mdanderson.org

Summary. When multiple drugs are administered simultaneously, investigators are often interested in assessing whether the drug combinations are synergistic, additive, or antagonistic. Based on the Loewe additivity reference model, many existing response surface models require constant relative potency and some of them use a single parameter to capture synergy, additivity, or antagonism. However, the assumption of constant relative potency is too restrictive, and these models using a single parameter to capture drug interaction are inadequate to describe the phenomenon when synergy, additivity, and antagonism are interspersed in different regions of drug combinations. We propose a generalized response surface model with a function of doses instead of one single parameter to identify and quantify departure from additivity. The proposed model can incorporate varying relative potencies among multiple drugs as well. Examples and simulations are given to demonstrate that the proposed model is effective in capturing different patterns of drug interaction.

Key words: Additivity; Antagonism; Dose–response curve; Dose–response surface; Interaction index; Loewe additivity model; Synergy.

1. Introduction

Studies of interactions among biologically active agents, such as drugs, carcinogens, or environmental pollutants, have become increasingly important in many branches of biomedical research (Suhnel, 1998). An effective and accurate evaluation of drug interaction for in vitro and/or in vivo studies can help to determine whether a combination therapy should be further investigated in clinical trials.

The literature supports the notion that the Loewe additivity model can be considered as the "gold standard" to define drug interactions (Berenbaum, 1989; Greco, Bravo, and Parsons, 1995). Based on the Loewe additivity model, we focus on applying the response surface method (RSM) to study drug interaction. The RSM, which involves an estimation of the $(n + 1)$-dimensional response surface in n drug combinations, can take all of the information present in the full dose-effect data set for n drugs to give a complete picture of drug interactions over all possible drug combinations. In addition, the RSM can be used to determine the optimal combination therapy. Many examples of the RSM (e.g., Finney, 1971; Greco, Park, and Rustum, 1990; Plummer and Short, 1990) used a single parameter to capture synergy, additivity, or antagonism. These approaches are valid if only either synergy, additivity, or antagonism exists throughout the whole surface. They are inadequate to describe the presence of pockets of local synergy or local antagonism when they are interspersed in different regions of drug combinations. White et al. (2004) proposed a nonlinear mixture response surface approach based on the assumption that the combination doses at each fixed ratio follow the median effect model (Chou and Talalay, 1984), and the parameters in the median effect model are assumed to be polynomials of the ratio. The resulting models capture synergy, additivity, or antagonism exclusively based on the 50% maximal effect isoboles. However, at a fixed ratio, the combination doses of two drugs do not necessarily yield the same mode of drug interactions as that at 50% maximal effect. For example, Savelev et al. (2003) showed that the combinations of 1,8-cineole and α-pinene at the fixed ratio 11:1 are synergistic for higher combination doses and additive for lower combination doses. To address this issue, we propose a generalized response surface (GRS) model for two drugs. Instead of using one single parameter, we construct a function of the doses of two drugs to capture synergy, additivity, and antagonism without assuming any fixed patterns of drug interactions. The model contains a rich class of dose–response relationships and allows the drug interaction patterns to be determined by the observed data.

Before we proceed, let us recall a widely used model that provides a dose–response curve for a single agent: Chou and Talalay's (1984) median effect equation,

$$E = \frac{\left(\frac{d}{D_m}\right)^m}{1 + \left(\frac{d}{D_m}\right)^m}. \quad (1)$$

Here d is the dose of a drug, D_m is the median effective dose of a drug, and m is a slope parameter depicting the shape

of the dose–response curve. All these dose–response curves can be rewritten as Y, a monotone function of E, having a linear relationship with $\log d$. For example, the median effect equation has the form

$$Y = \log \frac{E}{1-E} = m(\log d - \log D_m). \tag{2}$$

All the families described by Suhnel (1998), excluding the Weibull family, can take such form by establishing a linear relationship between a monotone transformation of E and $\log d$. Tallarida (2000, Chapter 2) pointed out that, in many settings, the data points in the mid range (say between 20% and 80% of the maximum effect) typically display a nearly linear trend between the response and the $\log d$ when responses are measured on a continuous scale. For quantal response data, Finney (1971) and Govindarajulu (2001) pointed out that the probit- or logistic-transformed response usually exhibits a linear relationship with $\log d$. Consequently, we assume that the response or transformed response follows a linear function of $\log d$ for each of the two drugs when acting alone. Without loss of generality, we denote the dose–response curve as $Y = \beta_0 + \beta_1 \log d$.

Suhnel (1998) explicitly derived the combined additive effect of two drugs under the Loewe additivity model and made the assumption that the slopes β_1 are the same for both drugs. Finney (1971) proposed an additivity model for two drugs as $Y = \beta_0 + \beta_1 \log(d_1 + \rho d_2)$ for the combination dose (d_1, d_2), where ρ is the relative potency of drug 2 versus drug 1 and is assumed to be a constant. The constant ρ again implies that the two dose–response curves have the same slope. To construct a generalized model, we would first loosen the parallel assumption by allowing a varying relative potency. Next, we propose the use of a quadratic function of two doses instead of one single parameter to depict different patterns of drug interactions. The proposed model can be considered as a generalization of Finney's model (1971) and the model derived by Plummer and Short (1990). We will describe our proposed model in Section 2, relate this new model to isoboles and interaction indices in Section 3, state how to make inference on drug combinations in Section 4, and give simulations and examples to illustrate how the new approach performs in Section 5. The last section is devoted to discussion.

2. Derivation of the Generalized Response Surface Model

Recall the Loewe additivity model (Loewe and Muischnek, 1926; Berenbaum, 1989; Greco et al., 1995)

$$\frac{d_1}{D_{y,1}} + \frac{d_2}{D_{y,2}} = 1, \tag{3}$$

where d_1, d_2 are doses of drug 1 and drug 2 in the mixture eliciting an effect y, and $D_{y,1}$ and $D_{y,2}$ are the respective single-agent doses of drug 1 and drug 2 that elicit the effect y. One can obtain the predicted additive effect based on the Loewe additivity model providing that the dose–effect curves for each of the two drugs are known. Suppose that the dose–effect curves are $F_1(D_1)$ for drug 1 and $F_2(D_2)$ for drug 2, then the predicted effect, say y, can be obtained by solving equation (3) after replacing $D_{y,1}$ by $F_1^{-1}(y)$ and $D_{y,2}$ by $F_2^{-1}(y)$, where F_i^{-1} is the inverse function of $F_i (i = 1, 2)$. If the observed effect at (d_1, d_2) is more than or less than the predicted effect, the combination dose (d_1, d_2) is correspondingly synergistic or antagonistic.

Note that the above additive equation (3) can be rewritten as

$$d_1 + d_2 \frac{D_{y,1}}{D_{y,2}} = D_{y,1}. \tag{4}$$

Denote $\frac{D_{y,1}}{D_{y,2}}$ as $\rho(y)$, which is the relative potency of drug 2 versus drug 1, meaning that 1 unit of drug 2 has the same effect as $\rho(y)$ units of drug 1. Grabovsky and Tallarida (2004) addressed the issue that the relative potency may vary. The nonparallel dose–effect curves introduced by Suhnel (1998) can also be interpreted as the varying relative potency. When the relative potency varies, finding a method to transform the combination dose (d_1, d_2) into the equivalent doses of drug 1 or drug 2 requires careful investigation. In the following derivation, we uphold the Loewe additivity model regardless of the shape of the dose–effect curve associated with each single drug. We expound the interpretation of the varying relative potency, its correct usage, and the relationship of various quantities in equation (4) in the Appendix. From the Appendix, it follows that the additive y-isobole is a straight line $\overline{PQ}$, which connects $P = (D_{y,1}, 0)$ and $Q = (0, D_{y,2})$ (Figure 1, panel A). Each drug combination (d_1, d_2) on the y-isobole shares the same relative potency $\rho(y)$, and its equivalent amount dose is $d_1 + \rho(y)d_2$ in terms of drug 1, or $\rho(y)^{-1}d_1 + d_2$ in terms of drug 2. On the other hand, the combination doses on different additive isoboles may have different relative potencies as shown in Figure 1, panel B.

In this article, we construct a GRS model which incorporates the varying relative potency. We assume that the log(dose)–response curves are linear. Without loss of generality, the model derivation begins with the assumptions of a constant relative potency and a log(dose)–effect curve for drug 1:

$$Y_1 = \beta_0 + \beta_1 \log D_{Y_1,1}. \tag{5}$$

Subsequently, the predicted additive effect of the combination can be written as $Y = \beta_0 + \beta_1 \log(d_1 + \rho d_2)$, where ρ is a constant relative potency parameter. In order to capture synergy, additivity, or antagonism, Finney (1971, Section 11.5) suggested a model of the form

$$Y = \beta_0 + \beta_1 \log\left(d_1 + \rho d_2 + \kappa (d_1 \rho d_2)^{\frac{1}{2}}\right). \tag{6}$$

Here the additional term $(d_1 \rho d_2)^{\frac{1}{2}}$ is the geometric mean of d_1 and ρd_2, and κ is the synergy-antagonism parameter with $\kappa = 0$ corresponding to additivity, $\kappa > 0$ to synergy, and $\kappa < 0$ to antagonism.

Plummer and Short (1990) extended model (6) to a case in which the relative potency ρ may be varying while keeping the same formulation as (6). Let us assume that the log(dose)–effect curve for drug 2 is

$$Y_2 = \alpha_0 + \alpha_1 \log D_{Y_2,2}. \tag{7}$$

The question is: what form should the relative potency take under the log(dose)–effect curves (5) for drug 1 and (7) for drug 2? Let $Y_1 = Y_2 = y$, we have $\beta_0 + \beta_1 \log D_{y,1} = \alpha_0 + \alpha_1 \log D_{y,2}$. Then, $\beta_1 \log \frac{D_{y,1}}{D_{y,2}} = \alpha_0 - \beta_0 + (\alpha_1 - \beta_1) \log D_{y,2}$.

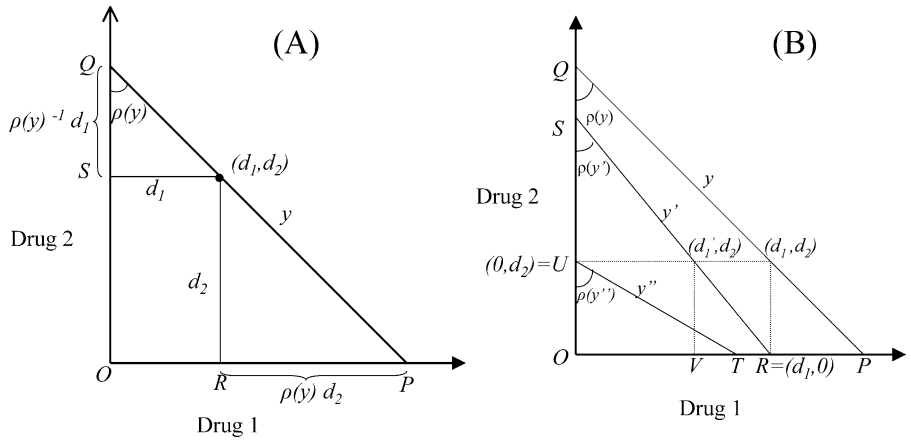

Figure 1. Relative potency and equivalent doses. $\overline{PQ}$ is an additive isobole, $P = (D_{y,1}, 0)$, $Q = (0, D_{y,2})$. The relative potency of drug 2 versus drug 1 is defined as $\rho(y) = \frac{D_{y,1}}{D_{y,2}}$. Under additive assumption the effect at (d_1, d_2) is the same as the effect of drug 1 alone at $d_1 + \rho(y)d_2$, and also the same as the effect of drug 2 alone at $\rho(y)^{-1}d_1 + d_2$ (panel A). Panel B shows that given drug 2 at dose d_2, its equivalent drug 1 dose may change when different amounts of drug 1 are added. Here $y = F_1(D_{y,1}) = F_2(D_{y,2})$, $y' = F_1(d_1)$, and $y'' = F_2(d_2)$. The equivalent amount of drug 1 doses of d_2 at combination doses (d_1, d_2), (d_1', d_2), and $(0, d_2)$ are $\rho(y)d_2(=\text{length}(\overline{RP}))$, $\rho(y')d_2(=\text{length}(\overline{VR}))$, and $\rho(y'')d2(=\text{length}(\overline{OT}))$, respectively.

Thus, the relative potency can be written as $\rho(y) = \frac{D_{y,1}}{D_{y,2}} = \exp(\frac{\alpha_0 - \beta_0}{\beta_1} + \frac{\alpha_1 - \beta_1}{\beta_1}\log D_{y,2})$. Introducing two parameters $\gamma_1(= \frac{\alpha_0 - \beta_0}{\beta_1})$ and $\gamma_2(= \frac{\alpha_1 - \beta_1}{\beta_1})$, we can write

$$\rho(y) = \exp(\gamma_1 + \gamma_2 \log D_{y,2}). \tag{8}$$

Here $D_{y,2}$ is the amount of the drugs in terms of drug 2, that is, $D_{y,2} = \rho(y)^{-1}d_1 + d_2$, which produces the same effect as the combination (d_1, d_2) under the additive assumption. Note that given one of the two, $D_{y,2}$ and y are uniquely determined, so we may suppress y to obtain the relative potency at combination dose (d_1, d_2) by solving $\rho = \exp(\gamma_1 + \gamma_2 \log D_2)$ subject to $D_2 = \rho^{-1}d_1 + d_2$.

Plummer and Short's model incorporates the varying relative potency. However, the model is inadequate to describe the phenomena when synergy and antagonism are interspersed in different regions of the drug combinations. To overcome this limitation, we propose the GRS model of the following form,

$$Y = \beta_0 + \beta_1 \log\left(d_1 + \rho d_2 + f(d_1, d_2; \gamma, \kappa)(d_1 \rho d_2)^{\frac{1}{2}}\right) \tag{9}$$

using $f(d_1, d_2; \gamma, \kappa)$ to capture local synergy, local additivity, or local antagonism. In this article we take

$$f(d_1, d_2; \gamma, \kappa) = \kappa_0 + \kappa_1 d_1^{\frac{1}{2}} + \kappa_2(\rho d_2)^{\frac{1}{2}} + \kappa_3 d_1 + \kappa_4 \rho d_2 + \kappa_5(d_1 \rho d_2)^{\frac{1}{2}}, \tag{10}$$

where f is a function of d_1 and d_2 with parameters γ's capturing the varying relative potency ρ as described above and κ's being the coefficients of the quadratic function.

Our main considerations for using the term $f(d_1, d_2; \gamma, \kappa)(d_1 \rho d_2)^{\frac{1}{2}}$ are: (i) the marginal dose–effect curves are easily obtained and are impacted as little as possible by this extra term, and (ii) the function f can have enough flexibility to capture the departure from the predicted additivity effect, $\beta_0 + \beta_1 \log(d_1 + \rho d_2)$. For the first consideration, we used the factor $(d_1 \rho d_2)^{\frac{1}{2}}$, and for the second consideration, we adopted the complete quadratic form of $d_1^{\frac{1}{2}}$ and $(\rho d_2)^{\frac{1}{2}}$ for $f(d_1, d_2; \gamma, \kappa)$. Extensive search and simulations show that the proposed model parameterization is reasonable and appropriate. One caveat is that the current parameterization may contain more parameters than necessary; therefore, model selection procedures need to be developed.

The following equations demonstrate how the GRS model captures different patterns of drug interaction: for each fixed effect level y, setting $d_2 = 0$ in (9), we obtain $D_{y,1} = \exp(\frac{y - \beta_0}{\beta_1})$; setting $d_1 = 0$, we obtain $D_{y,2} = \rho^{-1}\exp(\frac{y - \beta_0}{\beta_1})$; and the combination dose (d_1, d_2) satisfies $\exp(\frac{y - \beta_0}{\beta_1}) = d_1 + \rho d_2 + f(d_1, d_2; \gamma, \kappa)(d_1 \rho d_2)^{\frac{1}{2}}$. Dividing both sides by $\exp(\frac{y - \beta_0}{\beta_1})$ and rearranging the equality, the interaction index, $\frac{d_1}{D_{y,1}} + \frac{d_2}{D_{y,2}}$, could be written as

$$\begin{aligned}
&\text{Interaction index} \\
&= \frac{d_1}{D_{y,1}} + \frac{d_2}{D_{y,2}} = \frac{d_1}{\exp\left(\dfrac{y - \beta_0}{\beta_1}\right)} + \frac{d_2}{\rho^{-1}\exp\left(\dfrac{y - \beta_0}{\beta_1}\right)} \\
&= 1 - \frac{f(d_1, d_2; \gamma, \kappa)(d_1 \rho d_2)^{\frac{1}{2}}}{\exp\left(\dfrac{y - \beta_0}{\beta_1}\right)} \\
&= \left[1 + \frac{f(d_1, d_2; \gamma, \kappa)(d_1 \rho d_2)^{\frac{1}{2}}}{d_1 + \rho d_2}\right]^{-1}.
\end{aligned} \tag{11}$$

From (11), the polynomial function $f(d_1, d_2; \gamma, \kappa)$ being greater than, equal to, or less than 0 corresponds to the interaction index being less than, equal to, or greater than 1, and consequently, this combination is synergistic, additive, or antagonistic, respectively.

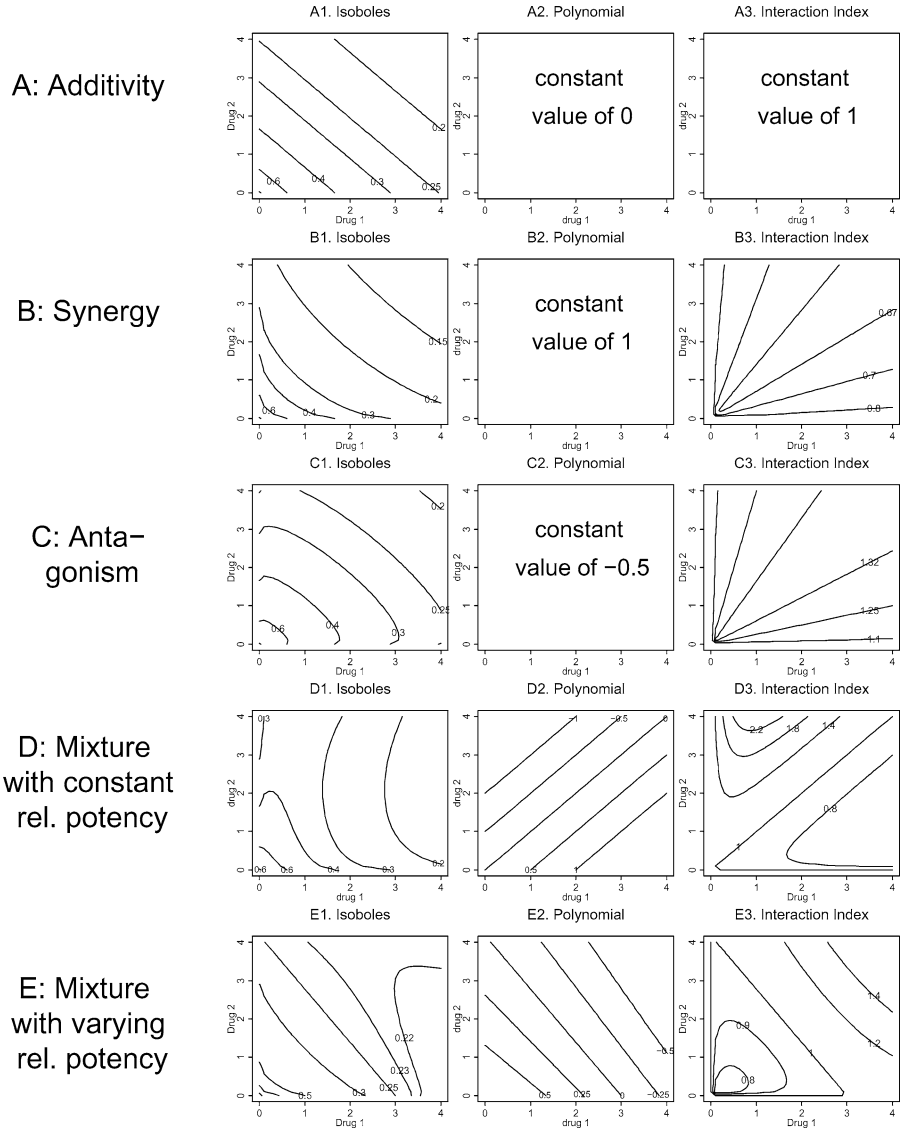

Figure 2. Contour plots of the response surfaces (i.e., isoboles), contour plots of the polynomial function $f(d_1, d_2; \gamma, \kappa)$, and contour plots of the interaction indices under different parameters. For all panels, $\beta_0 = 0$, $\beta_1 = -1$. For panels A, B, and C, $\kappa_0 = 0$, 1, and -0.5, respectively, while $\gamma_1 = \gamma_2 = 0$, $\kappa_i = 0$ for $i = 1, \ldots, 5$. Parameters in panel D are the same as in panel A except $\kappa_3 = 0.5$ and $\kappa_4 = -0.5$. In panel E we set $\gamma_1 = 0.1$, $\gamma_2 = -0.4$, $\kappa_0 = 0.9$, $\kappa_3 = \kappa_4 = -0.3$, and $\kappa_1 = \kappa_2 = \kappa_5 = 0$.

3. Relating the GRS Model to Isoboles and Interaction Indices

Recall that an isobole consists of all the drug combinations which elicit the same effect y. So, each curve in the contour plot of the response surface (9) can be viewed as an isobole. To better understand the proposed GRS model, we examine the relationship between the contour plots of the response surface, the polynomial function, and the interaction index. Chou and Talalay's (1984) median effect equation (2) is used to model the dose–effect curve for each single drug. We begin by taking the simplest case that the two dose–effect curves are the same with the slope being -1 and the median effective dose being 1, which yields $\beta_0 = \gamma_1 = \gamma_2 = 0$, $\beta_1 = -1$, and $\rho = 1$. In this special case the relative potency is constant, and the model conforms to equation (6). This model can be represented in the GRS model (9) by taking $\kappa_i = 0\,(i = 1, \ldots, 5)$ with different values of κ_0 in $f(d_1, d_2; \gamma, \kappa)$. In Figure 2, panels A, B, and C illustrate the cases for $\kappa_0 = 0$, 1, $-$ 0.5, respectively. In panel A, the contour plot of the response surface shows that the isoboles are straight lines (subpanel A1); $f(d_1, d_2; \gamma, \kappa)$ is a constant at 0 (subpanel A2); and the interaction index is a constant at 1 (subpanel A3). All three subpanels indicate that the combination doses are additive. In panel B, the contour plot of the response surface shows that the isoboles are concave down (subpanel B1); $f(d_1, d_2; \gamma, \kappa)$ is a constant at 1 (subpanel B2); and the interaction indices are less than 1 (subpanel B3). All three subpanels indicate that the combination doses are synergistic. Similarly, subpanel C1 shows that the

isoboles are concave up, subpanel C2 shows $f(d_1, d_2; \gamma, \kappa) = -0.5$, and subpanel C3 shows that the interaction indices are greater than 1, indicating that the combination doses are antagonistic. These special cases of our proposed model with $\kappa_i = 0$ $(i = 1, \ldots, 5)$ use a single parameter κ_0 to capture synergy, additivity, or antagonism and they reduce to Finney's model and Plummer and Short's model. Beyond these three special cases, the proposed model can be used more broadly, in particular when synergy and antagonism appear in different combination doses. We construct a case in panel D by setting $\kappa_0 = \kappa_1 = \kappa_2 = 0$, $\kappa_3 = 0.5$, $\kappa_4 = -0.5$, and $\kappa_5 = 0$, that is, $f(d_1, d_2; \gamma, \kappa) = 0.5d_1 - 0.5d_2$. The contour plot of the response surface is shown in subpanel D1. The contour plot of the polynomial function forms straight lines at a 45° angle (subpanel D2). The diagonal line $0.5d_1 - 0.5d_2 = 0$ separates the space into two parts. In the area below this 45° diagonal line, the polynomial is positive and the interaction index is less than 1 (subpanel D3), indicating that the combination doses in this area are synergistic. On the other hand, in the area above this 45° diagonal line, the polynomial is negative and the interaction index is greater than 1, indicating that the combination doses in this area are antagonistic. Furthermore, to show the varying relative potency, we set $\gamma_1 = 0.1$, $\gamma_2 = -0.4$ with $\kappa_0 = 0.9$, $\kappa_3 = -0.3$, and $\kappa_4 = -0.3$ (panel E). The isobole with effect level 0.25 is a straight line (subpanel E1), the corresponding polynomial is a constant at 0 (subpanel E2), and the interaction index is a constant at 1 (subpanel E3), indicating that all the combination doses on this line are additive. The isoboles with effect levels greater than 0.25 are concave down, the corresponding polynomial is positive, and the interaction index is less than 1, indicating that the combination doses in these regions are synergistic. In contrast, the isoboles with effect levels less than 0.25 are concave up, the corresponding polynomial is negative, and the interaction index is greater than 1, indicating that the combination doses in the other areas are antagonistic.

4. Statistical Consideration of the GRS Model

First we may consider whether the new model (9)-(10) provides a significant improvement of Plummer and Short's model by testing $H_0 : \kappa_1 = \kappa_2 = \kappa_3 = \kappa_4 = \kappa_5 = 0$ against $H_1 : \kappa_i \neq 0$ for any $i (i = 1, \ldots, 5)$ using the F-statistics (Gallant, 1987):

$$F = \frac{(\mathrm{RSS}_{\mathrm{P-S}} - \mathrm{RSS}_{\mathrm{full}})/q}{\mathrm{RSS}_{\mathrm{full}}/(n-p)} \tag{12}$$

with $q = 5$ and $n - p$ degrees of freedom. Here n is the number of observations and $p = 10$ is the number of parameters in model (9)-(10). $\mathrm{RSS}_{\mathrm{full}}$ is the residual sum of squares of our GRS model, and $\mathrm{RSS}_{\mathrm{P-S}}$ is the residual sum of squares of Plummer and Short's model. Rejecting H_0 suggests that Plummer and Short's model does not provide adequate fit to the data. On the other hand, failing to reject H_0 suggests that Plummer and Short's model is sufficient and there is no need to add more terms to the model. Note that the F-test requires that the responses on Y-scale are normally distributed. One should check the normality assumption, for example, applying the Q–Q plot to the residuals to examine whether the assumption is reasonable. If not, proper transformation should be sought.

The true model may include only a few terms in the GRS model (9)-(10). To avoid overparameterization, we remove the unnecessary terms by using the Akaike information criterion (AIC) (Venables and Ripley, 2002) and a backward elimination procedure. For the backward elimination procedure, a constraint is added that no lower-order terms can be removed until after the corresponding higher-order terms are removed. Here, AIC = $-2 \times$ maximized log likelihood + $2p$, which can be written as AIC = $n\log(\mathrm{RSS}/n) + 2p + C(n)$ under the normality assumption for the response Y. For a data set, the number of observations, n, remains constant, so, comparing AIC values under different parameterization is the same as comparing the sum of the first two terms, which is referred to as AIC later. To remove the unnecessary terms, we first fit the full model, calculate AIC, and then remove the parameter with the smallest absolute t-value among γ, β, and the higher-order terms of κ's in f if the parameter has a p-value greater than the level of significance α, say, $\alpha = 0.10$ (Hocking, 1976). We repeat the procedure, refit the reduced model, calculate the AIC for the reduced model, and check the t-values until either all the remaining parameters among γ, β, and the higher-order terms κ's in f have p-values smaller than α or when the AIC value increases.

As described in Section 3, the different patterns of drug interactions could be detected by observing the sign and magnitude of the polynomial function $f(d_1, d_2; \gamma, \kappa)$. Because the parameters γ and κ in the polynomial are estimated, their asymptotic properties follow the standard results from a nonlinear regression. For each combination dose (d_1, d_2), the variance of the estimated polynomial $f(d_1, d_2; \gamma, \kappa)$ can be approximated by $\widehat{\mathrm{Var}}_f = (\frac{\partial f}{\partial(\gamma,\kappa)})' \Sigma (\frac{\partial f}{\partial(\gamma,\kappa)})|_{(\gamma,\kappa)=(\hat{\gamma},\hat{\kappa})}$, where

$$\begin{aligned}\frac{\partial f}{\partial(\gamma,\kappa)} &= \left(\frac{\partial f}{\partial\gamma_1}, \frac{\partial f}{\partial\gamma_2}, \frac{\partial f}{\partial\kappa_0}, \frac{\partial f}{\partial\kappa_1}, \frac{\partial f}{\partial\kappa_2}, \frac{\partial f}{\partial\kappa_3}, \frac{\partial f}{\partial\kappa_4}, \frac{\partial f}{\partial\kappa_5}\right)' \\ &= \left(\frac{\partial f}{\partial\rho}\frac{\partial\rho}{\partial\gamma_1}, \frac{\partial f}{\partial\rho}\frac{\partial\rho}{\partial\gamma_2}, 1, d_1^{\frac{1}{2}}, (\rho d_2)^{\frac{1}{2}}, d_1, \rho d_2, (d_1\rho d_2)^{\frac{1}{2}}\right)'\end{aligned}$$

with $\frac{\partial f}{\partial\rho} = \frac{1}{2}\kappa_2(\frac{d_2}{\rho})^{\frac{1}{2}} + \kappa_4 d_2 + \frac{1}{2}\kappa_5(\frac{d_1 d_2}{\rho})^{\frac{1}{2}}$, $\frac{\partial\rho}{\partial\gamma_1} = \frac{\rho^2(d_2 + d_1\rho^{-1})}{\rho(d_2+d_1\rho^{-1})+\gamma_2 d_1}$, and $\frac{\partial\rho}{\partial\gamma_2} = \frac{\rho^2(d_2+d_1\rho^{-1})}{\rho(d_2+d_1\rho^{-1})+\gamma_2 d_1}\log(d_2 + d_1\rho^{-1})$. Σ is the estimated covariance matrix of the parameters (γ_1, γ_2, κ_0, κ_1, κ_2, κ_3, κ_4, κ_5). Thus, we may construct $(1 - \alpha) \times 100\%$ lower and upper confidence surfaces for $f(d_1, d_2; \gamma, \kappa)$:

$$f_{l,u}(d_1, d_2) = \hat{f}(d_1, d_2) \mp t_{\frac{\alpha}{2}, n-p}\sqrt{\widehat{\mathrm{Var}}_f(d_1, d_2)},$$

where $t_{\frac{\alpha}{2}, n-p}$ is the upper $\frac{\alpha}{2}$ percentile of a t-distribution with $n - p$ degrees of freedom. The intercepts of the lower and upper confidence surfaces of $f(d_1, d_2; \gamma, \kappa)$ with the dose plane form a bound which embraces the curve $f(d_1, d_2; \gamma, \kappa) = 0$. The combination doses beyond the bound with positive polynomial values are synergistic. Conversely, the combination doses beyond the other side of the bound with negative polynomial values are antagonistic. Inside the bound, the drug combinations are considered additive because the responses are not significantly different from the predicted effect based on the additive model. When the final model is a subset of the full model, a similar approach can be used to construct the confidence bound for $f(d_1, d_2, \gamma, \kappa) = 0$ in the final model.

Table 1
Simulation results from fitting the full model and the true model with $\sigma = 0.1$

	Set 1 $f(d_1, d_2; \gamma, \kappa) = 0.5d_1 - 0.5d_2$							Set 2 $f(d_1, d_2; \gamma, \kappa) = 0.9 - 0.3d_1 - 0.3\rho d_2$						
		Full model			True model				Full model			True model		
Parameters	True value	Est.	SE	CR	Est.	SE	CR	True value	Est.	SE	CR	Est.	SE	CR
β_0	0	0.002	0.044	0.950				0	0.002	0.043	0.957			
β_1	−1	−0.999	0.034	0.951	−1.000	0.020	0.954	−1.0	−0.999	0.033	0.956	−0.999	0.031	0.959
γ_1	0	0.002	0.062	0.957				0.1	0.102	0.062	0.958	0.100	0.041	0.953
γ_2	0	0.002	0.046	0.952				−0.3	−0.299	0.040	0.955	−0.299	0.038	0.952
κ_0	0	0.003	0.324	0.946				0.9	0.901	0.553	0.953	0.900	0.138	0.949
κ_1	0	−0.001	0.478	0.956				0	0.018	0.577	0.952			
κ_2	0	0.004	0.499	0.942				0	0	0.850	0.948			
κ_3	0.5	0.515	0.227	0.946	0.502	0.049	0.944	−0.3	−0.298	0.195	0.958	−0.298	0.047	0.945
κ_4	−0.5	−0.500	0.188	0.933	−0.500	0.022	0.963	−0.3	−0.293	0.366	0.958	−0.297	0.063	0.955
κ_5	0	−0.013	0.236	0.953				0	−0.017	0.312	0.950			

Est. = parameter estimate; SE = standard error; CR = coverage rate.

In medical research and its applications, the inferences should be made considering both clinical and statistical significance. Although the above inferences on synergy and antagonism are primarily based on statistical significance, the importance of clinical significance, that is, the magnitude of drug interaction to be considered clinically meaningful, should also be considered. Chou and Hayball (1996) recommended that the synergy, antagonism, and additivity at a combination dose should be made based on whether interaction index at this combination is less than 0.9, greater than 1.1, or in between. Our method provides a more rigorous way to assess statistical significance and also provides a venue for gauging the magnitude of clinical significance.

5. Simulation and Data Analysis

5.1 *Simulation*

We performed simulation studies to examine the finite-sample properties of the estimates of the proposed model. We took two sets of parameters, as shown in Figure 2, panel D (set 1) and panel E (set 2). The corresponding response surface models are

$$\text{Set 1: } Y = \log\frac{E}{1-E} = -\log\left(d_1 + d_2 + (0.5d_1 - 0.5d_2)(d_1 d_2)^{\frac{1}{2}}\right) + \epsilon$$

and

$$\text{Set 2: } Y = \log\frac{E}{1-E} = -\log\left(d_1 + \rho d_2 + (0.9 - 0.3d_1 - 0.3\rho d_2)(d_1 \rho d_2)^{\frac{1}{2}}\right) + \epsilon$$

with $\rho = \exp(0.1 - 0.3 \log D_2)$, where $\epsilon \sim N(0, \sigma^2)$. For each model we generated 1000 random samples with $\sigma = 0.1$, and d_1 and d_2 taking values among (0, 0.1, 0.5, 1, 2, 4). The sample size in each simulation run was $6 \times 6 = 36$. We fitted each random sample to the full model and then the true model (i.e., only fitting the nonzero parameters), and obtained the estimated parameters and their corresponding standard errors (SE). For each parameter, we constructed the 95% confidence interval and observed whether the true parameter lies in the confidence interval. We report the averages of the estimated parameters, SE, and the coverage rate of the confidence intervals for the 1000 random samples in Table 1. We conclude that (1) the parameters are very well estimated; (2) the coverage rates are close to the nominal 95% coverage; (3) in the full model, the standard errors of β_0, β_1, γ_1, and γ_2 are close to half of $\sigma(=0.1)$, while the SE of $\kappa_i (i = 0, \ldots, 5)$ are two- to eightfold of σ. In the true model, the standard errors for β's, γ's, and κ's are all with similar magnitude, ranging from 0.020 to 0.063 with an exception of $\hat{\kappa}_0$ in set 2 (SE = 0.138). These facts reflect that including unnecessary parameters increases the uncertainty of estimating all parameters, especially those in the quadratic function f. Therefore, it is important to develop an appropriate procedure to remove unnecessary parameters. A parsimonious model can increase the accuracy of the estimated parameters; hence, it provides a better estimator for the dose–response relationship.

We also performed simulated case studies to examine whether the estimation and the backward elimination procedure described in Section 4 can recover the true dose–response function, that is, all the zero parameters are removed, the 95% confidence bounds for $f = 0$ have proper coverage rates, and the contours of the fitted response surfaces are similar to the underlying response surface. These simulations showed that the estimation and the backward elimination procedure work well (data not shown).

5.2 *Data Analysis*

We analyzed data sets from cell lines in a study conducted by Dr. Reuben Lotan and his colleagues at M. D. Anderson Cancer Center. The study aimed to evaluate the efficacy of combination therapy with two novel agents, SCH66336 and 4-HPR, in a number of squamous cell carcinoma cell lines (unpublished data). Cell lines of human squamous cell carcinoma were treated with SCH66336 and 4-HPR separately and in combination. After 6 hours, the proportions of surviving cells were calculated. To illustrate, we present the results for the cell line UMSCC22B, after treating with SCH66336 at

Table 2
Fractions of cells surviving (UMSCC22B) *treated by single and combination doses of* SCH66336 *and* 4-HPR

SCH66336 dose (μM)	4-HPR dose (μM)				
	0	0.1	0.5	1	2
0	1	0.7666	0.5833	0.5706	0.4934
0.1	0.6701	0.6539	0.4767	0.5171	0.3923
0.5	0.6289	0.6005	0.4919	0.4625	0.3402
1	0.5577	0.5102	0.4541	0.3551	0.2851
2	0.455	0.4203	0.3441	0.3082	0.2341
4	0.3755	0.3196	0.2978	0.2502	0.1578

doses ranging from 0 to 4 μM and 4-HPR at doses ranging from 0 to 2 μM, alone and in combination, respectively. The corresponding fractions of cells surviving at each combination dose are shown in Table 2.

We analyzed these data sets using different methods. We calculated the interaction indices and their associated confidence intervals at the combination doses at the fixed ratio 1:1 by first fitting the respective dose–effect curves for SCH66336 and 4-HPR. We concluded that the combination doses (0.1, 0.1) and (0.5, 0.5) are additive, and the combination doses (1, 1) and (2, 2) are synergistic. The contour plot of the raw data is shown in Figure 3, panel A. Based on Plummer and Short's model, the combinations are synergistic ($\hat{\kappa} = 2.146$ with SE = 1.102). The contour plot, interaction indices, and residual plot of the fitted response surface of Plummer and Short's model are shown in Figure 3, panels B1, B2, and B3, respectively. The contour plot in panel B1 differs from the raw data contour plot in panel A. We fitted the data to our proposed full model, and found that the contour plot of the fitted response surface (panel C1) is more similar to the raw data contour plot. The contour plot of the polynomial function $f(d_1, d_2; \gamma, \kappa)$ is shown in panel C2, where the dotted curve is the upper boundary of the 95% confidence bound for $f(d_1, d_2; \gamma, \kappa) = 0$, and the lower boundary is below the illustrated region. The combination doses above the dotted line are synergistic. Panel C3 shows the contour plot of the interaction indices, and panel C4 shows the residual plot of the full model. We used the aforementioned backward elimination procedure with an order constraint to remove γ_2, κ_4, and β_0 sequentially, and the corresponding AIC values were -106.28, -106.39, and -106.72, respectively. The backward elimination procedure stopped when AIC increased. The results of the final model are shown in panels D1–D4. Panel D2 shows that the combination doses above the confidence bound are synergistic, inside the bound are additive, and below the bound are antagonistic. The residual plots show that the full model (panel C4) and the final model (panel D4) provide better fit for the data than Plummer and Short's model

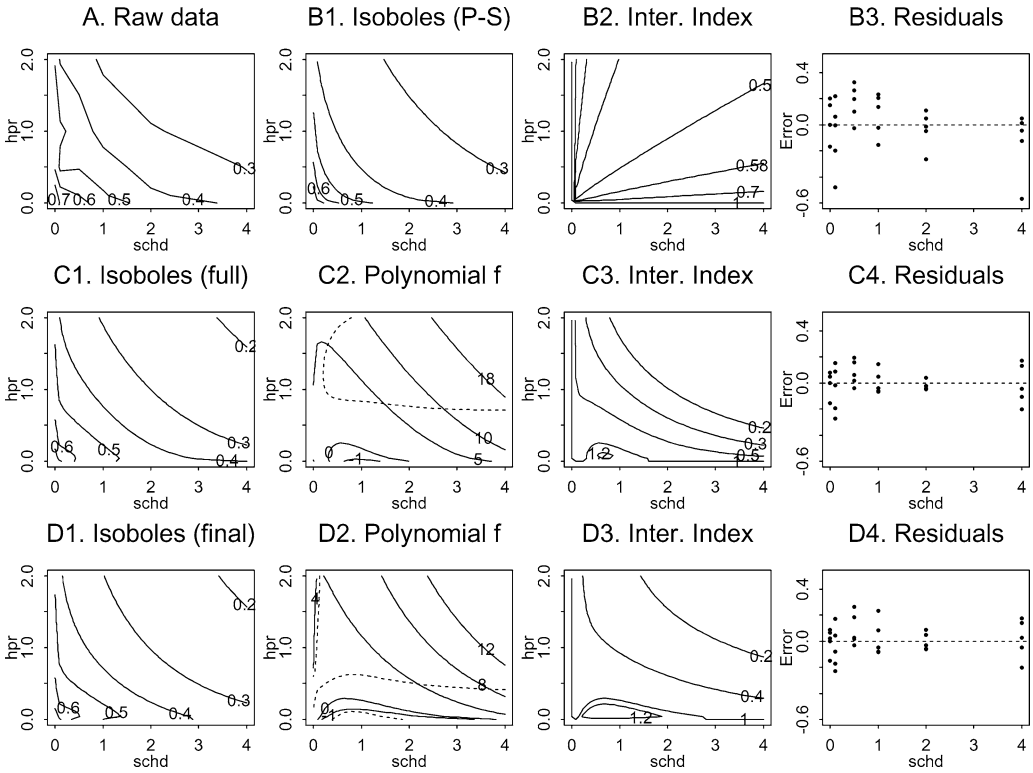

Figure 3. Results for cell line UMSCC22B: panel A is the contour plot of the raw data; panels B1–B3 show the results from Plummer and Short's model; panels C1–C4 show the results from the proposed full model; panels D1–D4 show the results from the final model. The dotted line in panel C2 is the upper boundary of the 95% confidence bound for $f(d_1, d_2; \gamma, \kappa) = 0$, and the lower boundary is out of the dose range. The two dotted lines in panel D2 are the two boundaries of a 95% confidence bound for $f(d_1, d_2; \gamma, \kappa) = 0$.

Table 3
The estimated parameters and their standard errors of different models for the data set shown in Table 2

		β_0	β_1	γ_1	γ_2	κ_0	κ_1	κ_2	κ_3	κ_4	κ_5	RSE
P-S	Est.	0.099	−0.473	−0.083	0.120	2.146						0.227
model	SE	0.093	0.062	0.292	0.259	1.102						
Full	Est.	0.088	−0.354	−0.339	0.148	5.735	−14.104	−5.539	7.114	5.283	7.021	0.143
model	SE	0.064	0.046	0.289	0.242	3.510	6.668	8.230	3.743	6.593	5.446	
Final	Est.		−0.384	−0.575		3.220	−12.368	1.195	5.492		8.250	0.143
model	SE		0.035	0.212		2.268	5.169	3.672	2.682		5.126	

P-S model = Plummer and Short's model; Est. = parameter estimate; SE = standard error; RSE = residual standard error.

(panel B3). The results from the final model are consistent with the results achieved by directly calculating the interaction indices and their associated confidence intervals.

In this example, $\mathrm{RSS}_{\mathrm{P-S}} = 1.238$, $\mathrm{RSS}_{\mathrm{full}} = 0.390$, and $n = 29$ (the model automatically assumed the fraction of cell survival being 1 at the combination dose $d_1 = d_2 = 0$ and this observation did not participate in the calculation). The Q–Q plots (not shown) indicated that the normality holds for the responses on Y-scale, therefore the F-test can be carried out. The F-statistic was 8.250 with degrees of freedom (5, 19), corresponding to $p < 0.003$. Hence, we rejected H_0 at $\alpha = 0.05$, that is, the new model (9)-(10) provides a significant improvement of Plummer and Short's model. The estimated parameters and their standard errors for Plummer and Short's model, the full model, and the final model are listed in Table 3. The residual standard error (RSE), which is an estimate of σ, is shown in the last column in Table 3 for each model. Figure 3 and Table 3 indicate that the final model fits the data as well as the full model, and the precisions on parameter estimation in the final model were improved over the full model. We conclude that the proposed model and procedure work well for this data set.

6. Discussion and Further Extension

One important contribution of this article is that the proposed model can incorporate varying relative potency. Although varying relative potency has been investigated by Tallarida (2000) and Grabovsky and Tallarida (2004), their interpretations resulted in inconsistent predicted additive effects for combination doses (Jonker et al., 2005). In the Appendix, we expound a method to correctly incorporate varying relative potency to predict the additive effect based on the Loewe additivity model. Using the proposed varying relative potency formulation, one can extend the additive response surface for k ($k \geq 2$) drug combinations as follows:

$$Y = \beta_0 + \beta_1 \log(d_1 + \rho_2 d_2 + \cdots \rho_k d_k), \tag{13}$$

where $\rho_i = \exp(\gamma_{i0} + \gamma_{i1} \log D_1)$ $(i = 2, \ldots, k)$ is the relative potency of drug i versus drug 1, and D_1 is the amount of drug 1 having an equivalent effect to that of the combination $(d_1, \ldots, d_k)$ under the additive assumption. D_1 can be obtained by solving the following equation:

$$d_1 + \rho_2 d_2 + \cdots + \rho_k d_k = D_1.$$

Here γ_{i0} and γ_{i1} are uniquely determined by the two dose–effect curves for drug 1 and drug i $(i = 2, \ldots, k)$. The additive response surface model constructed this way is consistent with the Loewe additivity model.

In this article, we assume that the effect or transformed effect has a linear relationship with $\log d$. Although a broad class of dose–effect models satisfies this assumption, there are still some exceptions. One important exception is that the logit transform of the effect has a linear relationship with the dose, say $\log \frac{E}{1-E} = \alpha_0 + \alpha_1 d$. In that case, the relative potency for the two drugs is constant, and the additive response for the two drugs can be predicted by $\log \frac{E}{1-E} = \alpha_0 + \alpha_1 d_1 + \alpha_2 d_2$ (Carter et al., 1988). One can still use a quadratic function of d_1 and d_2 to detect different patterns of drug interactions by adding the product of the quadratic function and $(d_1 d_2)^{\frac{1}{2}}$ to the above model.

Suhnel (1990) used bivariate splines to fit dose–response data. The determination of drug interaction was based on the visualization of whether the contours of the response surface (i.e., isoboles) were concave up or concave down. The approach did not give any summary measure on drug interaction. Kelly and Rice (1990) used a monotone spline-based procedure to fit marginal dose–response curves first, then predicted the additive effect of the combination dose based on the Loewe additivity model. Extrapolation beyond the observed dose range is dangerous in this spline-based approach and, therefore, this approach has limited usage. Tan et al. (2003) proposed an optimal experimental design in the sense that it reduces the variability in modeling synergy while allocating the doses to minimize the sample size and to extract maximum information on the joint action of the compounds. The method uses a nonparametric function to detect drug interactions. Semiparametric approaches, as the format (9) or the format given by Tan et al. (2003), which combine parametric marginal dose–response curves with a nonparametric function to detect different patterns of drug interaction, provide logical extension to the current model and are appropriate topics for future research.

Acknowledgements

This research was supported in part by grants from the National Cancer Institute CA16672, CA97007, and CA91844, and the Department of Defense W81XWH-04-1-0142 and W81XWH-05-2-0027. The authors are thankful to the reviewers for their constructive comments, to Dr Reuben Lotan for providing the data, and to Lee Ann Chastain for editorial assistance.

References

Berenbaum, M. C. (1989). What is synergy? *Pharmacological Reviews* **41,** 93–141.

Carter, W. H., Jr., Gennings, C., Staniswalis, J. G., Cambell, E. D., and White, K. L., Jr. (1988). A statistical approach to the construction and analysis of isobolograms. *Journal of American College Toxicology* **7,** 963–973.

Chou, T. C. and Hayball, M. (1996). *CalcuSyn for Windows: Multiple-Drug Dose-Effect Analyzer and Manual*. Cambridge, U.K.: Biosoft.

Chou, T. C. and Talalay, P. (1984). Quantitative analysis of dose-effect relationships: The combined effects of multiple drugs or enzyme inhibitors. *Advances in Enzyme Regulation* **22,** 27–55.

Finney, D. J. (1971). *Probit Analysis*. Cambridge, U.K.: Cambridge University Press.

Gallant, A. R. (1987). *Nonlinear Statistical Models*. New York: Wiley.

Govindarajulu, Z. (2001). *Statistical Techniques in Bioassay*. Basel: Karger.

Grabovsky, Y. and Tallarida, R. J. (2004). Isobolographic analysis for combinations of a full and partial agonist: Curved isoboles. *Journal of Pharmacology and Experimental Therapeutics* **310,** 981–986.

Greco, W. R., Park, H. S., and Rustum, Y. M. (1990). Application of a new approach for the quantitation of drug synergy to the combination of cis-diamminedichloroplatinum and 1-β-D-arabinofuranosylcytosine. *Cancer Research* **50,** 5318–5327.

Greco, W. R., Bravo, G., and Parsons, J. C. (1995). The search of synergy: A critical review from a response surface perspective. *Pharmacological Reviews* **47,** 331–385.

Hocking, R. R. (1976). The analysis and selection of variables in linear regression. *Biometrics* **32,** 1–49.

Jonker, D. M., Visser, S. A. G., Van der Graaf, P. H., Voskuyl, R. A., and Danhof, M. (2005). Towards a mechanism-based analysis of pharmacodynamic drug-drug interactions in vivo. *Pharmacology and Therapeutics* **106,** 1–18.

Kelly, C. and Rice, J. (1990). Monotone smoothing with application to dose-response curves and the assessment of synergism. *Biometrics* **46,** 1071–1085.

Loewe, S. and Muischnek, H. (1926). Effect of combinations: Mathematical basis of problem. *Archives of Experimental Pathology and Pharmacology* **11,** 313–326.

Plummer, J. L. and Short, T. G. (1990). Statistical modeling of the effects of drug combinations. *Journal of Pharmacological Methods* **23,** 297–309.

Savelev, S., Okello, E., Perry, N. S. L., Wilkins, R. M., and Perry, E. K. (2003). Synergistic and antagonistic interactions of anticholinesterase terpenoids in *Salvia lavandulaefolia* essential oil. *Pharmacology, Biochemistry and Behavior* **75,** 661–668.

Suhnel, J. (1990). Evaluation of synergism or antagonism for the combined action of antiviral agents. *Antiviral Research* **13,** 23–40.

Suhnel, J. (1998). Parallel dose-response curves in combination experiments. *Bulletin of Mathematical Biology* **60,** 197–213.

Tallarida, R. J. (2000). *Drug Synergy and Dose-Effect Data Analysis*. Boca Raton, Florida: Chapman Hall/CRC Press.

Tan, M., Fang, H., Tian, G., and Houghton, P. J. (2003). Experimental design and sample size determination for testing synergism in drug combination studies based on uniform measures. *Statistics in Medicine* **22,** 2091–2100.

Venables, W. N. and Ripley, B. D. (2002). *Modern Applied Statistics with S*, 4th edition. New York: Springer-Verlag.

White, D. B., Faessel, H. M., Slocum, H. K., Khinkis, L., and Greco, W. R. (2004). Nonlinear response surface and mixture experiment methodologies applied to the study of synergy. *Biometrical Journal* **46,** 56–71.

Received July 2005. *Revised February* 2006. *Accepted February* 2006.

Appendix

Varying Relative Potency and Its Application

Figure 1, panel A shows that for each fixed effect y, as long as the dose–effect curves for each drug are known, $D_{y,1}$ and $D_{y,2}$ will be known and fixed, thus the relative potency defined by $\frac{D_{y,1}}{D_{y,2}}$ is fixed. Any combination dose (d_1, d_2) on the line $\overline{PQ}$ connecting $P(=(D_{y,1}, 0))$ and $Q(=(0, D_{y,2}))$ has the same relative potency, and d_2 units of drug 2 is equivalent to $\rho(y)d_2$ units of drug 1. Therefore the combination dose (d_1, d_2) is equivalent to $d_1 + \rho(y)d_2$ units of drug 1, which is exactly $D_{y,1}$, and the predicted effect is $F_1(d_1 + \rho(y)d_2)$, which is $F_1(D_{y,1})$. Similarly, for any combination dose (d_1, d_2) on the line $\overline{PQ}, d_1$ units of drug 1 is equivalent to $\rho(y)^{-1}d_1$ units of drug 2, thus the combination dose (d_1, d_2) is equivalent to $\rho(y)^{-1}d_1 + d_2$ units of drug 2, which is $D_{y,2}$. Consequently, the predicted effect is $F_2(\rho^{-1}(y)d_1 + d_2)$, that is, $F_2(D_{y,2})$. Hence, the predicted effect either by $F_1(d_1 + \rho(y)d_2)$ or by $F_2(\rho(y)^{-1}d_1 + d_2)$ is the same.

We then pay special attention to the fact that, for a given dose d_2 of drug 2, its equivalent amount of drug 1 may be different depending on the existing amount of drug 1 due to a varying relative potency. For example, suppose from the two marginal dose–effect curves we learn that the effects of drug 1 at doses $D_{y,1}$, d_1, and $D_{y'',1}$ are the same as the effects of drug 2 at doses $D_{y,2}$, $D_{y',2}$, and d_2, respectively. When two drugs are used, the three corresponding additive isoboles (Figure 1, panel B) are $\overline{PQ}$ connecting $P = (D_{y,1}, 0)$ and $Q = (0, D_{y,2}), \overline{RS}$ connecting $R = (d_1, 0)$ and $S = (0, D_{y',2})$, and $\overline{TU}$ connecting $T = (D_{y'',1}, 0)$ and $U = (0, d_2)$. All the combinations on $\overline{PQ}$ share the relative potency $\rho(y)$, all the combinations on $\overline{RS}$ share the relative potency $\rho(y')$, and all the combinations on $\overline{TU}$ share the relative potency $\rho(y'')$. Thus, in terms of drug 1 the equivalent dose of d_2 in the combinations (d_1, d_2), (d_1', d_2), and $(0, d_2)$ will be $\rho(y)d_2$, $\rho(y')d_2$, and $\rho(y'')d_2$, which can be illustrated by the length of $\overline{RP}, \overline{VR}$, and $\overline{OT}$, respectively. Here $y = F_1(D_{y,1}) = F_2(D_{y,2})$, $y' = F_1(d_1)$, and $y'' = F_2(d_2)$. Grabovsky and Tallarida (2004) proposed a model to

incorporate the varying relative potency, but they interpret the relative potency as $\rho(y'')$ at all three combinations, namely, (d_1, d_2), (d_1', d_2), and $(0, d_2)$. Consequently, the equivalent amount of drug 1 will be the dose of drug 1 plus $\rho(y'')d_2$ no matter the dose of drug 1. Their interpretation may result in two inconsistent additive effects, say $F_1(d_1 + \rho(y'')d_2)$ and $F_2(\rho(y')^{-1}d_1 + d_2)$ (Jonker et al., 2005), and curved additive isoboles (Grabovsky and Tallarida, 2004). Therefore, their approach is questionable. On the other hand, when combinations of two drugs are additive with varying relative potency, our formulation shows straight line isoboles, which are consistent with the Loewe additivity model.

Biometrics 64, 396–405
June 2008

DOI: 10.1111/j.1541-0420.2007.00882.x

A Semiparametric Response Surface Model for Assessing Drug Interaction

Maiying Kong[1,2] and J. Jack Lee[1,*]

[1]Department of Biostatistics, University of Texas M.D. Anderson Cancer Center, Unit 447, 1515 Holcombe Boulevard, Houston, Texas 77030, U.S.A.
[2]Department of Bioinformatics and Biostatistics, University of Louisville, Louisville, Kentucky 40292, U.S.A.
[*]*email:* jjlee@mdanderson.org

Summary. When multiple drugs are administered simultaneously, investigators are often interested in assessing whether the drug combinations are synergistic, additive, or antagonistic. Existing response surface models are not adequate to capture the complex patterns of drug interactions. We propose a two-component semiparametric response surface model with a parametric function to describe the additive effect of a combination dose and a nonparametric function to capture the departure from the additive effect. The nonparametric function is estimated using the technique developed in thin plate splines, and the pointwise bootstrap confidence interval for this function is constructed. The proposed semiparametric model offers an effective way of formulating the additive effect while allowing the flexibility of modeling a departure from additivity. Example and simulations are given to illustrate that the proposed model provides an excellent estimation for different patterns of interactions between two drugs.

Key words: Additivity; Antagonism; Loewe additivity model; Synergy; Thin plate splines; Wild bootstrap.

1. Introduction

Studies of interactions among biologically active agents, such as drugs, carcinogens, or environmental pollutants, have become increasingly important in many branches of biomedical research. For example, in cancer chemotherapy the therapeutic effect of many anticancer drugs is limited when they are used as a single drug (Kanzawa et al., 1999). Finding the combination therapies with increasing treatment efficacy and reduced toxicity is an active and promising research area. In this article, we focus on assessing drug interactions for experiments performed in in vitro and/or in vivo studies to help determine whether a combination therapy should be further investigated in a clinical trial.

The literature supports the notion that the Loewe additivity model (Berenbaum, 1989; Greco, Bravo, and Parsons, 1995 and references therein; Lee et al., 2007) can be considered as the "gold standard" to define drug interactions. Based on the Loewe additivity model, the following two approaches are often used: (1) the marginal dose–effect curve model method (MDECM), or (2) the response surface method (RSM). The MDECM (Kelly and Rice, 1990) fits a dose–effect curve for each single drug, uses the fitted dose–effect curves to calculate the expected additive effect to a particular combination, and then compares the expected additive effect to the observed effect. The MDECM methods can only assess drug interactions at observed combinations, and do not give a complete picture of drug interactions over all possible combination doses. The RSM (Greco et al., 1995), which involves an estimation of the $k + 1$ dimensional response surface in k drug combinations, can take all of the information present in the full dose–effect data set for k drugs to assess drug interactions at all levels of combination doses. However, most of the RSMs either use a single parameter (e.g., Carter et al., 1988) or use a 50% maximal effect isobole (White et al., 2004) to capture synergy, additivity, or antagonism. These approaches are not adequate to capture different patterns of drug interactions.

To overcome this limitation, we recently developed a parametric response surface model with a complete quadratic function of combination doses to capture synergy, additivity, and antagonism (Kong and Lee, 2006). Similar to many other settings, these parametric models are efficient when the model assumptions hold but not necessarily robust when the assumptions fail. Therefore, our goal in the article is to develop a semiparametric model to capture complex patterns of drug interactions and provide statistical inference. Although fully nonparametric models have been explored in the literature, the accomplishment is quite limited. Suhnel (1990) used bivariate splines to fit dose effect data. The determination of drug interactions was based on the visualization of whether the contours of the response surface were concave up or concave down. Prichard and Shipman (1990) proposed using the differences of the theoretical additive surface and the experimental data surface to reveal regions of synergy and antagonism. However, the theoretical additive surface was not constructed accurately, and the assessment of drug interaction was not derived from a statistical point of view. Kelly and

Rice (1990) and Kong and Eubank (2006) proposed using B-spline to estimate a marginal dose–effect curve. However, the fitted smoothing curve cannot be extrapolated beyond the observed range of effects for each single drug. Thus, the additive effects for those combination doses beyond the range of the effects produced by each single drug cannot be modeled. To predict the additive effects for all combination doses, our idea in this article is to use parametric model to estimate dose–effect curve for single drug. Based on the reasonably chosen parametric dose–effect curve model and the Loewe additivity model, we can estimate the theoretical additive surface. Subsequently, we use a nonparametric function to describe the effect beyond the additive model. The confidence surfaces for the nonparametric function are constructed so that the local synergy or local antagonism can be estimated from the statistical point of view. This approach not only combines the idea used in the MDECM but also incorporates the advantages of the RSM. We describe our model and its estimation in Sections 2 and 3, and give a case study in Section 4 and simulations in Section 5. The last section is devoted to discussion.

2. The Proposed Model

Recall the Loewe additivity model (Berenbaum, 1989; Greco et al., 1995 and references therein)

$$\frac{d_1}{D_{y,1}} + \frac{d_2}{D_{y,2}} = 1, \tag{1}$$

where d_1, d_2 are doses of drugs 1 and 2 in the mixture, y is the theoretic additive effect at $(d_1,\ d_2)$, and $D_{y,1}$ and $D_{y,2}$ are the respective single-agent doses of drugs 1 and 2 that elicit the effect y. The theoretic additive effect y at $(d_1,\ d_2)$ can be predicted as long as the dose–effect curves for each of the two drugs are known. Denote the dose–effect curves for drugs 1 and 2 used alone as $F_1(D_1)$ and $F_2(D_2)$, respectively. Then, the predicted additive effect, say y, can be obtained by solving equation (1) after replacing $D_{y,1}$ by $F_1^{-1}(y)$ and $D_{y,2}$ by $F_2^{-1}(y)$, where F_i^{-1} is the inverse function of F_i $(i = 1, 2)$. If the effect measured at $(d_1,\ d_2)$ is more than or less than the predicted effect, the combination dose $(d_1,\ d_2)$ corresponds to synergy or antagonism. We denote the predicted effect at the combination dose $(d_1,\ d_2)$ by $F_p(d_1,\ d_2)$.

To capture different patterns of drug interaction, we propose a two-component model to describe the effect of combination treatment:

$$Y = F_p(d_1, d_2) + f(d_1, d_2). \tag{2}$$

Please note that in equation (2) and equations (3), (4), and (6) below, a mean zero random error term is suppressed from the right-hand side of the model. Here $f(d_1,\ d_2)$ is a function that is estimated nonparametrically to capture local synergy and local antagonism, that is, drug effect beyond the additive effect. To see this point, suppose the marginal dose–effect curves are decreasing, then $f(d_1,\ d_2) < 0$ implies that the effect at $(d_1,\ d_2)$ is more than the predicted effect $F_p(d_1,\ d_2)$, thus the combination dose $(d_1,\ d_2)$ is synergistic. On the other hand, $f(d_1,\ d_2) > 0$ implies that the effect at $(d_1,\ d_2)$ is less than the predicted effect, thus the combination dose $(d_1,\ d_2)$ is antagonistic. Contrarily, in the case of increasing marginal dose–effect curves, $f(d_1,\ d_2) > 0$ or $f(d_1,\ d_2) < 0$ implies that the combination dose $(d_1,\ d_2)$ is synergistic or antagonistic, respectively.

3. Estimation for the Proposed Model

From this point on we assume that the observed data are $(d_{1i},\ d_{2i},\ E_i)$ for $i = 1, \ldots, n$. Here $(d_{1i},\ d_{2i})$ $(i = 1, \ldots, n)$ is the observed combination dose, and $E_i\,(i = 1, \ldots, n)$ is the corresponding observed effect. If the data contain enough observations for each drug when used alone, then, the marginal dose–effect curves, and subsequently, predicted additive effects, may be estimated with small error. The choices of the dose–effect curves may be based on the biology-driven mechanistic models, such as the median effect model by Chou and Talalay (1984), if the model provides adequate fit. Once we obtain an appropriate dose–effect curve for each drug, the predicted effects based on the Loewe additivity model can be obtained. In the literature, two commonly used classes of marginal dose–effect curves are reported. We illustrate how to obtain the predicted effect $\hat{F}_p(d_1, d_2)$ under each class in Section 3.1. Next, we can obtain the difference of the observed effect and the predicted effect at each observed combination dose $(d_{1i},\ d_{2i})$ $(i = 1, \ldots, n)$. Based on this information, we can then estimate the function $f(d_1,\ d_2)$ using the technique described in Section 3.2. To account for the variability in estimation, the bootstrap confidence interval (CI) for $f(d_1,\ d_2)$ is given in Section 3.3.

3.1 *Estimation of the Marginal Dose–Effect Curves and the Predicted Effects*

One class of commonly used dose–effect curves is based upon a linear relationship between the effect or transformed effect and the dose or concentration. The dose–effect curves for drugs 1 and 2 have the following form:

$$\begin{aligned} Y = g(E) &= \beta_0 + \beta_1 D_{y,1} \quad \text{for drug 1, and} \\ Y = g(E) &= \beta_0 + \beta_2 D_{y,2} \quad \text{for drug 2,} \end{aligned} \tag{3}$$

where $g(E)$ is a monotonic function of E, for example, we may take $g(E) = \log \frac{E}{1-E}$ (Carter et al., 1988). The intercepts in (3) are assumed to be the same because the baseline effects without drugs (i.e., $D_{y,1} = D_{y,2} = 0$) should be the same. We refer to Y as the transformed effect. Based on the Loewe additivity model, the predicted effect in Y-scale can be obtained from $\frac{d_1}{(Y-\beta_0)/\beta_1} + \frac{d_2}{(Y-\beta_0)/\beta_2} = 1$. The resulting predicted additive response function of the combination dose is, then,

$$Y = g(E) = F_p(d_1, d_2) = \beta_0 + \beta_1 d_1 + \beta_2 d_2. \tag{4}$$

In application, we may first regress $g(E)$ on dose with the observations of each drug when used alone to see whether the fit is adequate and the intercepts of the two regression lines for the two drugs are close. If so, we may force the intercepts to be the same by regressing $g(E)$ on d_1 and d_2 using only the marginal data (i.e., the data with $d_1 = 0$ or $d_2 = 0$). Thus, we obtain the estimates of β_0, β_1, and β_2. Plugging these estimates in equation (4), we obtain the theoretic additive effect $\hat{F}_p(d_1, d_2)$ in the transformed scale for each combination

dose (d_1, d_2). The predicted additive effect in the original scale at (d_1, d_2) is obtained by the inverse transformation

$$\hat{E}_{d_1,d_2} = g^{-1}(\hat{F}_p(d_1, d_2)). \tag{5}$$

Another class of dose–effect curves is based upon a linear relationship between the effect or transformed effect and the log(dose) or log(concentration). This class is very general and includes many families (Kong and Lee, 2006). We assume that the effect or transformed effect follows a linear function of log(dose) for each of the two drugs when acting alone:

$$\begin{aligned} Y = g(E) &= \beta_0 + \beta_1 \log D_{y,1} \quad \text{for drug 1,} \quad \text{and} \\ Y = g(E) &= \alpha_0 + \alpha_1 \log D_{y,2} \quad \text{for drug 2.} \end{aligned} \tag{6}$$

Again $g(E)$ is a monotonic function of E, and Y is the transformed effect. Kong and Lee (2006) showed that, based on the Loewe additivity model, the predicted effect at combination dose (d_1, d_2) is $Y = F_p(d_1, d_2) = \beta_0 + \beta_1 \log(d_1 + \rho d_2)$, where ρ can be obtained by solving $\rho = \exp(\frac{\alpha_0 - \beta_0}{\beta_1} + \frac{\alpha_1 - \beta_1}{\beta_1} \log(\rho^{-1} d_1 + d_2))$.

3.2 *Estimation of* $f(d_1, d_2)$

In the previous section, we illustrated how to estimate the additive effect for each combination dose. Particularly, we can estimate the additive effect, $\hat{F}_p(d_{1i}, d_{2i})$, for each observed combination dose (d_{1i}, d_{2i}) ($i = 1, \ldots, n$). Then we can easily compute the difference of the observed effect and the predicted additive effect, $Y_i - \hat{F}_p(d_{1i}, d_{2i})$, at each observed combination dose (d_{1i}, d_{2i}) ($i = 1, \ldots, n$), where $Y_i = g(E_i)$. Note that $f(d_1, d_2)$ in (2) is used to capture the departure from the additive effect, which only exists for nonmarginal combination dose, that is, (d_1, d_2) with $d_1 \neq 0$ and $d_2 \neq 0$, because by definition, there is no interaction when a drug is used alone. Theoretically, $f(d_1, d_2)$ should be set as zero whenever $d_1 = 0$ or $d_2 = 0$. However, as far as we know, in the framework of bivariate splines, there are no basis functions such that their linear combination is zero at (d_1, d_2) whenever $d_1 = 0$ or $d_2 = 0$. In order to estimate $f(d_1, d_2)$ as close to zero as possible whenever $d_1 = 0$ or $d_2 = 0$, we force the differences between the observed and predicted effects at the marginal observations to be zero. Thus, we define an indicator function

$$1_{\{d_1 \neq 0 \,\&\, d_2 \neq 0\}} = \begin{cases} 1, & \text{if } d_1 \neq 0 \,\&\, d_2 \neq 0 \\ 0, & \text{Otherwise.} \end{cases}$$

Then, we can proceed to estimate the function $f(d_1, d_2)$ based on the observed doses (d_{1i}, d_{2i}) and the estimated differences $\left(Y_i - \hat{F}_p(d_{1i}, d_{2i})\right) 1_{\{d_{1i} \neq 0 \,\&\, d_{2i} \neq 0\}}$ for $i = 1, \ldots, n$.

We use thin plate splines (Green and Silverman, 1994) to represent $f(d_1, d_2)$. The thin plate splines can incorporate observations from any kind of design, such as a factorial design, ray design (Chou and Talalay, 1984), and a uniform design (Tan et al., 2003). We adopted the techniques developed in a mixed effect model (Ruppert, Wand, and Carroll, 2003) to select the smoothing parameter and to estimate the function $f(d_1, d_2)$.

The estimated function $f(d_1, d_2)$ can be obtained by minimizing the following penalized residual sum of squares (PRSS; Green and Silverman, 1994):

$$\begin{aligned} PRSS = &\sum_{i=1}^{n} ((Y_i - \hat{F}_p(d_{1i}, d_{2i})) 1_{\{d_{1i} \neq 0 \,\&\, d_{2i} \neq 0\}} - f(d_{1i}, d_{2i}))^2 \\ &+ \lambda J(f), \end{aligned} \tag{7}$$

where the first term measures the goodness of fit, the second term, $J(f)$, measures the smoothness of the function $f(d_1, d_2)$, and the smoothing parameter, λ, measures the tradeoff between the goodness of fit and the smoothness of the function f. The minimizer of PRSS is necessarily a natural thin plate spline, which can be expressed as a linear combination of the radial basis functions:

$$\begin{aligned} f(d_1, d_2) = &\gamma_0 + \gamma_1 d_1 + \gamma_2 d_2 \\ &+ \sum_{k=1}^{K} v_k \eta\left(||(d_1, d_2)^T - (\kappa_{1k}, \kappa_{2k})^T||\right), \end{aligned} \tag{8}$$

where the radial basis function

$$\begin{aligned} \eta(r) &= \frac{1}{16\pi} r^2 \log r^2 \quad \text{for } r > 0, \\ &= 0 \qquad\qquad\quad \text{for } r = 0. \end{aligned} \tag{9}$$

The knots, say, $(\kappa_{1k}, \kappa_{2k})^T$ ($k = 1, \ldots, K$), are all the distinct values among $(d_{1i}, d_{2i})^T$ ($i = 1, \ldots, n$), and the distance between two combination doses is defined as the Euclidean distance:

$$||(d_1, d_2)^T - (\kappa_{1k}, \kappa_{2k})^T|| = \sqrt{(d_1 - \kappa_{1k})^2 + (d_2 - \kappa_{2k})^2}.$$

If we define a $K \times K$ matrix $\Omega = [\eta(||(\kappa_{1k}, \kappa_{2k})^T] - (\kappa_{1k'}, \kappa_{2k'})^T||)_{1 \leq k, k' \leq K}]$, a $K \times 3$ matrix $T^T = [1, \kappa_{1k}, \kappa_{2k}]_{1 \leq k \leq K}$, and a vector $v = (v_1, \ldots, v_K)^T$, then the minimizer of (7) satisfies $J(f) = v^T \Omega v$ and $Tv = 0$. Let us denote

$$\begin{aligned} Y_R = \big[&(Y_1 - \hat{F}_p(d_{11}, d_{21})) 1_{\{d_{11} \neq 0 \,\&\, d_{21} \neq 0\}}, \ldots, \\ &(Y_n - \hat{F}_p(d_{1n}, d_{2n})) 1_{\{d_{1n} \neq 0 \,\&\, d_{2n} \neq 0\}}\big]^T, \end{aligned}$$

$$X = [1, d_{1i}, d_{2i}]_{1 \leq i \leq n} \in R^{n \times 3},$$

$$Z_1 = \left[\eta\left(||(d_{1i}, d_{2i})^T - (\kappa_{1k}, \kappa_{2k})^T||\right)_{1 \leq k \leq K}\right]_{1 \leq i \leq n} \in R^{n \times K},$$

and

$$\gamma = (\gamma_0, \gamma_1, \gamma_2)^T.$$

Consider a QR decomposition of T^T, say, $T^T = FG$, where F is an $K \times K$ orthogonal matrix and G is $K \times 3$ upper triangular. Let F_1 be the first three columns and F_2 be the remaining $K - 3$ columns of F, respectively. Following the argument in Green and Silverman (1994, p. 166), we can show that $Tv = 0$ if and only if v can be expressed as $F_2 \xi$, where ξ is a $K - 3$ vector. Thus the minimizer of (7) is essentially equivalent to minimizing

$$\begin{aligned} &(Y_R - X\gamma - Z_1 F_2 \xi)^T (Y_R - X\gamma - Z_1 F_2 \xi) \\ &\quad + \lambda \xi^T F_2^T \Omega F_2 \xi. \end{aligned} \tag{10}$$

Set $u = (F_2^T \Omega F_2)^{\frac{1}{2}} \xi$, where $(F_2^T \Omega F_2)^{\frac{1}{2}}$ is the matrix square root of $F_2^T \Omega F_2$ (Ruppert et al., 2003, p. 329). Thus minimizing (10) is equivalent to minimizing

$$(Y_R - X\gamma - Zu)^T (Y_R - X\gamma - Zu) + \lambda u^T u, \qquad (11)$$

where $Z = Z_1 F_2 (F_2^T \Omega F_2)^{-\frac{1}{2}}$. Expression (11) is proportional to the negative exponential part of the joint distribution of Y_R and u under the following model assumption:

$$\begin{aligned} Y_R &= X\gamma + Zu + \epsilon \qquad \text{with} \\ \begin{pmatrix} u \\ \epsilon \end{pmatrix} &\sim N\left(\begin{pmatrix} 0 \\ 0 \end{pmatrix}, \begin{pmatrix} \sigma_u^2 I_{K-3} & 0 \\ 0 & \sigma_\epsilon^2 I_n \end{pmatrix} \right), \end{aligned} \qquad (12)$$

where λ is replaced by $\sigma_\epsilon^2/\sigma_u^2$. The solution of minimizing (11) is the same as the best linear unbiased predictor (BLUP) for γ and u in the mixed model (12). This solution can be written as

$$\begin{pmatrix} \tilde{\gamma} \\ \tilde{u} \end{pmatrix} = \text{BLUP} \begin{pmatrix} \gamma \\ u \end{pmatrix} = (C^T C + \lambda D)^{-1} C^T Y_R, \qquad (13)$$

with $C = [X \;\; Z]$ and $D = \text{diag}\,(0, 0, 0, 1, \ldots, 1)$, where the number of zeros in the matrix D corresponds to the number of γ_i's ($i = 0, 1, 2$), and the number of ones corresponds to the number of u_i's ($i = 1, \ldots, K-3$).

For any combination dose (d_1, d_2), if we denote $f(d_1, d_2) = \gamma_0 + \gamma_1 d_1 + \gamma_2 d_2 + Z_0 u$ with $Z_0 = [\eta(||(d_1, d_2)^T - (\kappa_{1k}, \kappa_{2k})^T||)]_{1 \le k \le K} F_2 (F_2^T \Omega F_2)^{-\frac{1}{2}}$, then $\hat{f}(d_1, d_2) = \tilde{\gamma}_0 + \tilde{\gamma}_1 d_1 + \tilde{\gamma}_2 d_2 + Z_0 \tilde{u}$ is the BLUP for $f(d_1, d_2)$. Usually σ_ϵ^2 and σ_u^2 are unknown, and consequently, $\lambda = \sigma_\epsilon^2/\sigma_u^2$ is unknown, therefore, $\tilde{\gamma}$ and $\tilde{u}$ are unknown. Let $\hat{\sigma}_\epsilon^2$ and $\hat{\sigma}_u^2$ be the restricted maximum likelihood estimators (REML) of σ_ϵ^2 and σ_u^2 in the mixed model (12). Replacing λ by $\hat{\lambda} = \hat{\sigma}_\epsilon^2/\hat{\sigma}_u^2$ in (13), we can obtain the estimated BLUP for γ and u, say $\hat{\gamma}$ and $\hat{u}$. Thus the estimated BLUP for $f(d_1, d_2)$ is $\hat{f}(d_1, d_2) = \hat{\gamma}_0 + \hat{\gamma}_1 d_1 + \hat{\gamma}_2 d_2 + Z_0 \hat{u}$. Especially, the fitted value $\hat{f}(d_{1i}, d_{2i})$ $(i = 1, \ldots, n))$ is the ith component of $C(C^T C + \hat{\lambda} D)^{-1} C^T Y_R$.

To assess drug interactions from the statistical point of view, we need to examine the variability of $\hat{f}(d_1, d_2)$. To our knowledge, it is rather difficult to derive a theoretic formula for the variance of the estimated function $f(d_1, d_2)$ in the framework of two-stage estimation. Therefore, we use the bootstrap method (Davison and Hinkley, 1997; Liang, Hardle, and Sommerfeld, 2000) to estimate the variance of $f(d_1, d_2)$, and then construct the corresponding confidence interval for $f(d_1, d_2)$ accordingly.

3.3 *Estimate the Variance of $f(d_1, d_2)$ Using Bootstrap Method*

Under the semiparametric framework, Liang et al. (2000) presented a bootstrap approximation for a partially linear regression model. However, in our setting, the standard errors of the residuals from estimating dose–effect curves and from estimating the function $f(d_1, d_2)$ may be quite different. Hence, a wild bootstrap method (Davison and Hinkley, 1997), which can account for the different error structures, would be more appropriate. Instead of simply resampling the residuals, the wild bootstrap uses the product of each residual and a random number that has mean zero and standard deviation 1; thus the different error structures can be maintained (Hardle and Marron, 1991, and references therein). In addition, we adopted the recommendation by Davison and Hinkley (1997, Section 7.6) to reduce the biases in estimating the standard error for $\hat{f}(d_1, d_2)$. We summarize the procedure as following:

Step 1. Fit the model based on the original observations, obtain $\hat{f}(d_{1i}, d_{2i})$ and $\hat{\lambda}$, where $\hat{f}(d_{1i}, d_{2i})$ is the ith components of $C(C^T C + \hat{\lambda} D)^{-1} C^T Y_R$.

Step 2. Obtain the residuals from the undersmoothed estimation of $f(d_1, d_2)$, that is, $\hat{\epsilon}_i = Y_i - \hat{F}_p(d_{1i}, d_{2i}) - \hat{f}_{0.5\hat{\lambda}}(d_{1i}, d_{2i})$. Here $\hat{f}_{0.5\hat{\lambda}}(d_{1i}, d_{2i})$ is the ith component of $C(C^T C + 0.5\hat{\lambda} D)^{-1} C^T Y_R$.

Step 3. Generate n i.i.d. (independent and identically distributed) random variables $\epsilon_1^*, \ldots, \epsilon_n^*$ with mean 0 and variance 1, for example, $\epsilon_i^* = -\frac{\sqrt{5}-1}{2}$ with probability $\frac{\sqrt{5}+1}{2\sqrt{5}}$ and $\epsilon_i^* = \frac{\sqrt{5}+1}{2}$ with probability $\frac{\sqrt{5}-1}{2\sqrt{5}}$ (Hardle and Marron, 1991).

Step 4. Obtain the fitted value from the oversmoothed estimation of $f(d_1, d_2)$, say, $Y_i^* = \hat{F}_p(d_{1i}, d_{2i}) + \hat{f}_{2\hat{\lambda}}(d_{1i}, d_{2i}) + \hat{\epsilon}_i \epsilon_i^*$ for $i = 1, \ldots, n$. Here $\hat{f}_{2\hat{\lambda}}(d_{1i}, d_{2i})$ is the ith component of $C(C^T C + 2\hat{\lambda} D)^{-1} C^T Y_R$.

Step 5. Fit the model using the generated data (d_{1i}, d_{2i}, Y_i^*) $(i = 1, \ldots, n)$, and then obtain the estimated function $f^*(d_1, d_2)$.

Step 6. Repeat step 2 to step 5 B (say, 50) times.

If we denote the estimated $f(d_1, d_2)$ in the bth $(b = 1, \ldots, B)$ iteration as $f^{*b}(d_1, d_2)$, the standard deviation for $f(d_1, d_2)$ will be estimated by

$$\widehat{SD}^{*B}(\hat{f}(d_1, d_2)) = \left(\frac{1}{B} \sum_{b=1}^{B} \left(f^{*b}(d_1, d_2) - \hat{f}(d_1, d_2) \right)^2 \right)^{\frac{1}{2}},$$

thus a $100(1-\alpha)\%$ pointwise confidence interval for $f(d_1, d_2)$ can be constructed as

$$\begin{aligned} \big[\hat{f}(d_1, d_2) - z_{\frac{\alpha}{2}} \times \widehat{SD}^{*B}(\hat{f}(d_1, d_2)), \hat{f}(d_1, d_2) + z_{\frac{\alpha}{2}} \\ \times \widehat{SD}^{*B}(\hat{f}(d_1, d_2)) \big], \end{aligned} \qquad (14)$$

where $z_{\frac{\alpha}{2}}$ is the upper $\frac{\alpha}{2} \times 100\%$ percentile of the standard normal distribution, and $\hat{f}(d_1, d_2)$ is the estimated BLUP for $f(d_1, d_2)$ in Section 3.2. Our case study in Section 4 showed that the estimated variance for $f(d_1, d_2)$ can account for the carry-over errors from estimating the marginal dose–effect curves. Our simulations given in Section 5 showed that the proposed bootstrap CIs have good coverage properties.

4. Case Study

Table 1 shows the fractions of surviving cells after cancer cells from cell line UMSCC22B were treated with SCH66336, a farnesyl transferase inhibitor, and 4-HPR, a retinoid, alone and in combinations (data were provided by Dr Reuben Lotan at M.D. Anderson Cancer Center). Both agents have a role in producing apoptosis. The objective was to study the efficacy and quantify the drug interaction when the two agents were used in combination. The experiment was conducted in six trays as shown in Table 1. The cells were untreated (control group), or were treated with single-drug doses or combination

Table 1
Observed fractions of surviving cells from cell line UMSCC22B after treatment with SCH66336 and 4-HPR

Tray	(0, 0)		(0.1, 0)		(0.5, 0)		(1.0, 0)		(2.0, 0)		(4.0, 0)	
1	0.422	0.498	0.328	0.345	0.383	0.306	0.255	0.303	0.202	0.235	0.163	0.205
	0.473	0.453	0.335	0.336	0.282	0.329	0.297	0.228	0.258	0.229	0.213	0.196
	0.491	0.623	0.307	0.346	0.297	0.277	0.296	0.283	0.223	0.209	0.180	0.162
Tray	(0, 0)		(0.1, 0.1)		(0.5, 0.1)		(1.0, 0.1)		(2.0, 0.1)		(4.0, 0.1)	
2	0.456	0.513	0.317	0.312	0.303	0.236	0.256	0.212	0.163	0.233	0.133	0.168
	0.479	0.458	0.322	0.310	0.234	0.307	0.255	0.213	0.226	0.178	0.121	0.166
	0.456	0.429	0.255	0.309	0.262	0.334	0.252	0.236	0.202	0.171	0.149	0.155
Tray	(0, 0)		(0.1, 0.5)		(0.5, 0.5)		(1.0, 0.5)		(2.0, 0.5)		(4.0, 0.5)	
3	0.33	0.335	0.187	0.176	0.185	0.175	0.163	0.158	0.133	0.116	0.083	0.108
	0.392	0.36	0.176	0.216	0.182	0.221	0.143	0.205	0.151	0.145	0.123	0.108
	0.439	0.448	0.168	0.185	0.186	0.194	0.174	0.212	0.134	0.121	0.152	0.118
Tray	(0, 0)		(0.1, 1.0)		(0.5, 1.0)		(1.0, 1.0)		(2.0, 1.0)		(4.0, 1.0)	
4	0.358	0.382	0.215	0.215	0.176	0.186	0.145	0.176	0.148	0.108	0.130	0.093
	0.361	0.447	0.162	0.222	0.159	0.181	0.107	0.125	0.165	0.07	0.089	0.100
	0.431	0.367	0.187	0.212	0.187	0.196	0.134	0.146	0.112	0.120	0.068	0.107
Tray	(0, 0)		(0.1, 2.0)		(0.5, 2.0)		(1.0, 2.0)		(2.0, 2.0)		(4.0, 2.0)	
5	0.380	0.386	0.173	0.165	0.165	0.135	0.157	0.113	0.073	0.115	0.066	0.067
	0.417	0.409	0.157	0.153	0.140	0.133	0.116	0.114	0.087	0.103	0.051	0.071
	0.393	0.411	0.136	0.156	0.127	0.115	0.097	0.086	0.098	0.085	0.075	0.048
Tray	(0, 0)		(0, 0.1)		(0, 0.5)		(0, 1.0)		(0, 2.0)			
6	0.558	0.573	0.515	0.509	0.347	0.396	0.371	0.422	0.332	0.292		
	0.638	0.619	0.397	0.372	0.407	0.348	0.368	0.209	0.281	0.328		
	0.569	0.655	0.402	0.574	0.306	0.303	0.338	0.353	0.276	0.273		

doses. The fraction of surviving cells was recorded. We fitted the marginal data to model (6) by taking $g(E) = \log \frac{E}{E_{\max} - E}$ with $E_{\max}$ as the mean of the control group (solid curves in Figure 1, panels A and B), and the model (3) with $g(E) = \log \frac{E}{1-E}$ (dashed curves in Figure 1, panels A and B). In these two panels, the observed data are shown as "+" for SCH66336 and "×" for 4-HPR, respectively. From the two panels, it is clear that model (6) fits the data better. Therefore, we choose model (6) as the marginal dose–effect curve. Taking $E_{\max}$ as the mean of the control group, fitting model (6) with $g(E) = \log \frac{E}{E_{max} - E}$ is equivalent to fitting this model with $g(E) = \log \frac{E}{1-E}$ and effect as the surviving cell fraction divided by the mean of the control. In the following data analysis, the effects will be taken as the observed fractions of surviving cells divided by the mean of the corresponding control group in each tray (c.f., Kanzawa et al. [1999] for a similar procedure). Based on the processed data, we obtained the two marginal dose–effect curves: $Y = \log \frac{E}{1-E} = 0.0973 - 0.3373 \log D_{y,1}$ for SCH66336 with a residual error of 0.2684 (i.e., $\hat{\sigma} = 0.2684$), and $Y = \log \frac{E}{1-E} = 0.2303 - 0.4672 \log D_{y,2}$ for 4-HPR with a residual error of 0.5618. Then, we can obtain the predicted effect in the E-scale using the inverse transformation (5; panel E). The differences between the observed effects and predicted effects in logit scale versus SCH66336 doses, 4-HPR doses, and the observed effects (in logit scale) are plotted in panels C, D, and F, respectively. Here the circles correspond to the nonmarginal data. Panels C and D show that the differences for the lower combination doses are roughly centered around zero, indicating additivity of the associated combination doses, and the differences for the median to large combination doses are less than zero, indicating synergy of the associated combination doses. The results indicate that the additive model is not adequate to explain the observed data.

Now, we proceed to estimate $f(d_1, d_2)$. The estimated residual error $\hat{\sigma}_\epsilon = 0.217$ and the estimated smoothing parameter $\hat{\lambda} = 0.1326$. The final residuals (i.e., $Y_i - \hat{F}_p(d_{1i}, d_{2i}) - \hat{f}(d_{1i}, d_{2i})$ for $i = 1, \ldots, n$) versus the observed effects (i.e., Y_i for $i = 1, \ldots, n$) are plotted in panel G, which indicates that the fit has improved compared to panel F under the additive model. The contour plot of the estimated $f(d_1, d_2)$ is shown in panel H. The 95% pointwise confidence surfaces for $f(d_1, d_2)$ are constructed based on the bootstrap method (14). The 95% confidence bound for $f(d_1, d_2) = 0$ can be formed by taking the intersection lines of the upper and lower confidence surfaces with the dose plane. The dashed line in panel H is the intersection line of the upper confidence surface based on the bootstrap confidence interval (14) with the dose plane. From panel H, we conclude that the combination doses above the dashed line are synergistic (i.e., $f(d_1, d_2) < 0$), and the combination doses below the dashed line are additive (i.e., $f(d_1, d_2)$ is not significantly different from zero). To show the contour plot of the fitted response surface in the original effect scale, we add $f(d_1, d_2)$ to the predicted effect surface, and then use the inverse transformation (5) to obtain the fitted response surface on the original scale (panel I). The contour plot in panel I based on the model is similar to the contour

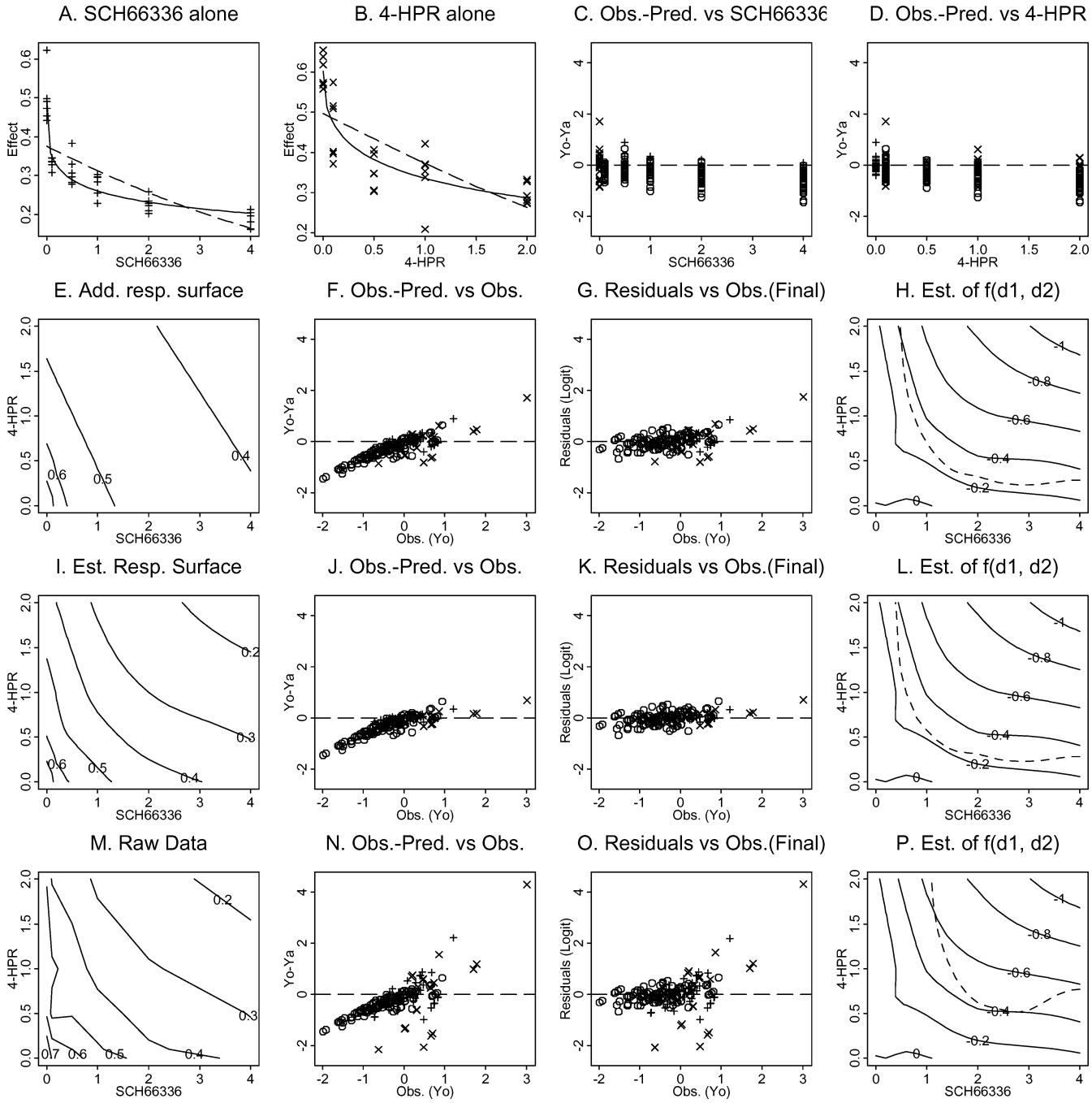

Figure 1. The results from analyzing the data set derived from cell line UMSCC22B treated with SCH66336 and 4-HPR. Panels A and B show the fitted dose–effect curves for SCH66336 and 4-HPR, respectively. The solid lines are based on model (6) whereas the dashed lines are based on model (3). Panels C, D, and F are the plots of the differences between the observed and the predicted effects in logit scale versus the SCH66336 doses, the 4-HPR doses, and the observed effects, respectively. Panel E is the contour plot of the predicted additive surface. Panel G is the plot of the final residuals versus the observed effects. Panel H is the contour plot of the estimated $f(d_1, d_2)$ along with the intersection line of its upper 95% bootstrap confidence surface based on (14) with the dose plane shown in the dashed line. Panel I is the contour plot of the estimated response surface based on the semiparametric model. Panel M is the contour plot of the raw data. Panels J, K, and L are results parallel to panels F, G, and H but in the case of the decreased marginal residuals (0.4 times of the original residuals), whereas panels N, O, and P are the parallel results in the case of the increased marginal residuals (2.5 times of the original residuals).

plot of the raw data in panel M, which indicates that the fit is reasonable.

Further, in order to examine whether the proposed bootstrap procedure can account for the errors from estimating the marginal dose–effect curves, we performed additional analysis for our case study by keeping the fitted marginal dose–effect curves the same as above, while perturbing the residuals of the marginal observations. In the first case, we changed the marginal observations (fractions of cell survival using one agent alone) to yield the same estimated marginal dose–effect curves but with smaller residuals (0.4 times of the original residuals). The data for the combination doses remained unchanged. Under this new setting, we estimated the predicted effects, and plotted the differences of observed effects and predicted effects versus observed effect, in logit scale (panel J). Then we estimated the function $f(d_1, d_2)$, panel K shows the final residual plot, and panel L shows the contour plot of the estimated $f(d_1, d_2)$ along with its 95% confidence bound for $f(d_1, d_2) = 0$ based on the bootstrap method (14) in dashed line. To compare, in the second case, we increased the residuals by 2.5-fold from estimating marginal dose–effect curves. Panels N, O, and P are the parallel results as panels J, K, and L, respectively. Comparing the dashed lines in panels H, L, and P, it is clear that even when the estimated marginal dose–effect curves are all the same, the larger the estimated errors from estimating the marginal dose–effect curves, the wider the confidence bound is. Note that because the marginal dose–effect curves and the effects of combination doses in the two new settings are the same as the original case study, the predicted additive effect surfaces as well as the estimated $f(d_1, d_2)$ would remain the same. However, the bootstrap confidence bounds would account for the errors from estimating the marginal dose–effect curves. In the next section, we illustrate that the confidence interval based on the bootstrap method has a coverage rate that is close to the nominal coverage rate 95%.

5. Simulation Studies

We use simulations to examine whether the estimation of the function f in our semiparametric model is accurate, and whether the semiparametric model can detect different patterns of drug interactions successfully.

To examine whether or not the function $f(d_1, d_2)$ can be estimated accurately, we generated data based on the marginal dose–effect curves estimated in the previous studied case, but take

$$f(d_1, d_2) = -0.2 * (d_1 d_2)^{\frac{1}{4}} \left(d_2 - 1.5d_1^2 + 4.5d_1 - 2.125\right), \quad (15)$$

shown in Figure 2, panel A. The construction of $f(d_1, d_2)$ mimics the scenario that there are different patterns of drug interactions within the same data. Note that the shape of $f(d_1, d_2)$ chosen in the simulation studies here is quite different from the case study presented in Section 4. We generated the marginal data by adding the white noise from $N(0, \sigma_1^2)$ to the "true" effect on the logit scale. Similarly, we generated the nonmarginal data by adding the white noise from $N(0, \sigma_2^2)$ to the sum of the additive effect and $f(d_1, d_2)$, where the additive response surface is constructed based on the underlying marginal dose–effect curves. We took the same settings as those in the studied case in Section 4 except that we added one more dose level for drug 1 at $d_1 = 3$. Including dose 0, there were seven levels for drug 1 and five levels for drug 2. The sample size for each sample is $7 \times 5 = 35$, which includes $6 \times 4 = 24$ combination doses. For each dose or combination dose, we generated six replicates as were done in the experiment except for $d_1 = d_2 = 0$, the fraction of cell survival is set to 1. We took $\sigma_1 = 0.3$, which lies between the estimated residual errors for SCH66336 and 4-HPR, and $\sigma_2 = 0.217$, which is the estimated residual error for f. We generated 20 samples, estimated $f(d_1, d_2)$, and plotted the $\hat{f}(d_1, d_2)$ at each unique d_2 level (Figure 2, panel B1 through panel B5). In each panel, the solid line is the underlying $f(d_1, d_2)$ by varying d_1, and the dotted lines are the estimated curves for each of the 20 samples. In addition, for a particular sample, we estimated $f(d_1, d_2)$ and constructed its bootstrap confidence interval based on (14). Figure 2, panel C3 through panel C5 show the underlying $f(d_1, d_2)$ (solid line), the estimated $f(d_1, d_2)$ (dotted line), and their 95% pointwise bootstrap confidence bound based on (14) with $B = 50$ (dashed lines) for this particular sample. It is evident that the fitted curves are close to the underlying curves, and the bootstrap confidence interval (14) performs well.

To further examine the performance of the bootstrap confidence interval (14), and also to examine whether the semiparametric method can detect different patterns of drug interactions, we generated data from the same scenario as above with $f(d_1, d_2)$ shown in (15) and ran 150 simulated samples. For each sample, we estimated the marginal dose–effect curves, estimated the predicted additive effects and the function $f(d_1, d_2)$ at (d_{1i}, d_{2i}) for $i = 1, \ldots, n$, and constructed the 95% bootstrap confidence interval based on (14) with $B = 50$. For each sample, we recorded (a) the estimated function $\hat{f}(d_{1i}, d_{2i})$ and the squared difference $\hat{f}(d_{1i}, d_{2i}) - f(d_{1i}, d_{2i})(i = 1, \ldots, n)$, (b) whether $f(d_{1i}, d_{2i})$ lies inside its associated confidence interval (14), (c) whether the associated bootstrap confidence interval (CI) contained zero (additivity), the lower limit of the associated bootstrap CI was greater than zero (antagonism), or the upper limit of the bootstrap CI was less than zero (synergy). Table 2 shows the combination dose (d_1, d_2), the underlying function $f(d_1, d_2)$, and the averages of the above quantities over the simulated samples, which include (a) the average of the 150 estimated $f(d_1, d_2)$ (denoted as f.ave); the mean squared error (denoted as f.mse), and the estimated variance based on the simulated samples (denoted as f.var), (b) the percentage of counts of the underlying value lying inside the bootstrap confidence interval (14; denoted as cr.bci); (c) the percentage of counts of the lower limit being greater than zero (denoted as p.ant), the confidence interval containing zero (denoted as p.add), and the upper limit being less than zero (denoted as p.syn), indicating predicted antagonism, additivity, and synergy, respectively. From Table 2, we conclude that (i) overall, the averages of the estimated function $f(d_1, d_2)$ are close to the underlying function values, and the mean square errors are similar to the variance estimates except that at the combination dose (4.0, 0.1) the mean square error is much bigger, indicating bias of the estimation; (ii) the coverage rates based on the bootstrap method (cr.bci) are close to the nominal coverage rate of 95%; (iii) when $f(d_1, d_2) > 0$, the larger the $f(d_1, d_2)$ is, the higher the percentage (p.ant) of the lower limit of the bootstrap confidence interval (14) being greater than 0, indicating the correct assessment of drug

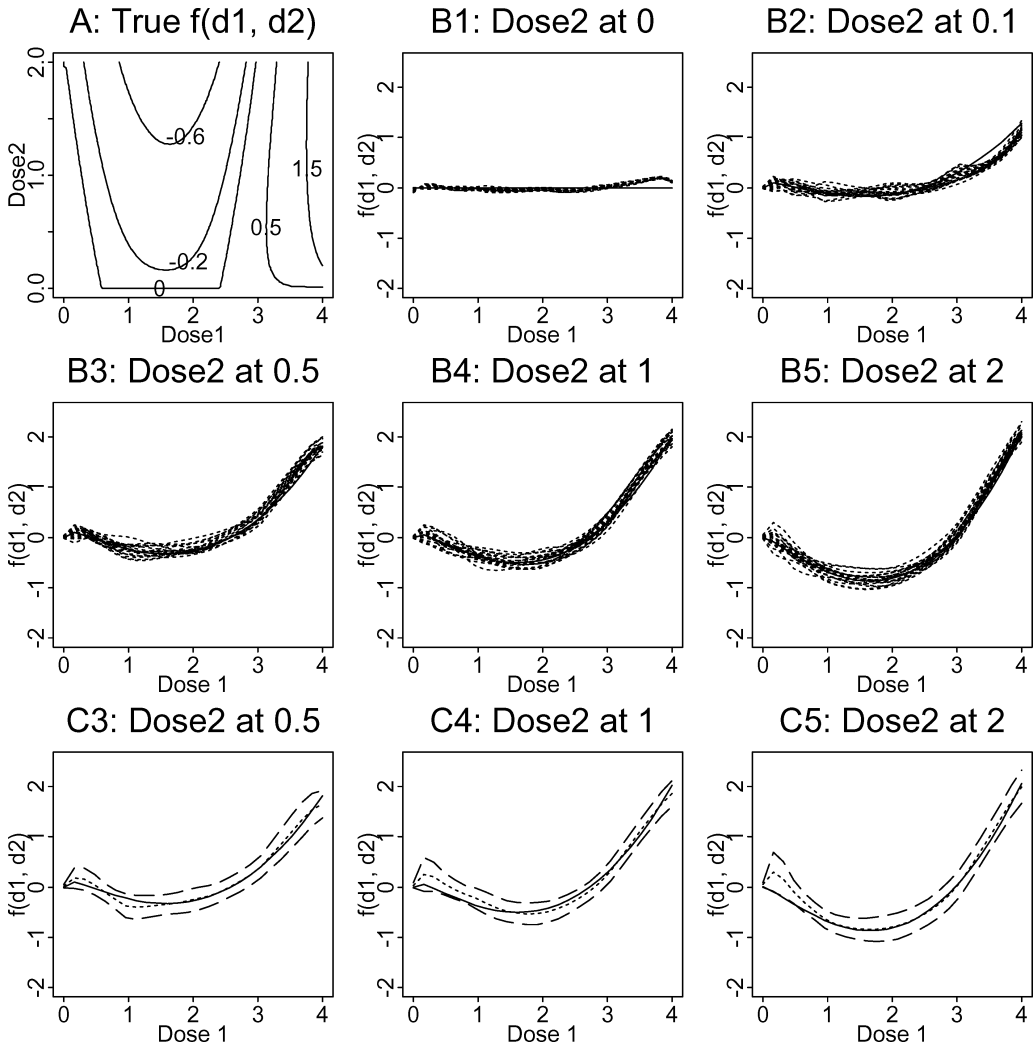

Figure 2. The results from simulation studies presented in Section 5. Panel A shows the contour plot of the underlying true function $f(d_1, d_2)$. Each panel of panels B1–B5 shows the underlying curve (solid lines) and the fitted curves (dotted lines) based on a sample of 35 doses with six replicates for each dose level and 20 simulation runs under the setting $\sigma_1 = 0.3$ and $\sigma_2 = 0.217$. Each panel of panels C3–C5 shows the underlying curve (solid lines), the fitted curve (dotted line), and the 95% pointwise bootstrap confidence bound (dashed lines) for a particular sample.

interaction as antagonism at (d_1, d_2); (iv) when $f(d_1, d_2) < 0$, the larger the absolute value of $f(d_1, d_2)$ is, the higher the percentage (p.syn) of the upper limit being less than 0, indicating the correct assessment of drug interaction as synergy at (d_1, d_2); (v) when $f(d_1, d_2)$ is close to zero, the percentage of the CIs containing zero (p.add) is close to 95%, indicating the correct assessment of drug interaction as additivity at (d_1, d_2). These facts illustrated that both the estimation for the model and the constructed bootstrap CIs perform well.

6. Discussion

The case study in Section 4 and the simulations in Section 5 indicate that our proposed method can be used to successfully assess drug interaction even when different patterns of drug interactions exist within the same data. In addition, the fitted dose–response surface $\hat{F}_p(d_1, d_2) + \hat{f}(d_1, d_2)$ gives an overall picture of the dose–effect relationship, which can help us to identify the optimal combination therapy.

In our two-stage procedure, because both the errors from estimating the dose–effect curves and the errors for measuring the effects at combination doses impact the precision of the estimated $f(d_1, d_2)$, in the case that the errors are large, further efforts, such as better control of experimental conditions and increasing the number of replicates will be required to improve the assessment of drug interaction. As in any data analysis, model fitting needs to be examined carefully, for example, by plotting residuals and predicted values versus observed values, etc. Sensitivity analysis can be done by removing or down weighing suspected outliers. Statistical inference should be made in conjunction with meaningful biological evidence and knowledge.

In the semiparametric model, we use a function f to capture the patterns of drug interactions. The estimated

Table 2
Simulation results for evaluating mixed pattern of drug interaction with 24 *combination doses and* 150 *runs under the setting* $\sigma_1 = 0.3$ *and* $\sigma_2 = 0.217$

(d_1, d_2)	$f(d_1, d_2)$	f.ave	f.mse	f.var	cr.bci	p.ant	p.add	p.syn
(0.1, 0.1)	0.101	0.080	0.0074	0.0070	0.97	5	95	0
(0.1, 0.5)	0.113	0.092	0.0076	0.0072	0.91	17	82	1
(0.1, 1.0)	0.078	0.053	0.0088	0.0082	0.90	2	97	1
(0.1, 2.0)	−0.041	−0.052	0.0098	0.0097	0.95	1	93	6
(0.5, 0.1)	0.014	0.015	0.0070	0.0070	0.97	1	97	2
(0.5, 0.5)	−0.035	−0.039	0.0083	0.0083	0.92	0	89	11
(0.5, 1.0)	−0.126	−0.136	0.0107	0.0107	0.90	0	66	34
(0.5, 2.0)	−0.350	−0.380	0.0131	0.0123	0.92	0	15	85
(1.0, 0.1)	−0.110	−0.093	0.0073	0.0071	0.96	0	77	23
(1.0, 0.5)	−0.231	−0.241	0.0090	0.0089	0.95	0	33	67
(1.0, 1.0)	−0.375	−0.384	0.0101	0.0100	0.95	0	3	97
(1.0, 2.0)	−0.684	−0.690	0.0120	0.0120	0.94	0	0	100
(2.0, 0.1)	−0.130	−0.109	0.0082	0.0072	0.96	0	68	32
(2.0, 0.5)	−0.275	−0.277	0.0076	0.0081	0.97	0	28	72
(2.0, 1.0)	−0.446	−0.452	0.0081	0.0129	0.91	0	5	95
(2.0, 2.0)	−0.813	−0.816	0.0129	0.0129	0.92	0	0	100
(3.0, 0.1)	0.300	0.271	0.0094	0.0086	0.97	47	53	0
(3.0, 0.5)	0.360	0.365	0.0094	0.0094	0.95	91	9	0
(3.0, 1.0)	0.296	0.287	0.0116	0.0115	0.95	71	29	0
(3.0, 2.0)	0.039	0.028	0.0115	0.0115	0.97	2	95	3
(4.0, 0.1)	1.276	1.115	0.0406	0.0146	0.99	100	0	0
(4.0, 0.5)	1.814	1.826	0.0113	0.0113	0.97	100	0	0
(4.0, 1.0)	2.015	2.007	0.0124	0.0125	0.94	100	0	0
(4.0, 2.0)	2.060	2.042	0.0114	0.0111	0.97	100	0	0

function f and its 95% confidence surfaces can guide us to explore whether some parametric models are sufficient to describe the data. If the fitted function f and its confidence surfaces indicate that the modes of drug interactions for all combination doses are similar, a parametric model with a single parameter capturing drug interaction may suffice. If the fitted function f and its confidence surfaces indicate that the modes of drug interactions for the combination doses at each fixed ratio are unique, the parametric models based on a 50% maximal effect isobole may be appropriate. We advocate the use of our proposed semiparametric method for model building because we typically do not know the true patterns of drug interactions. Blindly using any parametric model can be dangerous and may lead to the wrong conclusions of drug interactions. In our proposed model, we do not assume any parametric patterns for $f(d_1, d_2)$. The conclusions of drug interactions are based on the estimated f and its confidence surfaces, which are determined by the underlying data.

Our current model can be extended in several ways. One extension is that we may use nonparametric dose–effect curves to describe the marginal dose–effect relationship. Then, we can use the same procedure to estimate the function $f(d_1, d_2)$ and construct its confidence surfaces, and assess drug interactions accordingly. However, because the curves estimated nonparametrically cannot be extrapolated, larger range of dose levels for each single drug is needed so that the range of effects from each single drug covers the range of the effect for the combination doses so that the additive effect can be estimated for each combination dose (Kelly and Rice, 1990).

Another extension of the current model is that the two-stage model can be extended to assess multiple drug interactions (say, $k > 2$ drugs). The predicted additive effect can be obtained from $\frac{d_1}{\hat{F}_1^{-1}(y_p)} + \cdots + \frac{d_k}{\hat{F}_k^{-1}(y_p)} = 1$, and $f(d_1, \ldots, d_k)$ can be estimated by using high-dimensional thin plate spline (Green and Silverman, 1994).

In the current setting, we first estimate the parameter's β's, and then estimate $f(d_1, d_2)$. Here $f(d_1, d_2)$ is used to characterize drug interaction, which should be zero whenever $d_1 = 0$ or $d_2 = 0$. Currently, we forced the difference between observed effect and predicted additive effect to be zero for each marginal dose so that the estimated $f(d_1, d_2)$ could be as close to zero as possible. However, it will be beneficial to research how this constraint could be transferred to the constraint on γ's and v's. In addition, whether and how to estimate β's and $f(d_1, d_2)$ simultaneously may be further investigated. We may also consider formulating the response surface model in a different manner, such that $Y = \beta_0 + \beta_1 \log(d_1 + \rho d_2 + f(d_1, d_2)(d_1 \rho d_2)^{\frac{1}{2}})$ (Kong and Lee, 2006). In that setting, β's and $f(d_1, d_2)$ may be estimated simultaneously. But how to estimate them remains a very challenging and interesting problem. Last but not the least, further research is needed to develop the theoretical properties of the bootstrap method for constructing the confidence interval for $f(d_1, d_2)$ in the current setting.

7. Supplementary Materials

The data and `S-PLUS` are available under the Paper Information link at the Biometrics website `http://www.biometrics.tibs.org`.

Acknowledgements

This research was supported in part by grants from the National Cancer Institute CA106451, CA97007, CA91844,

and the Department of Defense W81XWH-04-1-0142 and W81XWH-05-2-0027. The authors are thankful to Dr Reuben Lotan for providing data, to Dr Raymond Carroll and Dr Somnath Datta for their discussion, to Lee Ann Chastain for editorial assistance, and to the two reviewers, the associate editor, and the editor for their constructive comments.

References

Berenbaum, M. C. (1989). What is synergy? *Pharmacological Reviews* **41,** 93–141.

Carter, W. H., Jr., Gennings, C., Staniswalis, J. G., Cambell, E. D., and White, K. L., Jr. (1988). A statistical approach to the construction and analysis of isobolograms. *Journal of the American College of Toxicology* **7,** 963–973.

Chou, T. C. and Talalay, P. (1984). Quantitative analysis of dose-effect relationships: The combined effects of multiple drugs or enzyme inhibitors. *Advances in Enzyme Regulation* **22,** 27–55.

Davison, A. C. and Hinkley, D. V. (1997). *Bootstrap Methods and their Application.* Cambridge, U.K.: Cambridge University Press.

Greco, W. R., Bravo, G., and Parsons, J. C. (1995). The search of synergy: A critical review from a response surface perspective. *Pharmacological Reviews* **47,** 331–385.

Green, P. J. and Silverman, B. W. (1994). *Nonparametric Regression and Generalized Linear Models.* London: Chapman & Hall.

Hardle, W. and Marron, J. S. (1991). Bootstrap simultaneous error bars for nonparametric regression. *Annals of Statistics* **19,** 778–796.

Kanzawa, F., Nishio, K., Fukuoka, K., Sunami, T., and Saijo, N. (1999). In vitro interactions of a new derivative of spicamycin, KRN5500, and other anticancer drugs using a three-dimensional model. *Cancer Chemotherapy and Pharmacology* **43,** 353–363.

Kelly, C. and Rice, J. (1990). Monotone smoothing with application to dose-response curves and the assessment of synergism. *Biometrics* **46,** 1071–1085.

Kong, M. and Eubank, R. L. (2006). Monotone smoothing with application to dose-response curve. *Communications in Statistics—Simulation and Computation* **35,** 991–1004.

Kong, M. and Lee, J. J. (2006). A generalized response surface model with varying relative potency for assessing drug interactions. *Biometrics* **62,** 986–995.

Lee, J. J., Kong, M., Ayers, G. D., and Lotan, R. (2007). Interaction index and different methods for determining drug interaction in combination therapy. *Journal of Biopharmaceutical Statistics* **17,** 461–480.

Liang, H., Hardle, W., and Sommerfeld, V. (2000). Bootstrap approximation in partially linear regression model. *Journal of Statistical Planning and Inference* **91,** 413–426.

Prichard, M. N. and Shipman, C., Jr. (1990). A three-dimensional model to analyze drug-drug interactions. *Antiviral Research* **14,** 181–206.

Ruppert, D., Wand, M. P., and Carroll, R. J. (2003). *Semiparametric Regression.* Cambridge, U.K.: Cambridge University Press.

Suhnel, J. (1990). Evaluation of synergism or antagonism for the combined action of antiviral agents. *Antiviral Research* **13,** 23–40.

Tan, M., Fang, H., Tian, G., and Houghton, P. J. (2003). Experimental design and sample size determination for testing synergism in drug combination studies based on uniform measures. *Statistics in Medicine* **22,** 2091–2100.

White, D. B., Faessel, H. M., Slocum, H. K., Khinkis, L., and Greco, W. R. (2004). Nonlinear response surface and mixture experiment methodologies applied to the study of synergy. *Biometrical Journal* **46,** 56–71.

Received March 2006. *Revised May* 2007.
Accepted May 2007.

Available online at www.sciencedirect.com
SCIENCE DIRECT®
Biochemical Pharmacology 68 (2004) 1119–1124
Biochemical Pharmacology
www.elsevier.com/locate/biochempharm

Molecular mechanisms of deguelin-induced apoptosis in transformed human bronchial epithelial cells

Ho-Young Lee*

Department of Thoracic/Head and Neck Medical Oncology, The University of Texas, M. D. Anderson Cancer Center, 1515 Holcombe Boulevard, Houston, TX 77030, USA

Received 5 March 2004; accepted 4 May 2004

Abstract

Increasing evidence has demonstrated that the phosphatidylinositol-3 kinase (PI3K)/Akt signaling pathway plays an important role in cell proliferation, apoptosis, angiogenesis, adhesion, invasion, and migration, functions that are critical to cancer cell survival and metastasis. Increased expression of activated Akt has been observed in the early stages of tobacco-induced lung carcinogenesis. Moreover, blocking the PI3K/Akt pathway specifically inhibits the proliferation of non-small cell lung cancer (NSCLC) cells, indicating that the PI3K/Akt pathway is a potential target for chemoprevention and therapy in lung cancer. The aim of this work is to study the lung cancer chemopreventive potential of PI3K/Akt inhibitors using an in vitro lung carcinogenesis model. We found that genetic or pharmacologic approaches targeting the PI3K/Akt pathway inhibited the proliferation of premalignant and malignant human bronchial epithelial (HBE) cells. After screening several natural products to identify a potential lung cancer chemopreventive agent, we have found that deguelin, a rotenoid isolated from *Mundulea sericea* (Leguminosae), specifically inhibits the growth of transformed HBE and NSCLC cells by inducing cell-cycle arrest in the G2/M phase and apoptosis, with no detectable toxic effects on normal HBE cells, most likely due to the agent's ability to inhibit PI3K/Akt-mediated signaling pathways. The specific sensitivity of premalignant and malignant HBE and NSCLC cells to deguelin suggests that this drug could be clinically useful for chemoprevention in early-stage lung carcinogenesis and for therapy in confirmed lung cancer.

Keywords: Chemoprevention; Apoptosis; Phosphatidylinositol-3 kinase; Akt; Deguelin; Lung cancer

1. Introduction

Despite recent advances in radiotherapy and chemotherapy, the severe morbidity from lung cancer and the low 5-year survival rates have improved modestly and lung cancer remains the primary cause of cancer-related deaths in both men and women in the United States [1]. Cancer chemoprevention is therefore a logical strategy to help alleviate this disease. However, all trials of lung cancer chemoprevention agents performed in the United States and Europe have been unsuccessful to date [2]. Most of these trials examined the chemopreventive efficacy of retinoid-based regimens, indicating the need to develop novel chemopreventive approaches for lung cancer. Because exposure to cigarette smoke confers the greatest risk, with approximately 90% of all lung cancers occurring in smokers, smoking-cessation campaigns have been a major focus of effort to prevent the disease. However, approximately 25% of adults in the United States continue to smoke cigarettes [3]. Furthermore, the risk of lung cancer does not diminish during the first 5 years after smoking cessation and remains higher among former smokers than among people who have never smoked [3]. Additional preventive strategies for former and current smokers are therefore needed.

It is known that the metabolites of tobacco carcinogens such as 4-(methylnitrosamino)-1-(3-pyridyl)-1-butanone (NNK) and polyaromatic hydrocarbons induce DNA mutations in tumor suppressor genes and oncogenes [4]. Cells with mutated DNA are normally removed via apoptosis

Abbreviations: HBE, human bronchial epithelial; IGF-1, insulin-like growth factor-1; MAPK, mitogen-activated protein kinase; MEK, MAPK/extracellular signal-regulated kinase (ERK) kinase; NHBE, normal human bronchial epithelial; NSCLC, non-small cell lung cancer; PI3K, phosphatidylinositol-3 kinase; PKB, protein kinase B; TGF, transforming growth factor; TK, tyrosine kinase

* Tel.: +1 713 792 6363; fax: +1 713 796 8655.
E-mail address: hlee@mdanderson.org (H.-Y. Lee).

0006-2952/$ – see front matter © 2004 Elsevier Inc. All rights reserved.
doi:10.1016/j.bcp.2004.05.033

[4]; however, if the survival pathway is active, cells with damaged DNA persist, resulting in loss of growth control and, ultimately, lung cancer formation. On the basis of this notion, we have investigated novel agents targeting signaling mechanisms that play an important role in survival of premalignant and malignant human bronchial epithelial (HBE) cells as well as lung cancer cells. This commentary presents evidence that the PI3K/Akt pathway plays a central role in the proliferation and survival of preneoplastic cells and that deguelin, a natural product, inhibits Akt activation and has potential as a novel chemopreventive agent in lung cancer.

2. Activation of the PI3K/Akt signaling pathway and biological effects of Akt activation

Growing evidence has demonstrated that a receptor signaling system mediated by receptor and nonreceptor tyrosine kinase (TK) plays a critical role in cellular proliferation and survival and in the inhibition of apoptosis [5]. Signaling by receptor TK requires ligand-induced receptor oligomerization, which results in tyrosine autophosphorylation of the receptor subunits that mediate the specific binding of cytoplasmic signaling proteins containing Src homology-2 and protein tyrosine-binding domains, such as Grb2, Shc, IRS, Src, RasGAP, SHP-1, and PI3K [6]. Strict regulation of TK activity controls cell-cycle progression and cell proliferation, differentiation, motility, and survival [5–7]. Therefore, overexpression of receptor TK, ligand, or both could lead to deregulated TK-mediated signaling, resulting in the imbalance between the rates of cell-cycle progression (cell division) and cell growth (cell mass) on the one hand and programmed cell death (apoptosis) on the other that is characteristic of all neoplasms [8]. Two distinct signal transduction pathways, PI3K/Akt and Ras/Raf/MAPK, are crucial effectors in oncogenic TK signaling [8,9]. RTKs can also activate PI3K indirectly through Ras, which can bind and activate the p110 subunit [9], indicating a cross-talk between these two signaling pathways.

The PI3K/Akt pathway has been involved in several types of carcinogenesis. Findings from in vitro models indicate that activation of the PI3K/Akt pathway is sufficient to induce malignant transformation of human cells [10,11]. PIK3CA, which encodes p110α, has been amplified in human ovarian cancer cell lines [12]. A partially transformed phenotype has been demonstrated in mammalian fibroblasts transfected with the constitutively active form of p110α [13]. Moreover, an oncogenic mutant of p85 that can, in collaboration with the v-*raf* oncogene, transform mammalian fibroblasts has been isolated [14]. The transforming activity of PI3K is associated with its ability to activate Akt (also known as protein kinase B), a cellular homologue of the viral oncogenic protein v-Akt. Akt, a subfamily of serine/threonine protein kinases, is now known to define a family of closely related, highly conserved cellular homologues consisting of Akt1/protein kinase B (PKB)α, Akt2/PKBβ, and Akt3/PKBγ [9]. Akt is activated by growth factors, adhesive interactions with int7egrins, and signals initiated by stimulation of G-protein-coupled receptor (GPCR) [15]. Akt is also activated by isoproterenol stimulation of the β3 adrenergic receptor and Ca^{2+}/calmodulin-dependent protein kinase kinase (CaMKK) in a PI3K-independent manner [16]. 3-Phosphatidylinositol-dependent protein kinase (PDK)-1 and integrin link kinase (ILK) have been found to activate Akt by phosphorylating Thr308 and Ser473, respectively [9]. PTEN regulates Akt activity by dephosphorylating the lipid product of PI3K [16]. Activated Akt promotes cell proliferation and survival by directly phosphorylating several components involved in cell-cycle and cell-death machinery, such as glycogen synthase kinase (GSK)-3, the mammalian target of rapamycin, BAD, caspase-9, human telomerase reverse transcriptase subunit β, and IκB kinases [17–22]. Akt also induces phosphorylation of FKHR – a member of the Forkhead family of transcription factors – and thus prevents its induction of several pro-apoptotic protein expression, such as BIM and FAS ligand. In addition, Akt indirectly influence cell survival by phosphorylating IκB kinase (IKK) and MDM2, affecting the level of two central regulators of cell death – nuclear factor of κB (NF-κB) and p53, and negatively regulates the expression of CDK inhibitors (CKIs), such as KIP1 (also known as p27) and WAF1 (also known as CIP1 or p21). The effects on KIP1 seem to be transcriptional and mediated by FKHR (reviewed in Ref. [9]).

3. Involvement of Akt activation in lung carcinogenesis

Activation of Akt causes malignant transformation in vitro and in vivo in mouse models of various human cancers [23–25]. We and others have previously reported evidence that Akt activation is an early event in lung carcinogenesis; expression of pAkt is increased in premalignant and malignant HBE cells [26], reactive epithelium specimens (bronchial hyperplasia and squamous metaplasia), bronchial dysplasia, and NSCLC cells [26–28]. West et al. [29] recently reported that activation of Akt is an early biochemical effect of tobacco components in normal human lung epithelial cells that is induced by nicotine and NNK in pharmacologically relevant concentrations both in vitro in normal HBE cells and small airway epithelial cells (SAECs) and in vivo in the lungs of NNK-treated mice and human smokers with lung cancers. Lung cancer cells produce insulin-like growth factor (IGF), a major survival factor, at higher levels than do normal lung cells and exhibit a mitogenic response to exogenous IGF [30,31]. Moreover, increased expressions of epidermal growth factor receptor (EGFR) and transforming growth

factor (TGF), mutations of k-*ras*, reduced expression of PTEN, and amplification of a region of chromosome 3q that includes the p110 catalytic subunit of PI3K – all of which could induce activation of PI3K/Akt pathway – have been observed in bronchial preneoplastic lesions, NSCLC, or both [32–36]. Together, these findings indicated that Akt activation is an early event in lung tumorigenesis and, therefore, development of new chemopreventive agents that suppress the PI3K/Akt pathway may abrogate lung carcinogenesis.

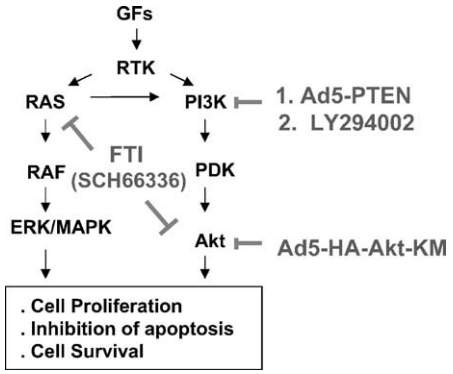

Fig. 1. Strategies to inhibit PI3K/Akt pathway; PI3K activities suppressed by LY294002 or an adenoviruses expressing PTEN (Ad5-PTEN). Akt was blocked by an adenoviruses expressing dominant negative Akt (K179M). Ras is inactivated by SCH66336, a farnesyl transferase inhibitor that was designed to inhibit Ras activation.

4. Targeting the PI3K/Akt signaling pathway in lung cancer

The effects of the PI3K/Akt pathway on the proliferation of normal (NHBE), premalignant, and malignant HBE

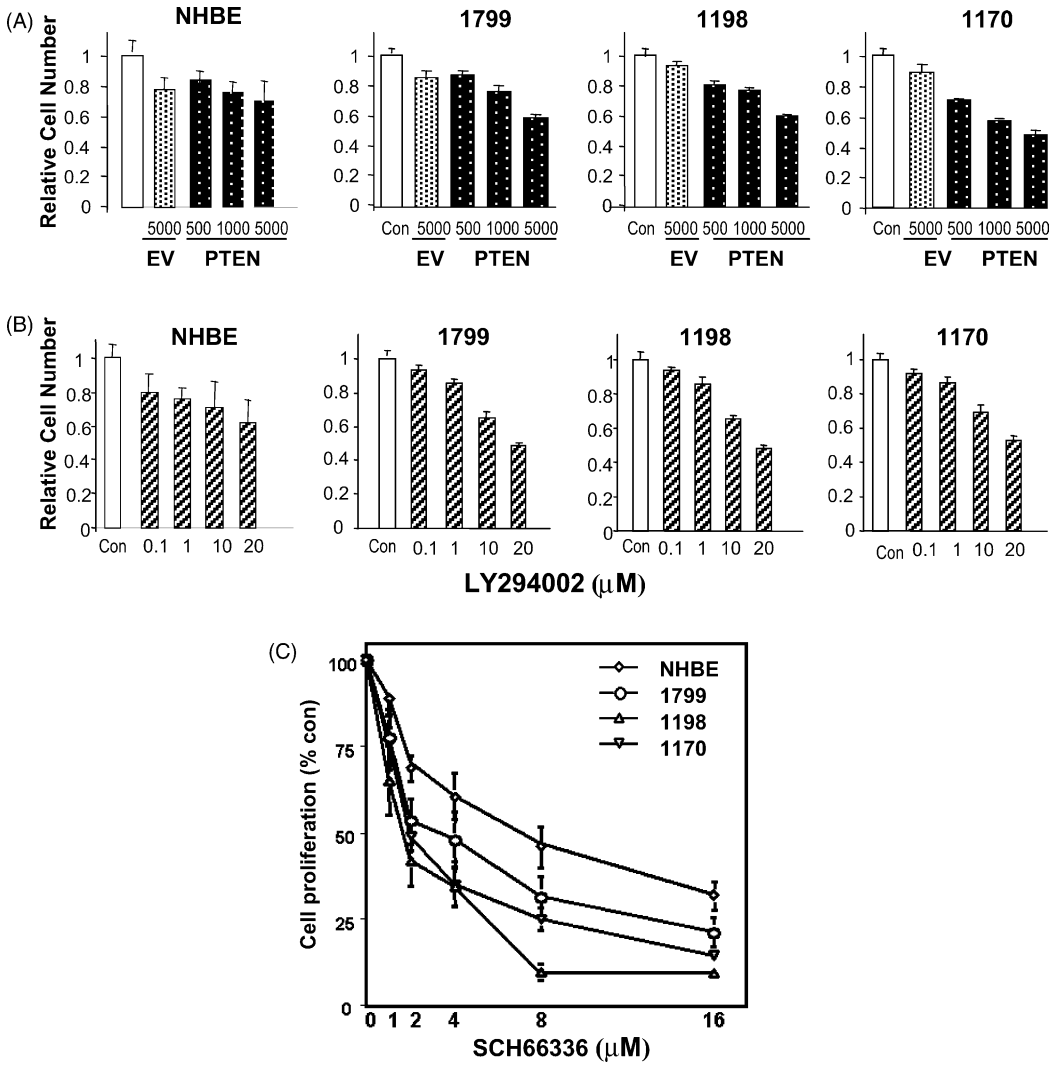

Fig. 2. Effect of the PI3K/Akt pathway on HBE cell proliferation. (B) NHBE cells and the indicated HBE cell lines were seeded in 96-well culture plates (2000–5000 cells/well), incubated with the indicated titers of (A) Ad5-CMV (EV), an empty virus, or Ad5-PTEN (PTEN) (particles/cell), (B) LY294002 (μM), or (C) SCH66336 (μM). After incubation of the cells for 3 days, they were subjected to MTT assay. Results are expressed relative to the number of cells infected with EV (A) or cells treated with medium alone (B, C). Each value is the mean (±S.D.) from five identical wells.

cells were investigated using genetic approaches with adenoviral vectors and pharmacologic approaches (Fig. 1) in normal, premalignant (1799 and 1198 cells), and malignant HBE (1170-1) cells. Specifically, the cells were treated with the PI3K inhibitor LY294002 or an adenovirus expressing either PTEN (Ad5-PTEN) [28] or dominant-negative Akt (Ad5-HA-Akt-KM) [37]. The results showed that Ad5-PTEN (Fig. 2A), LY294002 (Fig. 2B), or Ad5-HA-Akt-KM (data not shown) effectively suppressed the proliferation of 1179, 1198, and 1170-1 cells compared with NHBE cells. However, SCH66336, a farnesyl transferase inhibitor that was originally designed to inhibit Ras activation but also inhibited Akt activation [38], resulted in marginally selective inhibition of the growth of transformed HBE cells (Fig. 2C). Thus, interrupting the PI3K/Akt pathway is, in this model of lung cancer, a potentially effective chemopreventive strategy. Targeting this pathway could be extremely useful in clinical settings, especially in the treatment of NSCLC, in which constitutive activation of Akt occurs at a high frequency [39]. Moreover, manipulating Akt activity alters the sensitivity of cells to chemotherapy and irradiation [39]. Therefore, targeting Akt might enhance the efficacy of chemotherapy and radiotherapy, and increase the apoptotic potential of NSCLC cells.

5. Chemopreventive and chemotherapeutic potential of deguelin in lung cancer

Since the publication of clinical studies showing the efficacy and feasibility of chemoprevention of aerodigestive tract cancer [40], researchers have devoted much effort to the discovery and development of new chemopreventive agents. Many compounds with varied mechanisms, including retinoids, tyrosine kinase inhibitors, farnesyl transferase inhibitors, non-steroidal anti-inflammatory agents (NSAIDs), and the polyamine synthase inhibitor have been used successfully as chemopreventive agents in either animal carcinogenesis models or clinical trials [41]. However, undesirable side effects or resistance of lung cancer cells to these agents limit their long-term clinical use as chemopreventive therapy. Furthermore, all clinical trials of lung cancer chemopreventive agents performed in the United States and Europe have failed to show that such therapy benefits individuals at increased risk of developing lung cancer, thus emphasizing the need for novel lung cancer chemopreventive strategies.

Since we and others have found that one of the most promising molecules for chemoprevention and treatment of lung cancer is targeting of Akt, several natural plant products and dietary constituents have been screened to identify those with inhibitory effects on proliferation of transformed HBE cells by blocking Akt activation. Among many tested natural products, deguelin (Fig. 3), a rotenoid isolated from several plant species including *Mundulea sericea* (Leguminosae), has shown potential cancer chemopreventive activity. Deguelin effectively prevented 7,12-dimethyl(*a*)benzanthracene-induced preneoplastic lesions in mouse mammary organ culture [42]. Further, in a murine two-stage DMBA/TPA skin carcinogenesis model, treatment with topical deguelin markedly suppressed disease induction of papillomas in mice treated at a low dose (33 μg) and completely suppressed disease (i.e., no tumors in any mice) at a high dose (330 μg) [43]. The antitumor efficacy of deguelin was also shown in an NMU-induced rat mammary carcinogenesis model: although deguelin had no effect on tumor incidence, the mean tumor number was reduced from 6.8 to 3.2 tumors per rat in the group treated with high-dose deguelin [43].

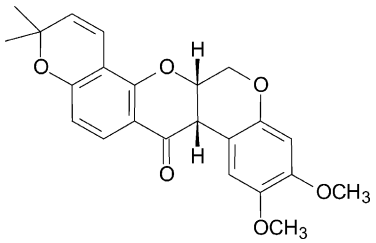

Fig. 3. Structure of deguelin.

We have demonstrated that deguelin has potent apoptotic activities in transformed HBE cells and a variety of NSCLC cell lines at doses attainable in vivo, with minimal effects on NHBE viability [44]. Deguelin treatment induced both cell-cycle arrest in the G2/M phase and apoptosis [26,44]. In addition, deguelin inhibited PI3K activity and reduced pAkt levels and activity but had minimal effects on the MAPK pathway; furthermore, overexpression of a constitutively active Akt blocked deguelin-induced growth arrest and apoptosis [44]. These findings indicate that the proapoptotic activity of deguelin results from its ability to inhibit PI3K/Akt-mediated signaling pathways. In addition, deguelin induced a partial and delayed inhibition of PI3K activity, compared with stronger, earlier inhibition of Akt activity, suggesting that more than one mechanism mediates deguelin-induced suppression of Akt activity. Deguelin also inhibits the expression of cyclooxygenase (COX)-2 [44], which is largely regulated by Akt activity [45], without affecting the COX-1 protein level. COX catalyzes the conversion of arachidonic acid to prostaglandins, which can cause tumor cell growth, suppress immune surveillance [46], and induce metabolic activation of the tobacco components PAH and NNK [47]. Other PI3K/Akt inhibitors, such as LY294002 and farnesyltransferase inhibitor SCH66336 [38], were less effective than deguelin at inhibiting the growth of premalignant HBE cells (unpublished data); LY294002 and SCH66336 required more than 10 and 1 μM, respectively, to induce detectable growth inhibition in premalignant and malignant HBE cells. The difference in the effects on COX-2 expression between deguelin and these PI3K/Akt inhibitors warrants further investigation.

All these findings indicate that deguelin is a potentially useful chemopreventive agent in lung cancer. In addition, since malignant HBE cells and NSCLC cell lines are also sensitive to deguelin, this proapoptotic drug has potential as a therapeutic agent against lung cancer.

6. Conclusion

The evidence presented herein suggests that Akt is activated at an early stage of lung carcinogenesis through a variety of mechanisms. Because Akt activity is crucial for cell proliferation and survival of transformed HBE and NSCLC cells, Akt is likely to be an important factor in early progression of lung carcinoma. Interestingly, activation of Akt is an early biochemical effect of tobacco components on human lung epithelial cells in vitro and in vivo [36]. Thus, suppression of Akt activation could be an effective preventive strategy, especially for smokers. The potential of inhibitors of PI3K/Akt activities for treatment of lung cancer should also be considered.

Given this evidence of Akt's involvement in lung cancer and the fact that this malignancy is the leading cause of cancer death worldwide, the need to develop small molecules such as deguelin that target Akt activation is urgent. The present data provide evidence that deguelin selectively inhibits the proliferation of transformed HBE cells by blocking Akt activation and that inhibition of Akt by deguelin is the mechanism that mediates its apoptotic effects in transformed HBE cells. Because Akt activity alters the sensitivity of NSCLC cells to chemotherapeutic agents and irradiation [39], treatment with deguelin may enhance the efficacy of chemotherapy and radiotherapy, and increase the apoptotic potential of NSCLC cells.

The potential of deguelin as a chemopreventive and chemotherapeutic agent in lung cancer has recently attracted much attention. Before this approach is used clinically, more experimental studies, especially in animal models, are needed to provide in vivo evidence of efficacy in preventing early disease progression and potential to increase the effectiveness of current chemotherapy and radiation therapy. Since rotenoids inhibit NADH:ubiquinone oxidoreductase activity, an enzyme complex in mitochondrial oxidative phosphorylation, which is associated with cardiotoxicity, respiratory depression, and nerve conduction blockade at high doses ($LD_{50} = 10–100$ g in humans) [42,43], additional studies are needed to evaluate any potential systemic toxicity of deguelin. In addition, further studies to define the relation between structure and activity of analogues of the rotenoids are warranted.

Acknowledgments

This work was supported by National Institutes of Health Grants1RO1 CA100816-01A1 (to H.-Y. Lee), National American Cancer Society, RSG-04-082-01-TBE 01(to H.-Y. Lee), DAMD17-01-1-0689 from the Department of Defense (to W.K. Hong); W.K.H. is an American Cancer Society clinical research professor.

References

[1] Khuri FR, Herbst RS, Fossella FV. Emerging therapies in non-small-cell lung cancer. Ann Oncol 2001;12:739–44.
[2] Khuri FR, Lippman SM. Lung cancer chemoprevention. Semin Surg Oncol 2000;18:100–5.
[3] Burns DM. Primary prevention, smoking, and smoking cessation: implications for future trends in lung cancer prevention. Cancer 2000;89:2506–9.
[4] Hecht S. Tobacco smoke carcinogens and lung cancer. J Natl Cancer Inst 1999;91:1194–210.
[5] Blume-Jensen B, Hunter T. Oncogenic kinase signaling. Nature 2001;411:355–65.
[6] Heldin CH. Dimerization of cell surface receptors in signal transduction. Cell 1995;80:213–23.
[7] Vlahovic G, Crawford J. Activation of tyrosine kinases in cancer. Oncologist 2003;8:531–8.
[8] Reed JC. Dysregulation of apoptosis in cancer. J Clin Oncol 1999;17:2941–53.
[9] Vivanco I, Sawyers CL. The phosphatidylinositol 3-kinase-Akt pathway in human cancer. Nat Rev Cancer 2002;2:489–501.
[10] Bellacosa A, Testa JR, Staal SP, Tsichlis PN. A retroviral oncogene, Akt, encoding a serine–threonine kinase containing an SH2-like region. Science 1991;254:274–7.
[11] Chang HW, Aoki M, Fruman D, Auger KR, Bellacosa A, Tsichlis PN, et al. Transformation of chicken cells by the gene encoding the catalytic subunit of PI 3-kinase. Science 1997;276:1848–50.
[12] Shayesteh L, Lu Y, Kuo WL, Baldocchi R, Godfrey T, Collins C, et al. PIK3CA is implicated as an oncogene in ovarian cancer. Nat Genet 1999;21:99–102.
[13] Klippel A, Escobedo MA, Wachowicz MS, Apell G, Brown TW, Giedlin MA, et al. Activation of phosphatidylinositol 3-kinase is sufficient for cell cycle entry and promotes cellular changes characteristic of oncogenic transformation. Mol Cell Biol 1998;18:5699–56711.
[14] Jimenez C, Jones DR, Rodriguez-Viciana P, Gonzalez-Garcia A, Leonardo E, Wennstrom S, et al. Identification and characterization of a new oncogene derived from the regulatory subunit of phosphoinositide 3-kinase. EMBO J 1998;17:743–53.
[15] Chan TO, Rittenhouse SE, Tsichlis PN. AKT/PKB and other D3 phosphoinositide-regulated kinases: kinase activation by phosphoinositide-dependent phosphorylation. Annu Rev Biochem 1999;68:965–1014.
[16] Alessi DR, Cohen P. Mechanism of activation and function of protein kinase B. Curr Opin Genet Dev 1998;8:55–62.
[17] Cross DAE, Alessi DR, Cohen P, Andjelkovich M, Hemmings BA. Inhibition of glycogen synthase kinase-3 by insulin mediated by protein kinase B. Nature 1995;378:785–9.
[18] Brunet A, Bonni A, Zigmond MJ, Lin MZ, Juo P, Hu LS, et al. Akt promotes cell survival by phosphorylating and inhibiting a forkhead transcription factor. Cell 1999;96:857–68.
[19] Cardone MH, Roy N, Stennicke HR, Salvesen GS, Franke TF, Stanbridge E, et al. Regulation of cell death protease caspase-9 by phosphorylation. Science 1998;282:1318–21.
[20] Datta SR, Dudek H, Tao X, Masters S, Fu H, Gotoh Y, et al. Akt phosphorylation of BAD couples survival signals to the cell-intrinsic death machinery. Cell 1997;91:231–41.
[21] Del Peso L, Gonzalez-Garcia M, Page C, Herrera R, Nunez G. Interleukin-3-induced phosphorylation of BAD through the protein kinase Akt. Science 1997;278:687–9.

[22] Krasilnikov MA. Phosphatidylinositol-3 kinase dependent pathways: the role in control of cell growth, survival, and malignant transformation. Biochemistry 2000;65:59–67.
[23] Chang HW, Aoki M, Fruman D, Auger KR, Bellacosa A, Tsichlis PN, et al. Transformation of chicken cells by the gene encoding the catalytic subunit of PI 3-kinase. Science (Washington, DC) 1997;276:1848–50.
[24] Hutchinson J, Jin J, Cardiff RD, Woodgett JR, Mueller WJ. Activation of AKT (protein kinase B) in mammary epithelium provides a critical cell survival signal required for tumor progression. Mol Cell Biol 2001;21:2203–12.
[25] Podsypanina K, Ellenson LH, Nemes A, Gu J, Tamura M, Yamada KM, et al. Mutation of Pten/MMAC1 in mice causes neoplasia in multiple organs. Proc Natl Acad Sci USA 1999;96:1563–8.
[26] Chun K-H, Kosmeder JW, Sun S, Pezzuto JM, Lotan R, Hong WK, et al. Chemopreventive effects of deguelin, a naturally occurring PI3K/Akt inhibitor, during the malignant transformation of human bronchial epithelial cells. J Nat Cancer Inst 2003;95:291–302.
[27] Tsao AS, McDonnell T, Lam S, Putnam JB, Bekele N, Hong WK, et al. Increased phospho-AKT (Ser473) expression in bronchial dysplasia. Cancer Epidemiol Biomarkers Prev 2003;12:660–4.
[28] Lee H-Y, Srinivas H, Xia D, Ling Y, Superty R, LaPushin R, et al. Evidence that phosphatidylinositol 3-kinase- and mitogen-activated protein kinase kinase-4/c-jun nh2-terminal kinase-dependent pathways cooperate to maintain lung cancer cell survival. J Biol Chem 2003;278:23630–8.
[29] West KA, Brognard J, Clark AS, Linnoila IR, Yang X, Swain SM, et al. Akt activation by nicotine and a tobacco carcinogen modulates the phenotype of normal human airway epithelial cells. J Clin Invest 2003;111:81–90.
[30] Zia F, Jacobs S, Kull Jr F, Cuttita F, Mulshine JL, Moody TW. Monoclonal antibody alphaIR3 inhibits non-small cell lung cancer growth in vitro and in vivo. J Cell Biochem Suppl 1996;24:269–75.
[31] Quinn KA, Treston AM, Unsworth EJ, Miller MJ, Vos M, Grimley C, et al. Insulin-like growth factor expression in human cancer cell lines. J Biol Chem 1996;271:11477–83.
[32] Sugio K, Kishimoto Y, Virmani AK, Hung JY, Gazdar AF. K-ras mutations are a relatively late event in the pathogenesis of lung carcinomas. Cancer Res 1994;54:5811–55.
[33] Soria JC, Lee HY, Lee JI, Wang L, Issa JP, Kemp BL, et al. Lack of PTEN expression in non-small cell lung cancer could be related to promoter methylation. Clin Cancer Res 2002;8:1178–84.
[34] Massion PP, Kuo WL, Stokoe D, Olshen AB, Treseler PA, Chin K, et al. Genomic copy number analysis of non-small cell lung cancer using array comparative genomic hybridization: implications of the phosphatidylinositol 3-kinase pathway. Cancer Res 2002;62:3636–40.
[35] Lin X, Bohle AS, Dohrmann P, Leuschner I, Schulz A, Kremer B, et al. Overexpression of phosphatidylinositol 3-kinase in human lung cancer. Langenbecks Arch Surg 2001;386:293–301.
[36] Moore SM, Rintoul RC, Walker TR, Chilvers ER, Haslett C, Sethi T. The presence of a constitutively active phosphatidylinositol 3-kinase in small cell lung cancer cells mediates anchorage-independent proliferation via a protein kinase B and $p70^{S6K}$ pathway. Cancer Res 1998;58:5239–47.
[37] Lee H-Y, Chun K-H, Wiehle S, Rristiano R, Hong WK, Kurie JM. The effects of insulin-like growth factor binding protein-3 on lung cancer. Cancer Res 2002;62:3530–7.
[38] Lee H-Y, Chang YS, Chun K-H, Hassan K, Moon HJ, Wiehle S, et al. Apoptotic activity of NSCLC cells enhanced by synergy of IGFBP-3 with farnesyl transferase inhibitor SCH66336. JNCI, in press.
[39] Brognard J, Clark AS, Ni Y, Dennis PA. Akt/protein kinase B is constitutively active in non-small cell lung cancer cells and promotes cellular survival and resistance to chemotherapy and radiation. Cancer Res 2001;61:3986–97.
[40] Hong WK, Sporn MB. Recent advances in chemoprevention of cancer. Science 1997;278:1073–7.
[41] McWilliams A, Lam S. New approaches to lung cancer prevention. Curr Oncol Rep 2002;4:487–94.
[42] Gerhäuser C, Lee SK, Kosmeder JW, Moriarty RM, Hamel E, Mehta RG, et al. Regulation of ornithine decarboxylase induction by deguelin, a natural product cancer chemopreventive agent. Cancer Res 1997;57:3429–35.
[43] Udeani GO, Gerhauser C, Thomas CF, Moon RC, Kosmeder JW, Kinghorn AD, et al. Cancer chemopreventive activity of deguelin, a naturally occurring rotenoid. Cancer Res 1997;57:3424–8.
[44] Lee H-Y, Suh Y-A, Kosmeder JW, Pezzuto JM, Kurie JM. Deguelin-induced inhibition of cyclooxygenase-2 expression in human bronchial epithelial cells, Clin Cancer Res, in press.
[45] Sheng H, Shao J, DuBois RN. K-Ras-mediated increase in cyclooxygenase 2 mRNA stability involves activation of the protein kinase B. Cancer Res 2001;61:2670–5.
[46] Taketo MM. Cyclooxygenase-2 inhibitors in tumorigenesis (Part I). J Natl Cancer Inst 1998;90:1529–36.
[47] El-Bayoumy K, Iatropoulos M, Amin S, Hoffmann D, Wynder EL. Increased expression of cyclooxygenase-2 in rat lung tumors induced by the tobacco-specific nitrosamine 4-(methylnitrosamino)-4-(3-pyridyl)-1-butanone: the impact of a high-fat diet. Cancer Res 1999;59:1400–3.

VOLUME 23 · NUMBER 19 · JULY 1 2005

JOURNAL OF CLINICAL ONCOLOGY ORIGINAL REPORT

Effects of 9-*cis*-Retinoic Acid on the Insulin-Like Growth Factor Axis in Former Smokers

Ho-Young Lee, Yoon Soo Chang, Ji-Youn Han, Diane D. Liu, J. Jack Lee, Reuben Lotan, Margaret R. Spitz, and Waun Ki Hong

From The University of Texas Graduate School of Biomedical Sciences at Houston and The University of Texas M.D. Anderson Cancer Center, Houston, TX.

Submitted November 9, 2004; accepted January 24, 2005.

Supported in part by National Institutes of Health Grants U19 CA68437 (W.K.H.), R01 CA109520-01 (H.-Y.L.), CA-100816-01A1 (H.-Y.L), American Cancer Society grant RSG-04-082-01-TBE 01(H.-Y.L), and W81XWH-04-1-0142-01-VITAL from the Department of Defense (W.K.H.). W.K.H. is an American Cancer Society Clinical Research Professor.

Presented in part at the 40th Annual Meeting of the American Society of Clinical Oncology, New Orleans, LA, June 5-8, 2004.

Authors' disclosures of potential conflicts of interest are found at the end of this article.

Address reprint requests to Ho-Young Lee, PhD, Department of Thoracic/Head & Neck Medical Oncology, and the Program in Cancer Biology, Unit 432, The University of Texas M.D. Anderson Cancer Center, 1515 Holcombe Blvd, Houston, TX 77030; e-mail: hlee@mdanderson.org.

0732-183X/05/2319-4439/$20.00

DOI: 10.1200/JCO.2005.04.572

ABSTRACT

Purpose
Insulin-like growth factor (IGF) axis has been associated with the risk of lung cancer. 9-*cis*-retinoic acid (9-*cis*-RA) has shown potential chemopreventive activities in former smokers. This study was designed to evaluate the effects of 9-*cis*-RA on IGF axis in former smokers to identify any benefit the retinoid may have in preventing lung cancer.

Patients and Methods
Serum concentrations of IGF-I, IGF binding protein (IGFBP)-3, and their molar ratio (IGF-I/IGFBP-3) were measured with radioimmunoassay kits in stored blood samples from the participants of an original chemoprevention trial. The participants had ceased smoking for at least 12 months and were randomly assigned to receive 3 months of daily oral 9-*cis*-RA (100 mg) or placebo. All statistical tests were two-sided.

Results
A total of 111 samples from the study's baseline and 84 samples from the 3 months treatment were analyzed. The serum concentrations of IGF-I and IGF-I/IGFBP-3 at baseline were significantly lower in female than in male participants. After 3 months of treatment, the serum level of IGF-I and IGF-I/IGFBP-3 were significantly lower in the 9-*cis*-RA group than in the placebo group ($P = .03$ and $P < .01$, respectively), but the IGFBP-3 level was significantly higher ($P = .03$).

Conclusion
9-*cis*-RA treatment modulated the IGF axis in former smokers, suggesting that the IGF axis is a potential target for the chemopreventive activities of 9-*cis*-RA and that the serum concentrations of IGF, IGFBP-3, and IGF-I/IGFBP-3 could serve as surrogate end point biomarkers of 9-*cis*-RA treatment.

J Clin Oncol 23:4439-4449. © 2005 by American Society of Clinical Oncology

INTRODUCTION

Lung cancer is the leading cause of cancer death in men and women in the United States,[1,2] and cigarette smoking is the predominant risk factor for lung cancer. Therefore, smoking cessation campaigns have been a major focus of preventive effort.[3,4] However, the risk for lung cancer does not diminish during the first 5 years after smoking cessation[5,6]: former smokers continue to have an increased risk compared with people who have never smoked.[7] These findings indicate that additional preventive strategies for former smokers are needed. One effective strategy is the administration of agents that suppress the promotion or progression steps of lung carcinogenesis by inhibiting the proliferation and survival of preneoplastic cells that have acquired genomic DNA damage as a result of exposure to cigarette carcinogens.

An increasingly recognized mediator of cell proliferation and survival is insulin-like growth factor (IGF).[8,9] IGFs can also inhibit apoptosis and play an important role in

differentiation of many normal and cancer cell types and in neoplastic transformation and metastasis.[9-11] The IGF system is regulated by IGF binding proteins (IGFBPs), especially IGFBP-3, which bind to IGFs in the extracellular milieu with high affinity and specificity, thus reducing the bioavailability of IGFs; more than 90% of circulating IGF-I is bound within a large complex containing IGFBP-3 and its acid-labile subunit.[9] A growing number of epidemiologic studies have suggested that increased serum concentrations of IGFs, altered concentrations of IGFBP-3, or both, are associated with an increased risk for several types of cancer, including lung cancer, and that high IGFBP-3 concentrations can attenuate this risk.[12-17] We have shown that loss of IGFBP-3 expression, due partly to hypermethylation of its promoter,[18] is a marker of poor prognosis in patients with early-stage non–small-cell lung cancer (NSCLC).[19,20] We have also demonstrated that overexpression of IGFBP-3 inhibits the growth of NSCLC cells in vitro and in vivo by inducing apoptosis.[21] These data indicate that for high-risk patients, the IGF system is a potential target for preventive strategies, for novel antineoplastic therapies, or for both.

An increasing body of evidence has suggested that retinoids, the most frequently studied chemopreventive agents for lung cancer, modulate the IGF axis.[22-24] Results of several in vivo studies in experimental animals have shown that retinoids suppress carcinogenesis in a variety of tissue types, including the lung.[25,26] Of the naturally occurring retinoids, all-*trans*-retinoic acid (all-*trans*-RA) binds to RA receptors (RARs), and 9-*cis*-retinoic acid (9-*cis*-RA) binds to RARs, retinoid X receptors (RXRs), and other nuclear receptor complexes in which the RXR is a ligand-binding partner, such as the vitamin D receptor and the peroxisome proliferator–activated receptor.[27] 13-*cis*-RA binds to RAR and, after stereoisomerization, to either all-*trans*-RA or 9-*cis*-RA in a process that occurs intracellularly.[28]

We demonstrated in a clinical lung cancer chemoprevention trial that 9-*cis*-RA treatment can restore RARβ expression in former smokers after 3 months of treatment.[29] RARβ expression has been implicated in the prevention of tumor development and has shown growth-inhibitory and apoptotic effects on the bronchial epithelia of former smokers.[30] These previous findings thus raised the possibility that 9-*cis*-RA has potential chemopreventive properties in former smokers.

To shed more light on the beneficial effects of 9-*cis*-RA on former smokers, we analyzed the effects of 9-*cis*-RA on the IGF axis, especially on the serum concentrations of IGF-I and IGFBP-3 and on the molar ratio of IGF-I to IGFBP-3, which has been proposed to reflect tissue bioactivity, in a previously studied population of former smokers.[31] We found that 9-*cis*-RA treatment modulated the IGF axis in these former smokers, suggesting that the serum IGF axis is a target of the potential chemopreventive activities of 9-*cis*-RA in former smokers.

PATIENTS AND METHODS

Patients

The original study from which we derived our data was a three-arm, randomized, double-blinded, placebo-controlled trial comparing the effects of 9-*cis*-RA (100 mg) with those of 13-*cis*-RA (1 mg/kg) plus α-tocopherol (AT; 1,200 U) administered for 3 months. In this study, a significant increase in RARβ expression and a reduction of metaplasia were observed in individuals treated with 9-*cis*-RA, but not with 13-*cis*-RA plus AT, compared with those treated with placebo. Because antioxidants such as AT can affect the concentrations of the components of the IGF axis,[32] we decided not to include the 13-*cis*-RA plus AT treatment group in our analysis. The eligibility criteria were previously described.[29] Briefly, the study population consisted of former heavy smokers clinically free of any cancer, who were registered in the Departments of Thoracic/Head and Neck Medical Oncology and of Thoracic Surgery at The University of Texas M.D. Anderson Cancer Center. To be eligible, subjects had to have adequate renal, hematologic, and hepatic function and must not have taken more than 25,000 U of vitamin A or other retinoids daily for at least 3 months before study entry. Subjects were allowed to have had a prior smoking-related cancer, but they had to have been tumor free for 6 months before enrollment in the study. Subjects were required to abstain from consuming dietary vitamin supplements while on the study. The treatment duration was 3 months, based on the toxicity data from a previous phase I trial that included 9-*cis*-RA treatment.[33] Subjects were seen monthly and were evaluated for compliance with the trial protocol, drug-related toxic effects, and serum cotinine concentrations.

The clinical trial from which the samples analyzed in this study were derived indicated that 9-*cis*-RA had some side effects. Specifically, subjects in the 9-*cis*-RA group experienced grade 2 (46 subjects) and grade 3 (nine subjects) toxic effects typical of retinoid treatment, including skin rash, hypertriglyceridemia, headache, cheilitis, conjunctivitis, arthralgia, and myalgia.[29] Drug-related toxicity was graded according to the National Cancer Institute's Common Toxicity Criteria.[34]

The original study had been approved by the institutional review board of The M.D. Anderson Cancer Center and by the US Department of Health and Human Services. Our current study was also approved by the institutional review board at M.D. Anderson.

IGF-I and IGFBP-3 Measurements

For analysis of serum concentrations of IGF-I and IGFBP-3, blood samples were drawn from nonfasting subjects and collected in heparinized tubes that were transported immediately to the laboratory, where the samples were immediately centrifuged for 10 minutes at 4,000 $\times$ *g* and then stored at -80°C until the assays were performed. The serum concentration of IGF-I was measured by a specific radioimmunoassay (Diagnostic Systems Laboratories Inc, Webster, TX) with intra-assay and interassay coefficients of variation of less than 4% and 8%, respectively. To separate IGFs from their binding proteins, we mixed serum specimens with an acid-ethanol extraction buffer before measurement. The extraction procedure had been previously evaluated, and the efficiency of the extraction was identical to that for acid-column chromatography.[35] The IGFBP-3 concentration was also measured by a specific radioimmunoassay (Diagnostic Systems Laboratories Inc) with intra-assay and interassay coefficients of variation of less than 3.5% and 7.5%, respectively, and no cross-reaction with other

members of the IGFBP family. The assays were performed according to the instructions of the manufacturer and without knowledge of who the subject was. The molar ratio of IGF-I to IGFBP-3 was calculated as (0.130 × IGF-I concentration [ng/mL])/(0.036 × IGFBP-3 concentration [ng/mL]).

Statistical Analysis

The characteristics of the study subjects were compared pre–random assignment, according to sex or study group, by using Fisher's exact test for dichotomous characteristics and the Kruskal-Wallis test for quantitative characteristics. Because the distributions of serum concentrations of IGF-I and IGFBP-3 were skewed, the differences between groups were tested by using the Wilcoxon rank sum test. An overall treatment effect over time was determined by comparing the modulation (ie, the value at the subsequent visit minus the value at the baseline evaluation) in serum concentrations of IGF-I and IGFBP-3 and in the molar ratio of IGF-I to IGFBP-3 between the 9-*cis*-RA and placebo groups. All *P* values were determined by two-sided tests. Associations were considered statistically significant at *P* values less than .05. In the multivariate analysis, the variables of sex, age, smoking status, and body mass index (body weight in kg/height in m^2) were included in the model.

RESULTS

Subject Characteristics

The characteristics of eligible subjects were described in detail previously.[29] Of the 226 former smokers enrolled in the original chemoprevention trial, 149 were randomly assigned to placebo or 9-*cis*-RA treatments, and 113 of them completed 3 months of treatment. The characteristics of subjects assessable for our study are detailed in Table 1. Each treatment group was well balanced for sex, race, age, body mass index, and history of smoking. Blood samples from 111 of these subjects (52 women and 59 men; 56 from the 9-*cis*-RA group and 55 from the placebo group) at the baseline of the study, and from 84 (40 women and 44 men; 41 from the 9-*cis*-RA group and 43 from the placebo group) after 3 months of treatment were assessable for serum concentrations of IGF-I and IGFBP-3. The two treatment groups had comparable baseline mean serum concentrations of IGF-I and IGFBP-3 and similar molar ratios of IGF-I to IGFBP-3 (Table 2).

To determine whether subject characteristics affected the baseline serum concentrations of IGF-I or IGFBP-3, we evaluated the correlation between certain variables (eg, sex, race, age, body mass index, pack-years of smoking, and number of years since stopping smoking) and the baseline serum concentrations of IGF-I and IGFBP-3 and the molar ratio of IGF-I to IGFBP-3 (Table 3). The baseline serum concentration of IGF-I and the molar ratio of IGF-I to IGFBP-3 were significantly lower in women, whereas the IGFBP-3 concentration was slightly higher, though the difference did not reach statistical significance. Moreover, the serum concentration of IGF-I and the molar ratio of IGF-I to IGFBP-3 in women significantly decreased with increasing age (Fig 1A). Because serum concentrations of IGF-I are reduced in women treated with hormone replacement therapy (HRT),[36,37] we analyzed whether the changes in the baseline serum concentration of IGF-I and the baseline molar ratio of IGF-I to IGFBP-3 were associated with HRT use among women. Self-reported data for HRT use were available for 38 of the 52 women (Table 3). Overall, baseline serum concentrations IGF-I and molar ratios of IGF-I to IGFBP-3 concentrations were significantly lower in the HRT users than the non–HRT users (Fig 1B). Among HRT users, differences in the IGFBP-3 concentrations were not significantly different. The mean baseline serum concentrations of IGF-I and IGFBP-3, and the molar ratio of IGF-I to IGFBP-3 in the HRT users are summarized in Table 3. Race, body mass index, number of pack-years, and years since stopping smoking did not affect the serum concentrations of IGF-I and IGFBP-3 or the molar ratio of IGF-I to IGFBP-3 in the study population.

Effect of 9-cis-RA on IGF-I and IGFBP-3 Serum Concentrations and on the IGF-I to IGFBP-3 Molar Ratio

The primary end point of the original lung cancer chemoprevention trial was restoration of RARβ expression in the bronchial epithelium.[29] In the previous study, we demonstrated that, compared with the effect of placebo, the median change in receptor index was significantly different from placebo for 9-*cis*-RA but not for 13-*cis*-RA plus AT,[29] raising the possibility that 9-*cis*-RA has potential chemopreventive properties in former smokers.

In the current study, we evaluated the serum concentrations of the IGF axis in former smokers during treatment with 9-*cis*-RA. The modulations in mean serum concentrations of IGF-I and IGFBP-3 and in the molar ratio of IGF-I to IGFBP-3 in the two treatment groups during 3 months of treatment are illustrated in Figure 2. The mean changes in the placebo and 9-*cis*-RA groups are summarized in Table 4. Compared with the placebo group, the 9-*cis*-RA group exhibited a statistically significant modulation in the IGF axis. The mean changes from the study's baseline to the end of 3 months of treatment in the placebo and 9-*cis*-RA groups were as follows: IGF-I, 14.3 and −19.2, respectively; IGFBP-3, −175.1 and 196.6, respectively; and molar ratio of IGF-I to IGFBP-3, 0.05 and −0.06, respectively. These findings suggested that 9-*cis*-RA increases serum concentrations of IGFBP-3 and decreases serum concentrations of IGF-I, thus reducing the molar ratio of IGF-I to IGFBP-3.

To determine whether the differences in the serum concentrations of IGFBP3 between untreated and treated groups reflected differences at the tissue level, we also performed immunohistochemical analysis of IGFBP3, using the methodology described previously for lung cancer

Table 1. Characteristics of Subjects According to Treatment Group

Characteristic	Placebo (n = 61) No.	Placebo (n = 61) %	9-*cis*-RA (n = 52) No.	9-*cis*-RA (n = 52) %	*P**
Sex					
Male	37	60.7	27	51.9	.35
Female	24	39.3	25	48.1	
Race					
White	52	85.3	49	94.2	
African American	6	9.8	2	3.9	.35
Hispanic	3	4.9	1	1.9	
Asian	0	0.0	0	0.0	
Smoking-related cancer					
No	54	88.5	48	92.3	.54
Yes	7	11.5	4	7.7	
Age, years					
Mean	58.1		55.7		.12
SD	8.9		9.2		
Median	58.8		54.9		
Range	34.9-73.6		35.9-74.5		
BMI					
Mean	27.8		28.1		.92
SD	4.1		5.38		
Median	27.1		27.3		
Range	20.6-39.4		19.4-44.4		
Smoking years					
Mean	29.1		27.3		.39
SD	9.8		9.5		
Median	30		26		
Range	15-50		10-50		
PPD					
Mean	1.7		1.9		.23
SD	0.7		0.8		
Median	1.5		2		
Range	1-4		0.8-4		
Pack-years					
Mean	50.2		52.6		.94
SD	27.2		30.5		
Median	42.5		42		
Range	20-135		20-136		
Smoking quit years					
Mean	10.4		11.0		.56
SD	8.8		8.7		
Median	10.1		7.8		
Range	1.1-35.2		1.0-38.2		

Abbreviations: 9-*cis*-RA, 9-*cis*-retinoic acid; SD, standard deviation; BMI, body mass index; PPD, packs per day.
*The Wilcoxon rank-sum test was performed to test continuous variables between two treatment groups. The χ^2 test (for sex) and Fisher's exact test (for race and smoking-related cancer) were performed to test the association between two categorical variables.

samples,[20] in more than 90% of the cases. The intensity of IGFBP-3 expression in the normal and hyperplastic epithelial tissue samples was high, and differences between placebo– and 9-*cis*-RA–treated groups were not significant (data not shown). We suggest that the reason for the apparent discrepancy between the results of the plasma concentration analysis reported in this article and the tissue analysis is the higher sensitivity and dynamic range of the enzyme-linked immunosorbent assay for the plasma IGFBP3 and IGF1 compared with the limited dynamic range of the immunohistochemical analysis. In addition, the sources of IGF1 and IGFBP-3 in the blood include the liver and other tissues and is not expected to be directly related to expression in bronchial epithelial cells.

Correlation Between Changes in Tissue Level of RAR-β and Modulation of the IGF Axis Induced by 9-cis-RA

We further evaluated the association between the changes in serum concentrations of the IGF axis peptides

Table 2. The Baseline Serum Concentration of IGF-I, IGFBP-3, and IGF-I:IGFBP-3 Molar Ratio in the Study Population According to Treatment Group

	Placebo (n = 55)			9-*cis*-RA (n = 56)			
	Mean	SD	95% CI	Mean	SD	95% CI	*P**
IGF-I, ng/mL	208.8	123.3	175.4 to 242.1	236.0	117.8	204.4 to 267.5	.87
IGFBP-3, ng/mL	2,416.5	826.2	2,193.2 to 2,639.9	2,415.5	636.2	2,245.1 to 2,585.9	.23
IGF-I:IGFBP-3	0.33	0.20	0.28 to 0.39	0.38	0.20	0.32 to 0.43	.22

Abbreviations: 9-*cis*-RA, 9-*cis*-retinoic acid; SD, standard deviation; IGFBP-3, insulin-like growth factor binding protein 3; IGF-I, insulin-like growth factor I.
**P* was obtained from the Wilcoxon rank sum test.

and changes in the tissue expression level of RARβ during 9-*cis*-RA treatment. To determine the effect of treatment on loss of RARβ expression at any biopsy site, the subjects were grouped according to whether their biopsy samples were positive (ie, RARβ was detected in all six biopsy sites) or negative (ie, RARβ was not detected in at least one biopsy site) for RARβ expression, and the effects of treatment on RARβ expression was determined as a binary variable (ie, loss of RARβ expression at any biopsy site). The modulation of serum concentrations of IGF-I and IGFBP-3 and the molar ratio of IGF-I to IGFBP-3 were not significantly correlated with baseline RARβ expression (Fig 3A) or with the changes in tissue RARβ expression induced by 9-*cis*-RA (Fig 3B).

DISCUSSION

Our main finding in this analysis of data collected from a completed chemoprevention trial assessing the benefits of 9-*cis*-RA for former smokers was that the IGF axis can be modulated by 9-*cis*-RA in a population of former smokers. To our knowledge, this is the first report showing modulation of the IGF axis by 9-*cis*-RA in the setting of a chemoprevention trial.

Growing evidence supports an association between the IGF axis and the risk for lung cancer[8] and suggests that the development of agents targeting the IGF axis could be an effective strategy in chemoprevention of the disease. Therefore, retinoids, shown to regulate the IGF axis in vitro[22,38,39]

Table 3. Association Between Baseline IGF-I, IGFBP-3, and IGF-I:IGFBP-3 Molar Ratio and Subjects' Demographic Characteristics

	IGF-I			IGFBP-3			IGF-I:IGFBP-3		
Characteristic	Mean	SD	*P*	Mean	SD	*P*	Mean	SD	*P*
Sex									
Male (n = 59)	261.3	108.2	.0002	2,373.4	784.7	.52	0.43	0.19	< .0001
Female (n = 52)	178.5	120.1		2,464.4	674.2		0.28	0.19	
HRT									
HRT use (n = 23)	139.9	89.22	.004	2,331	770.6	.16	0.23	0.13	.009
No HRT use (n = 15)	282.9	139.8		2,523	556.4		0.43	0.25	
Race									
White (n = 98)	220.0	122.4	.51	2,439.1	732.2	.51	0.35	0.21	.46
African American (n = 9)	261.6	107.4		2,356.3	740.0		0.39	0.06	
Hispanic (n = 4)	196.3	118.6		1,983.8	798.3		0.35	0.23	
Age, years									
< 60 (n = 71)	228.2	118.8	.47	2,353.6	658.3	.43	0.37	0.21	.22
≥ 60 (n = 40)	212.4	125.1		2,526.8	847.6		0.32	0.20	
BMI									
< 28 (n = 64)	235.1	117.4	.20	2,360.9	660.6	.51	0.38	0.20	.16
≥ 28 (n = 42)	206.7	129.8		2,483.4	854.0		0.33	0.22	
Pack-years									
< 40 (n = 46)	234.3	125.9	.39	2,388.9	624.2	.81	0.37	0.20	.44
≥ 40 (n = 65)	214.2	117.3		2,435.2	805.6		0.35	0.20	
Years quit smoking									
< 10 (n = 61)	216.8	121.7	.60	2,434.8	770.0	.85	0.35	0.21	.89
≥ 10 (n = 50)	229.4	120.5		2,393.1	692.6		0.36	0.20	

NOTE. *P* was obtained from the Wilcoxon rank sum test.
Abbreviations: IGF-I, insulin-like growth factor-I; IGFBP-3, insulin-like growth factor binding protein-3; SD, standard deviation; BMI, body mass index.

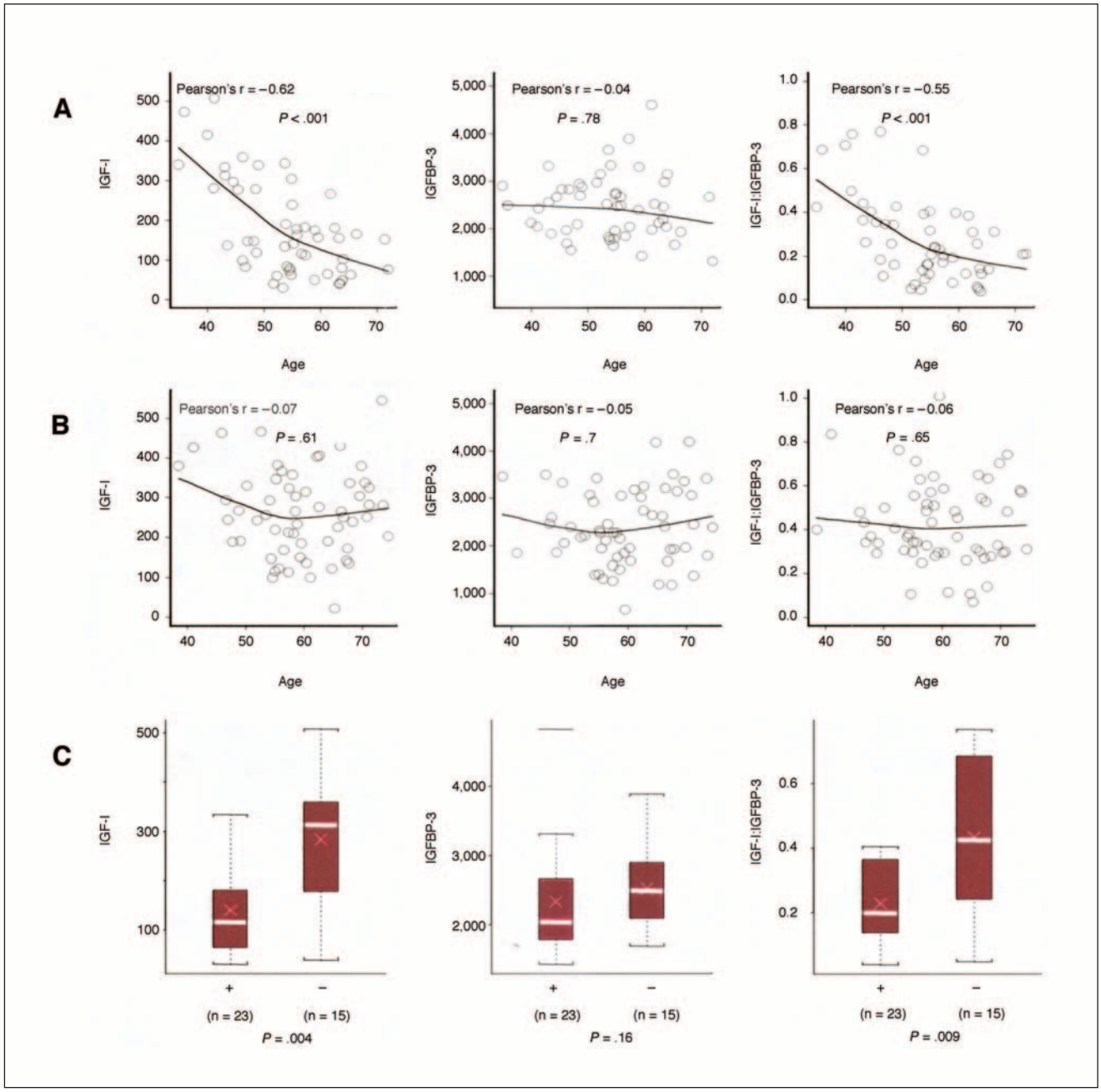

Fig 1. Effect of subject characteristics on the baseline serum concentrations of IGF-I and IGFBP-3 the molar ratio of IGF-I to IGFBP-3. Correlation between age and the baseline serum concentrations of IGF-1 (ng/mL) and IGFBP-3 (ng/mL) and the molar ratio of IGF-I to IGFBP-3 by increasing age in (A) female and (B) male subjects. (C) Effect of HRT use on the baseline serum concentrations of IGF-1 (ng/mL) and IGFBP-3 (ng/mL) and on the IGF-I to IGFBP-3 ratio. "+" indicates HRT use and "−" indicates no HRT use. IGF, insulin-like growth factor; IGFBP, IGF binding protein; HRT, hormone replacement therapy.

have a potential to exert chemopreventive activities. Indeed, several findings have demonstrated the potential use of retinoids as chemopreventive agents. For example, 9-*cis*-RA has shown antiproliferative activity against a broad range of neoplastic cells, including those from prostate cancer,[40] breast cancer,[41,42] leukemia and lymphoma,[43] lung cancer,[44] and head and neck cancer.[45] In vivo, 9-*cis*-RA has substantial anticarcinogenic activity in rat mammary glands[46,47] and rat colons.[48] More recently, the synthetic retinoid fenretinide has been shown to modulate circulating IGF-I and IGFBP-3 concentrations in breast cancer patients,[49,50] and the relative risk of a second breast cancer was 35% lower in premenopausal women treated with fenretinide than in those who received no treatment.[51] Thus, from the standpoint of directing future chemoprevention trials, our findings are important because we have

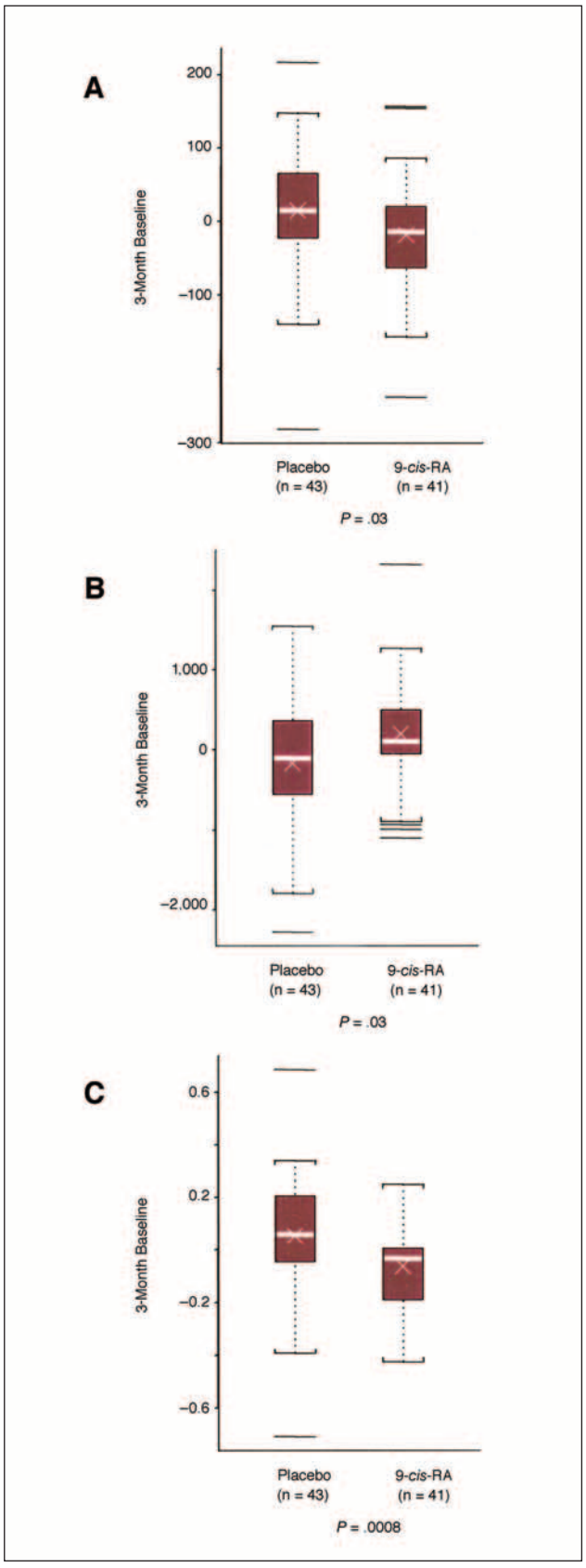

shown both that clinical trials targeting the IGF axis in former smokers are feasible and that 9-*cis*-RA can modulate the IGF axis in this population.

To determine whether the characteristics of subjects affected the baseline IGF axis, we evaluated many variables, such as sex, age, nutritional status, and growth hormone secretion level, which have all been shown to affect the serum concentrations of IGF-I.[52] The baseline serum level of IGF-I and the molar ratio of IGF-I to IGFBP-3 were significantly lower in women than in men. Estrogen is most likely responsible for the sex-related difference in the serum concentration of IGF-I. Endogenous estrogens have been shown to directly regulate circulating IGF-I synthesis[53] and oral administration of estrogen decreases IGF-I serum concentrations.[54,55] In our study, 38 of the 52 women took HRT during the treatment period, and the serum concentrations of IGF-I were significantly lower for HRT users than for non-HRT users. Therefore, the significant difference in serum concentrations of IGF-I and the molar ratio of IGF-I to IGFBP-3 might have resulted from the HRT. The role of estrogen in regulating the IGF-I level is further supported by the recent finding that the IGF-I concentrations of women using HRT were significantly lower than those of women not using HRT.[37] Studies have suggested that HRT use is associated with a decreased risk for several types of cancer, including lung cancer, through decreases in the production of IGF-I.[56,57] Therefore, if a high level of IGF-I is a putative risk factor for lung cancer, HRT use appears to lower IGF-I concentrations, thereby decreasing lung cancer risk.

We also observed that baseline serum concentrations of IGF-I and the molar ratio of IGF-I to IGFBP-3 were significantly decreased with increasing age in women. Duration of HRT use is also likely responsible for the age-related difference in the serum concentration of IGF-I in a female population because older women may conceivably have used HRT for a longer time. The decrease in IGF-I concentrations with aging has been described many times,[49,58,59] and may be due in part to decreased growth hormone levels.[60] In normal subjects, the interaction between growth hormone

Fig 2. Effect of 9-*cis*-retinoic acid (9-*cis*-RA) on the modulation of the IGFBP-3 concentration, IGF-I concentration, and the IGF-I to IGFBP-3 ratio after the 3 months of treatment. The distributions of serum concentrations of IGF-I and IGFBP-3 and of the IGF-I to IGFBP-3 ratio are presented using box plots. The top and bottom edges of the box portion of the plots represent the 75th and 25th percentiles, respectively, of the distributions. The vertical bars extend to the 90th and 10th percentiles. The *P* value was obtained by using the Wilcoxon rank sum test comparing baseline values and the modulation of IGFBP-3 concentration, IGF-I concentration, and the IGF-I to IGFBP-3 ratio between the 9-*cis*-RA and placebo groups. After 3 months of treatment with 9-*cis*-RA, the serum level of IGF-I and the IGF-I to IGFBP-3 ratio were significantly lower ($P = .03$ and $P < .01$, respectively) in the group receiving 9-*cis*-RA than in the placebo group, whereas the serum level of IGFBP-3 was significantly higher ($P = .03$). X, variables; horizontal line, medians of the variables; IGF, insulin-like growth factor; IGFBP, IGF binding protein.

Table 4. Modulation of Serum Concentration of IGF-I, IGFBP-3, and IGF-I:IGFBP-3 Molar Ratio in the Study Population According to Treatment Group

	Placebo (n = 43)				9-*cis*-RA (n = 41)				
	Mean	SD	Median	Range	Mean	SD	Median	Range	*P**
IGF-I (ng/mL)	14.3	85.0	14.5	−282.4-216.5	−19.2	78.3	−14.7	−238.9-156.1	.03
IGFBP-3 (ng/mL)	−175.1	790.9	−109.7	−2,277.2-1,548.9	196.6	657.5	100.1	−1,099.4-2,325.7	.03
IGF-I:IGFBP-3†	0.05	0.2	0.06	−0.7-0.7	−0.06	0.2	−0.03	−0.4-0.3	.0008

Abbreviations: 9-*cis*-RA, 9-*cis*-retinoic acid; SD, standard deviation; IGFBP-3, insulin-like growth factor binding protein 3; IGF-I, insulin-like growth factor I.
**P* comparing the differences between the baseline and the 3rd month values were obtained from the Wilcoxon rank sum test.
†IGF-I:IGFBP-3 = 0.13 IGF-I/0.036 IGFBP3.

and its specific hepatic receptor stimulates expression of the *IGF-I* gene and the release of the IGF-I polypeptide.[52] Therefore, it is likely that the concentration of IGF-I declines with age, as do secretions of growth hormone. However, we have not observed a significant correlation between the age of the study population in men and serum concentrations of IGF-I and IGFBP-3 or the molar ratio of IGF-I to IGFBP-3 in our study.

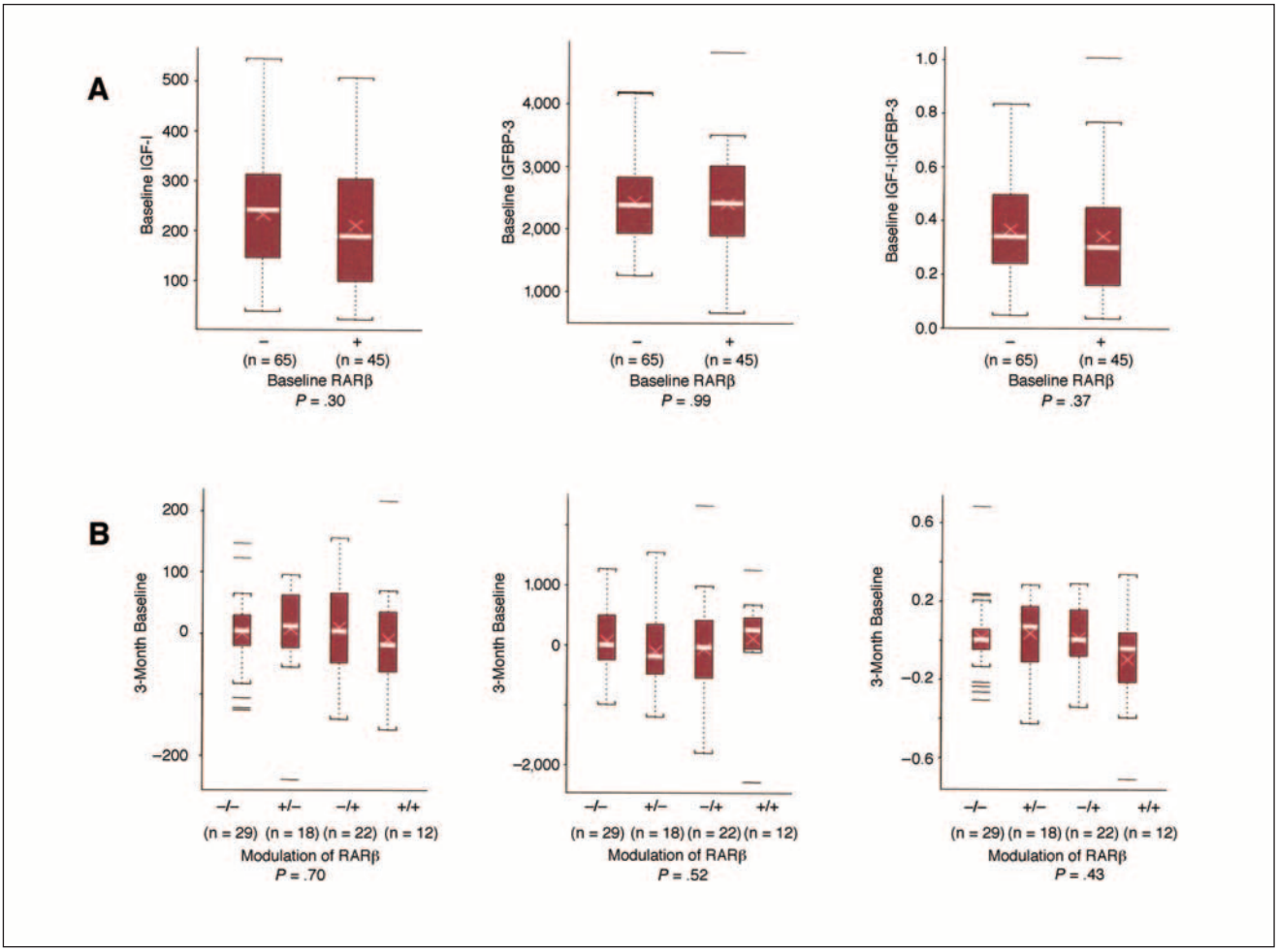

Fig 3. Correlation between RARβ expression in tissue and modulation of the IGF-axis. (A) A Wilcoxon rank sum test was performed to test the statistical significance of the changes in the median RARβ expression in tissues from baseline to after 3 months of treatment. (B) Kruskal-Wallis test was performed comparing the modulations in the median IGFBP-3 concentration, IGF-I concentration, and IGF-I to IGFBP-3 ratio from baseline to 3 months after treatment with the modulation in median RARβ expression in tissue. Subjects were grouped according to their levels of RARβ expression at baseline and at 3 months after treatment (+/+, +/−, −/+, −/−), "+" indicates that RARβ was detected in all six biopsy sites; "−" indicates that RAR-β was not detected in at least one biopsy site. The number of subjects with each combination of RARβ expression is given. RARβ, retinoic acid receptor; IGF, insulin-like growth factor; IGFBP, IGF binding protein.

Growth hormone deficiency is also associated with a decreased muscle mass and increased body fat,[61] and it has been hypothesized that low IGF-I concentrations are associated with high body fat, weight gain over time, and high body mass index.[62] This hypothesis was supported by a study of Swedish men and women, which showed an inverse association between IGF-I concentrations and body mass index.[53] However, we have not observed such correlation between IGF-I and body mass index, similar to the Rancho Bernardo study.[59]

The effects of smoking on serum concentrations of IGF-I are unclear. A positive association between IGF-I concentrations and pack-years of smoking and a negative association between pack-years or the number of cigarettes/d and concentrations of IGFBP-3 have been shown.[63] However, an inverse association between IGF-I concentrations and smoking has been also reported among men, although not among women.[53] Recently, Holmes et al[58] showed that lower serum concentrations of IGF-I are significantly associated with smoking. In our study subjects, we observed a very modest decrease in IGF-I concentrations and an increase in IGFBP-3 concentrations associated with pack-years. However, smoking history generally did not affect the serum concentrations of IGF-I and IGFBP-3 or the molar ratio of IGF-I to IGFBP-3.

We observed that subjects in the 9-*cis*-RA group had a significant decrease in their IGF-I serum concentration, an increase in their IGFBP-3 serum concentration, and a decrease in the molar ratio of IGF-I to IGFBP-3 compared with subjects in the placebo group. The magnitude of the 9-*cis*-RA–induced changes in the IGF axis was moderate. This may be a consequence of the substantial interindividual variability in concentrations of 9-*cis*-RA and IGFs, which is at least in part genetically driven.[33] Given the potential therapeutic activity of both exogenous growth hormone and IGF-I against heart failure[64] and the long-term positive association between the decline in serum IGF-I concentrations and aging,[65] a moderate yet durable effect of 9-*cis*-RA on the IGF axis may be desirable in a preventive context.

Although the exact mechanisms underlying the modulation of the IGF axis by 9-*cis*-RA are unclear, several in vitro results suggest the ability of retinoids to regulate the IGF axis; retinoids have been shown to regulate the expression of IGFBPs[22,23,66]; likewise, IGFs have been shown to modulate the cellular response of RAs, and vice versa.[24] The induction of IGFBP-3 expression is activated by retinoids. We previously demonstrated that all-*trans*-RA increases *IGFBP-3* expression at a transcriptional level through a RAR-α-dependent signaling pathway.[22] It is well known that the cellular effects of RAs are mediated by RXRs and RARs. 9-*cis*-RA is a ligand for both RXRs and RARs, but its affinity for RXRs is 40-fold higher than for RARs. On the other hand, RA is primarily a ligand for RARs and only activates RXRs at high concentrations.[67] Recently, the vitamin D receptor has been identified in the *IGFBP-3* promoter, and RXR has been shown to be required for 1,25-dihydroxyvitamin D_3–induced gene transcription.[68] Therefore, treatment with 9-*cis*-RA could lead to there being available ligand for activation of both the RAR:RXR and the VDR:RXR heterodimeric complex, so that *IGFBP-3* gene transcription could be efficiently activated.

Given the inverse association between estrogen and serum IGF-I concentrations, the ability of 9-*cis*-RA to regulate type 1 17β-hydroxysteroid dehydrogenases,[69] which catalyzes the conversion of estrone and 17β-estradiol, could increase the level of 17β-estradiol, the physiologically significant molecule of estrogen, and thereby decrease IGF-I concentrations. The ability of estrogens to increase the expression of vitamin D receptors in vitro[70] may also contribute to decreased concentrations of IGF-I by inducing IGFBP-3 expression.[71] Additional work will be necessary to investigate the mechanism that mediates the regulation of the IGF axis by 9-*cis*-RA in former smokers.

Because 9-*cis*-RA treatment increased the tissue expression of RARβ, we also explored the correlation between tissue levels of RARβ and serum concentrations of the IGF axis. However, we did not find any significant correlation between the modulation of the serum concentrations of IGF-I or IGFBP-3 and RARβ expression in the tissue. These findings provide evidence that the mechanisms involved in 9-*cis*-RA–mediated gene expression are diverse and complex.

In conclusion, we are the first to show that 3 months of treatment with 9-*cis*-RA decreased the serum level of IGF-I and the molar ratio of IGF-I to IGFBP-3 and increased the serum level of IGFBP-3 in former smokers. These effects may contribute to the chemopreventive benefit of 9-*cis*-RA to former smokers. Despite these promising findings, enthusiasm for the use of 9-*cis*-RA as a chemopreventive agent for lung cancer could be tempered by the toxic effects of the agent.[29] Although there were no serious side effects such as cardiovascular problems, pancreatitis, or death in the subjects treated with 9-*cis*-RA in our previous prevention study, and only one patient with grade 4 hypertriglyceridemia stopped 9-*cis*-RA treatment, it would be better to develop newer agents that are related to 9-*cis*-RA but that do not have the toxic effects of 9-*cis*-RA. Because 9-*cis*-RA can activate both RARs and RXRs and because the toxicities are thought to be mediated by RAR-RXR heterodimers, it had been suggested that "pure" RXR selective synthetic retinoids may exert the beneficial effects of retinoids without the toxicities. Indeed, a group of RXR-selective retinoids ("rexinoids") has demonstrated efficacy with fewer adverse effects in patients with NSCLC in early clinical trials.[72] Therefore, whether rexinoids regulate the IGF axis and thereby reduce lung cancer risk would be a worthwhile topic for future chemoprevention trials in former smokers. In addition, because Ras-mediated signaling pathways may participate in the development of resistance to IGFBP-3,[73] the combination

of RXR-selective agonists and inhibitors of the Ras-mediated signaling pathway could also be considered. Clearly, additional work will be necessary to determine whether the modulation of the IGF axis by 9-*cis*-RA correlates with the ability to reduce lung cancer risk in former smokers. In addition, further investigation into the role of serum concentrations of IGF-I and IGFBP-3 as surrogate biomarkers in determining the chemopreventive effects of retinoids are warranted.

Authors' Disclosures of Potential Conflicts of Interest

The authors indicated no potential conflicts of interest.

REFERENCES

1. Khuri FR, Herbst RS, Fossella FV: Emerging therapies in non-small-cell lung cancer. Ann Oncol 12:739-744, 2001

2. Parkin DM, Pisani P, Ferlay J: Estimates of the worldwide incidence of 25 major cancers in 1990. Int J Cancer 80:827-841, 1999

3. Ginsberg RJ, Vokes EE, Kenneth R: Non-small cell lung cancer, in DeVita VT Jr, Hellman S, Rosenberg SA (eds): Cancer: Principles and Practice of Oncology (ed 6). Philadelphia, PA, Lippincott Williams & Wilkins, 2001, pp 925-983

4. Mattson ME, Pollack ES, Cullen JW: What are the odds that smoking will kill you? Am J Public Health 77:425-431, 1987

5. Wistuba II, Lam S, Behrens C, et al: Molecular damage in the bronchial epithelium of current and former smokers. J Natl Cancer Inst 89:1366-1373, 1997

6. Sekido Y, Fong KM, Minna JD: Progress in understanding the molecular pathogenesis of human lung cancer. Biochim Biochim Biophys Acta 1378:21-59, 1998

7. Burns DM: Primary prevention, smoking, and smoking cessation: Implications for future trends in lung cancer prevention. Cancer 89: 2506-2509, 2000

8. Ibrahim YH, Yee D: Insulin-like growth factor-I and cancer risk. Growth Horm IGF Res 14:261-269, 2004

9. Butt AJ, Firth SM, Baxter RC: The IGF axis and programmed cell death. Immunol Cell Biol 77:256-262, 1999

10. Lopez T, Hanahan D: Elevated levels of IGF-1 receptor convey invasive and metastatic capability in a mouse model of pancreatic islet tumorigenesis. Cancer Cell 1:339-353, 2002

11. Samani AA, Chevet E, Fallavollita L, et al: Loss of tumorigenicity and metastatic potential in carcinoma cells expressing the extracellular domain of the type 1 insulin-like growth factor receptor. Cancer Res 64:3380-3385, 2004

12. Yu H, Spitz MR, Mistry J, et al: Plasma levels of insulin-like growth factor-I and lung cancer risk: A case-control analysis. J Natl Cancer Inst 91:151-156, 1999

13. Wu X, Tortolero-Luna G, Zhao H, et al: Serum levels of insulin-like growth factor I and risk of squamous intraepithelial lesions of the cervix. Clin Cancer Res 9:3356-3361, 2003

14. Pollak M: Insulin-like growth factors (IGFs) and prostate cancer. Epidemiol Rev 23:59-66, 2001

15. Lukanova A, Lundin E, Toniolo P, et al: Circulating levels of insulin-like growth factor-1 and risk of ovarian cancer. Int J Cancer 101:549-554, 2002

16. Zhao H, Grossman HB, Spitz MR, et al: Plasma levels of insulin-like growth factor-1 and binding protein-3, and their association with bladder cancer risk. J Urol 169:714-717, 2003

17. Kaaks R, Toniolo P, Akhmedkhanov A, et al: Serum C-peptide, insulin-like growth factor (IGF)-I, IGF binding proteins, and colorectal cancer risk in women. J Natl Cancer Inst 92:1592-1600, 2000

18. Chang YS, Wang L, Mao L, et al: Mechanisms underlying lack of insulin like-growth factor binding protein-3 expression in NSCLC cells. Oncogene 23:6569-6580, 2004

19. Chang YS, Wang L, Liu D, et al: Correlation between IGFBP-3 promoter methylation and prognosis of patients with stage I non-small cell lung cancer. Clin Cancer Res 8:3669-3675, 2002

20. Chang YS, Gong K, Sun S, et al: Clinical significance of IGFBP-3 expression in stage I non-small cell lung cancer. Clin Cancer Res 8:3796-3802, 2002

21. Lee HY, Chun KH, Liu B, et al: Insulin-like growth factor binding protein-3 inhibits the growth of non-small cell lung cancer. Cancer Res 62:3530-3537, 2002

22. Han G-R, Dohi DF, Lee H-Y, et al: All-trans-retinoic acid increases transforming growth factor-β2 and insulin-like growth factor binding protein-3 expression through a retinoic acid receptor-β-dependent signaling pathway. J Biol Chem 272:13711-13716, 1997

23. Fontana JA, Burrows-Mezu A, Clemmons DR, et al: Retinoid modulation of insulin-like growth factor-binding proteins and inhibition of breast carcinoma proliferation. Endocrinology 128:1115-1122, 1991

24. Bentel JM, Lebwohl DE, Cullen KJ, et al: Insulin-like growth factors modulate the growth inhibitory effects of retinoic acid on MCF-7 breast cancer cells. J Cell Physiol 165:212-221, 1995

25. Nagy L, Thomazy VA, Heyman RA, et al: Retinoid-induced apoptosis in normal and neoplastic tissues. Cell Death Differ 5:11-19, 1998

26. Hansen LA, Sigman CC, Andreola F, et al: Retinoids in chemoprevention and differentiation therapy. Carcinogenesis 21:1271-1279, 2000

27. Mangelsdorf DJ, Evans RM: The RXR heterodimers and orphan receptors. Cell 83:841-850, 1995

28. Marchetti MN, Samplo E, Bun H, et al: In vitro metabolism of three major isomers of retinoic acid in rats: Intersex and interstrain comparison. Drug Metab Dispos 25:637-646, 1997

29. Kurie JM, Lotan R, Lee JJ, et al: Treatment of former smokers with 9-cis-retinoic acid reverses loss of retinoic acid receptor-βexpression in the bronchial epithelium: Results from a randomized placebo-controlled trial. J Natl Cancer Inst 95:206-214, 2003

30. Seewaldt VL, Johnson BS, Parker MB, et al: Expression of retinoic acid receptor beta mediates retinoic acid-induced growth arrest and apoptosis in breast cancer cells. Cell Growth Differ 6:1077-1088, 1995

31. Juul A, Dalgaard P, Blum W, et al: Serum levels of insulin-like growth factor (IGF)-binding protein-3 (IGFBP-3) in healthy infants, children, and adolescents: The relation to IGF-I, IGF-II, IGFBP-1, IGFBP-2, age, sex, body mass index, and pubertal maturation. J Clin Endocrinol Metab 80:2534-2542, 1995

32. Zi X, Zhang J, Agarwal R, et al: Silibinin up-regulates insulin-like growth factor-binding protein 3 expression and inhibits proliferation of androgen-independent prostate cancer cells. Cancer Res 60:5617-5620, 2000

33. Miller VA, Rigas JR, Benedetti FM, et al: Initial clinical trial of the retinoid receptor pan agonist 9-cis retinoic acid. Clin Cancer Res 6:471-475, 1996

34. National Cancer Institute: Common toxicity criteria, version 2.0. http://ctep.cancer.gov/forms/CTCv20_4-30-992.pdf

35. Baxter RC, Martin JL: Radioimmunoassay of growth hormone-dependent insulin-like growth factor binding protein in human plasma. J Clin Invest 78:1504-1512, 1986

36. Campagnoli C, Biglia N, Altare F, et al: Differential effects of oral conjugated estrogens and transdermal estradiol on insulinlike growth factor 1, growth hormone and sex hormone binding globulin serum levels. Gynecol Endocrinol 7:251-258, 1993

37. Schabath MB, Wu X, Sellin RV, et al: Hormone replacement therapy and lung cancer risk: A case-control analysis. Clin Cancer Res 10:113-123, 2004

38. Zhou Y, Mohan S, Linkhart TA, et al: Retinoic acid regulates insulin-like growth factor-binding protein expression in human osteoblast cells. Endocrinology 137:975-983, 1996

39. Gabbitas B, Canalis E: Retinoic acid regulates the expression of insulin-like growth factors I and II in osteoblasts. J Cell Physiology 172:253-264, 1997

40. Blutt SE, Allegretto EA, Pike JW, et al: 1,25-Dihydroxyvitamin D3 and 9-*cis*-retinoic acid act synergistically to inhibit the growth of LNCaP prostate cells and cause accumulation of cells in G1. Endocrinology 138:1491-1497, 1997

41. Rubin M, Fenig E, Rosenauer A, et al: 9-*cis*-Retinoic acid inhibits growth of breast cancer cells and down-regulates estrogen receptor RNA and protein. Cancer Res 54:6549-6556, 1994

42. Gottardis MM, Lamph WW, Shalinsky DR, et al: The efficacy of 9-*cis*-retinoic acid in experimental models of cancer. Breast Cancer Res Treat 38:85-96, 1996

43. Lutzky J, Vujicic M, Yamanishi DT, et al: Antiproliferative effects of all-*trans*-retinoic acid (tRA) and 9-*cis*-retinoic acid (9-cisRA) on human

lymphoid cell lines. Proc Am Assoc Cancer Res 34:292, 1993 (abstr 1738)

44. Guzey M, Demirpence E, Criss W, et al: Effects of retinoic acid (all-*trans* and 9-*cis*) on tumor progression in small-cell lung carcinoma. Biochem Biophys Res Commun 242:369-375, 1998

45. Giannini F, Maestro R, Vukosavljevic T, et al: All-*trans*, 13-*cis*, and 9-*cis* retinoic acids induce a fully reversible growth inhibition in HNSCC cell lines: Implications for *in vivo* retinoic acid use. Int J Cancer 70:194-200, 1997

46. Anzano MA, Byers SW, Smith JM, et al: Prevention of breast cancer in the rat with 9-*cis*-retinoic acid as a single agent and in combination with tamoxifen. Cancer Res 54:4614-4617, 1994

47. Anzano MA, Peer CW, Smith JM, et al: Chemoprevention of mammary carcinogenesis in the rat: Combined use of raloxifene and 9-*cis*-retinoic acid. J Natl Cancer Inst 88:123-125, 1996

48. Zheng Y, Kramer PM, Olson G, et al: Prevention by retinoids of azoxymethane-induced tumors and aberrant crypt foci and their modulation of cell proliferation in the colon of rats. Carcinogenesis 18:2119-2125, 1997

49. Decensi A, Johansson H, Miceli R, et al: Long-term effects of fenretinide, a retinoic acid derivative, on the insulin-like growth factor system in women with early breast cancer. Cancer Epidemiol Biomarkers Prev 10:1047-1053, 2001

50. Torrisi R, Parodi S, Fontana V, et al: Effect of fenretinide on plasma IGF-I and IGFBP-3 in early breast cancer patients. Int J Cancer 76:787-790, 1998

51. Veronesi U, De Palo G, Marubini E, et al: Randomized trial of fenretinide to prevent second breast malignancy in women with early breast cancer. J Natl Cancer Inst 91:1847-1856, 1999

52. Le Roith D: Seminars in medicine of the Beth Israel Deaconess Medical Center: Insulin-like growth factors. N Engl J Med 336:633-640, 1997

53. Landin-Wilhelmsen K, Wilhelmsen L, Lappas G, et al: Serum insulin-like growth factor I in a random population sample of men and women: Relation to age, sex, smoking habits, coffee consumption and physical activity, blood pressure and concentrations of plasma lipids, fibrinogen, parathyroid hormone and osteocalcin. Clin Endocrinol (Oxf) 41:351-357, 1994

54. Helle SI, Omsjo IH, Hughes SC, et al: Effects of oral and transdermal oestrogen replacement therapy on plasma levels of insulin-like growth factors and IGF binding proteins 1 and 3: a cross-over study. Clin Endocrinol (Oxf) 45:727-732, 1996

55. Raudaskoski T, Knip M, Laatikainen T: Plasma insulin-like growth factor-I and its binding proteins 1 and 3 during continuous non-oral and oral combined hormone replacement therapy. Menopause 5:217-222, 1998

56. Janne PA, Mayer RJ: Chemoprevention of colorectal cancer. N Engl J Med 342:1960-1968, 2000

57. Grodstein F, Newcomb PA, Stampfer MJ: Postmenopausal hormone therapy and the risk of colorectal cancer: A review and meta-analysis. Am J Med 106:574-578, 1999

58. Holmes MD, Pollak MN, Hankinson SE: Lifestyle correlates of plasma insulin-like growth factor I and insulin-like growth factor binding protein 3 concentrations. Cancer Epidemiol Biomarkers Prev 11:862-867, 2002

59. Goodman-Gruen D, Barrett-Connor E: Epidemiology of insulin-like growth factor-I in elderly men and women: The Rancho Bernardo Study. Am J Epidemiol 146:970-976, 1997

60. Bondy CA, Underwood LE, Clemmons DR, et al: Clinical uses of insulin-like growth factor I. Ann Intern Med 120:593-601, 1994

61. Sonksen PH, Salomon F, Cuneo R: Metabolic effects of hypopituitarism and acromegaly. Horm Res 36:27-31, 1991 (suppl 1)

62. Harris T, Kiel D, Roubenoff R, et al: Association of insulin-like growth factor-I with body composition, weight history, and past health behaviors in the very old: The Framingham Heart Study. J Am Geriatr Soc 45:133-139, 1997

63. Kaklamani VG, Linos A, Kaklamani E, et al: Age, sex, and smoking are predictors of circulating insulin-like growth factor 1 and insulin-like growth factor-binding protein 3. J Clin Oncol 17:813-817, 1999

64. Fazio S, Sabatini D, Capaldo B, et al: A preliminary study of growth hormone in the treatment of dilated cardiomyopathy. N Engl J Med 334:809-814, 1996

65. Janssen JA, Stolk RP, Pols HA, et al: Serum free IGF-I, total IGF-I, IGFBP-1 and IGFBP-3 levels in an elderly population: Relation to age and sex steroid levels. Clin Endocrinol (Oxf) 48:471-478, 1998

66. Woodward TL, Turner JD, Hung HT, et al: Inhibition of cellular proliferation and modulation of insulin-like growth factor binding proteins by retinoids in a bovine mammary epithelial cell line. J Cell Physiol 167:488-499, 1996

67. Heyman RA, Mangelsdorf DJ, Dyck JA, et al: 9-*cis* Retinoic acid is a high affinity ligand for the retinoid X receptor. Cell 68:397-406, 1992

68. Pathrose P, Barmina O, Chang CY, et al: Inhibition of 1,25-dihydroxyvitamin D3-dependent transcription by synthetic LXXLL peptide antagonists that target the activation domains of the vitamin D and retinoid X receptors. J Bone Miner Res 17:2196-2205, 2002

69. Piao Y-S, Peltoketo H, Jouppila A, et al: Retinoic acids increase 17β-hydroxysteroid dehydrogenase type 1 expression in JEG-3 and T47D cells, but the stimulation is potentiated by epidermal growth factor, 12-O-tetradecanoulphorbol-13-acetate, and cyclic adenosine 3′, 5′-monophosphate only in JEG-3 cells. Endocrinology 138:898-904, 1997

70. Smirnoff P, Liel Y, Gnainsky J, et al: The protective effect of estrogen against chemically induced murine colon carcinogenesis is associated with decreased CpG island methylation and increased mRNA and protein expression of the colonic vitamin D receptor. Oncol Res 11:255-264, 1999

71. Boyle BJ, Zhao XY, Cohen P, et al: Insulin-like growth factor binding protein-3 mediates 1α,25-dihydroxyvitamin D_3 growth inhibition in the LNCaP prostate cancer cell line through p21/WAF1. J Urol 165:1319-1324, 2001

72. Rizvi NA, Marshall JL, Dahut W, et al: A phase I study of LGD1069 in adults with advanced cancer. Clin Cancer Res 5:1658-1664, 1999

73. Lee H-Y, Moon HJ, Chun K-H, et al: Effects of insulin-like growth factor binding protein-3 and farnesyltransferase inhibitor SCH66336 on Akt expression and apoptosis in non–small-cell lung cancer cells. J Natl Cancer Inst 96:1536-1548, 2004

BRIEF COMMUNICATIONS

Chemopreventive Effects of Deguelin, a Novel Akt Inhibitor, on Tobacco-Induced Lung Tumorigenesis

Ho-Young Lee, Seung-Hyun Oh, Jong K. Woo, Woo-Young Kim, Carolyn S. Van Pelt, Roger E. Price, Dianna Cody, Hai Tran, John M. Pezzuto, Robert M. Moriarty, Waun Ki Hong

Tobacco carcinogens induce Akt activation and lung carcinogenesis. We previously demonstrated that deguelin, a natural plant product, specifically inhibits the proliferation of premalignant and malignant human bronchial epithelial cells by blocking Akt activation. To evaluate the ability of deguelin to block tobacco carcinogen-induced lung tumorigenesis, we evaluated the in vivo effects of deguelin on Akt activation and lung tumorigenesis in transgenic mice in which Akt expression was induced by tamoxifen and in 4-(methylnitrosoamino)-1-(3-pyridyl)-1-butanone (NNK)/benzo(a) pyrene (BaP)-treated A/J mice. Deguelin suppressed Akt activation in vivo, as measured by immunohistochemistry and immunoblotting, and statistically significantly reduced NNK/BaP-induced lung tumor multiplicity, volume, and load in A/J mice, as monitored by microcomputed tomography image analysis, with no detectable toxicity. These results indicate that deguelin warrants consideration as a chemopreventive agent for early-stage lung carcinogenesis in a clinical lung cancer chemoprevention trial. [J Natl Cancer Inst 2005;97:1695–9]

In the United States and western Europe, lung cancer leads all other cancers in both incidence and mortality rate *(1)*, underscoring the need for effective lung cancer chemopreventive agents. Because tobacco smoking confers the greatest risk of developing lung cancer *(2)*, molecules that target pathways involved in tobacco-mediated lung carcinogenesis could be effective lung cancer chemopreventive agents. The PI3K/Akt pathway could be such a target because Akt is activated in premalignant and malignant human bronchial epithelial cells, as well as non–small-cell lung cancer cells, through the activating mutation of ras, overexpression of the epidermal growth factor receptor and subunits of PI3K, inactivation of tumor suppressor genes such as PTEN, or exposure to tobacco carcinogens, all of which are frequent events in lung cancer *(3–9)*. Akt is activated by phosphorylation at two key regulatory sites, Thr^{308} and Ser^{473} *(10)*. Akt promotes cell survival by phosphorylating proapoptotic and antiapoptotic proteins, including the Bcl-2 family member BAD, caspase-9, cAMP response element-binding protein, inhibitor of kappaB kinase complex α, and forkhead transcription factor-1 *(11–19)*.

We and others have shown that pharmacologic and genetic approaches targeting Akt suppress the proliferation of premalignant and malignant human bronchial epithelial cells and reverse characteristics of transformed human bronchial epithelial cells *(20,21),* indicating that inhibitors of Akt could be effective lung cancer chemopreventive agents. We have previously found that deguelin, isolated from several plant species, including *Mundulea sericea* (*Leguminosae*), inhibits the PI3K/Akt pathway and decreases the expression of cyclooxygenase-2, which participates in xenobiotic metabolism, angiogenesis, and inhibition of immune surveillance and apoptosis during tumorigenesis *(22)*. Importantly, deguelin induces apoptosis in premalignant and malignant human bronchial epithelial cells, with minimal effects on normal human bronchial epithelial cells in vitro at dosages attainable in vivo *(23)*. Deguelin has been shown to have cancer chemopreventive activities in the two-stage skin carcinogenesis model *(24)* and in the N-nitroso-N-methylurea-induced rat mammary carcinogenesis model *(25)*. It also exhibits therapeutic activities in colon cancer, melanoma, and lung cancer *(22,26,27)*. These findings led us to hypothesize that deguelin could be an effective lung cancer chemopreventive agent by blocking Akt activation. In the present study, we attempted to test our hypothesis in Akt-inducible transgenic mice, in which Akt is activated by tamoxifen (tmaAkt/Z;CAG::Cre) *(28)*, and in A/J mice, in which lung tumors are induced by 4-(methylnitrosoamino)-1-(3-pyridyl)-1-butanone (NNK) and benzo(a)pyrene (BaP) *(20,29)*.

To test the effects of deguelin on Akt activation in tmaAkt/Z;CAG::Cre mice, we performed immunohistochemical (Fig. 1, A) and immunoblot (Fig. 1, B) analyses with phosphorylated (p)Akt (at Ser473) on lung tissues from tmaAkt/Z;CAG::Cre mice treated with 4 mg/kg of deguelin for 3 days. pAkt staining was homogeneous in the bronchial epithelium of the control and deguelin-treated mice; however, levels of pAkt in the lung tissues of control mice were higher than in that of deguelin-treated mice. Western blot analysis also showed decreased expression of pAkt in the lungs of deguelin-treated mice, indicating that deguelin affects Akt activation in vivo.

To evaluate the chemopreventive effects of deguelin in the A/J mice, we first evaluated the serum and tissue distribution of deguelin in A/J mice. Fig. 2, A, shows the concentration-time curve of deguelin in serum and various organs after oral gavage administration of 4 mg/kg deguelin, the maximum tolerated dose in rats *(25)*. The total body clearance of deguelin was 0.33 L/kg/hour, the apparent volume of distribution was 1.86 L/kg, and the half-life was 3.98 hours. One hour after the treatment, concentrations of deguelin in

Affiliations of authors: Departments of Thoracic/Head and Neck Medical Oncology (H-YL, S-HO, JKW, W-YK, HT, WKH), Imaging Physics (REP, DC), and Veterinary Medicine and Surgery (CSVP), The University of Texas M. D. Anderson Cancer Center, Houston, TX; Pharmacy Nursing Health Science, Purdue University, West Lafayette, IN (JMP); Department of Medicinal Chemistry and Pharmacognosy, University of Illinois at Chicago, Chicago, IL (RMM).

Correspondence to: Ho-Young Lee, PhD, Department of Thoracic/Head and Neck Medical Oncology, Unit 432, The University of Texas M. D. Anderson Cancer Center, 1515 Holcombe Boulevard, Houston, TX 77030 (e-mail: hlee@mdanderson.org).

See "Notes" following "References."

DOI: 10.1093/jnci/dji377

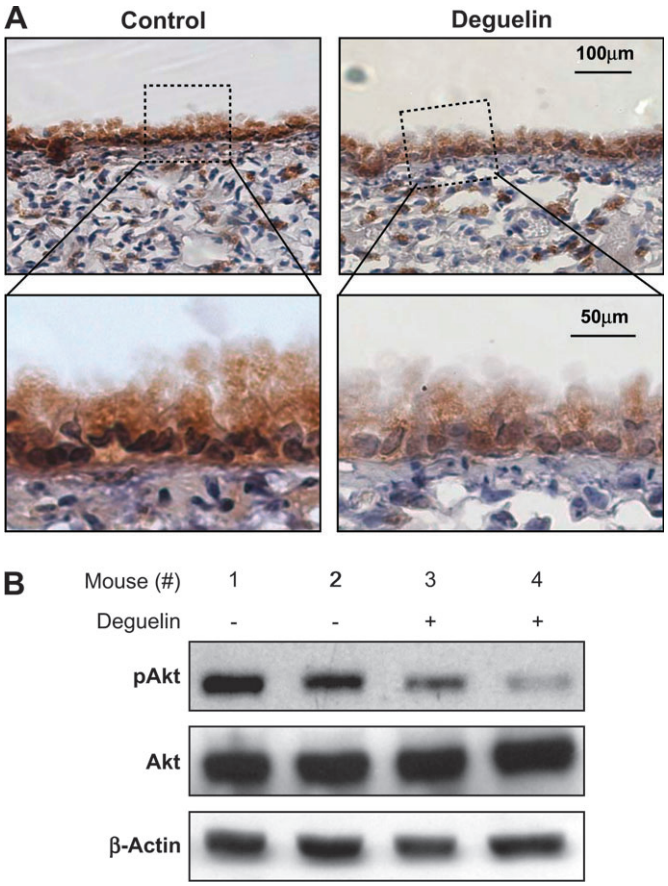

Fig. 1. Effects of deguelin on Akt activation in the transgenic mice expressing tamoxifen-inducible Akt. The mouse line expressing tamoxifen-inducible Akt (tmaAkt/Z;CAG::Cre) was generated by crossing the "master" line (CAG::loxP::CAT::loxP::tmaAkt::IRESLacZ) (provided by Thomas N. Sato, Weill Medical College of Cornell University, New York, NY) to CMV:Cre (distributed by the Mouse Resource Facility at M. D. Anderson Cancer Center, Houston, TX), which led to the expression of inactive (not phosphorylated) Akt by excising the floxed CAT. Six-week-old tmaAkt/Z;CAG::Cre mice were orally treated with deguelin (4 mg/kg) during feeding twice a day for 3 days (five mice/group) and then were injected intraperitoneally with 5 mg of tamoxifen (Sigma, St. Louis, MO). The next day, the mice were killed by CO_2 asphyxiation. Lungs were surgically removed, and **A**) half of each lung was fixed with 10% formaldehyde, embedded in paraffin, sectioned (5-μm thick), and processed for immunohistochemical analysis. The sections were deparaffinized, immersed in methanol containing 0.3% hydrogen peroxide to block endogenous peroxidase activity, and then incubated in blocking serum (Vector Laboratories, Burlingame, CA) to reduce nonspecific antibody binding. The sections were incubated overnight at 4 °C with rabbit polyclonal anti-Akt (diluted 1:100 in 2.5% blocking serum) or rabbit polyclonal anti-phosphorylated Akt (pAkt, Ser473) (diluted 1:200) (Cell Signaling Technology, Beverly, MA) and were then processed using standard avidin-biotin immunohistochemical techniques according to the manufacturer's recommendations (Vector Laboratories, Burlingame, CA). Diaminobenzidine was used as a chromogen, and commercial hematoxylin was used as a counterstain. **B**) The other half of each lung was lysed in 150 m*M* NaCl, 20 m*M* Tris-HCl, pH 7.5, 1% Triton X-100, 1 m*M* phenylmethylsulfonyl fluoride, 10 m*M* EDTA, 0.1 m*M* vanadate, and 1 μg/mL aprotinin by mechanical homogenization. Equivalent amounts of protein were resolved on sodium dodecyl sulfate–polyacrylamide gels (10%) and electrophoretically transferred to nitrocellulose membranes. After membranes were blocked in Tris-buffered saline (TBS) containing 0.05% Tween-20 (TBST) and 5% (w/v) nonfat powdered milk, they were incubated with primary antibodies against pAkt (Ser473) (1:1000) and unphosphorylated Akt (1:1000) (Cell Signaling Technology, Beverly, MA) or with a goat polyclonal anti-β–Actin (1:4000) (Santa Cruz Biotechnology, Inc., Santa Cruz, CA) in TBS–5% nonfat milk at 4 °C for 16 hours. The membranes were then washed three times with TBST and incubated with secondary antibody for 1 hour at room temperature. The goat anti-rabbit immunoglobulin G (IgG) or bovine anti-goat IgG horseradish peroxidase-conjugated complexes were detected using the enhanced chemiluminescence kit (Amersham, Arlington Heights, IL) according to the manufacturer's recommended protocol.

various organs ranged from less than 1 ng/mL in the brain tissue to 57.1 ng/mL in the kidneys. The peak concentration in these organs occurred between 1 hour (lung, heart, and kidney) and 6 hours (liver) after administration. These studies indicate that oral deguelin administration can achieve effective absorption and distribution in several organs, including the lung.

We next tested the chemopreventive effects of deguelin in the A/J mice, in which lung carcinogenesis was induced by NNK and BaP, as previously described *(30)*. Cancer chemopreventive agents are classified as either blocking or suppressing agents *(31)*. Blocking agents, which prevent the metabolic activation of carcinogens and reduce DNA damage, are tested by administering them before or simultaneously with the carcinogen. Suppressing agents, which inhibit the neoplastic progression of premalignant cells, are usually tested by administering them after the carcinogen *(32)*. Hence, deguelin (4 mg/kg twice a day) was administered either 1 week after the first dose of NNK/BaP (entire period, group 3) or after completion of carcinogen administration (postcarcinogen, group 4) (Fig. 2, B). A/J mice untreated (group 1) or treated with NNK plus BaP (group 2) received only the vehicle (corn oil) during this period. Sixteen and/or 20 weeks after the first dose of NNK and BaP, representative A/J mice from groups 1, 2, and 3 were analyzed by microcomputed tomography to monitor changes in the number and size of lung tumor nodules. The lung structure in a control mouse (Fig. 2, C, 1) and tumor nodules (Fig. 2, C, 2) less than 1 mm in diameter in a NNK/BaP-treated mouse *(10)* were easily detected and were consistent with the block-faced image (Fig. 2, C, 3) at 16 weeks. A second NNK/BaP-treated mouse *(33)* had two tumor nodules (0.4 mm and 0.55 mm) at 16 weeks (Fig. 2, C, 4) that became larger (0.4 mm to 0.6 mm and 0.55 mm to 1 mm) at 20 weeks (Fig. 2, C, 5), when a new tumor nodule (0.8 mm) was observed. In contrast, a tumor nodule (1.1 mm) detected at 16 weeks (Fig. 2, C, 6) in the deguelin-treated mouse was not detectable at 20 weeks (Fig. 2, C, 7). All mice were killed at 20 weeks. Gross evaluation revealed no tumors in the lungs of control mice (group 1) and 100% lung tumor formation in NNK/BaP-treated mice (group 2) (Supplementary Fig. 1 and Supplementary Table 1 available at http://jncicancerspectrum.oxfordjournals.org/jnci/content/vol97/issue22). Deguelin-treated mice had fewer lung tumors (Supplementary Fig. 1 and Supplementary Table 1 available at http://jncicancerspectrum.oxfordjournals.org/jnci/content/vol97/issue22); mice in groups 3 and 4 had fewer lung tumor nodules than NNK/BaP-treated mice in group 2 (mean = 4.57 versus mean = 11.0, difference = 6.43, 95% confidence intervals

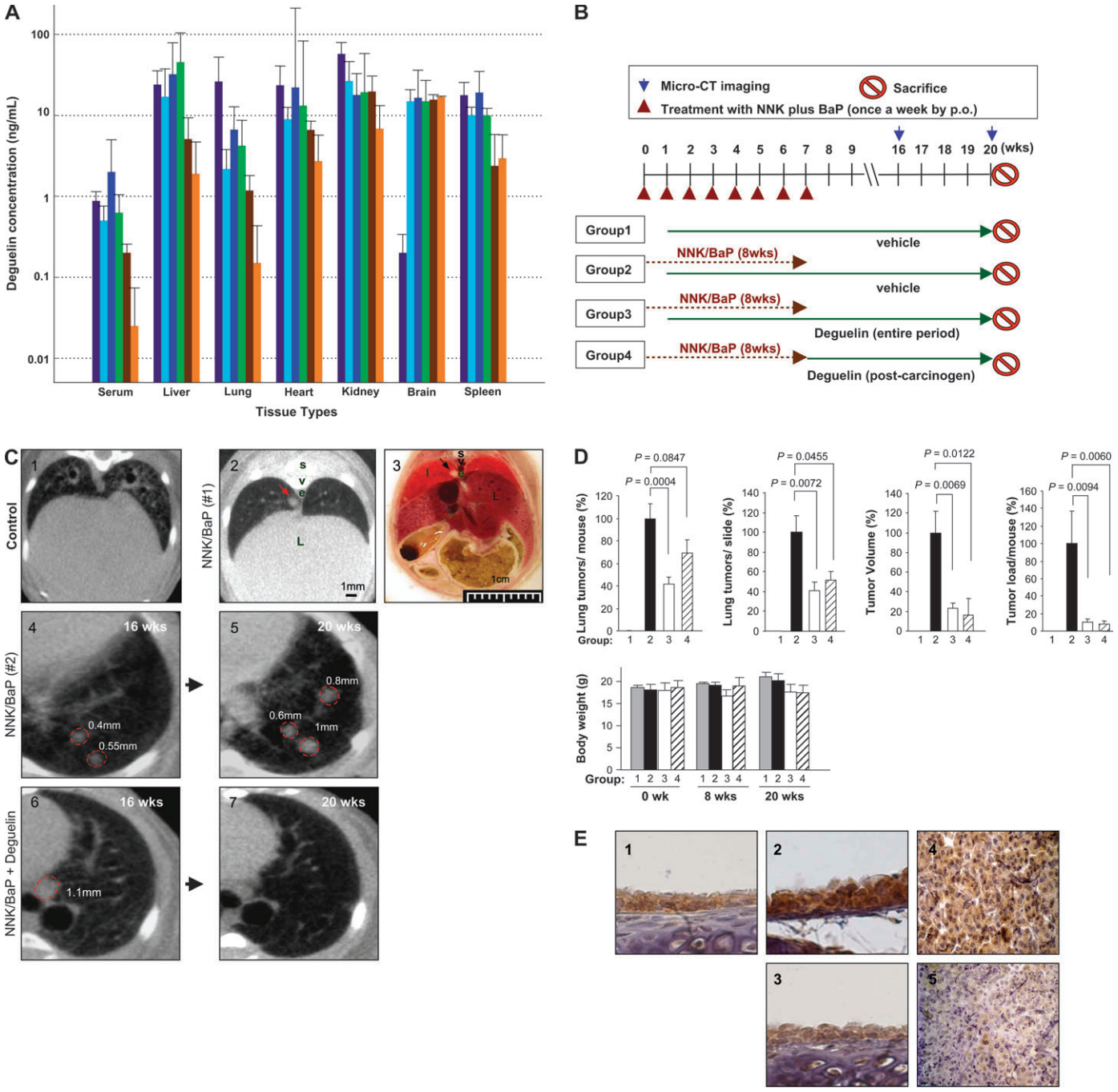

Fig. 2. Evaluation of the chemopreventive effects of deguelin in the A/J mice. **A**) Six-week-old A/J mice were given 4 mg/kg deguelin orally. The serum and indicated organ samples were collected at 0 (baseline), 1 (**purple**), 2 (**turquoise**), 4 (**blue**), 6 (**green**), 12 (**brown**), or 24 (**orange**) hours after deguelin administration. Blood samples were immediately placed on ice and centrifuged at 2000*g* at 4 °C for 15 minutes, and the serum was stored at −70 °C until analysis. The mice were killed prior to organ sample collection. Each organ sample was suspended in acetonitrile, sonicated, and then centrifuged at 1500*g* for 3 minutes at 4 °C. The liquid-tissue extraction process was repeated three times, and each time, 100 μL of supernatant was collected. To the final 300-μL sample, 2700 μL of 0.1 *M* ammonium acetate, pH 5.5, was added. Deguelin was isolated from both serum and organ (liquid-extracted) samples by solid-phase chromatography (tC18 solid-phase extraction [SPE] cartridge, 100 mg, Waters Corp, Millford, MA). After the SPE cartridge was conditioned with 2 mL of methanol and 2 mL of high-performance liquid chromatography-grade water, either 100 μL of serum or 3 mL (a volume of 1 mL pulled through the column each time) of liquid-extracted sample was placed into the SPE cartridge. Deguelin was eluted with 1 mL of methanol, dried, and then reconstituted with a 100-μL mixture of methanol and 0.1% formic acid (50:50, v/v). Thirty microliters of the reconstituted sample was then injected onto a high-performance liquid chromatography mass spectrometer (LC/MS-ES+, MicroMass, Beverly, MA). Standard calibration curves for deguelin ranged from 5 to 1000 ng/mL. The lower limit of quantitation was 0.01 ng/mL. Pharmacokinetic modeling was completed using a noncompartment method (WinNonlin version 3.1, Pharsight Corporation, Mountain View, CA). The results are expressed as means and 95% confidence intervals (CIs), four mice/group. **B–E**) Six-week-old male A/J mice (Jackson Laboratories, Bar Harbor, ME) were randomized into three groups of 12–14 mice (groups 2–4). We included five untreated A/J mice (group 1) as a negative control. Except for group 1, all mice were treated with 4-(methylnitrosoamino)-1-(3-pyridyl)-1-butanone (NNK)/benzo(a)pyrene (BaP) (3 μmol each in 0.1 mL cottonseed oil) once per week for 8 weeks by oral gavage. Vehicle (groups 1 and 2) or deguelin (groups 3 and 4) was administered by oral gavage (4 mg/kg twice a day) beginning 1 week after the first dose of NNK/BaP (entire period) (group 3) or after the last dose of NNK/BaP treatment (postcarcinogen) (group 4) until the end of the experiment. The experimental design is summarized in (**B**). During the experiments, drinking water was available ad libitum, and the body weights of the mice were measured at 0, 8, and 20 weeks. Arrows indicate the time points at which microcomputed tomography (CT) image analysis was performed. **C**) Registered axial respiratory-gated micro-CT image and block-faced image analyses were performed in one of the A/J mice at 16 and 20 weeks

[CIs] on the difference = 3.25 to 9.60, P = <.001 for group 3; mean = 7.60 versus mean = 11.0, difference = 3.4, 95% CIs on the difference = −0.39 to 7.19, P = .085, Fig. 2, D). Microscopic evaluation of the lungs revealed a statistically significant decrease in tumor multiplicity, the number of tumors inside the lung (group 3: 59.4%; mean = 1.70 tumors/slide, difference = 2.48, 95% CIs on the difference = 0.97 to 4.0, P = .007; and group 4: 48.8%; mean = 2.14 tumors/slide, difference = 2.04, 95% CIs on the difference = 0.52 to 3.56, P = .046), volume (group 3: 76.1%; mean = 0.016 mm^3, difference = 0.051, 95% CIs on the difference = 0.021 to 0.082, P = .007; and group 4: 83.58%; mean = 0.011 mm^3, difference = 0.056, 95% CIs on the difference = 0.019 to 0.093, P = .012), and load (group 3: 89.3%; mean = 0.032 mm^3, difference = 0.27, 95% CIs on the difference = 0.051 to 0.48, P = .009; and group 4: 92.3%; mean = 0.023 mm^3, difference = 0.27, 95% CIs on the difference = 0.06 to 0.49, P = .006) in the deguelin-treated mice compared with the NNK/BaP-treated mice in group 2 (tumor multiplicity, mean = 4.182 tumors/slide; volume, mean = 0.067 mm^3; load, mean = 0.298 mm^3). Mice in groups 3 and 4 showed a statistically non-significant decrease in body weight compared with mice in groups 1 and 2.

Immunohistochemical analysis revealed stronger cytoplasmic and nuclear pAkt staining in airway epithelial cells (Fig. 2, E, 2) in mice in group 2 compared with those in group 1 (Fig. 2, E, 1) and group 3 (Fig. 2, E, 3). The tumors in group 2 (Fig. 2, E, 4) also showed stronger pAkt staining compared with those in group 3 (Fig. 2, E, 5).

In spite of its potential as a cancer chemopreventive/therapeutic agent, there is concern about possible side effects of deguelin treatment. Deguelin is derived from rotenone, which can inhibit NADH: ubiquinone oxidoreductase, an enzyme complex involved in mitochondrial oxidative phosphorylation *(34)*, and induce cardiotoxicity, respiratory depression, and nerve conduction blockade at high doses (a dose that is lethal to 50% of those exposed = 10–100 g in humans). However, we did not observe major toxicity or substantial loss of body weight in the deguelin-treated A/J mice at the dose used in this study. Deguelin is also safer in terms of its mechanism of action, which differs from that of rotenone, which inhibits tubulin polymerization. Additionally, deguelin rapidly decomposes in light and air. All of these results suggest that deguelin would be harmless when orally administered. Moreover, in contrast to some natural products presently used in cancer chemoprevention and therapy, deguelin could be easily synthesized using commercially available rotenone as a starting material; therefore, its clinical use as a lung cancer chemopreventive agent is feasible. These collective findings provide a strong rationale for testing deguelin in a phase I clinical trial of lung cancer chemoprevention after its complete toxicity profile in humans is known.

References

(1) Greenlee RT, Hill-Harmon MB, Murray T, Thun M. Cancer statistics, 2001. CA Cancer J Clin 2001;51:15–36.

(2) van Zandwijk N, Hirsch FR. Chemoprevention strategies for non-small cell lung cancer. Curr Opin Oncol 2002;14:185–90.

(3) Richardson CM, Sharma RA, Cox G, O'Byrne KJ. Epidermal growth factor receptors and cyclooxygenase-2 in the pathogenesis of non-small cell lung cancer: potential targets for chemoprevention and systemic therapy. Lung Cancer 2003;39:1–13.

(4) Rusch V, Klimstra D, Venkatraman E, Pisters PW, Langenfeld J, Dmitrovsky E. Overexpression of the epidermal growth factor receptor and its ligand transforming growth factor alpha is frequent in resectable non-small cell lung cancer but does not predict tumor progression. Clin Cancer Res 1997;3:515–22.

(5) Fontanini G, De Laurentiis M, Vignati S, Chine S, Lucchi M, Silvestri V, et al. Evaluation of epidermal growth factor-related growth factors and receptors and of neoangiogenesis in completely resected stage I-IIIA non-small-cell lung cancer: amphiregulin and microvessel count are independent prognostic indicators of survival. Clin Cancer Res 1998;4:241–9.

(6) Lin X, Bohle AS, Dohrmann P, Leuschner I, Schulz A, Kremer B, et al. Overexpression of phosphatidylinositol 3-kinase in human lung cancer. Langenbecks Arch Surg 2001;386:293–301.

(7) Mitsudomi T, Steinberg SM, Oie HK, Mulshine JL, Phelps R, Viallet J, et al. ras gene mutations in non-small cell lung cancers are associated with shortened survival irrespective of treatment intent. Cancer Res 1991;51:4999–5002.

(8) Mills NE, Fishman CL, Rom WN, Dubin N, Jacobson DR. Increased prevalence of K-ras oncogene mutations in lung adenocarcinoma. Cancer Res 1995;55:1444–7.

(9) Soria JC, Lee HY, Lee JI, Wang L, Issa JP, Kemp BL, et al. Lack of PTEN expression in non-small cell lung cancer could be related to promoter methylation. Clin Cancer Res 2002;8:1178–84.

(10) Alessi DR, James SR, Downes CP, Holmes AB, Gaffney PR, Reese CB, et al. Characterization of a 3-phosphoinositide-dependent protein kinase which phosphorylates and activates protein kinase Balpha. Curr Biol 1997;7:261–9.

(11) Cross DA, Alessi DR, Cohen P, Andjelkovich M, Hemmings BA. Inhibition of glycogen synthase kinase-3 by insulin mediated by protein kinase B. Nature 1995;378:785–9.

using a model RS-9 tabletop CT scanner (General Electric Medical Systems, London, Ontario) as previously described *(35,36)*. The technique used was 80 kVp and 450 μA, with 720 views obtained at 0.5-degree increments at 400 msec per view. The radiation dose delivered during this scan was approximately 0.26 Gy. Labview software (National Instruments, Austin, TX) provided an interface for selecting the mouse respiratory parameters. The Feldkamp reconstruction method was used to normalize the raw images and to correct for nonuniformities in the detector *(35)*. Images were formed with isotropic 91-mm voxels. NNK/BaP-treated mice sections *(10)* were fast-frozen immediately after their micro-CT scan session to confirm their position in the images relative to block-faced pathologic sections. A representative micro-CT (**1, 2, 4–7**) or block-faced (**3**) image analysis of the lungs from a control mouse (**1**) or mice treated with NNK/BaP alone (**2–5**) or with NNK/BaP plus deguelin (group 3) at 16 (**4, 6**) and 20 (**5, 7**) weeks is shown. l = lung; e = esophagus; v = thoracic vertebra; L = liver; s = spinal cord. **D**) Postmortem examinations were performed on the lungs of the A/J mice after mice were killed at 20 weeks. The lung tissues were fixed in Bouin's solution, and the gross tumor nodules (lung tumors/slide) were counted. Microscopic evaluation of lung tissues was also performed to measure mean tumor number (N), volume (V), and total tumor load (N × V) in a blinded fashion. The tumor volume was calculated by the formula of V (mm^3) = (long diameter × short $diameter^2$)/2. The number and size of tumors in five sections distributed uniformly through each lung were calculated. Body weight of the mice was measured at 0 (baseline), 8, and 20 weeks (wks). Effects of deguelin on lung tumorigenesis were expressed by means and 95% CIs of tumor nodules/mouse, tumor nodules/slide (multiplicity), volume, and load from 12 (group 2) or 14 (groups 3 and 4) samples. The data were analyzed in comparision with that from the mice treated with NNK/BaP (group 2). We set values from group 2 at 100% and then calculated the others as a percentage of that. Differences between groups were compared using the t test or Mann-Whitney statistical test. Differences were considered statistically significant if $P < .05$. Histopathologic evidence of pulmonary toxicity, i.e., edema or inflammation of the bronchial epithelium and alveoli and inflammation and injury in other organs were evaluated by a veterinary pathologist. These animal studies were approved by M. D. Anderson Cancer Center's Institutional Animal Care and Use Committee. **E**) After the evaluation of tumor nodules, lung tissues were surgically removed and paraffin embedded. Bronchial epithelium (**1, 2, 3**) and lung adenoma (**4, 5**) lesions in the A/J mice that were untreated (**1**) or treated with NNK/BaP alone (**2, 4**) or NNK/BaP plus deguelin (**3, 5**) were processed for immunohistochemical analysis with anti-pAkt (Ser473) as described in Fig. 1.

(12) Brunet A, Bonni A, Zigmond MJ, Lin MZ, Juo P, Hu LS, et al. Akt promotes cell survival by phosphorylating and inhibiting a Forkhead transcription factor. Cell 1999;96:857–68.
(13) Cardone MH, Roy N, Stennicke HR, Salvesen GS, Franke TF, Stanbridge E, et al. Regulation of cell death protease caspase-9 by phosphorylation. Science 1998;282:1318–21.
(14) Datta SR, Dudek H, Tao X, Masters S, Fu H, Gotoh Y, et al. Akt phosphorylation of BAD couples survival signals to the cell-intrinsic death machinery. Cell 1997;91:231–41.
(15) del Peso L, Gonzalez-Garcia M, Page C, Herrera R, Nunez G. Interleukin-3-induced phosphorylation of BAD through the protein kinase Akt. Science 1997;278:687–9.
(16) Krasilnikov MA. Phosphatidylinositol-3 kinase dependent pathways: the role in control of cell growth, survival, and malignant transformation. Biochemistry (Mosc) 2000;65:59–67.
(17) Brognard J, Clark AS, Ni Y, Dennis PA. Akt/protein kinase B is constitutively active in non-small cell lung cancer cells and promotes cellular survival and resistance to chemotherapy and radiation. Cancer Res 2001;61:3986–97.
(18) Kennedy SG, Kandel ES, Cross TK, Hay N. Akt/protein kinase B inhibits cell death by preventing the release of cytochrome *c* from mitochondria. Mol Cell Biol 1999;19: 5800–10.
(19) Chen RH, Su YH, Chuang RL, Chang TY. Suppression of transforming growth factor-beta-induced apoptosis through a phosphatidylinositol 3-kinase/Akt-dependent pathway. Oncogene 1998;17:1959–68.
(20) West KA, Linnoila IR, Belinsky SA, Harris CC, Dennis PA. Tobacco carcinogen-induced cellular transformation increases activation of the phosphatidylinositol 3′-kinase/Akt pathway in vitro and in vivo. Cancer Res 2004;64:446–51.
(21) Lee HY. Molecular mechanisms of deguelin-induced apoptosis in transformed human bronchial epithelial cells. Biochem Pharmacol 2004;68:1119–24.
(22) Lee HY, Suh YA, Kosmeder JW, Pezzuto JM, Hong WK, Kurie JM. Deguelin-induced inhibition of cyclooxygenase-2 expression in human bronchial epithelial cells. Clin Cancer Res 2004;10:1074–9.
(23) Chun KH, Kosmeder JW 2nd, Sun S, Pezzuto JM, Lotan R, Hong WK, et al. Effects of deguelin on the phosphatidylinositol 3-kinase/Akt pathway and apoptosis in premalignant human bronchial epithelial cells. J Natl Cancer Inst 2003;95:291–302.
(24) Gerhauser C, Lee SK, Kosmeder JW, Moriarty RM, Hamel E, Mehta RG, et al. Regulation of ornithine decarboxylase induction by deguelin, a natural product cancer chemopreventive agent. Cancer Res 1997;57:3429–35.
(25) Udeani GO, Zhao GM, Shin YG, Kosmeder JW, 2nd, Beecher CW, Kinghorn AD, et al. Pharmacokinetics of deguelin, a cancer chemopreventive agent in rats. Cancer Chemother Pharmacol 2001;47:263–8.
(26) Murillo G, Kosmeder JW, 2nd, Pezzuto JM, Mehta RG. Deguelin suppresses the formation of carcinogen-induced aberrant crypt foci in the colon of CF-1 mice. Int J Cancer 2003;104:7–11.
(27) Mehta RG, Pezzuto JM. Discovery of cancer preventive agents from natural products: from plants to prevention. Curr Oncol Rep 2002;4:478–86.
(28) Kroll J, Cobo P, Sato TN. Versatile inducible activation system of Akt/PKB signaling pathway in mice. Genesis 2003;35:160–3.
(29) Hecht SS, Isaacs S, Trushin N. Lung tumor induction in A/J mice by the tobacco smoke carcinogens 4-(methylnitrosamino)-1-(3-pyridyl)-1-butanone and benzo[a]pyrene: a potentially useful model for evaluation of chemopreventive agents. Carcinogenesis 1994;15:2721–5.
(30) Hoffmann D, Hecht SS. Advances in tobacco carcinogenesis. 1990;94:63–102.
(31) Wattenberg LW. Chemoprevention of cancer. Cancer Res 1985;45:1–8.
(32) Hecht SS, Upadhyaya P, Wang M, Bliss RL, McIntee EJ, Kenney PM. Inhibition of lung tumorigenesis in A/J mice by N-acetyl-S-(N-2-phenethylthiocarbamoyl)-L-cysteine and myo-inositol, individually and in combination. Carcinogenesis 2002;23: 1455–61.
(33) Beckett WS. Epidemiology and etiology of lung cancer. Clin Chest Med 1993;14:1–15.
(34) Fang N, Casida JE. Anticancer action of cube insecticide: correlation for rotenoid constituents between inhibition of NADH:ubiquinone oxidoreductase and induced ornithine decarboxylase activities. Proc Natl Acad Sci U S A 1998;95:3380–4.
(35) Cavanaugh D, Johnson E, Price RE, Kurie J, Travis EL, Cody DD. In vivo respiratory-gated micro-CT imaging in small-animal oncology models. Mol Imaging 2004; 3:55–62.
(36) Rivera B, Miller S, Brown E, Price R. A novel method for endotracheal intubation of mice and rats used in imaging studies. Contemp Top Lab Anim Sci 2005;44:52–5.

NOTES

Supported by National Institutes of Health grants R01 CA100816–01 and CA109520–01 (to H.-Y. Lee) and American Cancer Society grant RSG-04–082–01-TBE 01 (to H.-Y. Lee) and partly by Department of Defense grant W81XWH-04–1–0142–01-VITAL (to W. K. Hong) and National Institutes of Health Cancer core grant CA16672. We thank the staff of the Small Animal Cancer Research Imaging Facility for their diligence and devotion. WKH is an American Cancer Society clinical research professor.

Manuscript received March 29, 2005; revised August 23, 2005; accepted September 7, 2005.

Cancer Prevention Research

Prevention of Bronchial Hyperplasia by EGFR Pathway Inhibitors in an Organotypic Culture Model

Jangsoon Lee, Seung-Hee Ryu, Shin Myung Kang, et al.

Cancer Prev Res Published OnlineFirst April 19, 2011.

Published OnlineFirst on April 19, 2011; DOI:10.1158/1940-6207.CAPR-10-0364

Research Article

Cancer Prevention Research

Prevention of Bronchial Hyperplasia by EGFR Pathway Inhibitors in an Organotypic Culture Model

Jangsoon Lee[1], Seung-Hee Ryu[1], Shin Myung Kang[1], Wen-Cheng Chung[1], Kathryn Ann Gold[2], Edward S. Kim[1], Walter N. Hittelman[3], Waun Ki Hong[1], and Ja Seok Koo[1]

Abstract

Lung cancer is the leading cause of cancer-related mortality worldwide. Early detection or prevention strategies are urgently needed to increase survival. Hyperplasia is the first morphologic change that occurs in the bronchial epithelium during lung cancer development, followed by squamous metaplasia, dysplasia, carcinoma *in situ*, and invasive tumor. This study was designed to determine the molecular mechanisms that control bronchial epithelium hyperplasia. Using primary normal human tracheobronchial epithelial (NHTBE) cells cultured by using the 3-dimensional (3D) organotypic method, we found that the epidermal growth factor receptor (EGFR) ligands, EGF, TGF-α, and amphiregulin induced hyperplasia, as determined by cell proliferation and multilayered epithelium formation. We also found that EGF induced increased cyclin D1 expression, which plays a critical role in bronchial hyperplasia; this overexpression was mediated by activating the mitogen-activated protein kinase pathway but not the phosphoinositide 3-kinase/Akt signaling pathway. Erlotinib, an EGFR tyrosine kinase inhibitor, and U0126, a MAP/ERK kinase (MEK) inhibitor, completely inhibited EGF-induced hyperplasia. Furthermore, a promoter analysis revealed that the activator protein-1 transcription factor regulates EGF-induced cyclin D1 overexpression. Activator protein-1 depletion by using siRNA targeting its c-Jun component completely abrogated EGF-induced cyclin D1 expression. In conclusion, we showed that bronchial hyperplasia can be modeled *in vitro* by using primary NHTBE cells maintained in a 3D organotypic culture. EGFR and MEK inhibitors completely blocked EGF-induced bronchial hyperplasia, suggesting that they have a chemopreventive role. *Cancer Prev Res; 4(8); 1–10. ©2011 AACR.*

Introduction

Hyperplasia in the bronchial epithelium, as evidenced by increased cell proliferation, is associated with conditions such as trauma, smoking, chronic cough, chronic inflammatory airway disease, and cancer. It is the first of several progressive, cumulative, genetic, and morphologic changes associated with lung squamous cell carcinoma, followed by squamous metaplasia, dysplasia, and carcinoma *in situ* (1–3). These extensive, multifocal changes occur throughout the respiratory tree when the lungs are chronically exposed to common carcinogens, a phenomenon known as field cancerization (4).

In the developed lung, growth factors and their signaling receptors support cellular activities in equilibrium, preserving normal lung structure, and function (5). However, this homeostatic control can be compromised during the accumulation of genetic and molecular alterations that lead to lung cancer. Several decades of research have revealed that the ErbB system is a critical growth factor system in normal and abnormal epithelial cell proliferation (6, 7). The ErbB family, ErbB1-4, plays an important role in lung cancer development. In addition, several ErbB ligands are aberrantly regulated in cancer cells. Therefore, we hypothesized that bronchial hyperplasia results from ErbB hyperactivation in bronchial epithelial cells. To test this hypothesis, we evaluated ErbB ligands for their ability to induce bronchial hyperplasia by using a 3-dimensional (3D) organotypic air–liquid interface primary bronchial epithelial

Authors' Affiliations: [1]Department of Thoracic/Head and Neck Medical Oncology, [2]Hematology and Oncology, [3]Experimental Therapeutics, The University of Texas MD Anderson Cancer Center, Houston, Texas

Note: J. Lee and S-H. Ryu contributed equally to this work.

Current address for J. Lee: Breast Medical Oncology, The University of Texas MD Anderson Cancer Center, Houston, Texas.

Current address for S-H. Ryu: Department National Investment Project, Asan Institute for Life Sciences, Asan Medical Center, Seoul, Korea.

Current address for S.M. Kang: Center for Lung Cancer, National Cancer Center, Goyang-si, Korea.

Corresponding Author: Ja Seok Koo, Department of Thoracic/Head and Neck Medical Oncology, Unit 432, The University of Texas MD Anderson Cancer Center, 1515 Holcombe Blvd., Houston, TX 77030. Phone: 713-792-8454; Fax: 713-794-5997; E-mail: jskoo@mdanderson.org

doi: 10.1158/1940-6207.CAPR-10-0364

Published OnlineFirst on April 19, 2011; DOI:10.1158/1940-6207.CAPR-10-0364

cell culture system (8–10). We then determined which downstream signaling pathways and genes were involved in bronchial hyperplasia development. Epidermal growth factor receptor (EGFR) ligands induce bronchial hyperplasia via the MAP/ERK kinase (MEK)/extracellular signal regulated kinase (ERK) signaling pathway. EGF-induced cyclin D1 overexpression plays a critical role in the development of bronchial hyperplasia. EGFR and MEK inhibitors completely blocked EGF-induced bronchial hyperplasia.

As monotherapy, erlotinib, a small molecular inhibitor targeting the intracellular tyrosine kinase domain of EGFR, significantly prolonged survival in previously treated advanced non–small cell lung cancer (NSCLC) patients compared with placebo (13) and was recently approved by the Food and Drug Administration. Erlotinib has antiproliferative effects arising from G_1 arrest and proapoptotic effects on cancer cells (14). However, its effects on normal and hyperplastic bronchial epithelial cells are unknown. Our results showed that erlotinib blocks EGF-induced bronchial hyperplasia and can reverse hyperplasia, restoring normal bronchial epithelial morphologic characteristics. We identified several mechanisms involved in the onset of changes leading to lung cancer, such as abnormal cell proliferation, which may be targets for preventing malignant progression.

Materials and Methods

Chemicals

Erlotinib (LKT Laboratories, Inc.), U0126, LY294002, and Akt inhibitor VIII (Calbiochem) were dissolved in dimethylsulfoxide.

Cells

Normal human tracheobronchial epithelial (NHTBE) cells were obtained from the Lonza Walkersville, Inc. A549 lung cancer cells were obtained from the American Type Culture Collection. We authenticated A549 cell by genotyping through MD Anderson Cancer Center DNA analysis core facility.

3D organotypic air–liquid interface cell culture and treatment

We cultured NHTBE, or A549 cells by using the 3D organotypic air–liquid interface method described previously (9, 11). The medium in the bottom chamber was changed every 24 hours. We treated 7-day-old confluent NHTBE cells grown on a porous membrane of a Transwell plate with various ligands (Sigma-Aldrich) for ErbB receptors, EGF (10 ng/mL), TGF-α (10 ng/mL), amphiregulin (AR, 50 ng/mL), or heregulin (HR, 100 ng/mL) for 4 days. The ligands were included only in basal media, and the apical side of the cultures was exposed to air by removing the media overlaying the cells in the upper side of the well. For dose-dependent experiments, we used 0.5, 2.0, 5.0, 10, and 25 ng/mL of EGF. For time-dependent experiments, we cultured cells with 5 ng/mL of EGF for 1 to 4 days.

Western blot analysis

We prepared total protein extracts by using cold radioimmunoprecipitation assay lysis buffer (50 mmol/L HEPES, pH 7.4; 1% NP-40, 150 mmol/L NaCl, 1 mmol/L EDTA, phosphates inhibitors, and protease inhibitors). Protein (15 μg) was resolved by 10% SDS-PAGE gel. Membranes were incubated with rabbit polyclonal antibodies against cAMP responsive element binding protein (CREB), phospho-CREB-133 (Upstate Biotechnology), ERK, phospho-ERK-202/204, cyclin A1, cyclin B1, cyclin D1, cyclin E2, Akt, phospho-Akt-473, c-Jun, phospho-c-Jun-73, p-EGFR-1068, and EGFR (Cell Signaling Technology) overnight. β-Actin (clone AC-15; Sigma-Aldrich) was used as a loading control. The reaction of proteins with primary antibodies was visualized with horseradish peroxidase-conjugated secondary antibody and enhanced chemiluminescence reagents (GE Healthcare).

siRNA

Human c-Jun (accession no. NM_002228) siRNAs were used to knock down c-Jun expression (Sigma-Aldrich), according to the manufacturer's instructions. A mixture of several siRNAs ensured that the targeted gene product was effectively deleted. Cells at 60% to 70% confluency were transfected for 48 hours with a final concentration of 100 nmol/L c-Jun siRNA or nonspecific control pooled siRNAs by using the Dharmafect 1 transfection reagent (Dharmacon), according to the manufacturer's instructions. The cells were treated with EGF (5 ng/mL) for 24 hours, when target protein levels had been reduced more than 70%, as assessed by Western blot analysis.

Immunohistochemistry and immunofluorescence

The NHTBE cells were fixed in neutral-buffered formalin and embedded in paraffin. Sections (5 μm each) were prepared by using a microtome, mounted on slides, deparaffinized in xylene, rehydrated in graded alcohols, and washed in distilled water. Endogenous peroxidases were quenched by incubation in 3% H_2O_2. Antigens were retrieved by microwaving the sections in 10 mmol/L citric acid (pH 6.0) for 5 minutes. The slides were washed 3 times with PBS and blocked for 30 minutes with 10% normal goat serum in 1% bovine serum albumin (BSA)/PBS. Immunohistochemical staining was visualized by using the Histostain-Bulk–SP and the AEC red substrate kits (Zymed Laboratories). Immunohistochemical staining without a primary antibody was done as a negative control. Immunofluorescence staining was visualized by using Cy-3 (Jackson ImmunoResearch) and 4′,6-diamidino-2-phenylindole (Invitrogen). Stained slides were visualized with an Axioskop 40 fluorescence microscope (Carl Zeiss); the images were captured at a magnification of 200× and stored by using Axiovision LE software v4.5 (Carl Zeiss) according to the manufacturer's instructions.

Luciferase reporter assay

NHTBE cells (5×10^4) were cultured in 12-well tissue culture plates (Corning) overnight and cotransfected with

Published OnlineFirst on April 19, 2011; DOI:10.1158/1940-6207.CAPR-10-0364

cyclin D1 promoter-luciferase constructs (wild type, AP-1 site mutant, or CRE site mutant; kindly provided by Dr. Richard Pestell at Thomas Jefferson University) and *Renilla* luciferase control vector by using Lipofectamin 2000 (Invitrogen). After 24 hours, the culture medium was changed to 0.1% BSA in bronchial epithelial basal medium (BEBM; Lonza Walkersville, Inc.), and cells were treated with or without EGF (5 ng/mL) for 24 hours. Luciferase activity was detected by using the dual-luciferase reporter assay (Promega) and measured by using a Lumat LB 9507 tube luminometer (Berthold). All assays were done in triplicate and repeated at least 3 times. Figures show representative results.

Hyperplasia evaluation via cell layer thickness and cell number

To determine ErbB receptors ligands' effects on the histomorphologic characteristics of NHTBE cells, we incubated NHTBE cells with EGF (10 ng/mL), TGF-α (10 ng/mL), AR (50 ng/mL), or HR (100 ng/mL) for 4 days. After making paraffin-embedded blocks, we captured 3 images from each block within a 10-mm area from the center of the Transwell membrane with an Axioskop 40 microscope (Carl Zeiss) under light microscopy (200×). To evaluate hyperplasia, we measured thickness by using Axiovision LE software v4.5 (Carl Zeiss) according to the manufacturer's instructions. Total cell numbers in the captured area were counted manually under light microscopy (200×). Bars, SE; **, $P < 0.01$ and ***, $P < 0.001$.

Statistical analysis

For each experimental outcome, descriptive statistics (mean, SD, median, and range) were summarized for each group. An ANOVA model was used to detect any differences between treatment and control groups.

Results

EGFR ligands induce hyperplasia in bronchial epithelial cells grown in 3D organotypic culture

To determine whether ErbB receptors are involved in bronchial hyperplasia morphologic changes, we cultured NHTBE cells by using the organotypic air–liquid interface method with various ErbB receptor ligands, including EGF (10 ng/mL), TGF-α (10 ng/mL), AR (50 ng/mL), and HR (100 ng/mL), for 4 days. We histochemically evaluated ErbB ligands' effects on morphologic changes in NHTBE cells and found that the NHTBE cell layer was statistically significantly thicker after treatment with EGFR ligands, EGF, TGF-α, and AR but not with HR (Fig. 1A). Quantitative changes are shown as mean thicknesses: control = 13 (± 2) μm, EGF treated = 42 (±6) μm, TGF-α treated = 31 (±4) μm, AR treated = 28 (±3) μm, and HR treated = 15 (±2) μm cells. These data clearly show that high EGFR ligand concentrations induce bronchial epithelial cell hyperplasia. The most prominent hyperplastic morphologic changes in NHTBE cell culture histologic patterns were induced by EGF; therefore, we selected EGF for subsequent study.

To determine dose-dependent effects of EGF on NHTBE cell hyperplasia, we incubated NHTBE cells with EGF for 4 days. Immunohistochemical analysis and cell quantitation clearly indicated that EGF-induced hyperplasia in a dose-dependent manner. NHTBE cell layers were significantly thicker after treatment with 5 ng/mL of EGF, and cell quantitation showed a similar pattern (Fig. 1B). To determine time-dependent effects of EGF, we incubated NHTBE cells with 5 ng/mL of EGF for 1 to 4 days. The NHTBE cell layer expanded in a time-dependent manner. Four days of treatment resulted in an approximately 2.5-fold increase in cell number and cell layer thickness (Fig. 1C).

EGF induces cell proliferation at only the basal layer of NHTBE cell cultures

Multilayered hyperplasia is believed to result from uncontrolled bronchial epithelial cell proliferation. To identify the specific NHTBE cell population after EGFR ligand exposure, we conducted Ki-67 immunostaining in NHTBE cells grown in a 3D organotypic culture system. We used A549 cells as a positive control. As shown in Figure 2, immunohistochemical (Fig. 2A) and immunofluorescence (Fig. 2B) analyses of Ki-67 as a cell proliferation indicator revealed positive staining in cells in the basal layer of NHTBE cell cultures. In contrast, Ki-67–positive cells were detected randomly in both basal and parabasal layers in A549 cells. These results indicate that only NHTBE cells in the basal layer divide and grow in response to EGF; cancer cells are not limited to the basal layer.

MEK/ERK pathway is a critical signaling pathway for EGF-induced NHTBE cell hyperplasia

The MEK/ERK and PI3-K/Akt pathways are well-established downstream signaling pathways of the EGF–EGFR pathway (12). To determine the relative importance of these pathways for transmitting EGF-induced hyperplasia signals in NHTBE cells, we treated fully confluent 7-day-old NHTBE cells with 5 ng/mL of EGF for 2 hours. EGF induced Akt, ERK, and CREB phosphorylation in NHTBE cells (Fig. 3A), showing that the Akt and ERK pathways may participate in induction of cell proliferation of EGF and layer thickening. To further understand the relative role of these pathways, we treated 7-day-old NHTBE cells with EGF (5 ng/mL) alone or in combination with pharmacologic inhibitors targeting select molecules in the PI3-K/Akt and ERK signaling pathways: erlotinib (EGFR-TKI, 1 μmol/L), U0126 (MEK inhibitor, 5 μmol/L), LY294002 (PI3-K inhibitor, 10 μmol/L), and Akt inhibitor VIII (10 μmol/L) for 15 minutes. Inhibitors were pretreated for 30 minutes before EGF treatment. Erlotinib completely inhibited EGFR, Akt, and ERK phosphorylation (Fig. 3B). U0126 inhibited ERK and CREB phosphorylation. However, LY294002 and Akt inhibitor VIII had no effect on EGF-induced ERK and CREB phosphorylation (Fig. 3B).

Published OnlineFirst on April 19, 2011; DOI:10.1158/1940-6207.CAPR-10-0364

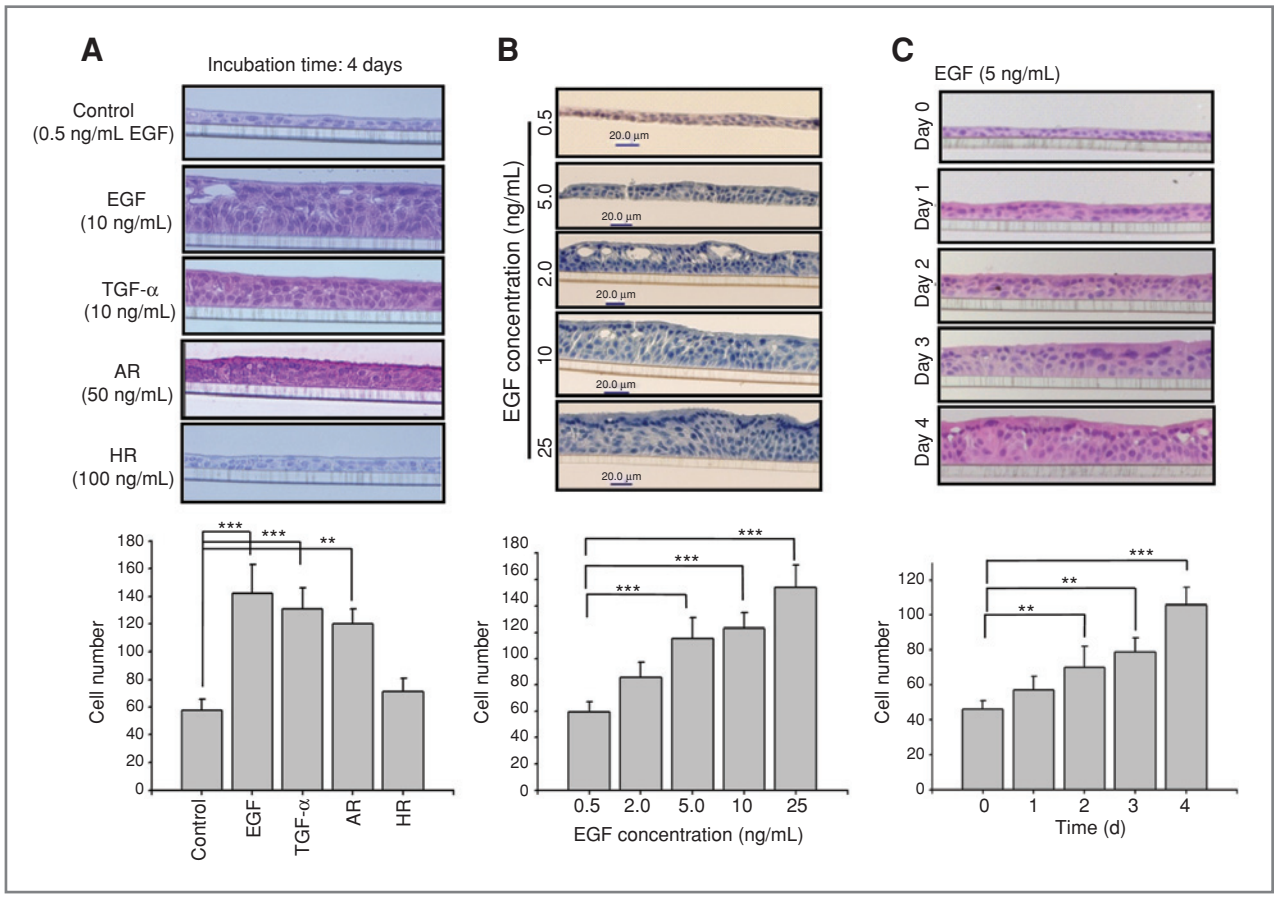

Figure 1. EGFR ligands induce hyperplasia in NHTBE cells. NHTBE cells were cultured on a Transwell plate until they formed a monolayer. The culture condition was changed to an air-liquid interface, as described in Materials and Methods. Starting at day 7, cells were treated with various ErbB-ligands (EGF 10 ng/mL, TGF-α 10 ng/mL, AR 50 ng/mL, and HR 100 ng/mL) for 4 days (A). EGF induces hyperplasia in a dose- (B) and time-dependent (C) manner. Seven-day-old NHTBE cell cultures were treated with indicated concentrations (B) of EGF for the indicated time periods (C). Cells were then fixed with phosphate-buffered formalin and embedded in paraffin. The result was visualized by using hematoxylin/eosin staining. Cells were counted as described in Materials and Methods. The results were summarized by descriptive statistics (mean, SD, and median), and box plots were generated for each experiment, with different cell groups compared side by side. Data shown are representative of 3 experiments with similar results.

To further determine the morphologic consequences of inhibiting critical molecules in signaling pathways, we cultured NHTBE cells for 7 days until they become confluent and then treated with EGF (5 ng/mL) alone or in the presence of various inhibitors for 4 days. NHTBE cells treated with EGF alone experienced hyperplastic changes and increased thickness, whereas those treated in the presence of erlotinib or U0126 underwent no such changes. However, LY294002- and Akt inhibitor VIII-treated NHTBE cells still showed hyperplasia and increased thickness (Fig. 3C). These results suggest that the MEK/ERK pathway is the main pathway by which EGF induces hyperplasia in NHTBE cells. We next determined whether inhibitors reverse EGF-induced hyperplasia in NHTBE cells. After they became hyperplastic, the cultures were maintained in media containing 0.5 ng/mL EGF in the absence or presence of erlotinib (1 μmol/L), LY294002 (10 μmol/L), U0126 (5 μmol/L), or Akt inhibitor VII (10 μmol/L) for 4 additional days. Only erlotinib successfully reverted EGF-induced hyperplasia such that normal morphologic characteristics were restored (Fig. 3D).

Cyclin D1 is increased during EGF-induced NHTBE cell hyperplasia

Increased cell proliferation is partly responsible for hyperplasia induction. Because elevated cyclin levels play a role in enhancing cell proliferation, we determined cyclin levels in NHTBE cells after EGF treatment. EGF robustly increased cyclin D1 and slightly increased cyclin E2 expression (Fig. 4A). However, A1 and B1 were not significantly increased. The EGFR and MEK inhibitors erlotinib and U0126, respectively, markedly blocked EGF-induced expression of cyclin D1, but LY294002 and Akt inhibitor VIII did not (Fig. 4B).

To determine which transcription factors are involved in EGF-induced *cyclin D1* gene expression, we conducted a *cyclin D1* promoter-luciferase activity assay (Fig. 4C).

Published OnlineFirst on April 19, 2011; DOI:10.1158/1940-6207.CAPR-10-0364

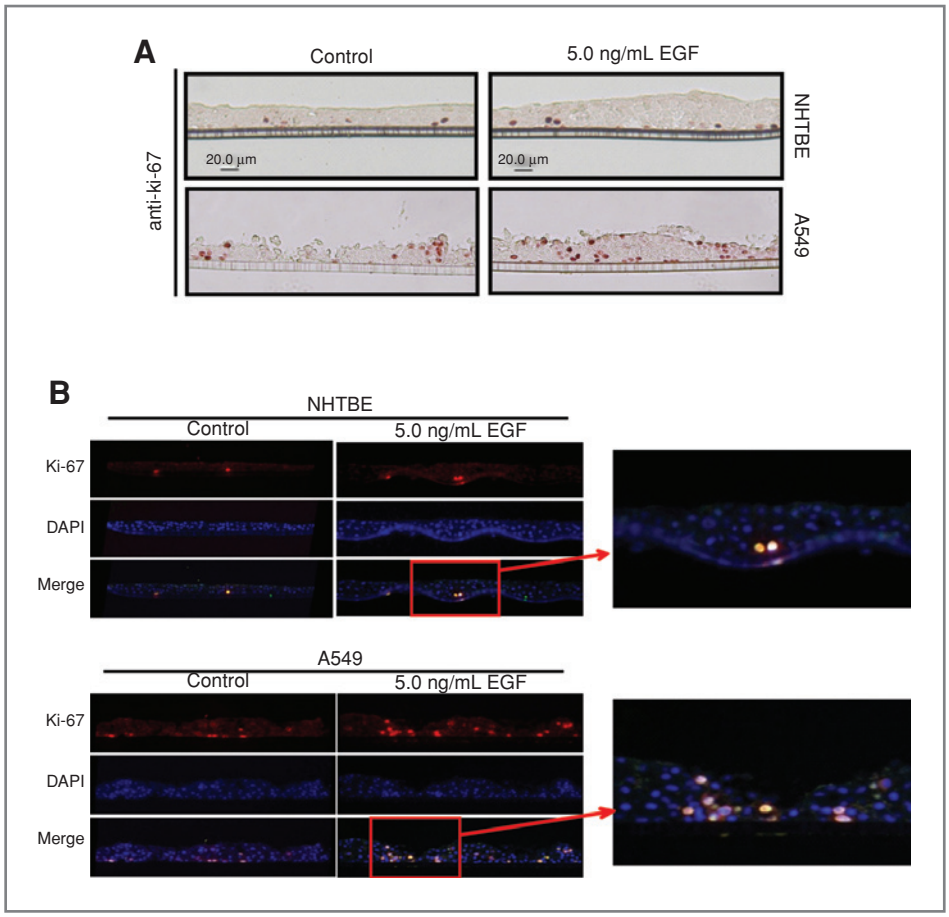

Figure 2. Proliferating cells are differentially localized in NHTBE or A549 cancer cells. Both cell lines were grown by using the ALI method, as described in Materials and Methods. The cultures were starved without supplements in their respective culture media for 24 hours and treated with 5 ng/mL of EGF (0.5 ng/mL as control). The cultures were fixed, and paraffin blocks were prepared. Slide sections were stained with anti-Ki-67. The result was visualized by using immunohistochemical (A) and immunofluorescence (B) analysis. Data shown are representative of 3 experiments with similar results.

We transfected NHTBE cells with various *cyclin D1* promoter-luciferase reporters (wild type, AP-1 site mutant, and CRE sites mutant in the cyclin D1 promoter region) and treated the transfected cells with or without EGF. EGF increased luciferase activity more than 20 times when wild-type or mutated CRE *cyclin D1* promoter reporters were introduced (Fig. 4C). However, when the AP-1 recognition sequence was mutated or removed, the EGF response was dramatically lower than that in the wild-type promoter. This result shows the importance of the AP-1 transcription factor in EGF-induced cyclin D1 overexpression.

Next, we investigated the activation status of AP-1 components c-Jun and c-Fos. EGF induced c-Jun expression and phosphorylation (Fig. 4D) but not c-Fos (data not shown). In addition, erlotinib and U0126 markedly blocked EGF-induced c-Jun phosphorylation (Fig. 4E). c-Jun knockdown with c-Jun siRNA prevented EGF-induced cyclin D1 expression, suggesting that EGF-induced cyclin D1 expression is mediated by c-Jun (Fig. 4F). Thus, we concluded that EGF induces cyclin D1 overexpression and that this overexpression is mediated by AP-1 (c-Jun) transcription factor. In addition, EGF-induced cyclin D1 overexpression is blocked by EGFR and MEK inhibitors.

Discussion

We showed that bronchial hyperplasia can be modeled and manipulated *in vitro* by using primary NHTBE cells maintained in a 3D organotypic air–liquid interface culture. The EGFR ligands EGF, TGF-α, and AR induce hyperplasia in NHTBE cells. This histomorphologic change is regulated by the MEK/ERK signaling pathway but not the PI3-K/Akt signaling pathway. The MEK/ERK signaling pathway induces cyclin D1 expression by activating AP-1 transcription factor. The EGFR and MEK inhibitors erlotinib and U0126 completely blocked EGF-induced hyperplasia.

In view of multistep lung carcinogenesis and field cancerization, our results suggest that erlotinib may be useful as a chemopreventive agent as such agents inhibit, delay, or reverse carcinogenesis. First, erlotinib may be beneficial for high-risk patients, such as those with a strong smoking history. Erlotinib is currently being studied in the adjuvant setting after surgery and chemotherapy in NSCLC. Lung cancer develops in a field with extensive and multifocal hot spots throughout the respiratory trees, which are consistently exposed to common carcinogens. Even after tumor resection, these hot spots can develop into lung cancer. After resection, the risk of a second primary lung cancer is

Published OnlineFirst on April 19, 2011; DOI:10.1158/1940-6207.CAPR-10-0364

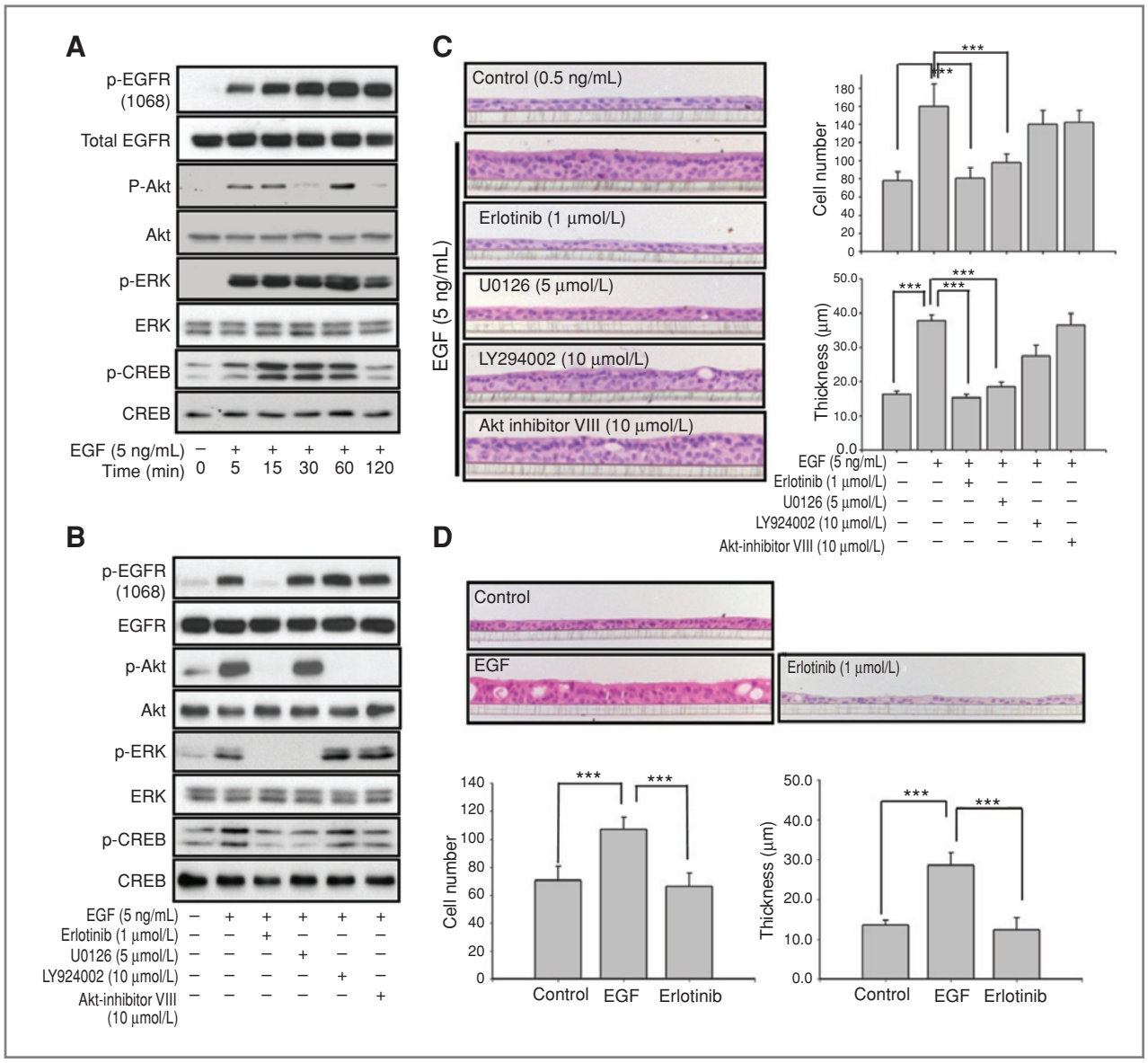

Figure 3. MEK/ERK pathway is involved in EGF-induced hyperplasia in NHTBE cells. A, EGF induced Akt, ERK, and CREB phosphorylation. Seven-day-old NHTBE cell cultures were maintained in BEBM without supplements overnight, and then treated with EGF (5 ng/mL) for the indicated time periods. B, effect of pharmacologic inhibitors on EGF-induced Akt, ERK, and CREB phosphorylation. The same 7-day-old NHTBE cell cultures maintained in BEBM without supplements overnight were treated with EGF (5 ng/mL) alone or in combination with the indicated pharmacologic inhibitors for 15 minutes. Inhibitors were pretreated 30 minutes before EGF treatment. C, histologic evaluation of pharmacologic inhibitors' effects. Seven-day-old NHTBE cell cultures were incubated with 5 ng/mL EGF alone or in combination with the various inhibitors for 4 days. Control cultures were maintained in 0.5 ng/mL EGF media. Cell numbers and thickness of cultures were determined as described in Materials and Methods. D, treatment effects of erlotinib on EGF-induced hyperplasia. Seven-day-old NHTBE cell cultures were treated with EGF (5 ng/mL) for 4 days to generate hyperplasia. The cultures were then maintained in culture media with 0.5 ng/mL EGF for 4 more days with or without inhibitors. The result was evaluated by using hematoxylin/eosin staining. Cells were counted, as described in Materials and Methods. The results were summarized by descriptive statistics (mean, SD, and median).

approximately 1% to 2% per patient per year, with a cumulative risk of up to 20% at 6 to 8 years after resection (15). Erlotinib would target 2 cell populations at once: micrometastatic NSCLC cells and evolving bronchial epithelial cells. Inhibition of erlotinib and reversal of the first step in lung carcinogenesis in NHTBE cells warrant further investigation. We are conducting a clinical study and have enrolled 50 patients with early-stage lung cancer who have undergone neoadjuvant chemotherapy with cisplatin and docetaxel, followed by surgical resection and 1 year of adjuvant erlotinib. Patients will undergo bronchoscopy at 6 months and 1 year to assess possible changes in the bronchial epithelium after erlotinib treatment (16).

Published OnlineFirst on April 19, 2011; DOI:10.1158/1940-6207.CAPR-10-0364

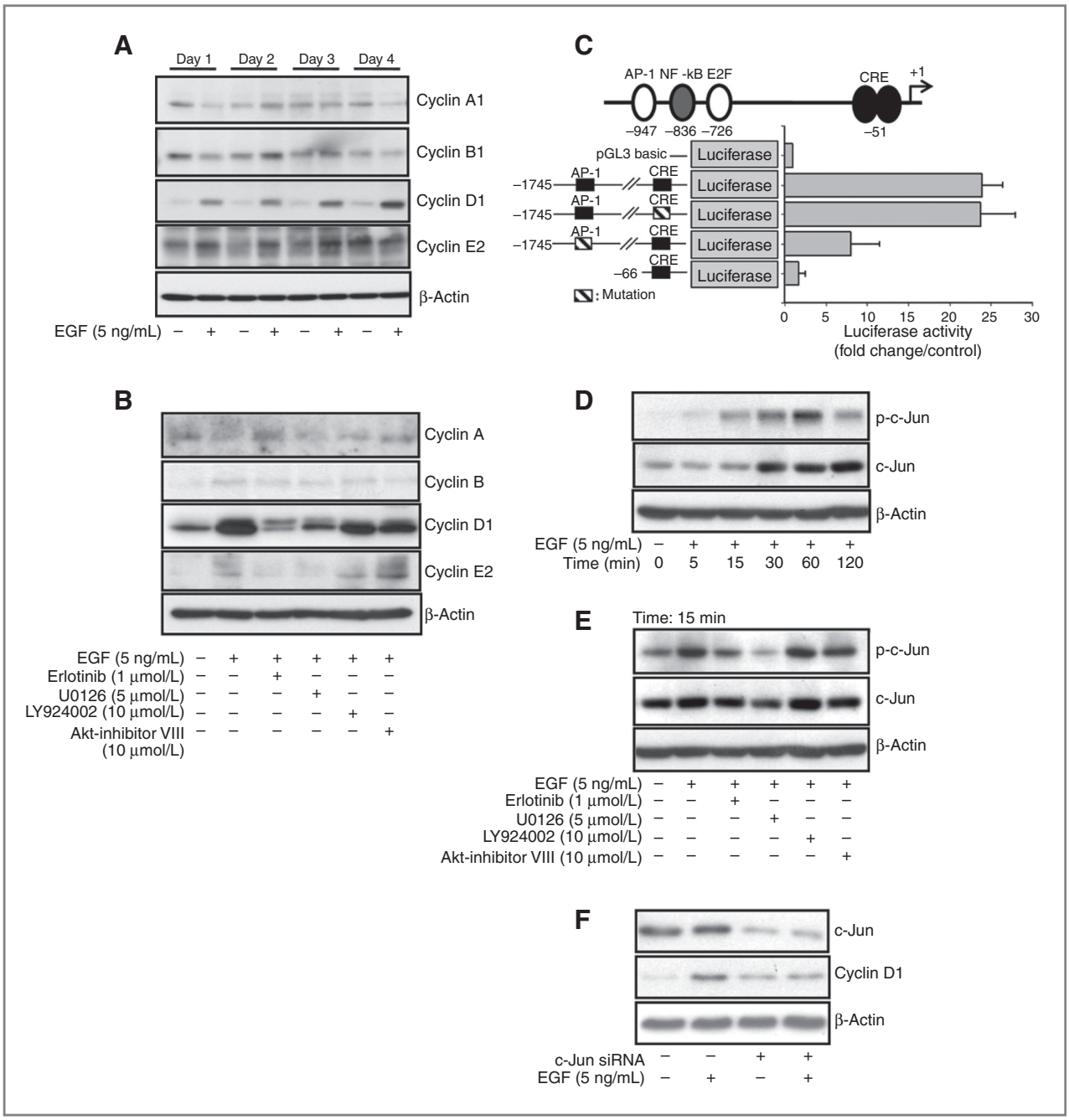

Figure 4. AP-1 is a critical transcription factor in EGF-induced cyclin D1 overexpression in NHTBE cells. A, B, D, and E, NHTBE cells were cultured on a Transwell plate until they formed a monolayer. The culture condition was changed to an air–liquid interface. Before EGF stimulation or pharmacologic inhibitor treatment, cells were incubated with 0.1% BSA/BEBM medium for 24 hours before treatment. A, EGF upregulates cyclin D1 expression in a time-dependent manner. B, erlotinib and U0126 inhibit EGF-induced cyclin D1 expression. C, the AP-1 binding site is important for cyclin D1 promoter activity. Cells were transfected with indicated plasmids by using a 12-well tissue culture plate. After 48 hours of incubation, cells were maintained in 0.1% BSA/BEBM without supplements overnight and treated with EGF (5 ng/mL) for 24 hours. D, EGF induces c-Jun phosphorylation in a time-dependent manner. E, erlotinib and U0126 inhibit EGF-induced c-Jun phosphorylation. F, c-Jun siRNA abrogated EGF-induced cyclin D1 expression. Cells were transfected with siRNA by using a 12-well tissue culture plate. After 48 hours incubation, cells were maintained in 0.1% BSA/BEBM without supplements overnight and treated with EGF (5 ng/mL) for 24 hours. Data shown are representative of 3 experiments with similar results.

We found that EGF robustly increased cyclin D1 in primary NHTBE cells grown in organotypic culture. The malignant transformation of bronchial epithelial cells is driven by the dysregulation of oncogenes, growth factors, or tumor suppressor genes. Cyclin D1 is strongly implicated as an oncogene in lung cancer and several other

Published OnlineFirst on April 19, 2011; DOI:10.1158/1940-6207.CAPR-10-0364

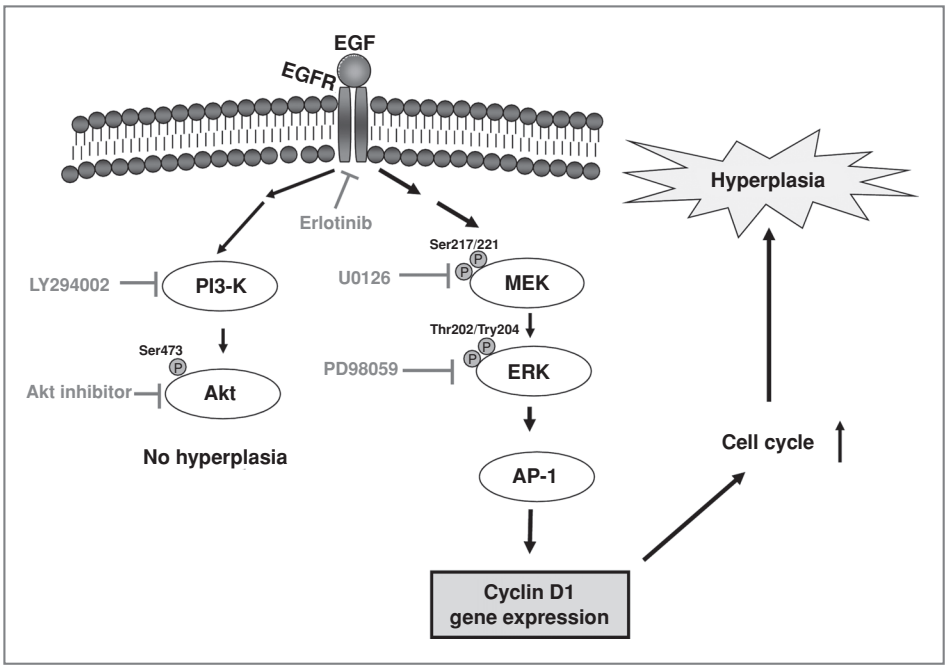

Figure 5. EGF induced increased cyclin D1 expression, which plays a critical role in bronchial hyperplasia; overexpression was mediated by activating the MAPK pathway.

human cancers, including B-cell lymphomas, head and neck squamous cell carcinomas, esophageal cancer, and breast cancer (17). Cyclin D1 is part of the cyclin-dependent kinase (CDK)-cyclin complex that increases retinoblastoma (Rb) protein phosphorylation at the G_1-S transition and may play a role in transcriptional regulation. Cyclin D deregulation, by amplification or transcriptional upregulation, has been found in many tumor types (18–22). The p53-Rb pathway that mediates G_1 arrest is the most commonly affected pathway in lung cancer. Defects in G_1-regulatory proteins, especially p53-p21WAF1, p16-Rb-cyclin D1, and cyclin E-p16 pathway deregulation, seem to be essential to lung cancer development (23, 24). An immunohistochemical analysis showed cyclin D1 and E overexpression in bronchial preneoplasia that precedes the development of squamous cell carcinoma (25). These data imply that increased cyclin levels play a critical role in preneoplastic bronchial lesion progression. This conclusion was confirmed in bronchial epithelial cellular models (14) and carcinogen-induced lung tumors in animal models (26, 27).

Cyclin D1 overexpression may portend a worse prognosis in patients with resected lung cancer (28), although results have not been consistent (29). Cyclin D1 seems to be regulated by EGFR in gefitinib-resistant EGFR mutant cell lines, and these cell lines are sensitive to flavopiridol, a CDK inhibitor (30). Cyclin D1 repression is an indirect marker of erlotinib treatment response in aerodigestive tract cancers (31). Chemoprevention trials have found that rexinoid, a selective retinoid X receptor agonist, suppresses cyclin D1 expression in NSCLC (32), and low cyclin D1 expression predicts longer cancer-free survival in laryngeal premalignancy patients (33). Thus, cyclin D1 levels have been studied as markers for abnormal cell growth in chemoprevention trials (34). Cyclin D1 gene expression regulation has been reported to include the ras/raf/mitogen-activated protein kinase (MAPK) cascade in fibroblast cells (35, 36), p60Src pathways through CREB/activating transcription factor 2 activation in breast cancer cells (37), and PI3-K/Akt/NF-κB pathway-involved prooncogenic effects in human bronchial epithelial cells (38). Our data showed that EGF activates the PI3-K/Akt and MEK/ERK pathways in a time-dependent manner. However, only the MEK/ERK pathway was involved in EGF-induced cyclin D1 expression, suggesting that it is involved in early-stage lung carcinogenesis.

As shown in Figure 5, we found that bronchial hyperplasia can be modeled *in vitro* by using a 3D organotypic culture method and prevented by blocking the EGFR/MEK signaling pathway. We further found that bronchial hyperplasia is dependent on cyclin D1, which is regulated by AP-1 activation through the MEK/ERK pathway rather than the PI3-K/Akt pathway. Our model system and results will help elucidate the molecular mechanisms of lung carcinogenesis at its early stages and may support the prophylactic use of EGFR-targeting agents in patients at high risk of tumor development.

Disclosure of Potential Conflicts of Interest

No potential conflicts of interest were disclosed.

Acknowledgment

We thank Dr. Richard Pestell (Thomas Jefferson University, Philadelphia, PA) for the gift of cyclin D1 luciferase vectors.

Grant Support

Department of Defense VITAL grant W81XW-04-1-0142 (J.S. Koo, E.S. Kim, and W.K. Hong), National Heart, Lung and Blood Institute grant R01-HL-077556 (J.S. Koo), and National Cancer Institute Cancer Center Support grant CA-16672 (The University of Texas MD Anderson Cancer Center).

The costs of publication of this article were defrayed in part by the payment of page charges. This article must therefore be hereby marked *advertisement* in accordance with 18 U.S.C. Section 1734 solely to indicate this fact.

Received December 8, 2010; revised March 23, 2011; accepted April 3, 2011; published OnlineFirst April 19, 2011.

References

1. Saccomanno G, Archer VE, Auerbach O, Saunders RP, Brennan LM. Development of carcinoma of the lung as reflected in exfoliated cells. Cancer 1974;33:256–70.
2. Auerbach O, Hammond EC, Garfinkel L. Changes in bronchial epithelium in relation to cigarette smoking, 1955–1960 vs. 1970–1977. N Engl J Med 1979;300:381–5.
3. Saccomanno G, Archer VE, Saunders RP, Auerbach O, Klein MG. Early indices of cancer risk among uranium miners with reference to modifying factors. Ann N Y Acad Sci 1976;271:377–83.
4. Strong MS, Incze J, Vaughan CW. Field cancerization in the aerodigestive tract–its etiology, manifestation, and significance. J Otolaryngol 1984;13:1–6.
5. Warburton D, Schwarz M, Tefft D, Flores-Delgado G, Anderson KD, Cardoso WV. The molecular basis of lung morphogenesis. Mech Dev 2000;92:55–81.
6. Scagliotti GV, Selvaggi G, Novello S, Hirsch FR. The biology of epidermal growth factor receptor in lung cancer. Clin Cancer Res 2004;10:4227s-32s.
7. Vlahovic G, Crawford J. Activation of tyrosine kinases in cancer. The Oncologist 2003;8:531–8.
8. Koo JS, Jetten AM, Belloni P, Yoon JH, Kim YD, Nettesheim P. Role of retinoid receptors in the regulation of mucin gene expression by retinoic acid in human tracheobronchial epithelial cells. Biochem J 1999;338:351–7.
9. Aggarwal S, Kim SW, Cheon K, Tabassam FH, Yoon JH, Koo JS. Nonclassical action of retinoic acid on the activation of the cAMP response element-binding protein in normal human bronchial epithelial cells. Mol Biol Cell 2006;17:566–75.
10. Kim SW, Cheon K, Kim CH, Yoon JH, Hawke DH, Kobayashi R, et al. Proteomics-based identification of proteins secreted in apical surface fluid of squamous metaplastic human tracheobronchial epithelial cells cultured by three-dimensional organotypic air-liquid interface method. Cancer Res 2007;67:6565–73.
11. Koo JS, Yoon JH, Gray T, Norford D, Jetten AM, Nettesheim P. Restoration of the mucous phenotype by retinoic acid in retinoid-deficient human bronchial cell cultures: changes in mucin gene expression. Am J Respir Cell Mol Biol 1999;20:43–52.
12. Loupakis F, Vasile E, Santini D, Masi G, Falcone A, Graziano F. EGF-receptor targeting with monoclonal antibodies in colorectal carcinomas: rationale for a pharmacogenomic approach. Pharmacogenomics 2008;9:55–69.
13. Shepherd FA, Rodrigues Pereira J, Ciuleanu T, Tan EH, Hirsh V, Thongprasert S, et al. Erlotinib in previously treated non-small-cell lung cancer. N Engl J Med 2005;353:123–32.
14. Moyer JD, Barbacci EG, Iwata KK, Arnold L, Boman B, Cunningham A, et al. Induction of apoptosis and cell cycle arrest by CP-358,774, an inhibitor of epidermal growth factor receptor tyrosine kinase. Cancer Res 1997;57:4838–48.
15. Johnson BE. Second lung cancers in patients after treatment for an initial lung cancer. J Natl Cancer Inst 1998;90:1335–45.
16. Gold KA, Lee JJ, Rice D, Tse W, Stewart D, Wistuba I, et al. Phase II pilot study of neoadjuvant docetaxel and cisplatin followed by adjuvant erlotinib in patients with stage I-III non-small cell lung cancer (NSCLC). J Clin Oncol ASCO Annu Meeting Proc (Post-Meeting Ed) 2009;27.
17. Motokura T, Arnold A. Cyclin D and oncogenesis. Curr Opin Genet Dev 1993;3:5–10.
18. Sheyn I, Noffsinger AE, Heffelfinger S, Davis B, Miller MA, Fenoglio-Preiser CM. Amplification and expression of the cyclin D1 gene in anal and esophageal squamous cell carcinomas. Hum Pathol 1997;28:270–6.
19. Bellacosa A, Almadori G, Cavallo S, Cadoni G, Galli J, Ferrandina G, et al. Cyclin D1 gene amplification in human laryngeal squamous cell carcinomas: prognostic significance and clinical implications. Clin Cancer Res 1996;2:175–80.
20. Yatabe Y, Nakamura S, Seto M, Kuroda H, Kagami Y, Suzuki R, et al. Clinicopathologic study of PRAD1/cyclin D1 overexpressing lymphoma with special reference to mantle cell lymphoma. A distinct molecular pathologic entity. Am J Surg Pathol 1996;20:1110–22.
21. Gillett C, Fantl V, Smith R, Fisher C, Bartek J, Dickson C, et al. Amplification and overexpression of cyclin D1 in breast cancer detected by immunohistochemical staining. Cancer Res 1994;54:1812–7.
22. Bartkova J, Lukas J, Strauss M, Bartek J. Cyclin D1 oncoprotein aberrantly accumulates in malignancies of diverse histogenesis. Oncogene 1995;10:775–8.
23. Reissmann PT, Koga H, Takahashi R, Figlin RA, Holmes EC, Piantadosi S, et al. Inactivation of the retinoblastoma susceptibility gene in non-small-cell lung cancer. The Lung Cancer Study Group. Oncogene 1993;8:1913–9.
24. Kratzke RA, Greatens TM, Rubins JB, Maddaus MA, Niewoehner DE, Niehans GA, et al. Rb and p16INK4a expression in resected non-small cell lung tumors. Cancer Res 1996;56:3415–20.
25. Lonardo F, Rusch V, Langenfeld J, Dmitrovsky E, Klimstra DS. Overexpression of cyclins D1 and E is frequent in bronchial preneoplasia and precedes squamous cell carcinoma development. Cancer Res 1999;59:2470–6.
26. Witschi H, Espiritu I, Suffia M, Pinkerton KE. Expression of cyclin D1/2 in the lungs of strain A/J mice fed chemopreventive agents. Carcinogenesis 2002;23:289–94.
27. Boyle JO, Langenfeld J, Lonardo F, Sekula D, Reczek P, Rusch V, et al. Cyclin D1 proteolysis: a retinoid chemoprevention signal in normal, immortalized, and transformed human bronchial epithelial cells. JNatl Cancer Inst 1999;91:373–9.
28. Ratschiller D, Heighway J, Gugger M, Kappeler A, Pirnia F, Schmid RA, et al. Cyclin D1 overexpression in bronchial epithelia of patients with lung cancer is associated with smoking and predicts survival. J Clin Oncol 2003;21:2085–93.
29. Filipits M, Pirker R, Dunant A, Lantuejoul S, Schmid K, Huynh A, et al. Cell cycle regulators and outcome of adjuvant cisplatin-based chemotherapy in completely resected non-small-cell lung cancer: the International Adjuvant Lung Cancer Trial Biologic Program. J Clin Oncol 2007;25:2735–40.
30. Kobayashi S, Shimamura T, Monti S, Steidl U, Hetherington CJ, Lowell AM, et al. Transcriptional profiling identifies cyclin D1 as a critical downstream effector of mutant epidermal growth factor receptor signaling. Cancer Res 2006;66:11389–98.
31. Petty WJ, Dragnev KH, Memoli VA, Ma Y, Desai NB, Biddle A, et al. Epidermal growth factor receptor tyrosine kinase inhibition represses cyclin D1 in aerodigestive tract cancers. Clin Cancer Res 2004;10:7547–54.
32. Dragnev KH, Petty WJ, Shah SJ, Lewis LD, Black CC, Memoli V, et al. A proof-of-principle clinical trial of bexarotene in patients with non-small cell lung cancer. Clin Cancer Res 2007;13:1794–800.
33. Papadimitrakopoulou V, Izzo JG, Liu DD, Myers J, Ceron TL, Lewin J, et al. Cyclin D1 and cancer development in laryngeal premalignancy patients. Cancer Prev Res 2009;2:14–21.
34. Freemantle SJ, Guo Y, Dmitrovsky E. Retinoid chemoprevention trials: cyclin D1 in the crosshairs. Cancer Prev Res 2009;2:3–6.

Published OnlineFirst on April 19, 2011; DOI:10.1158/1940-6207.CAPR-10-0364

35. Takuwa N, Takuwa Y. Ras activity late in G1 phase required for p27kip1 downregulation, passage through the restriction point, and entry into S phase in growth factor-stimulated NIH 3T3 fibroblasts. Mol Cell Biol 1997;17:5348–58.
36. Lavoie JN, L′Allemain G, Brunet A, Muller R, Pouyssegur J. Cyclin D1 expression is regulated positively by the p42/p44MAPK and negatively by the p38/HOGMAPK pathway. J Biol Chem 1996;271:20608–16.
37. Lee RJ, Albanese C, Stenger RJ, Watanabe G, Inghirami G, Haines GK, et al. pp60(v-src) induction of cyclin D1 requires collaborative interactions between the extracellular signal-regulated kinase, p38, and Jun kinase pathways. A role for cAMP response element-binding protein and activating transcription factor-2 in pp60(v-src) signaling in breast cancer cells. J Biol Chem 1999; 274:7341–50.
38. Han SW, Roman J. Fibronectin induces cell proliferation and inhibits apoptosis in human bronchial epithelial cells: pro-oncogenic effects mediated by PI3-kinase and NF-kappa B. Oncogene 2006;25:4341–9.

Journal of Biopharmaceutical Statistics, 17: 461–480, 2007

ISSN: 1054-3406 print/1520-5711 online
DOI: 10.1080/10543400701199593

Taylor & Francis
Taylor & Francis Group

INTERACTION INDEX AND DIFFERENT METHODS FOR DETERMINING DRUG INTERACTION IN COMBINATION THERAPY

J. J. Lee
Department of Biostatistics, University of Texas, M. D. Anderson Cancer Center, Houston, Texas, USA

M. Kong
Department of Biostatistics and Bioinformatics, University of Louisville, Kentucky, USA

G. D. Ayers
Department of Biostatistics, Vanderbilt University Medical Center, Nashville, Tennessee, USA

R. Lotan
Division of Cancer Medicine, University of Texas, M. D. Anderson Cancer Center, Houston, Texas, USA

Studying and understanding the joint effect of combined treatments is important in pharmacology and in the development of combination therapies. The Loewe additivity model is one of the best general reference models for evaluating drug interactions. Based on this model, synergy occurs when the interaction index is less than one, while antagonism occurs when interaction index is greater than one. We expound the meaning of the interaction index, and propose a procedure to calculate the interaction index and its associated confidence interval under the assumption that the dose-effect curve for a single agent follows Chou and Talalay's median effect equation. In addition, we review four response surface models based on the Loewe additivity model using a single parameter to determine drug interactions. We describe each of these models in the context of Loewe additivity model and discuss their relative advantages and disadvantages. We also provide S-PLUS/R code for each approach to facilitate the implementation of these commonly used methods.

Key Words: Antagonism; Drug interaction; Loewe additivity model; Response surface model; Synergy.

1. INTRODUCTION

Studying and understanding the combined effects of multiple concurrent treatments has a venerable history among basic scientists, clinicians, and statisticians

Received April 19, 2006; Accepted December 30, 2006
Address correspondence to J. J. Lee, Department of Biostatistics, University of Texas, M. D. Anderson Cancer Center, Houston, Texas, USA; Fax: 713-563-4242; E-mail: jjlee@mdanderson.org

with the goal to develop better treatment regimens with increased efficacy and reduced toxicity. Many such successful studies can be found in the literature including, for example, a study of the cocktail approach to control AIDS with nucleoside reverse transcriptase inhibitors, non-nucleoside reverse transcriptase inhibitors, and protease inhibitors (Sharma et al., 2004); studies of platinum-based doublets that include a taxane, vinorelbine, or gemcitabine (Evans, 2004) or the use of chemoradiation therapy (Curran, 2003) for non-small-cell lung cancer. Advents in molecular target-based treatments for cancer have rekindled an interest in studying combinations of targeting agents, chemotherapy, and/or radiation therapy (Herbst, 2005; Niyazi and Belka, 2006). In addition, examining adverse effects following the simultaneous administration of multiple drugs is important in toxicology studies to ensure that combination therapy can be given safely. Recent advancements in systems biology also point to a promising direction in developing and quantifying effective combination therapy (Fitzgerald et al., 2006).

Data from *in vitro* and *in vivo* assays are useful for screening out inefficacious and/or toxic combination regimens while selecting the promising ones for further development. Although it is generally recognized that *in vitro* data cannot be extrapolated directly to *in vivo* or clinical settings, there are many successful examples in which *in vitro* data predict *in vivo* drug interactions (Bachmann and Ghosh, 2001). Failure of accurate predictions may be caused by the methodology used, inappropriate model selection, errant scale-up factors, biological differences, etc.

A drug-induced effect may be expressed on a continuous scale or on a binary scale. For example, in cell line studies, percent cell survival or percent cell killed is commonly applied to measure the drug effect. In animal studies, when a binary response status is recorded, the response rate, i.e., the number of responses divided by the total number assigned to a dose, can be constructed as a measurement of treatment effect (Finney, 1971; Morgan, 1992).

To characterize drug interaction, we first need to define an appropriate reference model for additive effects of drug combinations. When the effect of a combination dose is greater (less) than that predicted by the additivity model, the combination dose is synergistic (antagonistic). Historically, three additivity reference models are commonly used (Berenbaum, 1989; Greco et al., 1995): 1) effect addition, 2) Bliss independence, and 3) Loewe additivity. Excellent and comprehensive reviews on drug interaction can be found in Berenbaum (1989), Greco et al. (1995), and Tallarida (2000). The effect addition model has a simple form: $E(d_1, d_2) = E(d_1) + E(d_2)$, where $E(d_1, d_2)$ is the effect at (d_1, d_2), and $E(d_i)$ is the effect of drug i alone at dose d_i with $i = 1, 2$. However, this model is not generally correct. For example, when $E(d_1) = E(d_2) = 70\%$, clearly $E(d_1, d_2)$ can not be 140% when the effect is measured as a proportion of cells killed. The Bliss independence model (Bliss, 1939; Greco et al., 1995; Webb, 1963) is also called effect multiplication or the fractional product, which has the form $f_{12} = f_1 f_2$. Here f_1, f_2, and f_{12} are the effects expressed as the fractions of the maximal effects for drug 1, drug 2, and the combination, and the maximal effect of a drug or combination is defined as the effect observed with an infinite amount of the drug or combination. For example, the Bliss independence model for percentage cell survival is $E(d_1, d_2) = E(d_1)E(d_2)$. Combination doses with effects less than predicted are

synergistic, and conversely, antagonistic. The Loewe additivity model to characterize drug interaction can be defined as:

$$\frac{d_1}{D_{y,1}} + \frac{d_2}{D_{y,2}} \begin{cases} =1, & \text{Additivity;} \\ <1, & \text{Synergy;} \\ >1, & \text{Antagonism,} \end{cases} \tag{1}$$

where d_1, d_2 are doses of drug 1 and drug 2 in mixture, which produces an effect y, while $D_{y,1}$ and $D_{y,2}$ are the doses of drug 1 and drug 2 that produce the same effect y when given alone. The term $\frac{d_1}{D_{y,1}} + \frac{d_2}{D_{y,2}}$ is also called the interaction index at the combination dose (d_1, d_2). If the interaction index at (d_1, d_2) is equal to, less than, or greater than 1, the combination dose (d_1, d_2) is claimed to be additive, synergistic, or antagonistic, respectively.

The Bliss independence and Loewe additivity models are the two most cited reference models for defining drug interactions (Fitzgerald et al., 2006; Greco et al., 1995; Jonker et al., 2005). The literature indicates that the Loewe additivity model works in the settings of mutually exclusive drugs while the Bliss independence model works in the settings of mutually nonexclusive drugs. However, the mechanism of drug interactions is often unknown. Debate continues over which is the better reference model for defining drug interaction. So far, there is no generally accepted agreement as to which of the two models is more appropriate. Both models were recommended by the so-called Saariselkaa agreement (Greco et al., 1992). Drebler et al. (1999) developed *CombiTool,* software to assess drug interactions based on both of the reference models. Berenbaum (1989) showed that the two reference models are the same if the dose-effect curves are in simple exponential family, i.e., $E(d) = \exp(-\beta d)$. The Bliss independence was originally derived from probability theory, and the effect scale can only be applied to fractional effects $0 < E < 1$. Although the Bliss independence has extensive mechanistic and probabilistic support, the underlying independence assumption may be difficult to verify. On the other hand, the Loewe additivity model was defined based on the dose scale no matter the measurements of the effects. Berenbaum (1989) used a "sham combination" (i.e., a drug is combined with itself or its diluted form) thought experiment to advocate the Loewe additivity model. Although supporters of the Bliss independence model question the validity of applying the "sham combination" to general drug combination because the "sham" treatments involve the same treatment and are not independent of each other, the Loewe additivity model gives an intuitively clear and reasonable explanation for experiments beyond the "sham combination". For example, when two non-interactive and equally potent drugs are applied together, we expect that the combination dose (d_1, d_2) will have the same effect as drug 1 alone or drug 2 alone at dose level $d_1 + d_2$. Drug additivity is substantiated under the Loewe additivity model but not the Bliss independence model. The Loewe additivity model is also consistent with the graphical isobologram approach (Martinez-Irujo et al., 1998). Hence, we conclude that the Loewe additivity model is one of the best general reference models for evaluating drug interactions.

In this paper, we intend to clarify the meaning of the interaction index and compare several commonly used methods on assessing drug interaction based

on the Loewe additivity model. In Section 2, we illustrate the meaning of the interaction index, and show that the interaction index can be used to characterize the magnitude of non-additive effects. In Section 3, we derive the interaction index and demonstrate how to construct its confidence interval under the assumption that the median-effect equation holds for both agents. In addition, we review the commonly applied approach to assess drug interactions by Chou and Talalay (1984). Based on the Loewe additivity model, response surface models (RSMs) can be constructed to describe the three dimensional dose-response surface in two drug combinations and can include all of the information present in the full dose-effect data set for two drugs. In addition, the RSM can be used to quantify the amount of drug interactions and to determine the optimal combination therapy. The RSM's of Finney (1971), Greco et al. (1990), Machado and Robinson (1994), Plummer and Short (1990), and Carter et al. (1988), use a single parameter to quantify synergy, additivity, or antagonism, and have been successfully applied in many reported case studies. We review those approaches in Section 4, taking the median-effect equation as the dose-effect model for each single agent except for the model by Carter et al. (1988), which uses a logistic model. We give an example of the combination of two agents to elicit cell death in a cancer cell line study in Section 5. The results of analysis using these methods are given in Section 6 to compare and contrast the properties of various methods. In addition, we supply S-PLUS/R code to provide investigators useful tools for studying drug interactions. In Section 7, we discuss our findings and make suggestions on future research areas.

2. INTERACTION INDEX AND ITS INTERPRETATION

Suppose that the combination dose (d_1, d_2) elicits the same effect y as drug 1 alone at dose $D_{y,1}$, and drug 2 alone at dose $D_{y,2}$, then $\frac{d_1}{D_{y,1}} + \frac{d_2}{D_{y,2}}$, the interaction index at dose (d_1, d_2),denoted by τ, measures additivity, synergy, or antagonism according to the relation shown in Eq. (1).

What does the interaction index τ mean? Note that $\frac{d_1}{D_{y,1}} + \frac{d_2}{D_{y,2}} = \tau$ can be rewritten as

$$d_1 + d_2 \frac{D_{y,1}}{D_{y,2}} = \tau D_{y,1}. \tag{2}$$

The ratio $\frac{D_{y,1}}{D_{y,2}}$ is defined as relative potency of drug 2 versus drug 1 (Morgan, 1992). Suppose the relative potency is a constant ρ at any level of effect, then one unit of drug 2 produces the same effect as ρ units of drug 1. Thus the total combined dose (d_1, d_2) will be $d_1 + \rho d_2$ in terms of drug 1 dose. Particularly, $\tau = 1$ implies $d_1 + \rho d_2 = D_{y,1}$, i.e., the total dose of the two drugs elicits the same effect as drug 1 is used alone at $D_{y,1}$, indicating additivity of the combination dose (d_1, d_2). $\tau < 1$ implies $d_1 + \rho d_2 = \tau D_{y,1} < D_{y,1}$, i.e., the total dose is less than that when drug 1 is used alone, indicating synergy of the combination dose (d_1, d_2); while $\tau > 1$ implies $d_1 + \rho d_2 = \tau D_{y,1} > D_{y,1}$, i.e., the total dose is more than that when drug 1 is used alone, indicating antagonism of the combination dose (d_1, d_2). Obviously, the smaller the τ is, the smaller is the total amount dose $d_1 + \rho d_2$, which produces the same effect as drug 1 alone at dose $D_{y,1}$. Therefore, the interaction

index, τ, is a quantitative measure capturing the mode and magnitude of drug interaction.

Geometrically, the drug interaction can be illustrated by constructing an isobole. An isobole corresponding to an effect y consists of all the combination doses (d_1, d_2) that elicit the effect y. In Fig. 1, suppose P is the point $(D_{y,1}, 0)$, Q is the point $(0, D_{y,2})$, and U is the point (d_1, d_2); all these points yield an effect y. Then, the relative potency $\rho = \frac{\text{length}(\overline{OP})}{\text{length}(\overline{OQ})}$, and the interaction index can be expressed as

$$\tau = \frac{d_1 + \rho d_2}{D_{y,1}} = \frac{\text{length}(\overline{OR})}{\text{length}(\overline{OP})} = \frac{\text{length}(\overline{OU})}{\text{length}(\overline{OV})} \quad \text{Fig. 1, Panel A}$$

The line $\overline{RS}$ is parallel to the line $\overline{PQ}$ (Fig. 1, Panel A), V is the intersection of $\overrightarrow{OU}$ and $\overline{PQ}$. So when U is on the straight line $\overline{PQ}$, the interaction index will be 1; when U is on the south-west side of the straight line $\overline{PQ}$, the interaction index will be less than 1; when U is on the north-east side of the straight line $\overline{PQ}$, the interaction index will be greater than 1. If the isobole is a straight line $\overline{PQ}$ (Fig. 1, Panel B), then any combination dose (d_1, d_2) on this line will have an interaction index at 1, indicating that the combination dose (d_1, d_2) is additive. If an isobole is concave down similar to the solid curve $\widehat{PNQ}$, then any combination dose (d_1, d_2) on this curve will have an interaction index less than 1, except at P and Q, indicating that these combination doses are synergistic. If an isobole is concave up similar to the solid curve $\widehat{PMQ}$, then any combination dose (d_1, d_2) on this curve will have an interaction index greater than 1, except at P and Q, indicating antagonism. However, the interaction indices for different combination doses on an isobole may

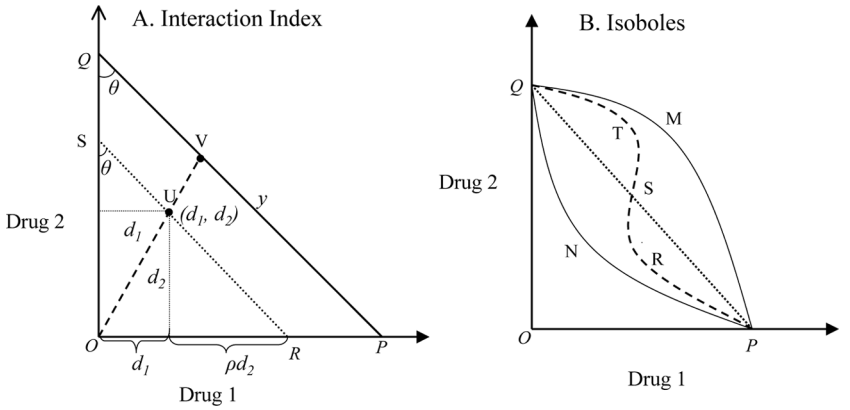

Figure 1 Geometric interpretation of the interaction index (Panel A) and examples of isoboles (Panel B). In both panels, $P = (D_{y,1}, 0)$ and $Q = (0, D_{y,2})$ showing the doses resulting effect y using single agent of drug 1 and drug 2. In Panel A, $U = (d_1, d_2)$, the effect $E(d_1, d_2) = y$, $\rho = tangent(\theta)$, and the interaction index $\tau = \frac{d_1+\rho d_2}{D_{y,1}} = \frac{\text{length}(\overline{OR})}{\text{length}(\overline{OP})} = \frac{\text{length}(\overline{OU})}{\text{length}(\overline{OV})}$. In Panel B, the dotted straight line $\overline{PQ}$ is a representation of a theoretical additive isobole. The solid curve $\widehat{PNQ}$ is a representation of an isobole with synergy, $\widehat{PMQ}$ is a representation of an isobole with antagonism, and the dashed curve $\widehat{PRSTQ}$ is a representation of an isobole with both synergy and antagonism.

be different. For example, the interaction index for the combination dose close to points P and Q on $\widehat{PNQ}$ will be less than 1 but close to 1, and the interaction index possibly has a minimum at point N, which means that the combination dose (d_1, d_2) at N is most synergistic among all the combination doses on $\widehat{PNQ}$. Similarly, the combination dose (d_1, d_2) at M may be most antagonistic among the combination doses on $\widehat{PMQ}$. An isobole may cross the additive isobole $\overline{PQ}$, e.g, the curve $\widehat{PRSTQ}$. In that case, the combination doses on the segment $\widehat{PRS}$ are synergistic, while the combination doses on the segment $\widehat{STQ}$ are antagonistic.

3. DERIVING INTERACTION INDEX AND CONSTRUCTING ITS CONFIDENCE INTERVAL

Generally, given the dose-effect curve for each single drug, the interaction index is determined by the combination dose (d_1, d_2) and its corresponding effect y. For example, if the effect at the combination dose (d_1, d_2) is y, and the dose-effect curve is $f_1(D_1)$ for drug 1, and $f_2(D_2)$ for drug 2, then $D_{y,1} = f_1^{-1}(y)$, and $D_{y,2} = f_2^{-1}(y)$, where f_i^{-1} $(i = 1, 2)$ is the inverse function of f_i. Thus we can estimate the value of the interaction index without specifying a joint model, $f(d_1, d_2)$, for the combination dose (d_1, d_2).

In the literature, there are different models to describe dose-effect curve, such as the probit model (Finney, 1971) and the logistic model (Morgan, 1992) for a binary response variable, and the $E_{\max}$ model, also known as Hill equation (Greco et al., 1995; Hill, 1910; Holford and Sheiner, 1981), for a continuous response variable. The $E_{\max}$ model has the following form:

$$E = \frac{E_{\max}\left(\frac{d}{D_m}\right)^m}{1 + \left(\frac{d}{D_m}\right)^m}, \tag{3}$$

where d is the dose of drug, D_m is the median effective dose of a drug, $E_{\max}$ is the maximal effect of the associated drug, and m is a slope parameter, also called the Hill coefficient, depicting the shape of the curve. When $E_{\max} = 1$, model ((3)) becomes Chou and Talalay's median effect equation (Chou and Talalay, 1984):

$$E = \frac{\left(\frac{d}{D_m}\right)^m}{1 + \left(\frac{d}{D_m}\right)^m}, \tag{4}$$

In our cell line study, we found the median effect Eq. (4) gave a reasonable estimation of the dose-effect curve. When m is negative, the measurements of effects described by Eqs. (3) and (4) decrease with increasing drug concentration; when m is positive, the curves rise with increasing drug concentration.

Equation (4) can be rewritten as

$$\log \frac{E}{1 - E} = m(\log d - \log D_m) = \beta_0 + \beta_1 \log d, \tag{5}$$

where $\beta_0 = -m \log D_m$ and $\beta_1 = m$. The dose producing effect E can be written as

$$d = D_m \left(\frac{E}{1-E} \right)^{\frac{1}{m}}, \tag{6}$$

$$\text{or} \quad d = \exp\left(-\frac{\beta_0}{\beta_1} \right) \left(\frac{E}{1-E} \right)^{\frac{1}{\beta_1}}. \tag{7}$$

Suppose model (5) has the form $\log \frac{E}{1-E} = \beta_0 + \beta_1 \log d + \epsilon$ with ϵ following $N(0, \sigma^2)$, we may regress $\log \frac{E}{1-E}$ on $\log d$ to get the marginal dose-effect curves $\log \frac{E}{1-E} = \hat{\beta}_{0,1} + \hat{\beta}_{1,1} \log d$ for drug 1 and $\log \frac{E}{1-E} = \hat{\beta}_{0,2} + \hat{\beta}_{1,2} \log d$ for drug 2. If the observed mean effect is y at a combination dose (d_1, d_2), then the associated interaction index can be estimated by

$$\hat{\tau} = \frac{d_1}{\widehat{D}_{y,1}} + \frac{d_2}{\widehat{D}_{y,2}} = \frac{d_1}{\exp\left(-\frac{\hat{\beta}_{0,1}}{\hat{\beta}_{1,1}}\right)\left(\frac{y}{1-y}\right)^{\frac{1}{\hat{\beta}_{1,1}}}} + \frac{d_2}{\exp\left(-\frac{\hat{\beta}_{0,2}}{\hat{\beta}_{1,2}}\right)\left(\frac{y}{1-y}\right)^{\frac{1}{\hat{\beta}_{1,2}}}} \tag{8}$$

Extensive simulations (Lee and Kong, 2006) indicate that $\log(\hat{\tau})$ is approximately normal distributed, even when $\hat{\tau}$ deviates from normal distribution for large σ's. A $(1-\alpha) \times 100\%$ confidence interval for $\log(\tau)$ can be constructed based on the delta method (Bickel and Doksum, 2001):

$$\left[\log(\hat{\tau}) - z_{\frac{\alpha}{2}} \sqrt{\text{Var}(\log(\hat{\tau}))}, \log(\hat{\tau}) + z_{\frac{\alpha}{2}} \sqrt{\text{Var}(\log(\hat{\tau}))} \right],$$

and, thus, a $(1-\alpha) \times 100\%$ confidence interval for τ can be formed as:

$$\left[\hat{\tau} \exp(-z_{\frac{\alpha}{2}} \sqrt{\text{Var}(\log(\hat{\tau}))}), \hat{\tau} \exp(z_{\frac{\alpha}{2}} \sqrt{\text{Var}(\log(\hat{\tau}))}) \right], \tag{9}$$

where $z_{\frac{\alpha}{2}}$ is the $1 - \frac{\alpha}{2}$ percentile of the standard normal distribution, and $\text{Var}(\log(\hat{\tau})) \backsimeq \frac{1}{\hat{\tau}^2} \text{Var}(\hat{\tau})$ with

$$\begin{aligned} \text{Var}(\hat{\tau}) \backsimeq & \sum_{i=1}^{2} \left(\frac{d_i}{\widehat{D}_{y,i}} \right)^2 \\ & \times \left(\frac{var(\hat{\beta}_{0,i})}{\hat{\beta}_{1,i}^2} + \frac{2cov(\hat{\beta}_{0,i}, \hat{\beta}_{1,i})(\log \frac{y}{1-y} - \hat{\beta}_{0,i})}{\hat{\beta}_{1,i}^3} + \frac{var(\hat{\beta}_{1,i})(\log \frac{y}{1-y} - \hat{\beta}_{0,i})^2}{\hat{\beta}_{1,i}^4} \right) \\ & + \left(\frac{1}{\hat{\beta}_{1,1}} \frac{d_1}{\widehat{D}_{y,1}} + \frac{1}{\hat{\beta}_{1,2}} \frac{d_2}{\widehat{D}_{y,2}} \right)^2 \left(\frac{1}{y(1-y)} \right)^2 var(y). \end{aligned} \tag{10}$$

Details of the derivation of the variance in Eq. (10) can be found in Lee and Kong (2006). We can estimate $var(y)$ in Eq. (10) in two ways. When there are replicates at the combination dose (d_1, d_2), we estimate $var(y)$ by the sample variance at (d_1, d_2). Otherwise, we may borrow the information from estimating the dose-effect curves. Note that $var(\log \frac{y}{1-y}) \backsimeq (\frac{1}{y(1-y)})^2 var(y)$ thus, we may simply substitute

$(\frac{1}{y(1-y)})^2 var(y)$ by the average of the squared residuals obtained from estimating the two dose-effect curves (Lee and Kong, 2006).

Chou and Talalay (1984) proposed to plot the interaction indices versus effects for combination doses at a fixed ratio. Their idea was to regress $\log \frac{E}{1-E}$ on $\log(d_1 + d_2)$ for the combination doses (d_1, d_2) with $\frac{d_1}{d_2} = \omega$, say, $\log \frac{E}{1-E} = \beta_{0,12} + \beta_{1,12} \log D_{12}$. Then for each fixed effect y, one may estimate the interaction index by

$$\widehat{II} = \frac{\widehat{D}_{y,12} \frac{\omega}{1+\omega}}{\widehat{D}_{y,1}} + \frac{\widehat{D}_{y,12} \frac{1}{1+\omega}}{\widehat{D}_{y,2}}, \tag{11}$$

where $\widehat{D}_{y,1} = \exp\left(-\frac{\hat{\beta}_{0,1}}{\hat{\beta}_{1,1}}\right)\left(\frac{y}{1-y}\right)^{\frac{1}{\hat{\beta}_{1,1}}}$, $\widehat{D}_{y,2} = \exp\left(-\frac{\hat{\beta}_{0,2}}{\hat{\beta}_{1,2}}\right)\left(\frac{y}{1-y}\right)^{\frac{1}{\hat{\beta}_{1,2}}}$, and $\widehat{D}_{y,12} = \exp\left(-\frac{\hat{\beta}_{0,12}}{\hat{\beta}_{1,12}}\right)\left(\frac{y}{1-y}\right)^{\frac{1}{\hat{\beta}_{1,12}}}$. A commercial software *CalcuSyn (http://www.biosoft.com/w/calcusyn.htm)* is available for estimating the interaction index and its confidence interval. However, the confidence interval for interaction index in Eq. (11) are constructed based on Monte Carlo techniques and the normal assumption on the parameters. We constructed the confidence interval for interaction index at observed data point based on the delta method and normal assumption on error in model (5). Extensive calculations involved in Monte Carlo techniques seem unnecessary. In a given experiment with varying doses of single agent and their combinations, we may calculate the interaction indices from Eq. (8) and theirs confidence intervals from Eq. (9) for the observed combination doses at the fixed ratio, and then plot the resulting interaction indices and their confidence intervals to Chou and Talalay's plot of interaction indices versus effects. Thus, the drug interactions for combination doses at the fixed ratio can be characterized.

4. COMPARISON OF FOUR APPROACHES TO DETECT DRUG INTERACTIONS

In this section, we review four response surface models. For comparison purposes we assume that the dose-effect curves follow median-effect Eq. (4) for the first three RSMs. When all the combination doses are synergistic or antagonistic, these approaches use a single synergy-antagonism parameter to summarize synergy or antagonism. In Section 5, we presented a data set from cancer cell line study (Chun et al., 2003). In Section 6, we give the results of data analysis using the method in Section 3 and the RSMs presented in this section, and illustrate the limitation of those methods, i.e., those RSMs are not adequate to capture different patterns of drug interactions when synergy, additivity, and antagonism intersperse.

4.1. Model of Greco et al. (1990)

Assume the dose-effect curves for both drugs follow the median effect Eq. (4), the model proposed by Greco et al. (1990) has the following form:

$$1 = \frac{d_1}{D_{m,1}\left(\frac{y}{1-y}\right)^{\frac{1}{m_1}}} + \frac{d_2}{D_{m,2}\left(\frac{y}{1-y}\right)^{\frac{1}{m_2}}} + \frac{\alpha d_1 d_2}{D_{m,1} D_{m,2}\left(\frac{y}{1-y}\right)^{\frac{1}{2m_1}}\left(\frac{y}{1-y}\right)^{\frac{1}{2m_2}}}. \tag{12}$$

Here, m_1, m_2 are the slopes of the dose-effect curves (4) for drug 1 and drug 2, respectively, and $D_{m,1}$ and $D_{m,2}$ are the median effect doses for drug 1 and drug 2, respectively. The parameter α captures the degree of synergism, additivity, or antagonism.

The dose level for each single drug producing effect y can be expressed as the right-hand side of Eq. (6), i.e., $D_{y,1} = D_{m,1}\left(\frac{y}{1-y}\right)^{\frac{1}{m_2}}$ and $D_{y,2} = D_{m,2}\left(\frac{y}{1-y}\right)^{\frac{1}{m_2}}$. The first two terms on the right-hand side of Eq. (12) are exactly the interaction index written as $\frac{d_1}{D_{y,1}}\frac{d_2}{D_{y,2}}$. So we can rewrite (12) as

$$\frac{d_1}{D_{y,1}} + \frac{d_2}{D_{y,2}} = 1 - \frac{\alpha d_1 d_2}{D_{m,1}^{\frac{1}{2}} D_{m,2}^{\frac{1}{2}} D_{y,1}^{\frac{1}{2}} D_{y,2}^{\frac{1}{2}}}$$

When $\alpha > 0$, the interaction index is less than one, synergism is detected. The larger α is, the smaller is the interaction index, therefore, the stronger is the synergy. When $\alpha < 0$, antagonism is detected; when $\alpha = 0$, additivity is detected. When we say $\alpha > 0$, or $\alpha < 0$, the inference should be made in the statistical point of view. For example, we claim $\alpha > 0$ only when the lower limit of the confidence interval for α is positive. We can estimate all five parameters ($m_1, m_2, D_{m,1}, D_{m,2}, \alpha$) by the least-squares method.

4.2. Model of Machado and Robinson

Of the several models investigated, Machado and Robinson (1994) recommended the following model which was originally derived by Plackett and Hewlett (1952):

$$\left(\frac{d_1}{D_{y,1}}\right)^{\eta} + \left(\frac{d_2}{D_{y,2}}\right)^{\eta} = 1, \tag{13}$$

Similar to the parameter α in the model of Greco et al. (1990), the parameter η captures synergism, additivity, or antagonism: when $0 < \eta < 1$, the combinations of the two drugs are synergistic; when $\eta = 1$, the combinations are additive; and when $1 < \eta < \infty$, the combinations are antagonistic. The smaller the value of η with $0 < \eta < 1$ is, the more synergistic are the combination doses. Again we should view these equalities or inequalities from the statistical point of view.

If one adopts the median effect Eq. (4) as the appropriate model of the dose-effect curve for each drug, then one can fit Machado and Robinson's model of the following form with five parameters ($m_1, m_2, D_{m,1}, D_{m,2}$, and η):

$$\left(\frac{d_1}{D_{m,1}\left(\frac{y}{1-y}\right)^{\frac{1}{m_1}}}\right)^{\eta} + \left(\frac{d_2}{D_{m,2}\left(\frac{y}{1-y}\right)^{\frac{1}{m_2}}}\right)^{\eta} = 1 \tag{14}$$

One can use the least-squares method to estimate the five parameters.

Remark 1. Note that for each fixed η, when re-scaled to pass through (1, 0) and (0, 1), all isoboles from a response surface are identical. Therefore, the model is very restrictive.

4.3. Model of Plummer and Short

Plummer and Short (1990) proposed a model of the form

$$Y = \beta_0 + \beta_1 \log(d_1 + \rho \cdot d_2 + \beta_4 (d_1 \cdot \rho \cdot d_2)^{\frac{1}{2}}) \tag{15}$$

to identify and quantify departures from additivity. This model was originally proposed by Finney (1971) with a fixed relative potency ρ, and was generalized by Plummer and Short to allow relative potency ρ to vary. Here, Y is the transformed effect, d_1 is the amount of drug 1 and d_2 is the amount of drug 2 in a combination, and ρ is a relative potency of drug 2 versus drug 1 given by $\log(\rho) = \beta_2 + \beta_3 \log D_2$, in which D_2 is the solution to $d_2 + \rho^{-1} d_1 = D_2$, To use this model, the plots of Y versus the $\log(d)$ for both drugs should be linear but need not be parallel. If we adopt the median effect Eq. (4) as the dose-effect relationship for each single drug, then Y as $\log \frac{E}{1-E}$ will have a linear relationship with $\log(d)$, so model (15) is applicable. When we take $Y = \log \frac{E}{1-E}$ model (15) contains five parameters ($\beta_0, \beta_1, \beta_2, \beta_3$, and β_4). One can use the least-squares method to estimate them. The parameter β_4 captures synergism ($\beta_4 > 0$), additivity ($\beta_4 = 0$), or antagonism ($\beta_4 < 0$). Again we should make significance inferences about these relations using confidence intervals, not point estimates.

Let us explore why β_4 can capture synergy and antagonism. If we set $d_2 = 0$ for Plummer and Short's model (15), we will get

$$D_{y,1} = \exp\left(\frac{Y - \beta_0}{\beta_1}\right).$$

which is the dose of drug 1 eliciting the effect Y. If we set $d_1 = 0$ we will get

$$D_{y,2} = \frac{\exp\left(\frac{Y-\beta_0}{\beta_1}\right)}{\rho}$$

which is the dose of drug 2 eliciting the effect of Y. From model (15) we can get

$$\frac{d_1}{\exp\left(\frac{Y-\beta_0}{\beta_1}\right)} + \frac{d_2 \cdot \rho}{\exp\left(\frac{Y-\beta_0}{\beta_1}\right)} + \beta_4 \frac{(d_1 \cdot \rho \cdot d_2)^{\frac{1}{2}}}{\exp\left(\frac{Y-\beta_0}{\beta_1}\right)} = 1,$$

that is,

$$\frac{d_1}{D_{y,1}} + \frac{d_2}{D_{y,2}} = 1 - \beta_4 \frac{(d_1 \cdot d_2)^{\frac{1}{2}}}{(D_{y,1} D_{y,2})^{\frac{1}{2}}} \tag{16}$$

Therefore β_4 captures synergy, additivity, or antagonism, coincident with the Loewe additivity model. Note that Eq. (16) is one of the models mentioned by Machado and Robinson (1994) and has the shortcoming, which we pointed out in Remark 1.

4.4. Model of Carter et al. (1988)

The model proposed by Carter et al. (1988) implies that the dose-effect for a single drug follows a logistic model. The model has the following form,

$$\log\left(\frac{E}{1-E}\right) = \beta_0 + \beta_1 d_1 + \beta_2 d_2 + \beta_{12} d_1 d_2 \tag{17}$$

By setting $d_2 = 0$ we can estimate the dose of drug 1 eliciting a fixed effect y

$$D_{y,1} = \frac{\log\left(\frac{y}{1-y}\right) - \beta_0}{\beta_1}$$

By setting $d_1 = 0$ we can estimate the dose of drug 2 eliciting the fixed effect y

$$D_{y,2} = \frac{\log\left(\frac{y}{1-y}\right) - \beta_0}{\beta_2}$$

From Carter's model (17) we can obtain the interaction index

$$\frac{d_1}{D_{y,1}} + \frac{d_2}{D_{y,2}} = \frac{\beta_1 d_1}{\log\left(\frac{y}{1-y}\right) - \beta_0} + \frac{\beta_2 d_2}{\log\left(\frac{y}{1-y}\right) - \beta_0} = 1 - \frac{\beta_{12} d_1 d_2}{\log\left(\frac{y}{1-y}\right) - \beta_0}. \tag{18}$$

Under the model, with a prerequisite that $\log\left(\frac{y}{1-y}\right) - \beta_0 > 0$, β_{12} captures synergy ($\beta_{12} > 0$), additivity ($\beta_{12} = 0$), or antagonism ($\beta_{12} < 0$).

5. DATA SET

A principal focus of chemoprevention research at M.D. Anderson Cancer Center is to identify efficient combinations of chemotherapeutic and biologic agents that eliminate precancerous cells or slow the carcinogenic processes in patients at high-risk for the development of cancer. Combinations of drugs acting synergistically have the primary benefits of improving therapeutic activity with lower toxicity. This is particularly important in the prevention setting because preventive regimen must elicit low toxicity profiles before they can be administered to relatively healthy subjects. For example, an experiment was conducted at M.D. Anderson Cancer Center (by Reuben Lotan) to evaluate the efficacy of two such novel agents, SCH66336 and 4-HPR, in squamous cell carcinoma cell lines (Chun et al., 2003). SCH66336, a tricyclic peptidomimetic compound, has extensive activity in preclinical studies in head and neck squamous cell carcinoma and in non-small-cell lung cancer cell lines. 4-HPR is a potent retinoid that induces apoptosis (cell death) in various malignant cells.

Cell lines of human squamous cell carcinoma were treated with SCH66336 and 4-HPR separately and in combination. After 72 h, the fractions of surviving cells at each single dose and combination dose levels were calculated. Table 1 shows the fractions of surviving cells from a human squamous cell carcinoma cell line (UMSCC22B) after treatment with SCH66336 (doses ranged from 0 to 4 μM) and 4-HPR (doses ranged from 0 to 2 μM) alone and in combination.

Table 1 Fractions of squamous cell carcinoma cells (UMSCC22B) surviving after 72 h of treatment by single and combination doses of SCH66336 and 4-HPR*

SCH66336 Dose (μM)	4-HPR Dose (μM)				
	0	0.1	0.5	1	2
0	1	0.7666	0.5833	0.5706	0.4934
0.1	0.6701	0.6539	0.4767	0.5171	0.3923
0.5	0.6289	0.6005	0.4919	0.4625	0.3402
1	0.5577	0.5102	0.4541	0.3551	0.2851
2	0.4550	0.4203	0.3441	0.3082	0.2341
4	0.3755	0.3196	0.2978	0.2502	0.1578

*The same data table was also shown in Kong and Lee (2006a), Table 2.

6. DATA ANALYSIS

We illustrate the methods described in Sections 3 and 4 to identify synergism, additivity, or antagonism by analyzing the data set in Table 1. The percentages of surviving cells ranged from 67% at 0.1 μM to only 38% at 4 μM by treating with SCH66336 alone. 4-HPR was slightly less effective as a single agent eliciting 77% surviving cells at 0.1 μM and 49% surviving cells at 2 μM. Equidose effects of the combination of the two agents ranged from 65% at 0.1 μM (total dose $= d_1 + d_2 =$ 0.2 μM) to 23% at 2 μM (total dose = 4μM). The data suggest some supra-additive effects by the combination. For example, a total dose of 2 μM of the combination dose with $d_1 = 1\mu M$ and $d_2 = 1\mu M$ elicited 36% surviving cells whereas the single agent effect at this dose was 46% and 49% for SCH66336 and 4-HPR, respectively. We treat the effect, i.e., fraction of surviving cells as a continuous variable and assume the stochastic error is linear in $\log \frac{E}{1-E}$. The least squares method was applied in solving the parameters for all methods described below.

The median effect plot can be obtained by a linear regression of $\log \frac{E}{1-E}$ on $\log d$ based on the data in Table 1. Recall that $\log \frac{E}{1-E} = m(\log d - \log D_m) = \beta_0 + \beta_1 \log d$. The estimates of β_0, $\beta_1 (=m)$, D_m, and r for drug 1, drug 2, and the mixture of the drugs with equal concentrations are summarized in Table 2.

Figure 2A shows the transformed data $\log \frac{E}{1-E}$ versus $\log d$ and the median effect plots for SCH66336 (open circles and a dashed line), 4-HPR (open triangles and a dotted line), and the mixture of the two drugs at the fixed ratio of 1:1 (filled circles and a solid line). Figure 2C shows the corresponding observed data and the fitted dose-effect curves for SCH66336, 4-HPR, and the mixture of the two drugs.

Table 2 Estimates based on Chou's median effect model

	i	$\beta_{0,i}$	Slope $\beta_{1,i}$ $(=m_i)$	D_{mi}	r_i
SCH66336	1	0.094	−0.335	1.326	0.946
4-HPR	2	0.217	−0.398	1.726	0.979
Mixture of the two drugs with equal concentrations	12	−0.225	−0.596	0.686	0.982

The median effect equation constrains the effect to be 1 at dose zero for $m < 0$. In fact only five observations were used to calculate the median effect model for SCH66336 alone, four observations for 4-HPR alone, and four observations for the mixture. The remaining 16 data points at other combination doses were not used, indicating that the method is not very efficient. The median effect plots in Fig. 2A and r values (correlation coefficients) in Table 2 indicate that the data follow the median effect Eq. (4) reasonably well. We plotted the interaction index versus the effect E for the combinations at the fixed ratio 1:1. From the fitted dose-effect curves for SCH66336 and 4-HPR, the four estimated interaction indices based on Eq. (8) at the four combination doses (0.1, 0.1), (0.5, 0.5), (1, 1), and (2, 2) were 0.791, 0.609, 0.256, and 0.103, respectively, and their corresponding 95% confidence intervals based on Eq. (9) were [0.341, 1.833], [0.283, 1.312], [0.101, 0.647], and [0.031, 0.335], respectively. The four pairs of interaction indices versus the effects

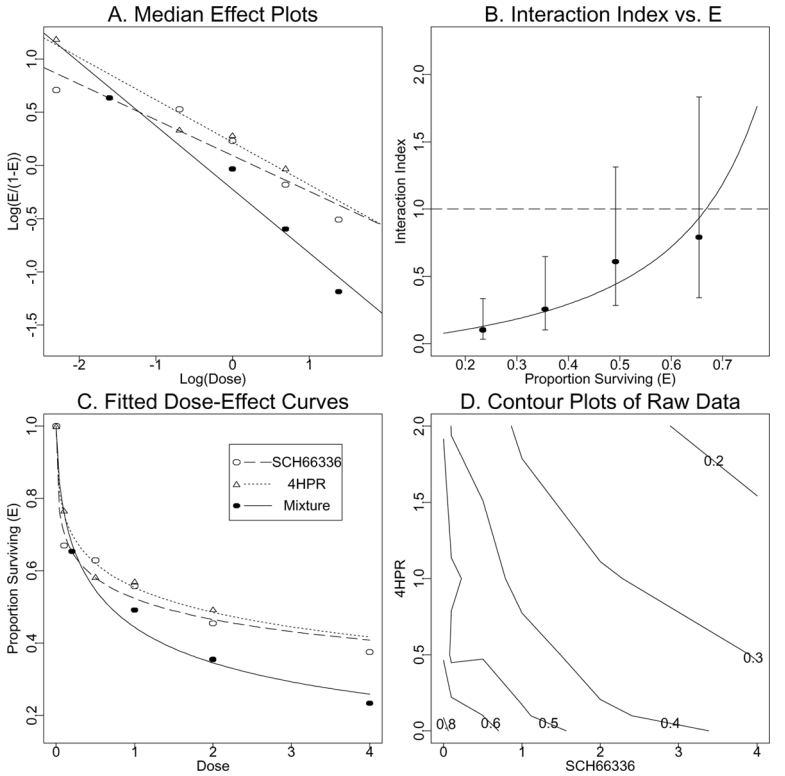

Figure 2 Results from fitting median effect equation models (Panels A and C), calculating interaction index and its confidence interval (Panel B), and the selected contour plot of the raw data (Panel D). Panel A shows the transformed observations $\log \frac{E}{1-E}$ versus $\log d$ and the median-effect plots for drug SCH66336, drug 4-HPR, and the mixture of the two drugs at the fixed ratio of 1:1. Panel B shows the curve of interaction index versus the effect E based on the three estimated median effect equations plotted in Panel A, the estimated interaction indices (in dots) along with their 95% confidence intervals (in vertical bars) at the four observations with the drug combinations at the fixed ratio of 1:1. Panel C shows the original observations effect versus dose level and the fitted dose-response curves using the median-effect equation. Panel D shows the contour plot of the raw data.

along with their 95% confidence intervals are shown in Fig. 2B. The 95% confidence intervals of the interaction indices at the combination doses (0.1, 0.1) and (0.5, 0.5) contain 1, indicating that the two combination doses are additive, while the 95% confidence intervals of the interaction indices at the combination doses (1, 1) and (2, 2) are below 1, indicating that the two combination doses are synergistic. Table 3 provides summaries of the estimated synergy-antagonism parameter, its 95% confidence interval, and the conclusion using each of the models described in Sections 3 and 4. We also assessed drug interactions for the combination doses at the fixed ratio 1:1 using the software CalcuSyn under the mutually exclusive assumption (Chou and Talalay, 1984) and concluded that the combination doses with effects less than 0.45 are synergistic, while the combination doses with effects greater than 0.45 are additive. The conclusions based on CalcuSyn are consistent with our findings based on the procedure in Section 3.

Since the data for each drug used alone follow the median effect equation reasonably well, we can use the median effect equation as dose-effect curve for the models described in Sections 4.1 to 4.3. The parameters estimated in the median effect plot could be used as the initial values for parameter estimation. We fitted each of the models mentioned in Sections 4.1 to Section 4.4, and plotted the observed values and the fitted dose-effect curves for SCH66336, 4-HPR, and the mixture of the drugs at the fixed ratio of 1:1 (Figures 3A, 3C, 4A, and 4C), where the fitted dose-response curves were obtained from the corresponding response surface models. Selected contours of each fitted response surface are shown in Figs. 3B, 3D, 4B, and 4D. Comparing these fitted curves with the raw data and comparing the contour plot of each fitted response surface with the contour plot of the raw data (Fig. 2D) provide a crude visual assessment of whether the fit is good or not. The residual sum of squares (RSS) is another useful measure of the goodness of fit.

For Greco's model, the initial values for m_1, m_2, D_{m1}, D_{m2}, are given in Table 2, and the initial value for α was set as 0. The two-component plot is shown in

Table 3 Summary statistics of the five methods for detecting drug interactions in the combined therapy of SCH66336 and 4-HPR on the UMSCC22B cell line

Model	Drug Syn.	Interaction Add.	Parameter Ant.	Estimated value	95% confidence interval	RSS	Conclusion
Direct	$II < 1$	$II = 1$	$II > 1$				
Calculation		$d_1 = 0.1$, $d_2 = 0.1$		0.791	[0.341, 1.833]	NA	Add.
		$d_1 = 0.5$, $d_2 = 0.5$		0.609	[0.283, 1.312]	NA	Add.
		$d_2 = 1.0$, $d_2 = 1.0$		0.256	[0.101, 0.647]	NA	Syn.
		$d_1 = 2.0$, $d_2 = 2.0$		0.103	[0.031, 0.335]	NA	Syn.
Greco's	$\alpha > 0$	$\alpha = 0$	$\alpha < 0$	5.622	[−0.464, 11.708]	0.618	Add.
Machado's	$0 < \eta < 1$	$\eta = 1$	$\eta > 1$	0.507	[0.327, 0.687]	1.232	Syn.
Plummer's	$\beta_4 > 0$	$\beta_4 = 0$	$\beta_4 < 0$	2.146	[−0.014, 4.305]	1.238	Add.
Carter's	$\beta_{12} > 0$	$\beta_{12} = 0$	$\beta_{12} < 0$	−0.003	[-0.087, 0.081]	1.399	Add.*

Note: II signifies the directly calculated Interaction Index; NA signifies not applicable; Syn. indicates synergy; Add. indicates additivity; Ant. indicates antagonism. RSS indicates residual sum of squares; Add.* indicates that Carter's model did not provide adequate fit to the data although the drug interaction parameter and its confidence interval show that the drug combinations are additive.

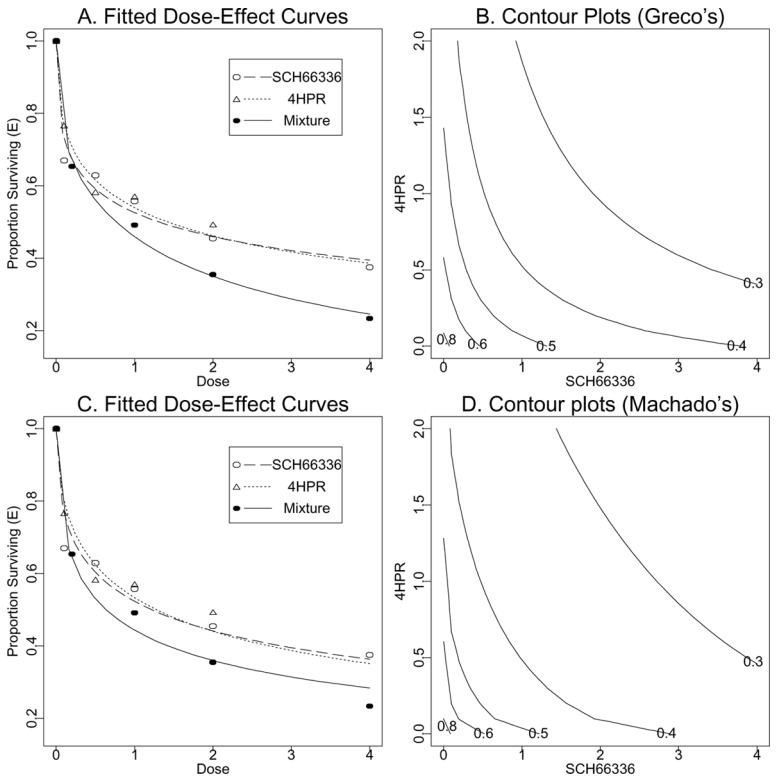

Figure 3 Results from Greco's model (Panels A and B) and Machado's model (Panel C and D): Panels A and C show the observations of effect E versus dose and the fitted dose effect curves for drug SCH66336, drug 4-HPR, and the mixture of the two drugs at the fixed ratio of 1:1. Panels B and D are the contour plots of the fitted response surfaces.

Fig. 3 (Panels A and B) and RSS = 0.618. The fitted parameters are $m_1 = -0.383$, $m_2 = -0.449$, $D_{m1} = 1.316$, $D_{m2} = 1.430$, and the estimated synergy-antagonism parameter $\alpha = 5.622$ with standard error 3.105. The 95% confidence interval for α is $[-0.464, 11.708]$. The confidence interval, which includes 0, precludes a statement of statistical significance for α being different from 0, and thus synergy. However, the confidence interval of α expands mostly in the positive range, suggesting that the combinations of the two drugs may have some synergistic effect instead of pure additive effect.

For Machado and Robinson's model, the initial values for m_1, m_2, D_{m1}, and D_{m2} were also taken from Table 2 with $\eta = 0.7$. The two plots are shown in Fig. 3 (Panels C and D) and RSS = 1.232. The fitted parameters are $m_1 = -0.471$, $m_2 = -0.538$, $D_{m1} = 1.220$, $D_{m2} = 1.282$, and the estimated synergy-antagonism parameter $\eta = 0.507$ with standard error 0.092, so the 95% confidence interval for η is [0.327, 0.687], which does not contain 1 and indicates synergy for the combinations of the two drugs.

For Plummer and Short's model, the initial values for β_0, β_1 could be taken as $\beta_{0,1}$ and slope m_1 in Table 2. The initial values for β_2 and β_3 were set at $\frac{\beta_{0,2}-\beta_{0,1}}{m_1}$ and

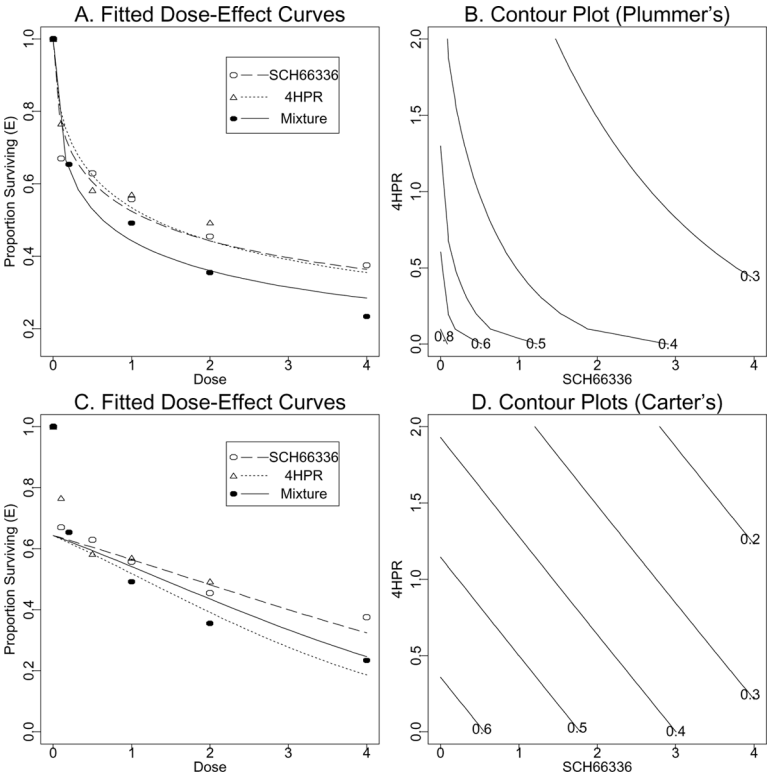

Figure 4 Results from Plummer's model (Panels A and B) and Carter's model (Panels C and D): Panels A and C show the observations of effect E versus dose and the fitted dose effect curves for drug SCH66336, drug 4-HPR, and the mixture of the two drugs at the fixed ratio of 1:1. Panels B and D are the contour plots of the fitted response surfaces.

$\frac{m_2-m_1}{m_1}$, respectively. We used the Newton–Raphson method to solve D_2 in Plummer and Short's model. The convergence of the algorithm is sensitive to the initial value of β_4. One should try different initial values for β_4 to see whether the solutions are obtainable and converge to the same value. In this example, we took 2.5 as the initial value for β_4. The corresponding two plots are shown in Fig. 4 (Panels A and B) and RSS = 1.238. The fitted parameters are $\beta_0 = 0.099$, $\beta_1 = -0.473$, $\beta_2 = -0.083$, $\beta_3 = 0.120$, and the estimated synergy-antagonism parameter $\beta_4 = 2.146$ with standard error 1.102, so the 95% confidence interval for β_4 is $[-0.014, 4.305]$. Similar to Greco's model, the confidence interval includes 0, but just barely. The conclusion is that these combinations of the two drugs are additive.

For Carter's model (17), the initial values can be obtained using logistic regression for each single drug. The two plots are shown in Fig. 4 (Panels C and D). The fitted parameters were $\beta_0 = 0.590$, $\beta_1 = -0.331$, and $\beta_2 = -0.516$. The estimated synergy-antagonism parameter $\beta_{12} = -0.003$ with standard error 0.043, thus the 95% confidence interval for β_{12}, $[-0.087, 0.081]$, contains zero, indicating the combinations are additive. From the plots in Fig. 4 (Panels C and D), we can see that the fit is not good either for a single drug or for the mixture of the two

drugs, and the contour plot of the fitted surface is far away from the contour of the raw data. These figures show that Carter's model does not provide a good fit for our data. Table 3 also shows that Carter's model yields the largest RSS(=1.399).

In conclusion, we have fitted five models to the data in Table 1 with summary statistics shown in Table 3. We compared the fitted dose-effect curves with raw data given in Figs. 2C, 3A, 3C, 4A, and 4C. In addition, the fitted contour plots in Figs. 3B, 3D, 4B, and 4D were compared to the raw data contour plot in Fig. 2D. The correlation coefficients in Table 2 and standard regression diagnostics indicated that the Chou and Talalay model fits the data well. Data analysis by the Machado and Robinson's model led us to the conclusion that the combinations of the two drugs are synergistic on the UMSCC22B cell line (Table 3). The directly calculated interaction indices and their confidence intervals based on the procedure in Section 3 indicate that the combination doses at moderate to high dose level are synergistic but the combination doses at low level are additive. The coexistence of synergy and additivity of the two agents probably explains why the confidence intervals for Greco's α and Plummer and Short's β_4 barely include zero but tend to be positive. These findings also indicate that the RSM using a single parameter to capture drug interactions is not adequate when synergy, additivity, and antagonism intersperse.

We developed S-PLUS/R programs to provide estimates for each of the five methods described. The S-PLUS/R code and the data example are available in *synergy* which can be downloaded from *http: //biostatistics.mdanderson.org/SoftwareDownload/*.

7. DISCUSSION AND FUTURE RESEARCH

Based on the directly calculated interaction indices and their confidence intervals in Section 3, one can only assess drug interactions for selected combination doses. More general approaches for estimating interaction indices and their associated confidence intervals should be derived to provide an efficient way to assess drug interaction in the situation when synergy, additivity, and antagonism intersperse. Furthermore, if the dose-effect curve for a single drug does not follow the median effect equation, alternative models with a better fit should be considered to provide a more accurate assessment of drug interaction.

Response surface models provide a reasonable overall picture of dose response relationships. However, our case study in Section 6 illustrates that these response surface models are not adequate to describe the pattern when some combination doses are synergistic while other combination doses are additive or antagonistic, e.g., in the case that a response surface has a similar contour as $\widehat{PRSTQ}$ (Fig. 1, Panel B). Generally speaking, such limitation exists for all response surface models using a single synergy-antagonism parameter. New methods are needed to identify and quantify departures from additivity when synergism and antagonism are inconsistent over all combination doses within the same data. Kong and Lee (2006a) extend Plummer and Short's approach and use a function of the two doses d_1 and d_2 instead of the single parameter β_4 to capture drug interactions. Kong and Lee (2006b) propose a two-component semiparametric model to capture the mixed patterns of drug interactions. These extended approaches can detect different patterns of synergy and antagonism among combination doses of two drugs.

For our data set, we had only a single outcome measure, i.e., fraction of surviving cells, at each combination dose. We used the least-squares method to estimate the parameters in the models as mentioned above. The results will be the same as the maximum likelihood estimate for normally distributed errors. If we have multiple observations for each drug combination, we can detect whether the variance is constant, and, if not, use the weighted least-squares method to improve the fit. Although we applied the above five methods to *in vitro* study data, these methods can be applied to *in vivo* studies as well. For example, if we know the total number of subjects (n) and the number of subjects (r) who respond to the treatment at each drug combination, we can assume that r follows a binomial distribution with parameter n and E, where E is the expected probability of response (i.e., the expected response rate) at the combination. Then we may use the maximum likelihood method to estimate the parameters in each model. Further statistical inferences can be made accordingly.

One of the important issues in studying drug synergy is to devise the most proper and efficient experimental design. Tan et al. (2003) proposed an optimal experimental design in the sense that it reduces the variability in modeling synergy while allocating the doses to minimize the sample size and to extract maximum information on the joint action of the drugs. Straetemans et al. (2005) gave a ray design for 96-well experiment and used a three-parameter log-logistic model to assess synergy. As the interest in combination therapy continues to increase, methodology development and experimental design for studying drug interaction deserve more attention.

ACKNOWLEDGMENTS

The research was supported in part by grants from the National Cancer Institute CA16672, CA97007, CA91844, and Department of Defense W81XWH-04-1-0142 and W81XWH-05-2-0027. The authors are thankful to Dr. Gary Rosner for his helpful comments, to John Boik for providing analysis results using *CalcuSyn,* and to Lee Ann Chastain for editorial assistance.

REFERENCES

Bachmann, K. A., Ghosh, R. (2001). The use of *in vitro* methods to predict *in vivo* pharmacokinetics and drug interactions. *Current Drug Metabolism* 2:299–314.

Berenbaum, M. C. (1989). What is synergy? *Pharmacological Reviews* 41:93–141.

Bickel, P. J., Doksum, K. A. (2001). *Mathematical Statistics: Basic Ideas and Selected Topics*. Vol. 1. Prentice Hall: New Jersey.

Bliss, C. I. (1939). The toxicity of poisons applied jointly. *Annals of Applied Biology* 26:585–615.

Carter, W. H. Jr., Gennings, C., Staniswalis, J. G., Cambell, E. D., White, K. L. Jr. (1988). A statistical approach to the construction and analysis of isobolograms. *Journal of American College Toxicology* 7:963–973.

Chou, T. C., Talalay, P. (1984). Quantitative analysis of dose-effect relationships: the combined effects of multiple drugs or enzyme inhibitors. *Advances in Enzyme Regulation* 22:27–55.

Chun, K. H., Lee, J. J., Ayers, G. D., Lotan, R. (2003). Synergistic induction of apoptosis in human head and neck squamous cell carcinoma (HNSCC) cell lines by the

combination of the synthetic retinoid 4HPR and the farnesyltransferase inhibitor SCH66336. Proceedings of American Association for Cancer Research 44.

Curran, W. J. Jr. (2003). Evolving chemoradiation treatment strategies for locally advanced non-small-cell lung cancer. *Oncology* (*Huntingt*) 17(12 Suppl 13):7–14.

Drebler, V., Muller, G., Suhnel, J. (1999). CombiTool-A new computer program for analyzing combination experiments with biologically active agents. *Computers and Biomedical Research* 32:145–160.

Evans, T. L. (2004). Highlights from the tenth world conference on lung cancer. *Oncologist* 9(2):232–238.

Finney, D. J. (1971). *Probit Analysis*. Cambridge: Cambridge University Press.

Fitzgerald, J. B., Schoeberl, B., Nielsen, U. B., Sorger, P. (2006). Systems biology and combination therapy in the quest for clinical efficacy. *Nature Chemical Biology* 2(9):458–466.

Greco, W. R., Park, H. S., Rustum, Y. M. (1990). Application of a new approach for the quantitation of drug synergism to the combination of cis-diamminedichloroplatinum and 1-β-D-arabinofuranosylcytosine. *Cancer Research* 50:5318–5327.

Greco, W. R., Bravo, G., Parsons, J. C. (1995). The search of synergy: a critical review from a response surface perspective. *Pharmacological Reviews* 47(2):331–385.

Greco, W. R., Unkelbach, H. D., Poch, G., Suhnel, J., Kundi, M., Bodeker, W. (1992). Consensus on concepts and terminology for combined-action assessment: the Saariselka Agreement. *Arch. Complex Environ. Stud.* 4:65–69.

Herbst, R. S. (2005). Role of novel targeted therapies in the clinic. *British Journal of Cancer* 92(Suppl 1):S21–27.

Hill, A. V. (1910). The possible effects of the aggregation of the molecules of haemoglobin on its dissociation curves. *The Journal of Physiology* 40:iv–vii.

Holford, N. H. G., Sheiner, L. B. (1981). Understanding the dose-effect relationship: clinical application of pharnacokinetic-Pharmacodynamic models. *Clinical Pharmcokinetics* 6:429–453.

Jonker, D. M., Visser, S. A. G., van der Graaf, P. H., Voskuyl, R. A., Danhof, M. (2005). Towards a mechanism-based analysis of pharmacodynamic drug–drug interactions *in vivo*. *Pharmacology and Therapeutics* 106:1–18.

Kong, M., Lee, J. J. (2006a). A general response surface model with varying relative potency for assessing drug interactions. *Biometrics* 62:986–995.

Kong, M., Lee, J. J. (2006b). A semiparametric response surface model for assessing drug interactions. (Submitted).

Lee, J. J., Kong, M. (2006). A confidence interval for interaction index for assessing multiple drug interaction. (Submitted).

Machado, S. G., Robinson, G. A. (1994). A direct, general approach based on isobolograms for assessing the joint action of drugs in pre-clinical experiments. *Statistics in Medicine* 13:2289–2309.

Martinez-Irujo, J. J., Villahermosa, M. L., Mercapide, J., Cabodevilla, J. F., Santiago, E. (1998). Analysis of the combined effect of two linear inhibitors on a single enzyme. *Biochemical Journal* 329:689–698.

Morgan, B. J. T. (1992). *Analysis of Quantal Response Data*. Chapman and Hall.

Niyazi, M., Belka, C. (2006). Isobologram analysis of triple therapies. *Radiation Oncology* Oct 17:1–39.

Plackett, R. L., Hewlett, P. S. (1952). Quantal responses to mixtures of poisons. *Journal of the Royal Statistical Society B* 14:141–163.

Plummer, J. L., Short, T. G. (1990). Statistical modeling of the effects of drug combinations. *Journal of Pharmacological Methods* 23:297–309.

Sharma, P. L., Nurpeisov, V., Hernandez-Santiago, B., Beltran, T., Schinazi, R. F. (2004). Nucleoside inhibitors of human immunodeficiency virus type 1 reverse transcriptase. *Current Topics in Medicinal Chemistry* 4(9):895–919.

Straetemans, R., O'Brien, T., Wouters, L., Dun, J. V., Janicot, M., Bijnens, L., Burzykowski, T., Aerts, M. (2005). Design and analysis of drug combination experiments. *Biometrical Journal* 47(3):299–308.

Tallarida, R. J. (2000). *Drug Synergism and Dose-Effect Data Analysis*. New York: Chapman and Hall.

Tan, M., Fang, H., Tian, G., Houghton, P. J. (2003). Experimental design and sample size determination for testing synergism in drug combination studies based on uniform measures. *Statistics in Medicine* 22:2091–2100.

Webb, J. L. (1963). *Enzyme and Metabolic Inhibitors*. New York: Academic Press.

DOI:10.1158/0008-5472.CAN-07-6209

Cancer Research

CAAT/Enhancer Binding Protein Homologous Protein–Dependent Death Receptor 5 Induction Is a Major Component of SHetA2-Induced Apoptosis in Lung Cancer Cells

Yi-Dan Lin, Shuzhen Chen, Ping Yue, et al.

Cancer Res 2008;68:5335-5344. Published online July 1, 2008.

DOI:10.1158/0008-5472.CAN-07-6209

Research Article

CAAT/Enhancer Binding Protein Homologous Protein–Dependent Death Receptor 5 Induction Is a Major Component of SHetA2-Induced Apoptosis in Lung Cancer Cells

Yi-Dan Lin,[1,2] Shuzhen Chen,[1] Ping Yue,[1] Wei Zou,[1] Doris M. Benbrook,[3] Shengquan Liu,[4] Thanh C. Le,[4] K. Darrell Berlin,[4] Fadlo R. Khuri,[1] and Shi-Yong Sun[1]

[1]Department of Hematology and Medical Oncology, Winship Cancer Institute, Emory University School of Medicine, Atlanta, Georgia; [2]Cardiothoracic Surgery Department, Daping Hospital, Third Military Medical University, Chongqing, P.R. China; [3]Department of Obstetrics and Gynecology, University of Oklahoma Health Science Center, Oklahoma City, Oklahoma; and [4]Department of Chemistry, Oklahoma State University, Stillwater, Oklahoma

Abstract

The flexible heteroarotinoids (Flex-Het) represent a novel type of atypical retinoids lacking activity in binding to and transactivating retinoid receptors. Preclinical studies have shown that Flex-Hets induce apoptosis of cancer cells while sparing normal cells and exhibit anticancer activity *in vivo* with improved therapeutic ratios over conventional retinoid receptor agonists. Flex-Hets have been shown to induce apoptosis through activation of the intrinsic apoptotic pathway. The present study has revealed a novel mechanism underlying Flex-Het–induced apoptosis involving induction of death receptor 5 (DR5). The representative Flex-Het SHetA2 effectively inhibited the growth of human lung cancer cells in cell culture and in mice. SHetA2 induced apoptosis, which could be abrogated by silencing caspase-8 expression, indicating that ShetA2 triggers a caspase-8–dependent apoptosis. Accordingly, SHetA2 up-regulated DR5 expression, including cell surface levels of DR5, and augmented tumor necrosis factor–related apoptosis-inducing ligand (TRAIL)–induced apoptosis. Importantly, small interfering RNA (siRNA)–mediated blockade of DR5 induction conferred cell resistance to SHetA2-induced apoptosis, as well as SHetA2/TRAIL-induced apoptosis. These results show that DR5 induction is a key component of apoptosis induced by SHetA2 or by SHetA2 combined with TRAIL. SHetA2 exerted CAAT/enhancer-binding protein homologous protein (CHOP)–dependent transactivation of the DR5 promoter. Consistently, SHetA2 induced CHOP expression, which paralleled DR5 up-regulation, whereas siRNA-mediated blockage of CHOP induction prevented DR5 up-regulation, indicating CHOP-dependent DR5 up-regulation by SHetA2. Collectively, we conclude that CHOP-dependent DR5 up-regulation is a key event mediating SHetA2-induced apoptosis. [Cancer Res 2008;68(13):5335–44]

Introduction

Retinoids, including natural retinoic acid and its synthetic derivatives, are a group of promising anticancer agents endowed with both therapeutic and chemopreventive potential (1). Treatment of acute promyelocytic leukemia with all-trans retinoic acid is a successful example (2). However, the exploitation of the full potential of retinoids as chemopreventive and/or therapeutic drugs, particularly against solid tumors, has been hampered largely by their local and systemic toxicity and side effects, which are often associated with their ability to activate nuclear retinoid receptors (1, 3). Thus, efforts have been made for the past decades to develop novel retinoid-like compounds or atypical retinoids, which retain anticancer activity of retinoids with minimal toxicity and side effects (3). SHetA2 (see structure in Fig. 1*A*) is such a compound because it did not activate retinoic acid receptor and retinoid X receptor receptors in receptor cotransfection assays and reporter cell lines (4), rescue or induce embryonic malformations in a RALDH knockout mouse model (5), or cause skin irritancy in a murine topical irritancy model (6). Thus, SHetA2 functions independently of retinoid receptors (7, 8). Accordingly, SHetA2 lacks conventional retinoid toxicities, such as skin irritation or teratogenecity, when tested in animal models (5, 6). However, SHetA2 has the ability to induce differentiation or reverse the cancerous phenotype (9). Moreover, SHetA2 induces apoptosis in cancer cells while sparing normal cells (7, 10). Importantly, SHetA2 effectively inhibits tumor growth *in vivo* without evidence of toxicity (6). Because of these encouraging results, SHetA2 was chosen for evaluation in the National Cancer Institute's Rapid Access to Intervention Development program (Application 196, compound NSC 726189) and is now in the Rapid Access to Preventive Intervention Development program, showing a potential as a cancer chemopreventive and therapeutic agent.

It is well known that there are two major apoptotic pathways: the extrinsic apoptotic pathway involving signals transduced through death receptors (DR) and the intrinsic apoptotic pathway relying on signals from the mitochondria. Both pathways involve the activation of a set of caspases, which in turn cleave cellular substrates and result in the characteristic morphologic and biochemical changes constituting the process of apoptosis (11, 12). The extrinsic pathway is characterized by the trimerization of cell surface DRs and activation of caspase-8, whereas the intrinsic pathway involves in the disruption of mitochondrial membranes, the release of cytochrome *c* from the mitochondria, and the activation of caspase-9. Through caspase-8–mediated cleavage or truncation of Bid, the extrinsic DR apoptotic pathway is linked to the intrinsic mitochondrial apoptotic pathway (11, 12).

The death ligand tumor necrosis factor–related apoptosis-inducing ligand (TRAIL) and its receptors have recently attracted much attention because TRAIL preferentially induces apoptosis in transformed or malignant cells while sparing most normal cells,

Note: Supplementary data for this article are available at Cancer Research Online (http://cancerres.aacrjournals.org/).

F.R. Khuri and S-Y. Sun are Georgia Cancer Coalition Distinguished Cancer Scholars.

Requests for reprints: Shi-Yong Sun, Winship Cancer Institute, Emory University School of Medicine, 1365-C Clifton Road NE, C3088, Atlanta, GA 30322. Phone: 404-778-2170; Fax: 404-778-5520; E-mail: shi-yong.sun@emoryhealthcare.org.

doi:10.1158/0008-5472.CAN-07-6209

DOI:10.1158/0008-5472.CAN-07-6209

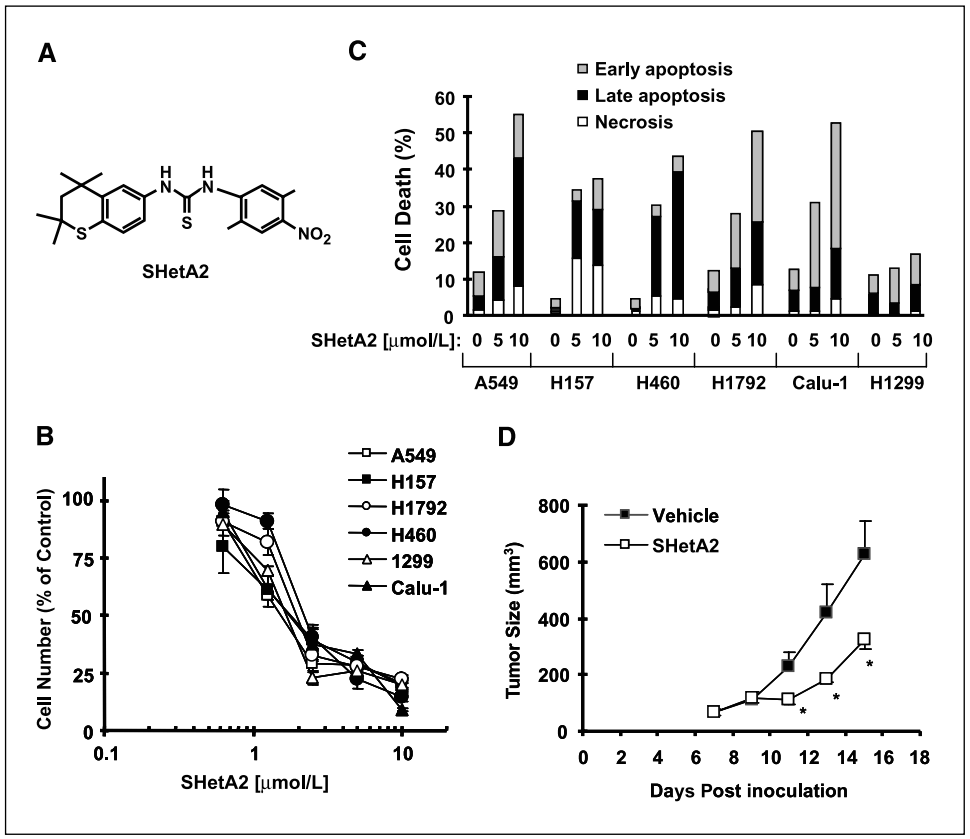

Figure 1. SHetA2 (*A*) decreases the survival (*B*) and induces apoptosis (*C*) of human NSCLC cells and inhibits the growth of lung cancer xenografts (*D*). *A,* chemical structure of SHetA2. *B,* the indicted NSCLC cell lines were seeded in 96-well cell culture plates and treated the next day with the given concentrations of SHetA2. After 3 d, cell number was estimated using the SRB assay. Cell survival was expressed as the percentage of control (DMSO-treated) cells. *Points,* means of four replicate determinations; *bars,* SDs. *C,* the indicated NSCLC cell lines were treated with the given concentrations of SHetA2 for 48 h. Cell death including apoptosis and necrosis from these cell lines were then determined by Annexin V staining. *D,* mice carrying A549 xenografts were treated with vehicle control or SHetA2 by oral gavage (daily) for 8 d. Tumor sizes were measured once every 2 d. *Points,* mean; *bars,* SE ($n = 6$). *, $P < 0.05$ compared with vehicle control using Student's *t* test.

demonstrating potential as a tumor-selective apoptosis-inducing cytokine for cancer treatment (13). Currently, both TRAIL and agonistic antibodies against DR4 or DR5 are being tested in cancer clinical trials (14). Importantly, certain cancer therapeutic agents sensitize various types of cancer cells to TRAIL-induced or agonistic anti-DR4 or DR5 antibody–induced apoptosis (13, 15). Thus, these agents are useful in combination with TRAIL or an agonistic anti-DR4 or DR5 antibody to augment induction of apoptosis. It is well known that TRAIL binds to its receptors: DR4 (also called TRAIL-R1) and DR5 (also named Apo2, TRAIL-R2, or Killer/DR5) to activate the extrinsic apoptotic pathway (13).

Both DR4 and DR5 expressions are modulated by some anticancer agents (16), including certain synthetic retinoids (17–23). As a result, these agents very often can sensitize cancer cells to TRAIL-induced or agonistic DR4 or DR5 antibody–induced apoptosis (17, 20, 21). Regulation of DR4 or DR5 occurs through p53-dependent mechanisms (24–26) and p53-independent mechanisms [e.g., nuclear factor-κB, activator protein 1, and CAAT/enhancer-binding protein homologous protein (CHOP); refs. 23, 27–30]. It has been recently shown that CHOP, also known as growth arrest and DNA damage gene 153 (GADD153), directly regulates DR5 expression through a CHOP binding site in the 5-flanking region of the DR5 gene (30, 31). Thus, certain drugs induce DR5 expression through CHOP-dependent transactivation of the DR5 gene (30–34).

The mechanism of SHetA2-induced apoptosis has been shown to occur through the intrinsic mitochondrial pathway associated with loss of mitochondrial membrane integrity, generation of reactive oxygen species, release of cytochrome *c* from the mitochondria, and activation of caspase-3 in head and neck cancer cell lines (7). Likewise, SHetA2 induces apoptosis in human ovarian cancer cells though targeting the mitochondria associated with alterations in the balance of Bcl-2 proteins, independent of generation of reactive oxygen species (10). It seems that the mechanisms of SHetA2 may vary in different types of cancer cells. The present study investigated the effects of SHetA2 on induction of apoptosis and examined the underlying mechanism in human non–small cell lung cancer (NSCLC) cells, which are typically insensitive to most of the conventional retinoids (35). Given that other synthetic atypical retinoids, such as CD437 and *N*-(4-hydroxyphenyl)retinamide (4HPR), modulate the expression of TRAIL DRs and TRAIL-induced apoptosis independent of the retinoid receptors (17–23), we focused on studying modulation of the extrinsic TRAIL DR-mediated apoptotic pathway in SHetA2-induced apoptosis.

Materials and Methods

Reagents. SHetA2 was described previously (6) and dissolved in DMSO at a concentration of 10 mmol/L, and aliquots were stored at −80°C. Stock solution was diluted to the appropriate concentrations with growth medium immediately before use. Human recombinant TRAIL was purchased from PeproTech, Inc.

Cell lines and cell culture. The human NSCLC cell lines used in this study were described previously (35). These cell lines were grown in monolayer culture in RPMI 1640 supplemented with glutamine and 5% fetal bovine serum at 37°C in a humidified atmosphere consisting of 5% CO_2 and 95% air.

Cell growth assay. Cells were cultured in 96-well cell culture plates and treated the next day with the agents indicated. Viable cell number was estimated using the sulforhodamine B assay, as previously described (35). Combination index (CI) for drug interaction (e.g., synergy) was calculated using the CompuSyn software (ComboSyn, Inc.).

DOI:10.1158/0008-5472.CAN-07-6209

Apoptosis assays. Apoptosis was detected either by analysis of caspase activation using Western blot analysis as described below or by Annexin V staining using Annexin V–phycoerythrin (PE) apoptosis detection kit (BD Bioscience) following the manufacturer's instructions and analyzed by flow cytometry using the FACScan (Becton Dickinson). In the Annexin V assay, the percentage of positive cells for Annexin V (PE) staining only in the bottom right quadrant and for both Annexin V and DNA (7-AAD) staining in the top right quadrant represents the early and late apoptotic populations, respectively. The percentage of positive cells for DNA staining only in the top left quadrant represents the necrotic population.

Western blot analysis. Preparation of whole-cell protein lysates and Western blot analysis were described previously (36). Mouse anti–caspase-3 monoclonal antibody was purchased from Imgenex. Rabbit polyclonal antibodies against caspase-8, caspase-9, Bid, and poly(ADP-ribose) polymerase (PARP), respectively, were purchased from Cell Signaling Technology. Mouse anti–caspase-10 monoclonal antibody was purchased from MBL International. Rabbit polyclonal anti-DR5 antibody was purchased from ProSci, Inc. Mouse monoclonal anti-DR4 antibody (B-N28) was purchased from Diaclone. Mouse anti-TRAIL monoclonal antibody was purchased from Imgenex. Mouse monoclonal anti-CHOP antibody (B-3) was purchased from Santa Cruz Biotechnology. Rabbit anti–β-actin polyclonal antibody and mouse anti-tubulin monoclonal antibody was purchased from Sigma Chemicals.

Detection of cell surface TRAIL receptors. The procedure for direct antibody staining and subsequent flow cytometric analysis of cell surface proteins was described previously (33). The mean fluorescent intensity (MFI) that represents antigenic density on a per cell basis was used to represent TRAIL receptor expression level. PE-conjugated mouse anti-human DR5 (DJR2-4), anti-human DR4 (DJR1), anti-human DcR1 (DJR3), and anti-human DcR2 (DJR4-1) monoclonal antibodies and PE mouse IgG1 isotype control (MOPC-21/P3) were purchased from eBioscience.

Gene silencing using small interfering RNAs. Silencing of caspase-8, DR5, and CHOP were achieved by transfecting small interfering RNA (siRNA) using RNAifect transfection reagent (Qiagen) following the manufacturer's instructions. Control (i.e., nonsilencing), caspase-8, DR5, and CHOP siRNAs were described previously (33, 37). These siRNAs were synthesized from Qiagen. Cells were plated in six-well cell culture plates and transfected the next day with the given siRNAs. After 24 h, the cells were trypsinized and replated in new plates and, on the second day, treated with SHetA2, as indicated. Gene silencing effects were evaluated by Western blot, as described above, after indicated times of treatment.

Construction of DR5 reporter plasmid, transient transfection, and luciferase activity assay. pGL3-DR5(−552) containing a wild-type CHOP binding site and pGL3-DR5(−552)CHOPm, in which the CHOP binding site was mutated, were generously provided by H.G. Wang (University of South Florida College of Medicine; ref. 30). The pGL3-DR5(−420) and pGL3-DR5(−240) reporter construct were described previously (33). The reporter constructs containing −1,400 and −810 bp 5′-flanking regions of the *DR5* gene upstream of the translation start site, respectively, were amplified by PCR using the plasmid containing a 5′-flanking region of *DR5* gene provided by Dr. G.S. Wu (Wayne State University School of Medicine) as a template. These amplified fragments were then subcloned into pGL3-basic reporter vector (Promega) through *Kpn*I and *Bgl*II restriction sites. In the PCR amplification, the same reverse primer 5′-CTTAAGATCTGGCGGTAGGGAACGCTCTTATAGTC-3′ was used to make these constructs. The upstream primers were 5′-CTTAGGTACCGCAATAAATCTTGCTACTGC-3′ (for −1,400) and 5′-CTTAGGTACCAGCTACATGGGAGGCTGAGG-3′ (for −810), respectively. These constructs were named pGL3-DR5(−1,400) and pGL3-DR5(−810), respectively. The plasmid transfection and luciferase assay were the same, as described previously (33).

Lung cancer xenograft and treatments. Animal experiments were approved by the Institutional Animal Care and Use Committee of Emory University. Four-week-old to 6-wk-old female athymic (nu/nu) mice (~20 g of body weight) were ordered from Taconic and housed under pathogen-free conditions in microisolator cages with laboratory chow and water *ad libitum*. The A549 cells (5×10^6) in serum-free medium were injected s.c. into the flank region of nude mice. When tumors reached certain size ranges (50–100 mm^3), the mice were randomized into two groups ($n = 6$ per group) according to tumor volumes and body weights for the following treatments: vehicle control and SHetA2 dissolved in sesame oil (oral gavage; daily). Tumor volumes were measured using caliper measurements once every 2 d and calculated with the formula $V = (\text{length} \times \text{width}^2) / 6$.

Results

SHetA2 inhibits the growth of human NSCLC cells *in vitro* and *in vivo* and induces apoptosis. We began our study by examining the effects of SHetA2 on the growth of a panel of human

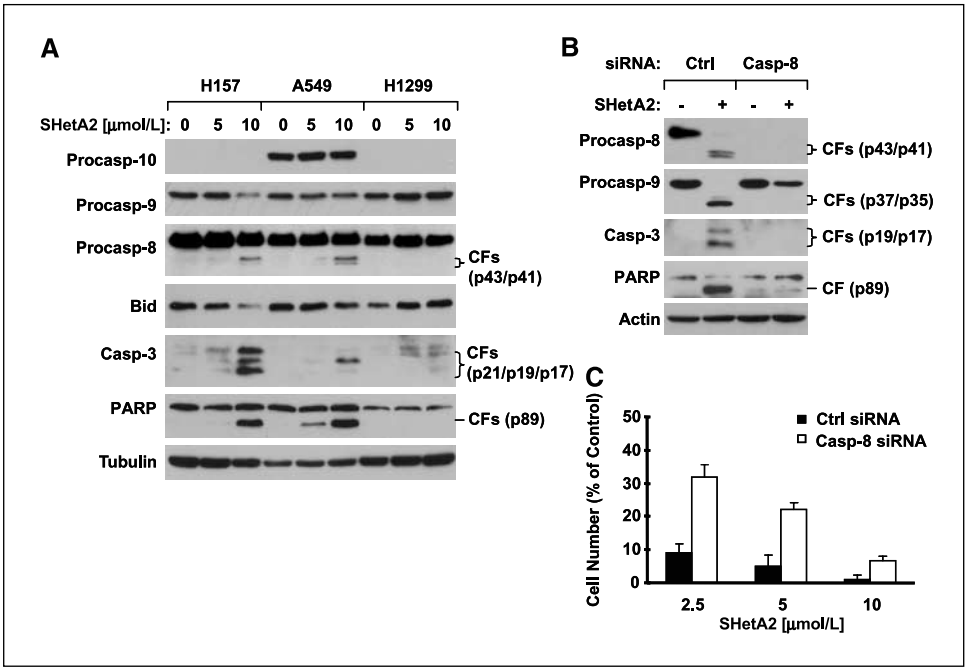

Figure 2. Effects of SHetA2 on cleavage of caspases and their substrates (*A*) and effect of caspase-8 silencing on SHetA2-induced caspase cleavage (*B*) and decrease in cell survival (*C*). *A,* the indicated cell lines were exposed to the given concentrations of SHetA2 for 30 h. The cells were then harvested for preparation of whole-cell protein lysates and subsequent Western blot analysis for detecting cleavage of caspases and their substrates. *B* and *C,* A549 cells were cultured in a six-well plate and the next day transfected with control (*Ctrl*) or caspase-8 siRNA. Twenty-four hours after transfection, the cells were re-seeded in a six-well plate or in a 96-well plate. On the second day, the cells were treated with DMSO or 10 μmol/L SHetA2 (in the six-well plate; *B*) or with the indicated concentrations of SHetA2 (in the 96-well plate; *C*). After 48 h, the cells were subjected to preparation of whole-cell protein lysates and subsequent Western blot analysis (*B*) or to an estimation of cell number using the SRB assay (*C*). *C, columns,* mean of four replicate determinations; *bars,* SD. *Procasp,* procaspase; *CF,* cleaved fragment.

DOI:10.1158/0008-5472.CAN-07-6209

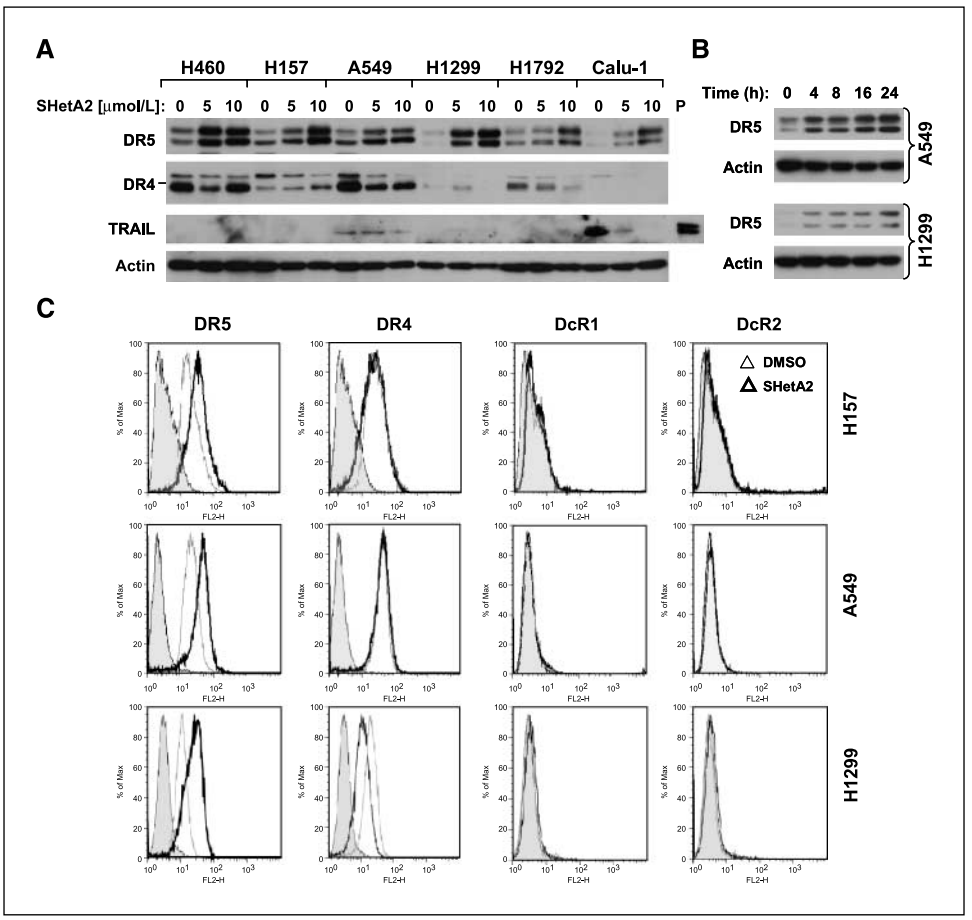

Figure 3. Effects of SHetA2 on the expression of DR5, DR4, and TRAIL (*A* and *B*) and cell surface distributions of TRAIL receptors (*C*) in human NSCLC cell lines. *A* and *B,* the indicated cell lines were treated with the given concentrations of SHetA2 for 16 h (*A*) or with 5 μmol/L SHetA2 for the given time as indicated (*B*). The cells were then subjected to preparation of whole-cell protein lysates and subsequent Western blot analysis. *P,* positive control lysates prepared from human HaCaT keratinocytes. *C*, the indicated cell lines were treated with 10 μmol/L SHetA2 for 16 h and then harvested for analysis of cell surface TRAIL receptors by immunofluorescent staining and subsequent flow cytometry. The filled gray peaks represented cells stained with a matched control PE-conjugated IgG isotype antibody. The open peaks were cells stained with PE-conjugated antibody against an individual TRAIL receptor.

NSCLC cell lines, which are typically resistant to the conventional retinoids (35). As presented in Fig. 1*B*, SHetA2 exhibited concentration-dependent effects on decreasing the number of six tested NSCLC cell lines with comparable activity, indicating that SHetA2 effectively inhibits the growth of human NSCLC cells. The IC_{50}s, which are the concentrations required for inhibiting cell growth by 50%, were ~2 μmol/L for all these cell lines after a 3-day exposure. Moreover, we showed that SHetA2 exerted concentration-dependent effects on increasing apoptotic cell death of the six NSCLC cell lines after a prolonged treatment (e.g., 48 h). Among these cell lines, H1299 cells were relatively less sensitive to SHetA2-induced apoptosis, because SHetA2 at 10 μmol/L induced <20% apoptotic cells (Fig. 1*C*). In addition to induction of apoptosis, SHetA2 induced either G_1 (e.g., H1299) or G_2-M (e.g., H460, A549, and H157) cell cycle arrest (see Supplementary Fig. S1). Together, these results suggest that SHetA2 inhibits the growth of NSCLC cells through both apoptosis induction and growth arrest.

Using a A549 xenograft model in nude mice, we found that SHetA2 significantly inhibited the growth of A549 xenografts ($P < 0.05$; Fig. 1*D*), indicating that SHetA2 also effectively inhibits the growth of human lung tumors *in vivo*. We noted that there was a reduction of mouse body weight (10–15%) during the treatment, suggesting that the current treatment schedule with the maximal tolerated dose of 60 mg/kg may have some toxicity.

SHetA2 induces caspase-8–dependent apoptosis. To show the mechanism by which SHetA2 induces apoptosis, we determined the effects of SHetA2 on the activation of intracellular caspase cascades and its dependence on caspase activation. Procaspase-10 was not detected in H157 and H1299 cells or was not altered in A549 cells. The levels of procaspase-9 and Bid were decreased in a dose-dependent manner in both H157 and A549 cell lines, but not in H1299 cells. Consistently, cleavage of procaspase-8, procaspase-3, and PARP was detected in SHetA2-treated H157 and A549 cell lines, but cleavage of these proteins was not detected or only minimally detected in SHetA2-treated H1299 cells (Fig. 2*A*). These results indicate that both caspase-8–mediated and caspase-9–mediated caspase cascades are activated during SHetA2-induced apoptosis. Because caspase-8 activation can result in activation of the caspase-9–mediated cascade, we questioned whether this was the case in SHetA-induced apoptosis. To this end, we inhibited caspase-8 activation by silencing caspase-8 expression using a caspase-8 siRNA. As shown in Fig. 2*B*, we detected pro-forms of caspase-8 and cleaved caspase-8 in control siRNA-transfected cells, but not in caspase-8 siRNA-transfected cells, indicating a successful silencing of caspase-8 expression. Correspondingly, we detected cleaved forms of caspase-9, caspase-3, and PARP in control siRNA-transfected cells, but not in caspase-8 siRNA-transfected cells. Moreover, the effect of SHetA2 on decreasing cell number was substantially attenuated in caspase-8 siRNA-transfected cells compared with that in control siRNA-transfected cells (Fig. 2*C*). Thus, these results collectively show that SHetA2 induces caspase-8–dependent apoptosis. In addition, caspase-9 activation induced by SHetA2 is secondary to caspase-8 activation.

DOI:10.1158/0008-5472.CAN-07-6209

SHetA2 up-regulates DR5 expression. Given that caspase-8 activation plays a critical role in mediating the extrinsic apoptotic pathway, we next asked whether SHetA2 activates the DR-mediated apoptotic pathway. Therefore, we examined the effects of SHetA2 on the expression of DR5, DR4, and their ligand TRAIL. As presented in Fig. 3*A*, SHetA2 at 5 or 10 μmol/L increased the levels of DR5 protein in all the tested cells lines. Under the same conditions, SHetA2 did not increase DR4 expression; interestingly, SHetA2 even decreased the levels of DR4 protein in some cell lines (e.g., A549 and H1792). We failed to detect the basal levels of TRAIL or increase in TRAIL expression in H460, H157, H1299, and H1792 cells. In cell lines that did express TRAIL (e.g., A549 and Calu-1), SHetA2 either did not alter TRAIL levels (e.g., A549) or decreased TRAIL expression (e.g., Calu-1). A time course analysis of DR5 expression in cells exposed to SHetA2 showed that DR5 up-regulation occurred 4 hours post–SHetA2 treatment and was sustained up to 24 hours (Fig. 3*B*). Given that functional DR5 and other TRAIL receptors are located on the cell surface, we further analyzed cell surface TRAIL receptor distributions in cells exposed to SHetA2. All three tested cell lines (i.e., H157, A549, and H1299) expressed basal levels of DR5 and DR4. Upon SHetA2 treatment, surface DR5 but DR4 levels were further increased. The MFIs of DR5 were 25 and 43 in DMSO-treated and SHetA2-treated H157 cells, respectively; 26 and 45, respectively, in A549 cells; and 11 and 27, respectively, in H1299 cells (Fig. 3*C*). In H1299 cells, we found that SHetA2 actually decreased the levels of cell surface DR4. The MFIs of DR4 in H1299 cells were 20 in DMSO-treated cells and 12 in SHetA2-treated cells (Fig. 3*C*). Cell surface DcR1 and DcR2 were

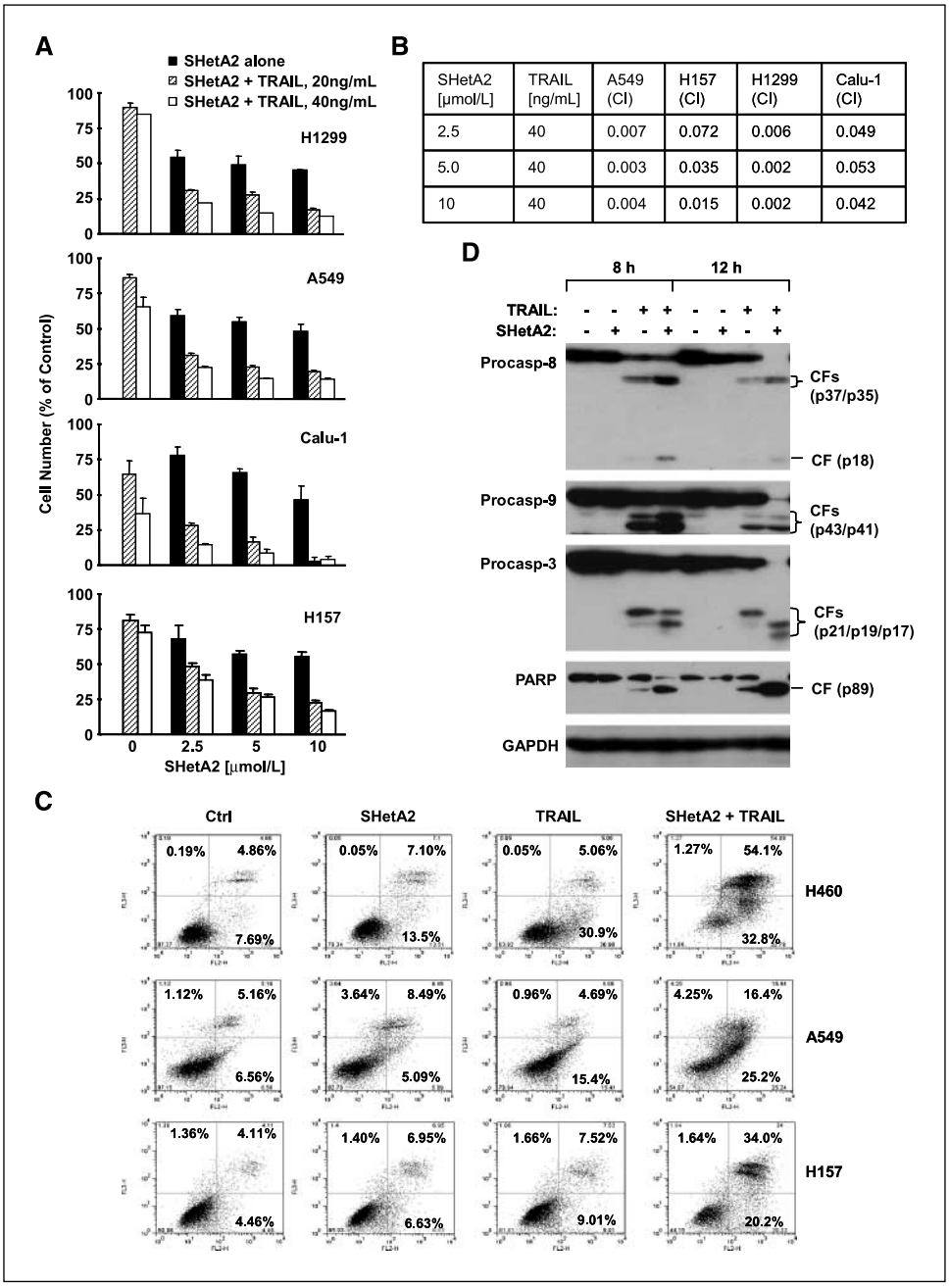

SHetA2 [μmol/L]	TRAIL [ng/mL]	A549 (CI)	H157 (CI)	H1299 (CI)	Calu-1 (CI)
2.5	40	0.007	0.072	0.006	0.049
5.0	40	0.003	0.035	0.002	0.053
10	40	0.004	0.015	0.002	0.042

Figure 4. SHetA2 combined with TRAIL synergistically decreases cell survival (*A* and *B*) and induces apoptosis (*C* and *D*) in human NSCLC cells. *A* and *B,* the indicated cell lines were treated with the given concentrations of SHetA2 alone, TRAIL alone, and their individual combinations as indicated. After 24 h, cell number was estimated using SRB assay for calculation of cell survival (*A*) and CI (*B*) with CompuSyn software. *Columns,* mean of four replicate determinations; *bars,* SDs. A CI smaller than 1 indicates synergy. *C,* the indicated cell lines were treated with 10 ng/mL (H460) or 20 ng/mL (A549 and H157) TRAIL alone, 10 μmol/L SHetA2 alone, and their respective combinations as indicated. After 24 h, the cells were subjected to measurement of apoptosis using Annexin V staining. The percentage of positive cells in the top right and bottom right quadrants were added to yield the total of apoptotic cells. *D,* A549 cells were treated with 10 μmol/L SHetA2 alone, 20 ng/mL TRAIL alone, and their combination. After the indicated times, the cells were subjected to preparation of whole-cell protein lysates and subsequent Western blot analysis.

DOI:10.1158/0008-5472.CAN-07-6209

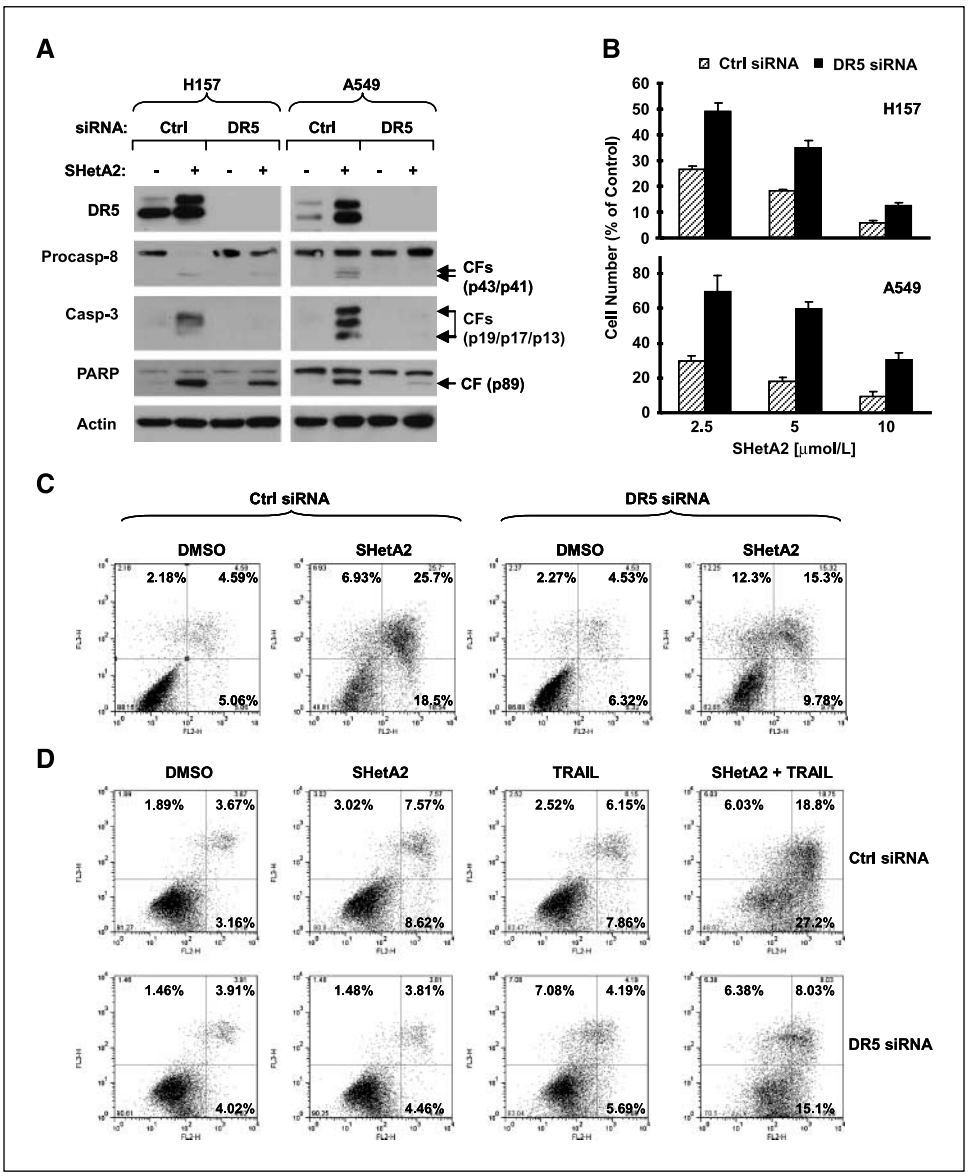

Figure 5. Blockage of DR5 induction (*A*) attenuates the ability of SHetA2 to activate caspases (*A*), decrease cell survival (*B*), induce apoptosis (*C*), and augment TRAIL-induced apoptosis (*D*) in human NSCLC cells. *A* and *B,* the indicated cell lines were cultured in six-well plates and the next day transfected with control or DR5 siRNA. Twenty-four hours after the transfection, cells were re-seeded in six-well plates (*A*) or 96-well plates (*B*) and treated with 10 μmol/L SHetA2 (*A*) or the indicated concentrations of SHetA2 (*B*). After 48 h (30 h for A549 in *A*), the cells were subjected to preparation of whole-cell lysates and Western blot analysis (*A*) or to the SRB assay for calculation of cell survival (*B*). *B, columns,* mean of four replicate determinations; *bars,* SD. *C* and *D,* H157 (*C*) or A549 (*D*) cells were cultured in six-well plates and the next day transfected with control or DR5 siRNA. Forty-eight hours after the transfection, the cells were exposed to DMSO or 10 μmol/L SHetA2 for 48 h (*C*) or treated with DMSO control, 10 μmol/L SHetA2 alone, 20 ng/mL TRAIL alone, or SHetA2 combined with TRAIL for 24 h (*D*). The cells were then harvested for Annexin V assay to detect apoptosis. The percentage of positive cells in the top right and bottom right quadrants were added to yield the total of apoptotic cells.

not or only minimally detected in these three cell lines and not increased by SHetA2 (Fig. 3*C*). Collectively, these results indicate that SHetA2 primarily up-regulates DR5 expression, including cell surface DR5 levels in human NSCLC cells.

SHetA2 cooperates with TRAIL to augment induction of apoptosis. If SHetA2-induced DR5 is functional, we speculated that inclusion of exogenous recombinant TRAIL in SHetA2 treatment would result in enhanced apoptosis induction. To test this hypothesis, we treated four NSCLC cell lines (i.e., H1299, Calu-1, A549, and H157) with SHetA2 alone, TRAIL alone, or both drugs combined and then assessed cell survival and apoptosis. As presented in Fig. 4*A*, the combination of SHetA2 at concentrations of 2.5 to 10 μmol/L with either dose of TRAIL (20 or 40 ng/mL) was much more effective in decreasing tumor cell number than either single agent alone. For example, in Calu-1 cells, both SHetA2 alone at 5 μmol/L and TRAIL (20 ng/mL) alone decreased cell number by ~30%, but the combination of the two agents reduced cell number by >80%, which is greater than the sum of the effects of each agent alone. The CIs for these combinations in all four cell lines were smaller than 1 (Fig. 4*B*), indicating that the combination of SHetA2 and TRAIL synergistically decreases cell survival. Moreover, we used Annexing V staining to detect apoptosis in three NSCLC cell lines (A549, H157, and H460) exposed to the combination of SHetA2 and TRAIL. During a 24-hour treatment, the SHetA2 and TRAIL combination was much more effective than each of the single agents alone in increasing apoptosis (Fig. 4*C*). For example, in H157 cells, 10 μmol/L SHetA2 alone and 20 ng/mL TRAIL alone induced ~14% and 17% apoptosis, respectively; however, their combination caused ~54% of cells to undergo apoptosis (Fig. 4*C*). By Western blotting, we also detected the strongest bands of cleaved caspases and PARP or the most reduction of procaspases and PARP in cells exposed to the combination of SHetA2 and TRAIL in comparison with those cells treated with SHetA2 or TRAIL alone (Fig. 4*D*). Collectively, these results clearly indicate that SHetA2 synergizes with TRAIL to augment induction of apoptosis in human NSCLC cells.

Induction of DR5 expression is required for SHetA2-induced apoptosis and augmentation of TRAIL-induced apoptosis. To

DOI:10.1158/0008-5472.CAN-07-6209

show the role of DR5 up-regulation in SHetA2-induced apoptosis and enhancement of TRAIL-induced apoptosis, we blocked DR5 induction through siRNA-mediated silencing of DR5 expression and examined its effect on the ability of SHetA2 to trigger apoptosis and to enhance TRAIL-induced apoptosis. As shown in Fig. 5*A*, in both H157 and A549 cells, DR5 siRNA transfection dramatically decreased basal levels of DR5 expression and, more importantly, abolished SHetA2-induced DR5 expression as detected by Western blot analysis (Fig. 5*A*). As a result, the cleavage of casapse-8, caspase-3, and PARP were substantially inhibited in cells transfected with DR5 siRNA, compared with control siRNA-transfected cells (Fig. 5*A*). Accordingly, SHetA2 had attenuated effects on decreasing cell number in DR5 siRNA-transfected cells compared with control siRNA-transfected cells (Fig. 5*B*). Consistently, we detected less apoptotic cells (~25%) in DR5 siRNA-transfected cells than in cells transfected with control siRNA (~45%; Fig. 5*C*). Collectively, these results indicate that DR5 induction is required for SHetA2-induced apoptosis.

In addition, we examined the effect of siRNA-mediated blockage of DR5 induction on cooperative induction of apoptosis by the combination of SHetA2 and TRAIL. As shown in Fig. 5*D*, the combination of SHetA2 and TRAIL induced ~46% apoptosis in control siRNA-transfected cells but only 23% apoptosis in DR5 siRNA-transfected cells, indicating that DR5 induction is also important for cooperative induction of apoptosis by the SHetA2 and TRAIL combination.

SHetA2-induced DR5 up-regulation is CHOP dependent. To understand how SHetA2 up-regulates DR5 expression, we examined the effects of SHetA2 on the transactivation of reporter constructs with different lengths of *DR5* 5′-flanking regions to identify the region responsible for SHetA2-mediated *DR5* transactivation. In a transient transfection and luciferase assay, SHetA2 minimally increased the luciferase activity of pGL3-DR5(−240) while drastically increasing the luciferase activity of pGL3-DR5(−420), pGL3-DR5(−810), and pGL3-DR5(−1400) (Fig. 6*A, left*), indicating that the region between −240 and −420 contains essential element(s) responsible for SHetA2-induced *DR5* transactivation. There is a CHOP binding site in this region, which has been shown to be responsible for DR5 up-regulation by several anticancer agents (30–32). Thus, we further compared the effects of SHetA2 on the transactivation of reporter constructs carrying wild-type and mutated CHOP binding sites, respectively. As presented in Fig. 6*A* (*right*), SHetA2 increased the luciferase activity of the constructs carrying the wild-type *DR5* promoter region, but did not increase the luciferase activity of the construct carrying the *DR5* promoter region with the mutated CHOP binding site. These results

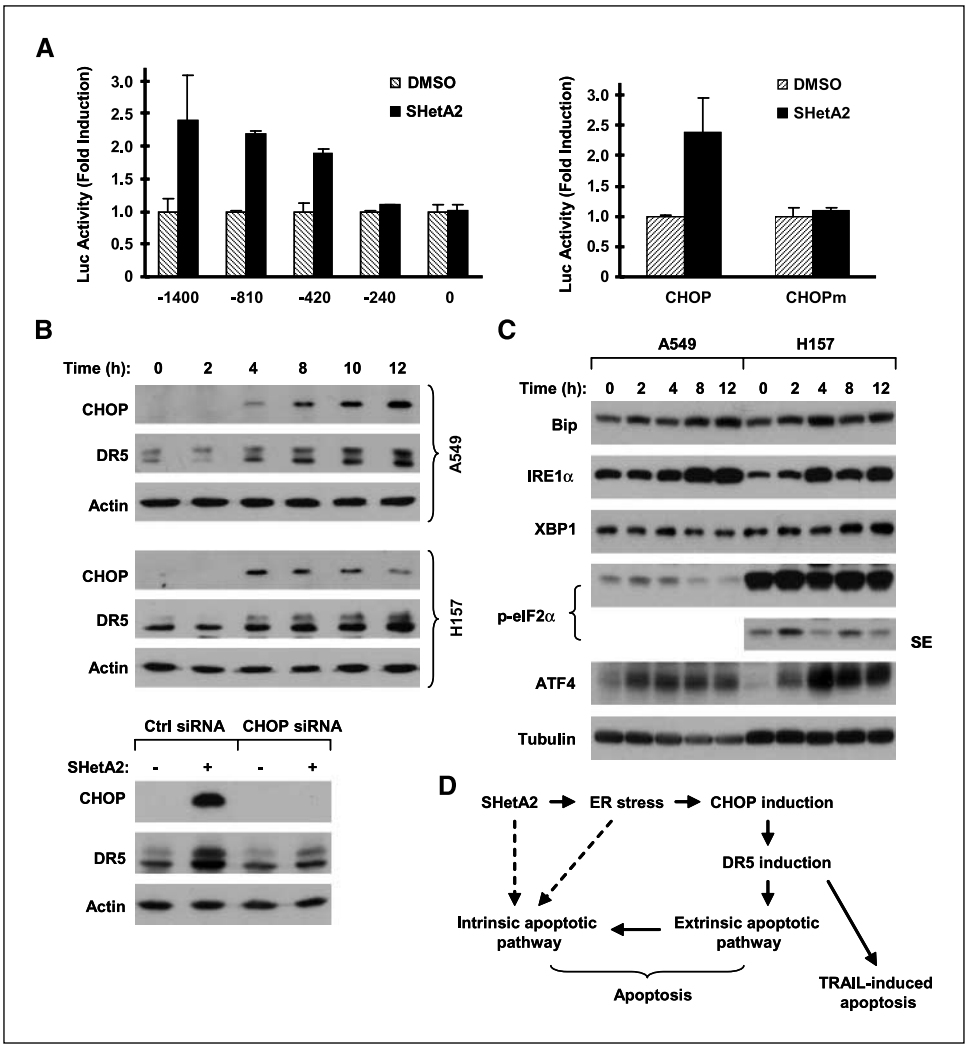

Figure 6. Induction of CHOP-dependent DR5 expression (*A* and *B*) and ER stress (*C*) by SHetA2 and schematic summary of signaling pathways involved in SHetA2-induced apoptosis (*D*). *A,* SHetA2 increases CHOP-dependent DR5 promoter activity. The given reporter constructs with different lengths of 5′-flanking region of the DR5 gene (*left*) or the reporter constructs with wild-type and mutated CHOP binding sites (*right*) were cotransfected with pCH110 plasmid into A549 cells. After 24 h, the cells were treated with DMSO or 5 μmol/L SHetA2 for 16 h and then subjected to luciferase assay. *Columns,* mean of triplicate determinations; *bars,* SDs. *B,* SHetA2 exerts time-dependent effects on inducing CHOP expression, which is responsible for DR5 up-regulation by SHetA2. The indicated cell lines (*top*) were treated with 10 μmol/L SHetA2 for the given times as indicated and then subjected to preparation of whole-cell protein lysates and subsequent Western blot analysis. A549 cells were transfected with control or CHOP siRNA (*bottom*). After 48 h, the cells were treated with the indicated concentrations of SHetA2 for 12 h and then subjected to preparation of whole-cell protein lysates and subsequent Western blot analysis. *C,* the indicated cell lines were treated with 10 μmol/L SHetA2 for the given times as indicated and subjected to preparation of whole-cell protein lysates and subsequent Western blot analysis. *SE,* short exposure. *D,* schematic summary of SHetA2-induced apoptosis. CHOP-dependent up-regulation of DR5 is important for SHetA2 to regulate the extrinsic apoptotic pathway, including TRAIL-induced apoptosis. This effect may eventually cooperate with other mechanisms, e.g., effects on the intrinsic apoptotic pathway (*dashed lines*), to fully activate apoptosis of cancer cells.

DOI:10.1158/0008-5472.CAN-07-6209

clearly indicate that the CHOP binding site in the *DR5* promoter region is responsible for SHetA2-mediated DR5 transactivation.

We next determined whether SHetA2 increased CHOP levels and, if so, whether CHOP is responsible for DR5 induction. By Western blot analysis, we detected a time-dependent DR5 induction accompanied by CHOP up-regulation in cells exposed to SHetA2, both of which occurred at 4 hours and were sustained up to 12-hour post–SHetA2 treatment (Fig. 6*B, top*). Moreover, we blocked SHetA2-induced CHOP expression using CHOP siRNA to see if blockage of CHOP induction abrogated the ability of SHetA2 to up-regulate DR5 expression. Indeed, blockage of the effect of SHetA2 on CHOP induction also abrogated the ability of SHetA2 to up-regulate DR5 expression in cells transfected with CHOP siRNA (Fig. 6*B, bottom*). Thus, these results clearly indicate that SHetA2-induced DR5 up-regulation is secondary to CHOP induction. Collectively, we conclude that SHetA2 induces a CHOP-dependent DR5 expression.

SHetA2 induces endoplasmic reticulum stress. It is well known that CHOP is one of the highest inducible genes during endoplasmic reticulum (ER) stress and a critical component of ER stress-induced apoptosis (38, 39). To determine whether SHetA2 induces ER stress, resulting in CHOP up-regulation, we further examined modulation of other featured proteins (e.g., Bip/GRP78, IRE1α, eIF2α, ATF4, and XBP1) of ER stress (39, 40) in cells exposed to SHetA2. As presented in Fig. 6*C*, SHetA2 increased the levels of Bip/GRP78, IRE1α, ATF4, and XBP1 in a time-dependent manner in both A549 and H157 cells, which occurred early at 2 hours and were sustained up to 12 hours. In addition, we found that SHetA2 weakly increased levels of p-eIF2α in these cell lines. However, these effects were transient because SHetA2 increased p-eIF2α levels only at early times (e.g., 2 hours). Collectively, these results suggest that SHetA2 induces ER stress in human NSCLC cells.

Discussion

By studying the effects of SHetA2 on the growth of human NSCLC cells, the present study has shown that SHetA2 effectively inhibits the growth of human NSCLC cells through induction of both apoptosis and cell cycle arrest. Importantly, SHetA2 significantly inhibits the growth of human lung cancer xenografts in nude mice. Thus, our results show the efficacy of SHetA2 for treatment of lung cancer and thereby warrant further evaluation of SHetA2 as a potential anticancer agent against lung cancer. We noted that, upon SHetA2 treatment, H1299 cells, which are the least sensitive to induction of apoptosis, primarily underwent G_1 arrest, whereas H460, A549 and H157 cells, which are relatively sensitive to induction of apoptosis, underwent G_2-M arrest. Whether G_1 arrest confers apoptosis resistance to SHetA2 in H1299 cells needs further investigation.

In this study, we found that SHetA2 increased cleavage of both caspase-8 and caspase-9. Importantly, silencing of caspase-8 using the caspase-8 siRNA abrogated SHetA2-induced cleavage of caspase-9, caspase-3, and PARP and attenuated the ability of SHetA2 to decrease the survival of lung cancer cells (Fig. 2). Thus, we conclude that SHetA2 induces caspase-8–dependent apoptosis. Given that silencing of caspase-8 prevents caspase-9 from activation, it seems that caspase-9 activation is secondary to caspase-8 activation during SHetA2-induced apoptosis. It has been shown that SHetA2 activates the mitochondrial apoptotic pathway in other types of cancer cells (8, 10). In our study, we also observed the cleavage of Bid, a caspase-8 substrate that mediates caspase-8–dependent activation of mitochondrial apoptosis, in SHetA2-treated cells. Thus, it is likely that SHetA2 induces apoptosis through activation of caspase-8 followed by activation of the mitochondrial apoptotic pathway involving cleavage of caspase-9 and caspase-3.

Moreover, we also found that SHetA2 up-regulated DR5 expression, including cell surface DR5 levels without increasing the expression of DR4, DcR1, and DcR2, as well as their ligand TRAIL (Fig. 3), suggesting that DR5 up-regulation may be important for SHetA2-induced caspase-8 activation and apoptosis. When combined with recombinant TRAIL, SHetA2 exerted augmented effects on induction of apoptosis (Fig. 4), suggesting that SHetA2-induced DR5 is functional. Moreover, siRNA-mediated blockade of DR5 induction attenuated the ability of SHetA2 to activate caspases, including caspase-8, to decrease cell survival, to induce apoptosis, and to augment induction of apoptosis when combined with TRAIL (Fig. 5). These results provide robust evidence for a critical role of DR5 up-regulation in mediating SHetA2-induced, caspase-8–dependent apoptosis, as well as cooperative induction of apoptosis by the SHetA2 and TRAIL combination. These findings indicate that SHetA2 is distinct from 4HPR, which induces caspase-8–dependent apoptosis independent of DRs (41). We noted that SHetA2 actually decreased the levels of DR4 and TRAIL in some cell lines. The underlying mechanism and their biological significance are currently unknown and need further investigation.

DR5 expression can be regulated through p53-dependent and p53-independent mechanisms (26, 42). In our study, SHetA2 induced DR5 expression in all of the tested human NSCLC cell lines (Fig. 3), among which only H460 and A549 have wild-type p53 gene (22, 25). Thus, it is likely that SHetA2 induces DR5 expression independent of p53. Recently, CHOP has been shown to regulate DR5 expression through the CHOP binding site in the DR5 gene (30, 31), revealing an important DR5 regulation mechanism. In our study, SHetA2 increased DR5 promoter activity, suggesting that DR5 induction occurs at the transcriptional level. The deletion and mutation analysis of the DR5 5′-flanking region revealed that the region containing the CHOP binding site is essential for SHetA2-mediated DR5 transactivation (Fig. 6). Moreover, SHetA2 induced a time-dependent CHOP expression, which was accompanied by the up-regulation of DR5 expression. Blockage of SHetA2-mediated CHOP induction by the CHOP siRNA accordingly inhibited DR5 up-regulation (Fig. 6). Collectively, we conclude that SHetA2 induces DR5 expression through a CHOP-dependent mechanism. It has been suggested that p53 regulates CHOP expression (43). In our study, SHetA2 increased CHOP expression in both p53 wild-type cells (e.g., A549) and p53 mutant cells (e.g., H157) in a similar fashion to DR5 up-regulation. Thus, it seems that SHetA2 induces CHOP independent of p53.

It is well known that CHOP is a featured ER stress-regulated protein involved in ER stress-induced apoptosis (38). Thus, our finding on CHOP induction by SHetA2 suggests that SHetA2 triggers ER stress. Indeed, SHetA2 increased the levels of Bip, IRE1α, p-eIF2α, ATF4, and XBP1 (Fig. 6), all of which are additional featured proteins accumulated or increased during ER stress (39, 40). Therefore, it seems that SHetA2 induces ER stress in NSCLC cells. Several studies have shown that 4HPR induces CHOP expression and ER stress, which are important for 4HPR-induced apoptosis (44–47). A recent study actually showed that 4HPR induces CHOP-dependent DR5 expression (17). In this regard, it seems that SHetA2 and 4HPR share similarities. Our preliminary

DOI:10.1158/0008-5472.CAN-07-6209

data show that cyclohexamide, an inhibitor of general protein synthesis that can decrease the overall protein burden, but not salubrinal, an inhibitor of eIF2α dephosphorylation that can protect cell from ER stress-induced apoptosis through temporary slow down of the global protein translation (48), abolished SHetA2-induced CHOP expression (see Supplementary Fig. S2). These results suggest that blockage of eIF2α-mediated protein translation is not sufficient to prevent CHOP induction by SHetA2, although eIF2α-signaling pathway is critical for CHOP induction in ER stress (38). Nevertheless, the relationship between ER stress and CHOP induction, as well as apoptosis by SHetA2, needs further investigation.

In practice, our findings that SHetA2 increases DR5 expression and enhances TRAIL-induced apoptosis have meaningful implications. Given the therapeutic potential of TRAIL and agonistic DR5 antibodies, both of which are being tested in phase I clinical trials, SHetA2 can be used in combination with TRAIL or an agonistic anti-DR5 antibody to achieve an enhanced cancer therapeutic effect through augmenting induction of apoptosis of human cancer cells.

In summary, our study has shown that the novel synthetic atypical retinoid compound SHetA2 effectively inhibits the growth of human NSCLC cells both *in vitro* and *in vivo*. For the first time, we have shown that SHetA2 triggers ER stress and induces CHOP-dependent DR5 expression, leading to caspase-8–dependent apoptosis. Given that SHetA2 also activates the intrinsic apoptotic pathways, as shown in other studies, we suggest that the intrinsic and extrinsic pathways may be simultaneously activated by an initiating stress induced by the drug or by cross-talk between the extrinsic and intrinsic apoptosis pathways (Fig. 6*D*).

Disclosure of Potential Conflicts of Interest

No potential conflicts of interest were disclosed.

Acknowledgments

Received 11/30/2007; revised 2/5/2008; accepted 3/31/2008.

Grant support: Georgia Cancer Coalition Distinguished Cancer Scholar award (S-Y. Sun) and Department of Defense grants W81XWH-04-1-0142-VITAL (S-Y. Sun and F.R. Khuri for Project 4).

The costs of publication of this article were defrayed in part by the payment of page charges. This article must therefore be hereby marked *advertisement* in accordance with 18 U.S.C. Section 1734 solely to indicate this fact.

We thank Dr. H-G. Wang (University of South Florida College of Medicine) for providing DR5 reporter constructs with wild-type and mutant CHOP binding sites, respectively; Dr. G.S. Wu (Wayne State University School of Medicine) for providing the plasmid containing a 5′-flanking region of the DR5 gene; M. Xia and L. Hu in our laboratory for excellent technical assistance; and Dr. H.A. Elrod for editing of the manuscript.

References

1. Sun SY, Lotan R. Retinoids and their receptors in cancer development and chemoprevention. Crit Rev Oncol Hematol 2002;41:41–55.
2. Lengfelder E, Saussele S, Weisser A, Buchner T, Hehlmann R. Treatment concepts of acute promyelocytic leukemia. Crit Rev Oncol Hematol 2005;56:261–74.
3. Garattini E, Gianni M, Terao M. Retinoid related molecules an emerging class of apoptotic agents with promising therapeutic potential in oncology: pharmacological activity and mechanisms of action. Curr Pharm Des 2004;10:433–48.
4. Dhar A, Liu S, Klucik J, et al. Synthesis, structure-activity relationships, and RARγ-ligand interactions of nitrogen heteroarotinoids. J Med Chem 1999;42:3602–14.
5. Mic FA, Molotkov A, Benbrook DM, Duester G. Retinoid activation of retinoic acid receptor but not retinoid X receptor is sufficient to rescue lethal defect in retinoic acid synthesis. Proc Natl Acad Sci U S A 2003; 100:7135–40.
6. Benbrook DM, Kamelle SA, Guruswamy SB, et al. Flexible heteroarotinoids (Flex-Hets) exhibit improved therapeutic ratios as anti-cancer agents over retinoic acid receptor agonists. Invest New Drugs 2005;23: 417–28.
7. Chun KH, Benbrook DM, Berlin KD, Hong WK, Lotan R. The synthetic heteroarotinoid SHetA2 induces apoptosis in squamous carcinoma cells through a receptor-independent and mitochondria-dependent pathway. Cancer Res 2003;63:3826–32.
8. Liu S, Brown CW, Berlin KD, et al. Synthesis of flexible sulfur-containing heteroarotinoids that induce apoptosis and reactive oxygen species with discrimination between malignant and benign cells. J Med Chem 2004; 47:999–1007.
9. Guruswamy S, Lightfoot S, Gold MA, et al. Effects of retinoids on cancerous phenotype and apoptosis in organotypic cultures of ovarian carcinoma. J Natl Cancer Inst 2001;93:516–25.
10. Liu T, Hannafon B, Gill L, Kelly W, Benbrook D. Flex-Hets differentially induce apoptosis in cancer over normal cells by directly targeting mitochondria. Mol Cancer Ther 2007;6:1814–22.
11. Ashkenazi A, Dixit VM. Death receptors: signaling and modulation. Science 1998;281:1305–8.
12. Hengartner MO. The biochemistry of apoptosis. Nature 2000;407:770–6.
13. Kelley SK, Ashkenazi A. Targeting death receptors in cancer with Apo2L/TRAIL. Curr Opin Pharmacol 2004;4: 333–9.
14. Rowinsky EK. Targeted induction of apoptosis in cancer management: the emerging role of tumor necrosis factor-related apoptosis-inducing ligand receptor activating agents. J Clin Oncol 2005;23:9394–407.
15. Wajant H, Gerspach J, Pfizenmaier K. Tumor therapeutics by design: targeting and activation of death receptors. Cytokine Growth Factor Rev 2005;16:55–76.
16. Elrod HA, Sun SY. Modulation of death receptors by cancer therapeutic agents. Cancer Biol Ther. Epub 2007 Nov 21.
17. Kouhara J, Yoshida T, Nakata S, et al. Fenretinide up-regulates DR5/TRAIL-R2 expression via the induction of the transcription factor CHOP and combined treatment with fenretinide and TRAIL induces synergistic apoptosis in colon cancer cell lines. Int J Oncol 2007;30:679–87.
18. Puduvalli VK, Li JT, Chen L, McCutcheon IE. Induction of apoptosis in primary meningioma cultures by fenretinide. Cancer Res 2005;65:1547–53.
19. Sun SY, Yue P, Chen X, Hong WK, Lotan R. The synthetic retinoid CD437 selectively induces apoptosis in human lung cancer cells while sparing normal human lung epithelial cells. Cancer Res 2002;62:2430–6.
20. Sun SY, Yue P, Hong WK, Lotan R. Augmentation of tumor necrosis factor-related apoptosis-inducing ligand (TRAIL)-induced apoptosis by the synthetic retinoid 6-[3-(1-adamantyl)-4-hydroxyphenyl]-2-naphthalene carboxylic acid (CD437) through up-regulation of TRAIL receptors in human lung cancer cells. Cancer Res 2000; 60:7149–55.
21. Sun SY, Yue P, Lotan R. Implication of multiple mechanisms in apoptosis induced by the synthetic retinoid CD437 in human prostate carcinoma cells. Oncogene 2000;19:4513–22.
22. Sun SY, Yue P, Wu GS, et al. Implication of p53 in growth arrest and apoptosis induced by the synthetic retinoid CD437 in human lung cancer cells. Cancer Res 1999;59:2829–33.
23. Jin F, Liu X, Zhou Z, et al. Activation of nuclear factor-κB contributes to induction of death receptors and apoptosis by the synthetic retinoid CD437 in DU145 human prostate cancer cells. Cancer Res 2005;65:6354–63.
24. Liu X, Yue P, Khuri FR, Sun SY. p53 upregulates death receptor 4 expression through an intronic p53 binding site. Cancer Res 2004;64:5078–83.
25. Guan B, Yue P, Clayman GL, Sun SY. Evidence that the death receptor DR4 is a DNA damage-inducible, p53-regulated gene. J Cell Physiol 2001;188:98–105.
26. Wu GS, Burns TF, McDonald ER III, et al. KILLER/DR5 is a DNA damage-inducible p53-regulated death receptor gene. Nat Genet 1997;17:141–3.
27. Guan B, Yue P, Lotan R, Sun SY. Evidence that the human death receptor 4 is regulated by activator protein 1. Oncogene 2002;21:3121–9.
28. Ravi R, Bedi GC, Engstrom LW, et al. Regulation of death receptor expression and TRAIL/Apo2L-induced apoptosis by NF-κB. Nat Cell Biol 2001;3:409–16.
29. Shetty S, Gladden JB, Henson ES, et al. Tumor necrosis factor-related apoptosis inducing ligand (TRAIL) up-regulates death receptor 5 (DR5) mediated by NFκB activation in epithelial derived cell lines. Apoptosis 2002;7:413–20.
30. Yamaguchi H, Wang HG. CHOP is involved in endoplasmic reticulum stress-induced apoptosis by enhancing DR5 expression in human carcinoma cells. J Biol Chem 2004;279:45495–502.
31. Yoshida T, Shiraishi T, Nakata S, et al. Proteasome inhibitor MG132 induces death receptor 5 through CCAAT/enhancer-binding protein homologous protein. Cancer Res 2005;65:5662–7.
32. Abdelrahim M, Newman K, Vanderlaag K, Samudio I, Safe S. 3,3′-diindolylmethane (DIM) and its derivatives induce apoptosis in pancreatic cancer cells through endoplasmic reticulum stress-dependent upregulation of DR5. Carcinogenesis 2006;27:717–28.
33. Sun SY, Liu X, Zou W, Yue P, Marcus AI, Khuri FR. The farnesyltransferase inhibitor lonafarnib induces CCAAT/enhancer-binding protein homologous protein-dependent expression of death receptor 5, leading to induction of apoptosis in human cancer cells. J Biol Chem 2007;282:18800–9.
34. Chen S, Liu X, Yue P, Schonthal AH, Khuri FR, Sun SY. CHOP-dependent DR5 induction and ubiquitin/proteasome-mediated c-FLIP downregulation contribute to enhancement of TRAIL-induced apoptosis by dimethylcelecoxib in human non-small cell lung cancer cells. Mol Pharmacol 2007;72:1269–79.
35. Sun SY, Yue P, Dawson MI, et al. Differential effects of

DOI:10.1158/0008-5472.CAN-07-6209

synthetic nuclear retinoid receptor-selective retinoids on the growth of human non-small cell lung carcinoma cells. Cancer Res 1997;57:4931–9.
36. Sun SY, Yue P, Wu GS, et al. Mechanisms of apoptosis induced by the synthetic retinoid CD437 in human non-small cell lung carcinoma cells. Oncogene 1999;18:2357–65.
37. Liu X, Yue P, Zhou Z, Khuri FR, Sun SY. Death receptor regulation and celecoxib-induced apoptosis in human lung cancer cells. J Natl Cancer Inst 2004;96:1769–80.
38. Oyadomari S, Mori M. Roles of CHOP/GADD153 in endoplasmic reticulum stress. Cell Death Differ 2004;11:381–9.
39. Szegezdi E, Logue SE, Gorman AM, Samali A. Mediators of endoplasmic reticulum stress-induced apoptosis. EMBO Rep 2006;7:880–5.
40. Ron D, Walter P. Signal integration in the endoplasmic reticulum unfolded protein response. Nat Rev Mol Cell Biol 2007;8:519–29.
41. Kalli KR, Devine KE, Cabot MC, et al. Heterogeneous role of caspase-8 in fenretinide-induced apoptosis in epithelial ovarian carcinoma cell lines. Mol Pharmacol 2003;64:1434–43.
42. Sheikh MS, Burns TF, Huang Y, et al. p53-dependent and -independent regulation of the death receptor KILLER/DR5 gene expression in response to genotoxic stress and tumor necrosis factor α. Cancer Res 1998;58:1593–8.
43. Zhan Q, Fan S, Smith ML, et al. Abrogation of p53 function affects gadd gene responses to DNA base-damaging agents and starvation. DNA Cell Biol 1996;15:805–15.
44. Xia Y, Wong NS, Fong WF, Tideman H. Upregulation of GADD153 expression in the apoptotic signaling of N-(4-hydroxyphenyl)retinamide (4HPR). Int J Cancer 2002;102:7–14.
45. Kim DG, You KR, Liu MJ, Choi YK, Won YS. GADD153-mediated anticancer effects of N-(4-hydroxyphenyl)retinamide on human hepatoma cells. J Biol Chem 2002;277:38930–8.
46. Kadara H, Lacroix L, Lotan D, Lotan R. Induction of endoplasmic reticulum stress by the pro-apoptotic retinoid N-(4-hydroxyphenyl)retinamide via a reactive oxygen species-dependent mechanism in human head and neck cancer cells. Cancer Biol Ther 2007;6:705–11.
47. Tiwari M, Kumar A, Sinha RA, et al. Mechanism of 4-HPR-induced apoptosis in glioma cells: evidences suggesting role of mitochondrial-mediated pathway and endoplasmic reticulum stress. Carcinogenesis 2006;27:2047–58.
48. Boyce M, Bryant KF, Jousse C, et al. A selective inhibitor of eIF2α dephosphorylation protects cells from ER stress. Science 2005;307:935–9.

DOI:10.1158/1535-7163.MCT-08-0648

Molecular Cancer Therapeutics

Involvement of c-FLIP and survivin down-regulation in flexible heteroarotinoid-induced apoptosis and enhancement of TRAIL-initiated apoptosis in lung cancer cells

Yidan Lin, Xiangguo Liu, Ping Yue, et al.

Mol Cancer Ther 2008;7:3556-3565. Published online November 11, 2008.

DOI:10.1158/1535-7163.MCT-08-0648

Involvement of c-FLIP and survivin down-regulation in flexible heteroarotinoid-induced apoptosis and enhancement of TRAIL-initiated apoptosis in lung cancer cells

Yidan Lin,[1,2] Xiangguo Liu,[1,3] Ping Yue,[1] Doris M. Benbrook,[4] K. Darrell Berlin,[5] Fadlo R. Khuri,[1] and Shi-Yong Sun[1]

[1]Department of Hematology and Medical Oncology, Winship Cancer Institute, Emory University School of Medicine, Atlanta, Georgia; [2]Thoracic Surgery Department, Daping Hospital, Third Military Medical University, Chongqing, People's Republic of China; [3]School of Life Sciences, Shandong University, Jinan, Shandong, People's Republic of China; [4]Departments of Obstetrics and Gynecology and Biochemistry and Molecular Biology, University of Oklahoma Health Science Center, Oklahoma City, Oklahoma; and [5]Department of Chemistry, Oklahoma State University, Stillwater, Oklahoma

Abstract

The flexible heteroarotinoid, SHetA2, is a novel compound with apoptosis-inducing and anticancer activities *in vitro* and *in vivo*. Our previous research showed that up-regulation of death receptor 5 plays a critical role in the mechanism of SHetA2-induced apoptosis in human lung cancer cells. The hypothesis of this study was that the mechanism of SHetA2-induced apoptosis requires modulation of additional proteins critical for regulation of apoptosis, including cellular FLICE-inhibitory protein (c-FLIP), survivin, X-linked inhibitor of apoptosis, Bcl-2, Bcl-X_L, Bax, and Bim. Western blot analysis showed that c-FLIP and survivin were substantially reduced in all of the tested cell lines exposed to SHetA2 compared with other proteins that were reduced only in a subset of the cell lines tested. Strikingly, overexpression of c-FLIP, but not survivin, protected cells from SHetA2-induced apoptosis and enhancement of TRAIL-initiated apoptosis, although knockdown of endogenous survivin did slightly sensitize cells to SHetA2-induced apoptosis. Consistent with these results, small interfering RNA-mediated reduction of c-FLIP was more effective than survivin down-regulation in triggering apoptosis in these cell lines. SHetA2 increased ubiquitination of c-FLIP and the consequent degradation was abrogated by the proteasome inhibitor MG132. Although SHetA2 treatment led to increased c-Jun phosphorylation, the JNK inhibitor SP600125 did not prevent c-FLIP down-regulation by SHetA2. Thus, it appears that SHetA2 down-regulates c-FLIP levels by facilitating its ubiquitin/proteasome-mediated degradation independent of JNK activation. Collectively, the present study indicates that, in addition to death receptor 5 up-regulation, c-FLIP down-regulation is another important component of flexible heteroarotinoid (SHetA2)-induced apoptosis as well as enhancement of TRAIL-induced apoptosis. [Mol Cancer Ther 2008;7(11):3556–65]

Introduction

Apoptosis is a genetically well-controlled mechanism essential for the maintenance of tissue homeostasis and proper development through the elimination of unwanted cells. Thus, it represents a universal and exquisitely efficient endogenous or induced cellular suicide pathway (1, 2). It is well known that cells can die of apoptosis primarily through the extrinsic death receptor-induced pathway and/or the intrinsic mitochondria-mediated pathway. Cross-talk between these two pathways is mediated by the truncated proapoptotic protein Bid (2). A central step in the execution of apoptosis is the activation of an unusual class of cysteine proteases, termed caspases, which are widely expressed as inactive forms (2). Thus, this step is negatively regulated by multiple antiapoptotic proteins to prevent unnecessary activation of these caspases.

Caspase-8 activation is a critical step in initiating the extrinsic apoptotic pathway (3). Cellular FLICE-inhibitory protein (c-FLIP) is the major protein that prevents caspase-8 from activation by death receptors through binding to Fas-associated death domain and caspase-8 at the death-inducing signaling complex (4). Although multiple splicing isoforms of c-FLIP mRNA have been described, only two of them, $FLIP_S$ and $FLIP_L$, have been significantly studied at the protein level (5). Both proteins can be recruited to the death-inducing signaling complex and inhibit death receptor-mediated apoptosis (6). Both $FLIP_L$ and $FLIP_S$ are quick turnover proteins; thus, their levels are subject to regulation by ubiquitin/proteasome-mediated degradation (7–9). Generally speaking, c-FLIP expression correlates with resistance against death receptor-induced apoptosis. Accordingly, down-regulation of c-FLIP confers sensitivity to death receptor-induced apoptosis (5). Additionally, c-FLIP expression is associated with chemoresistance. Thus, down-regulation of c-FLIP using antisense oligonucleotides

Received 5/5/08; revised 7/11/08; accepted 8/28/08.

Grant support: Georgia Cancer Coalition Distinguished Cancer Scholar award (S-Y. Sun) and Department of Defense VITAL award W81XWH-04-1-0142 (S-Y. Sun and F.R. Khuri for Project 4).

The costs of publication of this article were defrayed in part by the payment of page charges. This article must therefore be hereby marked *advertisement* in accordance with 18 U.S.C. Section 1734 solely to indicate this fact.

Note: Y. Lin and X. Liu share first authorship. F.R. Khuri and S-Y. Sun are Georgia Cancer Coalition Distinguished Cancer Scholars.

Requests for reprints: Shi-Yong Sun, Department of Hematology and Medical Oncology, Winship Cancer Institute, Emory University School of Medicine, 1365-C Clifton Road Northeast, C3088, Atlanta, GA 30322. Phone: 404-778-2170; Fax: 404-778-5520. E-mail: ssun@emory.edu

doi:10.1158/1535-7163.MCT-08-0648

DOI:10.1158/1535-7163.MCT-08-0648

or small interfering RNA (siRNA) sensitizes cancer cells to chemotherapeutic agent-induced apoptosis (10, 11), whereas overexpression of c-FLIP protects cells from apoptosis induced by certain cancer therapeutic agents such as etoposide and cisplatin (10–17).

Caspase-9 activation is an essential step in the intrinsic apoptotic pathway (3). Survivin is a protein belonging to the inhibitor of apoptosis (IAP) gene family. Like other IAPs, survivin acts downstream of mitochondria to prevent processing or activation of initiator caspase-9 in the apoptosome, leading to inhibition of the activity of the effector caspases. Thus, survivin modulates both extrinsic and intrinsic apoptotic pathways (18). Genetic studies have shown that survivin transgenic mice exhibit apoptotic resistance (19), whereas survivin knockout mice show increased sensitivity to apoptosis (20). Moreover, many studies have shown that induction of survivin expression causes cell resistance to drug-induced apoptosis (21), whereas down-regulation of survivin using various means such as siRNA either induces apoptosis or sensitizes cells to undergo drug-induced or death ligand/receptor-induced apoptosis (22–25).

Although heteroarotinoids were initially developed as retinoids, the flexible heteroarotinoids act independently of the retinoic acid receptors to regulate growth, differentiation, and apoptosis (26–29). Moreover, SHetA2 induces apoptosis in cancer cells while sparing normal cells (30, 31). Importantly, SHetA2 effectively inhibits tumor growth *in vivo* without evidence of toxicity (26). Because of these encouraging results, SHetA2 was chosen for evaluation in the National Cancer Institute Rapid Access to Intervention Development program (application 196, compound NSC 726189) and now is in the Rapid Access to Preventive Intervention Development program, showing a potential as a cancer chemopreventive and therapeutic agent.

The mechanism of SHetA2-induced apoptosis has been shown to occur through the intrinsic mitochondrial pathway associated with loss of mitochondrial membrane integrity, generation of reactive oxygen species, release of cytochrome *c* from the mitochondria, and activation of caspase-3 in head and neck cancer cell lines (31). Likewise, SHetA2 induces apoptosis in human ovarian cancer cells through targeting the mitochondria, which is associated with alterations in the balance of Bcl-2 proteins, independent of generation of reactive oxygen species (30). It appears that the mechanisms of SHetA2 may vary in different types of cancer cells. We have shown recently that SHetA2 effectively inhibits the growth and induces apoptosis of human non-small cell lung cancer (NSCLC; ref. 32). Moreover, SHetA2 cooperates with the death ligand tumor necrosis factor-related apoptosis-inducing ligand (TRAIL) to augment induction of apoptosis (32). These effects are tightly associated with death receptor 5 (DR5) up-regulation (32), implying the importance of activation of the extrinsic apoptotic pathway in SHetA2-induced apoptosis. The present study further determined whether SHetA2 modulates levels or expression of other proteins critical for regulation of apoptosis, including regulation of both intrinsic and extrinsic apoptotic pathways. In this study, we found that, of the critical apoptosis-regulating proteins,

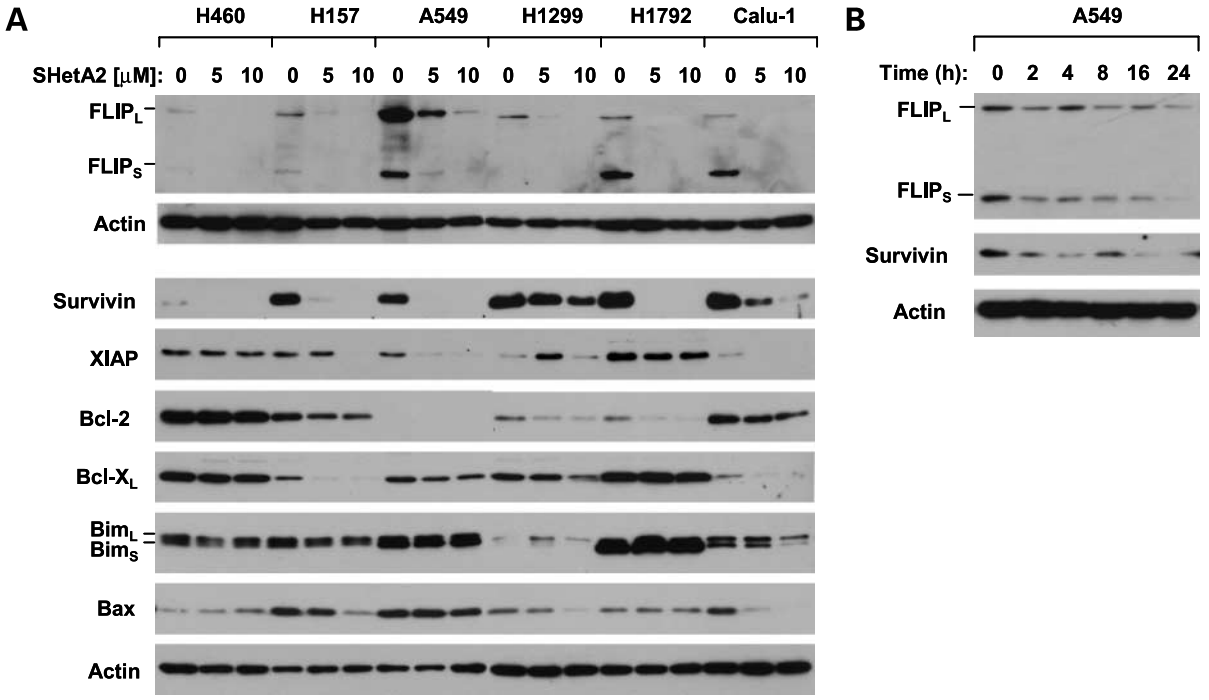

Figure 1. Modulatory effects of SHetA2 on c-FLIP, survivin, XIAP, Bcl-2, Bcl-X_L, Bim, and Bax in human NSCLC cell lines. The indicated cell lines were treated with the indicated concentrations of SHetA2 for 16 h (**A**) or with 5 μmol/L SHetA2 for the given time as indicated (**B**). The cells were then subjected to preparation of whole-cell protein lysates and subsequent Western blot analysis.

DOI:10.1158/1535-7163.MCT-08-0648

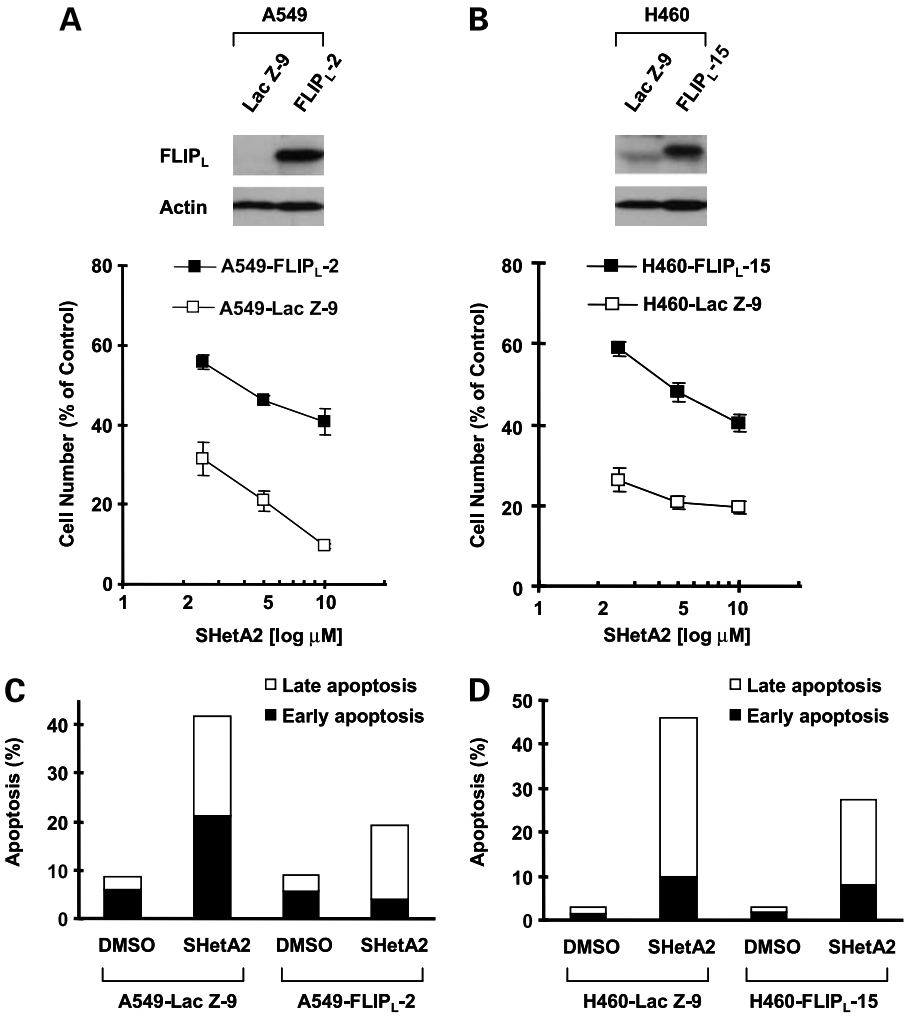

Figure 2. Enforced expression of ectopic c-FLIP protects cells from SHetA2-induced cell number decrease (**A** and **B**) and apoptosis (**C** and **D**). **A** and **B,** indicated transfectants were seeded in 96-well plates and treated with the indicated concentrations of SHetA2 ranging from 2.5 to 10 μmol/L. After 48 h, the cells were subjected to the sulforhodamine B assay for measurement of cell number. Mean of four replicate determinations. *Bars,* SD. **C** and **D,** indicated transfectants were treated with 10 μmol/L SHetA2 for 48 h and then harvested for detection of apoptotic cells using Annexin V staining. The percent positive cells in the top right and bottom right quadrants were added to yield the total of apoptotic cells.

c-FLIP was down-regulated consistently in all of the tested cell lines exposed to SHetA2 and contributed to SHetA2-induced apoptosis and enhancement of TRAIL-induced apoptosis. These results complement our previous findings to further support the importance of the activation of the extrinsic apoptotic pathway in SHetA2-induced apoptosis.

Materials and Methods

Reagents

SHetA2 was synthesized as described previously (27) and dissolved in DMSO at a concentration of 10 mmol/L, and aliquots were stored at −80°C. Stock solution was diluted to the appropriate concentrations with growth medium immediately before use. Human recombinant TRAIL was purchased from PeproTech. The specific JNK inhibitor SP600125 was purchased from Biomol. The proteasome inhibitor MG132 was purchased from Sigma. Mouse monoclonal anti-FLIP antibody (NF6) was purchased from Alexis Biochemicals. Rabbit polyclonal anti-X-linked IAP (XIAP), anti-Bim, anti-c-Jun, and anti-phospho-c-Jun (Ser^{63}) antibodies and mouse monoclonal anti-survivin antibody were purchased from Cell Signaling Technology. Mouse anti-Bax monoclonal antibody was purchased from Trevigen. Mouse anti-Bcl-2 and rabbit anti-Bcl-X_L antibodies were purchased from Santa Cruz Biotechnology. Rabbit polyclonal anti-β-actin antibody was purchased from Sigma.

Cell Lines and Cell Culture

The human NSCLC cell lines used in this study were described previously (33). A549-Lac Z-9, A549-FLIP$_L$-2, H460-Lac Z-9, and H460-FLIP$_L$-15 were described previously (15, 16). These cell lines were grown in monolayer culture in RPMI 1640 supplemented with glutamine and 5% fetal bovine serum at 37°C in a humidified atmosphere consisting of 5% CO_2 and 95% air.

Construction of Lentiviral Survivin Expression Vector and Establishment of Lung Cancer Cell Lines That Overexpress Survivin

Survivin cDNA was amplified by standard reverse transcription-PCR from RNA extracted from normal human bronchial epithelial cells using the following primers: sense 5′-CACTAGTGCCGCCACCATGGGTG-CCCCGACGTTGCCCCCTG-3′ and antisense 5′-CGGG-CCCTCAATCCATGGCAGCCAGCTGCTCG-3′. Following the amplification, the survivin cDNA was cloned into a

DOI:10.1158/1535-7163.MCT-08-0648

pT-easy vector (Promega) following the manufacturer's protocol as pT-easy-survivin. The pT-easy-survivin was then cut and cloned into a lentiviral vector using two restriction enzyme sites *Spe*I and *Apa*I as described previously (34). The newly generated plasmid was named lenti-survivin. In this study, we used pLenti-Lac Z as a vector control, which was included in the pLenti6/V5 Directional TOPO Cloning kit (Invitrogen). Lentiviruses were produced using ViraPower Lentiviral Expression System (Invitrogen) according to the manufacturer's instructions. The viral titers were determined following the manufacturer's manual. For infection, the viruses were added to the cells at the multiplicity of infection of 10. For stable expression, cells were infected and then selected in the presence of 50 μg/mL blasticidin for 1 week. The individual clones and pool were expanded and screened for survivin expression using Western blot analysis.

Cell Growth Assay

Cells were cultured in 96-well cell culture plates and treated the next day with the agents indicated. Viable cell number was estimated using the sulforhodamine B assay as described previously (33).

Apoptosis Assays

Apoptosis was detected either by analysis of caspase activation using Western blot analysis as described below or by Annexin V staining using Annexin V-PE apoptosis detection kit (BD Bioscience) following the manufacturer's instructions and analyzed by flow cytometry using FACScan (Becton Dickinson). In the Annexin V assay, the percent positive cells for Annexin V-PE staining only in the bottom right quadrant and for both Annexin V and DNA (7-amino-actinomycin D) staining in the top right quadrant represent the early and late apoptotic populations, respectively. The percent positive cells for DNA staining only in the top left quadrant represent the necrotic population.

Western Blot Analysis

Preparation of whole-cell protein lysates and Western blot analysis were described previously (35).

Silencing of c-FLIP and Survivin

c-FLIP and survivin gene silencing was achieved by transfecting the given cell lines with siRNA oligonucleotides using the HiperFect transfection reagent (Qiagen) following the manufacturer's instructions. The control (nonsilencing), c-FLIP, and survivin siRNA oligonucleotide duplexes that target the sequences 5′-AATTCTCCGAACGTGTCACGT-3′, 5′-AAGCAGTCTGTTCAAGGAGCA-3′ (12), and 5′-AAGCATTCGTCCGGTTGCGCT-3′ (36), respectively, were synthesized by Qiagen. The transfection was conducted in 6-well plates. Forty-eight hours after the transfection, the cells were harvested and subjected to Annexin V staining/flow cytometric analysis. The knockdown efficiency was evaluated by Western blotting.

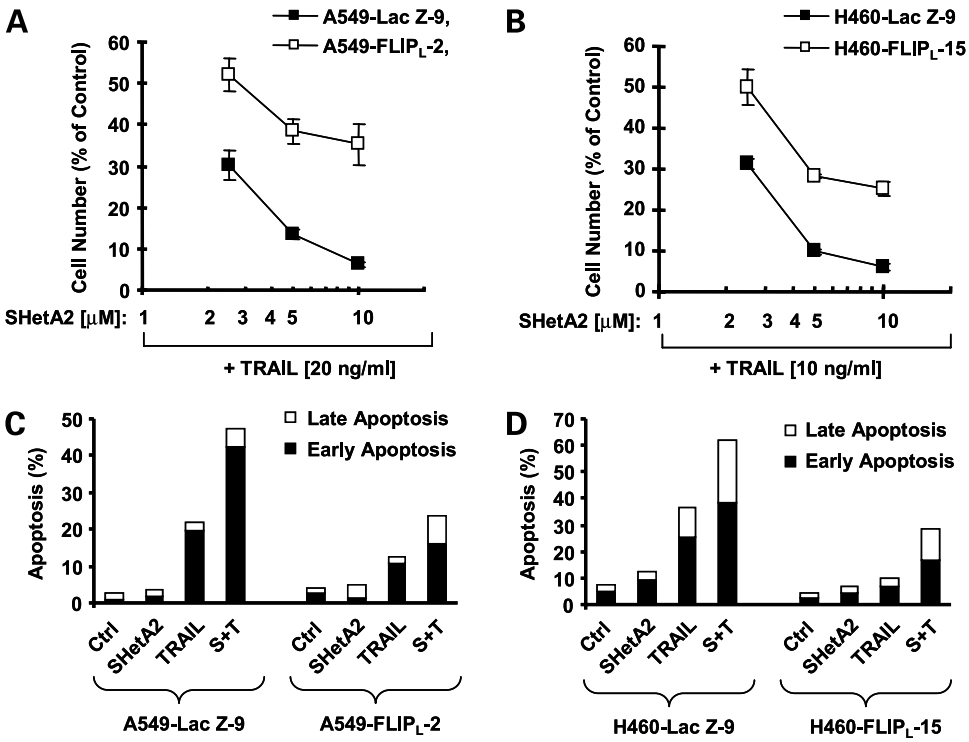

Figure 3. Enforced expression of ectopic c-FLIP confers resistance to induction of apoptosis by the combination of SHetA2 and TRAIL. **A** and **B,** indicated transfectants were seeded in 96-well plates and treated with the indicated concentrations of SHetA2 combined with 10 ng/mL TRAIL (H460) or 20 ng/mL TRAIL (A549). After 24 h, cells were subjected to the sulforhodamine B assay for measurement of cell survival. Mean of four replicate determinations. *Bars,* SD. **C** and **D,** indicated transfectants were treated with DMSO, 5 μmol/L SHetA2 alone, 10 ng/mL (H460) or 20 ng/mL (A549) TRAIL alone, or SHetA2 plus TRAIL for 24 h and then subjected to detection of apoptotic cells using Annexin V staining. The percent positive cells in the top right and bottom right quadrants were added to yield the total of apoptotic cells.

DOI:10.1158/1535-7163.MCT-08-0648

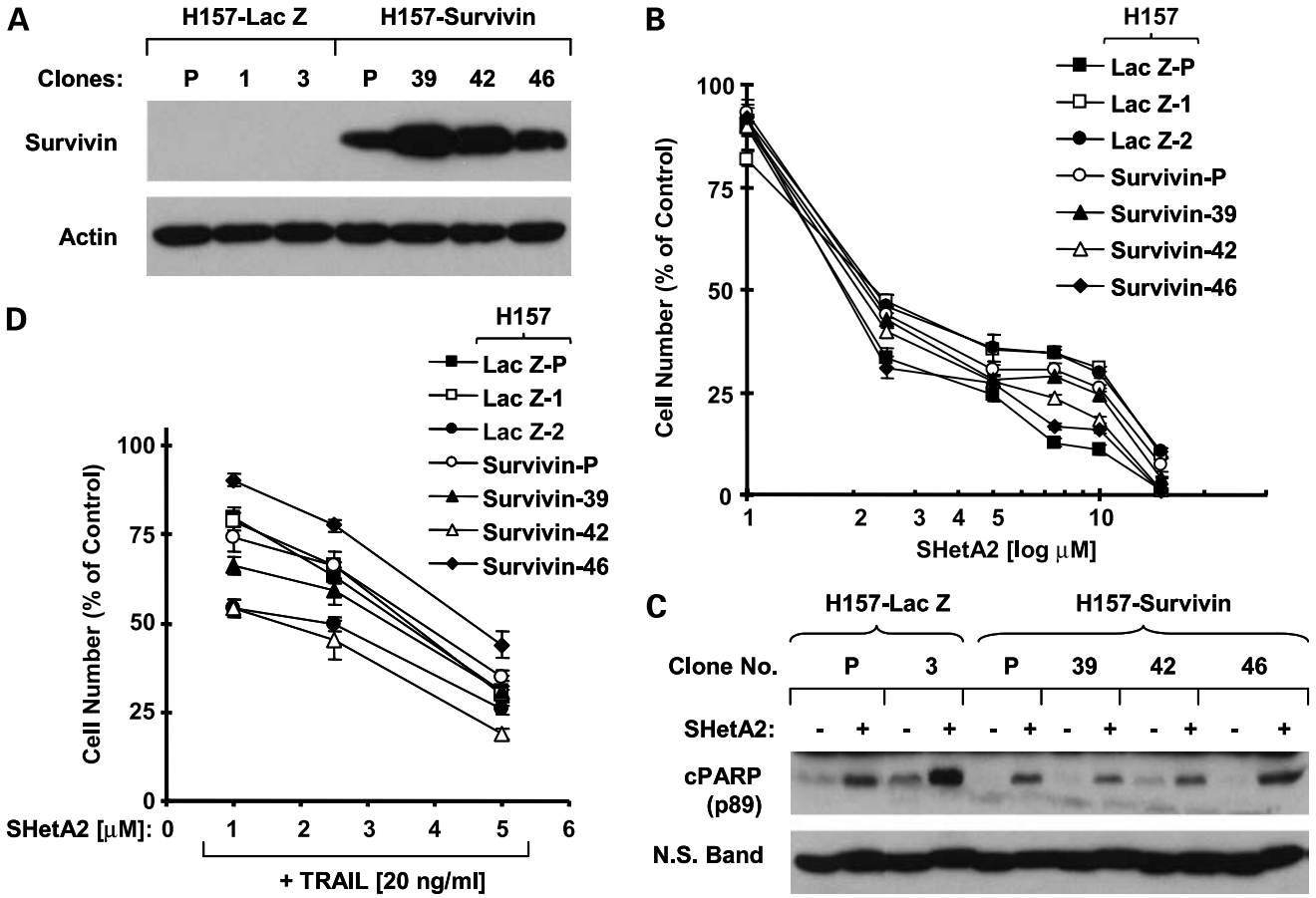

Figure 4. Enforced expression of ectopic survivin (**A**) does not confer resistance to ShetA2 (**B** and **C**) or the combination of SHetA2 and TRAIL (**D**). **A,** confirmation of ectopic survivin expression in H157 survivin transfectants by Western blotting using survivin antibody. *P,* pool. **B** and **D,** indicated transfectants from H157 cells were seeded in 96-well plates and treated with the given concentrations of SHetA2 (**B**) or the individual combination of SHetA2 and TRAIL as indicated (**D**) the next day. After 48 h (**B**) or 24 h (**D**), the cells were subjected to the sulforhodamine B assay for measurement of cell survival. Mean of four replicate determinations. *Bars,* SD. **C,** indicated transfectants were treated with 10 μmol/L SHetA2 for 48 h and then subjected to preparation of whole-cell protein lysates and subsequent Western blot analysis for detection of cleaved poly(ADP-ribose) polymerase (*cPARP*). *N.S.,* nonspecific.

Immunoprecipitation for Detection of Ubiquitinated c-FLIP

A549-FLIP$_L$-2 cells, which stably express FLIP$_L$, were transfected with HA-ubiquitin plasmid using the FuGENE 6 transfection reagent (Roche Diagnostics) following the manufacturer's instruction. After 24 h, the cells were treated with SHetA2 or MG132 plus SHetA2 for 4 h and then were lysed for immunoprecipitation of Flag-FLIP$_L$ using Flag M2 monoclonal antibody (Sigma), as described previously (37), followed by the detection of ubiquitinated FLIP$_L$ with Western blotting using anti-HA antibody (Abgent).

Results

SHetA2 Modulates the Levels of c-FLIP, Survivin, and Other Apoptosis-Related Proteins in Human NSCLC Cells

To better understand the mechanisms by which SHetA2 induces apoptosis, we examined the effects of SHetA2 on modulation of several important proteins involved in regulation of both extrinsic and intrinsic apoptotic pathways in a panel of human NSCLC cell lines. As presented in Fig. 1A, SHetA2 at 5 or 10 μmol/L effectively reduced the levels of c-FLIP (both FLIP$_L$ and FLIP$_S$) and survivin in all of the 6 tested cell lines. Compared with other cell lines, H1299 cells exhibited the least decrease in survivin levels on treatment with SHetA2. We also noted that the basal levels of FLIP$_S$ in H460, H157, and H1299 cells and the basal levels of survivin in H460 cells were very low or undetectable. The down-regulation of both c-FLIP and survivin occurred rapidly within 2 h and was sustained up to 24 h post-SHetA2 treatment (Fig. 1B).

SHetA2 also reduced the levels of XIAP, Bcl-2, and Bcl-X$_L$; however, these modulations occurred only in some of the tested cell lines (Fig. 1A). For example, SHetA2 decreased the levels of XIAP and Bcl-X$_L$ in H157, A549, and Calu-1 cell lines but not in H460 and H1792 cell lines. Bcl-2 levels were reduced in 4 of the 5 tested cell lines that

DOI:10.1158/1535-7163.MCT-08-0648

express detectable Bcl-2, except for H460 cells on treatment with SHetA2. SHetA2 did not modulate the levels of Bim in all of the tested cell lines. Bax levels were either not altered (e.g., H460 and A549) or even decreased (e.g., H157 and Calu-1) particularly by the high dose of SHetA2 (e.g., 10 μmol/L; Fig. 1A).

Collectively, it appears that down-regulation of c-FLIP and survivin is likely to be the common and important mechanism contributing to SHetA2-induced apoptosis. Therefore, the subsequent experiments focused on showing the importance of c-FLIP and survivin down-regulation in SHetA2-induced apoptosis as well as enhancement of TRAIL-induced apoptosis.

Enforced Expression of Ectopic c-FLIP Protects NSCLC Cells from Induction of Apoptosis by SHetA2 Alone or When Combined with TRAIL

To test the importance of c-FLIP in SHetA2-induced apoptosis, the effect of c-FLIP overexpression on induction of apoptosis by SHetA2 alone or combined with TRAIL was examined. As presented in Fig. 2, in both A549 and H460 cells, SHetA2 effectively decreased the numbers of control cells that expressed the control protein Lac Z (A549-Lac Z-9

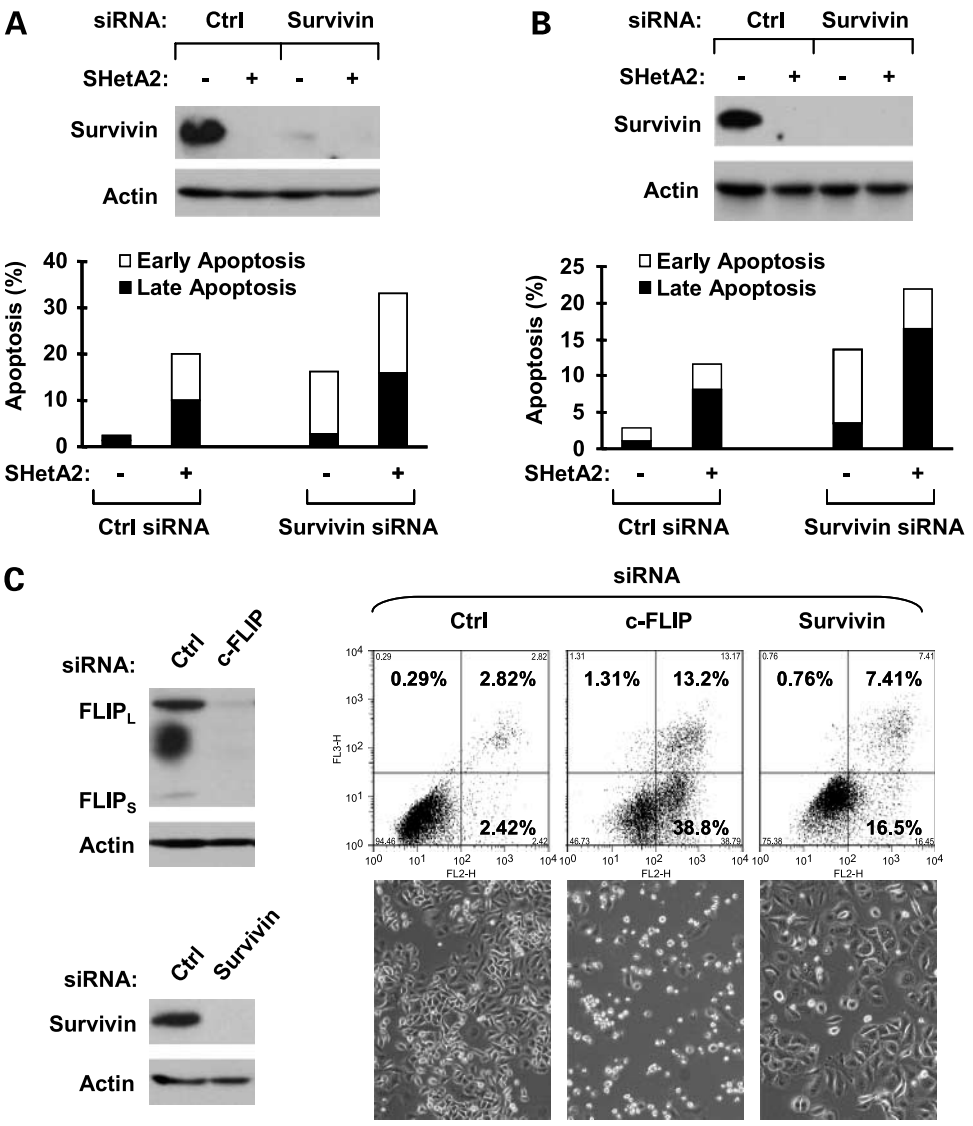

Figure 5. Effects of siRNA-mediated reduction of endogenous survivin on SHetA2-induced apoptosis (**A** and **B**) and comparison of the potencies of siRNA-mediated down-regulation of c-FLIP and survivin on triggering apoptosis (**C**). A549 (**A**) or H1299 (**B**) cells were seeded in 6-well plates and the next day transfected with 60 nmol/L control (*Ctrl*) and survivin siRNAs, respectively. Twenty-four hours later, the cells were treated with 10 μmol/L SHetA2. After an additional 48 h, the cells were harvested for evaluation of survivin knockdown efficiency by Western blotting (*top*) and apoptosis using Annexin V staining/flow cytometry (*bottom*), respectively. **C,** A549 cells were seeded in 6-well plates and the next day subjected to transfection with 60 nmol/L control, c-FLIP, and survivin siRNAs, respectively. After 48 h, the cells were harvested for evaluation of c-FLIP or survivin knockdown efficiency by Western blot analysis (*left*) and for detection of apoptotic cells using Annexin V staining/flow cytometry (*right*). In addition, the morphologic changes of the transfected cells were also documented (*right*).

DOI:10.1158/1535-7163.MCT-08-0648

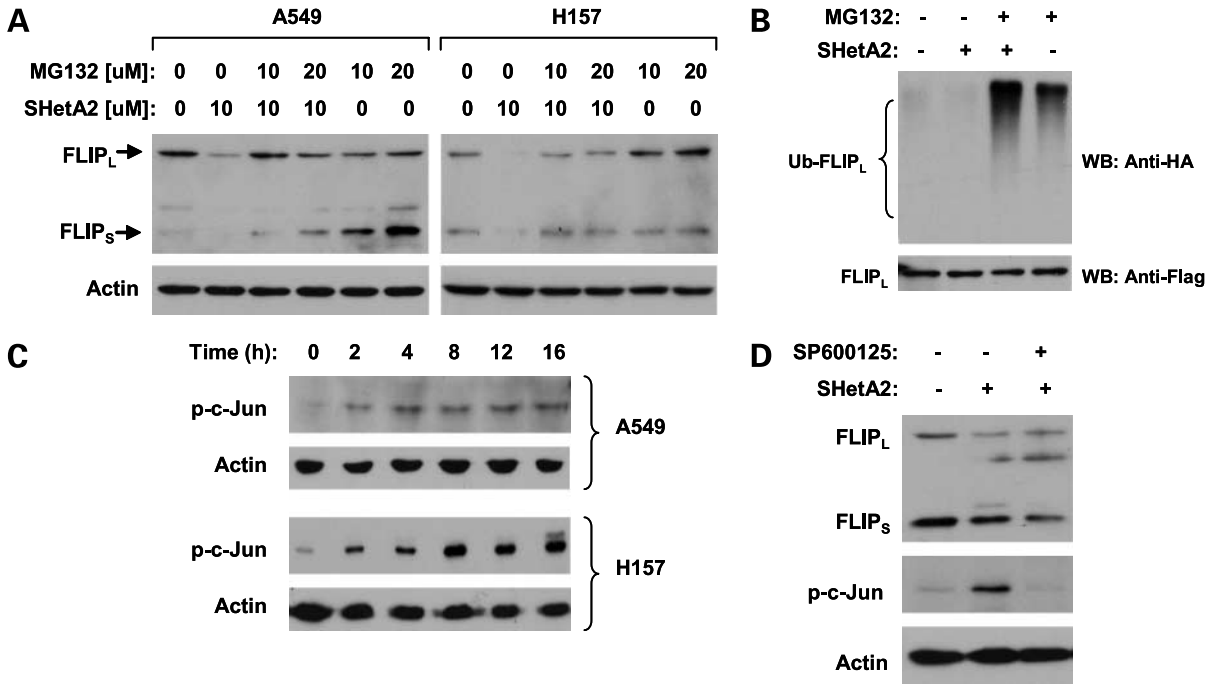

Figure 6. SHetA2 down-regulates c-FLIP levels through ubiquitin/proteasome-mediated protein degradation (**A** and **B**) independent of JNK (**C** and **D**). **A,** given cell lines were pretreated with 10 or 20 μmol/L MG132 for 30 min before the addition of 10 μmol/L SHetA2. After cotreatment for 4 h, the cells were harvested for preparation of whole-cell protein lysates and subsequent Western blot analysis. **B,** A549-FLIP$_L$-2 cells that stably express ectopic flag-FLIP$_L$ were transfected with HA-ubiquitin plasmid using FuGENE 6 transfection reagent for 24 h. The cells were then pretreated with 20 μmol/L MG132 for 30 min and then cotreated with 10 μmol/L SHetA2 for 4 h. Whole-cell protein lysates were then prepared for immunoprecipitation using anti-Flag antibody followed by Western blotting (*WB*) using anti-HA antibody for detection of ubiquitinated FLIP$_L$ (*Ub-FLIP$_L$*) and anti-Flag antibody for detection of ectopic FLIP$_L$. FLIP$_L$. **C,** indicated cell lines were treated with 10 μmol/L SHetA2 for the given times. **D,** A549 cells were pretreated with 20 μmol/L SP600125 for 30 min and then cotreated with 10 μmol/L SHetA2 for another 12 h. After the aforementioned treatments (**C** and **D**), the cells were then subjected to preparation of whole-cell protein lysates and subsequent Western blot analysis for detection of the indicated proteins.

and H460-Lac Z-9); however, this effect was substantially diminished in cell lines that overexpressed ectopic FLIP$_L$ (A549-FLIP$_L$-2 and H460-FLIP$_L$-15; Fig. 2A and B). Consistently, SHetA2 caused ~42% and 46% apoptotic cells in A549-Lac Z-9 and H460-Lac Z-9 cells, respectively, but only 19% and 27% apoptosis in A549-FLIP$_L$-2 and H460-FLIP$_L$-15 cells, respectively (Fig. 2C and D), indicating that enforced overexpression of c-FLIP confers cell resistance to SHetA2-induced apoptosis. Taken together, we conclude that c-FLIP overexpression partially protects NSCLC cells from SHetA2-induced apoptosis.

Moreover, we examined the effects of c-FLIP overexpression on SHetA2/TRAIL-induced apoptosis. As shown in Fig. 3A and B, SHetA2/TRAIL had much less effects on decreasing the numbers of A549-FLIP$_L$-2 and H460-FLIP$_L$-15 cells than those of A549-Lac Z-9 and H460-Lac Z-9 cells, indicating that the cell-killing effects of the SHetA2 and TRAIL combination were substantially inhibited in NSCLC cells that overexpress c-FLIP. In agreement, we detected ~62% and 48% apoptosis, respectively, in H460-Lac Z-9 and A549-Lac Z-9 cells but only 27% and 24% apoptosis, respectively, in H460-FLIP$_L$-15 and A549-FLIP$_L$-2 cells (Fig. 3C and D), showing that enforced expression of ectopic c-FLIP partially protected NSCLC cells from cooperative induction of apoptosis by the SHetA2 and TRAIL combination. Thus, c-FLIP overexpression decreases the sensitivity of NSCLC cells to SHetA2/TRAIL-induced apoptosis as well.

Enforced Overexpression of Ectopic Survivin Does Not Protect NSCLC Cells from SHetA2- or SHetA2/TRAIL-induced Apoptosis

Given that SHetA2 also effectively reduced the levels of survivin in human NSCLC cells, we further determined whether survivin reduction plays a role in regulation of SHetA2-induced apoptosis or SHetA2-mediated enhancement of TRAIL-induced apoptosis. To this end, we infected H157 cells, which have a high lentiviral infection efficiency, with lentiviral Lac Z (as a control) or survivin and established several sublines that stably express Lac Z or survivin as presented in Fig. 4A. After obtaining these cell lines, we then examined their sensitivity to SHetA2 or SHetA2/TRAIL. Unexpectedly, we found that the H157-survivin sublines, despite having high levels of survivin, were not different in their sensitivity to either SHetA2 or SHetA2/TRAIL compared with the Lac Z sublines albeit their sublines exhibited various sensitivity (Fig. 4B and D). Overall, it appears that survivin overexpression does not alter cell sensitivity to either SHetA2 or SHetA2/TRAIL. Moreover, we looked at poly(ADP-ribose) polymerase cleavage in these cell lines exposed to SHetA2 and found

DOI:10.1158/1535-7163.MCT-08-0648

that induction of poly(ADP-ribose) polymerase cleavage by SHetA2 between Lac Z and survivin sublines were overall comparable (Fig. 4C). These results further indicate that overexpression of survivin does not alter cell sensitivity to SHetA2-induced apoptosis.

Silencing of Endogenous Survivin Expression Slightly Enhances SHetA2-Induced Apoptosis

We also determined whether enforced reduction of endogenous survivin expression with transfection of survivin siRNA alters cell sensitivity to SHetA2. As presented in Fig. 5A and B, transfection of survivin siRNA in either A549 or H1299 cells substantially reduced basal levels of survivin. In A549 cells, SHetA2-induced apoptosis was increased from 20% in control siRNA-transfected cells to 33% in survivin siRNA-transfected cells (Fig. 5A). In H1299 cells, SHetA2-induced apoptosis was increased from 12% in control siRNA-transfected cells to 22% in survivin siRNA-transfected cells (Fig. 5B). Overall, data from both cell lines indicate that siRNA-mediated reduction of endogenous survivin results in ~10% increase in SHetA2-induced apoptosis. Thus, we conclude that enforced down-regulation of endogenous survivin slightly enhances SHetA2-induced apoptosis.

siRNA-Mediated Down-regulation of c-FLIP More Effectively Initiates Apoptosis Than Survivin Reduction

To further decipher the involvement or importance of c-FLIP and survivin in regulation of apoptosis, we used siRNA to silence c-FLIP or survivin and then examined their respective effect on induction of apoptosis. As presented in Fig. 5C, transfection of c-FLIP and survivin siRNA into A549 cells efficiently reduced the levels of c-FLIP and survivin proteins, respectively (*left*). However, c-FLIP down-regulation induced much more apoptotic cells than survivin reduction (~44% compared with 24%; *right*). These results again suggest that c-FLIP plays a more important role than survivin in regulation of apoptosis.

SHetA2 Down-regulates c-FLIP through Promoting Ubiquitin/Proteasome-Mediated Degradation Independent of JNK

Considering the importance of c-FLIP down-regulation in SHetA2-induced and SHetA2/TRAIL-induced apoptosis as shown above, we also questioned how SHetA2 reduced c-FLIP levels. Because c-FLIP proteins are known to be regulated by ubiquitin/proteasome-mediated degradation (7, 9), we then determined whether the observed down-regulation of c-FLIP by SHetA2 would be mediated via this process. To this end, we first treated cells with SHetA2 in the absence and presence of the proteasome inhibitor MG132 and then compared c-FLIP modulation under these conditions. In both A549 and H157 cells, SHetA2-induced down-regulation of c-FLIP was inhibited by MG132 (Fig. 6A), indicating that SHetA2-induced c-FLIP degradation is proteasome dependent. By immunoprecipitation/Western blotting, we detected the highest levels of ubiquitinated $FLIP_L$ in cells treated with SHetA2 plus MG132 compared with cells exposed to SHetA2 alone or MG132 alone (Fig. 6B), indicating that SHetA2 increases c-FLIP ubiquitination. Taken together, we conclude that SHetA2 initiates ubiquitin/proteasome-mediated c-FLIP degradation, leading to down-regulation of c-FLIP in human NSCLC cells.

Recently, JNK has been linked to tumor necrosis factor-induced, ubiquitin/proteasome-mediated $FLIP_L$ degradation (9). Therefore, we determined whether JNK activation is involved in mediating SHetA2-induced c-FLIP degradation. To this end, we first looked at whether SHetA2 increases JNK activity. As presented in Fig. 6C, SHetA2 caused a time-dependent increase in the levels of phospho-c-Jun, a well-known readout of JNK activity, indicating that SHetA2 treatment leads to activation of JNK. Following this study, we examined the effects of SHetA2 on c-FLIP down-regulation in the presence of the JNK-specific inhibitor SP600125. SP600125 at the concentration of 20 μmol/L blocked SHetA2-induced c-Jun phosphorylation, confirming that SP600125 worked as expected in our cell system. However, SP600125 did not block SHetA2-induced c-FLIP (both $FLIP_L$ and $FLIP_S$) down-regulation (Fig. 6D). Collectively, we suggest that SHetA2 down-regulates c-FLIP independent of JNK activation.

Discussion

By examining the modulatory effects of SHetA2 on the levels of several proteins involved in the regulation of both extrinsic and intrinsic apoptotic pathways, including c-FLIP, survivin, XIAP, Bcl-2, Bcl-X_L, Bim, and Bax, we noted that c-FLIP, a major inhibitor of the extrinsic apoptotic pathway, and survivin, a major inhibitor of the intrinsic apoptotic pathway, are the only proteins that were down-regulated in all of the tested NSCLC cell lines (Fig. 1). Thus, down-regulation of c-FLIP and survivin appears important for SHetA2 regulation of apoptosis.

It has been documented that modulation of either c-FLIP or survivin levels alters cell sensitivity to drug-induced or death receptor-mediated apoptosis (5–7, 38–40). In this study, enforced expression of ectopic $FLIP_L$ attenuated induction of apoptosis by SHetA2 or its combination with TRAIL (Figs. 2 and 3), suggesting a critical role of c-FLIP down-regulation in mediating SHetA2-induced apoptosis and the augmentation of TRAIL-induced apoptosis. In contrast, enforced expression of ectopic survivin did not protect cancer cells from either SHetA2-induced apoptosis or SHetA2/TRAIL-induced apoptosis (Fig. 4). Interestingly, siRNA-mediated reduction of endogenous survivin did slightly enhance SHetA2-induced apoptosis (Fig. 5A and B). Thus, it seems that survivin reduction plays a role, albeit limited, in this process. In our previous study, the proteasome inhibitor PS-341 induced apoptosis and augmented TRAIL-induced apoptosis despite up-regulation of survivin (41). In this study, we also showed that siRNA-mediated silencing of c-FLIP induced massive apoptosis, whereas silencing of survivin initiated limited apoptosis (Fig. 5C). These results suggest that cancer cells are more subject to undergo apoptosis by modulation of c-FLIP levels than by alteration of survivin levels, although both c-FLIP and survivin are involved in the regulation of apoptosis.

DOI:10.1158/1535-7163.MCT-08-0648

Our previous study showed that SHetA2 up-regulates DR5 expression, which contributes to SHetA2-induced apoptosis and enhancement of TRAIL-induced apoptosis in human NSCLC cells (32). The present findings on modulation of c-FLIP and its involvement in SHetA2-induced apoptosis alone and in combination with TRAIL further highlight the importance of the activation of the DR5-mediated extrinsic apoptotic pathway in SHetA2 mechanisms at least in NSCLC cells. Based on these previous (32) and current findings, we propose that SHetA2 induces apoptosis and enhances TRAIL-induced apoptosis primarily through activation of the extrinsic apoptotic pathway by induction of DR5 expression and down-regulation of c-FLIP in human NSCLC cells. In addition, down-regulation of survivin can further amplify death signaling from activation of the extrinsic apoptotic pathway.

It has been documented that both $FLIP_L$ and $FLIP_S$ are quick turnover proteins regulated by ubiquitin/proteasome-mediated degradation (7, 9). In the current study, SHetA2 down-regulated c-FLIP levels by facilitating ubiquitin/proteasome-mediated degradation of c-FLIP, as SHetA2 increased ubiquitinated c-FLIP levels and lost activity in reducing c-FLIP levels in the presence of the proteasome inhibitor MG132 (Fig. 6). JNK activation has been recently suggested to regulate ubiquitin/proteasome-dependent degradation of $FLIP_L$ (9). Although SHetA2 treatment leads to activation of the JNK pathway, the JNK inhibitor SP600125 did not prevent SHetA2-induced down-regulation of c-FLIP. Moreover, SHetA2 decreased both forms of c-FLIP ($FLIP_L$ and $FLIP_S$), whereas JNK regulates the degradation of only the long form of c-FLIP ($FLIP_L$; ref. 9). Thus, our results suggest that SHetA2 down-regulates c-FLIP independent of JNK.

We noted only in some of the tested cell lines that SHetA2 did down-regulate the expression of Bcl-2, Bcl-X_L, and XIAP, all of which are antiapoptotic proteins involved in regulation of the intrinsic apoptotic pathway (2). Thus, it appears that the modulation of these proteins may not be as important as c-FLIP down-regulation in mediating SHetA2-induced apoptosis. However, it is still possible that the modulation of these proteins contributes to SHetA2-induced apoptosis or augmentation of TRAIL-induced apoptosis, to a certain extent, in a specific cell line. It is likely that SHetA2-mediated induction of DR5 and down-regulation of c-FLIP initiates apoptosis, whereas down-regulation of other antiapoptotic proteins such as survivin and Bcl-2 lowers the cellular apoptotic threshold to further sensitize cancer cells to SHetA2-induced apoptosis. Nonetheless, the roles of these antiapoptotic proteins in regulating SHetA2-induced apoptosis including sensitization of TRAIL-induced apoptosis need further investigation.

In summary, the present study shows for the first time that SHetA2 down-regulates c-FLIP in human NSCLC cells; this down-regulation contributes to SHetA2-mediated induction of apoptosis and enhancement of TRAIL-induced apoptosis. The current results complement our previous finding that the DR5-mediated extrinsic apoptotic pathway plays a critical role in SHetA2-induced apoptosis in human NSCLC cells.

Disclosure of Potential Conflicts of Interest

No potential conflicts of interest were disclosed.

Acknowledgments

We thank Dr. H.A. Elrod in our laboratory for editing the article.

References

1. Song Z, Steller H. Death by design: mechanism and control of apoptosis. Trends Cell Biol 1999;9:M49 – 52.

2. Hengartner MO. The biochemistry of apoptosis. Nature 2000;407:770 – 6.

3. Green DR, Evan GI. A matter of life and death. Cancer Cell 2002;1:19 – 30.

4. Irmler M, Thome M, Hahne M, et al. Inhibition of death receptor signals by cellular FLIP. Nature 1997;388:190 – 5.

5. Wajant H. Targeting the FLICE inhibitory protein (FLIP) in cancer therapy. Mol Interv 2003;3:124 – 7.

6. Sharp DA, Lawrence DA, Ashkenazi A. Selective knockdown of the long variant of cellular FLICE inhibitory protein augments death receptor-mediated caspase-8 activation and apoptosis. J Biol Chem 2005;280:19401 – 9.

7. Kim Y, Suh N, Sporn M, Reed JC. An inducible pathway for degradation of FLIP protein sensitizes tumor cells to TRAIL-induced apoptosis. J Biol Chem 2002;277:22320 – 9.

8. Poukkula M, Kaunisto A, Hietakangas V, et al. Rapid turnover of c-FLIPshort is determined by its unique C-terminal tail. J Biol Chem 2005;280:27345 – 55.

9. Chang L, Kamata H, Solinas G, et al. The E3 ubiquitin ligase itch couples JNK activation to TNFα-induced cell death by inducing c-FLIP(L) turnover. Cell 2006;124:601 – 13.

10. Abedini MR, Qiu Q, Yan X, Tsang BK. Possible role of FLICE-like inhibitory protein (FLIP) in chemoresistant ovarian cancer cells *in vitro*. Oncogene 2004;23:6997 – 7004.

11. Kamarajan P, Sun NK, Chao CC. Up-regulation of FLIP in cisplatin-selected HeLa cells causes cross-resistance to CD95/Fas death signalling. Biochem J 2003;376:253 – 60.

12. Longley DB, Wilson TR, McEwan M, et al. c-FLIP inhibits chemotherapy-induced colorectal cancer cell death. Oncogene 2006;25:838 – 48.

13. Wilson TR, McLaughlin KM, McEwan M, et al. c-FLIP: a key regulator of colorectal cancer cell death. Cancer Res 2007;67:5754 – 62.

14. Rogers KM, Thomas M, Galligan L, et al. Cellular FLICE-inhibitory protein regulates chemotherapy-induced apoptosis in breast cancer cells. Mol Cancer Ther 2007;6:1544 – 51.

15. Liu X, Yue P, Schonthal AH, Khuri FR, Sun SY. Cellular FLICE-inhibitory protein down-regulation contributes to celecoxib-induced apoptosis in human lung cancer cells. Cancer Res 2006;66:11115 – 9.

16. Zou W, Chen S, Liu X, et al. c-FLIP downregulation contributes to apoptosis induction by the novel synthetic triterpenoid methyl-2-cyano-3,12-dioxooleana-1,9-dien-28-oate (CDDO-Me) in human lung cancer cells. Cancer Biol Ther 2007;6:1614 – 20.

17. Day TW, Najafi F, Wu CH, Safa AR. Cellular FLICE-like inhibitory protein (c-FLIP): a novel target for Taxol-induced apoptosis. Biochem Pharmacol 2006;71:1551 – 61.

18. Altieri DC. Validating survivin as a cancer therapeutic target. Nat Rev Cancer 2003;3:46 – 54.

19. Grossman D, Kim PJ, Blanc-Brude OP, et al. Transgenic expression of survivin in keratinocytes counteracts UVB-induced apoptosis and cooperates with loss of p53. J Clin Invest 2001;108:991 – 9.

20. Conway EM, Pollefeyt S, Steiner-Mosonyi M, et al. Deficiency of survivin in transgenic mice exacerbates Fas-induced apoptosis via mitochondrial pathways. Gastroenterology 2002;123:619 – 31.

21. Ling X, Bernacki RJ, Brattain MG, Li F. Induction of survivin expression by Taxol (paclitaxel) is an early event, which is

DOI:10.1158/1535-7163.MCT-08-0648

independent of Taxol-mediated G_2/M arrest. J Biol Chem 2004;279:15196 – 203.

22. Yonesaka K, Tamura K, Kurata T, et al. Small interfering RNA targeting survivin sensitizes lung cancer cell with mutant p53 to Adriamycin. Int J Cancer 2006;118:812 – 20.

23. Li JX, Zhou KY, Liang T, Zhang YF. Knockdown of survivin expression by small interfering RNA induces apoptosis in human breast carcinoma cell line MCF-7. Ai Zheng 2005;24:268 – 72.

24. Uchida H, Tanaka T, Sasaki K, et al. Adenovirus-mediated transfer of siRNA against survivin induced apoptosis and attenuated tumor cell growth *in vitro* and *in vivo*. Mol Ther 2004;10:162 – 71.

25. Chawla-Sarkar M, Bae SI, Reu FJ, Jacobs BS, Lindner DJ, Borden EC. Downregulation of Bcl-2, FLIP or IAPs (XIAP and survivin) by siRNAs sensitizes resistant melanoma cells to Apo2L/TRAIL-induced apoptosis. Cell Death Differ 2004;11:915 – 23.

26. Benbrook DM, Kamelle SA, Guruswamy SB, et al. Flexible heteroarotinoids (Flex-Hets) exhibit improved therapeutic ratios as anti-cancer agents over retinoic acid receptor agonists. Invest New Drugs 2005;23:417 – 28.

27. Liu S, Brown CW, Berlin KD, et al. Synthesis of flexible sulfur-containing heteroarotinoids that induce apoptosis and reactive oxygen species with discrimination between malignant and benign cells. J Med Chem 2004;47:999 – 1007.

28. Guruswamy S, Lightfoot S, Gold MA, et al. Effects of retinoids on cancerous phenotype and apoptosis in organotypic cultures of ovarian carcinoma. J Natl Cancer Inst 2001;93:516 – 25.

29. Mic FA, Molotkov A, Benbrook DM, Duester G. Retinoid activation of retinoic acid receptor but not retinoid X receptor is sufficient to rescue lethal defect in retinoic acid synthesis. Proc Natl Acad Sci U S A 2003;100:7135 – 40.

30. Liu T, Hannafon B, Gill L, Kelly W, Benbrook D. Flex-Hets differentially induce apoptosis in cancer over normal cells by directly targeting mitochondria. Mol Cancer Ther 2007;6:1814 – 22.

31. Chun KH, Benbrook DM, Berlin KD, Hong WK, Lotan R. The synthetic heteroarotinoid SHetA2 induces apoptosis in squamous carcinoma cells through a receptor-independent and mitochondria-dependent pathway. Cancer Res 2003;63:3826 – 32.

32. Lin YD, Chen S, Yue P, et al. CHOP-dependent death receptor 5 induction is a major component of SHetA2-induced apoptosis in lung cancer cells. Cancer Res 2008;68:5335 – 44.

33. Sun SY, Yue P, Dawson MI, et al. Differential effects of synthetic nuclear retinoid receptor-selective retinoids on the growth of human non-small cell lung carcinoma cells. Cancer Res 1997;57:4931 – 9.

34. Liu X, Yue P, Khuri FR, Sun SY. Decoy receptor 2 (DcR2) is a p53 target gene and regulates chemosensitivity. Cancer Res 2005;65:9169 – 75.

35. Sun SY, Yue P, Wu GS, et al. Mechanisms of apoptosis induced by the synthetic retinoid CD437 in human non-small cell lung carcinoma cells. Oncogene 1999;18:2357 – 65.

36. Retzer-Lidl M, Schmid RM, Schneider G. Inhibition of CDK4 impairs proliferation of pancreatic cancer cells and sensitizes towards TRAIL-induced apoptosis via downregulation of survivin. Int J Cancer 2007;121:66 – 75.

37. Chen C, Sun X, Ran Q, et al. Ubiquitin-proteasome degradation of KLF5 transcription factor in cancer and untransformed epithelial cells. Oncogene 2005;24:3319 – 27.

38. Xiao C, Yang BF, Song JH, Schulman H, Li L, Hao C. Inhibition of CaMKII-mediated c-FLIP expression sensitizes malignant melanoma cells to TRAIL-induced apoptosis. Exp Cell Res 2005;304:244 – 55.

39. Rippo MR, Moretti S, Vescovi S, et al. FLIP overexpression inhibits death receptor-induced apoptosis in malignant mesothelial cells. Oncogene 2004;23:7753 – 60.

40. Mathas S, Lietz A, Anagnostopoulos I, et al. c-FLIP mediates resistance of Hodgkin/Reed-Sternberg cells to death receptor-induced apoptosis. J Exp Med 2004;199:1041 – 52.

41. Liu X, Yue P, Chen S, et al. The proteasome inhibitor PS-341 (bortezomib) up-regulates DR5 expression leading to induction of apoptosis and enhancement of TRAIL-induced apoptosis despite up-regulation of c-FLIP and survivin expression in human NSCLC cells. Cancer Res 2007;67:4981 – 8.

DOI:10.1158/0008-5472.CAN-05-0939

Cancer Research

Decoy Receptor 2 (*DcR2*) Is a p53 Target Gene and Regulates Chemosensitivity

Xiangguo Liu, Ping Yue, Fadlo R. Khuri, et al.

Cancer Res 2005;65:9169-9175. Published online October 17, 2005.

DOI:10.1158/0008-5472.CAN-05-0939

Decoy Receptor 2 (*DcR2*) Is a p53 Target Gene and Regulates Chemosensitivity

Xiangguo Liu, Ping Yue, Fadlo R. Khuri, and Shi-Yong Sun

Department of Hematology and Oncology, Winship Cancer Institute, Emory University School of Medicine, Atlanta, Georgia

Abstract

Decoy receptor 2 (DcR2) is one of the tumor necrosis factor–related apoptosis-inducing ligand (TRAIL) receptors and suppresses TRAIL-induced apoptosis. Its expression, like the other three TRAIL receptors (i.e., DR4, DR5, and DcR1), is regulated by p53. Here, we report that *DcR2* is a p53 target gene and regulates chemosensitivity. In this study, we identified a p53-binding site (p53BS) in the first intron of the *DcR2* gene. This p53BS is almost identical to the ones found in the first introns of other three TRAIL receptor genes. By a chromatin immunoprecipitation assay, we detected that the p53 protein bound to the DcR2 p53BS in intact cells. Subcloning of the DcR2 p53BS into a luciferase reporter vector driven by a SV40 promoter exhibited enhanced luciferase activity when transiently cotransfected with a wild-type (wt) p53 expression vector in p53-null cell lines or stimulated with DNA-damaging agents in cell lines having wt p53. Moreover, when the DcR2 p53BS, together with its own corresponding promoter regions, was subcloned into a basic luciferase vector without a promoter element, its transcriptional activities were strikingly increased by cotransfection of the wt *p53* gene. However, when this p53BS was deleted from the construct, wt p53 failed to transactivate this reporter construct. Collectively, we conclude that p53 directly regulates the *DcR2* gene expression via an intronic p53BS. In addition, overexpression of DcR2 conferred resistance to TRAIL-mediated apoptosis and attenuated cell response to DNA-damaging agents, whereas silencing of DcR2 expression enhanced chemotherapeutic agent–induced apoptosis. These results suggest that DcR2 regulates chemosensitivity. (Cancer Res 2005; 65(20): 9169-75)

Introduction

p53 is the most commonly altered gene in human cancer. Thus, it plays a crucial role in protecting organisms from developing cancer (1). Compared with many normal tissues, aberrant cells with potentially malignant characteristics are highly sensitive to apoptotic signals and survive and further progress to malignancy only when they have acquired lesions, such as loss of p53, that prevent or impede cell death (2). Therefore, it is important to understand how cancer cells become resistant to apoptosis to pursue apoptosis-oriented cancer therapy. In fact, the most common antiapoptotic lesion that is detected in cancers is the inactivation of the p53 tumor suppressor pathway (2). It is well known that activation of p53 (e.g., stress-induced stabilization) leads to either growth arrest or induction of apoptosis (3, 4). The question is how p53 contributes to the activation of cell death and what determines whether induction of p53 will trigger apoptosis.

It is generally accepted that p53 primarily acts as a transcription factor and induces apoptosis by transcriptionally modulating the expression of its proapoptotic target genes, although it also induces apoptosis in a transcription-independent fashion (2–5). It is also clear that most functional genes regulated by p53 contain classic p53-binding sites (p53BSs) in their promoter or intronic regions (6). In the last few decades, multiple proapoptotic genes that serve as p53 target genes have been identified, among which some encode death domain–containing proteins including the death receptors Fas and DR5, whereas others encode mitochondria-related proteins, such as Bax, Noxa, Puma, and p53AIP1, along with others having known or speculated roles in different steps of the apoptotic cascades such as PIGs, caspase-6, Bid, and Apaf-1 (2–7). These genes may contribute to p53-mediated cell death under certain conditions, in certain specific tissues, or in different cell types; however, no single target gene is an absolute mediator for p53-dependent apoptotic cell death (6, 7). In addition, there are increased studies showing that p53 also transactivates some target genes that are antiapoptotic, such as heparin-binding epidermal growth factor (*HB-EGF*) and *DcR1* (8–10). The roles of these antiapoptotic genes in regulating p53-dependent apoptosis are less clear, which make p53-mediated apoptosis even more complex.

The tumor necrosis factor–related apoptosis-inducing ligand (TRAIL; also called APO-2L) is a newly identified member of the tumor necrosis factor family with great therapeutic potential for cancer treatment, because it induces apoptosis in a wide variety of transformed cells but does not seem cytotoxic to normal cells *in vitro* and *in vivo* (11–13). TRAIL induces apoptosis by interacting with two death domain–containing receptors: DR4 (also called TRAIL receptor-1) and DR5 (also called TRAIL receptor 2 and Killer/DR5; refs. 11, 12). In addition, TRAIL can bind to two decoy receptors DcR1 (also called TRAIL-R3) and DcR2 (also called TRAIL-R4). The former does not contain a cytoplasmic death domain, whereas the latter has a truncated death domain. Therefore, both DcR1 and DcR2 can compete with DR4 and DR5 for TRAIL binding and negatively regulate TRAIL-induced apoptosis (11, 12). Interestingly, *DcR1* and *DcR2* as antiapoptotic genes are expressed in many normal tissues, but their expressions are frequently lost in various types of human cancer (11, 12).

It has been documented that all the four TRAIL receptors are regulated by p53 (14). Among them, DR5 is the first to be shown that its transcription is directly transactivated by p53 through an intronic sequence–specific p53BS (15, 16). Very recently, we and others have shown that p53 also directly regulates the expression of both DR4 and DcR1 through the intronic p53BSs that are similar to the one identified in the *DR5* gene (10, 17). However, it is undetermined whether *DcR2* is also a p53 target gene.

Note: F.R. Khuri and S-Y. Sun are Georgia Cancer Coalition Distinguished Cancer Scholars.

Requests for reprints: Shi-Yong Sun, Winship Cancer Institute, Emory University School of Medicine, 1365-C Clifton Road Northeast, C3088, Atlanta, GA 30322. Phone: 404-778-2170; Fax: 404-778-5520; E-mail: shi-yong_sun@emoryhealthcare.org.

doi:10.1158/0008-5472.CAN-05-0939

DOI:10.1158/0008-5472.CAN-05-0939

It is known that the genes encoding DR4, DR5, DcR1, and DcR2 are highly homologous and map together to a tight cluster on human chromosome 8p21-22, suggesting that they arose from a common ancestral gene (6, 14). Because DR5, DR4, and DcR1 are directly regulated by p53 through similar p53BSs existing in their corresponding intronic region, we speculated that DcR2 might also be regulated by p53 through a similar intronic p53BS. In this study, we compared the sequences of first introns of these four genes and identified a similar p53BS in the first intron of the *DcR2* gene. Moreover, we have proven that it is a functional p53BS that mediates p53-dependent regulation of DcR2. In addition, we studied its roles in regulating TRAIL- and DNA-damaging agent–induced apoptosis.

Materials and Methods

Reagents. RPMI 1640 with glutamine and fetal bovine serum were obtained from Sigma Chemicals (St. Louis, MO). All restriction enzymes and T4 DNA ligase were purchased from New England Biolabs (Beverly, MA). PCR reagents were purchased from Invitrogen (Carlsbad, CA) or Eppendorf (Westbury, NY). iScript cDNA Synthesis Kit was purchased from Bio-Rad Laboratories (Hercules, CA). Etoposide (VP-16), doxorubicin, and other chemical reagents were purchased from Sigma Chemicals. Human recombinant TRAIL was purchased from PeproTech, Inc. (Rocky Hill, NJ).

Cell lines and cell culture. The human tumor cell lines H1299 (p53 null), H358 (p53 null), H460 (wild-type p53, wt p53), and MCF-7 (wt p53) were purchased from the American Type Culture Collection (Manassas, VA). HCT116 (wt p53) and HCT116 $p53^{-/-}$ cell lines were kindly provided by Dr. B. Vogelstein (Johns Hopkins University Medical Institutions, Baltimore, MD). These cell lines were grown in monolayer culture in RPMI 1640 with glutamine or McCoy's 5A medium (HCT116) supplemented with 5% fetal bovine serum at 37°C in a humidified atmosphere consisting of 5% CO_2 and 95% air.

Western blot analysis. Preparation of whole cell protein lysates and the procedures for the Western blotting were described previously (18). Whole cell protein lysates (50 μg) were electrophoresed through 10% or 12% denaturing polyacrylamide slab gels and transferred to a PROTRAN pure nitrocellulose transfer membrane (Schleicher & Schuell BioScience, Inc., Keene, NH) by electroblotting. The blots were probed or reprobed with the antibodies and then antibody binding was detected using the SuperSignal West Pico Chemiluminescent Substrate (Pierce Biotechnology, Inc., Rockford, IL) according to the manufacturer's protocol. Mouse monoclonal anti-p53 (Ab-6) antibody and rabbit polyclonal anti-DcR2 antibody were purchased from EMD Bioscience, Inc. (La Jolla, CA) and Imgenex (San Diego, CA), respectively. Anti-V5 antibody was purchased from Invitrogen. Rabbit polyclonal anti-human glyceraldehyde-3-phosphate dehydrogenase antibody was purchased from Trevigen (Gaithersburg, MD).

Adenoviral infection. H1299 or H358 cells were infected with the adenovirus carrying wt p53 (Ad5-CMV-hp53) or empty vector (Ad-CMV) as described previously (17). Ad5-CMV-hp53 and Ad-CMV were purchased from Qbiogene, Inc. (Carlsbad, CA).

Chromatin immunoprecipitation assay. Chromatin immunoprecipitation assay was conducted using the chromatin immunoprecipitation assay kit purchased from Upstate Biotechnology (Lake Placid, NY) following the manufacturer's instruction and was described previously (17). The following specific primers for DcR1 and DcR2 were used to amplify p53BS from genomic DNA immunoprecipitated with specific p53 antibody in the chromatin immunoprecipitation assay: DcR1 sense, 5′-CTCGAGAAGTTCGTCGTCGTCATCGT-3′; DcR1 antisense, 5′-GAGCTCACCCAGTTCTTCCCCTGACT-3′; DcR2 sense, 5′-CTCGAGTTCTGCTGCCGGTGAGTCT-3′; and DcR2 antisense, 5′-GAGCTCCCACTCTTCCCCTGACTC-3′.

Construction of reporter plasmids. The 196- and 170-bp DNA fragments containing intronic p53BSs of DcR1 and DcR2, respectively, were amplified from H1299 genomic DNA with PCR amplification using the primers described in the above chromatin immunoprecipitation assay. These fragments were then subcloned into pGL3-Promoter luciferase vector (pGL3-P-luc; Promega, Madison WI), which contains an SV40 promoter upstream of the luciferase gene, through *Xho*I and *Sac*I sites. The corresponding constructs were named pP-DcR1/p53BS-Luc and pP-DcR2/p53BS-Luc, respectively. In addition, a 1,443-bp DNA fragment spanning the DcR2 promoter, first exon, and partial p53BS-containing intron region and a 1,389-bp fragment spanning only the DcR2 promoter, first exon, and partial intron region without p53BS were amplified by PCR with the following primers: DcR2-BS-*Kpn*I sense, 5′-GGTACCCCTGCCATTGACCTTACTGCTT-3′, DcR2-BS(+)-*Bgl*II antisense, 5′-AGATCTCACCCCACTCTTCCCCTGACTCC-3′; and DcR2-BS(−)-*Bgl*II antisense, 5′-AGATCTGGCCGCAGGCGACCCGGGCCAAG-3′. These fragments were then cloned into a pGL3-basic vector, which has no promoter (Promega), using *Kpn*I and *Bgl*II restriction sites. These constructs were named pB-DcR2/p53BS(+)-luc and pB-DcR2/p53BS(−)-luc, respectively.

Construction of lentiviral expression vectors, virus preparation, and cell infection. DcR2 cDNA was amplified by standard reverse transcription-PCR (RT-PCR) from RNA extracted from normal human bronchial epithelia cells using the primers: sense, 5′-GACTAGTATGGGACTTTGGGGACAAAGCGTC-3′ and antisense, 5′-CGGGCCCTCTAGACTCGAGCCCTTCAGGCAGGACGTAGCAGAGCCTG-3′. The DcR2 cDNA was then cloned into a pT-easy vector (Promega) following the manufacturer's protocol as pT-easy-DcR2. Both pLenti-DcR1 (a lentiviral vector harboring DcR1, which was constructed using the pLenti6/V5 Directional TOPO Cloning kit purchased from Invitrogen) and pT-easy-DcR2 were cut with *Spe*I and *Apa*I. The released fragment containing DcR2 cDNA was then cloned into the digested pLenti6/V5 vector and the resultant construct was named pLenti-DcR2. In this study, we used pLenti-Lac Z as a vector control, which was included in the pLenti6/V5 Directional TOPO Cloning kit.

Lentiviruses were produced using ViraPower Lentiviral Expression System (Invitrogen) according to the manufacturer's directions. The supernatants containing lentiviral particles were filtered with MILLEX-HV Syringe Driven Filter Unit (Millipore, Billerica, MA) and followed by a concentration using Amicon Ultra Centrifugal Filter Devices (Millipore). The viral titers were determined following manufacturer's manual. For infection, the viruses were added to the cells at the multiplicity of infection of 10 with 10 μg/mL polybrene. For transient expression, cells were infected and then selected in the presence of 50 μg/mL blasticidin, 24 hours after infection. After 8 days, the cells were subjected to the given experiments.

Transient transfection and reporter activity assay. The information about the plasmids used in this study, including a p53-luc reporter plasmid, a pCH110 plasmid encoding β-galactosidase, pCMV-p53, and pCMV-p53mt135 expression vectors, the purification and transfection of these plasmids, and luciferase activity assay, were described in detail previously (17).

Detection of DcR2 mRNA expression. DcR2 mRNA was detected using RT-PCR described as follows. Total cellular RNA was isolated from cells using TRIzol reagent (Invitrogen) as instructed by the manufacturer. cDNA was synthesized using iScript cDNA Synthesis Kit (Bio-Rad Laboratories) following the manufacturer's instructions. cDNA was then amplified by PCR using the following primers: DcR2 sense, 5′-CCTGTACCACGACCAGAGACAC-3′; DcR2 antisense, 5′-GAACTCGTGAAGGACATGAACG-3′; β-actin sense, 5′-GAAACTACCTTCAACTCCATC-3′; and β-actin antisense, 5′-CTAGAAGCATTTGCGGTGGACGATGGAGGGGCC-5′. The 25-μL amplification mixture contained 1 μL of cDNA, 0.5 μL of deoxynucleotide triphosphate (25 mmol/L each), 1 μL each of the sense and antisense primers (20 μmol/L each), 5 μL of TaqMaster PCR enhancer, 1 μL of Taq DNA polymerase (5 units/μL; Eppendorf), 2.5 μL 10× reaction buffer, and sterile H_2O. PCR was done for 26 cycles. After an initial step at 95°C for 3 minutes, each cycle consisted of 45 seconds of denaturation at 94°C, 45 seconds of annealing at 58°C, and 1 minute of extension at 72°C. This was followed by an additional extension step at 72°C for 7 minutes. The housekeeping gene *β-actin* was also amplified as an internal reference. PCR products were resolved by electrophoresis on a 1.5% agarose gel, stained, and directly visualized under UV illumination.

Silencing of DcR2 expression using small interfering RNA. Stealth DcR2 small interfering RNA (siRNA) that targets sequence of 5′-CCAAGATCCTTAAGTTCGTCGTCTT-3′ and Stealth control siRNA that targets

DOI:10.1158/0008-5472.CAN-05-0939

sequence of 5′-CCTACCAGGGAATTTAAGAGTGTAT-3′ were synthesized by Invitrogen. The transfection of siRNA was conducted in a 24-well plate using LipofectAMINE 2000 (Invitrogen) following the manufacturer's instructions. We transfected the same cells twice with the same siRNA with a 48-hour interval in between the two transfections as described previously (19). Twenty-four hours after the second transfection, cells were replated in fresh medium and treated on the second day with chemotherapeutic agents as indicated. The gene-silencing effect was evaluated by RT-PCR and apoptosis was measured by a Cell Death Detection ELISA^{Plus} kit as described below.

Cell survival assay. Cells were seeded in 96-well cell culture plates and treated on the second day with the indicated agents. At the end of treatment, cell number was estimated by the sulforhodamine B assay as previously described (20).

Detection of apoptosis. Apoptosis was evaluated either by Annexin V staining using Annexin V-PE apoptosis detection kit purchased from BD Bioscience (San Jose, CA), or by a Cell Death Detection ELISA^{Plus} kit purchased from Roche Molecular Biochemicals (Indianapolis, IN), following the manufacturer's instructions.

Statistical analysis. Cell survival and apoptosis (i.e., DNA fragmentation) between two groups were analyzed with two-sided unpaired Student's *t* tests by use of Graphpad InStat 3 software (GraphPad Software, Inc., San Diego, CA). In all analyses, results were considered to be statistically significant at $P < 0.05$.

Results

Overexpression of p53 increases DcR2 expression in p53-null cancer cells. Up-regulation of DcR2 expression by 53 has been shown previously by Meng et al. (21). In this study, we also examined the effect of p53 overexpression via adenoviral infection on the expression of DcR2 in p53-null lung cancer cell lines. As shown in Fig. 1*A*, Ad-p53 infection resulted in increased expression of DcR2 in both H358 and H1299 cell lines evaluated by Western blot analysis. Thus, this result confirms the previous finding that *DcR2* is indeed a p53-regulated gene (21).

Sequence-based identification of a putative p53BS in the first intron of the *DcR2* gene. By comparing the first intron sequences of the four TRAIL receptor genes, we identified a similar p53BS (DcR2-p53BS) in the first intron of the *DcR2* gene. This p53BS is almost identical to the ones reported within the first introns of *DR4, DR5*, and *DcR1* genes (refs. 10, 16, 17; Fig. 1*B*). DcR2-p53BS shares 85% homology with the p53 consensus DNA-binding sequence (22). Among the p53BSs of the four TRAIL receptors, their sequences are at least 80% identical (Fig. 1*B*). Moreover, DcR2-p53BS and other receptor p53BSs are close to the boundary of first exon/intron and are only 107 to 109 bp away from the boundary (Fig. 1*B*), indicating that they are very close to their promoter regulatory regions. Considering the identical locations and similar sequences between DcR2-p53Bs and other receptor p53BSs, we speculate that the DcR2-p53BS is very likely to be functional and to mediate transcriptional regulation of the *DcR2* gene expression by p53.

Detection of DcR2-p53BS bound to p53 in intact cells using a chromatin immunoprecipitation assay. To determine whether p53 actually binds to DcR2-p53BS in cells on p53 activation, we did the chromatin immunoprecipitation assay to detect formation of DcR2-p53BS-binding complex with p53 in both H358 and H1299 p53-null cell lines infected with Ad-CMV-hp53. As a control, we also

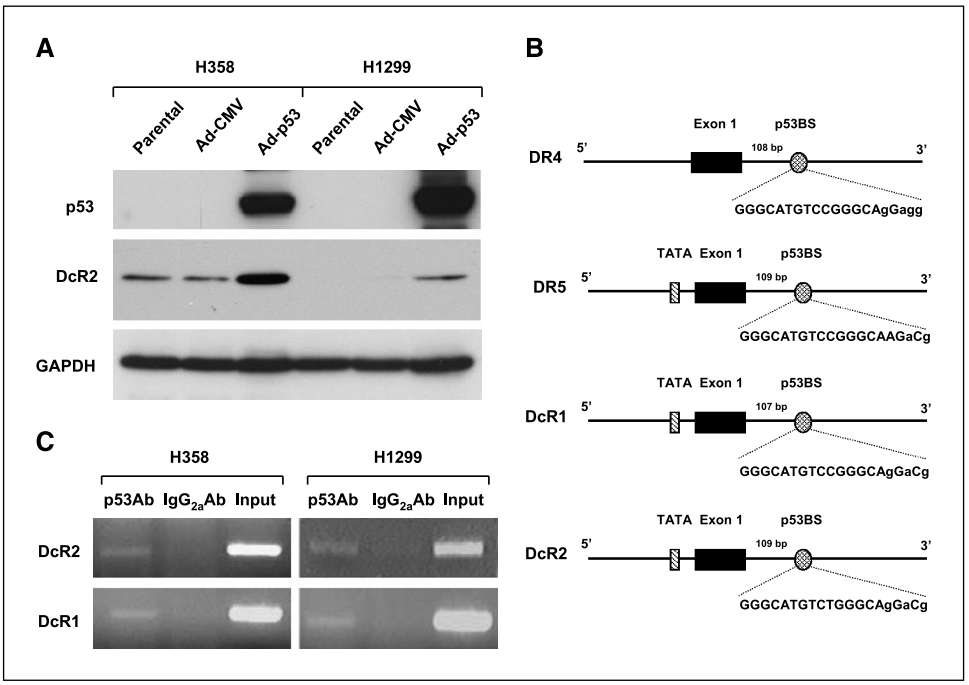

Figure 1. Up-regulation of DcR2 expression by p53 overexpression in p53-null cancer cells (*A*), identification of the putative DcR2-p5BS (*B*), and detection of DcR2-p53BS bound to p53 in intact cells upon p53 activation (*C*). *A,* H1299 or H358 cells were infected on the second day after seeding with adenovirus carrying an empty vector (Ad-CMV) or wt *p53* gene (Ad-p53). After 24 hours, cells were harvested for preparation of whole cell protein lysates. Western blot analysis was done to detect the expression of p53, DcR2, and glyceraldehyde-3-phosphate dehydrogenase (*GAPDH*) using antibodies against them. *B,* DcR2-p53BS is 85% identical to the classic p53BS that is defined as two copies of the 10-bp motif 5′-PuPuPuC(A/T)(T/A)GPyPyPy-3′ separated by 0 to 13 bp (22), where Pu represents purine and Py represents pyrimidine. In addition, DcR2-p53BS shares ≥90% sequence homology with the other three TRAIL receptors. *C,* H358 and H1299 p53-null cell lines were infected with Ad5-CMV-hp53 for 24 hours and subjected to chromatin immunoprecipitation assay as described in Materials and Methods. DcR1-p53BS here was detected as a known sequence bound to p53 when p53 is activated. The amplified DNA fragments for DcR1 and DcR2 by PCR were 196 and 170 bp, respectively. p53Ab, p53 antibody; IgG_{2a}Ab, isotype antibody.

DOI:10.1158/0008-5472.CAN-05-0939

detected DcR1-p53BS bound to p53. As shown in Fig. 1*C*, we detected DNA fragments containing DcR2-p53BS and DcR1-p53BS, respectively, from genomic DNA precipitated with p53-specific antibody but not from that pulled down with a control IgG2a isotype antibody in either cell line. This result clearly indicates that p53 protein binds to DcR2-p53BS as it does to DcR1-p53BS in intact cells upon p53 activation, indicating that DcR2-p53BS is a functional response element.

Reporter construct carrying DcR2-p53BS exhibits increased transcriptional activity in response to p53 overexpression or treatment with DNA-damaging agents. To examine whether DcR2-p53BS is functional in mediating p53-dependent up-regulation of the *DcR2* gene, we amplified ~170- and 196-bp intronic fragments carrying DcR2-p53BS and DcR1-p53BS, respectively, and cloned each of fragment into a pGL3-promoter luciferase vector upstream of minimal SV40 promoter (Fig. 2*A*). In this study, we used DcR1-p53BS, which is more related to DcR2 and known to be functional p53BS (10), as a positive control for comparison. When the individual reporter construct was transiently cotransfected with empty pCMV, pCMV-p53, or pCMV-p53mt135 vector into H1299 p53-null cells, we found that transfection of pCMV-p53 but not pCMV or pCMV-p53mt135 increased the luciferase activity of the reporter plasmid carrying either DcR2-p53B or DcR1-p53BS (Fig. 2*B*). The expression of p53 and p53mt135 after transient transfection in H1299 cells has been shown in our previous study (17). Therefore, our data indicate that overexpression of p53 enhances transcriptional activity of the reporter plasmid carrying either DcR2-p53BS or DcR1-p53BS. Similar results were also observed when we cotransfected these plasmids into H358 p53-null cells (data not shown). Moreover, we examined the effects of activation of endogenous p53 on transactivation of these reporter vectors by treating wt p53–containing cancer cells with DNA-damaging agents. In MCF-7 cells, both VP-16 and doxorubicin that are known to increase p53 levels (17) failed to increase luciferase activity of empty pGL3-P-luc lacking any p53BS. However, they increased transcriptional activities by >2-fold (VP-16) or 3-fold (doxorubicin) of the pGL3-P-luc reporter vector carrying DcR1-p53BS or DcR2-p53BS (Fig. 2*C*). We noted that the reporter vector carrying DcR2-p53BS exhibited a greater increase of luciferase activity than the reporter plasmid carrying DcR1-p53BS in response to activation of endogenous p53 induced by either VP-16 or doxorubicin, although the increase of luciferase activity was much greater in the reporter vector carrying DcR1-p53BS than in the reporter plasmid harboring DcR2-p53BS when stimulated with overexpression of an exogenous p53 (Fig. 2*B* and *C*). Collectively, these results suggest that DcR2-p53BS, like DcR1-p53BS, is functional to mediate p53-induced gene transactivation.

The intronic DcR2-p53BS is required for driving p53-mediated transactivation of DcR2 promoter. The aforementioned results clearly indicate that p53 protein binds to the intronic DcR2-p53BS in cells and confers p53 responsiveness when located upstream of a promoter (i.e., SV40) in a promoter-containing reporter vector (i.e., pGL3-P-luc). We next wanted to know whether DcR2-p53BS could also mediate p53-dependent transcriptional

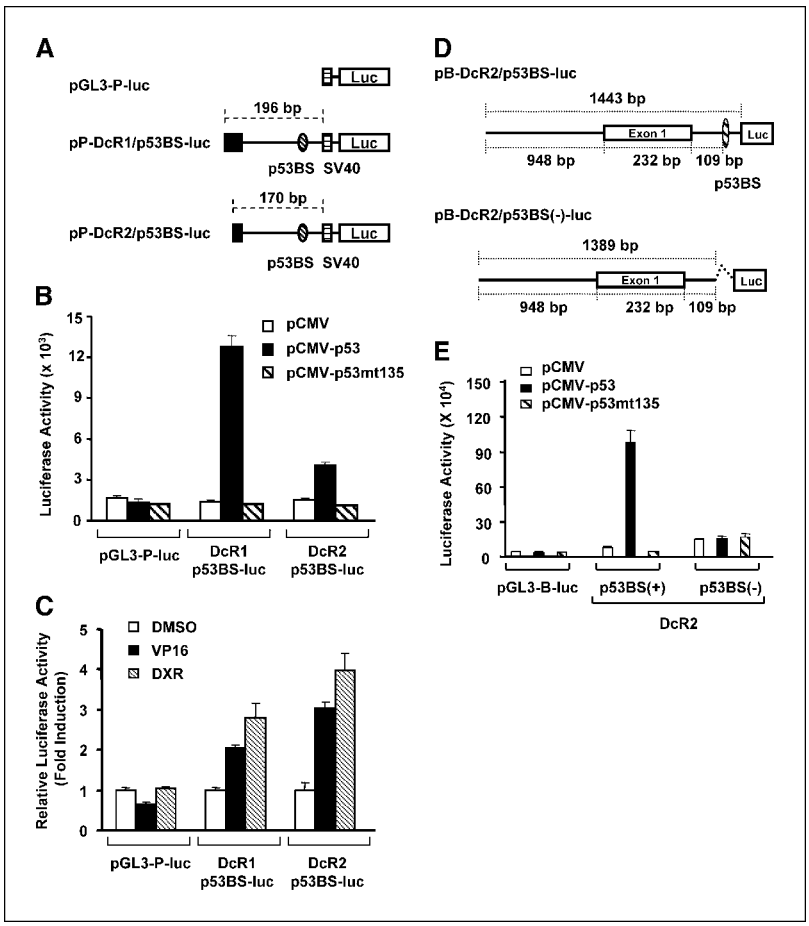

Figure 2. DcR2-p53BS is required for p53-dependent transactivation of DcR2 promoter. *A,* diagram illustrating cloning of DNA fragments containing DcR1-p53BS and DcR2-p53BS, respectively, into the pGL3-P-luc reporter vector. The DNA fragments containing DcR1-p53BS and DcR2-p53BS, respectively, were PCR amplified and cloned into pGL3-P-luc reported vector upstream of the SV40 promoter. *Black boxes,* partial exon 1 sequences. *B,* comparison of the activities of the reporter constructs (*A*) in response to p53 overexpression. The indicated reporter vector together with pCMV, pCMV-p53, or pCMV-p53mt135 and pCH110 β-galactosidase expression plasmids was cotransfected into H1299 cells using the FuGene 6 transfection reagent. After 24 hours, cells were harvested and subjected to a luciferase activity assay. *C,* comparison of the activities of the reporter constructs (*A*) in response to treatment with DNA-damaging agents. MCF-7 cells transfected with the indicated reporter vector and β-galactosidase expression plasmid using the FuGene 6 transfection reagent for 16 hours were treated with 10 μmol/L VP-16 or 1 μmol/L doxorubicin (*DXR*). After 8 hours, the cells were harvested and subjected to the luciferase activity assay. *Column,* means of triplicate treatments; *bars,* ±SD. *D,* diagram illustrating generation of a reporter vector that harbors a piece of natural DcR2 genomic sequence with DcR2 promoter region, exon 1, and partial intron 1 containing the DcR2-p53BS (pB-DcR2/p53BS-luc) and a corresponding construct lacking DcR2-p53BS [pB-DcR2/p53BS(−)-luc]. These DcR2 genomic fragments were PCR amplified and cloned into a pGL-3 basic luciferase vector as described in Materials and Methods. *E,* comparison of the activities of the reporter constructs (*D*) in response to p53 overexpression. The indicated reporter vector together with pCMV, pCMV-p53, or pCMV-p53mt135 and pCH110 β-galactosidase expression plasmids were cotransfected into H1299 cells using the FuGene 6 transfection reagent. After 24 hours, cells were harvested and subjected to luciferase activity assay. *Columns,* means of triplicate treatments; *bars,* ±SD.

DOI:10.1158/0008-5472.CAN-05-0939

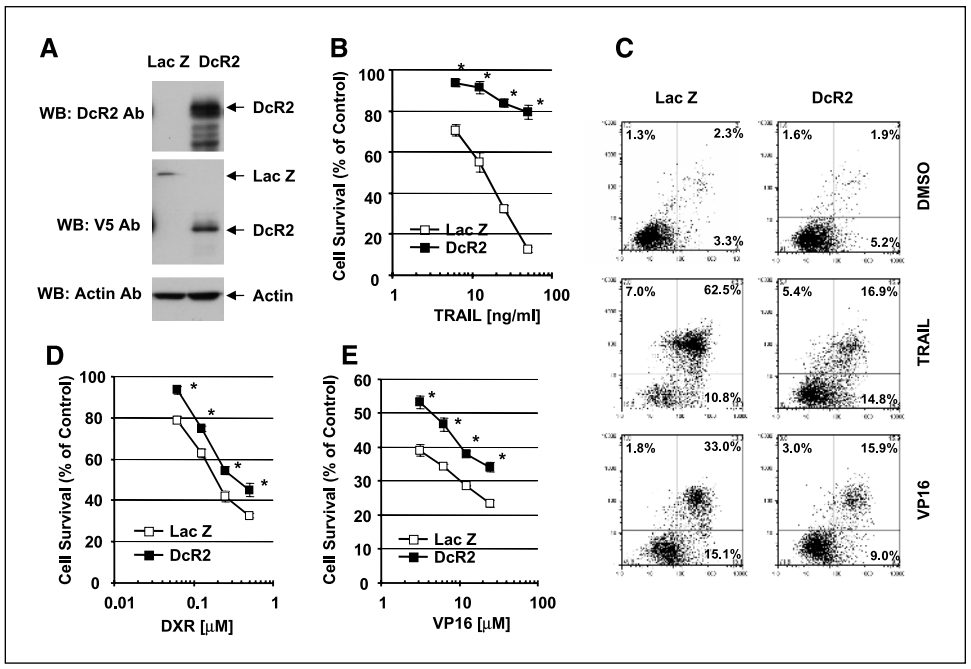

Figure 3. Lentivirus-mediated expression of exogenous DcR2 (*A*) and its effects on decrease of cell survival induced by TRAIL (*B*), doxorubicin (*DXR, D*), and VP-16 (*E*), respectively, and on induction of apoptosis by TRAIL and VP-16, respectively (*C*). H460 cells were infected with 10 multiplicity of infection of lentiviruses harboring Lac Z and DcR2, respectively. Twenty-four hours later, the cells were subjected to blasticidin selection (50 μg/mL). After 8 days, the cells were then subjected to the given experiments. The expression of DcR2 was detected by Western blot analysis using DcR2 and V5 antibody, respectively (*A*). Cell survival was estimated using the sulforhodamine B assay after the cells were exposed to the indicated concentrations of TRAIL (*B*), doxorubicin (*D*), and VP-16 (*E*), respectively, for 24 hours. Apoptosis was measured using Annexin V staining after the cells were treated with 20 ng/mL TRAIL or 25 μmol/L VP-16 for 24 hours (*C*). *Points,* means of four replicates; *bars,* ±SD. *, $P < 0.001$, compared with each corresponding control treatment with two-sided unpaired Student's *t* tests.

activity of its own gene promoter when located at a natural position relative to the promoter in its genomic locus. To do this, we amplified a 1,443-bp DcR2 genomic DNA fragment consisting of the 948-bp promoter region, a 232-bp exon 1, and a 263-bp fragment of the first intron harboring the DcR2-p53BS and an identical 1,389-bp DcR2 genomic DNA fragment lacking only 54 bp with the DcR2-p53BS, respectively. By cloning these fragments into the pGL3-B-luc vector, we generated luciferase reporter constructs with and without DcR2-p53BS. These constructs were named pB-DcR2/p53BS(+)-luc and pB-DR4/p53BS(−)-luc, respectively (Fig. 2*D*). When each of the aforementioned reporter plasmids together with the expression vector carrying no p53, a wt p53, or a mutant *p53* gene were cotransfected into H1299 cells, we found that the wt p53 but not mutant p53 increased transcriptional activity of pB-DcR2/p53BS(+) by >13-fold. In contrast, p53 completely lost its ability to increase transcriptional activity of the reporter vector with deleted DcR2-p53BS (pB-DcR2/p53BS(−)-luc; Fig. 2*E*). This result clearly indicates that the intronic DcR2-p53BS is essential for p53-mediated transactivation of the *DcR2* gene.

Overexpression of DcR2 confers resistance to chemotherapeutic agents. Other than its inhibitory function in negatively regulating TRAIL-induced apoptosis, the role of DcR2 in drug-induced apoptosis is largely unknown. Therefore, we examined the effect of DcR2 overexpression on apoptosis induction by chemotherapeutic agents in human cancer cells. Infection of H460 lung cancer cells with lentiviruses carrying the *DcR2* gene resulted in successful DcR2 expression evaluated by Western blot analysis using both V5 and DcR2 antibodies (Fig. 3*A*). Overexpression of DcR2 has been shown to inhibit TRAIL-induced apoptosis (21, 23–25). To assure the normal function of DcR2 expression in our cell system, we first determined whether cells infected with DcR2 lentiviruses were resistant to TRAIL treatment. Indeed, TRAIL effectively decreased the survival of cells infected with control lentiviruses carrying the *Lac Z* gene in a dose-dependent manner. In contrast, cells infected with lentiviruses harboring DcR2 were insensitive to TRAIL treatment. For example, TRAIL, at 50 ng/mL, rapidly decreased cell survival by >85% in cells infected with Lac Z lentiviruses, but only by 20% in cells infected with DcR2 lentiviruses (Fig. 3*B*). Moreover, TRAIL treatment induced 73% cells infected with Lac Z lentiviruses undergoing apoptosis, whereas it caused only 32% cells infected with DcR2 lentiviruses to die of apoptosis when evaluated using Annexin V staining (Fig. 3*C*). These results indicate that DcR2 expression in our system indeed confers cell resistance to TRAIL-induced apoptosis and thereby is functionally active.

Following these experiments, we examined the effects of DcR2 overexpression on cell responses to the chemotherapeutic agents doxorubicin and VP-16. Compared with control Lac Z lentivirus-infected cells, cells expressing DcR2 were significantly less sensitive to either doxorubicin (Fig. 3*D*; $P < 0.001$) or VP-16 (Fig. 3*E*; $P < 0.001$) by measuring overall cell survival. Moreover, following VP-16 treatment, we detected about 48% apoptotic cells from cells infected with control Lac Z lentiviruses, but only about 25% apoptotic cells from cells infected with DcR2 lentiviruses (Fig. 3*C*). Collectively, these results indicate that the enforced DcR2 expression reduces cell sensitivity to chemotherapeutic agents and thus affects chemosensitivity.

Silencing of DcR2 expression enhances chemotherapeutic agent–induced apoptosis. To further show the relationship between DcR2 expression and chemosensitivity, we determined whether manipulation of endogenous levels of DcR2-affected cell responses to chemotherapeutic agents. Meng et al. (21) reported that the chemotherapeutic agent doxorubicin induced p53-dependent expression of DcR2 in human cancer cells. We found that both doxorubicin and VP-16 increased DcR2 expression in HCT116 ($p53^{+/+}$) cells but not in p53 knockout HCT116 ($p53^{-/-}$) cells, although they had higher basal levels of DcR2 than did HCT116 ($p53^{+/+}$; Fig. 4*A*). Thus, our results confirmed p53-dependent up-regulation of endogenous DcR2 expression by chemotherapeutic agents. Transfection of the DcR2 siRNA but not the control siRNA into HCT116 cells substantially decreased basal levels of DcR2 expression and prevented DcR2 up-regulation

DOI:10.1158/0008-5472.CAN-05-0939

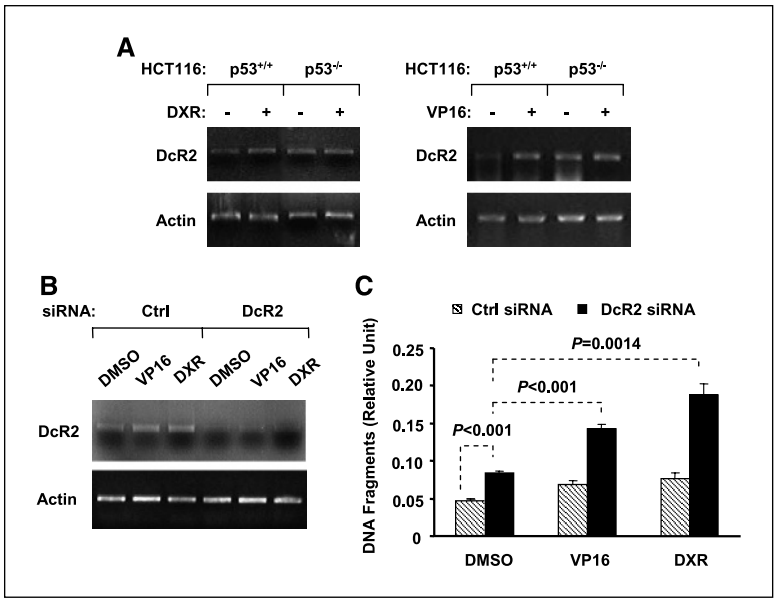

Figure 4. p53-dependent modulation of endogenous DcR2 expression by chemotherapeutic agents (*A*) and the effects of silencing DcR2 expression on chemotherapeutic agent–induced apoptosis (*B* and *C*). *A,* the indicated cell lines were treated with 50 μmol/L VP-16 or 0.5 μmol/L doxorubicin (*DXR*) for 24 hours and subjected to RNA extraction. DcR2 mRNA levels were detected using RT-PCR as described in Materials and Methods. *B* and *C,* HCT116 cells were transfected twice with control (*Ctrl*) or DcR2 siRNA in a 48-hour interval as described in Materials and Methods. Forty hours later after the second transfection, cells were treated with 50 μmol/L VP-16 or 1 μmol/L doxorubicin (*DXR*). After 24 hours, the cells were subjected to RNA extraction and subsequent detection of DcR2 expression by RT-PCR (*B*). In addition, the cells were subjected to estimation of DNA fragmentation using the Cell Death Detection ELISA kit (*C*). *Columns,* mean of triplicate treatments; *bars,* ±SD. The statistical differences between the two treatments were analyzed by two-sided unpaired Student's *t* tests.

by chemotherapeutic agents (Fig. 4*B*). In the control siRNA-transfected HCT116 cells, the amounts of DNA fragments were only slightly increased upon treatment with VP-16 or doxorubicin. In contrast, in the DcR2 siRNA-transfected HCT116 cells, the basal levels of DNA fragmentation were significantly increased ($P < 0.001$). When treated with VP-16 or doxorubicin, the amounts of DNA fragments were further significantly increased ($P < 0.001$; Fig. 4*C*). Thus, these results indicate that prevention or blockage of endogenous DcR2 up-regulation sensitizes cells to chemotherapeutic agent–induced apoptosis, furthering the notion that DcR2 regulates chemosensitivity.

Discussion

p53-dependent up-regulation of DcR2 expression has been shown previously (21). However, the mechanism underlying p53-dependent regulation of DcR2 is unknown. In the present study, we identified a putative p53BS in the first intron of the *DcR2* gene. This p53BS is almost identical to those found in the first introns of DR5, DR4, and DcR1 in terms of their sequences and locations. p53 overexpression or treatment with DNA-damaging agents enhanced transcriptional activity of the luciferase reporter construct carrying the DcR2-p53BS upstream of the SV40 promoter, indicating that this intronic p53BS is active for p53-dependent transactivation of the *DcR2* gene. Furthermore, the reporter construct carrying the fragment consisting of the endogenous promoter region, exon 1, and partial first intron region with DcR2-p53BS exhibited increased transcriptional activity upon p53 activation. However, its corresponding construct lacking DcR2-p53BS did not show any response to the same stimulus. This result further indicates that the DcR2-p53BS is essential for p53-mediated transactivation of the *DcR2* gene. Using a chromatin immunoprecipitation assay, we were able to detect the DNA fragment containing DcR2-p53BS from DNA/protein complex precipitated only with p53-specific antibody in Ad-p53-infected p53-null cell lines, indicating that the DcR2-p53BS binds to p53 in intact cells upon p53 activation. Taken together, we conclude that p53 directly regulates transcription of the *DcR2* gene via an intronic p53BS.

It has been noted that the genes encoding DR4, DR5, DcR1, and DcR2 are highly homologous and map together to a tight cluster on human chromosome 8p21-22, suggesting that they arose from a common ancestral gene (6, 14). The current study together with others (10, 16, 17) have shown that the four TRAIL receptors are all p53 target genes and their expression is regulated by p53 through similar intronic p53BSs. By comparing the sequences and locations of these p53BSs, we found that they share high homology (≥90%) and locate at almost the same positions that are only 107 bp (DcR1), 108 bp (DR4), or 109 bp (DR5 and DcR2) away from the exon 1 and intron 1 boundaries (Fig. 1). Thus, it seems that these p53BSs are well conserved during evolution.

It is clear that the four TRAIL receptors are critical for regulating TRAIL-induced apoptosis (11–13). Indeed, overexpression of DcR2 in our cell system protected cells from TRAIL-induced apoptosis as shown previously (21, 23–25). However, the biological significance of DcR2 as well as other TRAIL receptors as p53 target genes in regulation of p53-dependent apoptosis remains unclear. The only study dealing with this issue by Meng et al. (21) showed that overexpression of DcR2 delays p53-induced apoptosis in human colon cancer cells. In our current study, we found that overexpression of DcR2 in a human lung cancer cell line with wt p53 partially protected cells from induction of apoptosis by some chemotherapeutic agents. Although we used lentivirus to deliver DcR2 expression in our cell system, the infection or expression efficiency in this particular cell line was still <50%. The brief selection using blasticidin (8 days) after infection theoretically eliminates most cells that do not express DcR2, but there might be still significant portions of surviving cells that did not express DcR2 well. Therefore, the protection of DcR2 on chemotherapeutic agent–induced apoptosis may be underestimated. Nevertheless, our current results suggest that DcR2 expression levels may affect chemosensitivity. If high levels of DcR2 expression confer cell resistance to chemotherapeutic agents, down-regulation of DcR2 expression, or prevention of DcR2 up-regulation during chemotherapy should sensitize cells to chemotherapy. In this study, we found that prevention of DcR2 up-regulation using

DOI:10.1158/0008-5472.CAN-05-0939

siRNA-mediated gene silencing indeed enhanced chemotherapeutic agent–induced apoptosis. Thus, this result further supports the notion that DcR2 regulates chemosensitivity.

In contrast to DR4 and DR5 that are expressed widely in both normal and malignant cells, DcR2 as well as DcR1 are expressed preferentially in many normal tissues (11), and their expression is often silenced or down-regulated due to promoter hypermethylation in multiple cancer types, including neuroblastoma, malignant mesothelioma, breast cancers, and lung cancers (26, 27), although they are generally considered as antiapoptotic genes (11–13). Currently, it is unknown why DcR1 and DcR2 but not DR4 and DR5 are frequently down-regulated in cancer cells. This raises a relevant question as to the normal function and importance of DcR2 as well as DcR1 in homeostasis and carcinogenesis. It seems that this needs to be further investigated in the future. Nevertheless, the down-regulation of DcR1 and DcR2 expression in cancer cells may present an opportunity for TRAIL-based cancer therapy.

In summary, this report provides compelling evidence showing that *DcR2* is a p53 target gene, which is regulated by p53 through an intronic p53BS. In addition, we also suggest that DcR2 regulates chemosensitivity. Currently, the biological significance of DcR2 in p53-regulated apoptosis and carcinogenesis has not been elucidated.

Acknowledgments

Received 3/21/2005; revised 7/14/2005; accepted 8/16/2005.

Grant support: Winship Cancer Institute faculty start-up research fund (S-Y. Sun), Georgia Cancer Coalition Distinguished Cancer Scholar award (S-Y. Sun), and Department of Defense VITAL grant W81XWH-04-1-0142 (S-Y. Sun for Project 4).

The costs of publication of this article were defrayed in part by the payment of page charges. This article must therefore be hereby marked *advertisement* in accordance with 18 U.S.C. Section 1734 solely to indicate this fact.

We thank Dr. B. Vogelstein for providing us with HCT116 and HCT115 p53-null cell lines.

References

1. Levine AJ. p53, the cellular gatekeeper for growth and division. Cell 1997;88:323–31.
2. Vousden KH, Lu X. Live or let die: the cell's response to p53. Nat Rev Cancer 2002;2:594–604.
3. Oren M. Decision making by p53: life, death and cancer. Cell Death Differ 2003;10:431–42.
4. Vogelstein B, Lane D, Levine AJ. Surfing the p53 network. Nature 2000;408:307–10.
5. Manfredi JJ. p53 and apoptosis: it's not just in the nucleus anymore. Mol Cell 2003;11:552–4.
6. El-Deiry WS. Insights into cancer therapeutic design based on p53 and TRAIL receptor signaling. Cell Death Differ 2001;8:1066–75.
7. Benchimol S. p53-dependent pathways of apoptosis. Cell Death Differ 2001;8:1049–51.
8. Fang L, Li G, Liu G, Lee SW, Aaronson SA. p53 induction of heparin-binding EGF-like growth factor counteracts p53 growth suppression through activation of MAPK and PI3K/Akt signaling cascades. EMBO J 2001;20:1931–9.
9. Sheikh MS, Huang Y, Fernandez-Salas EA, et al. The antiapoptotic decoy receptor TRID/TRAIL-R3 is a p53-regulated DNA damage-inducible gene that is overexpressed in primary tumors of the gastrointestinal tract. Oncogene 1999;18:4153–9.
10. Ruiz De Almodovar C, Ruiz-Ruiz C, Rodriguez A, Ortiz-Ferron G, Redondo JM, Lopez-Rivas A. TRAIL decoy receptor TRAIL-R3 is upregulated by p53 in breast tumor cells through a mechanism involving an intronic p53 binding site. J Biol Chem 2004;279:4093–101.
11. Ashkenazi A, Dixit VM. Death receptors: signaling and modulation. Science 1998;281:1305–8.
12. Kelley SK, Ashkenazi A. Targeting death receptors in cancer with Apo2L/TRAIL. Curr Opin Pharmacol 2004;4:333–9.
13. Bouralexis S, Findlay DM, Evdokiou A. Death to the bad guys: targeting cancer via Apo2L/TRAIL. Apoptosis 2005;10:35–51.
14. Sheikh MS, Fornace AJ, Jr. Death and decoy receptors and p53-mediated apoptosis. Leukemia 2000;14:1509–13.
15. Wu GS, Burns TF, McDonald ER III, et al. KILLER/DR5 is a DNA damage-inducible p53-regulated death receptor gene. Nat Genet 1997;17:141–3.
16. Takimoto R, El-Deiry WS. Wild-type p53 transactivates the KILLER/DR5 gene through an intronic sequence-specific DNA-binding site. Oncogene 2000;19:1735–43.
17. Liu X, Yue P, Khuri FR, Sun SY. p53 upregulates death receptor 4 expression through an intronic p53 binding site. Cancer Res 2004;64:5078–83.
18. Sun SY, Yue P, Wu GS, et al. Mechanisms of apoptosis induced by the synthetic retinoid CD437 in human non-small cell lung carcinoma cells. Oncogene 1999;18:2357–65.
19. Liu X, Yue P, Zhou Z, Khuri FR, Sun SY. Death receptor regulation and celecoxib-induced apoptosis in human lung cancer cells. J Natl Cancer Inst 2004;96:1769–80.
20. Sun SY, Yue P, Dawson MI, et al. Differential effects of synthetic nuclear retinoid receptor-selective retinoids on the growth of human non-small cell lung carcinoma cells. Cancer Res 1997;57:4931–9.
21. Meng RD, McDonald ER III, Sheikh MS, Fornace AJ, Jr., El-Deiry WS. The TRAIL decoy receptor TRUNDD (DcR2, TRAIL-R4) is induced by adenovirus-p53 overexpression and can delay TRAIL-, p53-, and KILLER/DR5-dependent colon cancer apoptosis. Mol Ther 2000;1:130–44.
22. El-Deiry WS, Kern SE, Pietenpol JA, Kinzler KW, Vogelstein B. Definition of a consensus binding site for p53. Nat Genet 1992;1:45–9.
23. Degli-Esposti MA, Dougall WC, Smolak PJ, Waugh JY, Smith CA, Goodwin RG. The novel receptor TRAIL-R4 induces NF-κB and protects against TRAIL-mediated apoptosis, yet retains an incomplete death domain. Immunity 1997;7:813–20.
24. Marsters SA, Sheridan JP, Pitti RM, et al. A novel receptor for Apo2L/TRAIL contains a truncated death domain. Curr Biol 1997;7:1003–6.
25. Pan G, Ni J, Yu G, Wei YF, Dixit VM. TRUNDD, a new member of the TRAIL receptor family that antagonizes TRAIL signalling. FEBS Lett 1998;424:41–5.
26. van Noesel MM, van Bezouw S, Salomons GS, et al. Tumor-specific down-regulation of the tumor necrosis factor-related apoptosis-inducing ligand decoy receptors DcR1 and DcR2 is associated with dense promoter hypermethylation. Cancer Res 2002;62:2157–61.
27. Shivapurkar N, Toyooka S, Toyooka KO, et al. Aberrant methylation of trail decoy receptor genes is frequent in multiple tumor types. Int J Cancer 2004;109:786–92.

DOI:10.1158/0008-5472.CAN-06-4274

Cancer Research

The Proteasome Inhibitor PS-341 (Bortezomib) Up-Regulates DR5 Expression Leading to Induction of Apoptosis and Enhancement of TRAIL-Induced Apoptosis Despite Up-Regulation of c-FLIP and Survivin Expression in Human NSCLC Cells

Xiangguo Liu, Ping Yue, Shuzhen Chen, et al.

Cancer Res 2007;67:4981-4988. Published online May 17, 2007.

DOI:10.1158/0008-5472.CAN-06-4274

The Proteasome Inhibitor PS-341 (Bortezomib) Up-Regulates DR5 Expression Leading to Induction of Apoptosis and Enhancement of TRAIL-Induced Apoptosis Despite Up-Regulation of c-FLIP and Survivin Expression in Human NSCLC Cells

Xiangguo Liu, Ping Yue, Shuzhen Chen, Liping Hu, Sagar Lonial, Fadlo R. Khuri, and Shi-Yong Sun

Department of Hematology and Oncology, Winship Cancer Institute, Emory University School of Medicine, Atlanta, Georgia

Abstract

The proteasome inhibitor PS-341 (bortezomib or Velcade), an approved drug for treatment of patients with multiple myeloma, is currently being tested in clinical trials against various malignancies, including lung cancer. Preclinical studies have shown that PS-341 induces apoptosis and enhances tumor necrosis factor–related apoptosis-inducing ligand (TRAIL)–induced apoptosis in human cancer cells with undefined mechanisms. In the present study, we show that PS-341 induced caspase-8–dependent apoptosis, cooperated with TRAIL to induce apoptosis, and up-regulated death receptor 5 (DR5) expression in human non–small cell lung cancer (NSCLC) cells. DR5 induction correlated with the ability of PS-341 to induce apoptosis. Blockage of PS-341–induced DR5 up-regulation using DR5 small interfering RNA (siRNA) rendered cells less sensitive to apoptosis induced by either PS-341 or its combination with TRAIL, indicating that DR5 up-regulation mediates PS-341–induced apoptosis and enhancement of TRAIL-induced apoptosis in human NSCLC cells. We exclude the involvement of c-FLIP and survivin in mediating these events because c-FLIP (i.e., $FLIP_S$) and survivin protein levels were actually elevated on exposure to PS-341. Reduction of c-FLIP with c-FLIP siRNA sensitized cells to PS-341–induced apoptosis, suggesting that c-FLIP elevation protects cells from PS-341–induced apoptosis. Thus, the present study highlights the important role of DR5 up-regulation in PS-341–induced apoptosis and enhancement of TRAIL-induced apoptosis in human NSCLC cells. [Cancer Res 2007;67(10):4981–8]

Introduction

The tumor necrosis factor (TNF)–related apoptosis-inducing ligand (TRAIL) receptor death receptor 4 (DR4; also called TRAIL-R1) and death receptor 5 (DR5; also named Apo2, TRAIL-R2, TRICK2, or Killer/DR5) belong to the TNF receptor gene superfamily, all of which share a similar, cysteine-rich extracellular domain and additional cytoplasmic death domain (1). Both DR4 and DR5, located at the cell surface, become activated or trimerized on binding to their ligand TRAIL or overexpression and then signal apoptosis through caspase-8–mediated activation of caspase cascades (1). Recently, these death receptors have attracted much more attention because their ligand TRAIL preferentially induces apoptosis in transformed or malignant cells, showing potential as a tumor-selective apoptosis-inducing cytokine for cancer treatment. The expression of DR4 and DR5 is inducible by certain stimuli, including some cancer therapeutic agents (2, 3). It has been documented that induction of DR4 and/or DR5 accounts for induction of apoptosis and/or enhancement of TRAIL-induced apoptosis by certain cancer therapeutic agents (4–9).

Caspase-8 activation is a critical step in initiating death receptor–induced apoptosis (1). c-FLIP is the major protein that prevents caspase-8 from activation by death receptors. Although more than 10 isoforms of c-FLIP mRNA have been described, only 2 of them, $FLIP_S$ and $FLIP_L$, have been significantly studied at the protein level (10). Both proteins can be recruited to the death-inducing signaling complex (DISC) to inhibit caspase-8 activation (10, 11). There are an increasing number of studies showing that modulation of c-FLIP levels affects cell sensitivity to death receptor–mediated apoptosis (10, 11).

It is well known that the extrinsic death receptor–mediated pathway can activate the intrinsic mitochondria-mediated pathway, through caspase-8–mediated cleavage or truncation of Bid protein, leading to induction of apoptosis (12). Survivin, a family member of the inhibitor of apoptosis proteins, acts downstream of mitochondria to prevent processing of initiator caspase-9 from the apoptosome, leading to inhibition of the activity of the effector caspases. Thus, survivin modulates both the extrinsic and the intrinsic apoptotic pathways (13). Many studies have shown that induction of survivin expression causes cellular resistance to drug-induced apoptosis, whereas down-regulation of survivin using various means, such as small interfering RNA (siRNA), either induces apoptosis or sensitizes cells to undergo drug- or death ligand/receptor–induced apoptosis (13).

PS-341 (also called bortezomib or Velcade) is an approved drug for treatment of patients with relapsed multiple myeloma. Currently, there are many ongoing clinical trials that test the anticancer efficacy of PS-341 or its combinations with other agents in different types of cancers, including lung cancer (14, 15). Many preclinical studies documented that PS-341 alone or in combination with other cancer therapeutic agents, including TRAIL, induces apoptosis in a variety of human cancer cells *in vitro*, including both hematologic and solid tumor malignancies, and inhibits the growth of tumor xenografts *in vivo* (16, 17). However, the molecular mechanisms underlying PS-341–induced apoptosis and enhancement of apoptosis when combined with other agents, including TRAIL, particularly in human lung cancer

Note: Supplementary data for this article are available at Cancer Research Online (http://cancerres.aacrjournals.org/).

F.R. Khuri and S-Y. Sun are Georgia Cancer Coalition Distinguished Cancer Scholars.

Requests for reprints: Shi-Yong Sun, Winship Cancer Institute, Emory University School of Medicine, 1365-C Clifton Road Northeast, C3088, Atlanta, GA 30322. Phone: 404-778-2170; Fax: 404-778-5520; E-mail: shi-yong.sun@emoryhealthcare.org.

doi:10.1158/0008-5472.CAN-06-4274

DOI:10.1158/0008-5472.CAN-06-4274

cells, remain largely uncharacterized, although it seems to be associated with nuclear factor-κB inhibition (14, 18, 19), c-Jun NH_2-terminal kinase (JNK) activation (19–21), or Bik and Bim accumulation (22, 23) shown in certain types of cancer cells.

PS-341 has been shown to sensitize cells to TRAIL-induced apoptosis in certain types of cancer cells; this effect seems to be associated with Bik accumulation or c-FLIP down-regulation (22–24). Other proteasome inhibitors, such as MG132, increase DR5 expression, which mediates induction of apoptosis and enhances TRAIL-induced apoptosis by these inhibitors (25–27). To show the mechanism by which PS-341 induces apoptosis in human non–small cell lung cancer (NSCLC) cells, we studied the effects of PS-341 on the expression of DR4, DR5, c-FLIP, and survivin and their effect on PS-341–induced apoptosis and enhancement of TRAIL-induced apoptosis. Our results show that DR5 up-regulation plays an important role in PS-341–induced apoptosis and enhancement of TRAIL-induced apoptosis in human NSCLC cells.

Materials and Methods

Reagents. The powder of pure PS-341 was provided by Millennium Pharmaceuticals. It was dissolved in DMSO at a concentration of 1 mmol/L, and aliquots were stored at −80°C. Stock solutions were diluted to the desired final concentrations with growth medium just before use. MG132 and epoxomicin, two additional proteasome inhibitors, were purchased from Sigma Chemical Co. and Calbiochem, respectively. Human recombinant TRAIL was purchased from Biomol or PeproTech, Inc. Rabbit polyclonal anti-DR5 antibody was purchased from ProSci, Inc. Mouse monoclonal anti-DR4 antibody (B-N28) was purchased from Diaclone. Mouse monoclonal anti-FLIP antibody (NF6) was purchased from Alexis Biochemicals. Mouse monoclonal anti-caspase-3 was purchased from Imgenex. Rabbit anti-caspase-8, anti-caspase-9, anticaspase-6, anti-lamin A/C, and anti–poly(ADP-ribose) polymerase (PARP) antibodies and mouse monoclonal anti-survivin antibody were purchased from Cell Signaling Technology, Inc. Rabbit polyclonal anti-β-actin antibody was purchased from Sigma Chemical.

Cell culture. The human NSCLC cell lines used in this study were purchased from the American Type Culture Collection. They were grown in monolayer culture in RPMI 1640 with glutamine (Sigma Chemical) supplemented with 5% fetal bovine serum at 37°C in a humidified atmosphere consisting of 5% CO_2 and 95% air. The immortalized normal human bronchial epithelial cell lines BEAS-2B (28) and HBEC3KT (29) were provided by Dr. R. Lotan (M. D. Anderson Cancer Center, Houston, TX) and J.D. Minna (The University of Texas Southwestern Medical Center, Dallas, TX) and cultured as described previously (28, 29).

Cell survival assay. Cell survival was estimated by sulforhodamine B (SRB) assay as described previously (30).

Western blot analysis. Preparation of whole-cell protein lysates and the procedures for the Western blotting were described previously (4).

Detection of apoptosis. The amounts of cytoplasmic histone-associated DNA fragments (mononucleosome and oligonucleosomes) formed during apoptosis were measured using a Cell Death Detection ELISA^{Plus} kit (Roche Molecular Biochemicals) according to the manufacturer's instructions. The sub-G_1 population was analyzed using flow cytometry as described previously (31). In addition, caspase activation and their substrate cleavage were also detected by Western blot analysis as described above as another indicator of apoptosis.

Detection of cell surface death receptors. The procedure for direct antibody staining and subsequent flow cytometric analysis of cell surface protein was described previously (32). The mean fluorescence intensity (MFI) that represents antigenic density on a per cell basis was used to represent DR5 expression level. Phycoerythrin-conjugated mouse anti-human DR5 (DJR2-4) and anti-human DR4 (DJR1) monoclonal antibodies and phycoerythrin mouse IgG1 isotype control (MOPC-21/P3) were purchased from eBioscience.

Gene silencing using siRNA. The siRNA duplexes for control, *caspase-8*, *DR4*, and *DR5* genes were described previously (4, 5). c-FLIP siRNA duplex

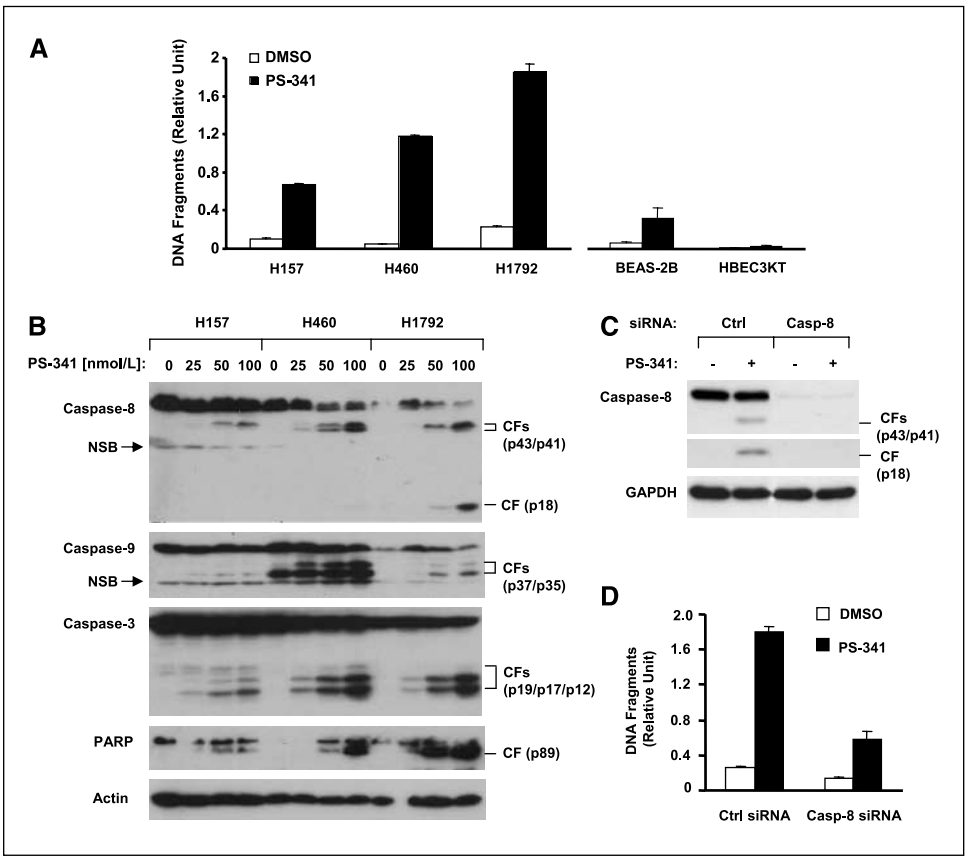

Figure 1. PS-341 induces DNA fragmentation (*A*), caspase activation (*B*), and caspase-8–dependent apoptosis (*C* and *D*). *A,* the indicated cell lines were treated with 50 nmol/L PS-341 for 24 h and then subjected to evaluation of DNA fragmentation. *B,* the indicated cell lines were treated with the given concentrations of PS-341 for 24 h and then subjected to preparation of whole-cell protein lysates and subsequent Western blot analysis. *C* and *D,* H157 cells were cultured in a 24-well plate and on the 2nd day transfected twice with control (*Ctrl*) or caspase-8 (*Casp-8*) siRNA with a 48-h interval between transfections. Forty hours after the second transfection, cells were treated with 50 nmol/L PS-341. The cells were either harvested for preparation of whole-cell protein lysates and subsequent Western blot analysis after an 8-h treatment (*C*) or subjected to estimation of DNA fragmentation using the Cell Death Detection ELISA^{Plus} kit after a 24-h treatment (*D*). *Columns,* mean of triplicate determinations; *bars,* SD. *CF,* cleaved fragment. *NSB*, nonspecific band.

DOI:10.1158/0008-5472.CAN-06-4274

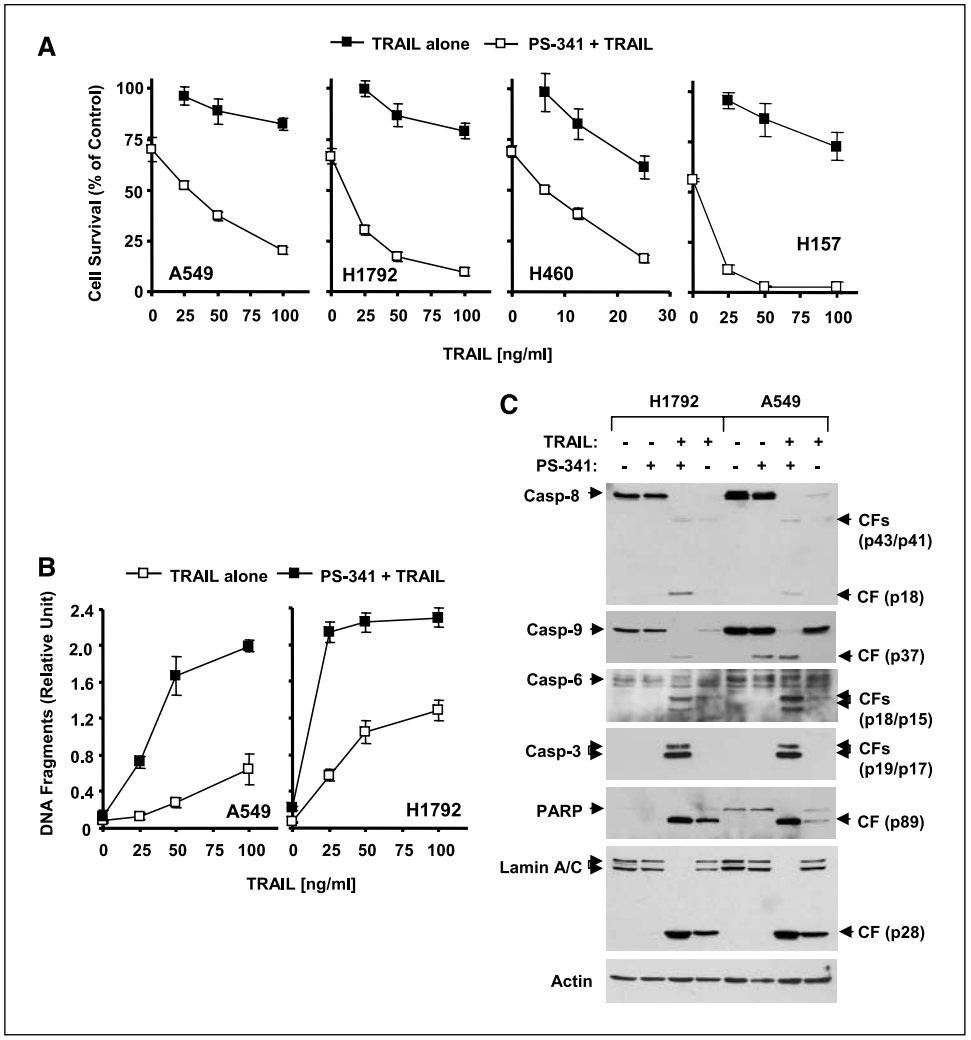

Figure 2. Combination of PS-341 and TRAIL exerts augmented effects on decreasing cell survival (*A*), increasing DNA fragmentation (*B*), and activating caspases (*C*). *A,* the indicated cell lines were treated with the given concentrations of TRAIL alone, 50 nmol/L PS-341 alone, and their respective combinations as indicated. After 24 h, cell number was estimated using the SRB assay for calculation of cell survival. *Points,* mean of four replicate determinations; *bars,* SD. *B,* the indicated cell lines were treated with the indicated concentrations of TRAIL alone, 50 nmol/L PS-341 alone, and their respective combinations as indicated. After 18 h, the cells were subjected to measurement of DNA fragmentation using the Cell Death Detection ELISA^{Plus} kit. *Points,* mean of triplicate determinations; *bars,* SD. *C,* the indicated cell lines were treated with 50 nmol/L PS-341 alone, 50 ng/mL TRAIL alone, and their combination. After 15 h, the cells were harvested for preparation of whole-cell protein lysates and subsequent Western blot analysis for detecting cleavage of caspases and their substrates.

targeting the sequence 5′-AATTCTCCGAACGTGTCACGT-3′ of *c-FLIP* gene (+514 to +534) was described previously (33). Transfection of these siRNA duplexes was conducted in 24-well or 96-well plates using the HiPerFect transfection reagent (Qiagen) following the manufacturer's manual. Gene silencing effects and caspase activation were evaluated by Western blot analysis, whereas DNA fragmentation and cell survival were measured by a Cell Death Detection ELISA^{Plus} kit and the SRB assay, respectively, as described above.

Results

PS-341 induces caspase-8–dependent apoptosis. To understand the mechanism by which PS-341 induces apoptosis in human NSCLC cells, we first determined the effects of PS-341 on induction of apoptosis by measuring DNA fragmentation in several NSCLC cell lines. As shown in Fig. 1*A*, PS-341 increased DNA fragmentation in H157, H460, and H1792 cell lines, indicating that these cell lines undergo apoptosis on PS-341 treatment. The sensitivities to undergo apoptosis of these cell lines are H1792 > H460 > H157. We also determined the effects of PS-341 on induction of apoptosis in BEAS-2B and HBEC3KT immortalized normal human bronchial epithelial cells. Compared with NSCLC cell lines, these normal cell lines were much less sensitive to PS-341–induced apoptosis (Fig. 1*A*).

We next determined the effects of PS-341 on activation of different caspases in the above human NSCLC cell lines. PS-341 at the tested concentration range (25–100 nmol/L) effectively induced cleavage of caspase-8, caspase-9, caspase-3, and PARP as indicated by appearance of the cleaved forms of these proteins in H157, H460, and H1792 cells treated with PS-341, showing that PS-341 activates these caspases (Fig. 1*B*). Moreover, it seemed that the degree of caspase-8 activation, but not caspase-9 activation, by PS-341 was associated with cell sensitivities to undergo cleavage of caspase-3 and PARP and DNA fragmentation (Fig. 1*B*), suggesting that caspase-8 activation may be important in PS-341–induced apoptosis. Thus, we further determined whether caspase-8 activation is required for PS-341–induced apoptosis. To this end, we used caspase-8 siRNA to block caspase-8 activation. As presented in Fig. 1*C*, the levels of uncleaved caspase-8 in caspase-8 siRNA-transfected cells were substantially decreased compared with those in cells transfected with control siRNA. Accordingly, we detected cleaved forms of caspase-8 in control siRNA-transfected cells, but not in cells transfected with caspase-8 siRNA, on PS-341 treatment, indicating a successful inhibition of caspase-8 activation induced by PS-341. Under these conditions, PS-341 efficiently increased levels of DNA fragments in control siRNA-transfected cells but only weakly in caspase-8 siRNA-transfected cells (Fig. 1*D*). These results indicate that caspase-8 activation is required for PS-341–induced apoptosis in human NSCLC cells.

PS-341 cooperates with TRAIL to enhance apoptosis. Sensitization of TRAIL-induced apoptosis by PS-341 has been

DOI:10.1158/0008-5472.CAN-06-4274

documented in other types of cancer cells but not in lung cancer cells. Thus, we examined the effects of PS-341 in combination with TRAIL on cell survival and apoptosis in several human NSCLC cell lines, including A549, which is relatively resistant to TRAIL-induced apoptosis (34). TRAIL at concentrations ranging from 25 to 100 ng/mL decreased cell survival by ≤25% in A549, H1792, and H157 cells, whereas PS-341 at 50 nmol/L alone decreased cell survival by <30% in A549 and H1792 cells and by <50% in H157 cells. However, the combination of PS-341 and TRAIL achieved 50% to 80% decreases in cell survival in A549 and H1792 cells and >90% in H157 cells (Fig. 2*A*). Similar result was also observed in TRAIL-sensitive H460 cells (Fig. 2*A*).

By specifically measuring DNA fragmentation, a hallmark of apoptosis, we detected enhanced DNA fragmentation in both H1792 and A549 cell lines treated with the combination of PS-341 and TRAIL (Fig. 2*B*). For example, TRAIL at 50 ng/mL alone and PS-341 at 50 nmol/L alone exerted limited effects on increasing DNA fragmentation (0.280 and 0.133 arbitrary units, respectively) in A549 cells. However, their combination increased DNA fragmentation up to 1.67 arbitrary unit (Fig. 2*B*). Collectively, these results clearly indicate that the combination of PS-341 and TRAIL exhibits a more than additive (synergistic) effect on induction of apoptosis in human NSCLC cells. Moreover, we also examined the effects of the combination on caspase activation in these cell lines. As presented in Fig. 2*C*, the combination of PS-341 and TRAIL was obviously more potent than each single agent in inducing cleavage of caspase-8, caspase-9, caspase-6, and caspase-3 and their substrates PARP and lamin A/C, evidenced by increased amounts of cleaved bands in cells treated with the combination in comparison with those in cells treated with either PS-341 or TRAIL alone. These data further support that the combination of PS-341 and TRAIL enhances apoptosis in human NSCLC cells.

PS-341 up-regulates the expression of DR5, $FLIP_S$, and survivin. Because both caspase-8 activation and enhancement of TRAIL-induced apoptosis involve TRAIL death receptors and c-FLIP, we next examined the effects of PS-341 on the expression of DR4, DR5, and c-FLIP in these NSCLC cell lines. By Western blot analysis, we detected increased and dose-dependent DR5 expression in the three NSCLC cell lines after exposure to PS-341. The degrees of DR5 induction in these cell lines were H1792 > H460 > H157 cells (Fig. 3*A*), which correlate with cell sensitivity to undergo apoptosis and caspase-8 activation as described above (Fig. 1*A* and *B*). PS-341 increased DR4 levels in H1792 cells but not in H157 and H460 cells (Fig. 3*A*). In agreement, cell surface DR5 levels were increased in the three cell lines treated with PS-341, whereas cell surface DR4 levels were substantially increased only in H1792 cells (Fig. 3*B*). PS-341 did not apparently alter $FLIP_L$ levels; instead, it increased $FLIP_S$ levels in the three cell lines, particularly in H157 and H460 cells (Fig. 3*A*), which were less sensitive to PS-341–induced apoptosis compared with H1792 cells (Fig. 1*A*). We noted that the basal levels of c-FLIP in H157 and H460 cells were much higher than in H1792 cells (Fig. 3*A*). These results suggest that c-FLIP up-regulation may protect cells from PS-341–induced apoptosis. Together, these results suggest that DR5 up-regulation, rather than c-FLIP modulation, plays an important role in PS-341–mediated apoptosis and enhancement of TRAIL-induced apoptosis in human NSCLC cells.

It is well known that survivin, Bcl-2, and Bcl-X_L are other important proteins involved in regulating apoptosis or enhancing TRAIL-induced apoptosis (13, 35, 36). Therefore, we also measured the levels of these proteins in cells exposed to PS-341. PS-341 did not alter the expression of either Bcl-2 or Bcl-X_L in human NSCLC cells even at concentrations up to 1 μmol/L (see Supplementary Fig. S1). In a similar fashion to $FLIP_S$ modulation, we found that PS-341 also increased the levels of survivin in the tested NSCLC cell lines, particularly in H460 and H1792 cells (Fig. 3*A*).

We also examined the effects of two other proteasome inhibitors, MG132 and epoxomicin, on the expression levels of DR5, c-FLIP, and

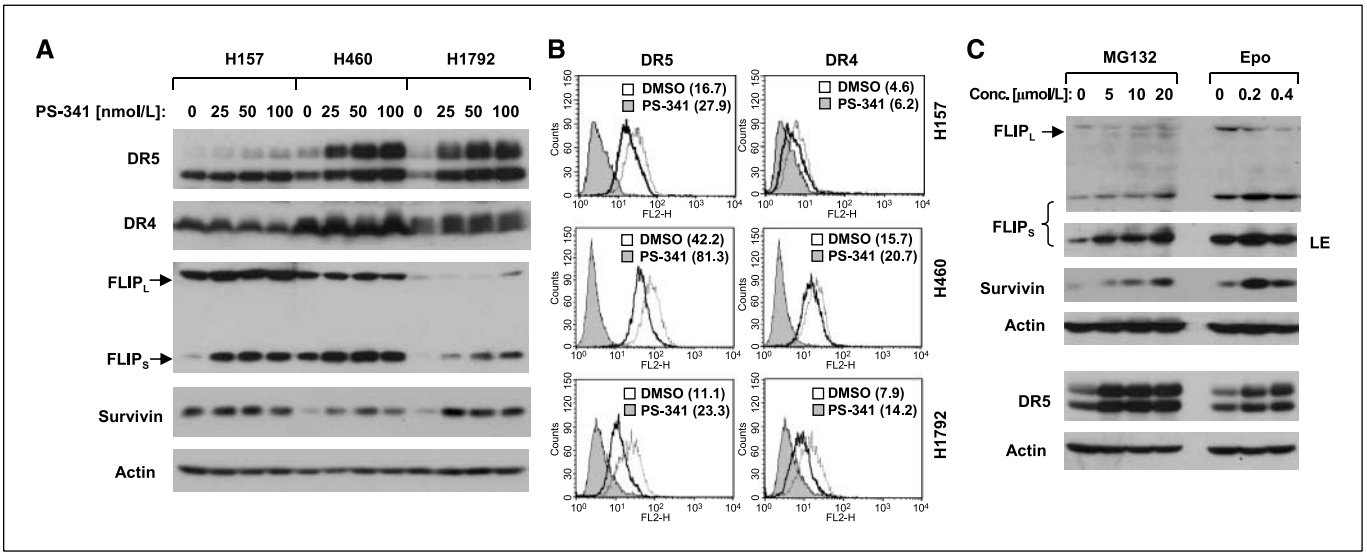

Figure 3. Effects of PS-341 as well as other proteasome inhibitors on the expression of DR5, DR4, c-FLIP, and survivin (*A* and *C*) and cell surface distributions of death receptors (*B*) in human NSCLC cell lines. *A,* the indicated cell lines were treated with the given concentrations of PS-341 for 8 h and then subjected to preparation of whole-cell protein lysates. The given proteins were detected using Western blot analysis. *B,* the indicated cell lines were treated with 50 nmol/L PS-341 for 12 h and then harvested for analysis of cell surface DR5 and DR4 by immunofluorescent staining and subsequent flow cytometry. *Filled gray peaks,* cells stained with a matched control phycoerythrin-conjugated IgG isotype antibody; *open peaks,* cells stained with phycoerythrin-conjugated anti-DR5 or DR4 antibody. The number in each parenthesis is the MFI. *C,* H460 cells were treated with the indicated concentrations of MG132 or epoxomicin (*Epo*) for 8 h and then subjected to preparation of whole-cell protein lysates. The given proteins were detected using Western blot analysis. *LE,* longer exposure.

DOI:10.1158/0008-5472.CAN-06-4274

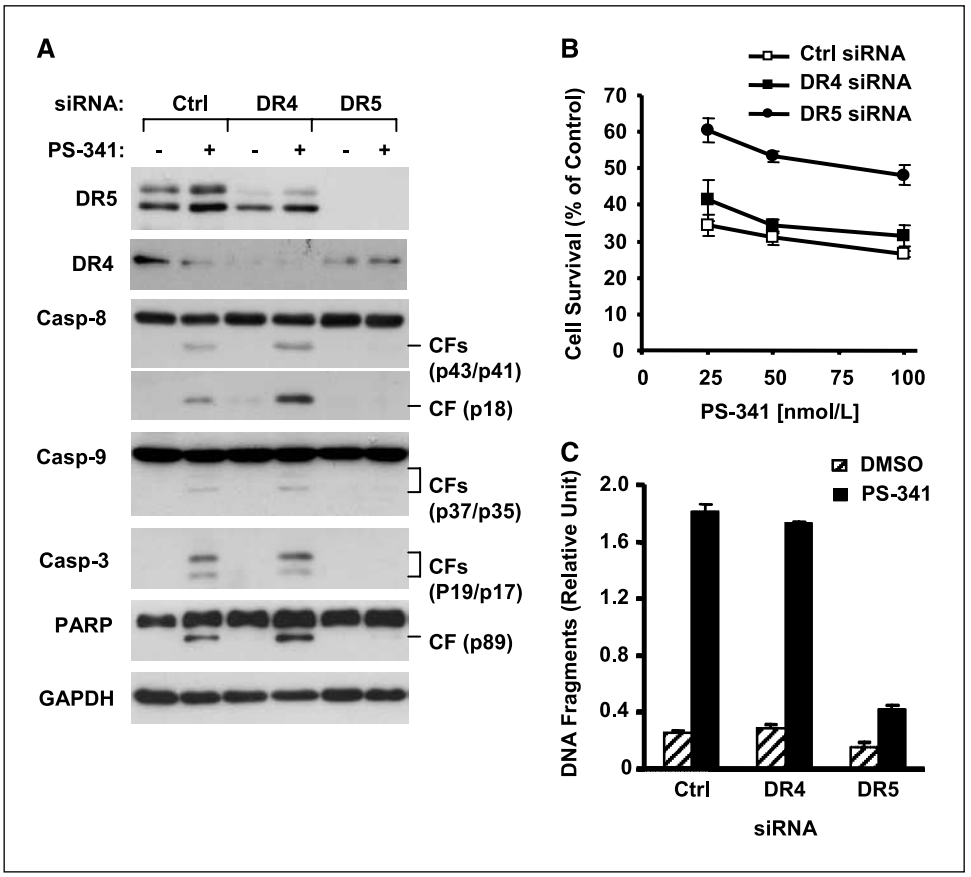

Figure 4. Silencing of DR5 expression protects cells from PS-341–induced activation of caspases (*A*), decrease in cell survival (*B*), and increase in DNA fragmentation (*C*) in H157 human NSCLC cells. H157 cells were cultured in a 24-well plate and on the 2nd day transfected twice with control, DR4, or DR5 siRNA with a 48-h interval between transfections. Forty hours after the second transfection, cells were treated with 50 nmol/L PS-341 (*A*), the indicated concentrations of PS-341 (*B*), or 25 nmol/L PS-341 (*C*). The cells were either harvested for preparation of whole-cell protein lysates and subsequent Western blot analysis after an 8-h treatment (*A*) or subjected to estimation of cell number by SRB assay (*B*) or measurement of DNA fragmentation using the Cell Death Detection ELISA^{Plus} kit (*C*) after a 24-h treatment. *Points* and *columns,* mean of four replicate (*B*) or triplicate (*C*) determinations; *bars,* SD.

survivin. As presented in Fig. 3*C*, $FLIP_S$, but not $FLIP_L$, was elevated in cells treated with either MG132 or epoxomicin. Similarly, we also detected increases in survivin levels in cells exposed to either MG132 or epoxomicin. In addition, we also found that both MG132 and epoxomicin induced DR5 expression. Collectively, these results suggest that elevation of $FLIP_S$ and survivin by PS-341 is likely to be a consequence of proteasome inhibition.

DR5 up-regulation contributes to PS-341–induced apoptosis. To determine whether DR5 up-regulation is involved in PS-341–induced apoptosis in human NSCLC cells, we used DR5 siRNA to block PS-341–induced DR5 up-regulation and then determined its effect on PS-341–induced apoptosis. As presented in Fig. 4*A*, transfection of DR5 siRNA into H157 cells effectively decreased the basal levels of DR5 expression and PS-341–induced DR5 up-regulation. In this experiment, we also included DR4 silencing as a control, transfection of which into H157 cells substantially reduces the basal levels of DR4 expression. These results indicate successful knockdown of either DR5 or DR4. Under these conditions, DR5 siRNA protected cells from PS-341–induced decrease in cell survival, whereas DR4 siRNA did not have such an effect (Fig. 4*B*). By measuring caspase activation using Western blot analysis, we found that PS-341 induced cleavage of caspase-8, caspase-9, caspase-3, and PARP in cells transfected with control or DR4 siRNA but not in DR5 siRNA-transfected cells (Fig. 4*A*). Accordingly, PS-341 increased DNA fragmentation in cells transfected with control or DR4 siRNA, but this effect was drastically inhibited in DR5 siRNA-transfected cells (Fig. 4*C*). In agreement, we observed that PS-341 also induced less amounts of cleaved forms of caspase-8, caspase-3, and PARP and DNA fragments in DR5 siRNA-transfected H460 cells than in control siRNA-transfected H460 cells (see Supplementary Fig. S2). Together, these results indicate that DR5 up-regulation plays a critical role in mediating PS-341–induced apoptosis in human NSCLC cells.

DR5 up-regulation contributes to PS-341–mediated enhancement of TRAIL-induced apoptosis. Because PS-341 increases $FLIP_S$ levels, we also determined whether PS-341 enhances TRAIL-induced apoptosis via up-regulation of DR5. The combination of PS-341 and TRAIL exhibited enhanced effects on cleavage of caspase-8, caspase-3, and PARP, as indicated by the levels of the cleaved bands by Western blotting, in control siRNA-transfected cells but not in cells transfected with DR5 siRNA (Fig. 5*A*). Accordingly, the combination of PS-341 and TRAIL was significantly less active in decreasing cell survival (Fig. 5*B*) and in increasing DNA fragmentation (Fig. 5*C*) in DR5 siRNA-transfected cells than in cells transfected with control siRNA. Together, these results indicate that PS-341 up-regulates DR5 expression, leading to enhancement of TRAIL-induced apoptosis.

PS-341 induces apoptosis independently of TRAIL ligand. The preceding data clearly indicate that PS-341 induces apoptosis in human NSCLC cells through a DR5-mediated mechanism, whereas others have shown that PS-341 increased TRAIL expression, which contributes to PS-341–induced apoptosis in primary chronic lymphocytic leukemia cells (37). Thus, we further determined if PS-341–induced DR5-dependent apoptosis involves the TRAIL ligand. By Western blot analysis, we observed that H157 cells expressed very low levels of TRAIL, which were not further increased by PS-341 (see Supplementary Fig. S3*A*). The presence of soluble recombinant DR5:Fc, which neutralizes TRAIL, abolished TRAIL-induced decrease in cell survival and increase in DNA fragmentation but failed to protect cells from PS-341–induced cell death (see Supplementary

DOI:10.1158/0008-5472.CAN-06-4274

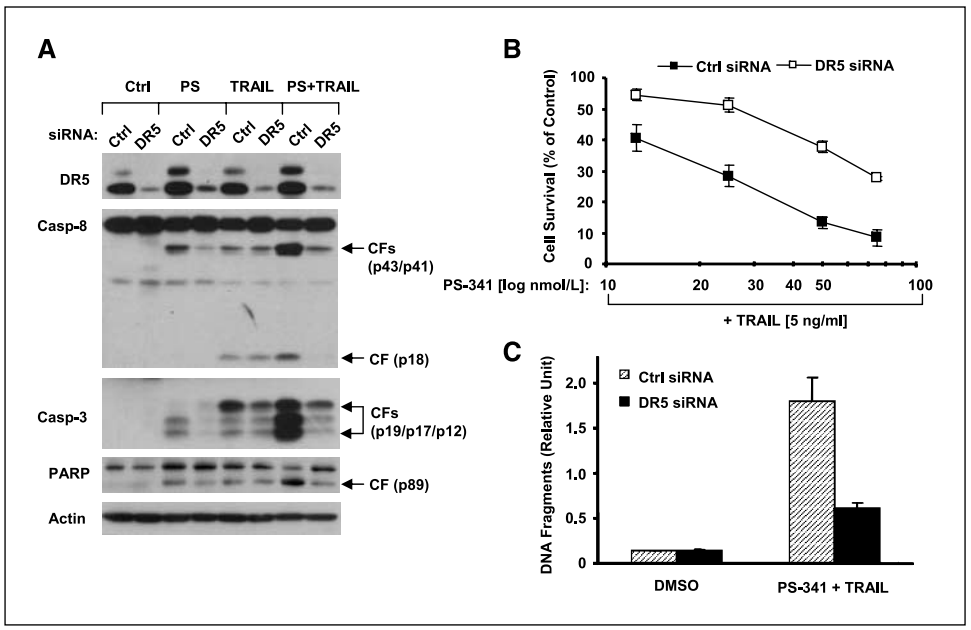

Figure 5. Silencing of DR5 expression attenuates the ability of PS-341 to cooperate with TRAIL to activate caspases (*A*), decrease cell survival (*B*), and increase DNA fragmentation (*C*). H157 cells were cultured in a 24-well plate and on the 2nd day transfected with control or DR5 siRNA. Twenty-four hours after the transfection, cells were reseeded in a 6-well plate (*A*) or 96-well plates (*B* and *C*) and treated with 50 nmol/L PS-341 (*PS*), 5 ng/mL TRAIL or PS-341, and TRAIL combination (*PS+TRAIL*; *A*), with 5 ng/mL TRAIL in combination with the indicated concentrations of PS-341, respectively (*B*), or with the solvent control DMSO or the combination of 50 nmol/L PS-341 and 10 ng/mL TRAIL (*C*) on the 2nd day after reseeding. After 24-h (*A* and *B*) or 12-h (*C*) treatment, the cells were either harvested for preparation of whole-cell protein lysates and subsequent Western blot analysis (*A*) or subjected to estimation of cell number by SRB assay (*B*) or measurement of DNA fragmentation using the Cell Death Detection ELISA^{Plus} kit (*C*). *Points* and *columns,* mean of triplicate (*B* and *C*) determinations; *bars,* SD.

Fig. S3*B* and *C*). Collectively, we conclude that PS-341 induces apoptosis in human NSCLC cells independently of TRAIL.

Blockage of FLIP$_S$ elevation sensitizes cells to PS-341 treatment. To determine whether FLIP$_S$ elevation by PS-341 is associated with cell resistance to PS-341, we used c-FLIP siRNA to block PS-341–induced FLIP$_S$ elevation and then examined cell sensitivity to PS-341 treatment. As presented in Fig. 6*A*, transfection of c-FLIP siRNA not only decreased basal levels of c-FLIP (both FLIP$_L$ and FLIP$_S$) but also more importantly abrogated PS-341–induced FLIP$_S$ elevation. Subsequently, the cell sensitivity to PS-341 treatment in c-FLIP siRNA-transfected cells was greatly increased in comparison with cells transfected with control siRNA (Fig. 6*B*). In both H157 and H460 cells, PS-341 induced more apoptosis in c-FLIP siRNA-transfected cells than in control siRNA-transfected cells (Fig. 6*C*). For example, PS-341 induced ~15% apoptosis in control siRNA-transfected cells but 30% apoptosis in c-FLIP siRNA-transfected cells, whereas transfection of c-FLIP siRNA alone caused only ~10% apoptosis (Fig. 6*C*). Thus, these results have proved our speculation that FLIP$_S$ elevation protects cells from PS-341–induced apoptosis.

Discussion

Induction of DR4 and/or DR5 and enhancement of TRAIL-induced apoptosis by PS-341 have been shown in certain types of cancer cells, including colon cancer, prostate cancer, bladder cancer, and chronic lymphocytic leukemia cells (37, 38). Moreover, a recent study has shown that the TRAIL/DR4 or DR5 apoptotic pathway mediates proteasome inhibitor (including PS-341)–induced apoptosis in primary chronic lymphocytic leukemia cells (37). In the present study, we have shown for the first time that PS-341 induces apoptosis in human NSCLC cells through a DR5-mediated mechanism because of the following findings: first, PS-341 induced the activation of caspase-8 and other caspases, whereas inhibition of caspase-8 activation diminished PS-341–induced apoptosis, indicating that PS-341 induces a caspase-8–dependent apoptosis; second, PS-341 induced DR5 expression, including cell surface DR5 and enhanced TRAIL-induced apoptosis; and last, blockage of DR5 up-regulation by siRNA-mediated DR5 silencing abrogated PS-341–induced apoptosis and enhancement of TRAIL-induced apoptosis, indicating that DR5 up-regulation is required for PS-341–induced apoptosis and sensitization to TRAIL-induced apoptosis. In this regard, our results partially agree with the findings by Kabore et al. (37) that PS-341–induced apoptosis in primary chronic lymphocytic leukemia cells involves up-regulation of DR4 and DR5, although we failed to show the role of DR4 in PS-341–induced apoptosis in H157 human NSCLC cells. In primary chronic lymphocytic leukemia cells, TRAIL was induced and is required for PS-341–induced apoptosis because soluble DR4:Fc inhibited PS-341–induced cell death (37). However, we failed to detect TRAIL up-regulation in cells treated with PS-341 and protective effects of soluble DR5:Fc on PS-341–induced cell death in human NSCLC cells, suggesting that PS-341 induces apoptosis independently of TRAIL ligand in human NSCLC cells.

DR5 expression is regulated through p53-dependent and p53-independent mechanisms (2, 39). Although PS-341 was reported to increase p53 expression (20, 40), we found that PS-341 increased DR5 expression in NSCLC cell lines with wild-type p53 (H460) and mutant p53 (H157 and H1792). Thus, PS-341 is likely to up-regulate DR5 expression through a p53-independent mechanism. Some studies have shown that JNK regulates DR5 expression (6, 41, 42). Although PS-341 indeed induced JNK activation in our cell lines as shown previously (20, 21), we found that the JNK inhibitor SP600125 only weakly attenuated PS-341–induced DR5 induction,[1] suggesting that other mechanism(s) beyond JNK may be involved in PS-341–induced DR5 expression in human NSCLC cells. Because PS-341 induces endoplasmic reticulum stress, including up-regulation of CHOP/GADD153 (43, 44), a transcriptional factor known to regulate DR5 expression (27, 45), it remains to be determined whether PS-341 induces a CHOP-dependent up-regulation of DR5.

c-FLIP is regulated by an ubiquitin-proteasome mechanism (46, 47), and certain cancer therapeutic agents stimulate down-regulation of c-FLIP expression through this mechanism (46). PS-341, as a proteasome inhibitor, was surprisingly reported to

[1] Unpublished data.

DOI:10.1158/0008-5472.CAN-06-4274

reduce c-FLIP levels (24), although other studies showed that PS-341 did not alter c-FLIP levels (38) or increased the levels of c-FLIP in the DISC (48). In our study, we clearly showed that PS-341 increased the levels of $FLIP_S$ without altering $FLIP_L$ levels in all of the tested NSCLC cell lines. Moreover, we also showed that other proteasome inhibitors, including MG132 and epoxomicin, exhibited similar effects on modulation of c-FLIP expression as PS-341. Therefore, this is the first study to show that PS-341 and other proteasome inhibitors selectively increase $FLIP_S$ levels, although the underlying mechanism is currently unclear. A recent study has shown that $FLIP_S$ is more prone to ubiquitination and has a considerably shorter half-life in comparison with $FLIP_L$ (47). Therefore, it would be interesting to investigate whether PS-341 increases $FLIP_S$ levels through inhibition of the proteasome. Nevertheless, our results indicate that it is unlikely for PS-341 to enhance TRAIL-induced apoptosis through modulation of c-FLIP in human NSCLC cells.

The basal levels of c-FLIP in H157 and H460 cells, which were less sensitive to PS-341–induced apoptosis, were much higher than in H1792 cells, which were more sensitive to PS-341–induced apoptosis. Moreover, $FLIP_S$ levels were greatly increased in H157 and H460 cells in comparison with those in H1792 cells (Fig. 3). Thus, it seems that the levels of c-FLIP, particularly $FLIP_S$ elevation during PS-341 treatment, may provide a protective mechanism for cells to counteract PS-341–induced apoptosis. Indeed, this notion was supported by our findings that reduction of c-FLIP levels, particularly prevention of PS-341–induced $FLIP_S$ elevation in both H157 and H460 cells, significantly sensitized cells to PS-341–induced apoptosis (Fig. 6).

Survivin, Bcl-2, and Bcl-X_L are known to regulate apoptosis or enhance TRAIL-induced apoptosis (13, 35, 36). In our study, we found that PS-341 did not alter the expression of either Bcl-2 or Bcl-X_L in human NSCLC cells, which agree with published results in other types of cancer cells (22, 23). In a similar fashion to $FLIP_S$ modulation, PS-341 also increased the levels of survivin in human NSCLC cells (Fig. 3*A*). To the best of our knowledge, this is the first study showing that PS-341 increases survivin expression. Given the antiapoptotic property of survivin, it is likely that survivin up-regulation, like $FLIP_S$ elevation, may counteract the apoptosis-inducing effect of PS-341. It has been shown that the ubiquitin-proteasome regulates survivin degradation (49). Given that other proteasome inhibitors (e.g., MG132 and epoxomicin) other than PS-341 also increased survivin levels (Fig. 3*C*), it is plausible to speculate that PS-341 may stabilize survivin through inhibition of the proteasome. Studies to evaluate this hypothesis are ongoing.

Our results clearly indicate that PS-341 treatment generates conflicting signals by activating both proapoptotic (e.g., DR5) and antiapoptotic signaling (e.g., c-FLIP and survivin). Despite up-regulation of c-FLIP and survivin, PS-341 indeed induced apoptosis and enhanced TRAIL-induced apoptosis in human NSCLC cells albeit with various degrees. Thus, it seems that PS-341–activated proapoptotic signaling, such as DR5 induction, can override activation of antiapoptotic signaling, such as up-regulation of $FLIP_S$ and survivin caused by PS-341, leading to induction of apoptosis and enhancement of TRAIL-induced apoptosis. Given that prevention of c-FLIP elevation during PS-341 treatment sensitized cells to PS-341–induced apoptosis, it may be possible to enhance the anticancer efficacy of PS-341 via combination with other agents, which decrease c-FLIP and survivin expression.

It is known that TRAIL functions as a DR5 ligand and rapidly induces apoptosis in a wide variety of transformed cells but is not cytotoxic in normal cells *in vitro* and *in vivo* (1, 2). Therefore, TRAIL is considered to be a tumor-selective, apoptosis-inducing cytokine and a promising new candidate for cancer treatment. Unfortunately, certain cancer cell lines and tumors are resistant to TRAIL-mediated cell killing (2). In addition, agonistic anti-DR5 antibodies can also induce DR5 trimerization, which triggers the extrinsic apoptotic pathway, thus having great cancer therapeutic potential (50). In fact, the agonistic anti-DR5 antibody is already being tested in phase I clinical trials. Therefore, PS-341 may be useful in combination with TRAIL or an agonistic anti-DR5

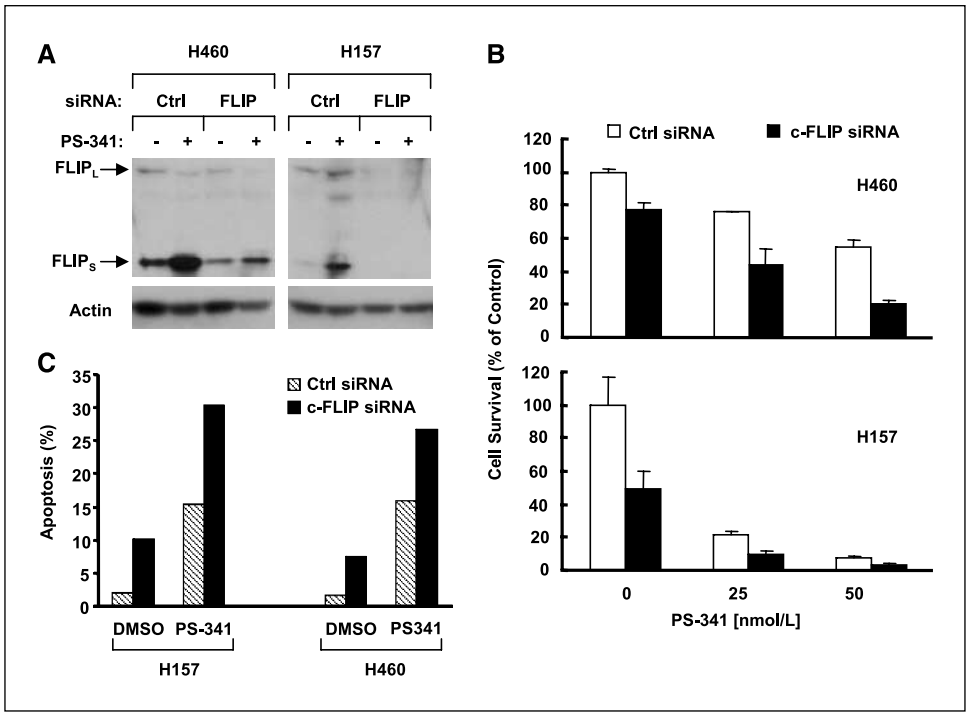

Figure 6. Silencing of c-FLIP sensitizes NSCLC cells to PS-341 treatment. H460 and H157 cells seeded in a 96-well plate or a 24-well plate were transfected with control or c-FLIP siRNA. Twenty-four hours after the transfection, cells were treated with 50 nmol/L PS-341 (in a 24-well plate) for 24 h (*A* and *C*) or with the given concentrations of PS-341 for 48 h (*B*). The cells were then harvested for preparation of whole-cell protein lysates and subsequent Western blot analysis to evaluate the silencing efficiency of c-FLIP (*A*) or subjected to the SRB assay for estimation of cell survival (*B*) or sub-G_1 analysis for measurement of apoptosis (*C*). *Columns,* mean of triplicate treatments (*B*); *bars,* SD.

DOI:10.1158/0008-5472.CAN-06-4274

antibody to achieve an enhanced effect on apoptosis induction or overcome TRAIL resistance in human cancer cells.

In summary, our study has shown that PS-341 induces DR5 expression, which contributes to PS-341–induced apoptosis and enhancement of TRAIL-induced apoptosis in human NSCLC cells despite up-regulation of $FLIP_S$ and survivin. Our findings provide novel insight into the mechanism by which PS-341 induces apoptosis and enhances TRAIL-induced apoptosis in human cancer cells.

Acknowledgments

Received 11/20/2006; revised 2/5/2007; accepted 3/14/2007.

Grant support: The Georgia Cancer Coalition Distinguished Cancer Scholar award (S-Y. Sun) and Department of Defense VITAL grant W81XWH-04-1-0142 (S-Y. Sun for Project 4).

The costs of publication of this article were defrayed in part by the payment of page charges. This article must therefore be hereby marked *advertisement* in accordance with 18 U.S.C. Section 1734 solely to indicate this fact.

We thank Dr. R. Lotan and J.D. Minna for providing immortalized normal bronchial epithelial cell lines.

References

1. Kelley SK, Ashkenazi A. Targeting death receptors in cancer with Apo2L/TRAIL. Curr Opin Pharmacol 2004;4:333–9.
2. Wang S, El-Deiry WS. TRAIL and apoptosis induction by TNF-family death receptors. Oncogene 2003;22:8628–33.
3. Sun SY. Chemopreventive agent-induced modulation of death receptors. Apoptosis 2005;10:1203–10.
4. Liu X, Yue P, Zhou Z, Khuri FR, Sun SY. Death receptor regulation and celecoxib-induced apoptosis in human lung cancer cells. J Natl Cancer Inst 2004;96:1769–80.
5. Jin F, Liu X, Zhou Z, et al. Activation of nuclear factor-κB contributes to induction of death receptors and apoptosis by the synthetic retinoid CD437 in DU145 human prostate cancer cells. Cancer Res 2005;65:6354–63.
6. Zou W, Liu X, Yue P, et al. c-Jun NH2-terminal kinase-mediated up-regulation of death receptor 5 contributes to induction of apoptosis by the novel synthetic triterpenoid methyl-2-cyano-3,12-dioxooleana-1, 9-dien-28-oate in human lung cancer cells. Cancer Res 2004;64:7570–8.
7. Nagane M, Pan G, Weddle JJ, et al. Increased death receptor 5 expression by chemotherapeutic agents in human gliomas causes synergistic cytotoxicity with tumor necrosis factor-related apoptosis-inducing ligand *in vitro* and *in vivo*. Cancer Res 2000;60:847–53.
8. Gibson SB, Oyer R, Spalding AC, Anderson SM, Johnson GL. Increased expression of death receptors 4 and 5 synergizes the apoptosis response to combined treatment with etoposide and TRAIL. Mol Cell Biol 2000;20:205–12.
9. Kim H, Kim EH, Eom YW, et al. Sulforaphane sensitizes tumor necrosis factor-related apoptosis-inducing ligand (TRAIL)-resistant hepatoma cells to TRAIL-induced apoptosis through reactive oxygen species-mediated up-regulation of DR5. Cancer Res 2006;66:1740–50.
10. Wajant H. Targeting the FLICE inhibitory protein (FLIP) in cancer therapy. Mol Interv 2003;3:124–7.
11. Krueger A, Baumann S, Krammer PH, Kirchhoff S. FLICE-inhibitory proteins: regulators of death receptor-mediated apoptosis. Mol Cell Biol 2001;21:8247–54.
12. Green DR. Apoptotic pathways: paper wraps stone blunts scissors. Cell 2000;102:1–4.
13. Altieri DC. Validating survivin as a cancer therapeutic target. Nat Rev Cancer 2003;3:46–54.
14. Adams J, Kauffman M. Development of the proteasome inhibitor Velcade (bortezomib). Cancer Invest 2004;22:304–11.
15. Richardson PG, Mitsiades C, Hideshima T, Anderson KC. Bortezomib: proteasome inhibition as an effective anticancer therapy. Annu Rev Med 2006;57:33–47.
16. Schenkein DP. Preclinical data with bortezomib in lung cancer. Clin Lung Cancer 2005;7 Suppl 2:S49–55.
17. Voorhees PM, Orlowski RZ. The proteasome and proteasome inhibitors in cancer therapy. Annu Rev Pharmacol Toxicol 2006;46:189–213.
18. An J, Sun Y, Fisher M, Rettig MB. Maximal apoptosis of renal cell carcinoma by the proteasome inhibitor bortezomib is nuclear factor-κB dependent. Mol Cancer Ther 2004;3:727–36.
19. Yin D, Zhou H, Kumagai T, et al. Proteasome inhibitor PS-341 causes cell growth arrest and apoptosis in human glioblastoma multiforme (GBM). Oncogene 2005;24:344–54.
20. Yang Y, Ikezoe T, Saito T, et al. Proteasome inhibitor PS-341 induces growth arrest and apoptosis of non-small cell lung cancer cells via the JNK/c-Jun/AP-1 signaling. Cancer Sci 2004;95:176–80.
21. Lauricella M, Emanuele S, D'Anneo A, et al. JNK and AP-1 mediate apoptosis induced by bortezomib in HepG2 cells via FasL/caspase-8 and mitochondria-dependent pathways. Apoptosis 2006;11:607–25.
22. Nikrad M, Johnson T, Puthalalath H, et al. The proteasome inhibitor bortezomib sensitizes cells to killing by death receptor ligand TRAIL via BH3-only proteins Bik and Bim. Mol Cancer Ther 2005;4:443–9.
23. Zhu H, Zhang L, Dong F, et al. Bik/NBK accumulation correlates with apoptosis-induction by bortezomib (PS-341, Velcade) and other proteasome inhibitors. Oncogene 2005;24:4993–9.
24. Sayers TJ, Brooks AD, Koh CY, et al. The proteasome inhibitor PS-341 sensitizes neoplastic cells to TRAIL-mediated apoptosis by reducing levels of c-FLIP. Blood 2003;102:303–10.
25. He Q, Huang Y, Sheikh MS. Proteasome inhibitor MG132 upregulates death receptor 5 and cooperates with Apo2L/TRAIL to induce apoptosis in Bax-proficient and -deficient cells. Oncogene 2004;23:2554–8.
26. Nencioni A, Wille L, Dal Bello G, et al. Cooperative cytotoxicity of proteasome inhibitors and tumor necrosis factor-related apoptosis-inducing ligand in chemoresistant Bcl-2-overexpressing cells. Clin Cancer Res 2005;11:4259–65.
27. Yoshida T, Shiraishi T, Nakata S, et al. Proteasome inhibitor MG132 induces death receptor 5 through CCAAT/enhancer-binding protein homologous protein. Cancer Res 2005;65:5662–7.
28. Sun SY, Kurie JM, Yue P, et al. Differential responses of normal, premalignant, and malignant human bronchial epithelial cells to receptor-selective retinoids. Clin Cancer Res 1999;5:431–7.
29. Ramirez RD, Sheridan S, Girard L, et al. Immortalization of human bronchial epithelial cells in the absence of viral oncoproteins. Cancer Res 2004;64:9027–34.
30. Sun SY, Yue P, Dawson MI, et al. Differential effects of synthetic nuclear retinoid receptor-selective retinoids on the growth of human non-small cell lung carcinoma cells. Cancer Res 1997;57:4931–9.
31. Sun SY, Zhou Z, Wang R, Fu H, Khuri FR. The farnesyltransferase inhibitor Lonafarnib induces growth arrest or apoptosis of human lung cancer cells without downregulation of Akt. Cancer Biol Ther 2004;3:1092–8; discussion 9–101.
32. Sun SY, Yue P, Hong WK, Lotan R. Induction of Fas expression and augmentation of Fas/Fas ligand-mediated apoptosis by the synthetic retinoid CD437 in human lung cancer cells. Cancer Res 2000;60:6537–43.
33. Longley DB, Wilson TR, McEwan M, et al. c-FLIP inhibits chemotherapy-induced colorectal cancer cell death. Oncogene 2006;25:838–48.
34. Sun SY, Yue P, Zhou JY, et al. Overexpression of BCL2 blocks TNF-related apoptosis-inducing ligand (TRAIL)-induced apoptosis in human lung cancer cells. Biochem Biophys Res Commun 2001;280:788–97.
35. Harada H, Grant S. Apoptosis regulators. Rev Clin Exp Hematol 2003;7:117–38.
36. Chawla-Sarkar M, Bae SI, Reu FJ, et al. Down-regulation of Bcl-2, FLIP, or IAPs (XIAP and survivin) by siRNAs sensitizes resistant melanoma cells to Apo2L/TRAIL-induced apoptosis. Cell Death Differ 2004;11:915–23.
37. Kabore AF, Sun J, Hu X, et al. The TRAIL apoptotic pathway mediates proteasome inhibitor induced apoptosis in primary chronic lymphocytic leukemia cells. Apoptosis 2006;11:1175–93.
38. Johnson TR, Stone K, Nikrad M, et al. The proteasome inhibitor PS-341 overcomes TRAIL resistance in Bax and caspase 9-negative or Bcl-xL overexpressing cells. Oncogene 2003;22:4953–63.
39. Sheikh MS, Fornace AJ, Jr. Death and decoy receptors and p53-mediated apoptosis. Leukemia 2000;14:1509–13.
40. Ling YH, Liebes L, Jiang JD, et al. Mechanisms of proteasome inhibitor PS-341-induced G(2)-M-phase arrest and apoptosis in human non-small cell lung cancer cell lines. Clin Cancer Res 2003;9:1145–54.
41. Higuchi H, Grambihler A, Canbay A, Bronk SF, Gores GJ. Bile acids up-regulate death receptor 5/TRAIL-receptor 2 expression via a c-Jun N-terminal kinase-dependent pathway involving Sp1. J Biol Chem 2004;279:51–60.
42. Chen D, Chan R, Waxman S, Jing Y. Buthionine sulfoximine enhancement of arsenic trioxide-induced apoptosis in leukemia and lymphoma cells is mediated via activation of c-Jun NH2-terminal kinase and up-regulation of death receptors. Cancer Res 2006;66:11416–23.
43. Nawrocki ST, Carew JS, Pino MS, et al. Bortezomib sensitizes pancreatic cancer cells to endoplasmic reticulum stress-mediated apoptosis. Cancer Res 2005;65:11658–66.
44. Fribley A, Zeng Q, Wang CY. Proteasome inhibitor PS-341 induces apoptosis through induction of endoplasmic reticulum stress-reactive oxygen species in head and neck squamous cell carcinoma cells. Mol Cell Biol 2004;24:9695–704.
45. Yamaguchi H, Wang HG. CHOP is involved in endoplasmic reticulum stress-induced apoptosis by enhancing DR5 expression in human carcinoma cells. J Biol Chem 2004;279:45495–502.
46. Kim Y, Suh N, Sporn M, Reed JC. An inducible pathway for degradation of FLIP protein sensitizes tumor cells to TRAIL-induced apoptosis. J Biol Chem 2002;277:22320–9.
47. Poukkula M, Kaunisto A, Hietakangas V, et al. Rapid turnover of c-FLIPshort is determined by its unique C-terminal tail. J Biol Chem 2005;280:27345–55.
48. Ganten TM, Koschny R, Haas TL, et al. Proteasome inhibition sensitizes hepatocellular carcinoma cells, but not human hepatocytes, to TRAIL. Hepatology 2005;42:588–97.
49. Zhao J, Tenev T, Martins LM, Downward J, Lemoine NR. The ubiquitin-proteasome pathway regulates survivin degradation in a cell cycle-dependent manner. J Cell Sci 2000;113 Pt 23:4363–71.
50. Ichikawa K, Liu W, Zhao L, et al. Tumoricidal activity of a novel anti-human DR5 monoclonal antibody without hepatocyte cytotoxicity. Nat Med 2001;7:954–60.

DOI:10.1158/0008-5472.CAN-06-2471

Cancer Research

Cellular FLICE-Inhibitory Protein Down-regulation Contributes to Celecoxib-Induced Apoptosis in Human Lung Cancer Cells

Xiangguo Liu, Ping Yue, Axel H. Schönthal, et al.

Cancer Res 2006;66:11115-11119. Published online December 4, 2006.

DOI:10.1158/0008-5472.CAN-06-2471

Cellular FLICE-Inhibitory Protein Down-regulation Contributes to Celecoxib-Induced Apoptosis in Human Lung Cancer Cells

Xiangguo Liu,[1] Ping Yue,[1] Axel H. Schönthal,[2] Fadlo R. Khuri,[1] and Shi-Yong Sun[1]

[1]Department of Hematology and Oncology, Winship Cancer Institute, Emory University School of Medicine, Atlanta, Georgia and
[2]Department of Molecular Microbiology and Immunology, University of Southern California, Los Angeles, California

Abstract

The cyclooxygenase-2 (COX-2) inhibitor celecoxib is an approved drug in the clinic for colon cancer chemoprevention and has been tested for its chemopreventive and therapeutic efficacy in various clinical trials. Celecoxib induces apoptosis in a variety of human cancer cells including lung cancer cells. Our previous work has shown that celecoxib induces death receptor 5 expression, resulting in induction of apoptosis and enhancement of tumor necrosis factor–related apoptosis-inducing ligand (TRAIL)–induced apoptosis in human lung cancer cells. In the current study, we further show that celecoxib down-regulated the expression of cellular FLICE-inhibitory protein (c-FLIP), a major negative regulator of the death receptor–mediated extrinsic apoptotic pathway, through a ubiquitin/proteasome–dependent mechanism independent of COX-2 in human lung cancer cells. Overexpression of c-FLIP, particularly $FLIP_L$, inhibited not only celecoxib-induced apoptosis but also apoptosis induced by the combination of celecoxib and TRAIL. These results thus indicate that c-FLIP down-regulation also contributes to celecoxib-induced apoptosis and enhancement of TRAIL-induced apoptosis, which complements our previous finding that the extrinsic apoptotic pathway plays a critical role in celecoxib-induced apoptosis in human lung cancer cells. Collectively, we conclude that celecoxib induces apoptosis in human lung cancer cells through activation of the extrinsic apoptotic pathway, primarily by induction of death receptor 5 and down-regulation of c-FLIP. (Cancer Res 2006; 66(23): 11115-9)

Introduction

Celecoxib, a marketed anti-inflammatory and anti-pain drug, is being tested in clinical trials for its chemopreventive and therapeutic effects against a broad spectrum of epithelial malignancies, including lung cancers, either as a single agent or in combination with other agents. The antitumor activity of celecoxib is thought to be associated with its ability to induce apoptosis in a variety of cancer cells (1). The molecular mechanism underlying celecoxib-mediated apoptosis remains largely uncharacterized, although it seems to be associated with inactivation of Akt, induction of endoplasmic reticulum stress involving up-regulation of CCAAT/enhancer-binding protein-homologous protein (CHOP)/GADD153 and increase in Ca^{2+} levels, or down-regulation of the antiapoptotic protein survivin (2). There are two major apoptotic pathways: the extrinsic death receptor–mediated pathway and the intrinsic mitochondria-mediated pathway, with truncated Bid protein accounting for the cross-talk between the two pathways (3). Our previous results have shown that celecoxib induces apoptosis in non–small-cell lung cancer cell lines primarily through the activation of the extrinsic death receptor pathway (4).

The cellular FLICE-inhibitory protein (c-FLIP) plays a key role in negatively regulating the extrinsic apoptotic pathway through inhibition of caspase-8 activation (5). c-FLIP has multiple splice variants, and two main forms have been well characterized: c-FLIP short form (c-$FLIP_S$) and long form (c-$FLIP_L$; ref. 5). It has been well documented that elevated c-FLIP expression protects cells from death receptor–mediated apoptosis, whereas down-regulation of c-FLIP by chemicals or small interfering RNA (siRNA) sensitizes cells to death receptor–mediated apoptosis (5). Moreover, overexpression of c-FLIP also protects cells from apoptosis induced by cancer therapeutic agents such as etoposide and cisplatin (6–8). In the present study, we show for the first time that celecoxib, in addition to up-regulating death receptor 5, down-regulates c-FLIP expression, which contributes to celecoxib-induced apoptosis in non–small-cell lung cancer cells. This further confirms and expands our previous finding that celecoxib induces apoptosis in non–small-cell lung cancer cell lines primarily through the activation of the extrinsic death receptor pathway (4).

Materials and Methods

Reagents. Celecoxib, other nonsteroidal anti-inflammatory drugs, and antibodies against caspases were the same as previously described (4). 2,5-Dimethyl-celecoxib was synthesized as previously described (9). Human recombinant tumor necrosis factor–related apoptosis-inducing ligand (TRAIL) was purchased from PeproTech, Inc. (Rocky Hill, NJ). Mouse monoclonal anti-FLIP antibody (NF6) was purchased from Alexis Biochemicals (San Diego, CA). MG132 and SP600125 were purchased from Sigma Chemicals (St. Louis, MO) and Biomol (Plymouth Meeting, PA), respectively.

Cell lines and cell culture. The human non–small-cell lung cancer cell lines used in this study were purchased from the American Type Culture Collection (Manassas, VA) and cultured as previously described (4). H157-V and H157-AS cell lines, in which retroviral vector and antisense cyclooxygenase-2 (COX-2) were stably transfected, respectively (10), were kindly provided by Dr. S.M. Dubinett.

Western blot analysis. Preparation of whole-cell protein lysates and the procedures for the Western blotting were previously described (4).

Immunoprecipitation. A549-$FLIP_L$-2 cells, which stably express $FLIP_L$, were transfected with hemagglutinin-ubiquitin plasmid using FuGENE 6 transfection reagent (Roche Diagnostics Corp., Indianapolis, IN) following the manufacturer's instruction. After 24 hours, the cells were treated with celecoxib or MG132 plus celecoxib for 4 hours and then were lysed for immunoprecipitation of Flag-$FLIP_L$ with Flag M2 monoclonal antibody (Sigma Chemicals) as previously described (11), followed by the detection of ubiquitinated $FLIP_L$ by Western blotting with antihemagglutinin antibody (Abgent, San Diego, CA).

Note: Supplementary data for this article are available at Cancer Research Online (http://cancerres.aacrjournals.org/).

F.R. Khuri and S-Y. Sun are Georgia Cancer Coalition Distinguished Cancer Scholars.

Requests for reprints: Shi-Yong Sun, Winship Cancer Institute, Emory University School of Medicine, 1365-C Clifton Road Northeast, C3088, Atlanta, GA 30322. Phone: 404-778-2170; Fax: 404-778-5520; E-mail: shi-yong.sun@emoryhealthcare.org.

doi:10.1158/0008-5472.CAN-06-2471

DOI:10.1158/0008-5472.CAN-06-2471

Silencing of COX-2 expression with siRNA. Stealth COX-2 siRNA that targets the sequence 5′-GCAGGCAGATGAAATACCAGTCTTT-3′ and Stealth control siRNA (12) were synthesized by Invitrogen (Carlsbad, CA). The transfection of siRNA was conducted as previously described (12).

Generation of lentiviral c-FLIP expression constructs and establishment of stable lines that overexpress c-FLIP. *c-FLIP$_L$* and *c-FLIP$_S$* coding regions were amplified by PCR using plasmids containing full-length cDNAs of *FLIP$_L$* and *FLIP$_S$*, respectively, which were provided by Dr. J. Tschopp. The amplified fragments were then ligated into the pT-easy vector (Promega, Madison, WI) following the manufacturer's protocol as pT-easy-FLIP$_L$ and pT-easy-FLIP$_S$, respectively, using the following primers: FLIP$_L$ sense, 5′-GACTAGTGCCGCCACCATGGATTACAAAGACGATGACG-3′; FLIP$_L$ antisense, 5′-CGGGCCCTTATGTGTAGGAGAGGATAAGTTTC-3′; FLIP$_S$ sense, 5′-GACTAGTGCCGCCACCATGTCTGCTGAAGTCATCCAT-CAGG-3′; and FLIP$_S$ antisense, 5′-CGGGCCCTCACATGGAACAATTTC-CAAG-3′. Both pLenti-DcR1 (a lentiviral vector harboring the *DcR1* gene, which was constructed using the pLenti6/V5 Directional TOPO Cloning kit purchased from Invitrogen) and pT-easy-FLIP$_L$ or pT-easy-FLIP$_S$ were cut with *Spe*I and *Apa*I restriction enzymes. The released fragment containing *c-FLIP$_L$* or *c-FLIP$_S$* gene was then cloned into the digested pLenti6/V5 vector and the resultant constructs were named pLenti-Flag-FLIP$_L$ and pLenti-FLIP$_S$, respectively. In this study, we used pLenti-LacZ as a vector control, which was included in the pLenti6/V5 Directional TOPO Cloning kit.

Lentiviral production and titer determination were previously described (12). For infection, the viruses were added to the cells at a multiplicity of infection of 10 with 10 μg/mL polybrene. For transient expression, cells were infected and then subjected to initial selection with 50 μg/mL blasticidin beginning at 24 hours after infection. Five days later, the cells were used for the given experiments. For stable expression, cell clones were picked after a 2-week selection with 50 μg/mL blasticidin postinfection and screened for FLIP expression by Western blotting with c-FLIP antibody. The clones with the highest levels of FLIP expression were used in the experiment.

Detection of apoptosis. Apoptosis was evaluated by Annexin V staining using Annexin V-PE apoptosis detection kit purchased from BD Biosciences (San Jose, CA) following the manufacturer's instructions. We also detected caspase activation by Western blotting (as described above) as an additional indicator of apoptosis.

Results and Discussion

Because c-FLIP levels are modulated by many cancer therapeutic agents, we were interested in determining whether celecoxib altered c-FLIP expression levels. Thus, we treated several non–small-cell lung cancer cell lines with increasing concentrations of celecoxib and then assessed c-FLIP levels. As presented in Fig. 1*A*, the expression levels of both FLIP$_L$ and FLIP$_S$ in these cell lines were reduced by celecoxib in a concentration-dependent manner after a 16-hour incubation. We noted that FLIP$_S$ levels were decreased after treatment with 10 μmol/L celecoxib, whereas FLIP$_L$ levels were reduced by relatively high concentrations of celecoxib (e.g., ≥25 μmol/L), suggesting that FLIP$_S$ is somewhat more sensitive to modulation by celecoxib than FLIP$_L$. The down-regulation of both FLIP$_L$ and FLIP$_S$ occurred as early as 3 hours and was sustained up to 48 hours after celecoxib treatment (Fig. 1*B*). We noted that the reduction of c-FLIP, particularly FLIP$_L$, at the late time points (e.g., 24 and 48 hours) was not as strong as that at the early time points (e.g., 3 and 6 hours). Nevertheless, these results clearly indicate that celecoxib down-regulates c-FLIP expression in human non–small-cell lung cancer cells, which represents an early event during celecoxib-induced apoptosis. We next determined whether other nonsteroidal anti-inflammatory drugs, including SC58125, NS-398, sulindac sulfide, and Dup697, down-regulated c-FLIP expression. As presented in Fig. 1*C*, these agents, particularly at 75 μmol/L, decreased the levels of both FLIP$_L$ and FLIP$_S$, albeit with weaker activity than celecoxib, which, at 50 μmol/L, effectively reduced c-FLIP levels. Thus, we conclude that other COX-2 inhibitors down-regulate c-FLIP expression as well.

c-FLIP is known to be regulated by a ubiquitin-proteasome mechanism (13, 14), and certain cancer therapeutic agents stimulate down-regulation of c-FLIP expression through this mechanism (13). To determine whether celecoxib induces proteasome-mediated c-FLIP degradation, we examined the effects of celecoxib on c-FLIP expression in the absence and presence of the proteasome inhibitor MG132 in A549 cells. As shown in Fig. 2*A*, MG132 at concentrations of ≥10 μmol/L abrogated the ability of celecoxib to reduce both FLIP$_L$ and FLIP$_S$, suggesting that celecoxib down-regulates c-FLIP through proteasome-mediated protein degradation. We also noted that MG132 alone did not increase the levels of FLIP$_L$ but strikingly increased the levels of FLIP$_S$, suggesting that FLIP$_S$ is more prone to proteasome-mediated

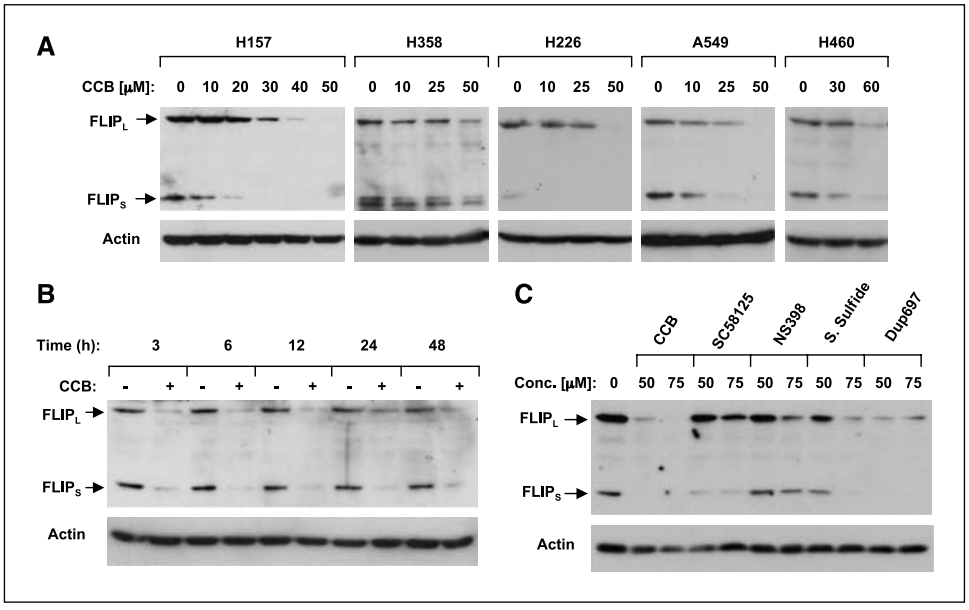

Figure 1. Down-regulation of c-FLIP expression by celecoxib (*A* and *B*) and other nonsteroidal anti-inflammatory drugs (*C*) in human non–small-cell lung cancer cells. *A,* the indicated cell lines were treated with the given concentrations of celecoxib (*CCB*) for 16 hours. *B,* H157 cells were treated with 50 μmol/L celecoxib for the indicated times. *C,* H157 cells were treated with the given concentrations of the indicated nonsteroidal anti-inflammatory drugs for 7 hours. Whole-cell protein lysates were prepared from the aforementioned treatments for detection of the given proteins using Western blot analysis, with actin serving as a loading control.

DOI:10.1158/0008-5472.CAN-06-2471

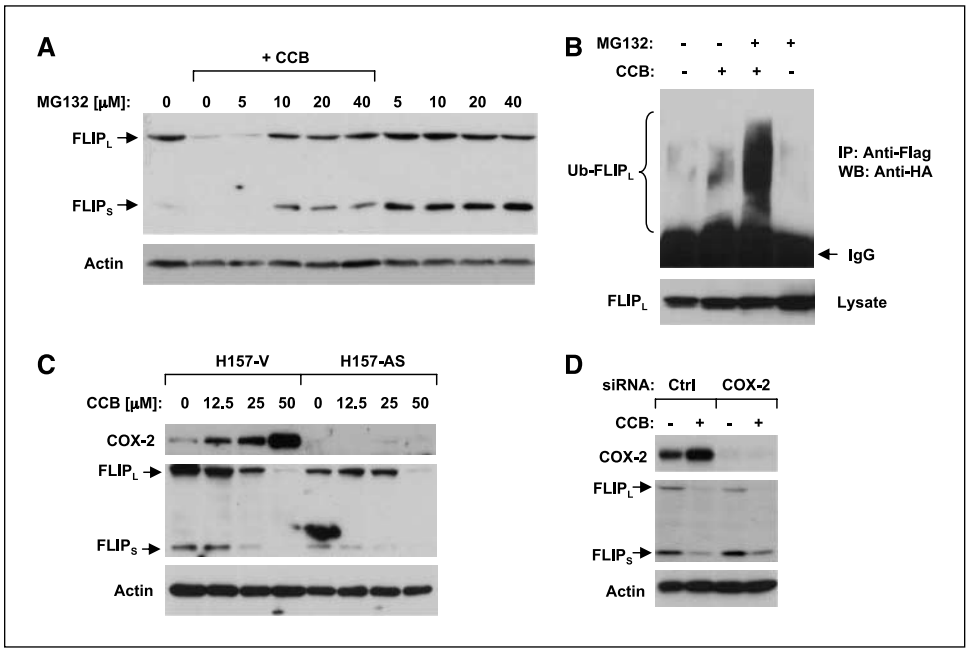

Figure 2. Celecoxib down-regulates c-FLIP through ubiquitin/proteasome–mediated protein degradation (*A* and *B*) independent of COX-2 (*C* and *D*). *A,* A549 cells were pretreated with the indicated concentrations of MG132 for 30 minutes and then cotreated with 50 μmol/L celecoxib (CCB) for another 4 hours. *B,* A549-FLIP$_L$-2 cells were transfected with hemagglutinin-ubiquitin plasmid using FuGENE 6 transfection reagent for 24 hours. The cells were then pretreated with 20 μmol/L MG132 for 30 minutes and then cotreated with 50 μmol/L celecoxib for 4 hours. *C,* H157-V (vector-control) and H157-AS (antisense COX-2) paired cell lines were treated with the given concentrations of celecoxib for 16 hours. *D,* A549 cells were transfected with control (*Ctrl*) or COX-2 siRNA for 48 hours and then treated with 50 μmol/L celecoxib for 16 hours. Whole-cell protein lysates were then prepared from the aforementioned treatments for detection of the given proteins by Western blot analysis (*A, C*, and *D*), with actin serving as the loading control, or immunoprecipitation (*IP*) with antihemagglutinin antibody followed by Western blotting (*WB*) for detection of ubiquitinated FLIP$_L$ (*Ub-FLIP$_L$*; *B*).

degradation, which is consistent to the recent findings by Poukkula et al. (14). Moreover, we examined the effects of celecoxib on overall proteasome activity and c-FLIP ubiquitination. Celecoxib did not increase proteasome activity (data not shown). However, it increased the levels of ubiquitinated c-FLIP, particularly in the presence of MG132 (Fig. 2*B*), indicating that celecoxib increases c-FLIP ubiquitination. Collectively, we suggest that celecoxib down-regulates c-FLIP levels through a ubiquitin-proteasome mechanism.

A recent study has shown that c-jun NH_2-terminal kinase (JNK) activation modulates FLIP$_L$ degradation (15). We then determined whether celecoxib down-regulates c-FLIP through a JNK-dependent mechanism. Celecoxib indeed increased the levels of phosphorylated c-Jun (p-c-Jun), an indicator of JNK activation, and decreased the levels of both FLIP$_L$ and FLIP$_S$. The JNK inhibitor SP600125 at concentrations up to 30 μmol/L abrogated celecoxib-induced c-Jun phosphorylation, but failed to block down-regulation of either FLIP$_L$ or FLIP$_S$ by celecoxib (Supplementary Fig. S1). Considering these findings and the fact that JNK does not modulate FLIP$_S$ turnover (15) whereas celecoxib down-regulates the levels of both FLIP$_L$ and FLIP$_S$ (Fig. 1), we conclude that celecoxib induces a JNK-independent degradation of c-FLIP.

It is well known that celecoxib is a specific COX-2 inhibitor. However, many studies show that celecoxib induces apoptosis independent of COX-2 inhibitory activity (2). To determine whether celecoxib decreases c-FLIP levels through its COX-2 inhibitory activity, we compared the modulatory effects of celecoxib on c-FLIP between H157 cells stably transfected with a retroviral vector harboring antisense COX-2 (H157-AS) and vector control cells (H157-V). As shown in Fig. 2*C*, the basal levels of COX-2 in H157 cell were reduced compared with H157-V cells. Interestingly, we found that celecoxib, albeit a COX-2 inhibitor, actually increased COX-2 protein levels in a concentration-dependent manner in H157-V cells; this effect was abolished in H157-AS cells. Together, these results validate the cell system in which COX-2 expression is inhibited due to the expression of antisense COX-2. In both cell lines, celecoxib still effectively reduced levels of FLIP$_L$ and FLIP$_S$, indicating that celecoxib modulates c-FLIP levels regardless of the presence of COX-2. Some nonsteroidal anti-inflammatory drugs were reported to induce COX-2 expression (16, 17). However, the inducing effect of celecoxib on COX-2 expression has not been reported. Currently, it is unclear what the implications of COX-2 induction are in celecoxib-mediated anticancer activity.

Moreover, we used siRNA to knockdown COX-2 expression in A549 cells and then examined its effect on celecoxib-induced c-FLIP down-regulation. Transfection of COX-2 siRNA inhibited not only the basal levels of COX-2 but also celecoxib-mediated COX-2 induction. However, it did not alter the effect of celecoxib on reduction of c-FLIP (Fig. 2*D*), furthering the notion that celecoxib down-regulates c-FLIP expression levels irrespective of COX-2 expression. In addition, we examined the effect of 2,5-dimethyl-celecoxib, a derivative of celecoxib completely lacking COX-2 inhibitory activity (9), on c-FLIP expression and found that 2,5-dimethyl-celecoxib still decreased c-FLIP levels, albeit with more potency than celecoxib (Supplementary Fig. S2). This result again suggests that celecoxib reduces c-FLIP levels independent of its COX-2-inhibitory activity. Collectively, we conclude that celecoxib down-regulates c-FLIP expression independent of COX-2.

To determine the involvement of c-FLIP down-regulation in celecoxib-induced apoptosis, we used a lentiviral expression system to enforce expression of c-FLIP in non–small-cell lung cancer cell lines and then analyzed its effect on celecoxib-induced caspase activation and apoptosis. Taking advantage of a lentiviral expression system that can achieve both transient and stable gene expression, we first transiently expressed FLIP$_L$ or FLIP$_S$ in H1792 cells. By Western blotting, we could detect high levels of ectopic FLIP$_L$ or FLIP$_S$ (Fig. 3*A*). Celecoxib induced cleavage of caspase-8, caspase-3, and poly(ADP-ribose) polymerase in lacZ-infected control cells, evidenced by the decrease in the levels of their proforms and the increase in the amounts of their cleaved bands. However, these effects were inhibited or diminished in cells infected with c-FLIP, particularly FLIP$_L$ (Fig. 3*A*). Consistently, we detected 34% apoptotic cells in lacZ-infected cells, but only 17% and 26% apoptosis in cells infected with FLIP$_L$ and FLIP$_S$,

DOI:10.1158/0008-5472.CAN-06-2471

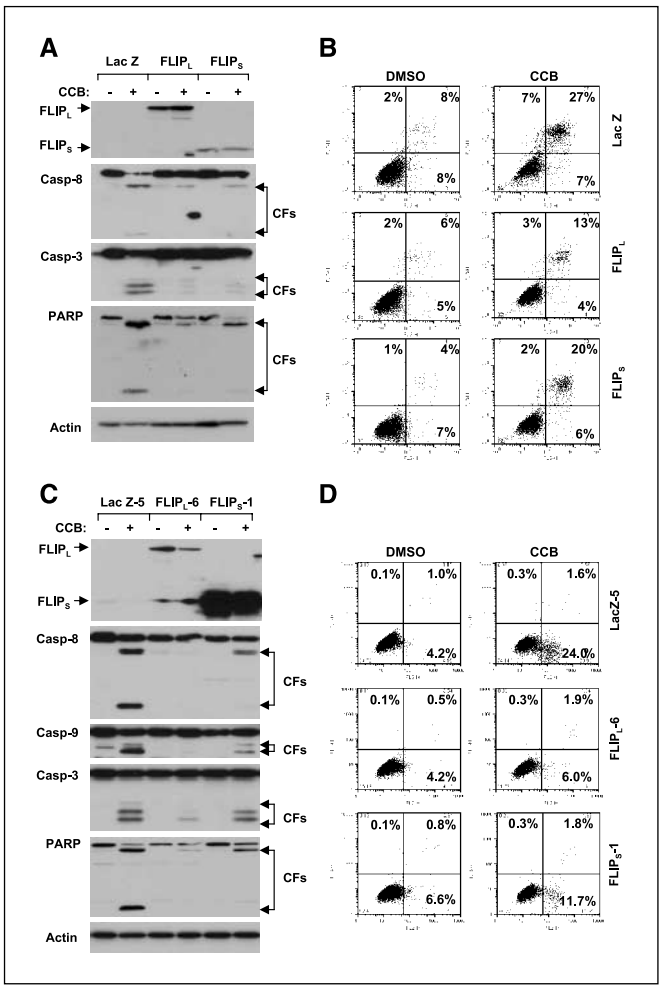

Figure 3. Both transient (*A* and *B*) and stable (*C* and *D*) overexpression of exogenous c-FLIP protect cells from celecoxib-induced caspase activation (*A* and *C*) and apoptosis (*B* and *D*) in human lung cancer cell lines. *A* and *B,* H1792 cells were infected with lentiviruses carrying lacZ, FLIP$_L$, and FLIP$_S$. After a brief selection with blasticidin for 5 days, the cells were treated with DMSO or 50 μmol/L celecoxib (CCB). Twenty-four hours later, the cells were subjected to preparation of whole-cell protein lysates and subsequent Western blot analysis for detection of caspase activation (*A*) or harvested for detection of apoptosis by Annexin V staining-flow cytometry (*B*). *C* and *D,* H157 stable transfectants expressing lacZ, FLIP$_L$, and FLIP$_S$ were treated with DMSO or 50 μmol/L celecoxib. Twenty-four hours later, the cells were subjected to preparation of whole-cell protein lysates and subsequent Western blot analysis for detection of caspase activation (*C*) or harvested for detection of apoptosis by Annexin V staining-flow cytometry (*D*). *CFs,* cleaved forms. Note that the endogenous levels of FLIP$_L$ and FLIP$_S$ proteins are not visible in these Western blots due to the short exposure times required to visualize the highly overexpressed exogenous forms of these proteins. In the Annexin V staining assay, the percent positive cells in the top right and bottom right quadrants were added to yield the total of apoptotic cells.

respectively, by Annexin V staining (Fig. 3*B*). Thus, these results show partial protective effects of c-FLIP, particularly FLIP$_L$, on celecoxib-induced apoptosis.

Following this study, we further established stable cell lines from H157 cells that expressed ectopic FLIP$_L$ or FLIP$_S$ and examined their responses to celecoxib-induced apoptosis. By Western blot analysis, we detected the expression of ectopic FLIP$_L$ and FLIP$_S$ in H157-FLIP$_L$-6 and H157-FLIP$_S$-1 transfectants, respectively (Fig. 3*C*), indicating the successful expression of ectopic FLIP$_L$ or FLIP$_S$ in H157 cells. Celecoxib treatment strongly increased amounts of cleaved forms of caspase-8, caspase-9, caspase-3, and poly(ADP-ribose) polymerase in the control H157-lacZ-5 cells; however, these effects were abrogated or diminished in either H157-FLIP$_L$-6 or H157-FLIP$_S$-1 cells. Accordingly, celecoxib caused 25.6% apoptosis in H157-lacZ-5 cells, but only 7.9% and 13.5% apoptosis in H157-FLIP$_L$-6 and H157-FLIP$_S$-1 transfectants, respectively (Fig. 3*D*). These results thus indicate that stable overexpression of c-FLIP, particularly, FLIP$_L$, protects cells from celecoxib-induced apoptosis. Taken together, we conclude that down-regulation of c-FLIP contributes to celecoxib-induced apoptosis. Because c-FLIP is a key regulatory protein that inhibits death receptor–mediated apoptosis (5), these findings further support our notion that the extrinsic apoptotic pathway plays a important role in celecoxib-induced apoptosis, at least in human non–small-cell lung cancer cells as previously shown (4). In agreement with our finding, a recent study has shown that celecoxib activates the death receptor–mediated apoptosis in hepatocellular carcinoma cells (18).

We previously reported that celecoxib in combination with TRAIL augmented the induction of apoptosis in human non–small-cell lung cancer cells (4). To determine whether down-regulation of c-FLIP also contributes to synergy between celecoxib and TRAIL on apoptosis induction, we examined the effects of enforced overexpression of c-FLIP on celecoxib-mediated enhancement of TRAIL-induced apoptosis in two non–small-cell lung cancer cell lines. To this end, we further established H460 transfectants that overexpressed ectopic FLIP$_L$ and FLIP$_S$ (Fig. 4*A*), in addition to the aforementioned H157 cells. In the two tested cell lines (i.e., H157 and H460), the combination of celecoxib and TRAIL induced more than additive effects on induction of apoptosis compared with each single agent in lacZ-infected control cells evaluated by Annexin V staining; however, these effects were either abrogated or

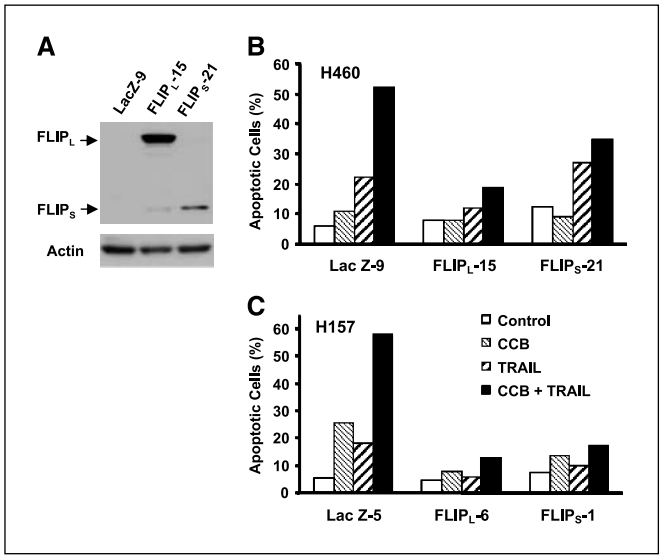

Figure 4. Overexpression of exogenous c-FLIP protects cells from induction of apoptosis by the combination of celecoxib (CCB) and TRAIL in H460 (*A* and *B*) and H157 (*C*) human lung cancer cell lines. *A* and *B,* the indicated H460 stable transfectants were treated with DMSO, 50 μmol/L celecoxib alone, 3 ng/mL TRAIL alone, or celecoxib and TRAIL combination for 24 hours (*B*). The expression of ectopic FLIP$_L$ and FLIP$_S$ was detected by Western blot analysis (*A*). *C,* the indicated H157 stable transfectants expressing lacZ, FLIP$_L$, and FLIP$_S$, as shown in Fig. 3, were treated with DMSO, 50 μmol/L celecoxib alone, 4 ng/mL TRAIL alone, or celecoxib and TRAIL combination for 24 hours. At the end of the aforementioned treatments (*B* and *C*), the cells were harvested for detection of apoptosis by Annexin V staining-flow cytometry.

DOI:10.1158/0008-5472.CAN-06-2471

inhibited in cells overexpressing c-FLIP, particularly $FLIP_L$ (Fig. 4*B* and *C*). For example, the combination of celecoxib and TRAIL caused ~58% apoptosis in H157-lacZ-5 cells, but only 13% apoptosis in H157-$FLIP_L$-6 cells and 17% apoptosis in H157-$FLIP_S$-1 cells (Fig. 4*C*). Thus, these results collectively show that down-regulation of c-FLIP also contributes to celecoxib-mediated enhancement of TRAIL-induced apoptosis.

We noted that the concentrations (≥10 μmol/L) required for celecoxib to down-regulate c-FLIP are higher than clinically achievable peak plasma concentrations (3.2-5.6 μmol/L) of celecoxib in humans after oral administration of a single dose of 800 mg (19). Given that celecoxib has been developed and marketed mainly for treatment of arthritis and pain, but not primarily for anticancer purposes, it is conceivable that this drug might be suboptimal for inclusion in the therapy of advanced cancers, such as non–small-cell lung cancer cells. In this regard, it might be beneficial to consider streamlined celecoxib derivatives that are optimized for anticancer applications, and some promising efforts have indeed been made in this direction. Certain novel non-COX-2 inhibitory celecoxib derivatives show better activity than celecoxib in inducing apoptosis and inhibiting the growth of tumors (9, 20), further emphasizing the need to explore and understand the underlying molecular mechanisms by which these drugs exert their proapoptotic, antitumor potential. In this regard, our finding that celecoxib and its COX-2-inactive derivative 2,5-dimethyl-celecoxib down-regulate c-FLIP provides a novel aspect of this process and is important for understanding the molecular mechanisms by which these drugs induce apoptosis. We noted that 2,5-dimethyl-celecoxib, which is more potent than celecoxib in down-regulating c-FLIP, was also more potent than celecoxib in decreasing cell survival and inducing apoptosis in human non–small-cell lung cancer cells,[3] suggesting that there is a inverse relationship between down-regulation of c-FLIP and induction of apoptosis by celecoxib and its derivatives. Therefore, we may consider modulation of c-FLIP as a screening tool for the development of novel celecoxib derivatives with better anticancer efficacy.

In conclusion, the present study shows for the first time that celecoxib down-regulates c-FLIP expression in human non–small-cell lung cancer cells; this down-regulation accounts for celecoxib-mediated induction of apoptosis and enhancement of TRAIL-induced apoptosis. These results complement our previous finding that the death receptor–mediated extrinsic apoptotic pathway plays a critical role in celecoxib-induced apoptosis in human lung cancer cells.

Acknowledgments

Received 7/7/2006; revised 9/27/2006; accepted 10/20/2006.

Grant support: Winship Cancer Institute faculty start-up research fund (S-Y. Sun), the Georgia Cancer Coalition Distinguished Cancer Scholar award (S-Y. Sun), and Department of Defense VITAL grant W81XWH-04-1-0142 (S-Y. Sun for Project 4).

The costs of publication of this article were defrayed in part by the payment of page charges. This article must therefore be hereby marked *advertisement* in accordance with 18 U.S.C. Section 1734 solely to indicate this fact.

We thank Dr. Steven M. Dubinett (University of California at Los Angeles, Los Angeles, CA) for providing cell lines expressing antisense COX-2, Dr. Jürg Tschopp (University of Lausanne, Lausanne, Switzerland) for c-FLIP cDNAs, and Dr. Ceshi Chen (Albany Medical College, Albany, NY) for hemagglutinin-ubiquitin plasmid.

[3] Our unpublished data.

References

1. Thun MJ, Henley SJ, Patrono C. Nonsteroidal anti-inflammatory drugs as anticancer agents: mechanistic, pharmacologic, and clinical issues. J Natl Cancer Inst 2002;94:252–66.
2. Schonthal AH. Antitumor properties of dimethyl-celecoxib, a derivative of celecoxib that does not inhibit cyclooxygenase-2: implications for glioma therapy. Neurosurg Focus 2006;20:E21.
3. Hengartner MO. The biochemistry of apoptosis. Nature 2000;407:770–6.
4. Liu X, Yue P, Zhou Z, Khuri FR, Sun SY. Death receptor regulation and celecoxib-induced apoptosis in human lung cancer cells. J Natl Cancer Inst 2004;96:1769–80.
5. Wajant H. Targeting the FLICE inhibitory protein (FLIP) in cancer therapy. Mol Interv 2003;3:124–7.
6. Kamarajan P, Sun NK, Chao CC. Up-regulation of FLIP in cisplatin-selected HeLa cells causes cross-resistance to CD95/Fas death signalling. Biochem J 2003;376:253–60.
7. Longley DB, Wilson TR, McEwan M, et al. c-FLIP inhibits chemotherapy-induced colorectal cancer cell death. Oncogene 2006;25:838–48.
8. Abedini MR, Qiu Q, Yan X, Tsang BK. Possible role of FLICE-like inhibitory protein (FLIP) in chemo-resistant ovarian cancer cells *in vitro*. Oncogene 2004; 23:6997–7004.
9. Kardosh A, Wang W, Uddin J, et al. Dimethyl-celecoxib (DMC), a derivative of celecoxib that lacks cyclooxygenase-2-inhibitory function, potently mimics the anti-tumor effects of celecoxib on Burkitt's lymphoma *in vitro* and *in vivo*. Cancer Biol Ther 2005; 4:571–82.
10. Dohadwala M, Luo J, Zhu L, et al. Non-small cell lung cancer cyclooxygenase-2-dependent invasion is mediated by CD44. J Biol Chem 2001;276:20809–12.
11. Chen C, Sun X, Ran Q, et al. Ubiquitin-proteasome degradation of KLF5 transcription factor in cancer and untransformed epithelial cells. Oncogene 2005;24: 3319–27.
12. Liu X, Yue P, Khuri FR, Sun SY. Decoy receptor 2 (DcR2) is a p53 target gene and regulates chemosensitivity. Cancer Res 2005;65:9169–75.
13. Kim Y, Suh N, Sporn M, Reed JC. An inducible pathway for degradation of FLIP protein sensitizes tumor cells to TRAIL-induced apoptosis. J Biol Chem 2002;277:22320–9.
14. Poukkula M, Kaunisto A, Hietakangas V, et al. Rapid turnover of c-FLIPshort is determined by its unique C-terminal tail. J Biol Chem 2005;280:27345–55.
15. Chang L, Kamata H, Solinas G, et al. The E3 ubiquitin ligase itch couples JNK activation to TNFα-induced cell death by inducing c-FLIP(L) turnover. Cell 2006;124: 601–13.
16. Paik JH, Ju JH, Lee JY, Boudreau MD, Hwang DH. Two opposing effects of non-steroidal anti-inflammatory drugs on the expression of the inducible cyclooxygenase. Mediation through different signaling pathways. J Biol Chem 2000;275:28173–9.
17. Pang L, Nie M, Corbett L, Knox AJ. Cyclooxygenase-2 expression by nonsteroidal anti-inflammatory drugs in human airway smooth muscle cells: role of peroxisome proliferator-activated receptors. J Immunol 2003;170: 1043–51.
18. Kern MA, Haugg AM, Koch AF, et al. Cyclooxygenase-2 inhibition induces apoptosis signaling via death receptors and mitochondria in hepatocellular carcinoma. Cancer Res 2006;66:7059–66.
19. Niederberger E, Tegeder I, Vetter G, et al. Celecoxib loses its anti-inflammatory efficacy at high doses through activation of NF-κB. FASEB J 2001;15:1622–4.
20. Zhu J, Song X, Lin HP, et al. Using cyclooxygenase-2 inhibitors as molecular platforms to develop a new class of apoptosis-inducing agents. J Natl Cancer Inst 2002;94: 1745–57.

Death Receptor Regulation and Celecoxib-Induced Apoptosis in Human Lung Cancer Cells

Xiangguo Liu, Ping Yue, Zhongmei Zhou, Fadlo R. Khuri, Shi-Yong Sun

Background: **Celecoxib, a cyclooxygenase 2 inhibitor, has chemopreventive and therapeutic activities toward lung cancer and other epithelial malignancies. Celecoxib can induce apoptosis in various cancer cell lines through a mechanism that is independent of its cyclooxygenase 2 inhibitory activity but is otherwise largely uncharacterized. We investigated the mechanism of celecoxib-induced apoptosis further.** ***Methods:*** **All experiments were conducted in human non-small-cell lung carcinoma (NSCLC) cell lines; results in celecoxib-treated and untreated cells were compared. Cell survival was assessed with a sulforhodamine B assay. Apoptosis was assessed by DNA fragmentation with an enzyme-linked immunosorbent assay, by terminal deoxynucleotidyltransferase-mediated dUTP nick-end-labeling (TUNEL) assay, and by western blot analysis of caspase activation. Death receptor gene and protein expression was detected by northern and western blot analysis, respectively. Gene silencing was achieved with small interfering RNA (siRNA) technology.** ***Results:*** **Celecoxib treatment decreased cell survival, activated caspase cascades, and increased DNA fragmentation, all of which were abrogated when caspase 8 expression was silenced with caspase 8 siRNA. Celecoxib treatment induced the expression of death receptors, particularly that of DR5. Overexpression of a dominant negative Fas-associated death domain mutant, but not of BCL2, reduced the level of celecoxib-induced apoptosis, and silencing of DR5 expression by DR5 siRNA suppressed celecoxib-induced caspase 8 activation and apoptosis. Combination treatment with celecoxib and tumor necrosis factor-related apoptosis-inducing ligand (TRAIL) induced additional apoptosis. For example, survival of A549 cells was decreased with 50 μM celecoxib alone by 38.7% (95% confidence interval [CI] = 35.2% to 42.2%), with TRAIL alone by 29.3% (95% CI = 25.1% to 33.6%), but with their combination by 77.5% (95% CI = 74.5% to 79.5%), a greater than additive effect.** ***Conclusion:*** **Celecoxib appears to induce apoptosis in human NSCLC through the extrinsic death receptor pathway. [J Natl Cancer Inst 2004;96:1769–80]**

Affiliation of authors: Winship Cancer Institute, Emory University School of Medicine, Atlanta, GA.

Correspondence to: Shi-Yong Sun, PhD, Winship Cancer Institute, Emory University School of Medicine, 1365-C Clifton Rd., C3088, Atlanta, GA 30322 (e-mail: shi-yong_sun@emoryhealthcare.org).

See "Notes" following "References."

DOI: 10.1093/jnci/djh322

Celecoxib was the first cyclooxygenase 2–selective nonsteroidal anti-inflammatory drug (NSAID) approved for the treatment of adult arthritis. Celecoxib exerts potent chemopreventive activity in chemical carcinogen–induced colon, bladder, and breast carcinogenesis *(1–4)* and UV-induced skin carcinogenesis *(5,6).* Celecoxib also effectively inhibits the growth of colon and breast cancer xenograft tumors in nude mice *(7–9)* and is a clinically effective chemoprevention agent for colon cancer *(10).* The U.S. Food and Drug Administration (FDA) has approved the use of celecoxib for the adjuvant treatment of familial adenomatous polyposis, an inherited syndrome that predisposes individuals to colon cancer. Currently, celecoxib is being tested in clinical trials for its chemopreventive or therapeutic activity against various cancers, including lung cancer, as a single agent or in combination with other agents.

Although celecoxib is a cyclooxygenase 2 inhibitor, it has been found to have antitumor activity in tumor cells and tissues that lack the cyclooxygenase 2 enzyme *(7–9,11,12).* Therefore, celecoxib appears to exert its chemopreventive and therapeutic activity through a mechanism that is independent of its cyclooxygenase 2 inhibitory activity. Celecoxib induces apoptosis in various cell types *(7,11–18),* and this activity may account for its chemopreventive and therapeutic activity *(19,20).* However, the mechanisms by which celecoxib induces apoptosis remain largely uncharacterized, although celecoxib-induced apoptosis appears to be associated with inactivation of the protein kinase Akt in prostate, colon, and liver cancer cells *(11,14,21)* and with inhibition of endoplasmic reticulum Ca^{2+}-ATPases in prostate cancer cells *(22).* Although celecoxib induces apoptosis when BCL2 is overexpressed *(11,17),* Jendrossek et al. *(17)* reported that celecoxib induced mitochondria-mediated apoptosis independent of the death receptor pathway in Jurkat T cells.

There are two major apoptotic signaling pathways, the intrinsic mitochondria-mediated pathway and the extrinsic death receptor–induced pathway, and cross-talk between these pathways is mediated by the truncation of the proapoptotic protein Bid *(23).* Steps in the intrinsic pathway include cytochrome *c* release from mitochondria, caspase 9 activation, and then activation of effector caspases, including caspase 3. Steps in the extrinsic pathway include the Fas-associated death domain (FADD)-dependent recruitment and activation of caspase 8 and/or caspase 10, triggered by the binding of a death receptor ligand to its death receptor, and then activation of the same effector caspases involved in the intrinsic pathway. The antiapoptotic molecules BCL2 and BCL-XL inhibit the intrinsic pathway by preventing cytochrome *c* release from mitochondria. Many chemicals or small molecules induce apoptosis through the intrinsic pathway *(24),* but other small molecules, including NSAIDs, induce apoptosis through the extrinsic pathway by increasing the expression of death ligands *(25)* or death receptors *(26,27).*

The importance of death receptors in NSAID-induced apoptosis has been described previously. Han et al. *(27)* reported that the NSAIDs indomethacin and sulindac activate caspase 8 and apoptosis by a FADD-dependent mechanism in Jurkat T cells. Huang et al. *(26)* found that sulindac induces DR5 expression in human prostate and colon cancer cells and that DR5 expression then contributes to sulindac-induced apoptosis.

Tumor necrosis factor–related apoptosis-inducing ligand (TRAIL, also called APO-2L) is a member of the tumor necrosis factor family that appears to induce apoptosis in a wide variety of transformed cells but does not appear to induce apoptosis in normal cells *(28,29).* TRAIL appears to be a tumor-selective, apoptosis-inducing cytokine and may be a potential agent for cancer treatment. TRAIL induces apoptosis by binding to one of the two death domain–containing receptors—DR4 (also called TRAIL receptor 1) and DR5 (also called TRAIL receptor 2). TRAIL can also bind to the decoy receptors DcR1 (also called TRAIL-R3) and DcR2 (also called TRAIL-R4), but these receptors contain either no cytoplasmic death domain or a truncated death domain and so cannot transmit a signal to induce apoptosis. Because DcR1 and DcR2 can compete with DR4 and DR5 for TRAIL binding, they act to inhibit TRAIL-induced apoptosis *(28,29).* TRAIL induces apoptosis by binding to its cognate death receptors (i.e., DR4 or DR5), which then recruit caspase 8 via the FADD. Activated caspase 8 then directly activates caspases 3, 6, and 7 or activates the intrinsic mitochondria-mediated pathway through caspase 8–mediated Bid cleavage, which indirectly activates caspases 3, 6, and 7 *(28,29).*

Both DR5 and DR4 are target genes of p53 *(30–33),* but they can also be regulated through p53-independent mechanisms *(34–36).* Therefore, drug-induced expression of DR5 and DR4 can be either p53-dependent or p53-independent. It has been reported that the NSAID sulindac induces DR5 expression in human colon and prostate cancer cells in an apparently p53-independent manner *(26).* In general, agents that increase the expression of TRAIL death receptors are able to enhance TRAIL-induced apoptosis in human cancer cells *(29).*

In this study, we examined the mechanism of celecoxib-induced apoptosis in four human non-small-cell lung cancer (NSCLC) cell lines. We were particularly interested in the roles of caspase 8 activation, death receptor DR5 and DR4 expression, and TRAIL in this mechanism.

Materials and Methods

Reagents

Celecoxib was purchased from LKT Laboratories (St. Paul, MN). The cyclooxygenase 2 inhibitor NS398 was purchased from Biomol (Plymouth Meeting, PA). DUP697 (a cyclooxygenase 2 inhibitor), SC-58125 (a cyclooxygenase 2 inhibitor), sulindac sulfide (a cyclooxygenase 1 and 2 inhibitor), sulindac sulfone (a sulindac sulfide metabolite without cyclooxygenase inhibitor activity), and SC-560 (a cyclooxygenase 1 inhibitor) were purchased from Cayman Chemical (Ann Arbor, MI). Each of these compounds was dissolved in dimethyl sulfoxide (DMSO) at a concentration of 100 m*M* and stored at −80 °C. Stock solutions were diluted to the appropriate concentrations with growth medium immediately before use. Other agents were purchased from Sigma Chemical (St. Louis, MO).

Cell Lines and Cell Culture

Human NSCLC cell lines H460, A549, H358, and H1792 were purchased from the American Type Culture Collection (Manassas, VA). Among these cell lines, A549 and H358 cells express high levels of cyclooxygenase 2, whereas H460 and H1792 cells express very low levels of cyclooxygenase 2 (data not shown). H460 cells stably transfected with control vector (H460/V) and with BCL2 expression vector (H460/Bcl2-6) were described previously *(37).* These cell lines were grown in mono-

layer culture in a 1:1 mixture of Dulbecco's modified Eagle medium and Ham's F12 medium supplemented with 5% fetal bovine serum at 37 °C in a humidified atmosphere of 5% CO_2/95% air.

Generation of Stable Transfectants That Overexpress a Dominant Negative FADD Mutant

NSCLC H460 cells were transfected with the control pcDNA3 empty vector or with the vector containing the dominant negative mutant FADDm, termed pcDNA-FADD-DN *(38),* by use of FuGene 6 (Roche Molecular Biochemicals, Indianapolis, IN), in accordance with the manufacturer's instructions. After selection in culture medium containing G418 (500 μg/mL; Gibco-BRL, Rockville, MD) for 2 weeks, individual G418-resistant clones were isolated with cloning cylinders and cultured to obtain adequate numbers of cells for other experiments. Expression of the dominant negative mutant FADDm was confirmed by western blot analysis with mouse anti-FADD monoclonal antibodies (Upstate Biotechnology, Placid Lake, NY). Cells transfected with the empty vector (that expressed no FADDm) were designated H460/V1, and cells transfected with the vector containing FADDm that expressed FADDm were designated H460/Fm6 and H460/Fm16.

Cell Viability and Death Assays

Cells were cultured in 96-well cell culture plates (viability assay) or in 10-cm diameter dishes (death assay), treated on the second day with the agents indicated, and then subjected to an assay. For the cell viability assay, the viable cell number was estimated by use of the sulforhodamine B assay, as previously described *(39).* For the cell death assay, the number of cells floating in the medium were directly counted with a hemacytometer.

Apoptosis Assays

Cells were cultured in 96-well cell culture plates or in 10-cm diameter dishes and treated with test agents on the second day as indicated, and then apoptosis was assessed by use of three assays. The first assay used the presence of cytoplasmic histone-associated DNA fragments (mononucleosome and oligonucleosomes) to identify apoptotic cells by use of an enzyme-linked immunosorbent assay (Cell Death Detection $ELISA_{Plus}$ kit; Roche Molecular Biochemicals), according to the manufacturer's instructions. The second assay for apoptotic cells was the terminal deoxynucleotidyltransferase-mediated dUTP nick-end-labeling (TUNEL) assay. For this assay, cells were cultured on 10-cm diameter dishes for 1 day, then treated with agents as indicated, and harvested by trypsinization. Cells were fixed with 1% paraformaldehyde, and cytoplasmic DNA fragments with 3′-hydroxyl ends were detected with an APO-Direct TUNEL kit (Phoenix Flow Systems, San Diego, CA) by following the manufacturer's protocol. The third assay for apoptosis measured the level of activated caspase. In this assay, cells were harvested, whole cell protein lysates were prepared, and activation of caspases was assessed in the lysates by western blot analysis as described below.

Western Blot Analysis

Preparation of whole cell protein lysates and western blot analysis were as described previously *(40).* Briefly, whole cell protein lysates (50 μg) were electrophoresed through 7.5%–12% denaturing polyacrylamide slab gels, and the protein bands were transferred to a Hybond enhanced chemiluminescence (ECL) membrane (Amersham, Arlington Heights, IL) by electroblotting. The blots were probed or re-probed with the appropriate primary antibodies, blots were incubated with the secondary antibodies, and then antibody binding was detected by the ECL system (Amersham), according to the manufacturer's protocol. Mouse anti-caspase 3 and anti-DR4 monoclonal antibodies and rabbit anti-DR5 polyclonal antibody were purchased from Imgenex (San Diego, CA). Rabbit anti-caspase 9, anti-caspase 8, anti-caspase 7, anti-caspase 6, anti-poly(ADP-ribose) polymerase (PARP), anti-lamin A/C, and anti-DNA fragmentation factor 45 (DFF45) polyclonal antibodies were purchased from Cell Signaling Technology (Beverly, MA). Rabbit anti-Bid polyclonal antibody was purchased from Trevigen (Gaithersburg, MD). Mouse anti-BCL2 monoclonal antibody was purchased from Santa Cruz Technology (Santa Cruz, CA). Rabbit anti-β-actin polyclonal antibody was purchased from Sigma. Secondary antibodies, goat anti-mouse immunoglobulin G (IgG)–horseradish peroxidase conjugates and anti-rabbit IgG–horseradish peroxidase conjugates, were purchased from Bio-Rad (Hercules, CA) and Pierce Biotechnology (Rockford, IL), respectively.

Northern Blot Analysis

Total cellular RNA was prepared and loaded (30 μg of RNA per lane) onto a formaldehyde-denatured agarose gel, and RNAs were separated by electrophoresis. Northern blot analysis was performed as described previously *(39).* The probes were human DR5 cDNA (obtained from Dr. W. S. El-Deiry, The University of Pennsylvania School of Medicine, Philadelphia, PA); human DR4 cDNA (purchased from Alexis Biochemicals, San Diego, CA); and human glyceraldehyde-3-phosphate dehydrogenase (GAPDH) cDNA (purchased from Ambion, Austin, TX).

Enzyme-Linked Immunosorbent Assay (ELISA) for Detection of DR5

Cells were cultured on 10-cm dishes in culture medium supplemented with 5% fetal bovine serum and treated with celecoxib, as indicated, on the second day. After a 24-hour incubation, the level of DR5 protein was measured in cells with an ELISA kit purchased from Biosource International (Camarillo, CA), by following the manufacturer's instructions.

Silencing of Gene Expression With Small Interfering RNA

Gene silencing by small interfering RNA (siRNA) technology uses a small double-stranded RNA (i.e., the siRNA) that triggers degradation of target mRNA. Gene silencing was achieved by transfecting cells with siRNAs by use of the RNAiFect transfection reagent (Qiagen, Valencia CA), following the manufacturer's instructions. High-purity control (i.e., non-silencing) siRNA oligonucleotides that target the sequence 5′-AATTCTCCGAACGTGTCACGT-3′ were purchased from Qiagen. This scrambled sequence does not match any human genome sequence. Caspase 8 and DR5 siRNA duplexes that target the sequences 5′-AACTACCAGAAAGGTATACCT-3′ and 5′-AAGACCCTTGTGCTCGTTGTC-3′, respectively, as described previously *(41,42),* were synthesized by Qiagen. To improve gene silencing, we transfected the same cells twice with the same siRNA with a 48-hour interval between the two trans-

fections. Twenty-four hours after the second transfection, cells were re-plated in fresh medium supplemented with 5% fetal bovine serum and treated on the second day with celecoxib, as indicated. Gene silencing effects were evaluated by western blot analysis.

Statistical Analysis

The statistical significance of differences in cell survival and apoptosis (i.e., DNA fragmentation) between two groups were analyzed with two-sided unpaired Student's *t* tests when the variances were equal or with Welch's corrected *t* test when the variances were not equal, by use of Graphpad InStat 3 software (GraphPad Software, San Diego, CA). Data were examined as suggested by the same software to verify that the assumptions for use of the *t* tests held. All means and 95% confidence intervals (CIs) from triplicate or four replicate samples were calculated with Microsoft Excel software, version 5.0 (Microsoft, Seattle, WA). Results were considered to be statistically significant at $P<.01$ to account for multiple comparisons. All statistical tests were two-sided.

Results

Celecoxib, Caspase 8, and Apoptosis in Human NSCLC Cell Lines

To determine the optimal celecoxib concentration and incubation time for our experiments, we treated the following four NSCLC cell lines H358, A549, H1792, and H460 with celecoxib and examined cell survival. The survival of all four cell lines was reduced by celecoxib in a concentration-dependent manner (Fig. 1, A) when incubated for 24, 48, or 72 hours. The concentration of celecoxib that resulted in a 50% decrease in cell survival after a 48-hour incubation averaged about 30 μ*M* in these cell lines. A 48-hour incubation with celecoxib reduced cell survival more effectively than a 24-hour incubation, but a 72-hour incubation did not reduce cell survival further. To achieve biologically significant effects in the subsequent experiments, we used a celecoxib concentration of 50 μ*M* and an incubation time of not more than 48 hours.

We next examined whether celecoxib treatment activated caspase cascades in these cell lines by monitoring the cleavage

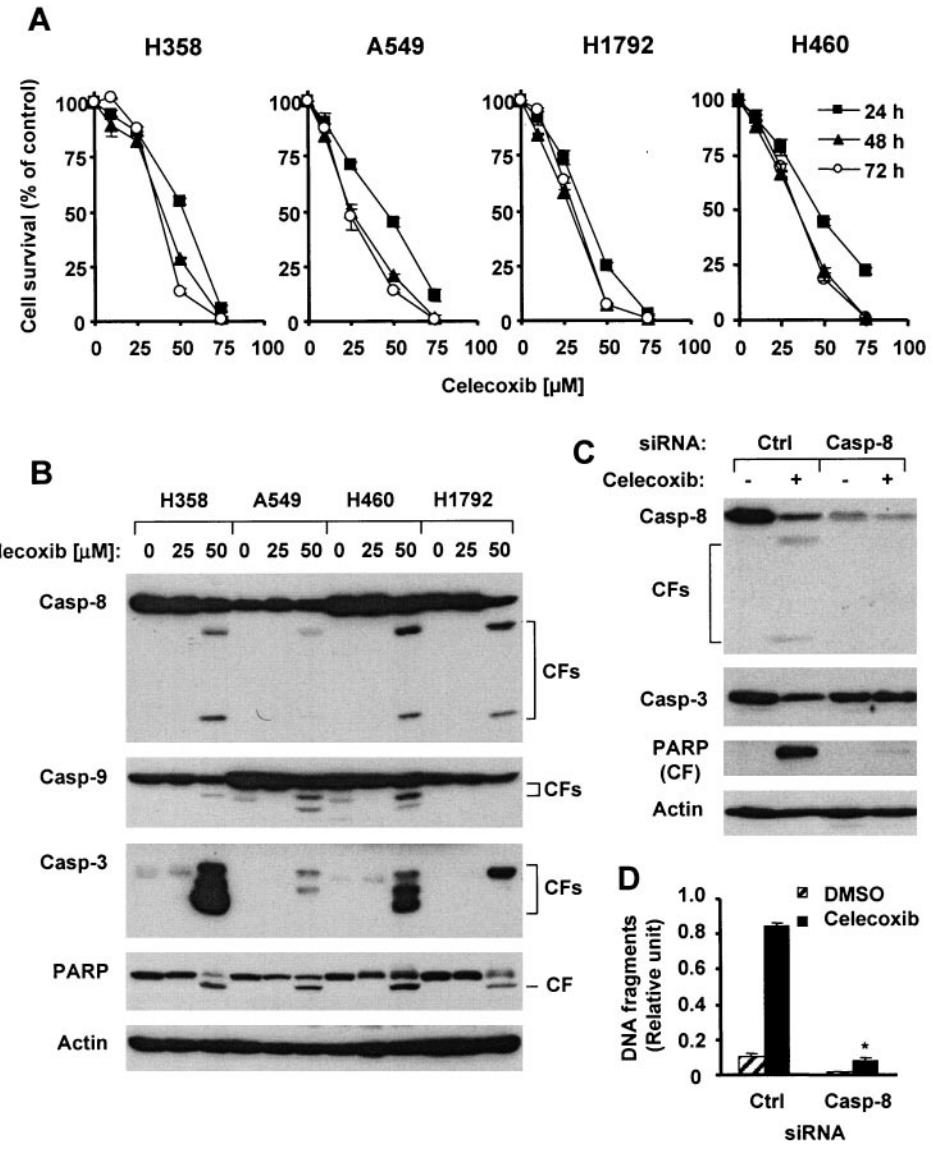

Fig. 1. Celecoxib and caspase 8-mediated apoptosis in human non-small-cell lung carcinoma (NSCLC) cell lines. **A**) Celecoxib and cell survival. NSCLC cell lines, as indicated, were cultured in 96-well cell culture plates and treated on the second day with celecoxib as indicated. After 24, 48, or 72 hours, cell numbers were estimated by use of the sulforhodamine B assay, as described *(39).* Cell survival is expressed as the percent of control (dimethyl sulfoxide [DMSO]-treated) cells (0 μ*M* celecoxib). Each point is the mean value from four identical wells. **Error bars** = 95% confidence intervals [CIs]. **B**) Celecoxib and caspase activation. NSCLC cell lines were treated with celecoxib, as indicated, for 31 hours, whole cell protein lysates were prepared, and cleavage of caspase 8 (Casp-8), caspase 9 (Casp-9), caspase 3 (Casp-3), and poly(ADP-ribose) polymerase (PARP) was detected by western blot analysis. (Cleaved forms of caspase 9 appeared with longer exposure in the H1792 cell line, as did the smaller cleaved form of caspase 8 in the A549 cell line; data not shown.) Actin expression was used as a loading control. CF = cleaved form. **C** and **D**) Silencing of caspase 8 expression and celecoxib-induced caspase activation and DNA fragmentation. H1792 cells were cultured in a 24-well cell culture plate and transfected with control (Ctrl) or caspase 8 small interfering RNA (siRNA) twice with a 48-hour interval between transfections. Forty hours after the second transfection, cells were treated with DMSO (0.05%) or 50 μ*M* celecoxib. Twenty-four hours later, caspase activation was assessed by western blot analysis (**C**), and DNA fragmentation was assessed with the Cell Death Detection enzyme-linked immunosorbent assay (ELISA) kit (Roche Molecular Biochemicals) (**D**). Data are the mean value of three identical wells, and error bars are the upper 95% CIs. *, $P<.001$ compared with that of control siRNA-transfected cells treated with celecoxib. All statistical tests were two-sided.

of upstream and downstream components of caspase cascades, caspases 3, 8, and 9 and PARP. Addition of 50 μ*M* celecoxib induced cleavage of caspases 8 and 9, as well as cleavage of caspase 3 and its substrate PARP (Fig. 1, B). Thus, celecoxib appears to activate the caspase cascade in NSCLC cells.

To determine whether caspase 8 activation is involved in celecoxib-induced apoptosis, we transfected H1792 cells (which tolerate transfection reagents better than other cell lines evaluated and have good transfection efficiency) with caspase 8 siRNA to silence caspase 8 expression and then assessed whether apoptosis was altered by examining levels of cleaved and uncleaved caspases 8 and 3 and PARP, as well as levels of DNA fragmentation. We found that, in the absence of celecoxib treatment, the level of caspase 8 was much lower in cells transfected with caspase 8 siRNA than in cells transfected with control siRNA (Fig. 1, C). After treatment of control siRNA-transfected cells with 50 μ*M* celecoxib, levels of uncleaved forms of caspase 8 decreased as levels of cleaved forms of caspase 8 increased, the level of uncleaved caspase 3 was reduced, and levels of cleaved PARP and DNA fragments were elevated, all compared with levels in corresponding untreated cells (Fig. 1, C and D). After caspase 8 siRNA-transfected cells were treated with 50 μ*M* celecoxib, the level of uncleaved caspase 3 appeared unchanged, cleaved PARP was faintly detected, and DNA fragmentation was statistically significantly less than that in celecoxib-treated control siRNA–transfected cells (Fig. 1, C and D). Similar results were obtained with H460 cells (data not shown). Thus, celecoxib appeared to activate apoptosis in a caspase 8–dependent manner in human NSCLC cells.

Celecoxib and DR5 Expression

To determine whether celecoxib induces DR5 expression and whether p53 status alters the effect of celecoxib, we examined the effect of celecoxib on DR5 expression in three human NSCLC cell lines, one carrying wild-type p53 (A549), one carrying mutant p53 (H1792), and one that is p53-null(H358) *(43).* We treated all three lines with celecoxib and then assessed DR5 mRNA and protein expression. The level of DR5 mRNA increased in a time-dependent manner in all three cell lines, regardless of p53 status, for at least 24 hours after celecoxib treatment, compared with that in untreated cells (Fig. 2, A). The level of DR5 protein also increased in all three cell lines after a 24-hour incubation with celecoxib, compared with that in untreated cells, particularly when cells were treated with 50 μ*M* celecoxib (Fig. 2, B and C). Thus, celecoxib appears to induce DR5 expression in a p53-independent manner in human NSCLC cells.

To determine whether celecoxib increases DR5 mRNA expression at the transcriptional level, we used the transcriptional inhibitor actinomycin D and the translational inhibitor cycloheximide. DR5 mRNA was not detected in cells treated with actinomycin D or in cells treated with the combination of actinomycin D and celecoxib. Treatment of cells with cycloheximide alone increased the level of DR5 mRNA, compared with that in untreated control cells, and treatment with both cycloheximide and celecoxib increased the level of DR5 mRNA even more (Fig. 2, D). We next examined whether celecoxib altered the stability of the DR5 mRNA. After cells were treated with DMSO (vehicle control) or with celecoxib for 24 hours, actinomycin D was then added, and mRNAs were isolated from cells after 0, 1,

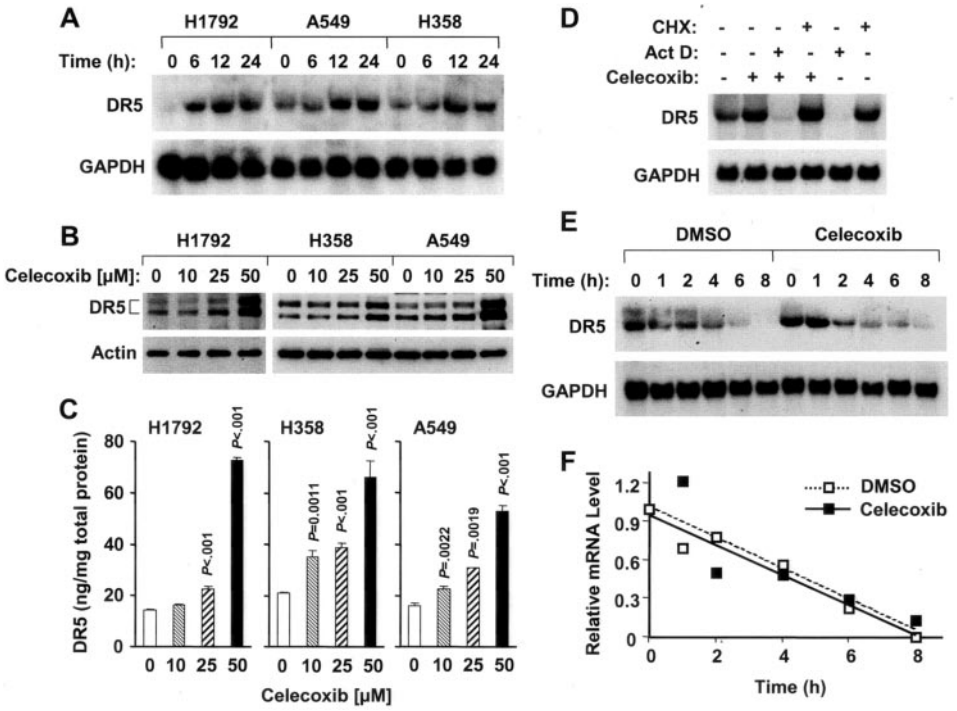

Fig. 2. Celecoxib and DR5 expression in human non-small-cell lung carcinoma (NSCLC) cells. **A–C**) Celecoxib and DR5 mRNA (**A**) and protein (**B** and **C**) expression. NSCLC cell lines were treated with 50 μ*M* celecoxib for the times indicated (**A**) or concentrations of celecoxib indicated for 24 hours (**B** and **C**). Total cellular RNA and whole cell protein lysates were then prepared, DR5 mRNA was detected by northern blot analysis (**A**), and DR5 protein was detected by western blot analysis (**B**) and by enzyme-linked immunosorbent assay (ELISA) (**C**). Data in **panel C** are the mean value of three identical treatments, and **error bars** are the upper 95% confidence intervals [CIs]. All *P* values were compared with control cells (0 μ*M* celecoxib) for all cells treated with the indicated concentrations of celecoxib compared with control cells. All statistical tests were two-sided. **D**) Celecoxib induction of DR5 expression. H358 cells were pretreated with the transcription inhibitor actinomycin D at 5 μg/mL or with the translational inhibitor cycloheximide (CHX) at 10 μg/mL for 30 minutes and then treated with the combination of actinomycin D (Act D) or cycloheximide and 50 μ*M* celecoxib for 24 hours. Total cellular RNA was then prepared and the expression of DR5 mRNA was detected bynorthern blot analysis. **E** and **F**) Celecoxib and the stability of DR5 mRNA in H358 cells. **E**) After a 24-hour treatment with 50 μ*M* celecoxib or dimethyl sulfoxide (DMSO), cells were exposed to actinomycin D at 5 μg/mL, and total cellular RNA was isolated and examined by northern blot analysis. **F**) Hybridization signals were quantitated with a PhosphorImager using ImageQuant software and were normalized to glyceraldehyde-3-phosphate dehydrogenase (GAPDH). Data are the relative level of mRNA (ratio of the value at time 0 of actinomycin D treatment) at the indicated times. The result reflects one gel scanning.

2, 4, 6, and 8 hours of incubation to assess the degradation rate of DR5 mRNA (Fig. 2, E and F). The rate of DR5 mRNA degradation in control (DMSO)-treated cells was similar to that in celecoxib-treated cells. Thus, celecoxib appeared to increase DR5 expression at the transcriptional level.

Celecoxib and the Expression of the Other TRAIL Receptors DR4 and the Decoy Receptors

To determine whether celecoxib also affects the expression of TRAIL receptors in addition to that of DR5, we treated cells with celecoxib for 24 hours and assessed the levels of DR5, DR4, DcR1, and DcR2 mRNAs. Celecoxib treatment increased the levels of DR4 and DR5 mRNAs in a concentration-dependent manner, particularly in H358 cells (Fig. 3, A) but did not change the levels of DcR1 and DcR2 mRNAs in all three cell lines tested. In H358 cells, celecoxib at concentrations from 5 μM through 50 μM increased the expression of DR4, whereas in A549 and H1792 cells, increased DR4 expression was detected even at celecoxib concentrations of 25 μM and 10 μM, respectively. Because celecoxib increased the DR4 mRNA level but did not change DcR1 and DcR2 mRNA levels, we also examined the effect of celecoxib on DR4 protein expression. Increased expression of DR4 protein was detected at 25 μM celecoxib in H358 cells and at 50 μM celecoxib in H1792 cells, but the expression of DR4 protein in A549 cells was not altered, even at 50 μM celecoxib (Fig. 3, B). Thus, we conclude that celecoxib also increased DR4 expression in some NSCLC cell lines.

NSAIDs, Induction of DR5 Expression, and Apoptosis

To determine whether other NSAIDs also modulate death receptor expression in human NSCLC cells, we treated H358 cells with celecoxib or another NSAID (NS398, DUP697, SC-58125, sulindac sulfide, sulindac sulfone, or SC-560; each at 50 μM) and then assessed death receptor protein expression and survival in these cells. Treatment with celecoxib, NS398, DUP697, or SC-58125 increased the expression of DR5 protein (Fig. 4, A), with celecoxib and DUP697 inducing the highest levels, and increased the expression of DR4 protein, with cele-

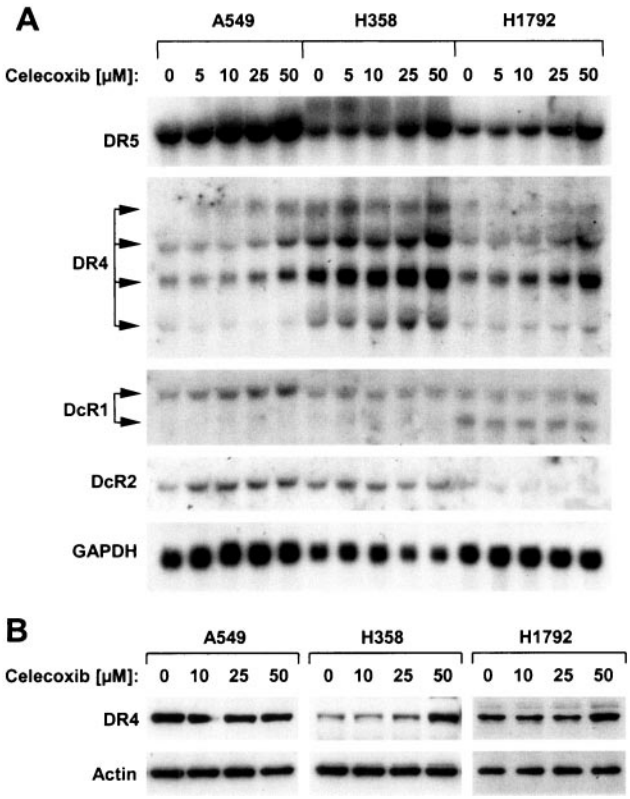

Fig. 3. Celecoxib and modulation of the expression of tumor necrosis factor-related apoptosis-inducing ligand (TRAIL) receptors (DR4, DR5, DcR1, and DcR2) in human non-small-cell lung carcinoma (NSCLC) cells. **A**) Celecoxib and the expression of TRAIL receptors. NSCLC cell lines as indicated were treated with celecoxib for 24 hours as indicated. Total cellular RNAs were prepared and subjected to northern blot analysis to detect TRAIL receptor expression. Glyceraldehyde-3-phosphate dehydrogenase (GAPDH) expression was used as a loading control. **B**) Celecoxib and DR4 protein expression. The indicated NSCLC cell lines were treated with celecoxib as indicated. After 24 hours, whole cell protein lysates were prepared, and DR4 protein was detected by western blot analysis. Actin expression level was used as a loading comparison.

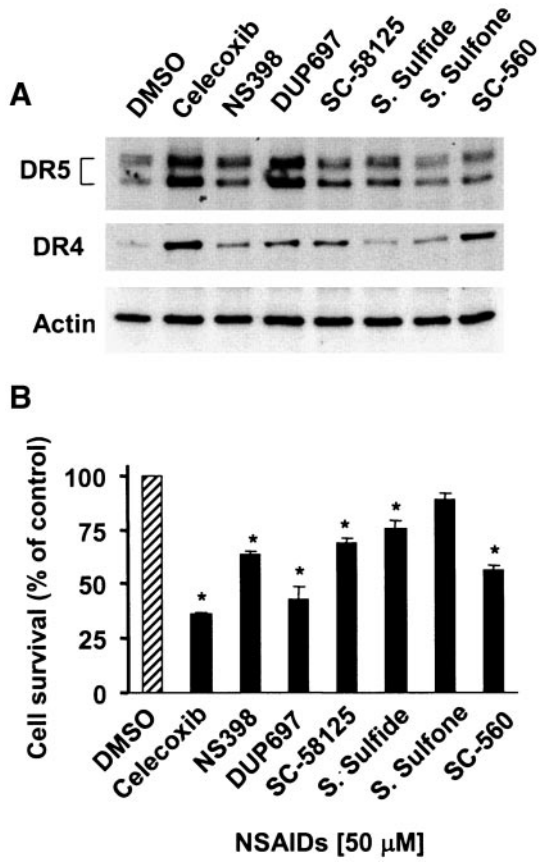

Fig. 4. Abilities of celecoxib and other nonsteroidal anti-inflammatory drugs (NSAIDs) to induce death receptor expression (**A**) and apoptosis (**B**). **A**) H358 cells were treated for 24 hours with dimethyl sulfoxide (DMSO), 50 μM celecoxib, or the indicated NSAIDs at 50 μM. Whole cell protein lysates were prepared, and DR4 or DR5 protein was detected with western blot analysis. Actin expression was used as a loading control. **B**) H358 cells were cultured in 96-well cell culture plates and treated with DMSO, 50 μM celecoxib, or other NSAIDs at 50 μM on the second day. After 48 hours, the cell number was estimated by use of the sulforhodamine B assay, as described *(39)*. Cell survival data are expressed as percent of control DMSO-treated cells and are the mean value of four identical wells. **Error bars** are the upper 95% confidence interval. *, $P<.001$ for survival cells treated with the indicated agent relative to control DMSO-treated cells. All statistical tests were two-sided. S. Sulfide = sulindac sulfide; S. Sulfone = sulindac sulfone.

coxib inducing the highest level. Although treatment with SC-560 did not increase DR5 expression, it did increase DR4 expression. Treatment with either sulindac sulfide or sulindac sulfone did not appear to induce DR4 expression, although treatment with sulindac sulfide increased the expression of DR5 slightly.

When the induction of DR4 protein expression was used to assess NSAID activity in H358 cells, the order from most active to least active was celecoxib, SC-560, DUP697, SC-58125, and NS398. When cell survival was used to assess NSAID activity in H358 cells, treatment with each NSAID decreased cell survival, with celecoxib and DUP697 having the highest activity and sulindac sulfone having the lowest activity (Fig. 4, B). The ability of each NSAID, except for SC-560, to decrease cell survival appeared to be associated with its ability to induce the expression of DR5 (Fig. 4). The ability of SC-560 to decrease cell survival may be related to its ability to induce DR4 expression. The inability of sulindac sulfone to increase the expression of DR5 and DR4 may account for its inability to decrease cell survival. Thus, the induction of death receptors, particularly DR5 induction, appeared to be important for NSAID-induced apoptosis, at least in human NSCLC cell lines.

BCL2 Overexpression and Resistance to Celecoxib-Induced Apoptosis

BCL2 is an antiapoptotic protein that inhibits the release of cytochrome *c* from mitochondria into the cytoplasm, thereby inhibiting intrinsic mitochondria-mediated apoptosis *(23,24)*. To determine whether BCL2 overexpression protects cells from celecoxib-induced apoptosis, we used H460 cells transfected with an empty control vector (H460/V) and H460 cells transfected with a vector containing the gene for BCL2 (H460/Bcl2-6). Treatment with increasing concentrations of celecoxib did not alter the expression of endogenous (i.e., genomic) or exogenous (i.e., transfected) BCL2 or of DR4 protein in either cell line (Fig. 5, B). Celecoxib did not differentially alter survival of either of the two cell lines (Fig. 5, A), and it increased the level of DR5 protein equally well in both cell lines (Fig. 5, B). Thus, overexpression of BCL2 did not appear to confer resistance to celecoxib.

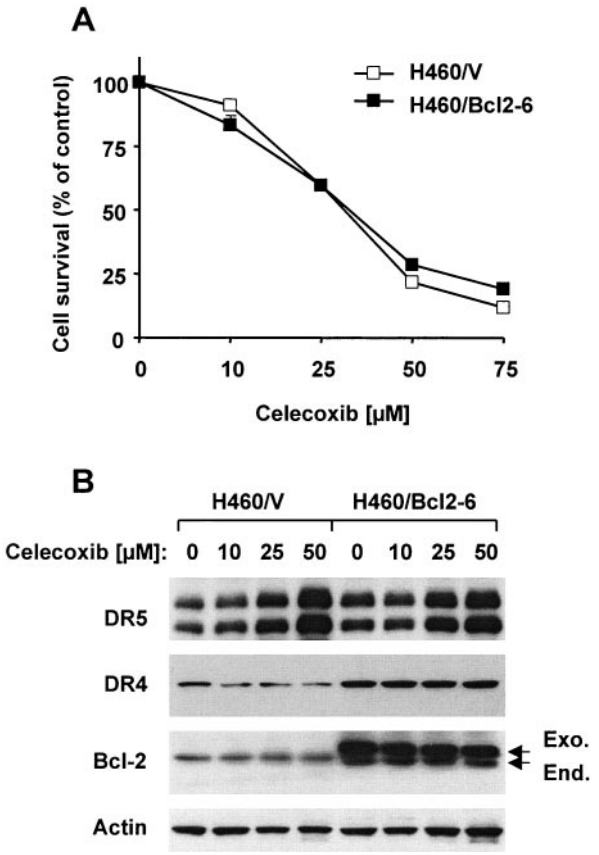

Fig. 5. BCL2 overexpression, celecoxib-induced apoptosis (**A**), and death receptor expression (**B**). **A**) Control vector-transfected H460/V and BCL2 vector-transfected H460/Bcl2–6 cells were cultured in 96-well plates and treated on the second day with celecoxib as indicated. After 3 days, cell number was estimated with the sulforhodamine B assay, as described *(39)*. Cell survival data are expressed as percent of control dimethyl sulfoxide-treated cells (0 μ*M* celecoxib). Data are the mean value of four identical wells, and **error bars** are the 95% confidence intervals (some error bars are too small to be seen). **B**) H460/V and H460/Bcl2–6 cells were cultured in 10-cm dishes and treated with celecoxib as indicated for 24 hours. Whole cell protein lysates were then prepared, and DR5, DR4, and BCL2 expression levels were detected by western blot analysis. Actin expression was used as a loading control. Positions of exogenous (Exo.) and endogenous (End.) BCL2, DR5, and DR4 are indicated.

Death Receptor Expression and Celecoxib-Mediated Apoptosis

The binding of TRAIL to DR5 or DR4 recruits and activates caspase 8 via the adaptor molecule FADD, and activated caspase 8 induces apoptosis by activating caspase cascades *(28,29)*. Death receptor–induced apoptosis can be disrupted by use of a dominant negative FADD mutant (FADDm) that blocks the recruitment of caspase 8 *(38)*. To determine whether increased death receptor expression contributes to celecoxib-induced apoptosis, we transfected cells with a FADDm expression vector or with an empty control vector (Fig. 6, A), treated the transfectants with celecoxib, and assessed their survival. Celecoxib decreased cell survival better in cells transfected with the empty vector (H460/V1) than in the two lines transfected with FADDm (H460/Fm6 and H460/Fm16) (Fig. 6, B). After a 24-hour treatment with 50 μ*M* celecoxib, survival of H460/V1 cells was 28.2% (95% CI = 28.0% to 29.6%) of that of untreated cells, survival of H460/Fm6 cells was 47.1% (95% CI = 45.0% to 49.2%) of that of untreated cells, and survival of H460/Fm16 was 44.5% (95% CI = 43.1% to 45.9%) of that of untreated cells, with the survival values of H460/Fm6 and H460/Fm16 being statistically significantly different from that of H460/V1 ($P<.001$).

In addition to measuring viable cells, we also measured dead cells by directly counting the number of floating cells in the medium. As shown in Fig. 6, C, the number of floating or dead cells was statistically significantly increased in cultures of H460/V1 cells but not in cultures of H460/Fm6 and H460/Fm16 cells after exposure to celecoxib. Thus, the overexpression of FADDm appeared to protect cells from celecoxib-induced cell death.

When we directly measured DNA fragmentation and caspase activation—hallmarks of apoptosis—we found that the differences in the response to celecoxib between empty vector–transfected and FADDm-transfected H460 cells were apparently larger than what we observed in the cell survival assay. After treatment with 50 μ*M* celecoxib, the amount of DNA fragmentation was increased in H460/V1 cells but not in H460/Fm6 cells

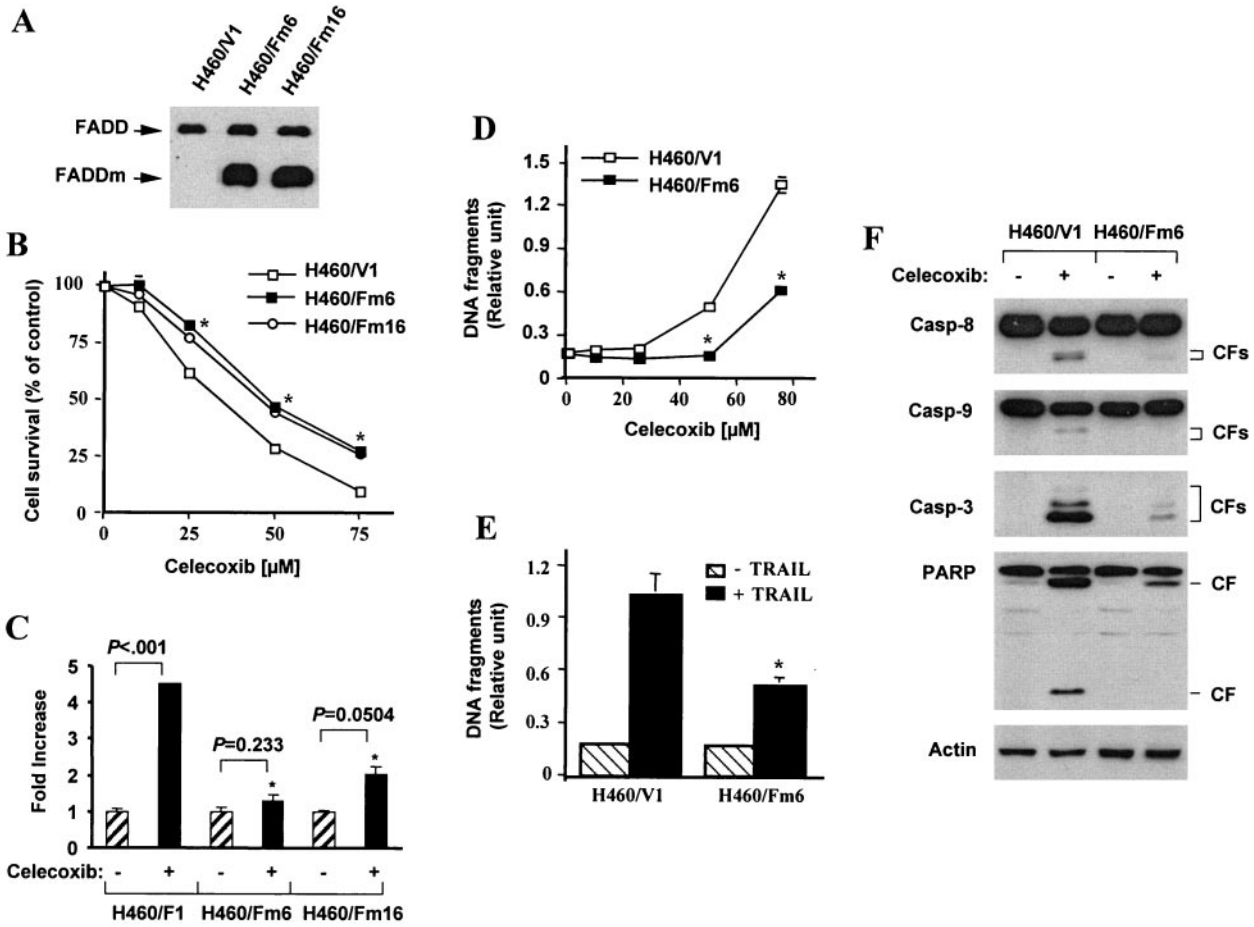

Fig. 6. Overexpression of a dominant negative Fas-associated death domain mutant (FADDm) and celecoxib-induced apoptosis. **A**) Detection of FADDm by western blot analysis. Whole cell protein lysates prepared from H460 transfectants as indicated were subjected to detection of endogenous FADD and FADDm by western blot analysis. **B**) Overexpression of FADDm and celecoxib-induced decrease of cell survival. H460 cells transfected with empty vector (H460/V1) or FADDm (H460/Fm6 and H460/Fm16) were cultured in 96-well plates and treated on the second day with celecoxib as indicated. After 24 hours, the cell number was estimated with the sulforhodamine B assay, as described *(39).* Cell survival data are expressed as percent of dimethyl sulfoxide-treated cells (0 μ*M* celecoxib). Data are the mean value of four identical wells, and **error bars** are the 95% confidence intervals. *, $P<.001$ compared with celecoxib-treated H460/V1 cells. **C**) Overexpression of FADDm and celecoxib-induced cell death. Cell lines, as indicated, were cultured in 10-cm diameter dishes and treated with 50 μ*M* celecoxib. After 24 hours, the floating or dead cells in the medium were counted directly with a hemacytometer. Data are the mean value of three identical dishes, and **error bars** are the upper 95% confidence intervals. *, $P<.001$, compared with the increase in H460/V1 cells. **D**) Overexpression of FADDm and celecoxib-induced DNA fragmentation. Cell lines were cultured in 96-well plates and treated on the second day with celecoxib as indicated. After 24 hours, DNA fragmentation was measured with the Cell Death Detection enzyme-linked immunosorbent assay (ELISA) kit (Roche Molecular Biochemicals). Data are the mean value of three identical wells, and **error bars** are the upper 95% confidence intervals. *, $P<.001$ compared with the value in H460/V1 cells. **E**) Overexpression of FADDm and tumor necrosis factor-related apoptosis-inducing ligand (TRAIL)-induced apoptosis. Cells were treated with TRAIL at 25 ng/mL for 24 hours, and then DNA fragmentation was measured by use of the Cell Death Detection ELISA kit. Data are the mean value of three identical wells, and **error bars** are the upper 95% confidence intervals. *, $P = .002$, compared with that of H460/V1 cell lines. **F**) Overexpression of FADDm and celecoxib-induced caspase activation. Cells, as indicated, were treated with 50 μ*M* celecoxib for 20 hours, whole cell protein lysates were then prepared, and cleaved caspase 8 (Casp-8), caspase 9 (Casp-9), caspase 3 (Casp-3), and poly(ADP-ribose) polymerase (PARP) were detected by western blot analysis. Actin expression was used as a loading control. CF = cleaved form. All statistical tests were two sided.

compared with that in the corresponding untreated cells. After treatment with 75 μ*M* celecoxib, the amount of DNA fragmentation in both cell lines was further increased, but the increase in DNA fragmentation was statistically significantly lower in H460/Fm6 cells than in H460/V1 cells ($P<.001$) (Fig. 6, D). As a control, the amount of DNA fragmentation was statistically significantly lower in TRAIL-treated H460/Fm6 cells than in TRAIL-treated H460/V1 cells ($P = .002$) (Fig. 6, E). Clearly, FADDm overexpression suppressed celecoxib-induced apoptosis.

Furthermore, we found that celecoxib consistently induced a much higher level of cleavage of caspases 9, 8, and 3 and of PARP in H460/V1 cells than in H460/Fm6 cells (Fig. 6, F), demonstrating that FADDm overexpression also suppressed celecoxib's ability to activate the caspase 8–mediated caspase cascade. Thus, overexpression of FADDm appeared to suppress celecoxib-induced apoptosis, indicating that increased expression of death receptors, particularly expression of DR5, contributes to celecoxib-induced apoptosis, at least in human NSCLC cells.

To further explore the relationship between DR5 expression and celecoxib-induced apoptosis, we used siRNA methodology to silence the DR5 gene. DR5 siRNA transfection decreased both the basal level of DR5 expression and the level of celecoxib-increased DR5 expression and decreased the celecoxib-increased levels of cleaved caspase 8 and PARP (Fig. 7, A). Transfection with control siRNA did not interfere with celecoxib-induced increased DR5 expression or activation of

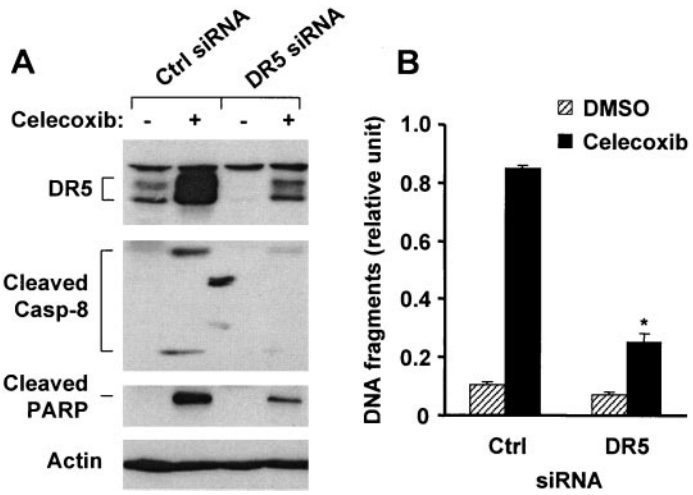

Fig. 7. Silencing of DR5 expression with small interfering RNA (siRNA) and celecoxib-induced caspase activation (**A**) and DNA fragmentation (**B**). H1792 cells were cultured in a 24-well plate and on the second day transfected twice with control (Ctrl) or DR5 siRNA with a 48-hour interval in between transfections. Forty hours after the second transfection, cells were treated with dimethyl sulfoxide (DMSO) or 50 μM celecoxib for 24 hours. **A**) DR5 expression and cleavage of caspase 8 (Casp-8) and poly(ADP-ribose) polymerase (PARP) were assessed by western blot analysis. The two sports between lanes 2 and 3 are nonspecific background material. **B**) DNA fragmentation was evaluated with the Cell Death Detection enzyme-linked immunosorbent assay (ELISA) kit (Roche Molecular Biochemicals). Data are the mean value of three identical wells or treatments, and **error bars** are the upper 95% confidence intervals. *, $P<.001$ compared with that of control (Ctrl) siRNA-transfected cells treated with celecoxib. All statistical tests were two-sided.

caspase 8 and PARP cleavage (Fig. 7, A). In addition, celecoxib-induced DNA fragmentation was statistically significantly lower in DR5 siRNA–transfected cells than in control siRNA–transfected cells ($P<.001$) (Fig. 7, B). When treated with celecoxib, the level of DNA fragments (arbitrary unit) increased from 0.107 U (95% CI = 0.018 U to 0.197 U) to 0.848 U (95% CI = 0.814 U to 0.882 U) in control siRNA–transfected cells, whereas it increased only from 0.070 U (95% CI = 0.045 U to 0.097 U) to 0.249 U (95% CI = 0.127 U to 0.327 U) in DR5 siRNA–transfected cells. Thus, DR5 appeared to play an important role in mediating celecoxib-induced apoptosis.

Celecoxib, TRAIL, and the Induction of Apoptosis

Agents that induce death receptor expression usually enhance TRAIL-induced apoptosis. To determine whether celecoxib enhances TRAIL-induced apoptosis in NSCLC cells, we treated cells with TRAIL and various concentrations of celecoxib and assessed apoptosis. Treatment with TRAIL alone decreased survival of H358, A549, and H460 cells, and cell survival was further decreased by treatment with TRAIL in the presence of different concentrations of celecoxib (Fig. 8, A). In A549 cells, for example, celecoxib alone at 50 μM decreased cell survival by 38.7% (95% CI = 35.2% to 42.2%), TRAIL alone decreased cell survival by 29.3% (95% CI = 25.1% to 33.6%), but a combination of the two decreased cell survival by 77.5% (95% CI = 74.5% to 79.5%), which is greater than the sum of the effects of each agent alone. Similar results were observed with H358 and H460 cell lines. In addition, when DNA fragmentation in H358 cells was directly measured with an ELISA (Fig. 8, B and C) or by the TUNEL method (Fig. 8, D), a greater than additive amount of DNA fragmentation was detected in cells treated with a combination of celecoxib and TRAIL than in cells treated with either agent alone. As assessed by an ELISA, for example, the levels of DNA fragments were 0.082 U (95% CI = 0.017 U to 0.147 U) in untreated cells, 0.153 U (95% CI = 0.074 U to 0.233 U) in cells treated with TRAIL alone at 100 ng/mL, 0.412 U (95% CI = 0.166 U to 0.659 U) in cells treated with 50 μM celecoxib alone, and 1.129 U (95% CI = 0.617 U to 1.641 U) in cells treated with the combination of celecoxib and TRAIL (Fig. 8, B). As assessed by the TUNEL assay, TRAIL alone at 100 ng/mL and celecoxib alone at 50 μM induced 32.4% and 3.62% of cells to undergo apoptosis, respectively, but the combination of celecoxib and TRAIL caused 58.5% of cells to undergo apoptosis (Fig. 8, D).

To determine whether the combination of celecoxib and TRAIL enhances caspase activation in a supra-additive fashion, we examined caspase activation and caspase substrate cleavage in H358 cells treated with celecoxib alone, TRAIL alone, and the combination of celecoxib and TRAIL. Celecoxib alone at 50 μM or TRAIL alone at 100 or 200 ng/mL activated low levels of caspases 9, 8, 7, 6, and 3, and apparently did not increase cleavage of caspase substrates, including Bid, PARP, lamin A/C, and DFF45. However, the combination of celecoxib at 50 μM and TRAIL at 100 ng/mL or 200 ng/mL resulted in clearly increased caspase activation, as shown by decreased levels of uncleaved forms and/or increased levels of cleaved forms and increased cleavage of their substrates (Fig. 8, E). TRAIL alone at 400 ng/mL activated these caspases and increased cleavage of their substrates (Fig. 8, E, lane 8); however, the addition of celecoxib further increased both activities (Fig. 8, E, lane 5). Thus, celecoxib appeared to cooperate with TRAIL to activate both caspase 8– and caspase 9–mediated caspase cascades.

Discussion

In this study, we provided several lines of evidences to demonstrate that the extrinsic death receptor apoptotic pathway, particularly that involving DR5, plays a critical role in mediating celecoxib-induced apoptosis in human NSCLC cells. First, celecoxib activated caspase 8, and silencing of caspase 8 by caspase 8 siRNA abrogated celecoxib-induced caspase activation and DNA fragmentation, indicating that celecoxib induces apoptosis in a caspase 8–dependent manner. Second, overexpression of a dominant negative FADDm suppressed the ability of celecoxib to decrease cell survival and to increase caspase activation and DNA fragmentation, indicating that celecoxib induces apoptosis through an extrinsic apoptotic pathway. Third, the expression of DR4 and particularly of DR5 were induced in cells treated with celecoxib, and the silencing of DR5 expression by DR5 siRNA transfection blocked caspase 8 activation and decreased cell sensitivity to celecoxib-induced apoptosis, indicating that DR5 induction contributes to celecoxib-induced caspase 8 activation and apoptosis. Fourth, overexpression of BCL2 did not inhibit celecoxib-induced apoptosis, suggesting a less important role for the intrinsic mitochondria-mediated apoptotic pathway than for the extrinsic pathway in celecoxib-induced apoptosis, at least in NSCLC cells.

We also found that other NSAIDs (including NS398, DUP697, SC-58125, sulindac sulfide, and SC-560) increased the expression of DR5 and/or DR4 in NSCLC cells to various levels. The ability of an NSAID to increase the expression of death receptors, particularly DR5, is associated with its ability to

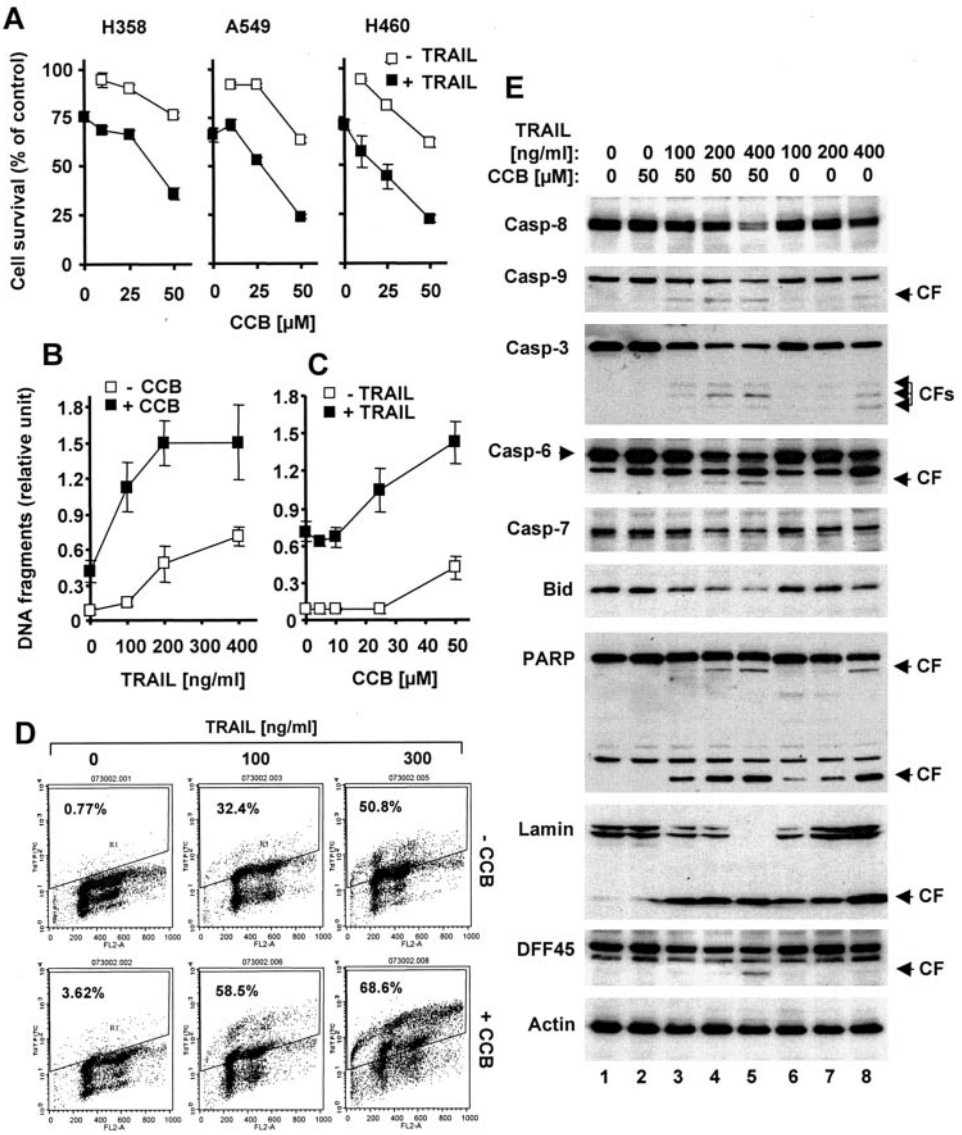

Fig. 8. Combination treatments with celecoxib and tumor necrosis factor-related apoptosis-inducing ligand (TRAIL) and human non-small-cell lung carcinoma (NSCLC) cells. **A**) Cell survival. NSCLC cell lines, as indicated, were cultured in 96-well plates and treated on the second day with TRAIL alone at 400 ng/mL (H358), 300 ng/mL (A549), or 25 ng/mL (H460), celecoxib alone as indicated, or celecoxib plus TRAIL. After 20 hours, cell numbers were estimated by use of the sulforhodamine B assay, as described *(39).* Cell survival data are expressed as percent control dimethyl sulfoxide-treated cells. Data are the mean value of four identical wells, and **error bars** are the 95% confidence intervals. **B** and **C**) DNA fragmentation detected with an enzyme-linked immunosorbent assay (ELISA). H358 cells were cultured in 96-well plates and treated with 50 μ*M* celecoxib alone, TRAIL alone as indicated, or celecoxib plus TRAIL (**B**) or with celecoxib alone as indicated, TRAIL alone at 400 ng/mL, or celecoxib plus TRAIL (**C**). After 20 hours, cells were harvested, and DNA fragmentation was measured with the Cell Death Detection ELISA kit (Roche Molecular Biochemicals). Data are the mean value of three identical wells, and **error bars** are the 95% confidence intervals. **D**) DNA fragmentation detected with the terminal deoxynucleotidyltransferase-mediated UTP nick-end-labeling (TUNEL) assay. H358 cells were cultured in 10-cm dishes and treated on the second day with 50 μ*M* celecoxib alone, TRAIL alone at 100 or 300 ng/mL, or celecoxib plus TRAIL. After 18 hours, cells were harvested, and DNA fragmentation was measured with an APO-DIRECT TUNEL kit (Phoenix Flow Systems) by the manufacturer's protocol. The percent of apoptotic cells with DNA fragmentation is shown. **E**) Apoptosis detected by cleavage of caspases and their substrates. H358 cells were treated with 50 μ*M* celecoxib alone, TRAIL alone as indicated, or the combination of celecoxib and TRAIL for 16 hours. Whole cell protein lysates were then prepared from both detached (i.e., apoptotic death cells) and attached cells (i.e., cells that are undergoing apoptosis), and cleavage of caspases and their substrates was detected by western blot analysis. CCB = celecoxib; Casp = caspase; CF = cleaved form. Cleaved forms are indicated to the right. Caspase activation or cleavage of caspase substrates is indicated by a decreased level of the pro-form of the component and/or the appearance of cleaved forms.

induce apoptosis. Among the NSAIDs tested, celecoxib induced the highest expression of both DR5 and DR4. DUP697, which is structurally closest to celecoxib, was almost as active as celecoxib in inducing DR5 expression and decreasing cell survival; the level of DR4 expression induced by DUP697, however, was lower than that induced by celecoxib. Celecoxib increased the level of DR5 protein in all four cell lines tested but increased the level of DR4 protein in only two of the four lines (Figs. 2 and 5). Thus, the induction of DR5 expression may be more important than that of DR4 expression in mediating celecoxib-induced apoptosis. This result may explain the association between the ability of an NSAID to induce DR5 expression and its ability to induce apoptosis. At present, it is not clear whether induction of death receptor expression by an NSAID, such as celecoxib, is associated with its ability to inhibit cyclooxygenase 2. Because sulindac sulfide and celecoxib induce apoptosis independent of cyclooxygenase 2 levels and their induction of DR5 contributes to induction of apoptosis, the induction of death receptor expression by celecoxib and other NSAIDs may also be independent of their cyclooxygenase 2 inhibitory activity.

Celecoxib appears to increase the expression of DR5 by acting at the transcriptional level because the transcription inhibitor actinomycin D blocked the increased DR5 expression induced by celecoxib and because celecoxib did not alter DR5 mRNA stability. At present, the mechanism by which celecoxib increases DR5 expression is unclear. However, this effect is most likely p53–independent because celecoxib increased DR5 expression regardless of the p53 status of the cells examined. We showed that the protein synthesis inhibitor cycloheximide increased the level of DR5 mRNA and further enhanced the celecoxib-induced increase in DR5 mRNA expression. Although the mechanism of this effect is unclear, uncharacterized proteins may mask or inhibit the transcription of DR5. Cycloheximide may block the synthesis of these proteins and consequently block their suppression of DR5 expression.

Overexpression of BCL2 generally suppresses mitochondria-mediated apoptosis induced by many chemicals or small molecules *(24)*. In our study, we found that BCL2 overexpression did not suppress celecoxib-induced apoptosis, as has been reported in prostate cancer cells *(11),* and that celecoxib induced the same level of DR5 expression in both cells transfected with empty control vector and cells transfected with BCL2 vector. These results indirectly support a role of a death receptor–mediated extrinsic apoptotic pathway in celecoxib-induced apoptosis in NSCLC cells. Jendrossek et al. *(17)* have reported that Jurkat T cells overexpressing BCL2 were sensitive to celecoxib-induced apoptosis, which is consistent with our findings. However, in contrast to our results in NSCLC cells, they found that celecoxib could induce apoptosis in Jurkat T cells that lacked caspase 8 or FADD but did not induce apoptosis in the presence of a caspase 9 inhibitor and a dominant negative caspase 9 mutant. Thus, in Jurkat T cells, celecoxib appears to act through a caspase 9–mediated mitochondrial signaling pathway that leads to the induction of apoptosis independent of BCL2– and death receptor–mediated apoptotic pathways.

It should be noted that the concentrations of celecoxib used by Jendrossek et al. (75–100 μM) were higher than the concentrations used in our study (50 μM or lower). At such high concentrations, celecoxib might still induce apoptosis in cells deficient in caspase 8 or FADD if the intrinsic mitochondrial pathway could override the death receptor pathway. In our study, overexpression of the dominant negative FADDm only partially suppressed apoptosis when cells were treated by 75 μM celecoxib (Fig. 6, D). Celecoxib may also induce apoptosis by cell type–specific mechanisms because other studies have shown that BCL2 overexpression exerted different impacts on induction of apoptosis in different types of cancer cells. For example, overexpression of BCL2 failed to block TRAIL-induced apoptosis in Jurkat or myeloma cells *(44–46)* but suppressed TRAIL-induced apoptosis in human lung and prostate cancer cells *(37,47,48)*.

FADDm overexpresssion apparently protected cells from celecoxib-induced apoptotic cell death, as indicated by the increased number of floating or dead cells, the increased amount of DNA fragmentation, and increased level of caspase cleavage or activation in celecoxib-treated cultures compared with untreated cells (Fig. 6, C, D, and F). The FADDm overexpresssion apparently protected cells from celecoxib-induced apoptotic cell death as indicated by detecting the increase in floating or dead cells, increase in DNA fragmentation, and caspase cleavage or activation (Fig. 6, C, D, and F). However, the protective effect of the FADDm overexpression on cell number decrease caused by celecoxib was limited (close to 20% protection) (Fig. 6, B). If decrease of cell number is an outcome of the mixed effects due to growth arrest (i.e., proliferation inhibition) and apoptotic death, we expect only a partial rescue of cell number decrease, even by a substantial blockade of apoptotic death unless cell number decrease is caused purely by apoptosis. Thus, our data suggest that apoptosis only partially accounts for cell number decrease caused by celecoxib.

A potential limitation of our study is that the peak human plasma concentration of celecoxib after oral administration of a single dose of 400–800 mg ranges from 3 to 8 μM *(49,50),* which is considerably lower than the concentrations required to induce apoptosis in our study with human NSCLC cells and in other studies with different types of cancer cells. Currently, the tissue level of such a dose has not been determined. Nevertheless, the approach of celecoxib-based combination regimens for cancer chemoprevention and therapy and identification of celecoxib-derived novel anticancer drugs with more potent efficacy should be explored further.

Our findings that celecoxib increases the expression of death receptors and increases TRAIL-induced apoptosis indicate that combined treatment with celecoxib and TRAIL or celecoxib and agonistic anti-DR4 or -DR5 antibodies may be therapeutically useful in certain cancers. In this study, we have demonstrated that DR5 induction is a critical event in celecoxib-mediated apoptosis. Therefore, we suggest that induction of DR5 expression be explored further as a possible predictive biomarker for evaluating celecoxib and its derivatives as chemopreventive or therapeutic agents in clinical trials. Currently, several ongoing clinical trials are evaluating celecoxib alone or in combination with other agents for prevention or treatment of lung cancer *(51)*. Celecoxib is an FDA-approved and widely marketed drug that was originally developed as an anti-inflammatory drug, not as an anticancer drug. Celecoxib has a simple chemical structure and should be an ideal lead compound for developing novel derivatives with more potent apoptosis-inducing activity. In fact, celecoxib analogs have been developed, and the proapoptotic activity of some analogs is higher than that of celecoxib *(52,53)*. We suggest that death receptor induction be evaluated as a target for screening novel celecoxib-based anticancer drugs.

REFERENCES

(1) Harris RE, Alshafie GA, Abou-Issa H, Seibert K. Chemoprevention of breast cancer in rats by celecoxib, a cyclooxygenase 2 inhibitor. Cancer Res 2000;60:2101–3.

(2) Reddy BS, Hirose Y, Lubet R, Steele V, Kelloff G, Paulson S, et al. Chemoprevention of colon cancer by specific cyclooxygenase-2 inhibitor, celecoxib, administered during different stages of carcinogenesis. Cancer Res 2000;60:293–7.

(3) Kawamori T, Rao CV, Seibert K, Reddy BS. Chemopreventive activity of celecoxib, a specific cyclooxygenase-2 inhibitor, against colon carcinogenesis. Cancer Res 1998;58:409–12.

(4) Grubbs CJ, Lubet RA, Koki AT, Leahy KM, Masferrer JL, Steele VE, et al. Celecoxib inhibits N-butyl-N-(4-hydroxybutyl)-nitrosamine-induced urinary bladder cancers in male B6D2F1 mice and female Fischer-344 rats. Cancer Res 2000;60:5599–602.

(5) Fischer SM, Lo HH, Gordon GB, Seibert K, Kelloff G, Lubet RA, et al. Chemopreventive activity of celecoxib, a specific cyclooxygenase-2 inhibitor, and indomethacin against ultraviolet light-induced skin carcinogenesis. Mol Carcinog 1999;25:231–40.

(6) Orengo IF, Gerguis J, Phillips R, Guevara A, Lewis AT, Black HS. Celecoxib, a cyclooxygenase 2 inhibitor as a potential chemopreventive to UV-induced skin cancer: a study in the hairless mouse model. Arch Dermatol 2002;138:751–5.

(7) Grosch S, Tegeder I, Niederberger E, Brautigam L, Geisslinger G. COX-2 independent induction of cell cycle arrest and apoptosis in colon cancer cells by the selective COX-2 inhibitor celecoxib. FASEB J 2001;15:2742–4.

(8) Williams CS, Watson AJ, Sheng H, Helou R, Shao J, DuBois RN. Celecoxib prevents tumor growth in vivo without toxicity to normal gut: lack of correlation between in vitro and in vivo models. Cancer Res 2000;60:6045–51.

(9) Blumenthal RD, Waskewich C, Goldenberg DM, Lew W, Flefleh C, Burton J. Chronotherapy and chronotoxicity of the cyclooxygenase-2 inhibitor, celecoxib, in athymic mice bearing human breast cancer xenografts. Clin Cancer Res 2001;7:3178–85.

(10) Steinbach G, Lynch PM, Phillips RK, Wallace MH, Hawk E, Gordon GB, et al. The effect of celecoxib, a cyclooxygenase-2 inhibitor, in familial adenomatous polyposis. N Engl J Med 2000;342:1946–52.

(11) Hsu AL, Ching TT, Wang DS, Song X, Rangnekar VM, Chen CS. The cyclooxygenase-2 inhibitor celecoxib induces apoptosis by blocking Akt activation in human prostate cancer cells independently of Bcl-2. J Biol Chem 2000;275:11397–03.

(12) Waskewich C, Blumenthal RD, Li H, Stein R, Goldenberg DM, Burton J. Celecoxib exhibits the greatest potency amongst cyclooxygenase (COX) inhibitors for growth inhibition of COX-2-negative hematopoietic and epithelial cell lines. Cancer Res 2002;62:2029–33.
(13) Leahy KM, Ornberg RL, Wang Y, Zweifel BS, Koki AT, Masferrer JL. Cyclooxygenase-2 inhibition by celecoxib reduces proliferation and induces apoptosis in angiogenic endothelial cells in vivo. Cancer Res 2002;62:625–31.
(14) Arico S, Pattingre S, Bauvy C, Gane P, Barbat A, Codogno P, et al. Celecoxib induces apoptosis by inhibiting 3-phosphoinositide-dependent protein kinase-1 activity in the human colon cancer HT-29 cell line. J Biol Chem 2002;277:27613–21.
(15) Song X, Lin HP, Johnson AJ, Tseng PH, Yang YT, Kulp SK, et al. Cyclooxygenase-2, player or spectator in cyclooxygenase-2 inhibitor-induced apoptosis in prostate cancer cells. J Natl Cancer Inst 2002;94:585–91.
(16) Kern MA, Schubert D, Sahi D, Schoneweiss MM, Moll I, Haugg AM, et al. Proapoptotic and antiproliferative potential of selective cyclooxygenase-2 inhibitors in human liver tumor cells. Hepatology 2002;36:885–94.
(17) Jendrossek V, Handrick R, Belka C. Celecoxib activates a novel mitochondrial apoptosis signaling pathway. FASEB J 2003;17:1547–9.
(18) Hashitani S, Urade M, Nishimura N, Maeda T, Takaoka K, Noguchi K, et al. Apoptosis induction and enhancement of cytotoxicity of anticancer drugs by celecoxib, a selective cyclooxygenase-2 inhibitor, in human head and neck carcinoma cell lines. Int J Oncol 2003;23:665–72.
(19) Thun MJ, Henley SJ, Patrono C. Nonsteroidal anti-inflammatory drugs as anticancer agents: mechanistic, pharmacologic, and clinical issues. J Natl Cancer Inst 2002;94:252–66.
(20) Mohan S, Epstein JB. Carcinogenesis and cyclooxygenase: the potential role of COX-2 inhibition in upper aerodigestive tract cancer. Oral Oncol 2003;39:537–46.
(21) Leng J, Han C, Demetris AJ, Michalopoulos GK, Wu T. Cyclooxygenase-2 promotes hepatocellular carcinoma cell growth through Akt activation: evidence for Akt inhibition in celecoxib-induced apoptosis. Hepatology 2003;38:756–68.
(22) Johnson AJ, Hsu AL, Lin HP, Song X, Chen CS. The cyclo-oxygenase-2 inhibitor celecoxib perturbs intracellular calcium by inhibiting endoplasmic reticulum Ca2+-ATPases: a plausible link with its anti-tumour effect and cardiovascular risks. Biochem J 2002;366:831–7.
(23) Hengartner MO. The biochemistry of apoptosis. Nature 2000;407:770–6.
(24) Costantini P, Jacotot E, Decaudin D, Kroemer G. Mitochondrion as a novel target of anticancer chemotherapy. J Natl Cancer Inst 2000;92:1042–53.
(25) Altucci L, Rossin A, Raffelsberger W, Reitmair A, Chomienne C, Gronemeyer H. Retinoic acid-induced apoptosis in leukemia cells is mediated by paracrine action of tumor-selective death ligand TRAIL. Nat Med 2001;7:680–6.
(26) Huang Y, He Q, Hillman MJ, Rong R, Sheikh MS. Sulindac sulfide-induced apoptosis involves death receptor 5 and the caspase 8-dependent pathway in human colon and prostate cancer cells. Cancer Res 2001;61:6918–24.
(27) Han Z, Pantazis P, Wyche JH, Kouttab N, Kidd VJ, Hendrickson EA. A Fas-associated death domain protein-dependent mechanism mediates the apoptotic action of non-steroidal anti-inflammatory drugs in the human leukemic Jurkat cell line. J Biol Chem 2001;276:38748–54.
(28) Ashkenazi A, Dixit VM. Death receptors: signaling and modulation. Science 1998;281:1305–8.
(29) Wang S, El-Deiry WS. TRAIL and apoptosis induction by TNF-family death receptors. Oncogene 2003;22:8628–33.
(30) Wu GS, Burns TF, McDonald ER 3rd, Jiang W, Meng R, Krantz ID, et al. KILLER/DR5 is a DNA damage-inducible p53-regulated death receptor gene. Nat Genet 1997;17:141–3.
(31) Takimoto R, El-Deiry WS. Wild-type p53 transactivates the KILLER/DR5 gene through an intronic sequence-specific DNA-binding site. Oncogene 2000;19:1735–43.
(32) Guan B, Yue P, Clayman GL, Sun SY. Evidence that the death receptor DR4 is a DNA damage-inducible, p53-regulated gene. J Cell Physiol 2001;188:98–105.
(33) Liu X, Yue P, Khuri FR, Sun SY. p53 upregulates death receptor 4 expression through an intronic p53 binding site. Cancer Res 2004;64:5078–83.
(34) Sheikh MS, Burns TF, Huang Y, Wu GS, Amundson S, Brooks KS, et al. p53-dependent and -independent regulation of the death receptor KILLER/DR5 gene expression in response to genotoxic stress and tumor necrosis factor alpha. Cancer Res 1998;58:1593–8.
(35) Ravi R, Bedi GC, Engstrom LW, Zeng Q, Mookerjee B, Gelinas C, et al. Regulation of death receptor expression and TRAIL/Apo2L-induced apoptosis by NF-kappaB. Nat Cell Biol 2001;3:409–16.
(36) Guan B, Yue P, Lotan R, Sun SY. Evidence that the human death receptor 4 is regulated by activator protein 1. Oncogene 2002;21:3121–9.
(37) Sun SY, Yue P, Zhou JY, Wang Y, Choi Kim HR, Lotan R, et al. Overexpression of BCL2 blocks TNF-related apoptosis-inducing ligand (TRAIL)-induced apoptosis in human lung cancer cells. Biochem Biophys Res Commun 2001;280:788–97.
(38) Chinnaiyan AM, O'Rourke K, Tewari M, Dixit VM. FADD, a novel death domain-containing protein, interacts with the death domain of Fas and initiates apoptosis. Cell 1995;81:505–12.
(39) Sun SY, Yue P, Dawson MI, Shroot B, Michel S, Lamph WW, et al. Differential effects of synthetic nuclear retinoid receptor-selective retinoids on the growth of human non-small cell lung carcinoma cells. Cancer Res 1997;57:4931–9.
(40) Sun SY, Yue P, Wu GS, El-Deiry WS, Shroot B, Hong WK, et al. Mechanisms of apoptosis induced by the synthetic retinoid CD437 in human non-small cell lung carcinoma cells. Oncogene 1999;18:2357–65.
(41) Chun HJ, Zheng L, Ahmad M, Wang J, Speirs CK, Siegel RM, et al. Pleiotropic defects in lymphocyte activation caused by caspase-8 mutations lead to human immunodeficiency. Nature 2002;419:395–9.
(42) Wang S, El-Deiry WS. Requirement of p53 targets in chemosensitization of colonic carcinoma to death ligand therapy. Proc Natl Acad Sci U S A 2003;100:15095–100.
(43) Mitsudomi T, Steinberg SM, Nau MM, Carbone D, D'Amico D, Bodner S, et al. p53 gene mutations in non-small-cell lung cancer cell lines and their correlation with the presence of ras mutations and clinical features. Oncogene 1992;7:171–80.
(44) Gazitt Y, Shaughnessy P, Montgomery W. Apoptosis-induced by TRAIL and TNF-alpha in human multiple myeloma cells is not blocked by BCL-2. Cytokine 1999;11:1010–9.
(45) Keogh SA, Walczak H, Bouchier-Hayes L, Martin SJ. Failure of Bcl-2 to block cytochrome c redistribution during TRAIL-induced apoptosis. FEBS Lett 2000;471:93–8.
(46) Walczak H, Bouchon A, Stahl H, Krammer PH. Tumor necrosis factor-related apoptosis-inducing ligand retains its apoptosis-inducing capacity on Bcl-2- or Bcl-xL-overexpressing chemotherapy-resistant tumor cells. Cancer Res 2000;60:3051–7.
(47) Rokhlin OW, Guseva N, Tagiyev A, Knudson CM, Cohen MB. Bcl-2 oncoprotein protects the human prostatic carcinoma cell line PC3 from TRAIL-mediated apoptosis. Oncogene 2001;20:2836–43.
(48) Munshi A, Pappas G, Honda T, McDonnell TJ, Younes A, Li Y, et al. TRAIL (APO-2L) induces apoptosis in human prostate cancer cells that is inhibitable by Bcl-2. Oncogene 2001;20:3757–65.
(49) Niederberger E, Tegeder I, Vetter G, Schmidtko A, Schmidt H, Euchenhofer C, et al. Celecoxib loses its anti-inflammatory efficacy at high doses through activation of NF-kappaB. FASEB J 2001;15:1622–4.
(50) Davies NM, Gudde TW, de Leeuw MA. Celecoxib: a new option in the treatment of arthropathies and familial adenomatous polyposis. Expert Opin Pharmacother 2001;2:139–52.
(51) Bunn PA Jr, Keith RL. The future of cyclooxygenease-2 inhibitors and other inhibition of the eicosanoid signal pathway in the prevention and therapy of lung cancer. Clin Lung Cancer 2002;3:271–7.
(52) Zhu J, Song X, Lin HP, Young DC, Yan S, Marquez VE, et al. Using cyclooxygenase-2 inhibitors as molecular platforms to develop a new class of apoptosis-inducing agents. J Natl Cancer Inst 2002;94:1745–7.
(53) Zhu J, Huang JW, Tseng PH, Yang YT, Fowble J, Shiau CW, et al. From the cyclooxygenase-2 inhibitor celecoxib to a novel class of 3-phosphoinositide-dependent protein kinase-1 inhibitors. Cancer Res 2004;64:4309–18.

NOTES

Supported in part by the Winship Cancer Institute faculty start-up research fund (to S.-Y. Sun), the American Cancer Society Institutional Seed Grant (to S.-Y. Sun), the Department of Defense VITAL grant W81XWH-04-1-0142 (to S.-Y. Sun for Project 4), and the Georgia Cancer Coalition Distinguished Cancer Scholar award (to S.-Y. Sun).

Drs. S.-Y. Sun and F. R. Khuri are Georgia Cancer Coalition Distinguished Cancer Scholars.

Manuscript received March 11, 2004; revised October 4, 2004; accepted October 7, 2004.

DOI:10.1158/1078-0432.CCR-06-2077

Clinical Cancer Research

Implication of the Insulin-like Growth Factor-IR Pathway in the Resistance of Non –small Cell Lung Cancer Cells to Treatment with Gefitinib

Floriana Morgillo, Woo-Young Kim, Edward S. Kim, et al.

Clin Cancer Res 2007;13:2795-2803. Published online May 1, 2007.

DOI:10.1158/1078-0432.CCR-06-2077

Implication of the Insulin-like Growth Factor-IR Pathway in the Resistance of Non–small Cell Lung Cancer Cells to Treatment with Gefitinib

Floriana Morgillo,[1] Woo-Young Kim,[1] Edward S. Kim,[1] Fortunato Ciardiello,[3] Waun Ki Hong,[1] and Ho-Young Lee[1,2]

Abstract

Purpose: Epidermal growth factor receptor (EGFR) tyrosine kinase inhibitors have been found to be effective against lung cancer *in vitro*, but clinical resistance to these agents has developed as their usage has increased. In this study, we determined whether the insulin-like growth factor I (IGF-I) signaling pathway induces resistance of non–small cell lung cancer (NSCLC) cells to the EGFR tyrosine kinase inhibitor gefitinib.

Experimental Design: The effects of gefitinib and cetuximab on NSCLC cells, alone or with an IGF-I receptor (IGF-IR) inhibitor, were assessed using the 3-(4,5-dimethylthiazol-2-yl)-2,5-diphenyltetrazolium bromide assay, the flow cytometry–based terminal nucleotidyl transferase–mediated nick end labeling assay, coimmunoprecipitation, and Western blot analysis. EGFR and IGFR expression in NSCLC tissues were examined by Western blot analysis.

Results: Gefitinib inhibited NSCLC cell proliferation by inducing apoptosis when IGF-IR signaling was suppressed. Treatment with gefitinib, but not cetuximab, induced EGFR:IGF-IR heterodimerization and activation of IGF-IR and its downstream signaling mediators, resulting in increased survivin expression in NSCLC cell lines with high levels of IGF-IR expression. Inhibition of IGF-IR activation and knockdown of survivin expression led to increased apoptosis. In contrast, overexpression of survivin protected cells with low IGF-IR expression from gefitinib-induced apoptosis. Most NSCLC tissues with EGFR overexpression had associated high levels of IGF-IR expression.

Conclusions: IGF-IR expression may be useful as a predictive marker for gefitinib treatment of NSCLC. Suppression of IGF-IR signaling pathways may prevent or delay development of gefitinib resistance in patients with NSCLC.

Lung cancer is the leading cause of cancer-related death in both sexes in the United States and throughout the world, and its overall mortality rate has not changed substantially in decades (1). Advances in the understanding of lung tumor biology and oncogenesis have provided several molecular targets for the treatment of non–small cell lung cancer (NSCLC). Of these, inhibitors of epidermal growth factor receptor (EGFR) tyrosine kinase pathways are the most extensively studied.

EGFR is overexpressed in several solid tumor types, including NSCLC (it has been found in 40-80% of cases; ref. 2). The EGFR signaling pathway activates the phosphoinositide-3-kinase/Akt and mitogen-activated protein kinase (MAPK) pathways, which mediate proliferation, differentiation, and survival in both normal and malignant epithelial cells (3, 4). Activated EGFR also promotes angiogenesis, tumor cell motility, and invasion by regulating the expression and activity of matrix metalloproteinases and by interacting with components of the integrin pathway (5). These findings indicate that EGFR-targeted agents would be effective against cancer.

Small-molecular-weight EGFR tyrosine kinase inhibitors (TKI) and anti-EGFR monoclonal antibodies have been in advanced clinical development (6, 7). Monoclonal antibodies bind to the extracellular domain of EGFR. The EGFR-antibody complex is subsequently internalized, causing decreases in EGFR expression and heterodimerization in a phosphorylation status–independent manner. Treatment with cetuximab, a chimeric human-mouse anti-EGFR monoclonal immunoglobulin G_1 (IgG_1) antibody, has been found to block cell cycle progression by inducing G_1 arrest and to inhibit human cancer xenograft growth in nude mice *in vivo* (8) by inhibiting tumor-induced angiogenesis (9). Treatment with cetuximab has shown therapeutic activities in patients with head and neck

Authors' Affiliations: [1]Department of Thoracic/Head and Neck Medical Oncology, M. D. Anderson Cancer Center, and [2]Graduate School of Biomedical Sciences at Houston, The University of Texas, Houston, Texas and [3]Dipartimento Medico-Chirurgico di Internistica Clinica e Sperimentale F. Magrassi e A. Lanzara, Seconda Universita degli Studi di Napoli, Naples, Italy

Received 8/18/06; revised 1/25/07; accepted 2/9/07.

Grant support: NIH grants R01 CA100816 and CA109520 (H.-Y. Lee), American Cancer Society grant RSG-04-082-01-TBE 01 (H.-Y. Lee), and partly by Department of Defense grants W81XWH-06-1-0303-BATTLE and W81XWH-04-1-0142-01-VITAL (W.K. Hong). W.K. Hong is an American Cancer Society Clinical Research Professor.

The costs of publication of this article were defrayed in part by the payment of page charges. This article must therefore be hereby marked *advertisement* in accordance with 18 U.S.C. Section 1734 solely to indicate this fact.

Requests for reprints: Ho-Young Lee, Department of Thoracic/Head and Neck Medical Oncology, Unit 432, The University of Texas M. D. Anderson Cancer Center, 1515 Holcombe Boulevard, Houston, TX 77030. Phone: 713-792-6363; Fax: 713-792-0430; E-mail: hlee@mdanderson.org.

doi:10.1158/1078-0432.CCR-06-2077

DOI:10.1158/1078-0432.CCR-06-2077

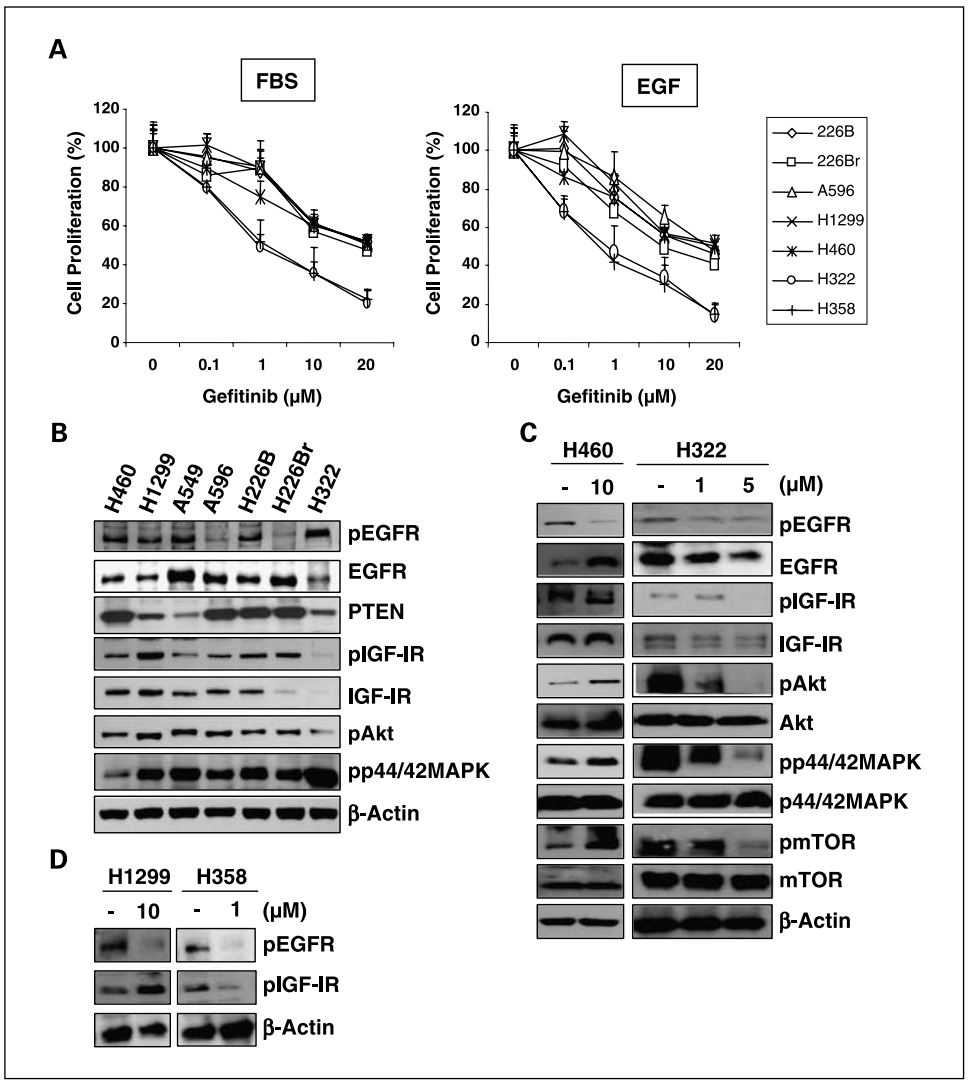

Fig. 1. Stimulation of IGF-IR signaling pathway in gefitinib-resistant NSCLC cell lines. *A,* results of the MTT assay of H460, H1299, A596, H226B, H226Br, H322, and H358 cell lines treated with the indicated concentrations of gefitinib in RPMI 1640 containing 10% FBS or EGF for 3 d. Independent experiments were repeated at least thrice each, and one representative result is shown. Points, mean value of eight identical wells of a single representative experiment; bars, upper 95% CIs. **, $P < 0.01$ and ***, $P < 0.001$ for comparisons between gefitinib-treated and control cells. *B,* basal expression of EGFR, IGF-IR, p44/42 MAPK, Akt, and their phosphorylated forms and PTEN in seven NSCLC cell lines. *C* and *D,* immunoblotting of EGFR, IGF-IR, and their downstream signaling components in H460, H322 (*C*), H1299, and H358 (*D*) cells treated with the indicated concentrations of gefitinib. *B* and *C,* Western blotting on β-actin was included as a loading control.

cancer or colorectal cancer (10, 11). Unlike monoclonal antibodies, TKIs do not affect internalization of the EGF receptor and are often not EGFR specific; thus, they affect the kinase activity of other ErbB family receptors. EGFR TKIs block the ATP pocket of EGFR, thereby inhibiting EGFR phosphorylation and downstream signal transduction (12).

Preclinical studies have shown that the EGFR TKI gefitinib, when used in combination with standard chemotherapeutic agents or radiotherapy, inhibits EGFR activation, causing G_1 arrest and additive-to-synergistic growth inhibition (6). However, negative results from clinical trials (13, 14) have diminished the enthusiasm for gefitinib and indicate that a better understanding is needed of the mechanisms of acquired resistance to this drug. The effectiveness of gefitinib is currently being studied in a population of patients who may have a biomarker that sensitizes their tumors to gefitinib. However, mechanistic studies of gefitinib resistance have not been completed.

Because recent studies have suggested that the insulin-like growth factor I receptor (IGF-IR) pathway is involved in NSCLC cells' resistance to EGFR-targeting agents (15, 16), we studied whether the IGF-IR–mediated signaling pathway influences the NSCLC response to gefitinib and cetuximab. We also sought to determine the proteins mediating survival of NSCLC cells against gefitinib treatment. In the present studies, we show that treatment with gefitinib but not cetuximab stimulates the IGF-IR pathway and its downstream signaling mediators via the EGFR:IGF-IR heterodimer and induces survivin expression that protects NSCLC cells from apoptosis.

Materials and Methods

Cells and reagents. The human NSCLC cell lines H596, H226B, H226Br, H460, H1299, H358, and H322 were purchased from the American Type Culture Collection and maintained in RPMI 1640 supplemented with 10% fetal bovine serum (FBS; Life Technologies-BRL) in a humidified atmosphere with 5% CO_2. EGF was purchased from R&D Systems. Gefitinib (AstraZeneca) was prepared as a 10 mmol/L stock solution in DMSO. Cetuximab was obtained from ImClone Systems and prepared as a 20 mmol/L stock solution. AG1024, an IGF-IR TKI, was purchased from Calbiochem-Novabiochem. Adenoviruses, with and without survivin (Ad-survivin and Ad-EV, respectively), were amplified as described previously (17).

Cell proliferation assay. To determine the effects of gefitinib and AG1024 on NSCLC cell proliferation, we plated 3×10^3 cells per well of the indicated NSCLC cell lines in 96-well plates. The next day, cells were

DOI:10.1158/1078-0432.CCR-06-2077

treated with either 0.1% DMSO as a diluent control or with different concentrations of drugs (0.1-10.0 μmol/L in a final DMSO concentration of 0.1%) in RPMI with 10% FBS or EGF (50 ng/mL). Cell medium was replaced with fresh medium containing gefitinib, AG1024, or both everyday for 3 days. At the end of the treatment period, cell proliferation was measured using the 3-(4,5-dimethylthiazol-2-yl)-2,5-diphenyltetrazolium bromide (MTT) assay. The drug concentrations required to inhibit cell growth by 50% were determined by interpolation from the dose-response curves. Eight replicate wells were used for each analysis, and at least three independent experiments were done. The data from replicate wells are presented as the mean numbers of cells remaining, with 95% confidence intervals (CI). To determine the effect of the combined drug treatments, any potentiation was estimated by multiplying the percentage of cells remaining (% growth) for each agent. The classification index was calculated as described previously (18). Supra-additivity was defined as $\%\ AB/(\%\ A \times \%\ B) > 1.0$; additivity was defined as $\%\ AB/(\%\ A \times \%\ B) = 0.9\text{-}1.0$; and subadditivity was defined as $\%\ AB/(\%\ A \times \%\ B) < 0.9$. (In these equations, *A* and *B* are the effects of individual agents, and *AB* is the effect of the combination of the two drugs.).

Cell cycle and apoptosis assays. For cell cycle and apoptosis assays, 2×10^5 NSCLC cells per well were plated in six-well plates. The next day, the cells were treated with various concentrations of gefitinib (5 μmol/L), AG1024 (5 μmol/L), or both. Both adherent and nonadherent cells were harvested, pooled, and fixed with 1% paraformaldehyde and 70% ethanol. To determine the percentages of cells in the phases of the cell cycle (G_1, S, and G_2-M), we stained cells with 50 μg/mL propidium iodide and analyzed them with a flow cytometer (Epics Profile II; Beckman Coulter Inc.) equipped with a 488-nm argon laser. Apoptosis was assessed using a modified flow cytometry–based terminal nucleotidyl transferase–mediated nick end labeling (TUNEL) assay with an APO-bromodeoxyuridine staining kit (Phoenix Flow Systems) as described previously (19). Data from at least three experiments are presented as means with 95% CIs.

Immunoblotting and coimmunoprecipitation. NSCLC cells were either left uninfected or infected with Ad-EV or Ad-survivin (50 infection-forming units) and then left untreated or treated with gefitinib (1-10 μmol/L), AG1024 (5 μmol/L), and cetuximab (1-10 μmol/L), alone or in combination, in growth medium that was changed daily. For growth factor stimulation, cells were cultured in serum-free medium for 1 day and then incubated with EGF (50 ng/mL). For small interfering RNA (siRNA) transfection, H460 cells in the logarithmic growth phase in six-well plates (5×10^5 cells per well) were transfected with 10 μL of 20 μmol/L survivin siRNA or control scrambled siRNA (Dharmacon) using LipofectAMINE 2000 (Invitrogen) according to the manufacturer's protocol. Cells were incubated for 24 h in growth medium, and gefitinib was added. Cells were harvested after 3 days of incubation.

We did a biochemical analysis of 14 lung tumor and 14 healthy adjacent tissue specimens from patients with NSCLC who had been treated at The University of Texas M.D. Anderson Cancer Center. This study was approved by the M.D. Anderson Cancer Center Institutional Review Board. All tissue specimens were frozen in liquid nitrogen immediately after being resected and rinsed in PBS; they were kept in a -80°C freezer until retrieved for the study. Total protein isolation and Western blot analyses were done as described previously (20).

Immunoprecipitation was done using 3 mg of protein from the total cell lysates and 3 μg of mouse monoclonal anti-EGFR antibody (Santa Cruz Biotechnology), mouse monoclonal anti–IGF-IR antibody (αIR-3; Oncogene Science), or healthy preimmune serum anti-mouse antibody (sc-2025) as the negative control, followed by incubation overnight at 4°C. The immunoprecipitates were resolved by 6% SDS-PAGE and then

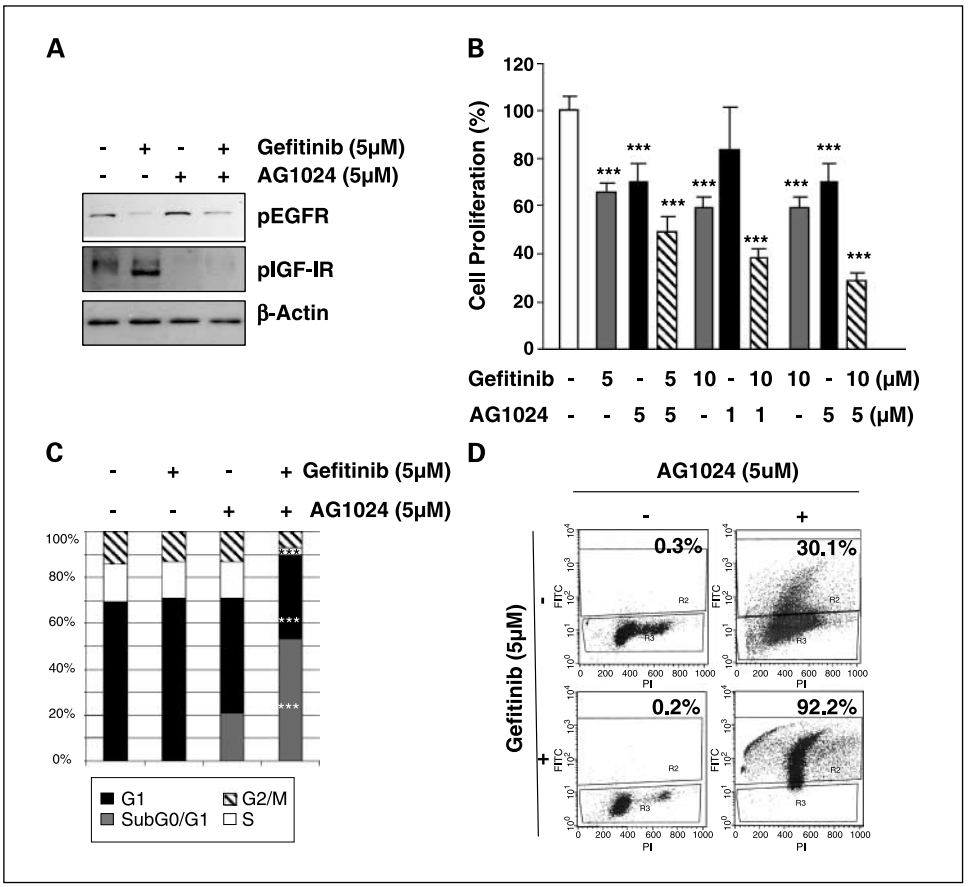

Fig. 2. Effects of combined blockade of EGFR and IGF-IR pathways on NSCLC cells. *A,* effects of treatment with 5 μmol/L gefitinib, 5 μmol/L AG1024, or both on the expression of pEGFR and pIGF-IR were determined in H460 cells by Western blot analysis. β-Actin was used as a loading control. *B,* effect of targeting EGFR and IGF-IR on cell proliferation. H460 cells were treated with the indicated concentrations of gefitinib, AG1024, or both in RPMI 1640 containing 10% FBS for 3 d. The results of the MTT assay are shown. Columns, mean value of eight (MTT) identical wells in a single representative experiment; $n = 3$. Bars, upper 95% CIs. ***, $P < 0.001$ for comparisons between cells treated with a single drug or both drugs. *C,* effects of treatment with the indicated concentrations of gefitinib, AG1024, or both on the cell cycle distribution of H460 cells. DNA content was evaluated by propidium iodide uptake, and the percentages of cells in specific phases of the cell cycle were determined using flow cytometry. Columns, mean value of three identical experiments. **, $P < 0.01$; ***, $P < 0.001$. *D,* apoptosis in H460 cells assessed using a modified TUNEL assay. Two independent experiments were done; the data shown are from a single representative experiment.

DOI:10.1158/1078-0432.CCR-06-2077

Table 1. Synergistic indices of combination treatment with gefitinib and AG1024

Treatment A				Treatment B				Combination treatment			Index*
Drug	Concentration (μmol/L)	MGI	*P* value†	Drug	Concentration (μmol/L)	MGI	*P* value†	Expected‡	Observed§	*P* value†	
Gefitinib	1	0.85	5.3E-05	AG1024	1	0.87	0.0299	0.73	0.69	0.000124	1.05
					5	0.70	7.5E-07	0.59	0.57	1.3E-09	1.03
	5	0.65	1.9E-09		1	0.87	0.0299	0.56	0.50	8.3E-08	1.12
					5	0.70	7.5E-07	0.45	0.44	1.9E-10	1.022
	10	0.59	4.3E-10		1	0.87	0.0299	0.51	0.32	1.2E-12	1.59
					5	0.70	7.5E-07	0.41	0.28	9.9E-14	1.46

NOTE: H460 cell proliferation treated with indicated concentrations of gefitinib, AG1024, or their combinations was calculated by the MTT assay.
Abbreviation: MGI, mean growth inhibition rate = growth rate of treated group/growth rate of untreated group.
*Calculated by dividing the expected growth inhibition rate by the observed growth inhibition rate. An index more than 1 indicates synergistic effect and <1 indicates less than additive effect.
† *P* value (two-sided) was calculated by *t* test compared with no treatment.
‡ Growth inhibition rate of treatment A × growth inhibition rate of treatment B.
§ Growth inhibition rate of combined treatment on treatments A and B.

analyzed by Western blot using rabbit polyclonal antibodies against human phosphorylated EGFR (pEGFR; Tyr^{1068}), EGFR, and phosphorylated IGFR (pIGF-IR and Tyr^{1131}/Tyr^{1146}; 1:1,000; Cell Signaling Technology); rabbit polyclonal antibodies against human IGFR (1:500; Santa Cruz Biotechnology); rabbit polyclonal antibodies against human phosphorylated Akt (pAkt; Ser^{473}; 1:1,000), and Akt (1:1,000) and a mouse monoclonal antibody against human anti-phosphorylated p44/42 MAPK (pp44/42MAPK and Thr^{202}/Tyr^{204}; 1:500; Cell Signaling Technology); goat polyclonal antibodies against p44/42 MAPK (1:1,000; Cell Signaling Technology); and a rabbit polyclonal anti–poly(ADP-ribose) polymerase antibody (1:1,000; VIC 5; Roche Molecular Biochemicals). Other products used in the Western blot analysis included rabbit polyclonal caspase-3 (1:1,000), rabbit polyclonal antibodies against X inhibitor of apoptosis protein (XIAP; 1:1,000; Cell Signaling Technology), rabbit polyclonal antibodies against mammalian target of rapamycin (mTOR; 1:1,000; Cell Signaling Technology), pmTOR (1:1,000; Cell Signaling Technology), mouse monoclonal survivin (1:1,000; Santa Cruz Biotechnology), goat polyclonal antibody against β-actin (1:4,000, Santa Cruz Biotechnology), and rabbit anti-mouse IgG-horseradish peroxidase conjugate (1:2,000; DakoCytomation).

Statistical analysis. The MTT assay data were analyzed using the Student's *t* test. Eight replicate wells were used for each analysis, and data from replicate wells are presented as mean values with 95% CIs. At least three independent experiments were done to obtain each result, and cell survival among groups was compared using ANOVA for a 2 × 2 factorial design. The mean values from three experiments with the eight replicates and 95% CIs were calculated using the SAS software (version 8.02; SAS Institute). In all statistical analyses, two-sided *P* values of <0.05 were considered statistically significant.

Results

Stimulation of the IGF-IR signaling pathway in gefitinib-resistant NSCLC cell lines. We determined the effects of gefitinib on cell proliferation in H596, H226B, H226Br, H460, H1299, H358, and H322 cell lines. We treated cells with gefitinib in the presence of 10% FBS or 50 ng/mL EGF. The MTT assay revealed that gefitinib decreased NSCLC cell proliferation in a dose-dependent manner (Fig. 1A). H322 and H358 cells were more sensitive to gefitinib than were the other cell lines [H322 in 10% FBS, 47.5% (95% CI, 41.5-53.5%; $P < 0.001$); H322 in EGF, 46.8% (95% CI, 40.8-52.8%; $P < 0.01$); H358 in 10% FBS, 52.1% (95% CI, 50.0-54.2%; $P < 0.001$); and H358 in EGF, 41.6% (95% CI, 37.3-45.9%; $P < 0.01$) after 72 h]. The gefitinib concentrations required to inhibit H596, H226B, H226Br, H460, and H1299 cell growth by 50.0% were 10 to 20 times higher than were those for H322 and H358 cells.

We next determined the mechanisms responsible for the sensitivity of NSCLC cells to gefitinib. We first measured the basal levels of EGFR and pEGFR in the cell lines. As shown in Fig. 1B, all cell lines except H322 had high levels of EGFR expression. Four of these six cell lines also had high levels of pEGFR expression, indicating that no relationship exists between gefitinib response and EGFR activation. Because of the role of phosphatase and tensin homologue (PTEN) in NSCLC cells' resistance to EGFR TKIs (21), we next determined

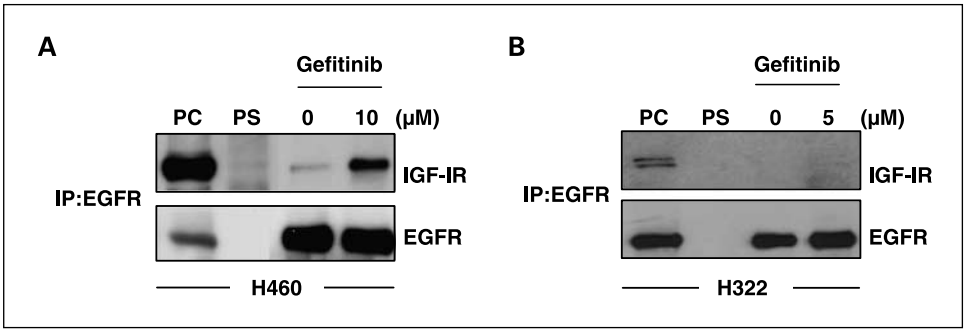

Fig. 3. Effect of gefitinib on EGFR:IGF-IR heterodimerization and activation of IGF-IR signaling pathway. Whole-cell extracts (3 mg) from (*A*) H460 and (*B*) H322 cells, left untreated or treated with gefitinib (10 and 5 μmol/L, respectively) for 3 d, were immunoprecipitated (*IP*) with anti-EGFR antibodies. The immunoprecipitates were subjected to Western blot analysis with the indicated antibodies. Input (*PC*) represents cell lysates (30 μg) that were not subjected to immunoprecipitation. Control immunoprecipitation was done using mouse preimmune serum.

DOI:10.1158/1078-0432.CCR-06-2077

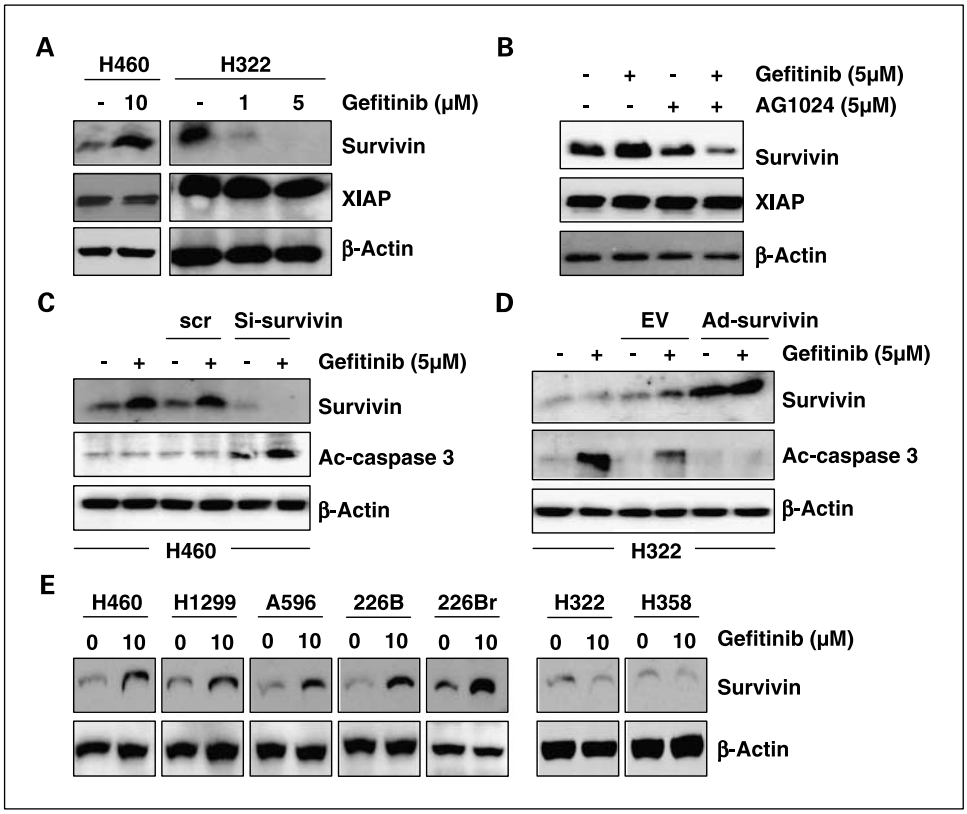

Fig. 4. Role of survivin in the resistance of NSCLC cells to gefitinib. *A,* immunoblotting of survivin and XIAP in H460 and H322 cells treated with the indicated concentrations of gefitinib. *B,* effects of treatment with 5 μmol/L gefitinib, 5 μmol/L AG1024, or both on the expression of survivin and XIAP in H460 cells. *C* and *D,* effect of knockdown of expression or overexpression of survivin on H460 and H322 cells treated with gefitinib. H460 cells were transfected with scrambled (*scr*) or survivin siRNA and left untreated or treated with gefitinib for 48 h. H322 cells were infected with a control virus (Ad-EV or Ad-survivin) and incubated for 3 d in the presence of gefitinib. The protein extracts were subjected to Western blotting for evaluation of survivin and active caspase-3. *E,* Western blot analysis of survivin expression in NSCLC cell lines treated with 10 μmol/L gefitinib. β-Actin was used as a loading control.

the level of PTEN protein expression. PTEN was expressed in all cell lines, suggesting that gefitinib resistance is not caused by a PTEN deficiency. We then determined the expression of IGF-IR, pIGF-IR, Akt, and pAkt and found that most cell lines had high levels of IGF-IR expression, which were associated with high levels of pIGF-IR expression. The levels of pIGF-IR, IGF-IR, and pAkt expression were higher in H460, H1299, A549, H226B, and H226Br cells than in H322 cells, and the levels of pEGFR, EGFR, and pp44/42MAPK expression did not substantially differ among these cell lines. H358 cells also had lower levels of IGFR expression than did H460, H1299, A549, H226B, and H226Br cells (data not shown). The two cell lines most sensitive to gefitinib treatment (H322 and H358) had the lowest level of IGF-IR expression, suggesting that IGF-IR is involved in NSCLC cells' sensitivity to gefitinib.

We selected four representative cell lines, two resistant (H1299 and H460) and two sensitive (H322 and H358) to gefitinib, to determine whether IGF-IR and its downstream signaling components confer resistance to gefitinib. We first determined the phosphorylated and unphosphorylated levels of IGF-IR, EGFR, Akt, and mammalian target of rapamycin (mTOR) in H460 and H322 cells after 72 h of treatment with gefitinib. The treatment (10 μmol/L for H460 cells and 1 or 5 μmol/L for H322 cells) resulted in the complete inhibition of pEGFR expression, verifying gefitinib's effects on EGFR tyrosine kinase activity (Fig. 1C). It was surprising that the levels of pIGF-IR, pAkt, pp44/42MAPK, and pmTOR expression increased in H460 cells after treatment with 10 μmol/L gefitinib, the drug concentration that had completely suppressed pEGFR expression. However, these proteins remained suppressed in gefitinib-treated H322 cells. A gefitinib-induced increase in pIGF-IR expression was observed in H1299 cells that had high levels of IGF-IR expression but not in H358 cells with low levels of IGF-IR expression (Fig. 1D). Taken together, these findings suggest that gefitinib treatment induces activation of the IGF-IR pathway and its downstream signaling components.

Effects of the combined blockade of the EGFR and IGF-IR pathways on the proliferation of NSCLC cells. To determine the roles of the IGF-IR signaling pathway in the development of gefitinib resistance, we evaluated the effects of gefitinib and AG1024, an IGF-IR TKI (22), on the proliferation and apoptosis of H460 cells.

Treatment with gefitinib and AG1024 efficiently blocked the gefitinib-induced increase in pIGF-IR expression in H460 cells (Fig. 2A). We observed more sensitivity to gefitinib when we simultaneously treated H460 cells with gefitinib and AG1024 than with either agent alone (Fig. 2B). In fact, the combined treatment resulted in synergistically enhanced antiproliferative effects on H460 cells [10 μmol/L gefitinib, 59% (95% CI, 55.9-62.1%; $P < 0.001$); 5 μmol/L AG1024, 70.1% (95% CI, 64.7-75.5%; $P < 0.001$); 10 μmol/L gefitinib plus 5 μmol/L AG1024, 28.5% (95% CI, 26-31%; $P < 0.001$; Table 1].

No obvious changes in cell cycle progression were found in H460 cells that had been treated with gefitinib for 3 days; however, a decrease in the G_1 phase population and an increase in the $subG_0/G_1$ phase population were found in those treated with AG1024. Combined treatment with gefitinib (5 μmol/L) and AG1024 (5 μmol/L) for the same duration led to a decrease in the S population, a further decrease in the G_1 population, and an increase in the $subG_0/G_1$ population ($P < 0.001$ for all; Fig. 2C). Moreover, TUNEL staining of cells treated with gefitinib and AG1024 showed a marked increase in apoptosis

DOI:10.1158/1078-0432.CCR-06-2077

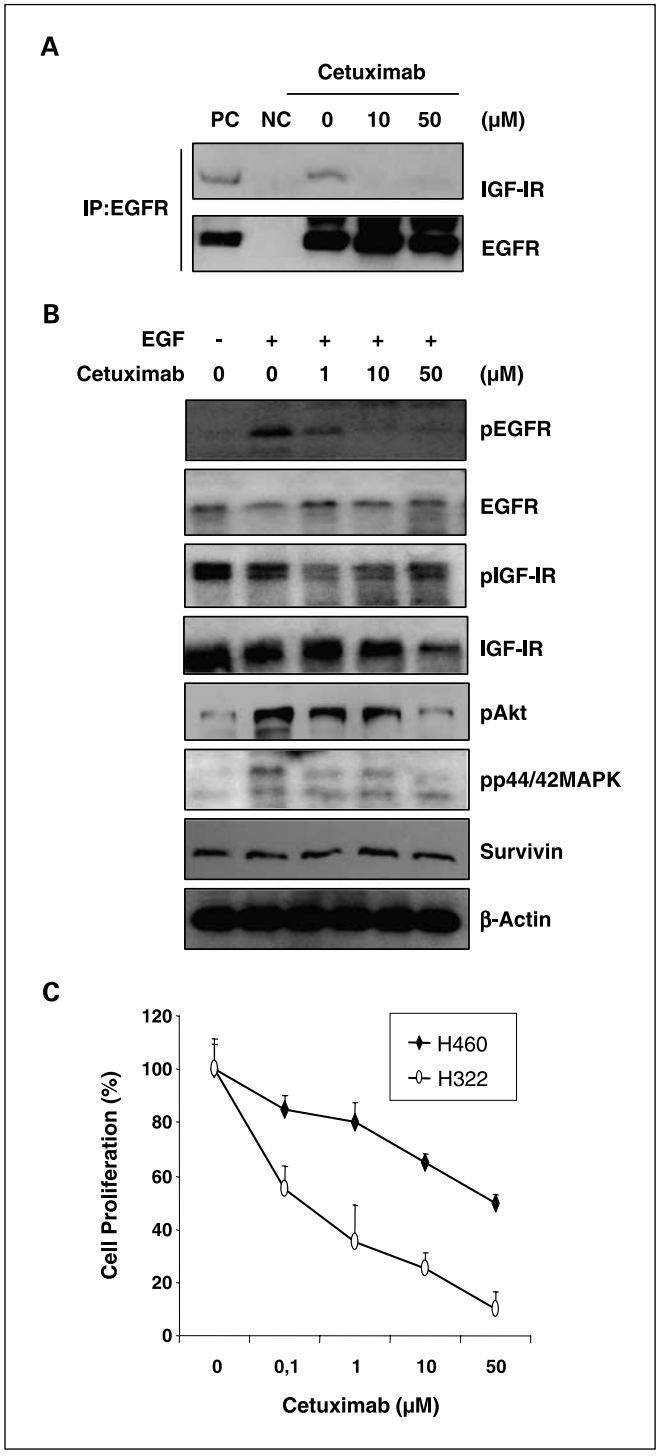

Fig. 5. Effects of cetuximab on EGFR:IGF-IR interaction in NSCLC cells. *A,* effect of cetuximab treatment on EGFR:IGF-IR heterodimerization and activation of the IGF-IR and EGFR signaling pathways. Whole-cell extracts (3 mg) from H460 cells were left untreated or treated with cetuximab (10 and 50 μmol/L) for 3 d. They were then immunoprecipitated with anti-EGFR antibodies, and the immunoprecipitates were subjected to Western blot analysis with the indicated antibodies. Input represents cell lysates (30 μg) that were not subjected to immunoprecipitation. Control immunoprecipitation was done using mouse preimmune serum (PS) as a negative control. *B,* Western blot analysis of survivin, pIGF-IR, IGF-IR, pEGFR, EGFR, pAkt, and pp44/42MAPK expression in H460 cells treated with cetuximab (1, 10, and 50 μmol/L) for 3 d in the absence or presence of EGF (50 ng/mL). *C,* results of the MTT assay of H460 and H322 cell lines after treatment with cetuximab in RPMI 1640 containing 10% FBS for 3 d. Points, mean value of eight identical wells of a single representative experiment; bars, upper 95% CIs.

(Fig. 2D); administration of 5 μmol/L of both gefitinib and AG1024 as single agents induced apoptosis in 0.2% (95% CI, 0.0-2.8%; $P > 0.05$) and 30.1% (95% CI, 14.3-37.6%; $P < 0.05$) of cells, respectively, whereas combined treatment with gefitinib and AG1024 induced apoptosis in more than 90% (95% CI, 64.4-89.8%; $P < 0.001$). These findings suggest that the IGF-IR pathway provides an alternative proliferation or survival mechanism for NSCLC cells in which the EGFR pathway is blocked by gefitinib treatment. Thus, cotargeting the IGF-IR and EGFR pathways may be an effective therapeutic strategy for NSCLC.

Gefitinib induces heterodimerization of IGF-IR and EGFR in H460 cells. EGFR signaling can be modulated by several mechanisms, including heterodimerization with other members of the EGFR family, such as HER-2, and other growth factor receptors, such as IGF-IR (15, 16, 23, 24). We recently observed increased heterodimerization between EGFR and IGF-IR in NSCLC cells after treating them with erlotinib, an EGFR TKI (25). In the current study, we determined the effects of gefitinib on the interaction between EGFR and IGF-IR in H460 and H322 cells. EGFR immunoprecipitates from gefitinib-treated H460 cells showed an obvious increase in IGF-IR binding, whereas control immunoprecipitates that had been treated with preimmune serum had no immunoreactive bands (Fig. 3A). In contrast, both EGFR and control immunoprecipitates from H322 cells lacked immunoreactive bands (Fig. 3B). These results suggest that EGFR and IGF-IR interact through physical contact, and that treatment with gefitinib increases the heterodimerization of EGFR and IGF-IR in H460 cells.

Role of survivin in resistance of NSCLC cells to gefitinib. We next evaluated the signaling mediator that connects gefitinib-induced IGF-IR pathway activation and H460 cell survival. Because inhibitors of apoptosis protein (IAP) such as survivin and XIAP play a role in tumor cells' resistance to chemotherapeutic drugs (26), we determined the effects of gefitinib on the expression of these proteins in H460 and H322 cells. As shown in Fig. 4A, the expression level of survivin but not XIAP markedly increased in H460 cells after treatment with gefitinib. In contrast, no changes were detected in the expression levels of survivin or XIAP in these cells. Moreover, treatment with gefitinib (5 μmol/L) and AG1024 (5 μmol/L) efficiently suppressed the gefitinib-induced increase in survivin expression (Fig. 4B). We then evaluated the influence of survivin on gefitinib-induced apoptosis in NSCLC cells by knockdown of expression or overexpression of survivin. H460 cells transfected with control scrambled or survivin siRNA before treatment with 10 μmol/L gefitinib (a concentration that did not induce apoptosis) had an obvious increase in the rate of apoptosis as determined by a Western blot analysis of an increase in activated caspase-3 expression (Fig. 4C). Furthermore, among H322 cells infected with Ad-survivin, the level of gefitinib-induced apoptosis was substantially reduced (Fig. 4D). These findings suggest that NSCLC cells can escape apoptosis by inducing survivin expression. To determine whether the induction of survivin by gefitinib is related to the resistance of cell lines to the drug, we compared the expression of survivin in a subset of NSCLC cell lines that had been treated with TKI. The five nonsensitive or resistant NSCLC cell lines (H460, H1299, A596, 226B, and 226Br cells) showed an increase in survivin expression after treatment with gefitinib; no increase

DOI:10.1158/1078-0432.CCR-06-2077

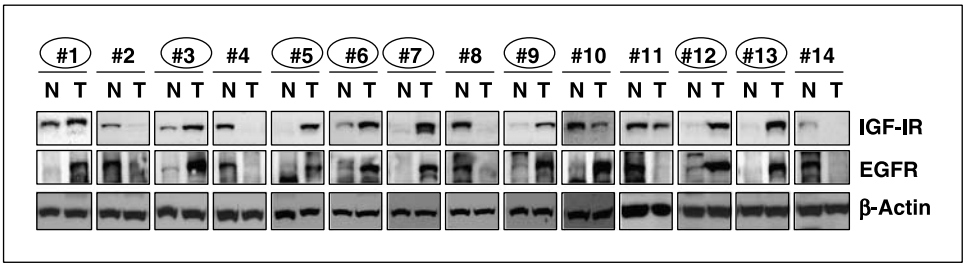

Fig. 6. Expression of EGFR and IGF-IR in paired lung tumor and normal tissue specimens from patients with NSCLC. Proteins were extracted from lung tumor and healthy lung tissue and subjected to Western blot analysis to determine the expression of EGFR and IGF-IR. β-Actin was used as a loading control. The samples marked with a circle had increased IGF-IR and EGFR expression.

was found in the two most sensitive NSCLC cell lines (H322 and H358; Fig. 4E). These results suggest that NSCLC cells' resistance to gefitinib can be mediated by survivin induction.

Effects of cetuximab on EGFR:IGF-IR interaction in NSCLC cells. We evaluated the effects of cetuximab on the interaction between IGF-IR and EGFR. EGFR precipitates from cetuximab-treated H460 cells showed no detectable binding to IGF-IR, suggesting that cetuximab suppressed the interaction between EGFR and IGF-IR (Fig. 5A). Moreover, treatment with cetuximab decreased EGF-stimulated pEGFR expression in H460 cells in a dose-dependent manner, without inducing pIGF-IR, pAkt, pp44/42MAPK, or survivin expression (Fig. 5B). A cell proliferation assay showed that H460 cells were more resistant to the antibody than were H358 cells (Fig. 5C). Overall, these findings suggest that heterodimerization between IGF-IR and EGFR, activation of IGF-IR, and induction of survivin expression are at least partly responsible for the induction of acquired resistance to EGFR TKIs, but not to the monoclonal antibody against EGFR in NSCLC cells.

Expression of EGFR and IGF-IR in human lung tissue. Our data suggested that IGF-IR expression has an important role in determining NSCLC cells' sensitivity to EGFR TKIs. Therefore, we determined the levels of EGFR and IGF-IR expression in NSCLC tissue. Nine of the fourteen tumor specimens had higher levels of EGFR expression than did normal tissue specimens from the same patients. Eight of those specimens also had higher levels of IGF-IR expression than those did in normal tissue (Fig. 6).

Discussion

We have previously shown that erlotinib, an EGFR TKI, induces heterodimerization of EGFR/IGF-IR, resulting in the activation of IGF-IR and induction of Akt/mTOR-mediated synthesis of survivin protein, which protects NSCLC cells from the drug-induced apoptosis (25). In the present study, we show that the activation of the IGF-IR via heterodimerization of EGFR/IGF-IR and consequent induction of survivin expression also mediate gefitinib resistance in NSCLC cells, confirming and extending our previous findings (25). Our studies also show that IGF-IR pathway did not affect antiproliferative activities of cetuximab, a monoclonal antibody blocking EGFR. Overall, these findings suggest that heterodimerization between IGF-IR and EGFR, activation of IGF-IR, and induction of survivin expression contribute to the acquired resistance to EGFR TKIs, but not to the monoclonal antibody against EGFR in NSCLC cells.

In clinical trials, the EGFR TKIs, such as erlotinib and gefitinib, were found to be effective in the treatment of patients with NSCLC (27, 28). These agents were approved for NSCLC treatment after resulting in response rates of 10% and survival advantages in patients previously treated with chemotherapy (29). However, large-scale phase III clinical trials in advanced NSCLC have had contrasting results (13, 14, 29, 30). In the current study, we found that gefitinib treatment did not inhibit NSCLC cell proliferation at doses sufficient to suppress EGFR activation, suggesting that the development of resistance to EGFR TKIs is caused by the activation of alternative cell survival signaling mechanisms.

To develop better anticancer therapeutic strategies using gefitinib, we sought to identify the pathways whereby NSCLC cell trigger alternative survival signaling. PTEN expression and EGFR and Kirsten ras (*KRAS*) somatic mutation have been involved in the cellular response to EGFR-targeted therapy (31–33). Bianco et al. (34) found that the loss of PTEN expression in the MDA-468 breast cancer cell line contributed to gefitinib resistance. These findings suggest that PTEN-deficient cell lines maintain their Akt activity and survive when EGFR is inactivated. However, deletion of PTEN does not frequently occur in NSCLC cells (31, 35). In fact, all NSCLC cell lines used in our study expressed PTEN, suggesting that gefitinib resistance in NSCLC cells is not caused by a PTEN deficiency. Similarly, the NSCLC cell lines without somatic mutations of *EGFR* responded to gefitinib, which is consistent with previously reported findings (36, 37). Moreover, in our study, gefitinib showed antiproliferative effects on H358 cells that have somatic mutation in *KRAS* (38). Together, these findings indicate that expression of PTEN and mutational status of *EGFR* and *KRAS* are not entirely responsible for NSCLC cells' resistance to gefitinib.

Our *in vitro* data suggest that the cross-talk between the IGF-IR and EGFR signaling pathways is involved in the development of gefitinib resistance in NSCLC cells. First, we found that the levels of IGF-IR and pIGF-IR expression in NSCLC cells were inversely associated with the antiproliferative effects of gefitinib. Second, gefitinib induced phosphorylation of IGF-IR and its downstream mediators in NSCLC cell lines with high levels of IGF-IR expression. Third, gefitinib induced heterodimerization between IGF-IR and EGFR and survivin expression in the high IGF-IR–expressing H460 cells but not in the low IGF-IR–expressing H322 cells. Finally, gefitinib exhibited apoptotic activity in H460 cells, in which IGF-IR activation was blocked. These NSCLC cell lines have shown a similar response to the erlotinib treatment (25). EGFR and IGF-IR have similar extracellular domain structures (39); therefore, it is plausible that EGFR TKIs induce a direct interaction between EGFR and IGF-IR, leading to the activation of IGF-IR pathways and induction of survivin expression and, thus, maintain NSCLC cell proliferation. Recent reports showing a direct interaction between EGFR and IGF-IR (40, 41) also support our hypothesis.

DOI:10.1158/1078-0432.CCR-06-2077

The induced expression of survivin found in our study seemed to protect H460 cell from apoptosis in the presence of gefitinib: survivin overexpression protected H322 cells from gefitinib-induced apoptosis. In addition, gefitinib induced apoptosis in H460 cells, in which transfection with survivin-specific siRNA silenced survivin expression. Survivin is a member of the IAP family and is associated with both cancer progression and drug resistance (42, 43). Therefore, the resistance and sensitivity of NSCLC cells to gefitinib may be determined, at least in part, by their ability to activate the IGF-IR–mediated pathway and induce survivin expression. Most strikingly, we found no evidence of EGFR and IGF-IR heterodimerization, IGF-IR activation, and induction of survivin expression in H460 cells after cetuximab treatment. These findings suggest that activation of the IGF-IR pathway and the subsequent expression of survivin are at least partly responsible for the sensitivity of NSCLC cells to EGFR TKIs but not to anti-EGFR monoclonal antibodies.

In summary, we showed that the cross-talk between IGF-IR and EGFR has a specific role in inducing gefitinib resistance in NSCLC cells. Gefitinib induced heterodimerization of EGFR and IGF-IR; stimulated IGF-IR and downstream pathways, including phosphoinositide-3-kinase/Akt/mTOR and p44/42 MAPK; and increased survivin expression in NSCLC cell lines. Overexpression of the EGFR family and its ligands have been found in 30% to 80% of NSCLC (30, 44, 45). However, we found no interaction between EGFR and IGF-IR in NSCLC cells with low levels of IGF-IR expression, suggesting that the basal level of IGF-IR expression is important for initiating the formation of the EGFR:IGF-IR complex. Nine of the fourteen (64%) tumor specimens in our study exhibited higher levels of EGFR expression, and eight of those had related higher IGF-IR expression compared with paired normal tissue. The number of IGF-IRs may determine the response to IGF-I; activated IGF-IRs in sufficient numbers change the mode of IGF's effect from nonmitogenic to mitogenic, resulting in cell cycle progression, translation, and DNA synthesis (46). Overexpression of IGF-IR has been associated with survival of NSCLC patients treated with gefitinib (47). Therefore, our newly identified mechanism of EGFR TKI resistance could provide new therapeutic avenues for NSCLC. Treatment with the anti-EGFR monoclonal antibody cetuximab may be effective once resistance to EGFR TKIs has been established, and the use of combination regimens with EGFR TKIs and IGF-IR inhibitors may be effective at treating NSCLC in patients with high levels of EGFR and IGF-IR expression. However, the results of an *in vitro* study with a limited number of cell lines are not sufficient to generalize the roles of the IGF-IR signaling pathway and survivin expression in gefitinib resistance in NSCLC cells. Further clinical trials are needed to determine whether combined treatment with EGFR TKIs and IGF-IR pathway inhibitors enhances objective responses and survival in patients with NSCLC.

References

1. Jemal. American Cancer Society: Cancer facts and figures 2006. Atlanta, GA: American Cancer Society; 2006.
2. Mendelsohn J. The epidermal growth factor receptor as a target for cancer therapy. Endocr Relat Cancer 2001;8:3–9.
3. Brognard J, Clark AS, Ni Y, Dennis PA. Akt/protein kinase B is constitutively active in non–small cell lung cancer cells and promotes cellular survival and resistance to chemotherapy and radiation. Cancer Res 2001;61:3986–97.
4. Brognard J, Dennis PA. Variable apoptotic response of NSCLC cells to inhibition of the MEK/ERK pathway by small molecules or dominant negative mutants. Cell Death Differ 2002;9:893–904.
5. Woodburn JR. The epidermal growth factor receptor and its inhibition in cancer therapy. Pharmacol Ther 1999;82:241–50.
6. Ciardiello F, Bianco R, Damiano V, et al. Antiangiogenic and antitumor activity of anti-epidermal growth factor receptor C225 monoclonal antibody in combination with vascular endothelial growth factor antisense oligonucleotide in human GEO colon cancer cells. Clin Cancer Res 2000;6:3739–47.
7. Fan Z, Lu Y, Wu X, Mendelsohn J. Antibody-induced epidermal growth factor receptor dimerization mediates inhibition of autocrine proliferation of A431 squamous carcinoma cells. J Biol Chem 1994;269:27595–602.
8. Goldstein NI, Prewett M, Zuklys K, Rockwell P, Mendelsohn J. Biological efficacy of a chimeric antibody to the epidermal growth factor receptor in a human tumor xenograft model. Clin Cancer Res 1995;1:1311–8.
9. Ciardiello F, Damiano V, Bianco R, et al. Antitumor activity of combined blockade of epidermal growth factor receptor and protein kinase A. J Natl Cancer Inst 1996;88:1770–6.
10. Bonner JA, Harari PM, Giralt J, et al. Radiotherapy plus cetuximab for squamous-cell carcinoma of the head and neck. N Engl J Med 2006;354:567–78.
11. Meyerhardt JA, Mayer RJ. Systemic therapy for colorectal cancer. N Engl J Med 2005;352:476–87.
12. Fry DW, Bridges AJ, Denny WA, et al. Specific, irreversible inactivation of the epidermal growth factor receptor and erbB2, by a new class of tyrosine kinase inhibitor. Proc Natl Acad Sci U S A 1998;95:12022–7.
13. Giaccone G, Herbst RS, Manegold C, et al. Gefitinib in combination with gemcitabine and cisplatin in advanced non–small-cell lung cancer: a phase III trial—INTACT 1. J Clin Oncol 2004;22:777–84.
14. Herbst RS, Giaccone G, Schiller JH, et al. Gefitinib in combination with paclitaxel and carboplatin in advanced non–small-cell lung cancer: a phase III trial—INTACT 2. J Clin Oncol 2004;22:785–94.
15. Jones HE, Goddard L, Gee JM, et al. Insulin-like growth factor-I receptor signalling and acquired resistance to gefitinib (ZD1839; Iressa) in human breast and prostate cancer cells. Endocr Relat Cancer 2004;11:793–814.
16. Chakravarti A, Loeffler JS, Dyson NJ. Insulin-like growth factor receptor I mediates resistance to anti-epidermal growth factor receptor therapy in primary human glioblastoma cells through continued activation of phosphoinositide 3-kinase signaling. Cancer Res 2002;62:200–7.
17. Lee CT, Park KH, Adachi Y, et al. Recombinant adenoviruses expressing dominant negative insulin-like growth factor-I receptor demonstrate antitumor effects on lung cancer. Cancer Gene Ther 2003;10:57–63.
18. Goldstein D, Bushmeyer SM, Witt PL, Jordan VC, Borden EC. Effects of type I and II interferons on cultured human breast cells: interaction with estrogen receptors and with tamoxifen. Cancer Res 1989;49:2698–702.
19. Chun KH, Kosmeder JW II, Sun S, et al. Effects of deguelin on the phosphatidylinositol 3-kinase/Akt pathway and apoptosis in premalignant human bronchial epithelial cells. J Natl Cancer Inst 2003;95:291–302.
20. Lee HY, Moon H, Chun KH, et al. Effects of insulin-like growth factor binding protein-3 and farnesyltransferase inhibitor SCH66336 on Akt expression and apoptosis in non–small-cell lung cancer cells. J Natl Cancer Inst 2004;96:1536–48.
21. Tang JM, He QY, Guo RX, Chang XJ. Phosphorylated Akt overexpression and loss of PTEN expression in non–small cell lung cancer confers poor prognosis. Lung Cancer 2006;51:181–91.
22. Parrizas M, Gazit A, Levitzki A, Wertheimer E, LeRoith D. Specific inhibition of insulin-like growth factor-1 and insulin receptor tyrosine kinase activity and biological function by tyrphostins. Endocrinology 1997;138:1427–33.
23. Balana ME, Labriola L, Salatino M, et al. Activation of ErbB-2 via a hierarchical interaction between ErbB-2 and type I insulin-like growth factor receptor in mammary tumor cells. Oncogene 2001;20:34–47.
24. Gilmore AP, Valentijn AJ, Wang P, et al. Activation of BAD by therapeutic inhibition of epidermal growth factor receptor and transactivation by insulin-like growth factor receptor. J Biol Chem 2002;277:27643–50.
25. Morgillo F, Woo JK, Kim ES, Hong WK, Lee HY. Heterodimerization of insulin-like growth factor receptor/epidermal growth factor receptor and induction of survivin expression counteract the antitumor action of erlotinib. Cancer Res 2006;66:10100–11.
26. Altieri DC. The molecular basis and potential role of survivin in cancer diagnosis and therapy. Trends Mol Med 2001;7:542–7.
27. Kris MG, Natale RB, Herbst RS, et al. Efficacy of gefitinib, an inhibitor of the epidermal growth factor receptor tyrosine kinase, in symptomatic patients with non–small cell lung cancer: a randomized trial. JAMA 2003;290:2149–58.
28. Fukuoka M, Yano S, Giaccone G, et al. Multi-institutional randomized phase II trial of gefitinib for previously treated patients with advanced non–small-cell lung cancer (the IDEAL 1 trial) [corrected]. J Clin Oncol 2003;21:2237–46.
29. Shepherd FA, Rodrigues Pereira J, Ciuleanu T, et al.

DOI:10.1158/1078-0432.CCR-06-2077

Erlotinib in previously treated non – small-cell lung cancer. N Engl J Med 2005;353:123 – 32.

30. Thatcher N, Chang A, Parikh P, et al. Gefitinib plus best supportive care in previously treated patients with refractory advanced non – small-cell lung cancer: results from a randomised, placebo-controlled, multicentre study (Iressa Survival Evaluation in Lung Cancer). Lancet 2005;366:1527 – 37.

31. Kohno T, Takahashi M, Manda R, Yokota J. Inactivation of the PTEN/MMAC1/TEP1 gene in human lung cancers. Genes Chromosomes Cancer 1998;22: 152 – 6.

32. Lynch TJ, Bell DW, Sordella R, et al. Activating mutations in the epidermal growth factor receptor underlying responsiveness of non – small-cell lung cancer to gefitinib. N Engl J Med 2004;350:2129 – 39.

33. Paez JG, Janne PA, Lee JC, et al. EGFR mutations in lung cancer: correlation with clinical response to gefitinib therapy. Science 2004;304:1497 – 500.

34. Bianco R, Shin I, Ritter CA, et al. Loss of PTEN/MMAC1/TEP in EGF receptor-expressing tumor cells counteracts the antitumor action of EGFR tyrosine kinase inhibitors. Oncogene 2003;22:2812 – 22.

35. Yokomizo A, Tindall DJ, Drabkin H, et al. PTEN/MMAC1 mutations identified in small cell, but not in non – small cell lung cancers. Oncogene 1998;17: 475 – 9.

36. Amann J, Kalyankrishna S, Massion PP, et al. Aberrant epidermal growth factor receptor signaling and enhanced sensitivity to EGFR inhibitors in lung cancer. Cancer Res 2005;65:226 – 35.

37. Tracy S, Mukohara T, Hansen M, Meyerson M, Johnson BE, Janne PA. Gefitinib induces apoptosis in the EGFRL858R non – small-cell lung cancer cell line H3255. Cancer Res 2004;64:7241 – 4.

38. Mitsudomi T, Steinberg SM, Nau MM, et al. p53 gene mutations in non – small-cell lung cancer cell lines and their correlation with the presence of ras mutations and clinical features. Oncogene 1992;7: 171 – 80.

39. Garrett TP, McKern NM, Lou M, et al. Crystal structure of the first three domains of the type-1 insulin-like growth factor receptor. Nature 1998;394:395 – 9.

40. Gschwind A, Zwick E, Prenzel N, Leserer M, Ullrich A. Cell communication networks: epidermal growth factor receptor transactivation as the paradigm for interreceptor signal transmission. Oncogene 2001;20: 1594 – 600.

41. Roudabush FL, Pierce KL, Maudsley S, Khan KD, Luttrell LM. Transactivation of the EGF receptor mediates IGF-I – stimulated shc phosphorylation and ERK1/2 activation in COS-7 cells. J Biol Chem 2000; 275:22583 – 9.

42. Adida C, Crotty PL, McGrath J, Berrebi D, Diebold J, Altieri DC. Developmentally regulated expression of the novel cancer anti-apoptosis gene survivin in human and mouse differentiation. Am J Pathol 1998; 152:43 – 9.

43. Zhang M, Latham DE, Delaney MA, Chakravarti A. Survivin mediates resistance to antiandrogen therapy in prostate cancer. Oncogene 2005;24: 2474 – 82.

44. Rusch V, Klimstra D, Venkatraman E, Pisters PW, Langenfeld J, Dmitrovsky E. Overexpression of the epidermal growth factor receptor and its ligand transforming growth factor α is frequent in resectable non – small cell lung cancer but does not predict tumor progression. Clin Cancer Res 1997;3: 515 – 22.

45. Fontanini G, De Laurentiis M, Vignati S, et al. Evaluation of epidermal growth factor-related growth factors and receptors and of neoangiogenesis in completely resected stage I-IIIA non – small-cell lung cancer: amphiregulin and microvessel count are independent prognostic indicators of survival. Clin Cancer Res 1998;4:241 – 9.

46. Kurmasheva RT, Houghton PJ. IGF-I mediated survival pathways in normal and malignant cells. Biochim Biophys Acta 2006;1766:1 – 22.

47. Cappuzzo F, Toschi L, Tallini G, et al. Insulin-like growth factor receptor 1 (IGFR-1) is significantly associated with longer survival in non – small-cell lung cancer patients treated with gefitinib. Ann Oncol 2006;17:1120 – 7.

DOI:10.1158/0008-5472.CAN-06-1684

Cancer Research

Heterodimerization of Insulin-like Growth Factor Receptor/Epidermal Growth Factor Receptor and Induction of Survivin Expression Counteract the Antitumor Action of Erlotinib

Floriana Morgillo, Jong Kyu Woo, Edward S. Kim, et al.

Cancer Res 2006;66:10100-10111. Published online October 17, 2006.

DOI:10.1158/0008-5472.CAN-06-1684

Research Article

Heterodimerization of Insulin-like Growth Factor Receptor/Epidermal Growth Factor Receptor and Induction of Survivin Expression Counteract the Antitumor Action of Erlotinib

Floriana Morgillo, Jong Kyu Woo, Edward S. Kim, Waun Ki Hong, and Ho-Young Lee

Department of Thoracic/Head and Neck Medical Oncology, The University of Texas M.D. Anderson Cancer Center, Houston, Texas

Abstract

Epidermal growth factor receptor (EGFR) tyrosine kinase inhibitors (TKIs) have been used to treat non–small cell lung cancer (NSCLC). However, the overall response rate to EGFR TKIs is limited, and the mechanisms mediating resistance to the drugs are poorly understood. Here, we report that insulin-like growth factor-I receptor (IGF-IR) activation interferes with the antitumor activity of erlotinib, an EGFR TKI. Treatment with erlotinib increased the levels of EGFR/IGF-IR heterodimer localized on cell membrane, activated IGF-IR and its downstream signaling mediators, and stimulated mammalian target of rapamycin (mTOR)–mediated *de novo* protein synthesis of EGFR and survivin in NSCLC cells. Inhibition of IGF-IR activation, suppression of mTOR-mediated protein synthesis, or knockdown of survivin expression abolished resistance to erlotinib and induced apoptosis in NSCLC cells *in vitro* and *in vivo*. Our data suggest that enhanced synthesis of survivin protein mediated by the IGFR/EGFR heterodimer counteracts the antitumor action of erlotinib, indicating the needs of integration of IGF-IR–targeted agents to the treatment regimens with EGFR TKI for patients with lung cancer. (Cancer Res 2006; 66(20): 10100-11)

Introduction

The 5-year survival rate for lung cancer patients remains extremely poor (≤15; ref. 1), underscoring the need for more effective treatment strategies. Recently, new therapeutic approaches targeting signaling pathways involved in cell proliferation, apoptosis, angiogenesis, and metastasis have been investigated (2). Among the many potential target pathways, the epidermal growth factor (EGF) receptor (EGFR) signaling pathway has been studied most extensively because EGFR overexpression has been observed in a number of solid tumors, including 40% to 80% of non–small cell lung cancers (NSCLC; ref. 3). The EGFR signaling pathway activates the phosphatidylinositol 3-kinase (PI3K)/Akt and mitogen-activated protein kinase (MAPK) pathways, which play major roles in cell proliferation, survival, and transformation and in therapeutic resistance (4, 5). In addition, the EGFR pathway is implicated in angiogenesis, and cell invasion by its regulation of the expression and activity of matrix metalloproteinases (6, 7).

These findings indicate the therapeutic potential of inhibitors of EGFR tyrosine kinase activation. EGFR tyrosine kinase activity can be inhibited by antibodies against the extracellular domain of EGFR, such as cetuximab, or by small molecules that block the ATP binding site of the cytoplasmic domain, such as gefitinib (ZD1839, Iressa; AstraZeneca Pharmaceuticals, Macclesfield, United Kingdom) and erlotinib (Tarceva®; OSI Pharmaceuticals; Genentech, South San Francisco, CA). Both forms of EGFR inhibition have single-agent antitumor activity against previously treated NSCLC (3, 8–10). Erlotinib exhibits an antiproliferative effect at nanomolar concentrations and has induced apoptosis and reversible cell cycle arrest at G_1 (11). *In vivo* preclinical models have shown that erlotinib administration markedly reduces EGFR autophosphorylation and growth in human head and neck cancer xenografts (HN5 and A431 cells) in nude mice (11, 12). In addition, gefitinib, combined with standard chemotherapeutic agents and/or radiotherapy in preclinical studies, has inhibited EGFR activation, thus causing G_1 cell cycle arrest and contributing to synergistic growth inhibition (13).

Despite a similar chemical structure, these two EGFR tyrosine kinase inhibitors (TKIs) have provided contrasting results in phase III clinical trials, in which only erlotinib showed significantly improved survival compared with placebo (14–16). The response to gefitinib and erlotinib has been suggested to be associated with sex, smoking status, tumor histology, and somatic mutations of the EGFR ATP binding site (17, 18). Recent data have suggested that the insulin-like growth factor-1 receptor (IGF-IR) pathway is also implicated in the resistance of gefitinib and anti-EGFR monoclonal antibody (19, 20). However, to our knowledge, the mechanisms involved in the IGF-IR–mediated acquired resistance to erlotinib in NSCLC cells have not been completely defined. In this article, we report that erlotinib induce EGFR/IGF-IR heterodimerization on the cell membrane, transmitting a survival signal through IGF-IR and its downstream mediators PI3K/Akt and p44/42 MAPK to stimulate mammalian target of rapamycin (mTOR)–mediated synthesis of EGFR and antiapoptotic survivin proteins. Consequently, inactivation of IGF-IR, suppression of mTOR-mediated protein synthesis, or knockdown of survivin protein renders EGFR-overexpressing NSCLC cells sensitive to the erlotinib treatment.

Materials and Methods

Cells, reagents, and animals. The human NSCLC cell lines H596, H226B, H226Br, H460, H1299, A549, H358, H661, and H322 were from the American Type Culture Collection (Manassas, VA) and maintained in RPMI 1640 supplemented with 10% fetal bovine serum (FBS; Life Technologies, Gaithersburg, MD) in a humidified atmosphere with 5% CO_2. IGF and EGF were from R&D Systems (Minneapolis, MN). Erlotinib were prepared as 10 mmol/L stock solution in DMSO and stored at −20°C. LY294002

Note: Supplementary data for this article are available at Cancer Research Online (http://cancerres.aacrjournals.org/).

W.K. Hong is an American Cancer Society Clinical Research Professor. H-Y. Lee is a faculty member at the Graduate School of Biomedical Sciences.

Requests for reprints: Ho-Young Lee, Department of Thoracic/Head and Neck Medical Oncology, The University of Texas M.D. Anderson Cancer Center, Box 432, 1515 Holcombe Boulevard, Houston, TX 77030. Phone: 713-792-6363; Fax: 713-792-0430; E-mail: hlee@mdanderson.org.

doi:10.1158/0008-5472.CAN-06-1684

DOI:10.1158/0008-5472.CAN-06-1684

(an inhibitor of PI3K), PD98059 (an inhibitor of the MEK1), rapamycin, and AG1024, a TKI of IGF-IR, were from Calbiochem-Novabiochem (Alexandria, New South Wales, Australia); these inhibitors were prepared as 20 mmol/L stock solutions in DMSO and also stored at −20°C. Adenoviral vectors expressing survivin (Ad-survivin; ref. 21) or dnIGF-IR/482 [adenovirus-expressing, dominant-negative IGF-IR (Ad-dnIGF-IR)], a soluble extracellular domain of IGF-IR with an engineered stop codon at amino acid residue 482 (22), and control adenoviral vector [adenovirus-expressing empty vector (Ad-EV)] were amplified as described elsewhere (23). We confirmed increases in the levels of IGF-IR protein by Western blot assay with an antibody for the α-subunit (anti-IGF-IRα N-20, Santa Cruz Biotechnology, Santa Cruz, CA) using medium from the cells that were infected with Ad-dnIGF-IR because IGF-IR/482 has been shown to produce and release the truncated α-subunit of IGF-IR into the medium (22). The effect of the combination of erlotinib and Ad-dnIGF-IR on established s.c. tumor nodules was studied in athymic nude mice (Harlan Sprague-Dawley, Indianapolis, IN) in a defined pathogen-free environment. Six-week-old female mice were used in this study; mice with necrotic tumors or tumors ≥1.5 cm in diameter were euthanized.

Cell proliferation assay. Cells were treated with erlotinib, rapamycin, LY294002, PD98059, AG1024, Ad-dnIGF-IR, Ad-EV, or their combinations in the absence or presence of 10% FBS, EGF (50 ng/mL), or IGF (50 ng/mL). For the experiments with the viruses, cells were infected with 5 and 10 particle forming unit (pfu) for Ad-dnIGF-IR or Ad-EV, in serum-free medium for 2 hours and then incubated for 3 days in RPMI medium supplemented with 10% FBS in the absence or presence of the indicated concentrations of erlotinib. Cell proliferation was measured with the 3-(4,5-dimethylthiazol-2-yl)-2,5-diphenyltetrazolium bromide (MTT) assay. The drug concentrations required to inhibit cell growth by 50% were determined by interpolation from the dose-response curves. For defining the effect of the combined drug treatments, any potentiation was estimated by multiplying the percentage of cells remaining by each individual agent. The synergistic index was calculated as previously described (24). In the following equations, A and B are the effects of each individual agent, and AB is the effect of the combination. Subadditivity was defined as %AB / (%A × %B) < 0.9; additivity was defined as %AB / (%A × %B) = 0.9-1.0; and supra-additivity was defined as %AB / (%A × %B) > 1.0.

Clonogenic growth assay. The anchorage-dependent clonogenic growth assay was done by seeding NSCLC cell lines into six-well plates at low density (≈3×10^3 cells per well). Cells were either left uninfected or infected with 5 or 10 pfu/cell of Ad-dnIGF-IR or Ad-EV, incubated for 72 hours with different concentrations of erlotinib (0.1, 1.0, and 5.0 μmol/L), AG1024 (5 μmol/L), or combinations of the two drugs in serum-free RPMI medium in the absence or presence of IGF (50 ng/mL). Cells were replated in six-well plates and cultured in growth medium for 7 to 10 days, in a humidified atmosphere with 5% CO_2, at 37°C, and then colonies were fixed with 0.1% Coomassie blue (Bio-Rad Laboratories, Hercules, CA) in 30% methanol and 10% acetic acid. We then counted the number of colonies with >50 cells. For the anchorage-independent clonogenic growth assay, ~3×10^3 cells were suspended in 0.75 mL of 0.22% soft agar that was layered on top of 1 mL of 1% solidified agar in each well of 24-well plates. The plates were then incubated for 10 to 15 days in serum-free RPMI medium containing 0.1 or 1.0 μmol/L concentrations of erlotinib in the absence or presence of 10% FBS or IGF (50 ng/mL). The medium was changed daily during this period, at the end of which tumor cell colonies measuring at least 80 μm were counted under using a dissection microscope.

Cell cycle and apoptosis assays. For cell cycle and apoptosis assays, both adherent and nonadherent cells were harvested, pooled, and fixed with 1% paraformaldehyde and 70% ethanol. For the cell cycle analysis, we stained cells with 50 μg/mL propidium iodide and determined the percentage of cells in specific cell cycle phases (G_1, S, and G_2-M) by using a flow cytometer equipped with a 488 nm argon laser (Epics Profile II; Beckman Coulter, Miami, FL). Approximately 1×10^4 cells were evaluated for each sample. Apoptosis was assessed with a flow cytometry–based terminal deoxyribonucleotide transferase–mediated nick-end labeling (TUNEL) assay processed with an APO-bromodeoxyuridine (APO-BrdUrd) staining kit (Phoenix Flow Systems, San Diego, CA); this assay was modified as previously described (25). Cells treated with DMSO were used as a negative control, and for a positive control, we used the HL-60 leukemic cells treated with camptothecin provided with the kit.

Establishment of resistant cell line. The H460 cell cultures were continuously exposed to erlotinib (10 μmol/L) in routine culture medium that was replaced every day for 5 months. Initially, H460 cell numbers were substantially reduced, and for the next 2 months, the surviving cells were passaged approximately every 10 days with a seeding ratio of 1:2. Cell proliferation slowly increased to allow a passage every 7 days with a seeding ratio of 1:4 over the next 2 months. A stable growth rate was reached after a total of 5 months with routine maintenance of the H460/TKI-R cells involving passage every 4 days with a seeding ratio of 1:8 of the confluent cell number.

Subcellular fractionation. The following procedures were done at 4°C. Cells were scraped into PBS [10 mmol/L sodium phosphate (pH 7.4) and 150 mmol/L NaCl] and then collected by centrifugation. Cell pellets were resuspended with 1 mL of hypotonic buffer [10 mmol/L Tris-HCl (pH 7.5), 1 mmol/L $MgCl_2$, 50 μg/mL leupeptin, 1 mmol/L phenylmethylsulfonyl fluoride, and 1 mmol/L Na_3VO_4]; 10 minutes later, the cells were transferred to a Dounce homogenizer and further disrupted by 25 strokes with a tight-fitting pestle. The homogenate was adjusted to the indicated NaCl concentration from a 5 mol/L stock solution, and nuclei were removed by centrifugation at 1,700 × g for 5 minutes. The postnuclear supernatant was centrifuged again at 10,000 rpm for 20 minutes to remove the mitochondrial fraction; the postmitochondrial supernatant was centrifuged at 45,000 × g for 60 minutes. The supernatant fraction, representing the cytosolic fraction, was adjusted to 1% NP40 from a 10% stock solution. The pellet, representing the plasma membrane fraction, was gently rinsed with 1 mL PBS and then resuspended in 1 mL hypotonic buffer containing 1% NP40.

Immunoblotting and coimmunoprecipitation. NSCLC cells (1×10^6 cells/100 mm^3 dish) were either left uninfected or infected with Ad-EV (50 pfu/cell) or Ad-survivin (50 pfu/cell) and then left untreated or treated with various concentrations of erlotinib (0.1-10.0 μmol/L), AG1024 (5.0 μmol/L), LY294002 (10.0 μmol/L), PD98059 (10.0 μmol/L), rapamycin (1.0 μmol/L), or their combinations in growth medium that was changed daily. When growth factor stimulation was done, cells were cultured in serum-free medium for 1 day and then incubated in EGF (50 ng/mL) or IGF (50 ng/mL) for 15 minutes. For the small interfering RNA (siRNA) transfection, H460 cells in the logarithmic growth phase in six-well plates (5×10^5 cells per well) were transfected with 10 μL of 20 μmol/L survivin siRNA or control scrambled siRNA (Dharmacon Research, Lafayette, CO) using LipofectAMINE 2000 (Invitrogen, Carlsbad, CA), according to the protocol of the manufacturer. After 24 hours of incubation in growth medium, erlotinib was added, and the cells were harvested after 3 days of incubation. Immunoprecipitations were done using 3 mg protein from the total cell lysates and 1 μg mouse monoclonal anti-EGFR antibody, mouse monoclonal anti-IGF-IR antibody (Oncogene Sciences, Uniondale, NY), or healthy preimmune serum anti-mouse for the negative control and by incubating overnight at 4°C. The immunocomplexes were precipitated with protein-G agarose (Pharmacia-LKB Biotechnology, Piscataway, NJ). The immunoprecipitates were resolved on 6% SDS-PAGE gels, followed by Western blotting as described elsewhere (25).

Metabolic labeling. Metabolic labeling was done with H460 and TKI-R cells (5×10^5 in six-well plates). Cells were washed in PBS and incubated in RPMI medium without methionine and cysteine (Sigma, St. Louis, MO) for 2 hours. Next, the medium was replaced with fresh medium containing methionine and cysteine, to final concentrations of 150 mg/L, and the cells were labeled with trans-^{35}S (0.5 mCi; ICN, MP Biomedicals, Irvine, CA). The cells were then treated with 0.1% DMSO or erlotinib (10 μmol/L) for 1, 3, 6, 12, and 24 hours. At harvesting time, the cells were washed in ice-cold PBS and lysed in radioimmunoprecipitation assay buffer. Lysates containing equal amounts of protein (100 μg) were immunoprecipitated using 1 μg of antibody to detect EGFR or 1 μg of antibody to detect survivin (both from Santa Cruz Biotechnology) and 30 μL of 50% slurry of protein G agarose beads (Pharmacia-LKB Biotechnology, Piscataway, NJ). The immunoprecipitates were washed five times with lysis buffer, separated by SDS-PAGE,

DOI:10.1158/0008-5472.CAN-06-1684

and analyzed autofluorographically. Cell extracts were also subjected to Western blot analysis for β-actin to ensure that equal amounts of protein had been used. Two independent experiments were done with similar results; representative results of one experiment are presented.

Northern blot analysis. H460 cells (1×10^6 in 10 mm^3 plates) were treated with erlotinib (10 μmol/L) for different times (0, 24, 48, and 72 hours). The total cellular RNA was isolated by the application of TRIzol. For the Northern blotting, 10 μg of the total cellular RNA prepared from each sample was subjected to electrophoresis on a 1% agarose gel containing 2% formaldehyde and then stained with ethidium bromide, photographed, transferred to a Z probe membrane (Bio-Rad Laboratories), and hybridized to an [α-^{32}P]dCTP-labeled EGFR cDNA probe.

***In vivo* model.** The effect of the combination of erlotinib and Ad-dnIGF-IR on established s.c. tumor nodules was studied in athymic nude mice (Harlan Sprague-Dawley) in a defined pathogen-free environment. Briefly, 6-week-old female nude mice were irradiated with 350 rad from a cesium-137 source and then were injected s.c. with 1×10^7 H1299 cells in 100 μL of growth medium at a single dorsal site. The mice were randomly assigned to one of four treatment groups, with each group containing eight mice. Group 1 (control mice) received 1× PBS and Ad-EV, group 2 received erlotinib and Ad-EV, group 3 received 1× PBS and Ad-dnIGF-IR, and group 4 received erlotinib and Ad-dnIGF-IR. Tumor growth was quantified by measuring the tumors in three dimensions with calipers for a total of 35 days. After the tumor volumes reached ~75 mm^3 (considered day 0), the mice were treated with p.o. administered erlotinib (100 mg/kg of body weight) twice a day. We chose this dosage of erlotinib because it had had no notable effect on H1299 tumor growth in preliminary experiments (data not shown). On day 23, when tumor volumes reached ~125 mm^3, each mouse was given a single intratumoral injection of 2×10^9 particles of Ad-dnIGF-IR or Ad-EV in 100 μL of PBS. Mice with necrotic tumors or tumors ≥1.5 cm in diameter were euthanized immediately. The results were expressed as the mean tumor volume ($n = 5$) with 95% confidence intervals (95% CI). On day 35, all mice were sacrificed and tumor tissues were collected from the xenografts to determine whether the combination of erlotinib and

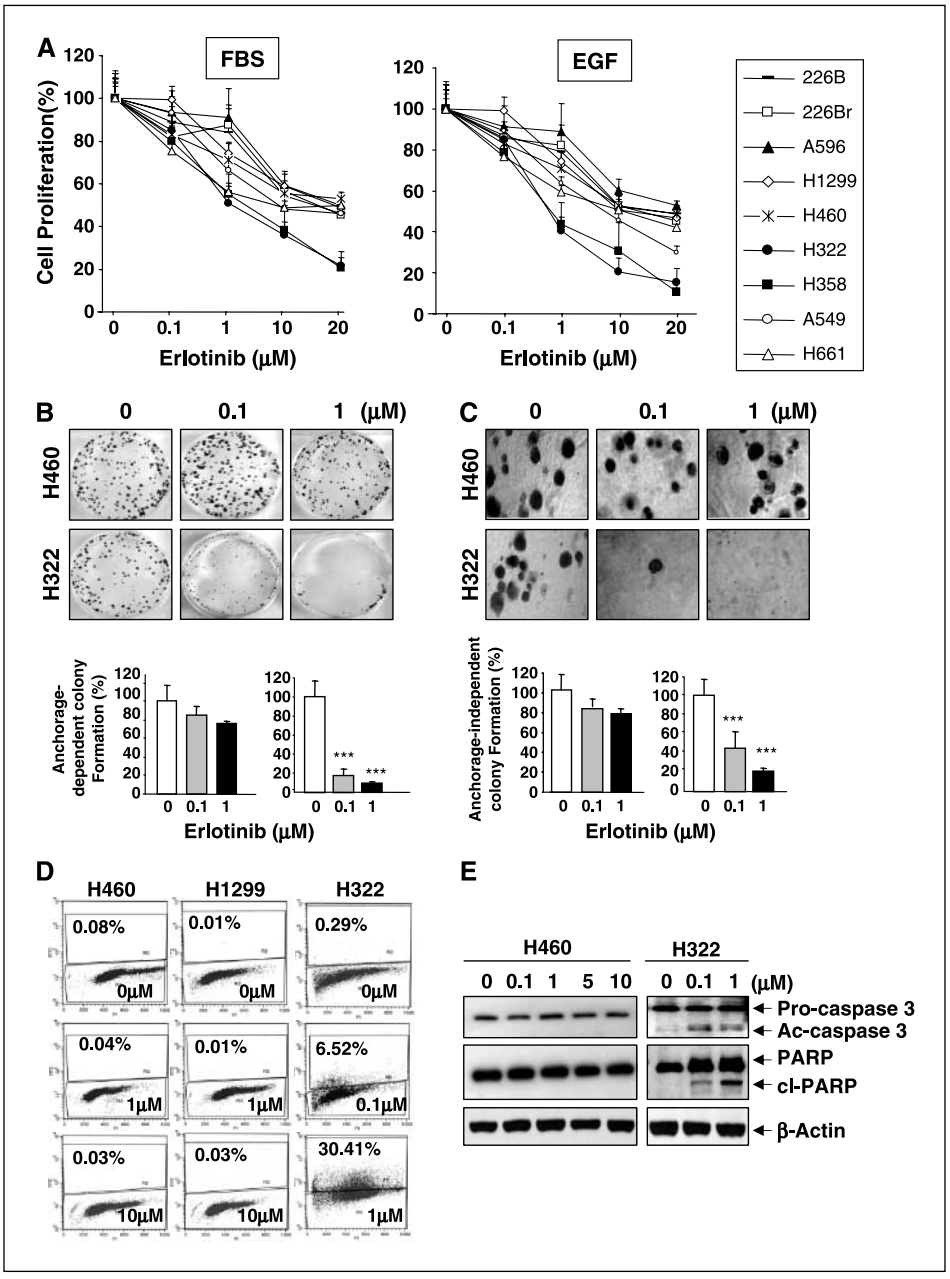

Figure 1. *A,* the MTT assay in NSCLC cell lines (H460, H1299, H661, A596, A549, H226B, H226Br, H322, and H358) treated with the indicated concentrations of erlotinib in RPMI 1640 containing 10% FBS or EGF for 3 days. *B,* clonogenic survival assay of H460 and H322 cells treated with the indicated concentrations of erlotinib. *C,* anchorage-independent growth assay of cells treated with the indicated concentrations of erlotinib. In (*A-C*), independent experiments were repeated thrice. *Columns,* mean of eight (*A*) or three (*B* and *C*) identical wells of a single representative experiment; *bars,* upper 95% CI; **, $P < 0.01$; ***, $P < 0.001$, for comparisons between erlotinib-treated and control cells. *D,* effects of the indicated concentrations of erlotinib on apoptosis in H322, H460, and H1299 NSCLC cells, assessed by a modified TUNEL assay. From a single representative experiment ($n = 2$). *E,* effects of the indicated concentrations of erlotinib on apoptosis-related enzyme expression in H322 and H460 NSCLC cells. The expression of caspase-3, PARP, and β-actin was assessed by Western blotting.

DOI:10.1158/0008-5472.CAN-06-1684

Ad-dnIGF-IR induced apoptosis *in vivo* by Western blot and immunohistochemical analyses as previously described (23).

Statistical analyses. The data acquired from the MTT assay were analyzed using Student's *t* test. All means and 95% CIs from eight samples were calculated using Microsoft Excel software (version 5.0; Microsoft Corporation, Seattle, WA). Cell survival comparisons among groups and statistical significance of differences in tumor growth in the combination treatment group and in the single-agent treatment groups were analyzed by ANOVA for 2×2 factorial design. All means from triplicate to eight samples and 95% CIs were calculated using SAS software (release 8.02; SAS Institute, Cary, NC). In all statistical analyses, two-sided *P* values of <0.05 were considered statistically significant.

Results

Differential apoptotic responses of NSCLC cells after treatment with erlotinib. To test the effects of EGFR TKIs on NSCLC cell proliferation, a subset of NSCLC cell lines (H460, H1299, H661, H596, H226B, H226Br, A549, H322, and H358) was treated with erlotinib in regular growth medium containing 10% FBS or in serum-free medium containing EGF. A MTT assay revealed that erlotinib has different levels of antiproliferative activities, depending on cell lines (Fig. 1*A*): Compared with the other NSCLC cell lines, H322 and H358 cells were more sensitive to the erlotinib treatment ($P < 0.001$). Approximately 1 μmol/L erlotinib significantly inhibited proliferation of H322 and H358 cells after 72 hours of treatment. In contrast, the drug concentrations required to inhibit cell growth by 50% for H460, H1299, H661, H596, H226B, H226Br, and A549 cells were 10 to 20 times higher than those needed to inhibit H322 and H358 cells. Consistent with the results from the MTT assay, erlotinib only slightly affected the anchorage-dependent and anchorage-independent colony-forming abilities of H460 and H1299 cells (data not shown) at concentrations <1 μmol/L, a concentration that significantly inhibited those abilities of H322 ($P < 0.001$; Fig. 1*B* and *C*; $P < 0.001$) and H358 (data not shown) cells.

We next asked whether the ability of 1 μmol/L erlotinib to inhibit H322 and H358 cell proliferation was due to decreased cell cycle progression and/or increased apoptosis. Flow cytometric analyses of propidium iodide–stained H460, H1299, and H322 cells revealed that treatment with 1 μmol/L erlotinib for 3 days resulted in no marked change in the cell cycle distribution (data not shown). However, fluorescence-activated cell sorter analysis followed by terminal deoxynucleotidyl transferase–mediated dUTP-biotin nick-end labeling (TUNEL) staining revealed induction of apoptosis in 30.4% of the H322 cells treated with 1 μmol/L erlotinib. In contrast, treatment with up to 10 μmol/L erlotinib did not detectably increase the apoptotic population of H1299 and H460 cells (Fig. 1*D*). In agreement with these findings, the protein levels of the active form of caspase-3 (Ac-caspase-3) and the cleaved form of poly(ADP-ribose) polymerase (PARP; cl-PARP, the 89 kDa fragment) increased in the H322 cells treated with >0.1 μmol/L erlotinib but not in the H460 cells, even after treatment with 10 μmol/L erlotinib (Fig. 1*E*). H358 cells also responded with apoptosis to similar concentrations of erlotinib (data not shown). Together, these findings indicated the presence of mechanisms that affect the response of NSCLC cells to erlotinib-mediated apoptosis.

Role of IGF-IR signaling pathways in the development of resistance to erlotinib treatment in NSCLC cells. To investigate the mechanisms involved in the sensitivity of NSCLC cells to erlotinib, we first tested whether erlotinib successfully blocks activation of EGFR and its downstream mediators in NSCLC cell lines. Figure 2*A* shows that 0.1 to 1.0 μmol/L erlotinib suppressed the levels of phosphorylated EGFR (pEGFR), phosphorylated Akt (pAkt), and phosphorylated p44/42 MAPK (pp44/42 MAPK) in H460 and H1299 cells (cell lines that are weakly sensitive to erlotinib) and H322 and H358 cells (cell lines that are very sensitive to the drug). However, comparable induction of pAkt and p44/42 MAPK was evident in H460 and H1299 cells after treatment with >5.0 μmol/L erlotinib, doses that induce apoptosis in most of the H322 and H358 cells. pAkt and p44/42 MAPK are located in the nodal points of growth factor–mediated cell survival signaling, and the IGF-IR pathway can modulate the action of the erbB family blocking agents in various cancer cells (25–27). Hence, we tested whether IGF-IR was involved in increases in pAkt and p44/42 MAPK. Indeed, erlotinib concentrations >5.0 μmol/L induced phosphorylated IGF-IR (pIGF-IR) in H460 and H1299 cells but not in H322 and H358 cells.

We then studied the influence of IGF-IR signaling pathways on the response of NSCLC cells to erlotinib. H460 cells exhibited significantly decreased proliferation and anchorage-dependent and anchorage-independent colony-forming abilities when the cells were treated with erlotinib in serum-free medium compared with when they were treated in the presence of IGF-I. H322 cells, however, showed statistically significant sensitivity to erlotinib in all conditions (Fig. 2*B*), suggesting that the induced activation of the IGF-IR signaling pathway allows NSCLC cells to survive and proliferate when the EGFR pathway is blocked by erlotinib treatment.

To test our hypothesis, we compare the effects of erlotinib, either single or in combination with AG1024, an IGF-IR TKI, on the proliferation, clonogenic survival ability, and apoptosis of H460 cells. AG1024 has shown significantly lower affinity for the insulin receptor than for the IGF-IR (26). Combined treatment with erlotinib and AG1024 synergistically enhanced the antiproliferative effects of erlotinib on H460 cells compared with single treatment with each drug when cultured in complete (FBS) or serum-free medium in the absence or presence of IGF ($P < 0.001$; Fig. 2*C*; Supplementary Table S1). Erlotinib also showed significantly enhanced antiproliferative properties in H460 cells infected with an Ad-dnIGF-IR compared with the control cells infected with Ad-EV ($P < 0.001$; Fig. 2*D*). Moreover, combined treatment with erlotinib and AG1024 (Fig. 2*E*) or Ad-dnIGF-IR (Fig. 2*F*) significantly suppressed the anchorage-dependent, colony-forming ability of H460 cells ($P < 0.001$; Supplementary Table S2). Furthermore, TUNEL staining and flow cytometric analysis revealed that ~1% of control H460 cells, 1.2% of erlotinib-treated cells, and 26% (95% CI, 14.3-37.6%, $P < 0.05$) of AG1024-treated cells underwent apoptosis. In contrast, combined treatment with both erlotinib and AG1024 significantly enhanced TUNEL staining (77.1%; 95% CI, 64.4-89.8%; $P < 0.001$; Fig. 2*G*) and induced cleavage of the 113-kDa PARP to the 89-kDa fragment in parallel with the concomitant decreases in the levels of pIGF-IR, pAkt, and p44/42 MAPK (Fig. 2*H*). These findings suggest that the IGF-IR pathway provides an alternative proliferation and/or survival mechanism for NSCLC cancer cells in which EGFR is blocked by erlotinib.

Evidence of increased heterodimerization and membrane localization of IGF-IR and EGFR in erlotinib-treated H460 cells. We investigated the mechanism underlying NSCLC cell resistance to erlotinib using *in vitro* model of the H460 cell line (H460/TKI-R) that had been continuously treated with erlotinib. Treatment with >10 μmol/L erlotinib decreased the number of H460 cells, but proliferation of the remaining cells gradually

DOI:10.1158/0008-5472.CAN-06-1684

increased after 3 months of erlotinib treatment. Compared with the parent H460 cells, the H460 cells treated with 10 μmol/L erlotinib for 5 months (H460/TKI-R) had higher levels of pIGF-IR, pAkt, and pp44/42MAPK, with no detectable differences in the expression of IGF-IR, Akt, and p44/42MAPK (Fig. 3*A*). The dose-response curves in Fig. 3*B* revealed no detectable cytotoxicity from erlotinib treatment of the H460/TKI-R cells up to a concentration of 20 μmol/L, whereas inhibition of IGF-IR activation by the AG1024 treatment induced greater antiproliferative effects on the H460/TKI-R cells than it did on the H460 cells. Moreover, compared with a single agent, combined treatment with erlotinib and AG1024 significantly suppressed the anchorage-dependent, colony-forming ability of H460/TKI-R as well as H460 cells ($P < 0.001$; Fig. 3*C*). The effects of combined treatment with erlotinib and AG1024 on colony formation was greater in H460/TKI-R cells than in H460 cells, indicating the dependence of H460/TKI-R cells on the IGF-IR signaling pathway for maintaining cell proliferation and tumorigenic potential.

We investigated the mechanism of erlotinib-mediated activation of IGF-IR in H460 cells. One mechanism by which the growth factor receptor is activated in tumor cells is by receptor dimerization; another is by overwhelming negative regulatory mechanisms that suppress receptor activation. Recent studies have revealed the interaction between the ErbB receptor families and IGF-IR in several tumor models, including breast cancer and oral cancer cell lines (19, 28–32). We, therefore, tested whether EGFR interacts with IGF-IR in H460/TKI-R cells by performing immunoprecipitation. EGFR immunoprecipitates from H460/TKI-R cells showed greater IGF-IR binding compared with that from the parental H460 cells (Fig. 3*D*). Control immunoprecipitates using preimmune serum exhibited no immunoreactive band. The interaction between EGFR and IGF-IR was observed as early as 30 minutes after the erlotinib treatment (Fig. 3*E*). In contrast, no detectable change was observed in the levels of EGFR-EGFR or EGFR-ErbB2 interaction in H460 cells treated with erlotinib for 3 days (Fig. 3*F, top*). Similarly, IGF-IR immunoprecipitates from erlotinib-treated H460 cells showed greater levels of EGFR binding than untreated cells did (Fig. 3*F, bottom*), whereas no detectable binding was observed when the IGF-IR immunoprecipitates were immunoblotted to ErbB2 or ErbB3. Increased EGFR/IGF-IR heterodimerization was also observed in H1299 cells treated with 10 μmol/L erlotinib (Fig. 3*G*). In contrast, the EGFR and control (preimmune serum) immunoprecipitates from untreated or erlotinib-treated H322 cells exhibited no immunoreactive band. These results suggested that erlotinib induces physical contact between EGFR and IGF-IR, which is accumulative.

Erlotinib treatment–induced expression of survivin protein protects NSCLC cells from apoptosis. We next attempted to find evidence connecting erlotinib-induced activation of the IGF-IR with survival of NSCLC cells. Because the inhibitor of apoptosis

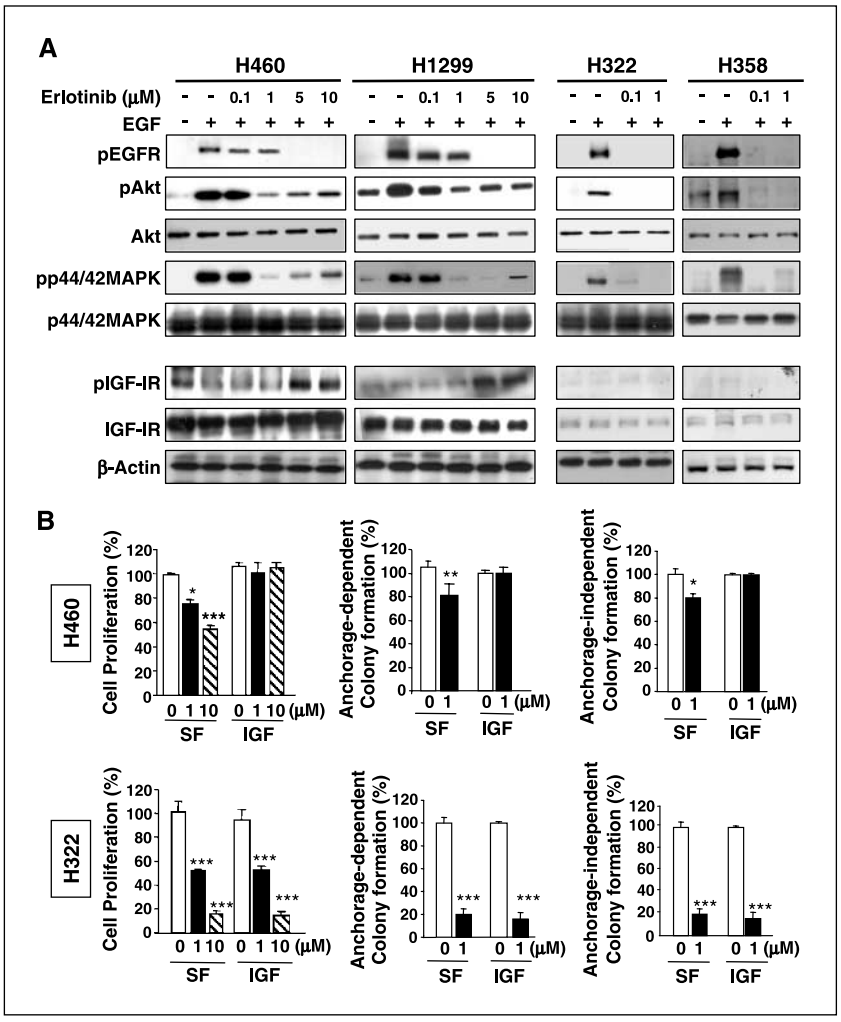

Figure 2. *A,* immunoblotting of the EGFR, IGF-IR, and their downstream signaling components in NSCLC cells treated with indicated concentrations of erlotinib. Western blotting on β-actin is included as a loading control. *B,* role of the IGF-I on the proliferation and survival of NSCLC cells. *Left,* MTT assay in H460 and H322 cells incubated in the serum-free medium without (*SF*) or with IGF-I (50 ng/mL) in the presence of indicated concentrations of erlotinib for 3 days. *Middle* and *right,* efficacy of the indicated concentrations of erlotinib in inhibiting anchorage-dependent and anchorage-independent growth of H460 and H322 cells, respectively, in serum-free and IGF-dependent conditions.

DOI:10.1158/0008-5472.CAN-06-1684

proteins, including survivin and XIAP, decrease the sensitivity of tumor cells to chemotherapeutic drugs, thereby conferring resistance to apoptosis (21, 33), we tested the effects of erlotinib on the expression of these proteins in a subset of NSCLC cells with weak or great sensitivity to erlotinib. We found that expression of survivin but not XIAP markedly increased in H1299, H460, H661, A549, A596, and 226B cells (Fig. 4*A, top*) during the time IGF-IR was phosphorylated by the erlotinib treatment (Fig. 4*A, bottom*). In contrast, H358 and H322 cells showed no detectable changes in the protein levels of survivin, XIAP, and pIGF-IR during the time EGFR was inactivated by erlotinib treatment. Erlotinib induced survivin expression in a time- and dose-dependent manner (Fig. 4*B*). Interestingly, a similar but less pronounced increase in EGFR expression was observed in H1299, H460, H661, A549, H596 H226Br, and H226B, H460/TKI-R cells but not in H358 and H322 cells. Increases in the survivin and EGFR expression were also observed in H460/TKI-R cells (Fig. 4*C*).

We then tested the response of H460 cells, in which survivin expression was abolished by siRNA transfection. Western blot analysis revealed an obvious increase in PARP cleavage in the 460 cells by the treatment with erlotinib (Fig. 4*D*). Among H322 cells, in which survivin overexpression was induced by the infection with Ad-survivin, the PARP cleavage was substantially reduced after the erlotinib treatment (Fig. 4*E*). These results indicated that increased expression of survivin protein protected NSCLC cells from the erlotinib-induced apoptosis.

mTOR pathway induces *de novo* protein synthesis of EGFR and survivin and protects NSCLC cells from apoptosis. We investigated the mechanisms of erlotinib-mediated increase in survivin and EGFR protein expression. According to Northern blot analysis, exposure of H460 cells to erlotinib resulted in no change in the mRNA levels of survivin (Fig. 5*A*) and EGFR (data not shown). We then determined the effects of erlotinib on the rates of survivin and EGFR protein synthesis. Metabolic labeling of the H460 cells with [^{35}S]Met-Cys revealed that the rate of [^{35}S]labeled survivin (Fig. 5*B*) and EGFR (data not shown) synthesis was remarkably greater in the erlotinib-treated H460 and H460/TKI-R cells than in the untreated parental H460 cells. We then determined whether

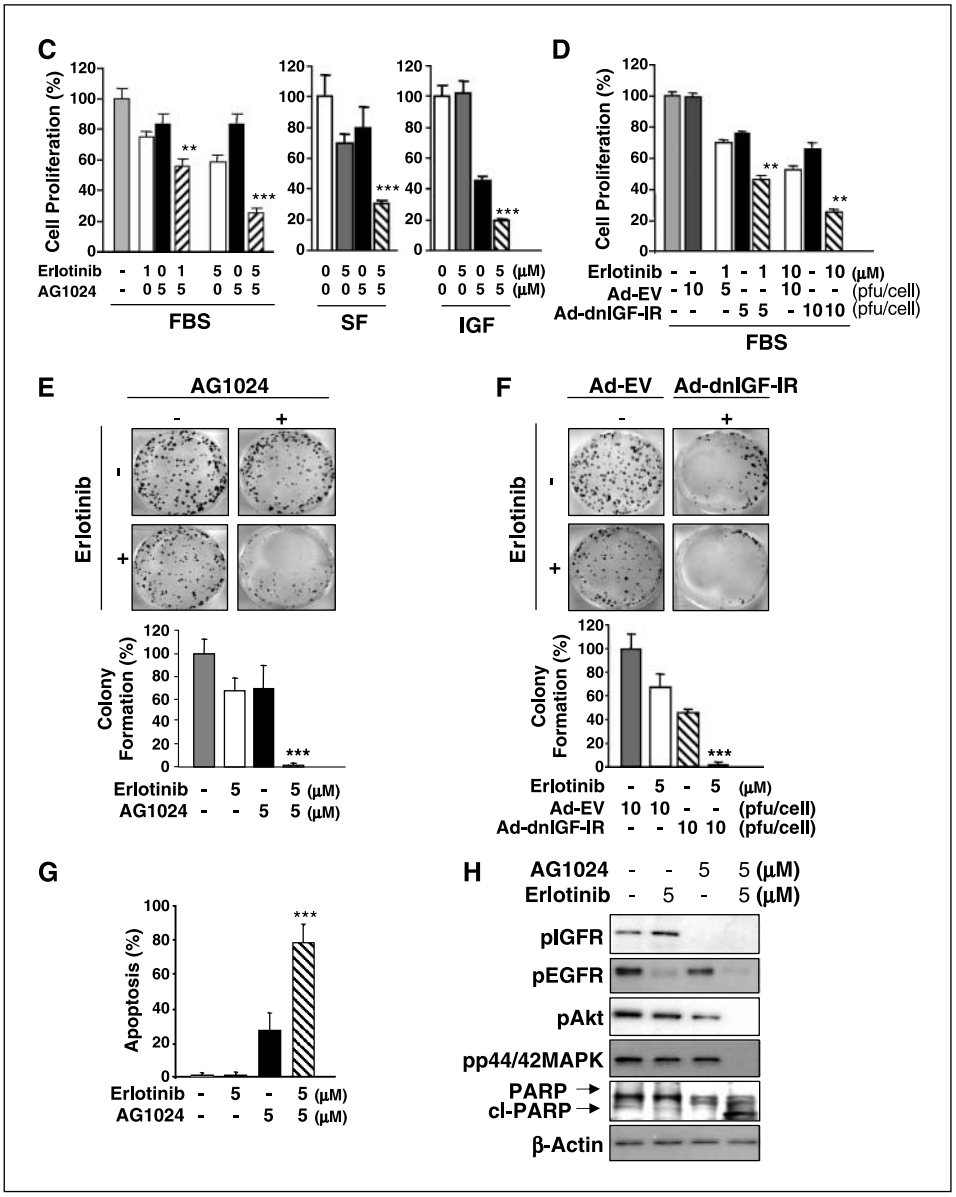

Figure 2 *Continued.* *C* and *D,* effect of targeting both the EGFR and the IGFR-IR on cell proliferation. MTT assay in H460 cells uninfected (*C*) or infected with 5 or 10 infectious forming unit of Ad-EV or Ad-dnIGF-IR (*D*) and treated with indicated concentrations of erlotinib, AG1024, or their combination in serum-free RPMI 1640 containing 10% FBS or IGF (50 ng/mL) for 3 days. *E* and *F,* survival of H460 cells treated with erlotinib (5 μmol/L), AG1024 (5 μmol/L), or their combination (*E*), or cells infected with 10 pfu/cell of Ad-EV or Ad-dnIGF-IR and then untreated or treated with erlotinib (5 μmol/L; *F*) were assessed by counting colonies consisting of >50 cells after 10 days of growth. *G* and *H,* effects of 5 μmol/L erlotinib, 5 μmol/L AG1024, or their combination on apoptosis (*G*) and expression of pEGFR, pIGF-IR, pp44/42MAPK, and pAkt (*H*) were analyzed in H460 cells by a flow cytometry–based TUNEL assay and Western blotting. β-Actin, loading control. *Columns,* mean value of eight (MTT) or three (clonogenic growth assay and TUNEL assay) identical wells of a single representative experiment ($n = 3$); *bars,* upper 95% CI (*B-G*). ***, $P < 0.001$ for comparisons between cells treated with drug combination and cells treated with single agent.

DOI:10.1158/0008-5472.CAN-06-1684

mTOR is involved in the erlotinib-induced protein synthesis of survivin and EGFR by determining the levels of phosphorylated 4E-BP1 and p70^{s6k}, downstream mediators of mTOR (27, 34), in the H460 cells treated with erlotinib alone or in combination with rapamycin, an mTOR inhibitor, or AG1024 for 3 days. Western blot analysis revealed that erlotinib up-regulated the protein levels of p4E-BP1, pp70^{s6k} in association with increases in survivin and EGFR expression, all of which were suppressed by

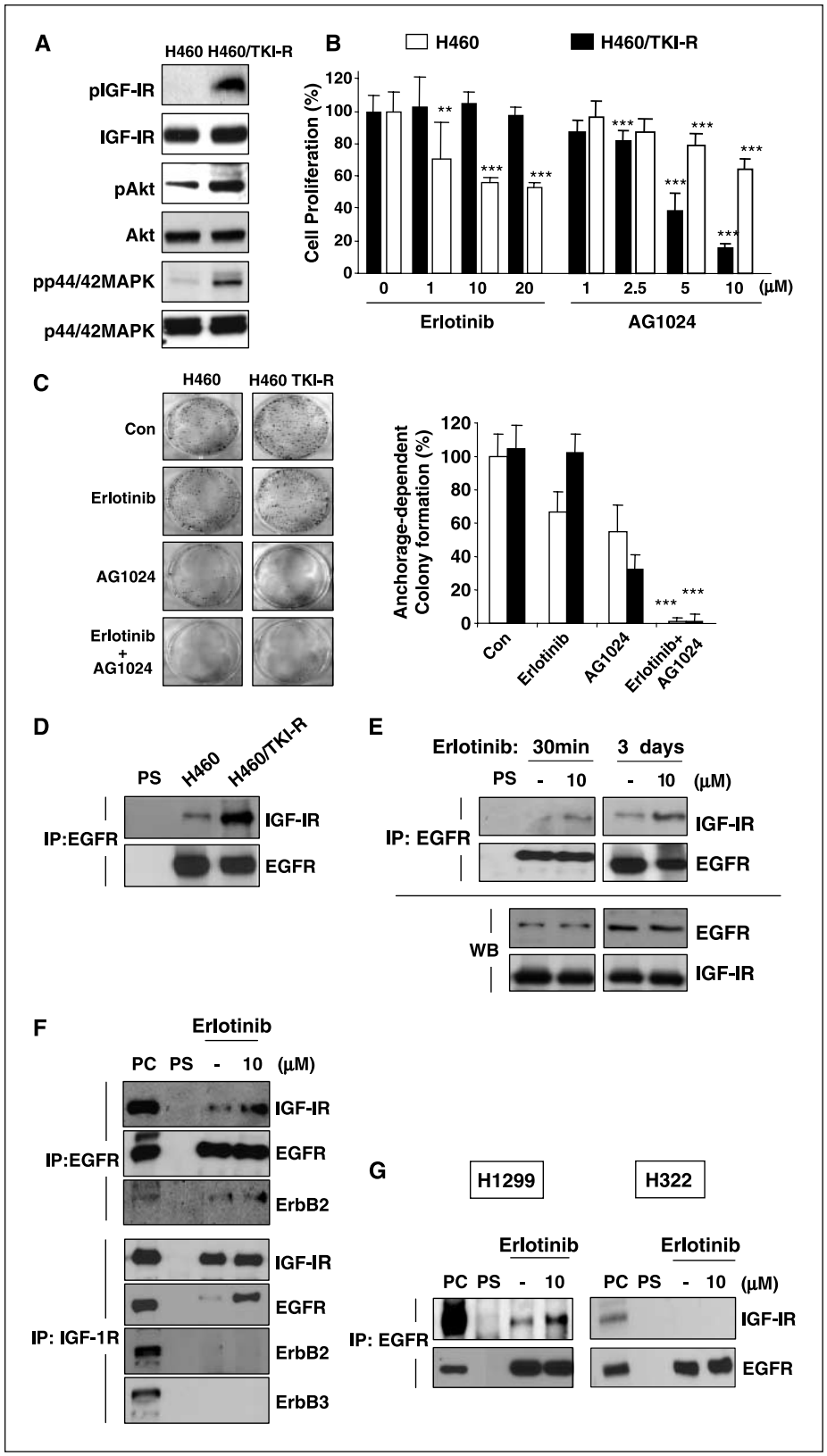

Figure 3. *A,* Western blot analysis of indicated protein expressions in H460 and H460/TKI-resistant (H460/TKI-R) cells. *B,* MTT assay on the proliferation of H460 and H460/TKI-R cells treated with erlotinib (1-20 μmol/L) or AG1024 (1-10 μmol/L). Cells treated with 0.1% DMSO were included as a control (0). *C,* survival of H460 and H460/TKI-R cells treated with erlotinib (5 μmol/L), AG1024 (5 μmol/L), or their combination. *Columns,* mean value of eight (MTT) or three (clonogenic assay) identical wells of a single representative experiment ($n = 3$); *bars,* upper 95% CI (*A* and *B*). ***, $P < 0.001$ compared with control. *D* to *G,* coimmunoprecipitation was done for the interaction between EGFR and IGF-IR. Whole-cell extracts from H460 and H460/TKI-R cells (*D*) or H460 cells, H1299, and H322 cells untreated or treated with erlotinib (10 μmol/L) for 30 minutes (*E*) or 3 days (*E-G*) were immunoprecipitated (*IP*) with anti-EGFR or anti-IGF-IR antibodies. The immunoprecipitates were subjected to Western blot analysis with indicated antibodies. Input (*PC*) represents cell lysates that were not subjected to immunoprecipitation. Control immunoprecipitation was done using control mouse preimmune serum (*PS*).

DOI:10.1158/0008-5472.CAN-06-1684

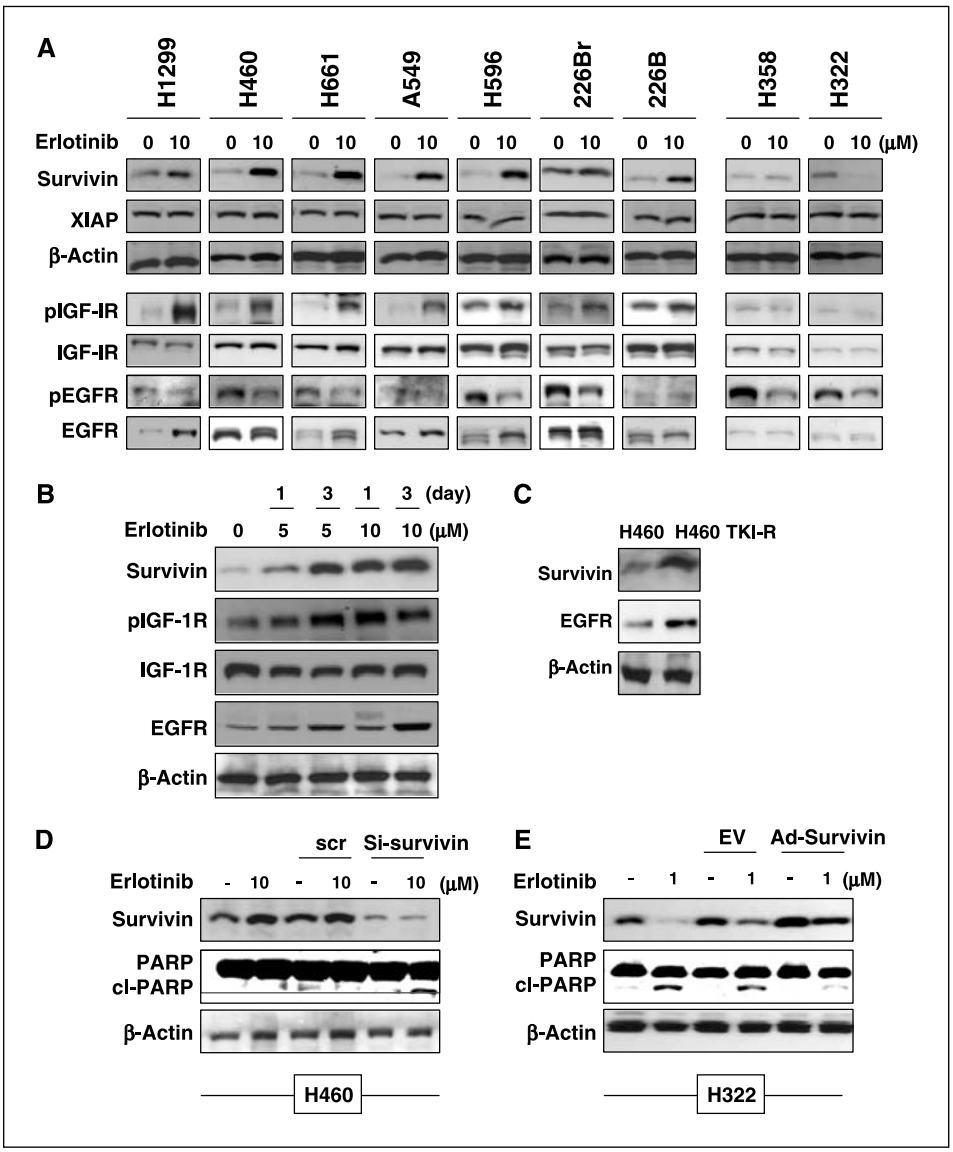

Figure 4. *A* and *B,* Western blot analysis on the survivin, XIAP, pIGF-IR, IGF-IR, pEGFR, EGFR protein expression in indicated NSCLC cell lines treated with erlotinib (1-10 μmol/L) for 1 (*B*) or 3 (*A, B*) days. *C,* Western blot analysis on the survivin and EGFR protein in H460 TKI/R cells. *D,* effect of the knockdown of survivin expression on H460 cells in the presence of erlotinib. H460 cells transfected with scramble (*scr*) or survivin siRNA (*si-survivin*), untreated and treated for 48 hours with erlotinib (10 μmol/L), were subjected to protein extraction and Western blotting for evaluation of caspase-3 (pro-caspase-3) and PARP. Loading control: β-actin. *E,* effects of overexpression of survivin in erlotinib-induced apoptosis in H322 cells. H322 cells were infected with 50 pfu/cell of control virus (Ad-EV) or Ad-survivin and incubated for 3 days in the presence of erlotinib (1 μmol/L). Protein extract was subjected to Western blotting for evaluation of survivin, caspase-3 (pro-caspase-3), and PARP. Loading control: β-actin.

treatment with AG1024 or rapamycin (Fig. 5*C*). Moreover, the combined treatment with AG1024, LY294002 (PI3K inhibitor), PD98059 (MEK inhibitor), or rapamycin reduced the levels of membranous EGFR expression (Fig. 5*D*) and of the EGFR and IGF-IR heterodimer (Fig. 5*E*) induced by the 3 days treatment of erlotinib. These findings suggested that the increases in the levels of EGFR/IGF-IR heterodimer on cell membrane and protein expressions of survivin and EGFR were mediated at least in part through translation-dependent events mediated by IGF-IR signaling pathways. We then tested whether inhibitors of the IGF-IR and mTOR pathways sensitize the H460 cells to the erlotinib treatment. H460 cells treated with erlotinib and AG1024 (Fig. 2*G* and *H*) or rapamycin (Fig. 5*F*) showed an increase in the PARP cleavage, suggesting that suppression of IGF-IR and mTOR pathways could restore the apoptotic activities of erlotinib in NSCLC cells.

Antitumor efficacy of dual targeting of EGFR and IGF-IR signaling pathways *in vivo*. To determine whether the inhibition of IGF-IR signaling can enhance the antitumor activities of erlotinib *in vivo*, we tested the effects of erlotinib, Ad-dnIGF-IR, and their combination on the growth of H1299 NSCLC xenograft tumors established in athymic nude mice. The mice treated with erlotinib plus Ad-dnIGF-IR showed synergistically reduced tumor growth compared with the control mice or the mice treated with erlotinib or Ad-dnIGF-IR alone (Fig. 6*A*; Supplementary Table S3). At the end of the study, the mean tumor volume in combined treatment group was 23% ($P < 0.001$) of the mean volume in the control group. Thus, the combination of erlotinib and Ad-dnIGF-IR enhanced the antitumor effects on the growth of NSCLC cells *in vivo*.

We then determined the effects of erlotinib, Ad-dnIGF-IR, and their combination on the activation of the IGF-IR and EGFR, the expression of survivin and EGFR, and the induction of apoptosis *in vivo*. According to Western blot analysis of total protein extracts harvested from the H1299 xenograft tumor tissues, the levels of pEGFR were decreased by erlotinib. In addition, erlotinib treatment induced marked increases in the levels of pIGF-IR, EGFR, and survivin, all of which were effectively blocked by Ad-dnIGF-IR (Fig. 6*B*). Combined treatment with erlotinib and Ad-dnIGF-IR also increased the levels of Ac-caspase-3, which is confirmed by the

DOI:10.1158/0008-5472.CAN-06-1684

immunohistochemical staining of the H1299 xenograft tumor tissues (Fig. 6*C*). Together, these findings suggested that the combined treatment with erlotinib and Ad-dnIGF-IR exert enhanced *in vivo* antitumor activities by decreased expression of survivin and EGFR and induction of apoptosis.

Discussion

Several preclinical and clinical discoveries have associated EGFR TKIs with antitumor activities. However, the limited response rates of patients to EGFR TKIs, even in patients with high levels of EGFR (15, 16, 35), have been raising questions about the mechanisms leading to the EGFR TKI resistance. Although somatic mutations of the EGFR ATP binding site have been associated with the response to the EGFR TKIs in some cases (17, 18), increasing number of evidence have suggested that the presence of other pathways that mediate the resistance of cancer cells to EGFR TKI therapy (36, 37). In this article, we have shown, to our knowledge for the first time, that erlotinib induces survival of NSCLC cells by inducing heterodimerization of EGFR/IGF-IR, activating IGF-IR pathway and its downstream mediators Akt and p44/42 MAPK, and thus stimulating mTOR-mediated protein synthesis of survivin that plays a crucial role in the blocking apoptosis. We showed here that the blockade of the IGF-IR to mTOR signaling pathway was sufficient to suppress *de novo* survivin protein synthesis and to restore apoptotic activities of erlotinib in NSCLC cells *in vitro* and *in vivo*. Our data present clear evidence that crosstalk between the IGF-IR and the EGFR signaling pathways and consequential survivin expression are involved in the NSCLC cell resistance to erlotinib. The erbB2/Her2/neu, a known preferred coreceptor for the EGFR, has been suggested to play a role in inducing NSCLC cell survival against EGFR TKIs (28). However, we found that the erbB2/Her2/neu was inactivated by the EGFR TKIs in NSCLC cells (data not shown), consistent with previous reports (38). In addition, an interaction between IGF-IR and erbB2 was undetectable, regardless of erlotinib treatment. Therefore, erbB2/Her2/neu is not likely to have a role in inducing EGFR TKI resistance in NSCLC cells.

We investigated the detailed mechanism that mediates IGF-IR activation by erlotinib and the consequent development of drug resistance. Given that gefitinib-resistant DU145/TKI-R prostate cells have shown considerably higher basal levels of IGF-II mRNA than wild-type cells (19), erlotinib might have increased the expression of IGF and conferred resistance to the drug to NSCLC cells. However, in gefitinib-resistant breast cancer cell lines, the IGF II mRNA level did not differ from that of the original clone (19), indicating that autocrine/paracrine production is not entirely responsible for the sensitivity of the cell to EGFR TKIs. Perhaps our most striking finding was that in H460 and H1299 cells, erlotinib induced heterodimerization between IGF-IR and EGFR. The interaction between EGFR and IGF-IR also has been observed in cancer cells (29–31). Given the considerable similarity between EGFR and IGF-IR in the sequence of their extracellular domain (39) and their reliance on EGF and IGF to achieve cell cycle progression and survival, it is plausible that erlotinib-mediated IGF-IR/EGFR heterodimerization can stimulate intracellular signaling components in a distinct pattern and allow NSCLC cells to resist the drug.

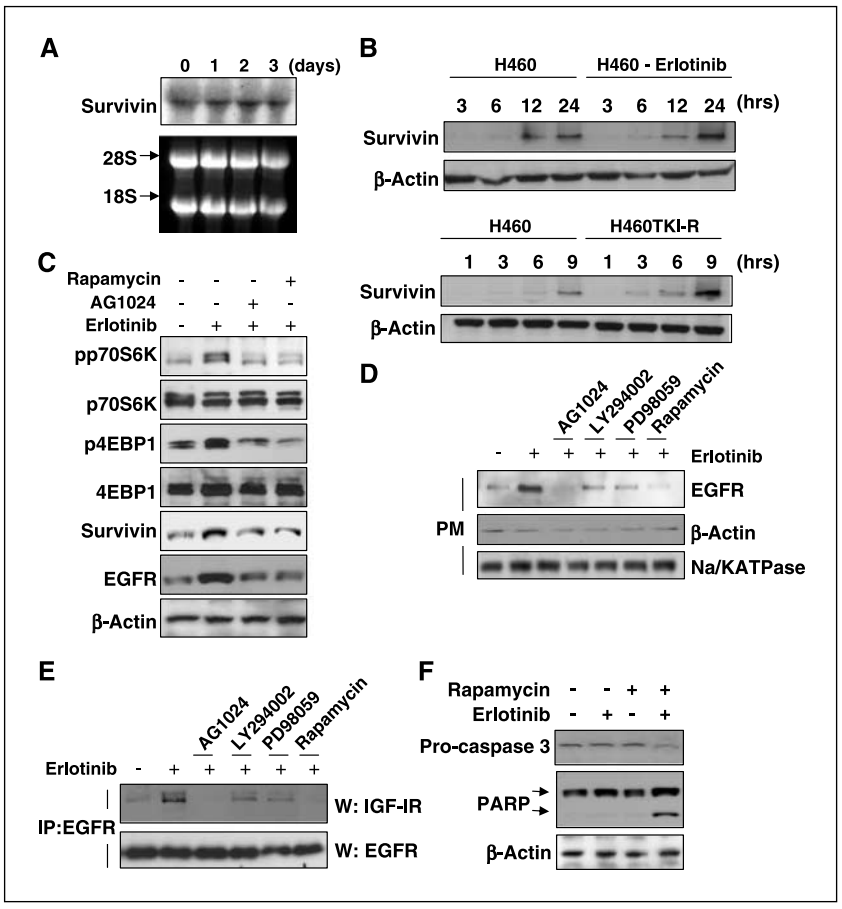

Figure 5. *A,* Northern blot analysis on survivin mRNA in H460 treated with erlotinib (10 μmol/L) for 1, 2, or 3 days. *B,* survivin and EGFR protein synthesis evaluated by metabolic labeling in untreated 460 cells, H460 cells treated with erlotinib (10 μmol/L), and H460TKI-R cells. Cell extracts were also subjected to Western blot analysis for β-actin to ensure that equal amounts of protein were used. *C,* expression of phosphorylated p70S6K (pp70S6k), p70S6K, phosphorylated 4EBP1 (p4EBP1), 4EBP1, survivin and EGFR in H460 cells treated with erlotinib (10 μmol/L), either single or in combination with AG1024 (5 μmol/L) or rapamycin (1 μmol/L), for 3 days. *D* and *E,* effects of erlotinib in combination with AG1024, LY294002, PD98059, or rapamycin on the plasma membrane (*PM*) localization of EGFR (*D*) and on the interaction between EGFR and IGF-IR (*E*). β-Actin, control for cytosol fraction; Na/K ATPase, control for plasma membrane fraction. *F,* effect of combined treatment with erlotinib (10 μmol/L) and rapamycin (1 μmol/L) for 3 days on apoptosis in H460 cells. Protein extract was subjected to Western blotting for the evaluation of pro-caspase-3 and PARP. Loading control: β-actin.

DOI:10.1158/0008-5472.CAN-06-1684

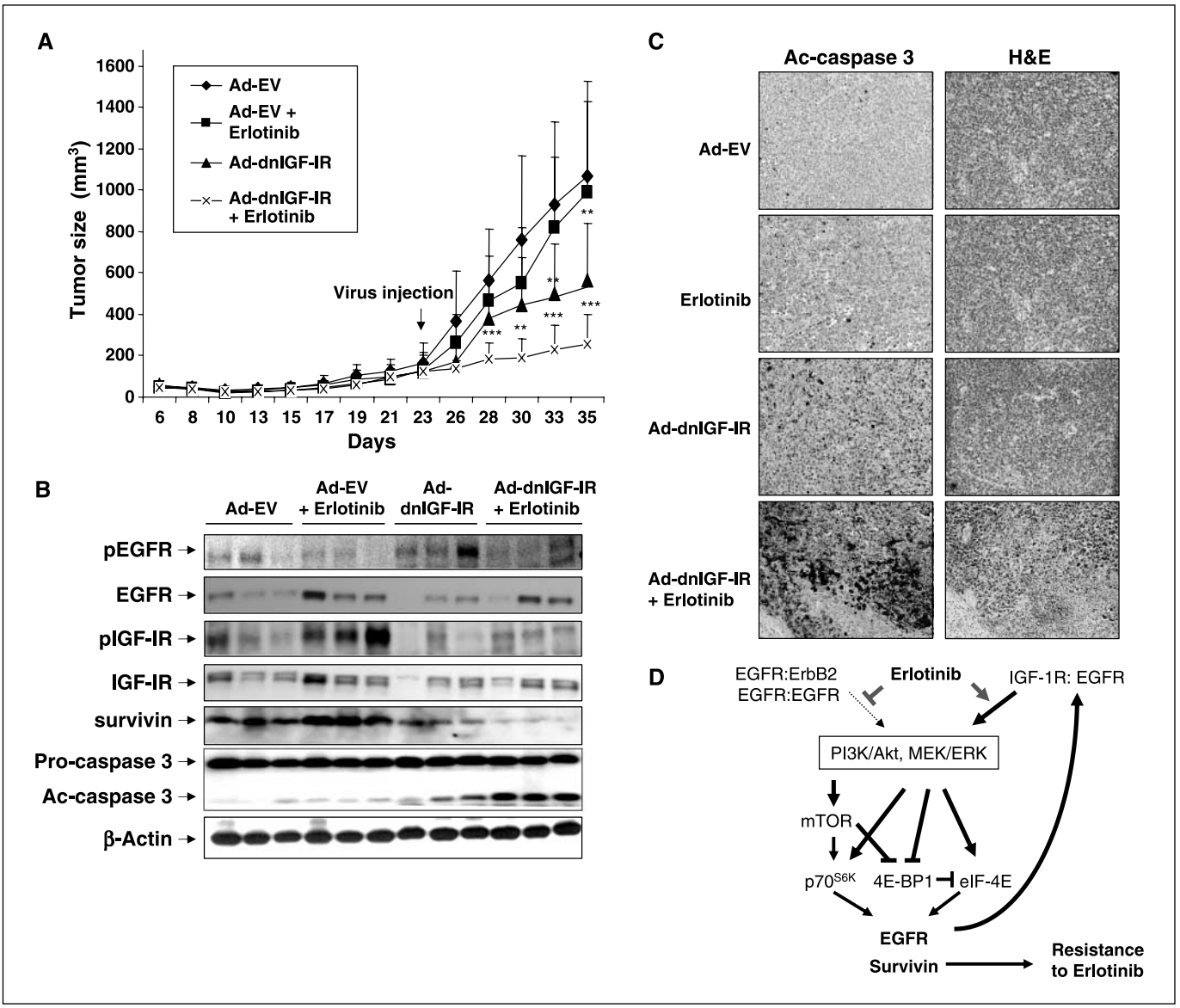

Figure 6. Effects of combined treatment with erlotinib and recombinant Ad-dnIGF-IR on growth of H1299 NSCLC xenograft tumors in athymic nude mice. The mice were randomly assigned to one of four treatment groups, with each group containing five mice. Group 1 (control mice) received 1× PBS and Ad-EV, group 2 received erlotinib and Ad-EV, group 3 received 1× PBS and Ad-dnIGF-IR, and group 4 received erlotinib and Ad-dnIGF-IR. *A,* effect of erlotinib (40 mg/kg body weight, administered p.o. twice daily) on tumor volume. When tumor volume was ~125 mm^3, mice were treated with Ad-IGF-IR or Ad-EV (control) in 100 μL PBS. *Points,* mean tumor volume (n = 5) with 95% CI; *bars,* SE. **, $P < 0.01$, ***, $P < 0.001$ for comparisons between drug-treated and control cells for each series of experiments. *B,* effects of erlotinib and Ad-dnIGF-IR on the expression of pEGFR, EGFR, pIGF-IR, IGF-IR, survivin, and pro-caspase-3 and Ac-caspase-3 in NSCLC xenograft tumors, assessed by Western blotting. β-Actin = loading control. *C,* effects of combined erlotinib and Ad-IGF-IR on expression of Ac-caspase-3. Tissues were stained with H&E. Representative section from each condition. *D,* schematic model of resistance mechanism to erlotinib.

Previous studies have shown the ability of erlotinib to induce EGFR mRNA and protein expression in the erlotinib-resistant biliary tract cancer cell line HuCCT1 but not in the susceptible A431 epidermoid cell line (40). In current study, we found that erlotinib induces mTOR-mediated *de novo* protein synthesis of survivin and EGFR with no detectable change in their mRNA levels, indicating diverse responses of different cancer cells to erlotinib. Our results may explain some apparently paradoxical findings in several clinical trials (41), in which up-regulation of pEGFR was observed after treatment of breast cancer patients with erlotinib. In another report, modifications of EGFR serum values during treatment of NSCLC seemed to reflect gefitinib activity; responding patients showed decreased serum levels of EGFR relative to those in patients with refractory disease (42). Our data also show the critical role of the induced survivin proteins in the development of resistance to erlotinib; (*a*) survivin expression was induced in NSCLC cell lines with weak sensitivity to the erlotinib treatment; (*b*) overexpression of survivin protected the sensitive NSCLC cells from erlotinib-induced apoptosis; and (*c*) knockdown survivin expression by siRNA provoked apoptosis in NSCLC cells with weak erlotinib sensitivity. mTOR has been known to regulate the translation of subsets of mRNA, many of which encode for proteins involved with driving cell growth, proliferation, and angiogenesis (43). Therefore, resistance and sensitivity to erlotinib in NSCLC may be determined at least in part by the ability of the cancer cells to stimulate mTOR-mediated synthesis of specific proteins that

DOI:10.1158/0008-5472.CAN-06-1684

have key roles in cell proliferation and/or survival and thus to adapt to a stressful environment.

In summary, our findings provide definitive *in vitro* and *in vivo* evidence that erlotinib induces heterodimerization of the EGFR/IGF-IR and stimulates IGF-IR and downstream pathways, including PI3K/Akt, MEK/extracellular signal-regulated kinase (ERK), resulting in the mTOR-mediated increases in EGFR and survivin proteins. On the basis of these findings, it is plausible to suggest that increased EGFR proteins further enhance the interplay between the EGFR and IGFR on the cell membrane, resulting in a further amplification of IGF-IR to mTOR signaling. In addition, the increased survivin proteins seem to provide survival potential to the NSCLC cells against the erlotinib treatment (Fig. 6*D*).

Our findings have direct effect to the treatment of NSCLC with erlotinib. The data showing no detectable interaction between EGFR/IGF-IR in NSCLC cell lines with low levels of IGF-IR expression suggests that the expression of IGF-IR is an important factor for the EGFR and IGF-IR complex and erlotinib sensitivity. Therefore, IGF-IR expression may serve as a predictor for erlotinib resistance in NSCLC. IGF-IR signaling pathway also plays a key role in the resistance to several therapeutic drugs (12, 27, 44–47). Overexpression of IGF-IR has been observed in various human cancers, including lung cancer (48), and is associated with a poor prognosis (49). Importantly, our unpublished data showed that clinical samples from NSCLC patients revealed that the majority of EGFR-overexpressing samples showed correlative increases in IGF-IR protein levels compared with their paired normal counterparts from the same patients. With this prospect, IGF-IR–targeting combination treatment may be required when erlotinib is considered as a therapeutic agent for NSCLC patients. Alternatively, mTOR inhibitors could confer benefit to erlotinib-resistant patients. In light of this notion, we have shown that combined treatment with erlotinib and inhibitors of IGF-IR or mTOR suppressed survivin and EGFR expression, decreased proliferation of NSCLC cells, and induced apoptosis in NSCLC cells *in vitro* and *in vivo*. Further studies are warranted to validate whether the erlotinib combined with inhibitors of IGF-IR or mTOR inhibitors could enhance the objective response and survival rates in NSCLC patients.

Acknowledgments

Received 5/10/2006; revised 7/6/2006; accepted 8/22/2006.

Grant support: NIH grant R01 CA100816 (H-Y. Lee), American Cancer Society grant RSG-04-082-01-TBE 01 (H-Y. Lee), Department of Defense grants W81XWH-04-1-0142-01-VITAL and W81XWH-06-1-0303-BATTLE, and partly by The National Foundation for Cancer Research Fellow grants (W.K. Hong).

The costs of publication of this article were defrayed in part by the payment of page charges. This article must therefore be hereby marked *advertisement* in accordance with 18 U.S.C. Section 1734 solely to indicate this fact.

References

1. Jemal A, Murray T, Samuels A, Ghafoor A, Ward E, Thun MJ. Cancer statistics, 2003. CA Cancer J Clin 2003;53:5–26.
2. Ferreira CG, Huisman C, Giaccone G. Novel approaches to the treatment of non-small cell lung cancer. Crit Rev Oncol Hematol 2002;41:57–77.
3. Mendelsohn J. The epidermal growth factor receptor as a target for cancer therapy. Endocr Relat Cancer 2001;8:3–9.
4. Brognard J, Clark AS, Ni Y, Dennis PA. Akt/protein kinase B is constitutively active in non-small cell lung cancer cells and promotes cellular survival and resistance to chemotherapy and radiation. Cancer Res 2001;61:3986–97.
5. Brognard J, Dennis PA. Variable apoptotic response of NSCLC cells to inhibition of the MEK/ERK pathway by small molecules or dominant negative mutants. Cell Death Differ 2002;9:893–904.
6. Khazaie K, Schirrmacher V, Lichtner RB. EGF receptor in neoplasia and metastasis. Cancer Metastasis Rev 1993;12:255–74.
7. Ellerbroek SM, Halbleib JM, Benavidez M, et al. Phosphatidylinositol 3-kinase activity in epidermal growth factor-stimulated matrix metalloproteinase-9 production and cell surface association. Cancer Res 2001;61:1855–61.
8. Sandler A. Clinical experience with the HER1/EGFR tyrosine kinase inhibitor erlotinib. Oncology (Huntingt) 2003;17:17–22.
9. Ready N. Inhibition of the epidermal growth factor receptor in combined modality treatment for locally advanced non-small cell lung cancer. Semin Oncol 2005;32:S35–41.
10. Hidalgo M. Erlotinib: preclinical investigations. Oncology (Huntingt) 2003;17:11–6.
11. Moyer JD, Barbacci EG, Iwata KK, et al. Induction of apoptosis and cell cycle arrest by CP-358,774, an inhibitor of epidermal growth factor receptor tyrosine kinase. Cancer Res 1997;57:4838–48.
12. Pollack VA, Savage DM, Baker DA, et al. Inhibition of epidermal growth factor receptor-associated tyrosine phosphorylation in human carcinomas with CP-358,774: dynamics of receptor inhibition *in situ* and antitumor effects in athymic mice. J Pharmacol Exp Ther 1999;291:739–48.
13. Albanell J, Rojo F, Baselga J. Pharmacodynamic studies with the epidermal growth factor receptor tyrosine kinase inhibitor ZD1839. Semin Oncol 2001;28:56–66.
14. Shepherd FA, Rodrigues Pereira J, Ciuleanu T, et al. Erlotinib in previously treated non-small-cell lung cancer. N Engl J Med 2005;14:123–32.
15. Giaccone G, Herbst RS, Manegold C, et al. Gefitinib in combination with gemcitabine and cisplatin in advanced non-small-cell lung cancer: a phase III trial-INTACT 1. J Clin Oncol 2004;22:777–84.
16. Herbst RS, Giaccone G, Schiller JH, et al. Gefitinib in combination with paclitaxel and carboplatin in advanced non-small-cell lung cancer: a phase III trial-INTACT 2. J Clin Oncol 2004;22:785–94.
17. Lynch TJ, Bell DW, Sordella R, et al. Activating mutations in the epidermal growth factor receptor underlying responsiveness of non-small-cell lung cancer to gefitinib. N Engl J Med 2004;350:2129–39. Epub 2004 Apr 29.
18. Paez JG, Janne PA, Lee JC, et al. EGFR mutations in lung cancer: correlation with clinical response to gefitinib therapy. Science 2004;304:1497–500. Epub 2004 Apr 29.
19. Jones HE, Goddard L, Gee JM, et al. Insulin-like growth factor-I receptor signalling and acquired resistance to gefitinib (ZD1839; Iressa) in human breast and prostate cancer cells. Endocr Relat Cancer 2004;11:793–814.
20. Liu B, Fang M, Lu Y, Mendelsohn J, Fan Z. Fibroblast growth factor and insulin-like growth factor differentially modulate the apoptosis and G1 arrest induced by anti-epidermal growth factor receptor monoclonal antibody. Oncogene 2001;20:1913–22.
21. Altieri DC. Survivin and apoptosis control. Adv Cancer Res 2003;88:31–52.
22. Lee CT, Park KH, Adachi Y, et al. Recombinant adenoviruses expressing dominant negative insulin-like growth factor-I receptor demonstrate antitumor effects on lung cancer. Cancer Gene Ther 2003;10:57–63.
23. Lee HY, Moon H, Chun KH, et al. Effects of insulin-like growth factor binding protein-3 and farnesyltransferase inhibitor SCH66336 on Akt expression and apoptosis in non-small-cell lung cancer cells. J Natl Cancer Inst 2004;96:1536–48.
24. Goldstein D, Bushmeyer SM, Witt PL, Jordan VC, Borden EC. Effects of type I and II interferons on cultured human breast cells: interaction with estrogen receptors and with tamoxifen. Cancer Res 1989;49:2698–702.
25. Chun KH, Kosmeder JW II, Sun S, et al. Effects of deguelin on the phosphatidylinositol 3-kinase/Akt pathway and apoptosis in premalignant human bronchial epithelial cells. J Natl Cancer Inst 2003;95:291–302.
26. Parrizas M, Gazit A, Levitzki A, Wertheimer E, LeRoith D. Specific inhibition of insulin-like growth factor-1 and insulin receptor tyrosine kinase activity and biological function by tyrphostins. Endocrinology 1997;138:1427–33.
27. Peterson RT, Desai BN, Hardwick JS, Schreiber SL. Protein phosphatase 2A interacts with the 70-kDa S6 kinase and is activated by inhibition of FKBP12-rapamycinassociated protein. Proc Natl Acad Sci U S A 1999;96:4438–42.
28. Chakravarti A, Loeffler JS, Dyson NJ. Insulin-like growth factor receptor I mediates resistance to anti-epidermal growth factor receptor therapy in primary human glioblastoma cells through continued activation of phosphoinositide 3-kinase signaling. Cancer Res 2002;62:200–7.
29. Balana ME, Labriola L, Salatino M, et al. Activation of ErbB-2 via a hierarchical interaction between ErbB-2 and type I insulin-like growth factor receptor in mammary tumor cells. Oncogene 2001;20:34–47.
30. Gilmore AP, Valentijn AJ, Wang P, et al. Activation of BAD by therapeutic inhibition of epidermal growth factor receptor and transactivation by insulin-like growth factor receptor. J Biol Chem 2002;277:27643–50. Epub 2002 May 13.
31. Ahmad T, Farnie G, Bundred NJ, Anderson NG. The mitogenic action of insulin-like growth factor I in normal human mammary epithelial cells requires the epidermal growth factor receptor tyrosine kinase. J Biol Chem 2004;279:1713–9. Epub 2003 Oct.
32. Kuribayashi A, Kataoka K, Kurabayashi T, Miura M. Evidence that basal activity, but not transactivation, of the epidermal growth factor receptor tyrosine kinase is required for insulin-like growth factor I-induced

DOI:10.1158/0008-5472.CAN-06-1684

activation of extracellular signal-regulated kinase in oral carcinoma cells. Endocrinology 2004;145:4976–84. Epub 2004 Jul 22.
33. Holcik M, Gibson H, Korneluk RG. XIAP: apoptotic brake and promising therapeutic target. Apoptosis 2001; 6:253–61.
34. Gingras AC, Gygi SP, Raught B, et al. Regulation of 4E-BP1 phosphorylation: a novel two-step mechanism. Genes Dev 1999;13:1422–37.
35. Herbst RS. Erlotinib (Tarceva): an update on the clinical trial program. Semin Oncol 2003;30:34–46.
36. Amann J, Kalyankrishna S, Massion PP, et al. Aberrant epidermal growth factor receptor signaling and enhanced sensitivity to EGFR inhibitors in lung cancer. Cancer Res 2005;65:226–35.
37. Tracy S, Mukohara T, Hansen M, Meyerson M, Johnson BE, Janne PA. Gefitinib induces apoptosis in the EGFRL858R non-small-cell lung cancer cell line H3255. Cancer Res 2004;64:7241–4.
38. Roskoski R, Jr. The ErbB/HER receptor protein-tyrosine kinases and cancer. Biochem Biophys Res Commun 2004;319:1–11.
39. Garrett TP, McKern NM, Lou M, et al. Crystal structure of the first three domains of the type-1 insulin-like growth factor receptor. Nature 1998;394: 395–9.
40. Jimeno A, Rubio-Viqueira B, Amador ML, et al. Epidermal growth factor receptor dynamics influences response to epidermal growth factor receptor targeted agents. Cancer Res 2005;65:3003–10.
41. Tan AR, Yang X, Hewitt SM, et al. Evaluation of biologic end points and pharmacokinetics in patients with metastatic breast cancer after treatment with erlotinib, an epidermal growth factor receptor tyrosine kinase inhibitor. J Clin Oncol 2004;22:3080–90.
42. Gregorc V, Ceresoli GL, Floriani I, et al. Effects of gefitinib on serum epidermal growth factor receptor and HER2 in patients with advanced non-small cell lung cancer. Clin Cancer Res 2004;10:6006–12.
43. Rao RD, Mladek AC, Lamont JD, et al. Disruption of parallel and converging signaling pathways contributes to the synergistic antitumor effects of simultaneous mTOR and EGFR inhibition in GBM cells. Neoplasia 2005;7:921–9.
44. Gschwind A, Zwick E, Prenzel N, Leserer M, Ullrich A. Cell communication networks: epidermal growth factor receptor transactivation as the paradigm for interreceptor signal transmission. Oncogene 2001;20: 1594–600.
45. Roudabush FL, Pierce KL, Maudsley S, Khan KD, Luttrell LM. Transactivation of the EGF receptor mediates IGF-1-stimulated shc phosphorylation and ERK1/2 activation in COS-7 cells. J Biol Chem 2000; 275:22583–9.
46. Pierce KL, Luttrell LM, Lefkowitz RJ. New mechanisms in heptahelical receptor signaling to mitogen activated protein kinase cascades. Oncogene 2001;20: 1532–9.
47. Marinissen MJ, Gutkind JS. G-protein-coupled receptors and signaling networks: emerging paradigms. Trends Pharmacol Sci 2001;22:368–76.
48. Pollak M. Insulin-like growth factor physiology and cancer risk. Eur J Cancer 2000;36:1224–8.
49. Merrill MJ, Edwards NA. Insulin-like growth factor-I receptors in human glial tumors. J Clin Endocrinol Metab 1990;71:199–209.

DOI:10.1158/1078-0432.CCR-05-1725

Clinical Cancer Research

Identification of Insulin-Like Growth Factor Binding Protein-3 as a Farnesyl Transferase Inhibitor SCH66336-Induced Negative Regulator of Angiogenesis in Head and Neck Squamous Cell Carcinoma

Seung-Hyun Oh, Woo-Young Kim, Jai-Hyun Kim, et al.

Clin Cancer Res 2006;12:653-661. Published online January 20, 2006.

DOI:10.1158/1078-0432.CCR-05-1725

Identification of Insulin-Like Growth Factor Binding Protein-3 as a Farnesyl Transferase Inhibitor SCH66336-Induced Negative Regulator of Angiogenesis in Head and Neck Squamous Cell Carcinoma

Seung-Hyun Oh,[1] Woo-Young Kim,[1] Jai-Hyun Kim,[1] Maher N. Younes,[2] Adel K. El-Naggar,[3] Jeffrey N. Myers,[2] Merril Kies,[1] Pinchas Cohen,[4] Fadlo Khuri,[5] Waun K. Hong,[1] and Ho-Young Lee[1]

Abstract The farnesyl transferase inhibitor (FTI) SCH66336 has been shown to have antitumor activities in head and neck squamous cell carcinoma (HNSCC) *in vitro* and *in vivo*. However, its mechanism of action has not been well defined. Here, we report that the insulin-like growth factor (IGF) binding protein (IGFBP)-3 mediates antitumor activities of SCH66336 in HNSCC by inhibiting angiogenesis. SCH66336 significantly suppressed HNSCC tumor growth and angiogenesis via mechanisms that are independent of H-Ras and RhoB. By inducing IGFBP-3 secretion from HNSCC cells, this compound suppresses angiogenic activities of endothelial cells, including vessel formation in chorioallantoic membranes of chick, endothelial cell sprouting from chick aorta, and capillary tube formation of human umbilical vascular endothelial cells (HUVEC). Knockdown of IGFBP-3 expression in HNSCC cells by RNA interference or depletion of IGFBP-3 in HUVECs by neutralizing antibody effectively blocked the effects of IGFBP-3 secreted from SCH66336-treated HNSCC cells on HUVECs. These findings suggest that IGFBP-3 could be a primary target for antitumor activities of FTIs and that IGFBP-3 is an effective therapeutic approach against angiogenesis in HNSCC.

Despite advances in therapy, including surgery, chemotherapy, and radiation, the survival rate of patients with head and neck squamous cell carcinoma (HNSCC) has not improved substantially (1). Conventional treatments have targeted tumor cells alone. In patients with HNSCC, however, the primary tumor has metastasized to regional lymph nodes, distant organs, or both by the time the diagnosis is made (2, 3). Angiogenesis is an essential step in the transition of a tumor from a small cluster of mutated cells to a large, malignant growth and subsequent metastasis to other organs throughout the body (4–6). It has been hypothesized, therefore, that the development of agents targeting tumor angiogenesis could be an effective strategy to control and treat various malignancies.

Increasing number of evidence implicate insulin-like growth factor (IGF) binding proteins (IGFBP) in regulating angiogenesis. IGFBPs modulate the bioactivity of IGFs by sequestering IGFs away from their receptors in the extracellular milieu, thereby regulating the stimulating action of IGF on angiogenesis and invasion (7). Some IGFBPs, however, in particular IGFBP-3, also have exhibited more active, IGF-independent antitumor activities, which are probably mediated by other cell surface receptors, such as the type V transforming growth factor-β receptor (8–11). IGFBP-3 has recently been identified as an IGF-independent inhibitor of vascular endothelial growth factor–induced endothelial cell proliferation (12).

While searching for agents that have antianiogenic activities in HNSCC cells, we found that farnesyl transferase inhibitors (FTI), especially SCH66336 (Lonafarnib, Sarasar) that has shown to induce tumor regression *in vitro* and *in vivo*, inhibit angiogenic activities of HNSCC cells by inducing IGFBP-3 expression. FTIs were originally designed to inhibit posttranslational activation of Ras by blocking farnesylation (13). Recent studies suggest, however, that the cytotoxic actions of FTIs are due not to the inhibition of Ras proteins exclusively but to the modulation of other targets, including RhoB, a G protein that regulates receptor trafficking; the centromere-binding proteins CENP-E and CENP-F; and/or other proteins that have not yet been identified (14). Our results show that SCH66336

Authors' Affiliations: Departments of [1]Thoracic/Head and Neck Medical Oncology, [2]Head and Neck Surgery, and [3]Pathology, The University of Texas M.D. Anderson Cancer Center, Houston, Texas; [4]Department of Pediatrics, University of California, Los Angeles, Los Angeles, California; and [5]The Winship Cancer Institute, Emory University, Atlanta, Georgia

Received 8/8/05; revised 10/7/05; accepted 11/9/05.

Grant support: NIH grants R01 CA100816-01A1 (H-Y. Lee) and R01 CA109520-01 (H-Y. Lee), American Cancer Society grant RSG-04-082-01-TBE 01 (H-Y. Lee), M.D. Anderson Cancer Center Specialized Programs of Research Excellence grant in head and neck cancer P50 CA 97007-01 (W.K. Hong), and Department of Defense grant W81XWH-04-1-0142-01-VITAL (W.K. Hong).

The costs of publication of this article were defrayed in part by the payment of page charges. This article must therefore be hereby marked *advertisement* in accordance with 18 U.S.C. Section 1734 solely to indicate this fact.

Note: W.K. Hong is an American Cancer Society clinical research professor.

Requests for reprints: Ho-Yung Lee, Department of Thoracic/Head and Neck Medical Oncology, Box 432, The University of Texas M.D. Anderson Cancer Center, 1515 Holcombe Boulevard, Houston, TX 77030. Phone: 713-745-0769; Fax: 713-796-8655; E-mail: hlee@mdanderson.org.

doi:10.1158/1078-0432.CCR-05-1725

DOI:10.1158/1078-0432.CCR-05-1725

induced expression of IGFBP-3 protein, which in turn blocked the PI3K/Akt pathway, resulting in the induction of apoptosis in vascular endothelial cells and regression of HNSCC tumor growth and angiogenesis.

Materials and Methods

Cells, animals, and materials. Human HNSCC cell lines UMSCC38, UMSCC22B, and SqCC/Y1, established originally by Dr. Michael Reiss (Yale University, New Haven, CT) and Dr. Thomas Carey (University of Michigan, Ann Arbor, MI), respectively, were obtained from Dr. Reuben Lotan (M.D. Anderson Cancer Center, Houston, TX). (15). Human non–small cell lung cancer (NSCLC) cell lines H460, Calu1, and H358 were purchased from the American Type Culture Collection (Manassas, VA). These cells were cultured in DMEM supplemented with 10% fetal bovine serum and antibiotics. Human umbilical vascular endothelial cells (HUVEC; Cambrex BioScience, Walkersville, MD) were maintained in a gelatin-coated dish in endothelial cell basal medium (Cambrex BioScience) containing endothelial cell growth supplement at 37°C in a humidified environment with 5% CO_2. HUVECs used in this study were from passages 2 to 7. Female nude mice, 6 weeks of age, were purchased from Harlan-Sprague-Dawley (Indianapolis, IN). Chick eggs were obtained from Charles River Laboratories (Wilmington, MA).

Expression vectors containing pH-ras-V12 or pRhoB-GG were kindly given by Dr. George C. Prendergast (Thomas Jefferson University, Philadelphia, PA). Bovine serum albumin, gelatin, and 3-(4,5-dimethylthiazol-2-yl)-2,5-diphenyltetrazolium bromide were obtained from Sigma-Aldrich (St. Louis, MO). IGF-1 and Des(1-3)IGF were purchased from R&D Systems (Minneapolis, MN). Amicon Ultra-4 was obtained from Millipore Co. (Bedford, MA). Cell culture inserts incorporating PET membranes (6.4-mm diameter, 8-μm pore size) and 24-well plates were from Costar (Cambridge, MA). Anti-pIGF-1R antibodies were purchased from Cell Signaling Technology (Beverly, MA). Antibodies against IGFBP-2, IGFBP-6, IGF-1R, H-Ras, RhoB, α-tubulin, and anti-β-actin were purchased from Santa Cruz Biotechnology, Inc. (Santa Cruz, CA), and anti-CD31 antibody was obtained from BD PharMingen (San Diego, CA). Anti-IGFBP-3 antibody was from Diagnostic Systems Laboratories, Inc. (Webster, TX). SCH66336 was provided by Schering-Plough Research Institute (Kenilworth, NJ). FTI-277 was purchased from Calbiochem (San Diego, CA). SCH66336 and FTI-277 were dissolved in DMSO at various concentrations to establish dose responses. Synthetic small interfering RNAs (siRNA) targeting H-Ras or RhoB were purchased from Ambion (Austin, TX), and IGFBP-3 and nonspecific control siRNA were from Dharmacon (Lafayette, CO).

To test the effects of conditioned medium on proliferation of vascular endothelial cells, HUVECs were plated at 3×10^3 per well in 96-well culture plates, untreated or preincubated with IgG or IGFBP-3 neutralizing antibody, and then treated with conditioned medium (10 μg) from the HNSCC cells. Cell proliferation was measured using the 3-(4,5-dimethylthiazol-2-yl)-2,5-diphenyltetrazolium bromide assay, as previously described (16).

In experiments assessing the effects of SCH66336 on protein and mRNA expression, HNSCC and NSCLC cell lines (1×10^6 in 100-mm^3 dishes) were treated with different concentrations of SCH66336 (0.5, 1, or 5 μmol/L) for indicated time periods in complete medium. When the effects of SCH66336 on pIGF-1R were tested, cells were serum starved for 1 day and stimulated with IGF-I (100 ng/mL, for 30 minutes) before harvest. For siRNA transfection, UMSCC38 cells were plated at concentrations of 1×10^6 per well in 10-cm plates. The next day, the cells were transfected with siRNA using Oligofectamine (Invitrogen, Carlsbad, CA) and cultured in growth medium with or without SCH66336 (5 μmol/L). One day after transfection, cells were changed to serum-free medium containing the same concentration of SCH66336. After 2 days of incubation, cells and conditioned media were collected. When HUVECs were treated with conditioned media from UMSCC38 cells, 1×10^5 per well in six-well plates were treated with conditioned media in endothelial cell basal medium in the absence or presence of IGFBP-3 neutralizing antibody for 12 hours.

Conditioned medium. To collect conditioned media from UMSCC38 cells, UMSCC38 cells (1×10^6 per plate) in 10-cm plates were incubated in growth medium containing SCH66336 (0.5, 1, or 5 μmol/L) for 1 day, washed with PBS, and then resupplied with serum-free medium containing the same concentrations of SCH66336. After 2 days of incubation, conditioned medium was collected and subjected to centrifugation through an Amicon Ultra-4 filter to remove any traces of SCH66336. Concentration of the conditioned medium was measured by the bicinchoninic acid assay (Pierce Biotechnology, Rockford, IL). The molecular mass cutoff of the filter was 5 kDa; the molecular mass of SCH66336 is 0.56 kDa, thus the flow-through containing excess SCH66336 was discarded, and the retentate was collected. Removal of SCH66336 from the conditioned medium was determined as previously described (17). The final filter retentate was concentrated 40-fold for several analyses, including Western blot, HUVEC proliferation and tube formation, chick aortic arch, and chorioallantoic membrane assays.

Animal care and injections. All animal procedures were done in accordance with a protocol approved by the Institutional Animal Care and Usage Committee. Orthotopic sublingual injections of tumor cells were described elsewhere (18). Female nude mice (6-week-old) under anesthesia were injected with UMSCC38 cells (2×10^6) into the lateral tongue ($n = 5$). One week later, when tumors started to develop, 40 mg/kg of SCH66336 or 20% hydroxyl-propyl-β-cyclodexatrin control vehicle was given orally twice a day for 3 weeks. Thirteen days after cell injection, when tumors reached at least 50 mm^3 in volume, tumor size was measured twice a week for 15 days. Tumor growth was quantified by measuring the tumors in two dimensions and calculating volume as described elsewhere (16). One week later, when tumors started to develop, the mouse food was replaced by commercially available soft food (transgenic mice dough; Bio-serv, Frenchtown, NJ), which the mice can ingest even when the oral cavity was blocked by tumor. The mice were humanely killed by CO_2 inhalation when they had lost >20% of their preinjection body weight (average 18.92 g). The tongues were removed and separated into two parts. One part was fixed, embedded in paraffin, and sectioned for active caspase-3 staining. The other part was frozen and sectioned for CD31 staining.

Western blot analysis. Preparation of whole-cell lysates, quantification of the proteins, gel electrophoresis, and Western blotting were done as described elsewhere (19). Equal amounts of proteins in conditioned medium samples were confirmed by Coomassie blue staining of the duplicate gels and Ponceau staining of membrane.

Immunohistochemistry. Immunohistochemical analysis on IGFBP-3 was done using tongue tumor tissues from mice as described elsewhere (17). For CD31 staining, frozen sections of tumor tissues were stained with anti-CD31 antibody (BD PharMingen; 1:100 dilution) and then detected by 3,3′-diaminobenzidine.

Chick aortic arch assay. Chick aortic arch assay was done as described elsewhere (20). Briefly, conditioned media collected from UMSCC38 cells were added to aortic rings from 14-day-old chick embryos. The plates were incubated for 48 hours at 37°C to allow microvessel sprouting from the adventitial layer. Average sprouting was measured with the imageJ program (NIH) after the plates were photographed under the stereomicroscope (Zeiss, Göttingen, Germany). Each condition was tested in six wells. The experiment was repeated thrice with similar results.

Tube formation assay. Tube formation assay was done as described elsewhere (21). HUVECs (5×10^4) were seeded on Matrigel surfaces and grown in the absence or presence of conditioned media from different treatment groups. After 18 hours, images were photographed at ×40 magnification, and tube formation was scored by blinded

DOI:10.1158/1078-0432.CCR-05-1725

observer as follows: a three-branch point event was scored as one tube, as described elsewhere (21). Each condition was tested in six wells. The experiment was repeated thrice with similar results.

Chorioallantoic membrane assay. Chorioallantoic membrane assay was conducted on 9-day-old chick embryos as described elsewhere (21). A coverslip loaded with 50 μg of conditioned medium was applied onto the surface of the chorioallantoic membrane. After 2 days of incubation, a fat emulsion was injected into the chorioallantoic membrane to allow visualization of the blood vessels, and chorioallantoic membranes were photographed with a stereomicroscope.

Reverse transcription-PCR. Total RNA was isolated from cells with the use of Trizol reagent (Invitrogen). cDNA was synthesized as previously described (17). Reverse transcription-PCR was done by coamplification of the genes together with a reference gene (*GAPDH*) using cDNA template generated as already described and corresponding gene-specific primer sets. The primer sequences were as follows: 5′-GAAGGGCGACACTGCTTTTTC-3′ (sense) and 5′-CCAGCTCCAGGAAATGCTAG-3′ (antisense) for *IGFBP-3*; 5′-CAAGAGTGCGCTGACCATCC-3′ (sense) and 5′-CCGGATCTCACGCACCAAC-3′ (antisense) for H-*ras*; 5′-GCGTGCGGCAAGACGTCTG-3′ (sense) and 5′-TCATAGCACCTTGCAGCAGTT-3′ (antisense) for *rho-B*; 5′-GGTGAAGGTCGGTGTGAACGGATTT-3′ (sense) and 5′-AATGCCAAAGTTGTCATGGATGACC-3′(antisense) for *GAPDH*. To avoid amplification of genomic DNA, the primers of each gene were chosen from different exons. Reverse transcription-PCR was done in a total volume of 25 μL containing 1 μL of cDNA solution and 0.2 μmol/L of sense and antisense primers. The reverse transcription-PCR exponential phase was determined on 28 to 38 cycles using cDNAs developed from identical reactions. The thermocycler condition used for amplification was as follows: 6 minutes at 94°C (one cycle), 6 minutes hot start at 94°C, 45 seconds at 56°C to 60°C (25-35 cycles), and 1 minute at 72°C (one cycle). Amplification products (8 μL) were resolved in 2% agarose gel, stained with ethidium bromide, and visualized in a transilluminator and photographed.

Immunoprecipitation. Equal amounts of protein samples were incubated with anti-pTyr antibody and protein A-Sepharose overnight and washed with lysis buffer thrice and 2× PBS twice. Proteins were eluted with 4× SDS loading buffer. Samples were boiled and subjected to electrophoresis on SDS-polyacrylamide gels, and binding was detected by using an enhanced chemiluminescence assay (Amersham Pharmacia Biotech, Piscataway, NJ).

Northern blot analysis. Total cellular RNA was prepared, as previously described (22). Twenty micrograms of total RNA were subjected to electrophoresis in denaturing agarose gels and transferred to a Zeta-probe membrane (Bio-Rad Laboratories, Hercules, CA). Membranes were hybridized with [^{32}P]dCTP random-primed *IGFBP-3* cDNA, washed, and subjected to autoradiography. An equal amount of RNA loading was monitored by ethidium bromide staining of the gels.

Luciferase assay. Cells were seeded in 24-well tissue culture plates and transfected with 500 ng of IGFBP-3 reporter plasmid (pGL2 or pGL2-BP3) and 20 ng of *Renilla* luciferase control vector (pRL-SV40) using LipofectAMINE (Life Technologies/Bethesda Research Laboratories, Grand Island, NY). The total amount of plasmid DNA was equally adjusted with vector DNA. The transfection solution was removed after 6 hours of transfection, and the cells were changed to complete medium with or without different concentrations of SCH66336. Following 2 days of incubation, cells were harvested. The cells were washed with PBS and subjected to lysis in 0.1 mL of 1× passive lysis buffer (Promega, Madison, WI). Cell extracts were assayed for firefly and *Renilla* luciferase activities using the Dual-luciferase reporter assay system according to the manufacturer's instruction (Promega). Firefly luciferase activities were normalized by *Renilla* luciferase activities. Luciferase activities were expressed as the means and SD from three identical wells.

Statistical analysis. Data are shown as means ± SD. For statistical significance between groups, the paired Student's *t* test was done.

Results

SCH66336 inhibits angiogenic activities of HNSCC. We tested the effects of SCH66336 on HNSCC tumor growth by establishing orthotopic tongue tumors of UMSCC38 HNSCC cells in nude mice and treating the mice with SCH66336. Representative tongue tissues from a healthy mouse (*Normal*), and tongue tumors from SCH66336-untreated (*Con*) and SCH66336-treated mice (*SCH66336*) are shown (Fig. 1A). Oral treatment with SCH66336 (40 mg/kg) almost completely suppressed tumor growth ($P < 0.005$). On day 25, the average tumor volume for untreated control mice had increased to 287.86 ± 53.93% (mean ± SD) of the volume on day 13, whereas that for SCH66336-treated mice showed 123.20 ± 14.67% of the volume before the SCH66336 treatment (Fig. 1B, *left*). The average body weight of SCH66336-treated mice was not remarkably changed during the treatment (Fig. 1B, *right*) compared with that of control mice. These findings suggest that FTI SCH66336 is an efficient therapeutic agent in head and neck tumors.

We studied the mechanism of the antitumor activities of SCH66336 in HNSCC. Several HNSCC cell lines treated with as much as 5 μmol/L SCH66336 yielded neither a terminal deoxynucleotidyl transferase–mediated nick end labeling–positive cell population nor changes in expression of caspase-3 and poly (ADP-ribose) polymerase (data not shown), indicating that SCH66336 induces little apoptotic activities in HNSCC cells. Given this finding and the critical role of angiogenesis in tumor growth, we evaluated the effects of SCH66336 on angiogenic activities of HNSCC cells. As shown in Fig. 1C, SCH66336 significantly decreased tumor vascularization ($P < 0.01$) as determined by microvessel density in anti-CD31-stained tongue tumor tissues from control and SCH6636-treated nude mice. We then did a series of *in vitro* and *in vivo* experiments to test the antiangiogenic activities of SCH66336. We directly applied conditioned media from UMSCC38 cells to HUVECs. The proliferation (Fig. 1D) and capillary tube formation (Fig. 1E) of HUVECs were significantly stimulated by conditioned media from the untreated UMSCC38 cells but not by conditioned media from SCH66336 (5 μmol/L)–treated cells ($P < 0.01$). The *ex vivo* chick aortic ring arch assay revealed that conditioned media from untreated UMSCC38 cells also stimulated endothelial cell sprouts ($P < 0.01$), whereas conditioned media from SCH66336-treated cells did not exhibit stimulating effects on endothelial cell sprouting (Fig. 1F). The chorioallantoic membrane assay, an established *in vivo* angiogenesis model, revealed that treatment with conditioned media from untreated UMSCC38 cells but not conditioned media from SCH66336-treated cells significantly induced new vessel formation in chorioallantoic membranes of chick embryos ($P < 0.05$; Fig. 1G). We did not find any signs of toxicity, such as thrombosis, hemorrhage, or egg lethality, in the chorioallantoic membrane assay. Together, this data indicate that SCH66336 can elicit antiangiogenic activities in HNSCC.

Antiangiogenic activities of SCH66336 in HNSCC cells are independent of H-Ras and RhoB. We investigated the mechanisms by which SCH66336 elicits antiangiogenic activities in HNSCC cells. Because FTIs are designed to inhibit Ras farnesylation, the most important step in ras activation (13), we first tested the effects of SCH66336 on Ras in HNSCC cells. Western blot analysis revealed that SCH66336 induced

DOI:10.1158/1078-0432.CCR-05-1725

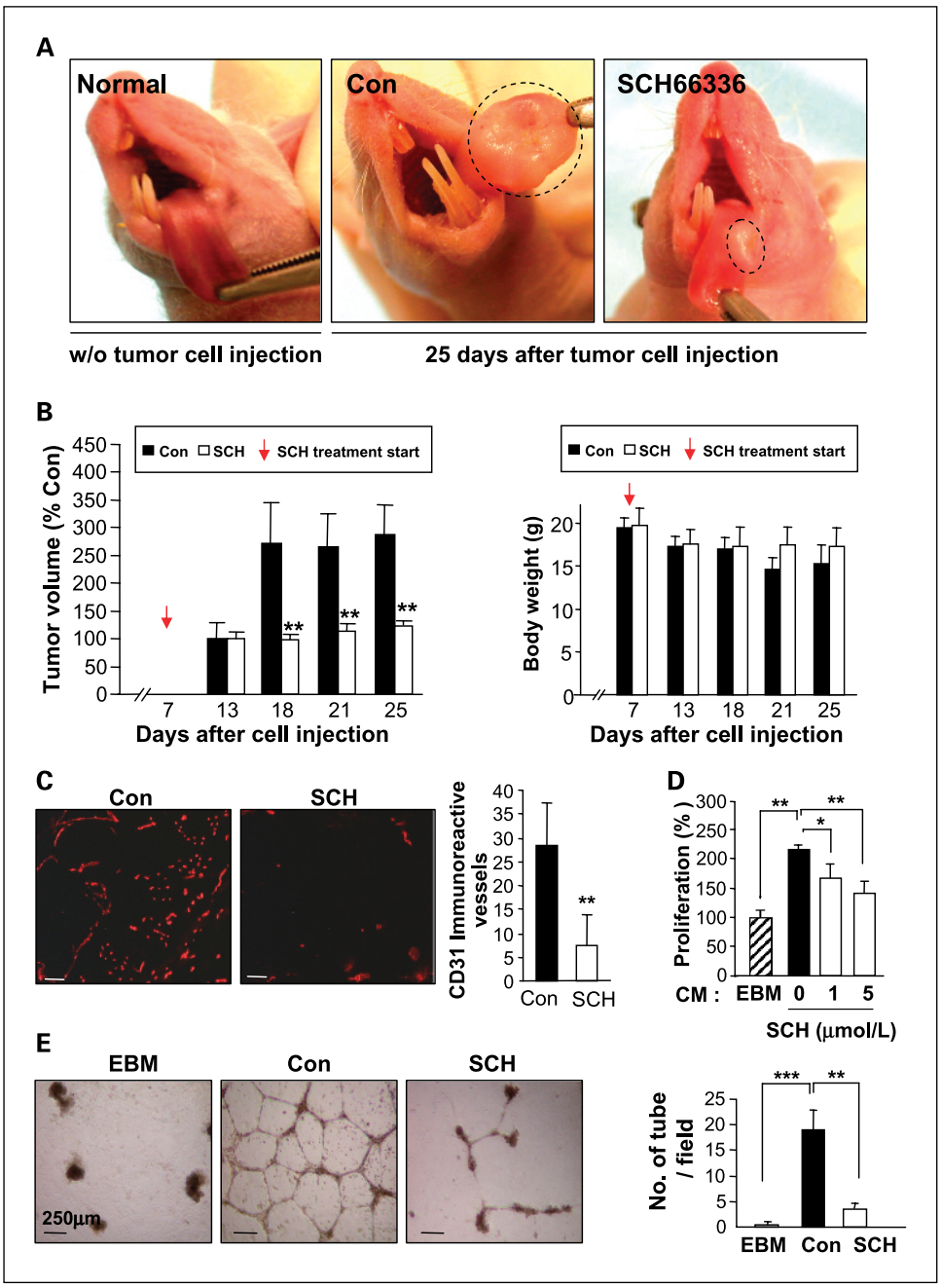

Fig. 1. Antiangiogenic activities of SCH66336 in HNSCC cells. *A,* photograph of normal tongue from nude mice that was not inoculated with UMSCC38 cells (*left*). Nude mice bearing UMSCC38 orthotopic tongue tumors were given 40 mg/kg SCH66336 orally twice a day on days 7 to 25 after tumor cell injection. Orthotopic tongue tumors from vehicle-treated (*middle, Con*) and SCH66336-treated (*right, SCH66336*) nude mice on day 25 after injection of UMSCC38 cells. *B,* effects of SCH66336 (*SCH*) on growth of orthotopic tongue tumors were tested. Relative tumor growth and changes in body weight in the control and the treatment groups compared with control tumor volumes at the time of SCH66336 treatment (day 13). Columns, mean tumor volumes (calculated from five mice); bars, SD. **, $P < 0.01$ compared with control. *C,* orthotopic mouse tongue tissues were stained with an anti-CD31 antibody. The slides were examined at ×100 under fluorescent microscope and analyzed for red (CD31) fluorescence. The number of microvessels per field was counted. Columns, mean of three slides per tumor (calculated from five mice); bars, SD. **, $P < 0.01$ compared with control-treated tumors. *D,* HUVECs were allowed to grow in 100 μL endothelial cell basal medium (*EBM*) containing 10 μL conditioned medium (*CM*) from untreated or SCH66336-treated UMSCC cells. Cell proliferation was analyzed by 3-(4,5-dimethylthiazol-2-yl)-2,5-diphenyltetrazolium bromide assay. Independent experiments were repeated three times. Columns, mean % of eight samples; bars, SD. *, $P < 0.05$; **, $P < 0.01$; ***, $P < 0.001$ compared with negative control. *E,* angiogenic activities of conditioned media from UMSCC38 cells were tested by tube formation assay. Columns, mean of three samples; bars, SD. **, $P < 0.01$; ***, $P < 0.001$ compared with control.

dose-dependent decreases in farnesylated H-Ras (H-Ras-F) in UMSCC38, UMSCC22B, and SqCC/Y1 cells (Fig. 2A). None of these cells have a *ras* mutation (data not shown), suggesting that the antiangiogenic activities of SCH66336 could be traced to proteins other than Ras. One potential target is RhoB, a 21-kDa G-protein, that is both farnesylated and geranylgeranylated by FTase and GGTase I (23), respectively. Recent evidence indicates that RhoB is a mediator of the antitumor activities of FTIs in mouse and rodent model systems and in human cancer cells (24, 25). Indeed, treatment with SCH66336 elicited elevations in the levels of RhoB (Fig. 2A), presumably due to the increased expression of the geranylgeranylated isoform of RhoB (RhoB-GG), as was observed previously (26).

To understand whether decreases in H-Ras-F or induction of RhoB mediated the antiangiogenic activity of SCH66336, we determined whether silencing H-Ras or RhoB expression by siRNA could abolish the activities of SCH66336 in UMSCC38 cells. Transfection with siRNAs targeting H-*ras* or *RhoB* specifically inhibited H-Ras or RhoB protein expression in UMSCC38 cells, whereas control scrambled (*scr*) siRNA did not affect the expression of these genes (Fig. 2B). Two different siRNAs induced similar degrees of gene silencing. These siRNAs also specifically inhibited mRNA expression of target genes regardless of the presence of SCH66336 (Fig. 2C). Cell viability was not specifically altered in any of these cells (data not shown). According to the 3-(4,5-dimethylthiazol-2-yl)-2,5-diphenyltetrazolium bromide assay (Fig. 2D) and

DOI:10.1158/1078-0432.CCR-05-1725

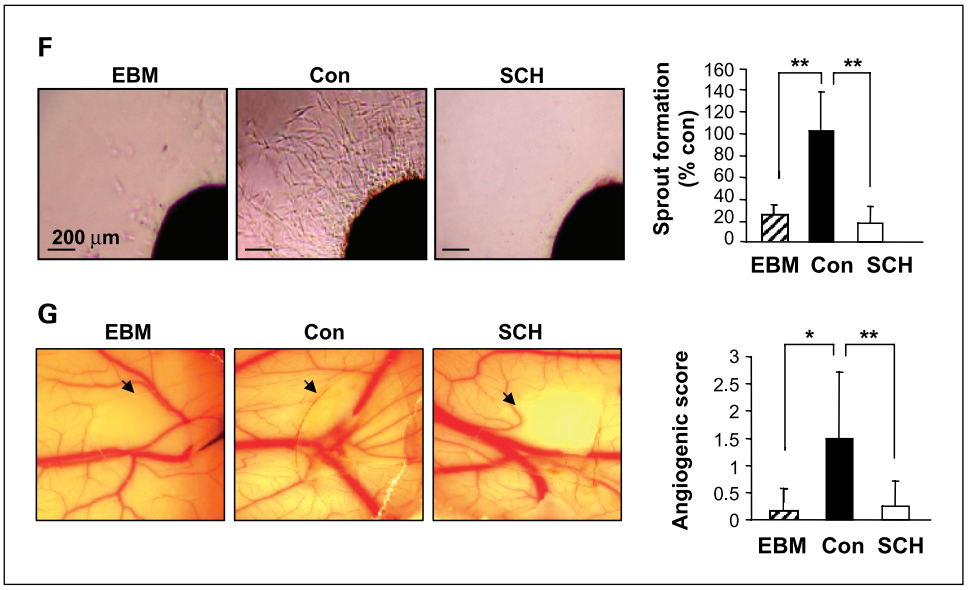

Fig. 1 *Continued. F,* endothelial cell sprouting from chick aortic rings that were incubated with conditioned medium from SCH66336-treated or untreated UMSCC38 cells. Columns, means from six samples; bars, SD. Representative group from each condition. Bar, 200 μm. **, $P < 0.01$ compared with negative control. *G,* in a chorioallantoic membrane assay, angiogenesis stimulated by conditioned media from UMSCC38 cells was photographed (*left*) or quantitatively evaluated (*right*). Independent experiments were repeated three times. Columns, mean of >30 eggs; bars, SD/95% confidence intervals. *, $P < 0.05$; **, $P < 0.01$; ***, $P < 0.001$ compared with negative control.

tube formation assays (Fig. 2E), HUVEC proliferation and morphogenesis were stimulated by conditioned media from control UMSCC 38 cells transfected with *scr*. Conditioned media from SCH66336-treated UMSCC38 cells did not show these angiogenic activities. The effects of SCH66336 were still consistent in UMSCC38 cells, which had been transfected with siRNA targeting H-ras or RhoB. Two different siRNAs for H-Ras and RhoB showed similar results (data not shown). All of these findings indicate that SCH66336 suppressed the angiogenic activities of HNSCC cells via H-Ras-independent and RhoB-independent mechanisms.

FTI induces IGFBP-3 expression* in vitro *and* in vivo *via mechanisms that are independent of H-Ras or RhoB. Because the IGF system has an important role in regulating4 proliferation and angiogenesis (27–29), we determined whether SCH66336 treatment stimulates the expression of IGFBPs. An obvious increase in IGFBP-3 protein level was observed in UMSCC38, UMSCC22B, and SqCC/Y1 cells treated with SCH66336 or FTI-277, another FTI (Fig. 3A). Increased levels of the IGFBP-3 protein were also observed in conditioned media from these cells (data not shown). No change was detected in the expression of other IGFBP subfamily members, including IGFBP-2 and IGFBP-6, after SCH66336 treatment (Fig. 3A). Because IGFBP-3 is supposed to control IGF-1–induced IGF-1R activation (30), we next determined the effects of SCH66336 on the levels of phosphorylated IGF-1R (pIGF-1R) in UMSCC38 cells. Western blot analysis revealed that treatment with IGF-1 caused increases in pIGF-1R, which is inhibited by SCH66336 in UMSCC38 cells (Fig. 3B, *left*). Whereas phosphorylation of IGF-1R stimulated by Des(1-3) (10 nmol/L), a mutant IGF-I that has a vastly diminished affinity for the IGFBPs but retains high avidity for IGF-1R (31), was marginally affected by SCH66336 in UMSCC38 cells (Fig. 3B, *middle*), indicating that secretion of functional IGFBP-3 by SCH66336-treated cells down-regulated pIGF-IR. Immunoprecipitation analysis using an antiphosphotyrosine antibody followed by Western blot analysis with an anti-IGF-1Rβ antibody confirmed that SCH66336 inhibited IGF-stimulated IGF-1R phosphorylation (Fig. 3B, *right*). Induction of IGFBP-3 by SCH66336 also found in H460, Calu1, and H358 NSCLC cell lines (Fig. 3C).

We further studied the mechanism by which SCH66336 activates IGFBP-3 expression. Northern and Western blot analyses of UMSCC38 cells revealed that *IGFBP-3* gene expression is induced within 1.5 hours after the SCH66336 treatment, respectively (Fig. 3D). Moreover, a transient transfection experiment done with a luciferase reporter plasmid containing 1.8-kb *IGFBP-3* promoter (pGL2-BP3; ref. 32) indicated that SCH66336 increased *IGFBP-3* promoter activity in UMSCC38 and H460 cells in a dose-dependent manner (Fig. 3E). IGFBP-3 promoter activity was also increased in UMSCC38 cells by the treatment with FTI-277. These findings indicate that SCH66336 induced IGFBP-3 expression at a transcriptional level and that the induction of IGFBP-3 expression is a generic response to FTIs. Blockade of H-Ras or RhoB expression by siRNA (Fig. 3F and G) or overexpression of pH-Ras-V12 or pRhoB-GG (Fig. 3H) did not affect the ability of SCH66336 to induce IGFBP-3 promoter activity and protein expression, indicating that induction of IGFBP-3 expression by SCH66336 is independent of H-Ras or RhoB.

Oral administration of FTI SCH66336 induces IGFBP-3 expression* in vivo *in tongue tumor tissues. We tested whether SCH66336 could increase IGFBP-3 expression *in vivo*. We found obviously higher levels of IGFBP-3 in orthotopic tongue tumor tissues removed from SCH66336-treated mice than in tongue tumor tissues from untreated control mice (Fig. 4A). IGFBP-3 expression was also analyzed in the tissue samples from patients who had received SCH66336. Results are shown from the pretreatment and/or posttreatment matched tumor tissues from three patients. Prominent IGFBP-3 expression was observed in the first patient (33) in histologically normal cells of the anterior tongue (Fig. 4B, *left*), but only focal or no IGFBP-3 expression was found in their squamous carcinoma tumor cells (*SCC*, Fig. 4B, *right*). Tumor tissues from this patient were not available after the SCH66336 treatment. Very low or undetectable levels of IGFBP-3 were also observed in squamous carcinoma tumor cells of the other two patients (patients 2 and 3) who had not been treated with SCH66336 (Fig. 4C, *left*). Three months after

DOI:10.1158/1078-0432.CCR-05-1725

these patients' treatment with SCH66336, however, IGFBP-3 expression was strongly induced in the membranes of the cancer cells undergoing karyolysis (Fig. 4C, *right*). These findings indicate that oral administration of SCH66336 was sufficient to induce IGFBP-3 expression *in vivo*.

IGFBP-3 secreted from SCH66336-treated HNSCC cells inhibits angiogenic activities in HUVECs by blocking Akt activation. To investigate whether IGFBP-3 secreted from SCH66336-treated HNSCC cells inhibited angiogenesis, we determined whether the blockade of IGFBP-3 secretion from SCH66336-treated UMSCC38 cells could restore the angiogenic effects of conditioned media from these cells. To this end, UMSCC38 cells were transfected with *IGFBP-3* siRNA, and the conditioned medium from these cells was applied to HUVECs. *IGFBP-3* siRNA specifically inhibited *IGFBP-3* mRNA expression (Fig. 5A, *left*) as well as protein expression in the untreated and SCH66336-treated UMSCC38 cells (Fig. 5A, *right*). Conditioned media from UMSCC38 cells transfected with *IGFBP-3* siRNA before the SCH66336 treatment (*SCH*) did not show significant effects on tube formation (Fig. 5B) and proliferation (Fig. 5C) of HUVECs compared with conditioned media from *scr*–transfected cells. To mask the effect of IGFBP-3 secreted from UMSCC38 cells on HUVECs, HUVECs were preincubated with IGFBP-3 neutralizing antibody (αBP3) before conditioned medium treatment. Stimulation of HUVECs proliferation by the conditioned media from control UMSCC38 cells was not affected with αBP3 (Fig. 5D). In contrast, proliferation-stimulating activities of conditioned media from SCH66336-treated UMSCC38 cells were almost completely blocked. These findings indicate that IGFBP-3 secreted from SCH66336-treated cells played a major role in inhibiting HUVECs proliferation and morphogenesis.

It has been shown that IGFBP-3 induces apoptosis in endothelial cells by inhibiting activation of Akt, a key enzyme for cell survival (12). Thus, we next tested whether IGFBP-3 secreted from SCH66336-treated HNSCC cells could inhibit activation of Akt. Western blot assays showed that conditioned media from control UMSCC38 cells stimulated phosphorylation of Akt (*pAkt*, Ser^{473}) in HUVECs (Fig. 5E), which was not affected by the αBP3 treatment. Conditioned media from SCH66336-treated UMSCC38 cells marginally stimulated phophorylation of Akt; however, pAkt levels were obviously induced by the incubation of HUVECs with αBP3. Phosphorylation of extracellular signal-regulated kinase (*pERK*) was stimulated in HUVECs by conditioned media from control or SCH66336-treated UMSCC cells but was not affected by the αBP3 (Fig. 5E). These findings suggest that IGFBP-3 secreted from SCH66336-treated HNSCC cells inhibited proliferation of HUVECs by inhibiting Akt activation.

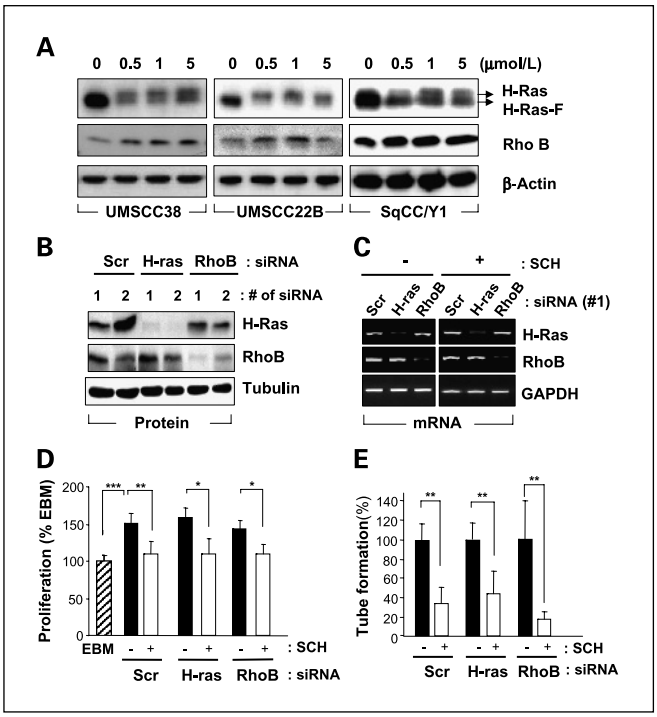

Fig. 2. Role of H-Ras and RhoB in the antiangiogenic and anti-invasive activities of SCH66336 in HNSCC cells. *A,* effects of SCH66336 on levels of unfarnesylated H-Ras and farnesylated H-Ras (H-Ras-F) were examined in UMSCC38, UMSCC22B, and SqCC/Y1 cells treated with indicated doses of SCH66336 for 3 days. *B-C,* effects of scrambled siRNA (*scr*) or siRNA targeting H-*ras* or *RhoB* on protein (*B*) and mRNA (*C*) levels of H-Ras and RhoB were examined. Expression of tubulin or GAPDH was included as loading controls. Lanes 1 and 2, siRNA with different sequence targeting same gene. *D-E*, proliferation (*D*) and morphogenesis (*E*) of HUVECs stimulated by conditioned media from UMSCC38 cells, which were transfected with the indicated siRNA and treated with SCH66336 (5 μmol/L), were tested by 3-(4,5-dimethylthiazol-2-yl)-2,5-diphenyltetrazolium bromide and tube formation assays, respectively. Independent experiments were repeated three times. Columns, means of three samples; bars, SD. *, $P < 0.05$; **, $P < 0.01$; ***, $P < 0.001$ compared with untreated cells from each transfection.

Discussion

In this article, we have shown for the first time that the FTI SCH66336 has antitumor activities, especially those related to angiogenesis, by inducing IGFBP-3 expression. The increased IGFBP-3 in turn induces tumor regression by inhibiting tumor angiogenesis via a mechanism that is independent of H-Ras and RhoB. We were encouraged to pursue this line of research by early observations of tumor regression in a clinical trial in which patients with advanced HNSCC were randomized to receive a short 8- to 14-day course of SCH66336 in the preoperative setting.[6] Our *in vivo* results also clearly show that SCH66336 induces efficient antitumor activities; daily oral administration of SCH66336 (40 mg/kg) was sufficient to suppress growth of implanted UMSCC38 tumors in the tongues of nude mice. SCH66336 was active at a concentration of 1 μmol/L, which is well below the concentration reported to be achievable *in vivo* (about 8 μmol/L) in mice given a single oral dose of 25 mg/kg SCH66336 (34). SCH66336 inhibits proliferation of HNSCC cells (15); similar results have been observed in cell lines derived from breast, colon, pancreas, brain, and lung cancers (35–37).

Despite these promising results, the mechanism of action of FTIs in tumors is still incompletely understood. We did not find evidence of SCH66336-mediated apoptotic activities in most of the HNSCC cell lines used in our study, results which are consistent with previous findings that SCH66336 as a single agent cannot induce apoptosis at doses similar to those we used (38). This led us to investigate the antiangiogenic activities of SCH66336 in HNSCC cells. SCH66336 inhibited the angiogenic activities of HNSCC cells *in vitro* and *in vivo*: (*a*)

[6] Unpublished data.

DOI:10.1158/1078-0432.CCR-05-1725

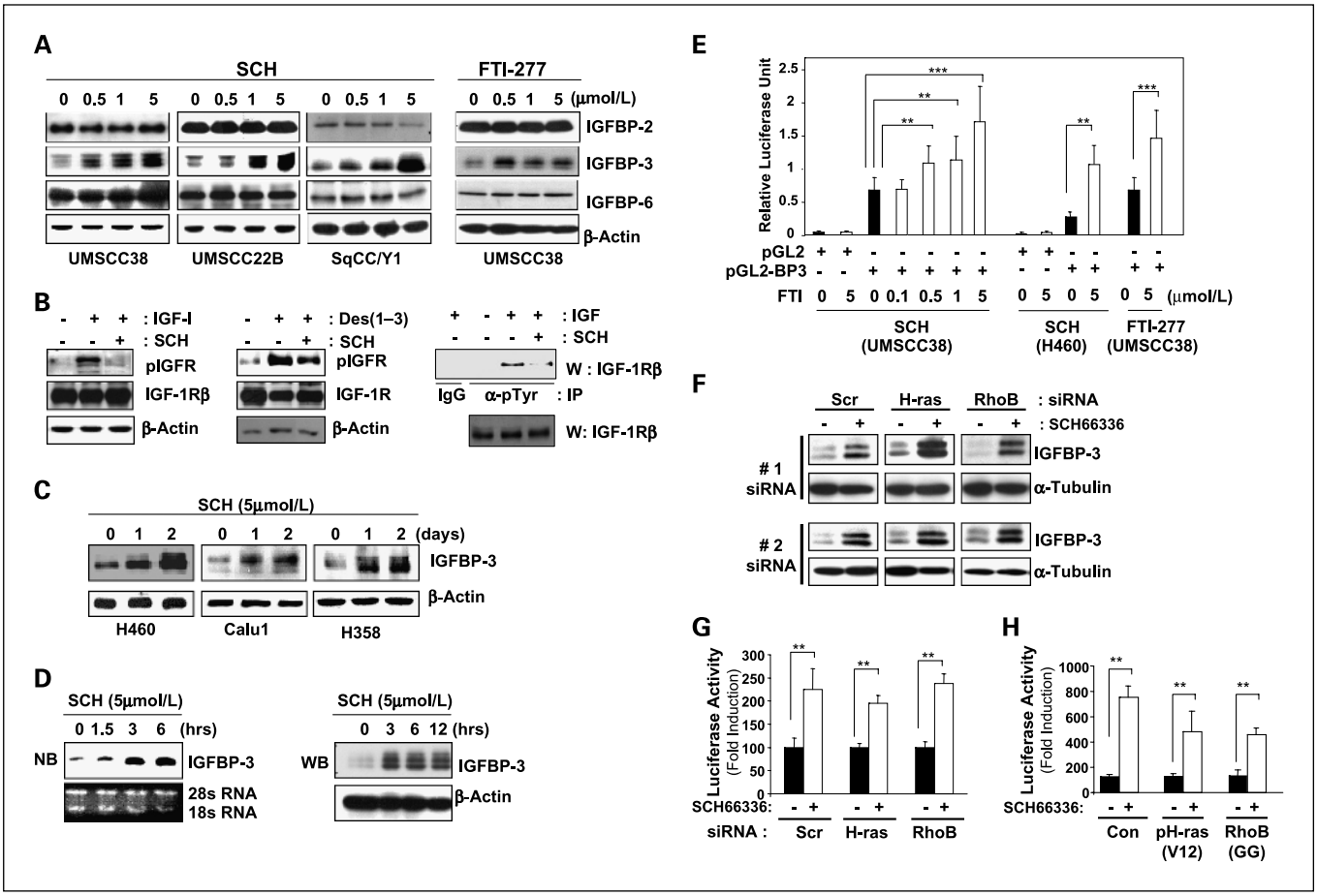

Fig. 3. Effects of FTIs on the expression of IGFBP-3 in HNSCC cells *in vitro* and *in vivo*. *A,* expression of IGFBP-2, IGFBP-3, and IGFBP-6 in UMSCC38, UMSCC22B, and SqCC/Y1 cells, untreated or treated with indicated concentrations of SCH66336 or FTI-277 for 3 days. *B,* Western blot analysis on expression of phosphorylated IGF-1R (Tyr^{1184}; pIGF-1R) and unphosphorylated IGF-1Rβ in UMSCC38 cells that were untreated or treated with SCH66336 and then activated with IGF-I (*left*) or Des(1-3) IGF-I (*middle*). β-Actin was also detected as a loading control. Total protein extracts (500 μg) of UMSCC38 cells that were untreated or treated with SCH66336 before the activation with IGF-1 were subjected to immunoprecipitation (*IP*) with IgG or anti-phosphotyrosine (*pTyr*) antibody. Western blot analysis (*WB*) on immunoprecipitates was done using an anti-IGF-1Rβ antibody (*right*). Equal amount of protein for immunoprecipitation was confirmed by Western blot analysis on IGF-1Rβ expression. *C,* H460, Calu1, and H358 cells treated with 5 μmol/L SCH66336 for 1 or 2 days were also analyzed for IGFBP-3 expression. β-Actin was included as a loading control. *D,* Northern blot (*NB*) and Western blot (*WB*) analyses were done to analyze the effect of SCH66336 on *IGFBP-3* mRNA and protein expression in UMSCC38 cells that were treated with SCH66336 (5 μmol/L) for the indicated time periods. The ethidium bromide – stained RNA gel is illustrated to show the relative amounts of total RNA loaded per well (*top*). *E,* luciferase analysis was done in UMSCC38 and H460 cells that were transiently transfected with pGL2 or pGL2-BP-3 reporter plasmid and then treated with indicated concentrations of SCH66336 or FTI-277. Columns, means of six different samples from three independent experiments; bars, SD. **, $P < 0.01$; ***, $P < 0.001$ compared with pGL2-BP3-transfected cells (*bottom*). *F,* Western blot analysis on expression of IGFBP-3 after transfection H-ras or RhoB siRNA and SCH66336 (5 μmol/L) treatment for 2 days in UMSCC38 cells. *G,* effects of siRNA targeting H-Ras or RhoB on SCH66336-mediated induction of IGFBP-3 promoter activities in UMSCC38 cells that were transfected with scr, H-Ras, or RhoB siRNA. *H,* luciferase analysis in UMSCC38 cells that were transiently cotransfected with reporter plasmid (pGL2 or pGL2-BP3) and expression vector (Control vector, pH-Ras-V12, or pRhoB-GG) and then treated with 5 μmol/L SCH66336. Columns, means of six different wells from three independent experiments; bars, SD. **, $P < 0.01$ compared with untreated control cells.

administration of SCH6636 significantly reduced tumor vascularization in HNSCC orthotopic tongue tumors; (*b*) pretreatment with SCH66336 effectively suppressed angiogenesis-stimulating effects of the conditioned media from HNSCC38 cells on HUVECs in several *in vitro* and *in vivo* angiogenesis assays. The antiangiogenic activities of SCH66336 in HNSCC cells did not correlate with mutation and expression of Ras and RhoB in our study, suggesting that FTIs have mechanisms of action other than inhibiting Ras or RhoB.

We found that FTIs, including SCH66336 and FTI-277, induced expression of IGFBP-3, a major IGFBP in serum (39), in several different cancer cell lines, orthotopic tongue tumor tissues from mice, and a subset of patients with HNSCC. These findings revealed that the effect of FTIs on IGFBP-3 expression is a generic response to FTI treatment, and that oral administration of SCH66336 is sufficient to induce IGFBP-3 expression *in vivo*. Because FTIs up-regulated promoter activities and transcription of the *IGFBP-3* gene, FTIs seemed to induce *IGFBP-3* gene expression at transcription level. The effects of FTIs on IGFBP-3 expression could be mediated by novel farnesylated proteins (37) or by farnesyl transferase – independent off-target activity of FTIs. It is also possible that FTIs may activate various transcription factors that stimulate the IGFBP-3 promoter, such as Sp-1/Sp-3, p53, vitamin D receptor, and retinoid X receptors. A detailed mechanism that is critical for the induction of IGFBP-3 expression by SCH66336 is currently under active investigation in our laboratory.

Perhaps most strikingly, our findings presented here show the role of IGFBP-3 as the functional basis for the use of FTIs in HNSCC targeting tumor angiogenesis; inhibition of

DOI:10.1158/1078-0432.CCR-05-1725

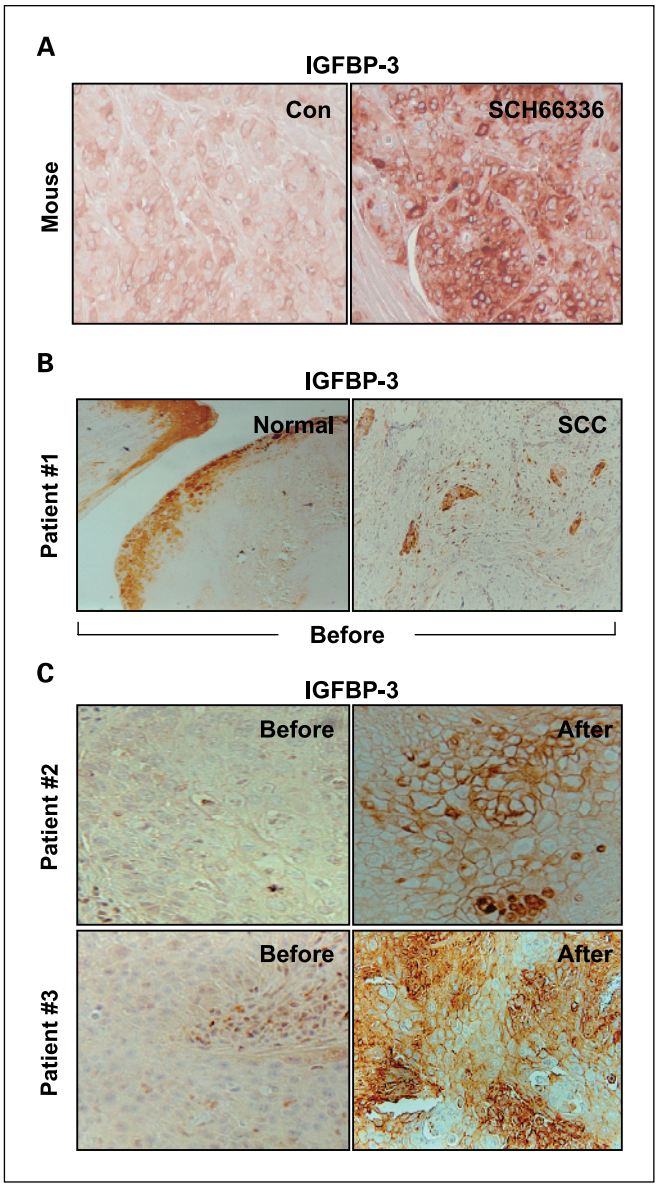

Fig. 4. Immunohistochemical analysis of IGFBP-3 in tongue tumor tissues. *A,* IGFBP-3 expression in orthotopic tongue tumor tissues from control nude mice (*left*) and SCH66336-treated mice (*right*) at 25 days. *B,* IGFBP-3 expression in normal and SCC tissues from a patient with HNSCC. *C,* IGFBP-3 expression was also tested in two patients before (*left*) or after 3 months of treatment with SCH66336 (*right*), ×400.

the secretion of SCH66336-induced IGFBP-3 from UMSCC38 cells by RNA interference or depletion of IGFBP-3 in HUVECs by neutralizing antibody significantly restored angiogenic effects of conditioned media from SCH66336-treated UMSCC38 cells on HUVECs. Consistent with previous findings (12), we also observed that IGFBP-3 secreted from FTI-treated HNSCC cells inhibited endothelial cell proliferation by blocking PI3K/Akt pathways: (*a*) conditioned media from control UMSCC38 cells, but not conditioned media from SCH66336-treated cells, induced phosphorylation of Akt in HUVECs; (*b*) depletion of IGFBP-3 in HUVECs by the IGFBP-3 neutralizing antibody effectively restored mitogenic activities and the levels of pAkt in HUVECs when incubated with conditioned media from SCH66336-treated UMSCC38 cells. Therefore, it is plausible to say that FTIs induce IGFBP-3 expression, which in turn regulate tumor angiogenesis by inhibiting Akt, a key enzyme for cell survival, and thus inducing apoptosis in endothelial cells.

In conclusion, our results reveal, for the first time, that the FTIs have potent antiangiogenic activities in HNSCC cells through the induction of IGFBP-3 expression. Our results could explain the antitumor activities of FTIs in the cancer cells that do not harbor activated Ras oncogene (40–43). IGFBP-3 has been also identified as having antitumor activities in a variety of cancers (16, 44, 45). Several case control studies have shown that serum IGFBP-3 levels inversely correlate with the risk of numerous cancers, including prostate (46), bladder (46), and colon (46). Smoking reduces IGFBP-3 levels (46) and low

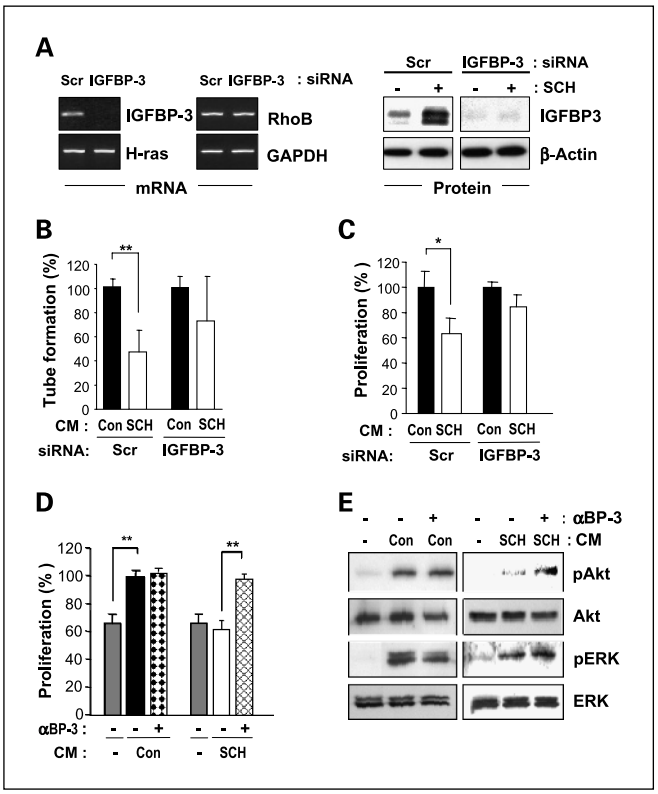

Fig. 5. IGFBP-3 secreted from SCH66336-treated HNSCC cells inhibits angiogenic activities in HUVECs by blocking Akt activation. *A-C,* effects of knock down of IGFBP-3 expression on antiangiogenic activities of SCH66336. *A,* semiquantitative reverse transcription-PCR analysis for *IGFBP-3*, *H-ras*, and *RhoB* mRNA expression (*left*) and Western blot analyses for IGFBP-3 protein expression (*right*) were done in UMSCC38 cells transfected with control (*scr*) or *IGFBP-3* siRNAs for 1 day before the SCH66336 (5 μmol/L) treatment. *GAPDH* mRNA and β-actin protein expression were also detected as controls for reverse transcription-PCR and Western blot analyses, respectively. Effects of conditioned media (*CM*) from these cells on HUVEC morphogenesis (*B*) and proliferation (*C*) were tested by tube formation and 3-(4,5-dimethylthiazol-2-yl)-2,5-diphenyltetrazolium bromide analyses, respectively. Independent experiments were repeated three times. Columns, percentages of eight samples; bars, SD/95% confidence intervals. *, $P < 0.05$; **, $P < 0.01$ compared with control. *D-E*, 3-(4,5-dimethylthiazol-2-yl)-2,5-diphenyltetrazolium bromide (*D*) and Western blot analyses (*E*) were performed in HUVECs, which were untreated or preincubated with IGFBP-3 neutralizing antibody (αBP-3) for 2 hours and then treated with EBM (−) or conditioned media from control UMSCC38 cells (*Con*) or from SCH66336-treated UMSCC38 cells (*SCH*). Independent experiments on cell proliferation were repeated three times. Columns, percentages of eight samples; bars, SD. αBP-3, antibody neutralizing IGFBP-3. **, $P < 0.01$ compared with HUVECs treated with control conditioned media.

DOI:10.1158/1078-0432.CCR-05-1725

IGFBP-3 concentrations are associated with increased risk of head and neck (46) as well as lung cancers (24). Furthermore, a decrease in IGFBP-3 expression due to the methylation or polymorphisms of the IGFBP-3 promoter is associated with an increased risk of lung, breast, and prostate cancers (46). Considering all of these promising results, IGFBP-3 should be critically evaluated in translational clinical trials against pathologic angiogenesis.

References

1. Horiot JC, Bontemps P, van den Bogaert W, et al. Accelerated fractionation (AF) compared to conventional fractionation (CF) improves loco-regional control in the radiotherapy of advanced head and neck cancers: results of the EORTC 22851 randomized trial. Radiother Oncol 1997;44:111–21.
2. Day GL, Blot WJ. Second primary tumors in patients with oral cancer. Cancer 1992;70:14–9.
3. Gupta AK, McKenna WG, Weber CN, et al. Local recurrence in head and neck cancer: relationship to radiation resistance and signal transduction. Clin Cancer Res 2002;8:885–92.
4. Fidler IJ. Critical factors in the biology of human cancer metastasis: twenty-eighth G.H.A. Clowes memorial award lecture. Cancer Res 1990;50:6130–8.
5. Folkman J. Angiogenesis in cancer, vascular, rheumatoid and other disease. Nat Med 1995;1:27–31.
6. Zetter BR. Angiogenesis and tumor metastasis. Annu Rev Med 1998;49:407–24.
7. Moschos SJ, Mantzoros CS. The role of the IGF system in cancer: from basic to clinical studies and clinical applications. Oncology 2002;63:317–32.
8. Leal SM, Liu Q, Huang SS, Huang JS. The type V transforming growth factor β receptor is the putative insulin-like growth factor-binding protein 3 receptor. J Biol Chem 1997;272:20572–6.
9. Valentinis B, Bhala A, DeAngelis T, Baserga R, Cohen P. The human insulin-like growth factor (IGF) binding protein-3 inhibits the growth of fibroblasts with a targeted disruption of the IGF-I receptor gene. Mol Endocrinol 1995;9:361–7.
10. Zadeh SM, Binoux M. The 16-kDa proteolytic fragment of insulin-like growth factor (IGF) binding protein-3 inhibits the mitogenic action of fibroblast growth factor on mouse fibroblasts with a targeted disruption of the type 1 IGF receptor gene. Endocrinology 1997;138:3069–72.
11. Hong J, Zhang G, Dong F, Rechler MM. Insulin-like growth factor (IGF)-binding protein-3 mutants that do not bind IGF-I or IGF-II stimulate apoptosis in human prostate cancer cells. J Biol Chem 2002;277:10489–97.
12. Franklin SL, Ferry RJ, Jr., Cohen P. Rapid insulin-like growth factor (IGF)-independent effects of IGF binding protein-3 on endothelial cell survival. J Clin Endocrinol Metab 2003;88:900–7.
13. Kohl NE, Mosser SD, deSolms SJ, et al. Selective inhibition of ras-dependent transformation by a farnesyltransferase inhibitor. Science 1993;260:1934–7.
14. Crespo NC, Ohkanda J, Yen TJ, Hamilton AD, Sebti SM. The farnesyltransferase inhibitor, FTI-2153, blocks bipolar spindle formation and chromosome alignment and causes prometaphase accumulation during mitosis of human lung cancer cells. J Biol Chem 2001;276:16161–7.
15. Chun KH, Lee HY, Hassan K, Khuri F, Hong WK, Lotan R. Implication of protein kinase B/Akt and Bcl-2/Bcl-XL suppression by the farnesyl transferase inhibitor SCH66336 in apoptosis induction in squamous carcinoma cells. Cancer Res 2003;63:4796–800.
16. Lee HY, Chun KH, Liu B, et al. Insulin-like growth factor binding protein-3 inhibits the growth of non-small cell lung cancer. Cancer Res 2002;62:3530–7.
17. Han JY, Oh SH, Morgillo F, et al. Hypoxia-inducible factor 1α and antiangiogenic activity of farnesyltransferase inhibitor SCH66336 in human aerodigestive tract cancer. J Natl Cancer Inst 2005;97:1272–86.
18. Myers JN, Holsinger FC, Jasser SA, Bekele BN, Fidler IJ. An orthotopic nude mouse model of oral tongue squamous cell carcinoma. Clin Cancer Res 2002;8:293–8.
19. Chun KH, Kosmeder JW, Il, Sun S, et al. Effects of deguelin on the phosphatidylinositol 3-kinase/Akt pathway and apoptosis in premalignant human bronchial epithelial cells. J Natl Cancer Inst 2003;95:291–302.
20. Min JK, Han KY, Kim EC, et al. Capsaicin inhibits *in vitro* and *in vivo* angiogenesis. Cancer Res 2004;64:644–51.
21. Reimer CL, Agata N, Tammam JG, et al. Antineoplastic effects of chemotherapeutic agents are potentiated by NM-3, an inhibitor of angiogenesis. Cancer Res 2002;62:789–95.
22. Chang YS, Wang L, Suh YA, et al. Mechanisms underlying lack of insulin-like growth factor-binding protein-3 expression in non-small-cell lung cancer. Oncogene 2004;23:6569–80.
23. Armstrong SA, Hannah VC, Goldstein JL, Brown MS. CAAX geranylgeranyl transferase transfers farnesyl as efficiently as geranylgeranyl to RhoB. J Biol Chem 1995;270:7864–8.
24. Liu A, Du W, Liu JP, Jessell TM, Prendergast GC. RhoB alteration is necessary for apoptotic and antineoplastic responses to farnesyltransferase inhibitors. Mol Cell Biol 2000;20:6105–13.
25. Du W, Lebowitz PF, Prendergast GC. Cell growth inhibition by farnesyltransferase inhibitors is mediated by gain of geranylgeranylated RhoB. Mol Cell Biol 1999;19:1831–40.
26. Lebowitz PF, Casey PJ, Prendergast GC, Thissen JA. Farnesyltransferase inhibitors alter the prenylation and growth-stimulating function of RhoB. J Biol Chem 1997;272:15591–4.
27. Poulaki V, Mitsiades CS, McMullan C, et al. Regulation of vascular endothelial growth factor expression by insulin-like growth factor I in thyroid carcinomas. J Clin Endocrinol Metab 2003;88:5392–8.
28. Long L, Navab R, Brodt P. Regulation of the M_r 72,000 type IV collagenase by the type I insulin-like growth factor receptor. Cancer Res 1998;58:3243–7.
29. Zhao WQ, Chen GH, Chen H, et al. Secretion of Annexin II via activation of insulin receptor and insulin-like growth factor receptor. J Biol Chem 2003;278:4205–15.
30. Devi GR, Yang DH, Rosenfeld RG, Oh Y. Differential effects of insulin-like growth factor (IGF)-binding protein-3 and its proteolytic fragments on ligand binding, cell surface association, and IGF-I receptor signaling. Endocrinology 2000;141:4171–9.
31. Clemmons DR, Dehoff ML, Busby WH, Bayne ML, Cascieri MA. Competition for binding to insulin-like growth factor (IGF) binding protein-2, 3, 4, and 5 by the IGFs and IGF analogs. Endocrinology 1992;131:890–5.
32. Walker GE, Wilson EM, Powell D, Oh Y. Butyrate, a histone deacetylase inhibitor, activates the human IGF binding protein-3 promoter in breast cancer cells: molecular mechanism involves an Sp1/Sp3 multiprotein complex. Endocrinology 2001;142:3817–27.
33. Carmeliet P, Dor Y, Herbert JM, et al. Role of HIF-1α in hypoxia-mediated apoptosis, cell proliferation and tumour angiogenesis. Nature 1998;394:485–90.
34. Liu M, Bryant MS, Chen J, et al. Antitumor activity of SCH 66336, an orally bioavailable tricyclic inhibitor of farnesyl protein transferase, in human tumor xenograft models and wap-ras transgenic mice. Cancer Res 1998;58:4947–56.
35. Loprevite M, Favoni RE, De Cupis A, et al. *In vitro* study of farnesyltransferase inhibitor SCH 66336, in combination with chemotherapy and radiation, in non-small cell lung cancer cell lines. Oncol Rep 2004;11:407–14.
36. Shi B, Yaremko B, Hajian G, et al. The farnesyl protein transferase inhibitor SCH66336 synergizes with taxanes *in vitro* and enhances their antitumor activity *in vivo*. Cancer Chemother Pharmacol 2000;46:387–93.
37. Feldkamp MM, Lau N, Roncari L, Guha A. Isotype-specific Ras.GTP-levels predict the efficacy of farnesyl transferase inhibitors against human astrocytomas regardless of Ras mutational status. Cancer Res 2001;61:4425–31.
38. Hoover RR, Mahon FX, Melo JV, Daley GQ. Overcoming STI571 resistance with the farnesyl transferase inhibitor SCH66336. Blood 2002;100:1068–71.
39. Baxter RC. Signalling pathways involved in antiproliferative effects of IGFBP-3: a review. Mol Pathol 2001;54:145–8.
40. Ashar HR, James L, Gray K, et al. The farnesyl transferase inhibitor SCH 66336 induces a G(2) → M or G(1) pause in sensitive human tumor cell lines. Exp Cell Res 2001;262:17–27.
41. End DW, Smets G, Todd AV, et al. Characterization of the antitumor effects of the selective farnesyl protein transferase inhibitor R115777 *in vivo* and *in vitro*. Cancer Res 2001;61:131–7.
42. Karp JE, Kaufmann SH, Adjei AA, Lancet JE, Wright JJ, End DW. Current status of clinical trials of farnesyltransferase inhibitors. Curr Opin Oncol 2001;13:470–6.
43. Karp JE, Lancet JE, Kaufmann SH, et al. Clinical and biologic activity of the farnesyltransferase inhibitor R115777 in adults with refractory and relapsed acute leukemias: a phase 1 clinical-laboratory correlative trial. Blood 2001;97:3361–9.
44. Prieur A, Tirode F, Cohen P, Delattre O. EWS/FLI-1 silencing and gene profiling of Ewing cells reveal downstream oncogenic pathways and a crucial role for repression of insulin-like growth factor binding protein 3. Mol Cell Biol 2004;24:7275–83.
45. Ali O, Cohen P, Lee KW. Epidemiology and biology of insulin-like growth factor binding protein-3 (IGFBP-3) as an anti-cancer molecule. Horm Metab Res 2003;35:726–33.
46. Wu X, Zhao H, Do KA, et al. Serum levels of insulin growth factor (IGF-I) and IGF-binding protein predict risk of second primary tumors in patients with head and neck cancer. Clin Cancer Res 2004;10:3988–95.

Erlotinib Combined with Cyclosporine in a Liver-Transplant Recipient with Epidermal Growth Factor Receptor-Mutated Non-small Cell Lung Cancer

To the Editor:

Management of cancer in transplant recipients is highly complicated by concomitant clinical situations which often require conflicting therapeutic approaches.

Distinctive from general population, non-small cell lung cancer which occurs in transplant recipients is often associated with nonsmoker status and adenocarcinoma histology[1] which are well established predictive factors for response to Epidermal Growth Factor Receptor (EGFR) –Tyrosine Kinase inhibitor drugs. Moreover, these drugs represent an attractive treatment for this set of patients thanks to their very low toxicity profile and to the fact that they do not induce immunosuppression and should not increase the risk of graft rejection.

Unfortunately, to our knowledge, no data on the interaction between immunosuppressive treatment and EGFR-tyrosine kinase inhibitors nor clinical reports on the safety of this combination are available. Moreover, considering that 70% of the metabolism of erlotinib is sustained by cytochrome P450 3A4 and CYP1A, its use in combination with cyclosporine (a known CYP 3A4 substrate), could induce unexpected and increased side effects.[2,3]

Here we describe a case of a liver-transplant recipient with advanced non-small cell lung cancer who received prolonged concomitant and uneventful administration of erlotinib and cyclosporine obtaining a long-lasting tumor response.

A 53-year-old nonsmoker male had received a liver transplantation for Hepatitis B virus- and Hepatitis D virus-related cirrhosis in February 2002, followed by continuous immunosuppressive treatment with cyclosporine.

On July 2007 he was diagnosed with an EGFR positive pulmonary adenocarcinoma with brain, bone, and pleural metastases. Molecular analysis of the tumor indicated an EGFR mutation (deletion of exon 19: leucine 747–752 serine) and the absence of k-Ras mutations (exons: 12, 13, 61).

First-line chemotherapy with carboplatin and paclitaxel was interrupted after the first administration because of severe toxicity, including grade 3 (G3) diarrhea and G3 neutropenia, concomitantly with a high variability of cyclosporinemia.

After whole-brain irradiation, the patient was given erlotinib (150 mg daily). Cyclosporine dosage was tailored to maintain a blood level of the drug between 60 and 90 ng/ml.

At the time of this report, the patient has been receiving erlotinib and cyclosporine for 1 year, with a maintained Response Evaluation Criteria in Solid Tumors partial response on all the disease parameters.

Treatment was very well tolerated, with only G1 skin toxicity and a persistent nonfebrile G1 neutropenia, appearing 11 weeks after the onset of treatment. No erlotinib-dose reduction or discontinuation was required. To maintain the cyclosporine blood levels in the established range, the dosage of administered drug was progressively increased from 50 mg bid to 75 mg bid (Figure 1), then to 100 mg bid (data not shown in the Figure).

Plasma levels of gamma-glutamyltransferase, monitored every 2 to 3 weeks to assess the efficacy of immunosuppression, were always within the normal range.

These data together indicate the absence of any clinically relevant interference between cyclosporine and erlotinib. However, the need of increasing the drug dosage over time could suggest that long-term exposure of erlotinib might induce CYP 3A4 and suggest the usefulness of monitoring cyclosporine blood levels.

To our knowledge, this is the first report of concomitant administration of erlotinib and cyclosporine. The absence of relevant toxicity, despite a full dose of erlotinib over a 1-year period and the lack of any sign of graft loss, indicate that cyclosporine use should not be considered a contraindication to erlotinib administration.

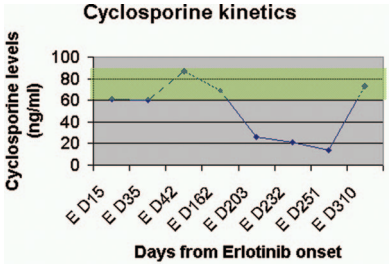

FIGURE 1. Cyclosporine kinetics during erlotinib treatment (E = erlotinib). The range outlined in green is the optimal range we aimed to maintain. The patient received 50 mg bid cyclosporine for the first 27 weeks of treatment with erlotinib, then 75 mg twice daily.

Tommaso De Pas, MD

Gianluca Spitaleri, MD
Department of Medicine, New Drugs Development and Clinical Pharmacology Unit, European Institute of Oncology, Milan, Italy

Giuseppe Pelosi, MD
Department of Pathology, European Institute of Oncology, Milan, Italy

Luciano De Carlis, MD
Niguarda Hospital, Milan, Italy

Katia Lorizzo, MD

Marzia Locatelli, MD

Giuseppe Curigliano, MD, PhD

Francesca Toffalorio, MD, PhD

Chiara Catania, MD

Filippo de Braud, MD
Department of Medicine, New Drugs Development and Clinical Pharmacology Unit, European Institute of Oncology, Milan, Italy

REFERENCES

1. Ajithkumar T, Parkinson C, Butler A, Hatchet H. Management of solid tumours in organ-transplant recipients. *Lancet Oncol* 2007; 8:921–932.
2. Li J, Zhao M, He P, et al. Differential metabolism of gefitinib and erlotinib by human cytochrome P450 enzymes. *Clin Cancer Res* 2007;13:3731–3737.
3. Zhou SF, Zhou ZW, Li CG, et al. Identification of drugs that interact with herbs in

Disclosure: The authors declare no conflicts of interest.

ISSN: 1556-0864/09/0401-0138

drug development. *Drug Discovery Today* 2007;12:664–673.

Germ-Line and Somatic Presentations of the *EGFR* T790M Mutation in Lung Cancer

To the Editor:

Somatic mutations in the kinase domain of the epidermal growth factor receptor (*EGFR*) gene are found in about 10% of lung adenocarcinomas that have been sequenced from Western countries and in about 30% of those that have been sequenced from Asia.[1] *EGFR* mutations are associated with sensitivity to the EGFR tyrosine kinase inhibitors gefitinib and erlotinib. However, many patients who initially respond to treatment with gefitinib or erlotinib develop resistance to these inhibitors and subsequently relapse. This process has been associated with point mutations in the kinase domain of mutant *EGFR*.[2,3] The most common *EGFR* mutation associated with treatment resistance involves a C-to-T change at nucleotide 2369 in exon 20, which results in threonine-to-methionine substitution at the amino acid position 790 (T790M). This amino acid change does not seem to diminish EGFR's catalytic activity, but the presence of the T790M mutation is predicted to impair binding of either gefitinib or erlotinib to the EGFR adenosine triphosphate-binding pocket.[2,3] In addition, emerging data suggest that the T790M change may potentiate oncogenic activity. For example, a T790M germ-line mutation was found in one family with a high incidence of lung cancer,[4] and somatic T790M mutations have been occasionally detected in tumors from patients who never received EGFR inhibitors.[5] In fact, it may be likely that all T790M mutations are present in a small subset of tumor cells before treatment and they expand selectively with EGFR tyrosine kinase inhibitors treatment. Using deoxyribonucleic acid (DNA) extracted from formalin-fixed and paraffin-embedded tissues from 240 patients with lung adenocarcinomas that had never received treatment with EGFR inhibitors, we sequenced the *EGFR* exons 18 to 21 and identified 2 tumor cases (1%) harboring the T790M mutation. Here, we report those two cases with an unusual presentation of the T790M mutation, including a germ-line and a somatic mutation (Figure 1).

The first case of T790M-associated lung cancer occurred in a 72-year-old female never smoker presented with 3 synchronous lung tumors, 2 adenocarcinomas, and 1 large-cell neuroendocrine carcinoma with hilar lymph node metastasis (Figures 1*A–C*). In addition to the malignant tissue from the three tumors, microdissected cells from normal bronchiolar epithelium, pleural connective tissue, and nonmetastatic lymph nodes showed the presence of both the *EGFR* T790M and wild-type alleles. No other *EGFR* mutations were detected in the patient's tissue specimens. We confirmed the presence of a germ-line mutation by sequencing the DNA extracted from the patient's peripheral mononuclear blood cells. Although we were unable to examine DNA from other family members, this patient represents, to our knowledge, the second case[4] of a T790M germ-line mutation ever reported and confirms the possibility that this phenomenon confers lung cancer susceptibility.

The second case of T790M-associated lung cancer occurred in a 62-year-old female never smoker diagnosed with stage IA adenocarcinoma; no other *EGFR* activating mutation was seen (Figures 1*D–F*). The T790M mutation was not detected in the DNA extracted from multiple microdissected tissue samples, including nonmalignant pleural connective tissue, lung hilar lymph nodes, and breast connective tissue obtained during a previous breast cancer resection showing that mutation was somatic. However, *EGFR* mutation analysis of microdissected epithelium obtained from bronchiolar structures adjacent to the tumor showed the T790M mutation in three out of five histologically normal epithelium sites. We previously demonstrated that *EGFR* kinase domain mutations in exons 19 and 21 are sometimes detected in normal bronchial and bronchiolar epithelium adjacent to *EGFR* mutant lung tumors, indicating that the development of such mutations may be an early event in the pathogenesis of lung adenocarcinoma as a filed cancerization phenomenon.[6] The presence of the T790M mutation in the normal bronchial epithelium in this patient confirms this mutation's potential oncogenic effect, and its role in preneoplastic lesions, which is supported by the report that in vitro human bronchial epithelial cells overexpressing the T790M mutation showed a growth advantage over cells expressing the wild-type form.[7]

Although the *EGFR* T790M mutation has been identified in the context of EGFR resistance to tyrosine kinase inhibitors, it is usually found in conjunction with a classific EGFR TK domain activating mutation. In the two cases described in this report, only the T790M mutation was found. The presence of the mutation alone and also its presence in prenoplastic lesions, indicate that the T790M mutation can occasionally be found in patients whose lung tumors exhibit primary drug resistance and that this mutation may have an oncogenic effect in lung respiratory epithelial cells.

ACKNOWLEDGMENTS

This work was supported, in part, by a grant from the Specialized Program of Research Excellence (SPORE) in Lung Cancer (grant P50 CA70907), National Cancer Institute, Bethesda, MD, and Department of Defense (grant W81XWH-04-1-0142). The authors thank Dr. Margaret Spitz for contributing the DNA specimen extracted from blood.

Ludmila Prudkin, MD
Ximing Tang, MD
Ignacio I. Wistuba, MD
Department of Pathology
The University of Texas M. D. Anderson Cancer Center
Houston, Texas
iiwistuba@mdanderson.org

REFERENCES

1. Shigematsu H, Lin L, Takahashi T, et al. Clinical and biological features associated with epidermal growth factor receptor gene mutations in lung cancers. *J Natl Cancer Inst* 2005;97:339–346.
2. Pao W, Miller VA, Politi KA, et al. Acquired Resistance of Lung Adenocarcinomas to Gefitinib or Erlotinib Is Associated with a Sec-

Disclosure: The authors declare no conflict of interest.

ISSN: 1556-0864/09/0401-0139

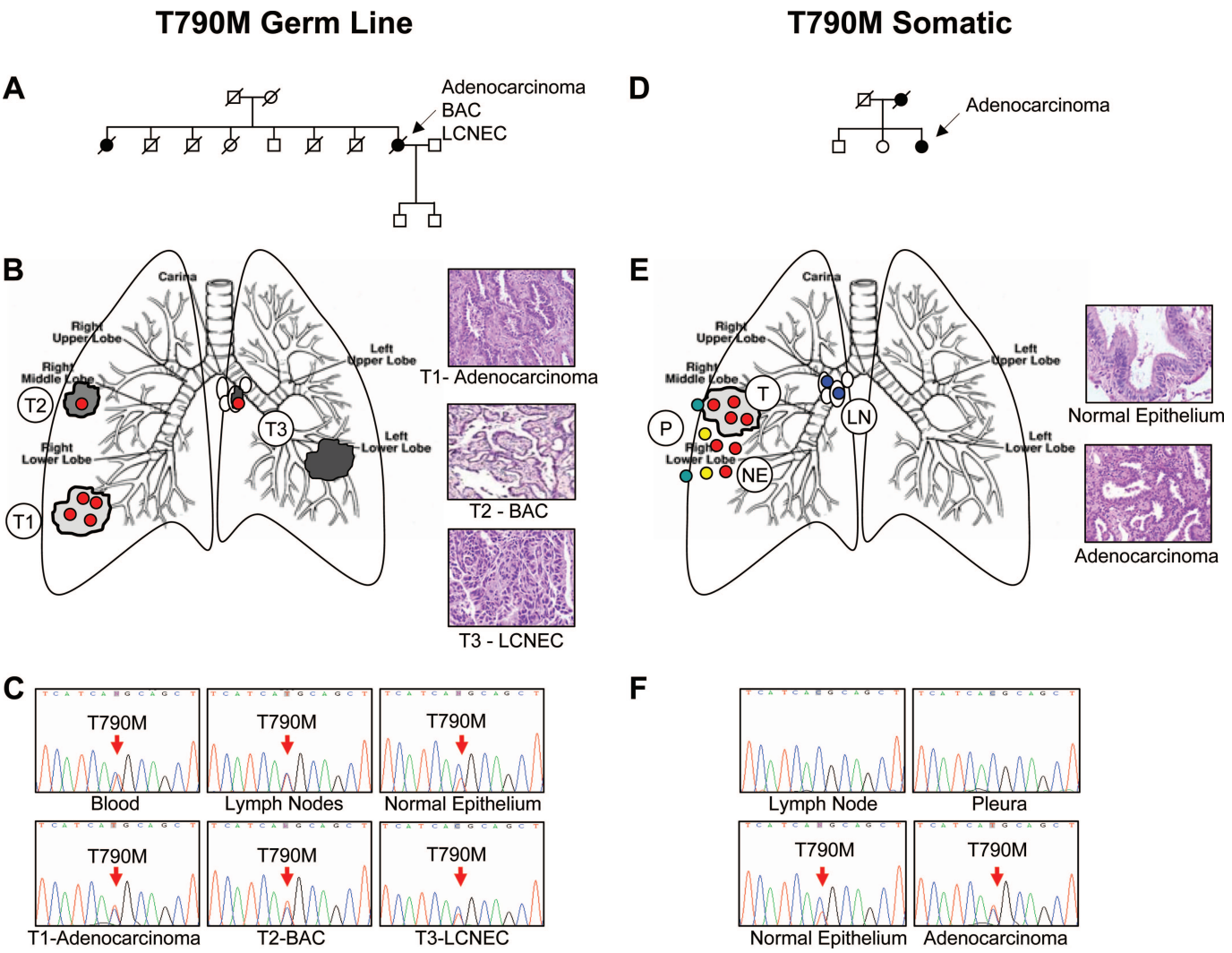

FIGURE 1. Epidermal growth factor receptor (*EGFR*) T790M Mutation in Two Patients with Lung Cancer. Panel *A*, shows the pedigree of the patient with the germ-line *EGFR* T790M mutation (the patient is indicated by the arrow, and lung cancer is indicated by solid symbols). Panel *B*, shows a diagram of the patient's lungs illustrating the three synchronous lung tumors and representative microphotographs from histologic analysis (hematoxylin and eosin, magnification ×400). Tumor 1 (T1) was an invasive adenocarcinoma located in the right lower lobe, tumor 2 (T2) was a pure (noninvasive) bronchioloalveolar carcinoma (BAC) located in the right middle lobe, and tumor 3 (T3) was a large-cell neuroendocrine carcinoma (LCNEC) located in the left lower lobe with hilar lymph node metastasis. Deoxyribonucleic acid (DNA) was extracted from about 1000 microdissected cells from four sites in T1 and 1 site each from the T2 and T3 lymph node metastases (red circles) and then examined for *EGFR* mutations in exons 18 to 21. In addition, microdissected connective pleural tissue (two sites), nonmetastatic lymph node (two sites), and normal bronchial epithelium adjacent to T1 and T2 (7 sites) were also examined (sites not indicated). All the specimens, nonmalignant and malignant, demonstrated the T790M mutation. Panel *C*, shows examples of nucleotide sequence tracings illustrating heterozygosity with respect to the T790M mutation in DNA extracted from the peripheral mononuclear blood cells and the tissue sites examined. Panel *D*, shows the pedigree of the patient with the somatic *EGFR* T790M mutation (the patient is indicated by the arrow, and lung cancer is indicated by the solid symbols). Panel *E*, shows a diagram of the patient's lungs illustrating the tumor and representative microphotographs from histologic analysis of the normal epithelium and tumor (hematoxylin and eosin, magnification ×400). In this case, the T790M mutation was detected in four of the four tumor sites (T, red circles) and three of the five normal bronchial epithelium sites (NE, mutant: red circles, wild-type: yellow circles). Microdissected tissue from two pleural (P, green circles) and lymph node (LN, blue circles) sites without tumor involvement had the wild-type allele. Panel *F*, shows examples of nucleotide sequence tracings illustrating heterozygosity with respect to the T790M variant in normal bronchiolar epithelium and tumor specimen sites. The lymph node sites and pleural tissues had the wild-type allele.

ond Mutation in the EGFR Kinase Domain. *PLoS Med* 2005;2:1–11.
3. Kobayashi S, Boggon TJ, Dayaram T, et al. EGFR mutation and resistance of non-small-cell lung cancer to gefitinib. *N Engl J Med* 2005;352:786–792.
4. Bell DW, Gore I, Okimoto RA, et al. Inherited susceptibility to lung cancer may be associated with the T790M drug resistance

mutation in EGFR. *Nat Genet* 2005;37: 1315–1316.
5. Inukai M, Toyooka S, Ito S, et al. Presence of epidermal growth factor receptor gene T790M mutation as a minor clone in non-small cell lung cancer. *Cancer Res* 2006;66:7854–7858.
6. Tang X, Shigematsu H, Bekele BN, et al. EGFR tyrosine kinase domain mutations are detected in histologically normal respiratory epithelium in lung cancer patients. *Cancer Res* 2005;65:7568–7572.
7. Vikis H, Sato M, James M, et al. EGFR-T790M is a rare lung cancer susceptibility allele with enhanced kinase activity. *Cancer Res* 2007;67:4665–4670.

Complete Response of Recurrent Squamous Cell Carcinoma of the Lung: Dose the Dose Matter?

To the Editor:

Bevacizumab is a humanized monoclonal antibody against vascular endothelial growth factor and has shown significant clinical benefit in patients with various cancers.[1] A randomized phase II study comparing carboplatin plus paclitaxel with or without bevacizumab in non-small cell lung cancer patients demonstrated that the addition of bevacizumab results in an increase in time to disease progression.[2] However, because of an increased risk of pulmonary hemorrhage with bevacizumab treatment, a subsequent large phase III study excluded patients with squamous cell histology.[3] In this report, we present an elderly patient with recurrent squamous cell carcinoma of the lung who achieved complete response after treatment with bevacizumab plus carboplatin and paclitaxel without developing any hemorrhagic complications.

A 79-year-old man visited our hospital in July of 2007 with cough and sputum for a month. The patient underwent a left upper lobe lobectomy in May of 2005. Pathology revealed poorly differentiated squamous cell carcinoma, and was staged as T2N1M0. After surgery, four cycles of vinorelbine plus cisplatin adjuvant chemotherapy were administered.

Upon admission, his Eastern Cooperative Oncology Group (ECOG) performance status was 2. Chest computed tomography (CT) scan revealed recurrence of the disease in the left main bronchus involving the carina, and a large intraluminal-protruding mass formation with internal necrosis (Figure 1). Biopsy revealed a squamous cell carcinoma, pathologically confirming disease recurrence. Chemotherapy with bevacizumab 7.5 mg/kg combined with carboplatin, area under the curve 4, and paclitaxel 175 mg/m^2 was given once every 3 weeks for 4 cycles. CT scan after the second cycle showed complete response (Figure 2) without any evidence of pulmonary hemorrhage. The CT scan after the fourth cycle showed that complete remission was maintained. After completing the regimen, the patient has been receiving bevacizumab alone for an additional eight cycles without evidence of recurrence.

The efficacy of bevacizumab in angiogenesis inhibition in non-small cell lung cancer has already been documented,[3,4] but comes at a significant price; it is often associated with adverse side effects, including pulmonary hemorrhage, which may be a life-threatening condition. A randomized phase II study conducted by Johnson et al.[2] warned of the risk of bleeding in tumors of the squamous cell histology, tumors located close to major vessels, and tumors with necrosis or cativation. Thus, a phase III trial (ECOG 4599) of bevacizumab excluded patients with squamous cell histology, brain metastasis, or anticoagulation medications.[3]

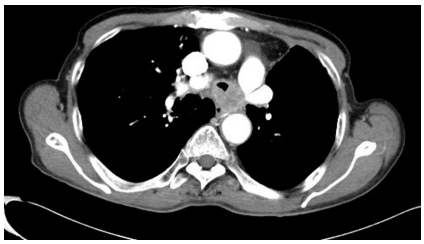

FIGURE 1. Computed tomography (CT) scan at the time of recurrence. Necrotic mass involved the posterior wall of the proximal left main bronchus. Biopsy was positive for recurrent squamous cell carcinoma.

FIGURE 2. Computed tomography (CT) scan after the second cycle of bevacizumab, carboplatin, and paclitaxel chemotherapy. There was complete resolution of the necrotic mass involving the left main stem bronchus.

This is the first case report of an elderly patient with squamous cell histology who showed complete response after being treated by bevacizumab combined with carboplatin and paclitaxel. This finding is significant in that the patient had a higher risk for pulmonary hemorrhage because he was elderly, had poor performance status, and had squamous cell histology, which was centrally located and showed necrosis. A recent subset analysis of the ECOG 4599 trial revealed no survival benefits of bevacizumab plus caboplatin and paclitaxel for elderly patients (>70 years). This finding can be explained by the higher toxicity when adding bevacizumab to chemotherapy compared with chemotherapy alone.[5]

In our case, we used a lower dose of bevacizumab (7.5 mg/kg), and an attenuated dose of carboplatin (area under the curve 4) and paclitaxel (175 mg/m^2) compared with the ECOG 4599 trial.[3] It seems that an attenuated dose of chemotherapy and a lower dose of bevacizumab can reduce the complications and the toxicity. Further clinical studies will be warranted to determine whether bevacizumab is indeed a safe regimen in the management of squamous cell carcinoma of the lung and whether an attenuated dose plays an important role in elderly patients.

Sanghoon Shin, MD
Kwang Joon Kim, MD
Department of Internal Medicine, Yonsei University College of Medicine
Seoul, Korea
Young Joo Lee
Hye Jin Choi
Yonsei Cancer Center
Seoul, Korea

Disclosure: The authors declare no conflicts of interest.

ISSN: 1556-0864/09/0401-0141

Hyunki Kim
Department of Pathology
Yonsei University College of Medicine
Seoul, Korea

Joo Hang Kim

Byoung Chul Cho, MD
Yonsei Cancer Center
Seoul, Korea

REFERENCES

1. Miller KD, Chap LI, Holmes FA, et al. Randomized phase III trial of capecitabine compared with bevacizumab plus capecitabine in patients with previously treated metastatic breast cancer. *J Clin Oncol* 2005;23: 792–799.
2. Johnson DH, Fehrenbacher L, Novotny WF, et al. Randomized phase II trial comparing bevacizumab plus carboplatin and paclitaxel with carboplatin and paclitaxel alone in previously untreated locally advanced or metastatic non-small-cell lung cancer. *J Clin Oncol* 2004;22:2184–2191.
3. Sandler A, Gray R, Perry MC, et al. Paclitaxel-carboplatin alone or with bevacizumab for non-small-cell lung cancer. *N Engl J Med* 2006;355:2542–2550.
4. Cohen MH, Gootenberg J, Keegan P, et al. FDA drug approval summary: bevacizumab (Avastin) plus Carboplatin and Paclitaxel as first-line treatment of advanced/metastatic recurrent nonsquamous non-small cell lung cancer. *Oncologist* 2007;12:713–718.
5. Ramalingam SS, Dahlberg SE, Langer CJ, et al. Outcomes for elderly, advanced-stage non small-cell lung cancer patients treated with bevacizumab in combination with carboplatin and paclitaxel: analysis of eastern cooperative oncology group trial 4599. *J Clin Oncol* 2008;26:60–65.

Wood-Smoke Exposure (WSE) as a Predictor of Response and Survival in Erlotinib-Treated Non-small Cell Lung Cancer (NSCLC) Patients

To the Editor:

Coal and biomass serves as a major fuel source for >50% of the world's population.[1] In Colombia the prevalence of wood-smoke exposure (WSE) in areas having less economic development is around 24%. The amount of pollution due to wood-smoke (WS) is elevated; moreover, it has been calculated that cooking with wood for 3 h/d, exposes people to similar amounts of benzo-pyrene as smoking 3 packs of cigarettes/d.[1,2] This confirms, at least in part, that carcinogens present in WS are similar to those associated with tobacco. There is biologic plausibility for the association of WSE and non-small cell lung cancer because of a similar effect on p53, phospho-p53, and MDM2 protein expression as occurs in tobacco smokers.[3] Another's, have shown an abnormal GSTP-1 genotype, matrix metalloproteinase expression, and DNA adduct formation.[4]

In a previous issue of the JTO, Arrieta et al.[5] described the results of 42 non-small cell lung cancer patients who were being treated with erlotinib and had been exposed to WS for approximately 40 years; 14% of these subgroup patients had been smokers, overall response rate was 34% and clinical benefit was 67%. Histologic subtype and WSE were the variables positively influencing erlotinib response. The study also showed that the independent factor which most affected progression-free survival (PFS) and overall survival was WSE, and a mean of 17.6 and 19.2 months has being found for each of these outcomes, respectively. Nevertheless, response rate to erlotinib among smokers was strikingly high (19%), 16% of the subjects included had stage IIIB disease and PFS rate for patients with WSE curiously proved to be greater than in patients having epidermal growth factor receptor mutations. Mean follow-up time was short (4.5 months) and possible confusion variables (mutational profile, smoking history, comorbidity) were not suitably debugged.

These findings go against the scientific aphorisms used for predicting epidermal growth factor receptor-tyrosine kinase inhibitors response in patients suffering from lung adenocarcinoma, thereby supporting a theory regarding an alternative route for tumors being produced by WSE. The main outcomes in a series of 156 patients suffering from lung adenocarcinoma treated in Bogotá (Colombia) were analyzed in an attempt to ascertain the clinical findings and the biologic hypothesis advanced by Arrieta's group. Average age was 64 years, 53% were female, 39% had never been smokers, 24% had been considerably exposed to WS, and 23% of patients had received erlotinib during some stage of the disease. Nine of these subjects had been exposed to WS and 27 had not been. Seven patients having WSE had been smoking for an average of 14 years.

Overall response rate to erlotinib among patients with and without WSE was 5% and 47% ($p = 0.0023$), respectively. PFS was also significantly higher among patients who had no history of WSE and who had received erlotinib as first-line ($p = 0.037$) and second-line intervention ($p = 0.044$). Among patients having WSE history, overall survival was 6.6 months (5.8–7.3) for those treated with erlotinib and 15.4 months (10.7–20.1) for those not treated with this compound ($p = 0.0022$) (Figure 1). Such difference could be attributed to greater compromise of performance status in the group with WSE (61% Eastern Cooperative Oncology Group ≥2) due to the marked deterioration of pulmonary function.

In line with Arrieta's proposal, a multivariate analysis was carried out for determining the factors influencing mortality among patients with WSE. Only performance status ($p = 0.053$) and gender ($p = 0.044$) were seen to be significant. Our data did not support the findings described by Arrieta et al., highlighting the need for more consistent studies in this field to be carried out further.

Andrés Felipe Cardona, MD, MSc
Department of Medical Oncology
Catalan Institute of Oncology, Hospital Germans Trias i Pujol, Badalona
Barcelona, Spain
Latin American Clinical Trials Register (LATINREC), Cochrane Colombian Group
Bogotá, Colombia
On behalf of the ONCOLGroup (Colombian Group for the Clinical and Molecular Investigation of Cancer) and the Medical Oncology Department of the Hospital San Ignacio, Pontificia Universidad Javeriana, Bogotá, Colombia

Disclosure: The authors declare no conflicts of interest.

ISSN: 1556-0864/09/0401-0142

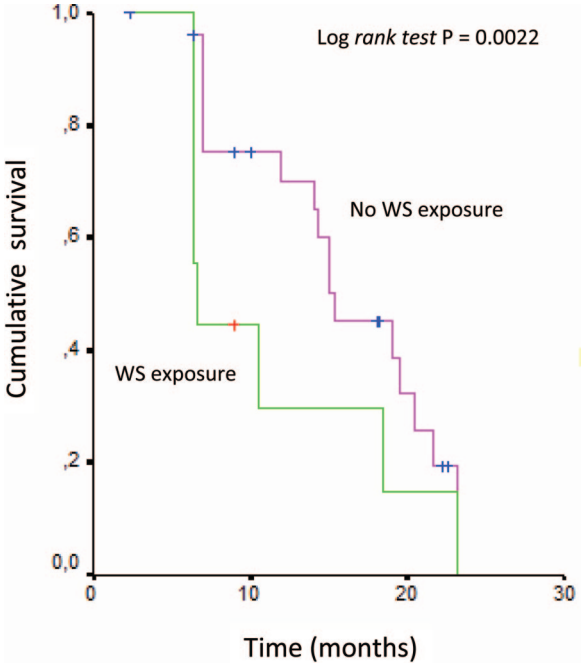

FIGURE 1. Overall survival in patients treated with erlotinib.

Noemí Reguart, MD, PhD
Department of Medical Oncology
Clinic Hospital
Barcelona, Spain

Ludovic Reveiz, MD, MSc
Department of Clinical Epidemiology
Latin American Clinical Trials Register (LATINREC)
Cochrane Colombian Group
Bogotá, Colombia

REFERENCES

1. Bruce N, Perez-Padilla R, Albalak R. Indoor air pollution in developing countries: a major environmental and public health challenge. *Bull World Health Organ* 2000;78:1078–1092.
2. Barcenas CH, Delclos GL, El-Zein R, Tortolero-Luna G, Whitehead LW, Spitz MR. Wood dust exposure and the association with lung cancer risk. *Am J Ind Med* 2005;47:349–357.
3. Delgado J, Martinez LM, Sánchez TT, Ramirez A, Iturria C, González-Avila G. Lung cancer pathogenesis associated with wood smoke exposure. *Chest* 2005;128:124–131.
4. Hosgood HD III, Berndt SI, Lan Q. GST genotypes and lung cancer susceptibility in Asian populations with indoor air pollution exposures: a meta-analysis. *Mutat Res* 2007; 636:134–143.
5. Arrieta O, Martinez-Barrera L, Treviño S, et al. Wood-smoke exposure as a response and survival predictor in erlotinib-treated non-small cell lung cancer patients: an open label phase II study. *J Thorac Oncol* 2008; 3:887–893.

Current Approach to Treatment of Non-small Cell Lung Cancer in Developing Countries—Time for a Rethink?

To the Editor:

Results of several recently published randomized trials (RTs), suggest that non-small cell lung cancer (NSCLC) with different histologic patterns may respond differently to various treatment modalities and thus may represent different disease entities. In a phase III RT comparing pemetrexed-cisplatin versus gemcitabine-cisplatin for previously untreated advanced NSCLC, it was observed that among patients with adenocarcinoma, overall survival was statistically superior for pemetrexed compared with gemcitabine (12.6 versus 10.9 months; hazards ratio [HR] = 0.84; 95% CI = 0.71–0.99; $p = 0.031$) while the reverse was seen with squamous histology (9.4 versus 10.8 months; HR = 1.23; 95% CI = 1.00–1.51; $p = 0.05$).[1] Nonsquamous histology (as a group) had results similar to adenocarcinoma.[1] Differences in progression free survival based on histology have also been observed in other RTs using third-generation platinum-based doublets for chemo-naive patients with advanced NSCLC.[2,3] Even in the second line setting, pemetrexed has been demonstrated to result in superior median overall survival and progression free survival for patients with adenocarcinoma.[4] However, for squamous or large-cell histology, the drug fared no better than placebo.[4] An individual patient data meta-analysis involving 2968 patients from 9 RTs compared the efficacy of cisplatin versus carboplatin when used in first line chemotherapy for advanced NSCLC.[5] Here also, carboplatin was associated with increased mortality for nonsquamous histology (HR = 1.12; 95% CI = 1.01–1.23).[5]

In addition, there is evidence to suggest that vascular endothelial growth factor receptor antagonists and tyrosine kinase inhibitors seem to exert beneficial effects predominantly in patients with adenocarcinoma and nonsquamous histologic types. Bevacizumab has in fact been shown to be detrimental in squamous histology. Squamous histology remains a favorable prognostic factor for patients undergoing lung resectional surgery in both prospective and retrospective studies. The converse has, however, been observed in unresectable disease. Thus, besides being an important predictive factor for different therapeutic modalities, histologic type remains an important prognostic factor as well.

With the growing body of evidence to suggest that NSCLC is a heterogeneous disease, an important question that arises is that are we still justified in clubbing all the different histologic types as one disease entity? Identification of genomic, proteomic and/or pharmacogenomic differences between different histologic patterns could be helpful in practicing 'personalized medicine.' However, carrying out such kind of analyses for each patient is usually not possible in health

Disclosure: The authors declare no conflict of interest.

ISSN: 1556-0864/09/0401-0143

care resource and economically constrained countries.

The next question is whether, in the absence of any or all of these, can NSCLC be reclassified or sub classified so that therapeutic decision making does not get unnecessarily complicated? One can debate whether it would be more appropriate to classify lung cancer into three main groups namely small-cell, adenocarcinoma, and non-adenocarcinoma (or alternatively, into small-cell, squamous, and nonsquamous). A second option could even be to keep NSCLC as a broad group intact but divide it further into adenocarcinoma, squamous, and nonadeno-nonsquamous subtypes for the purpose of management decision making.

It is not easy to resolve this issue and conduct of RTs in the future on patients with a particular histology is therefore required. The ultimate aim of classification is that each patient can be offered treatment that is likely to produce the most clinical benefit with the least possible toxicity profile even if genomic, proteomic or pharmacogenomic analyses are not available.

Navneet Singh, MD, DM, FCCP

Ashutosh N. Aggarwal, MD, DM, FCCP

Department of Pulmonary Medicine
Postgraduate Institute of Medical Education and Research (PGIMER)
Chandigarh, India
navneetchd@yahoo.com

REFERENCES

1. Scagliotti GV, Parikh P, von Pawel J, et al. Phase III study comparing cisplatin plus gemcitabine with cisplatin plus pemetrexed in chemotherapy-naive patients with advanced-stage non-small-cell lung cancer. *J Clin Oncol* 2008;26:3543–3551.
2. Park JO, Kim SW, Ahn JS, et al. Phase III trial of two versus four additional cycles in patients who are nonprogressive after two cycles of platinum-based chemotherapy in non small-cell lung cancer. *J Clin Oncol* 2007;25:5233–5239.
3. Lilenbaum R, Axelrod R, Thomas S, et al. Randomized phase II trial of erlotinib or standard chemotherapy in patients with advanced non-small-cell lung cancer and a performance status of 2. *J Clin Oncol* 2008;26:863–869.
4. Ciuleanu TE, Brodowicz T, Belani CP, et al. Maintenance pemetrexed plus best supportive care (BSC) versus placebo plus BSC: a phase III study. *J Clin Oncol* 2008;26:abstract 8011.
5. Ardizzoni A, Boni L, Tiseo M, et al. Cisplatin-versus carboplatin-based chemotherapy in first-line treatment of advanced non-small-cell lung cancer: an individual patient data meta-analysis. *J Natl Cancer Inst* 2007;99:847–857.

DOI:10.1158/0008-5472.CAN-06-4044

Cancer Research

The Farnesyltransferase Inhibitor R115777 Up-regulates the Expression of Death Receptor 5 and Enhances TRAIL-Induced Apoptosis in Human Lung Cancer Cells

Yuanzheng Qiu, Xiangguo Liu, Wei Zou, et al.

Cancer Res 2007;67:4973-4980. Published online May 17, 2007.

DOI:10.1158/0008-5472.CAN-06-4044

Research Article

The Farnesyltransferase Inhibitor R115777 Up-regulates the Expression of Death Receptor 5 and Enhances TRAIL-Induced Apoptosis in Human Lung Cancer Cells

Yuanzheng Qiu,[1,2] Xiangguo Liu,[1] Wei Zou,[1] Ping Yue,[1] Sagar Lonial,[1] Fadlo R. Khuri,[1] and Shi-Yong Sun[1]

[1]Department of Hematology and Oncology, Winship Cancer Institute, Emory University School of Medicine, Atlanta, Georgia and [2]Department of Otolaryngology-Head and Neck Surgery, Xiang-Ya Hospital, Central South University, Changsha, Hunan, P.R. China

Abstract

Tumor necrosis factor–related apoptosis-inducing ligand (TRAIL) preferentially induces apoptosis in transformed or malignant cells, thus exhibiting potential as a tumor-selective apoptosis-inducing cytokine for cancer treatment. Many studies have shown that the apoptosis-inducing activity of TRAIL can be enhanced by various cancer therapeutic agents. R115777 (tipifarnib) is the first farnesyltransferase inhibitor (FTI) that showed clinical activity in myeloid malignancies. In general, R115777, like other FTIs, exerts relatively weak effects on the induction of apoptosis in cancer cells with undefined mechanism(s). In the current study, we studied its effects on the growth of human lung cancer cells, including induction of apoptosis, and examined potential underlying mechanisms for these effects. We showed that R115777 induced apoptosis in human lung cancer cells, in addition to inducing G_1 or G_2-M arrest. Moreover, we found that R115777 up-regulated the expression of death receptor 5 (DR5), an important death receptor for TRAIL, and exhibited an augmented effect on the induction of apoptosis when combined with recombinant TRAIL. Blockage of DR5 induction by small interfering RNA (siRNA) abrogated the ability of R115777 to enhance TRAIL-induced apoptosis, indicating that R115777 augments TRAIL-induced apoptosis through up-regulation of DR5 expression. Thus, our findings show the efficacy of R115777 in human lung cancer cells and suggest that R115777 may be used clinically in combination with TRAIL for treatment of human lung cancer. [Cancer Res 2007;67(10):4973–80]

Introduction

The tumor necrosis factor–related apoptosis-inducing ligand (TRAIL) receptor death receptor 5 (DR5, also named TRAIL-R2, TRICK2, or Killer/DR5) is one of the death receptors that share a similar, cysteine-rich extracellular domain and additional cytoplasmic death domain (1). DR5 locates at the cell surface, becomes activated or oligomerized (trimerized) upon binding to its ligand TRAIL or overexpression, and then signals apoptosis through caspase-8–mediated rapid activation of caspase cascades (1, 2). Recently, DR5 has attracted much more attention because its ligand TRAIL preferentially induces apoptosis in transformed or malignant cells, thus demonstrating potential as a tumor-selective apoptosis-inducing cytokine for cancer treatment (3, 4). Certain cancer therapeutic agents induce the expression of DR5 in cancer cells and are thereby able to augment TRAIL-induced apoptosis or initiate apoptosis (5–7).

Farnesyltransferase inhibitors (FTI) are a class of agents that suppress the farnesytltransferase enzyme to prevent certain proteins such as the Ras oncoprotein from undergoing farnesylation (8–10). These agents inhibit proliferation and induce apoptosis in various types of cancer cell lines in culture or suppress the growth of xenografts in nude mice with limited toxicity (8–10). In the clinic, FTIs are well tolerated and have some positive outcomes in certain settings, such as hematologic malignancies and breast cancer, although the response rates to FTIs alone are generally poor. When combined with other therapeutic agents or radiotherapy, FTIs exhibits some encouraging clinical responses (8, 10). Although FTIs were historically developed as anti-Ras agents, it is now generally agreed upon that FTIs exert their antitumor activity independent of their activity on inhibiting Ras farnesylation (8, 9). Otherwise, the mechanisms underlying the antitumor effects of FTIs remain largely undefined.

R115777 is one of the clinically tested FTIs and is the first one to show clinical activity in myeloid malignancies (11). Preclinical studies have shown that this agent inhibited the growth of the majority of tested human cancer cell lines (12), induced apoptosis in certain types of cancer cells (13–15), and suppressed the growth of tumor xenografts in nude mice with an increase in apoptotic index (12, 16). When R115777 was combined with other therapeutic agents, such as taxol and the proteasome inhibitor bortezomib, enhanced effects on growth inhibition or apoptosis induction were observed (17–19). Moreover, R115777 was also effective in inhibiting the growth of chemical-induced lung carcinogenesis in mice (20), suggesting potential activity as a chemopreventive agent. In the clinic, the most promising activity of R115777 has been seen primarily in hematologic malignancies (8, 11). Although R115777 as a single agent exhibited limited clinical activity in solid tumors, when used in combination with other agents such as tamoxifen, it did induce responses in some patients with solid tumors (8).

In an effort to elucidate the molecular mechanisms of FTI-induced growth arrest and apoptosis and to develop mechanism-oriented, FTI-based combination regimens for effective treatment of cancer, we found that R115777 up-regulated DR5 expression, including causing an increase in cell surface DR5 levels. Accordingly, R115777 cooperated with TRAIL to enhance induction of apoptosis in human lung cancer cells. Thus, our findings in this

Note: S.-Y. Sun and F.R. Khuri are Georgia Cancer Coalition Distinguished Cancer Scholars.

Requests for reprints: Shi-Yong Sun, Winship Cancer Institute, Emory University School of Medicine, 1365-C Clifton Road, C3088, Atlanta, GA 30322. Phone: 404-778-2170; Fax: 404-778-5520; E-mail: shi-yong.sun@emoryhealthcare.org.

doi:10.1158/0008-5472.CAN-06-4044

DOI:10.1158/0008-5472.CAN-06-4044

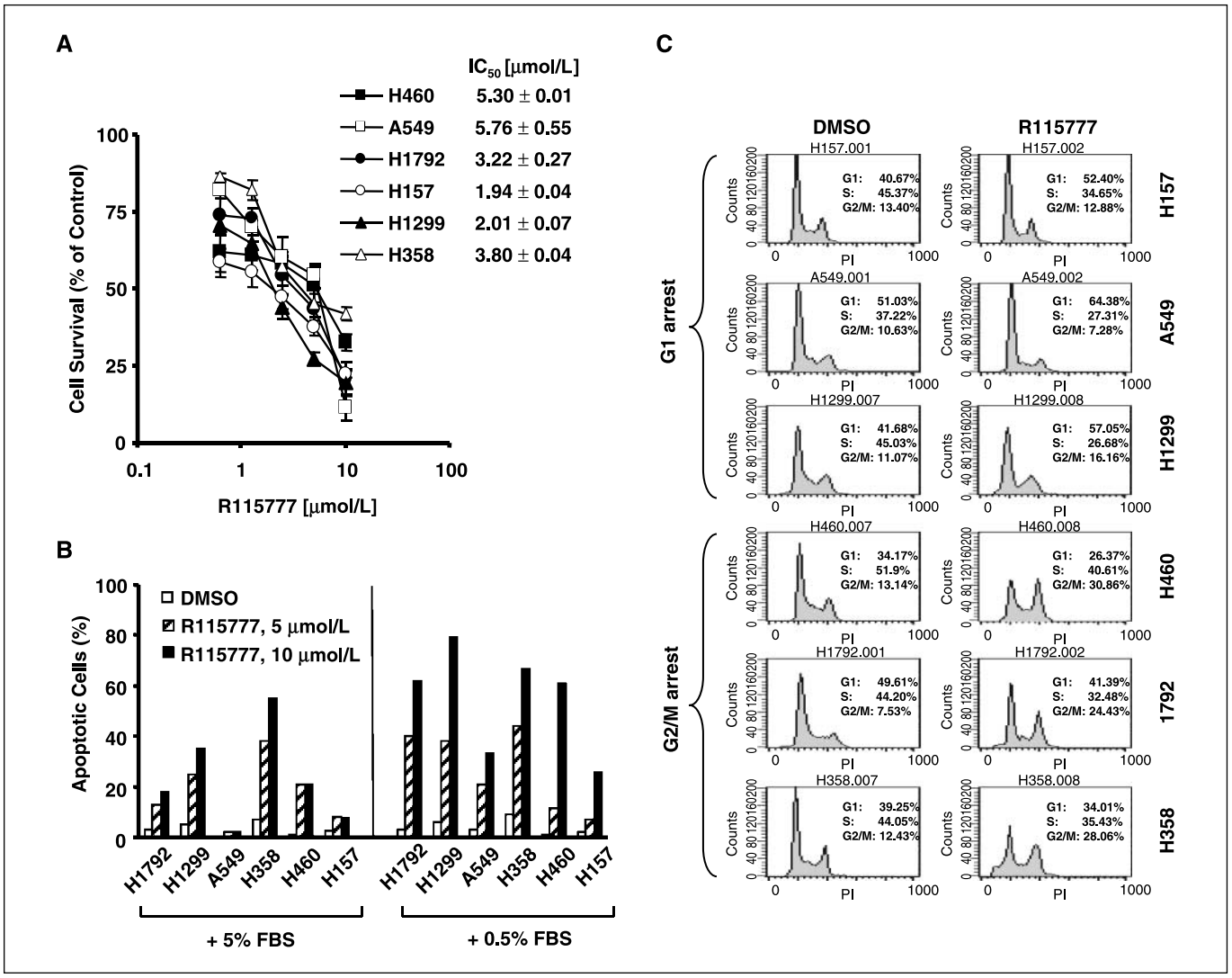

Figure 1. R115777 inhibits cell growth (*A*) and induces apoptosis (*B*) and cell cycle arrest (*C*) in human lung cancer cells. *A,* the indicated cell lines were seeded in 96-well plates. On the second day, the cells were treated with different concentrations of R115777. After 3 d, the cells were fixed and subjected to estimation of cell number using the sulforhodamine B assay. IC_{50} refers to the concentration that decreases cell number by 50%; *B,* the indicated cell lines were treated with 0, 5, and 10 μmol/L of R115777 in medium with either 5% or 0.1% FBS. After 48 h, the cells were harvested for analysis of sub-G_1 population by flow cytometry; *C,* the indicated cell lines were treated with DMSO or 5 μmol/L of R115777 in medium with 5% FBS. After 48 h, the cells were harvested for analysis of cell cycle distribution by flow cytometry.

study provide a scientific rationale for the combination of R115777 and TRAIL for the treatment of human lung cancer and possibly other types of cancer as well.

Materials and Methods

Reagents. R115777 was provided by Johnson & Johnson Pharmaceutical Research and Development, LLC. It was dissolved in DMSO at a concentration of 10 mmol/L, and aliquots were stored at −80°C. Stock solutions were diluted to the desired final concentrations with growth medium just before use. Soluble recombinant human TRAIL was purchased from PeproTech Inc. Rabbit polyclonal anti-DR5 antibody was purchased from ProSci Inc. Mouse monoclonal anti–caspase-3 was purchased from Imgenex. Rabbit polyclonal anti–caspase-9, anti–caspase-8, and anti–poly(ADP-ribose) polymerase (PARP) antibodies were purchased from Cell Signaling Technology, Inc.. Mouse monoclonal anti-RasGAP antibody (B4F8) was purchased from Santa Cruz Biotechnology. Mouse monoclonal anti–HDJ-2 antibody (clone KA2A5.6) was purchased from Lab Vision Corp. Mouse monoclonal anti–FLICE inhibitory protein (FLIP) antibody (NF6) was purchased from Alexis Biochemicals. Rabbit polyclonal anti–β-actin antibody was purchased from Sigma Chemical Co.

Cell lines and cell cultures. All human lung cancer cell lines used in this study were purchased from the American Type Culture Collection. H157-Lac Z-5 and H157-$FLIP_L$-6, which stably express Lac Z and $FLIP_L$, respectively, were described previously (21). These cell lines were grown in monolayer culture in RPMI 1640 supplemented with glutamine and 5% fetal bovine serum (FBS) at 37°C in a humidified atmosphere consisting of 5% CO_2 and 95% air.

Western blot analysis. The procedures for preparation of whole-cell protein lysates and Western blot analysis were described previously (22, 23).

Detection of DR5 mRNA expression. DR5 mRNA was detected using reverse transcription-PCR (RT-PCR) described as follows. Total RNA was isolated from cells using TRI Reagent (Sigma Chemical Co.) as instructed by the manufacturer. First-strand cDNA was synthesized from 2 μg of total RNA using iScript cDNA Synthesis Kit (Bio-Rad Laboratories) following the manufacturer's instructions. The given cDNAs were then amplified by PCR

DOI:10.1158/0008-5472.CAN-06-4044

using the following primers: DR5 sense 5′-GACCTAGCTCCCCAGCAGAGAG-3′, DR5 antisense 5′-CGGCTGCAACTGTGACTCCTAT-3′, β-actin sense, 5′-GAAACTACCTTCAACTCCATC-3′, and β-actin antisense 5′-CTAGAAGCATTTGCGGTGGACGATGGAGGGGCC-5′. The 25-μL amplification mixture contained 2 μL of cDNA, 0.5 μL of deoxynucleotide triphosphate (25 mmol/L each), 1 μL each of the sense and antisense primers (20 μmol/L each), 5 μL of TaqMaster PCR enhancer, 1 μL of Taq DNA polymerase (5 units/μL; Eppendorf), 2.5 μL 10× reaction buffer, and sterile H_2O. PCR was done for 28 cycles. After an initial step at 95°C for 3 min, each cycle consisted of 50 s of denaturation at 94°C, 50 s of annealing at 58°C, and 55 s of extension at 72°C. This was followed by an additional extension step at 72°C for 10 min. The housekeeping gene β-actin was also amplified as an internal reference. PCR products were resolved by electrophoresis on a 2% agarose gel, stained, and directly visualized under UV illumination.

Construction of DR5 reporter plasmids, transient transfection, and luciferase activity assay. The plasmid containing a 5′-flanking region of *DR5* gene was kindly provided by Dr. G.S. Wu (Wayne State University School of Medicine, Detroit, MI). We then used this plasmid as a template to amplify different lengths of the 5′-flanking region of the *DR5* gene by PCR and then subcloned these fragments, respectively, into pGL3-basic reporter vector (Promega) through *Kpn*I and *Bgl*II restriction sites. In the PCR amplification, the reverse primer 5′-CTTAAGATCTGGCGGTAGGGAACGCTCTTATAGTC-3′ was used to make all deletion constructs. The upstream primers used were 5′-CTTAGGTACCTGGCTCGTCTGTTCCTCTACGGCCCC-3′ (−3,070), 5′-CTTAGGTACCTCAACTCATTTCCCCCAAGTTTC-3′ (−420), and 5′-CTTAGGTACCACCCAGAAACAAACCACAGCCCGGG-3′ (−373), respectively. These constructs were then named pGL3-DR5(−3070), pGL3-DR5(−420), and pGL3-DR5(−373), respectively.

For examining the effect of R115777 on *DR5* transactivation activity, cells were seeded in 24-well plates and cotransfected with the given reporter plasmid (0.5 μg per well) and pCH110 plasmid encoding β-galactosidase (β-gal; Pharmacia Biotech; 0.2 μg per well) using FuGene 6 transfection reagent (3:1 ratio; Roche Molecular Biochemicals) following the manufacturer's protocol. Twenty-four hours later, the cells were treated with R115777. After 12 h, the cells were lysed and subjected to luciferase activity assay using Luciferase Assay System (Promega) in a luminometer. Relative luciferase activity was normalized to β-gal activity, which was measured as described previously (24).

Detection of cell surface DR5. Cell surface DR5 expression was analyzed using flow cytometry as described previously (25). The mean fluorescence intensity (MFI) that represents antigenic density on a per-cell basis was used to represent DR5 expression level. Phycoerythrin-conjugated mouse anti-human DR5 monoclonal antibody (DJR2-4), anti-human DR4 monoclonal antibody (DJR1), and mouse immunoglobulin G_1 (IgG_1) isotype control (MOPC-21/P3) were purchased from eBioscience.

Detection of caspase activation and apoptosis. Caspase activation and their substrate cleavage were detected by Western blot analysis as described above. Apoptosis was detected using an annexin V:phycoerythrin Apoptosis Detection kit purchased from BD Biosciences following the manufacturer's instructions. In addition, sub-G_1 was also measured by flow cytometry as described previously (26) as another indication of apoptosis.

Cell survival assay. Cells were seeded in 96-well cell culture plates and treated on the second day with the indicated agents. At the end of treatment, cell number was estimated by the sulforhodamine B assay as previously described (27). The cell survival was presented as the percentage

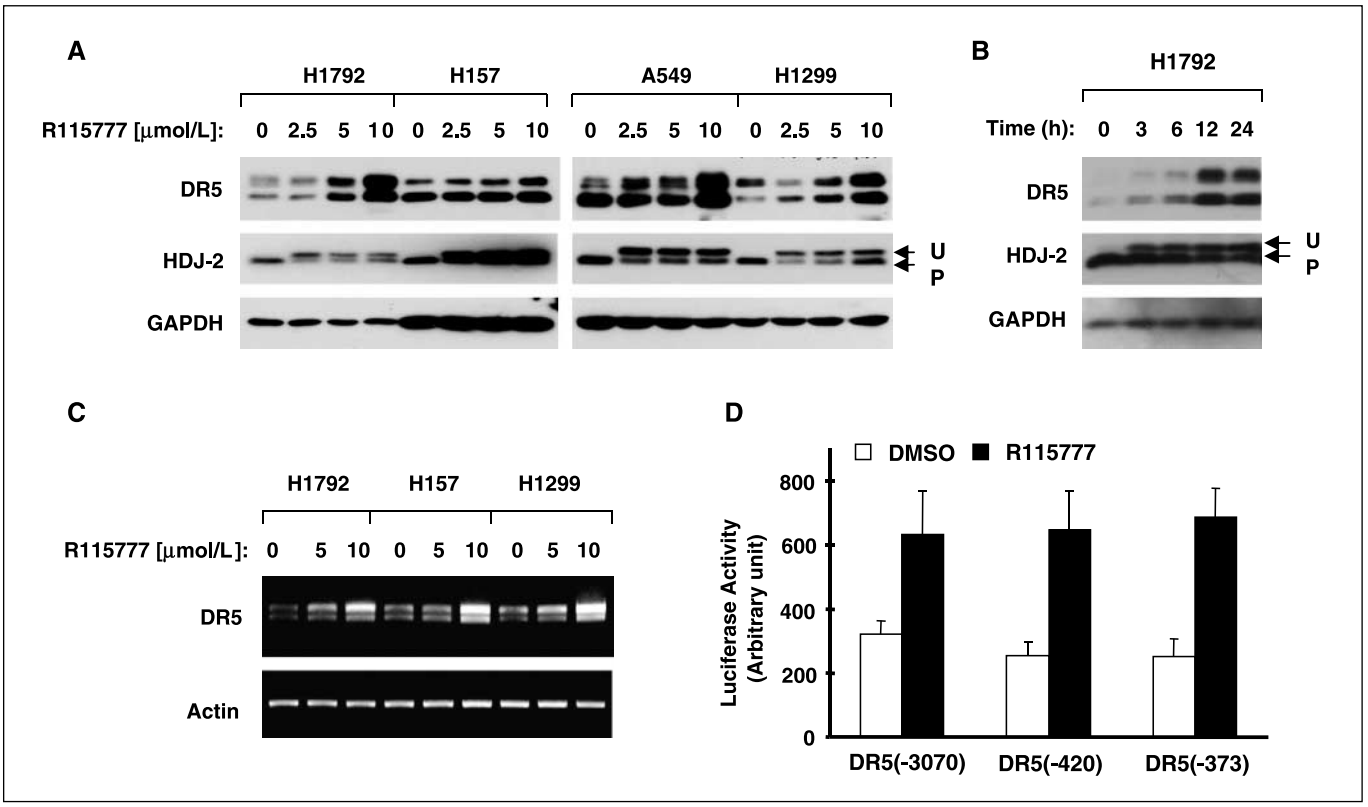

Figure 2. R115777 increases DR5 expression at both protein (*A* and *B*) and mRNA (*C*) levels and transactivates DR5 promoter (*D*) in human lung cancer cells. *A* and *B,* the indicated cell lines were treated with the given concentrations of R115777 for 16 h (*A*), or H1792 cells were treated with 5 μmol/L R115777 for the indicated times (*B*). Whole-cell protein lysates were then prepared from aforementioned treatments for detection of DR5 and HDJ-2 using Western blot analysis. *U,* unprocessed; *P,* processed; *C,* the indicated cell lines were exposed to the given concentrations of R115777 for 12 h. Cellular total RNA was then prepared for detection of DR5 mRNA using RT-PCR. Actin levels were used as an internal control. *D,* the given reporter constructs with different lengths of the 5′-flanking region of the *DR5* gene were cotransfected with pCH110 plasmid into H1792 cells. After 24 h, the cells were treated with DMSO or 10 μmol/L R115777 for 12 h and then subjected to luciferase assay. *Columns,* means of triplicate determinations; *bars,* SD.

DOI:10.1158/0008-5472.CAN-06-4044

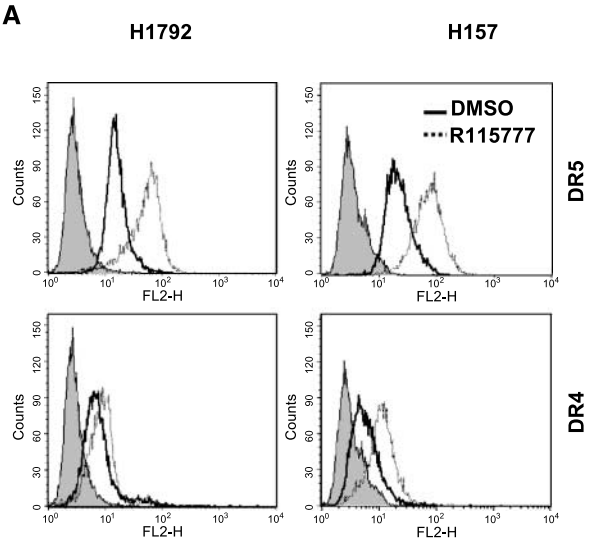

B

		Mean Fluorescent Intensity (MFI)			
		H1792		H157	
			Fold Change		Fold Change
DR5	DMSO	14.3		18.77	
	R115777	55.2	**3.85**	68.5	**3.65**
DR4	DMSO	6.67		6.64	
	R115777	8.82	**1.32**	12.98	**1.95**

Figure 3. R115777 increases cell surface DR5 distribution. Both H1792 and H157 cell lines were exposed to 10 μmol/L for 16 h. *A,* the cells were then harvested, stained with phycoerythrin-conjugated DR5 or DR4 antibody, and analyzed by flow cytometry. *Filled gray peak,* cells stained with matched phycoerythrin-conjugated IgG isotype. *Open peaks,* cells stained with phycoerythrin-conjugated anti-DR5 or anti-DR4 antibody. *B,* summary of changes in MFIs from cells treated with R115777 as presented in (*A*).

of control as calculated by using the equation: $A_t/A_c \times 100$, where A_t and A_c represent the absorbance in treated and control cultures, respectively.

Cell cycle analysis. Cell were seeded in 10-cm-diameter cell culture dishes and treated on the second day with DMSO control or R115777. At the end of treatment, cells were trypsinized, and single-cell suspensions were subjected to staining and subsequent analysis of cell cycle by flow cytometry as described previously (28).

Silencing of DR5 expression using small interfering RNA. High-purity control (nonsilencing) and DR5 small interfering RNA (siRNA) oligos were described previously (23) and synthesized from Qiagen. The transfection of siRNA was conducted in a 24-well plate (1 μg per well) using Lipofect-AMINE transfection reagent purchased from Invitrogen following the manufacturer's instruction. Forty-eight hours after the transfection, cells were treated with R115777 alone, TRAIL alone, and their combination. Gene-silencing effect was evaluated by Western blot analysis, and apoptosis was measured with annexin V staining.

Results

R115777 effectively inhibits the growth of human lung cancer cells through induction of apoptosis and growth arrest. The effects of R115777 on the growth of human lung cancer cells have not been systemically evaluated. Therefore, we examined the effects of R115777 on the growth of a panel of human non–small cell lung cancer cells by different assays. R115777 effectively inhibited the growth of six tested cell lines by measuring cell number, with IC_{50}s ranging from 2 to 6 μmol/L after a 3-day exposure (Fig. 1*A*). Under normal culture condition (i.e., 5% FBS), R115777 in general was a weak inducer of apoptosis because it induced apoptosis in some cell lines (e.g., H358 and H1299) but not in others (e.g., A549 and H157). However, under low-serum (i.e., 0.1%) culture conditions, the effects of R115777 on apoptosis induction were substantially enhanced in all of the tested cell lines. Under both culture conditions, A549 and H157 were relatively resistant to R115777-induced apoptosis (Fig. 1*B*). In addition to induction of apoptosis, R115777 induced cell cycle arrest either at the G_1 phase (i.e., H157, A549, and H1299) or at the G_2-M phase (i.e., H460, H1792, and H358), indicating that R115777 induces growth arrest. Collectively, these results show that R115777 inhibits the growth of human lung cancer cells through the induction of apoptosis and/or growth arrest.

R115777 induces DR5 expression in human lung cancer cells. To understand the mechanism by which R115777 induces apoptosis, we screened its effects on the expression of certain genes related to apoptosis. Our preliminary results indicate that DR5 is a gene up-regulated in cells exposed to R115777. Therefore, we did detailed experiments to study the effects of R115777 on the expression of DR5 in a panel of human lung cancer cells. We found that R115777 at concentrations ranging from 2.5 to 10 μmol/L increased DR5 protein levels in a concentration-dependent manner. The most dramatic increase in DR5 levels post–R115777 exposure were observed in H1792 cells and H1299 cell lines (Fig. 2*A*). R115777 induced a weak increase in DR5 levels in H157 cells. Time course analysis indicated that R115777 started to increase DR5 levels at 3 h, which was sustained up to 24 h (Fig. 2*B*). Under these conditions, the farnesylation of HDJ-2 protein was apparently inhibited (Fig. 2*A* and *B*), indicating that R115777 indeed inhibits protein farnesylation in the tested cell lines. Moreover, we determined whether R115777 up-regulated DR5 at the transcriptional level. R115777 increased not only DR5 mRNA levels evaluated by RT-PCR (Fig. 2*C*), but also the luciferase activity of the cells transfected with reporter plasmids with different lengths of the 5′-flanking region of the *DR5* gene ranging from 3,070 to 373 bp upstream of the translation start site (Fig. 2*D*). These results show that R115777 induces DR5 expression at the transcriptional level.

R115777 induces cell surface DR5 distribution. Because DR5 is a functional protein on the cell surface, we then analyzed cell surface DR5 levels in cells exposed to R115777. As shown in Fig. 3*A*, both H1792 and H157 cells treated with R115777 exhibited increased fluorescent intensity of DR5 staining in comparison with DMSO-treated cells (i.e., DR5 staining peak shifted to the right). The MFIs in both H1792 and H157 cells were increased close to 4-fold over those in DMSO-treated cells (Fig. 3*B*). These results clearly indicate that R115777 increases the amounts of DR5 on the cell surface. We also analyzed the effects of R115777 on the distribution of cell surface DR4, a protein with similar functions to DR5, in these cell lines. R115777 increased cell surface DR4 in H157 cells (1.95-fold), but only minimally in H1792 cells (1.32-fold; Fig. 3). Thus, these results indicate that R115777 primarily increases cell surface DR5 in human lung cancer cells.

R115777 cooperates with TRAIL to induce apoptosis in human lung cancer cells. Because R115777 increases cell surface DR5, we hypothesized that R115777 would sensitize cells to TRAIL-induced apoptosis. Therefore, we examined the effects of the

DOI:10.1158/0008-5472.CAN-06-4044

combination of R115777 and TRAIL on cell survival and apoptosis in human lung cancer cells. As presented in Fig. 4*A*, the combination of R115777 and TRAIL worked better than each single agent in decreasing cell survival. Accordingly, the combination was more potent than each single agent in inducing apoptosis estimated by annexin V staining (Fig. 4*B*). For example, R115777 at 5 μmol/L and TRAIL at 20 ng/mL alone induced 11.5% and 22.4% of cells to undergo apoptosis, respectively, whereas their combination induced 40% of cells to undergo apoptosis. Thus, it seems that the combination of R115777 and TRAIL synergistically induces apoptosis. Moreover, we examined the effects of R115777 and TRAIL combination on the activation of caspase cascades. R115777 alone at concentrations ranging from 2.5 to 10 μmol/L did not cause cleavage of the tested caspases. TRAIL alone at 20 ng/mL weakly induced cleavage of caspases and caspase-3 substrates, PARP, and RasGAP. However, their combinations exhibited enhanced effects on cleavage of these proteins (Fig. 4*C*). As the concentrations of R115777 in the combinations were increased, the cleavage of the caspases and related proteins were more pronounced. Thus, the combination of R115777 and TRAIL augments activation of caspases, further indicating that R115777 cooperates with TRAIL to induce apoptosis.

R115777 enhances TRAIL-induced apoptosis through up-regulation of DR5. To determine whether R115777 enhances TRAIL-induced apoptosis through DR5 up-regulation, we examined the effects of R115777 and TRAIL combination on apoptosis induction in cells where DR5 expression was silenced with DR5 siRNA. In control siRNA-transfected cells, R115777 increased DR5 levels (Fig. 5*A, lane 2*). In DR5 siRNA-transfected cells, the basal levels of DR5 were reduced (Fig. 5*A, lane 5*) and not increased further by R115777 (Fig. 5*A, lane 6*). These results indicate a successful silencing of DR5 expression. By apoptotic assay, we detected up to 70% apoptotic cells in control siRNA-transfected cells, but only 28% apoptotic cells in DR5 siRNA-transfected cells

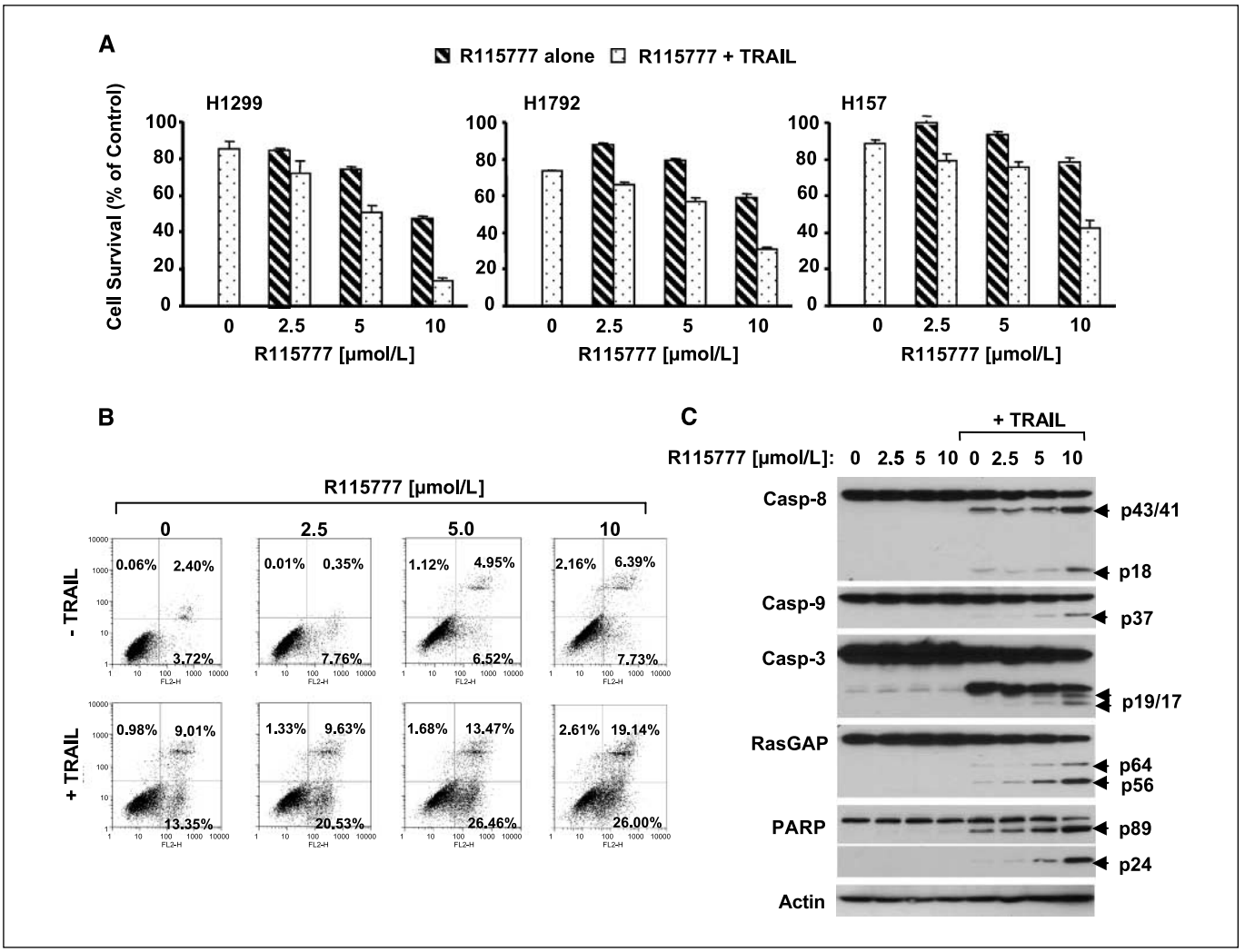

Figure 4. Combination of R115777 and TRAIL exerts augmented effects on decreasing cell survival (*A*), inducing apoptosis (*B*), and activating caspases (*C*). *A,* the indicated cell lines were treated with the indicated concentrations of R115777 alone, 25 ng/mL TRAIL alone, and their respective combinations as indicated. After 24 h, cell number was estimated using sulforhodamine B assay for calculation of cell survival; *B,* H157 cells were treated with the indicated concentrations of R115777 alone, 20 ng/mL TRAIL alone, and their respective combinations as indicated. After 24 h, the cells were harvested for measurement of apoptosis using annexin V staining. The percent positive cells in the top right and bottom right quadrants were added to yield the total of apoptotic cells. The cells in the bottom left quadrant were surviving cells; *C,* H157 cells were treated with the indicated concentrations of R115777 alone, 20 ng/mL TRAIL alone, and their respective combinations for 16 h. The cells were then subjected to preparation of whole-cell protein lysates and subsequent Western blot analysis for detecting cleavage of caspases and their substrates. *Casp,* caspase.

DOI:10.1158/0008-5472.CAN-06-4044

upon treatment with R115777 and TRAIL combination (Fig. 5*B*). Collectively, these results clearly indicate that up-regulation of DR5 is a key event that mediates augmentation of apoptosis induced by the combination of R115777 and TRAIL. We noted that more apoptotic cells were detected in control siRNA-transfected H157 cells treated with either TRAIL or the combination of R115777 and TRAIL compared with the result presented in Fig. 4*B* generated from the same cell line exposed to the similar treatment. In another transfection experiments, we generated identical results from control siRNA-transfected H157 cells treated with the same combination. Therefore, it is possible that the transfected cells are somehow more susceptible than their parental cells to undergo apoptosis upon treatment with TRAIL or the combination of R115777 and TRAIL. Of course, the discrepancy may also be caused by varied activities of different batches of recombinant TRAIL.

R115777 modulates c-FLIP expression in a cell line–dependent manner. c-FLIP including $FLIP_L$ and $FLIP_S$ are key proteins that negatively regulate the extrinsic death receptor–mediated apoptotic pathway by inhibiting caspase-8 activation (29). Some cancer therapeutic agents enhance cell sensitivity to TRAIL-induced apoptosis via down-regulation of c-FLIP expression (30–33). Therefore, we further examined the effects of R115777 on c-FLIP expression in human lung cancer cells. In H1792 cells, R115777 at the given concentrations decreased the levels of both $FLIP_L$ and $FLIP_S$. However, R115777 slightly increased the levels of both forms of c-FLIP in H157 and A549 cells. We detected neither basal levels of c-FLIP nor clear modulation by R115777 in H1299 cells (Fig. 6*A*). Thus, it seems that R115777 exerts a cell line–dependent modulation of c-FLIP in human lung cancer cells.

Enforced expression of exogenous c-FLIP protects cells from apoptosis induced by the combination of R115777 and TRAIL. Because the combination of R115777 and TRAIL still augmented apoptosis in the H157 cell line, in which c-FLIP levels were increased, we examined whether enforced expression of exogenous c-FLIP inhibited apoptosis induced by the combination of R115777 and TRAIL. By means of lentiviral infection, we established a stable H157 cell line that expressed high levels of exogenous $FLIP_L$ (Fig. 6*B*). In Lac Z (control)–transfected cell line, we detected ~2%, 10%, 14%, and 42% annexin V–positive (apoptotic) cells from cells treated with DMSO, R115777, TRAIL, and the combination of R115777 and TRAIL, respectively. However, annexin V–positive cells were ~2%, 3%, 2%, and 6% in $FLIP_L$-transfected H157 cells treated with DMSO, R115777, TRAIL, and the combination of R115777 and TRAIL, respectively (Fig. 6*C*). These results clearly indicate that enforced expression of $FLIP_L$ abolished apoptosis induced by R115777 and TRAIL.

Discussion

The effects of R115777 on the growth including apoptosis and cell cycle distribution of human lung cancer cells have not been fully evaluated in a preclinical setting. In this study, we show that R115777, at a clinically achievable and safe concentration range (2–6 μmol/L; refs. 34–37), effectively inhibited the growth of human lung cancer cells, primarily through inducing growth arrest and apoptosis. In general, R115777 was not a potent inducer of apoptosis under normal serum culture condition, although its apoptosis-inducing effects could be substantially enhanced by low-serum culture condition. Moreover, R115777 induced cell cycle arrest either at the G_1 phase or at the G_2-M phase depending on cell lines. All of these phenomena are consistent with those observed from other FTIs (26, 38, 39).

In this study, we show, for the first time, that R115777 induces DR5 expression not only at protein levels but also at mRNA levels. Moreover, R115777 increased transactivation of the DR5 promoter, indicating that R115777 modulates DR5 expression at the transcriptional level. In addition, we showed that R115777 increased amounts of DR5 at the cell surface, indicating that R115777 induces cell surface DR5 distribution. We noted that R115777 exerted only a moderate effect on modulation of DR5 protein levels in H157 cells (Fig. 1*A*). However, it increased cell surface DR5 in H157 cells as strongly as in H1792 cells (Fig. 3). These results suggest that R115777 induces DR5 redistribution at the cell surface in addition to increasing DR5 expression.

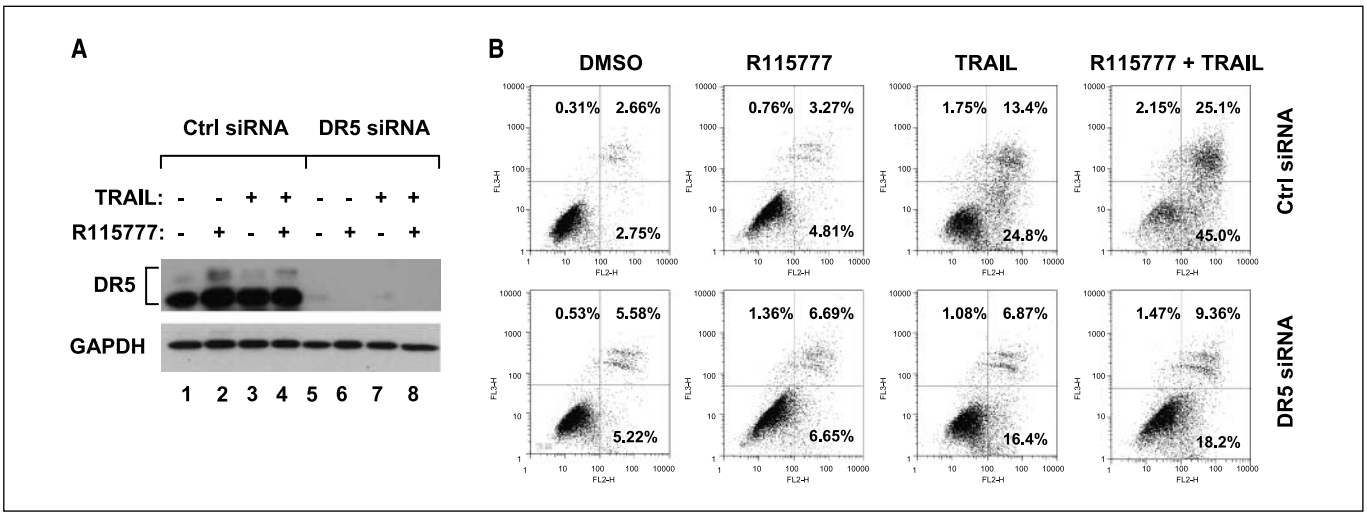

Figure 5. Silencing of DR5 expression by siRNA (*A*) attenuates apoptosis induced by the combination of R115777 and TRAIL (*B*). H157 cells were seeded in a 24-well cell culture plate and on the second day transfected with control (*Ctrl*) or DR5 siRNA. Forty hours later, the cells were treated with 10 μmol/L R115777, 20 ng/mL TRAIL, and their combination. After 15 h, the cells were harvested for preparation of whole-cell protein lysates and subsequent Western blot analysis (*A*) or for detection of apoptotic cells using annexin V staining (*B*). In annexin V assay, the percent positive cells in the top right and bottom right quadrants were added to yield the total of apoptotic cells. The cells in the bottom left quadrant were surviving cells.

DOI:10.1158/0008-5472.CAN-06-4044

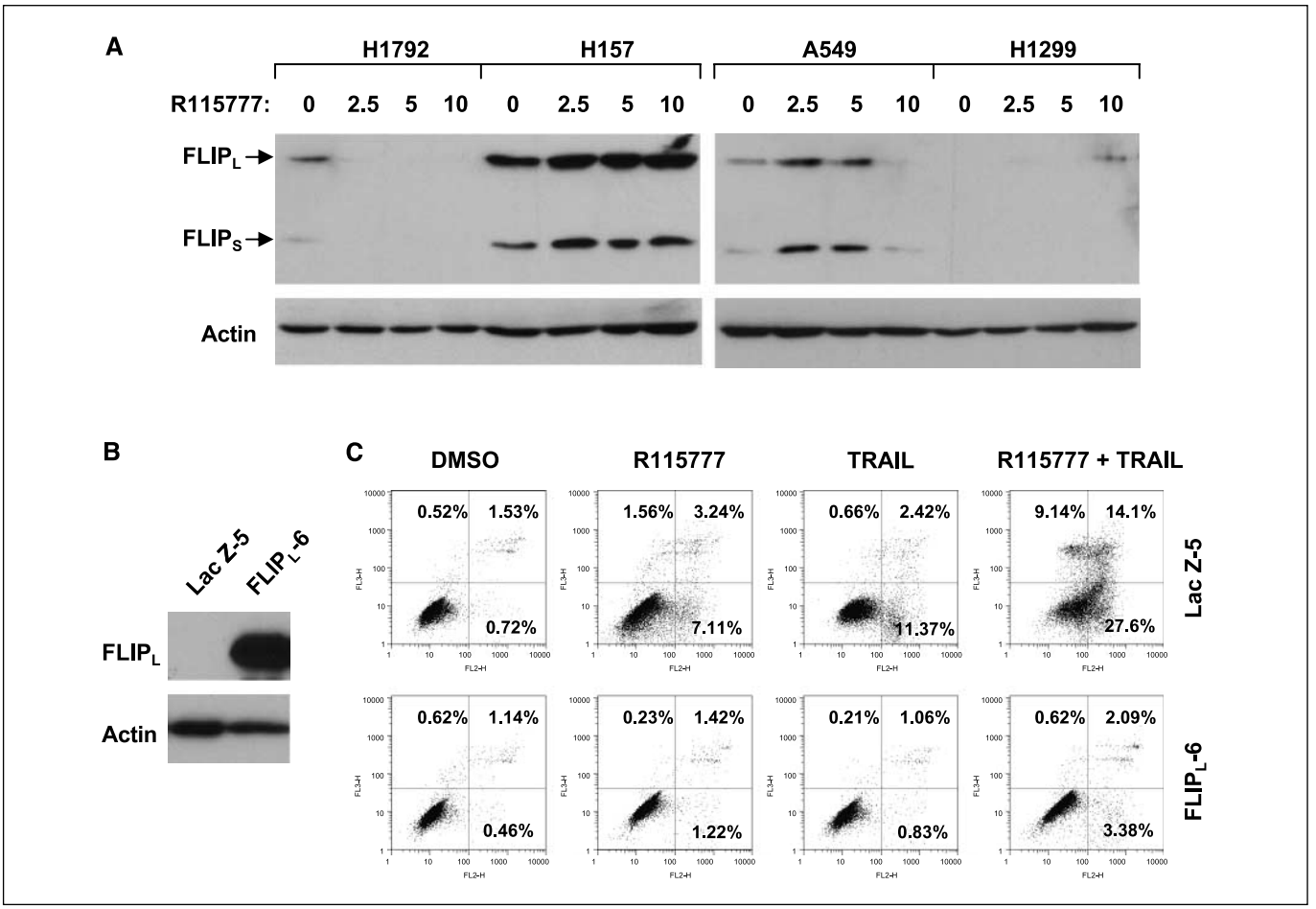

Figure 6. Differential effects of R115777 on c-FLIP levels (*A*) and protection of enforced c-FLIP expression (*B*) on apoptosis induced by the combination of R115777 and TRAIL (*C*). *A,* the indicated cell lines were treated with the given concentrations of R115777. After 16 h, the cells were subjected to preparation of whole-cell protein lysates and subsequent Western blot analysis. *B,* whole-cell protein lysates were prepared from H157 cells transfected with Lac Z and FLIP$_L$, respectively, and then subjected to detection of FLIP$_L$ expression by Western blot analysis. *C,* H157-Lac Z-5 or H157-FLIP$_L$-6 cells were treated with DMSO, 10 μmol/L R115777, 5 ng/mL TRAIL, and the combination of R115777 and TRAIL, respectively. After 24 h, the cells were harvested and subjected to detection of apoptotic cells using annexin V staining. The percent positive cells in the top right and bottom right quadrants were added to yield the total of apoptotic cells. The cells in the bottom left quadrant were surviving cells.

In addition to R115777, we found that another FTI called SCH66336 (lonafarnib) also induced DR5 expression and cell surface DR5 distribution.[3] Both agents have farnesyltransferase-inhibitory activity; however, they have distinct chemical structures. In our study, R115777 rapidly increased DR5 expression at 3 h posttreatment, which was accompanied by inhibition of HDJ-2 protein farnesylation (Fig. 3*B*). Therefore, we suggest that DR5 up-regulation by R115777 is associated with its ability to inhibit protein farnesylation. Because R115777 functions like SCH66336 to increase DR5 mRNA as well, it is unlikely that R115777 directly modulates DR5 protein. Rather, it may inhibit the farnesylation of an unknown protein, leading to increased DR5 transcription. Nevertheless, our findings on R115777 as well as SCH66336 warrant further study on the relationship between protein farnesylation and DR5 modulation.

Preliminary results from clinical trials have shown that R115777 exhibits promising efficacy in hematologic malignancies with a favorable toxicity profile (8, 11). R115777, at a clinically achievable and safe concentration range (2–6 μmol/L; refs. 34–37), up-regulated DR5 expression and induced cell surface DR5 distribution. Accordingly, we showed that the combination of a clinically achievable concentration of R115777 with TRAIL exhibited augmented effects on decreasing cell survival and inducing apoptosis (Fig. 4). Given that TRAIL is considered as a cancer-selective cytokine with cancer therapeutic potential and is being tested in phase I clinical trails, our current finding that R115777 enhances TRAIL-induced apoptosis clearly has translational significance in the clinic.

Some studies have shown that certain cancer therapeutic agents enhance TRAIL-induced apoptosis via down-regulation of c-FLIP expression (30–32, 40). In our study, we found that R115777 induced DR5 expression and cell surface distribution in all of the tested cell lines. However, it modulated c-FLIP expression in a cell line–dependent manner. R115777 even slightly increased c-FLIP levels in some cell lines (e.g., H157), whereas it decreased c-FLIP expression in other cell lines (e.g., H1792). Regardless of the differential modulation of c-FLIP expression, the combination of R115777 and TRAIL exerted augmented effects on decreasing cell survival and inducing apoptosis in these lung cancer cell lines, suggesting that it is unlikely for R115777 to enhance TRAIL-induced apoptosis via modulation of c-FLIP levels in certain cell lines in which c-FLIP levels are not decreased. Through

[3] S.Y. Sun, X. Liu, W. Zou, P. Yue, A.I. Marcus, and F.R. Khuri, unpublished data.

DOI:10.1158/0008-5472.CAN-06-4044

silencing DR5 expression and blocking DR5 induction by R115777 using siRNA targeting DR5, our data clearly show that apoptosis induced by the combination of R115777 and TRAIL was substantially attenuated. This result thus indicates that R115777 enhances TRAIL-induced apoptosis primarily via up-regulation of DR5.

Our results show that the combination of R115777 and TRAIL augmented induction of apoptosis in H157 cells, in which c-FLIP levels were actually increased upon R115777 treatment. When $FLIP_L$ expression was enforced to high levels in this cell line, either TRAIL alone or the combination of R115777 and TRAIL failed to induce apoptosis, indicating that $FLIP_L$ overexpression indeed inhibits TRAIL/death receptor–mediated apoptosis. Therefore, we suggest that R115777-induced DR5 expression and cell surface distribution override c-FLIP up-regulation, leading to enhancement of TRAIL-induced apoptosis in cell lines where c-FLIP expression is high or increased by R115777. If this is correct, we assume that cell lines in which c-FLIP levels are reduced upon R115777 treatment (e.g., H1792) will be more susceptible than other cell lines where c-FLIP expression is increased or not altered by R115777 (e.g., H157) to apoptosis induction by the combination of R115777 and TRAIL as shown in Fig. 4*A*.

Among the tested lung cancer cell lines, A549 and H157 cell lines are the least sensitive to R115777-induced apoptosis even under low-serum culture condition (Fig. 1*C*). We noted that these two cell lines had relatively higher levels of c-FLIP compared with H1792 and H1299 cells (Fig. 6*A*), which are sensitive to R115777-induced apoptosis (Fig. 1*C*). Whether these results suggest that the levels of c-FLIP determine cell sensitivity to R115777-induced apoptosis needs to be investigated in the future.

In summary, we have shown that R115777 increases DR5 expression, induces DR5 distribution at the cell surface, and subsequently enhances TRAIL-induced apoptosis. These findings warrant clinical evaluation of the efficacy of R115777 and TRAIL in the treatment of human lung and other types of cancer in the future.

Acknowledgments

Received 11/1/2006; revised 1/19/2007; accepted 3/2/2007.

Grant support: Georgia Cancer Coalition Distinguished Cancer Scholar award (S.-Y. Sun) and Department of Defense grant W81XWH-04-1-0142-VITAL (S.-Y. Sun for Project 4).

The costs of publication of this article were defrayed in part by the payment of page charges. This article must therefore be hereby marked *advertisement* in accordance with 18 U.S.C. Section 1734 solely to indicate this fact.

References

1. Ashkenazi A, Dixit VM. Death receptors: signaling and modulation. Science 1998;281:1305–8.
2. Wajant H, Gerspach J, Pfizenmaier K. Tumor therapeutics by design: targeting and activation of death receptors. Cytokine Growth Factor Rev 2005;16:55–76.
3. Almasan A, Ashkenazi A. Apo2L/TRAIL: apoptosis signaling, biology, and potential for cancer therapy. Cytokine Growth Factor Rev 2003;14:337–48.
4. Kelley SK, Ashkenazi A. Targeting death receptors in cancer with Apo2L/TRAIL. Curr Opin Pharmacol 2004; 4:333–9.
5. Wu GS, Burns TF, McDonald ER III, et al. KILLER/DR5 is a DNA damage-inducible p53-regulated death receptor gene. Nat Genet 1997;17:141–3.
6. Debatin KM, Krammer PH. Death receptors in chemotherapy and cancer. Oncogene 2004;23:2950–66.
7. Sheikh MS, Huang Y. Death receptors as targets of cancer therapeutics. Curr Cancer Drug Targets 2004; 4:97–104.
8. Basso AD, Kirschmeier P, Bishop WR. Thematic review series: lipid posttranslational modifications. Farnesyl transferase inhibitors. J Lipid Res 2006;47:15–31.
9. Sebti SM, Adjei AA. Farnesyltransferase inhibitors. Semin Oncol 2004;31:28–39.
10. Brunner TB, Hahn SM, Gupta AK, et al. Farnesyltransferase inhibitors: an overview of the results of preclinical and clinical investigations. Cancer Res 2003; 63:5656–68.
11. Jabbour E, Kantarjian H, Cortes J. Clinical activity of farnesyl transferase inhibitors in hematologic malignancies: possible mechanisms of action. Leuk Lymphoma 2004;45:2187–95.
12. End DW, Smets G, Todd AV, et al. Characterization of the antitumor effects of the selective farnesyl protein transferase inhibitor R115777 *in vivo* and *in vitro*. Cancer Res 2001;61:131–7.
13. Le Gouill S, Pellat-Deceunynck C, Harousseau JL, et al. Farnesyl transferase inhibitor R115777 induces apoptosis of human myeloma cells. Leukemia 2002;16: 1664–7.
14. Ochiai N, Uchida R, Fuchida S, et al. Effect of farnesyl transferase inhibitor R115777 on the growth of fresh and cloned myeloma cells *in vitro*. Blood 2003; 102:3349–53.
15. Beaupre DM, Cepero E, Obeng EA, Boise LH, Lichtenheld MG. R115777 induces Ras-independent apoptosis of myeloma cells via multiple intrinsic pathways. Mol Cancer Ther 2004;3:179–86.
16. Kelland LR, Smith V, Valenti M, et al. Preclinical antitumor activity and pharmacodynamic studies with the farnesyl protein transferase inhibitor R115777 in human breast cancer. Clin Cancer Res 2001;7:3544–50.
17. Yanamandra N, Colaco NM, Parquet NA, et al. Tipifarnib and bortezomib are synergistic and overcome cell adhesion-mediated drug resistance in multiple myeloma and acute myeloid leukemia. Clin Cancer Res 2006;12:591–9.
18. Zhu K, Gerbino E, Beaupre DM, et al. Farnesyltransferase inhibitor R115777 (Zarnestra, tipifarnib) synergizes with paclitaxel to induce apoptosis and mitotic arrest and to inhibit tumor growth of multiple myeloma cells. Blood 2005;105:4759–66.
19. Caraglia M, Giuberti G, Marra M, et al. Docetaxel induces p53-dependent apoptosis and synergizes with farnesyl transferase inhibitor r115777 in human epithelial cancer cells. Front Biosci 2005;10:2566–75.
20. Gunning WT, Kramer PM, Lubet RA, et al. Chemoprevention of benzo(*a*)pyrene-induced lung tumors in mice by the farnesyltransferase inhibitor R115777. Clin Cancer Res 2003;9:1927–30.
21. Liu X, Yue P, Schonthal AH, Khuri FR, Sun SY. Cellular FLICE-inhibitory protein down-regulation contributes to celecoxib-induced apoptosis in human lung cancer cells. Cancer Res 2006;66:11115–9.
22. Sun SY, Yue P, Wu GS, et al. Mechanisms of apoptosis induced by the synthetic retinoid CD437 in human non–small cell lung carcinoma cells. Oncogene 1999;18: 2357–65.
23. Liu X, Yue P, Zhou Z, Khuri FR, Sun SY. Death receptor regulation and celecoxib-induced apoptosis in human lung cancer cells. J Natl Cancer Inst 2004;96: 1769–80.
24. Pfahl M, Tzukerman M, Zhang XK, et al. Nuclear retinoic acid receptors: cloning, analysis, and function. Methods Enzymol 1990;189:256–70.
25. Sun SY, Yue P, Hong WK, Lotan R. Induction of Fas expression and augmentation of Fas/Fas ligand-mediated apoptosis by the synthetic retinoid CD437 in human lung cancer cells. Cancer Res 2000;60:6537–43.
26. Sun SY, Zhou Z, Wang R, Fu H, Khuri FR. The farnesyltransferase inhibitor lonafarnib induces growth arrest or apoptosis of human lung cancer cells without down-regulation of Akt. Cancer Biol Ther 2004;3:1092–8; discussion 9–101.
27. Sun SY, Yue P, Dawson MI, et al. Differential effects of synthetic nuclear retinoid receptor-selective retinoids on the growth of human non–small cell lung carcinoma cells. Cancer Res 1997;57:4931–9.
28. Sun SY, Yue P, Shroot B, Hong WK, Lotan R. Induction of apoptosis in human non–small cell lung carcinoma cells by the novel synthetic retinoid CD437. J Cell Physiol 1997;173:279–84.
29. Wajant H. Targeting the FLICE inhibitory protein (FLIP) in cancer therapy. Mol Interv 2003;3:124–7.
30. Chawla-Sarkar M, Bae SI, Reu FJ, et al. Down-regulation of Bcl-2, FLIP or IAPs (XIAP and survivin) by siRNAs sensitizes resistant melanoma cells to Apo2L/TRAIL-induced apoptosis. Cell Death Differ 2004;11: 915–23.
31. Hyer ML, Croxton R, Krajewska M, et al. Synthetic triterpenoids cooperate with tumor necrosis factor–related apoptosis-inducing ligand to induce apoptosis of breast cancer cells. Cancer Res 2005;65:4799–808.
32. Kim Y, Suh N, Sporn M, Reed JC. An inducible pathway for degradation of FLIP protein sensitizes tumor cells to TRAIL-induced apoptosis. J Biol Chem 2002;277:22320–9.
33. Olsson A, Diaz T, Aguilar-Santelises M, et al. Sensitization to TRAIL-induced apoptosis and modulation of FLICE-inhibitory protein in B chronic lymphocytic leukemia by actinomycin D. Leukemia 2001;15: 1868–77.
34. Zujewski J, Horak ID, Bol CJ, et al. Phase I and pharmacokinetic study of farnesyl protein transferase inhibitor R115777 in advanced cancer. J Clin Oncol 2000; 18:927–41.
35. Crul M, de Klerk GJ, Swart M, et al. Phase I clinical and pharmacologic study of chronic oral administration of the farnesyl protein transferase inhibitor R115777 in advanced cancer. J Clin Oncol 2002;20:2726–35.
36. Karp JE, Lancet JE, Kaufmann SH, et al. Clinical and biologic activity of the farnesyltransferase inhibitor R115777 in adults with refractory and relapsed acute leukemias: a phase 1 clinical-laboratory correlative trial. Blood 2001;97:3361–9.
37. Widemann BC, Salzer WL, Arceci RJ, et al. Phase I trial and pharmacokinetic study of the farnesyltransferase inhibitor tipifarnib in children with refractory solid tumors or neurofibromatosis type I and plexiform neurofibromas. J Clin Oncol 2006;24:507–16.
38. Du W, Liu A, Prendergast GC. Activation of the PI3K-AKT pathway masks the proapoptotic effects of farnesyltransferase inhibitors. Cancer Res 1999;59: 4208–12.
39. Jiang K, Coppola D, Crespo NC, et al. The phosphoinositide 3-OH kinase/AKT2 pathway as a critical target for farnesyltransferase inhibitor–induced apoptosis. Mol Cell Biol 2000;20:139–48.
40. Longley DB, Wilson TR, McEwan M, et al. c-FLIP inhibits chemotherapy-induced colorectal cancer cell death. Oncogene 2006;25:838–48.

DOI:10.1158/0008-5472.CAN-05-2521

Cancer Research

Multiple Oncogenic Changes (*K-RAS*^{V12}, p53 Knockdown, *Mutant EGFRs, p16* Bypass, Telomerase) Are Not Sufficient to Confer a Full Malignant Phenotype on Human Bronchial Epithelial Cells

Mitsuo Sato, Melville B. Vaughan, Luc Girard, et al.

Cancer Res 2006;66:2116-2128. Published online February 17, 2006.

DOI:10.1158/0008-5472.CAN-05-2521

Research Article

Multiple Oncogenic Changes (*K-RAS^{V12}*, p53 Knockdown, *Mutant EGFRs, p16* Bypass, Telomerase) Are Not Sufficient to Confer a Full Malignant Phenotype on Human Bronchial Epithelial Cells

Mitsuo Sato,[1] Melville B. Vaughan,[4] Luc Girard,[1] Michael Peyton,[1] Woochang Lee,[1] David S. Shames,[1] Ruben D. Ramirez,[1,2,6] Noriaki Sunaga,[1] Adi F. Gazdar,[1,3] Jerry W. Shay,[4] and John D. Minna[1,2,5]

[1]Hamon Center for Therapeutic Oncology Research and Departments of [2]Internal Medicine, [3]Pathology, [4]Cell Biology, and [5]Pharmacology, The University of Texas Southwestern Medical Center; and [6]Dallas Veterans Administration Medical Center, Dallas, Texas

Abstract

We evaluated the contribution of three genetic alterations (p53 knockdown, *K-RAS^{V12}*, and *mutant EGFR*) to lung tumorigenesis using human bronchial epithelial cells (HBEC) immortalized with telomerase and Cdk4-mediated p16 bypass. RNA interference p53 knockdown or oncogenic *K-RAS^{V12}* resulted in enhanced anchorage-independent growth and increased saturation density of HBECs. The combination of p53 knockdown and K-RAS^{V12} further enhanced the tumorigenic phenotype with increased growth in soft agar and an invasive phenotype in three-dimensional organotypic cultures but failed to cause HBECs to form tumors in nude mice. Growth of HBECs was highly dependent on epidermal growth factor (EGF) and completely inhibited by EGF receptor (EGFR) tyrosine kinase inhibitors, which induced G_1 arrest. Introduction of EGFR mutations E746-A750 del and L858R progressed HBECs toward malignancy as measured by soft agar growth, including EGF-independent growth, but failed to induce tumor formation. Mutant EGFRs were associated with higher levels of phospho-Akt, phospho–signal transducers and activators of transcription 3 [but not phospho-extracellular signal-regulated kinase (ERK) 1/2], and increased expression of *DUSP6/MKP-3* phosphatase (an inhibitor of phospho-ERK1/2). These results indicate that (*a*) the HBEC model system is a powerful new approach to assess the contribution of individual and combinations of genetic alterations to lung cancer pathogenesis; (*b*) a combination of four genetic alterations, including human telomerase reverse transcriptase overexpression, bypass of p16/RB and p53 pathways, and mutant K-RAS^{V12} or mutant EGFR, is still not sufficient for HBECs to completely transform to cancer; and (*c*) EGFR tyrosine kinase inhibitors inhibit the growth of preneoplastic HBEC cells, suggesting their potential for chemoprevention. (Cancer Res 2006; 66(4): 2116-28)

Introduction

Human lung cancer develops as a multistep process, usually occurring because of years of smoking-related tobacco exposure that results in specific proto-oncogene and tumor suppressor gene alterations in lung epithelial cells (1). In fact, the majority of lung cancers have many such changes (1). Identifying the minimal and most crucial set of changes required for lung tumorigenesis and the effect each of these alterations has on the carcinogenic process is vital to develop the best targets for early detection and therapeutic intervention. To address this issue, an *in vitro* model system using human bronchial epithelial cells (HBEC) was recently developed to assess the contribution of specific genetic alterations to lung cancer progression (2, 3). We accomplished this by overexpressing Cdk4 to abrogate the p16/Rb cell cycle checkpoint pathway and ectopic expression of human telomerase reverse transcriptase (hTERT) to bypass replicative senescence, allowing us to develop a series of immortalized HBEC lines without using viral oncoproteins. These HBECs have epithelial morphology, express epithelial markers, are able to differentiate into mature airway cells in organotypic cultures, have minimal genetic changes, and do not exhibit a transformed phenotype (2, 3). We have HBEC lines that are derived from patients with a variety of smoking histories, with and without lung cancer, which also allows us to explore interindividual variation in the tumor formation process.

Two of the genetic alterations that occur almost universally in human lung cancer, inactivation of the p16/pRb pathway and expression of hTERT, were used for establishment of immortalized HBECs and so are already present. The pRb pathway ($p16^{INK4a}$-cyclinD1-Cdk4-pRB pathway) is a key cell cycle regulator at the G_1-S phase transition. Absence of expression or structural abnormality of Rb protein is seen in >90% of small-cell lung cancers (SCLC) and loss of p16 protein expression by several mechanisms, including methylation or homozygous deletion of *$p16^{INK4a}$*, is seen in >70% of non-SCLC (NSCLC), both of which result in the inactivation of this pathway (1, 4, 5). Expression of high levels of telomerase is almost universal in lung cancer (1). hTERT is the key determinant of the enzymatic activity of human telomerase and its transcriptional control is a major contributor to the regulation of telomerase activity in many types of human cells (6–10). Because of the central role of the pRb pathway and telomerase expression, we initially evaluated the contribution of ectopically expressing Cdk4 and hTERT on lung cancer development. However, we found that such cells, although immortal and clonable, did not show anchorage-independent growth or an ability to form tumors *in vivo* (2). Other investigators and our group had also immortalized HBECs but these were made using viral oncoproteins, such as human papillomavirus E6/E7 or SV40 large T antigen with or without hTERT (2, 11, 12). These oncoproteins are known to cause

Requests for reprints: John D. Minna, Hamon Center for Therapeutic Oncology Research NB8.206, The University of Texas Southwestern Medical Center at Dallas, 6000 Harry Hines Boulevard, Dallas, TX 75390-8593. Phone: 214-648-4900; Fax: 214-648-4940; E-mail: John.Minna@UTsouthwestern.edu.

doi:10.1158/0008-5472.CAN-05-2521

DOI:10.1158/0008-5472.CAN-05-2521

malignant transformation through their ability to inactivate Rb and/or p53, as well as provide multiple other functions, which are not characterized. These "other functions" make it difficult to estimate the importance of added genetic or epigenetic changes in HBECs immortalized by viral oncoproteins.

Thus, we designed the current study to determine if the HBECs were genetically tractable and to analyze the effect of additional genetic alterations frequently observed in lung cancer on tumorigenic transformation of HBECs. First, we introduced two well-known genetic alterations seen in lung cancer, one of which is the loss of p53 function, which is observed in 90% of SCLCs and 50% of NSCLCs (1). The other is oncogenic K-RAS, which is frequently seen in NSCLCs (~ 30%), especially in adenocarcinomas but probably never in SCLCs (1, 13, 14). Furthermore, we introduced a mutant epidermal growth factor (EGF) receptor (EGFR) that has recently been reported in NSCLCs and shown to be correlated with tumor sensitivity to the EGFR tyrosine kinase inhibitors (15, 16). We report here that HBECs immortalized by overexpression of Cdk4 and hTERT and subsequently manipulated to have oncogenic K-RAS, knockdown of p53, or mutant EGFR have acquired part, but not all, of the malignant phenotype by the combination of these genetic alterations. These partially progressed lung epithelial cells show that more changes are needed for the full malignant phenotype. In addition, we have found that these preneoplastic cells are exquisitely sensitive to EGFR inhibition.

Materials and Methods

Cells and culture conditions. The HBEC3 (HBEC3-KT) immortalized normal HBEC line was established by introducing mouse Cdk4 and hTERT into normal HBECs obtained from a 65-year-old woman without cancer (2). NSCLC, NCI-H441, NCI-H358, NCI-H1299, and NCI-H2122 cell lines were obtained from Hamon Center Collection (University of Texas Southwestern Medical Center). HBEC3 was cultured with K-SFM (Life Technologies, Gaithersburg, MD) medium containing 50 μg/mL bovine pituitary extract (Life Technologies) with or without 5 ng/mL EGF (Life Technologies). These cells are resistant to G418 due to the neomycin-resistant gene introduced with the Cdk4 expression vector and to puromycin due to the puromycin-resistant gene introduced with the hTERT expression vector.

Viral vector construction and viral transduction. We used the pSUPER vector (OligoEngine, Seattle, WA) of Brummelkamp et al. (17, 18) as the basis for generating small interfering RNA for stable p53 knockdown. To generate pSUPER.retro-zeocin (pSRZ), *Sac*II and *Eco*RI sites were introduced into zeocin-resistant gene fragment amplified from pVgRXR (a gift from Dr. Preet Chaudhary) and the fragment was cloned into pSUPER.retro using *Sac*II and *Eco*RI sites, resulting in the replacement of the puromycin-resistant gene with a zeocin-resistant gene. To generate pSRZ-p53 for p53 knockdown, *Eco*RI- and *Hin*dIII-digested inserts from pSUPER-p53 (OligoEngine; ref. 18) was cloned into the same sites of pSRZ. pBabe-hyg and an oncogenic K-RAS^{V12}, pBabe-hyg-KRAS2-V12, vectors were provided by Dr. Michael White (The University of Texas Southwestern Medical Center, Dallas, TX). To produce viral-containing medium, 293T cells were transiently transfected with viral vector together with pVpack-VSVG and pVpack-GP vectors (Stratagene, La Jolla, CA). Forty-eight hours after the transfection, supernatant of the 293T cells was harvested and passed through a 0.45 μm filter and the viral supernatant was frozen at −80°C. The supernatant was used for infection after adding 4 μg/mL polybrene (Sigma, St. Louis, MO). Forty-eight hours after the infection, drug selection for infected cells was started with 12.5 μg/mL zeocin (Invitrogen, Carlsbad, CA) or 18 μg/mL hygromycin (Clontech, Palo Alto, CA) and continued for 7 to 11 days. HBEC3 cells were infected with four different combinations of the two retroviral vectors: (*a*) pSRZ and pBabe-hyg (vector control); (*b*) pSRZ-p53 and pBabe-hyg; (*c*) pSRZ and pBabe-hyg-KRAS2-V12; and (*d*) pSRZ-p53 and pBabe-hyg-K-RAS2-V12.

To introduce wild and mutant EGFRs into HBEC3 cells, we used the pLenti6/directional TOPO cloning kit. Full-length fragment of wild-type EGFR was amplified from pcDNA3.1-EGFR-wt (a gift from Dr. Joachim Herz, University of Texas Southwestern Medical Center) and cloned into pLenti6/directional TOPO vector according to the instructions of the manufacturer (pLenti-wt-EGFR). The L858R mutation was introduced into pLenti-wt-EGFR by using site-directed mutagenesis kit (Stratagene). The full length of E746-A750 del mutation was amplified from cDNA from HCC827 NSCLC cell line (19) and cloned into pLenti6/directional TOPO vector. Correct sequences were confirmed by sequencing for all vectors. Viral transduction was done following the instructions of the manufacturer. Briefly, the 293FT cells were transiently transfected with viral vector together with viral power (Invitrogen). Forty-eight hours after the transfection, supernatant of the 293FT cells was harvested and passed through a 0.45 μm filter, and frozen at −80°C. The supernatant was used for infection after adding 4 μg/mL polybrene (Sigma). Forty-eight hours after the infection, drug selection for infected cells was started with 5 μg/mL blasticidin (Invitrogen) and continued for 7 days.

Western blot analysis. Preparation of total cell lysates and Western blotting were done as described previously (20). Primary antibodies used were mouse monoclonal anti-p53 (Santa Cruz, Santa Cruz, CA), mouse monoclonal anti-p21 (BD Transduction Laboratories, Lexington, KY), mouse monoclonal anti-K-RAS (Santa Cruz), mouse monoclonal anti-EGFR (BD Transduction Laboratories), rabbit polyclonal anti-phospho-EGFR-Tyr^{1068} (Y1068), rabbit polyclonal anti-phospho-EGFR-Tyr^{845} (Y845), rabbit polyclonal anti-phospho-EGFR-Tyr^{992} (Y992), rabbit polyclonal anti-phospho-EGFR-Tyr^{1045} (Y1045; Cell Signaling, Beverly, MA), rabbit polyclonal anti-MEK1/2 (Cell Signaling), rabbit polyclonal anti-phospho-MEK1/2 (Cell Signaling), rabbit polyclonal anti–extracellular signal-regulated kinase (ERK) 1 (Cell Signaling), rabbit polyclonal anti-phospho-ERK1 (Cell Signaling), rabbit polyclonal anti-Akt (Cell Signaling), rabbit polyclonal anti-phospho-Akt (Thr^{308}), rabbit polyclonal anti-phospho-Akt (Ser^{473}), mouse monoclonal anti-phospho-signal transducers and activators of transcription (STAT) 3 (Tyr^{705}; Cell Signaling), poly(ADP-ribose) polymerase (PARP; Cell Signaling), and mouse monoclonal antiactin (Sigma) antibodies. Actin protein levels were used as a control for adequacy of equal protein loading. Antirabbit or antimouse antibody (1:2,000 dilution: Amersham, Piscataway, NJ) was used as the second antibody.

Immunofluorescence staining. Cells were washed with PHEM [60 mmol/L PIPES, 25 mmol/L HEPES, 10 mmol/L EGTA, and 1 mmol/L $MgCl_2$ (pH 7.4)] solution, and fixed in 3% paraformaldehyde for 10 minutes at 37°C in PHEM. After additional washes with PBS, the cells were permeabilized with 0.1% Triton in PBS for 10 minutes, blocked with 3% gelatin/3% bovine serum albumin (BSA)/0.2% Tween 20 for 1 hour at 37°C, and incubated with mouse polyclonal anti-p63 antibody (BD Transduction Laboratories) and rhodamine phalloidin (Molecular Probes, Eugene, OR) in gelatin/BSA blocking solution for 16 hours at 4°C. The cells were then incubated with the Alexa Fluor 568 anti-mouse IgG (H + L; Molecular Probes) secondary antibody for 1 hour at 37°C. Finally, cells were stained with 0.5 μg/mL Hoechst 33258 and examined in a fluorescence microscope.

RNA extraction and reverse transcription-PCR/RFLP analysis. We modified previously reported reverse transcription-PCR (RT-PCR)/RFLP method designed to distinguish mutated from wild-type *K-RAS* alleles (21). Total RNA was extracted using RNeasy mini kit (Qiagen, Valencia, CA). Four micrograms of total RNA were reverse transcribed with Superscript II First-Strand Synthesis using oligo-dTMP primer system (Invitrogen). PCR amplification was carried out with 3,704 K-RASTN sense (GACTGAATAT-AAACTTGTGGTAGTTGGACCT) and 3,672 K-RAS-RT-R antisense (5-TCC-TCTTGACCTGCTGTGTCG-3) primers, creating *Bst*NI restriction patterns that distinguished mutated from wild-type *K-RAS* alleles. PCR reactions were done in a 25 μL reaction mixture containing 1.5 mmol/L $MgCl_2$, 187.5 μmol/L of each deoxynucleotide triphosphate, 10 pmol of each primer, and 1.25 units of HotStar Taq DNA Polymerase (Qiagen). Cycling conditions were one incubation of 15 minutes at 95°C, followed by 35 cycles of a 20-second denaturation at 94°C, 60-second annealing at 58°C, and 90-second extension at 72°C, and a final elongation at 72°C for 7 minutes. PCR products were cut with *Bst*NI, electrophoresized on 1% agarose gel with

DOI:10.1158/0008-5472.CAN-05-2521

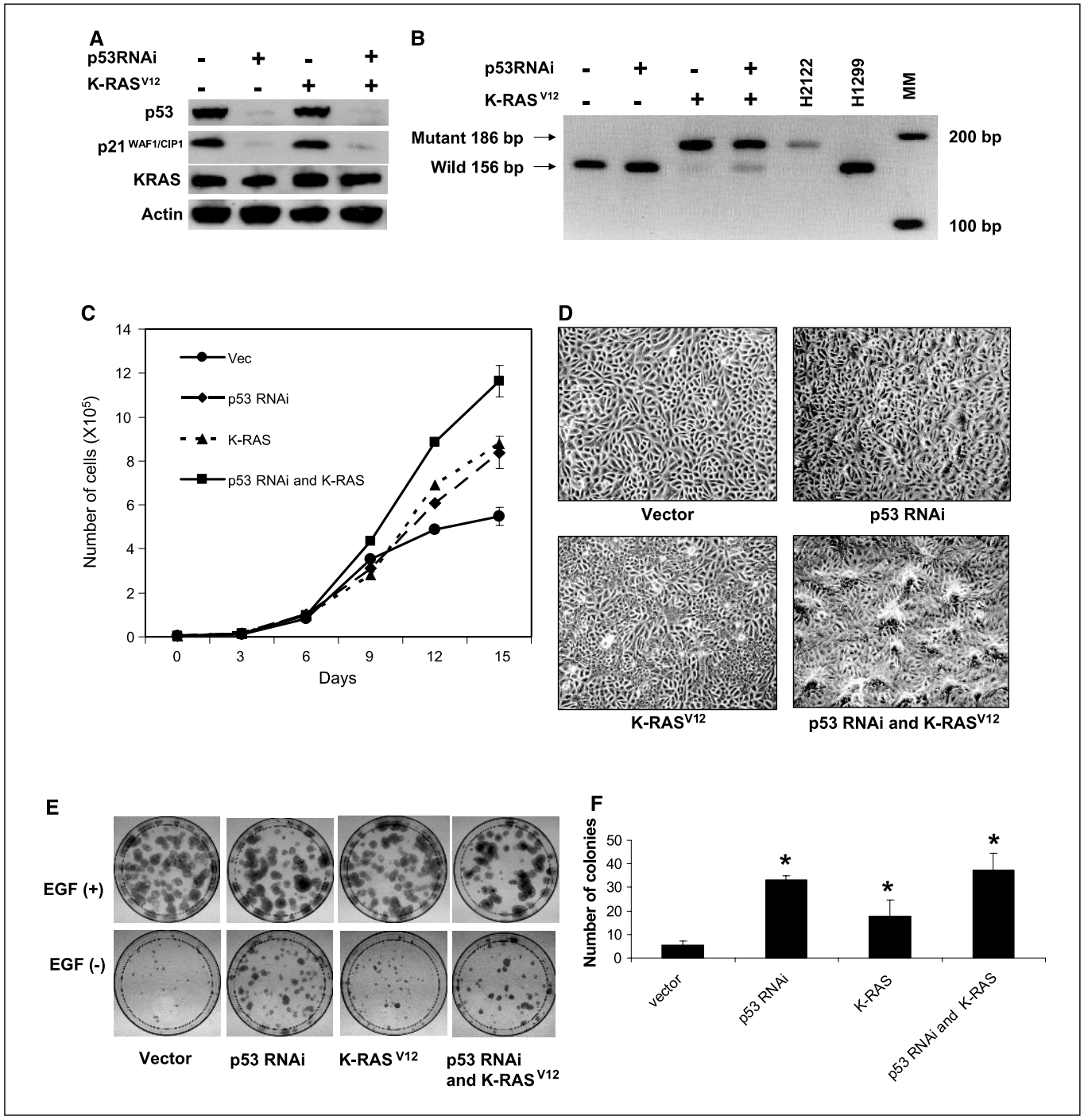

Figure 1. Characterization of p53 knocked down and K-RAS^{V12}–expressing HBEC3 cells. *A,* Western blots showing the suppression of p53, p21$^{WAF1/CIP1}$, and K-RAS in p53RNAi-, mutant K-RAS^{V12}–, and p53RNAi and mutant K-RAS^{V12}–expressing HBEC3 cells. p53 and p21$^{WAF1/CIP1}$ are clearly knocked down in p53RNAi-expressing cells, whereas the expression levels of K-RAS in K-RAS^{V12}–transfected and p53RNAi and K-RAS^{V12}–transfected HBEC3 cells approximate that of vector alone–transfected HBEC3 cells. *B,* RFLP analysis of K-RAS cDNA showing mutant K-RAS^{V12} transcripts are predominantly expressed in mutant K-RAS^{V12}–expressing and p53RNAi and mutant K-RAS^{V12}–expressing HBEC3 cells. H2122 and H1299 are used as positive controls for mutant K-RAS^{V12} and wild-type K-RAS, respectively. Brummelkamp et al. (18) reported a new vector system, named pSUPER, which generated small interfering RNAs in mammalian cells to functionally inactivate p53. Subsequently, they developed a retroviral version of pSUPER, named pSUPER.ret (pRS), to obtain stable knockdowns and showed stable and specific knockdown of oncogenic K-RAS^{V12} (17). To see the long-term effect of p53 inactivation, we used the pSUPER.ret system for p53 knockdown. Because a puromycin-resistant gene in pRS was already integrated in HBEC3 in the process of introducing Cdk4, we developed pRS-zeocin vector (pSRZ) by replacing the puromycin-resistant gene in pRS vector with a zeocin-resistant gene. Subsequently, the published p53 target small interfering RNA sequence was cloned into pSRZ (17, 18), yielding pSRZ-p53 vector. *C,* increased saturation density in p53 RNAi and mutant K-RAS^{V12}–expressing HBECs. HBEC3 cells (2,000) were cultured in triplicate 12-well plates and counted every 3 days. ●, vector–expressing HBEC3 cell; ◆, p53RNAi-expressing HBEC3 cells; ▲, mutant K-RAS^{V12}–expressing HBEC3 cells; ■, p53RNAi and mutant K-RAS^{V12}–expressing HBEC3 cells. *D,* cells were grown as described in (*C*) and pictures were taken on day 12. *E,* liquid colony formation assay for vector-, p53RNAi-, mutant K-RAS^{V12}–, and p53RNAi and mutant K-RAS^{V12}–expressing HBEC3 cells in the presence or absence of EGF (5 ng/mL). A total of 200 cells were plated per dish and cultured for 2 weeks before staining with methylene blue. *F,* quantitation of the number of colonies in the absence of EGF. *Columns,* mean of three independent experiments; *bars,* SD. *, $P < 0.01$, one-way ANOVA with Bonferroni's posttest.

DOI:10.1158/0008-5472.CAN-05-2521

Table 1. Tumorigenicity assay in nude mice for HBEC3 cells

Cell line	No. nude mice injected	No. cells per mouse	Observation period (d)	Percentage of tumors
NCI-H358	10	5×10^6	90	100
NCI-H441	5	5×10^6	61	100
NCI-H1299	40	5×10^6	17-38	100
HBEC3				
Nontreated	5	1×10^7	90	0
K-RAS^{V12}	5	5×10^6	90	0
p53RNAi	5	5×10^6	90	0
p53RNAi and K-RAS^{V12}	5	5×10^6	90	0
p53RNAi and K-RAS^{V12}	5	2.5×10^6	90	0
With Matrigel				
p53 RNAi and EGFR-L858R	5	2.5×10^6	90	0

ethidium bromide, and visualized by UV. NCI-H2122 cell line containing a endogenous mutant K-RAS at codon 12 was used as a control for *K-RAS^{V12}* allele, and NCI-H1299 cell was used as a control for the wild-type *K-RAS* allele.

***In vitro* and *in vivo* cell growth assays.** To determine growth curves, cells were cultured in triplicate wells in 12-well plates and counted every 3 days. Liquid colony formation assays were done as previously described (22). Briefly, 200 viable cells were plated in triplicate 100 mm plates and were cultured in K-SFM medium supplemented with 50 μg/mL bovine pituitary extract with or without 5 ng/mL EGF. To measure the effect of gefitinib or erlotinib, 1 μmol/L of each drug was added to the medium and the medium was replaced every 3 days. Surviving colonies were counted 14 days later after staining with methylene blue. For soft agar growth assays, 1,000 viable cells were suspended and plated in 0.37% Sea Kem agar (FMC, Philadelphia, PA) in K-SFM medium supplemented with 20% of fetal bovine serum and 50 μg/mL bovine pituitary extract with or without 5 ng/mL EGF in triplicate 12-well plates, and were layered over a 0.50% agar base in the same medium as the one used for suspending the cells. To measure

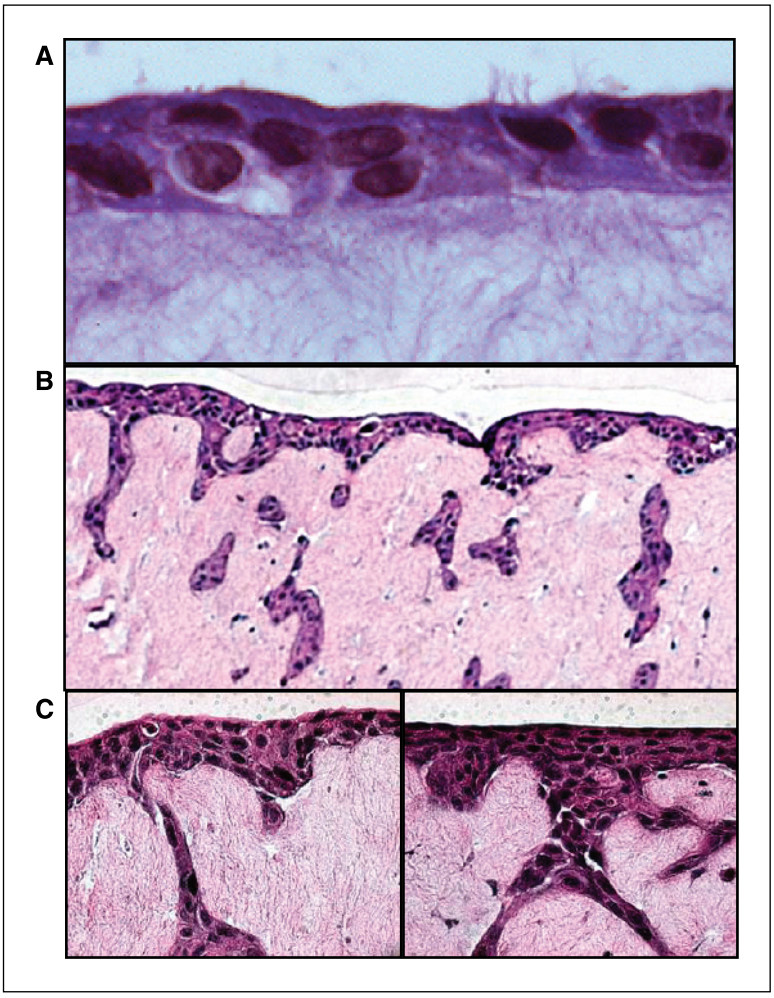

Figure 2. Effect of p53 knock down and mutant K-RAS^{V12} on three-dimensional organotypic culture of HBEC3 cells. *A,* stained paraffin cross-sections of organotypic cultures of HBEC3 cells showed that they formed a confluent layer of cells on the upper surface of the culture with the presence of cilia-like structures. Low-magnification (*B*) and high-magnification (*C*) p53RNAi and mutant K-RAS^{V12}–expressing HBEC3 cells showed a histologic change similar to metaplasia and dysplasia and they invaded into the fibroblast and collagen underlayer.

DOI:10.1158/0008-5472.CAN-05-2521

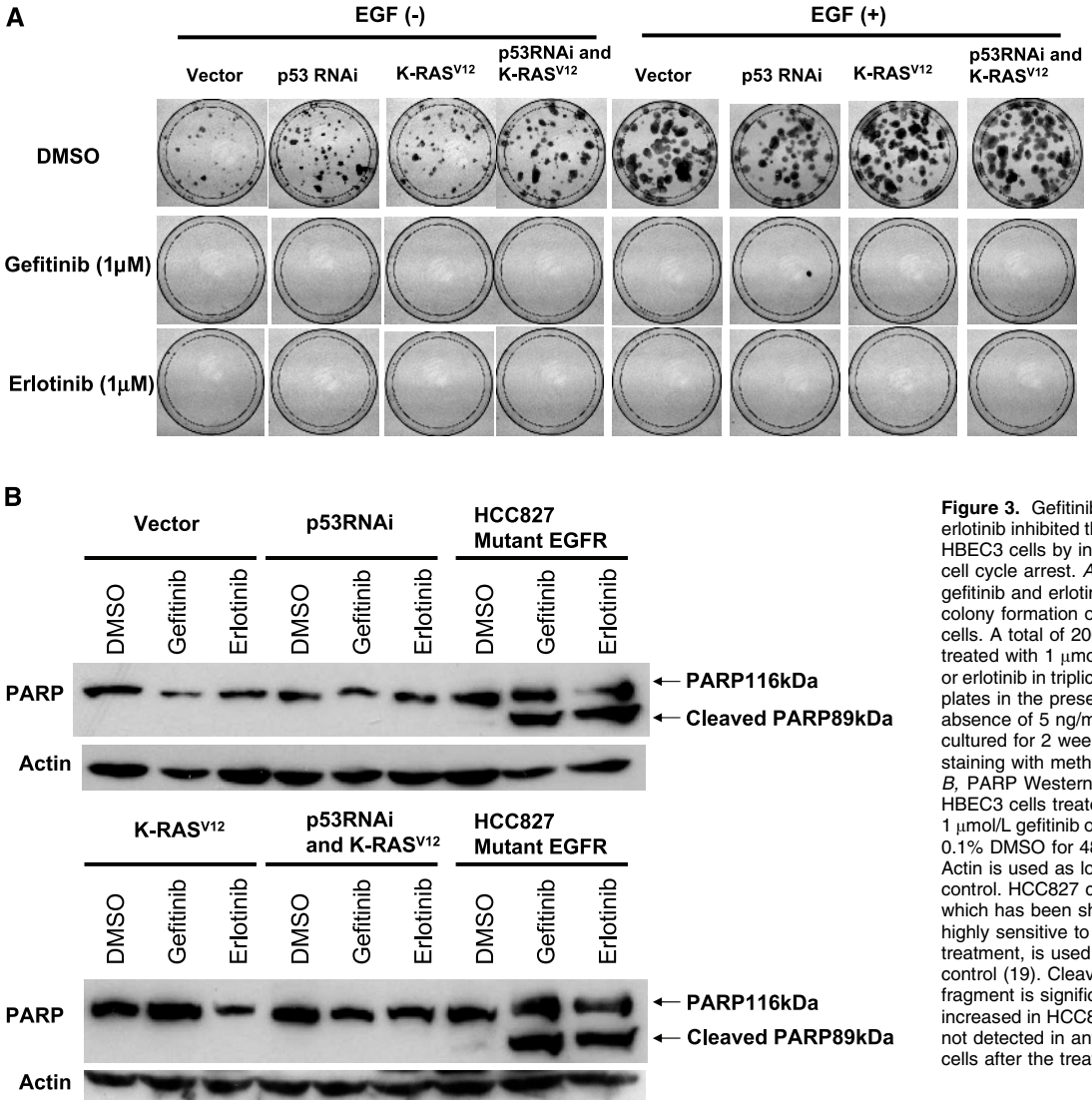

Figure 3. Gefitinib and erlotinib inhibited the growth of HBEC3 cells by inducing G_1 cell cycle arrest. *A,* effect of gefitinib and erlotinib on liquid colony formation of HBEC3 cells. A total of 200 cells were treated with 1 μmol/L gefitinib or erlotinib in triplicate 100 mm plates in the presence or the absence of 5 ng/mL EGF and cultured for 2 weeks before staining with methylene blue. *B,* PARP Western blot for HBEC3 cells treated with 1 μmol/L gefitinib or erlotinib or 0.1% DMSO for 48 hours. Actin is used as loading control. HCC827 cell line, which has been shown to be highly sensitive to gefitinib treatment, is used as positive control (19). Cleaved 89 kDa fragment is significantly increased in HCC827 cells but not detected in any of HBEC3 cells after the treatment.

the effect of gefitinib or erlotinib, 1 μmol/L of each drug was drug added to agar base layer. The number of microscopically visible colonies (>50 cells) was counted 4 weeks later. *In vivo* tumorigenicity was evaluated by injection of cells in nude mice. Male BALB/c nude (*nu/nu*) 3- to 6-week-old mice (Charles River Laboratories, Wilmington, DE) were irradiated on day 0 of the experiment in groups of five animals by a 5-minute exposure to 350 cGy from a cesium source. The next day, each mouse was given an injection s.c. on its flank 0.25×10^7 to 1×10^7 viable HBEC3 cells in 0.2 mL PBS containing different combinations of ectopically introduced genes. Coinjection of Matrigel (BD Bioscience, San Jose, CA) was also tested for HBEC3 cells expressing p53 RNA interference (RNAi) and K-RAS^{V12}. Mice were monitored every 2 to 3 days for tumor size. All animal care was in accord with institutional guidelines and approved Institutional Animal Care and Research Advisory Committee protocols. The NSCLC, NCI-H358, NCI-H441, and NCI-H1299 cell lines (5×10^6 cells) were used as positive controls.

Three-dimensional organotypic culture assay. Cultures were established as previously described for skin equivalents (23) except that airway fibroblasts were used in place of skin cells. Briefly, type I collagen and IMR90 fibroblasts were mixed and were allowed to polymerize. The collagen gels were released and incubated for a period of 4 to 10 days to allow the fibroblasts to contract the gels, creating a "submucosa." Cloning rings were then placed atop the gels and HBEC cells were plated into the rings at a concentration of $2 \times 10^5/cm^2$. After allowing the cells to attach for 4 hours, the rings were removed and organotypic cultures submerged for 4 days in keratinocyte feeder layer medium containing ascorbic acid, then emerged to the air-liquid interface for up to 28 days in culture, after which time the cultures were harvested, fixed, and prepared for histology. Organotypic cultures were immersed in 10% neutral buffered formalin overnight at 4°C followed by dehydration, paraffin embedding, and thin sectioning; 5 and 10 μM sections were then rehydrated and stained with H&E to view overall morphology (http://www.protocol-online.org/prot/Histology/Staining/). Stained slides were then viewed using an Axioscop-2 or Axioplan-2E microscope (Carl Zeiss, Thornwood, NY; www.zeiss.com) and photographed with Hamamatsu ORCA monochrome charge-coupled device camera (Hamamatsu, Bridgewater, NJ; www.hamamatsu.com).

Cell cycle analysis. Cells were harvested 48 hours after the treatment of 1 μmol/L gefitinib, erlotinib, or 0.1% DMSO, fixed with 70% ethanol, treated with 5 mg/mL RNase A (Roche Molecular Biochemicals), stained with 50 μg/mL propidium iodide, and analyzed by flow cytometry for DNA synthesis and cell cycle status [FACSCalibur instrument, (Becton Dickinson) with FlowJo software].

DOI:10.1158/0008-5472.CAN-05-2521

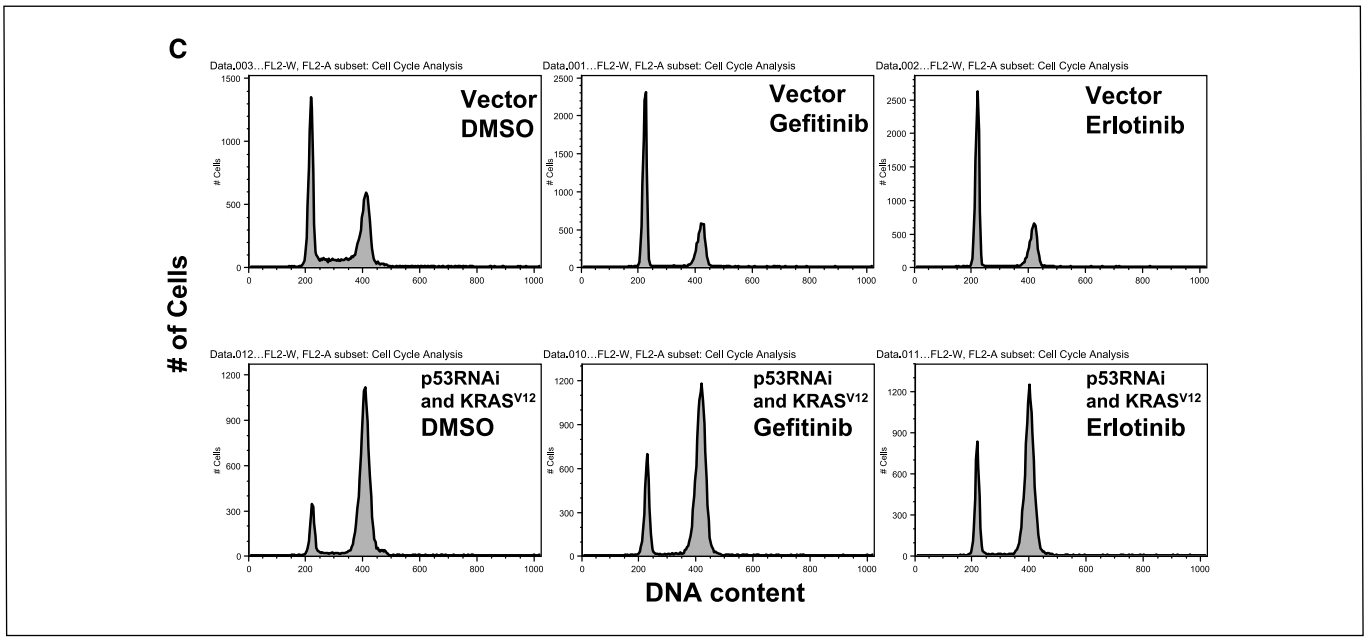

Figure 3 *Continued. C,* FACS profiles of vector (control) or p53 RNAi and mutant K-RAS^{V12}–expressing HBEC3 cells treated with 1 μmol/L of gefitinib or erlotinib or 0.1% DMSO for 48 hours. Cells were harvested after the treatment, stained with propidium iodide, and analyzed by using the flow cytometer. *X axis,* DNA content; *Y axis,* cell number. The fractions of cells in G_1 phase are significantly increased in both vector and the combined HBEC3 p53 knock down and mutant K-RAS cells, with the reduction of S-phase cells after the treatment of gefitinib or erlotinib. Compared with vector cells treated with DMSO, the combined HBEC3 p53 knockdown and mutant K-RAS cells treated with DMSO show a significant increase in G_2-M phase cells.

Microarray analysis. RNAs were labeled and hybridized to Affymetrix HG-U133-Plus2 GeneChips according to the protocol of the manufacturer (http://www.affymetrix.com). This array contains 54,675 genes (29,180 unique genes). Microarray analysis was done using Affymetrix MicroArray Suite 5.0 and in-house Visual Basic software MATRIX 1.26.

Real-time RT-PCR for DUSP6/MKP-3. The expression of *DUSP6/MKP-3* was analyzed by quantitative real-time RT-PCR. Primers were designed to ensure a single 107 bp amplicon using the standard Taqman assay-on-demand PCR protocol with a 10-minute hot start. Products were resolved on 2% agarose (Sigma). A probe sequence was designed using Primer-Express software (Applied Biosystems). The probe was labeled with TAMRA (quencher) and FAM (reporter) and synthesized by Integrated DNA Technologies. To establish the efficiency of this assay, we used a 5-fold serial dilution of cDNA over six concentrations. These samples were run on the Gene Amp 7700 Sequence Detection System (Applied Biosystems) in triplicate. The resultant curve had a slope of −3.396 and R^2 coefficient of 0.9939. For quantitative analysis of *DUSP6/MKP-3*, we used *GAPDH* (Applied Biosystems assay-on-demand) as an internal reference gene to normalize input cDNA. Quantitative real-time RT-PCR was done in a reaction volume of 25 μL, including 1 μL cDNA. We used the comparative C_t method to compute relative expression values.

Statistical analyses. For comparison of saturation density and colony formation between the different genetically manipulated cell strains, we used one-way ANOVA with Bonferroni's *post hoc* test correction and for comparisons of the effect of EGFR on growth the Mann-Whitney *U* test.

Results

RNAi-mediated p53 knockdown and K-RAS^{V12} introduction in HBEC3s. We used retroviral vector–mediated RNAi technology to generate HBEC3 clones stably knocked down for p53. HBEC3-expressing Cdk4 and hTERT cells were infected with pSRZ-p53 (see Materials and Methods and Fig. 1 caption), selected with zeocin, and tested for p53 and p21^{WAF1} protein expression. Western blot analysis showed clear suppression of p53 and p21^{WAF1} (Fig. 1*A*). Next, we introduced mutant K-RAS^{V12} into pSRZ-expressing and pSRZ-p53-expressing HBEC3 cells using pBabe-hyg-KRAS2-V12 retroviral vector followed by hygromycin selection. Western blot analysis showed that the expression levels of K-RAS in K-RAS^{V12}–transfected and p53RNAi and K-RAS^{V12}–transfected HBEC3 cells approximated that of vector alone–transfected HBEC3 cells (Fig. 1*A*). Because antibodies that recognize only wild or mutant K-RAS are not available, we did RT-PCR/RFLP analysis to distinguish between K-RAS^{V12} and wild-type K-RAS mRNA expression. The analysis revealed that mutant K-RAS^{V12} transcripts were the predominant form expressed in the K-RAS^{V12}–transfected HBEC3 alone or with p53 RNAi cells (Fig. 1*B*), indicating that most of the K-RAS protein expressed in HBEC3 cells infected with pBabe-hyg-KRAS2-V12 was the mutant form. We also did immunocytochemistry of p63 (a stem cell marker) and found that mutant K-RAS and/or p53 knockdown did not alter the p63 expression levels of HBEC3 cells (data not shown).

p53 knockdown and K-RAS^{V12} introduction into HBEC3s increase saturation density. We assessed the effect of p53 knockdown and expression of mutant K-RAS^{V12} on cell growth and found no significant difference in growth rate in the exponential growth phase between p53RNAi-expressing, K-RAS^{V12}-expressing, p53RNAi and K-RAS^{V12}–expressing, and vector-expressing HBEC3 cells. However, p53RNAi-expressing ($P < 0.01$), K-RAS^{V12}–expressing ($P < 0.01$), and p53RNAi and K-RAS^{V12}–expressing ($P < 0.001$) HBEC3 cells achieved significantly higher final saturation densities in confluent cultures compared with vector-transfected control (in all cases here and below using one-way ANOVA with Bonferroni's *post hoc* test; Fig. 1*C* and *D*). Also, the final density of the combined p53RNAi and K-RAS^{V12}–expressing HBEC3 cells was significantly higher than that of HBEC3 cells with either p53 knockdown ($P < 0.01$) or mutant K-RAS^{V12} ($P < 0.01$) alone (Fig. 1*C* and *D*). We conclude from these studies that introduction of these

DOI:10.1158/0008-5472.CAN-05-2521

Table 2. Soft agar colony formation assay for HBEC3 cells treated with gefitinib or erlotinib

	HBEC3			
	Vector	p53RNAi	K-RASV12	p53RNAi and K-RASV12
EGF(+)				
DMSO	1.3 ± 0.47	11 ± 1.6	5.7 ± 1.2	23 ± 2.1
Gefitinib (1 μmol/L)	0	0	0	0
Erlotinib (1 μmol/L)	0	0	0	0
EGF(−)				
DMSO	0	0	0	1.3 ± 0.94
Gefitinib (1 μmol/L)	0	0	0	0
Erlotinib (1 μmol/L)	0	0	0	0

NOTE: Number of colonies after 14 days are shown as average ± SD. HBEC3 cells (1,000) were plated in agar and treated with 1 μmol/L gefinitib or erlotinib in triplicate 12-well plates for up to 2 weeks in the presence or the absence of EGF and colonies (50-100 cells) were counted.

genetic changes produced part of the malignant phenotype, increased saturation density.

p53 knockdown and K-RAS^{V12} introduction permits anchorage-independent growth and partial bypass of EGF dependence. HBEC3 cells are able to form colonies in liquid medium but not in soft agar (i.e., they do not display anchorage-independent growth). We then tested the p53 and K-RAS^{V12}–manipulated variants to see if they had acquired this ability. In addition, because HBEC3 cells express robust levels of EGFR (Fig. 4*A*) and EGF is in the K-SFM synthetic medium, we tested the dependence of colony formation in liquid and semisolid medium on EGF. Supplementation of EGF dramatically enhanced liquid colony formation in all HBEC3 cells (Fig. 1*E*). In liquid colony formation in the presence of EGF, no significant difference in the number of colonies was seen between p53RNAi-expressing, K-RAS^{V12}–expressing, p53RNAi and K-RAS^{V12}–expressing, and vector-expressing HBEC3 cells. In contrast, there were significant differences in the number of colonies in the absence of EGF between these four strains (Fig. 1*F*). In the absence of EGF, p53RNAi-expressing (5.9 fold, $P < 0.001$) and p53RNAi and K-RAS^{V12}–expressing (6.6-fold, $P < 0.001$) HBEC3 cells formed a markedly increased number of colonies compared with vector control, whereas K-RAS^{V12}–expressing HBEC3 cells formed significantly increased (3.2-fold, $P < 0.001$) number of colonies compared with vector control (in all cases here and below using one-way ANOVA with Bonferroni's *post hoc* test; Fig. 1*F*). In the presence of EGF, p53RNAi-expressing, K-RAS^{V12}–expressing, and p53RNAi and K-RAS^{V12}–expressing HBEC3 cells formed a significantly increased number of soft agar colonies compared with vector control, 7.3-fold ($P < 0.001$), 6.7-fold ($P < 0.001$), and 16.5-fold ($P < 0.001$), respectively, whereas in the absence of EGF, p53 RNAi and p53RNAi and K-RAS^{V12}–expressing HBEC3 cells formed very few colonies (Fig. 4*C*). We conclude from these studies that introduction of these genetic changes led to anchorage-independent growth and both oncogenic K-RAS or p53 knockdown led to partial bypass of dependence on EGF. However, the cells still remain dependent on EGF signaling to express this anchorage-independent growth although an unexpected finding was the ability of p53 knockdown to partially alleviate this EGF dependence.

p53 knockdown and expression of mutant K-RAS^{V12} does not give a full malignant phenotype. In tumorigenicity assays, none of HBEC3 derivatives formed s.c. tumors in nude mice. Because Matrigel (BD Bioscience) accelerates tumor growth when coinjected with cells in athymic mice (24), we injected HBEC3 cells expressing p53 RNAi and K-RAS^{V12} together with Matrigel. However, even with Matrigel, the HBEC3 cells expressing p53 RNAi and

Table 3. Effect of gefitinib and erlotinib on cell cycle progression in HBEC3 cells

	Nontreated (DMSO)			Gefitinib/erlotinib		
	G_1	S	G_2-M	G_1	S	G_2-M
Vector	45.4 ± 0.2	27.5 ± 6.0	28.7 ± 3.9	76.6 ± 5.6*	2.6 ± 0.5†	28.0 ± 2.0
p53RNAi	41.4 ± 2.9	27.6 ± 3.7	31.0 ± 4.5	69.5 ± 0.2*	7.4 ± 2.8*	27.0 ± 3.4
K-RAS^{V12}	49.5 ± 6.3	31.7 ± 10.6	17.8 ± 12.2	81.4 ± 4.6*	7.7 ± 2.4	16.6 ± 2.8
p53RNAi and K-RAS^{V12}	12.9 ± 3.2	11.8 ± 6.2	73.7 ± 3.8	25.6 ± 4.8*	5.3 ± 1.2	70.8 ± 3.7

NOTE: Data are percentages (mean ± SD). Averaged values of three independent experiments are shown. Watson Pragmatic algorithm was used to calculate each cell cycle distribution. Because the algorithm contains approximations, the total of each distribution is not exactly 100%.
*$P < 0.01$ in comparison with the respective control.
†$P < 0.05$ in comparison with the respective control.

DOI:10.1158/0008-5472.CAN-05-2521

K-RAS^{V12} did not form tumors. In contrast, tests of 5×10^6 NSCLC, NCI-H358, NCI-H441, and NCI-H1299 cells reproductively formed progressively growing nude mouse xenograft tumors in the 17- to 90-day observation period (Table 1). We conclude from these studies that even with these gain-of-function and loss-of-function manipulations, a full malignant phenotype is not achieved (*in vivo* tumor formation).

Oncogenic manipulation leads to an invasive phenotype in a three-dimensional organotypic culture assay. To evaluate the effect of oncogenic manipulation in HBEC3s on their ability to differentiate and to invade, we did three-dimensional organotypic culture. HBEC3 cells only expressing hTERT and Cdk4 cells formed a confluent layer of cells on the upper surface of a fibroblast and collagen gel under layer and developed both ciliated (Fig. 2*A*) and mucous-producing cell types. In stark contrast, the cells expressing hTERT, Cdk4, K-RAS^{V12}, and p53 RNAi showed histologic change similar to metaplasia/dysplasia and they invaded into the fibroblast and collagen gel similar to cancer cells invading into the submucosal layer (Fig. 2*B* and *C*). We conclude from these studies that p53 knockdown and K-RAS^{V12} are additive in malignant transformation leading to the development of anchorage-independent growth and the ability to invade in a three-dimensional culture system.

Gefitinib and erlotinib inhibit proliferation and colony formation of HBEC3 cells by inducing G_1 cell cycle arrest. The dependency of HBEC3 cell on EGF signaling prompted us to investigate the effect of tyrosine kinase inhibitors, gefitinib and erlotinib, on cell proliferation in mass culture and colony formation of these cells. Both gefitinib and erlotinib at 1 μmol/L completely inhibited the mass culture proliferation of all HBEC3 cells both in the presence and the absence of EGF (data not shown). Gefitinib or erlotinib at 1 μmol/L also completely inhibited both anchorage-dependent and anchorage-independent colony formation in all HBEC3 cells (Fig. 3*A*; Table 2). Thus, although oncogenic manipulation partially relieved EGF dependence, EGF tyrosine kinase inhibitors remain potent inhibitors of HBEC growth. To investigate the mechanisms of this growth inhibition by tyrosine kinase inhibitors, we did apoptosis and cell cycle analyses. Western blot for PARP cleavage, an indicator of caspase-mediated apoptosis, showed that cleaved 89 kDa fragment was not detected in any of HBEC3 cells treated with tyrosine kinase inhibitors but was significantly increased in HCC827 EGFR mutant cells after the treatment with tyrosine kinase inhibitors for 48 hours (Fig. 3*B*). Cell cycle analysis also did not show sub-G_1 DNA fractions indicative of apoptosis in HBEC3 cells treated with tyrosine kinase inhibitors. Instead, the cell cycle analysis showed increase in the fraction of cells in G_1 phase in all the HBEC3 cells treated with either of the drugs, with reduction of S-phase cells (Fig. 3*C*; Table 3). These results suggest that growth inhibition for HBEC3 cells by tyrosine kinase inhibitors is mainly caused by G_1 cell cycle arrest and not apoptosis. Comparing the results of fluorescence-activated cell sorting (FACS) analysis for the control cells treated with DMSO, we found that the combined HBEC3 p53 knockdown and mutant K-RAS cells showed a significantly increase in G_2-M phase cells compared with either manipulation alone, suggesting dramatic cell cycle deregulation results from this oncogenic combination (Fig. 3*C*; Table 3).

Effect of K-RAS^{V12} and EGF supplementation on expression of phospho-EGFR, phospho-MEK, phospho-ERK, and phospho-Akt. We measured the expression of phosphorylated and total EGFR, mitogen-activated protein kinases (MAPK), and Akt proteins in the HBEC3 cells in the presence and absence of EGF. Addition of EGF resulted in massive induction of phospho-EGFR, a slight induction of phospho-ERK, and a modest induction of phospho-Akt^{Thr308} in all HBEC3 cells (Fig. 4*A*). In the absence of EGF, two immunoreactive phospho-MEK1/2 bands were detected whereas the faster migrating band was not detected in the presence of EGF, representing a shift to the hyper phosphorylated form (Fig. 4*A*). Surprisingly, introduction of K-RAS^{V12} did not show a significant effect on phosphorylation of MAPKs in the presence or absence of EGF but led to a slight increased phospho-Akt^{Thr308} in the absence of EGF (Fig. 4*A*). Also, surprisingly, both phospho-MEK1/2 and phospho-ERK were down-regulated in p53RNAi and K-RAS^{V12}–expressing HBEC3 cells compared with the other three cell lines in the absence of EGF (Fig. 4*A*).

Tyrosine kinase domain mutant EGFRs enhanced anchorage-independent growth of HBEC3 cells. EGFR with mutations in the tyrosine kinase domain have been discovered in lung cancers predominantly arising in never smokers (25). These mutant EGFRs are suspected as having oncogenic properties. To determine if mutant EGFRs commonly found in lung cancer (E746-A750, L858R) have oncogenic ability, we evaluated the tumorigenicity of wild-type and mutant EGFR transfected HBEC3s by soft agar colony formation assays. In the absence of EGF, E746-A750 del expressing HBEC3 cells formed significantly increased number of colonies compared with wild type–expressing cells in both p53 wild-type ($P < 0.001$ by Mann-Whitney *U* test) and p53 knocked down cells ($P < 0.01$ by Mann-Whitney *U* test), whereas L858R mutant-expressing HBEC3 cells increased the number of colonies only in p53 knocked down cells ($P < 0.001$ by Mann-Whitney *U* test; Fig. 4*C*). In contrast to p53 RNAi and mutant K-RAS–expressing HBEC3s that formed very few number of colonies (2.7 ± 2.0 of 1,000) in the absence of EGF, the E746-A750 del mutant transfectants formed substantial number of colonies even in the absence of EGF (Fig. 4*C*), suggesting that E746-A750 del mutant reduced the EGF dependence of HBEC3s in terms of anchorage-independent growth. Of interest, the L858R mutant only showed this independence when p53 was removed by knockdown (Fig. 4*C*). Again, in these p53 knocked down HBEC3s carrying a control vector (used for EGFR introduction), the cells remained dependent on EGF for soft agar growth. These results indicate that both types of mutant EGFRs possess oncogenic properties compared with wild-type EGFR. They also provide functional differences between the deletion and missense EGFR mutants, including differences in p53 interaction. We also did nude mice injection assays for p53 knocked down HBEC3s carrying L858R mutant, which formed the most number of colonies in the absence of EGF (Fig. 4*C*). However, they did not form tumor in nude mice (Table 1).

Introduction of both wild-type and mutant EGFR into HBEC3s resulted in constitutive activation of EGFR. Phosphorylation level of EGFR was evaluated by Western blotting with four (Y845, Y992, Y1045, and Y1068) phosphorylation-specific antibodies. To reduce the background for Western blotting, cells were first starved in the medium without bovine pituitary extract and EGF for 24 hours before harvest. In the absence of exogenous EGF, we found EGFR mutants and wild-type EGFR to exhibit induced levels of phosphorylated EGFR, suggesting the existence of autocrine ligands stimulating EGFR (Fig. 4*B*). In p53 wild-type cells, wild-type EGFR showed phosphorylation of Y845, Y992, and Y1068 to a lesser extent than when mutant EGFRs were present (Fig. 4*B*). In contrast, in p53 knocked down cells, such a difference

DOI:10.1158/0008-5472.CAN-05-2521

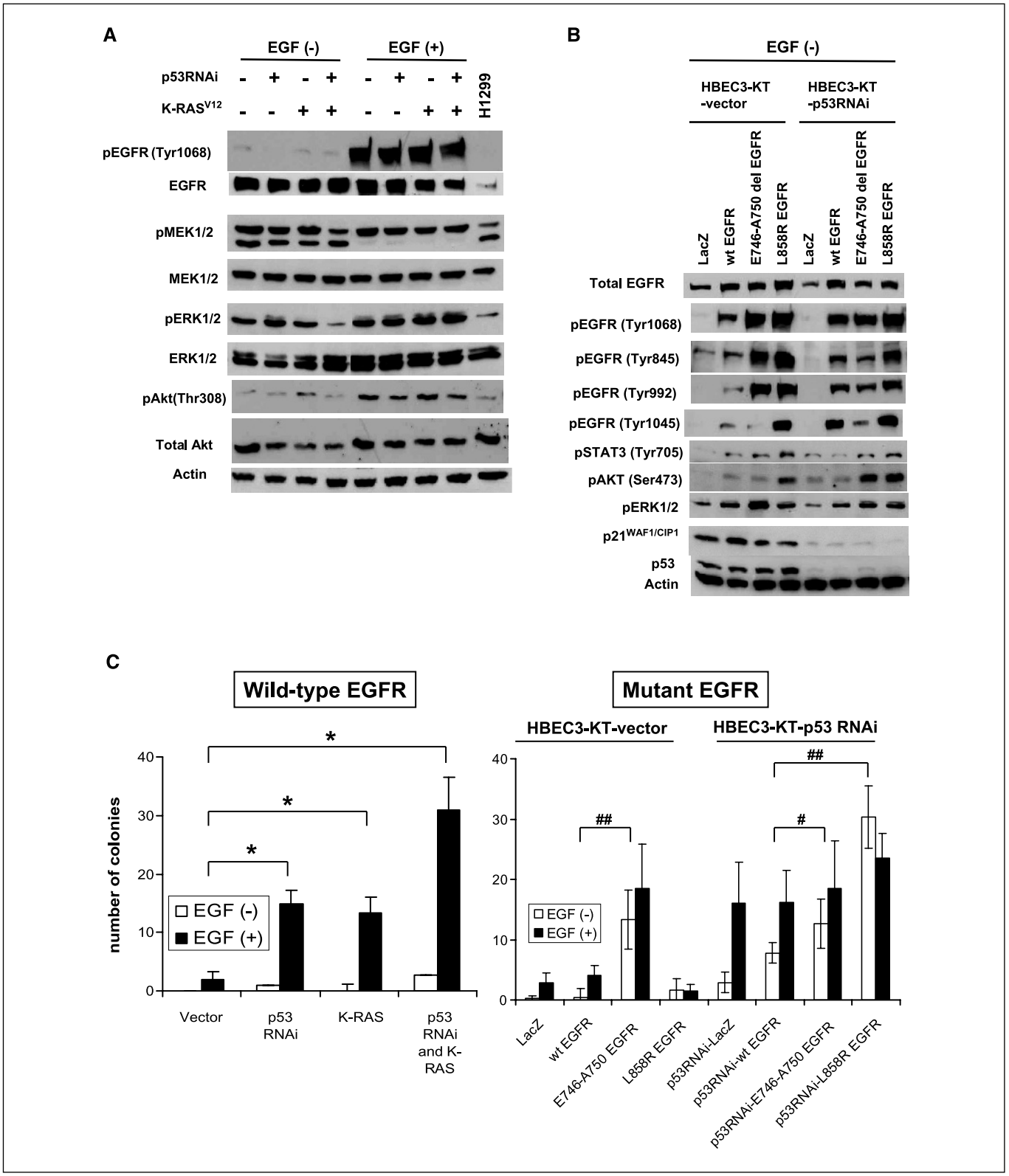

Figure 4. Transduction analysis for oncogenically manipulated HBEC3 cells. *A,* effect of K-RAS^{V12} and EGF supplementation on expression of phospho-EGFR, phospho-MEK, phospho-ERK, and phospho-Akt. HBEC3 cells were grown in the presence or absence of 5 ng/mL EGF and were immunoblotted to detect phospho-EGFR (*pEGFR*), EGFR, phospho-MEK1/2 (*pMEK1/2*), MEK1/2, phospho-ERK (*pERK*), ERK, phospho-Akt (*pAkt*; Thr^{308}), and Akt. Actin was used as loading control. *B,* effect of wild-type and mutant EGFR introduction on expression of phospho-EGFRs, phospho-STAT3, phospho-ERK, and phospho-Akt in HBEC3 cells. Wild type– or mutant EGFR–introduced HBEC3 cells were grown in the absence of EGF and were immunoblotted to detect phospho-EGFRs (Y1068, Y1045, Y992, and Y845), EGFR, phospho-STAT3, phospho-Akt (Y473), and phospho-ERK. Actin was used as loading control. *C,* soft agar colony formation assay for oncogenically manipulated HBEC3 cells. A total 1,000 of each HBEC3 cell strains were plated in agar and 4 weeks later microscopically visible colonies were counted. *Columns,* mean of three independent experiments; *bars,* SD. *, $P < 0.01$, one-way ANOVA with Bonferroni's posttest, #, $P < 0.01$, Mann-Whitney test; ##, $P < 0.001$, Mann-Whitney test.

DOI:10.1158/0008-5472.CAN-05-2521

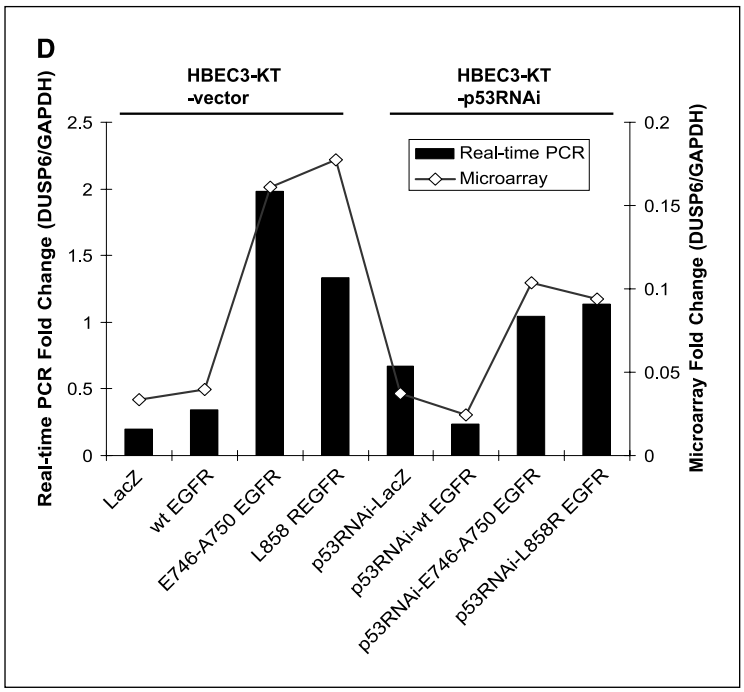

Figure 4 *Continued. D,* microarray analysis and real-time PCR validation for *DUSP6/MKP-3* gene. *Columns*, fold changes of the mRNA levels of *DUSP6/MKP-3* gene relative to those of *GAPDH* gene in HBEC3 cells transfected with wild-type or mutant EGFR.

was not seen (Fig. 4*B*). This result suggests that the activation of wild-type EGFR might be suppressed by p53. Interestingly, the Y1045 site was highly phosphorylated in L858R transfectants but not in E746-A750 del transfectant (Fig. 4*B*), indicating that Y1045 is unique in distinguishing between the two types of EGFR mutations (Fig. 4*B*).

AKT and STAT3 were phosphorylated at higher level in mutant EGFRs than wild-type EGFR. The EGFR L858R mutant showed increased level of phosphorylated Akt and STAT3 in both p53 wild-type and p53 knocked down cells, whereas the EGFR E746-A750 del mutant showed increased level of phosphorylated Akt only in p53 knocked down cells and slightly increased level of phosphorylated STAT3 in both p53 wild-type and p53 knocked down cells (Fig. 4*B*). By contrast, no significant difference in phosphorylated ERK was seen between wild-type and mutant EGFRs (Fig. 4*B*). These results suggest that mutant EGFRs selectively transduces signals through Akt and STAT3, which is consistent with previously reported data (26).

***DUSP6/MKP-3* gene was up-regulated in mutant EGFR transfected HBEC3 cells.** Microarray analysis for HBEC3 cells transfected with wild-type or mutant EGFRs shows that mRNA of DUSP6/MKP-3, whose protein is a dual-specificity phosphatase that dephosphorylate the active form of ERK (27, 28), is significantly up-regulated in mutant EGFR transfectants compared with wild-type and vector-transfected cells (Fig. 4*D*). Real-time PCR analysis for DUSP6/MKP-3 also showed this result (Fig. 4*D*).

Discussion

We have taken HBECs immortalized using overexpression of Cdk4 (to circumvent p16-mediated cell culture growth arrest) and hTERT (to prevent telomere erosion) and genetically manipulated them by stably knocking down p53, expressing oncogenic K-RAS^{V12} and mutant EGFR, alone or in combination. The results show that these additional genetic changes, commonly found in human lung cancer, progress the HBEC3 cells part, but not all, of the way toward malignancy. The human cells exhibit higher saturation density, anchorage-independent growth, invade in an organotypic culture assay but do not form tumors in mouse xenografts. Although, in general, the cells remain dependent on EGF, p53 knockdown and mutant EGFR reduce this EGF dependence. In addition, their growth and ability to form colonies in liquid and semisolid medium is dramatically reduced by EGFR-directed tyrosine kinase inhibitors. These studies indicate that more than four genetic alterations are required for the full cancer transformation of HBECs.

Several studies have reported that introduction of oncogenes, such as K-RAS or HRAS and c-myc, result in malignant transformation of HBECs (29–31). However, until the present study, there has not been immortalized cell lines with wild-type p53 function. (Prior studies were done with viral oncoprotein immortalized cells abrogating p53 function; refs. 11, 12, 29, 30, 32.) In the present study, we have shown that >90% inhibition of p53 protein in immortalized HBECs enhances the clonal and soft agar colony formation and results in partial loss of contact inhibition, indicating that loss of p53 function contributes importantly to the malignant progression of HBECs. In addition, the combination of p53 knockdown and oncogenic K-RAS^{V12} enhanced these changes further, suggesting these two genetic alterations have additive effects on tumorigenicity. Taken together, these results show that this model system provides a powerful new approach to assess the contribution of individual genetic alterations in HBECs in the malignant process.

RAS was first identified as an oncogene by virtue of its ability to overcome cell-to-cell contact inhibition of proliferation and this ability has been well documented in many types of cells (33, 34). In the present study, not only oncogenic K-RAS^{V12} but also p53 knockdown resulted in partial loss of contact inhibition and the combination of them enhanced this ability. Recently, Meerson et al. (35) reported results consistent with this finding. They showed that p53 knockdown in WI38 human embryonic lung fibroblasts

DOI:10.1158/0008-5472.CAN-05-2521

reduced density-dependent inhibition of growth by abolishing G_1 phase arrest. Although density-dependent inhibition of growth is a complex phenomenon and its precise mechanism is not well understood, this phenomenon is thought to be indicative of tumorigenic potential. Thus, their results and ours suggest that p53 may function as a tumor suppressor even when the cells are not under stresses, such as genotoxic damage and irradiation. Recently, other studies also reported that p53 function is involved in regulating cell motility and adhesion (36, 37).

It is unclear how the mutant K-RAS transfected HBECs preferentially express the mutant compared with wild-type *K-RAS* allele. These cells express mutant K-RAS mRNA predominantly without changing the total K-RAS protein levels, suggesting that wild-type K-RAS expression is suppressed at the transcriptional level in these cells. The mechanism of transcriptional regulation of K-RAS has not been fully elucidated and we are unable to explain the mechanism of this observation. However, the hypothesis that oncogenic RAS inhibits the transcription of wild-type RAS is compatible with our observations. Because the tumor suppressor function of wild-type K-RAS has been shown in mice, one possibility is that mutant RAS exerts its oncogenic ability in part by suppressing the expression of wild-type RAS. This hypothetical function of oncogenic RAS seems very attractive in terms of better understanding the mechanism of oncogenic RAS, and thus it will be of interest to further investigate these findings.

Previous studies have found high levels of EGFR expression in both immortalized and nonimmortalized HBECs (38). EGF supplementation also results in a slight increase of growth rate at normal cell density in HBECs (38). Several studies have shown the existence of an EGFR autocrine loop involving EGF, transforming growth factor-α, and amphiregulin in HBECs (39, 40). In addition, tobacco smoke induces proliferation of primary HBEC through an EGFR autocrine loop mediated by tumor necrosis factor-α–converting enzyme and amphiregulin, suggesting tobacco smoke induction of the EGFR autocrine loop in lung cancer pathogenesis (41). In the present study, we found that HBEC3 cells expressed high level of EGFR that was stimulated to phospho-EGFR with EGF whereas their colony-forming ability in both liquid and soft agar was highly dependent on EGF supplementation. Signal transduction studies in HBEC3 cells suggest that this may in part be due to the up-regulation of the Akt pathway. With p53 knockdown and K-RAS oncogenic manipulation, the EGF dependence was partially relieved, suggesting the potential for autocrine growth factor production. Thus, previous studies and our results suggest that EGF autocrine loop may play an important role in cell proliferation and tumorigenic progression of HBECs.

Gefitinib (Iressa) and erlotinib (Tarceva) are orally available tyrosine kinase inhibitors that target EGFR (42–45). Gefitinib has been approved as a third-line therapy for NSCLC patients. Erlotinib has been shown to be active and well tolerated in patients with NSCLC, providing survival benefit (46). Although these drugs are being developed as anticancer drugs, recent studies have shown that gefitinib inhibits cell proliferation in immortalized normal or precancerous breast cells, supporting its role as a chemopreventive agent (47). Because we found robust expression of EGFR in HBEC3 cells and their high dependency of growth on EGF, we considered the possibility that tyrosine kinase inhibitors are also effective in oncogenically manipulated HBEC3 cells. We observed that 1 μmol/L gefitinib or erlotinib dramatically inhibited both anchorage-dependent and anchorage-independent cell growth of HBEC3 cells. Apoptosis and cell cycle analyses showed that this inhibition was caused mainly by not apoptosis but G_1 cell cycle arrest, which is consistent with previous papers reporting that gefitinib and erlotinib induce G_1 cell cycle arrest in several types of cells (48–52). These results provide part of a preclinical rationale for the development of these drugs for the prevention of human lung cancer. It is important to point out that the concentrations used in the present studies are actually achieved in patients with current standard drug practices (53, 54). In addition, interestingly, we found that G_2-M fraction significantly increase with the combination of p53 knock down and mutant K-RAS cells compared with either oncogenic manipulation alone. We speculate that in the presence of intact p53 function, cell cycle progression induced by mutant K-RAS in HBECs is suppressed by the ability of p53 to induce G_1 arrest, whereas in the absence of p53, mutant K-RAS exerts its ability to progress the cell cycle from G_1 to S phases, resulting in significantly increased G_2-M phase fraction. Consistent with this hypothesis, one paper showed that ectopic expression of mutant N-RAS impaired the G_1 and G_2 cell cycle arrest only in p53-defective cells (55). In addition, it will be interesting to see whether similar types of cell cycle deregulation are also found when mutant EGFR is combined with loss of p53 function in these cells.

Introduction of tyrosine kinase domain EGFR mutants enhanced anchorage-independent growth of HBEC3s, providing evidence of their oncogenic properties. In addition, signal transduction analysis showed that they stimulated Akt and STAT3 but not Erk1/Erk2 signals, consistent with previously reported results (26). Our discovery of DUSP6/MKP-3 mRNA up-regulation in mutant EGFR transfectants provides an explanation for this. Because DUSP6/MKP-3 protein is a dual-specificity phosphatase that dephosphorylates the active form of ERK (27, 28), it is possible that Erk1/Erk2 phosphorylation in EGFR mutant cells is down-regulated by DUSP6/MKP-3. In addition, the findings that Akt and STAT3 were not highly phosphorylated in HBECs that showed robust level of phosphorylated EGFR suggests that a negative feedback regulatory pathway may be activated for Akt and STAT3 as well, and that the mutant EGFRs bypass this regulation.

Although p53 knockdown, K-RAS^{V12}, and mutant EGFR progress HBEC3 cells toward malignancy, the manipulated cells are not fully malignant. What additional genetic alterations are required for full malignant transformation in HBEC3 cells? For this question, there may be a clue from recent work of Hahn et al., who showed that defined genetic alterations, including the early region of the SV40 genome, the *hTERT* gene, and an oncogenic allele of H-ras, resulted in malignant transformation in human embryonic epithelial and fibroblast cells (56). By precisely analyzing the early region of SV40, they have shown that small T antigen, which is transcribed from the early region together with large T antigen, may play an important role in carcinogenesis. Small T antigen has been shown to bind and to target phosphatase 2A (PP2A), which regulates the RAS/MAPK cascade. Our unpublished studies have shown no mutation but frequent loss of PP2A expression in lung cancer, raising the possibility that PP2A is involved in lung carcinogenesis. Thus, a next step would be to inactivate PP2A in HBEC3 cells in addition to p53 knockdown and K-RAS^{V12}. It will also be of interest to introduce other genetic alterations observed in lung cancer, such as MYC family overexpression, FHIT inactivation, RASSF1A inactivation, and PTEN inactivation. Although we used a previously reported target sequence for p53 knockdown, which has also been used in several papers (17, 18, 57) and has no other BLAST hits, we are unable to completely exclude the possibility that off-target effects might affect our phenotypic analysis.

DOI:10.1158/0008-5472.CAN-05-2521

In conclusion, we have shown that using the immortalized HBEC model, p53 knockdown, K-RAS^{V12}, and mutant EGFR in the presence of p16 bypass and human telomerase contribute to lung cancer tumorigenesis, but additional genetic alterations are required for full malignant transformation of HBECs. In addition, we note that p53 knockdown relaxes the dependence on EGF in the presence of both wild-type and mutated EGFR. However, these oncogenically manipulated HBEC cells remain highly dependent on EGFR signaling for expression of key portion of the malignant phenotype. This dependence along with activated EGFR in bronchial preneoplasia suggests the use of EGFR inhibition by tyrosine kinase inhibitors as chemoprevention agents for lung cancer.

Acknowledgments

Received 7/18/2005; revised 11/22/2005; accepted 12/14/2005.

Grant support: Lung Cancer Specialized Programs of Research Excellence grants P50CA75907, CA71618, and NO1-CN-43301; Department of Defense VITAL grant W81XWH041014202PP; the Gillson Longenbaugh Foundation, and a NASA Specialized Center of Research (NSCOR) NNJ05HD36G.

The costs of publication of this article were defrayed in part by the payment of page charges. This article must therefore be hereby marked *advertisement* in accordance with 18 U.S.C. Section 1734 solely to indicate this fact.

References

1. Sekido Y, Fong KM, Minna JD. Molecular genetics of lung cancer. Annu Rev Med 2003;54:73–87.
2. Ramirez RD, Sheridan S, Girard L, et al. Immortalization of human bronchial epithelial cells in the absence of viral oncoproteins. Cancer Res 2004;64:9027–34.
3. Vaughan MB, Ramirez RD, Wright WE, Minna JD, Shay JW. A three-dimensional model of differentiation of immortalized human bronchial epithelial cells. Differentiation. In press 2006.
4. Geradts J. Abrogation of the RB-p16 tumor suppressor pathway in human lung cancer. Methods Mol Med 2003; 74:89–99.
5. Kaye FJ. RB and cyclin dependent kinase pathways: defining a distinction between RB and p16 loss in lung cancer. Oncogene 2002;21:6908–14.
6. Horikawa I, Barrett JC. Transcriptional regulation of the telomerase hTERT gene as a target for cellular and viral oncogenic mechanisms. Carcinogenesis 2003;24: 1167–76.
7. Meyerson M, Counter CM, Eaton EN, et al. hEST2, the putative human telomerase catalytic subunit gene, is up-regulated in tumor cells and during immortalization. Cell 1997;90:785–95.
8. Nakamura TM, Morin GB, Chapman KB, et al. Telomerase catalytic subunit homologs from fission yeast and human. Science 1997;277:955–9.
9. Nakayama J, Tahara H, Tahara E, et al. Telomerase activation by hTRT in human normal fibroblasts and hepatocellular carcinomas. Nat Genet 1998;18:65–8.
10. Kilian A, Bowtell DD, Abud HE, et al. Isolation of a candidate human telomerase catalytic subunit gene, which reveals complex splicing patterns in different cell types. Hum Mol Genet 1997;6:2011–9.
11. Reddel RR, Ke Y, Gerwin BI, et al. Transformation of human bronchial epithelial cells by infection with SV40 or adenovirus-12 SV40 hybrid virus, or transfection via strontium phosphate coprecipitation with a plasmid containing SV40 early region genes. Cancer Res 1988;48: 1904–9.
12. Lundberg AS, Randell SH, Stewart SA, et al. Immortalization and transformation of primary human airway epithelial cells by gene transfer. Oncogene 2002; 21:4577–86.
13. Barbacid M. ras genes. Annu Rev Biochem 1987;56: 779–827.
14. Bos JL. ras oncogenes in human cancer: a review. Cancer Res 1989;49:4682–9.
15. Paez JG, Janne PA, Lee JC, et al. EGFR mutations in lung cancer: correlation with clinical response to gefitinib therapy. Science 2004;304:1497–500.
16. Pao W, Miller V, Zakowski M, et al. EGF receptor gene mutations are common in lung cancers from "never smokers" and are associated with sensitivity of tumors to gefitinib and erlotinib. Proc Natl Acad Sci U S A 2004; 101:13306–11.
17. Brummelkamp TR, Bernards R, Agami R. Stable suppression of tumorigenicity by virus-mediated RNA interference. Cancer Cell 2002;2:243–7.
18. Brummelkamp TR, Bernards R, Agami R. A system for stable expression of short interfering RNAs in mammalian cells. Science 2002;296:550–3.
19. Amann J, Kalyankrishna S, Massion PP, et al. Aberrant epidermal growth factor receptor signaling and enhanced sensitivity to EGFR inhibitors in lung cancer. Cancer Res 2005;65:226–35.
20. Sato M, Girard L, Sekine I, et al. Increased expression and no mutation of the Flap endonuclease (FEN1) gene in human lung cancer. Oncogene 2003;22:7243–6.
21. Nishikawa T, Maemura K, Hirata I, et al. A simple method of detecting K-ras point mutations in stool samples for colorectal cancer screening using one-step polymerase chain reaction/restriction fragment length polymorphism analysis. Clin Chim Acta 2002; 318:107–12.
22. Burbee DG, Forgacs E, Zochbauer-Muller S, et al. Epigenetic inactivation of RASSF1A in lung and breast cancers and malignant phenotype suppression. J Natl Cancer Inst 2001;93:691–9.
23. Vaughan MB, Ramirez RD, Brown SA, Yang JC, Wright WE, Shay JW. A reproducible laser-wounded skin equivalent model to study the effects of aging *in vitro*. Rejuvenation Res 2004;7:99–110.
24. Fridman R, Giaccone G, Kanemoto T, Martin GR, Gazdar AF, Mulshine JL. Reconstituted basement membrane (Matrigel) and laminin can enhance the tumorigenicity and the drug resistance of small cell lung cancer cell lines. Proc Natl Acad Sci U S A 1990;87: 6698–702.
25. Shigematsu H, Lin L, Takahashi T, et al. Clinical and biological features associated with epidermal growth factor receptor gene mutations in lung cancers. J Natl Cancer Inst 2005;97:339–46.
26. Sordella R, Bell DW, Haber DA, Settleman J. Gefitinib-sensitizing EGFR mutations in lung cancer activate anti-apoptotic pathways. Science 2004;305:1163–7.
27. Muda M, Boschert U, Dickinson R, et al. MKP-3, a novel cytosolic protein-tyrosine phosphatase that exemplifies a new class of mitogen-activated protein kinase phosphatase. J Biol Chem 1996;271:4319–26.
28. Groom LA, Sneddon AA, Alessi DR, Dowd S, Keyse SM. Differential regulation of the MAP, SAP and RK/p38 kinases by Pyst1, a novel cytosolic dual-specificity phosphatase. EMBO J 1996;15:3621–32.
29. Reddel RR, Ke Y, Kaighn ME, et al. Human bronchial epithelial cells neoplastically transformed by v-Ki-ras: altered response to inducers of terminal squamous differentiation. Oncogene Res 1988;3:401–8.
30. Ura H, Bonfil RD, Reich R, et al. Expression of type IV collagenase and procollagen genes and its correlation with the tumorigenic, invasive, and metastatic abilities of oncogene-transformed human bronchial epithelial cells. Cancer Res 1989;49:4615–21.
31. Yoakum GH, Lechner JF, Gabrielson EW, et al. Transformation of human bronchial epithelial cells transfected by Harvey ras oncogene. Science 1985;227: 1174–9.
32. Reddel RR, Salghetti SE, Willey JC, et al. Development of tumorigenicity in simian virus 40-immortalized human bronchial epithelial cell lines. Cancer Res 1993; 53:985–91.
33. Hurlin PJ, Fry DG, Maher VM, McCormick JJ. Morphological transformation, focus formation, and anchorage independence induced in diploid human fibroblasts by expression of a transfected H-ras oncogene. Cancer Res 1987;47:5752–7.
34. Kinch MS, Clark GJ, Der CJ, Burridge K. Tyrosine phosphorylation regulates the adhesions of ras-transformed breast epithelia. J Cell Biol 1995;130:461–71.
35. Meerson A, Milyavsky M, Rotter V. p53 mediates density-dependent growth arrest. FEBS Lett 2004;559: 152–8.
36. Alexandrova A, Ivanov A, Chumakov P, Kopnin B, Vasiliev J. Changes in p53 expression in mouse fibroblasts can modify motility and extracellular matrix organization. Oncogene 2000;19:5826–30.
37. Sablina AA, Chumakov PM, Kopnin BP. Tumor suppressor p53 and its homologue p73α affect cell migration. J Biol Chem 2003;278:27362–71.
38. Tsao MS, Zhu H, Viallet J. Autocrine growth loop of the epidermal growth factor receptor in normal and immortalized human bronchial epithelial cells. Exp Cell Res 1996;223:268–73.
39. Plowman GD, Green JM, McDonald VL, et al. The amphiregulin gene encodes a novel epidermal growth factor-related protein with tumor-inhibitory activity. Mol Cell Biol 1990;10:1969–81.
40. Cook PW, Mattox PA, Keeble WW, et al. A heparin sulfate-regulated human keratinocyte autocrine factor is similar or identical to amphiregulin. Mol Cell Biol 1991; 11:2547–57.
41. Lemjabbar H, Li D, Gallup M, Sidhu S, Drori E, Basbaum C. Tobacco smoke-induced lung cell proliferation mediated by tumor necrosis factor α-converting enzyme and amphiregulin. J Biol Chem 2003;278:26202–7.
42. Glover KY, Perez-Soler R, Papadimitradopoulou VA. A review of small-molecule epidermal growth factor receptor-specific tyrosine kinase inhibitors in development for non-small cell lung cancer. Semin Oncol 2004; 31:83–92.
43. Perez-Soler R. The role of erlotinib (Tarceva, OSI 774) in the treatment of non-small cell lung cancer. Clin Cancer Res 2004;10:4238–40s.
44. Ciardiello F, Caputo R, Bianco R, et al. Antitumor effect and potentiation of cytotoxic drugs activity in human cancer cells by ZD-1839 (Iressa), an epidermal growth factor receptor-selective tyrosine kinase inhibitor. Clin Cancer Res 2000;6:2053–63.
45. Wakeling AE, Guy SP, Woodburn JR, et al. ZD1839 (Iressa): an orally active inhibitor of epidermal growth factor signaling with potential for cancer therapy. Cancer Res 2002;62:5749–54.
46. Perez-Soler R, Chachoua A, Hammond LA, et al. Determinants of tumor response and survival with erlotinib in patients with non-small-cell lung cancer. J Clin Oncol 2004;22:3238–47.
47. Lu C, Speers C, Zhang Y, et al. Effect of epidermal growth factor receptor inhibitor on development of estrogen receptor-negative mammary tumors. J Natl Cancer Inst 2003;95:1825–33.
48. Di Gennaro E, Barbarino M, Bruzzese F, et al. Critical role of both p27KIP1 and p21CIP1/WAF1 in the antiproliferative effect of ZD1839 ("Iressa"), an epidermal growth factor receptor tyrosine kinase inhibitor, in head and neck squamous carcinoma cells. J Cell Physiol 2003;195:139–50.
49. Sgambato A, Camerini A, Faraglia B, et al. Targeted inhibition of the epidermal growth factor receptor-tyrosine kinase by ZD1839 ("Iressa") induces cell-cycle arrest and inhibits proliferation in prostate cancer cells. J Cell Physiol 2004;201:97–105.

DOI:10.1158/0008-5472.CAN-05-2521

50. Shintani S, Li C, Mihara M, et al. Gefitinib ("Iressa", ZD1839), an epidermal growth factor receptor tyrosine kinase inhibitor, up-regulates p27KIP1 and induces G_1 arrest in oral squamous cell carcinoma cell lines. Oral Oncol 2004;40:43–51.

51. Chang GC, Hsu SL, Tsai JR, et al. Molecular mechanisms of ZD1839-induced G_1-cell cycle arrest and apoptosis in human lung adenocarcinoma A549 cells. Biochem Pharmacol 2004;68:1453–64.

52. Chinnaiyan P, Huang S, Vallabhaneni G, et al. Mechanisms of enhanced radiation response following epidermal growth factor receptor signaling inhibition by erlotinib (Tarceva). Cancer Res 2005;65:3328–35.

53. Zhang W, Siu LL, Moore MJ, Chen EX. Simultaneous determination of OSI-774 and its major metabolite OSI-420 in human plasma by using HPLC with UV detection. J Chromatogr B Analyt Technol Biomed Life Sci 2005;814:143–7.

54. Ranson M, Wardell S. Gefitinib, a novel, orally administered agent for the treatment of cancer. J Clin Pharm Ther 2004;29:95–103.

55. Agapova LS, Ivanov AV, Sablina AA, et al. P53-dependent effects of RAS oncogene on chromosome stability and cell cycle checkpoints. Oncogene 1999;18:3135–42.

56. Hahn WC, Dessain SK, Brooks MW, et al. Enumeration of the simian virus 40 early region elements necessary for human cell transformation. Mol Cell Biol 2002;22:2111–23.

57. Duursma A, Agami R. p53-Dependent regulation of Cdc6 protein stability controls cellular proliferation. Mol Cell Biol 2005;25:6937–47.

Primary Oncocytic Adenocarcinomas of the Lung

A Clinicopathologic, Immunohistochemical, and Molecular Biologic Analysis of 16 Cases

Luisa M. Solis, MD,[1] M. Gabriela Raso, MD,[1] Neda Kalhor, MD,[1] Carmen Behrens, MD,[2] Ignacio I. Wistuba, MD,[1,2] and Cesar A. Moran, MD[1]

Key Words: Oncocytic; Lung; Adenocarcinoma; Immunohistochemistry; Carcinoma

DOI: 10.1309/AJCPOQWPT1T1AJFT

Abstract

Sixteen cases of primary oncocytic adenocarcinomas of the lung are reported. The patients were 11 women and 5 men between the ages of 47 and 81 years (median, 75 years) with symptoms of cough, chest pain, and shortness of breath. Surgical staging disclosed 14 patients (88%) with stage I disease, 1 (6%) with stage II, and 1 (6%) with stage III. Histologically, all the cases displayed prominent oncocytic features with conventional growth patterns, including acinar, papillary, and bronchioloalveolar. Immunohistochemically, the tumors displayed positive staining for keratin 7, thyroid transcription factor-1, and mitochondrial antibody. Molecular studies showed 3 (20%) of 15 tumors with EGFR *mutations and 3 additional cases with* KRAS *mutations. Clinical follow-up of at least 24 months was obtained in all patients and showed that 5 patients had recurrences, 2 patients died of tumor, and 2 other patients died of unrelated conditions. These cases represent an unusual variant of pulmonary adenocarcinoma.*

Lung cancer is the most common cause of cancer-related mortality worldwide, and adenocarcinoma is currently the most common histologic subtype.[1] Conventionally, adenocarcinomas have been grouped into 3 distinct grades including well, moderately, and poorly differentiated. In addition, several distinct patterns of growth have been reported, including mucinous, papillary, micropapillary, hepatoid, and signet-ring cell among others.[2-13] However, primary oncocytic adenocarcinomas of the lung have not been addressed as a specific clinicopathologic entity. Oncocytic neoplasms are well recognized and accepted in other organ systems, including the salivary gland, thyroid, and kidney, where these tumors appear to be more common. Needless to say, owing to the unusual occurrence and lack of proper recognition, the presence of an oncocytic adenocarcinoma in the lung will inevitably lead to the possibility of metastatic disease to the lung.

Herein, we describe 16 primary oncocytic adenocarcinomas of the lung, which we consider represent a specific clinicopathologic entity and one that needs to be recognized and not mistaken for metastatic disease to the lung.

Materials and Methods

Sixteen cases of primary oncocytic adenocarcinomas of the lung represent the basis for this report. The cases were found in the files of the department of pathology at the M.D. Anderson Cancer Center, Houston, TX, during a review of 566 cases of primary adenocarcinomas of the lung in an 8-year period (1997 to 2005). All cases represent complete surgical resections, and no biopsy material was included. All available histologic material was reviewed, which included

3 to 22 H&E-stained glass slides of tumor. Detailed clinical and pathologic information was available in all cases, including demographic data, smoking history, clinical and surgical staging, overall survival, and recurrence data. Paraffin blocks were available in 14 cases to perform immunohistochemical studies and molecular analysis.

All tumors were evaluated following the subclassification proposed by the World Health Organization,[14] and, in addition, the percentage of necrosis and mitotic index were recorded in each case. The main criterion for inclusion in this study was more than 50% oncocytic differentiation in any of the recognized growth patterns. For immunohistochemical studies, antibodies for cytokeratin 7 (clone OV-TL 12/30, catalog No. M7018, dilution 1:100; DakoCytomation, Glostrup, Denmark), cytokeratin 20 (clone Ks 20.8, catalog No. M7019, dilution 1:100; DakoCytomation), thyroglobulin (polyclonal, catalog No. A0251, dilution 1:200; DakoCytomation), thyroid transcription factor (TTF)-1 (clone 8G7G3/1, catalog No. M3575, dilution 1:200; DakoCytomation), mitochondrial antigen (clone 113, catalog No. MU213-c, dilution 1:500; BioGenex, San Ramon, CA), dendritic cell lysosome-associated membrane protein (DC-LAMP [CD208], clone 104. G4, catalog No. IM-3448, dilution 1:50; Beckman Coulter, Fullerton, CA), and surfactant protein A (clone PE-10, catalog No. MS-703, dilution 1:150; Lab Vision, Fremont, CA) were evaluated in 14 tumors. Cytoplasmic staining was evaluated for cytokeratins 7 and 20 and nuclear staining for TTF-1, while granular or "spaghetti-like" cytoplasmic staining was used for mitochondrial antigen. The scoring system used was as follows: 0, no staining; 1+, weakly detectable staining; 2+, easily identifiable staining; and 3+, for dark, strong staining.

Molecular studies included *EGFR* mutation analysis of exons 18 through 21 and *KRAS* mutation analysis of exons 1 and 2 with polymerase chain reaction (PCR) amplification using intron-based primers, as previously described, using approximately 200 microdissected cells for each PCR amplification test.[15,16] All PCR products were directly sequenced using the Applied Biosystems PRISM dye terminator cycle sequencing method (Applied Biosystems, Foster City, CA). All sequence variants were confirmed by independent PCR amplification from at least 2 independent microdissections and DNA extraction and sequenced in both directions, as previously reported.[15,16]

After each of the aforementioned studies was performed, the 16 cases were further evaluated with the respective results. All cases selected on histologic evaluation were reevaluated after immunohistochemical and molecular biologic studies were completed.

Results

Clinical Features

The most important clinical features are given in **Table 1**. The patients included 11 women and 5 men between the ages of 47 and 81 years (median, 75 years; mean, 71 years). Of the 16 patients, 14 (88%) are tobacco users (10 former users and 4 current users), and 2 patients never used tobacco. Common symptoms for all patients included cough, shortness of breath, and chest pain. None of the patients had a history of malignancy elsewhere. Radiologically, all the patients were

Table 1
Clinicopathologic Characteristics and Follow-up of 16 Cases of Primary Oncocytic Lung Adenocarcinoma

Case No./ Sex/Age (y)	Surgical Procedure	Lobe	Tumor Localization	Tumor Size (cm)	Stage	Smoking Status	Recurrence (mo)	Outcome (mo)
1/M/78	Lobectomy	Left	Peripheral	2.1	IB	Former	Yes (14.55)	DOD (15.4)
2/F/74	Wedge resection	Left	Peripheral	1.3	IIIA	Former	Yes (3.6)	Died (7.0)
3/M/62	Wedge resection	Left	Peripheral	1.5	IA	Former	No	DOD (30.7)
4/F/76	Lobectomy	Left	Peripheral	3.8	IB	Former	No	Alive (61.1)
5/F/81	Lobectomy	Left	Perihilar	2.3	IA	Former	No	Alive (57.0)
6/F/74	Lobectomy	Right	Peripheral	1.2	IA	Current	No	Alive (48.1)
7/F/78	Lobectomy	Right	Peripheral	2.5	IB	Current	No	Alive (44.7)
8/M/75	Lobectomy	Right	Peripheral	2.3	IB	Former	Yes (32.1)	Alive (49.4)
9/F/65	Lobectomy	Left	Peripheral	2.0	IB	Former	Yes (9.7)	Alive (45.1)
10/F/75	Lobectomy	Right	Peripheral	3.5	IB	Current	No	Alive (37.5)
11/F/47	Wedge resection	Right	Peripheral	2.0	IA	Former	No	Alive (34.9)
12/M/79	Lobectomy	Left	Peripheral	3	IA	Former	No	DUC (44.9)
13/F/79	Lobectomy	Left	Peripheral	2.5	IA	Never	No	Alive (79.7)
14/F/54	Lobectomy	Right	Peripheral	2	IB	Current	No	Alive (92.1)
15/F/67	Lobectomy	Left	Peripheral	1.8	IA	Never	No	Alive (45.7)
16/M/76	Lobectomy	Right	Peripheral	4.9	IIB	Former	Yes (19.5)	Died (46.8)

DOD, died of other disease; DUC, died of unknown cause.

DOI: 10.1309/AJCPOQWPT1T1AJFT

shown to have an intrapulmonary mass, and all patients underwent surgical resection of the tumor mass. Of the patients, 13 patients underwent lobectomy and 3 underwent wedge resection as initial treatment. Disease stage was as follows: stage I, 14; stage II, 1; and stage III, 1.

Macroscopic Features

Of the tumors, 15 tumors were in the periphery of the lung parenchyma and 1 in the pulmonary hilum. In 1 case, there were 2 distinct contiguous tumor nodules, whereas in the remaining cases, there was a single pulmonary mass. The left lung was the site of 9 tumors, and 7 were located in the right lung. The tumors were described as well circumscribed, light tan, with and without areas of necrosis and/or hemorrhage. The tumors varied in size from 1.2 to 4.9 cm in greatest diameter.

Histologic Features

The 16 oncocytic adenocarcinomas were grouped in the conventional 3-tier category, showing 5 well-differentiated, 7 moderately differentiated, and 4 poorly differentiated adenocarcinomas. Four distinct growth patterns were observed in these adenocarcinomas: acinar, solid, papillary, and bronchioloalveolar in different percentages in a given tumor **Table 2**, **Image 1**, **Image 2**, **Image 3**, **Image 4**, **Image 5**, **Image 6**, and **Image 7**. A mixture of growth patterns was observed

Table 2
Tumor Growth Pattern Analysis of 16 Primary Oncocytic Lung Adenocarcinomas

Case No.	Subtype	Acinar (%)	Bronchioloalveolar (%)	Papillary (%)	Solid (%)
1	Mixed	90	0	0	10
2	Mixed	60	0	0	40
3	Mixed	70	0	30	0
4	Mixed	50	50	0	0
5	Mixed	10	10	80	0
6	Mixed	60	0	40	0
7	Mixed	60	40	0	0
8	Mixed	75	10	5	10
9	Acinar	100	0	0	0
10	Mixed	90	0	10	0
11	Acinar	100	0	0	0
12	Mixed	60	0	40	0
13	Acinar	100	0	0	0
14	Acinar	100	0	0	0
15	Mixed	95	5	0	0
16	Mixed	20	0	0	80

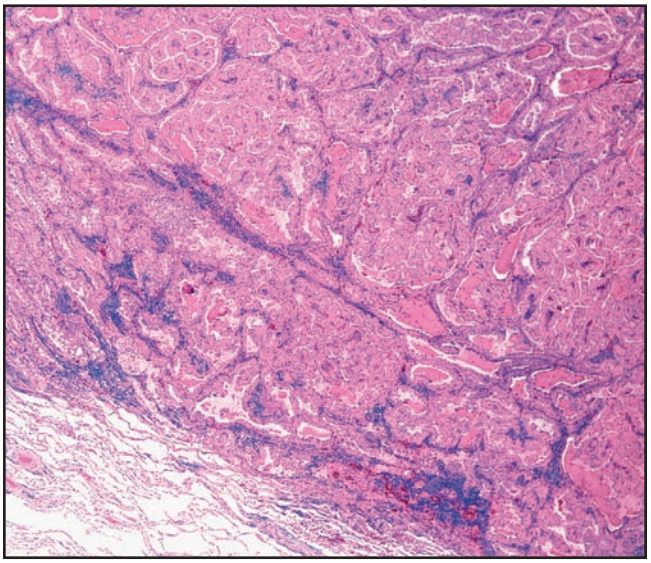

Image 1 Low-power view of an oncocytic adenocarcinoma with prominent papillary features (H&E, ×2).

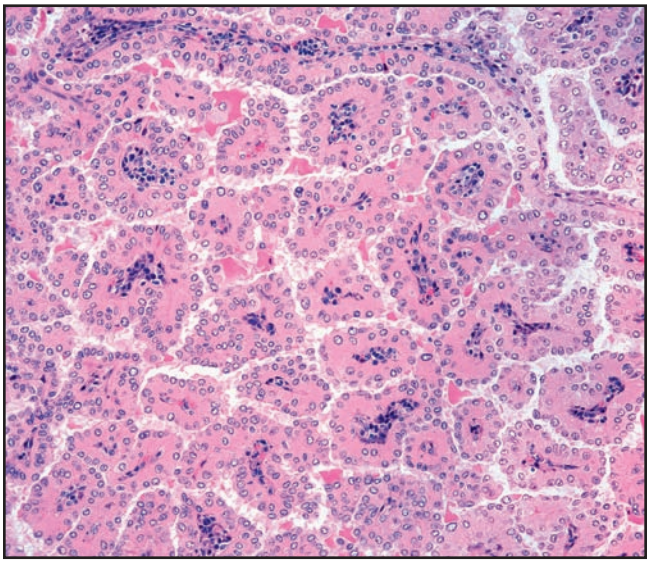

Image 2 Oncocytic papillary adenocarcinoma showing papillary structures with a homogeneous cellular proliferation (H&E, ×20).

DOI: 10.1309/AJCPOQWPT1T1AJFT

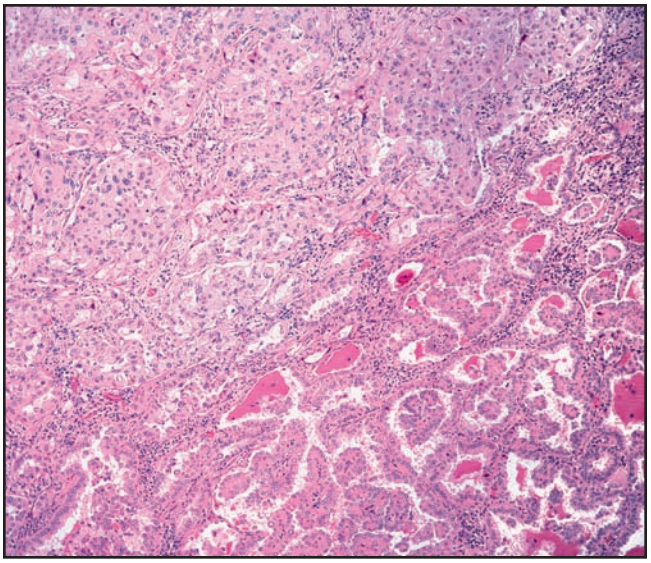

Image 3 Oncocytic adenocarcinoma showing a mixture of patterns, papillary and acinar (H&E, ×10).

in 12 cases, whereas only 4 tumors showed a single growth pattern. However, regardless of the growth pattern, the salient feature of all of these tumors was that they were composed of medium-sized cells with ample eosinophilic "oncocytic" cytoplasm, round nuclei, and conspicuous nucleoli. In some areas, larger polygonal cells resembling "oncoblasts" were also present. In tumors with a papillary pattern, the growth pattern resembled that described in the oncocytic variant of papillary carcinoma of the thyroid, ie, the presence of a prominent papillary configuration with anastomosing cords of neoplastic cells with little intervening stroma, whereas in tumors with a solid pattern, there were sheets of neoplastic cells without any particular arrangement. It is interesting that in some tumors, a prominent bronchioloalveolar pattern was also identified. Areas of necrosis were observed in 7 cases that ranged from approximately 10% to 50%, whereas mitotic figures ranged from 1 to 8 mitotic figures per 10 high-power fields.

Immunohistochemical Features

Immunohistochemical studies were performed in 14 cases. All tumors studied showed positive staining for cytokeratin 7 and for TTF-1 **Image 8A**, whereas thyroglobulin was negative in all cases. Cytokeratin 20 was focally positive in 2 cases. Mitochondrial antigen showed variable staining patterns; in 13 cases, the staining pattern was intense 2+ and 3+ **Image 8B**, whereas in 1 case, the staining pattern was 1+ and focal. In addition, other stains for the possibility of Clara cell differentiation were performed showing DC-LAMP with focal, positive staining in 2 cases and 2 additional cases with diffuse strong cytoplasmic staining, whereas surfactant protein A (PE-10) showed focal positive staining in 4 cases and strong positive cytoplasmic staining in only 1 case. In only 1 case did we observe the presence of DC-LAMP and PE-10+ staining **Table 3**.

Molecular Analysis

Mutation analyses for *EGFR* **Image 9A** and *KRAS* **Image 9B** were performed in 15 and 16 tumors, respectively, showing 3 cases (20%) harboring mutations in *EGFR*; 2 showing a 15-base-pair deletion in exon 19; and 1 showing a

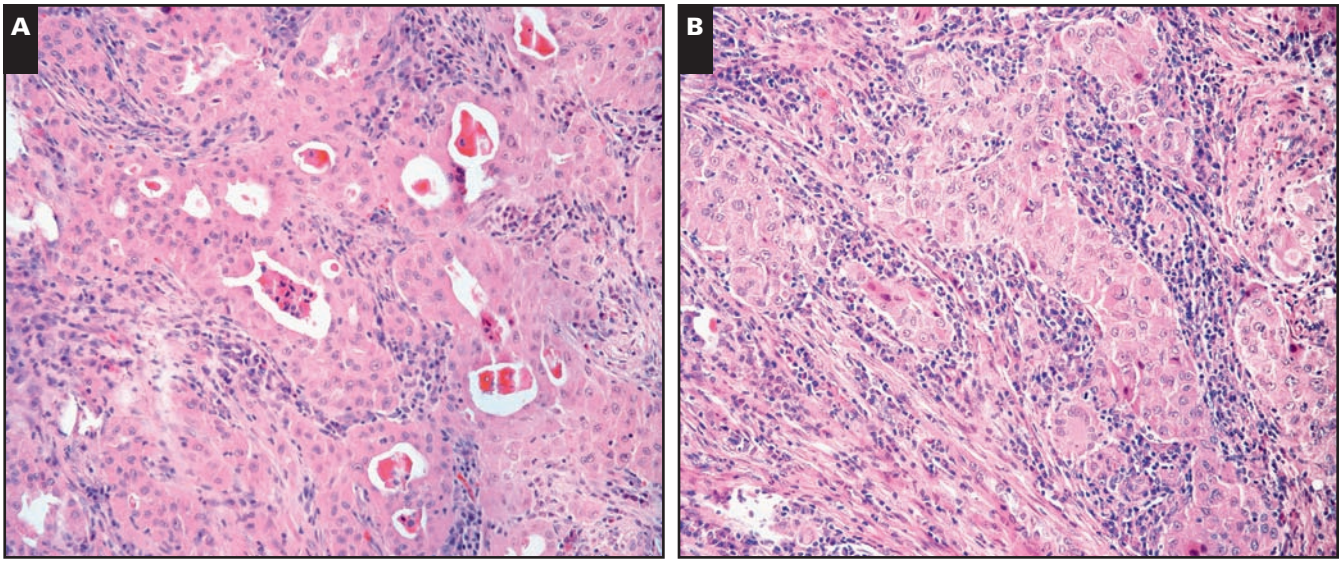

Image 4 Oncocytic adenocarcinoma showing an acinar growth pattern. **A**, Focal glandular formation with bright eosinophilic cytoplasm in the lumen. **B**, More solid proliferation with marked inflammatory reaction composed of plasma cells (**A** and **B**, H&E, ×20).

DOI: 10.1309/AJCPOQWPT1T1AJFT

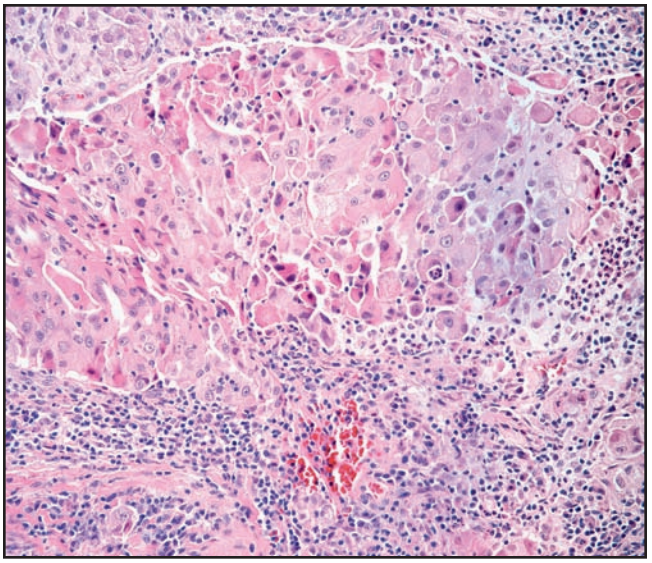

Image 5 High-power view of an acinar oncocytic adenocarcinoma showing larger cells with ample eosinophilic cytoplasm, oval nuclei, and prominent nucleoli resembling oncoblasts (H&E, ×40).

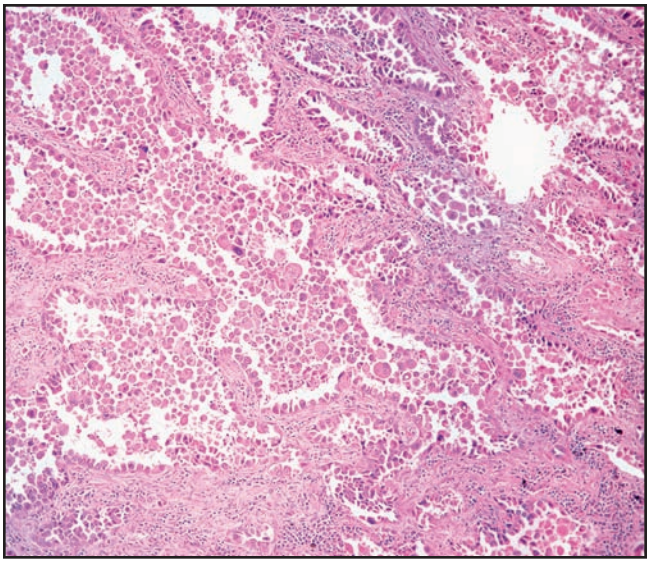

Image 6 Oncocytic adenocarcinoma with a bronchioloalveolar pattern (H&E, ×10).

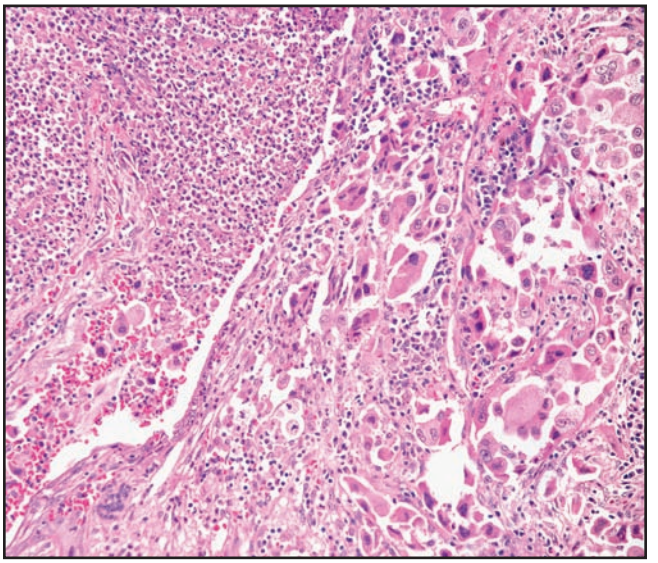

Image 7 Oncocytic adenocarcinoma showing necrosis. Note the adjacent oncocytic cellular proliferation (H&E, ×20).

point mutation in codon 21. Three cases (19%) were mutated for *KRAS*, 2 in codon 12 and 1 in codon 61 **Table 4**.

Follow-up Information

Clinical follow-up data for at last 24 months were available for all patients (Table 1). Recurrence-free survival at 2 years was 75% (12 patients), and overall survival was 88% (14 patients). Overall, 5 patients had recurrence (recurrence time ranged from 3.6 to 32 months). Two patients died of the tumor (~7 and 47 months), 2 died of unrelated conditions, and 1 died of unknown cause (~45 months) without evidence of recurrence.

Discussion

The existence of oncocytic features in primary tumors of the lung is well known, and in the majority of cases, such features have been reported in neuroendocrine tumors, including neuroendocrine carcinomas (carcinoid tumors) and primary paragangliomas of the lung. In addition, similar oncocytic features have also been described in salivary gland–type tumors, ie, acinic cell carcinoma and primary oncocytomas of the lung.[17-21] On the other hand, it is also well known that the lungs are a common place for metastatic neoplasms, ie, those originating in the thyroid, salivary gland, and kidney. Therefore, careful clinical and pathologic correlations must be undertaken to code a tumor as of lung origin.

It is interesting that although these oncocytic features are well recognized, they have been rarely mentioned or

Table 3
Immunohistochemical Analysis of 14 Primary Oncocytic Lung Adenocarcinomas

Antibody	No. (%) Positive
Cytokeratin 7	14 (100)
Cytokeratin 20	2 (14)
Thyroid transcription factor-1	14 (100)
Thyroglobulin	0 (0)
Antimitochondrial	
Negative	0 (0)
Intensity 1	1 (7)
Intensity 2	4 (29)
Intensity 3	9 (64)
DC-LAMP	4 (29)
PE-10 (surfactant protein A clone)	5 (36)

DC-LAMP, dendritic cell lysosome-associated membrane protein.

DOI: 10.1309/AJCPOQWPT1T1AJFT

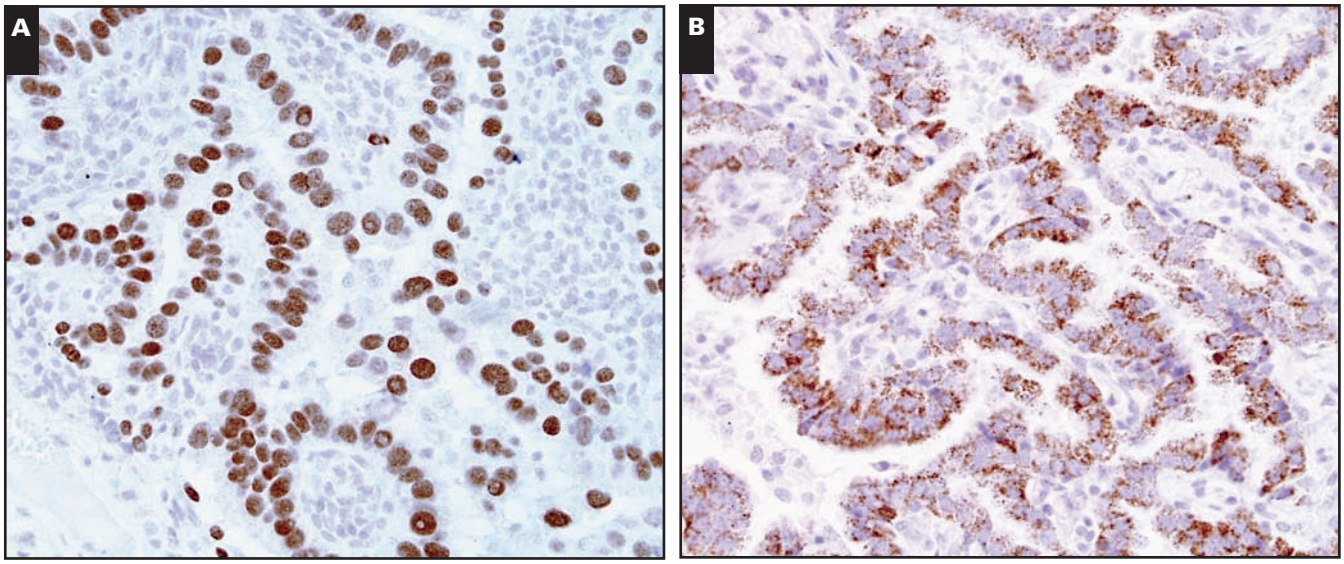

Image 8 **A**, Immunostain showing positive nuclear staining (thyroid transcription factor-1, ×10). **B**, Immunostain showing strong cytoplasmic staining (mitochondrial antibody, ×10).

Table 4
Mutation Analysis of *EGFR* and *KRAS* in Primary Oncocytic Lung Adenocarcinomas

Gene/Exon/Codon	No. (%)
EGFR (n = 15)	
Mutated	3 (20)
19/746-750 (15-base-pair deletion)	2 (13)
21/858 (CTG to CGG)	1 (7)
Wild type	12 (80)
KRAS (n = 16)	
Mutated	3 (19)
1/12 (GGT to GTT)	2 (13)
2/61 (CAA to CTA)	1 (6)
Wild type	13 (81)

addressed in the literature as a specific clinicopathologic entity. We have been able to document 16 such cases that, in our experience, represent approximately 3% of all primary adenocarcinomas of the lung. Similar to what occurs in other oncocytic neoplasms, the cells of oncocytic adenocarcinomas of the lung also are filled with mitochondria. However, the mitochondrial amount in cells varies from type to type and under different physiologic conditions in the same type of cells. Also, the occurrence of these oncocytic changes has been stated to be secondary to cell aging, degenerative process, and inflammation.[22,23]

In addition, the role of mitochondria in neoplasms is not clear, but it is has been proposed that an increase in number is secondary to a compensatory mechanism caused by defective organelles as a consequence of alteration in the mitochondrial

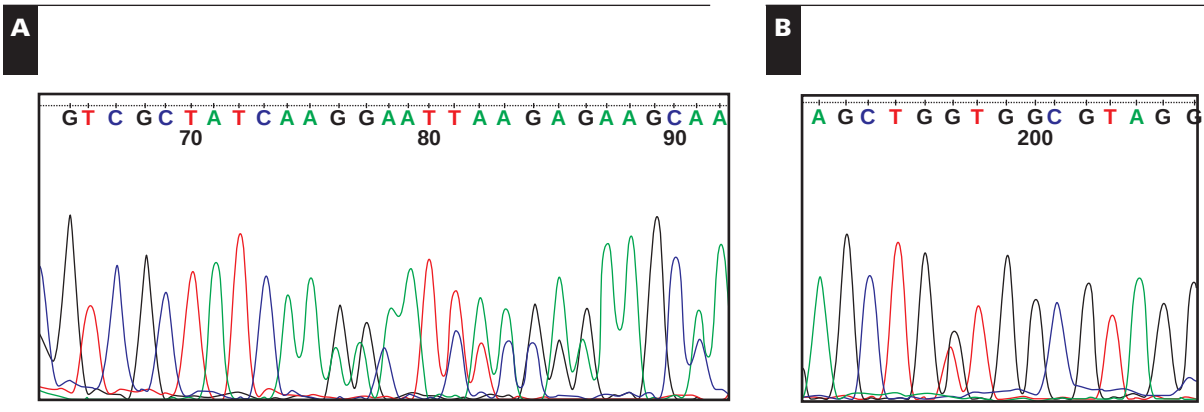

Image 9 Mutation analysis of *EGFR* and *KRAS*. **A**, *EGFR* 15-base-pair deletion in exon 19, codon 746-750. **B**, *KRAS* point mutation, GGT to GTT (glycine to valine) in exon 1, codon 12.

DOI: 10.1309/AJCPOQWPT1T1AJFT

DNA or in the DNA encoding for mitochondrial proteins.[24] Mitochondria can accumulate only in tumor cells that are not actively dividing, thus, the rationale for labeling oncocytic tumors as having low malignant potential.[25,26]

One other explanation for the oncocytic changes in a given tumor may be related to radiation and/or chemotherapy because those procedures may increase the number of mitochondria in cells.[27] The presence of an oncocytic growth pattern in pulmonary adenocarcinomas is clearly not a product of radiation or chemotherapy, because none of our patients was treated before surgical excision of the tumor was performed. In addition, we do not consider oncocytic adenocarcinoma of the lung as a low-malignant-potential neoplasm because in some of our cases, the patients died as a consequence of their tumor. We further stress that the behavior of these tumors is more closely linked to the clinical and pathologic staging of the tumor at the time of diagnosis.

One interesting feature that we observed was that oncocytic changes in adenocarcinomas of the lung were more likely to occur in tumors smaller than 5 cm in diameter, rather than in larger tumors. Even though we investigated the possibility of pneumocyte type II and/or Clara cell origin in these tumors, immunohistochemical studies did not show strong evidence of that possibility because only a minority of cases showed positive staining, and in most of the cases, the positivity was only focal and weak. Our study also showed that the molecular results in these cases closely mirror those in the general population and that the finding of oncocytic changes is not by any means a feature that can be correlated with specific molecular mutations.

More important, we consider that the different growth pattern observed in oncocytic adenocarcinomas of the lung may be mimicked by metastatic tumors to the lung, and, as such, the differential diagnosis of these tumors should include metastasis from thyroid, salivary gland, and renal tumors. In this setting, the use of immunohistochemical studies, ie, cytokeratin 7 and TTF-1, should be of great aid because oncocytic adenocarcinomas of the lung, as evidenced by our experience, would express positive staining for those markers. Nevertheless, in cases in which there is a history of a neoplasm of any of those organ systems (kidney, thyroid, or salivary gland), a complete panel of immunohistochemical studies needs to be undertaken before labeling a case as metastatic disease.

In addition, other primary tumors of the lung should also be considered in the differential diagnosis, including primary paraganglioma, oncocytic neuroendocrine carcinoma, and the oncocytic variant of acinic cell carcinoma of the lung. In the first 2 tumoral conditions, the use of neuroendocrine markers, essentially chromogranin, synaptophysin, and/or CD56, should aid in leading toward a more appropriate interpretation because paraganglioma and neuroendocrine carcinoma would express positive staining for neuroendocrine markers. On the other hand, the oncocytic variant of acinic cell carcinoma may be more problematic because acinic cell carcinoma not only may show an acinar growth pattern but also may show positive staining for cytokeratin and TTF-1. However, in cases of acinic cell carcinoma, the tumor may also show more conventional areas, which on histochemical stains for periodic acid–Schiff will show extensive deposition of intracellular glycogen.

Primary oncocytoma of the lung may pose a much more difficult problem in separating it from oncocytic adenocarcinoma. However, the presence of mixed patterns of growth such as acinar, papillary, and/or solid patterns in the same tumor would be unusual for oncocytoma. In addition, in our cases, we were able to observe that many cases also showed a bronchioloalveolar growth pattern, which would be unusual in primary oncocytomas of the lung. Needless to say, primary oncocytomas of the lung are exceedingly rare and have been reported only in rare instances.[19,20]

The cases herein presented are, in our experience, an unusual growth pattern of primary adenocarcinoma of the lung. The recognition of the oncocytic variant of adenocarcinoma of the lung is important to avoid confusion with metastatic neoplasms to the lung and other primary lung neoplasms. These adenocarcinomas, just like other types, may show similar immunohistochemical features and molecular mutations. Recognition is important to properly classify these tumors and for the proper treatment of the patients.

From the Departments of [1]Pathology and [2]Thoracic/Head and Neck Medical Oncology, The University of Texas M.D. Anderson Cancer Center, Houston.

Supported by grant DoD-W81XWH-04-1-0142, Department of Defense, Washington, DC.

Address reprint requests to Dr Moran: Dept of Pathology, M.D. Anderson Cancer Center, Houston, TX 77030.

References

1. Parkin DM, Bray F, Ferlay J, et al. Global cancer statistics, 2002. *CA Cancer J Clin*. 2005;55:74-108.
2. Moran CA. Pulmonary adenocarcinoma: the expanding spectrum of histologic variants. *Arch Pathol Lab Med*. 2006;130:958-962.
3. Moran CA. Mucin rich tumors of the lung. *Adv Anat Pathol*. 1995;2:299-305.
4. Graeme-Cook F, Mark EJ. Pulmonary mucinous cystic tumors of borderline malignancy. *Hum Pathol*. 1991;22:185-190.
5. Moran CA, Hochholzer L, Fishback N, et al. Mucinous (so-called colloid) carcinoma of the lung. *Mod Pathol*. 1992;5:634-638.
6. Silver S, Askin FB. True papillary carcinoma of the lung: a distinct clinicopathologic entity. *Am J Surg Pathol*. 1997;21:43-51.

DOI: 10.1309/AJCPOQWPT1T1AJFT

7. Moran CA, Jargidar J, Suster S. Papillary lung adenocarcinoma with prominent "morular" component. *Am J Clin Pathol*. 2004;122:106-110.
8. Amin M, Tamboli P, Merchant SH, et al. Micropapillary component in lung adenocarcinoma: a distinctive histologic feature with possible prognostic significance. *Am J Surg Pathol*. 2002;26:358-364.
9. Kish JK, Ro JY, Ayala AG, et al. Primary mucinous adenocarcinoma of the lung with signet-ring cells: a histochemical comparison with signet-ring cell carcinomas of other sites. *Hum Pathol*. 1989;20:1097-1102.
10. Castro CY, Moran CA, Flieder DG, et al. Primary signet ring cell adenocarcinoma of the lung: a clinicopathological study of 15 cases. *Histopathology*. 2001;39:397-401.
11. Steinhauer JR, Moran CA, Suster S. "Secretory endometrioid-like" adenocarcinoma of the lung [letter]. *Histopathology*. 2005;47:219-220.
12. Ishikura H, Kanda M, Ito M, et al. Hepatoid adenocarcinoma: a distinctive histological subtype of alpha-fetoprotein–producing lung carcinoma. *Virchows Arch A Pathol Anat Histopathol*. 1990;417:73-80.
13. Hayashi Y, Takanashi Y, Ohsawa H, et al. Hepatoid adenocarcinoma of the lung. *Lung Cancer*. 2002;38:211-214.
14. Travis WD, Brambilla E, Muller-Hermelink HK, et al, eds. *WHO Classification of Tumours: Pathology and Genetics of Tumours of the Lung, Pleura, Thymus and Heart*. Lyon, France: IARC Press; 2004.
15. Shigematsu H, Lin L, Takahashi T, et al. Clinical and biological features associated with epidermal growth factor receptor gene mutation in lung cancers. *J Natl Cancer Inst*. 2005;97:339-346.
16. Tang X, Shigematsu H, Bekele BN, et al. EGFR tyrosine kinase domain mutations are detected in histologically normal respiratory epithelium in lung cancer patients. *Cancer Res*. 2005;65:7568-7572.
17. Sklar JL, Churg A, Bensh KG. Oncocytic carcinoid tumor of the lung. *Am J Surg Pathol*. 1980;4:287-292.
18. Aubertine CL, Flieder DB. Primary paraganglioma of the lung. *Ann Diagn Pathol*. 2004;8:237-241.
19. Fechner RE, Bentnick BR. Ultrastructure of bronchial oncocytoma. *Cancer*. 1973;331:1451-1457.
20. Santos-Bris A, Jenron J, Sastre R, et al. Oncocytoma of the lung. *Cancer*. 1977;40:1330-1336.
21. Moran CA, Suster S, Koss MN. Acinic cell carcinoma of the lung ("Fechner tumor"): a clinicopathologic, immunohistochemical, and ultrastructural study of five cases. *Am J Surg Pathol*. 1992;16:1039-1050.
22. Nishioka H, Hirano A, Haraoka J, et al. Histological changes in the pituitary gland and adenomas following radiotherapy. *Neuropathology*. 2002;22:19-25.
23. Muller-Hocker J. Random cytochrome-C-oxidase deficiency of oxyphil cell nodules in the parathyroid gland: a mitochondrial cytopathy related to cell aging. *Pathol Res Pract*. 1992;188:701-706.
24. Tallini G. Oncocytic tumors. *Virchows Arch*. 1998;433:5-12.
25. Sobrinho-Simoes M, Maximo V. Warthin's tumor [letter]. *Virchows Arch*. 2006;448:877-878.
26. Teymoortash A, Werner JA. Tissue that has lost its track: Warthin's tumor. *Virchows Arch*. 2005;446:585-588.
27. Ambrosini-Spaltro A, Salvi F, Betts CM, et al. Oncocytic modifications in rectal adenocarcinoma after radio and chemotherapy. *Virchows Arch*. 2006;448:442-448.

DOI: 10.1309/AJCPOQWPT1T1AJFT

Apoptosis 2005; **10**: 1203–1210

DOI: 10.1007/s10495-005-2274-4

Chemopreventive agent-induced modulation of death receptors

S.-Y. Sun

Department of Hematology and Oncology, Winship Cancer Institute, Emory University School of Medicine, Atlanta, Georgia USA

Published online: 3 October 2005

The goals of chemoprevention of cancer are to inhibit the initiation or suppress the promotion and progression of preneoplastic lesions to invasive cancer through the use specific natural or synthetic agents. Therefore, a more desirable and aggressive approach is to eliminate aberrant clones by inducing apoptosis rather than merely slowing down their proliferation. The increased understanding of apoptosis pathways has directed attention to components of these pathways as potential targets not only for chemotherapeutic but also for chemopreventive agents. Activation of death receptors triggers an extrinsic apoptotic pathway, which plays a critical role in tumor immunosurveillance. An increasing number of previously identified chemopreventive agents were found to induce apoptosis in a variety of premalignant and malignant cell types *in vitro* and in a few animal models *in vivo*. Some chemopreventive agents such as non-steroidal anti-inflammatory drugs, tritepenoids, and retinoids increase the expression of death receptors. Thus, understanding the modulation of death receptors by chemopreventive agents and their implications in chemoprevention may provide a rational approach for using such agents alone or in combination with other agents to enhance death receptor-mediated apoptosis as a strategy for effective chemoprevention of cancer.

Keywords: apoptosis; chemoprevention; chemopreventive agents; death receptors.

Introduction

Epithelial carcinogenesis is a multi-year (sometime decade-long) process of clonal selection and evolution of genetically damaged cells, leading to the abnormal precancer phenotype that eventually becomes invasive cancer.[1] Therefore, carcinogenesis is a chronic disease process. This nature of carcinogenesis provides a strong rationale for cancer intervention or prevention as an attractive strategy to control cancer incidence and mortality. If such a process is arrested, delayed, or reversed, cancer incidence may be markedly reduced, eventually leading to a decline in cancer mortality rates. Such an approach is called chemoprevention, which is defined as the use of pharmacological or natural agents to inhibit the development of invasive cancer either by blocking the DNA damage that initiates carcinogenesis or by arresting or reversing the progression of premalignant cells in which such damage has already occurred.[2,3] Several thousand agents have been reported to have chemopreventive activity.[4] Some of the promising agents and agent combinations have been evaluated clinically for chemoprevention of major cancer types for the past few decades.[2] Clinical practice of chemoprevention has shown some success in reversing premalignant lesions, reducing the risk of developing second primary tumors, and decreasing cancer incidence.[4,5] Thus, chemoprevention has emerged as an integral part of cancer control.

Apoptosis or programmed cell death is a genetically controlled mechanism essential for the maintenance of tissue homeostasis, proper development, and the elimination of unwanted cells. Thus, it represents a universal and exquisitely efficient endogenous or induced cellular suicide pathway and can be induced in many cell types via numerous physiological, biochemical and/or noxious stimuli.[6,7] Because defects in apoptotic pathways or the inhibition of apoptosis play important roles in cancer development or carcinogenesis,[8] targeting the induction of apoptosis in premalignant or malignant lesions may selectively eliminate aberrant precancerous clones or cancer cells while sparing normal cells. Therefore, the induction of apoptosis should be efficient not only for chemotherapy but also for chemoprevention. In comparison with other strategies that merely slow down proliferation, the induction of apoptosis appears to be a more desirable and aggressive chemopreventive approach to eliminate aberrant clones (reviewed in[9]).

Death receptors are key components in the extrinsic apoptotic pathway.[10] Their activation due to ligand binding or increased expression triggers an extrinsic apoptotic signaling pathway leading to apoptosis. The expression of death receptors is inducible by many small molecules

Correspondence to: S.-Y. Sun, Winship Cancer Institute, Emory University School of Medicine, 1365-C Clifton Road, C3088, Atlanta, GA 30322, USA. Tel.: (404) 778-2170; Fax: (404) 778-5520; e-mail: shi-yong_sun@emoryhealthcare.org

including some chemopreventive agents. This review article will highlight the recent studies on the modulation of death receptors by chemopreventive agents and discuss their implications in chemoprevention.

Death receptor-mediated apoptotic pathway

There are generally two major apoptotic pathways: the first involves signals transduced through death receptors; the second relies on a signal from mitochondria. Both pathways are involved in a concerted activation of a set of cysteine proteases called caspases, which in turn cleave cellular substrates and result in the characteristic morphological and biochemical changes constituting the process of apoptosis (reviewed in[11,12]) (Figure 1).

Death receptors, including tumor necrosis factor (TNF) receptor (TNFR), Fas (CD95 or APO-1), DR3, DR4 (TRAIL-R1), DR5 (TRAIL-R2) and DR6, belong to the TNF receptor gene superfamily. They are defined by similar, cysteine-rich extracellular domains and additional cytoplasmic death domains (reviewed in[10]). The death domain is crucial for transmitting the death signal from the cell surface to intracellular signaling pathways. Upon ligand binding or overexpression, death receptors such as Fas are clustered to form a trimer in the cell membrane, which results in recruitment of adaptor proteins such as Fas-associated death domain (FADD) via death domain interactions. The FADD protein, containing both a death domain and an additional protein interaction domain called a death effector domain (DED), further binds via DED interactions to caspase-8, and possibly caspase-10, resulting in the recruitment and autoactivation of caspase-8. This process is referred to as the formation of the death-inducing signaling complex (DISC), an essential step in the activation of the extrinsic apoptotic pathway. The activated caspase-8 then acts to cleave and activate downstream effector caspases such as caspase-3.[10–12] In addition to directly activating the downstream effector caspases, death receptors also indirectly activate them through Bid-mediated cytochrome C release and subsequent caspase-9 activation because Bid is a substrate of caspase-8 and can be cleaved or activated by caspase-8.[10–12] Thus, Bid, a BH3-only protein of the bcl-2 family, provides a link and an integration between the extrinsic death receptor and intrinsic mitochondrial apoptotic pathways.

Although TNFR and Fas have been extensively studied, DR4 and DR5 recently have attracted considerable attention since their ligand TNF-related apoptosis-inducing ligand (TRAIL) has been shown to predominantly induce apoptosis of cancer cells, while sparing normal cells, showing a great potential in cancer therapy (reviewed in[13–15]). Like Fas, both DR4 and DR5 primarily act as inducers of apoptosis, distinguishing them from TNFR, which mainly activates the non-apoptotic gene-inducing functions such as NF-κB and JNK activation.[10] Currently, DR4 and DR5 are important targets for cancer therapy (reviewed in[13,16,17]).

Figure 1. Schema for basic apoptotic signaling pathways. Ligation of death ligands (*e.g.* FasL or TRAIL) with their receptors (*e.g.* Fas or DR4 and DR5) results in activation of caspase-8 (Casp-8) through a death adaptor protein FADD. Certain stress signals (*e.g.* DNA damage) can target mitochondria and induce cytochrome C (Cyt. C) release from mitochondria into cytosol leading to caspase-9 (Casp-9) activation via binding to Apaf-1. Both caspase-8 and caspase-9 activate downstream caspase-3 (Casp-3), caspase-6 (Casp-6) and caspase-7 (Casp-7) leading to cleavages of their target proteins such as PARP, DFF45 and lamins. In addition, truncated Bid (tBid), activated by caspase-8 via cleavage, facilitates insertion of BAX into mitochondrial membrane leading to Cyt. C release. Therefore, tBid may serve as a link between death receptor- and mitochondria-mediated apoptotic pathways. Inhibitors of apoptosis proteins (IAPs) can bind to activated Casp-9 and prevent its action on effector caspases (*e.g.* Casp-3), whereas Smac binds to IPAs, leaving Casp-9 free to activate Casp-3.

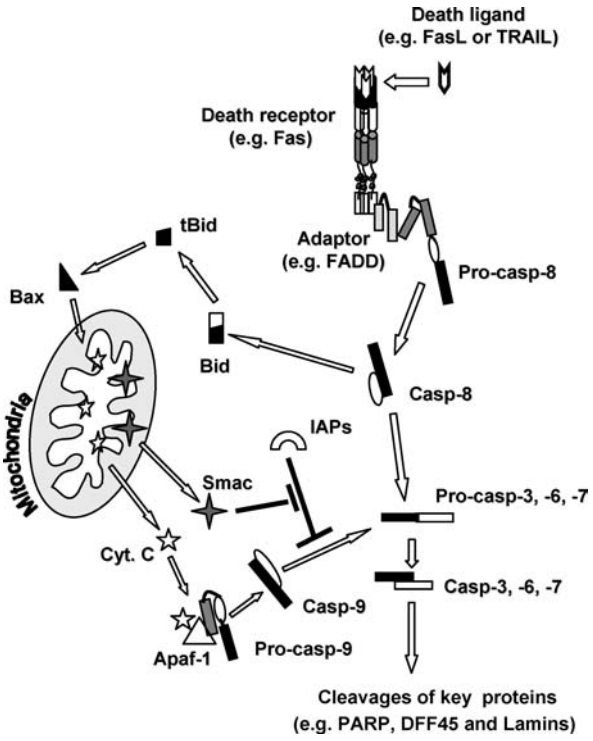

Death receptors, tumor immunosurveillance, and carcinogenesis

Cancer can be considered a cell clonal expansion disease. The process of clonal expansion involves genetic instability, which may result in some clones becoming predominant and tumorigenic. The growth advantage of aberrant cells or clones results from uncontrolled proliferation and

a loss of the ability to undergo differentiation and apoptosis. Very importantly, the aberrant cells or clones must build up immunosuppressive barriers to withstand or overcome host immune defense or surveillance mechanism (reviewed in[18,19]).

Immune surveillance against tumors is mediated by both innate and adaptive components of cellular immunity.[20] The most crucial guardians seem to be natural killer (NK) cells (innate immunity) and cytotoxic T-cells (CTLs) (adaptive immunity). One of the mechanisms by which activated NK cells or CTLs destroy malignant (or virus-infected) cells is mediated through membra-bound variants of the death ligands CD95L and TRAIL, which induce apoptosis in the target cells via activation of their corresponding death receptors (reviewed in[15,17,19,20]). This process can be further enhanced by interferon γ produced by activated NK- and T cells by sensitizing for death receptor-induced apoptosis and by upregulation of TRAIL.[21] Thus, the expression of death receptors (*e.g.*, Fas or DR4 and DR5) in premalignant and malignant cells is a prerequisite for immune cells to recognize and eliminate premalignant and malignant cells through death ligand and death receptor interaction.

Accordingly, it is understandable that one effective way for premalignant and malignant cells to escape immunosurveillance is to downregulate or inactivate death receptors on their membrane surface. Mutation analyses of the Fas gene have demonstrated that Fas mutation occurs in 0–65% of hematopoietic malignancies and 0–28% of solid tumors. Among the hematopoietic malignancies, high frequencies of Fas mutations occur in thyroid lymphoma (65.4%), cutaneous T-cell lymphoma (59%), and nasal NK/T cell lymphoma (50%). Among solid tumors, Fas mutations occurs frequently in bladder transitional cell carcinoma (28%) and burn scar-related squamous cell carcinoma (14.3%) (reviewed in[22]). Compared to Fas, mutation analyses of DR4 and DR5 have been performed less widely in human cancers. In general, the frequencies of DR4 and DR5 mutations in detected cancers are low (0–10.6%) (reviewed in[22]).

In addition to mutations, downregulation of death receptor expression has also been documented. Decreased expression of Fas was observed in hepatomas compared to normal hepatocytes.[23] Analysis of clinical cancer tissues in normal cervical samples and different grades of cervical intraepithelial neoplasia (CIN) samples revealed that the frequency of Fas-positive staining decreased with the increasing severity of CIN.[24] Analysis of small cell lung cancer (SCLC) tumors revealed reduced levels of Fas and DR4 mRNA compared to non-small cell lung cancer (NSCLC) tumors.[25,26] The downregulation of Fas and DR4 expression was likely the consequence of methylation of their gene promoters.[25] Although methylation of DR4 and DR5 are generally rare in many cancer types,[27] a recent study identified a high frequency of DR4 methylation (41%) in sporadic phaeochromocytomas.[28]

Rather than downregulate death receptors, tumor cells sometimes overexpress decoy receptors (DcRs), which lack a functional intracellular death domain and thereby compete with death receptors for death ligands to antagonize apoptosis mediated by the binding of death ligands and death receptors.[10] The gene coding for DcR3, a secreted protein that binds FasL, is amplified in about 50% of lung and colon cancers.[29] In addition, DcR3 is overexpressed in carcinomas of the stomach, esophagus and rectum independently of gene amplification.[30] Cells that overexpress DcR3 presumably have a survival advantage because of their ability to resist FasL-mediated attack by cytotoxic lymphocytes, although the role of DcR3 in tumorigenesis remains unclarified. Although DcR1 and DcR2 are generally downregulated in many types of cancer,[27] one study showed that DcR1 expression was enhanced in primary tumors of the gastrointestinal tract.[31] It is possible that DcR overexpressing tumors may gain a selective growth advantage by escaping from death ligand/death receptor-induced apoptosis.

Signaling through death receptors can also be negatively regulated by proteins such as FLIP that prevent interaction between FADD and caspase-8.[11,12] High FLIP expression existing in many tumor cells has been correlated with resistance to death ligand/death receptor-induced apoptosis (reviewed in[32,33]). In addition, FLIP expression was associated with tumor escape from T-cell immunity and enhanced tumor progression in experimental studies *in vivo* (reviewed in[34]).

Modulation of death receptors by chemopreventive agents

Many studies have demonstrated that the expression of death receptors, including Fas, DR4 and DR5, is inducible by many small molecules, particularly chemotherapeutic agents. Increased evidence indicates that activation of death receptors positively impacts cancer chemotherapy (reviewed in[16]). An increased number of recent studies also show that some chemopreventive agents such as non-steroidal anti-inflammatory drugs (NSAIDS), retinoids and tritepenoids, induce death receptor expression and enhance death ligand-induced apoptosis as well.

NSAIDS. Sulindac sulfide is one of the major metabolites of sulindac that is believed to mediate its antitumorigenic effects by inducing apoptosis. Sulindac sulfide specifically upregulates DR5 and activates the proximal caspase-8 in various colon and prostate cancer cell lines. Overexpression of a dominant-negative FADD (FADD-DN) suppresses sulindac sulfide-induced apoptosis and combination of sulindac sulfide with TRAIL exhibits an enhanced

apoptosis-inducing effect, suggesting the involvement of DR5 in sulindac sulfide-induced apoptosis.[35] Induction of DR5 by sulindac sulfide in gastric cancer cells was also reported recently. In this study, DR4 expression was also induced by sulindac sulfide.[36] Related to these findings, indomethacin and sulindac sulfide were reported to induce apoptosis of human leukemic Jurkat cells by a mechanism that requires the FADD-mediated activation of a caspase-8-dependent pathway,[37] implying the importance of a death receptor-mediated apoptotic pathway in their actions.

Celecoxib is another apoptosis-inducing NSAID with cyclooxygenase-2 (COX-2) activity and has been approved by the U.S. Food and Drug Administration (FDA) for the chemoprevention of colon cancer (*i.e.*, treatment of familial adenomatous polyposis, an inherited syndrome that predisposes individuals to colon cancer). Our recent work found that celecoxib increased the expression of DR4 and particularly DR5 at both mRNA and protein levels in human lung cancer cells. This effect appears to be independent of its COX-2 inhibitory activity and occurs at the transcriptional level. Both overexpression of FADD-DN and silencing of DR5 expression using small interfering RNA (siRNA) attenuated celecoxib-induced apoptosis. Moreover, celecoxib cooperated with TRAIL to augment the induction of apoptosis. These results indicate that the expression of death receptors, particularly DR5, contributes to celecoxib-induced apoptosis.[38]

Retinoids. Retinoids refer to an entire group of natural and synthetic retinol (vitamin A) metabolites and analogues and have long been considered promising chemopreventive agents.[39] The synthetic retinoid CD437 potently induces apoptosis in a variety of human cancer cells. Our studies showed that CD437 induced Fas, DR4 and DR5 expression primarily in lung cancer cell lines with wild-type p53.[40–43] The induction of these death receptors correlated with their potencies in inducing apoptosis in these cell lines.[40–42] Inactivation of p53 using HPV16 E6 abrogated CD437's ability to upregulate the expression of Fas, DR4, and DR5.[41–43] Thus, it appears that CD437 induces the expression of death receptors via a p53-dependent mechanism, at least in human lung cancer cells. Fas and DR5 are known to be p53 target genes.[44,45] Our recent work has demonstrated that DR4 is also a p53 target gene.[46]

Due to the above findings, we also determined whether CD437 induced the expression of death receptors and apoptosis in normal human lung epithelial cells, which possess wild-type p53. Significantly, CD437 did not induce the expression of Fas, DR4, and DR5, and apoptosis in both normal human bronchial epithelial (NHBE) cells and small airway epithelial cells.[47] The failure of CD437 to induce death receptor expression and apoptosis in normal lung epithelial cells may be related to its inability to increase or stabilize p53 protein in these cells.[47]

Although CD437 induces a p53-dependent expression of death receptors in human lung cancer cells, our studies showed that p53 was not important for the upregulation of death receptors by CD437 in human prostate or head and neck cancer cells because CD437 induced the expression of death receptors regardless of p53 status in these cell lines.[48,49] Thus, it appears that CD437 induces a p53-dependent and/or -independent death receptor expression depending on cell types or even cell lines. Currently, it remains unclear how CD437 upregulates the expression of death receptors through p53-independent mechanism(s) (reviewed in[43]).

It is generally thought that nuclear retinoid receptors mediate the major biological effects of retinoids.[39] To determine whether nuclear retinoid receptors play any role in mediating the upregulation of death receptors by CD437, we examined the effect of CD437 on the expression of death receptors in the presence of the pan RAR-specific antagonist AGN193109. We found that AGN193109 failed to block or suppress Fas, DR4, or DR5 induction by CD437, indicating that CD437 induces death receptor expression independent of nuclear retinoid receptors ([42], our unpublished data). This conclusion is further supported by the determination that other receptor-selective retinoids, except for those having similar parent structures to CD437, failed to induce the expression of death receptors ([42], our unpublished data).

N-(4-hydroxyphenyl) retinamide (4HPR; fenretinide), another synthetic retinoid that induces apoptosis in various types of cancer cells, has been evaluated in numerous clinical trials for its chemopreventive activity. A recent study has shown that 4HPR induced DR5 expression in primary meningioma cultures.[50] Another study did not find that 4HPR modulated the expression of DR4 or DR5. However, 4HPR enhanced TRAIL-mediated apoptosis in ovarian cancer cell lines but not in immortalized non-tumorigenic ovarian epithelial cells.[51]

Triterpenoids. Triterpenoids are another group of natural and synthetic compounds with chemopreventive potentials.[52] The natural triterpenoids betulinic acid and boswellic acid were reported to induce DR5 expression in melanoma, glioblastoma, and leukemia cells, respectively.[53,54] Our recent study has shown that the synthetic triterpenoid methyl-2-cyano-3,12-dioxooleana-1,9-dien-28-oate (CDDO-Me) increased the expression of DR4 and particularly DR5, and enhanced TRAIL-induced apoptosis in human lung cancer cells. Silencing of DR5 expression using siRNA inhibited both CDDO-Me-induced apoptosis and CDDO-Me-mediated enhancement of TRAIL-induced apoptosis, indicating the involvement of DR5 in both activities.[55] Induction of DR5 by betulinic acid and CDDO-Me is independent

of p53.[53,55] We found that CDDO-Me rapidly activated c-Jun NH_2-terminal kinase (JNK) before DR5 up-regulation. Moreover, application of the JNK-specific inhibitor SP600125 blocked CDDO-Me-induced DR5 upregulation. These results indicate that CDDO-Me induces a JNK-dependent DR5 upregulation.[55]

Polyphenols. Resveratrol, a polyphenol found in grape skin and various other food products, exhibits cancer chemopreventive activity in animal models of carcinogensis, likely through its ability to trigger apoptosis.[56] Studies in a human colon cancer cell line show that resveratrol does not modulate the expression of Fas, DR4, and DR5 at the surface of cancer cells. However, it induces the clustering of these death receptors and their redistribution in cholesterol and sphingolipid-rich fractions (lipid rafts) of cancer cells, together with FADD and procaspase-8. These redistributions are associated with the formation of a DISC and contribute to the induction of apoptosis and sensitization of cells to death ligand- or death receptor activation-mediated apoptosis.[57,58] (-)-Epigallocatechin-3-gallate (EGCG), a polyphenolic compound found in green tea, was reported to increase Fas protein levels in Hep G2 human liver cancer.[59] Another study reported that EGCG also bond to cell surface Fas, triggering Fas-mediated apoptosis in human monocytic leukemia U937 cells.[60]

Vitamin E and its derivatives. Vitamin E (α-tocopherol) is a dietary antioxidant with chemopreventive activity. Vitamin E succinate was reported to increase not only total protein levels of Fas but also cell surface levels of Fas in human breast cancer cells.[61,62] The upregulation of Fas is involved in vitamin E succinate-induced apoptosis[61] or associated with the enhancement of Fas-induced apoptosis[62] in these cells. Increases in cell surface Fas and enhancement of Fas-induced apoptosis by vitamin E succinate were also observed in human prostate cancer cells.[63] A recent study shows that the semisynthetic analogue of vitamin E, α-tocopheryl succinate, increases the expression of both DR4 and DR5 in human malignant mesothelioma cells; this increased expression is associated with its ability to enhance TRAIL-induced apoptosis.[64] Currently, it is unknown how vitamin E and its analogues upregulate the expression of death receptors.

Others. Selenium is an essential micronutrient that is currently being tested for prostate cancer chemoprevention. A recent study shows that selenium-mediated apoptosis appears to involve a DR5-dependent pathway in human prostate cancer cells. Selenium specifically induced DR5 expression, which coupled with caspase-8 activation and Bid cleavage.[65] Bovine lactoferrin, a multifunctional glycoprotein, has been shown to strongly inhibit the development of azoxymethane-induced rat colon tumors. Lactoferrin was shown to enhance Fas expression in the colon mucosa during both early and late stages of carcinogenesis. The elevation of Fas expression correlates with the activation of caspase-8 and caspase-3, suggesting that apoptosis caused by elevated expression of Fas is involved in chemoprevention by lactoferrin of colon carcinogenesis.[66] Curcumin, an antioxidant with chemopreventive and apoptosis-inducing activity, was reported to increase Fas expression and induce Fas clustering in human melanoma cells, leading to the induction of apoptosis.[67] Curcumin also increased cell surface DR4 and augmented TRAIL-induced apoptosis in prostate cancer cells.[68] Interferons have been used in some chemopreventive trials. Interferon-γ was shown to induce DR5 expression in cancer cell lines independent of p53.[53] Interferon-α was also reported to increase DR5 expression in human hepatoma cells; this increased expression is associated with its ability to enhance TRAIL-induced apoptosis.[69]

Implication of death receptor modulation in chemoprevention

Activation of death receptors with either ligand binding or receptor overexpression triggers the extrinsic apoptotic pathway. Apoptosis induced by the interaction between death ligand (from NK cells or T cells) and death receptors (from target cells) is the primary mechanism underlying tumor immunosurveillance (reviewed in [19–21]). In death ligand-expressing premalignant or malignant cells, the binding of death ligands such as Fas ligand (FasL) and TRAIL to an increased number of death receptors due to treatment with chemopreventive agents may trigger the apoptotic signal leading to the apoptotic death of these aberrant cells. Moreover, upregulation of death receptors in premalignant and malignant cells may cause these cells to become more susceptible targets for immune cells (*i.e.*, NK and T cells) that express and secrete death ligands such as TRAIL. In other words, chemopreventive agents with death receptor-inducing activity can sensitize premalignant and malignant cells to death receptor-mediated immune clearance or surveillance.

Some chemopreventive agents have been demonstrated to induce the expression of death ligands such as TRAIL. The examples of the agents are retinoic acid,[70,71] interferons,[71,72] and PI3 kinase inhibitors.[73] Therefore, it is plausible to speculate that the combination of a death receptor-inducing chemopreventive agent with a death ligand-inducing agent may enhance the killing or elimination of premalignant and malignant cells or lesions via death ligand/death receptor-mediated apoptosis. Studying the effect of this kind of combination may develop an effective and mechanism-driven combination regimen for cancer chemoprevention.

Conclusions and perspective

Chemoprevention has emerged as an essential part of cancer control. Many chemopreventive agents are thought to act as cytostatic agents. Therefore, they are traditionally suggested to be administered chronically to individuals at increased risk to develop cancer. A more desirable and aggressive approach is to use agents that can eliminate aberrant clones by inducing apoptosis rather than inhibit their proliferation. Such agents could be administered for shorter periods of time and at higher doses. Short-term treatment would allow the inclusion of agents with some reversible or moderate side effects for the prevention of premalignant lesions.

It appears that apoptosis is a useful target for the development of chemopreventive agents. Elucidation of the mechanism of chemopreventive agent-induced apoptosis in premalignant or malignant cells clearly will be helpful for developing new agents with better activity, selectivity and less toxicity. Some chemopreventive agents with apoptosis-inducing activity induce apoptosis through an intrinsic mitochondrial pathway involving the promotion of reactive oxygen species (ROS) generation (reviewed in[9]). Given that ROS-induced oxidative stress is involved in carcinogenesis, particularly in tumor promotion (reviewed in[74,75]), a concern is whether this kind of chemopreventive agent has a potential to promote carcinogenesis rather than prevention of cancer. From this point of view, chemopreventive agents with death receptor-inducing activity appear to have the advantage over others that induce apoptosis by promoting ROS generation. Therefore, future studies should focus on identifing and developing chemopreventive agents that, ideally, can selectively induce the expression of death receptors in preneoplastic or premaligant cells or induce the redistribution and clustering of death receptors on the membrane surface of these cells.

Acknowledgments

Works in author's laboratory were supported by Winship Cancer Institute faculty start-up research fund, the Georgia Cancer Coalition Distinguished Cancer Scholar award, and the Department of Defense VITAL grant W81XWH-04-1-0142 (for Project 4). The author is a Georgia Cancer Coalition Distinguished Cancer Scholar.

References

1. Kelloff GJ, Sigman CC, Greenwald P. Cancer chemoprevention: Progress and promise. *Eur J Cancer* 1999; **35**: 1755–1762.
2. Hong WK, Sporn MB. Recent advances in chemoprevention of cancer. *Science* 1997; **278**: 1073–1077.
3. Sporn MB, Suh N. Chemoprevention: An essential approach to controlling cancer. *Nat Rev Cancer* 2002; **2**: 537–543.
4. Kelloff GJ, Crowell JA, Steele VE, *et al.* Progress in cancer chemoprevention. *Ann N Y Acad Sci* 1999; **889**: 1–13.
5. Tsao AS, Kim ES, Hong WK. Chemoprevention of cancer. *CA Cancer J Clin* 2004; **54**: 150–180.
6. Steller H. Mechanisms and genes of cellular suicide. *Science* 1995; **267**: 1445–1449.
7. Metcalfe A, Streuli C. Epithelial apoptosis. *BioEssays* 1997; **19**: 711–720.
8. Green DR, Evan GI. A matter of life and death. *Cancer Cell* 2002; **1**: 19–30.
9. Sun SY, Hail N Jr, Lotan R. Apoptosis as a novel target for cancer chemoprevention. *J Natl Cancer Inst* 2004; **96**: 662–672.
10. Ashkenazi A, Dixit VM. Death receptors: Signaling and modulation. *Science* 1998; **281**: 1305–1308.
11. Hengartner MO. The Biochemistry of apoptosis. *Nature* 2000; **407**: 770–776.
12. Green DR. Apoptotic pathways: Paper wraps stone blunts scissors. *Cell* 2000; **102**: 1–4.
13. Kelley SK, Ashkenazi A. Targeting death receptors in cancer with Apo2L/TRAIL. *Curr Opin Pharmacol* 2004; **4**: 333–339.
14. Bouralexis S, Findlay DM, Evdokiou A. Death to the bad guys: Targeting cancer via Apo2L/TRAIL. *Apoptosis* 2005; **10**: 35–51.
15. Yagita H, Takeda K, Hayakawa Y, Smyth MJ, Okumura K. TRAIL and its receptors as targets for cancer therapy. *Cancer Sci* 2004; **95**: 777–783.
16. Debatin KM, Krammer PH. Death receptors in chemotherapy and cancer. *Oncogene* 2004; **23**: 2950–2966.
17. Wajant H, Gerspach J, Pfizenmaier K. Tumor therapeutics by design: Targeting and activation of death receptors. *Cytokine Growth Factor Rev* 2005; **16**: 55–76.
18. Reed JC. Mechanisms of apoptosis avoidance in cancer. *Curr Opin Oncol* 1999; **11**: 68–75.
19. Smyth MJ, Hayakawa Y, Takeda K, Yagita H. New aspects of natural-killer-cell surveillance and therapy of cancer. *Nat Rev Cancer* 2002; **2**: 850–861.
20. Smyth MJ, Takeda K, Hayakawa Y, Peschon JJ, van den Brink MR, Yagita H. Nature's TRAIL—on a path to cancer immunotherapy. *Immunity* 2003; **18**: 1–6.
21. Smyth MJ, Cretney E, Kershaw MH, Hayakawa Y. Cytokines in cancer immunity and immunotherapy. *Immunol Rev* 2004; **202**: 275–293.
22. Lee SH, Yoo NJ, Lee JY. Death receptor mutations. In: El-Deiry WS, ed. *Cancer drug discovery and development: Death receptors in cancer biology*. New Jersey: Humana Press Inc. 2005: 149–162.
23. Strand S, Hofmann WJ, Hug H, *et al.* Lymphocyte apoptosis induced by CD95 (APO-1/Fas) ligand-expressing tumor cells—A mechanism of immune evasion? *Nat Med* 1996; **2**: 1361–1366.
24. Reesink-Peters N, Hougardy BM, van den Heuvel FA, *et al.* Death receptors and ligands in cervical carcinogenesis: An immunohistochemical study. *Gynecol Oncol* 2005; **96**: 705–713.
25. Hopkins-Donaldson S, Ziegler A, Kurtz S, *et al.* Silencing of death receptor and caspase-8 expression in small cell lung carcinoma cell lines and tumors by DNA methylation. *Cell Death Differ* 2003; **10**: 356–364.
26. Shivapurkar N, Reddy J, Matta H, *et al.* Loss of expression of death-inducing signaling complex (DISC) components in lung cancer cell lines and the influence of MYC amplification. *Oncogene* 2002; **21**: 8510–8514.

27. Shivapurkar N, Toyooka S, Toyooka KO, *et al.* Aberrant methylation of trail decoy receptor genes is frequent in multiple tumor types. *Int J Cancer* 2004; **109**: 786–792.
28. Margetts CD, Astuti D, Gentle DC, *et al.* Epigenetic analysis of HIC1, CASP8, FLIP, TSP1, DCR1, DCR2, DR4, DR5, KvDMR1, H19 and preferential 11p15.5 maternal-allele loss in von Hippel-Lindau and sporadic phaeochromocytomas. *Endocr Relat Cancer* 2005; **12**: 161–172.
29. Pitti RM, Marsters SA, Lawrence DA, *et al.* Genomic amplification of a decoy receptor for Fas ligand in lung and colon cancer. *Nature* 1998; **396**: 699–703.
30. Bai C, Connolly B, Metzker ML, *et al.* Overexpression of M68/DcR3 in human gastrointestinal tract tumors independent of gene amplification and its location in a four-gene cluster. *Proc Natl Acad Sci USA* 2000; **97**: 1230–1235.
31. Sheikh MS, Huang Y, Fernandez-Salas EA, *et al.* The antiapoptotic decoy receptor TRID/TRAIL-R3 is a p53-regulated DNA damage-inducible gene that is overexpressed in primary tumors of the gastrointestinal tract. *Oncogene* 1999; **18**: 4153–4159.
32. Wajant H. Targeting the FLICE Inhibitory Protein (FLIP) in cancer therapy. *Mol Interv* 2003; **3**: 124–127.
33. Roth W, Reed JC. FLIP protein and TRAIL-induced apoptosis. *Vitam Horm* 2004; **67**: 189–206.
34. French LE, Tschopp J. Defective death receptor signaling as a cause of tumor immune escape. *Semin Cancer Biol* 2002; **12**: 51–55.
35. Huang Y, He Q, Hillman MJ, Rong R, Sheikh MS. Sulindac sulfide-induced apoptosis involves death receptor 5 and the caspase 8-dependent pathway in human colon and prostate cancer cells. *Cancer Res* 2001; **61**: 6918–6924.
36. Jang TJ, Kang HJ, Kim JR, Yang CH. Non-steroidal anti-inflammatory drug activated gene (NAG-1) expression is closely related to death receptor-4 and -5 induction, which may explain sulindac sulfide induced gastric cancer cell apoptosis. *Carcinogenesis* 2004; **25**: 1853–1858.
37. Han Z, Pantazis P, Wyche JH, Kouttab N, Kidd VJ, Hendrickson EA. A Fas-associated death domain protein-dependent mechanism mediates the apoptotic action of non-steroidal anti-inflammatory drugs in the human leukemic Jurkat cell line. *J Biol Chem* 2001; **276**: 38748–38754.
38. Liu X, Yue P, Zhou Z, Khuri FR, Sun SY. Death receptor regulation and celecoxib-induced apoptosis in human lung cancer cells. *J Natl Cancer Inst* 2004; **96**: 1769–1780.
39. Sun SY, Lotan R. Retinoids and their receptors in cancer development and chemoprevention. *Crit Rev Oncol Hematol* 2002; **41**: 41–55.
40. Sun SY, Yue P, Wu GS, *et al.* Mechanisms of apoptosis induced by the synthetic retinoid CD437 in human non-small cell lung carcinoma cells. *Oncogene* 1999; **18**: 2357–2365.
41. Sun SY, Yue P, Wu GS, *et al.* Implication of p53 in growth arrest and apoptosis induced by the synthetic retinoid CD437 in human lung cancer cells. *Cancer Res* 1999; **59**: 2829–2833.
42. Sun SY, Yue P, Hong WK, Lotan R. Induction of Fas expression and eugmentation of Fas/FasL-mediated apoptosis by the synthetic retinoid CD437 in human lung cancer cells. *Cancer Res* 2000; **60**: 6537–6543.
43. Sun SY. Regulation of death receptors by synthetic retinoids. In: El-Deiry WS, ed. *Cancer drug discovery and development: Death receptors in cancer biology*. New Jersey: Humana Press Inc. 2005: 189–200.
44. Muller M, Wilder S, Bannasch D, *et al.* p53 activates the CD95 (APO-1/Fas) gene in response to DNA damage by anticancer drugs. *J Exp Med* 1998; **188**: 2033–4205.
45. Takimoto R, El-Deiry WS. Wild-type p53 transactivates the KILLER/DR5 gene through an intronic sequence-specific DNA-binding site. *Oncogene* 2000; **19**: 1735–1743.
46. Liu X, Yue P, Khuri FR, Sun SY. p53 upregulates death receptor 4 expression through an intronic p53 binding site. *Cancer Res* 2004; **64**: 5078–5083.
47. Sun SY, Yue P, Chen X, Hong WK, Lotan R. The synthetic retinoid CD437 selectively induces apoptosis in human lung cancer cells while sparing normal human lung epithelial cells. *Cancer Res* 2002; **62**: 2430–2436.
48. Sun SY, Yue P, Mao L, *et al.* Identification of receptor-selective retinoids that are potent inhibitors of the growth of human head and neck squamous cell carcinoma cells. *Clin Cancer Res* 2000; **6**: 1563–1573.
49. Sun SY, Yue P, Lotan R. Implication of multiple mechanisms in apoptosis induced by the synthetic retinoid CD437 in human prostate carcinoma cells. *Oncogene* 2000; **19**: 4513–4522.
50. Puduvalli VK, Li JT, Chen L, McCutcheon IE. Induction of apoptosis in primary meningioma cultures by fenretinide. *Cancer Res* 2005; **5**: 1547–1553.
51. Cuello M, Coats AO, Darko I, *et al. N*-(4-hydroxyphenyl) retinamide (4HPR) enhances TRAIL-mediated apoptosis through enhancement of a mitochondrial-dependent amplification loop in ovarian cancer cell lines. *Cell Death Differ* 2004; **1**: 527–551.
52. Sporn MB, Suh N. Chemoprevention of cancer. *Carcinogenesis* 2000; **1**: 525–550.
53. Meng RD, El-Deiry WS. p53-independent upregulation of KILLER/DR5 TRAIL receptor expression by glucocorticoids and interferon-gamma. *Exp Cell Res* 2001; **262**: 154–169.
54. Xia L, Chen D, Han R, Fang Q, Waxman S, Jing Y. Boswellic acid acetate induces apoptosis through caspase-mediated pathways in myeloid leukemia cells. *Mol Cancer Ther* 2005; **4**: 381–388.
55. Zou W, Liu X, Yue P, *et al.* c-Jun NH2-terminal kinase-mediated up-regulation of death receptor 5 contributes to induction of apoptosis by the novel synthetic triterpenoid methyl-2-cyano-3,12-dioxooleana-1, 9-dien-28-oate in human lung cancer cells. *Cancer Res* 2004; **64**: 7570–7578.
56. Aggarwal BB, Bhardwaj A, Aggarwal RS, Seeram NP, Shishodia S, Takada Y. Role of resveratrol in prevention and therapy of cancer: Preclinical and clinical studies. *Anticancer Res* 2004; **24**: 2783–2840.
57. Delmas D, Rebe C, Lacour S, *et al.* Resveratrol-induced apoptosis is associated with Fas redistribution in the rafts and the formation of a death-inducing signaling complex in colon cancer cells. *J Biol Chem* 2003; **278**: 41482–41490.
58. Delmas D, Rebe C, Micheau O, *et al.* Redistribution of CD95, DR4 and DR5 in rafts accounts for the synergistic toxicity of resveratrol and death receptor ligands in colon carcinoma cells. *Oncogene* 2004; **23**: 8979–8986.
59. Kuo PL, Lin CC. Green tea constituent (−)-epigallocatechin-3-gallate inhibits Hep G2 cell proliferation and induces apoptosis through p53-dependent and Fas-mediated pathways. *J Biomed Sci* 2003; 10: 219–227.
60. Hayakawa S, Saeki K, Sazuka M, *et al.* Apoptosis induction by epigallocatechin gallate involves its binding to Fas. *Biochem Biophys Res Commun* 2001; **285**: 1102–1106.
61. Turley JM, Fu T, Ruscetti FW, Mikovits JA, Bertolette DC 3rd, Birchenall-Roberts MC. Vitamin E succinate induces Fas-mediated apoptosis in estrogen receptor-negative human breast cancer cells. *Cancer Res* 1997; **57**: 881–890.
62. Yu W, Israel K, Liao QY, Aldaz CM, Sanders BG, Kline K. Vitamin E succinate (VES) induces Fas sensitivity in human

breast cancer cells: Role for Mr 43,000 Fas in VES-triggered apoptosis. *Cancer Res* 1999; **59**: 953–961.
63. Israel K, Yu W, Sanders BG, Kline K. Vitamin E succinate induces apoptosis in human prostate cancer cells: Role for Fas in vitamin E succinate-triggered apoptosis. *Nutr Cancer* 2000; **36**: 90–100.
64. Tomasetti M, Rippo MR, Alleva R, *et al.* Alpha-tocopheryl succinate and TRAIL selectively synergise in induction of apoptosis in human malignant mesothelioma cells. *Br J Cancer* 2004; **90**: 1644–1653.
65. He Q, Rashid A, Rong R, Hillman MJ, Huang Y, Sheikh MS. Death receptor 5 regulation during selenium-mediated apoptosis in human prostate cancer cells. *Cancer Biol Ther* 2002; **1**: 287–290.
66. Fujita K, Matsuda E, Sekine K, Iigo M, Tsuda H. Lactoferrin enhances Fas expression and apoptosis in the colon mucosa of azoxymethane-treated rats. *Carcinogenesis* 2004; **25**: 1961–1966.
67. Bush JA, Cheung KJ Jr, Li G. Curcumin induces apoptosis in human melanoma cells through a Fas receptor/caspase-8 pathway independent of p53. *Exp Cell Res* 2001; **271**: 305–314.
68. Deeb D, Jiang H, Gao X, *et al.* Curcumin sensitizes prostate cancer cells to tumor necrosis factor-related apoptosis-inducing ligand/Apo2L by inhibiting nuclear factor-kappaB through suppression of IkappaBalpha phosphorylation. *Mol Cancer Ther* 2004; **3**: 803–812.
69. Shigeno M, Nakao K, Ichikawa T, *et al.* Interferon-alpha sensitizes human hepatoma cells to TRAIL-induced apoptosis through DR5 upregulation and NF-kappa B inactivation. *Oncogene* 2003; **22**: 1653–1662.
70. Altucci L, Rossin A, Raffelsberger W, Reitmair A, Chomienne C, Gronemeyer H. Retinoic acid-induced apoptosis in leukemia cells is mediated by paracrine action of tumor-selective death ligand TRAIL. *Nat Med* 2001; **7**: 680–686.
71. Clarke N, Jimenez-Lara AM, Voltz E, Gronemeyer H. Tumor suppressor IRF-1 mediates retinoid and interferon anticancer signaling to death ligand TRAIL. *EMBO J* 2004; **23**: 3051–3060.
72. Wang Q, Ji Y, Wang X, Evers BM. Isolation and molecular characterization of the 5′-upstream region of the human TRAIL gene. *Biochem Biophys Res Commun* 2000; **276**: 466–471.
73. Wang Q, Wang X, Hernandez A, Hellmich MR, Gatalica Z, Evers BM. Regulation of TRAIL expression by the phosphatidylinositol 3-kinase/Akt/GSK-3 pathway in human colon cancer cells. *J Biol Chem* 2002; **277**: 36602–36610.
74. Klaunig JE, Xu Y, Isenberg JS, *et al.* The role of oxidative stress in chemical carcinogenesis. *Environ Health Perspect* 1998; **106**: 289–295.
75. Vallyathan V, Shi X, Castranova V. Reactive oxygen species: Their relation to pneumoconiosis and carcinogenesis. *Environ Health Perspect* 1998; **106**: 1151–1155.

THE JOURNAL OF BIOLOGICAL CHEMISTRY VOL. 282, NO. 26, pp. 18800–18809, June 29, 2007

The Farnesyltransferase Inhibitor Lonafarnib Induces CCAAT/Enhancer-binding Protein Homologous Protein-dependent Expression of Death Receptor 5, Leading to Induction of Apoptosis in Human Cancer Cells*[S]

Received for publication, December 13, 2006, and in revised form, May 8, 2007 Published, JBC Papers in Press, May 9, 2007, DOI 10.1074/jbc.M611438200

Shi-Yong Sun[1,2], **Xiangguo Liu, Wei Zou, Ping Yue, Adam I. Marcus, and Fadlo R. Khuri**[1]

From the Department of Hematology and Oncology, Winship Cancer Institute, Emory University School of Medicine, Atlanta, Georgia 30322

Pre-clinical studies have demonstrated that farnesyltransferase inhibitors (FTIs) induce growth arrest or apoptosis in various human cancer cells independently of Ras mutations. However, the underlying mechanism remains unknown. Death receptor 5 (DR5) is a pro-apoptotic protein involved in mediating the extrinsic apoptotic pathway. Its role in FTI-induced apoptosis has not been reported. In this study, we investigated the modulation of DR5 by the FTI lonafarnib and the involvement of DR5 up-regulation in FTI-induced apoptosis. Lonafarnib activated caspase-8 and its downstream caspases, whereas the caspase-8-specific inhibitor benzyloxycarbonyl-Ile-Glu(methoxy)-Thr-Asp(methoxy)-fluoromethyl ketone or small interfering RNA abrogated lonafarnib-induced apoptosis, indicating that lonafarnib induces caspase-8-dependent apoptosis. Lonafarnib up-regulated DR5 expression, increased cell-surface DR5 distribution, and enhanced tumor necrosis factor-related apoptosis-inducing ligand-induced apoptosis. Overexpression of a dominant-negative Fas-associated death domain mutant or silencing of DR5 expression using small interfering RNA attenuated lonafarnib-induced apoptosis. These results indicate a critical role of the DR5-mediated extrinsic apoptotic pathway in lonafarnib-induced apoptosis. By analyzing the DR5 promoter, we found that lonafarnib induced a CCAAT/enhancer-binding protein homologous protein (CHOP)-dependent transactivation of the DR5 promoter. Lonafarnib increased CHOP expression, whereas silencing of CHOP expression abrogated lonafarnib-induced DR5 expression. These results thus indicate that lonafarnib induces CHOP-dependent DR5 up-regulation. We conclude that CHOP-dependent DR5 up-regulation contributes to lonafarnib-induced apoptosis.

Farnesyltransferase inhibitors (FTIs)[3] are a class of agents that suppress the farnesyltransferase enzyme to prevent farnesylation of certain proteins such as the Ras oncoprotein (1, 2). These agents inhibit proliferation and induce apoptosis in various cancer cell lines in culture or suppress the growth of xenografts in nude mice with limited toxicity (1, 2). In the clinic, FTIs are well tolerated and have some positive outcomes in certain settings such as hematological malignancies and breast cancer, although the response rates to FTIs alone are generally poor. When combined with other therapeutic agents or radiotherapy, FTIs exhibit some encouraging clinical responses (1, 2).

Lonafarnib (LNF; also called SCH66336 and Sarasar), a nonpeptide tricyclic FTI, was one of the first FTIs to undergo clinical testing and to exhibit significant activity (3). *In vitro*, this agent, either alone or in combination with other therapeutic agents, inhibits the growth or induces apoptosis of several types of human cancer cells (4–12). In animal models, LNF demonstrates potent oral activity in a wide array of human tumor xenograft models including tumors of colon, lung, pancreas, prostate, and urinary bladder origin (12). When LNF is combined with other chemotherapeutic agents, enhanced antitumor activity is observed (4, 6). In a phase I trial enrolling individuals with lung or aerodigestive tract cancer, a provocative clinical activity was observed when LNF was combined with paclitaxel (13). In a recent phase II trial, LNF plus paclitaxel achieved significant clinical activity with a favorable safety profile in patients with taxane-refractory/resistant metastatic non-small cell lung cancer (14), and these results were later supported by pre-clinical data in cell lines (15).

There are two major apoptotic pathways: one involves death signals transduced through death receptors (extrinsic apoptotic pathway), and the other relies on mitochondrial signals (intrinsic apoptotic pathway) (16). Both pathways are involved in an ordered activation of a set of caspases, which in turn cleave cellular substrates, leading to apoptosis. The activation of caspase-8 and caspase-9 has been documented to play a central

* This work was supported by a Georgia Cancer Coalition Distinguished Cancer Scholar award (to S.-Y. S.) and by Department of Defense TARGET Grant DAMD 17-02-1-0706 (to F. R. K. for Project 6) and VITAL Grant W81XWH-04-1-0142 (to S.-Y. S. for Project 4). The costs of publication of this article were defrayed in part by the payment of page charges. This article must therefore be hereby marked "*advertisement*" in accordance with 18 U.S.C. Section 1734 solely to indicate this fact.

[S] The on-line version of this article (available at http://www.jbc.org) contains supplemental Figs. S1–S3.

[1] Georgia Cancer Coalition Distinguished Cancer Scholars.

[2] To whom correspondence should be addressed: Winship Cancer Inst., Emory University School of Medicine, 1365-C Clifton Rd., C3088, Atlanta, GA 30322. Tel.: 404-778-2170; Fax: 404-778-5520; E-mail: shi-yong.sun@emoryhealthcare.org.

[3] The abbreviations used are: FTIs, farnesyltransferase inhibitors; LNF, lonafarnib; TRAIL, tumor necrosis factor-related apoptosis-inducing ligand; DR5, death receptor 5; CHOP, CCAAT/enhancer-binding protein homologous protein; ER, endoplasmic reticulum; OMe, methoxy; RasGAP, Ras GTPase-activating protein; FADDm, Fas-associated death domain mutant; FBS, fetal bovine serum; PE, phycoerythrin; PIPES, 1,4-piperazinediethanesulfonic acid; siRNA, small interfering RNA.

role in mediating apoptosis signaled by death receptors and by mitochondria, respectively; however, caspase-8 can activate the caspase-9-mediated apoptotic pathway by activating or cleaving Bid protein (16).

The tumor necrosis factor-related apoptosis-inducing ligand (TRAIL) receptor, death receptor 5 (DR5; also named Apo2, TRAIL receptor 2, TRICK2, or Killer/DR5), belongs to the tumor necrosis factor receptor gene superfamily, the members of which all share a similar cysteine-rich extracellular domain and an additional cytoplasmic death domain (17). DR5 localizes to the cell surface, becomes activated or oligomerized (trimerized) upon binding to its ligand TRAIL or through overexpression, and then signals an apoptotic response through caspase-8-mediated rapid activation of caspase cascades (17). DR5 has recently attracted more attention because its ligand TRAIL preferentially induces apoptosis in transformed or malignant cells, demonstrating potential as a tumor-selective apoptosis-inducing cytokine for cancer treatment (18, 19). Certain cancer therapeutic agents induce the expression of DR5 in various types of cancer cells and thus are able to augment TRAIL-induced apoptosis or to initiate apoptosis (20).

The CCAAT/enhancer-binding protein homologous protein (CHOP), also known as GADD153 (growth arrest and DNA damage gene 153), is an endoplasmic reticulum (ER) stress-induced transcription factor involved in the regulation of apoptosis, particularly ER stress-associated apoptosis (21). Recent studies have demonstrated that CHOP directly regulates DR5 expression through a CHOP-binding site in the 5-flanking region of the DR5 gene (22, 23). Certain drugs induce DR5 expression through CHOP-dependent transactivation of the DR5 gene (22–24).

The mechanisms underlying FTI-mediated growth arrest and apoptosis induction are largely undefined (1). Several non-Ras targets such as RhoB and Rab geranylgeranyltransferase have been proposed (25, 26). In addition, Akt inactivation appears to play a role in apoptosis induced by a subset of FTIs (5, 27, 28), although some studies have been unable to demonstrate this role (29–31). However, DR5 has not been suggested to be involved in the biological actions of FTIs. In this study, we reveal, for the first time, a novel mechanism in human cancer cells by which FTIs, particularly LNF, induce apoptosis via the CHOP-dependent up-regulation of DR5 expression and subsequent caspase-8 activation.

EXPERIMENTAL PROCEDURES

Reagents—LNF and its analog SCH66337 were provided by Schering-Plough Research Institute (Kenilworth, NJ). They were dissolved in Me_2SO at a concentration of 10 mM, and aliquots were stored at −80 °C. Stock solutions were diluted to the desired final concentrations with growth medium just before use. Soluble human recombinant TRAIL was purchased from BIOMOL International (Plymouth Meeting, PA). The caspase inhibitors benzyloxycarbonyl-Val-Ala-Asp-fluoromethyl ketone and benzyloxycarbonyl-Ile-Glu(OMe)-Thr-Asp(OMe)-fluoromethyl ketone were purchased from Enzyme System Products (Livermore, CA). Staurosporine and other chemicals were purchased from Sigma. Rabbit polyclonal anti-DR5 antibody was purchased from ProSci Inc. (Poway, CA). Mouse monoclonal anti-caspase-3 antibody was purchased from Imgenex (San Diego, CA). Rabbit polyclonal anti-caspase-9, anti-caspase-8, and anti-poly(ADP-ribose) polymerase antibodies were purchased from Cell Signaling Technology, Inc. (Beverly, MA). Mouse monoclonal anti-Ras GTPase-activating protein (RasGAP) antibody B4F8 was purchased from Santa Cruz Biotechnology, Inc. (Santa Cruz, CA). Mouse monoclonal anti-HDJ-2 antibody (clone KA2A5.6) was purchased from Lab Vision Corp. (Fremont, CA). Mouse monoclonal anti-BiP/GRP78 antibody was purchased from BD Transduction Laboratories.

Cell Lines and Cell Cultures—All cell lines were purchased from American Type Culture Collection (Manassas, VA). H460 cell lines stably expressing a dominant-negative Fas-associated death domain mutant (FADDm) were described previously (32). These cell lines were grown in monolayer culture in RPMI 1640 medium supplemented with glutamine and 5% fetal bovine serum (FBS) at 37 °C in a humidified atmosphere consisting of 5% CO_2 and 95% air.

Western Blot Analysis—The procedures for preparation of whole cell protein lysates and Western blot analysis were described previously (32, 33).

Detection of DR5 mRNA Expression—DR5 mRNA was detected by reverse transcription-PCR as follows. Total RNA was isolated from cells using TriReagent (Sigma) as instructed by the manufacturer. First-strand cDNA was synthesized from 2 μg of total RNA in a volume of 20 μl containing 1 μl of avian myeloblastosis virus reverse transcriptase, 0.5 μl of dNTP (25 mM each), 0.5 μl of random primer (0.5 μg/μl), 4 μl of 5× reverse transcription buffer, and sterile H_2O, followed by incubation at 42 °C for 60 min and inactivation by heating at 70 °C for 15 min. cDNA was then amplified by PCR using the following primers: DR5, 5′-GACCTAGCTCCCCAGCAGAGAG-3′ (sense) and 5′-CGGCTGCAACTGTGACTCCTAT-3′ (antisense); and β-actin, 5′-GAAACTACCTTCAACTCCATC-3′ (sense) and 5′-CTAGAAGCATTTGCGGTGGACGATGGAGGGGCC-5′ (antisense). The 25-μl amplification mixture contained 2 μl of cDNA, 0.5 μl of dNTP (25 mM each), 1 μl each of the sense and antisense primers (20 μM each), 1 μl of *Taq* DNA polymerase (5 units/μl; Promega, Madison, MI), 2.5 μl of 10× reaction buffer, and sterile H_2O. PCR was performed for 28 cycles. After an initial step at 95 °C for 3 min, each cycle consisted of 50 s of denaturation at 94 °C, 50 s of annealing at 58 °C, and 55 s of extension at 72 °C. This was followed by an additional extension step at 72 °C for 10 min. The housekeeping gene β-actin was also amplified as an internal reference. PCR products were resolved by electrophoresis on a 4% agarose gel, stained, and directly visualized under UV illumination.

Construction of DR5 Reporter Plasmid, Transient Transfection, and Luciferase Activity Assay—The plasmid containing a 5′-flanking region of the DR5 gene was kindly provided by Dr. G. S. Wu (Wayne State University School of Medicine, Detroit, MI). We used this plasmid as a template to amplify a series of deletion fragments of the 5′-flanking region of the DR5 gene ranging from 3070 to 120 bp upstream of the translation start site by PCR and then subcloned these fragments into the pGL3-Basic reporter vector (Promega) through KpnI and

BglII restriction sites. In the PCR amplification, the reverse primer 5′-CTTAAGATCTGGCGGTAGGGAACGCTCTTATAGTC-3′ was used to make all deletion constructs. The upstream primers used were 5′-CTTAGGTACCTGGCTCGTCTGTTCCTCTACGGCCCC-3′ (−3070), 5′-CTTAGGTACCTCAACTCATTTCCCCCAAGTTTC-3′ (−420), 5′-CTTAGGTACCACCCAGAAACAAACCACAGCCCGGG-3′ (−373), 5′-CTTAGGTACCCTTATTTATTGTCACCAACCTGTGG-3′ (−240), and 5′-CTTAGGTACCGCACGCGGCCGGAGAACCCC-3′ (−120). These constructs were named pGL3-DR5(−3070), pGL3-DR5(−420), pGL3-DR5(−373), pGL3-DR5(−240), and pGL3-DR5(−120), respectively. The reporter constructs containing a 552-bp 5′-flanking region of the DR5 gene with a wild-type or mutated CHOP-binding site, an NF-κB-binding site, or an Elk-binding site were generously provided by Dr. H.-G. Wang (University of South Florida College of Medicine, Tampa, FL) (22). In this study, we also used the pGL3-Promoter luciferase vector (pGL3-SV40-Luc; Promega), which contains an SV40 promoter, as a control. A pCH110 plasmid encoding β-galactosidase (GE Healthcare) was used in the cotransfection for normalization. These plasmids were purified with a Qiafilter plasmid maxi kit (Qiagen Inc.).

To examine the effect of LNF on DR5 transactivation activity, cells were seeded in 24-well plates and cotransfected with the given reporter plasmid (0.5 μg/well) and the pCH110 plasmid (0.2 μg/well) using FuGENE 6 transfection reagent (3:1 ratio; Roche Applied Science) following the manufacturer's protocol. Twenty-four hours later, the cells were treated with LNF. After 12 h, the cells were lysed and subjected to luciferase activity assay using a luciferase assay system (Promega) in a luminometer. Relative luciferase activity was normalized to β-galactosidase activity, which was measured as described previously (34).

Detection of Cell-surface DR5—In this study, cell-surface DR5 expression was analyzed by both flow cytometry and immunofluorescent staining. The procedure for direct antibody staining and subsequent flow cytometric analysis of cell-surface protein was described previously (35). The mean fluorescent intensity that represents antigenic density on a per cell basis was used to represent DR5 expression levels. Phycoerythrin (PE)-conjugated mouse monoclonal anti-human DR5 (clone DJR2-4), anti-human DR4 (clone DJR1), anti-human decoy receptor 1 (clone DJR3), anti-human decoy receptor 2 (clone DJR4-1), and anti-human Fas (clone DX2) antibodies and PE-conjugated mouse IgG1 isotype control (MOPC21/P3) were purchased from eBioscience (San Diego, CA). For immunofluorescent staining, cells were plated overnight on coverslips in 24-well plates and treated with different concentrations of LNF. Cells were then fixed in 68 mM PIPES, 25 mM HEPES, 15 mM EGTA, and 3 mM $MgCl_2$ with 3.7% formaldehyde, 0.05% glutaraldehyde, and 0.5% Triton X-100 for 10 min; washed three times with phosphate-buffered saline; and then blocked for 15 min with 10% normal goat serum. Next, cells were incubated with PE-conjugated mouse monoclonal anti-DR5 antibody (clone DJR2-4) diluted 1:15 in 5% normal goat serum for 1 h at room temperature. After the cells were washed three times, coverslips were removed from wells, inverted, and placed on slides. Images were acquired using a ×63 Zeiss Plan-Apochromat oil lens (numerical aperture = 1.4) mounted on a Zeiss LMS 510 confocal laser scanning microscope.

Detection of Apoptosis—The amounts of cytoplasmic histone-associated DNA fragments (mono- and oligonucleosomes) formed during apoptosis were measured using a Cell Death Detection ELISA^{Plus} kit (Roche Applied Science) according to the manufacturer's instructions. Caspase activation and substrate cleavage were detected by Western blot analysis as described above. In addition, we also counted floating cells in the medium as another indicator of apoptotic cell death. Because the albumin in the serum attenuates the FTI effect in culture (31), we performed these experiments in 0.1% serum-containing medium to increase induction of apoptosis.

Cell Survival Assay—Cells were seeded in 96-well cell culture plates and treated on the 2nd day with the indicated agents. At the end of treatment, the cell number was estimated by the sulforhodamine B assay as described previously (36).

Small Interfering RNA (siRNA)-mediated Gene Silencing—High purity control (non-silencing) siRNA oligonucleotides that target sequence 5′-AATTCTCCGAACGTGTCACGT-3′ was purchased from Qiagen Inc. Caspase-8, DR5, and CHOP siRNA duplexes that target sequences 5′-AACTACCAGAAAGGTATACCT-3′, 5′-AAGACCCTTGTGCTCGTTGTC-3′ (32, 37), and 5′-AAGAACCAGCAGAGGUCACAA-3′ (22), respectively, were synthesized by Qiagen Inc. The additional DR5 siRNA-2, which targets sequence 5′-AAGTTGCAGCCGTAGTCTTGA-3′ (22), was also synthesized by Qiagen Inc. Transfection of siRNA was performed as described previously (32). Gene silencing effects and caspase activation were evaluated by Western blot analysis, whereas DNA fragmentation was measured using the Cell Death Detection ELISA^{Plus} kit as described above.

Statistical Analysis—Cell survival and apoptosis (*i.e.* DNA fragmentation) between two groups were analyzed with two-sided unpaired Student's *t* tests when the variances were equal or with Welch's corrected *t* test when the variances were not equal using GraphPad InStat Version 3 software. The assumption for use of the *t* tests was calculated and suggested by the same software. All means ± S.D. from triplicate or quadruplicate samples were calculated with Microsoft Excel Version 5.0 software. In all statistical analyses, results were considered to be statistically significant at $p < 0.05$.

RESULTS

LNF Induces Caspase-8-dependent Apoptosis—Our previous study has shown that LNF induces apoptosis, particularly in low serum culture medium (31). Here, we examined further the effects of LNF on caspase activation and its involvement in LNF-induced apoptosis in human lung cancer cells. In both H157 and H1792 human lung cancer cell lines, LNF decreased the levels of the proforms of caspase-8, -9, and -3; increased the levels of their cleaved forms; and induced cleavage of poly(ADP-ribose) polymerase and RasGAP, both of which are caspase-3 substrates (38), in a concentration-dependent manner (Fig. 1*A*). These results indicate that LNF activates both caspase-8- and caspase-9-mediated activation of caspase cascades. Because caspase-8 activation is a critical event in the extrinsic apoptotic signaling pathway, we tested

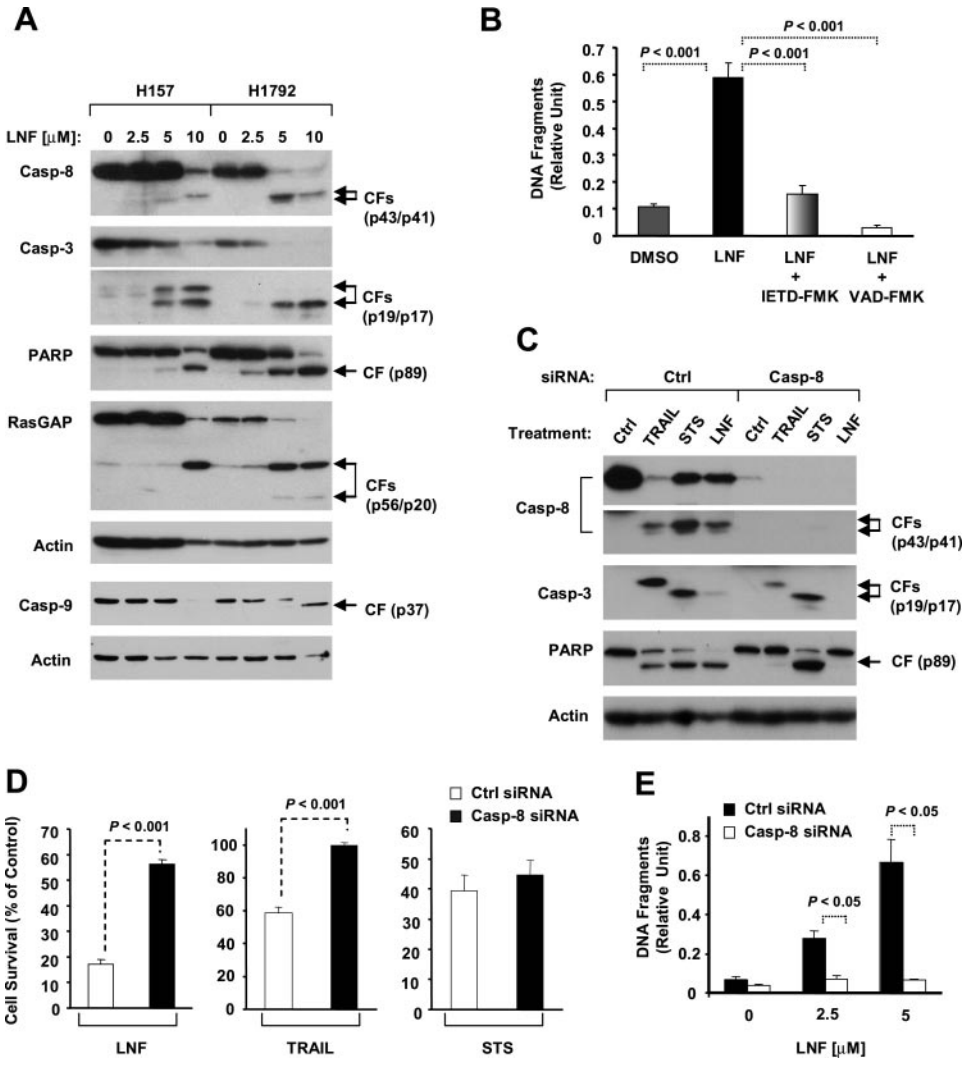

FIGURE 1. **LNF induces caspase-8-mediated apoptosis.** *A*, LNF induces caspase activation. The indicated lung cancer cell lines were treated with the indicated concentrations of LNF in 0.1% FBS for 24 h. Whole cell protein lysates were then prepared from these cell lines and subjected to detection of cleavage of caspase (*Casp*)-8, caspase-9, caspase-3, RasGAP, and poly(ADP-ribose) polymerase (*PARP*) by Western blot analysis. Actin expression was used as a loading control. *CFs*, cleaved forms. *B*, suppression of LNF-induced DNA fragmentation by caspase inhibitors. H1792 cells were pretreated with 50 μM caspase inhibitors as indicated and then cotreated with the given caspase inhibitor and 5 μM LNF in 0.1% FBS. After 24 h, the cells were subjected to estimation of DNA fragmentation using the Cell Death Detection ELISA^{plus} kit. Data are the means ± S.D. of three identical wells. *DMSO*, Me_2SO; *IETD-FMK*, benzyloxycarbonyl-Ile-Glu(OMe)-Thr-Asp(OMe)-fluoromethyl ketone; *VAD-FMK*, benzyloxycarbonyl-Val-Ala-Asp-fluoromethyl ketone. *C* and *D*, silencing of caspase-8 expression (*C*) decreases cell sensitivity to LNF-induced cell death (*D*) and inhibits LNF-induced caspase activation (*C*). H1792 cells were seeded in a 24-well cell culture plate and transfected with control (*Ctrl*) or caspase-8 siRNA. After 48 h, the cells were treated with the Me_2SO control (*Ctrl*), 7.5 μM LNF, 40 ng/ml TRAIL, or 0.5 μM staurosporine (*STS*) in 0.1% fetal calf serum for 24 h. The cells were then subjected to preparation of whole cell protein lysates and subsequent Western blot analysis (*C*). In addition, cells were also seeded in 96-well plates and treated with the solvent control, 7.5 μM LNF, 80 ng/ml TRAIL, or 0.25 μM staurosporine. After 24 h, the cell numbers were estimated using the sulforhodamine B assay (*D*). Data are the means ± S.D. of four identical wells. *E*, silencing of caspase-8 expression abrogates LNF-induced DNA fragmentation. H1792 cells were seeded in a 24-well cell culture plate and transfected twice with control or caspase-8 siRNA in a 48-h interval. Forty hours later after the second transfection, the cells were treated with the indicated concentrations of LNF in 0.1% FBS for 24 h and then subjected to evaluation of DNA fragmentation using the Cell Death Detection ELISA^{plus} kit. Data are the means ± S.D. of three identical wells.

whether caspase-8 activation is required for LNF-induced apoptosis. LNF significantly increased the amount of DNA fragments ($p < 0.001$), but in the presence of the pan-caspase inhibitor benzyloxycarbonyl-Val-Ala-Asp-fluoromethyl ketone or the caspase-8 inhibitor benzyloxycarbonyl-Ile-Glu-(OMe)-Thr-Asp(OMe)-fluoromethyl ketone, LNF failed to increase the levels of DNA fragments ($p < 0.001$) (Fig. 1*B*), indicating that LNF-induced apoptosis is caspase-dependent, particularly caspase-8-dependent. To further demonstrate the importance of caspase-8 activation in LNF-induced apoptosis, we silenced the expression of caspase-8 and then examined its impact on LNF-induced apoptosis. As shown in Fig. 1*C*, caspase-8 levels were dramatically decreased in H1792 cells transfected with the caspase-8 siRNA in comparison with caspase-8 levels in those cells transfected with the control siRNA. By measuring cell survival, we found that LNF caused significantly less cell death in caspase-8 siRNA-transfected cells than in control siRNA-transfected cells (Fig. 1*D*). Accordingly, we detected cleaved forms of caspase-8, caspase-3, and poly(ADP-ribose) polymerase (Fig. 1*C*) and increased amounts of DNA fragments (Fig. 1*E*) in control siRNA-transfected cells but not in caspase-8 siRNA-transfected cells after exposure to LNF. These results clearly indicate that silencing of caspase-8 expression inhibits LNF-induced apoptosis, further supporting the essential role of caspase-8 activation in LNF-induced apoptosis. Used as control treatments, TRAIL, a cytokine known to trigger the extrinsic apoptotic pathway, failed to decrease cell survival (Fig. 1*D*) and exhibited attenuated effects on the cleavage of caspase-8, caspase-3, and poly-(ADP-ribose) polymerase (Fig. 1*C*) in caspase-8 siRNA-transfected cells, whereas staurosporine, a small molecule known to induce apoptosis through the mitochondrial apoptotic pathway, was equally active in inducing cell death (Fig. 1*D*) and cleavage of caspase-3 and poly-(ADP-ribose) polymerase in both control and caspase-8 siRNA-transfected cells, although caspase-8 cleavage was inhibited in caspase-8 siRNA-transfected cells (Fig. 1*C*).

LNF Induces DR5 Expression—Because caspase-8 activation is an essential step in the extrinsic death receptor-mediated apoptotic pathway, we next tested whether LNF affects the expression of death receptors. By Western blot analysis, we found that LNF increased DR5 expression in a time- and concentration-dependent manner (Fig. 2, *A* and *B*). Specifically,

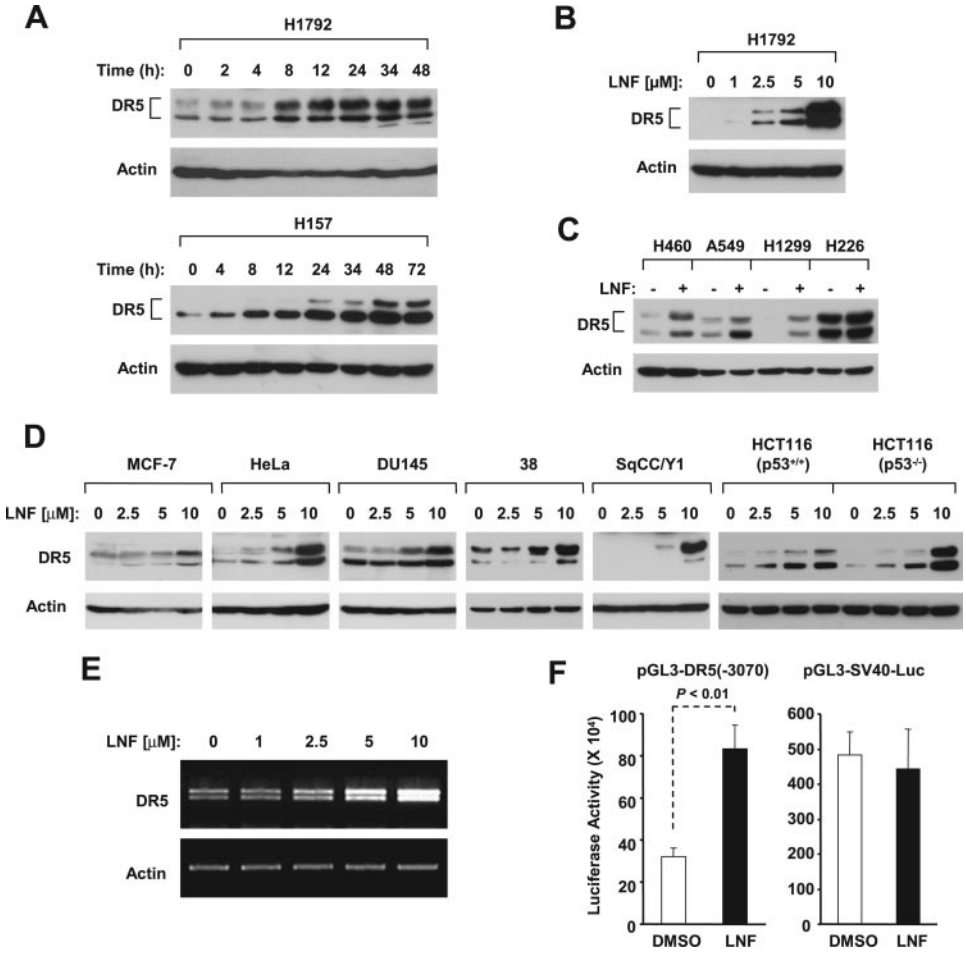

FIGURE 2. **LNF increases DR5 expression at both the protein (*A–D*) and mRNA (*E* and *F*) levels in human cancer cells.** *A*, the indicated cell lines were treated with 5 μM LNF for the indicated times. *B*, H1792 cells were treated with the indicated concentrations of LNF for 24 h. *C*, the indicated human lung cancer cell lines were treated with 5 μM LNF for 16 h. *D*, the indicated cell lines were treated with the given concentrations of LNF for 16 h. Whole cell protein lysates were then prepared from the aforementioned treatments for detection of DR5 expression by Western blot analysis. *E*, H1792 cells were exposed to the indicated concentrations of LNF for 8 h. Cellular total RNA was then prepared for detection of DR5 mRNA by reverse transcription-PCR. Actin levels were used as an internal control. *F*, H1792 cells were transiently transfected with pGL3-DR5(−3070) or pGL3-SV40-Luc for 24 h and then treated with Me_2SO (*DMSO*) or 10 μM LNF for an additional 12 h. The cells were subjected to a luciferase assay. Data are the means ± S.D. of three identical determinants.

LNF-induced DR5 expression occurred at 8 h, reached a peak at 24 h (H1792 cells) or 48 h (H157 cells), and was sustained up to 48 h (H1792 cells) or 72 h (H157 cells) post-LNF treatment (Fig. 2*A*). The highest levels of DR5 expression were observed with 10 μM LNF; however, 2.5 μM LNF was sufficient to increase DR5 expression relative to untreated cells (Fig. 2*B*). Therefore, it appears that, at clinically achievable and tolerable concentrations (2–5 μM) (39, 40), LNF induces rapid but sustained up-regulation of DR5 expression. Moreover, we found that LNF also increased DR5 expression in other human lung cancer cell lines, as shown in Fig. 2*C*, as well as in other types of cancer cell lines, including breast (MCF-7), cervical (HeLa), prostate (DU145), head and neck (38 and SqCC/Y1), and colon (HCT116) (Fig. 2*D*). We also compared the effects of LNF on DR5 induction in HCT116($p53^{+/+}$) and HCT116($p53^{-/-}$) cell lines and found that LNF up-regulated DR5 expression in both cell lines (Fig. 2*D*). These findings indicate that DR5 induction by LNF commonly occurs in human cancer cells. We noted that LNF also increased DR4 expression; however, it did not occur in all tested cell lines (data not shown). Thus, we focused our subsequent studies on DR5 induction.

To determine whether DR5 induction by LNF occurs at the transcriptional level, we detected DR5 mRNA levels in cells exposed to different concentrations of LNF using reverse transcription-PCR. As shown in Fig. 2*E*, LNF at concentrations ranging from 2.5 to 10 μM increased DR5 mRNA levels in a concentration-dependent manner. Moreover, we examined the effect of LNF on DR5 promoter activity and observed that LNF significantly increased luciferase activity in cells transfected with a luciferase reporter plasmid carrying a DR5 5′-flanking region (*i.e.* pGL3-DR5(−3070)), but not in cells transfected with a reporter plasmid driven by the SV40 promoter (*i.e.* pGL3-SV40-Luc) (Fig. 2*F*), indicating that LNF enhances DR5 transactivation. Collectively, these results clearly show that LNF up-regulates DR5 expression at the transcriptional level.

LNF Increases Cell-surface DR5 Levels—It is known that DR5 functions as a cell-surface protein (17). Thus, we were interested in determining whether LNF increases cell-surface DR5 levels. In this study, we treated cells with LNF, stained the cells with PE-conjugated anti-DR5 antibody, and analyzed PE-positive cells by flow cytometry and confocal microscopy. By flow cytometry, we detected a dramatic increase in fluorescent intensity in both H1792 and H157 cells treated with LNF compared with cells exposed to the Me_2SO control (Fig. 3*A*). The mean fluorescent intensities were 22.82, 60.01, and 142.71 in H1792 cells treated with the Me_2SO control, 5 μM LNF, and 10 μM LNF, respectively, and 29.44, 67.70, and 109.96 in H157 cells, respectively. By confocal microscopy, we observed low levels of cytoplasmic DR5 protein in control cells without cell-surface staining of DR5. After treatment with LNF, we observed clear DR5 staining on the cell surface, particularly at 5 and 10 μM (Fig. 3*B*), indicating that LNF induces cell-surface localization of DR5. Collectively, these data clearly demonstrate that LNF increases cell-surface DR5 levels.

In addition, we determined whether LNF alters the levels of other death or TRAIL receptors. H1792 cells expressed cell-surface DR4 and Fas, but very low levels of decoy receptors 1 and 2. Upon treatment with either 5 or 10 μM LNF, the levels of these surface receptors were not further increased (supplemental Fig. S1). Thus, it is clear that LNF does not affect the levels of

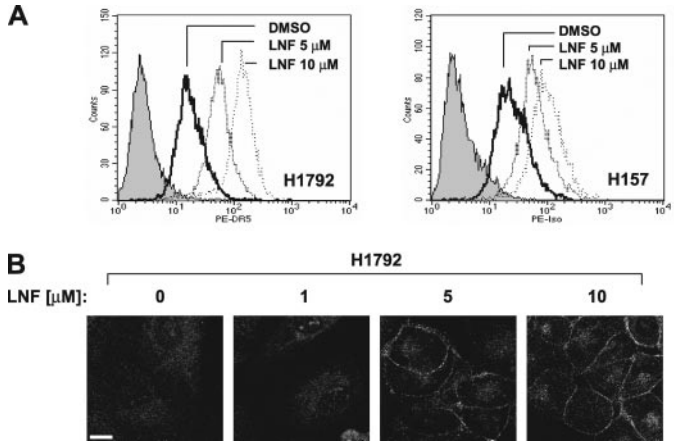

FIGURE 3. **LNF increases cell-surface DR5 levels.** *A*, H1792 and H157 cell lines were exposed to the indicated concentrations of LNF for 24 h. The cells were then harvested, stained with PE-conjugated DR5 antibody, and analyzed by flow cytometry. The *shaded peak* represents cells stained with a matched PE-conjugated IgG isotype control (*PE-Iso*). The *open peaks* were cells stained with PE-conjugated anti-DR5 antibody. *DMSO*, Me_2SO. *B*, H1792 cells were treated with the indicated concentrations of LNF for 16 h and then stained with PE-conjugated DR5 antibody. DR5 expression was visualized under a confocal microscope.

other death or TRAIL receptors at the cell surface. Collectively, these data further suggest the importance of DR5 up-regulation in LNF-induced apoptosis.

LNF Induces DR5 Expression through a CHOP-dependent Mechanism—To determine how FTIs increase DR5 expression at the transcriptional level, we examined the effects of LNF on the transactivation of reporter constructs with different lengths of DR5 5′-flanking regions (Fig. 4*A*) to identify the region responsible for LNF-mediated DR5 transactivation. In this transient transfection and luciferase assay, LNF failed to increase the luciferase activity of pGL3-DR5(−240) and pGL3-DR5(−120) while significantly increasing the luciferase activity of pGL3-DR5(−373), pGL3-DR5(−420), and pGL3-DR5(−3070) (Fig. 4*A*), indicating that the region between −240 and −373 contains essential element(s) responsible for LNF-induced DR5 transactivation. We identified a CHOP-binding site in this region, which has been demonstrated to be responsible for DR5 up-regulation by several cancer therapeutic agents (22–24). Thus, we further compared the effects of LNF on the transactivation of reporter constructs carrying wild-type and mutated CHOP-binding sites. We also included constructs carrying mutated NF-κB- and Elk-binding sites as controls (Fig. 4*B*). As shown in Fig. 4*B*, LNF increased the luciferase activity of the constructs carrying the wild-type DR5 promoter region or the DR5 promoter region with a mutated NF-κB- or Elk-binding site. However, LNF failed to increase the luciferase activity of the construct carrying the DR5 promoter region with a mutated CHOP-binding site. These results clearly indicate that the CHOP-binding site in the DR5 promoter region is required for LNF-mediated DR5 transactivation.

We next examined whether LNF actually modulates the expression of CHOP. By Western blot analysis, we detected a time-dependent DR5 induction accompanied by CHOP up-regulation in cells exposed to LNF, both of which occurred at 3 h and were sustained up to 24 h post-LNF treatment (Fig. 4*C*). The cleavage of caspase-8, caspase-3, and poly(ADP-ribose) polymerase was detected at 12 h after LNF treatment (Fig. 4*C*). Thus, the up-regulation of both CHOP and DR5 appears to be an early event that occurs before induction of apoptosis. By blocking LNF-induced CHOP expression using CHOP siRNA, we detected that DR5 induction by LNF was also accordingly diminished (Fig. 4*D*), indicating that LNF-induced DR5 up-regulation is secondary to CHOP induction. We conclude that LNF induces CHOP-dependent DR5 expression.

Given that CHOP is an ER stress-associated protein (21), we further examined whether LNF alters the expression levels of BiP/GRP78, another key protein marker of ER stress (21). As shown in Fig. 4*C*, under the same conditions used to test CHOP and DR5, LNF did not alter the levels of BiP/GRP78 from 3 to 16 h post-treatment. At 24 h, LNF only slightly increased the BiP/GRP78 levels. Together, these data clearly show that LNF increases the levels of CHOP, but not BiP/GRP78.

Induction of DR5 Contributes to LNF-induced Apoptosis—It is well known that DR5 activation (*e.g.* ligation with TRAIL) recruits and activates caspase-8 via the adaptor molecule FADD, leading to induction of apoptosis (18, 19). One common strategy to disrupt death receptor-induced apoptosis is to use a dominant-negative FADDm, which prevents death receptors from recruiting caspase-8 (41). To determine whether DR5 up-regulation contributes to LNF-induced apoptosis, we compared the effects of LNF on apoptosis induction in vector-transfected H460 cells (H460/V1) and FADDm-transfected cells (H460/Fm6 and H460/Fm16). These cell lines were equally sensitive to staurosporine in terms of decreasing cell survival. However, both H460/Fm6 and H460/Fm16 cell lines were significantly less sensitive to TRAIL in comparison with H460/V1 cells (Fig. 5*A*). LNF effectively increased the number of floating (dead) cells (Fig. 5*B*) and the levels of DNA fragments (Fig. 5*C*) in H460/V1 cells. However, these effects were significantly diminished in H460 cells expressing FADDm (*i.e.* H460/Fm6 and H460/Fm16; $p < 0.05$), indicating that FADDm overexpression abrogates the ability of LNF to induce apoptotic cell death, suggesting that the death receptor-mediated extrinsic apoptotic pathway is critical for LNF-induced apoptosis.

To further decipher the role of DR5 in LNF-induced apoptosis, we knocked down DR5 gene expression using siRNA and then examined its impact on LNF-induced apoptosis. In both H1792 and H157 cells, DR5 siRNA transfection dramatically decreased the basal levels of DR5 expression and, more important, abolished LNF-induced DR5 expression as detected by Western blot analysis (Fig. 5*D*). Furthermore, in cells transfected with DR5 siRNA, LNF-induced DNA fragmentation was significantly suppressed compared with cells transfected with control siRNA (Fig. 5*E*). To avoid possible off-target effects of siRNA, we also used a second DR5 siRNA (*i.e.* DR5 siRNA-2) that targets a different sequence of the DR5 gene to reproduce the aforementioned results. Similarly, blockage of DR5 induction by silencing DR5 using DR5 siRNA-2 significantly inhibited LNF-induced DNA fragmentation (supplemental Fig. S2). Collectively, these results further support the critical role of the DR5-mediated extrinsic apoptotic pathway in LNF-induced apoptosis.

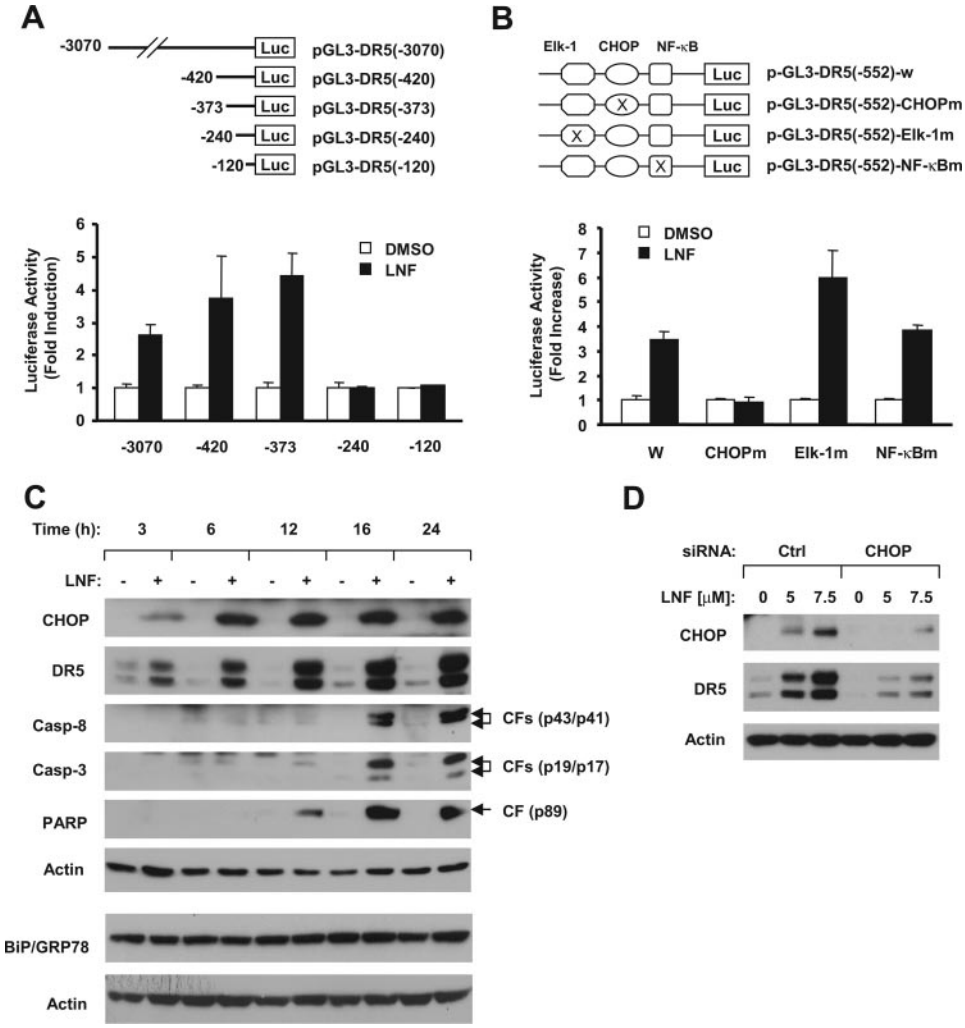

FIGURE 4. **LNF up-regulates DR5 expression through a CHOP-dependent mechanism.** *A*, identification of the region in the DR5 5′-flanking region that is responsible for LNF-induced DR5 transactivation. The given reporter constructs with different lengths of the 5′-flanking region of the DR5 gene were cotransfected with the pCH110 plasmid into H1792 cells. After 24 h, the cells were treated with Me_2SO (*DMSO*) or 10 μM LNF for 12 h and then subjected to luciferase (*Luc*) assay. Each *bar* represents the mean ± S.D. of triplicate determinations. *B*, the CHOP-binding site is required for LNF-induced DR5 transactivation. The given reporter constructs with and without different mutated (*m*) binding sites were cotransfected with the pCH110 plasmid into H1792 cells. After 24 h, the cells were treated with Me_2SO or 10 μM LNF for 12 h and then subjected to luciferase assay. Each *bar* represents the mean ± S.D. of triplicate determinations. *W*, wild-type. *C*, effects of LNF on the expression of CHOP, DR5, and Bip/GRP78 and cleavage of caspase (*Casp*)-8, caspase-3, and poly(ADP-ribose) polymerase (*PARP*). H1792 cells were treated with Me_2SO or 5 μM LNF in 0.1% FBS for the indicated times and then subjected to preparation of whole cell protein lysates and subsequent Western blot analysis. *CFs*, cleaved fragments. *D*, blockage of CHOP induction inhibits LNF-induced DR5 up-regulation. H1792 cells were transfected with control (*Ctrl*) or CHOP siRNA. After 48 h, the cells were treated with the indicated concentrations of LNF for 12 h and then subjected to preparation of whole cell protein lysates and subsequent Western blot analysis.

Combination of LNF and TRAIL Enhances Induction of Apoptosis—Because LNF increases cell-surface DR5 expression, we speculated that LNF would cooperate with exogenous TRAIL to augment induction of apoptosis if the induced DR5 is functional. Thus, we examined the effect of the combination of LNF with exogenous human recombinant TRAIL on apoptosis in two human lung cancer cell lines. As shown in Fig. 6*A*, 5 μM LNF alone did not apparently induce cleavage of caspase-8, caspase-3, poly(ADP-ribose) polymerase, and RasGAP, whereas TRAIL at the tested doses, particularly 10 and 20 ng/ml, caused only weak cleavage of the caspases and their substrates. Notably, the combination of LNF and TRAIL induced obvious cleavage of not only caspase-8, but also caspase-3 and its substrate poly(ADP-ribose) polymerase, as indicated by the dramatic decreases in their proforms (uncleaved forms) and/or increase in the cleaved bands. LNF alone did not affect RasGAP levels, and TRAIL alone at 20 and 30 ng/ml caused only weak cleavage of RasGAP. However, the combination of LNF with TRAIL, even at 10 ng/ml TRAIL, induced cleavage of RasGAP (Fig. 6*A*). Therefore, it appears that LNF cooperates with TRAIL to enhance activation of caspase-8 and its downstream caspase-3.

In addition, both LNF alone (1–5 μM) and TRAIL alone (25 ng/ml) did not increase or only slightly increased the amount of DNA fragments; however, the combination of the two agents induced a striking increase in DNA fragment levels, which were apparently greater than the sums of the levels caused by each single agent alone in both cell lines (Fig. 5*B*). For example, in H1792 cells, LNF at 5 μM increased DNA fragmentation by <0.2 arbitrary units, whereas TRAIL at 25 ng/ml increased DNA fragmentation by ~0.3 arbitrary units. However, the combination of these two agents increased DNA fragmentation by ~1.4 arbitrary units. Therefore, it appears that LNF synergizes with TRAIL to induce apoptosis in human cancer cells.

DISCUSSION

Although FTIs were historically developed as anti-Ras agents, it is now generally agreed that FTIs exert their antitumor activity independently of their inhibition of Ras farnesylation (1, 2, 25). In this study, we have demonstrated that induction of DR5 and its mediated activation of the extrinsic apoptotic pathway play critical roles in LNF-induced apoptosis in human lung cancer cells due to the following findings. First, LNF activated caspase-8, which is required for LNF-induced apoptosis because inhibition of caspase-8 activation by either a caspase-8 inhibitor or siRNA-mediated caspase-8 silencing abolished LNF-induced apoptosis. Second, overexpression of FADDm abrogated LNF-induced caspase activation and apoptotic cell death, suggesting that the activation of the extrinsic apoptotic pathway is critical for LNF-induced apoptosis. Finally,

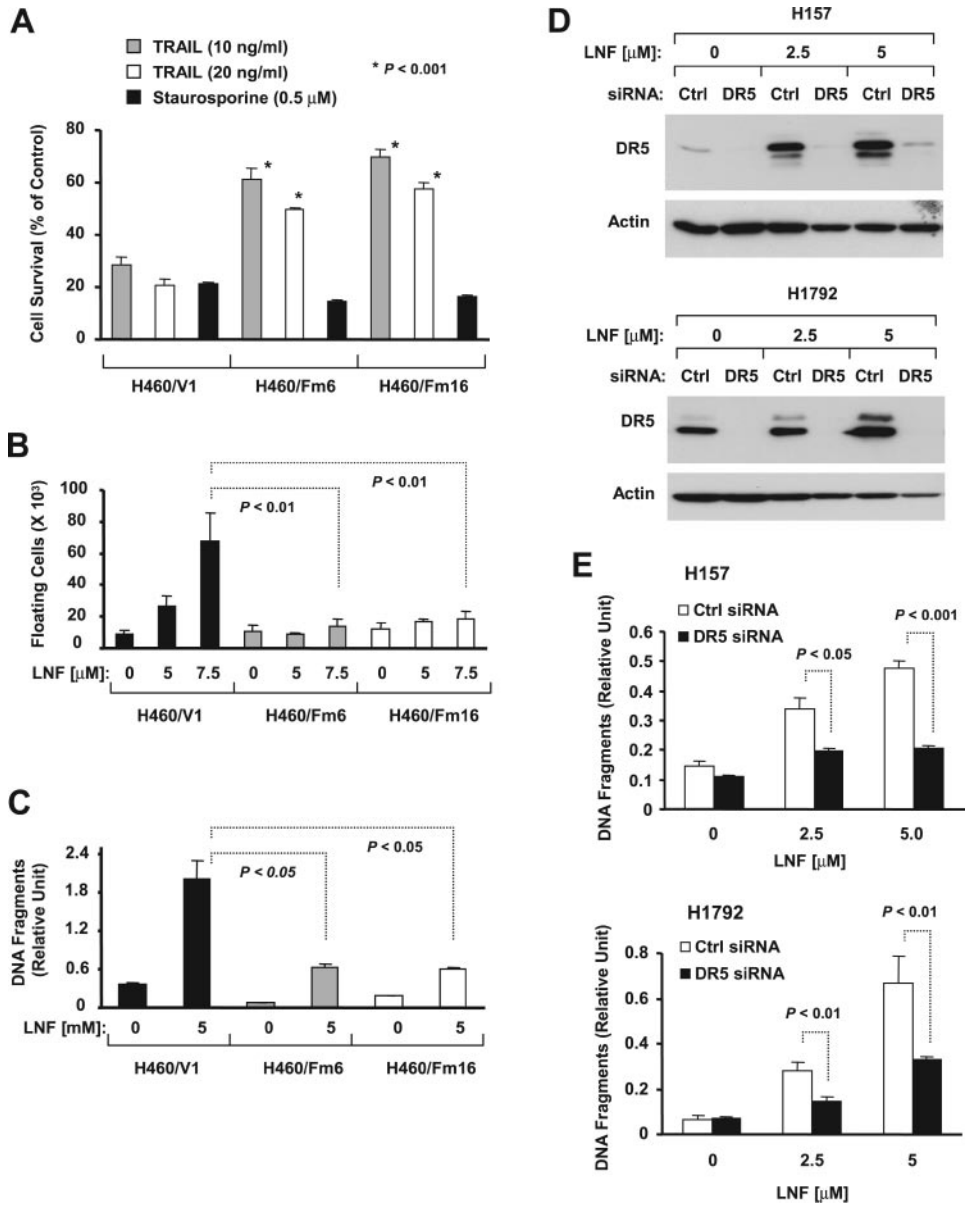

FIGURE 5. **Overexpression of a dominant-negative FADDm (*A–C*) or silencing of DR5 expression by siRNA (*D* and *E*) protects cells from LNF-induced apoptosis.** *A*, overexpression of FADDm protects cells from death induced by TRAIL, but not by staurosporine. The indicated cell lines were treated with the given concentrations of TRAIL or staurosporine for 24 h. The cells were then subjected to measurement of cell survival by the sulforhodamine B assay. Data are the means ± S.D. of four identical treatments. *B* and *C*, overexpression of FADDm protects cells from LNF-induced apoptosis. The indicated cell lines were exposed to the given concentrations of LNF in 0.1% FBS for 24 h. The cells were then subjected to detection of floating or dead cells in the medium by direct cell counting (*B*) and evaluation of DNA fragmentation using the Cell Death Detection ELISA^{plus} kit (*C*). *D*, the indicated cell lines were seeded in a 24-well cell culture plate and transfected twice on the 2nd day with control (*Ctrl*) or DR5 siRNA in a 48-h interval. Forty hours later after the second transfection, cells were treated with the indicated concentrations of LNF in 0.1% FBS. After 24 h, DR5 expression was assessed by Western blot analysis. *E*, the indicated cell lines were transfected with control or DR5 siRNA as aforementioned and then treated with the indicated concentrations of LNF in 0.1% FBS. After 24 h, cells were subjected to estimation of DNA fragmentation using the Cell Death Detection ELISA^{plus} kit. Data in *C* and *E* are the means ± S.D. of three identical wells.

LNF primarily induced DR5 expression (including an increase in cell-surface DR5), whereas DR5 silencing using DR5 siRNA attenuated LNF-induced caspase activation and apoptosis, indicating that DR5 induction contributes to LNF-induced apoptosis. Thus, our study is the first to demonstrate that an FTI induces DR5-mediated, caspase-8-dependent apoptosis in human cancer cells.

DR5 expression is regulated through p53-dependent and -independent mechanisms (42, 43). In our study, most of the cell lines used for examining DR5 up-regulation, including H1792, H157, H1299, H226, DU145, HeLa, and SqCC/Y1, have mutant or deleted p53 (44–47). Because LNF still increased DR5 expression in these cell lines (Fig. 2), we conclude that LNF induces DR5 expression independently of p53. This is further supported by our observation that LNF up-regulated DR5 expression with equal potency in both HCT116 and p53 knock-out HCT116 cell lines (Fig. 2). Currently, it is known that DR5 can be regulated in a p53-independent manner (43, 48), but the underlying mechanisms remain largely unclear.

CHOP has been demonstrated recently to regulate DR5 expression through the CHOP-binding site in the DR5 gene (22, 23), revealing a novel p53-independent regulation of DR5 expression. In our study, LNF appeared to increase DR5 expression at the transcriptional level because it increased DR5 mRNA levels and the activity of the DR5 promoter (Fig. 2). The deletion and mutation analyses of the DR5 5′-flanking region revealed that the region containing the CHOP-binding site is essential for LNF-mediated DR5 transactivation (Fig. 4). Indeed, LNF induced a time-dependent CHOP expression accompanied by the up-regulation of DR5 expression. Blockage of LNF-mediated CHOP induction by the CHOP siRNA accordingly inhibited DR5 up-regulation (Fig. 4). We conclude that LNF induces DR5 expression through a CHOP-dependent mechanism.

It is known that CHOP is an ER stress-regulated protein (21). It was reported that another FTI called R115777 induces ER stress in myeloma cells because it increased the levels of both CHOP and particularly BiP/GRP78 after a prolonged treatment (*i.e.* 72 h) (49). In our system, LNF at a concentration that induces DR5 expression (*e.g.* 5 μM) increased the levels of CHOP, but not BiP/GRP78 (Fig. 4), arguing that LNF induces ER stress in our system. Nonetheless, whether

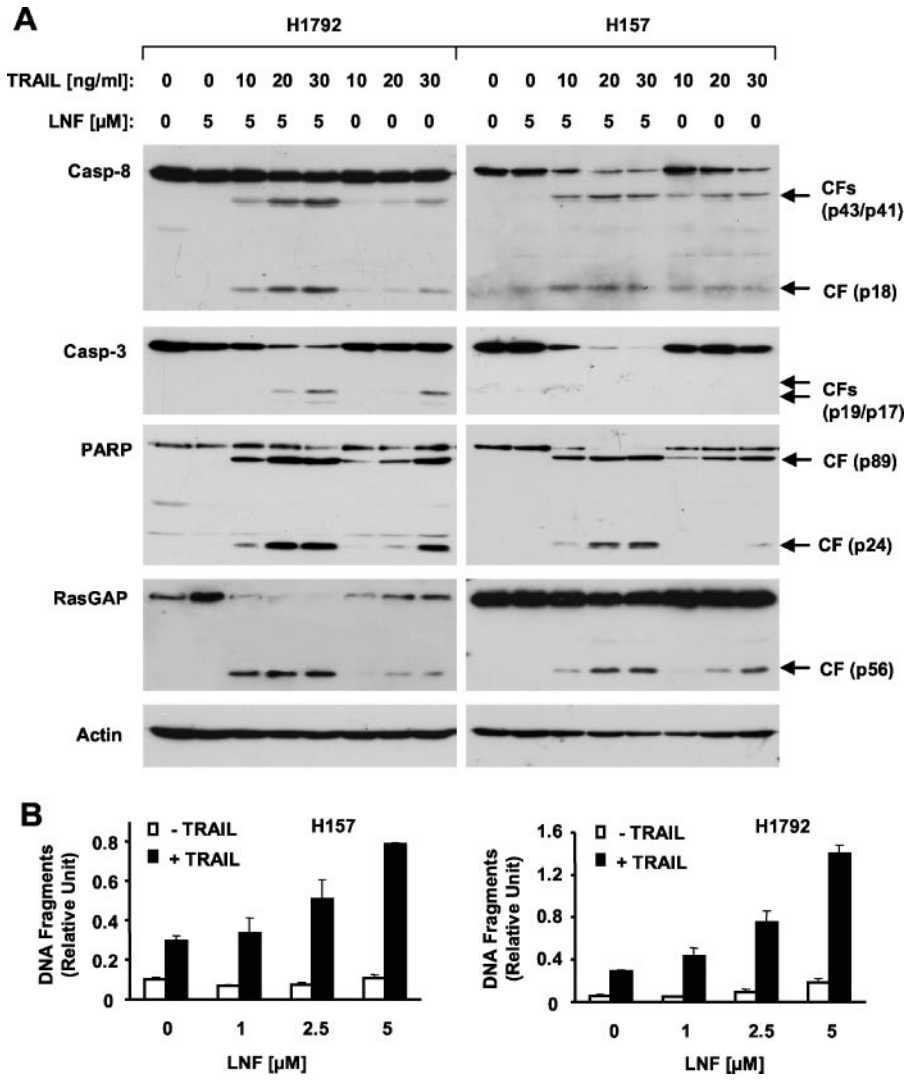

FIGURE 6. **Combination of LNF and TRAIL augments caspase activation (*A*) and DNA fragmentation (*B*).** *A*, the indicated cell lines were treated with LNF alone, TRAIL alone, and their combinations as indicated. After 14 h, whole cell protein lysates were prepared from both detached and attached cells and subjected to Western blot analysis to detect cleavage of caspases and their substrates. *Casp*, caspase; *PARP*, poly(ADP-ribose) polymerase; *CFs*, cleaved forms. *B*, the indicated cell lines were seeded in a 96-well plate and treated on the 2nd day with the indicated concentrations of LNF alone, TRAIL at 25 ng/ml alone, and their combinations. After 24 h, cells were subjected to measurement of DNA fragments using the Cell Death Detection ELISA^{plus} kit. Data are the means ± S.D. of three identical wells.

CHOP elevation by LNF is due to ER stress or other mechanisms needs to be studied further.

In addition to LNF, R115777 also increased DR5 expression.[4] The LNF analog SCH66337, which was much weaker than LNF in inhibiting protein farnesylation, also showed weaker activity than LNF in inducing DR5 expression and enhancing TRAIL-induced apoptosis (supplemental Fig. S3). Therefore, future studies should address whether there is a relationship between inhibition of protein farnesylation and induction of CHOP and DR5.

Although R115777 was reported to induce apoptosis in the presence of a caspase-8 inhibitor in myeloma cells (49), this FTI did enhance death receptor-induced apoptosis mediated by Fas ligand or TRAIL in myeloma cells (50) and lung cancer cells.[4] These findings are in agreement with our current finding that LNF enhances TRAIL-induced apoptosis in human lung cancer cells. In our study, we have clearly shown that LNF induces caspase-8-dependent apoptosis through both pharmacological (inhibitor) and molecular (siRNA) approaches (Fig. 1). Because both LNF and R115777 induced DR5 expression in myeloma cells,[4] further studies are needed to address whether the death receptor-mediated apoptotic pathway is also involved in FTI-induced apoptosis in myeloma cells as well as in other types of cancer cells.

Our findings that FTIs increase DR5 expression and enhance TRAIL-induced apoptosis have clinically meaningful implications. It is known that TRAIL functions as the DR5 ligand and rapidly induces apoptosis in a wide variety of transformed cells, but is not cytotoxic in normal cells *in vitro* and *in vivo* (18, 19). Therefore, TRAIL is considered to be a tumor-selective, apoptosis-inducing cytokine and a promising new candidate for cancer treatment. In addition, agonistic anti-DR5 antibodies can also induce DR5 trimerization, which triggers the extrinsic apoptotic pathway, thus having great cancer therapeutic potential (51). In fact, the agonistic anti-DR5 antibody is already being tested in phase I clinical trials. Therefore, LNF, as well as other FTIs that increase cell-surface DR5 expression, can be used in combination with TRAIL or an agonistic anti-DR5 antibody to achieve an enhanced effect on apoptosis induction in human cancer cells. In summary, our study has demonstrated, for the first time, that an FTI (*e.g.* LNF) induces CHOP-dependent DR5 expression at a clinically achievable concentration range, contributing to FTI-induced apoptosis.

Acknowledgments—We are grateful to Zhongmei Zhou for excellent technical support. We thank Drs. G. S. Wu and H.-G. Wang for providing some plasmids.

REFERENCES

1. Sebti, S. M. (2005) *Cancer Cell* **7,** 297–300
2. Brunner, T. B., Hahn, S. M., Gupta, A. K., Muschel, R. J., McKenna, W. G., and Bernhard, E. J. (2003) *Cancer Res.* **63,** 5656–5668
3. Adjei, A. A., Erlichman, C., Davis, J. N., Cutler, D. L., Sloan, J. A., Marks,

[4] Y. Qiu, X. Liu, P. Yue, F. R. Khuri, and S.-Y. Sun, unpublished data.

R. S., Hanson, L. J., Svingen, P. A., Atherton, P., Bishop, W. R., Kirschmeier, P., and Kaufmann, S. H. (2000) *Cancer Res.* **60,** 1871–1877
4. Adjei, A. A., Davis, J. N., Bruzek, L. M., Erlichman, C., and Kaufmann, S. H. (2001) *Clin. Cancer Res.* **7,** 1438–1445
5. Chun, K. H., Lee, H. Y., Hassan, K., Khuri, F., Hong, W. K., and Lotan, R. (2003) *Cancer Res.* **63,** 4796–4800
6. Smalley, K. S., and Eisen, T. G. (2003) *Int. J. Cancer* **105,** 165–175
7. Nakajima, A., Tauchi, T., Sumi, M., Bishop, W. R., and Ohyashiki, K. (2003) *Mol. Cancer Ther.* **2,** 219–224
8. Hoover, R. R., Mahon, F. X., Melo, J. V., and Daley, G. Q. (2002) *Blood* **100,** 1068–1071
9. Feldkamp, M. M., Lau, N., Roncari, L., and Guha, A. (2001) *Cancer Res.* **61,** 4425–4431
10. Reichert, A., Heisterkamp, N., Daley, G. Q., and Groffen, J. (2001) *Blood* **97,** 1399–1403
11. Shi, B., Yaremko, B., Hajian, G., Terracina, G., Bishop, W. R., Liu, M., and Nielsen, L. L. (2000) *Cancer Chemother. Pharmacol.* **46,** 387–393
12. Liu, M., Bryant, M. S., Chen, J., Lee, S., Yaremko, B., Lipari, P., Malkowski, M., Ferrari, E., Nielsen, L., Prioli, N., Dell, J., Sinha, D., Syed, J., Korfmacher, W. A., Nomeir, A. A., Lin, C. C., Wang, L., Taveras, A. G., Doll, R. J., Njoroge, F. G., Mallams, A. K., Remiszewski, S., Catino, J. J., Girijavallabhan, V. M., Kirschmeier, P., and Bishop, W. R. (1998) *Cancer Res.* **58,** 4947–4956
13. Khuri, F. R., Glisson, B. S., Kim, E. S., Statkevich, P., Thall, P. F., Meyers, M. L., Herbst, R. S., Munden, R. F., Tendler, C., Zhu, Y., Bangert, S., Thompson, E., Lu, C., Wang, X. M., Shin, D. M., Kies, M. S., Papadimitrakopoulou, V., Fossella, F. V., Kirschmeier, P., Bishop, W. R., and Hong, W. K. (2004) *Clin. Cancer Res.* **10,** 2968–2976
14. Kim, E. S., Kies, M. S., Fossella, F. V., Glisson, B. S., Zaknoen, S., Statkevich, P., Munden, R. F., Summey, C., Pisters, K. M., Papadimitrakopoulou, V., Tighiouart, M., Rogatko, A., and Khuri, F. R. (2005) *Cancer* **104,** 561–569
15. Marcus, A. I., O'Brate A, M., Buey, R. M., Zhou, J., Thomas, S., Khuri, F. R., Andreu, J. M., Diaz, F., and Giannakakou, P. (2006) *Cancer Res.* **66,** 8838–8846
16. Green, D. R. (2000) *Cell* **102,** 1–4
17. Ashkenazi, A., and Dixit, V. M. (1998) *Science* **281,** 1305–1308
18. Wang, S., and El-Deiry, W. S. (2003) *Oncogene* **22,** 8628–8633
19. Almasan, A., and Ashkenazi, A. (2003) *Cytokine Growth Factor Rev.* **14,** 337–348
20. Debatin, K. M., and Krammer, P. H. (2004) *Oncogene* **23,** 2950–2966
21. Oyadomari, S., and Mori, M. (2004) *Cell Death Differ.* **11,** 381–389
22. Yamaguchi, H., and Wang, H.-G. (2004) *J. Biol. Chem.* **279,** 45495–45502
23. Yoshida, T., Shiraishi, T., Nakata, S., Horinaka, M., Wakada, M., Mizutani, Y., Miki, T., and Sakai, T. (2005) *Cancer Res.* **65,** 5662–5667
24. Abdelrahim, M., Newman, K., Vanderlaag, K., Samudio, I., and Safe, S. (2006) *Carcinogenesis* **27,** 717–728
25. Lebowitz, P. F., and Prendergast, G. C. (1998) *Oncogene* **17,** 1439–1445
26. Lackner, M. R., Kindt, R. M., Carroll, P. M., Brown, K., Cancilla, M. R., Chen, C., de Silva, H., Franke, Y., Guan, B., Heuer, T., Hung, T., Keegan, K., Lee, J. M., Manne, V., O'Brien, C., Parry, D., Perez-Villar, J. J., Reddy, R. K., Xiao, H., Zhan, H., Cockett, M., Plowman, G., Fitzgerald, K., Costa, M., and Ross-Macdonald, P. (2005) *Cancer Cell* **7,** 325–336
27. Du, W., Liu, A., and Prendergast, G. C. (1999) *Cancer Res.* **59,** 4208–4212
28. Jiang, K., Coppola, D., Crespo, N. C., Nicosia, S. V., Hamilton, A. D., Sebti, S. M., and Cheng, J. Q. (2000) *Mol. Cell. Biol.* **20,** 139–148
29. Edamatsu, H., Gau, C. L., Nemoto, T., Guo, L., and Tamanoi, F. (2000) *Oncogene* **19,** 3059–3068
30. Marzo, I., Perez-Galan, P., Giraldo, P., Lopez-Royuela, N., Gomez-Benito, M., Larrad, L., Lasierra, P., Rubio-Felix, D., Anel, A., and Naval, J. (2004) *Leukemia* (*Basingstoke*) **18,** 1599–1604
31. Sun, S.-Y., Zhou, Z., Wang, R., Fu, H., and Khuri, F. R. (2004) *Cancer Biol. Ther.* **3,** 1092–1098; Discussion 1099–1101
32. Liu, X., Yue, P., Zhou, Z., Khuri, F. R., and Sun, S.-Y. (2004) *J. Natl. Cancer Inst.* **96,** 1769–1780
33. Sun, S.-Y., Yue, P., Wu, G. S., El-Deiry, W. S., Shroot, B., Hong, W. K., and Lotan, R. (1999) *Oncogene* **18,** 2357–2365
34. Pfahl, M., Tzukerman, M., Zhang, X. K., Lehmann, J. M., Hermann, T., Wills, K. N., and Graupner, G. (1990) *Methods Enzymol.* **189,** 256–270
35. Sun, S.-Y., Yue, P., Hong, W. K., and Lotan, R. (2000) *Cancer Res.* **60,** 6537–6543
36. Sun, S.-Y., Yue, P., Dawson, M. I., Shroot, B., Michel, S., Lamph, W. W., Heyman, R. A., Teng, M., Chandraratna, R. A., Shudo, K., Hong, W. K., and Lotan, R. (1997) *Cancer Res.* **57,** 4931–4939
37. Zou, W., Liu, X., Yue, P., Zhou, Z., Sporn, M. B., Lotan, R., Khuri, F. R., and Sun, S.-Y. (2004) *Cancer Res.* **64,** 7570–7578
38. Wen, L. P., Madani, K., Martin, G. A., and Rosen, G. D. (1998) *Cell Death Differ.* **5,** 729–734
39. Awada, A., Eskens, F. A., Piccart, M., Cutler, D. L., van der Gaast, A., Bleiberg, H., Wanders, J., Faber, M. N., Statkevich, P., Fumoleau, P., and Verweij, J. (2002) *Eur. J. Cancer* **38,** 2272–2278
40. Sharma, S., Kemeny, N., Kelsen, D. P., Ilson, D., O'Reilly, E., Zaknoen, S., Baum, C., Statkevich, P., Hollywood, E., Zhu, Y., and Saltz, L. B. (2002) *Ann. Oncol.* **13,** 1067–1071
41. Chinnaiyan, A. M., O'Rourke, K., Tewari, M., and Dixit, V. M. (1995) *Cell* **81,** 505–512
42. Wu, G. S., Burns, T. F., McDonald, E. R., III, Jiang, W., Meng, R., Krantz, I. D., Kao, G., Gan, D. D., Zhou, J. Y., Muschel, R., Hamilton, S. R., Spinner, N. B., Markowitz, S., Wu, G., and El-Deiry, W. S. (1997) *Nat. Genet.* **17,** 141–143
43. Sheikh, M. S., Burns, T. F., Huang, Y., Wu, G. S., Amundson, S., Brooks, K. S., Fornace, A. J., Jr., and El-Deiry, W. S. (1998) *Cancer Res.* **58,** 1593–1598
44. Mitsudomi, T., Steinberg, S. M., Nau, M. M., Carbone, D., D'Amico, D., Bodner, S., Oie, H. K., Linnoila, R. I., Mulshine, J. L., Minna, J. D., and Gazdar, A. F. (1992) *Oncogene* **7,** 171–180
45. Sun, S.-Y., Yue, P., Mao, L., Dawson, M. I., Shroot, B., Lamph, W. W., Heyman, R. A., Chandraratna, R. A., Shudo, K., Hong, W. K., and Lotan, R. (2000) *Clin. Cancer Res.* **6,** 1563–1573
46. Sun, S.-Y., Yue, P., and Lotan, R. (2000) *Oncogene* **19,** 4513–4522
47. Bohnke, A., Westphal, F., Schmidt, A., El-Awady, R. A., and Dahm-Daphi, J. (2004) *Int. J. Radiat. Biol.* **80,** 53–63
48. Meng, R. D., and El-Deiry, W. S. (2001) *Exp. Cell Res.* **262,** 154–169
49. Beaupre, D. M., Cepero, E., Obeng, E. A., Boise, L. H., and Lichtenheld, M. G. (2004) *Mol. Cancer Ther.* **3,** 179–186
50. Beaupre, D. M., McCafferty-Grad, J., Bahlis, N. J., Boise, L. H., and Lichtenheld, M. G. (2003) *Leuk. Lymphoma* **44,** 2123–2134
51. Ichikawa, K., Liu, W., Zhao, L., Wang, Z., Liu, D., Ohtsuka, T., Zhang, H., Mountz, J. D., Koopman, W. J., Kimberly, R. P., and Zhou, T. (2001) *Nat. Med.* **7,** 954–960

DOI:10.1158/0008-5472.CAN-05-1705

Cancer Research

EGFR Tyrosine Kinase Domain Mutations Are Detected in Histologically Normal Respiratory Epithelium in Lung Cancer Patients

Ximing Tang, Hisayuki Shigematsu, B. Nebiyou Bekele, et al.

Cancer Res 2005;65:7568-7572. Published online September 1, 2005.

DOI:10.1158/0008-5472.CAN-05-1705

Priority Report

EGFR Tyrosine Kinase Domain Mutations Are Detected in Histologically Normal Respiratory Epithelium in Lung Cancer Patients

Ximing Tang,[1] Hisayuki Shigematsu,[5] B. Nebiyou Bekele,[2] Jack A. Roth,[3] John D. Minna,[5,6,7] Waun Ki Hong,[1] Adi F. Gazdar,[5,8] and Ignacio I. Wistuba[1,4]

Departments of [1]Thoracic/Head and Neck Medical Oncology, [2]Biostatistics and Applied Mathematics, [3]Thoracic Surgery, and [4]Pathology, University of Texas M.D. Anderson Cancer Center, Houston, Texas and [5]Hamon Center for Therapeutic Oncology Research, Departments of [6]Internal Medicine, [7]Pharmacology, and [8]Pathology, University of Texas Southwestern Medical Center, Dallas, Texas

Abstract

To determine whether *EGFR* tyrosine kinase domain mutations are early events in the pathogenesis of lung adenocarcinomas, we tested for the presence of *EGFR* mutations in histologically normal bronchial and bronchiolar epithelia from lung adenocarcinomas bearing the common *EGFR* mutations. DNA was extracted from microdissected tissue obtained from 21 tumors with known *EGFR* mutations, 16 tumors without mutation, and 90 sites of normal bronchial and bronchiolar epithelium from the same surgical specimens. With the use of PCR and direct DNA sequencing, *EGFR* mutations identical to the tumors were detected in the normal respiratory epithelium in 9 of 21 (43%) patients with *EGFR* mutant adenocarcinomas but none in patients without mutation in the tumors. The finding of mutations being more frequent in normal epithelium within tumor (43%) than in adjacent sites (24%) suggests a localized field effect phenomenon. Our findings indicate that mutation of the tyrosine kinase domain of *EGFR* is an early event in the pathogenesis of lung adenocarcinomas, and suggest *EGFR* mutations as an early detection marker and chemoprevention target. (Cancer Res 2005; 65(17): 7568-72)

Introduction

Four major histologic types compose the majority of lung cancers, and adenocarcinoma histology is currently the type most frequently diagnosed (1). It has been established that adenocarcinomas usually arise from the peripheral airway; however, the specific airway structure (bronchus, bronchiole, and alveolus) and the respiratory epithelium cell type (ciliated, goblet, Clara, and type II alveolar cells) from which most adenocarcinomas develop have not been established. Recent findings indicate that clinically evident lung adenocarcinomas are the results of the accumulation of numerous genetic and epigenetic changes, including abnormalities for the inactivation of tumor suppressor genes and the activation of oncogenes (2). Despite these advances, there is extremely limited information available on the early molecular pathogenesis of lung adenocarcinomas.

Somatic mutations of *EGFR*, a tyrosine kinase of the ErbB family, recently have been reported in specific subsets of lung adenocarcinomas (3–9). The mutations are clinically relevant because most of them have been associated with patient tumor sensitivity to small molecule tyrosine kinase inhibitors gefitinib and erlotinib (3–5, 10). About 90% of the mutations detected in *EGFR* are composed either of in-frame deletions in exon 19 or a specific missense mutation in exon 21 (L858R; refs. 3–9). The mutations are significantly associated with adenocarcinoma histology, never or light smoker status, female gender, and East Asian ethnic origin (9). However, there is no information available on the stage of lung adenocarcinoma development when *EGFR* mutation develops. Thus, to investigate the stage of lung adenocarcinoma pathogenesis when *EGFR* mutations commence, we tested for the presence of *EGFR* mutations in peripheral airway respiratory epithelium (small bronchi and bronchioles) obtained from 21 patients with lung adenocarcinoma harboring *EGFR* mutations. We compared the findings with similar samples obtained from 16 lung cancer patients whose tumors had wild-type *EGFR*.

Materials and Methods

Case selection. Tumor tissue specimens obtained from 120 surgically resected lung adenocarcinomas, pathology stages I to IIIA, were obtained from the Lung Cancer Specialized Program of Research Excellence Tissue Bank at the M.D. Anderson Cancer Center (Houston, TX), and were examined for *EGFR* gene mutation in exons 18 to 21 (9). We selected 20 cases of adenocarcinoma and one adenosquamous carcinoma with *EGFR* mutation in exon 19 (n = 13) and exon 21 (n = 8) in which archival formalin-fixed paraffin-embedded tissues from which surgically resected lobectomy specimens were available (Table 1). Most patients were women of East Asian ethnicity and never or former smokers (Table 1). All *EGFR* mutated lung adenocarcinomas were of mixed histologic subtype (WHO classification, 2004; ref. 1). Two patients with *EGFR* mutant lung cancers were current smokers, but with only 5 and 12 pack-year exposures. None of the patients had received prior cytotoxic therapy. Patients who had smoked at least 100 cigarettes in their lifetime were defined as smokers, and smokers who quit smoking at least 12 months before lung cancer diagnosis were defined as former smokers. As a control group, 16 cases of adenocarcinoma without *EGFR* mutation, divided into 8 never and 8 former smokers, were selected. Clinical staging was based on the revised in International System for Stating Lung Cancer (11).

Respiratory epithelium foci selection. H&E-stained histology sections of archival specimens having tumor and adjacent normal lung tissues were reviewed to identify available foci of respiratory epithelium containing at least 1,000 cells. From the 21 *EGFR* mutated lung cancers, we identified noncontiguous small bronchial (n = 26) or bronchiolar (n = 38) sites suitable for microdissection. All the foci harbored histologically normal-appearing respiratory epithelium, without identifiable dysplastic or neoplastic cells (Fig. 1). No atypical adenomatous hyperplasias, putative precursors of a subset of lung adenocarcinomas, were detected. The microdissected specimens were obtained from three different locations

Requests for reprints: Ignacio I. Wistuba, Department of Pathology, Unit 85, University of Texas M.D. Anderson Cancer Center, 1515 Holcombe Boulevard, Houston, TX 77030-4009. Phone: 713-563-9184; Fax: 713-563-1848; E-mail: iiwistuba@mdanderson.org.

doi:10.1158/0008-5472.CAN-05-1705

DOI:10.1158/0008-5472.CAN-05-1705

Table 1. Clinicopathologic data of *EGFR* mutant resected lung adenocarcinomas studied

Case no.	Age	Gender	Race	Smoking status	Stage	EGFR mutation	Mutation in normal epithelium
1	55	Female	Caucasian	Never	IIB	15 bp del (746-750)	Yes
2	70	Female	Hispanic	Never	IIIA	15 bp del (746-750)	No
3	64	Male	Caucasian	Never	IA	15 bp del (746-750)	No
4	66	Female	Caucasian	Never	IB	18 bp del (746-751) and S752V	No
5	52	Female	Hispanic	Never	IIIA	L858R	Yes
6	70	Female	Caucasian	Never	IA	L858R	Yes
7	65	Female	Caucasian	Never	IA	L858R	No
8	45	Female	East Asian	Never	IA	L858R	No
9	61	Female	East Asian	Never	IIIA	L858R	No
10	49	Female	East Asian	Never	IIIA	L858R	No
11	35	Female	East Asian	Never	IA	15 bp del (746-750)	Yes
12	62	Female	East Asian	Never	IA	L858R	No
13	66	Female	Caucasian	Former	IV	15 bp del (746-750)	No
14	58	Female	Caucasian	Former	IA	15 bp del (746-750)	Yes
15	65	Male	East Asian	Former	IIB	18 bp del (746-751) and S752I	Yes
16	72	Female	Caucasian	Former	IB	15 bp del (746-750)	Yes
17	69	Male	East Asian	Former	IIIA	L858R	No
18	56	Male	East Asian	Former	IIB	18 bp del (747-752) and P753Q	Yes
19	69	Male	East Asian	Former	IB	15 bp del (747-751)	No
20	73	Male	East Asian	Current	IIB	15 bp del (746-750)	Yes
21	68	Female	Caucasian	Current	IIIA	15 bp del (746-750)	No

based on their relationship to the tumors: within the tumor (21 foci), <5 mm apart from the tumor margin (adjacent to tumor; 29 sites), and from sites located >5 mm from the tumor margin ("distant" lung; 14 sites). From the 16 non-*EGFR* mutated lung adenocarcinoma cases, we selected 26 (10 small bronchi and 16 bronchioles) sites of histologically normal respiratory epithelium (Table 2). Averages of 3.1 (range, 2-6) and 1.6 (range, 1-3) respiratory epithelium foci were examined from *EGFR* mutated and nonmutated cases, respectively. Small bronchi were identified as having well-defined smooth muscle and discontinuous cartilage layers. Bronchioles were defined as small conducting airways lacking well-defined smooth muscle wall or cartilage layers. As internal negative controls, stromal tissue obtained from bronchial walls was also selected for microdissection. As these were retrospectively collected specimens, location of the small bronchial and bronchiolar respiratory epithelium examined for mutations was assessed based on their location with respect to tumor tissue in the corresponding histology sections.

Microdissection and DNA extraction. Approximately 1,000 cells (tumor, respiratory epithelium, or stromal) were precisely microdissected from sequential 8-μm-thick H&E-stained, formalin-fixed paraffin-embedded histology sections, using laser capture microdissection (Arcturus Engineering Laser Microdissection System, Mountain View, CA; Fig. 1). To avoid possible nonspecific binding of mutant tumor cells to the microdissection cap film, the specifically microdissected epithelial cells were redissected from the film under stereomicroscope visualization using fine needles (25G5/8). DNA was extracted using 25 μL of Pico Pure DNA Extraction solution (Arcturus) containing proteinase K and incubated at 65°C for 24 hours. Subsequently, proteinase K inactivation was done by heating samples at 95°C for 10 minutes.

***EGFR* mutation analysis.** Exons 19 and 21 of *EGFR* were PCR amplified using intron-based primers as previously described (10). From microdissected formalin-fixed paraffin-embedded cells, ~100 cells were used for each PCR amplification. Each amplification was done in 25 μL volume containing 2.5 μL DNA, 0.5 μL each primer (20 pmol/L), 12.5 μL HotStarTaq Master Mix (Qiagen, Valencia, CA), and 9 μL DNase-free water. DNA was amplified for 38 cycles at 94°C for 30 seconds, 65°C for 30 seconds, and 72°C for 45 seconds, followed by 7-minute extension at 72°C. All PCR products were directly sequenced using Applied Biosystems PRISM dye terminator cycle sequencing method (Perkin-Elmer Corp., Foster City, CA). All sequence variants were confirmed by independent PCR amplifications from at least two independent microdissections, and sequenced in both directions.

Statistical analysis. For data in which there is one record per patient, all relationships between categorical variables were assessed via the Fisher's exact test (12). For continuous outcomes, differences between cohorts were assessed via the Wilcoxon rank-sum test. Data in which there are multiple records per patient, relationships between binary variables were assessed via generalized estimating equation models.

Results

***EGFR* mutation in histologically normal epithelium.** Mutation analysis of the microdissected tumor tissue confirmed the mutational pattern originally identified using frozen and non-microdissected formalin-fixed paraffin-embedded tissues in all 21 cases (Table 1). Of interest, *EGFR* mutations were detected in at least one sample of corresponding histologically normal small bronchial and bronchiolar epithelia in 9 of 21 (43%) *EGFR* mutant lung adenocarcinoma patients (Tables 1 and 2). By contrast, no mutations in exons 19 and 21 of the *EGFR* gene were detected in 26 respiratory epithelium foci obtained from 16 lobectomy specimens of cancers having wild-type *EGFR* ($P = 0.005$). In *EGFR* mutant lung adenocarcinomas, 16 of 64 (25%) normal respiratory epithelium foci microdissected showed *EGFR* mutations. Five of nine cases showing mutations in normal respiratory epithelium showed two or three microdissected sites with *EGFR* mutation. In all cases, the mutational patterns in the tumors and corresponding nonmalignant respiratory epithelial specimens were identical. All mutations detected were confirmed using additional microdissected samples and multiple independent sequencing experiments in both sense and antisense directions. Importantly, no mutations were detected in stromal cells microdissected from bronchial walls in five cases in which adjacent lung normal epithelium and tumor showed *EGFR* mutations.

DOI:10.1158/0008-5472.CAN-05-1705

The frequency of mutations in the histologically normal respiratory epithelium was higher in samples microdissected within the tumor (9 of 21, 43%) than samples obtained from tissue adjacent to tumor (distance of <5 mm from the tumor margin; 7 of 29, 24%; $P = 0.013$; Table 2). No mutation was detected in 14 distant bronchial and bronchiolar samples. Although not statistically significant, a higher incidence of mutation was detected in small bronchial (9 of 26, 35%) compared with bronchiolar structures (7 of 38, 18%; $P = 0.093$). More frequent mutations affecting normal epithelium were found in *EGFR* exon 19 (14 of 16, 54%) compared with exon 21 (2 of 28, 7%; $P = 0.02$). There was no correlation noted between mutations in the normal epithelium and age, gender, ethnic background, former or never smoker status, or lung cancer clinical stage in our patients.

Discussion

This is the first report of the presence of *EGFR* mutations in histologically normal bronchial and bronchiolar epithelium in patients with lung adenocarcinomas. Our findings of identical *EGFR* mutations in normal-appearing respiratory epithelium in 9 of 21 (43%) patients with mutant tumors suggest that the mutations occur as early events in the pathogenesis of a subset of lung adenocarcinomas, commencing in histologically normal peripheral airways. These findings impact our understanding of the early pathogenesis of *EGFR* mutant lung adenocarcinomas, and may lead to clinical applications, such as targeted early detection and chemoprevention strategies.

It has been proposed that lung cancer cells with mutant *EGFR* might become physiologically dependent on the continued activity of the gene for the maintenance of their malignant phenotype (13). Mutant *EGFR* selectively transduces survival signals, specifically Akt, and signal transduction and activator of transcription signaling pathways, on which lung cancer tumor cells become dependent (14). Our finding of identical *EGFR* mutations (15 or 18 bp in-frame deletion and L858R mutation) in lung adenocarcinoma cells and in 25% of the corresponding adjacent histologically normal epithelial sites examined indicates that *EGFR* tyrosine kinase mutations also may play an important role in the initiation of the malignant phenotype. This notion is further supported by the absence of *EGFR* mutations in normal-appearing epithelium from 16 lung adenocarcinomas with wild-type *EGFR* from never and former smokers.

Clinically and pathologically (1), most adenocarcinomas of the lung are considered to arise from the peripheral lung airway compartment (small bronchi/bronchioles and alveoli; ref. 15), which arise by division of the tertiary bronchi (16). Whereas bronchi are lined by pseudostratified ciliated epithelium with occasional mucin-producing cells, bronchioles contain ciliated cells and secretory Clara cells (16). The latter are believed to be

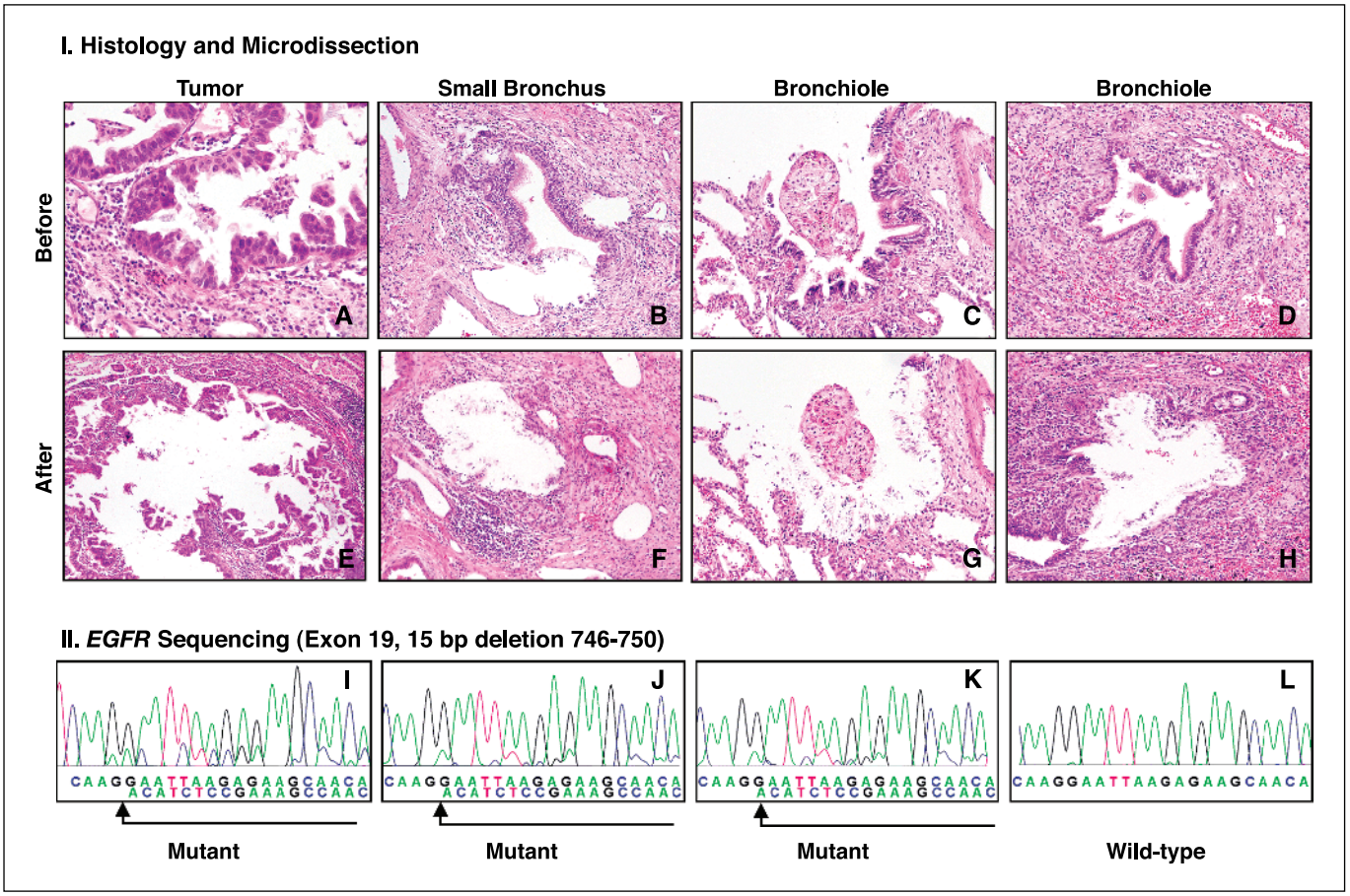

Figure 1. *I,* examples of tumor and histologically normal airway structures harboring the mutations are illustrated before (*A-D*) and after microdissection (*E-H*). *II,* sequencing chromatograms showing the presence of wild-type and mutant forms in the tumor (*I*), a small bronchus (*J*), and bronchiole (*K*), whereas only wild-type form is present in another bronchiole (*L*). *Arrow,* in-frame deletion mutation sequence.

DOI:10.1158/0008-5472.CAN-05-1705

Table 2. Frequency of *EGFR* tyrosine kinase domain mutations in microdissected histologically normal bronchial and bronchiolar epithelium in lung adenocarcinoma patients

Cases/samples	Mutated tumors			Wild-type tumors
	Exon 19 deletion	Exon 21 mutation	Total mutated	
Patients by smoking status (n = 30)				
Never	2 of 5	2 of 7	4 of 12	0 of 8
Former	4 of 6	0 of 1	4 of 7	0 of 8
Current	1 of 2	—	1 of 2	—
Total patients	7 of 13 (54%)	2 of 8 (25%)	9 of 21 (43%)*	0 of 16*
Foci by location compared with tumor (n = 90)				
Within	8 of 14 (57%)	1 of 7 (14%)	9 of 21 (43%)†	0 of 8
Near (<5 mm)	6 of 13 (46%)	1 of 16 (6%)	7 of 29 (24%)†	0 of 13
Distant	0 of 9	0 of 5	0 of 14 †	0 of 5
Foci by respiratory structure (n = 90)				
Small bronchus	8 of 17 (47%)	1 of 9 (11%)	9 of 26 (35%)	0 of 10
Bronchiole	6 of 19 (32%)	1 of 19 (5%)	7 of 38 (18%)	0 of 16
Total foci	14 of 36 (39%)‡	2 of 28 (7%)‡	16 of 64 (25%)	0 of 26

*P value of comparison: 0.0046.
†P value of comparison: 0.013.
‡P value of comparison: 0.021.

the progenitor cells of the bronchiolar epithelium. Respiratory bronchioles terminate in alveolar ducts and alveolar sacs, which are lined by type I and II pneumocytes (16). Our finding of *EGFR* mutations in microdissected histologically normal epithelial cells obtained from small bronchi and bronchioles supports the concept of adenocarcinomas arising from the peripheral lung airway compartment. The tendency of higher frequency of *EGFR* mutations in normal epithelium obtained from small bronchi (35%) compared with bronchioles (18%) may correlate with different cell types populating those epithelia, which could represent the site of the cell of origin for *EGFR* mutant adenocarcinomas. However, the possibility that common stem or progenitor cells for both bronchial and bronchiolar epithelia are the cell type bearing *EGFR* mutation cannot be excluded.

The finding of *EGFR* mutations in small bronchial and bronchiolar epithelium obtained from sites within (43%) and adjacent (24%) to tumors, but none in the distant peripheral lung sites, suggests that a localized type of field effect phenomenon may exist for *EGFR* mutations in the lung respiratory epithelium. A widespread field effect phenomenon with several molecular changes affecting histologically normal and abnormal bronchial and bronchiolar epithelium has been previously shown by us (17, 18) and others (19) in the smoking-damaged respiratory epithelium from lung cancer patients and from smokers without lung cancer. Therefore, our findings extend the field theory from centrally arising squamous carcinomas to peripheral occurring adenocarcinomas arising both in smokers and never smokers.

Our findings of *EGFR* mutations present in histologically normal epithelium of patients with lung adenocarcinomas bearing identical mutations open new avenues of investigation in the early pathogenesis of lung adenocarcinoma, including the identification of specific epithelial cell types hit by crucial genetic abnormalities involved in lung tumorigenesis.

Acknowledgments

Received 5/18/2005; revised 6/14/2005; accepted 6/22/2005.

Grant support: Specialized Program of Research Excellence in Lung Cancer grant P50CA70907, National Cancer Institute (Bethesda, MD), and Department of Defense grant W81XWH-04-1-0142.

The costs of publication of this article were defrayed in part by the payment of page charges. This article must therefore be hereby marked *advertisement* in accordance with 18 U.S.C. Section 1734 solely to indicate this fact.

References

1. Travis WD, Brambilla E, Muller-Hermelink HK, Harris CC, editors. World Health Organization classification of tumours, pathology and genetics: tumours of the lung, pleura, thymus and heart. Lyon: IARC Press; 2004. p. 9–124.
2. Minna JD, Gazdar A. Focus on lung cancer. Cancer Cell 2002;1:49–52.
3. Paez JG, Janne PA, Lee JC, et al. EGFR mutations in lung cancer: correlation with clinical response to gefitinib therapy. Science 2004;304:1497–500.
4. Lynch TJ, Bell DW, Sordella R, et al. Activating mutations in the epidermal growth factor receptor underlying responsiveness of non-small-cell lung cancer to gefitinib. N Engl J Med 2004;350:2129–39.
5. Pao W, Miller V, Zakowski M, et al. EGF receptor gene mutations are common in lung cancers from "never smokers" and are associated with sensitivity of tumors to gefitinib and erlotinib. Proc Natl Acad Sci U S A 2004;101:13306–11.
6. Huang SF, Liu HP, Li LH, et al. High frequency of epidermal growth factor receptor mutations with complex patterns in non-small cell lung cancers related to gefitinib responsiveness in Taiwan. Clin Cancer Res 2004;10:8195–203.
7. Kosaka T, Yatabe Y, Endoh H, Kuwano H, Takahashi T, Mitsudomi T. Mutations of the epidermal growth factor receptor gene in lung cancer: biological and clinical implications. Cancer Res 2004;64:8919–23.
8. Tokumo M, Toyooka S, Kiura K, et al. The relationship between epidermal growth factor receptor mutations and clinicopathologic features in non-small cell lung cancers. Clin Cancer Res 2005;11:1167–73.
9. Shigematsu H, Lin L, Takahashi T, et al. Clinical and biological features associated with epidermal growth factor receptor gene mutations in lung cancers. J Natl Cancer Inst 2005;97:339–46.
10. Amann J, Kalyankrishna S, Massion PP, et al.

DOI:10.1158/0008-5472.CAN-05-1705

Aberrant epidermal growth factor receptor signaling and enhanced sensitivity to EGFR inhibitors in lung cancer. Cancer Res 2005;65:226–35.
11. Mountain CF. Revisions in the International System for Staging Lung Cancer. Chest 1997;111:1710–7.
12. Snedecor GW, Cochran WG. Statistical method. 7th ed. Ames: Iowa State University Press; 1980.
13. Gazdar AF, Shigematsu H, Herz J, Minna JD. Mutations and addiction to EGFR: the Achilles "heal" of lung cancers? Trends Mol Med 2004;10:481–6.
14. Sordella R, Bell DW, Haber DA, Settleman J. Gefitinib-sensitizing EGFR mutations in lung cancer activate anti-apoptotic pathways. Science 2004;305:1163–7.
15. Yatabe Y, Mitsudomi T, Takahashi T. TTF-1 expression in pulmonary adenocarcinomas. Am J Surg Pathol 2002;26:767–73.
16. Gartner LP, Hiatt JL. Respiratory system. In: Gartner LP, Hiatt JL, editors. Color textbook of histology. Philadelphia: W.B. Saunders Company; 2001. p. 343–64.
17. Wistuba II, Lam S, Behrens C, et al. Molecular damage in the bronchial epithelium of current and former smokers. J Natl Cancer Inst 1997;89:1366–73.
18. Wistuba II, Behrens C, Virmani AK, et al. High resolution chromosome 3p allelotyping of human lung cancer and preneoplastic/preinvasive bronchial epithelium reveals multiple, discontinuous sites of 3p allele loss and three regions of frequent breakpoints. Cancer Res 2000;60:1949–60.
19. Mao L, Lee JS, Kurie JM, et al. Clonal genetic alterations in the lungs of current and former smokers. J Natl Cancer Inst 1997;89:857–62.

DOI:10.1158/1940-6207.CAPR-08-0032

Cancer Prevention Research

Epidermal Growth Factor Receptor Abnormalities in the Pathogenesis and Progression of Lung Adenocarcinomas

Ximing Tang, Marileila Varella-Garcia, Ana C. Xavier, et al.

Cancer Prev Res 2008;1:192-200. Published online July 25, 2008.

DOI:10.1158/1940-6207.CAPR-08-0032

Epidermal Growth Factor Receptor Abnormalities in the Pathogenesis and Progression of Lung Adenocarcinomas

Ximing Tang,[1] Marileila Varella-Garcia,[3] Ana C. Xavier,[3] Erminia Massarelli,[1] Natalie Ozburn,[1] Cesar Moran[2] and Ignacio I. Wistuba[1,2]

Abstract To identify the characteristics and sequence of epidermal growth factor receptor (EGFR) abnormalities relevant to the pathogenesis and progression of lung adenocarcinoma, we performed a precise mapping analysis of *EGFR* mutation, gene copy number, and total and phosphorylated EGFR protein expression for the same tissue sites. We examined normal bronchial and bronchiolar epithelium (NBE) and tumor tissues obtained from 50 formalin-fixed lung adenocarcinomas, including 24 *EGFR*-mutant primary tumors with nine corresponding lymph node metastases and 26 wild-type primary tumors. NBE in 12 of 24 (50%) mutant and 3 of 26 (12%) wild-type tumors harbored *EGFR* mutations; these NBE also showed a lack of *EGFR* copy number increase and frequent EGFR (69%) and phosphorylated EGFR (33%) overexpression. *EGFR* mutation and protein overexpression were more frequent in NBE sites within tumors than in NBE sites adjacent to and distant from tumors, suggesting a localized field effect. Sites with high and low *EGFR* copy numbers were heterogeneously distributed in six of nine primary tumors and in one of eight metastases. EGFR protein overexpression was significantly higher in metastasis sites than in primary tumors. We conclude from our findings that *EGFR* mutations and protein overexpression are early phenomena in the pathogenesis of lung adenocarcinoma and that *EGFR* mutation precedes an increase in gene copy number. In *EGFR*-mutant adenocarcinoma metastases, the higher levels of EGFR overexpression and more homogeneously distributed high gene copy numbers suggest tumor progression. Our findings have important implications for the development of new strategies for targeted chemoprevention and therapy in lung adenocarcinoma using EGFR inhibitors.

Epidermal growth factor receptor (EGFR), a tyrosine kinase (TK) member of the ErbB family, has shown frequent abnormalities in non–small cell lung carcinomas. These abnormalities include protein overexpression, gene amplification, and mutation (1–3). Somatic *EGFR* mutations have been identified in specific subsets of patients with lung adenocarcinoma, including never or light smokers, women, and patients of East Asian descent (4). The mutations cluster in the first four exons (18–21) of the TK domain of the gene, and ~90% of the mutations are composed of either an in-frame deletion in exon 19 or a specific missense mutation in exon 21 (4). An increase in *EGFR* gene copy number, including high polysomy and gene amplification shown by fluorescent *in situ* hybridization (FISH), has been detected in 22% of patients with surgically resected (stages I-IIIA) non–small cell lung carcinomas and correlated with EGFR protein overexpression (2). Higher frequencies (40-50%) of *EGFR* high copy number have been reported in patients with advanced non–small cell lung carcinomas (5–10). Despite this knowledge, limited information is available on the role of EGFR abnormalities in the early pathogenesis and progression of lung adenocarcinomas.

Recently, we showed that mutation of the *EGFR* TK domain is an early event in the pathogenesis of lung adenocarcinoma and is detected in histologically normal bronchial and bronchiolar epithelium (NBE) in 43% of patients with *EGFR*-mutant tumors (11). We found that *EGFR* mutations were more frequent in normal epithelium within the tumor (43%) than in adjacent sites (24%), suggesting a localized field effect (11). However, no comprehensive information is available regarding the role of *EGFR* abnormalities, including gene mutation, increased copy number, and protein overexpression in the early pathogenesis and progression of lung adenocarcinomas.

Both *EGFR* gene mutations and high copy number (gene amplification and high polysomy identified by FISH) have been associated with sensitivity to the small-molecule TK inhibitors gefitinib and erlotinib in patients with lung

Authors' Affiliations: Departments of [1]Thoracic/Head and Neck Medical Oncology and [2]Pathology, The University of Texas M. D. Anderson Cancer Center, Houston, Texas, and [3]Department of Medicine/Medical Oncology and Pathology, University of Colorado Cancer Center, Aurora, Colorado
Received 02/09/2008; revised 03/28/2008; accepted 04/23/2008.

Grant support: Department of Defense grants W81XWH-04-1-0142 and W81XWH-05-2-0027, the Specialized Program of Research Excellence in Lung Cancer grant P50CA70907, and Cancer Center Support grant CA-16672 from the National Cancer Institute.

Requests for reprints: Ignacio I. Wistuba, Department of Pathology, Unit 85, The University of Texas M. D. Anderson Cancer Center, 1515 Holcombe Boulevard, Houston, TX 77030-4009. Phone: 713-563-9184; Fax: 713-792-0309; E-mail: iiwistuba@mdanderson.org.

doi:10.1158/1940-6207.CAPR-08-0032

DOI:10.1158/1940-6207.CAPR-08-0032

adenocarcinoma (5–18). However, some of these results have been rather controversial (9, 10, 19, 20). In these studies of gefitinib and erlotinib, most of the *EGFR* mutation and copy number analyses were done in very small tissue samples or in cytologic specimens obtained from primary tumor and metastasis sites in patients with advanced-stage lung cancer (5–9, 12–16). To date, no studies have been done to identify the characteristics of *EGFR* gene and protein expression abnormalities at different sites with respect to primary lung adenocarcinomas and in corresponding sites of metastasis, information that might resolve some of the controversy.

To identify the sequence of EGFR abnormalities involved in the pathogenesis and progression of lung adenocarcinoma, we did a precise mapping analysis correlating *EGFR* mutation, gene copy number, and protein expression in NBE fields, primary tumors, and corresponding lymph node metastases that were obtained from 50 patients with lung adenocarcinomas, including 24 patients with *EGFR*-mutant primary tumors with nine corresponding lymph node metastasis sites and 26 patients with *EGFR*–wild-type primary tumors.

Table 1. Clinicopathologic features of patients with lung adenocarcinomas examined for *EGFR* abnormalities in tumors and adjacent normal epithelium

Features/samples	*EGFR* status		
	Mutant (*n* = 24)	Wild-type (*n* = 26)	Total (*n* = 50)
Mean age (y)	61.3	62.7	62.1
Gender			
Female	19 (79%)	13 (50%)	32
Male	5 (21%)	13 (50%)	18
Ethnicity			
East Asian	13 (54%)	9 (35%)	22
Not East Asian	11 (56%)	17 (65%)	28
Smoking history			
Never	16 (67%)	9 (35%)	25
Former	7 (29%)	10 (38%)	17
Current	1 (4%)	7 (27%)	8
Stage of disease			
I	11 (46%)	15 (58%)	26
II	5 (21%)	4 (15%)	9
IIIA	8 (33%)	7 (27%)	15

Materials and Methods

Case selection

To map *EGFR* gene and protein expression abnormalities, we obtained formalin-fixed, paraffin-embedded lung adenocarcinoma tissue specimens from the Lung Cancer Specialized Program of Research Excellence Tissue Bank at The University of Texas M. D. Anderson Cancer Center (Houston, TX). The tumor tissue specimens came from 50 patients with surgically resected lung adenocarcinomas (tumor-node-metastasis stage I-IIIA) with known *EGFR* mutations in exons 18 to 21, as described previously (3, 11). This bank was approved by the M. D. Anderson Cancer Center Institutional Review Board.

Of these 50 patients, 24 patients had lung adenocarcinoma with *EGFR* mutations in exon 18 (n = 1), exon 19 (n = 13), and exon 21 (n = 10), and 26 patients had *EGFR*–wild-type lung adenocarcinoma. The patients' clinicopathologic features are summarized in Table 1. All lung adenocarcinomas were of mixed histologic subtype (WHO classification; ref. 21). None of the patients had received cytotoxic and/or targeted therapy. Clinical staging was based on the revised International System for Staging Lung Cancer (22).

EGFR abnormality mapping

We retrospectively reviewed H&E-stained histology sections of primary tumor, lymph node metastases, and adjacent normal lung tissue specimens to identify tissue foci available for EGFR abnormality analyses. The EGFR abnormalities included *EGFR* mutations in exons 18 and 21, as shown by microdissection and PCR-based sequencing; *EGFR* copy number, as shown by FISH; and total EGFR and phosphorylated EGFR (pEGFR), as shown by immunohistochemical analyses. Representative examples of these molecular changes are illustrated in Fig. 1.

We used serial 5-μm-thick histology sections for the tissue microdissection, FISH, and immunohistochemical analyses. We identified a total of 316 noncontiguous tumor and epithelial foci from among 142 NBE specimens (obtained from 50 patients; 2.84 sites/patient), 144 primary tumors (from 50 patients; 2.88 sites/patient), and 30 lymph node metastases (from 9 patients; 3.3 sites/patient). We examined NBE and primary tumors in both *EGFR*-mutant and *EGFR*–wild-type cases and metastasis sites in *EGFR*-mutant cases only. All epithelial foci consisted of normal or mildly hyperplastic epithelia that harbored small bronchi (65 sites) and bronchioles (77 sites).

The NBE specimens were obtained from three different locations based on their relationship to the tumors: within the tumor (47 sites), ≤5 mm from the tumor margin (adjacent to tumor; 63 sites), and >5 mm from the tumor margin ("distant" lung; 32 sites). We did not detect squamous metaplastic or dysplastic lesions in the bronchial structures or atypical adenomatous hyperplasias in the alveolar tissue. We identified small bronchi on the basis of well-defined smooth muscle and discontinuous cartilage layers. Bronchioles were defined as small conducting airways lacking well-defined smooth muscle wall or cartilage layers. We assessed the location of the small bronchial and bronchiolar respiratory epithelium examined for *EGFR* abnormalities based on the epithelia's location in relation to the tumor tissue in the corresponding histology sections, as previously described (11).

Microdissection and DNA extraction

Approximately 1,000 cells were precisely microdissected from 8-μm-thick, H&E-stained, formalin-fixed, paraffin-embedded histology sections for each site using laser capture microdissection (Arcturus Engineering Laser Capture Microdissection System; MDS Analytical Technologies), as previously described (11). To prevent the nonspecific binding of the mutant cells to the microdissection cap film, the microdissected tissue samples were redissected from the film under stereomicroscope visualization using fine needles (25-gauge 5/8-inch needles). We then extracted the DNA using 25 μL of PicoPure DNA Extraction solution containing proteinase K and incubated the DNA at 65°C for 20 h. Subsequently, proteinase K was inactivated by heating samples at 95°C for 10 min.

EGFR mutation analysis

Exons 18 and 21 of *EGFR* were PCR-amplified using DNA extracted from microdissected NBE and tumor cells, as previously described (3, 11). Each PCR was done using HotStarTaq Master Mix (Qiagen) for 40 cycles at 94°C for 30 s, 63°C for 30 s, and 72°C for 30 s, followed by a 7-min extension at 72°C. PCR products were directly sequenced using the Applied Biosystems PRISM dye terminator cycle sequencing method (Perkin-Elmer Corp.). We confirmed all sequence variants by independent PCR amplifications from at least two independent microdissections and sequenced the variants in both directions.

DOI:10.1158/1940-6207.CAPR-08-0032

EGFR FISH analysis

We analyzed the gene copy number per cell using the LSI EGFR SpectrumOrange/CEP 7 SpectrumGreen Probe (Abbott Molecular), as previously described (5). Histology sections were incubated at 56°C overnight and deparaffinized by washing in CitriSolv (Fisher Scientific). After incubation in 2× SSC buffer (pH 7.0) at 75°C for 15 to 25 min, the histology sections were digested with proteinase K (0.25 mg/mL in 2× SSC) at 37°C for 15 to 25 min, rinsed in 2× SSC (pH 7.0) at room temperature for 5 min, and dehydrated using ethanol in a series of increasing concentrations (70%, 85%, 100%). We applied the EGFR SpectrumOrange/CEP 7/SpectrumGreen probe set (Abbott Molecular) onto the selected area, according to the manufacturer's instructions, on the basis of the tumor foci seen on each slide. We then covered the hybridization area with a glass coverslip and sealed the coverslip with rubber cement. The slides were incubated at 80°C for 10 min for codenaturation of chromosomal and probe DNA and then placed in a humidified chamber at 37°C for 20 to 24 h to allow hybridization to occur. Posthybridization washes were done in 1.5 mol/L of urea and 0.1× SSC (pH 7.0-7.5) at 45°C for 30 min and in 2× SSC for 2 min at room temperature. After the samples were dehydrated in a series of increasing ethanol concentrations, 4′,6′-diamidino-2-phenylindole (0.15 mg/mL in Vectashield Mounting Medium; Vector Laboratories) was applied for chromatin counterstaining. FISH analysis was done independently by two authors (M. Varella-Garcia and A. C. Xavier), who were blinded to the patients' clinical characteristics and all other molecular variables. Patients were classified into six FISH strata according to the frequency of cells with the *EGFR* gene copy number and referred to the chromosome 7 centromere, as follows: (*a*) disomy (≥3 copies in <10% of cells); (*b*) low trisomy (3 copies in 10% to 40% of the cells, ≥4 copies in <10% of cells); (*c*) high trisomy (3 copies in ≥40% of cells, ≥4 copies in <10% of cells); (*d*) low polysomy (≥4 copies in 10–40% of cells); (*e*) high polysomy (≥4 copies in ≥40% of cells); and (*f*) gene amplification (ratio of *EGFR* gene to chromosome ≥2, presence of tight *EGFR* gene clusters and 15 copies of *EGFR* per cell in 10% of the analyzed cells). The high polysomy and gene amplification categories were considered to be high *EGFR* copy number, and the other categories were considered to be nonincreased *EGFR* copy number, as previously published (5). Analysis was done in approximately 50 nuclei per tumor and epithelial site, and the section of the area was guided by image captured in the H&E-stained section.

Immunohistochemical staining

Tissue histology sections for immunohistochemical analyses were deparaffinized, hydrated, heated in a steamer for 10 min with 10 mmol/L of sodium citrate (pH 6.0) for antigen retrieval, and washed in Tris buffer. Peroxide blocking was done with 3% H_2O_2 in methanol at room temperature for 15 min, followed by 10% bovine serum albumin in TBS with Tween 20 for 30 min at room temperature. For the EGFR analysis, tissue sections were incubated for 2 h with primary antibodies against the EGFR clone 31G7 (1:100 dilution; Zymed) and pEGFR Tyr 1086 (1:100 dilution; Invitrogen). Tissue sections were then incubated for 30 min with the secondary antibody (EnVision+ Dual Link labeled polymer; DAKO), after which diaminobenzidine chromogen was applied for 5 min. The slides were then

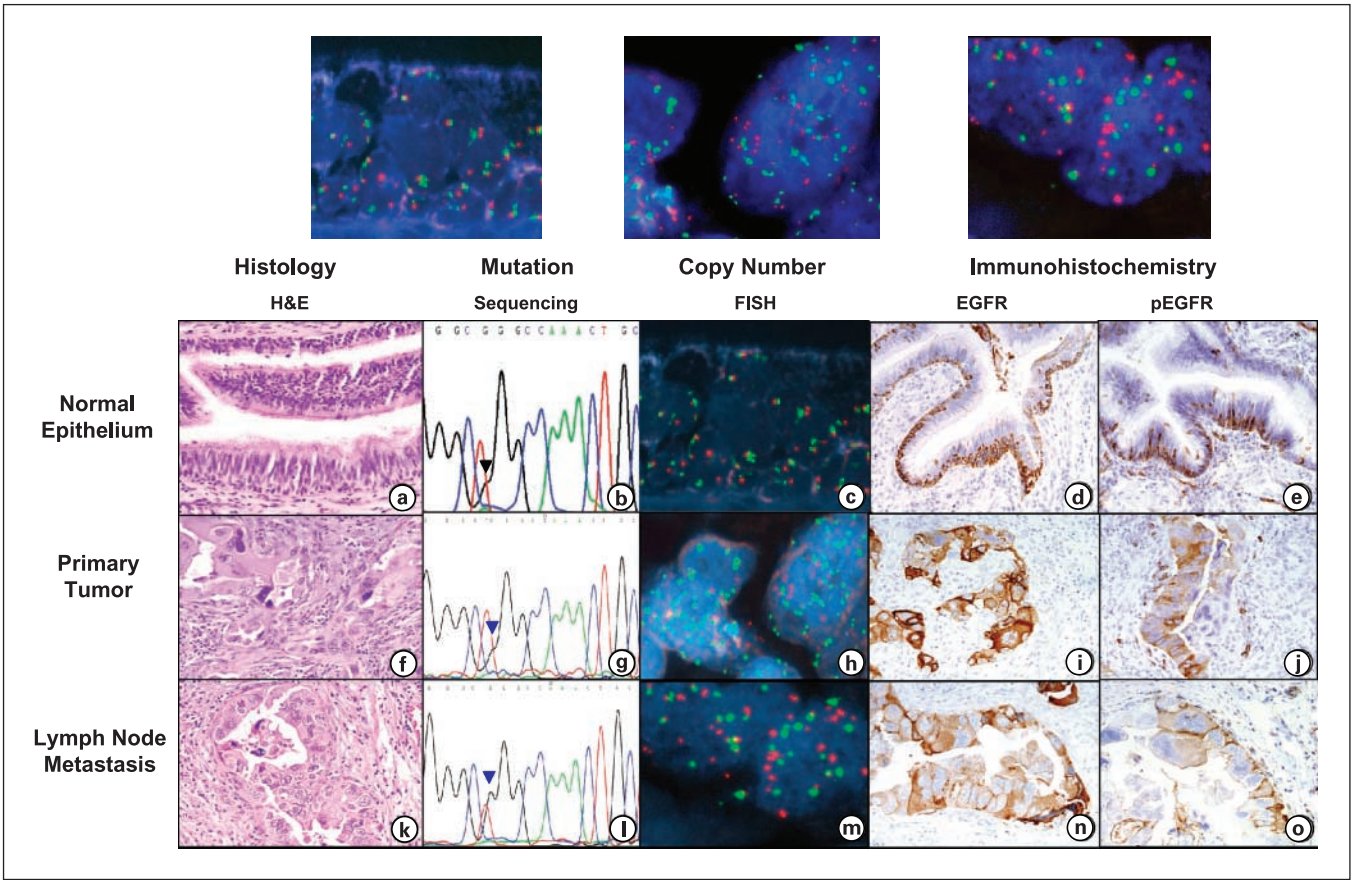

Fig. 1. A representative case of *EGFR*-mutant lung adenocarcinoma: *EGFR* gene and protein expression abnormalities in NBE (*A–E*), primary tumor (*F–J*), and lymph node metastasis (*K–O*) sites. Histologic characteristics (*A*, *F*, and *K*) of tissue sections stained with H&E (magnification, ×100). PCR-based *EGFR* sequencing (*B*, *G* and *L*) of the same *EGFR* mutation in exon 21 (L858R, *black arrowhead*) in NBE (*B*), primary tumor (*G*), and lymph node metastasis sites (*L*). *EGFR* FISH analysis (*C*, *H* and *M*) of low trisomy (low copy number) in the NBE sample (*C*), high polysomy in the primary tumor site (*H*), and gene amplification (*M*) in the metastasis site. Immunohistochemical analysis (*D, I, N, E, J*, and *O*) of high EGFR and pEGFR expression in the membrane and cytoplasm in all three types of samples.

DOI:10.1158/1940-6207.CAPR-08-0032

Table 2. Frequency of *EGFR* gene mutation and protein overexpression in histologically normal bronchial and bronchiolar epithelium obtained from *EGFR*-mutant and wild-type lung adenocarcinomas

EGFR abnormality in NBE	Cases			Sites		
	Mutant	Wild-type	Total	Mutant	Wild-type	Total
Mutation by sequencing						
Number	24	26	50	85	57	142
Mutant	12 (50%)*	3 (12%)*	15 (30%)	22 (26%)	8 (14%)	30 (21%)
Protein overexpression by immunohistochemistry†						
Number	23	26	49	78	56	134
EGFR	19 (83%)	15 (58%)	34 (69%)	52 (67%)	35 (63%)	87 (65%)
pEGFR	10 (44%)	6 (23%)	16 (33%)	24 (31%)	12 (21%)	36 (27%)

*$P = 0.003$.
†Positive immunohistochemical overexpression score >200 (range, 0-400).

counterstained with hematoxylin and topped with a coverslip. For EGFR and pEGFR expression, antibody specificity was confirmed using blocking peptide and phosphatase incubation experiments. For the control experiments, we used formalin-fixed and paraffin-embedded pellets from lung cancer cell lines with confirmed EGFR and pEGFR overexpression. Thyroid transcription factor-1 (TITF-1) antibody (1:100 dilution, Cell Marque) was used for the identification of TITF-1–positive cells. All four antibodies were incubated for 1.5 h at room temperature. Immunohistochemistry results were scored jointly by two authors (X. Tang and I.I. Wistuba), who were blinded to clinical and other molecular variables. Immunostaining of the cell membrane and cytoplasm for EGFR and pEGFR was evaluated by light microscopy (magnification, ×20). A semiquantitative approach was used to generate a score for each tissue site, as previously described (2, 23, 24). Membrane and cytoplasm stains were recorded separately. We defined the intensity score as follows: 0, no appreciable staining in the NBE or malignant cells; 1, barely detectable staining in NBE or malignant cells compared with the stromal elements; 2, readily appreciable staining; 3, dark brown staining of cells; and 4, very strong staining of cells. The score was also based on the fraction of cells showing a given staining intensity (0-100%). We calculated the immunohistochemical scores by multiplying the intensity and extension, and the scores ranged from 0 to 400. For the statistical analyses, scores of 0 to 200 signified negative/low expression, and scores >200 indicated positive/overexpression, as previously reported (2, 23, 24). For the evaluation of nuclear TITF-1 immunohistochemical expression, 200 epithelial cells were quantified by light microscopy (magnification, ×20), and a score (range, 0-100) expressing the percentage of positive cells was obtained.

Statistical analysis

All relationships between categorical variables were assessed using χ^2 and Fisher's exact tests. $P < 0.05$ values were considered statistically significant.

Table 3. *EGFR* mutation and protein overexpression in histologically normal epithelium by location

EGFR abnormality in NBE	Location in relation to the tumor			Structure	
	Inside	Adjacent	Distant	Bronchiole	Small bronchus
Mutation					
Mutant tumor	11/31 (36%)*	10/35 (29%)	1/17 (6%)*	10/43 (23%)	12/42 (29%)
Wild-type tumor	2/15 (13%)	3/28 (11%)	1/15 (7%)	4/34 (12%)	2/23 (9%)
All tumors	13/46 (28%)	13/63 (21%)	2/32 (6%)	14/77 (19%)	14/65 (22%)
EGFR overexpression†					
Mutant tumor	24/29 (83%)‡	20/33 (61%)‡	8/16 (50%)‡	18/38 (47%)§	34/40 (85%)§
Wild-type tumor	10/15 (67%)	17/28 (61%)	8/13 (62%)	14/33 (42%)§	21/23 (91%)§
All tumors	34/44 (77%)	37/61 (61%)	16/29 (55%)	32/71 (45%)§	55/63 (87%)§
pEGFR overexpression†					
Mutant tumor	13/29 (45%)‖	5/33 (15%)‖	6/16 (38%)‖	10/38 (26%)	14/40 (35%)
Wild-type tumor	5/15 (33%)	5/28 (18%)	2/13 (15%)	2/33 (6%)§	10/23 (44%)§
All tumors	18/44 (41%)	10/61 (16%)	8/29 (28%)	12/71 (17%)¶	24/63 (38%)¶

*Comparison of NBE from inside tumor vs. NBE distant ($P = 0.02$).
†Positive immunohistochemical overexpression score >200 (range 0-400).
‡Comparison of NBE from inside tumor vs. NBE adjacent + distant ($P = 0.02$)
§Comparison of NBE from bronchiole vs. small bronchus ($P < 0.001$).
‖Comparison of NBE from inside tumor vs. NBE adjacent + distant ($P = 0.038$).
¶Comparison of NBE from bronchiole vs. small bronchus ($P = 0.006$).

DOI:10.1158/1940-6207.CAPR-08-0032

Results

EGFR abnormalities in the early pathogenesis of lung adenocarcinomas

Patterns of EGFR mutation in NBE. We previously reported our finding of mutations in exons 19 and 21 of *EGFR* in at least one site of microdissected NBE obtained from lung cancer specimens from 9 of 21 (43%) patients with *EGFR*-mutant adenocarcinomas, with no such mutations found in any of 26 respiratory epithelium foci from 16 patients with wild-type tumors (11). In the present study, using the same methodology, we analyzed for *EGFR* mutation in NBE obtained from an additional 3 patients with an *EGFR*-mutant and 10 patients with *EGFR*–wild-type lung adenocarcinomas. Combining both data sets, the overall rate of mutation in NBE from *EGFR*-mutant tumors was 50%. In the wild-type tumor cases, we detected *EGFR* exon 19 deletions (15 bp, 746-750) in six sites of small bronchial (n = 4) and bronchiolar (n = 2) NBE obtained from three wild-type tumors (Table 2). Thus, an *EGFR* mutation was found in NBE in 3 of 26 (12%) wild-type adenocarcinomas and in 8 of 57 (14%) of the microdissected epithelial sites (Table 2).

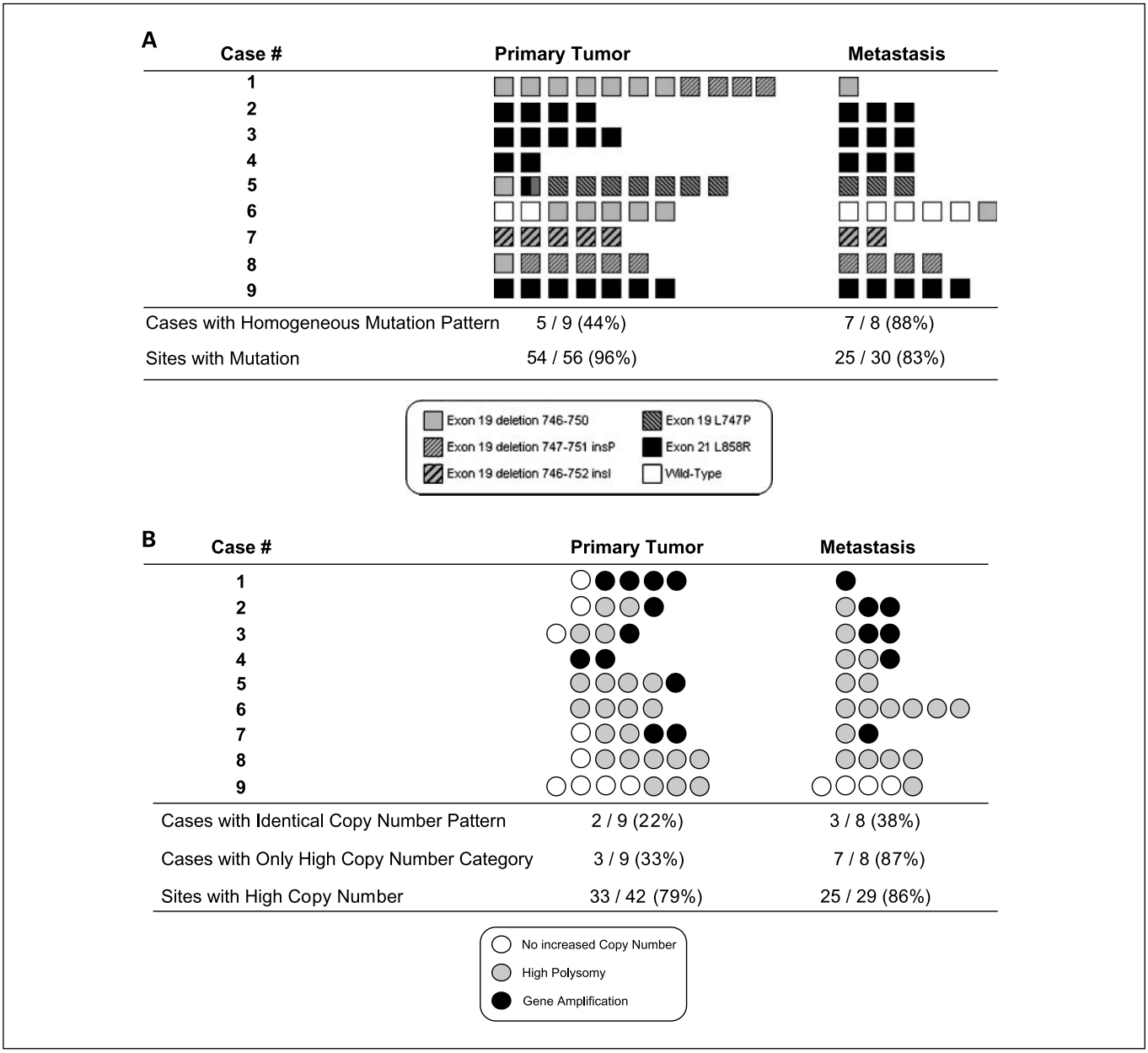

Fig. 2. *A, EGFR* mutation pattern in 56 primary tumor and 30 lymph node metastasis sites obtained from nine patients with *EGFR*-mutant lung adenocarcinomas. A homogeneous mutation pattern was detected in five primary tumors (*cases 2, 3, 4, 7*, and *9*) and all but one (*case 6*) metastasis case. *Case 6*, mixed wild-type and mutant sites in both primary tumor sites and corresponding metastases. *B, EGFR* copy number pattern shown by FISH in 42 primary tumor and 29 lymph node metastasis sites obtained from nine patients with *EGFR*-mutant lung adenocarcinomas. Different FISH copy number categories (low vs. high) were found in six of nine primary tumors and in one of eight corresponding metastases. Positive *EGFR* FISH expression included high polysomy and gene amplification, and negative *EGFR* FISH expression included disomy and trisomy.

DOI:10.1158/1940-6207.CAPR-08-0032

Table 4. Summary of *EGFR* abnormalities by sites in nine primary lung adenocarcinomas and corresponding lymph node metastases

EGFR abnormality/ number of sites	Primary tumor	Metastases
Mutation		
Number of sites examined	56	30
Mutation positive	54 (96%)*	25 (83%)*
Copy no.		
Number of sites examined	42	29
Low copy no.	9 (21%)	4 (14%)
High copy no.	33 (79%)	25 (86%)
High polysomy	22 (52%)	18 (62%)
Gene amplification	11 (26%)	7 (24%)
Protein overexpression†		
Number of sites examined	65	31
EGFR	42 (65%)‡	30 (97%)‡
pEGFR	9 (14%)§	21 (68%)§

*The same case harbored two primary tumor and five metastasis sites with *EGFR*-wild-type sequence.
†Positive immunohistochemical expression score >200 (range 0-400).
‡Primary tumor vs. metastasis ($P = 0.02$).
§Primary tumor vs. metastasis ($P = 0.00001$).

The combined data showed that NBE with mutant *EGFR* was detected in the small bronchi (13 of 64, 20%) and bronchioles (17 of 78, 22%) of both mutant and wild-type tumor cases. Overall, however, the mutation frequency was higher in NBE samples microdissected from within the tumor (13 of 47, 28%) than in samples obtained from adjacent tissue and tissue distant from the tumors (17 of 95, 18%; Table 3).

In our previously reported comparison of NBE and corresponding tumors (16 specimens), we always observed identical *EGFR* mutations in both sites examined (11). In this study, we have expanded the number of NBE sites ($n = 85$) examined for the mutation in patients with *EGFR*-mutant adenocarcinomas and detected five sites (6%) from three cases in which NBE showed mutations different from the ones detected in the corresponding tumor specimens (data not shown). Importantly, in all cases with a mutation in NBE, an identical mutation was detected in at least one site of the corresponding tumor specimen. Thus, in this expansion of our previous study (11), a relatively more heterogeneous *EGFR* mutation pattern of the respiratory field was detected in NBE microdissected from mutant lung adenocarcinomas, but most NBE and corresponding tumors shared the same mutation.

EGFR copy number and correlation with gene mutation in NBE. To determine the morphologic stage at which *EGFR* copy abnormalities arise in *EGFR*-mutant adenocarcinomas, we did a precise mapping analysis and examined *EGFR* copy number in 21 NBE sites obtained from nine mutant adenocarcinomas using FISH. All nine tumor specimens showed at least one site with a high copy number. These epithelial sites were also examined in the *EGFR* mutation analysis. Most NBE (14 of 21, 67%) showed no *EGFR* FISH abnormalities (disomy), including four *EGFR*-mutant sites with exon 19 (15 bp) deletions and exon 21 (L858R) point mutations. Trisomy was detected in seven (33%) NBE sites obtained from six (67%) cases. We did not identify any NBE with *EGFR* amplifications or a high level of polysomy, which have been defined as high gene copy number. In contrast, the nine tumors mapped showed significantly higher frequency of *EGFR* amplification (11 of 42 sites, 26%; $P < 0.018$) or a high level of polysomy (22 of 42, 52%; $P < 0.001$) compared with NBE. Our findings indicate that high *EGFR* copy number does not occur in peripheral NBE in *EGFR*-mutant lung adenocarcinomas and that gene mutations precede copy number abnormalities in the sequential pathogenesis of these tumors.

EGFR immunohistochemical expression and correlation with gene mutation in NBE. We evaluated the level of EGFR and pEGFR protein expression in 134 NBEs obtained from *EGFR*-mutant and wild-type lung adenocarcinomas. Overall, a

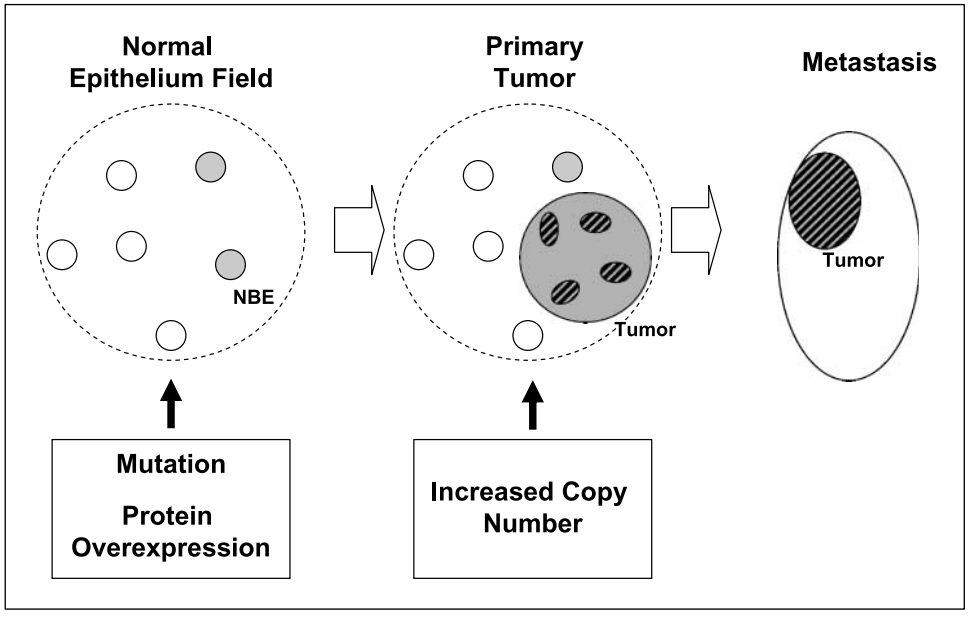

Fig. 3. Proposed sequence of *EGFR* abnormalities occurring in the early pathogenesis and progression of *EGFR*-mutant lung adenocarcinomas. NBE field, primary tumor, and metastasis sites. *Small circles*, NBE, which acquires *EGFR* mutations and EGFR protein (total and phosphorylated) overexpression (*gray circles*). In the primary tumor stage, the *EGFR* copy number increases (high polysomy and gene amplification) in small tumor foci (*striped ovals*). In the metastasis site, tumor cells show both *EGFR* mutation and high copy number throughout most of the lesion.

DOI:10.1158/1940-6207.CAPR-08-0032

high level of EGFR (69%) and a moderate level of pEGFR (33%) expression were detected in NBE from patients with tumors (Table 2). However, EGFR and pEGFR were expressed to a greater degree in NBE sites obtained from patients with *EGFR*-mutant tumors than in patients with wild-type tumors (Table 2), although these differences were not statistically significant. The frequency of EGFR, but not of pEGFR, overexpression was higher in *EGFR*–wild-type NBE sites (85 of 111, 77%) than in mutant sites (14 of 24, 58%; $P = 0.039$). Of interest, NBE located inside tumors showed the highest frequency of EGFR and pEGFR overexpression compared with NBE located adjacent to and distant from tumors, especially in *EGFR*-mutant tumors (Table 3). Small bronchi also showed a higher frequency of overexpression of both markers compared with bronchioles (Table 3). Thus, the overexpression of EGFR and pEGFR is a common event in NBE from patients with lung adenocarcinomas, especially in *EGFR*-mutant tumors, and shows a localized field phenomenon effect similar to gene mutation.

TITF-1 immunohistochemical expression and* EGFR *mutation in NBE. Recently, on the basis of immunohistochemical findings of higher levels of nuclear TITF-1 expression, a crucial transcription factor of the lung, in *EGFR*-mutant lung adenocarcinomas compared with in wild-type tumors, it has been suggested that *EGFR*-mutant lung adenocarcinoma originates from the terminal respiratory unit (25), which is composed of alveolar cells and nonciliated bronchiolar epithelium. Its characteristics are highlighted by the expression of TITF-1 (25). We therefore investigated the correlation between *EGFR* mutation and TITF-1 nuclear expression in tumor and normal epithelium sites. *EGFR*-mutant lung adenocarcinomas (18 of 20 cases, 90%) showed higher expression of TITF-1 than did wild-type tumors (10 of 26 cases, 38%; $P < 0.001$). However, in immunohistochemical studies, we did not see a significant difference in the frequency of TITF-1 expression between *EGFR*-mutant (11 of 25 sites, 44%) and *EGFR*–wild-type (34 of 105 sites, 33%; $P = 0.273$) respiratory epithelia. Our findings therefore indicate that NBE cells expressing TITF-1 are not the exclusive precursors of *EGFR*-mutant adenocarcinomas. From these results, it is clear that these tumors do not originate exclusively from terminal respiratory unit structures.

EGFR abnormalities in the progression of lung adenocarcinomas

EGFR mutation pattern in primary tumors and corresponding metastasis. To identify the characteristics of EGFR abnormalities in the progression of mutant lung adenocarcinomas, we examined *EGFR* gene mutation, gene copy number, and protein expression in primary tumors and corresponding metastases by performing a detailed mapping analysis of tumor specimens. For this study, we selected nine lung adenocarcinomas with known *EGFR* mutations in exon 19 ($n = 5$) and exon 21 ($n = 4$), and with lymph node metastases for which there was sufficient tissue to perform our mapping analysis.

For the mutation analysis of *EGFR* exons 19 and 21, we did precise tissue microdissection from noncontiguous primary tumor foci ($n = 56$ sites, 6.2 sites/tumor; range 2-11 sites) containing at least 1,000 cells. Surprisingly, four of the nine primary tumorsexamined showed mixed *EGFR* gene patterns (Fig. 2A): three showed two or more types of mutations, and one showed five sites with exon 19 (15 bp, 746-750) deletion and two sites with the wild-type *EGFR* gene. *EGFR* mutation analysis of 30 corresponding lymph node metastasis sites from the nine *EGFR*-mutant cases (3.3 sites/case; range 1-6 sites) detected only one type of *EGFR* mutation in all tumor sites in each case, and the mutation was always present in at least one site of the corresponding primary tumor. Similar to the corresponding primary tumor, one metastasis case showed *EGFR*–wild-type (five sites) and *EGFR*-mutant [one site, exon 19 (15 bp, 746-750) deletion] tumor sites (Fig. 2A). All these findings were confirmed by sequencing analyses of independently microdissected samples. In summary, our findings showed a relatively high level of heterogeneity for the *EGFR* mutation, and several tumor cell clones had mutation patterns in the primary tumor specimens that differed from the mutation patterns in the lymph node metastasis sites.

EGFR copy number abnormalities in primary tumors and corresponding metastasis. We used FISH to investigate the *EGFR* gene copy number abnormalities in 42 primary tumor sites (2.1 sites/case; range 2-7 sites) and 29 metastasis sites (3.2sites/case; range 1-6 sites), which were also examined for the mutation analysis. Overall, all primary tumors and corresponding metastases showed at least one site of high gene copy number (high polysomy or gene amplification; Fig. 2B). However, six (67%) primary tumor cases and one (11%) metastasis case showed at least one site without high copy number (disomy in one primary tumor site, high trisomy in one metastasis site, and low polysomy in seven primary and three metastasis sites; Fig. 2B). Thus, *EGFR* copy number heterogeneity was higher in primary tumor sites than in corresponding metastasis sites.

EGFR immunohistochemical expression in primary tumors and corresponding metastasis sites. In the nine *EGFR*-mutant lung adenocarcinoma cases mapped for *EGFR* abnormalities, we examined both primary tumors and the corresponding lymph node metastases for EGFR and pEGFR immunohistochemical expression. For both tumor locations combined, 96 distinct tumor sites were examined ($n = 65$ primary tumor sites, 7.2 sites/case; and $n = 31$ metastasis sites, 3.4 sites/case). Significantly higher levels of EGFR and pEGFR expression were detected in metastasis sites compared with primary tumor sites (Table 4). No correlation between EGFR and pEGFR expression and *EGFR* copy number status by FISH was detected.

Discussion

Using a detailed molecular pathology mapping strategy, we determined the sequence of EGFR abnormalities in the early pathogenesis of *EGFR*-mutant lung adenocarcinomas and identified the pattern of EGFR changes in the progression of *EGFR*-mutant lung adenocarcinomas from primary tumors to lymph node metastasis. First, we showed that *EGFR* mutations precede gene copy number abnormalities in the pathogenesis of these tumors and that EGFR and pEGFR immunohistochemical protein expressions are frequent events in histologically normal peripheral bronchial and bronchiolar epithelium adjacent to lung adenocarcinomas. Second, our data indicated that although primary lung adenocarcinomas show some degree of *EGFR* gene copy number heterogeneity, this phenomenon is rare in metastases. Although these findings can be considered tumor progression phenomena, they also have important clinical implications from the standpoint of making decisions regarding the use of EGFR TK inhibitor therapy on the basis of the finding of *EGFR* gene abnormalities.

DOI:10.1158/1940-6207.CAPR-08-0032

Despite the evidence showing that atypical adenomatous hyperplasia is a precursor of peripheral lung adenocarcinomas (26), there is consensus that the pathogenesis of most adenocarcinomas is unknown. Our previously reported findings of an *EGFR* mutation in NBE in 9 of 21 (43%) patients with *EGFR*-mutant adenocarcinomas indicated that the *EGFR* gene mutation is an early event in the pathogenesis of lung adenocarcinoma (11). In this study, we have investigated normal epithelium from additional patients with *EGFR*-mutant or wild-type lung adenocarcinomas and specifically have two new findings in this study; (*a*) we detected an *EGFR* mutation (exon 19, 15 bp deletion, 746-751) in six sites of small bronchial and bronchiolar epithelium obtained from three patients with wild-type adenocarcinoma, and (*b*) whereas an identical mutation was detected in the majority of specimens of mutant normal epithelium compared with the corresponding invasive tumor (75% of cases and 94% of sites), we found few normal epithelium sites (6%) in three of 12 cases (25%) of *EGFR*-mutant tumors, demonstrating the existence of a different mutation pattern between normal epithelium and the corresponding invasive tumor. All these data reinforce the concept of a field effect phenomenon in *EGFR* mutations in lung adenocarcinoma pathogenesis that affects histologically normal bronchial and bronchiolar respiratory epithelia.

We have previously shown that molecular abnormalities occur in a stepwise fashion in the sequential pathogenesis of squamous cell carcinoma of the lung, with molecular changes commencing in histologically normal bronchial epithelium in smokers and in patients with lung cancer (27, 28). Our findings suggest that *EGFR* abnormalities also occur sequentially in the early pathogenesis of lung adenocarcinoma, with a mutation commencing in histologically normal epithelium and a high *EGFR* copy number appearing at the invasive tumor stage. A recent report (29) of selective gene amplification of the shorter allele of the *EGFR* intron 1 polymorphism CA simple sequence repeat 1, which is the allele more frequently mutated in tumors harboring an *EGFR* mutation, also suggests that mutations occur earlier than copy number abnormalities in the pathogenesis of lung adenocarcinoma. Our findings of frequent EGFR (69%) and pEGFR (33%) protein overexpression in normal distal bronchial and bronchiolar epithelium from patients with either *EGFR*-mutant or *EGFR*–wild-type lung adenocarcinomas indicate a field phenomenon in the peripheral airway. A relatively high frequency of EGFR protein expression has also been reported in centrally located, histologically normal (42%) and hyperplastic (54%) bronchial epithelium from smokers (23). In addition, our data indicate that the mechanisms of protein overexpression seem to be unassociated with high gene copy number and mutation in NBE. Other mechanisms can explain EGFR overexpression in normal epithelial cells, including ligand-dependent up-regulation and activation, as well as inhibition of endocytosis-related protein down-regulation in the cell membrane (30).

Based on findings of higher levels of immunohistochemical expression of nuclear TITF-1, a crucial transcription factor of the lung, in *EGFR*-mutant lung adenocarcinomas compared with wild-type tumors, it has been suggested that *EGFR*-mutant lung adenocarcinoma originates from the terminal respiratory unit (25). We found *EGFR* mutations in microdissected histologically normal epithelial cells from small bronchi and bronchioles, which supports the concept of adenocarcinomas arising from the peripheral lung airway. Our findings indicate that NBE cells expressing TITF-1 are not the exclusive precursors of *EGFR*-mutant adenocarcinomas. From this finding, it is clear that these tumors do not originate exclusively from terminal respiratory unit structures. In addition, we cannot exclude the possibility that common stem or progenitor cells for both bronchial and bronchiolar epithelium bear *EGFR* mutations.

It has been suggested that activating TK *EGFR* mutations are a potent oncogenic event by which mutant tumor cells become physiologically dependent on the continued activity of the phosphorylated protein for the maintenance of their malignant phenotype (31). Our detailed mapping analysis of the *EGFR* gene mutation and copy number of multiple precisely microdissected sites in nine mutant primary tumors and corresponding lymph node metastases showed an identical or monoclonal pattern of mutation in most (n = 5) primary tumors and all metastases. These findings corroborate the monoclonal concept of tumor development and the monoclonal evolution of metastases (32, 33). However, two primary tumors lacking identical or monoclonal *EGFR*-mutant patterns harbored different sizes of exon 19 deletions (12 versus 15 bp and 15 versus 18 bp deletions). This finding could be explained by a tumor progression phenomenon in which the deletion size changed during the evolution of the malignancy. However, two very interesting primary tumors in our study exhibited findings that challenged the concept of the monoclonal evolution of tumors. One case showed a single site with an exon 19 (15 bp) deletion, whereas the remaining eight sites lacked the deletion but showed a point mutation (TTA747CCA) in the same exon. Of interest, the three metastasis sites examined harbored the most frequent mutation detected in the primary lung tumor. The other case showed areas of wild-type and mutant *EGFR* in both primary tumors and metastases, a phenomenon that is difficult to explain and suggests that molecular events other than an *EGFR* mutation may be responsible for tumor development in lung adenocarcinomas. These findings were confirmed by the sequencing of independently microdissected samples. In the latter case, the finding of a high *EGFR* copy number (high polysomy) in wild-type tumor sites raises the possibility of an alternative explanation—that the wild-type allele is preferentially amplified in some tumor cells. As a result, the mutant allele is underrepresented and is not detectable by our current sequencing methodology.

Retrospective studies have provided data suggesting that a high *EGFR* gene copy number shown by FISH is associated with treatment response, time to progression, and survival in patients with advanced non–small cell lung carcinoma treated with EGFR TK inhibitors (5-7, 10, 17). In these studies, high *EGFR* copy number as shown by FISH was defined as true gene amplification or high polysomy with equal to or more than four *EGFR* copies in ≥40% of cells (5, 34). Our mapping analysis of primary tumors and corresponding lymph node metastases in which we used the same *EGFR* FISH criteria showed that a frequent high copy number in mutant tumors was the most frequent pattern detected. Despite the fact that most primary tumor sites and nearly all metastasis sites showed high copy numbers, high polysomy and gene amplification were heterogeneously distributed in both tumor locations. More importantly, five of nine (56%)

DOI:10.1158/1940-6207.CAPR-08-0032

primary tumors and one metastasis (13%) showed one or more sites without an increased copy number (FISH negative). Similarly, EGFR and pEGFR immunohistochemical expression was less heterogeneous in primary tumors and more frequent in metastases. Taken together, these data suggest that *EGFR* copy number analyzed by FISH and protein expression analyzed by immunohistochemistry in small core biopsy or fine-needle aspiration specimens obtained from primary tumors, and more rarely from metastases, could miss these molecular changes, especially if only a small number of malignant cells are available for examination. In addition, if the suggested presence of *EGFR* high copy number correlates with sensitivity to EGFR TK inhibitors (5–7, 17), it is likely that metastases will show a better response to therapy than will primary tumors. This is an important consideration, in light of the fact that the site of origin (primary versus metastasis) of the tumor specimen was not reported and factored into the biomarker analyses in any of the clinical trials testing the efficacy of EGFR TK inhibitors in patients with advanced non–small cell lung carcinoma in whom *EGFR* copy number determined by FISH was examined as a predictor of response and prognosis (5–7). Our results show that a better understanding of the pattern of molecular abnormalities and their corresponding biomarker expression, including primary tumors and the frequent metastases seen for this tumor type, is important in lung cancer.

In summary, our data suggest that gene mutations and protein overexpression are the earliest phenomena in *EGFR*-mutant lung adenocarcinoma, occurring at the NBE stage, and that this is followed by the development of a focal increase in copy number at the tumor stage (Fig. 3). At the metastasis sites, however, all three abnormalities were more frequent than they were in the primary tumors and were homogeneously distributed throughout the malignant cells.

Disclosure of Potential Conflicts of Interest

No potential conflicts of interest were disclosed.

References

1. Scagliotti GV, Selvaggi G, Novello S, Hirsch FR. The biology of epidermal growth factor receptor in lung cancer. Clin Cancer Res 2004;10:4227s–32s.
2. Hirsch FR, Varella-Garcia M, Bunn PA, Jr., et al. Epidermal growth factor receptor in non-small-cell lung carcinomas: correlation between gene copy number and protein expression and impact on prognosis. J Clin Oncol 2003;21:3798–807.
3. Shigematsu H, Lin L, Takahashi T, et al. Clinical and biological features associated with epidermal growth factor receptor gene mutations in lung cancers. J Natl Cancer Inst 2005;97:339–46.
4. Shigematsu H, Gazdar AF. Somatic mutations of epidermal growth factor receptor signaling pathway in lung cancers. Int J Cancer 2006;118:257–62.
5. Cappuzzo F, Hirsch FR, Rossi E, et al. Epidermal growth factor receptor gene and protein and gefitinib sensitivity in non-small-cell lung cancer. J Natl Cancer Inst 2005;97:643–55.
6. Tsao MS, Sakurada A, Cutz JC, et al. Erlotinib in lung cancer—molecular and clinical predictors of outcome. N Engl J Med 2005;353:133–44.
7. Hirsch FR, Varella-Garcia M, McCoy J, et al. Increased epidermal growth factor receptor gene copy number detected by fluorescence *in situ* hybridization associates with increased sensitivity to gefitinib in patients with bronchioloalveolar carcinoma subtypes: a Southwest Oncology Group Study. J Clin Oncol 2005;23:6838–45.
8. Jackman DM, Holmes AJ, Lindeman N, et al. Response and resistance in a non-small-cell lung cancer patient with an epidermal growth factor receptor mutation and leptomeningeal metastases treated with high-dose gefitinib. J Clin Oncol 2006; 24:4517–20.
9. Massarelli E, Varella-Garcia M, Tang X, et al. KRAS mutation is an important predictor of resistance to therapy with epidermal growth factor receptor tyrosine kinase inhibitors in non-small-cell lung cancer. Clin Cancer Res 2007;13:2890–6.
10. Bunn PA, Jr., Dziadziuszko R, Varella-Garcia M, et al. Biological markers for non-small cell lung cancer patient selection for epidermal growth factor receptor tyrosine kinase inhibitor therapy. Clin Cancer Res 2006;12:3652–6.
11. Tang X, Shigematsu H, Bekele BN, et al. EGFR tyrosine kinase domain mutations are detected in histologically normal respiratory epithelium in lung cancer patients. Cancer Res 2005;65:7568–72.
12. Paez JG, Janne PA, Lee JC, et al. EGFR mutations in lung cancer: correlation with clinical response to gefitinib therapy. Science 2004;304: 1497–500.
13. Lynch TJ, Bell DW, Sordella R, et al. Activating mutations in the epidermal growth factor receptor underlying responsiveness of non-small-cell lung cancer to gefitinib. N Engl J Med 2004;350: 2129–39.
14. Mitsudomi T, Kosaka T, Endoh H, et al. Mutations of the epidermal growth factor receptor gene predict prolonged survival after gefitinib treatment in patients with non-small-cell lung cancer with postoperative recurrence. J Clin Oncol 2005;23: 2513–20.
15. Han SW, Kim TY, Hwang PG, et al. Predictive and prognostic impact of epidermal growth factor receptor mutation in non-small-cell lung cancer patients treated with gefitinib. J Clin Oncol 2005;23: 2493–501.
16. Taron M, Ichinose Y, Rosell R, et al. Activating mutations in the tyrosine kinase domain of the epidermal growth factor receptor are associated with improved survival in gefitinib-treated chemorefractory lung adenocarcinomas. Clin Cancer Res 2005; 11:5878–85.
17. Han SW, Kim TY, Jeon YK, et al. Optimization of patient selection for gefitinib in non-small cell lung cancer by combined analysis of epidermal growth factor receptor mutation, K-ras mutation, and Akt phosphorylation. Clin Cancer Res 2006; 12:2538–44.
18. Pugh TJ, Bebb G, Barclay L, et al. Correlations of EGFR mutations and increases in EGFR and HER2 copy number to gefitinib response in a retrospective analysis of lung cancer patients. BMC Cancer 2007;7:128.
19. Sequist LV, Haber DA, Lynch TJ. Epidermal growth factor receptor mutations in non-small cell lung cancer: predicting clinical response to kinase inhibitors. Clin Cancer Res 2005;11:5668–70.
20. Johnson BE, Janne PA. Selecting patients for epidermal growth factor receptor inhibitor treatment: a FISH story or a tale of mutations? J Clin Oncol 2005;23:6813–6.
21. Travis WD, Brambilla E, Muller-Hermelink HK, Harris CC. Tumours of the lung. In: W.D. Travis E, Brambilla HK, Muller-Hermelink, C.C. Harris, editors. Pathology and genetics: Tumours of the lung, pleura, thymus and heart. Lyon: IARC; 2004. p. 9-124.
22. Mountain CF. Revisions in the International System for Staging Lung Cancer. Chest 1997;111: 1710–7.
23. Merrick DT, Kittelson J, Winterhalder R, et al. Analysis of c-ErbB1/epidermal growth factor receptor and c-ErbB2/HER-2 expression in bronchial dysplasia: evaluation of potential targets for chemoprevention of lung cancer. Clin Cancer Res 2006;12:2281–8.
24. Tsao AS, Tang XM, Sabloff B, et al. Clinicopathologic characteristics of the EGFR gene mutation in non-small cell lung cancer. J Thorac Oncol 2006;1:231–9.
25. Yatabe Y, Kosaka T, Takahashi T, Mitsudomi T. EGFR mutation is specific for terminal respiratory unit type adenocarcinoma. Am J Surg Pathol 2005;29:633–9.
26. Westra WH. Early glandular neoplasia of the lung. Respir Med 2000;1:163–9.
27. Wistuba II, Behrens C, Milchgrub S, et al. Sequential molecular abnormalities are involved in the multistage development of squamous cell lung carcinoma. Oncogene 1999;18:643–50.
28. Wistuba II, Behrens C, Virmani AK, et al. High resolution chromosome 3p allelotyping of human lung cancer and preneoplastic/preinvasive bronchial epithelium reveals multiple, discontinuous sites of 3p allele loss and three regions of frequent breakpoints. Cancer Res 2000;60:1949–60.
29. Nomura M, Shigematsu H, Li L, et al. Polymorphisms, mutations, and amplification of the EGFR gene in non-small cell lung cancers. PLoS Med 2007;4:e125.
30. Grandal MV, Madshus IH, Epidermal growth factor receptor and cancer: control of oncogenic signalling by endocytosis. J Cell Mol Med 2008 [Epub ahead of print].
31. Gazdar AF, Shigematsu H, Herz J, Minna JD. Mutations and addiction to EGFR: the Achilles 'heal' of lung cancers? Trends Mol Med 2004;10:481–6.
32. Fearon ER, Hamilton SR, Vogelstein B. Clonal analysis of human colorectal tumors. Science 1987;238:193–7.
33. Garcia SB, Novelli M, Wright NA. The clonal origin and clonal evolution of epithelial tumours. Int J Exp Pathol 2000;81:89–116.
34. Varella-Garcia M. Stratification of non-small cell lung cancer patients for therapy with epidermal growth factor receptor inhibitors: the EGFR fluorescence *in situ* hybridization assay. Diagn Pathol 2006;1:19.

Clinicopathologic Characteristics of the *EGFR* Gene Mutation in Non–small Cell Lung Cancer

*Anne S. Tsao, MD, * Xi Ming Tang, MD, PhD,* Bradley Sabloff, MD,† Lianchun Xiao, MS,‡ Hisayuki Shigematsu, MD,** Jack Roth, MD,§ Margaret Spitz, MD, MPH,‖ Waun Ki Hong, MD,* Adi Gazdar, MD,#** and Ignacio Wistuba, MD*¶*

Background: The authors sought to define clinicopathologic features associated with mutations of the epidermal growth factor receptor (*EGFR*) gene in non–small cell lung cancer (NSCLC).

Methods: The authors evaluated surgically resected NSCLC tumors for *EGFR* (exons 18–21) and *KRAS* (codons 12–13) mutations and immunohistochemistry (EGFR, phosphorylated-EGFR, and HER2/Neu), and correlated results with clinical outcome and patient and disease features. After their analysis on 159 patients was completed, they selected a second cohort of Asian patients ($n = 22$) and compared *EGFR* mutation results to place of birth and immigration to the United States.

Results: Of 159 patients, 14 had *EGFR* mutations and 18 had *KRAS* mutations. *EGFR* mutations were associated with adenocarcinoma ($p = 0.002$), female gender ($p = 0.02$), never-smoking ($p < 0.0001$), Asian ethnicity ($p = 0.005$), air bronchograms ($p = 0.004$), and multiple wedge resections ($p = 0.03$). Although statistical significance was not reached, a higher incidence of synchronous primary cancers (36% versus 17%; $p = 0.09$) and a smaller median tumor size (11.8 cm^3 versus 24.0 cm^3; $p = 0.24$) were seen. There was no difference in disease-free survival; however, median overall survival in patients with *EGFR* mutations was shorter (3.49 versus 4.29 years; $p = 0.85$). *EGFR* mutation did not correlate with immunohistochemistry. In the second cohort of 22 Asian patients, 12 (55%) had the mutation. Of interest, there was no geographic difference in incidence of *EGFR* mutation. Asian women with the *EGFR* mutation developed adenocarcinoma at an earlier age than other lung cancer patients.

Conclusion: There is a distinct clinical profile for NSCLC patients with the *EGFR* mutation. However, this mutation does not alter disease-free survival and is likely attributable to an inherited susceptibility instead of an environmental effect.

(*J Thorac Oncol.* 2006;1: 231–239)

The epidermal growth factor receptor (EGFR) has been the recent subject of great interest in lung cancer treatment. EGFR is overexpressed in 40 to 80% of non–small cell lung cancer (NSCLC) patients and regulates cell proliferation, cell survival, angiogenesis, and tumor metastasis.[1] Recently, critical mutations in the adenosine triphosphate pocket of the tyrosine kinase–binding region were reported in patients with NSCLC.[2,3] These mutations are suspected to cause constitutive activation of the receptor and confer susceptibility to EGFR tyrosine kinase inhibitors.[2] *EGFR* exons 18 through 21 encode for structures around the adenosine triphosphate–binding cleft within the tyrosine kinase domain.[2–5] This is the binding area for the EGFR tyrosine kinase small molecule inhibitors gefitinib and erlotinib.

Based on the prior studies (Iressa Dose Evaluation in Advanced Lung cancer) using EGFR tyrosine kinase inhibitors, approximately 9 to 12% of European patients and 18 to 19% of Asian patients with NSCLC experienced a tumor response to these agents.[6,7] Subpopulation analyses revealed that responders were more likely to be female and nonsmokers and to have adenocarcinoma with bronchioloalveolar features.[8] However, more specific predictors of response were unknown, as immunohistochemical studies of EGFR were not reliable in predicting response to therapy.[9] The discovery of *EGFR* mutations in the tyrosine kinase domain provides some insight into why only a small proportion of patients benefit from EGFR targeted therapy. We sought to further define the clinical, pathologic, and biological features associated with the *EGFR* mutation in lung cancer to determine the most likely population to benefit from screening for the mutation.

MATERIALS AND METHODS

Methodology and Case Selection

We evaluated *EGFR* and *KRAS* gene mutations in archived frozen and paraffin-embedded NSCLC tumor specimens obtained from patients who underwent resection at The University of Texas M. D. Anderson Cancer Center. This

*Departments of Thoracic/Head & Neck Medical Oncology, †Diagnostic Radiology, ‡Biostatistics and Applied Mathematics, §Thoracic and Cardiovascular Surgery, ‖Epidemiology, and ¶Pathology, The University of Texas M. D. Anderson Cancer Center, Houston; #Hamon Center for Therapeutic Oncology Research; and **Department of Pathology, The University of Texas Southwestern Medical Center, Dallas, Texas.

Address for correspondence: Ignacio I. Wistuba, MD, Department of Pathology, Unit 85, The University of Texas M. D. Anderson Cancer Center, 1515 Holcombe Blvd., Houston, TX 77030-4009; email: iiwistuba@mdanderson.org.

ISSN: 1556-0864/06/0103-0231

retrospective study was approved by our institutional review board. One hundred fifty-nine tumor specimens were selected from The University of Texas M. D. Anderson Cancer Center Lung Specialized Program of Research Excellence Tissue Bank based on equal numbers of squamous cell and adenocarcinoma histologies. Patients with medical histories of never- and long-term former smoking were also selected to increase the likelihood of locating tumors with the *EGFR* mutation. The *EGFR* and *KRAS* mutation data from this first cohort of 159 patients have been previously published as part of a larger series.[4]

We determined the association between the mutation analysis results with immunohistochemical expression of EGFR, phosphorylated EGFR (p-EGFR, Y1086), and HER2/Neu. In addition, all laboratory results were compared to detailed clinical and pathologic disease features and outcome. After the analysis on the first 159 patients was completed, we selected a second group of patients ($n = 22$) from our archived Lung Specialized Program of Research Excellence Tissue Bank based on Asian ethnicity to conduct the *EGFR* mutation analysis. In this Asian cohort, we determined the association between mutation status and focused clinical information regarding smoking history, place of birth, and time lived in the United States or Asian country.

Clinical Information Collection

Patient charts were reviewed and demographic data were collected, including age, gender, and ethnicity. We also collected patients' medical history, including an extensive history of previous cancers and cancer therapies. A breakdown of aerodigestive tract cancers compared with hematologic and other solid tumors was performed. Extensive family medical histories, including immediate family member cancer histories, were obtained. We also collected data on disease characteristics including pathologic confirmation of primary tumor sites, areas of clinical metastasis, histologic pattern (including extensiveness of the bronchioloalveolar component), level of aggressiveness (lymphatic or vascular invasion, extracapsular invasion, microscopic lymph node metastasis, and pleural invasion), and tumor size. Bronchioloalveolar carcinoma was defined using the 2004 World Health Organization classification for lung cancer[10] and characterized by the growth of neoplastic cells along preexisting alveolar structures without evidence of stromal, pleural, or vascular invasion and in the absence of metastasis. Both clinical and pathologic TNM staging data were obtained. Radiographic clinical information before surgery was collected, including chest computed tomographic location of tumor, presence of air bronchograms, quality of tumor margins (smooth or ill-defined), extension to pleura, amount of solid component to the tumor, presence of pseudocavitation, amount of pleural thickening, and degree of tumor spiculation. Data on induction therapies used and response were tabulated, as were type of surgical resection, adjuvant therapy, and response to adjuvant therapy. Information on postoperative complications was also collected and categorized into cardiovascular, pulmonary, gastrointestinal, neurologic, hematologic, or wound infection. The duration of both disease-free and overall survival from the time of diagnosis was evaluated.

EGFR and *KRAS* Mutation Analysis

For the gene mutation analyses, genomic DNA was obtained from frozen normal and primary lung tumor specimens by overnight digestion with sodium dodecyl sulfate and proteinase K digestion (Life Technologies, Inc., Rockville, MD) at 37°C, followed by standard phenol-chloroform (1:1) extraction and ethanol precipitation. *EGFR* mutation analysis of four tyrosine kinase domain exons (18–21), that are frequently mutated in lung cancer was performed using an intron-based polymerase chain reaction (PCR) as previously reported.[4] All PCRs were carried out in 25 μl of solution containing 100 ng of genomic DNA using HotStarTaq DNA polymerase (QIAGEN, Inc., Valencia, CA). DNA was amplified for 33 cycles at 95°C for 30 seconds, 65°C for 30 seconds, and 72°C for 45 seconds, followed by 7 minutes' extension at 72°C. The intron-based PCR primer sequences for exon 2 of KRAS were as previously published.[4] For the *KRAS* mutation analysis, DNA was amplified for 33 cycles at 95°C for 30 seconds, 55°C for 30 seconds, and 72°C for 30 seconds, followed by 7 minutes' extension at 72°C. All PCR products were incubated using exonuclease I and shrimp alkaline phosphatase (Amersham Biosciences, Inc., Piscataway, NJ) and sequenced directly using Applied Biosystems PRISM dye terminator cycle sequencing method (Perkin-Elmer Corp., Foster City, CA). All sequence variants were confirmed by independent PCR amplifications and sequenced in both directions.

Immunohistochemical Analysis

Immunohistochemical analyses were performed on formalin-fixed, paraffin-embedded specimens from surgically resected primary lung NSCLC. Tissue microarrays were prepared using 1-mm core sections in triplicate. Four-micron-thick histology sections from tissue microarrays were prepared for immunohistochemical analysis. Antibodies against the EGFR clone 31G7 (Zymed, catalog no. 36-9700), Her2/Neu (DAKO catalog no. A0485), and p-EGFR (Tyr 1086; Zymed catalog no. 36-9700) were used as the primary antibodies. Tissue slides were baked at 67°C for 30 minutes and deparaffinized in xylene, followed by graded alcohol and DI H_2O washes, and rehydrated in TBS-t buffer. Slides were placed in 10% DAKO Target Retrieval Solution 10× and then steamed for 30 minutes in a 10-mM sodium citrate bath (pH 6.0) at 95°C. The bath and slides were removed from the steamer and cooled for 30 minutes until the temperature reached 50°C. Endogenous peroxidase activity was then blocked by incubating the slides for 15 minutes in a 3% H_2O_2 solution and 50 μl of Tween-20. Nonspecific protein–protein interaction was blocked with the addition of 200 μl of 10% fetal bovine serum/protein block solution to each slide for 35 minutes. The primary antibody was then added (200 μl of 1:100 dilution with 10% fetal bovine serum/protein block solution), and slides were incubated at room temperature for 90 minutes. Slides were washed and placed in a TBS-t bath. DAKO Envision plus Dual-link labeled polymer was added directly to the slides, which were then incubated for 30

minutes. After the slides were washed, 200 μl of DAKO substrate buffer/DAB plus chromogen substrate was added to the slides, and the slides were incubated for 5 minutes at room temperature. Slides were immersed in H_2O to stop the reaction, counterstained in 1:3 diluted hematoxylin (DAKO catalog no. S3301) for 6 minutes, and rinsed in H_2O. Scott's Bluing reagent was applied for 1 minute, followed by graded alcohol washes and then xylene incubation for 4 minutes. Immunostaining of the cell membrane and cytoplasm for EGFR, p-EGFR, and Her2/Neu was evaluated by light microscopy using a 20× magnification objective. A semiquantitative approach was used to generate a score for each tissue core, as previously described.[11] The percentage of positive tumor and epithelial cells per focus (0–100%) was multiplied by the dominant intensity pattern of staining (1, negative or trace; 2, weak; 3, moderate; and 4, intense); therefore, the overall score ranged from 0 to 400. Antibody specificity was confirmed using blocking peptide and phosphatase incubation experiments. For controls, we used formalin-fixed and paraffin-embedded pellets from lung cancer cell lines with p-EGFR overexpression confirmed by Western blot analysis.

Statistical Analysis

Fisher's exact test or the chi-square test was used to evaluate the association between *EGFR* mutations and clinical, pathologic, and demographic features. Kaplan-Meier survival curves were estimated, and the log-rank test was applied to assess the differences in survival distributions by *EGFR* mutations and clinical and pathologic variables. The Cox proportional hazards model was modeled to estimate the effect of *EGFR* mutation, *KRAS* mutation, and other covariates on survival.

RESULTS

Clinicopathologic Associations

Of our first cohort of 159 patients, 14 had *EGFR* mutations and 18 had *KRAS* mutations. Patient and disease characteristics are summarized in Table 1. Eight *EGFR* mutations occurred in exon 19 (15- to 18-bp in-frame deletions), one occurred in exon 20 (exon 20 insertion), and five occurred in exon 21 (L858R point mutation). Table 2 provides details on the 14 patients with *EGFR* mutations. Fifteen *KRAS* mutations occurred in exon 12 and three occurred in exon 13. None of the patients had both *EGFR* and *KRAS* mutations. *EGFR* mutations were associated with adenocarcinoma histology ($p = 0.002$), female gender ($p = 0.02$), never-smoker status ($p < 0.0001$), and Asian ethnicity ($p = 0.005$). Four of 10 adenocarcinomas with a bronchioloalveolar component demonstrated *EGFR* mutations (range, 20–50%) (Figure 1 and Table 2), but none of the patients with pure bronchioloalveolar histology ($n = 7$) had an *EGFR* mutation. All *EGFR* mutated lung adenocarcinomas where mixed histologic subtype (World Health Organization Classification, 2004), with acinar predominant component in 11, papillary in one, and solid in two.

Patients with *EGFR* mutations were more likely to have undergone multiple wedge resections than were noncarriers (28.5% versus 7.5%; $p = 0.03$). No differences in any other type of surgical resection were found. This was supported by a trend toward having synchronous primary disease or lung metastases in patients with *EGFR* mutations (36% compared with 17% of those without the mutation; $p = 0.09$). Air bronchograms were the only significant radiographic findings associated with the *EGFR* mutations (22% versus 2%; $p = 0.004$), as depicted in Figure 2.

There were no differences between patients with *EGFR* mutations and those without in tumor location, tumor margin characteristics, amount of extension to pleura, pseudocavitation, amount of solid tumor component within the tumors, presence of spiculation, or amount of pleural thickening. Although statistically not significant, the median pathologic tumor size was smaller in patients with *EGFR* mutations (11.8 cm^3 versus 24.0 cm^3; $p = 0.24$). There was no association between *EGFR* mutation and age; clinical or pathologic TNM stage; complications of surgery; location of the primary tumor; pathologic features of tumor aggressiveness; or response to adjuvant or neoadjuvant therapy. *EGFR* mutations were not associated with family history of cancer, number of immediate family members with cancer, or personal history of cancer. Four of the patients with *EGFR* mutations had prior cancers: one breast ductal carcinoma in situ, one follicular lymphoma, one lung cancer, and one basal cell carcinoma of the skin.

We conducted a limited multivariate logistic regression analysis to determine the independent predictors for the *EGFR* mutation. This analysis determined that Asian ethnicity ($p = 0.0004$), never-smoking ($p = 0.0001$), and multiple wedges ($p = 0.004$) were the only features that predicted for the *EGFR* mutation. However, this reduced model was handicapped by the small number of patients analyzed.

Survival Analysis

The median overall survival duration in patients with *EGFR* mutations was shorter than that in patients without the mutation (3.49 years versus 4.29 years). However, this difference was not statistically significant ($p = 0.85$) and did not account for the effect of stage (Figure 3). After adjustment for stage, the presence of the *EGFR* mutations did not appear to affect survival duration, although the number of events was small (figures not shown). A Cox proportional hazard model showed that pathologic stage independently determined outcome in our population: a higher stage conferred a hazard ratio of 3.54 ($p < 0.0001$).

Selected Asian Population Analysis

As we found an association between the *EGFR* mutations and Asian ethnicity in our first patient cohort, we selected tissue samples from an additional second cohort of 22 Asian patients from the tissue bank for *EGFR* analysis. Twelve patients (55%) had the mutation (Table 3). Detailed information on patient ethnicity, place of birth, and length of time they had lived in the United States was known for 20 patients. Eleven of 12 patients with *EGFR* mutations were born in Far East Asian nations (three from China, four from Vietnam, one from the Philippines, and three from Korea). The one patient born in the United States was of Greek and Filipino descent. Six of these patients with the *EGFR* muta-

TABLE 1. Patient and Tumor Characteristics by *EGFR* Mutation Status

	Patients with *EGFR* Mutation Characteristics ($n = 14$)	Patients without *EGFR* Mutation ($n = 145$)	p Value
Age (yr)			
Mean	64	66	
Median	66	68	
Range	45–77	40–90	
Gender			
Female	11	63	0.02
Male	3	82	
Ethnicity			
African American	0	8	
Asian	3	1	0.005
White	10	129	
Hispanic	1	7	
Prior cancer history			
Yes	5	44	
No	9	101	
Smoking status			
Never	8	15	<0.0001
Current	0	49	
Former	6	81	
Histology			
Adenocarcinoma*	14	75	0.002
Bronchioloalveolar	0	7	
Squamous cell	0	63	
Pathologic stage			
I	11	80	
II	0	28	
III	3	30	
IV	0	7	
Synchronous primary or lung metastasis			
Present	6	25	
Absent	8	120	
Tumor size (cm^3)			
Median	11.8	24	
Range	5.1–1080	0.36–2178	
Overall survival (yr)			
Median	3.49	4.29	

*Includes 10 adenocarcinomas with bronchioloalveolar features, four with and six without the *EGFR* mutation.

tion had lived in the United States for more than 28 years, and the other six patients had lived most of their lives in Asian countries. Of the patients who did not have *EGFR* mutations, all were born in Far East Asian countries, and more than 50% had lived in the United States for more than 20 years (range, 21–44 years). Two patients had never lived in the United States. Data on length of time lived in the United States and Asia were missing for two patients. In patients who had lived in the United States for more than 20 years (range, 21–46 years; $n = 12$) and in patients who had lived in their home countries most of their lives ($n = 8$), the incidence of *EGFR* mutation was similar, six of 12 (50%) and six of eight (67%), respectively.

The median age at lung cancer diagnosis was 64 years (range, 36–84 years) for the entire Asian cohort, with equal numbers of men and women. The median age at diagnosis of patients with *EGFR* mutations was slightly lower than in those who did not have the mutation (58.6 versus 64 years). A subset analysis of patient age and gender (Table 4) showed that the median age of diagnosis of Asian women with *EGFR* mutations was lower than that of Asian men who have the mutations and Asian patients without mutations. However, this did not reach statistical significance because of the small number of patients involved in this study ($p = 0.4$).

Immunohistochemistry Analysis

Tumors with *EGFR* mutations did not overexpress cytoplasmic or membranous EGFR or p-EGFR (Y1086). Patients who had *EGFR* mutations were more likely to have low immunohistochemical expression of EGFR when com-

TABLE 2. Clinicopathologic Features of Patients with Lung Adenocarcinoma *EGFR* Mutants from the First Cohort

Patient Age and Gender	Ethnicity	Smoking History	Pack-Years	Prior Cancer	Stage	Site* of Tumor	BAC (%)	Air† Bronchogram	Multiple Lesions	Surgical Resection	Type of *EGFR* Mutation
72 F	White	Former	25	No	1B	LUL	50	INEV	No	Lobectomy	Exon 19/15-bp del (746-750)
66 F	White	Former	20	No	4	RLL	30	Yes	Yes	Lobectomy, multiple wedges	Exon 19/15-bp del (746-750)
68 F	White	Current	80	No	4	RUL	20	INEV	Yes	Multiple wedges	Exon 19/15-bp del (746-750)
58 F	White	Current	37.5	No	1A	LLL	20	No	Yes	Lobectomy	Exon 19/15-bp del (746-750)
66 F	White	Never	0	No	1B	RUL	0	INEV	No	Lobectomy	Exon 19/18-bp del (746-751) and S752V
64 M	White	Never	0	No	1A	RLL	0	Yes	Yes	Lobectomy, multiple wedges	Exon 19/15-bp del (746-750)
65 M	Asian	Former	0.8	Yes	2B	RML, RLL	0	No	Yes	Bilobectomy	Exon 19/18-bp del (746-751) and S752I
70 F	White	Never	0	Yes	3A	LLL	0	Yes	No	Lobectomy	Exon 19/15-bp del (746-750)
55 F	White	Never	0	No	2B	RML	0	INEV	No	Lobectomy	Exon 20
70 F	White	Never	0	Yes	1A	LUL	0	INEV	No	Lobectomy	Exon 21/L858R
69 M	Asian	Former	42	No	3A	RUL	0	INEV	No	Lobectomy	Exon 21/L858R
52 F	Hispanic	Never	0	No	4	RUL	0	No	No	Lobectomy, multiple wedges	Exon 21/L858R
65 F	White	Never	0	Yes	1A	RUL	0	Yes	Yes	Lobectomy	Exon 21/L858R
45 F	Asian	Never	0	No	1A	LUL	0	INEV	No	Lobectomy	Exon 21/L858R

*Site of primary lung tumor location. †Presence of air bronchograms on radiographic imaging. F, female; M, male; RUL, right upper lobe; RML, right middle lobe; RLL, right lower lobe; LUL, left upper lobe; LLL, left lower lobe; Yes, present; No, not present; INEV, not assessable because of a lack of adequate radiographic imaging; bp, base pair.

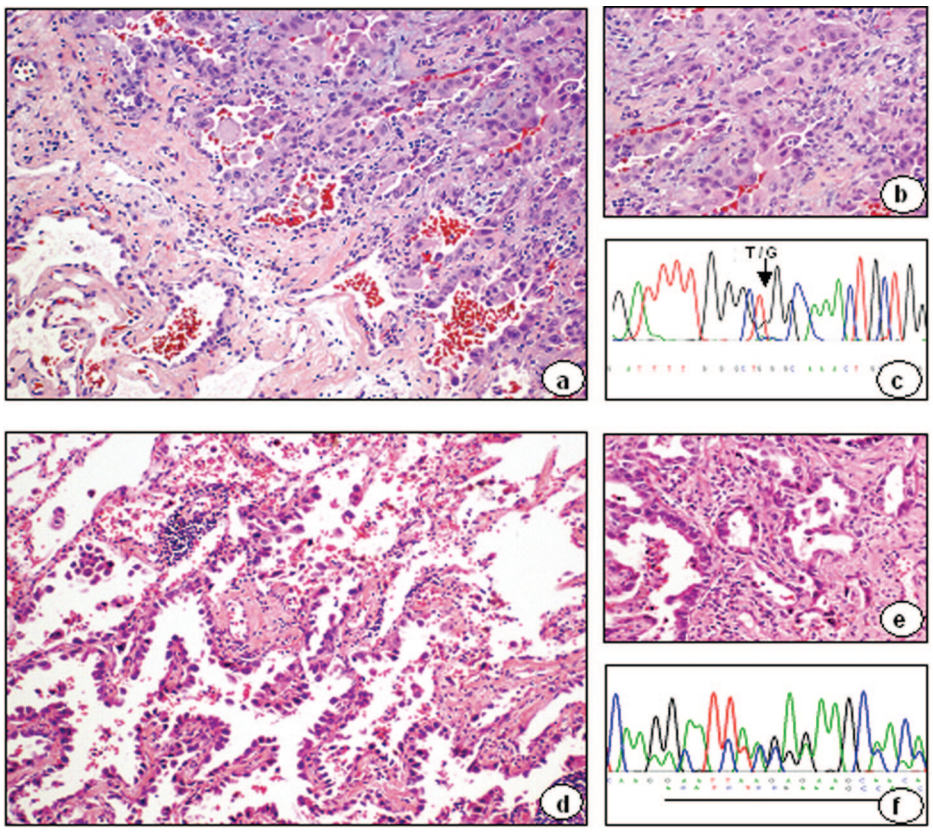

FIGURE 1. Microphotographs of two representative lung adenocarcinomas with *EGFR* mutations (hematoxylin and eosin stained). Panels *a* (100×) and *b* (200×) are from a lung adenocarcinoma with a point mutation L858R (T to G) in exon 21 (*c*) and with invasive acinar and solid patterns (*a* and *b*), and without any bronchioloalveolar component in the periphery. Panels *d* (100×) and *e* (200×) were obtained from a lung adenocarcinoma having a 15–base pair (746-750) in-frame deletion mutation in exon 19 (*f*), and with a predominant invasive acinar component (*e*) and some areas of bronchioloalveolar-like pattern (<20%) in the periphery (*d*).

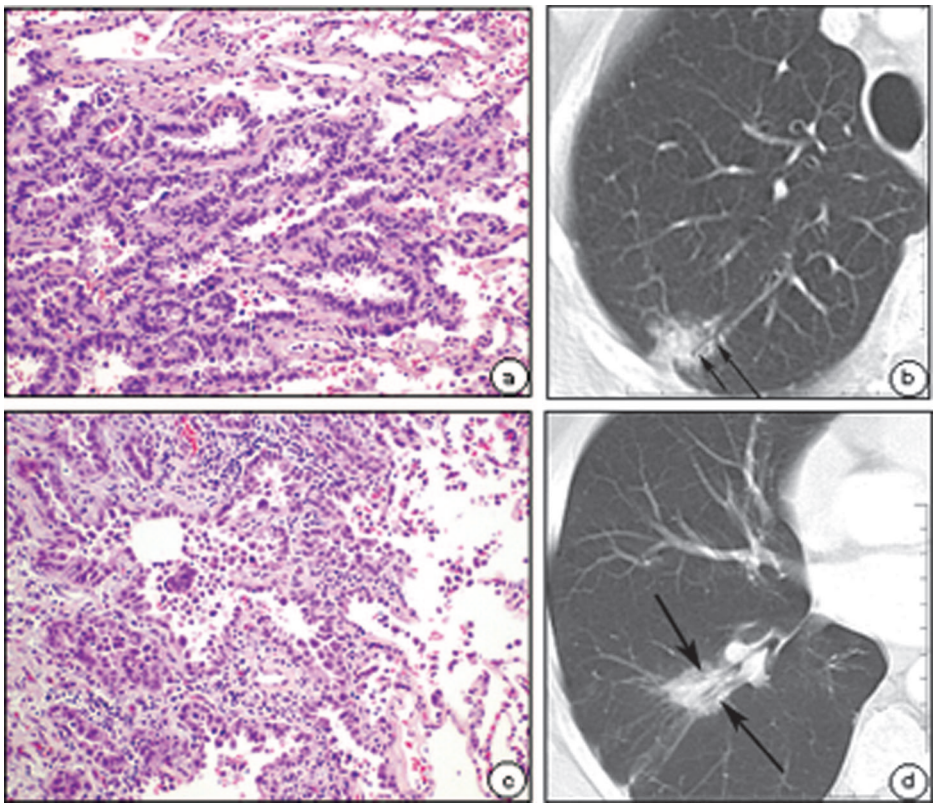

FIGURE 2. Two lung tumor cases with *EGFR* mutations showing invasive adenocarcinoma histologic features (mostly acinar pattern, *a* and *c*) and corresponding chest computed tomographic images (*b* and *f*). Computed tomographic scans (*b* and *d*) show two cases of NSCLC, (*b*) right upper lobe, (*d*) right lower lobe, manifesting as ill-defined nodules. Note air bronchograms, which correlate with *EGFR* mutation status (*black arrows*).

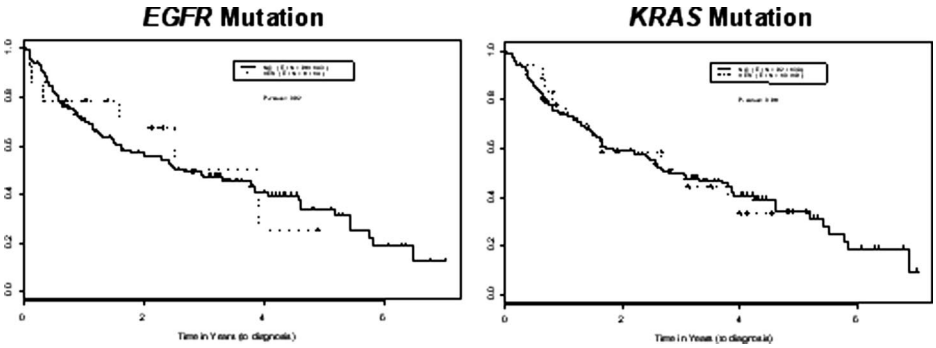

FIGURE 3. Survival by presence of *EGFR* and *KRAS* mutations.

pared with patients who did not have *EGFR* mutations (77% versus 35%; $p = 0.02$). However, there was no difference between the two groups in level of phosphorylated EGFR expression in both the cytoplasm and membrane. There was also no association between *EGFR* mutations and the presence or level of HER2/Neu expression.

DISCUSSION

Prior clinical studies on *EGFR* mutations in NSCLC report a higher frequency in women with adenocarcinoma, Asian patients, and nonsmokers.[2–5,8,12] Although our retrospective analysis was limited by small sample sizes and availability of patient medical records, we were able to confirm the clinical findings of earlier studies and also expand the clinical profile of patients likely to harbor *EGFR* mutations. In our study, tumors with these mutations were more likely to be associated with air bronchograms but no other distinguishing radiographic features. This finding should be considered with caution, as there are so few patients evaluated. Although the differences were not statistically significant, tumors with the *EGFR* mutation were smaller in volume and were more likely to metastasize to the lung or present as synchronous tumors. Patients with *EGFR* mutations did not have more previous malignancies, indicating that these mutations arise de novo in the majority of cases. Also, the lack of family history of cancer suggests that a germ-line predisposition to acquiring these mutations is not present.

Our second cohort of Asian patients was limited in number ($n = 22$) and by the nature of a retrospective analysis. However, two important observations are seen from this

TABLE 3. Patient Demographics of the Asian Cohort

Patient Age and Gender	Ethnicity	Place of Birth	Number of Years Lived in the United States	Smoking Status	Type of *EGFR* Mutation
63 F	Filipino	Philippines	32	Never	None
43 F	Filipino	Philippines	35	Never	None
65 M	Filipino	Philippines	35	Current	None
64 M	Filipino	Philippines	>32	Current	None
70 F	Japanese	Japan	44	Former	None
84 M	Chinese	China	21	Former	None
57 M	Chinese	China	28	Former	Exon 19/18-bp del (747-752) and P753Q
68 M	Chinese	China	31	Former	Exon 19/15-bp del (747-751)
36 F	Vietnamese	Vietnam	30	Never	Exon 19/15-bp del (746-750)
52 M	Vietnamese	Vietnam	33	Former	Exon 19/15-bp del (746-750)
65 M	Korean	Korea	39	Former	Exon 19/18-bp del (746-751)
46 F	Filipino/Greek	United States	46	Never	Exon 21/L858R
64 M	Filipino	Philippines	Unknown	Current	None
63 M	Taiwan	Taiwan	Unknown	Unknown	None
68 F	Korean	Korea	0	Never	None
62 F	Korean	Korea	0	Never	None
66 F	Vietnamese	Vietnam	0	Unknown	Exon 19/15-bp del (746-750)
74 M	Vietnamese	Vietnam	Lived mostly in Vietnam	Current	Exon 19/15-bp del (746-750)
72 F	Chinese	China	Lived mostly in China	Never	Exon 21/L858R
49 F	Korean	Korea	0	Never	Exon 21/L858R
49 F	Korean	Korea	0	Never	Exon 21/L858R
69 M	Filipino	Philippines	0	Former	Exon 21/L858R

M, male; F, female; bp, base pair.

study. First, our analysis showed a similar incidence of *EGFR* mutations in Asian patients who had lived in the United States for more than 20 years (50%) as compared with patients living in Asian countries most of their lives (67%). This finding suggests that the development of a mutation in the *EGFR* gene is not related to the environment but is instead dependent on a strong genetic predisposition. This concept is supported by the differences in the length of the *EGFR* intron 1 polymorphic CA dinucleotide repeat (CA-SSR 1) between Japanese and Chinese and white and African American populations.[13] In Asian patients, the repeat lengths are considerably longer than are those found in white and African American patients. It is of interest that the length of repeat sequences influences *EGFR* gene expression, with longer lengths leading to less gene transcription.[14] The effect that these and other genetic polymorphisms have on the rate of mutation in the *EGFR* gene is unknown and provides a strong rationale for conducting further molecular epidemiologic studies.

Second, we report a younger median age of developing lung cancer in Asian women with the *EGFR* mutation (Table 4). This result should be viewed with caution because of the very small sample size and the lack of statistical significance. However, this observation is important, as it suggests that the estrogen pathway (patients were in the premenopausal age group) may play a critical role in the early onset of carcinogenesis in Asian patients with *EGFR* gene mutations. We did not see this wide age difference between the genders in our first cohort of predominantly white patients, but it is interesting that the one Asian woman in that first cohort was 45 years old. There may also be some variation in the effect of gender among the Asian ethnicities. A previous report by a Japanese group[15] noted no difference in age between the women with *EGFR* mutations and other male patients. Our cohort did not include any Japanese female patients, but instead consisted of women of Chinese, Vietnamese, Filipino, and Korean ethnicities. A recent report by a group from Taiwan evaluated 39 Chinese patients with *EGFR* mutations[16] and found that the median age in women was 62 years compared with 68 years in men.

TABLE 4. Age Analysis of the Asian Cohort of Patients with and without *EGFR* Mutations

Gender/Age	Positive *EGFR* Mutation	Negative *EGFR* Mutation
Female	$n = 6$*	$n = 5$
Median (yr)	49	63
Mean (yr)	53	61
Range (yr)	36–72	43–70
Male	$n = 6$	$n = 5$
Median (yr)	66.5	64
Mean (yr)	64	68
Range (yr)	52–74	63–84

*$p = 0.4$.

Although our findings of Asian women with the *EGFR* mutation developing NSCLC at an earlier age are preliminary, there is compelling evidence to consider the role of estrogen as a carcinogenic promoter in these patients. First, it is well known that female gender is an independent risk factor for the development of NSCLC and that premenopausal women present with more aggressive disease.[17–21] Second, estrogens may act as tumor promoters or direct carcinogens with DNA adduct formation.[22–27] Third, Stabile et al. reported a functional interaction between the estrogen receptor and the EGFR pathways in NSCLC.[22,28] This study also found synergistic antitumor effects with fulvestrant (an estrogen receptor antagonist) and gefitinib (an EGFR tyrosine kinase inhibitor) in murine xenografts and NSCLC cell lines. Although this analysis did include a cell line with an *EGFR* mutation (273T heterozygous point mutation at exon 18 nucleotide 2180), conclusions on the effect of estrogen cannot be drawn, as it is not one of the typical mutations found in patients with NSCLC. The role of gender on *EGFR* mutation is unclear at this time but should be explored further.

In our laboratory analysis, we found low immunohistochemical expression of both EGFR and phosphorylated EGFR at site Y1086 in tumors of patients with *EGFR* mutations. This apparently conflicts with the premise that the mutations in the EGFR tyrosine kinase domain are activating mutations (L747-P753insS, L858R) with higher phosphorylation capability.[2] Our study is not the first to report this difference. Pao et al.[5] conducted functional studies on receptor mutations in exon 19 (del L747-S752, del E746-A750) and reported low kinase activity. This was seen with both low autophosphorylation Y1092 (p-EGFR) and low tyrosine-phosphorylated proteins when compared with wild-type EGFR assays. It is therefore possible that the mechanism of EGFR tyrosine kinase inhibitor sensitivity does not occur by means of intrinsic enhanced receptor tyrosine kinase activity but may be caused by altered receptor-substrate–binding capability. It is also plausible that de novo mutations in the *EGFR* gene may lead to variable protein expression with some dominant activating mutations and others that affect substrate binding. In support of this premise, there are at least seven different phosphorylation sites for EGFR, and the distinct mutations appear to have preferential phosphorylation patterns. The L858R mutation is associated with phosphorylation at sites Y845 and Y1092, whereas phosphorylation of sites Y992 and Y1068 is associated with both the L858R mutation and deletion of exon 19.[2,5,29] Phosphorylation at sites Y1173 and Y1045 do not appear to be associated with either mutation.[29] The lack of association found in our study between p-EGFR and *EGFR* mutation could be explained by the fact that our analysis focused solely on the Y1086 phosphorylation site. We plan to further document the preferential phosphorylation patterns of the distinct *EGFR* mutations. Further molecular studies to clarify the biology of these mutations is necessary to understand the efficacy of tyrosine kinase inhibitor treatment and development of tumor resistance.

CONCLUSION

In conclusion, our analysis reports the following characteristics to be associated with the *EGFR* mutation: female gender, Asian ethnicity, adenocarcinoma histology, never-smoker status, presence of multiple lung lesions, and air bronchograms on imaging. In our Asian cohort, the results suggest an inherent and nonenvironmental susceptibility to development of *EGFR* mutations. There is also some speculation that Asian women with *EGFR* mutations may develop adenocarcinoma at an earlier age than other patients. Further studies on the interaction of estrogen with the *EGFR* pathway are warranted, and continued efforts to define the mechanism of tyrosine kinase inhibitor sensitivity are needed to optimize cancer therapy.

ACKNOWLEDGMENTS

Supported by Department of Defense grant W81XWH-04-1-0142 and by grant 5U01CA8497102 from the Specialized Program of Research Excellence in Lung Cancer P50CA70907, National Cancer Institute. We thank Natalie Ozburn and Xiaoquin (Rachel) Bi for technical assistance.

REFERENCES

1. Mendelsohn J, Baselga J. The EGF receptor family as targets for cancer therapy. *Oncogene* 2000;19:6550–6565.
2. Lynch TJ, Bell DW, Sordella R, et al. Activating mutations in the epidermal growth factor receptor underlying responsiveness of non-small-cell lung cancer to gefitinib. *N Engl J Med* 2004;350:2129–2139.
3. Paez JG, Janne PA, Lee JC, et al. EGFR mutations in lung cancer: correlation with clinical response to gefitinib therapy. *Science* 2004;304: 1497–1500.
4. Shigematsu H, Lin L, Takahashi M, et al. Clinical and biological features of epidermal growth factor receptor mutations in lung cancers. *J Natl Cancer Inst* 2006;97:339–346.
5. Pao W, Miller V, Zakowski M, et al. EGF receptor gene mutations are common in lung cancers from "never smokers" and are associated with sensitivity of tumors to gefitinib and erlotinib. *Proc Natl Acad Sci USA* 2004;101:13306–13311.
6. Fukuoka M, Yano S, Giaccone G, et al. Multi-institutional randomized phase II trial of gefitinib for previously treated patients with advanced non-small-cell lung cancer (the IDEAL 1 trial). *J Clin Oncol* 2003;21: 2237–2246.
7. Kris MG, Natale RB, Herbst RS, et al. Efficacy of gefitinib, an inhibitor of the epidermal growth factor receptor tyrosine kinase, in symptomatic patients with non-small cell lung cancer: a randomized trial. *JAMA* 2003;290:2149–2158.
8. Miller VA, Kris MG, Shah N, et al. Bronchioloalveolar pathologic subtype and smoking history predict sensitivity to gefitinib in advanced non-small-cell lung cancer. *J Clin Oncol* 2004;22:1103–1109.
9. Bailey R, Kris MG, Wolf MK, et al. Gefitinib ("Iressa," ZD1839) monotherapy for pretreated advanced non-small cell lung cancer in IDEAL 1 and 2: tumor response is not clinically relevantly predictable from tumor EGFR membrane staining alone (Abstract O/242). *Lung Cancer* 2003:41(Suppl 2):71s.
10. Travis W, Brambilla E, Muller-Hermelink H, et al. Tumours of the lung. In World Health Organization Classification of Tumours. Lyon: IARC Press, 2004.
11. Hirsch FR, Varella-Garcia M, Bunn PA Jr, et al. Epidermal growth factor receptor in non-small-cell lung carcinomas: correlation between gene copy number and protein expression and impact on prognosis. *J Clin Oncol* 2003;21:3798–3807.
12. Kris MG, Sandler A, Miller VA, et al. EGFR and Kras mutations in patients with bronchioloalveolar carcinoma treated with erlotinib in a phase II multicenter study (Abstract 7029). In: *Proceedings of the American Society of Clinical Oncology* 2005.
13. Tidow N, Boecker A, Schmidt H, et al. Distinct amplification of an

untranslated regulatory sequence in the egfr gene contributes to early steps in breast cancer development. *Cancer Res* 2003;63:1172–1178.
14. Gebhardt F, Zanker KS, Brandt B. Modulation of epidermal growth factor receptor gene transcription by a polymorphic dinucleotide repeat in intron 1. *J Biol Chem* 1999;274:13176–13180.
15. Kosaka T, Yatabe Y, Endoh H, Kuwano H, Takahashi T, Mitsudomi T. Mutations of the epidermal growth factor receptor gene in lung cancer: biological and clinical implications. *Cancer Res* 2004;64:8919–8923.
16. Huang SF, Liu HP, Li LH, et al. High frequency of epidermal growth factor receptor mutations with complex patterns in non-small cell lung cancers related to gefitinib responsiveness in Taiwan. *Clin Cancer Res* 2004;10:8195–8203.
17. Zang EA, Wynder EL. Differences in lung cancer risk between men and women: examination of the evidence. *J Natl Cancer Inst* 1996; 88:183–192.
18. Gasperino J, Rom WN. Gender and lung cancer. *Clin Lung Cancer* 2004;5:353–359.
19. Patel JD, Bach PB, Kris MG. Lung cancer in US women: a contemporary epidemic. *JAMA* 2004;291:1763–1768.
20. Taioli E, Wynder EL. Re: Endocrine factors and adenocarcinoma of the lung in women. *J Natl Cancer Inst* 1994;86:869–870.
21. Moore KA, Mery CM, Jaklitsch MT, et al. Menopausal effects on presentation, treatment, and survival of women with non-small cell lung cancer. *Ann Thorac Surg* 2003;76:1789–1795.
22. Siegfried JM. Women and lung cancer: does oestrogen play a role? *Lancet Oncol* 2001;2:506–513.
23. Cheng YW, Hsieh LL, Lin PP, et al. Gender difference in DNA adduct levels among nonsmoking lung cancer patients. *Environ Mol Mutagen* 2001;37:304–310.
24. Toyooka S, Tsuda T, Gazdar AF. The TP53 gene, tobacco exposure, and lung cancer. *Hum Mutat* 2003;21:229–239.
25. Shriver SP, Bourdeau HA, Gubish CT, et al. Sex-specific expression of gastrin-releasing peptide receptor: relationship to smoking history and risk of lung cancer. *J Natl Cancer Inst* 2000;92:24–33.
26. Omoto Y, Kobayashi Y, Nishida K, et al. Expression, function, and clinical implications of the estrogen receptor beta in human lung cancers. *Biochem Biophys Res Commun* 2001;285:340–347.
27. Stabile LP, Davis AL, Gubish CT, et al. Human non-small cell lung tumors and cells derived from normal lung express both estrogen receptor alpha and beta and show biological responses to estrogen. *Cancer Res* 2002;62:2141–2150.
28. Stabile LP, Lyker JS, Gubish CT, Zhang W, Grandis JR, Siegfried JM. Combined targeting of the estrogen receptor and the epidermal growth factor receptor in non-small cell lung cancer shows enhanced antiproliferative effects. *Cancer Res* 2006;65:1459–1470.
29. Sordella R, Bell DW, Haber DA, Settleman J. Gefitinib-sensitizing EGFR mutations in lung cancer activate anti-apoptotic pathways. *Science* 2004;305:1163–1167.

DOI:10.1158/0008-5472.CAN-07-0217

Cancer Research

EGFR-T790M Is a Rare Lung Cancer Susceptibility Allele with Enhanced Kinase Activity

Haris Vikis, Mitsuo Sato, Michael James, et al.

Cancer Res 2007;67:4665-4670. Published online May 17, 2007.

DOI:10.1158/0008-5472.CAN-07-0217

EGFR-T790M Is a Rare Lung Cancer Susceptibility Allele with Enhanced Kinase Activity

Haris Vikis,[1] Mitsuo Sato,[2] Michael James,[1] Daolong Wang,[1] Yian Wang,[1] Min Wang,[1] Dongmei Jia,[1] Yan Liu,[1] Joan E. Bailey-Wilson,[3] Christopher I. Amos,[4] Susan M. Pinney,[5] Gloria M. Petersen,[6] Mariza de Andrade,[6] Ping Yang,[6] Jonathan S. Wiest,[7] Pamela R. Fain,[8] Ann G. Schwartz,[9] Adi Gazdar,[2] Colette Gaba,[10] Henry Rothschild,[11] Diptasri Mandal,[11] Elena Kupert,[5] Daniela Seminara,[7] Avinash Viswanathan,[1] Ramaswamy Govindan,[1] John Minna,[2] Marshall W. Anderson,[5] and Ming You[1]

[1]Washington University, St. Louis, Missouri; [2]University of Texas Southwestern Medical Center, Dallas, Texas; [3]National Human Genome Research Institute, Bethesda, Maryland; [4]M. D. Anderson Cancer Center, Houston, Texas; [5]University of Cincinnati, Cincinnati, Ohio; [6]Mayo Clinic College of Medicine, Rochester, Minnesota; [7]National Cancer Institute, Rockville, Maryland; [8]University of Colorado, Denver, Colorado; [9]Karmanos Cancer Institute, Detroit, Michigan; [10]Medical University of Ohio, Toledo, Ohio; and [11]Louisiana State University Health Science Center, New Orleans, Louisiana

Abstract

The use of tyrosine kinase inhibitors (TKI) has yielded great success in treatment of lung adenocarcinomas. However, patients who develop resistance to TKI treatment often acquire a somatic resistance mutation (T790M) located in the catalytic cleft of the epidermal growth factor receptor (EGFR) enzyme. Recently, a report describing EGFR-T790M as a germ-line mutation suggested that this mutation may be associated with inherited susceptibility to lung cancer. Contrary to previous reports, our analysis indicates that the T790M mutation confers increased Y992 and Y1068 phosphorylation levels. In a human bronchial epithelial cell line, overexpression of EGFR-T790M displayed a growth advantage over wild-type (WT) EGFR. We also screened 237 lung cancer family probands, in addition to 45 bronchoalveolar tumors, and found that none of them contained the EGFR-T790M mutation. Our observations show that EGFR-T790M provides a proliferative advantage with respect to WT EGFR and suggest that the enhanced kinase activity of this mutant is the basis for rare cases of inherited susceptibility to lung cancer. [Cancer Res 2007;67(10):4665–70]

Introduction

Recent work has identified a series of somatic mutations in exons 18 to 21 of epidermal growth factor (EGF) receptor (*EGFR*) that render lung tumors responsive to the gefitinib and erlotinib therapeutics (1–3). However, in patients that progress after drug treatment, it has been observed that a secondary "resistance" mutation is often acquired in exon 20 (4–6). This mutation, T790M, arises somatically in ~50% of these cases (4–6). In chronic myelogenous leukemia (CML) patients, an estimated 50% to 90% of tumors with acquired resistance have the analogous resistance mutation (T315I) in BCR-ABL (7). Interestingly, Bell et al. (8) report the first identification of the T790M mutation in the germ line of a European family that developed lung adenocarcinoma with bronchoalveolar (BAC) differentiation. This observation suggests that this mutation may be associated with genetic susceptibility to lung cancer and may underlie familial predisposition to the disease. The allele, although common in drug-treated tumors, seems extremely rare in the germ line of the general population, as the authors report no mutation observed in 782 alleles sequenced. Many groups have reported that the kinase activity of the EGFR-T790M–resistant mutant is indistinguishable from wild-type (WT) EGFR (4–6, 9, 10). What is somewhat perplexing is how T790M would confer susceptibility if its activity were identical to the WT molecule. Our analysis shows that T790M in fact does exhibit enhanced autophosphorylation at Y992 and Y1068, and this mutation is associated with a proliferative advantage in a human bronchial epithelial cell line. Interestingly, the mutation seems to be rare as it was not found in any of the familial or sporadic lung cancer populations we screened.

Materials and Methods

Cell lines. HEK293T, HEK293FT, and COS-7 cells were maintained in DMEM supplemented with 10% fetal bovine serum. Immortalized human bronchial epithelial cells (HBEC3-KT) were maintained in keratinocyte serum-free medium (with 50 μg/mL bovine pituitary extract and 5 ng/mL EGF). All cells were grown at 37°C in a humidified incubator with 5% CO_2.

Plasmids, transfection, and viral infection. Mammalian expression plasmids encoding for human EGFR, EGFR-T790M, and EGFR-L858R were kind gifts from William Pao (Memorial Sloan-Kettering Cancer Center, New York, NY). HEK293T and COS-7 cells were transfected with the indicated EGFR plasmids using LipofectAMINE 2000 (Invitrogen). Gefitinib was obtained from Chemoprevention Branch, National Cancer Institute (Bethesda, MD) and added to cells 10 h before lysis.

To introduce WT and mutant EGFRs into HBEC3 cells, we used the pLenti6/V5 Directional TOPO Cloning kit (Invitrogen). Construction of pLenti-wt-EGFR was described previously (11). The T790M and L747_E749 deletion mutations were introduced into pLenti-wt-EGFR by using site-directed mutagenesis (Stratagene). pLenti-KRASV12 vector was constructed by cloning KRASV12 fragment from pBabe-KRASV12-hyg (11) into pLenti6/V5 vector. pLenti6/V5-GW/*lacZ* (Invitrogen) was used as a control. Viral transduction of HBEC3 cells was done following the manufacturer's instructions. Briefly, the 293FT cells were transiently transfected with viral vector together with ViraPower (Invitrogen). Forty-eight hours after transfection, the supernatant of the 293FT cells was harvested and passed through a 0.45-μm filter and frozen at −80°C. The supernatant was used for infection after addition of 4 μg/mL polybrene (Sigma). Forty-eight hours after infection, drug selection of infected cells was started with 5 μg/mL blasticidin (Invitrogen) and continued for 7 days.

Note: H. Vikis, M. Sato, M. James, and D. Wang contributed equally to this work.

Requests for reprints: Ming You, Department of Surgery and The Alvin J. Siteman Cancer Center, Washington University, 660 Euclid Avenue, Box 8109, St. Louis, MO 63110. Phone: 314-362-9294; Fax: 314-362-9366; E-mail: youm@wustl.edu.

doi:10.1158/0008-5472.CAN-07-0217

DOI:10.1158/0008-5472.CAN-07-0217

Colony formation assays. Liquid colony formation assays were done as described previously (11). Briefly, 200 viable cells were plated in triplicate on 100-mm plates and cultured in keratinocyte serum-free medium supplemented with 50 μg/mL of bovine pituitary extract without EGF. Surviving colonies were counted 10 days later after staining with methylene blue, and colonies >3 mm in diameter were counted.

Western blot and antibodies. Cell lysates were prepared in LDS sample buffer (Invitrogen) and electrophoresed on NuPAGE gels (Invitrogen). Protein was transferred to polyvinylidene difluoride membranes and blotted using the antibodies as indicated: anti-EGFR (Cell Signaling Technology), anti–EGFR-Y1068 (Cell Signaling Technology), anti–EGFR-Y992 (Cell Signaling Technology), anti–mitogen-activated protein kinase (MAPK; Cell Signaling Technology), anti–phosphorylated MAPK (Thr^{202}/Tyr^{204}; Cell Signaling Technology), anti–phosphorylated AKT (Ser^{473}; Cell Signaling Technology), anti-AKT (Cell Signaling Technology), anti–α-tubulin (Santa Cruz Biotechnology), and anti–cyclin D1 (Santa Cruz Biotechnology).

***EGFR* exon 20 genotyping.** Amplification of human EGFR exon 20 was done via standard PCR methods using forward (5′-GACACTGACGTGCCTCTCC-3′) and reverse (5′-TTATCTCCCCTCCCCGTATC-3′) primers. PCR products were electrophoresed on agarose gels, purified, and subjected to standard DNA sequencing. The EGFR-T790M mutation is deduced by the genotype (C/T) at position 86 in exon 20.

Lung cancer DNAs. The Genetic Epidemiology of Lung Cancer Consortium (GELCC) has accrued over 700 families with three or more first-degree relatives with lung cancer (12), of which this study genotyped 237 individual probands. Paraffin blocks of lung tumors (45) with BAC differentiation (and 32 corresponding normals), in addition to the fresh frozen lung tumor DNAs, were obtained from the Washington University Tissue Procurement Center as paraffin blocks. For the blocks, genomic DNA was prepared by slicing several paraffin curls and adding xylenes to dissolve the paraffin. The remaining tissue was washed with ethanol, dried, and resuspended in PCR buffer (0.5% Tween 20, 0.5% NP40) and digested in proteinase K (1 mg/mL) at 55°C overnight. Chloroform/isoamyl alcohol (24:1) was added to the digest and soluble DNA was isolated from the aqueous phase.

Results

To address previous observations that EGFR-T790M activity is the same as the WT molecule, we did transient transfections of EGFR and EGFR-T790M expression constructs in COS-7 and 293T cells. Overexpression of EGFR and the T790M mutant in these cell lines clearly indicated that the phosphorylation status at Y1068 is enhanced with respect to WT (Fig. 1*A–E*). Tyr^{1068} is an EGFR autophosphorylation site that couples receptor activation to Ras signaling (13). Interestingly, our observations are in disagreement with previously published reports (4–6, 9, 10). Our data also show that phosphorylation levels between WT and T790M are indistinguishable at higher expression levels (Fig. 1*C*), yet differences are more apparent at lower expression levels. As a control, we also showed the drug-resistant nature of EGFR-T790M in comparison with WT EGFR (Fig. 1*D*). We further addressed the activation status of MAPK, a downstream molecule phosphorylated and activated by EGFR. We observed that phosphorylated MAPK

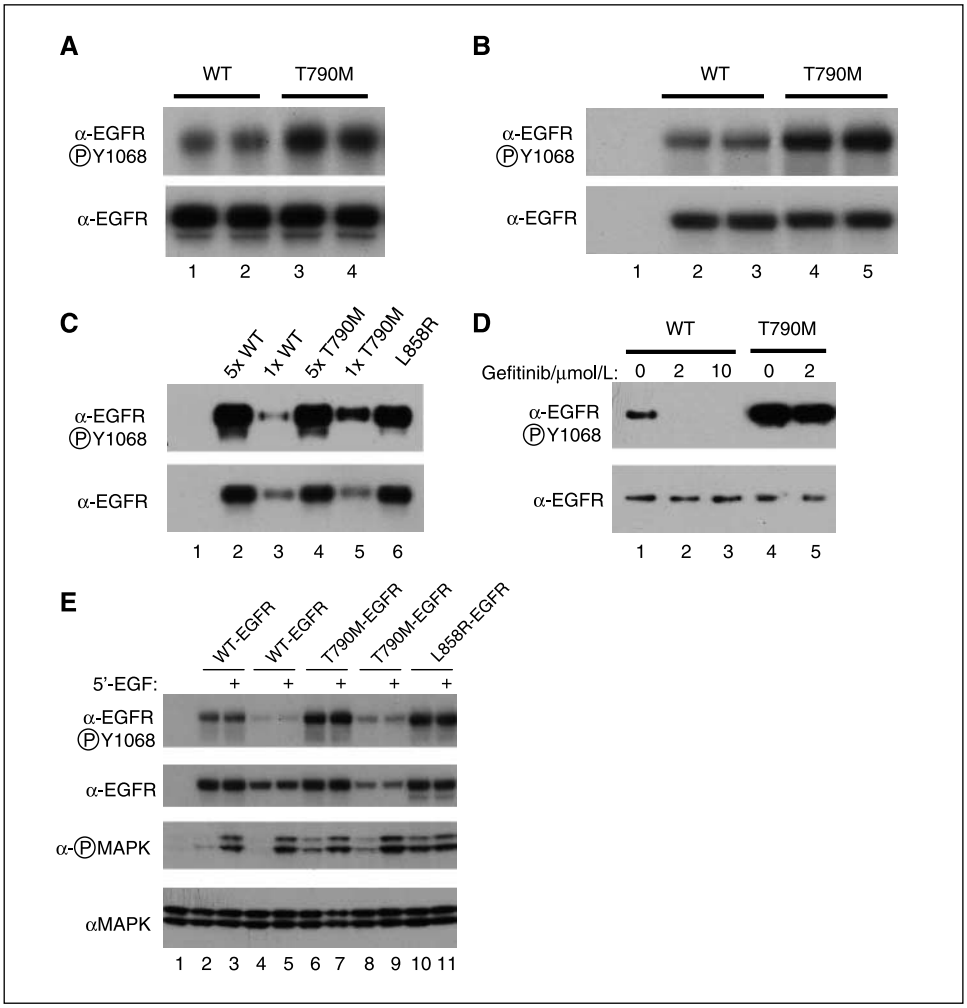

Figure 1. Phosphorylation of Y1068 is enhanced in EGFR-T790M. HEK293 cells (*A*) and COS-7 cells (*B*) were transfected with the indicated DNAs and lysed 48 h after transfection. Lysates were immunoblotted with anti-EGFR and anti–EGFR-Y1068 as indicated. Phosphorylation of Y1068 is enhanced in the EGFR-T790M mutant. *C,* phosphorylation and activation of EGFR-T790M are evident at lower levels of protein expression compared with higher levels in COS-7 cells (*lane 3* versus *lane 5*). *D,* gefitinib does not affect the phosphorylation status of T790M-EGFR. *E,* phosphorylation of MAPK is enhanced in EGFR-T790M–expressing (versus EGFR-WT expressing) cells. Cells were stimulated with EGF (10 ng/mL) for 5 min.

DOI:10.1158/0008-5472.CAN-07-0217

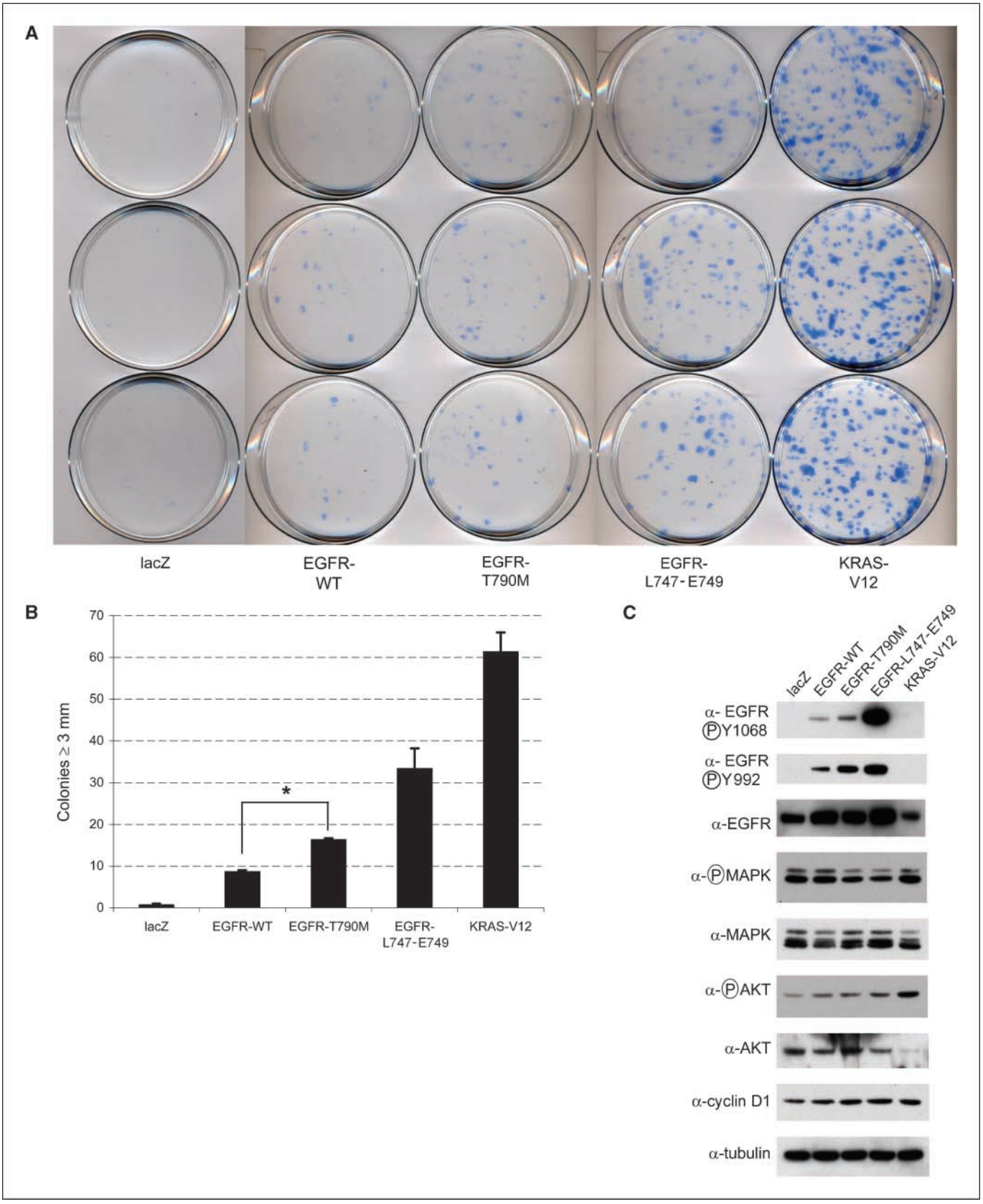

Figure 2. Colony formation growth assay for EGFR-T790M. Viral transduction and selection of HBEC cells stably expressing EGFR were done as described previously (11). *A,* cells (200) were plated in triplicate and grown in keratinocyte serum-free medium (with 50 μg/mL bovine pituitary extract and without EGF). After 10 d, cells were stained with methylene blue. *B,* stained cell colonies >3 mm in diameter were counted. *, $P < 0.0001$, two-tailed *t* test. *C,* Western blots for EGFR, EGFR-Y1068, EGFR-Y992, MAPK, MAPK (T202/Y204), AKT, AKT (S473), cyclin D1, and α-tubulin in the HBEC stable cell lines were done as indicated.

DOI:10.1158/0008-5472.CAN-07-0217

(Thr^{202}/Tyr^{204}) levels were enhanced in the T790M mutant compared with WT EGFR (Fig. 1*E*).

We also tested whether EGFR-T790M expression in an immortalized human bronchial epithelial cell (HBEC3) line affected growth properties of these cells. Cells were transduced by lentivirus expressing EGFR and EGFR mutants and selected for stable integration as done previously (11). Two hundred cells were seeded on plates without EGF supplementation and allowed to grow for

A

	Familial Lung Cancer Families	BAC tumors	BAC normal tissue	Fresh-Frozen Resected Tumors
EGFR T790M	0 / 237	0 / 45	0 / 32	0 / 60

B

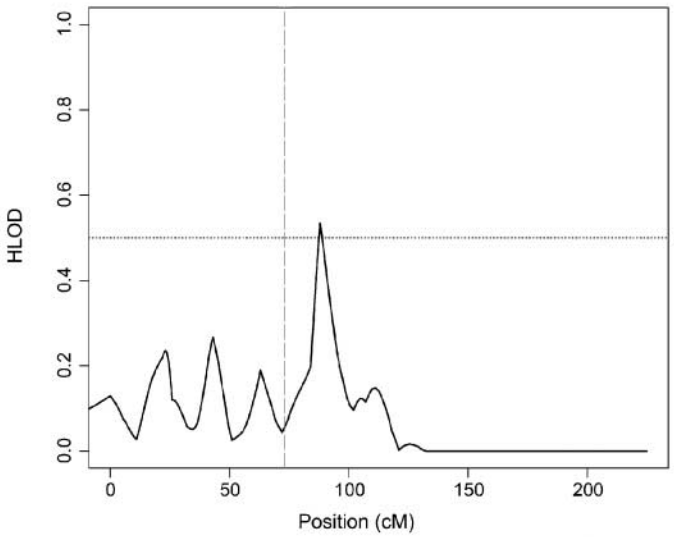

C

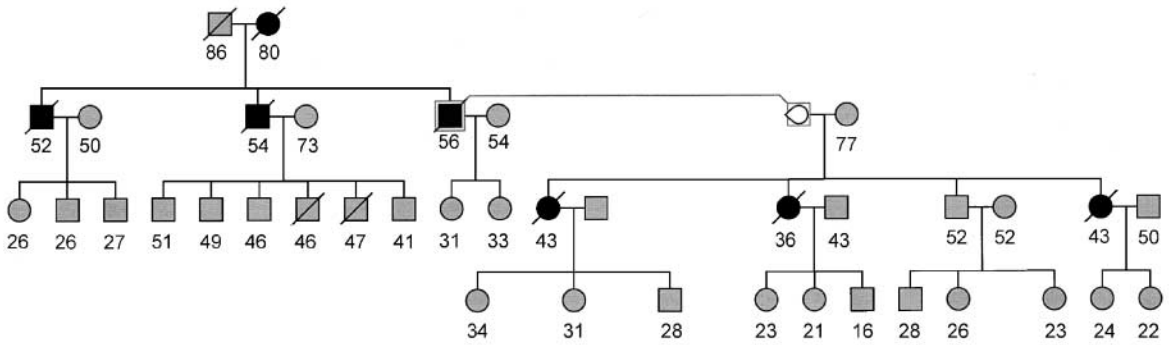

D

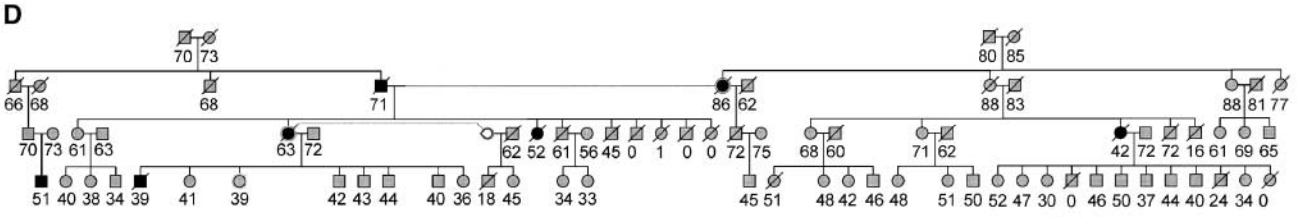

Figure 3. EGFR genotyping and linkage analysis for chromosome 7 with SimWalk2. *A,* the EGFR-T790M mutation was not observed in familial lung cancer blood DNA, BAC tumors and normals, or fresh-frozen resected tumors. *B,* the genetic position for EGFR is at ~73 cM (based on interpolation), between markers D7S1818 (70 cM) and D7S3046 (79 cM). Simwalk2 analysis was based on the parametric method using the genetic model reported by Moscatello et al. (18). Fifty-five pedigrees with five or more affected members were used. *C* and *D,* two representative pedigrees of GELCC collected families with predisposition to lung cancer. In (*C*) and (*D*), ● (females) or ■ (males) represent lung, throat, or laryngeal cancer. *Numbers below each individuals,* sample numbers; *numbers in brackets,* individual ages at the time the pedigree was constructed; *slashes,* dead individuals.

DOI:10.1158/0008-5472.CAN-07-0217

10 days. We observed that the EGFR-T790M–expressing cells had a greater number of large (≥3 mm in diameter) colonies compared with WT EGFR but less than the activated L747-E749 deletion (Fig. 2*A* and *B*). These results indicate that EGFR-T790M does in fact provide a growth advantage over WT EGFR. When we analyzed the status of EGFR phosphorylation at Y992 and Y1068 in these cells, we saw an increase in the EGFR-T790M mutant (Fig. 2*C*), consistent with what was observed in HEK293T and COS-7 cells (Fig. 1*A–D*).

To address possible downstream signaling mechanisms that are affected by mutant EGFR, we looked at the phosphorylation/activation status of MAPK and AKT (Fig. 2*C*). In contrast to our observations in 293T cells, we did not see MAPK activation induced by T790M. However, this is consistent with previously published results where no obvious changes are seen with the deletion mutant, yet colony formation is enhanced (11). Transcriptional changes, such as up-regulation of cyclin D1 levels, were recently reported to be a result of EGFR mutant signaling (14); however, we observed no changes induced by the mutants (Fig. 2*C*).

If *EGFR-T790M* is a human susceptibility allele, it is necessary to determine its prevalence in families with high susceptibility to lung cancer. With these families, a set of 52 extended pedigrees was used to show linkage on chromosome 6q23-25 (12). A concerted effort by the GELCC has attempted to identify the gene(s) associated with this susceptibility. We proposed that if the T790M mutation is a common variant for predisposition to lung cancer, it could potentially be enriched in probands from lung cancer families. Genomic DNA from 237 probands representing lung cancer families with more than three affected individuals was analyzed. PCR amplification and DNA sequencing of the resistance mutation in exon 20 were done. Interestingly, we did not observe the T790M mutation in any of the family probands analyzed or in any of 60 random fresh-frozen resected lung tumors (Fig. 3*A*). This would suggest that the T790M mutation is not enriched in our population and is likely a minor contributor to genetic susceptibility in familial lung cancers. Furthermore, in the aforementioned GELCC linkage study, the analysis of 52 families (and family subsets within) did not reveal a significant logarithm of odds score on or near 7p11, where the *EGFR* gene is located, which also suggests that the mutation is not a major contributor to familial predisposition to lung cancer (Fig. 3*B*; ref. 12). Representative families used in this study are indicated in Fig. 3*C* and *D*. We further tested to see if T790M might in fact be solely responsible for predisposition to adenocarcinomas with BAC differentiation. We sequenced 45 BAC tumors and 32 of the corresponding normal tissues and did not observe the T790M mutation in any of these samples (Fig. 3*A*). This further suggests the rarity of this potential predisposing mutation.

Discussion

Several lines of evidence exist that lend support to T790M as a putative susceptibility allele. T790M has been detected somatically in tumors that have not been treated with gefitinib or erlotinib, which may suggest that this mutant may have arisen during drug-free cancer progression (15). Furthermore, the NCI-H1975 BAC cell line, which has never undergone tyrosine kinase inhibitor treatment, has both activating L858R and resistant T790M mutations, suggestive that T790M may be growth promoting (5). Bell et al. (8) also have observed that the T790M mutation seems to occur in *cis* with the activating mutations. Perhaps more persuasive is that the analogous resistance mutation in CML patients, BCR-ABL-T315I, displays increased *in vitro* kinase activity (16). Similarly, the analogous mutations in Src (T341M) and FGFR1 (V561M) also result in increased phosphorylation and activation (10). Why T790M in EGFR does not reportedly function in a similar manner is unclear.

Our results suggest that the T790M mutation may in fact provide a proliferative advantage in normal cells by increasing kinase activity and downstream signaling. Our data suggest that EGFR-T790M does in fact exhibit higher kinase activity than WT molecule in HEK293T and COS-7 cell lines. Overexpression in our HBEC3 cell line showed increased tyrosine phosphorylation at Y992 and Y1068 and increased colony formation. Increased proliferation is most evident in the absence of EGF in the medium, suggesting that the activating T790M EGFR mutation is involved in the proliferative effects observed. EGFR kinase activity is essential for oncogenic transformation. EGFR extracellular domain deletion mutants and overexpression of EGFR are commonly found in human cancers (17, 18). Our data also show that phosphorylation levels between WT and T790M are indistinguishable at higher expression levels (Fig. 1*C*), yet differences are more apparent at lower expression levels. We believe this may be an explanation why others have seen no difference between EGFR and T790M.

EGFR signaling activates many pathways that lead to proliferative advantages. The Ras/MAPK pathway is activated via ligation of Grb2 to an activated EGFR molecule. In our 293T overexpression system, we observed that MAPK activity is increased by T790M versus WT EGFR. However, a significant effect of T790M on these downstream kinases was not evident in our HBEC3 system, which might suggest that other signaling/transcriptional events are responsible for the proliferative changes. Recent work has revealed transcriptional changes in cyclin D1, may be a key response to gefitinib resistance by T790M and susceptibility to the irreversible inhibitor CL-387,785 (14). We did not observe changes in cyclin D1 levels in the HBEC3 system and believe other, yet unidentified, mechanisms exist to account for the proliferative advantages caused by mutant EGFR.

A recent study, using a mutant-enriched PCR system, revealed the presence of the T790M mutation as a minor clone in non–small cell lung cancer tumors (19). It is suggested that these clones are selected for during gefitinib treatment and are enriched in the resistant tumor but do not provide the main proliferative function for oncogenesis. Our observations suggest that T790M as a germline mutation (i.e., in all cells) may provide the mild proliferative push for lung cancer development.

Many lines of evidence suggest the existence of a limited number of genetic factors that control susceptibility to lung cancer (20–22). However, due to a high-case fatality rate (5-year survival rate of 15%), obtaining biospecimen samples for DNA analysis is particularly difficult (23). A collaborative effort of GELCC has accrued DNA from families with lung, throat, and laryngeal cancers since the early 1990s. At present, 771 families with three or more first-degree relatives affected with lung cancer have been collected, of which 11% have sufficient family-wide biospecimen availability for any future studies. Subsequent sequencing of 237 families with predisposition to lung cancer, 45 BAC tumors and 60 fresh-frozen resected tumors, did not reveal any mutations, suggesting that T790M is likely a rare mutation. Nevertheless, our data provide a basis for *EGFR-T790M* as a rare susceptibility allele in human lung cancer.

Acknowledgments

Received 1/17/2007; revised 2/20/2007; accepted 3/9/2007.

Grant support: NIH grants U01CA76293 (Genetic Epidemiology of Lung Cancer Consortium), R01CA058554, R01CA093643, R01CA099147, R01CA099187, R01ES012063, R01ES013340, R03CA77118, R01CA80127, P30ES06096, P50CA70907 (Specialized Program of Research Excellence), and N01HG65404 and Department of Defense VITAL

DOI:10.1158/0008-5472.CAN-07-0217

grant. This study was supported in part by NIH, the Intramural Research Programs of National Cancer Institute, and National Human Genome Research Institute.

The costs of publication of this article were defrayed in part by the payment of page charges. This article must therefore be hereby marked *advertisement* in accordance with 18 U.S.C. Section 1734 solely to indicate this fact.

We thank W. Pao (Memorial Sloan-Kettering Cancer Center, New York, NY) for providing mammalian expression plasmids encoding for human EGFR, EGFR-T790M, and EGFR-L858R; R. Lubet (Chemoprevention Branch, National Cancer Institute, Bethesda, MD) for providing gefinitib; and J. Clark, Q. Chen, and M. Watson for their assistance in various aspects of this work.

References

1. Lynch TJ, Bell DW, Sordella R, et al. Activating mutations in the epidermal growth factor receptor underlying responsiveness of non-small-cell lung cancer to gefitinib. N Engl J Med 2004;350:2129–39.

2. Paez JG, Janne PA, Lee JC, et al. EGFR mutations in lung cancer: correlation with clinical response to gefitinib therapy. Science 2004;304:1497–500.

3. Pao W, Miller V, Zakowski M, et al. EGF receptor gene mutations are common in lung cancers from "never smokers" and are associated with sensitivity of tumors to gefitinib and erlotinib. Proc Natl Acad Sci U S A 2004; 101:13306–11.

4. Kobayashi S, Boggon TJ, Dayaram T, et al. EGFR mutation and resistance of non-small-cell lung cancer to gefitinib. N Engl J Med 2005;352:786–92.

5. Pao W, Miller VA, Politi KA, et al. Acquired resistance of lung adenocarcinomas to gefitinib or erlotinib is associated with a second mutation in the EGFR kinase domain. PLoS Med 2005;2:e73.

6. Kwak EL, Sordella R, Bell DW, et al. Irreversible inhibitors of the EGF receptor may circumvent acquired resistance to gefitinib. Proc Natl Acad Sci U S A 2005; 102:7665–70.

7. Deininger M, Buchdunger E, Druker BJ. The development of imatinib as a therapeutic agent for chronic myeloid leukemia. Blood 2005;105:2640–53.

8. Bell DW, Gore I, Okimoto RA, et al. Inherited susceptibility to lung cancer may be associated with the T790M drug resistance mutation in EGFR. Nat Genet 2005;37:1315–6.

9. Blencke S, Ullrich A, Daub H. Mutation of threonine 766 in the epidermal growth factor receptor reveals a hotspot for resistance formation against selective tyrosine kinase inhibitors. J Biol Chem 2003;278:15435–40.

10. Blencke S, Zech B, Engkvist O, et al. Characterization of a conserved structural determinant controlling protein kinase sensitivity to selective inhibitors. Chem Biol 2004;11:691–701.

11. Sato M, Vaughan MB, Girard L, et al. Multiple oncogenic changes (K-RAS(V12), p53 knockdown, mutant EGFRs, p16 bypass, telomerase) are not sufficient to confer a full malignant phenotype on human bronchial epithelial cells. Cancer Res 2006;66:2116–28.

12. Bailey-Wilson JE, Amos CI, Pinney SM, et al. A major lung cancer susceptibility locus maps to chromosome 6q23-25. Am J Hum Genet 2004;75:460–74.

13. Rojas M, Yao S, Lin YZ. Controlling epidermal growth factor (EGF)-stimulated Ras activation in intact cells by a cell-permeable peptide mimicking phosphorylated EGF receptor. J Biol Chem 1996;271:27456–61.

14. Kobayashi S, Shimamura T, Monti S, et al. Transcriptional profiling identifies cyclin D1 as a critical downstream effector of mutant epidermal growth factor receptor signaling. Cancer Res 2006;66:11389–98.

15. Kosaka T, Yatabe Y, Endoh H, et al. Mutations of the epidermal growth factor receptor gene in lung cancer: biological and clinical implications. Cancer Res 2004;64: 8919–23.

16. Yamamoto M, Kurosu T, Kakihana K, Mizuchi D, Miura O. The two major imatinib resistance mutations E255K and T315I enhance the activity of BCR/ABL fusion kinase. Biochem Biophys Res Commun 2004;319:1272–5.

17. Garcia de Palazzo IE, Adams GP, Sundareshan P, et al. Expression of mutated epidermal growth factor receptor by non-small cell lung carcinomas. Cancer Res 1993;53: 3217–20.

18. Moscatello DK, Holgado-Madruga M, Godwin AK, et al. Frequent expression of a mutant epidermal growth factor receptor in multiple human tumors. Cancer Res 1995;55:5536–9.

19. Inukai M, Toyooka S, Ito S, et al. Presence of epidermal growth factor receptor gene T790M mutation as a minor clone in non-small cell lung cancer. Cancer Res 2006;66:7854–8.

20. Sellers TA, Bailey-Wilson JE, Elston RC, et al. Evidence for mendelian inheritance in the pathogenesis of lung cancer. J Natl Cancer Inst 1990;82:1272–9.

21. Yang P, Schwartz AG, McAllister AE, Swanson GM, Aston CE. Lung cancer risk in families of nonsmoking probands: heterogeneity by age at diagnosis. Genet Epidemiol 1999;17:253–73.

22. Chen PL, Sellers TA, Bailey-Wilson JE, Rothschild H, Elston RC. Segregation analysis of smoking-associated malignancies: evidence for mendelian inheritance. Am J Hum Genet 1991;49.

23. Bunn PAJ, Soriano A. New therapeutic strategies for lung cancer: biology and molecular biology come of age. Chest 2000;117:163–8S.

Inhibition of Stat3 activation and tumor growth suppression of non-small cell lung cancer by G-quartet oligonucleotides

PRIYA WEERASINGHE[1], GABRIELA E. GARCIA[1], QIQING ZHU[1], PING YUAN[3], LILI FENG[1], LI MAO[3] and NAIJIE JING[1,2]

[1]Department of Medicine, and [2]Dan Duncan Cancer Center, Baylor College of Medicine; [3]Department of Thoracic/Head and Neck Medical Oncology, The University of Texas MD Anderson Cancer Center, Houston, TX, USA

Received February 20, 2007; Accepted April 12, 2007

Abstract. Lung cancer is the leading cause of cancer mortality in the United States. Despite advances made over the past decades, the overall survival of patients with lung cancer remains dismal. Here we report novel G-quartet oligodeoxynucleotides (GQ-ODN) that were designed to selectively target signal transducer and activator of transcription 3 (Stat3), in the treatment of human non-small cell lung cancer (NSCLC). The objective of this study was to evaluate the effects of two novel GQ-ODN STAT3 inhibitors, T40214 and T40231, on NSCLC bearing nude mice. NSCLC bearing nude mice were assigned to 5 groups, which were treated by vehicle, control ODN, T40214, T40231, and Paclitaxel, respectively. Tumors were measured, isolated and analyzed using Western blotting, immuno-histochemistry, RPA and TUNEL. Results show that GQ-ODN T40214 and T40231 significantly suppress the growth of NSCLC tumors in nude mice by selectively inhibiting the activation of Stat3 and its downstream proteins Bcl-2, Bcl-x_L, Mcl-1, survivin, VEGF, Cyclin D1 and c-myc; thereby, promoting apoptosis and reducing angiogenesis and cell proliferation. These findings validate Stat3 as an important molecular target for NSCLC therapy and demonstrate the efficacy of GQ-ODN in inhibiting Stat3 phosphorylation.

Introduction

Lung cancer is one of the most prevalent cancers and a leading cause of cancer mortality worldwide. In the United States, approximately 170,000 people are diagnosed with lung cancer each year (1,2); approximately 85% of those diagnosed die of the disease. The number of lung cancer deaths exceeds those due to breast, prostate, and colon cancers combined (3). Lung cancer has two major subtypes based on histology, i.e. small cell lung cancer (SCLC) and non-small cell lung cancer (NSCLC) which account for 85% of all lung cancers. More than 60% of all NSCLC patients have advanced or metastatic tumors at the time of diagnosis and are not suitable for surgery (3). Despite advances made in treating the disease over the past two decades, the overall survival of patients with NSCLC remains extremely poor (4). Therefore, innovative treatment approaches that employ new agents targeting novel molecules are urgently needed. In this regard, Stat3, a critical mediator of oncogenic signaling that is highly activated in a wide variety of human tumors (5), may hold promise.

Signal transducer and activator of transcription (STAT) proteins were discovered as latent cytoplasmic transcription factors (6). Seven known mammalian STAT proteins (i.e., Stat1, 2, 3, 4, 5a, 5b, and 6) are involved in immune response, inflammation, proliferation, differentiation, development, cell survival, and apoptosis (5). These proteins contain several domains: a tetramerization domain, a coil-coil domain, a DNA-binding domain, a linker domain, an Src-homology 2 (SH2) domain, a critical tyrosine residing near the C-terminal end, and a C-terminal transactivation domain (7,8). STAT proteins are activated in response to the binding of a number of ligands, including cytokines (e.g., IL-6) and growth factors (e.g., EGF), to their cognate cell surface receptors, and are recruited to specific phosphotyrosine residues within receptor complexes through their SH2 domains; they subsequently become phosphorylated on the tyrosine residue within their C-terminus and dimerize through reciprocal interactions between the SH2 domain of one monomer and the phosphorylated tyrosine of the other. The activated dimers translocate to the nucleus, where they bind to DNA-response elements in the promoters of target genes and activate specific gene expression programs (9).

Stat3 has been identified as an important target for cancer therapy, since it participates in oncogenesis through the upregulation of genes encoding apoptosis inhibitors (Bcl-x_L, Mcl-1, and survivin), cell-cycle regulators (cyclin D1 and c-*myc*), and inducers of angiogenesis (VEGF) (9). Mounting evidence has shown that Stat3 is also constitutively activated in many human cancers, including 82% of prostate cancers, 70% of breast cancers, over 90% of head and neck cancers, and more than 50% of lung cancers (10-13). These findings provide a strong rationale for targeting Stat3 to treat human cancers.

Correspondence to: Dr Naijie Jing, Department of Medicine, Baylor College of Medicine, Houston, TX 77030, USA
E-mail: njing@bcm.tmc.edu

Key words: G-quartet oligonucleotides, signal transducer and activator of transcription 3, non-small cell lung cancer, apoptosis, angiogenesis

Recently, we laid the groundwork to develop G-quartet oligodeoxynucleotide (GQ-ODN), which forms G-quartet helical DNA structures, as a potent inhibitor of Stat3 activation. In our preliminary studies, we have: i) demonstrated that GQ-ODN selectively inhibits Stat3 activation in cancer cells; ii) developed a novel delivery system for GQ-ODN, to increase drug activity in cells and *in vivo*; and iii) shown that GQ-ODN T40214 and T40231 significantly suppress tumor growth and greatly increase the survival of nude mice with tumors in which Stat3 is activated (14-16). This report is a part of our systematic *in vivo* examination, which aims to determine whether Stat3 as an oncogenic signaling molecule will have the same influence on tumor progression in different human cancers and whether GQ-ODN will have a similar effect on suppressing tumor growth in different xenografted models under the same conditions. Here we have demonstrated that: i) as a critical oncogenic signaling pathway, Stat3 strongly influences the progression of NSCLC *in vivo*; and ii) targeting the Stat3 molecule with GQ-ODN constitutes a novel and potent therapeutic treatment for NSCLC. We also provide experimental evidence for the proposed mechanism, that a tyrosine-phosphorylated STAT dimer is quickly dephosphorylated when the STAT dimer is dissociated from DNA in cells (17,18). Based on the results, we suggest that GQ-ODN is a novel and promising class of anti-cancer drug in the treatment of metastatic tumors.

Materials and methods

Materials. The following polyclonal antibodies were obtained from Santa Cruz Biotechnology, Inc. (Santa Cruz, CA): anti-Stat3; anti-Stat1; anti-Cyclin D1 against amino acids 1-295, which represents full-length cyclin D1 of human origin; anti-VEGF; anti-Bcl-x_L; and anti-Bcl-2. Phospho-specific antibodies, p-Stat1 and p-Stat3, were purchased from Cell Signaling Technology (Beverly, MA). Goat anti-rabbit horseradish peroxidase (HRP) conjugate was purchased from Bio-Rad Laboratories (Hercules, CA), goat anti-mouse HRP conjugate was purchased from BD Transduction Laboratories (Lexington, KY). Penicillin, streptomycin, RPMI-1640 medium, fetal bovine serum (FBS), and 0.4% trypan blue vital stain were obtained from Invitrogen Corporation/Life Technologies, Inc. (Grand Island, NY). Oligonucleotides were synthesized by The Midland Certified Reagent Company, Inc. (Midland, TX), dissolved in Polyethylenimine (PEI) (Aldrich Chemical, WI) as a 1 μg/μl stock solution, and stored at room temperature (RT).

Cell lines and cell culture. The cell lines used in our studies included: A549 (human non-small cell lung carcinoma); H292 (human lung epithelial cell carcinoma); and H359, H596, H1792, and H1299 cells, which were purchased from ATCC (Manassas, VA). These cell lines were cultured in DMEM medium supplemented with 10% FBS, 100 units/ml penicillin, and 100 μg/ml streptomycin.

Western blot analysis. To determine the effect of GQ-ODN on Stat3 phosphorylation, cytoplasmic extracts were prepared, as previously described (14), from murine tumor tissue or A549 lung cancer cells that had been pretreated with GQ-ODN. Lung tumor cells (1 million cells per well in 6-well plates) were first pre-treated with IL-6 (25 ng/ml) or EGF (25 ng/ml) for 30 min. Cells were then washed in serum-free medium and incubated with various concentrations (1.4-142 μM) of GQ-ODN/PEI complexes for 24 h. Cells were lysed with cell lysis buffer and 30 μg of whole cell protein was resolved on 10% SDS-PAGE gel, transferred to a nitrocellulose membrane, blocked with 5% nonfat milk, and probed with specific antibody against Stat3 and tyrosine-phosphorylated Stat3 (p-Stat3). Xenografted tumors were harvested at the end of treatment, diced into small pieces, and sonicated on ice for 2 min. Tumor tissue (100 mg) was lysed in 300 μl of lysis buffer containing protease and phosphatase inhibitors. Tumor tissue protein (50 μg) was resolved on SDS-PAGE and probed by specific antibodies, as previously described. The bands were quantitated using a Personal Densitometer Scanner (version 1.30) and ImageQuant software (version 3.3) (GE Healthcare/Amersham Biosciences).

Animal/xenograft model. Athymic nude mice (Balb-nu/nu, 4 weeks old, weighing approximately 20 g) were obtained from Charles River Laboratories, Inc. (Wilmington, MA); 2.5 million A549 NSCLC cells in 200 μl of PBS were then injected subcutaneously into the right flank of each mouse. After the NSCLC tumors were established (50-150 mm^3), the nude mice were randomly assigned to 5 groups of 5 (or 4): Group 1, was treated with PEI (2.5 mg/kg) (vehicle) alone; Group 2 was treated with paclitaxel (a conventional chemotherapeutic agent) at 10 mg/kg; Group 3 was treated with GQ-ODN T40214/PEI (10 mg/kg/+2.5 mg/kg); and Group 4 was treated with GQ-ODN T40231/PEI (10 mg/kg/+2.5 mg/kg) and Group 5 was treated with ns-ODN/PEI (10 mg/kg/+2.5 mg/kg) (control ODN). PEI and ODNs were administered every other day and paclitaxel was injected intraperitoneally (IP) every 4 days. Weight and tumor size were measured every other day. Tumor size was calculated by using the function [a x $(0.5^b)2$], where a equals the length and b equals the width of tumors.

RNase protection assay (RPA). RPA was performed, as previously described (19,20). Briefly, for each sample prepared from NSCLC tumor tissue, five micrograms of total RNA were used in the RNase protection assay. Probes specific to survivin, c-*myc*, and Mcl-1 mouse genes were prepared. Mouse Angio-1, Apo-2, and CYC-1 multi-probes were obtained from BD Biosciences/Pharmingen (San Diego, CA). An RNase protection assay was performed using a kit (Torrey Pines Biolabs, Inc.; Houston, TX), in accordance with the manufacturer's instructions. The ^{32}P[UTP] (3000 Ci/mmol, ICN)-labeled antisense RNA probes were synthesized using mCK5 multi-probes (BD Biosciences/Pharmingen) as templates, through an *in vitro* transcription system (Promega Corporation; Madison, WI). Antisense RNA probes were hybridized with the RNA samples at 90˚C for 25 min. Unhybridized single-stranded RNA was digested by ribonuclease A/T1 (Sigma-Aldrich; St. Louis, MO) for 30 min. Double-stranded RNA was precipitated by stop solution at -80˚C for 15-30 min, and centrifuged at maximum speed for 30 min. The samples were resolved by 6% sequencing gel. Subsequently, the gels were dried and exposed to X-ray film.

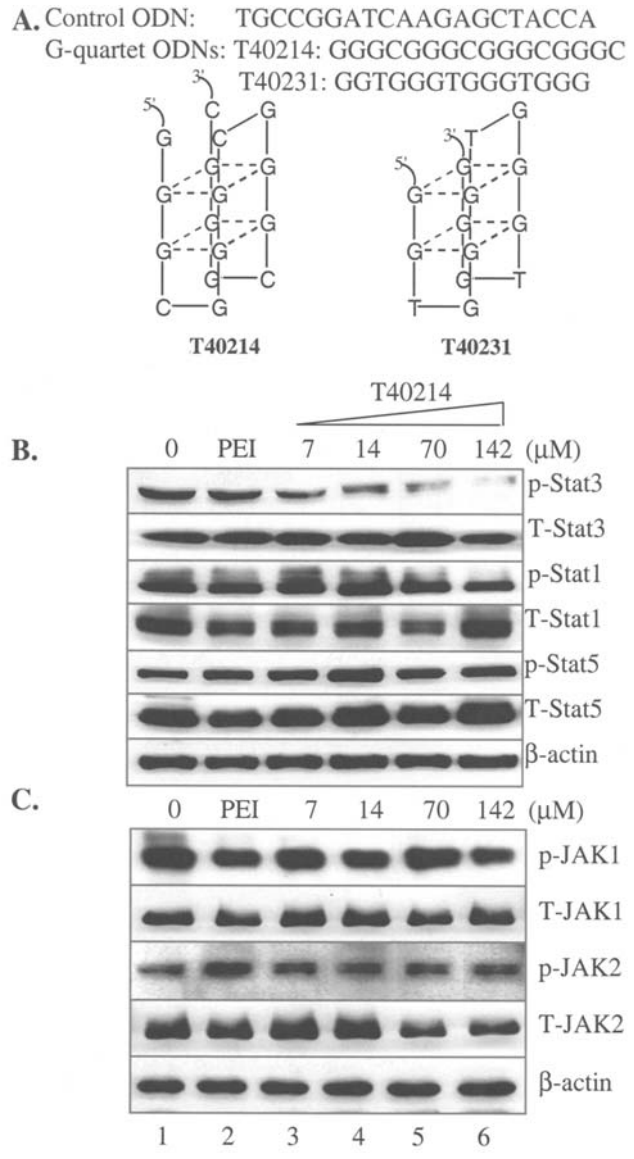

Figure 1. (A) The structures of GQ-ODN T40214 and T40231. (B) Western blot analysis shows the inhibition of Stat3 phosphorylation by GQ-ODNs T40214 and T40231 in NSCLC cells (A549). Comparing with the control band (lane 1), T40214 significantly inhibited the expression of p-Stat3 in NSCLC cells (A549) (IC_{50} = 5.4 μM). p-Stat3 and T-Stat3, phosphorylated Stat3 and total Stat3, respectively. PEI did not inhibit p-Stat3 (lane 2), and GQ-ODN T40214 did not inhibit p-Stat1 and p-Stat5 in A549 cells. (C) T40214 did not inhibit the expression of p-JAK1 and p-JAK2 in A549 cells. ß actin served as the internal control.

Hematoxylin and eosin staining. Xenografted tumors were harvested from athymic mice treated with vehicle alone (PEI), GQ-ODN T40214, GQ-ODN T40231, and paclitaxel, fixed (with 10% formaldehyde in paraffin), sectioned (5-μm tissue sections) and stained with hematoxylin and eosin (H&E).

Terminal deoxyribonucleotidyl transferase-mediated dUTP nick end labeling (TUNEL) analysis. Tissue sections (5 μm) were mounted on siliconized glass slides, air dried, and heated at 45˚C overnight. After deparaffinization and rehydration, the sections were digested with proteinase K (120 μg/ml) for 20 min at room temperature. Following quenching of the endogenous peroxidase activity, the sections were washed in PBS, and subsequently incubated with equilibration buffer for 10 min at room temperature. Sections were boiled and 50 μl of a mix containing terminal deoxynucleotidyl transferase, reaction buffer containing dATP, and digoxigenin-11-dUTP was then added. The sections were covered with a plastic coverslip, washed in stop/wash buffer for 10 min at room temperature, and subsequently washed in PBS. The sections were then incubated with anti-digoxigenin peroxidase for 30 min at room temperature and washed in PBS. Color development was accomplished through immersion of the slides in 3'3 diaminobenzidine/0.1% H_2O_2 for 3-7 min. Sections were counterstained with ethyl green, washed in butanol, cleared in xylol and mounted with permount.

Results

Inhibition of Stat3 activation by GQ-ODN. Recently, we have developed GQ-ODNs as a new class of Stat3 inhibitors. We have previously reported that the leading compounds, T40214 and T40231, selectively inhibit Stat3 activity (IC_{50} = 5 μM) in the cells of prostate, breast and head and neck cancers (14,16). Here we employed Western blotting to ascertain if GQ-ODN inhibits Stat3 phosphorylation in NSCLC cells. The sequences and structures of GQODN T40214 and T40231 have been previously delineated (Fig. 1A) (14). PEI (polyethylenimine) was used as vehicle for intracellular delivery of ODN at the ODN/PEI ratio of 4:1. ß-actin was used as the loading control. When compared to the tyrosine-phosphorylated Stat3 (p-Stat3) band in lane 1, lane 2 shows that PEI alone has no inhibitory effect on p-Stat3 in NSCLC cells. The p-Stat3 was significantly reduced when the concentration of T40214 increased (lanes 3 to 6). The IC_{50} of p-Stat3 dephosphorylation for T40214 was ~5.4 μM. Along with p-Stat3, we also detected tyrosine-phosphorylated Stat1 (p-Stat1) and Stat5 (p-Stat5) in NSCLC cells under similar experimental conditions. Importantly, we found that GQ-ODN T40214 does not inhibit the activation of p-Stat1 nor p-Stat5 in NSCLC cells, showing that GQ-ODN T40214 selectively inhibits p-Stat3 activation (Fig. 1B). Furthermore, tyrosine-phosphorylated JAK1 (p-JAK1) and JAK2 (p-JAK2) were also detected in NSCLC cells; and were not found to be inhibited by GQ-ODN T40214. This further reinforces the specificity of GQ-ODN to the selective inhibition of Stat3 protein (Fig. 1C).

GQ-ODN suppressed the growth of NSCLC tumors. Assessing the effectiveness of a drug in animal models is an important step toward establishing its potential clinical utility. To this end, we utilized nude mice xenografts as animal models of *in vivo* drug testing in order to evaluate the anti-cancer potential of GQ-ODN. First, nude mice were injected subcutaneously with NSCLC cells (e.g., A549) in which Stat3 is constitutively active. After tumors were established (vol. 50~150 mm^3), treatment of nude mice with NSCLC (A549) tumors was performed by intraperitoneal (IP) injection. The nude mice were randomly assigned to 5 groups (4 or 5 mice in each group): Group 1 was treated with PEI alone (2.5 mg/kg); Group 2 was treated with paclitaxel (a clinical drug) (10 mg/kg); Groups 3 and 4 were treated with T40231/PEI and T40214/PEI (10 mg/kg/+2.5 mg/kg), respectively; and Group 5 was treated by ns-ODN/PEI (10 mg/kg/+2.5 mg/kg). PEI and ODNs were administered every two days; paclitaxel was

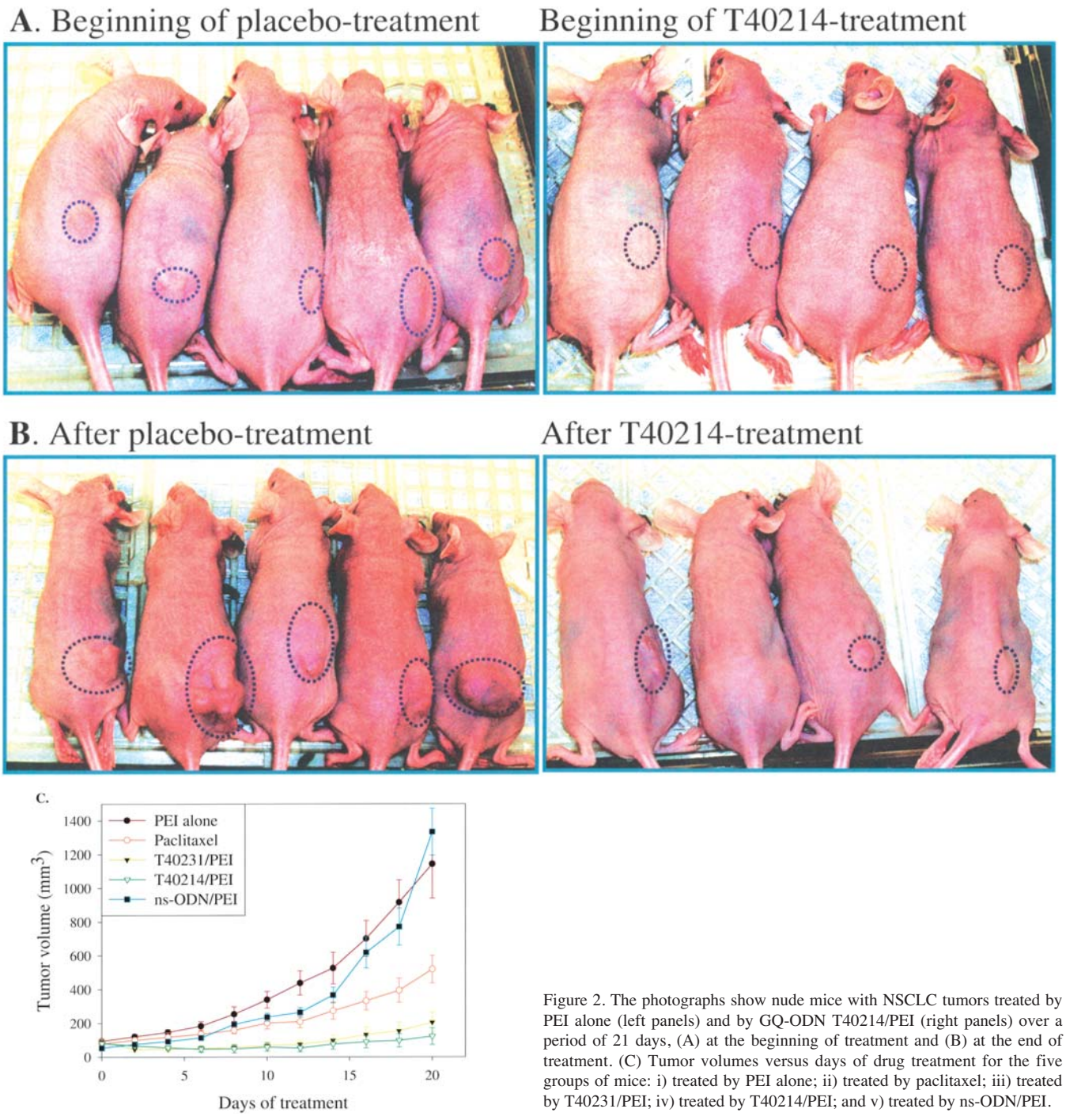

Figure 2. The photographs show nude mice with NSCLC tumors treated by PEI alone (left panels) and by GQ-ODN T40214/PEI (right panels) over a period of 21 days, (A) at the beginning of treatment and (B) at the end of treatment. (C) Tumor volumes versus days of drug treatment for the five groups of mice: i) treated by PEI alone; ii) treated by paclitaxel; iii) treated by T40231/PEI; iv) treated by T40214/PEI; and v) treated by ns-ODN/PEI.

injected every four days, to ensure safety of the mice from toxicity. Results demonstrate that, over the 21-day treatment period, i) the mean size of NSCLC tumors in the PEI- and ns-ODN-treated mice increased from 93 to 1144 mm^3 and from 53 to 1334 mm^3, respectively; ii) the mean size of NSCLC tumors in the paclitaxel-treated mice increased from 88 to 519 mm^3; and iii) the mean size of NSCLC tumors in the mice treated with T40231 and T40214 only increased from 89 to 204 mm^3 and from 83 to 123 mm^3, respectively (Fig. 2). Significant differences in tumor growth were observed between PEI-treated mice and T40214-treated (p=0.002) or T40231-treated mice (p=0.004) and between the mice treated by ns-ODN (a control ODN) and by T40214 (p=0.019) or by T40231 (p=0.028) as well.

Targets of GQODN. To determine the targets of GQ-ODN and possible mechanism of GQ-ODN suppressing tumor growth, we performed immunoblotting assays on tumor tissue, as described in Materials and methods. Results demonstrate the expression of p-Stat3 and its regulated proteins in NSCLC tumors (Fig. 3A). An equal amount of protein from each tumor sample was loaded, and the intensities of the bands from mice treated with T40214/PEI (lane 2), T40231/PEI (lane 3) or paclitaxel (lane 4), were compared with that from the PEI-treated mice (lane 1). We found that GQ-ODN T40214 and T40231 totally blocked expression of phosphorylated Stat3 (p-Stat3) and its downstream proteins (i.e., Bcl-2, Bcl-x_L, Mcl-1, survivin, VEGF, Cyclin D1, and c-myc) in NSCLC tumors. However, paclitaxel did not inhibit p-Stat3, and only

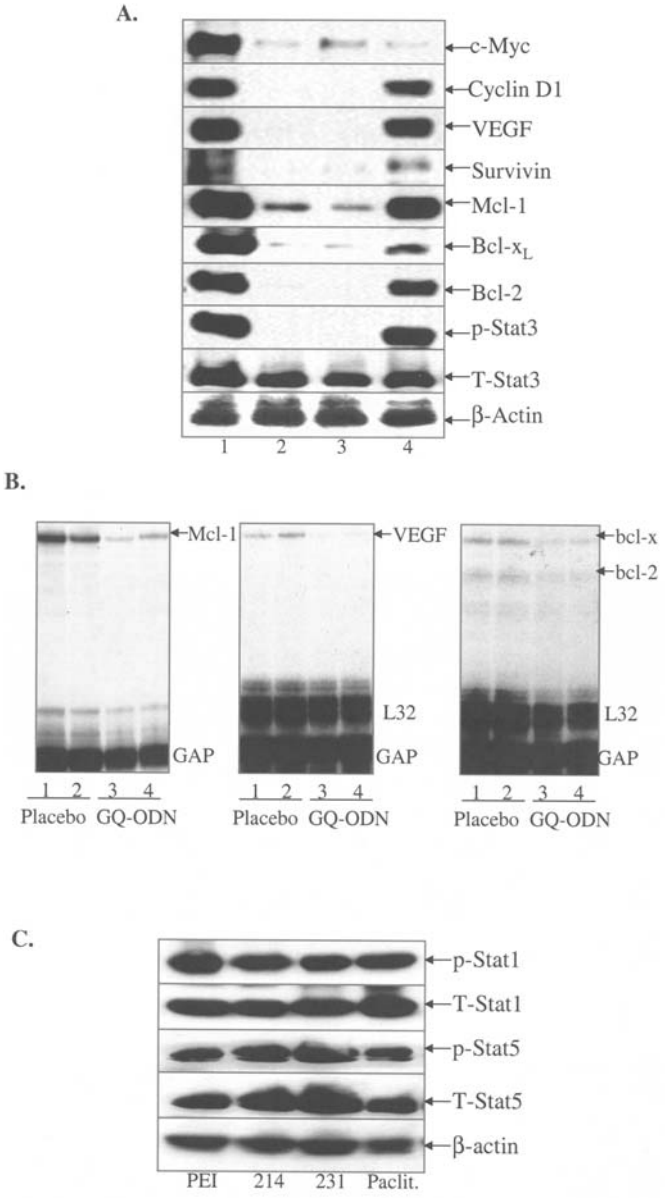

Figure 3. (A) Western blots obtained from NSCLC tumors demonstrate the expression of total Stat3 (T-Stat3), phosphorylated Stat3 (p-Stat3), and its downregulated proteins, including Bcl-2, Bcl-x_L, Mcl-1, survivin, VEFG, Cyclin D1 and c-myc. Lane 1, tumor treated by PEI alone; lane 2, tumor treated by T40214/PEI; lane 3, tumor treated by T40231/PEI; and lane 4, tumor treated by paclitaxel. ß actin serves as the internal control. (B) RPA results were obtained from tumors of two PEI-treated mice (lanes 1 and 2) and two T40214-treated mice (lanes 3 and 4). The mRNA levels of the Stat3-regulated genes in T40214-treated tumors were much less than in the PEI-treated control tumors, showing that Stat3-regulated transcription of candidate genes, i.e. Mcl-1 (left), VEGF (middle), survivin (middle), Bcl-x_L, and Bcl-2 (right), was inhibited by GQ-ODNs. L32 and GAPDH represent internal controls. (C) GQ-ODN T40214 did not inhibit p-Stat1 and p-Stat5 activation *in vivo*. (C) The proteins of Stat1 and Stat5 were obtained from the same tumor samples and under the same experimental conditions as Stat3. Comparing with proteins of total Stat1 (T-Stat1) and Stat5 (T-Stat5), T40214 and T40231 did not inhibit p-Stat1 and p-Stat5 in NSCLC tumors.

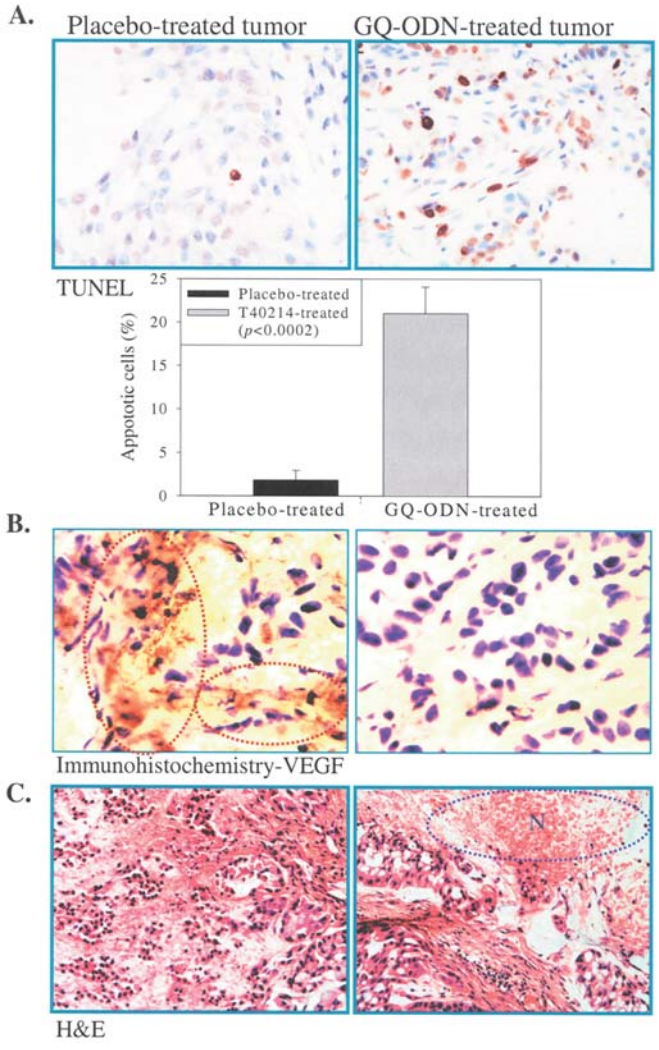

Figure 4. (A) Apoptosis of cells induced by GQ-ODN T40214 in NSCLC tumors. TUNEL-stained slides demonstrate an absence of TUNEL-positive cells (i.e., no cells are stained dark brown) in placebo-treated tumors (top left panel), whereas GQ-ODN-treated tumors (top right panel) exhibited a high number of TUNEL-positive tumor cells (photographs x400 magnification). The ratio of apoptotic cells to total cells increased 10-fold from placebo-treated tumor (1.9%) to T40214-treated tumor (21%). (B) Immunohistochemistry data show that VEGF, which appears brown in the images, was highly expressed in the tissue of NSCLC tumors treated by PEI (the cycled areas); however, tumors treated by GQ-ODN T40214 showed no evidence of VEGF (photographs x400 magnification). (C) H&E images show that in PEI-treated tumors (left), all NSCLC cells were intact. In contrast, in GQ-ODN-treated tumors (right) most NSCLC cells shrunk, partially resulting in necrosis (the circled area) (photographs x100 magnification).

partially blocked expression of Bcl-x_L, Bcl-2, survivin, and c-myc in NSCLC tumors.

To determine whether the Stat3-regulated proteins (e.g., Bcl-2, Bcl-x_L, Mcl-1, VEGF, and others) are inhibited by blocking Stat3 DNA transcription or directly by GQ-ODN, an RNase protection assay (RPA) was employed to test the mRNA of the Stat3-regulated genes in NSCLC tumors. The results, obtained from the tumors of two PEI-treated mice (lanes 1 and 2) and two T40214/PEI-treated mice (lanes 3 and 4), clearly show that the level of mRNA of Mcl-1, VEGF, bcl-x, and bcl-2 in T40214/PEI-treated tumors were much lower than those in the PEI-treated tumors (Fig. 3B). The mRNAs of L32 and GAP were equally loaded as controls. The RPA data provide solid evidence that GQ-ODNs inhibit the activation of Bcl-2, Bcl-x_L, Mcl-1, survivin, VEGF, Cyclin D1, and c-*myc* in NSCLC tumors through the disruption of Stat3 transcription.

Independent of Stat3, Stat1 and Stat5 are also active in human cancers, including NSCLC; and therefore the selective

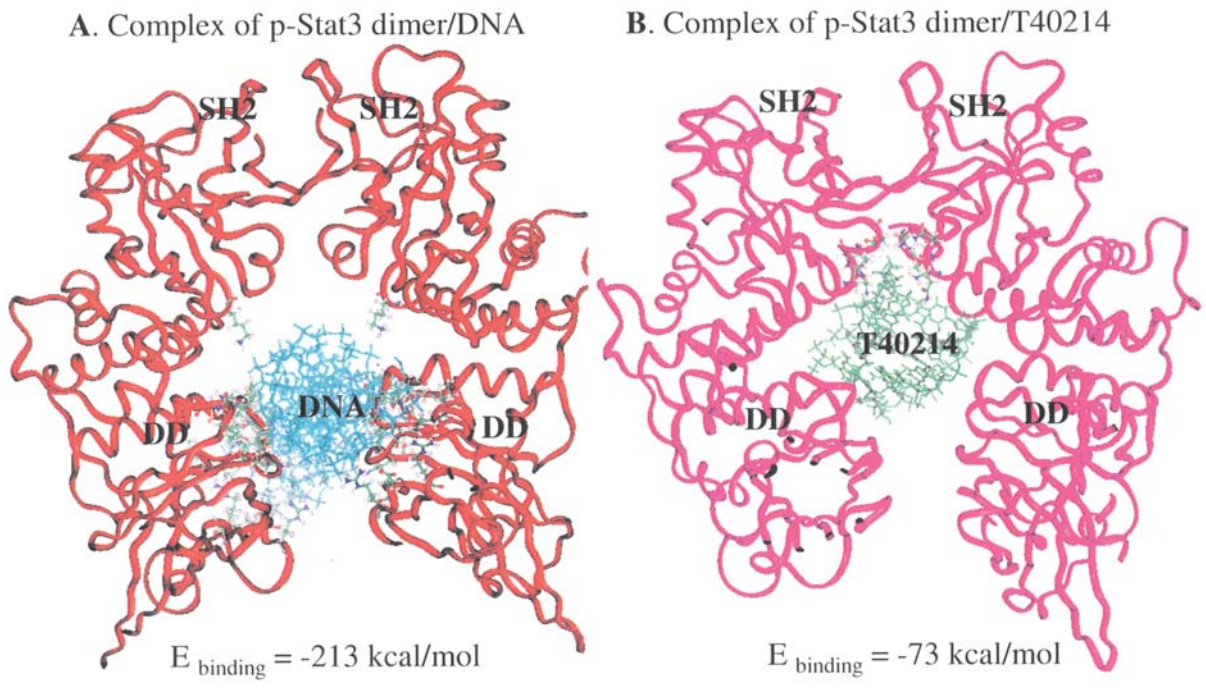

Figure 5. The complexes of p-Stat3 dimer with DNA and of p-Stat3 dimer with T40214 are demonstrated in A and B, respectively. The binding energies between Stat3 dimer and DNA and between Stat3 dimer and T40214 were calculated as -231 kal/mol and -73 kal/mol, respectively. (A) 30 H-bonds are formed between p-Stat3 dimer and DNA in the residues of M331 to V432 of DNA binding domains (7), and (B) seven H-bonds are formed between p-Stat3 dimer and T40214 in the residues of Q643 to N647 of SH2 domains. The residues in Stat3 forming H-bonds with DNA or T40214 are shown in stick and ball types. DD denotes DNA binding domain and SH2 denotes SH2 domain.

targeting of Stat3 becomes a key factor in the development of a potent Stat3 inhibitor. Using Western blot analysis we have shown that GQ-ODN T40214 and T40231 do not target Stat1 and Stat5. A comparison of the bands was made between T-Stat1 (total Stat1) and p-Stat1 and between T-Stat5 (total Stat5) and p-Stat5 of each tumor treated with PEI, T40214, T40231 and paclitaxel, respectively. Results demonstrate an absence of inhibition of Stat1 and Stat5 activation in GQ-ODN T40214- and T40231-treated NSCLC tumors (Fig. 3C). These results from tumor tissues are consistent with that obtained from NSCLC cells.

Tumor apoptosis and angiogenesis. We set out to determine if suppression of tumor-growth by GQ-ODN T40214 and T40231 was associated with an increase in apoptosis and reduction in angiogenesis in tumors. The TUNEL assay based on labeling the apoptotic cells with cleaved DNA fragments at the single cell level was performed to quantify apoptosis in tumors and light microscopy was used for data analysis. The apoptotic tumor cells were stained dark brown via TUNEL-positive staining, and the normal tumor cells remained unstained. Results show significant apoptosis in NSCLC tumors treated by GQ-ODN T40214 (Fig. 4A, right panel), when compared with NSCLC tumors treated by PEI alone (Fig. 4A, left panel). The analyses of the TUNEL-positive cells among total cells indicated that the percentage of apoptotic cells in PEI-treated tumors was 1.9% while that in T40214-treated tumors increased to 21.1% ($p<0.0002$, Wilcoxin rank sum test) (Fig. 4A, bottom panel).

VEGF staining was performed using immunohistochemistry with peroxidase-labeled secondary antibodies; negative controls (first incubation step, without primary antibody) were also included. When no staining was observed, the result was considered negative, whereas, moderate staining in the majority of the cells was considered positive. Slides were incubated with a mouse anti-VEGF monoclonal antibody. VEGF was highly expressed in the tissue of NSCLC tumors treated by PEI alone (the cycled areas) (Fig. 4B, left panel); however, VEGF was not observed in the tumors treated by GQ-ODN (Fig. 4B, right panel). These observations are consistent with the Western blotting results, which indicate that the expression of VEGF was totally blocked in GQ-ODN-treated tumors, but not in PEI-treated tumors. Microscopy with H&E staining clearly showed GQ-ODN-treatment to cause tumor cell shrinkage with chromatin condensation and partial necrosis (Fig. 4C, right panel); in contrast, PEI-treatment did not result in such changes in tumors (Fig. 4C, left panel).

Discussion

Although chemotherapy provides a clinically significant benefit for patients with advanced NSCLC, the improvement of survival for these patients is only modest (21); thus, there is a need to search for novel therapeutics. Haura *et al* showed that p-Stat3 was highly expressed in 54% of NSCLC primary tumors, suggesting that Stat3 is a promising molecular target for lung cancer (22). Our results show that when GQ-ODN was incubated with NSCLC cells for 24 h, T40214 selectively inhibited Stat3 phosphorylation. Moreover, GQ-ODN T40214 did not inhibit the activation of JAK kinases, the upstream proteins of STAT. In addition, our results in cell and tumor clearly show that GQ-ODN selectively inhibits the activation of Stat3, but not Stat1 and Stat5, both *in vitro* and *in vivo*. The selective inhibition of Stat3 activation for GQ-ODN *in vivo*

is considered beneficial to prospective clinical studies with regard to GQ-ODN since this selective targeting of Stat3 becomes a key factor in the development of a potent Stat3 inhibitor. Independent of Stat3, Stat1 and Stat5 are also active in many human cancers (5). Stat5-induced cell survival promotion has a potent oncogenic role similar to Stat3 (21). Stat1, which acts in a pro-apoptotic and anti-proliferative manner, seems to be a tumor suppressor whose functions totally differ from those of Stat3 (22,23).

In our previous studies (14,16), we demonstrated that GQ-ODN predominantly interacts with the p-Stat3 dimer in the range of amino acid residues 638 to 652, within the SH2 domains. The selective inhibition of p-Stat3 activity by GQ-ODN is based upon a few critical residues that form a local structure different from that of p-Stat1 dimer. In the p-Stat3 dimer, the paired residues of Q643 and N646 repel one another to form a channel conformation, in which GQ-ODN is held by seven H-bonds. However, the corresponding paired-residues of Stat1 dimer, K637 and S640, lock the dimer together; thereby, blocking the interaction of GQ-ODN with Stat1. Destabilizing the complex between p-Stat3 dimer and DNA is a critical step for the dephosphorylation of p-Stat3 by GQ-ODN. GQ-ODN T40214 promotes p-Stat3 dephosphorylation by blocking DNA binding to p-Stat3 dimer and forming an unstable complex between GQ-ODN T40214 and p-Stat3 dimer (3D model shown in Fig. 5). This unstable complex will dephosphorylate faster than the DNA complex. Computational energy calculation supported this hypothesis. The binding energy for the complexes DNA/p-Stat3 dimer and GQ-ODN T40214/p-Stat3 dimer are -213 kcal/mol and -73 kcal/mol, respectively. This selective inhibition of Stat3 phosphorylation observed in GQ-ODN-treated tumors (Fig. 3) is one of the greatest advantages of GQ-ODN as an anti-cancer drug.

We have demonstrated that T40214 and its analog T40231 totally blocked p-Stat3 and its downstream target proteins, including anti-apoptotic proteins: Bcl-2, Bcl-x_L, Mcl-1, and survivin; inducer of angiogenesis, VEGF; and the proteins for cell proliferation: Cyclin D1, and c-myc in tumor tissue (Fig. 3A). Additionally, we also have demonstrated that GQ-ODN also blocks the transcription of Stat3-regulated genes: Bcl-2, Bcl-x_L, Mcl-1, survivin, and VEGF in tumor tissue (Fig. 3B). To our knowledge, this is the first report to provide *in vivo* evidence of the relationship between Stat3 and its regulated genes and proteins, although it has been observed in cell culture previously (5). The inhibition of Stat3 protein induced a tremendous increase in apoptosis (Fig. 4A) and a concomitant decrease in angiogenesis (Fig. 4B) and cell proliferation in tumors, all of which strongly deter tumor growth. Consequently, the inhibition of Stat3 activation, which significantly promotes apoptosis and reduces angiogenesis and cell proliferation, strongly suppressed tumor growth.

Molecules of JAK/STAT signaling pathways, in particular Stat3, have been validated to be potential targets for cancer therapy and much effort has been made to develop novel anticancer drugs targeting Stat3 (24-49). Our systematic *in vivo* analysis (14,16) has shown that GQ-ODN as an anti-cancer agent selectively targeted Stat3 and significantly suppressed the tumor growth of a variety of tumors in nude mouse xenografts: prostate cancer (p=0.001); breast cancer (p=0.001); head and neck squamous cell carcinoma (HNSCC) (p<0.001); and NSCLC (p=0.002). This demonstrates that GQ-ODN has the capacity to be a potent Stat3 inhibitor, and represents a novel and promising class of anti-cancer drug in the treatment of metastatic human tumors.

Acknowledgments

The authors wish to thank Maryann Mastrangelo for assisting in immuno-histochemistry and Judy Young for assisting in the revision of the manuscript. This study was in part supported by R01 CA104035, SPORE CA97007, SPORE CA58204 (to NJ) and DOD W81XWH-04-1-0142 (to LM).

References

1. Stewart BW and Kleihues P: Lung Cancer. World Cancer Report. IARC Press, Lyon, France, 2003.
2. Greenlee RT, Murray T, Bolden S and Wingo PA: Cancer statistics, 2000. CA Cancer J Clin 50: 7-33, 2000.
3. Cohen V and Khuri FR: Chemoprevention of lung cancer: current status and future prospects. Cancer Metastasis Rev 21: 349-362, 2002.
4. Ginsberg RJ, Goldberg M and Waters PF: Surgery in non-small cell lung cancer. In: Thoracic Oncology. Roth JA RJ, Weisenburger TH (eds). 2nd edition. W.B. Saunders Company, Philadelphia, PA, pp124-126, 1995.
5. Yu H and Jove R: The STATs of cancer - new molecular targets come of age. Nat Rev Cancer 4: 97-105, 2004.
6. Darnell JE Jr: STATs and gene regulation. Science 277: 1630-1635, 1997.
7. Becker S, Groner B and Muller CW: Three-dimensional structure of the Stat3beta homodimer bound to DNA. Nature 394: 145-151, 1998.
8. Chen X, Vinkemeier U, Zhao Y, Jeruzalmi D, Darnell JE Jr and Kuriyan J: Crystal structure of a tyrosine phosphorylated STAT-1 dimer bound to DNA. Cell 93: 827-839, 1998.
9. Buettner R, Mora LB and Jove R: Activated STAT signaling in human tumors provides novel molecular targets for therapeutic intervention. Clin Cancer Res 8: 945-954, 2002.
10. Mora LB, Buettner R, Seigne J, Diaz J, Ahmad N, Garcia R, Bowman T, Falcone R, Fairclough R, Cantor A, Muro-Cacho C, Livingston S, Karras J, Pow-Sang J and Jove R: Constitutive activation of Stat3 in human prostate tumors and cell lines: direct inhibition of Stat3 signaling induces apoptosis of prostate cancer cells. Cancer Res 62: 6659-6666, 2002.
11. Dolled-Filhart M, Camp RL, Kowalski DP, Smith BL and Rimm DL: Tissue microarray analysis of signal transducers and activators of transcription 3 (Stat3) and phospho-Stat3 (Tyr705) in node-negative breast cancer shows nuclear localization is associated with a better prognosis. Clin Cancer Res 9: 594-600, 2003.
12. Nagpal JK, Mishra R and Das BR: Activation of Stat-3 as one of the early events in tobacco chewing-mediated oral carcinogenesis. Cancer 94: 2393-2400, 2002.
13. Song L, Turkson J, Karras JG, Jove R and Haura EB: Activation of Stat3 by receptor tyrosine kinases and cytokines regulates survival in human non-small cell carcinoma cells. Oncogene 22: 4150-4165, 2003.
14. Jing N, Li Y, Xiong W, Sha W, Jing L and Tweardy DJ: G-quartet oligonucleotides: a new class of signal transducer and activator of transcription 3 inhibitors that suppresses growth of prostate and breast tumors through induction of apoptosis. Cancer Res 64: 6603-6609, 2004.
15. Jing N, Sha W, Li Y, Xiong W and Tweardy DJ: Rational drug design of G-quartet DNA as anti-cancer agents. Curr Pharm Des 11: 2841-2854, 2005.
16. Jing N, Zhu Q, Yuan P, Li Y, Mao L and Tweardy DJ: Targeting signal transducer and activator of transcription 3 with G-quartet oligonucleotides: a potential novel therapy for head and neck cancer. Mol Cancer Ther 5: 279-286, 2006.
17. Zhong M, Henriksen MA, Takeuchi K, Schaefer O, Liu B, ten Hoeve J, Ren Z, Mao X, Chen X, Shuai K and Darnell JE Jr: Implications of an antiparallel dimeric structure of nonphosphorylated STAT1 for the activation-inactivation cycle. Proc Natl Acad Sci USA 102: 3966-3971, 2005.

18. Darnell JE: Validating Stat3 in cancer therapy. Nat Med 11: 595-596, 2005.
19. Feng L, Garcia GE, Yang Y, Xia Y, Gabbai FB, Peterson OW, Abraham JA, Blantz RC and Wilson CB: Heparin-binding EGF-like growth factor contributes to reduced glomerular filtration rate during glomerulonephritis in rats. J Clin Invest 105: 341-350, 2000.
20. Chen S, Bacon KB, Li L, Garcia GE, Xia Y, Lo D, Thompson DA, Siani MA, Yamamoto T, Harrison JK and Feng L: *In vivo* inhibition of CC and CX3C chemokine-induced leukocyte infiltration and attenuation of glomerulonephritis in Wistar-Kyoto (WKY) rats by vMIP-II. J Exp Med 188: 193-198, 1998.
21. Debierre-Grockiego F: Anti-apoptotic role of STAT5 in haematopoietic cells and in the pathogenesis of malignancies. Apoptosis 9: 717-728, 2004.
22. Reck M and Gatzemeier U: Chemotherapy in stage-IV NSCLC. Lung Cancer 45 (suppl 2): S217-S222, 2004.
23. O'Shea JJ, Gadina M and Schreiber RD: Cytokine signaling in 2002: new surprises in the Jak/Stat pathway. Cell 109 (suppl): S121-S131, 2002.
24. Turkson J, Ryan D, Kim JS, Zhang Y, Chen Z, Haura E, Laudano A, Sebti S, Hamilton AD and Jove R: Phosphotyrosyl peptides block Stat3-mediated DNA binding activity, gene regulation, and cell transformation. J Biol Chem 276: 45443-45455, 2001.
25. Stahl N, Farruggella TJ, Boulton TG, Zhong Z, Darnell JE Jr and Yancopoulos GD: Choice of STATs and other substrates specified by modular tyrosine-based motifs in cytokine receptors. Science 267: 1349-1353, 1995.
26. Shao H, Cheng HY, Cook RG and Tweardy DJ: Identification and characterization of signal transducer and activator of transcription 3 recruitment sites within the epidermal growth factor receptor. Cancer Res 63: 3923-3930, 2003.
27. Wiederkehr-Adam M, Ernst P, Muller K, Bieck E, Gombert FO, Ottl J, Graff P, Grossmuller F and Heim MH: Characterization of phosphopeptide motifs specific for the Src homology 2 domains of signal transducer and activator of transcription 1 (STAT1) and STAT3. J Biol Chem 278: 16117-16128, 2003.
28. Coleman DR, Ren Z, Mandal PK, Cameron AG, Dyer GA, Muranjan S, Campbell M, Chen X and McMurray JS: Investigation of the binding determinants of phosphopeptides targeted to the SRC homology 2 domain of the signal transducer and activator of transcription 3. Development of a high-affinity peptide inhibitor. J Med Chem 48: 6661-6670, 2005.
29. Grandis JR, Drenning SD, Zeng Q, Watkins SC, Melhem MF, Endo S, Johnson DE, Huang L, He Y and Kim JD: Constitutive activation of Stat3 signaling abrogates apoptosis in squamous cell carcinogenesis *in vivo*. Proc Natl Acad Sci USA 97: 4227-4232, 2000.
30. Niu G, Shain KH, Huang M, Ravi R, Bedi A, Dalton WS, Jove R and Yu H: Overexpression of a dominant-negative signal transducer and activator of transcription 3 variant in tumor cells leads to production of soluble factors that induce apoptosis and cell cycle arrest. Cancer Res 61: 3276-3280, 2001.
31. Epling-Burnette PK, Liu JH, Catlett-Falcone R, Turkson J, Oshiro M, Kothapalli R, Li Y, Wang JM, Yang-Yen HF, Karras J, Jove R and Loughran TP Jr: Inhibition of STAT3 signaling leads to apoptosis of leukemic large granular lymphocytes and decreased Mcl-1 expression. J Clin Invest 107: 351-362, 2001.
32. Leong PL, Andrews GA, Johnson DE, Dyer KF, Xi S, Mai JC, Robbins PD, Gadiparthi S, Burke NA, Watkins SF and Grandis JR: Targeted inhibition of Stat3 with a decoy oligonucleotide abrogates head and neck cancer cell growth. Proc Natl Acad Sci USA 100: 4138-4143, 2003.
33. Meydan N, Grunberger T, Dadi H, Shahar M, Arpaia E, Lapidot Z, Leeder JS, Freedman M, Cohen A, Gazit A, Levitzki A and Roifman CM: Inhibition of acute lymphoblastic leukaemia by a Jak-2 inhibitor. Nature 379: 645-648, 1996.
34. Faderl S, Ferrajoli A, Harris D, Van Q, Priebe W and Estrov Z: WP-1034, a novel JAK-STAT inhibitor, with proapoptotic and antileukemic activity in acute myeloid leukemia (AML). Anticancer Res 25: 1841-1850, 2005.
35. Blaskovich MA, Sun J, Cantor A, Turkson J, Jove R and Sebti SM: Discovery of JSI-124 (cucurbitacin I), a selective Janus kinase/signal transducer and activator of transcription 3 signaling pathway inhibitor with potent antitumor activity against human and murine cancer cells in mice. Cancer Res 63: 1270-1279, 2003.
36. Rajasingh J, Raikwar HP, Muthian G and Johnson C: Curcumin induces growth-arrest and apoptosis in association with the inhibition of constitutively active JAK-STAT pathway in T cell leukemia. Biochem Biophys Res Commun 340: 359-368, 2006.
37. Shi X, Franko B, Frantz C, Amin HM and Lai R: JSI-124 (cucurbitacin I) inhibits Janus kinase-3/signal transducer and activator of transcription-3 signalling, downregulates nucleophosmin-anaplastic lymphoma kinase (ALK), and induces apoptosis in ALK-positive anaplastic large cell lymphoma cells. Br J Haematol 135: 26-32, 2006.
38. Song L, Morris M, Bagui T, Lee FY, Jove R and Haura EB: Dasatinib (BMS-354825) selectively induces apoptosis in lung cancer cells dependent on epidermal growth factor receptor signaling for survival. Cancer Res 66: 5542-5548, 2006.
39. Lee YK, Isham CR, Kaufman SH and Bible KC: Flavopiridol disrupts STAT3/DNA interactions, attenuates STAT3-directed transcription, and combines with the Jak kinase inhibitor AG490 to achieve cytotoxic synergy. Mol Cancer Ther 5: 138-148, 2006.
40. Chakravarti N, Myers JN and Aggarwal BB: Targeting constitutive and interleukin-6-inducible signal transducers and activators of transcription 3 pathway in head and neck squamous cell carcinoma cells by curcumin (diferuloylmethane). Int J Cancer 119: 1268-1275, 2006.
41. Cuevas P, Diaz-Gonzalez D, Sanchez I, Lozano RM, Gimenez-Gallego G and Dujovny M: Dobesilate inhibits the activation of signal transducer and activator of transcription 3, and the expression of cyclin D1 and bcl-XL in glioma cells. Neurol Res 28: 127-130, 2006.
42. Kotha A, Sekharam M, Cilenti L, Siddiquee K, Khaled A, Zervos AS, Carter B, Turkson J and Jove R: Resveratrol inhibits Src and Stat3 signaling and induces the apoptosis of malignant cells containing activated Stat3 protein. Mol Cancer Ther 5: 621-629, 2006.
43. Amit-Vazina M, Shishodia S, Harris D, Van Q, Wang M, Weber D, Alexanian R, Talpaz M, Aggarwal BB and Estrov Z: Atiprimod blocks STAT3 phosphorylation and induces apoptosis in multiple myeloma cells. Br J Cancer 93: 70-80, 2005.
44. Nam S, Buettner R, Turkson J, Kim D, Cheng JQ, Muehlbeyer S, Hippe F, Vatter S, Merz KH, Eisenbrand G and Jove R: Indirubin derivatives inhibit Stat3 signaling and induce apoptosis in human cancer cells. Proc Natl Acad Sci USA 102: 5998-6003, 2005.
45. Venkatasubbarao K, Choudary A and Freeman JW: Farnesyl transferase inhibitor (R115777)-induced inhibition of STAT3(Tyr705) phosphorylation in human pancreatic cancer cell lines require extracellular signal-regulated kinases. Cancer Res 65: 2861-2871, 2005.
46. Sun J, Blaskovich MA, Jove R, Livingston SK, Coppola D and Sebti SM: Cucurbitacin Q: a selective STAT3 activation inhibitor with potent antitumor activity. Oncogene 24: 3236-3245, 2005.
47. Turkson J, Zhang S, Palmer J, Kay H, Stanko J, Mora LB, Sebti S, Yu H and Jove R: Inhibition of constitutive signal transducer and activator of transcription 3 activation by novel platinum complexes with potent antitumor activity. Mol Cancer Ther 3: 1533-1542, 2004.
48. Barton BE, Murphy TF, Shu P, Huang HF, Meyenhofer M and Barton A: Novel single-stranded oligonucleotides that inhibit signal transducer and activator of transcription 3 induce apoptosis *in vitro* and *in vivo* in prostate cancer cell lines. Mol Cancer Ther 3: 1183-1191, 2004.
49. Bharti AC, Donato N and Aggarwal BB: Curcumin (diferuloylmethane) inhibits constitutive and IL-6-inducible STAT3 phosphorylation in human multiple myeloma cells. J Immunol 171: 3863-3871, 2003.

Annals of Oncology Advance Access published March 23, 2011

original article

Annals of Oncology
doi:10.1093/annonc/mdr036

The impact of phosphorylated AMP-activated protein kinase expression on lung cancer survival

W. N. William[1†], J.-S. Kim[1†], D. D. Liu[2], L. Solis[3], C. Behrens[1], J. J. Lee[2], S. M. Lippman[1], E. S. Kim[1], W. K. Hong[1], I. I. Wistuba[1,3] & H.-Y. Lee[1,4*]

Departments of [1]Thoracic/Head & Neck Medical Oncology; [2]Biostatistics; [3]Pathology, The University of Texas MD Anderson Cancer Center, Houston, USA; [4]College of Pharmacy, Seoul National University, Seoul, Republic of Korea

Received 11 November 2010; revised 18 January 2011; accepted 21 January 2011

Background: The aim of this study is to investigate the prognostic role of phosphorylated AMP-activated protein kinase (pAMPK) in surgically resected non-small-cell lung cancer (NSCLC).
Methods: Immunohistochemical staining of pAMPK was carried out on tissue microarrays containing 463 samples obtained from patients with NSCLC and correlated with clinicopathological characteristics and survival.
Results: pAMPK expression levels were significantly higher in never smokers versus former smokers versus current smokers ($P = 0.045$). A positive pAMPK expression was associated with increased overall survival (OS) and recurrence-free survival (RFS) ($P = 0.0009$ and $P = 0.0007$, respectively). OS and RFS were statistically superior in pAMPK-positive than in pAMPK-negative patients with adenocarcinoma (ADC; median OS: 5.6 and 4.2 years, respectively, $P = 0.0001$; median RFS: 5.0 and 2.4 years, respectively, $P = 0.001$), whereas they were similar in those patients with squamous cell carcinoma. Multivariate analysis confirmed that pAMPK positivity was associated with OS [hazard ratio (HR) = 0.574, 95% confidence interval (CI) 0.418–0.789, P = 0.0006) and RFS (HR = 0.608, 95% CI 0.459–0.807, and P = 0.0006), independent of clinical covariates.
Conclusions: High pAMPK expression levels are associated with increased survival in patients with NSCLC, especially those with ADC. Our results support further evaluation of AMP-activated protein kinase as a potential prognostic and therapeutic target for lung cancer.
Key words: AMP-activated protein kinase, LKB1, non-small-cell lung cancer, tobacco smoking

introduction

Lung cancer is a leading cause of cancer death worldwide. Non-small-cell lung cancer (NSCLC) accounts for ~75%–80% of lung cancer cases and carries a 5-year survival rate of ~10%–15% for all stages. Unfortunately, most patients with NSCLC are diagnosed in an advanced stage with local or distant metastases. Therefore, development of new therapeutic strategies is urgently needed for the treatment of NSCLC. Because cancer has been envisioned as a signaling disease, identification of biochemical signaling molecules that have a critical role in cell growth, survival, and metabolism would provide valuable prognostic and predictive biomarkers for the strategies.

In the past few years, several lines of evidence implicate AMP-activated protein kinase (AMPK) in many human malignancies, including NSCLC. AMPK is a serine/threonine protein kinase that acts as a cellular fuel sensor and intermediary metabolism regulator. AMPK is allosterically activated under conditions that decrease the ATP : AMP ratio, such as glucose deprivation, hypoxia, ischemia, and heat shock [1]. AMPK is also activated by phosphorylation following activation of the upstream serine/threonine kinase LKB1 [2] or of other receptor-mediated signal transduction cascades by extracellular hormonal stimuli such as adiponectin [3] and leptin [4]. AMPK has been suggested as a key cellular fuel sensor and may couple energy metabolism with cell proliferation. Once activated, AMPK phosphorylates and inactivates several metabolic enzymes involved in ATP-consuming events (e.g. synthesis of fatty acids, cholesterol, and protein) and activates metabolic pathways involved in ATP production (e.g. glucose uptake, glucose and fatty acid oxidation) [5].

Researchers have recently implied that AMPK is involved in carcinogenesis. AMP-mimetic 5-aminoimidazole-4-carboxamide ribonucleoside (AICAR) is a potent AMPK activator that can inhibit the proliferation of various cancer cell lines *in vitro* and *in vivo* by increasing $p21^{CIP}$, $p27^{KIP}$, and p53 levels and attenuating Akt and mammalian target of rapamycin (mTOR) phosphorylation [6–8]. The mTOR pathway integrates nutrient and mitogen signals to regulate cell growth and division by stimulating the initiation of translation [9], and activation of AMPK can suppress mTOR signaling by hormones and amino acids [7], leading to

*Correspondence to: Dr H.-Y. Lee, College of Pharmacy, Seoul National University, 599 Gwanak-ro, Gwanak-gu, Seoul 151-742, Republic of Korea. Tel:+82-2-880-9277; Fax: +82-2-880-6988; E-mail: hylee135@snu.ac.kr

†These two authors equally contributed to this work

impairment of cell growth and proliferation by down-regulating protein synthesis [9]. The relationship between AMPK and LKB1, which functions as a tumor suppressor [10], further supports its potential role in carcinogenesis. Mutated *Lkb1* loses its kinase activity and impairs downstream signaling of AMPK, leading to unsuppressed cell proliferation [11]. *Lkb1* is mutated in patients with Peutz–Jeghers syndrome, who have an increased risk of cancer (including lung cancer) [12]. Sporadic mutations of the *Lkb1* gene occur in up to 34% of patients with lung adenocarcinomas (ADCs) [13, 14].

In fact, surprisingly little is known about the role of phosphorylated AMP-activated protein kinase (pAMPK) in NSCLC. In this context, we designed the current study to address this paucity of translational information. Here, we sought to identify the expression of pAMPK in lung tumor samples in a large patient cohort and to correlate the expression pattern of pAMPK with clinicopathological data and patient survival.

methods

case selection and tissue microarray construction

Archived, formalin-fixed paraffin-embedded (FFPE) tumor samples resected from patients with NSCLC were obtained from previously described tissue banks at The University of Texas MD Anderson Cancer Center [15]. Samples obtained from patients with available staging information were included in our analysis ($N = 463$). The tissue samples were collected from 1997 to 2005 and classified using the 2004 World Health Organization classification system. The patients' baseline characteristics are listed in Table 1. Tissue microarrays (TMAs) containing three 1-mm-diameter cores from each tumor were constructed. The TMAs were prepared using a manual tissue arrayer (Advanced Tissue Arrayer ATA100; Chemicon International, Temecula, CA). A chart review was carried out to retrieve detailed clinical and pathological information, including demographic data, smoking history, pathologic TNM (tumor–node–metastasis) stage [16], and overall survival (OS) and recurrence-free survival (RFS) duration.

immunohistochemistry

Expression of pAMPK was measured via immunostaining with an anti-pAMPKα antibody (Thr172; Cell Signaling Technology, Danvers, MA) at a dilution of 1 : 100. Five-micron-thick FFPE TMA histological sections of the samples were deparaffinized, hydrated, heated in a steamer for 10 min with 10 mM sodium citrate (pH 6.0) for antigen retrieval, and washed in Tris buffer. Peroxide blocking was carried out with 3% H_2O_2 in methanol at room temperature for 15 min followed by 10% bovine serum albumin in Tris-buffered saline with Tween 20 for 30 min at room temperature. The slides were incubated with a primary antibody at room temperature; afterward, they were washed with phosphate-buffered saline (PBS) and then incubated with a biotin-labeled secondary antibody for 30 min. Finally, the samples were incubated with a 1 : 40 solution of streptavidin–peroxidase for 30 min. The stains were then developed with 0.05% 3′,3-diaminobenzidine tetrahydrochloride that had been freshly prepared in 0.05 mol/l Tris buffer (pH 7.6) containing 0.024% H_2O_2 and then counterstained with hematoxylin, dehydrated, and mounted. FFPE lung tissue samples containing normal bronchial epithelia were used as positive controls. Also, the primary antibody in each positive control was replaced with PBS; the resulting samples were used as negative controls.

scoring of pAMPK expression in TMAs

pAMPK expression was predominantly detected in the cytoplasm of tumor cells (Figure 1). The expression of pAMPK was quantified by two independent observers (CB and IIW) who were unaware of the patients' outcomes. Cytoplasmic expression of pAMPK was quantified using a four-value intensity score (0, 1+, 2+, and 3+) and the percentage of the extent of reactivity. Next, the cytoplasmic expression score was calculated by multiplying the intensity and reactivity extension values (range 0–300). Tumors with pAMPK score >1 were considered positive staining.

statistical analysis

Summary statistical analysis of pAMPK expression levels was carried out according to patient baseline characteristics. Associations between categorical variables were assessed by χ^2 test or Fisher's exact test. The Wilcoxon rank sum test or Kruskal–Wallis test was used to compare pAMPK expression in different subgroups defined by categorical variables, such as gender or smoking history, when appropriate. Spearman's rank correlation coefficient was used to estimate the correlation between age and pAMPK expression score. The OS and RFS durations in patients positive and negative for pAMPK expression were estimated using the Kaplan–Meier method and compared using the log-rank test. Cox proportional hazards models were used for multivariate analysis of the prognostic impact of pAMPK positivity, adjusting for other important covariates, such as age, gender, histology, pathologic stage and adjuvant/neoadjuvant treatment. All the statistical tests carried out were two sided, and P values ≤0.05 were considered statistically significant.

role of the funding source

The funding sources had no role in the study design, data analysis, data interpretation, or writing of this report. The corresponding author had full access to all data and final responsibility for the decision to submit for publication.

results

pAMPK expression in TMAs

There were significantly more female patients ($P = 0.0032$, χ^2 square test) and never smokers ($P < 0.0001$, Fisher's exact test) in patients with ADC (Table 1). The numbers of patients who received adjuvant and/or neoadjuvant treatment were similar between histologies ($P = 0.87$). The proportion of pN0 was not statistically different between histologies ($P = 0.20$). The cytoplasmic pAMPK expression according to the patients' baseline characteristics is listed in Table 2. We observed no statistically significant differences in the distribution of pAMPK score according to cancer type, race, tumor stage, nodal status, adjuvant or neoadjuvant treatment, sex, or age. pAMPK expression levels were significantly higher in never smokers than in former and current smokers [$P = 0.0319$ (Wilcoxon rank sum test)]. The direction was consistent when we carried out the analysis after stratification of the pAMPK expression scores according to sex (data not shown). We observed that 65.2% (195 of 299) of the patients with ADC and 73.8% (121 of 164) of those with squamous cell carcinoma (SCC) had positive pAMPK expression scores, a difference that was not statistically significant [Table 2; $P = 0.058$ (χ^2 test)].

survival

After a median follow-up duration of 4.1 years for the censored observations (data cut-off: September 2010), the median OS duration was 5.6 years and the 3- and 5-year survival rates were 76.1% [95% confidence interval (CI) 71.5% to 81.1%] and 59.9% (95% CI 53.8% to 66.8%), respectively, in patients with positive pAMPK expression scores. In comparison, the median OS duration was 4.1 years and the 3- and 5-year survival rates were 62.1% (95% CI 54.6% to 70.7%) and 40.9% (95% CI

Table 1. Patients' characteristics

Feature	NSCLC histologic type[a]			
	Adenocarcinoma ($n = 299$), n (%)	Squamous carcinoma ($n = 164$), n (%)	P value	Total ($N = 463$), n (%)
Median age (range), years	65 (32–89)	68 (44–90)	0.0353	66 (32–89)
Sex			0.0032	
Male	134 (44.8)	97 (59.1)		232 (50.1)
Female	165 (55.2)	67 (40.9)		231 (49.9)
Smoking status[b]			<0.0001	
Never	48 (16.1)	1 (0.6)		49 (10.6)
Former	133 (44.5)	79 (48.2)		212 (45.8)
Current	118 (39.5)	84 (51.2)		202 (43.6)
Race			0.87	
Caucasian	273 (91.3)	149 (90.9)		422 (91.1)
Others	26 (8.7)	15 (9.1)		41 (8.9)
(Neo)adjuvant treatment			0.0159	
No	140 (46.8)	73 (44.5)		213 (46.0)
Adjuvant	19 (6.4)	21 (12.8)		40 (8.6)
Neoadjuvant	84 (28.1)	45 (27.4)		129 (27.9)
Both	26 (8.7)	5 (3.0)		31 (6.7)
Unknown	30 (10.0)	20 (12.2)		50 (10.8)
T category[c]			0.35	
1	120 (40.1)	58 (35.4)		178 (38.4)
2	145 (48.5)	85 (51.8)		230 (49.7)
3	11 (3.7)	11 (6.7)		22 (4.8)
4	23 (7.7)	10 (6.1)		33 (7.1)
N category[c]			0.0460	
0	214 (71.8)	107 (65.6)		321 (69.6)
1	42 (13.8)	37 (22.7)		78 (16.9)
2	43 (14.4)	19 (11.7)		62 (13.4)
x	1 (0.3)	1 (0.6)		2 (0.4)
Final stage[c]			0.25	
I	184 (61.5)	93 (56.7)		277 (59.8)
II	82 (27.4)	58 (35.4)		140 (30.2)
III	21 (7.0)	10 (6.1)		31 (6.7)
IV	12 (4.0)	3 (1.8)		15 (3.2)

Never smoker: an adult who has never smoked or who has smoked <100 cigarettes in his or her lifetime; former smoker: an adult who has smoked at least 100 cigarettes in his or her lifetime but who had quit smoking at the time of interview; current smoker: an adult who has smoked 100 cigarettes in his or her lifetime and who currently smokes cigarettes.

[a]Values are number of cases unless otherwise indicated.

[b]Smoking history was assigned based on the CDC definitions (http://www.cdc.gov/nchs/nhis/tobacco/tobacco_glossary.htm, accessed on 29 June 2010).

[c]According to the American Joint Committee on Cancer Staging Manual sixth edition.

CDC, Center for Disease Control and Prevention; N, node; NSCLC, non-small-cell lung cancer; T, tumor.

32.3% to 51.9%), respectively, in patients with negative pAMPK expression scores. The unadjusted hazard ratio (HR) for death associated with positive pAMPK expression scores was 0.615 [95% CI 0.460–0.822; $P = 0.0009$ (log-rank test)] (Figure 2A). Similarly, the 5-year RFS rate was 26.7% in patients with negative pAMPK expression scores versus 46.1% in patients with positive pAMPK expression scores [HR 0.642 (95% CI 0.496–0.831); $P = 0.0007$ (log-rank test)] (Figure 2B). Interestingly, OS durations were longer in patients with ADC who had positive pAMPK expression scores than in those who had negative pAMPK scores (median OS duration: 5.6 and 4.2 years, respectively; $P = 0.0001$) (Figure 3A). We also observed a significant difference in RFS durations in patients with ADC who had positive and negative pAMPK expression scores (median RFS duration: 5.0 and 2.4 years, respectively; $P = 0.001$) (Figure 3C), whereas OS and RFS were similar but not significantly different between negative and positive pAMPK groups in patients with SCC (Figure 3B and D). We observed no similar interactions of pAMPK expression with sex or smoking history (data not shown).

We carried out a multivariate analysis to determine whether the pAMPK expression level was an independent prognostic factor in the study population. Younger age, female sex, and earlier stage were all associated with increased OS duration, thus validating our retrospectively selected cohort of patients. Adjuvant and/or neoadjuvant treatment was not significantly affecting the patient survival. After adjusting for these known prognostic factors, the HR for death in patients with positive

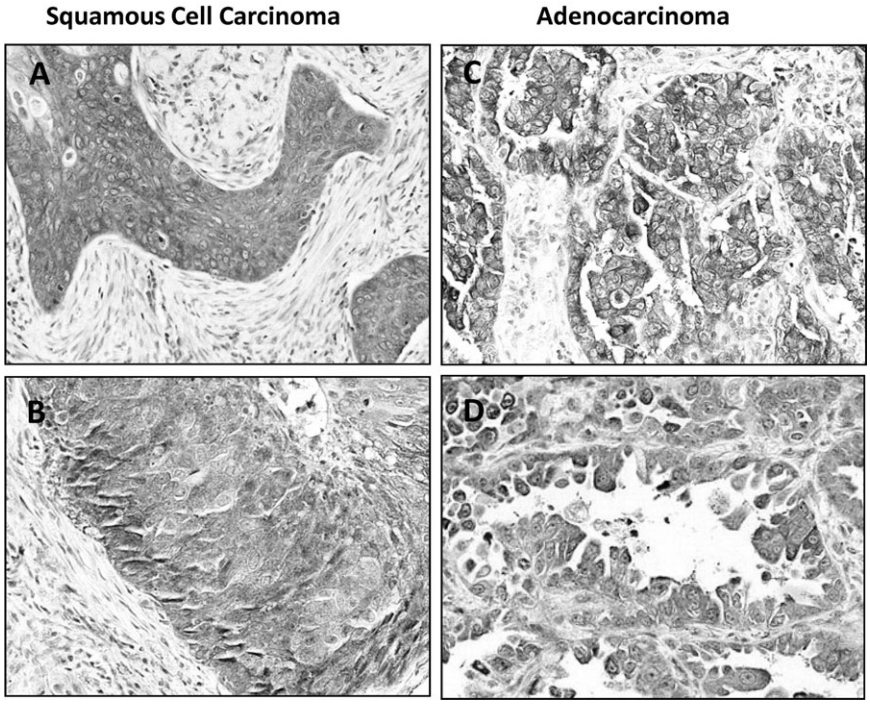

Figure 1. Representative microphotographs of cytoplasmic expression of pAMPK in samples of primary NSCLCs. Expression of pAMPK in SCC and ADC: (A and B) pAMPK staining in SCC with ×100 magnification (A) and ×400 magnification (B); (C and D) pAMPK staining in ADC with ×100 magnification (C) and ×400 magnification (D). pAMPK, phosphorylated AMP-activated protein kinase; NSCLC, non-small-cell lung cancer; SCC, squamous cell carcinoma; ADC, adenocarcinoma.

pAMPK expression scores to that in patients with negative pAMPK expression scores was 0.574 (95% CI 0.418–0.789; $P = 0.0006$) (Table 3). Similarly, the adjusted HR for recurrence in patients with positive pAMPK expression scores to that in patients with negative pAMPK expression scores was 0.608 (95% CI 0.459–0.807; $P = 0.0006$). When we carried out the multivariate analysis in each histology subgroup, the benefit of positive pAMPK was significant in patients with ADC [HR for OS: 0.456 (0.303–0.686), $P = 0.0002$ and HR for RFS: 0.576 (0.403–0.823), $P = 0.0025$] but not significant in patients with SCC (Tables 4 and 5).

discussion

Although growing evidence supports a role of AMPK in human cancers, researchers have placed little emphasis on the prognostic value of AMPK activation. The aim of the present study was to elucidate the potential implications of pAMPK, as a surrogate marker for activated AMPK, in the survival of patients with NSCLC. Notably, we observed that pAMPK expression levels were significantly higher in lung tumors obtained from never smokers than in those obtained from ever smokers. Most importantly, patients with particularly positive expression of pAMPK showed significantly improved survival durations. In our subgroup analysis, we found that the survival benefit of high pAMPK expression may be limited in patients with ADC. These findings indicate that pAMPK is a potential prognostic biomarker for NSCLC patients, especially those with ADC. To our knowledge, this is the first study to examine the expression of pAMPK in a large cohort of patients with NSCLC.

A number of studies in the literature have suggested that AMPK is a key cellular fuel sensor and may couple energy metabolism with cell proliferation. Li et al. [17] demonstrated that induced overexpression of AMPK-b1 inhibited growth of H1299 human lung carcinoma cells. In the study of Han and Roman [18], rosiglitazone (a peroxisome proliferator-activated receptor-γ agonist) had antiproliferative effects that were mediated by peroxisome proliferator-activated receptor-γ-independent activation of AMPK and consequent inhibition of mTOR in H1792 and H1838 human NSCLC cells. Furthermore, our previous study has recently demonstrated that the cancer-preventing properties and proapoptotic activities of deguelin, a natural product with cancer chemopreventive and therapeutic activities, were mediated by activation of AMPK, ultimately leading to inhibition of mTOR and suppression of survivin expression in an *in vitro* model of lung carcinogenesis [8]. While most of these findings support the function of AMPK as a tumor suppressor [8, 17, 19], some studies have suggested that activation of AMPK may protect cells against apoptosis under special conditions, such as metabolic stress [20, 21]. Carretero et al. [11], for example, demonstrated that AMPK has a dual effect on survival of lung cancer cell lines depending on the activation status of the upstream molecule LKB1. They observed that following glucose withdrawal, the AMPK activator AICAR significantly reduced cell death in *Lkb1* wild-type cell lines. In contrast, following glucose deprivation, AICAR did not improve cell viability in lines with an inactivating mutation of *Lkb1*. These results indicate that in the presence of LKB1 signaling, activated AMPK may protect cells against nutrient deprivation-induced apoptosis.

Table 2. Patients' characteristics according to pAMPK expression

	Negative pAMPK (n = 147), n (%)	Positive pAMPK (n = 316), n (%)	P value[a]
Age, median age (range), years	65 (39–87)	66 (32–90)	0.45
Gender			0.47
Female	70 (47.6)	162 (51.2)	
Male	77 (52.4)	154 (48.8)	
Race			0.08
Caucasian	129 (87.8)	293 (92.7)	
Non-Caucasian	18 (12.2)	23 (7.3)	
Histology			0.06
Adenocarcinoma	104 (70.7)	195 (61.7)	
Squamous cell carcinoma	43 (29.3)	121 (38.3)	
Smoking			0.045
Never smoker	10 (6.8)	39 (12.3)	
Former smoker	62 (42.2)	150 (47.5)	
Current smoker	75 (51.0)	127 (40.2)	
(Neo)adjuvant treatment			0.47
No	65 (44.2)	148 (46.8)	
Neoadjuvant	10 (6.8)	30 (9.5)	
Adjuvant	38 (25.9)	91 (28.8)	
Both	13 (8.8)	18 (5.7)	
Unknown	21 (14.3)	29 (9.2)	
T category[b]			0.61
T1	63 (42.9)	115 (36.4)	
T2	68 (46.3)	162 (51.3)	
T3	6 (4.1)	16 (5.1)	
T4	10 (6.8)	23 (7.3)	
N category[b]			0.66
N0	97 (66.9)	224 (70.1)	
N1	26 (17.9)	52 (16.5)	
N2	22 (15.2)	40 (12.7)	
Nx	2 (1.4)	0 (0.0)	
Final stage[b]			0.45
I	82 (55.8)	195 (61.7)	
II	50 (34.0)	90 (28.4)	
III and IV	15 (10.2)	31 (9.8)	

[a]P values are calculated by Wilcoxon rank sum test for age and by chi-square test for all the other variables.

[b]According to the American Joint Committee on Cancer Staging Manual sixth edition.

pAMPK, phosphorylated AMP-activated protein kinase; T, tumor; N, node.

Our attempt to further understand the role of AMPK in lung cancers has led us to evaluate the expression of pAMPK in lung cancer. In a recent study, Conde et al. [22] evaluated the expression of phosphorylated acetyl-CoA carboxylase (pACC), a substrate of active AMPK, by immunohistochemistry (IHC) in surgically resected lung cancer patients (N = 159). The investigators observed elevated pACC expression in patients with ADC than in patients with SCC. Furthermore, they observed significantly longer survival durations in ADC patients with high pACC (96 months) than in those with low pACC (44 months), even though the number of patients was quite small (N = 28 and 18, respectively). Although the result of OS analysis in the whole study population was not statistically significant, their data suggest that pACC might be a clinically relevant prognostic marker for the patients with NSCLC. In the present study, patients with high levels of pAMPK expression exhibited improved RFS. These findings are consistent with the previous report showing a favorable prognostic impact of pACC expression in NSCLC.

We observed a significantly greater expression of pAMPK in never smokers than in smokers. Given the inhibitory function of Akt on AMPK activity [23], one possible explanation for this observation may be via the activation of Akt by tobacco components, including 4-(methylnitrosamino)-1-(3-pyridyl)-1-butanone and nicotine [24]. Interestingly, we observed that elevated pAMPK expression was significantly associated with histological feature of ADC patients. In a recent pivotal trial [25], patients with nonsquamous cell lung cancer exhibited survival benefit from treatment with pemetrexed, which is also known to activate AMPK [26]. This is consistent with the present study and suggests a different role of AMPK according to the histologies.

Given the role of LKB1 in AMPK activation, researchers have assessed LKB1-inactivating mutations in NSCLC. A previous study observed LKB1-inactivating mutations in 34% of patients with lung ADC and 19% of patients with lung SCC (N = 144), although rare in patients with other forms of sporadic cancers [14]. Another report confirmed that LKB1-inactivating mutations were not uncommon in lung cancer cases (18.1% of 188 lung ADC cases) [27]. In general, investigators have frequently detected *Lkb1* mutations in male, white patients, and smokers with ADC [28–30], although the *Lkb1* mutations were not prognostic in those patients. Considering the small number of lung tumor samples analyzed to date, however, cautious interpretation of the associations of *Lkb1* mutation with ethnicity and tobacco exposure in these early studies is warranted. The clinical implication of this finding is that the function of pAMPK *in vivo* may depend on the presence or absence of inactivating *Lkb1* mutations. Unfortunately, one limitation of our study is the lack of information on *Lkb1* mutational status, which could, in conjunction with pAMPK expression, further refine the prognostic roles of these biomarkers and potentially identify the subset of patients for whom pAMPK could serve as a therapeutic target. Also, in this preliminary study, we did not examine the expression levels of downstream effectors of AMPK, which could provide further evidence (or lack thereof) of the functional status of pAMPK. We acknowledge, however, that other molecules of signaling pathways certainly correlate with prognosis as well and may directly or indirectly interact with pAMPK to ultimately determine the natural history of NSCLC. In the future, we plan to expand IHC analyses to include other markers in these samples as well, and results will be reported in future publications.

In summary, this is the first study to investigate the distribution of pAMPK expression in clinical lung tumor samples. We provide evidence of an association of pAMPK expression with increased survival durations in patients with NSCLC. At this point, the biological significance of pAMPK expression will require further studies in cell lines and animal models to better understand the impact of AMPK activation in NSCLC. We also show significantly higher pAMPK expression levels in never smokers than in smokers. While we speculate that AMPK signaling is abrogated in the NSCLC tumors from

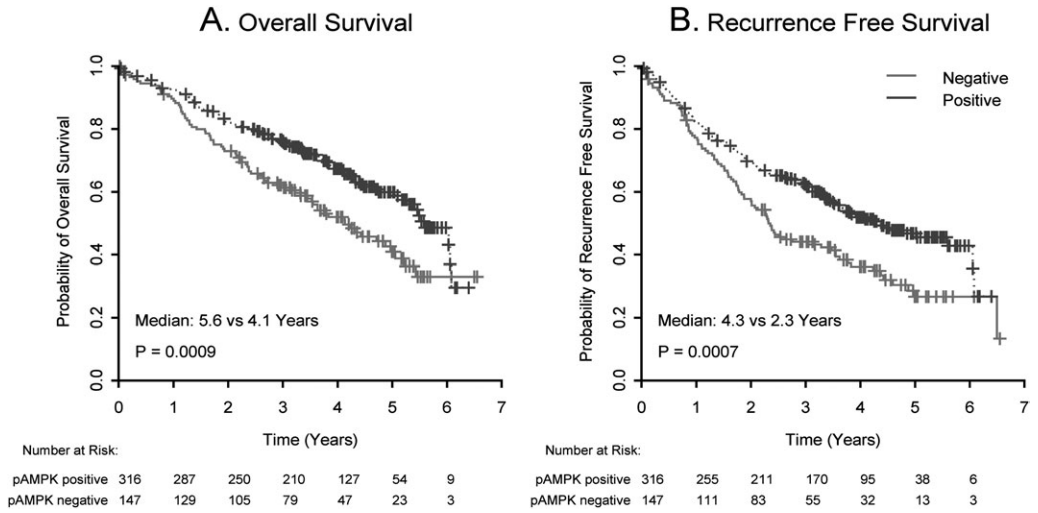

Figure 2. Kaplan–Meier (A) OS and (B) RFS curves for patients with NSCLC who had positive versus negative pAMPK expression scores. Kaplan–Meier curves depicting OS and RFS according to the expression levels of pAMPK. The patient groups were compared using the log-rank test. OS, overall survival; RFS, recurrence-free survival; NSCLC, non-small-cell lung cancer; pAMPK, phosphorylated AMP-activated protein kinase.

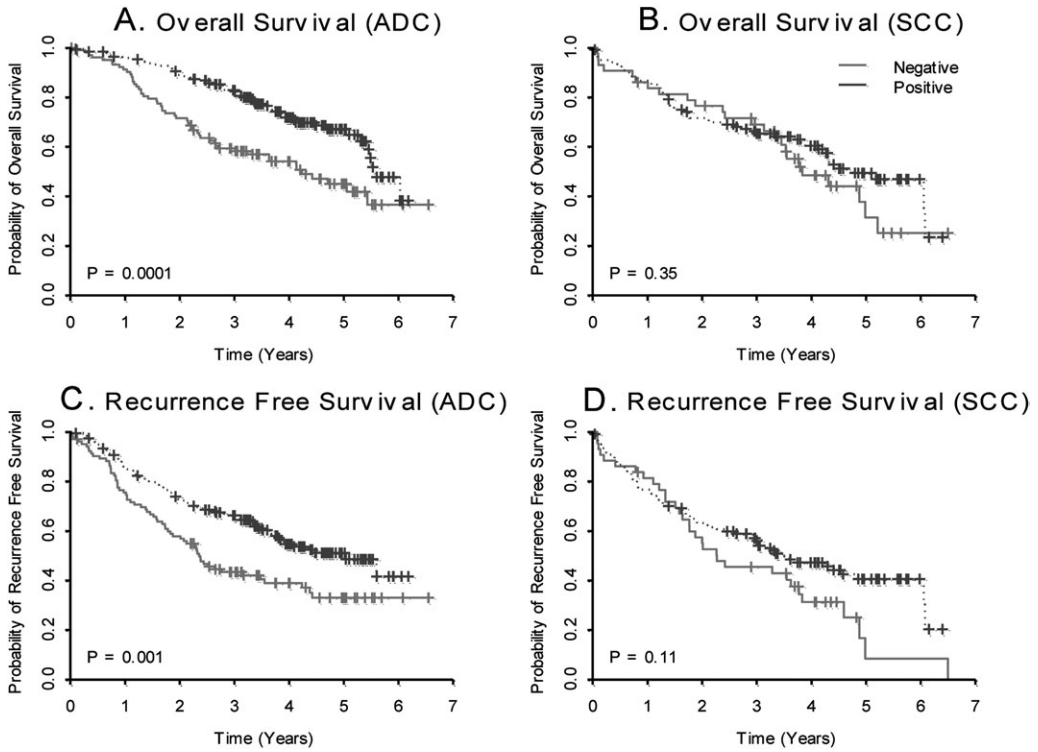

Figure 3. Kaplan–Meier OS curves for patients with (A) ADC versus (B) SCC and RFS curves for patients with (C) ADC versus (D) SCC. Kaplan–Meier curves depicting OS and RFS according to the expression levels of pAMPK in ADC (A and C) and SCC (B and D). The patient groups were compared using the log-rank test. OS, overall survival; ADC, adenocarcinoma; SCC, squamous cell carcinoma; RFS, recurrence-free survival; pAMPK, phosphorylated AMP-activated protein kinase.

nonsmokers, further mechanistic studies will be vital to facilitate our understanding of this phenomenon. In addition, correlation between pAMPK expression and *Lkb1* mutation remains intriguing and potentially important. Further studies are also needed to assess the role of AMPK according to histological subtype of human NSCLC. These efforts should help in determining whether AMPK is a valid prognostic marker and therapeutic target for NSCLC in specific patient subpopulations.

acknowledgements

Contributors—WNW and J-SK, who contributed equally to this work, were involved in the data analysis, interpretation and drafting the article. LS, CB and IIW were involved in the acquisition of data. DDL and JJL were involved in the data analysis and interpretation. SML, ESK, WKH and H-YL were involved in conception and design. All authors were involved in writing or critical review of the draft report and all approved the

Table 3. Multivariate analysis (Cox proportional hazards model) for overall population

Variable	HR for OS (95% CI)	*P* value	HR for RFS (95% CI)	*P* value
Age	1.023 (1.006–1.040)[a]	0.0066	1.019 (1.004–1.033)	0.0108
Histology				
ADC versus SCC	0.706 (0.515–0.969)	0.0313	0.760 (0.575–1.005)	0.0546
Gender				
Male versus female	1.476 (1.081–2.017)	0.0144	1.388 (1.055–1.826)	0.0190
Stage				
II versus I	1.761 (1.238–2.503)	0.0016	1.756 (1.289–2.392)	0.0004
III/IV versus I	2.753 (1.709–4.435)	<0.0001	2.530 (1.624–3.942)	<0.0001
Any treatment versus none	1.228 (0.877–1.718)	0.23	1.344 (0.998–1.810)	0.0519
pAMPK				
Positive versus negative	0.608 (0.444–0.832)	0.0006	0.624 (0.427–0.825)	0.0009

P values are calculated by Cox proportional hazards model.
[a]Risk of death 1.023 times higher for each year increase.
HR, hazard ratio; OS, overall survival; CI, confidence interval; RFS, recurrence-free survival; ADC, adenocarcinoma; SCC, squamous cell carcinoma; pAMPK, phosphorylated AMP-activated protein kinase.

Table 4. Multivariate analysis (Cox proportional hazards model) for OS and RFS in patients with adenocarcinoma ($N = 299$)

Variable	HR for OS (95% CI)	*P* value	HR for RFS (95% CI)	*P* value
Age	1.026 (1.004–1.048)	0.0192	1.020 (1.002–1.039)	0.0317
Gender				
Male versus female	1.909 (1.265–2.880)	0.0021	1.571 (1.106–2.230)	0.0116
Stage				
II versus I	2.154 (1.346–3.445)	0.0014	1.925 (1.288–2.878)	0.0014
III/IV versus I	2.294 (1.247–4.219)	0.0076	2.073 (1.198–3.585)	0.0091
Any treatment versus none	1.056 (0.678–1.644)	0.81	1.324 (0.902–1.945)	0.15
pAMPK				
Positive versus negative	0.459 (0.307–0.688)	0.0002	0.574 (0.402–0.818)	0.0021

P values are calculated by Cox proportional hazards model.
OS, overall survival; RFS, recurrence-free survival; HR, hazard ratio; CI, confidence interval; pAMPK, phosphorylated AMP-activated protein kinase.

Table 5. Multivariate analysis (Cox proportional hazards model) for OS and RFS in patients with squamous cell carcinoma ($N = 164$)

Variable	HR for OS (95% CI)	*P* value	HR for RFS (95% CI)	*P* value
Age	1.016 (0.989–1.044)	0.24	1.012 (0.998–1.035)	0.33
Gender				
Male versus female	1.168 (0.720–1.895)	0.53	1.163 (0.749–1.806)	0.50
Stage				
II versus I	1.416 (0.824–2.433)	0.21	1.615 (0.989–2.635)	0.06
III/IV versus I	3.968 (1.859–8.470)	0.0004	4.158 (1.946–8.882)	0.0002
Any treatment versus none	1.354 (0.797–2.301)	0.26	1.264 (0.787–2.029)	0.33
pAMPK				
Positive versus negative	0.888 (0.523–1.505)	0.66	0.747 (0.470–1.187)	0.22

P values are calculated by Cox proportional hazards model.
OS, overall survival; RFS, recurrence-free survival; HR, hazard ratio; CI, confidence interval; pAMPK, phosphorylated AMP-activated protein kinase.

final version. The authors had full access to the study data and had final responsibility for the decision to submit for publication.

funding

National Institutes of Health (R01 CA109520, CA100816 to H.-Y.L.); Department of Defense (W81XWH-04-1-0142-01-VITAL to W.K.H.); National Institutes of Health through MD Anderson's Cancer Center Support Grant (CA016672).

disclosure

The authors have declared no conflicts of interest.

references

1. Hardie DG, Carling D. The AMP-activated protein kinase—fuel gauge of the mammalian cell? Eur J Biochem 1997; 246: 259–273.
2. Hong SP, Leiper FC, Woods A et al. Activation of yeast Snf1 and mammalian AMP-activated protein kinase by upstream kinases. Proc Natl Acad Sci U S A 2003; 100: 8839–8843.

3. Yamauchi T, Kamon J, Minokoshi Y et al. Adiponectin stimulates glucose utilization and fatty-acid oxidation by activating AMP-activated protein kinase. Nat Med 2002; 8: 1288–1295.
4. Minokoshi Y, Kim YB, Peroni OD et al. Leptin stimulates fatty-acid oxidation by activating AMP-activated protein kinase. Nature 2002; 415: 339–343.
5. Luo Z, Saha AK, Xiang X, Ruderman NB. AMPK, the metabolic syndrome and cancer. Trends Pharmacol Sci 2005; 26: 69–76.
6. Rattan R, Giri S, Singh AK, Singh I. 5-Aminoimidazole-4-carboxamide-1-beta-D-ribofuranoside inhibits cancer cell proliferation in vitro and in vivo via AMP-activated protein kinase. J Biol Chem 2005; 280: 39582–39593.
7. Kimura N, Tokunaga C, Dalal S et al. A possible linkage between AMP-activated protein kinase (AMPK) and mammalian target of rapamycin (mTOR) signalling pathway. Genes Cells 2003; 8: 65–79.
8. Jin Q, Feng L, Behrens C et al. Implication of AMP-activated protein kinase and Akt-regulated survivin in lung cancer chemopreventive activities of deguelin. Cancer Res 2007; 67: 11630–11639.
9. Mamane Y, Petroulakis E, LeBacquer O, Sonenberg N. mTOR, translation initiation and cancer. Oncogene 2006; 25: 6416–6422.
10. Tiainen M, Ylikorkala A, Makela TP. Growth suppression by Lkb1 is mediated by a G(1) cell cycle arrest. Proc Natl Acad Sci U S A 1999; 96: 9248–9251.
11. Carretero J, Medina PP, Blanco R et al. Dysfunctional AMPK activity, signalling through mTOR and survival in response to energetic stress in LKB1-deficient lung cancer. Oncogene 2007; 26: 1616–1625.
12. Giardiello FM, Brensinger JD, Tersmette AC et al. Very high risk of cancer in familial Peutz-Jeghers syndrome. Gastroenterology 2000; 119: 1447–1453.
13. Sanchez-Cespedes M, Parrella P, Esteller M et al. Inactivation of LKB1/STK11 is a common event in adenocarcinomas of the lung. Cancer Res 2002; 62: 3659–3662.
14. Ji H, Ramsey MR, Hayes DN et al. LKB1 modulates lung cancer differentiation and metastasis. Nature 2007; 448: 807–810.
15. Yuan P, Kadara H, Behrens C et al. Sex determining region Y-Box 2 (SOX2) is a potential cell-lineage gene highly expressed in the pathogenesis of squamous cell carcinomas of the lung. PLoS One 2010; 5: e9112.
16. Mountain CF. Revisions in the International System for Staging Lung Cancer. Chest 1997; 111: 1710–1717.
17. Li J, Jiang P, Robinson M et al. AMPK-beta1 subunit is a p53-independent stress responsive protein that inhibits tumor cell growth upon forced expression. Carcinogenesis 2003; 24: 827–834.
18. Han S, Roman J. Rosiglitazone suppresses human lung carcinoma cell growth through PPARgamma-dependent and PPARgamma-independent signal pathways. Mol Cancer Ther 2006; 5: 430–437.
19. Han S, Khuri FR, Roman J. Fibronectin stimulates non-small cell lung carcinoma cell growth through activation of Akt/mammalian target of rapamycin/S6 kinase and inactivation of LKB1/AMP-activated protein kinase signal pathways. Cancer Res 2006; 66: 315–323.
20. Ido Y, Carling D, Ruderman N. Hyperglycemia-induced apoptosis in human umbilical vein endothelial cells: inhibition by the AMP-activated protein kinase activation. Diabetes 2002; 51: 159–167.
21. Park HU, Suy S, Danner M et al. AMP-activated protein kinase promotes human prostate cancer cell growth and survival. Mol Cancer Ther 2009; 8: 733–741.
22. Conde E, Suarez-Gauthier A, Garcia-Garcia E et al. Specific pattern of LKB1 and phospho-acetyl-CoA carboxylase protein immunostaining in human normal tissues and lung carcinomas. Hum Pathol 2007; 38: 1351–1360.
23. Hahn-Windgassen A, Nogueira V, Chen CC et al. Akt activates the mammalian target of rapamycin by regulating cellular ATP level and AMPK activity. J Biol Chem 2005; 280: 32081–32089.
24. West KA, Brognard J, Clark AS et al. Rapid Akt activation by nicotine and a tobacco carcinogen modulates the phenotype of normal human airway epithelial cells. J Clin Invest 2003; 111: 81–90.
25. Scagliotti GV, Parikh P, von Pawel J et al. Phase III study comparing cisplatin plus gemcitabine with cisplatin plus pemetrexed in chemotherapy-naive patients with advanced-stage non-small-cell lung cancer. J Clin Oncol 2008; 26: 3543–3551.
26. Racanelli AC, Rothbart SB, Heyer CL, Moran RG. Therapeutics by cytotoxic metabolite accumulation: pemetrexed causes ZMP accumulation, AMPK activation, and mammalian target of rapamycin inhibition. Cancer Res 2009; 69: 5467–5474.
27. Ding L, Getz G, Wheeler DA et al. Somatic mutations affect key pathways in lung adenocarcinoma. Nature 2008; 455: 1069–1075.
28. Matsumoto S, Iwakawa R, Takahashi K et al. Prevalence and specificity of LKB1 genetic alterations in lung cancers. Oncogene 2007; 26: 5911–5918.
29. Onozato R, Kosaka T, Achiwa H et al. LKB1 gene mutations in Japanese lung cancer patients. Cancer Sci 2007; 98: 1747–1751.
30. Koivunen JP, Kim J, Lee J et al. Mutations in the LKB1 tumour suppressor are frequently detected in tumours from Caucasian but not Asian lung cancer patients. Br J Cancer 2008; 99: 245–252.

Genetics of Preneoplasia: Lessons from Lung Cancer

Ignacio I. Wistuba*

Departments of Pathology and Thoracic/Head and Neck Medical Oncology, The University of Texas M. D. Anderson Cancer Center, Houston, Texas 77030, USA

Abstract: From biological, histopathologic, and clinical perspectives, lung cancer is a highly complex neoplasm probably having multiple preneoplastic pathways. The sequence of histopathologic changes in the bronchial mucosa that precedes the development of squamous carcinomas of the lung has been identified. For the other major forms of lung cancer, however, such sequences have been poorly documented. This review summarizes the current knowledge regarding the molecular and histopathologic pathogenesis of lung cancer and discusses the complexity of identifying novel molecular mechanisms involved in the development of the lung premalignant disease, and their relevance to the development of new strategies for early detection and chemoprevention. Although our current knowledge of the molecular pathogenesis of lung cancer is still meager, work over the last decade has taught several important lessons about the molecular pathogenesis of this tumor, including the following: a) Better characterization of the high-risk population is needed. b) There are several histopathologic and molecular pathways associated with the development of the major types of non-small cell lung cancer. c) Although there is a field effect phenomenon for lung preneoplastic lesions, recent data suggest that there are at least two distinct lung airway compartments (central and peripheral) for lung cancer pathogenesis. d) Inflammation may play an important role in lung cancer development and could be an important component of the field effect phenomenon. e) For lung adenocarcinoma, at least two pathways (smoking-related and nonsmoking-related) have been identified. f) Finally, the identification of deregulated molecular signaling pathways in lung cancer preneoplasias may provide a rationale for designing novel strategies for early detection and targeted chemoprevention of lung cancer.

Keywords: Preneoplasias, field effect, lung cancer risk, inflammation, smoking, NF-kB, EGFR, KRAS.

INTRODUCTION

Lung cancer is the leading cause of cancer deaths in the United States and worldwide [1,2]. This high mortality is attributed to diagnosis at advanced stages, when the options for treatment are mostly palliative. Thus, to reduce the mortality of lung cancer, new approaches must be developed to prevent, diagnose, and treat premalignant lesions, shifting the paradigm to consider premalignancy as the disease and lung cancer as the endpoint. However, the identification of the early molecular and histopathologic pathogenesis of lung cancer represents an enormous challenge.

From biological, histopathologic, and clinical perspectives, lung cancer is a highly complex neoplasm [1], probably having multiple preneoplastic pathways. Lung cancer consists of several histological types, including small cell lung carcinoma (SCLC, 25% of cases) and the non-small cell lung carcinoma (NSCLC, 75%) types of squamous cell carcinoma, adenocarcinoma (including the non-invasive type of bronchioloalveolar carcinoma) and large cell carcinoma [3]. Lung cancers may arise from the major bronchi (central tumors) or from the small bronchi, bronchioles, or alveoli (peripheral tumors) of the distant airway of the lung. Squamous cell carcinomas and SCLCs usually arise centrally, whereas adenocarcinomas and large cell carcinomas usually arise peripherally [3]. The population of normal respiratory epithelial cells varies along different compartments of the respiratory tree, and the specific respiratory epithelial cell type from which each lung cancer type develops has not been established with certainty.

The sequence of histopathologic changes in the bronchial mucosa that precedes the development of squamous carcinomas of the lung has been identified (Fig. **1**) [4]. For the other major forms of lung cancer, however, such sequences have been poorly documented [5]. Although many molecular abnormalities have been described in clinically evident lung cancers [1], relatively little is known about the molecular events preceding the development of lung carcinomas and the underlying molecular basis of lung carcinogenesis. Although several studies have provided relevant information regarding the molecular characterization of the premalignant changes involved in the pathogenesis of lung cancer, especially for squamous cell carcinoma [6], that information has proven insufficient to identify with certainty the molecular pathogenetic pathways or molecular markers useful for risk assessment, targeted chemoprevention or treatment, and early detection of lung premalignant

*Address correspondence to this author at the Department of Pathology – Unit 85, M. D. Anderson Cancer Center, 1515 Holcombe Blvd., Houston, TX 77030-4009, USA; Tel: 713-563-9184; Fax: 713-563-1848; E-mail: iiwistuba@mdanderson.org

1566-5240/07 $50.00+.00

lesions. Attempts to better define the pathogenesis of lung premalignancy have been thwarted by the relative invisibility of the cellular lesions and their random distribution throughout the respiratory airway field, and new methodologies, including computed tomography (CT) imaging [7] and fluorescence bronchoscopy [8], has been introduced to better identify and visualize lung premalignant lesions. Because examination of the sputum and bronchoscopy specimens examines the central airways, whereas spiral CT detects mainly peripheral tumors, different approaches are required to detect tumors in different compartments of the lung.

This review summarizes the current knowledge regarding the molecular and histopathologic pathogenesis of lung cancer and discusses the complexity of identifying novel molecular mechanisms involved in the development of the lung premalignant disease, and their relevance to the development of new strategies for early detection and chemoprevention. Although our current knowledge of the molecular pathogenesis of lung cancer is still meager, work over the last decade has taught several important lessons about the molecular pathogenesis of this tumor, including the following: a) Better characterization of the high-risk population is needed. b) There are several histopathologic and molecular pathways associated with the development of the major types of NSCLC. c) Although there is a field effect phenomenon for lung preneoplastic lesions, recent data suggest that there are at least two distinct lung airway compartments (central and peripheral) for lung cancer pathogenesis. d) Inflammation may play an important role in lung cancer development and could be an important component of the field effect phenomenon. e) For lung adenocarcinoma, at least two pathways (smoking-related and nonsmoking-related) have been identified. f) Finally, the identification of deregulated molecular signaling pathways in lung cancer preneoplasias may provide a rationale for designing novel strategies for early detection and targeted chemoprevention of lung cancer.

HIGH-RISK POPULATION

In lung cancer, there is a consensus that the high-risk population targeted for early detection and chemoprevention efforts has been identified: heavy smokers and patients who have survived a cancer of the upper aerodigestive tract [2,9-13]. Evidence for the relationship between lung cancer and smoking is

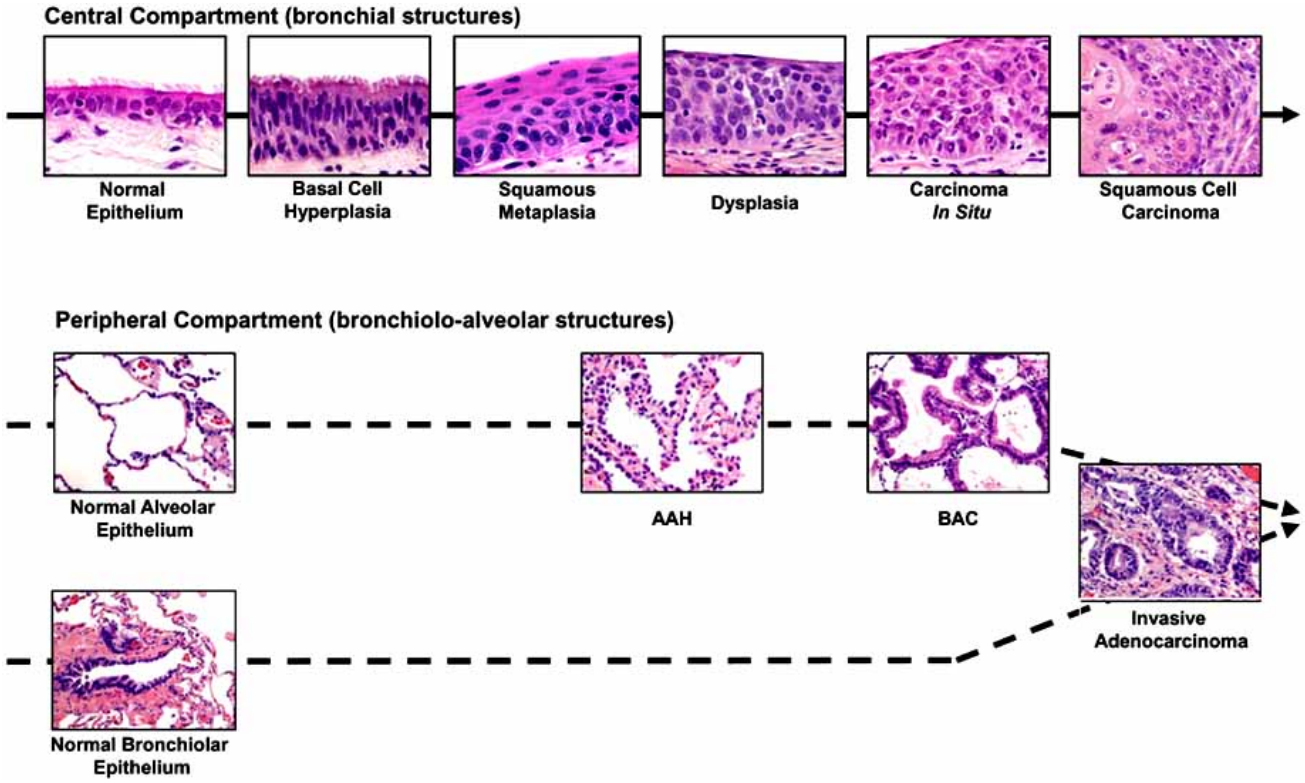

Fig. (1). Summary of the histopatholologic changes during the pathogenesis of squamous cell carcinoma and adenocarcinoma of the lung. At least two types of epithelial cells (alveolar and bronchiolar/bronchial) have been suggested as precursor of lung adenocarcinoma. (AAH = atypical adenomatous hyperplasia; BAC = bronchioloalveolar carcinoma).

clear. The risk of lung cancer increases with the number of cigarettes smoked, the years of smoking, an earlier age of onset of smoking, the degree of inhalation, the tar and nicotine content of the cigarettes smoked, and the use of unfiltered cigarettes [2,9-13]. However, based on the fact that only 11% of smokers develop lung cancer, better criteria are needed for the identification of the subset of smokers that will develop lung cancer.

Lung premalignant lesions of the central airway are frequent in smokers and rare in never-smokers [4-6]. Precisely how much smoking is necessary to develop lung premalignant changes is unknown, but there is consensus that the frequency and severity of those lesions increases with increasing tobacco exposure [13]. In the effort to characterize better the population of smokers at higher risk to develop lung cancer, research has been focused on, among other characteristics, sex, lung function abnormalities, and duration of cessation of smoking. However, the data available are somehow controversial. Although there is evidence that at every level of exposure to cigarette smoke, the risk of lung cancer (especially SCLC and adenocarcinoma) is 1.2-fold to 1.7-fold higher in women than in men [14], a study of central bronchial premalignant lesions using fluorescent bronchoscopy indicated that men had a higher prevalence of high-grade squamous premalignant lesions [13]. In addition to smoking, the presence of chronic obstructive pulmonary disease (COPD) with different levels of airway obstruction is a strong indicator for the subsequent development of lung cancer, with a 1.3-fold to 4.9-fold increased risk [15]. The risk of lung cancer increases in proportion to the degree of airway obstruction, indicating that smokers with ventilatory obstruction are at greater risk for lung cancer than are smokers without obstruction [16]. Notably, although smoking causes most cases of COPD, only 15% of smokers develop COPD. Although a high proportion (~67%) of smokers with COPD demonstrate cytological atypia compatible with mild or worse dysplastic changes [17], approximately 50% of smokers demonstrating histologically documented squamous premalignant lesions by fluorescence bronchoscopy examination do not have airway obstruction consistent with COPD [13]. It has been established that in terms of reduced risk of lung cancer mortality, smoking cessation is beneficial at any age, with much greater benefits accruing to those quitting at younger ages [10]. Although the risk decreases proportionately with the number of years after quitting [18], for men the risk was still significantly elevated even 10 years after smoking cessation [12]. This phenomenon correlates with the finding that the prevalence of high-grade premalignant lesions is not reduced significantly for more than 10 years after cessation of smoking [13]. Consequently, former smokers make up a large proportion (~50%) of lung cancer patients in the United States [11].

Despite intense epidemiological and clinical research, the subset of smokers with a greater risk of developing lung cancer has not been identified with certainty, and novel approaches to identify the best population to be targeted for early detection and chemoprevention strategies should be devised. Those novel approaches could be based on the detection of lung cancer precursors using histopathologic, imaging, or molecular methodologies. For these purposes, a better understanding of the biology and molecular pathology of the early pathogenesis of lung cancer, including premalignancy, is needed.

HISTOPATHOLOGIC AND MOLECULAR PATHWAYS FOR LUNG CANCER DEVELOPMENT

Most of the molecular and histopathologic changes in the respiratory epithelium associated with lung cancer pathogenesis have been related to smoking [6]. However, the recent discovery of frequent ***EGFR*** gene mutations in lung cancer and adjacent normal epithelium in never-smokers or light smokers suggests the presence of at least two distinct pathways for the molecular pathogenesis of lung cancer, smoking- and nonsmoking-related [19,20]. Because a relatively small subset of smokers develops lung cancer, attention has been focused on the identification of specific molecular and histopathologic pathways that can predict lung cancer development in high risk-populations. One of those key pathways, currently under intense investigation, is the activation of inflammation-related pathways. We will focus this review on the discussion of the major molecular and histopathologic pathways at different compartments of the lung airway that have been identified in the pathogenesis of the major types of lung cancer. A summary of our current understanding of the molecular pathways involved in the pathogenesis of lung cancer is shown in Fig. (**2**).

INFLAMMATION AND LUNG CANCER

Accumulating evidence suggests that tumor progression is governed not only by genetic changes intrinsic to cancer cells but also by epigenetic and environmental factors. Chronic inflammation has been hypothesized as one of the most important epigenetic and environmental factors contributing to epithelial cancer development and tumor progression [21]. A chronic inflammatory process enhances cell proliferation, cell survival, and cell migration in epithelial cells, as well as angiogenesis in the adjacent stroma, thereby promoting epithelial tumor development [21]. In the last decades, inflammation and related pathways have been suggested to play an important role in the pathogenesis of lung cancer, particularly in smoking-damaged respiratory epithelium [22,23]. However, the mechanisms involved are not well understood.

The specific cellular and molecular pathways that link such inflammatory responses to malignant transformation vary depending on the

microorganism, target organ, and tumor subtype [21,23]. However, despite these differences, several common features exist. A microbial presence in or near epithelia provides a stimulus for recruitment and activation of inflammatory cells (macrophages, neutrophils, and lymphocytes) from the blood stream [21]. Cytokines, chemokines, and free radicals initiate and perpetuate inflammatory responses. This process leads to the release of free radicals that contribute to the malignant transformation of epithelial cells by peroxidazing lipids and inducing genetic mutations [21]. Such damage to epithelial cells stimulates apoptotic cell death and reactive epithelial hyperproliferation that promotes further mutation. In epithelial sites, the nature of the inflammatory response is governed initially by the dominant type of T helper lymphocyte cells recruited to the epithelium in response to inflammation [24]. Moreover, inflammation-related carcinogenesis results from the stimulation of angiogenesis and from inflammatory cells and mediators that act directly on epithelial cells and indirectly on stromal cells and extracellular matrix components [21].

The association between chronic inflammatory conditions of the lung and cancer has been studied extensively [23]. As stated above, several studies have found that smokers with COPD have an increased risk of lung cancer compared with smokers without COPD [23]. In persons with COPD, at the level of the alveoli, inflammation leads to protease release and oxidative inactivation of antiproteases by inflammatory cells, contributing to degradation of the extracellular matrix [25,26]. At the level of the conducting airways, there is metaplasia of the airway epithelium to a mucus-secreting phenotype, thickening of the airway wall from the increased deposition of matrix molecules and the proliferation of mesenchymal cells, and narrowing from fibrosis [25,26]. These changes are also present in the

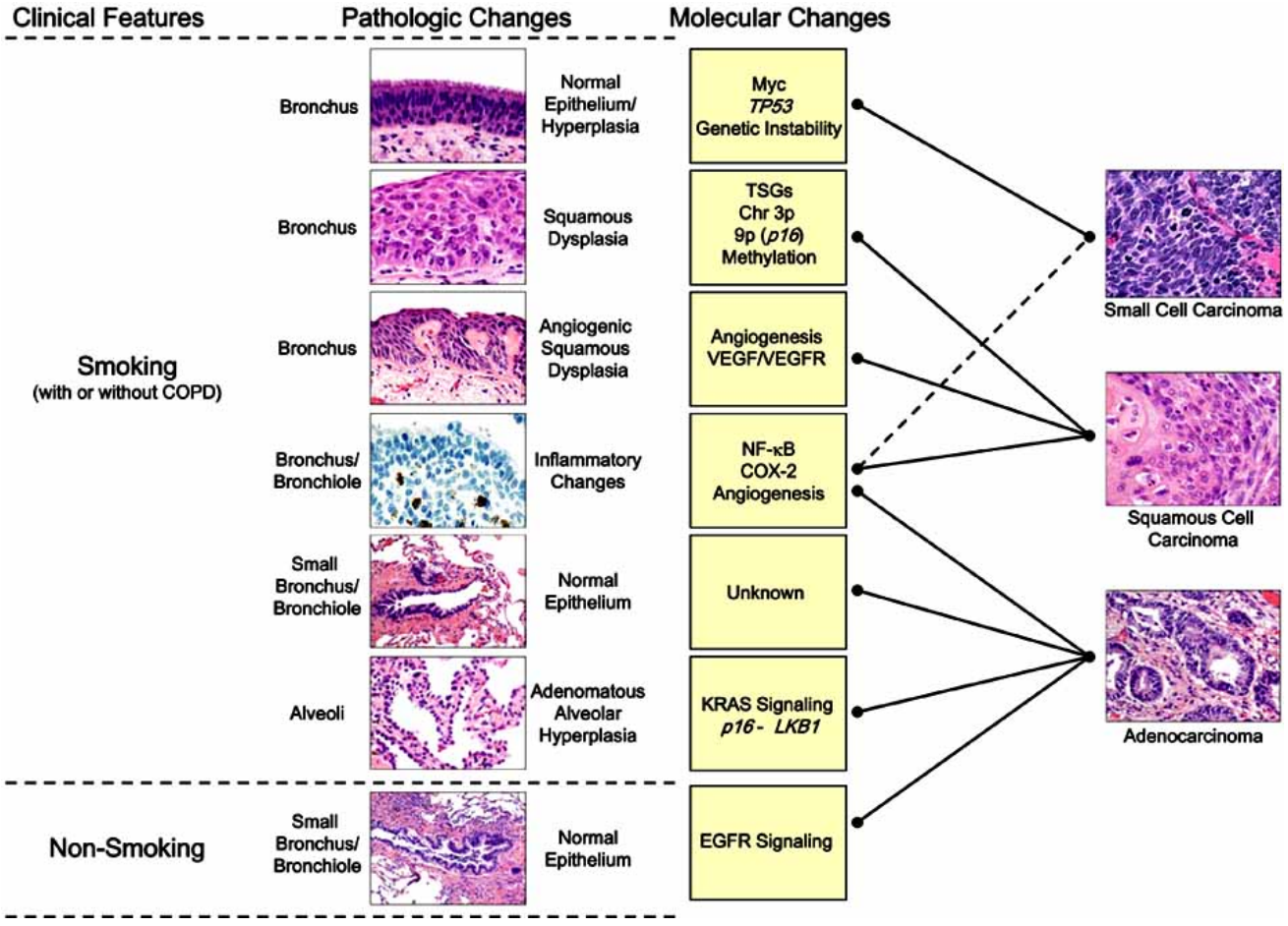

Fig. (2). Schema showing the association between histopathologic and molecular pathways known to be involved in the pathogenesis of lung carcinomas. At least, two pathways, smoking and nonsmoking-associated, are involved. The smoking pathway includes several distinct mechanisms, including inactivation of tumor suppressor genes (TSG), inflammation, angiogenesis and activation of several signaling pathways. However, currently the pathologic and molecular mechanisms responsible of lung adenocarcinoma pathogenesis are mostly unknown. The smoking pathway includes smokers with and without chronic obstructive pulmonary disease (COPD).

lungs of smokers without COPD, but they are not as severe [27]. COPD patients with 40 or more pack-years of smoking history have demonstrated a high prevalence of premalignant dysplasia (24% severe and carcinoma ***in situ***) detectable through sputum cytology [28].

A number of lines of evidence suggest that chronic inflammation contributes to the process of lung carcinogenesis through activation of a number of molecular pathways, including the nuclear factor kappa B (NF-κB) [22,23]. In NSCLC cell lines, it has been demonstrated that tobacco components stimulate NF-κB-dependent survival [29], and the cyclooxygenase (COX)-2 inhibitor celecoxib suppresses NF-κB activation induced by various carcinogens [30]. To date, however, the activation of NF-κB has not been studied comprehensively in lung cancer tumors and lung preneoplastic lesion tissues. Recently, Tichelaar ***et al***. [31], reported findings of increased nuclear NF- κB expression in a limited number of squamous moderate and severe dysplasias obtained from smokers without cancer compared with normal epithelium specimens. NF- κB has recently been identified as a molecular link between chronic inflammation and cancer [32,33], suggesting that NF-κB exerts its oncogenic effects in both the tumor and the microenvironment, promoting the survival of premalignant epithelial cells [34]. NF-κB has been shown to suppress apoptosis and induce expression of proto-oncogenes such as c-myc and cyclin D1, which directly stimulate cell proliferation [35]. In addition, NF- κB regulates the expression of various molecules important in tumorigenesis, such as matrix metalloproteinases, COX-2, inducible nitric oxide synthase, chemokines, and inflammatory cytokines, all of which promote tumor cell invasion and angiogenesis [36].

The eicosanoid pathway, specifically COX-2, is involved in the pathogenesis of lung cancer. COX-2, an intermediate early response gene induced by growth factors, oncogenes, carcinogens, and tumor-promoter phorbol esters [37], has been shown to be overexpressed in lung adenocarcinoma and squamous cell carcinoma [38]. Cyclooxygenase catalyzes the synthesis of prostaglandins from arachidonic acid, and both arachidonic acid and eicosanoids are potent inflammatory and growth agents. Both preclinical and clinical trials of the effect of celecoxib on lung cancer prevention have shown a marked reduction in prostaglandin E_2 production [39]. COX-2 immunohistochemical expression has shown to be highly expressed in bronchial squamous dysplasias, especially those having high-grade histology (severe dysplasia and carcinoma ***in situ***) [40]. Recent findings suggest that the COX-2 inhibitor celecoxib may modulate the proliferation indices and apoptotic balance in the bronchial tissue of active smokers [41].

However, it is currently unknown whether NF- κB or COX-2 activity itself plays a causal role in the initiation event leading to lung cancer or whether it may participate in tumor promotion and progression. Clearly, despite recent advances, the role of inflammation in lung cancer pathogenesis still remains an open question.

FIELD DEFECT PHENOMENON

Current information suggests that lung premalignant lesions are frequently extensive and multifocal throughout the respiratory epithelium, indicating a field effect [42]. In this phenomenon, called field cancerization, much of the respiratory epithelium has been mutagenized, presumably from exposure to tobacco-related carcinogens [43]. Several studies performed in the respiratory epithelium of lung cancer patients and smokers have demonstrated that multiple molecularly altered foci of bronchial epithelium are present throughout the airway [44-46]. A detailed analysis of premalignant and malignant epithelium from patients with squamous cell carcinoma indicated that multiple, sequentially occurring allele-specific chromosomal deletions (loss of heterozygosity [LOH]) commence in widely dispersed, apparently clonally independent foci, early in the multistage pathogenesis of squamous cell carcinoma of the lung [44,45]. These observations were extended to former and current smokers [47,48], whose bronchial epithelia demonstrate multiple foci of genetic changes, similar to those found in lung cancers, that may persist for many years after smoking cessation [47]. One of the most intriguing findings regarding the molecular field effect in lung cancer patients and smokers is the high frequency of multiple foci of histologically normal and mildly abnormal (hyperplasia and squamous metaplasia) epithelia exhibiting molecular abnormalities [44,45,47-49]. Because at least some degree of inflammation and inflammatory-related damage is almost invariably present in the central and peripheral airway of smokers [26,50], and because these changes precede the development of lung cancer, the field cancerization phenomenon can be explained both by a direct effect of smoking carcinogens on the epithelial cell and by the initiation of inflammatory response in the epithelial mucosa that may perpetuate the epithelial genetic damage. However, as discussed below, some evidence suggests that there are two distinct lung airways compartments (central and peripheral) for lung cancer pathogenesis (Fig. **3**). This concept is supported by the findings of low frequency of molecular abnormalities detected in the centrally located bronchial respiratory epithelium in patients with peripheral lung adenocarcinomas, compared with specimens from patients with squamous cell carcinomas and SCLC [46] indicating the presence of two compartments in the lung with different degrees of smoking-related genetic damage. Recently, the ***EGFR*** mutation detected in the normal airway of non-smokers has shown to be a “localized” field effect phenomenon affecting the peripheral airway (see below) [20].

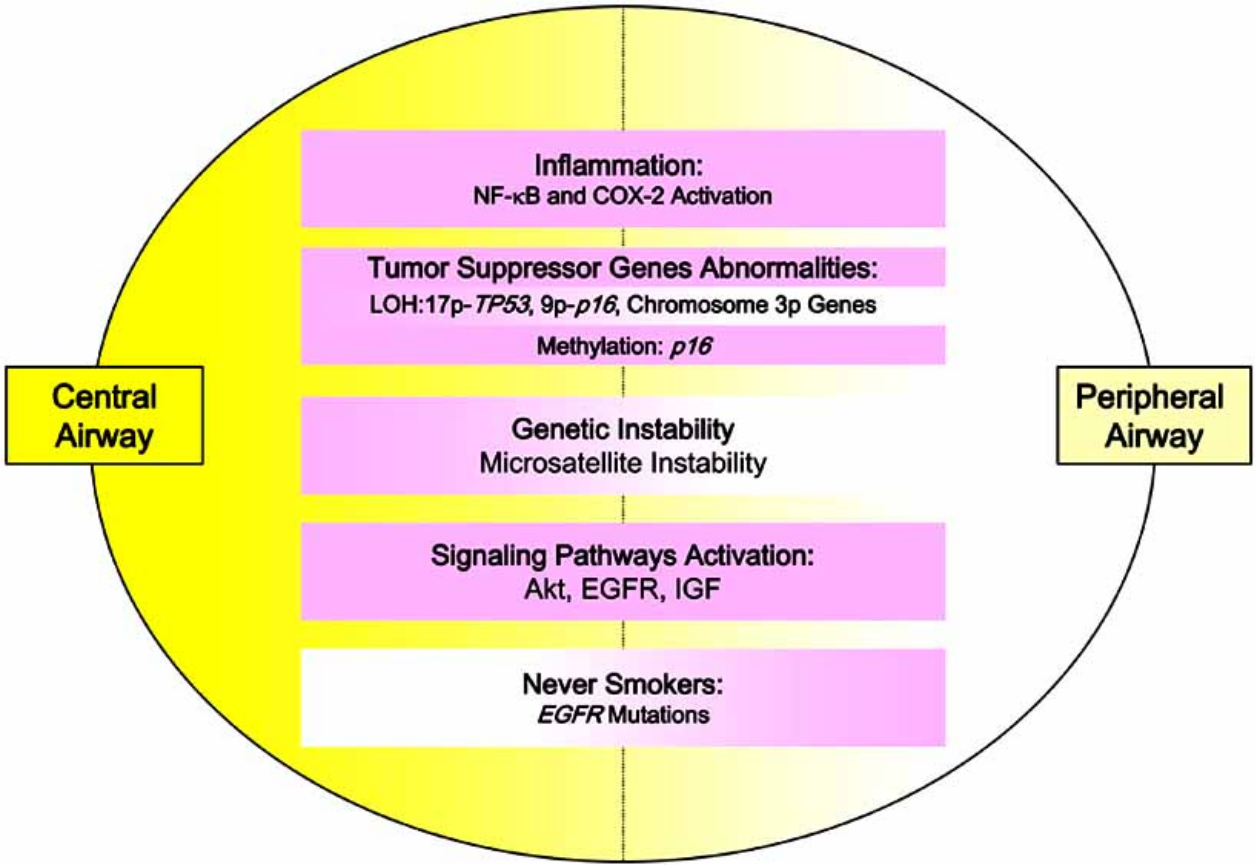

Fig. (3). The field effect phenomenon is called field cancerization, by which much of the respiratory epithelium has been mutagenized, presumably from exposure to tobacco-related carcinogenesis. However, localized field effect has been also detected for ***EGFR*** mutations in never smokers. While some molecular changes (i.e., inflammation and some signaling pathways activation) have been detected throughout the lung airway and including both compartments (central and peripheral airway), others have been more frequently altered in either central (i.e., loss of heterozygosity, LOH, and genetic instability) or peripheral (i.e., EGFR mutations) airway.

MOLECULAR ABNORMALITIES IN THE PATHOGENESIS OF LUNG CANCER

Multiple genetic changes have been found in clinically evident lung cancers in several studies, and these changes have involved known and putative tumor-suppressor genes as well as several dominant oncogenes [1]. Lung cancers arise after a series of molecular changes that commence in histologically normal epithelium and demonstrate a specific sequence [6,44]. There is a preferred order of these allele loss changes, with 3p allele loss (several 3p sites) followed by 9p (***p16^{INK4a}*** locus) as the earliest changes occurring in histologically normal epithelium [44,45,51]. Telomerase activation has been also implicated as an early event in lung cancer pathogenesis [52,53]. Telomerase shortening is an early genetic abnormality in bronchial carcinogenesis, preceding telomerase expression and p53/Rb inactivation, and predominates in high - grade squamous preinvasive lesions [54]. Precise microscopic-based microdissection of epithelial tissue followed by allelotyping of smoking-damaged lung from lung cancer patients or from current or former smokers without lung cancer has found multiple lesions containing clonal abnormalities of allele loss, occurring in both histologically normal as well as mildly abnormal (hyperplasia and squamous metaplasia) and preneoplastic (dysplasia) respiratory epithelium [49]. Although those changes are found in the lungs of current and former smokers without lung cancer, they are almost never found in life-time never-smokers [47,48]. Interestingly, those clonal changes persist for decades after smoking cessation [47].

Similar evidence exists for multiple promoter methylation changes in smoking-damaged lung epithelium and sputum specimens [55,56]. Recent results for methylation analyses of several genes, including ***RARβ-2***, ***H-cadherin***, ***APC***, ***p16^{INK4a},*** and ***RASFF1A***, indicate that abnormal gene methylation is relatively frequent (one or more genes in 48%) in oropharyngeal and bronchial epithelial cells in heavy smokers with evidence of sputum atypia [56]. Methylation in one or more of three genes tested (***p16^{INK4a}***, ***GSTP1***, and ***DAPK***) has been demonstrated in bronchial brush specimens in about one third of smokers [57]. Results from another study indicated that aberrant promoter hypermethylation of

the ***p16^{INK4a}*** gene occurs frequently in the bronchial epithelium of lung cancer patients and smokers without cancer and persists after smoking cessation [58,59]. Aberrant promoter methylation of ***p16^{INK4a}*** was seen in at least one bronchial epithelial site from 44% of lung cancer patients and cancer-free smokers. A recent nested case-control study [60] of incident lung cancer cases from an extremely high - risk cohort for evaluating promoter methylation of 14 genes in sputum showed that the prevalence for methylation of gene promoters increased as the time to lung cancer diagnosis decreased. Six (***p16^{INK4a}***, ***MGMT***, ***DAPK***, ***RASSF1A***, ***PAX5***β, and ***GATA5***) of 14 genes were associated with a >50% increased risk of lung cancer. In addition, in the same study, the concomitant methylation of three or more of these six genes was associated with a 6.5-fold increased risk and a sensitivity and specificity of 64%.

Considerable attention has been given to the identification of the 3p genes involved in lung cancer pathogenesis, including ***RAR***β at 3p24, ***FHIT*** at 3p14.2, ***RASSF1A***, ***BLU***, ***FUS1***, and ***SEMA3B*** located at 3p21.3, and potentially ***ROBO1*** at 3p12 [45,55,61]. Their expression is frequently lost in lung cancer, usually by promoter methylation [62]. However, specific roles of the genes undergoing activation or inactivation and the order of cumulative molecular changes that lead to the development of each lung tumor histologic type remain to be elucidated.

Profiling studies using high-throughput technologies for the identification of molecular signatures associated with the development and progression of lung cancer precursor lesions are extremely difficult to perform, because usually such lesions are small and need histological confirmation by tissue fixation and histopathologic processing. Although some profiling studies have been performed using ***in vitro*** cultured human normal bronchial epithelial cells [63,64], recently a specific pattern of protein expression using proteomic methodology of the airway epithelium that accurately classified bronchial and alveolar tissue with normal histology from preinvasive bronchial lesions and from invasive lung cancer was reported [63]. Although these findings need to be further validated, this represents a first step toward a new proteomic characterization of the human model of lung cancer development.

PRENEOPLASTIC LESIONS AT THE CENTRAL LUNG AIRWAY

Squamous Metaplasia and Dysplasia

Mucosal changes in the large airways that may precede or accompany invasive squamous cell carcinoma include hyperplasia, squamous metaplasia, squamous dysplasia, and carcinoma ***in situ*** [4,5,65]. Dysplastic squamous lesions are considered true preneoplastic lesions and may be of various degrees (i.e., mild, moderate, and severe); however, these lesions represent a continuum of cytologic and histologic atypical changes that may show some overlapping features between categories. These lesions are often not detected by conventional white light bronchoscopy or gross examination. However, the use of fluorescent bronchoscopy greatly increases the sensitivity for detection of squamous dysplastic and carcinoma ***in situ*** lesions [66-68]. Little is known about the rate and risks of progression of squamous dysplasia to carcinoma ***in situ*** and ultimately to invasive squamous cell carcinoma.

There are no squamous cells in the normal airways. The progenitor or stem cells for the squamous metaplastic epithelium for the proximal airway are not known, but it is presumed that the basal cells represent a relatively quiescent zone that is the precursor of preneoplastic epithelium. In fact, squamous metaplasia is usually preceded and accompanied by basal cell hyperplasia. It is of interest that these cells express significant levels of Egfr protein and increased proliferative activity as measured by Ki-67 staining [69,70].

The current working model of the sequential molecular abnormalities in the pathogenesis of squamous cell lung carcinoma indicates the following: (a) Genetic abnormalities commence in histologically normal epithelium and increase with increasing severity of histologic changes [44]. (b) Mutations follow a sequence, with progressive allelic losses at multiple 3p (3p21, 3p14, 3p22-24, and 3p12) chromosome sites and 9p21 (***p16 ^{INK4a}***) as the earliest detected changes. Later changes include 8p21-23, 13q14 (***RB***), and 17p13 (***TP53***) [44,45,51]. ***p16^{INK4a}*** methylation has been also detected at an early stage of squamous preinvasive lesions with a frequency that increases during histopathologic progression (24% in squamous metaplasia and 50% in carcinoma ***in situ***) [58]. (c) Molecular changes in the respiratory epithelium are extensive and multifocal throughout the bronchial tree of smokers and lung cancer patients, indicating a field effect or field cancerization [44,45,47,48]. (d) Multiple clonal and subclonal patches of molecular abnormalities not much larger in size than the average bronchial biopsy obtained by fluorescent bronchoscopy (estimated to be approximately 40,000 to 360,000 cells) can be detected in the normal and slightly abnormal bronchial epithelium of patients with lung cancer [49]. Despite encouraging results from isolated studies [60], most of these findings have not been useful for the development of successful strategies for lung cancer risk assessment, early detection, or chemoprevention.

Angiogenic Squamous Dysplasia

Interestingly, in a subset of squamous metaplastic and dysplastic changes, the basal membrane becomes thickened and there is vascular budding in the subepithelial tissues that results in papillary protrusions of the epithelium, lesions that Keith ***et al***.

termed angiogenic squamous dysplasia (ASD) [71]. ASD lesions are more frequently detected by using fluorescent bronchoscopy than by using white-light conventional bronchoscopy [69]. In the bronchial biopsies of these lesions, microvessel density is elevated compared with normal mucosa but not compared with other forms of hyperplasia or dysplasia. ASD thus represents a qualitatively distinct form of angiogenesis in which there is architectural rearrangement of the capillary microvasculature. Genetic analysis of surface epithelium in a subset of lesions found a LOH at chromosome 3p in 53% of lesions, and compared with normal epithelium, proliferative activity was markedly elevated in ASD lesions. ASD was found in approximately 19% of high-risk smokers without carcinoma who underwent fluorescence bronchoscopy [68] and was not present in biopsy specimens from 16 normal nonsmoker control subjects [71]. The presence of this lesion in high-risk smokers suggests that aberrant patterns of microvascularization may occur at an early stage of bronchial carcinogenesis. The finding of vascular endothelial growth factor (VEGF) isoforms and VEGF receptors (VEGFR) by semiquantitative reverse transcriptase-PCR, confirmed by immunohisto-chemistry in bronchial squamous dysplastic epithelia compared with normal bronchial epithelia [72], supports the notion that angiogenesis develops early in lung carcinogenesis and that these abnormalities provide a rationale for the develo-pment of targeted antiangiogenic chemopre-vention strategies.

PRENEOPLASTIC LESIONS AT THE PERIPHERAL LUNG AIRWAY

Despite the evidence that atypical adenomatous hyperplasia (AAH) is a precursor lesion for peripheral lung adenocarcinomas [5,73], there is consensus that the pathogenesis of many adenocarcinomas is still unknown. AAH is a discrete parenchymal lesion arising in the alveoli close to terminal and respiratory bronchioles, and AAH may be single or multiple. These lesions maintain an alveolar structure lined by rounded, cuboidal, or low columnar cells. The postulated progression of AAH to adenocarcinoma especially the bronchioloalveolar (BAC) subtype, is supported by morphometric, cytofluorometric, and molecular studies [65,73]. AAH is most frequently detected in lung from patients bearing lung cancers (9-20%), especially adenocarcinomas (up to 40%) compared with squamous cell carcinomas (11%) [65,74-77]. In contrast, autopsy studies have reported AAH in approximately 3% of persons without cancer [78]. It is extremely difficult to know the progression rate of AAH to lung adenocarcinoma, and it is also currently almost impossible to determine whether AHH may regress. Because they are air-filled structures, they may appear as ground glass opacities on CT scans. However, the location, size, and relative invisibility of AHH by most imaging methods make longitudinal studies of AAH even more difficult than studies of centrally located squamous preneoplastic lesions. Another type of lung peripheral lesion, termed bronchiolization of the alveoli [79,80], which is characterized by replacement of the alveolar epithelium by columnar bronchiolar-type epithelium with and without cytological atypia and which may exhibit molecular abnormalities such as chromosomal abnormalities by comparative genome hybridization (CGH) [79], has been also associated with the pathogenesis of lung adenocarcinoma.

Several molecular changes frequently present in lung adenocarcinomas are also present in AAH lesions, and they are further evidence that AAH may represent true preneoplastic lesions [73,81]. The most important finding is the presence of KRAS (codon 12) mutations, which are also relatively frequent alterations in lung adenocarcinomas, in up to 39% of AAH [73]. Other molecular alterations detected in AAH are overexpression of cyclin D1 (~70%), p53 (ranging from 10% to 58%), survivin (48%), and Her-2/neu (7%) proteins [73,82,83]. Some AAH lesions have demonstrated LOH in chromosomes 3p (18%), 9p (***p16^{INK4a}***, 13%), 9q (53%), 17q, and 17p (***TP53***, 6%), changes that are frequently detected in lung adenocarcinomas [84,85]. A study of lung adenocarcinoma with synchronous multiple AAH showed frequent LOH of tuberous sclerosis complex (TSC)-associated regions (***TSC1*** at 9q, 53%, and ***TSC2*** at 16p, 6%), suggesting that these are candidate loci for a tumor - suppressor gene in a subset of adenocarcinomas of the lung [85]. Activation of telomerase, expressed by expression of human telomerase RNA component (hTERC) and telomerase reverse transcriptase (hTERT) mRNA, has been detected in 27% to 78% of AAH lesions, depending on their atypia level [86]. Recently, it has been shown that loss of LKB1, a serine/threonine kinase that functions as a tumor - suppressor gene, is frequent in lung adenocarcinomas (25%) and in AAH with severe cytological atypia (21%), while it is rare in mild atypical AAH lesions (5%), suggesting that ***LKB1*** inactivation may play a role in the AAH progression to malignancy [87].

Several mouse models have been developed to better study various oncogenic molecular signaling pathways and the sequence of molecular events involved in the pathogenesis of peripheral lung tumors and to test novel chemopreventive agents [88]. The ***K-RAS*** oncogenic mouse model is characterized by the development of the peripheral alveolar type of proliferations, including AAH, adenoma, and adenocarcinoma [88]. Using this mouse model, several important findings that need to be further validated in human tissues have been reported. Kim ***et al***. [89] identified the potential stem cell population (expressing Clara cells-specific protein and surfactant protein-C, termed bronchioalveolar stem cell, BASC) that maintains the bronchiolar Clara cells and alveolar cells of the distal respiratory epithelium and which could be considered the

precursors of lung ***K-RAS*** neoplastic lesions in mice. Wislez ***et al***. [90] provided evidence that the expansion of lung adenocarcinoma precursors induced by oncogenic ***K-RAS*** requires mammalian target of rapamycin (mTOR)-dependent signaling and, most importantly, that inflammation-related host factors, including factors derived from macrophages, play a critical role in adenocarcinoma progression in mice. Recent findings reported by Collado ***et al***. [91] suggest that ***K-RAS*** oncogene-induced senescence may help restrict tumor progression of lung peripheral lesions in mice. They discovered that a substantial number of cells in mouse premalignant alveolar-type lesions undergo oncogene-induced senescence, but the cells that escape senescence by loss of oncogene-induced senescence effectors, such as $p16^{INK4a}$ or p53, progress to malignancy. Thus, senescence is a defining feature of premalignant lung lesions but not invasive tumors.

NONSMOKING-RELATED PATHWAYS

Although most lung cancers are smoking-related tumors, a subset of NSCLCs arises in never-smokers. Adenocarcinoma histology is the tumor type most frequently detected in never-smokers. Recently, somatic mutations of ***EGFR*** and ***HER-2/NEU***, tyrosine kinase (TK) members of the ErbB family, have been reported in a subset of lung adenocarcinoma patients having never-smoker or light-smoker status, female sex, and East Asian ethnicity [92-99]. The ***EGFR*** mutations are clinically relevant because most of them have been associated with sensitivity of lung adenocarcinoma to small-molecule TK inhibitors (gefitinib and erlotinib) [92-94,100]. More than 80% of the mutations detected in ***EGFR*** are in-frame deletions in exon 19 and a single missense mutation in exon 21 (L858R) [92-98]. It has been proposed that lung cancer cells with mutant ***EGFR*** might become physiologically dependent on the continued activity of the gene for the maintenance of their malignant phenotype, leading to accelerated development of lung adenocarcinoma [19]. Recent studies have demonstrated that tumor cell high ***EGFR*** copy number, identified by the fluorescent ***in situ*** hybridization (FISH) technique, may also be a predictor for response to EGFR TK inhibitors [101-103] and be involved in the pathogenesis of lung adenocarcinoma.

To better understand the pathogenesis of ***EGFR*** mutant lung adenocarcinomas, we investigated the presence of ***EGFR*** mutations in the normal bronchial and bronchiolar epithelium adjacent to mutant tumors. We detected ***EGFR*** mutations in normal-appearing peripheral respiratory epithelium in nine (44%) of 21 adenocarcinoma patients, but not in patients without mutations in the tumors [20]. Our finding of more frequent ***EGFR*** mutations in normal epithelium within the tumor (43%) than in adjacent sites (24%) suggests a localized field effect phenomenon, probably affecting preferentially the peripheral lung airway compartment, for this abnormality in the respiratory epithelium of the lung. Although the cell type having those mutations is unknown, we have hypothesized that stem or progenitor cells of the bronchial and bronchiolar epithelium are the cell type bearing such mutations. The finding of relatively infrequent ***EGFR*** mutations in AAH lesions (three out of 40 examined) [104,105] and the finding of no mutation [98] or a relatively low frequency of mutation in true BACs of the lung support the concept that genetic abnormalities of ***EGFR*** are not relevant in the pathogenesis of alveolar-type lung neoplasia. Our recent unpublished data suggest that ***EGFR*** mutation precedes increased copy number of the gene in the pathogenesis of lung adenocarcinoma. Thus, two different molecular pathways have been identified in the pathogenesis of lung adenocarcinoma, a smoking-associated activation of KRAS signaling and a nonsmoking-associated activation of EGFR signaling, the latter detected in histologically normal bronchial and bronchiolar epithelium.

SIGNALING PATHWAY ACTIVATION IN LUNG CANCER PRENEOPLASTIC LESIONS

The recent developments in molecular biology have increased our knowledge of critical biological pathways that are deregulated in lung cancer cells, and they have provided a rationale for the development of targeted therapy in human tumors, including lung cancer [106]. Activation of tyrosine kinases, particularly receptor tyrosine kinases, is increasingly recognized as a common cause for deregulation of these pathways, and inhibiting tyrosine kinases has proven to be an effective strategy for a number of malignancies, including lung cancer [107]. Thus, the possible activation of signaling pathways early in the pathogenesis of lung cancer has created an opportunity for the design of targeted chemoprevention strategies [108,109]. Of interest, most important signaling pathways that are being targeted in lung cancer have been shown to be also deregulated in lung cancer preneoplastic lesions, mostly in the squamous cell carcinoma pathway, including (among others) the inflammation-related polyunsaturated fatty acid metabolic pathways [110], retinoic acid signaling [109], and pathways involving Ras [73,90,111,112], EGFR [20,113], phosphoinositide 3-kinase (PI3K)/Akt [114-116], insulin-like growth (IGF) factor axis [117], VEGF/VEGFR [72], and mTOR [90].

PERSPECTIVE

During the last decade, encouraged by the development of methodologies such as laser microdissection for the isolation of cells from small histologic lesions, combined with techniques to perform genomic studies from minute amounts of DNA, RNA, and protein, several groups have made substantial progress in discovering the molecular and

genetic abnormalities of lung cancer precursor lesions, including those evolving to centrally located squamous cell carcinoma and peripheral adenocarcinoma. However, it seems that the enthusiasm has somehow substantially decreased, for in the last few years little progress has been made. The recent development of a panel of human normal bronchial epithelial cells immortalized with telomerase and CdK4-mediated ***p16^{INK4a}*** bypass, which can be modified with a combination of oncogene activation and tumor-suppressor gene knockdowns for ***in vitro*** discovery work [118], coupled with the development of more relevant lung cancer animal models [119] and new high-throughput genomic [120] and proteomic [63,121] profiling techniques that can be applied to small amounts of microdissected tissues, may stimulate the scientific community to perform innovative investigations in the fields of molecular and pathologic research to understand the molecular malignant potential of respiratory epithelium even before histologic changes occur. Currently, two major National Cancer Institute programs, Specialized Programs of Research Excellence and the Early Detection Research Network, are concentrating on a search for new biomarkers in lung cancer. All these efforts may help us to better characterize the malignant potential of lung cancer preneoplastic lesions and to understand the field cancerization compartmental (central versus periphery) phenomenon in lung cancer pathogenesis.

ACKNOWLEDGEMENT

Supported by grant Department of Defense W81XWH-04-1-0142.

ABBREVIATIONS

SCLC = small cell lung carcinoma

NSCLC = non-small cell lung carcinoma

CT = computed tomography

COPD = chronic obstructive pulmonary disease

EGFR = epidermal growth factor receptor

COX-2 = cyclooxigenase-2

NF-κB = nuclear factor kappa B

LOH = loss of heterozygosity

ASD = angiogenic squamous dysplasia

AAH = atypical adenomatous hyperplasia

REFERENCES

[1] Minna, J.D. and Gazdar, A. (2002) ***Cancer Cell***., **1,** 49-52.

[2] Jemal, A., Murray, T., Ward, E., Samuels, A., Tiwari, R.C., Ghafoor, A., Feuer, E.J. and Thun, M.J. (2005)***C.A. Cancer J. Clin***., **55,** 10-30.

[3] Travis, W.D., Brambilla, E., Muller-Hermelink, H.K. and Harris, C.C. (2004). Pathology and Genetics: Tumours of the Lung, Pleura, Thymus and Heart: World Health Orgnaziation Classification of Tumours. Pathology & Genetics. Travis Wd, Brambilla E, Muller-Hermelink Hk and Harris Cc (eds). International Agency for Research on Cancer (IARC): Lyon, pp. 9-124.

[4] Franklin, W., Wistuba, I., Geisinger, K., Lam, S., Hirsch, F., Muller, K.M., Sozzi, G., Brambilla, E. and Gazdar, A. (2004). ***Pathology and Genetics. Tumors of the Lung, Pleura, Thymus and Heart: World Health Organization Classification of Tumours***. Travis W, Brambilla E, Muller-Hermelink Hk and Harris Cc (eds). International Agency for Research on Cancer (IARC): Lyon, pp. 68-72.

[5] Colby, T.V., Wistuba, I.I. and Gazdar, A. (1998) ***Adv. Anat. Pathol.,*** **5,** 205-215.

[6] Wistuba, I.I., Mao, L. and Gazdar, A.F. (2002) ***Oncogene***, **21,** 7298-7306.

[7] Mulshine, J.L. (2005) ***Oncol. (Williston Park),*** **19,**1724-1730; discussion 1730-1721.

[8] Lam, S., MacAulay, C., leRiche, J.C. and Palcic, B. (2000) ***Cancer***, **89,** 2468-2473.

[9] Lubin, J.H. and Blot, W.J. (1993) ***J. Natl. Cancer Inst***., **85,** 422-423.

[10] Halpern, M.T., Gillespie, B.W. and Warner, K.E. (1993) ***J. Natl. Cancer Inst***., **85,** 457-464.

[11] Tong, L., Spitz, M.R., Fueger, J.J. and Amos, C.A. (1996) ***Cancer,*** **78,** 1004-1010.

[12] Risch, H.A., Howe, G.R., Jain, M., Burch, J.D., Holowaty, E.J. and Miller, A.B. (1993) ***Am. J. Epidemiol***., **138,** 281-293.

[13] Lam, S., leRiche, J.C., Zheng, Y., Coldman, A., MacAulay, C., Hawk, E., Kelloff, G. and Gazdar, A.F. (1999) ***J. Natl. Cancer Inst***, **91,** 691-696.

[14] Zang, E.A. and Wynder, E.L. (1996) ***J. Natl. Cancer Inst***., **88,** 183-192.

[15] O'Byrne, P M. and Postma, D.S. (1999) ***Am. J. Respir. Crit. Care Med***., **159,** S41-63.

[16] Tockman, M.S., Anthonisen, N.R., Wright, E.C. and Donithan, M.G. (1987) ***Ann. Intern. Med***., **106,** 512-518.

[17] Prindiville, S.A., Byers, T., Hirsch, F.R., Franklin, W.A., Miller, Y.E., Vu, K.O., Wolf, H.J., Baron, A.E., Shroyer, K.R., Zeng, C., Kennedy, T.C. and Bunn, P.A. (2003) ***Cancer Epidemiol. Biomarkers Prev***., **12,** 987-993.

[18] Garfinkel, L. and Stellman, S.D. (1988) ***Cancer Res***., **48,** 6951-6955.

[19] Gazdar, A.F., Shigematsu, H., Herz, J. and Minna, J.D. (2004) ***Trends Mol. Med***., **10,** 481-486.

[20] Tang, X., Shigematsu, H., Bekele, B.N., Roth, J.A., Minna, J.D., Hong, W.K., Gazdar, A.F. and Wistuba, II. (2005) ***Cancer Res***., **65,** 7568-7572.

[21] Coussens, L.M. and Werb, Z. (2002) ***Nature,*** **420,** 860-867.

[22] Ballaz, S. and Mulshine, J.L. (2003) ***Clin. Lung Cancer,*** **5,** 46-62.

[23] Anderson, G.P. and Bozinovski, S. (2003) ***Trends Pharmacol. Sci***., **24,** 71-76.

[24] Suzuki, H., Graziano, D.F., McKolanis, J. and Finn, O.J. (2005) ***Clin. Cancer Res***., **11,** 1521-1526.

[25] Hogg, J.C. (2004) ***Lancet,*** **364,** 709-721.

[26] Barnes, P.J. (2000) ***N. Engl. J. Med***., **343,** 269-280.

[27] Hida, T., Kozaki, K., Muramatsu, H., Masuda, A., Shimizu, S., Mitsudomi, T., Sugiura, T., Ogawa, M. and Takahashi, T. (2000) ***Clin. Cancer Res***., **6,** 2006-2011.

[28] Kennedy, T.C., Proudfoot, S.P., Franklin, W.A., Merrick, T.A., Saccomanno, G., Corkill, M.E., Mumma, D.L., Sirgi, K.E., Miller, Y.E., Archer, P.G. and Prochazka, A. (1996) ***Cancer Res***., **56,** 4673-4678.

[29] Tsurutani, J., Castillo, S.S., Brognard, J., Granville, C.A., Zhang, C., Gills, J.J., Sayyah, J. and Dennis, P.A. (2005) ***Carcinogenesis,*** **26,** 1182-1195.

[30] Shishodia, S., Koul, D. and Aggarwal, B.B. (2004) ***J. Immunol***., **173,** 2011-2022.

[31] Tichelaar, J.W., Zhang, Y., leRiche, J.C., Biddinger, P.W., Lam, S. and Anderson, M.W. (2005) ***BMC Cancer,*** **5,** 155.

[32] Aggarwal, B.B. (2004) ***Cancer Cell,*** **6,** 203-208.

[33] Karin, M. and Greten, F.R. (2005) ***Nat. Rev. Immunol***., **5,** 749-759.

[34] Pikarsky, E., Porat, R.M., Stein, I., Abramovitch, R., Amit, S., Kasem, S., Gutkovich-Pyest, E., Urieli-Shoval, S., Galun, E. and Ben-Neriah, Y. (2004) ***Nature,*** **431,** 461-466.

[35] Kumar, A., Takada, Y., Boriek, A.M. and Aggarwal, B.B. (2004) ***J. Mol. Med***., **82,** 434-448.

[36] Shishodia, S. and Aggarwal, B.B. (2004) ***Biochem. Pharmacol***., **68,** 1071-1080.

[37] Dannenberg, A.J., Altorki, N.K., Boyle, J.O., Dang, C., Howe, L.R., Weksler, B.B. and Subbaramaiah, K. (2001) ***LancetOncol***., **2,** 544-551.

[38] Hasturk, S., Kemp, B., Kalapurakal, S.K., Kurie, J.M., Hong, W.K. and Lee, J.S. (2002) ***Cancer,*** **94,** 1023-1031.

[39] Mao, J.T., Cui, X., Reckamp, K., Liu, M., Krysan, K., Dalwadi, H., Sharma, S., Hazra, S., Strieter, R., Gardner, B. andDubinett, S.M. (2005) ***Clin. Lung Cancer,*** **7,** 30-39.

[40] Mascaux, C., Martin, B., Verdebout, J.M., Ninane, V. and Sculier, J.P. (2005) ***Eur. Respir. J***., **26,** 198-203.

[41] Mao, J.T., Fishbein, M.C., Adams, B., Roth, M.D., Goodglick,L., Hong, L., Burdick ,M., Strieter, E.R., Holmes, C., Tashkin, D.P. and Dubinett, S.M. (2006) ***Clin. Cancer Res***., **12,** 314-320.

[42] Auerbach, O., Stout, A.P., Hammond, E.C. and Garfinkel, L. (1961) ***N. Engl. J. Med***., **265,** 253-267.

[43] Slaughter, D.P., Southwick, H.W. and Smejkal, W. (1954) ***Cancer,*** **6,** 963-968.

[44] Wistuba, I.I., Behrens, C., Milchgrub, S., Bryant, D., Hung, J., Minna, J.D. and Gazdar, A.F. (1999) ***Oncogene,*** **18,** 643-650.

[45] Wistuba, I.I., Behrens, C., Virmani, A.K., Mele, G., Milchgrub, S., Girard, L., Fondon, J.W., Garner, H.R., McKay, B., Latif, F., Lerman, M.I., Lam, S., Gazdar, A.F. and Minna, J.D. (2000) ***Cancer Res***., **60,** 1949-1960.

[46] Wistuba, I.I., Berry, J., Behrens, C., Maitra, A., Shivapurkar, N., Milchgrub, S., Mackay, B., Minna, J.D. and Gazdar, A.F. (2000) ***Clin. Cancer Res***., **6,** 2604-2610.

[47] Wistuba, I.I., Lam, S., Behrens, C., Virmani, A.K., Fong, K.M., LeRiche, J., Samet, J.M., Srivastava, S., Minna, J.D. and Gazdar, A.F. (1997) ***J. Natl. Cancer Inst***., **89,** 1366-1373.

[48] Mao, L., Lee, J.S., Kurie, J.M., Fan, Y.H., Lippman,S.M., Lee, J.J., Ro, J.Y., Broxson, A., Yu, R., Morice, R.C., Kemp, B.L., Khuri, F.R., Walsh, G.L., Hittelman, W.N. and Hong, W.K. (1997) ***J. Natl. Cancer Inst***., **89,** 857-862.

[49] Park, I.W., Wistuba, I.I., Maitra, A., Milchgrub, S., Virmani, A.K., Minna, J.D. and Gazdar, A.F. (1999) ***J. Natl. Cancer Inst***., **91,** 1863-1868.

[50] Sin, D.D., Man, S.F., McWilliams, A. and Lam, S. (2006) ***Am. J. Respir. Crit. Care Med***., **173,** 535-539.

[51] Wistuba, I.I., Behrens, C., Virmani, A.K., Milchgrub, S., Syed, S., Lam, S., Mackay, B., Minna, J.D. and Gazdar, A.F. (1999) ***Cancer Res***., **59,** 1973-1979.

[52] Yashima, K., Milchgrub, S., Gollahon, L.S., Maitra, A., Saboorian,M.H., Shay, J.W. and Gazdar, A.F. (1998) ***Clin. Cancer Res***., **4,** 229-234.

[53] Miyazu, Y.M., Miyazawa, T., Hiyama, K., Kurimoto, N., Iwamoto, Y., Matsuura ,H., Kanoh, K., Kohno, N., Nishiyama, M. and Hiyama, E. (2005) ***Cancer Res***., **65,** 9623-9627.

[54] Lantuejoul, S., Soria, J.C., Morat, L., Lorimier, P., Moro-Sibilot, D., Sabatier, L., Brambilla, C. and Brambilla, E. (2005) ***Clin. Cancer Res***., **11,** 2074-2082.

[55] Zochbauer-Muller, S., Fong, K.M., Maitra, A., Lam, S., Geradts, J., Ashfaq, R., Virmani, A.K., Milchgrub, S., Gazdar, A.F. and Minn, J.D. (2001) ***Cancer Res***., **61,** 3581-3585.

[56] Zochbauer-Muller, S., Lam, S., Toyooka, S., Virmani, A.K., Toyooka, K.O., Seidl, S., Minna, J.D. andGazdar, A.F. (2003) ***Int. J. Cancer,*** **107,** 612-616.

[57] Soria, J.C., Rodriguez, M., Liu, D.D., Lee, J.J., Hong, W.K. and Mao, L. (2002) ***Cancer Res***., **62,** 351-355.

[58] Belinsky, S.A., Nikula, K.J., Palmisano, W.A., Michels, R., Saccomanno, G., Gabrielson, E., Baylin, S.B. and Herman, J.G. (1998) ***Proc. Natl. Acad. Sci. USA***, **95,** 11891-11896.

[59] Belinsky, S.A., Palmisano, W.A., Gilliland, F.D., Crooks, L.A., Divine, K.K., Winters, S.A., Grimes M.J., Harms H.J., Tellez C.S., Smith T.M., Moots P.P., Lechner J.F., Stidley, C.A. and Crowell, R.E. (2002) ***Cancer Res***., **62,** 2370-2377.

[60] Belinsky, S.A., Liechty, K.C., Gentry, F.D., Wolf, H.J., Rogers, J., Vu, K., Haney, J., Kennedy, T.C., Hirsch, F.R., Miller, Y., Franklin, W.A., Herman, J.G., Baylin, S.B., Bunn, P.A. and Byers, T. (2006) ***Cancer Res***., **66,** 3338-3344.

[61] Lerman, M.I. and Minna, J.D. (2000) ***Cancer Res***., **60,** 6116-6133.

[62] Zabarovsky, E.R., Lerman, M.I. and Minna, J.D. (2002) ***Oncogene,*** **21,** 6915-6935.

[63] Rahman, S.M., Shyr, Y., Yildiz, P.B., Gonzalez, A.L., Li, H., Zhang, X., Chaurand, P., Yanagisawa, K., Slovis, B.S., Miller, R.F., Ninan, M., Miller, Y.E., Franklin, W.A., Caprioli, R.M., Carbone, D.P. and Massion, P.P. (2005) ***Am. J. Respir. Crit. Care Med***., **172,** 1556-1562.

[64] Jorgensen, E.D., Dozmorov, I., Frank, M.B., Centola, M. and Albino, A.P. (2004) ***Cell Cycle,*** **3,** 1154-1168.

[65] Kerr, K.M. (2001) ***J. Clin. Pathol***., **54,** 257-271.

[66] Lam, S., Kennedy, T., Unger, M., Miller, Y.E., Gelmont, D., Rusch, V., Gipe, B., Howard, D., LeRiche, J.C., Coldman, A. and Gazdar, A.F. (1998) ***Chest,*** **113,** 696-702.

[67] Kennedy, T.C., Lam, S. and Hirsch, F.R. (2001) ***Oncologist***, **6,** 257-262.

[68] Hirsch, F.R., Prindiville, S.A., Miller, Y.E., Franklin, W.A., Dempsey, E.C., Murphy J.R., Bunn, P.A., Jr. and Kennedy, T.C. (2001) ***J. Natl. Cancer Inst***., **93,** 1385-1391.

[69] Hirsch, F.R., Franklin, W.A., Gazdar, A.F. and Bunn, P.A., Jr. (2001) ***Clin. Cancer Res***., **7,** 5-22.

[70] Lee, J.J., Liu, D., Lee, J.S., Kurie, J.M., Khuri, F.R., Ibarguen,H., Morice, R.C., Walsh, G., Ro, J.Y., Broxson, A., Hong, W.K. and Hittelman, W.N. (2001) ***J. Natl. Cancer Inst***., **93,** 1081-1088.

[71] Keith, R.L., Miller, Y.E., Gemmill, R.M., Drabkin, H.A., Dempsey, E.C., Kennedy, T.C., Prindiville, S. and Franklin, W.A. (2000) ***Clin. Cancer Res***., **6,** 1616-1625.

[72] Merrick, D.T., Haney, J., Petrunich, S., Sugita, M., Miller, Y.E., Keith, R.L., Kennedy ,T.C. and Franklin, W.A. (2005) ***Lung Cancer,*** **48,** 31-45.

[73] Westra, W.H. (2000) ***Respir. Med***., **1,** 163-169.

[74] Weng, S.Y., Tsuchiya, E., Kasuga, T. and Sugano, H. (1992) ***Virchows Arch. A. Pathol. Anat. Histopathol***., **420,** 463-471.

[75] Nakanishi, K. (1990) ***Arch. Pathol. Lab. Med***., **114,** 363-368.

[76] Chapman, A.D. and Kerr, K.M. (2000) ***Br. J. Cancer,*** **83,** 632-636.

[77] Koga, T., Hashimoto, S., Sugio, K., Yonemitsu, Y., Nakashima, Y., Yoshino, I., Matsuo , Y., Mojtahedzadeh, S., Sugimachi, K. and Sueishi, K. (2002) ***Am. J. Clin. Pathol***., **117**, 464-70.

[78] Yokose, T., Doi, M., Tanno, K., Yamazaki, K. and Ochiai, A. (2001) ***Lung Cancer,*** **33,** 155-161.

[79] Jensen-Taubman, S.M., Steinberg, S.M. and Linnoila, R.I. (1998) ***Int. J. Cancer,*** **75,** 489-496.

[80] Ullmann, R., Bongiovanni, M., Halbwedl, I., Petzmann, S., Gogg-Kammerer, M., Sapino, A., Papotti, M., Bussolati, G. and Popper, H.H. (2003) ***Virchows Arch***., **442,** 429-436.

[81] Kitamura, H., Kameda, Y., Ito, T. and Hayashi, H. (1999) ***Am. J. Clin. Pathol***., **111,** 610-622.

[82] Tominaga, M., Sueoka, N., Irie, K., Iwanaga, K., Tokunaga,O., Hayashi, S.I., Nakachi, K. and Sueoka, E. (2003)***LungCancer,*** **40,** 45-53.

[83] Nakanishi, K., Kawai, T., Kumaki, F., Hiroi, S., Mukai, M. and Ikeda, E. (2003) ***Am. J. Clin. Pathol***., **120,** 712-719.

[84] Kitaguchi, S., Takeshima, Y., Nishisaka, T. and Inai,K. (1998) ***Hiroshima. J. Med. Sci***., **47,** 17-25.

[85] Takamochi, K., Ogura, T., Suzuki, K., Kawasaki, H., Kurashima, Y., Yokose, T., Ochiai, A., Nagai, K., Nishiwaki, Y. and Esumi, H. (2001) ***Am. J. Pathol***., **159,** 1941-1948.

[86] Nakanishi, K., Kawai, T., Kumaki, F., Hirot, S., Mukai, M. and Ikeda, E. (2002) ***Hum. Pathol***., **33,** 697-702.

[87] Ghaffar, H., Sahin, F., Sanchez-Cespedes, M., Su, G.H., Zahurak, M., Sidransky, D. and Westra, W.H. (2003) ***Clin. Cancer Res***., **9,** 2998-3003.

[88] Nikitin, A.Y., Alcaraz, A., Anver, M.R., Bronson, R.T., Cardiff, R.D., Dixon, D., Fraire, A.E., Gabrielson, E.W., Gunning, W.T., Haines, D.C., Kaufman, M.H., Linnoila, R.I., Maronpot, R.R., Rabson, A.S., Reddick, R.L., Rehm, S., Rozengurt, N., Schuller, H.M., Shmidt, E.N., Travis, W.D., Ward, J.M. and Jacks, T. (2004) ***Cancer Res***., **64,** 2307-2316.

[89] Kim, C.F., Jackson, E.L., Woolfenden, A.E., Lawrence, S., Babar, I., Vogel, S., Crowley, D., Bronson, R.T. and Jacks, T. (2005) ***Cell,*** **121,** 823-835.

[90] Wislez, M., Spencer, M.L., Izzo, J.G., Juroske, D.M., Balhara, K., Cody, D.D., Price, R.E., Hittelman, W.N., Wistuba, I.I. and Kurie, J.M. (2005) ***Cancer Res***., **65,** 3226-3235.

[91] Collado, M., Gil, J., Efeyan, A., Guerra, C., Schuhmacher, A.J., Barradas, M., Benguria, A., Zaballos, A., Flores, J.M., Barbacid, M., Beach, D. and Serrano, M. (2005) ***Nature,*** **436,** 642.

[92] Paez, J.G., Janne, P.A., Lee, J.C., Tracy, S., Greulich, H., Gabriel ,S., Herman, P., Kaye, F.J., Lindeman, N., Boggon, T.J., Naoki, K., Sasaki, H., Fujii, Y., Eck, M.J., Sellers, W.R.,

Johnson, B.E. and Meyerson, M. (2004) ***Science,*** **304,** 1497-1500.

[93] Lynch, T.J., Bell, D.W., Sordella, R., Gurubhagavatula, S., Okimoto, R.A., Brannigan, B.W., Harris, P.L., Haserlat, S.M., Supko, J.G., Haluska, F.G., Louis, D.N., Christiani, D.C., Settleman, J. and Haber, D.A. (2004) ***N. Engl. J. Med***., **350,** 2129-2139.

[94] Pao, W., Miller, V., Zakowski, M., Doherty, J., Politi, K., Sarkaria, I., Singh, B., Heelan, R., Rusch, V., Fulton, L., Mardis, E., Kupfer, D., Wilson, R., Kris, M. and Varmus, H. (2004) ***Proc. Natl. Acad. Sci. USA***, **101,** 13306-13311.

[95] Huang, S.F., Liu, H.P., Li, L.H., Ku, Y.C., Fu, Y.N., Tsai, H.Y., Chen, Y.T., Lin, Y.F., Chang, W.C., Kuo, H.P., Wu, Y.C., Chen, Y.R. and Tsai, S.F. (2004) ***Clin. Cancer Res***., **10,** 8195-8203.

[96] Kosaka, T., Yatabe, Y., Endoh, H., Kuwano, H., Takahashi, T. and Mitsudomi, T. (2004) ***Cancer Res***., **64,** 8919-8923.

[97] Tokumo, M., Toyooka, S., Kiura K., Shigematsu, H., Tomii, K., Aoe, M., Ichimura, K., Tsuda, T., Yano, M., Tsukuda, K., Tabata, M., Ueoka, H., Tanimoto, M., Date, H., Gazdar, A.F. and Shimizu, N. (2005) ***Clin. Cancer Res***., **11,** 1167-1173.

[98] Shigematsu, H., Lin, L., Takahashi, T., Nomura, M., Suzuki, M., Wistuba, II, Fong, K.M., Lee, H., Toyooka, S., Shimizu, N., Fujisawa, T., Feng, Z., Roth, J.A., Herz, J., Minna, J.D. and Gazdar, A.F. (2005) ***J. Natl. Cancer Inst***., **97,** 339-346.

[99] Shigematsu, H., Takahashi, T., Nomura, M., Majmudar, K., Suzuki, M., Lee, H., Wistuba, II, Fong, K.M., Toyooka, S., Shimizu, N., Fujisawa, T., Minna, J.D. and Gazdar, A.F. (2005) ***Cancer Res***., **65,** 1642-1646.

[100] Amann, J., Kalyankrishna, S., Massion, P.P., Ohm, J.E., Girard, L., Shigematsu, H., Peyton, M., Juroske, D., Huang, Y., Stuart Salmon, J., Kim, Y.H., Pollack, J.R., Yanagisawa, K., Gazdar, A., Minna, J.D., Kurie, J.M. and Carbone, D.P. (2005) ***Cancer Res***., **65,** 226-235.

[101] Cappuzzo, F., Hirsch, F.R., Rossi, E., Bartolini, S., Ceresoli, G.L., Bemis, L., Haney, J., Witta, S., Danenberg, K., Domenichini, I., Ludovini, V., Magrini, E., Gregorc, V., Doglioni, C., Sidoni, A., Tonato, M., Franklin, W.A., Crino, L., Bunn, P.A., Jr. and Varella-Garcia, M. (2005) ***J. Natl. Cancer Inst***., **97,** 643-655.

[102] Hirsch, F.R., Varella-Garcia, M., McCoy, J., West, H., Xavier, A.C., Gumerlock, P., Bunn, P.A., Jr., Franklin, W.A., Crowley, J. and Gandara, D.R. (2005) ***J. Clin. Oncol***., **23**, 6838-6845.

[103] Tsao, M.S., Sakurada, A., Cutz, J.C., Zhu, C.Q., Kamel-Reid, S., Squire, J., Lorimer, I., Zhang, T., Liu, N., Daneshmand, M., Marrano, P., da Cunha Santos, G., Lagarde, A., Richardson, F., Seymour, L., Whitehead, M., Ding, K., Pater, J. and Shepherd, F.A. (2005) ***N. Engl. J. Med***., **353,** 133-144.

[104] Yatabe, Y., Kosaka, T., Takahashi, T. and Mitsudomi, T. (2005) ***Am. J. Surg. Pathol***., **29,** 633-639.

[105] Yoshida, Y., Shibata, T., Kokubu, A., Tsuta, K., Matsuno, Y., Kanai, Y., Asamura, H., Tsuchiya, R. and Hirohashi, S. (2005) ***Lung Cancer***. **50**, 1-8.

[106] Massarelli, E. and Herbst, R.S. (2006) ***Semin. Oncol***., **33,** S9-16.

[107] Santarpia, M., Altavilla, G., Salazar, F., Taron, M. and Rosell, R. (2006) ***Clin. Transl. Oncol***., **8,** 71-76.

[108] Abbruzzese, J.L. and Lippman, S.M. (2004) ***Cancer Cell,*** **6,** 321-326.

[109] Khuri, F.R. and Cohen, V. (2004) ***Clin. Cancer Res***., **10,** 4249s-4253s.

[110] Hirsch, F.R. and Lippman, S.M. (2005) ***J. Clin. Oncol***., **23,** 3186-3197.

[111] Westra, W.H., Baas, I.O., Hruban, R.H., Askin, F.B., Wilson, K., Offerhaus, G.J. and Slebos, R.J. (1996) ***Cancer Res***., **56,** 2224-2228.

[112] Wislez, M., Fujimoto, N., Izzo, J.G., Hanna, A.E., Cody, D.D., Langley, R.R., Tang, H., Burdick, M.D., Sato, M., Minna, J.D., Mao, L., Wistuba, I., Strieter, R.M. and Kurie, J.M. (2006) ***Cancer Res***., **66,** 4198-4207.

[113] Merrick, D.T., Kittelson, J., Winterhalder, R., Kotantoulas, G., Ingeberg, S., Keith, R.L., Kennedy, T.C., Miller, Y.E., Franklin, W.A. and Hirsch, F.R. (2006) ***Clin. Cancer Res***., **12,** 2281-2288.

[114] Tsao, A.S., McDonnell, T., Lam, S., Putnam, J.B., Bekele, N., Hong, W.K. and Kurie, J.M. (2003) ***Cancer Epidemiol. Biomarkers Prev***., **12,** 660-664.

[115] Balsara, B.R., Pei, J., Mitsuuchi, Y., Page, R., Klein-Szanto, A., Wang, H., Unger, M. and Testa, J.R. (2004) ***Carcinogenesis,*** **25,** 2053-2059.

[116] Lee, H.Y., Oh, S.H., Woo, J.K., Kim, W.Y., Van Pelt, C.S., Price, R.E., Cody, D., Tran , H., Pezzuto, J.M., Moriarty, R.M. and Hong, W.K. (2005) ***J. Natl. Cancer Inst***., **97,** 1695-1699.

[117] Lee, H.Y., Moon, H., Chun, K.H., Chang Y.S., Hassan, K., Ji, L., Lotan, R., Khuri, F.R. and Hong, W.K. (2004) ***J. Natl. Cancer Inst***, **96,** 1536-1548.

[118] Sato, M., Vaughan, M.B., Girard, L., Peyton, M., Lee, W., Shames, D.S., Ramirez, R.D., Sunaga, N., Gazdar, A.F., Shay, J.W. and Minna, J.D. (2006) ***Cancer Res***., **66,** 2116-2128.

[119] Kwak, I., Tsai, S.Y. and DeMayo, F.J. (2004) ***Annu. Rev. Physiol***., **66,** 647-663.

[120] Kobayashi, K., Nishioka, M., Kohno, T., Nakamoto, M., Maeshima, A., Aoyagi, K., Sasaki, H., Takenoshita, S., Sugimura, H. and Yokota, J. (2004) ***Oncogene,*** **23,** 3089-3096.

[121] Yanagisawa, K., Shyr, Y., Xu, B.J., Massion, P.P., Larsen, P.H., White, B.C., Roberts, J.R., Edgerton, M., Gonzalez, A., Nadaf, S., Moore, J.H., Caprioli, R.M. and Carbone, D.P. (2003) ***Lancet,*** **362,** 433-439.

Received: June 28, 2006 **Revised: July 15, 2006** **Accepted: July 31, 2006**

Lung Cancer Preneoplasia

Ignacio I. Wistuba[1] and Adi F. Gazdar[2]

[1]Departments of Pathology and Thoracic/Head and Neck Medical Oncology, M.D. Anderson Cancer Center, University of Texas, Houston, Texas 77030; email: iiwistuba@mdanderon.org

[2]Hamon Center for Therapeutic Oncology Research and Department of Pathology University of Texas Southwestern Medical Center, Dallas, Texas 75390; email: adi.gazdar@utsouthwestern.edu

Annu. Rev. Pathol. Mech. Dis.
2006. 1:331–48

First published online as a Review in Advance on October 26, 2005

The *Annual Review of Pathology: Mechanisms of Disease* is online at pathmechdis.annualreviews.org

doi: 10.1146/annurev.pathol.1.110304.100103

1553-4006/06/0114-0331$20.00

Key Words

smoking, bronchial dysplasia, atypical adenomatous hyperplasia, EGFR mutations

Abstract

From histological and biological perspectives, lung cancer is a complex neoplasm. Although the sequential preneoplastic changes have been defined for centrally arising squamous carcinomas of the lung, they have been poorly documented for the other major forms of lung cancers, including small cell lung carcinoma and adenocarcinomas. There are three main morphologic forms of preneoplastic lesions recognized in the lung: squamous dysplasias, atypical adenomatous hyperplasia, and diffuse idiopathic pulmonary neuroendocrine cell hyperplasia. However, these lesions account for the development of only a subset of lung cancers. Several studies have provided information regarding the molecular characterization of lung preneoplastic changes, especially for squamous cell carcinoma. These molecular changes have been detected in the histologically normal and abnormal respiratory epithelium of smokers. Two different molecular pathways have been detected in lung adenocarcinoma pathogenesis: smoking-associated activation of RAS signaling, and nonsmoking-associated activation of EGFR signaling; the latter is detected in histologically normal respiratory epithelium.

INTRODUCTION

SCLC: small cell lung carcinoma

NSCLC: non-small cell lung carcinoma

CIS: carcinoma in situ

AAH: atypical adenomatous hyperplasia

Lung cancer is the leading cause of cancer deaths in the United States and worldwide (1). The high mortality rate of this disease is due primarily to the fact that the majority of lung cancers are diagnosed at advanced stages when the options for treatment are mostly palliative. Experience with other epithelial tumors, such as uterine, cervical, esophageal, and colon carcinomas, has shown that if neoplastic lesions can be detected and treated at their intraepithelial stage the chances for survival can be improved significantly. Thus, to reduce the mortality rate of lung cancer, new techniques and approaches must be developed to diagnose and treat pre-invasive lesions. However, the early diagnosis of lung cancer represents an enormous challenge. From histopathological and biological perspectives, lung cancer is a highly complex neoplasm (2), probably having multiple preneoplastic pathways.

Lung cancer consists of several histological types, including small cell lung carcinoma (SCLC) and non-small cell lung carcinoma (NSCLC) types of squamous cell carcinoma, adenocarcinoma (including the noninvasive type of bronchioloalveolar carcinoma), and large cell carcinoma (3). Lung cancers may arise from the major bronchi (central tumors) or small bronchi, bronchioles, or alveoli (peripheral tumors) of the distant airway of the lung. Squamous cell carcinomas and SCLCs usually arise centrally, whereas adenocarcinomas and large cell carcinomas usually arise peripherally. However, the specific respiratory epithelial cell type from which each lung cancer type develops has not been established. As with other epithelial malignancies, researchers believe lung cancers arise after a series of progressive pathological changes, known as preneoplastic or premalignant lesions (4). Although the sequential preneoplastic changes have been defined for centrally arising squamous carcinomas of the lung, they have been poorly documented for the other major forms of lung cancers (4).

Although many molecular abnormalities have been described in clinically evident lung cancers (2), relatively little is known about the molecular events preceding the development of lung carcinomas and the underlying genetic basis of lung carcinogenesis. In the past decade, several studies have provided information regarding the molecular characterization of the preneoplastic changes involved in the pathogenesis of lung cancer, especially squamous cell carcinoma and adenocarcinoma (5, 6). Many of these molecular changes have been detected in the histologically normal respiratory mucosa of smokers (5).

The high-risk population targeted for early detection efforts are heavy smokers and patients who have survived a cancer of the upper aerodigestive tract. However, conventional morphologic methods for the identification of premalignant cell populations in the lung airways have important limitations. This has led to research in biological properties, including molecular and genetic changes, of the respiratory epithelium and its corresponding preneoplastic cells and lesions. Further research in this area may provide new methods for assessing the likehood of developing invasive lung cancer in smokers and allow for early detection and monitoring of their response to chemopreventive regimens.

In this review we will describe the recognized preneoplastic lesions for major types of lung cancers, such as bronchial squamous dysplasia and carcinoma in situ (CIS) for squamous cell carcinoma (7); atypical adenomatous hyperplasia (AAH), a putative preneoplastic lesion, for a subset of adenocarcinomas (6); and neuroendocrine cell hyperplasia for neuroendocrine lung carcinomas (7). In addition, we will review the current concepts of early pathogenesis and the progression of lung cancer.

OVERVIEW OF LUNG CANCER MOLECULAR PATHOLOGY

Several molecular and genetic studies have revealed that multiple genetic and epigentic changes are found in clinically evident lung cancers, involving known and putative recessive oncogenes (tumor suppressor genes, TSGs) as well as several dominant oncogenes (8). Most of the molecular and genetic studies of lung cancers have been performed on the major types of lung cancer (2). Many growth factors or regulatory peptides and their receptors are overexpressed by cancer cells and adjacent normal-appearing cells in the lung, and thus provide a series of autocrine and paracrine growth stimulatory loops in this neoplasm (9). The list of recessive oncogenes involved in lung cancer is likely to include as many as 10 to 15 known and putative genes (2), and possibly many more. Oncogenes that contribute to the pathogenesis of lung cancer include *CMYC*, mutated *KRAS* (10% to 20%, predominantly adenocarcinomas), overexpression of *Cyclin D1* and *BCL2*, and mutations in *ERBB* family genes such as *EGFR* (epidermal growth factor receptor) (10–12) and *HER2/neu* (12, 13). The latter two oncogenes occur almost exclusively in adenocarcinomas, patients of East Asian ethnic groups, and non- or light smokers (12). Several TSGs, such as *TP53* (17p13), *RB* (13q14), $p16^{INK4a}$ (9p21), and new candidate TSGs at several chromosomal regions, including the short arm of chromosomes 3 (3p12, *DUTT1* gene; 3p14.2, *FHIT* gene; 3p21, *RASFF1A* and *FUS-1* gene; 3p22–24, *BAP-1* gene), show frequent abnormalities in lung cancer (2). Recessive oncogenes are believed to be inactivated via a two-step process involving both alleles. Knudson has proposed that the first hit is frequently a point mutation, whereas the second allele is subsequently inactivated via a chromosomal deletion, translocation, or other event such as methylation of gene promoter regions (14). In addition to those specific genetic changes, other evidence indicates that genetic instability is concurrent with lung cancer. This evidence includes changes in the number of short-tandem DNA repeats (also known as microsatellites), which are frequently present in a wide variety of cancer types, including lung. Overall, an average of 35% (range 0%–76%) of SCLCs and 22% (range 2%–49%) of NSCLCs show some evidence of genetic instability at individual loci (8).

TSG: tumor suppressor gene

EGFR: epidermal growth factor receptor

Studies of many lung cancers have demonstrated different patterns of molecular alterations between the two major groups of lung carcinomas (SCLC and NSCLC) (15, 16) and among the two major histologic types of NSCLC (squamous cell carcinomas and adenocarcinomas) (17–20). Allelic loss analyses at different chromosomal regions and the methylation status of multiple genes have provided clear evidence, on a genome-wide scale, that SCLC and NSCLC differ significantly in the TSGs that are inactivated during their pathogenesis (21–24). In addition, a variety of studies on gene expression profiles have sought to identify specific profiles and new molecular markers for histologically different lung cancers, including adenocarcinomas (25, 26). Specifically, we have found different patterns of allelic loss involving the two major histologic types of NSCLC, with higher incidences of deletions at 17p13 (*TP53*), 13q14 (*RB*), 9p21 ($p16^{INK4a}$), 8p21–23, and several 3p regions in squamous cell carcinomas (17, 27, 28). Recently, differences in $p16^{INK4a}$, *APC*, and *H-cadherin* gene methylation frequencies have been detected between squamous cell and adenocarcinoma, suggesting that different gene methylation patterns characterize the two major histologic types of NSCLC (24). Recent findings indicate that mutations in three genes, *KRAS*, *EGFR*, and *Her2/neu*, occur almost exclusively in lung cancers of adenocarcinoma histology (12, 29). In lung adenocarcinoma, *KRAS* and *EGFR* mutations are mutually exclusive, which indicates two distinct pathways for lung adenocarcinoma development (12, 30). Whereas in smokers tobacco-related carcinogens favor *KRAS* mutations, in nonsmokers unidentified

carcinogens induce *EGFR* mutations (30). We refer to nonsmokers as people who have never smoked.

LUNG CANCER PRENOPLASTIC LESIONS

Lung cancers are believed to arise after a series of progressive pathological changes (preneoplastic or precursor lesions) in the respiratory mucosa. Although the sequential preneoplastic changes have been defined for centrally arising squamous carcinomas, they have been poorly documented for large cell carcinomas, adenocarcinomas, and SCLCs (4, 7). Mucosal changes in the large airways that may precede invasive squamous cell carcinoma include squamous dysplasia and CIS (4, 7). Adenocarcinomas may be preceded by morphological changes including AAH (4, 6) in peripheral airway cells. For SCLC, no specific preneoplastic changes have been described in the respiratory epithelium. Current information suggests that preneoplastic lesions are frequently extensive and multifocal throughout the lung, indicating a field effect (field cancerization) by which much of the respiratory epithelium has been mutagenized, presumably from exposure to tobacco-related carcinogens (5).

The recent histological classification of pre-invasive lung lesions by the World Health Organization (WHO) lists three main morphologic forms of preneoplastic lesions (3): (*a*) squamous dysplasia and CIS, (*b*) AAH, and (*c*) diffuse idiopathic pulmonary neuroendocrine cell hyperplasia (DIPNECH). However, as we will explain in this review, these lesions account for the development of only a subset of lung cancers.

Squamous Cell Carcinoma Preneoplastic Lesions

Mucosal changes in the large airways that may precede or accompany invasive squamous cell carcinoma include hyperplasia, squamous metaplasia, squamous dysplasia, and CIS (**Figure 1**) (4, 7). Two types of bronchial epithelial hyperplasia that are thought to be reactive lesions, goblet cell hyperplasia and basal cell (reserve cell) hyperplasia, may occur. Dysplastic squamous lesions are considered true preneoplastic lesions and may vary in degree (i.e., mild, moderate, or severe); however, these lesions represent a continuum of cytologic and histologic atypical changes that may show some overlapping features between categories. Whereas mild squamous dysplasia is characterized by minimal architectural and cytological disturbance, moderate dysplasia exhibits more cytological irregularity, which is even higher in severe dysplasia and is accompanied by considerable cellular polymorphism. In a subset of squamous dysplastic changes, the basal membrane thickens and there is vascular budding in the subepithelial tissues that results in papillary protrusions of the epithelium, lesions that have been termed angiogenic squamous dysplasia (31). CIS demonstrates extreme cytological aberrations with almost complete architectural disarray, but with an intact basement membrane and absence of stromal invasion. Foci of CIS usually arise near bifurcations in the segmental bronchi, subsequently extending proximally into the adjacent lobar bronchus and distally into subsegmental branches. These lesions are often not detected by conventional white-light bronchoscopy or gross examination. However, the utilization of fluorescent bronchoscopy, such as lung-imaging fluorescent endoscopy (LIFE), greatly increases the sensitivity for detection of squamous dysplastic and CIS lesions (32–34). Little is known about the rate and risks of progression from squamous dysplasia to CIS and ultimately to invasive squamous cell carcinoma. Recently, a longitudinal study addressing the natural histopathologic course of squamous preneoplastic lesions in bronchial epithelium using white-light and fluorescent bronchoscopy examinations was reported (35). In this study, the progression rate to CIS and invasive carcinoma was significantly higher in lesions with severe dysplasia (32%) compared with squamous metaplasias (4%) and low-grade

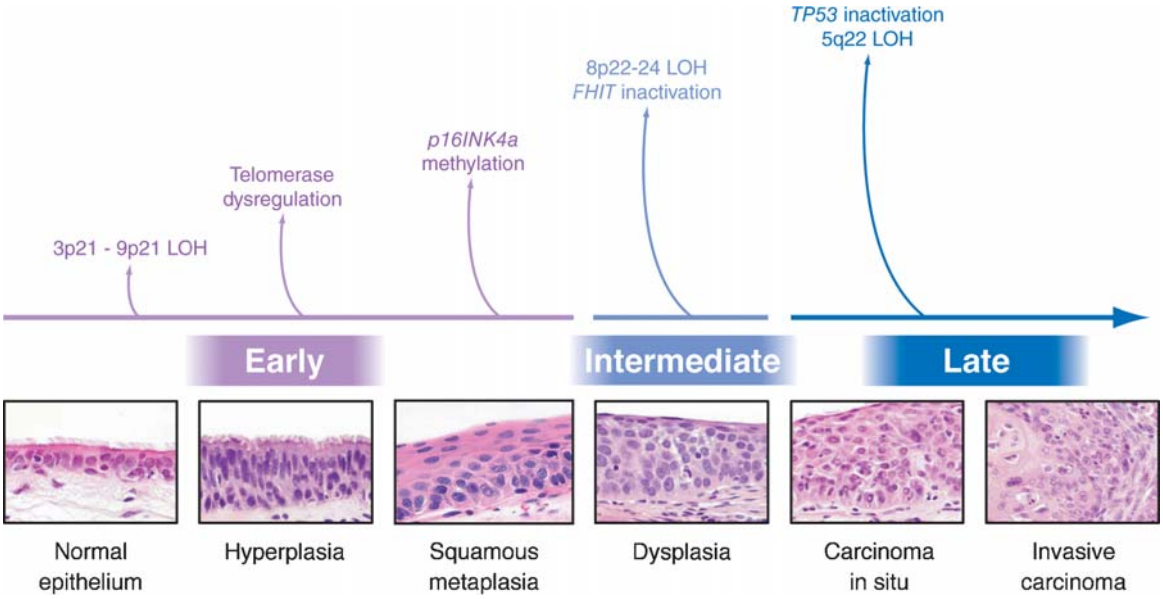

Figure 1

Histopatholological and molecular changes during the pathogenesis of squamous cell carcinoma of the lung with molecular changes commencing at early stages, and a histologically normal respiratory epithelium. There is stepwise molecular and histopathological sequence of events leading to dysplastic and invasive carcinoma stages. LOH, loss of heterozygosity.

dysplasias (9%). Somewhat striking, at the individual level, the rates of progression to squamous carcinoma were not significantly higher in individuals harboring high-grade dysplastic lesions (39%) compared with individuals having only lower-grade lesions (26%). In addition, the study detected the progression from squamous metaplasia and low-grade dysplasias (mild and moderate) to CIS and invasive carcinoma, suggesting that a stepwise histopathologic multistage development of lung squamous cell carcinoma does not always occur, or it is not always detected because of rapid progression. These findings suggest that the current histologic classification of preneoplastic squamous lesions of the bronchial epithelia may not be a reliable guide for risk assessment of lung cancer. Other types of biomarkers, including molecular and genetic markers, are needed.

There are no squamous cells in the normal airways. The progenitor or stem cells for the squamous metaplastic epithelium of the proximal airway is not known, but it is presumed that the basal cells represent a relatively quiescent zone that is the precursor of preneoplastic epithelium. In fact, squamous metaplasia usually precedes and accompanies basal cell hyperplasia. Interestingly, these cells express significant levels of Egfr protein and increased proliferative activity measured by Ki-67 staining (36, 37).

The current working model of the sequential molecular abnormalities in the pathogenesis of squamous cell lung carcinoma (**Figure 1**) indicates the following: (*a*) Genetic abnormalities commence in histologically normal epithelium and grow with increasing severity of histologic changes (27). (*b*) Mutations follow a sequence, with progressive allelic losses at multiple 3p (3p21, 3p14, 3p22–24, and 3p12) chromosome sites and 9p21 ($p16^{INK4a}$) as the earliest detectable changes. Later changes occur at 8p21–23, 13q14 (*RB*), and 17p13 (*TP53*) (17, 27, 28). $p16^{INK4a}$ methylation has also been detected at an early

BAC: bronchioloalveolar carcinoma

stage of squamous pre-invasive lesions with a frequency that increases during histopathologic progression (by 24% in squamous metaplasia and 50% in CIS) (38). (*c*) Molecular changes in the respiratory epithelium are extensive and multifocal throughout the bronchial tree of smokers and lung cancer patients, indicating a field cancerization effect by which much of the respiratory epithelium has been mutagenized, presumably from exposure to tobacco-related carcinogens (27, 28, 39, 40). (*d*) Multiple small patches of histologically normal and hyperplastic epithelium with clonal and subclonal molecular abnormalities, not much larger in size than the average bronchial biopsy obtained by fluorescent bronchoscopy and estimated to be approximately 40,000 to 360,000 cells, such as allelic loss (chromosome 3p and 9p21 regions) and genetic instability, can be detected in the normal and slightly abnormal bronchial epithelium of patients with lung cancer (41). These findings are consistent with evidence of numerous small monosomic and trisomic clonal and subclonal patches present in smoking-damaged upper aerodigestive epithelium as determined by fluorescent in situ hybridization (FISH) analyses (42).

Adenocarcinoma Precursor Lesions

In alveoli, type I pneumocytes are involved in respiratory gas exchange whereas type II cells produce surfactant proteins, essential for preventing alveoli from collapsing (43). In bronchioles, short, stubby ciliated cells and the secretory Clara cells are present. The Clara cells and the type II pneumocytes are believed to be the progenitor cells of the peripheral airways, and peripherally arising adenocarcinomas often express markers of these cell types (44, 45). Researchers suggest that adenocarcinomas may be preceded by AAH in peripheral airway cells (4, 6); however, the respiratory structures and the specific epithelial cell types involved in the origin of most lung adenocarcinomas are unknown. Although there is only one sequence of morphologic change identified so far for the development of invasive lung adenocarcinomas (AAH and bronchioloalveolar carcinoma, BAC), recent data indicate that at least two molecular pathways are involved, the *KRAS* and *EGFR* pathways in smoker and nonsmoker populations, respectively (**Figure 2**).

Atypical adenomatous hyperplasia. AAH is considered a putative precursor of adenocarcinoma (4, 6). AAH is a discrete parenchymal lesion arising in alveoli near terminal and respiratory bronchioles (**Figure 2**) and may be single or multiple lesions. These lesions maintain an alveolar structure lined by rounded, cuboidal, or low columnar cells. The alveolar walls may be slightly thickened by collagen, occasional fibroblasts, and lymphocytes. Cellularity and cytological atypia vary from minimal to high grade. The postulated progression of AAH to adenocarcinoma with BAC features, which is characterized by the growth of neoplastic cells along preexisting alveolar structures without evidences of stromal, pleural, or vascular invasion and without metastasis, is supported by morphometric, cytofluorometric, and molecular studies (6, 7). Distinction between highly atypical AAH and BAC is sometimes difficult. Somewhat arbitrarily, BAC are considered generally >10 mm in diameter, with more pleomorphism, mild stratification, packed cells, and abrupt transitions to adjacent alveolar lining cells. However, the distinction may, on occasion, be difficult. The differentiation phenotype derived from immunohistochemical and ultrastructural features indicates that AAHs originate from the progenitor cells of the peripheral airways (46, 47). Surfactant apoprotein and Clara cell–specific 10-kDd protein are expressed in almost all AAHs (46). As many as 25% of the cells show ultrastructural features of Clara cells and type II pneumocytes (47). Recent results from a study (48) performed in mice and lung cancer mouse models suggest that peripheral bronchioalveolar cells expressing Clara cell–specific protein and surfactant protein-C, and having in vitro stem

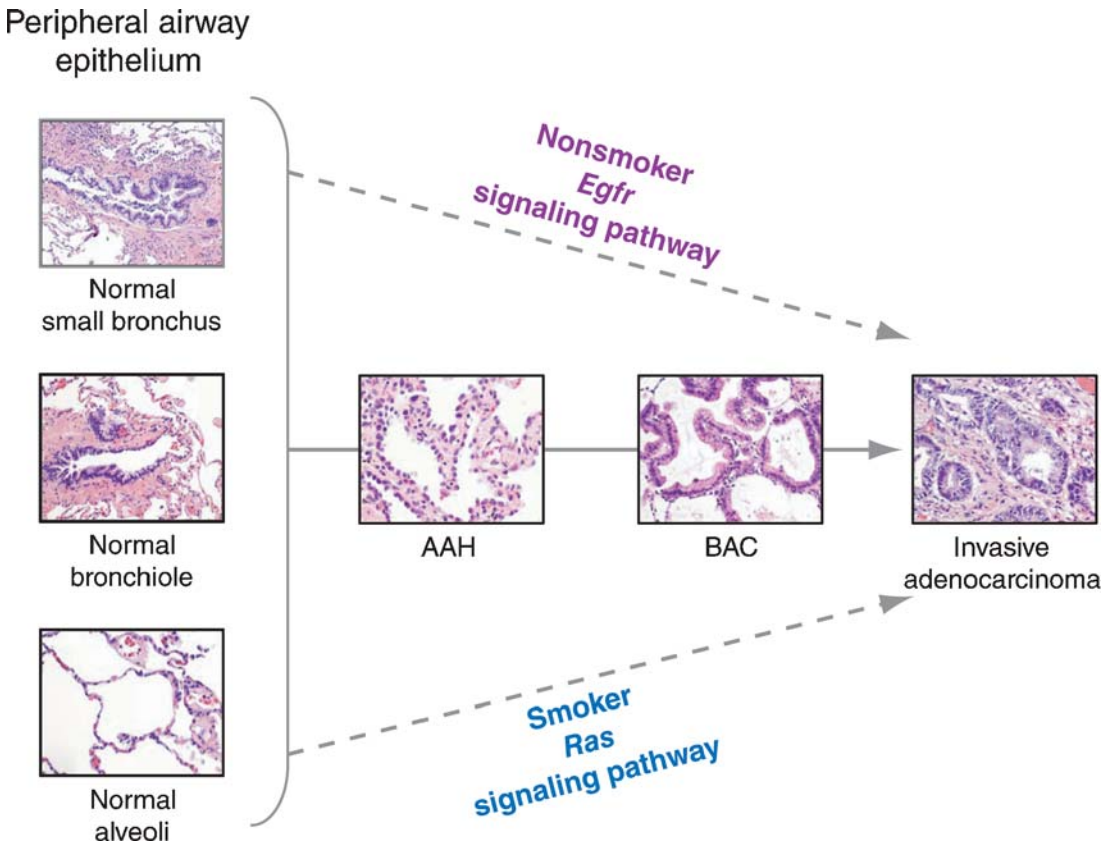

Figure 2

Two molecular pathways involved in the development of lung cancer have been recognized. AAH, atypical adenomatous hyperplasia; BAC, bronchioloalveolar carcinoma.

cell properties (termed bronchioalveolar stem cell, BASC), are the stem cell population that maintains the bronchiolar Clara cells and alveolar cells of the distal respiratory epithelium. In vitro studies performed in the same study indicated that the BASC-transformed counterpart gives rise to adenocarcinoma of the lung. BASCs expanded in response to oncogenic *KRAS* in culture and in precursors of mouse lung tumors in vivo (48).

An increasing body of evidence supports the concept of AAH as the precursor of at least a subset of adenocarcinomas. AAH is most frequently detected in lungs of patients bearing lung cancers (9%–20%), especially adenocarcinomas (as many as 40%), compared with squamous cell carcinomas (11%) (7, 49–52). In contrast, autopsy studies have reported AAH in ~3% of noncancer patients (53). Because inflation of the lungs prior to sectioning (a practice not common in the United States) aids identification, their true incidence may be higher than indicated. Some patients display a large number of AAH lesions (>40) in conjunction with multiple synchronous peripheral lung adenocarcinomas or BACs (51). However, it is extremely difficult to know the progression rate of AAH to lung adenocarcinoma, and it is also currently almost impossible to determine if AAHs may regress. Because they are air-filled structures, they may appear as ground glass opacities on computed tomography scans. However, AAH location, size, and relative invisibility to most imaging

methods make longitudinal studies even more difficult than centrally located squamous preneoplastic lesions.

Several molecular changes frequently present in lung adenocarcinomas are also present in AAH lesions, and they are further evidence that AAH may represent true preneoplastic lesions (46). The most important finding is the presence of *KRAS* (codon 12) mutations in as many as 39% of AAHs, which are also a relatively frequent alteration in lung adenocarcinomas (6, 54). Other molecular alterations detected in AAH are overexpression of Cyclin D1 (~70%), p53 (ranging from 10% to 58%), survivin (48%), and HER2/neu (7%) proteins (6, 55, 56). Some AAH lesions have demonstrated loss of heterozygosity (LOH) in chromosomes 3p (18%), 9p ($p16^{INK4a}$, 13%), 9q (53%), 17q, and 17p (*TP53*, 6%), changes that are frequently detected in lung adenocarcinomas (57, 58). A study on lung adenocarcinoma with synchronous multiple AAHs showed frequent LOH of tuberous sclerosis complex (TSC)-associated regions (*TSC1* at 9q, 53%, and *TSC2* at 16p, 6%), suggesting that these are candidate loci for TSG in a subset of adenocarcinomas of the lung (58). Some cases of AAH have been monoclonal, suggesting that it may be a true preneoplastic lesion (59). Activation of telomerase, required for the perpetuation of cancer cells and expressed by human telomerase RNA component and telomerase reverse transcriptase mRNA, has been detected in 27% to 78% of AAH lesions, depending on their atypia level (60). Recently, it was shown that loss of *LKB1*, a serine/threonine kinase that functions as a TSG, is frequent in lung adenocarcinomas (25%) and AAH (21%) with severe cytological atypia, whereas it is rare in mild atypical AAH lesions (5%), suggesting that *LKB1* inactivation may play a role in the AAH progression to malignancy (61).

Bronchial and bronchiolar epithelium as precursors of adenocarcinomas. Despite evidence that AAH is a precursor lesion for peripheral lung adenocarcinomas, there is general consensus that the pathogenesis of many adenocarcinomas, especially those of central origin, is still unknown. The presence of *KRAS* mutations in bronchiolar epithelium with atypical changes raised the possibility that non-AAH lesions could also be the origin of lung adenocarcinomas (62). The recent findings of several distinct genetic changes specifically associated with lung adenocarcinoma, such as *EGFR* (10–12), *Her2/neu* (29), and *BRAF* (63) genes mutations, represent a unique opportunity to study further the pathogenesis of adenocarcinomas of the lung.

Somatic mutations of *EGFR*, a tyrosine kinase (TK) of the *ERBB* family, have been reported recently in a subset of lung adenocarcinomas (10–12, 64–67) (**Figure 3**). Those mutations are clinically relevant because most of them have been associated with sensitivity of lung adenocarcinoma to small molecule TK inhibitors (gefitinib and erlotinib) (10, 11, 64, 68). The mutations are associated significantly with adenocarcinoma histology, non- or light-smoker status, females, and East Asian ethnic groups (12). Data analysis from 13 (10, 12, 45, 65–67, 69–75) recently published studies on *EGFR* mutations in surgically resected specimens in more than 1600 lung cancers indicates that the incidence of mutations in adenocarcinomas is at least fourfold higher in East Asian populations (China, Japan, Korea, and Taiwan) compared with Western populations (Australia, Italy, and the United States) (**Figure 3*a***). Analysis of 721 *EGFR* mutations reported from surgically resected (12, 65–67, 69–71, 73–75) and small-biopsy lung cancer specimens (10, 11, 71, 76–82) demonstrated that more than 90% of the mutations detected in *EGFR* are in-frame deletions in exon 19, and there was a single missense mutation in exon 21 (L858R) (10–12, 64–67) (**Figure 3*b***). Researchers propose that lung cancer cells with mutant *EGFR* may become physiologically dependent on the continued activity of the gene for the maintenance of their malignant phenotype, which leads to accelerated development of lung adenocarcinoma (30). Recent studies indicate that

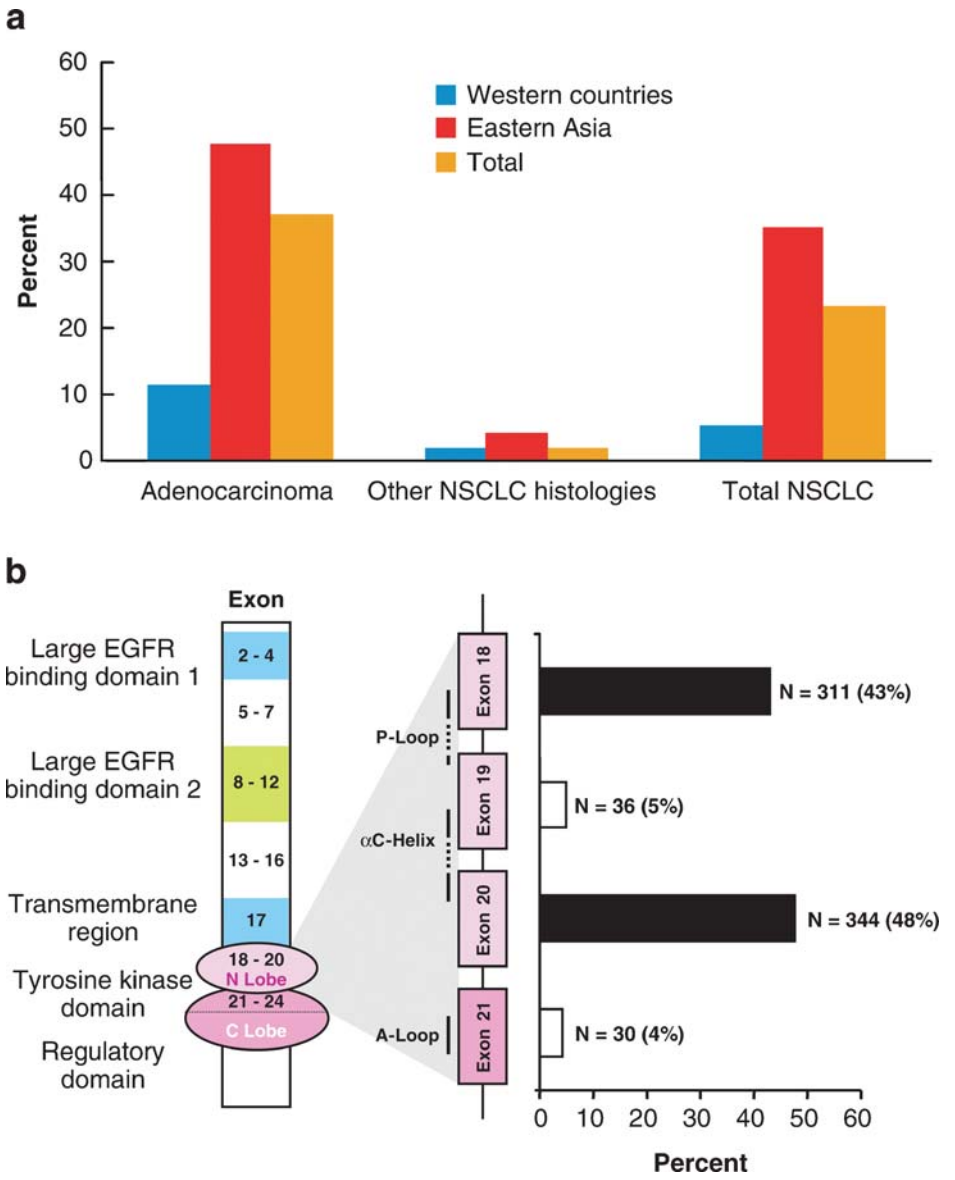

Figure 3

(*a*) Summary of epidermal growth factor receptor (*EGFR*) gene mutation frequency in lung cancer by histology and country of origin. Data analysis from 13 (10, 12, 45, 65–67, 69–75) recently published studies examining more than 1600 lung cancers have been summarized. (*b*) Summary of exon distribution of 721 *EGFR* mutations reported from surgically resected (12, 65–67, 69–71, 73–75) and small-biopsy (10, 11, 71, 76–82) lung cancer specimens.

tumor cell high *EGFR* copy number, identified by FISH technique and Egfr immunohistochemical expression, may also be effective predictors for EGFR TK inhibitors (76, 79, 83).

Some studies have investigated Egfr expression in centrally located bronchial preneoplastic lesions of the lung (36, 84), which are considered markers for squamous metaplasia (84). In lung adenocarcinoma, recent studies indicate that the recently identified TK domain of *EGFR* mutations is an early development in the pathogenesis of lung cancer, being identified in histologically normal epithelium of small bronchi and bronchioles adjacent to *EGFR* mutant adenocarcinomas (85). We have detected *EGFR* mutations in normal-appearing peripheral respiratory epithelium in 9 out of 21 (43%) adenocarcinoma patients (85), but not in patients without

DIPENECH: diffuse idiopathic pulmonary neuroendocrine cell hyperplasia

mutation in the tumor (85). Our finding of more frequent *EGFR* mutations in normal epithelium within the tumor (43%) than in adjacent sites (24%) suggests a localized field effect phenomenon for this abnormality in the respiratory epithelium of the lung. A higher frequency of mutations in cells obtained from small bronchi (35%) compared with bronchioles (18%) was detected. This finding may correlate with different cell types populating those epithelia, which could represent the site of the cell of origin for *EGFR* mutant adenocarcinomas of the lung. Although the cell type having those mutations is unknown, we hypothesize that stem or progenitor cells of the bronchial and bronchiolar epithelium bear such mutations. The finding of relatively infrequent *EGFR* mutations in AAH lesions (3 out of 40 examined) (45, 86) and the finding of no mutation (12) or relatively low frequency of mutation in true BACs of the lung (86) support the concept that genetic abnormalities of *EGFR* are not relevant in the pathogenesis of alveolar-type lung neoplasia.

The low frequency of molecular abnormalities detected in the centrally located bronchial respiratory epithelium in patients with peripheral lung adenocarcinomas, compared with specimens from patients with squamous cell carcinomas and SCLC (87), suggests the presence of two compartments in the lung with different degrees of smoking-related genetic damage. Thus, smokers who develop squamous cell carcinoma and SCLC have more smoking-related genetic damage in the respiratory epithelium of the central airway, whereas patients who develop adenocarcinoma have damage mainly in the peripheral airways (small bronchus, bronchioles, and alveoli).

Precursor Lesions of Neuroendocrine Tumors

As stated above, the precursor lesions for the most common type of neuroendocrine carcinoma of the lung, the SCLC, are unknown (4, 7). However, a rare lesion termed diffuse idiopathic pulmonary neuroendocrine cell hyperplasia (DIPENECH) has been associated with the development of other neuroendocrine tumors of the lung, typical and atypical carcinoids (4, 88, 89) (**Figure 4**). DIPENECH consists of a generalized proliferation of scattered single cells, small nodules, or linear proliferations of neuroendocrine cells present in the bronchial and bronchiolar epithelium. These lesions include local extraluminal proliferations in the form of tumorlets.

Small cell lung carcinoma precursors. As the development of epithelial cancers requires the stepwise accumulation of multiple mutations, which may represent a mutator phenotype, it is possible that those epithelial cell clones that have accumulated multiple mutations are at higher risk for developing malignant transformation (90). As stated before, no phenotypically identifiable epithelial lesion has been identified as a precursor for SCLC. We performed a study comparing the molecular changes (LOH at several chromosomal sites and microsatellite instability) occurring in histologically normal and mildly abnormal (hyperplastic), centrally located bronchial epithelium accompanying SCLCs and NSCLCs (squamous cell carcinomas and adenocarcinoma) (87). Normal and hyperplastic bronchial epithelium accompanying SCLC demonstrated a significantly higher incidence of genetic abnormalities than those adjacent to NSCLC tumor types (19). These findings indicate that more widespread and more extensive genetic damage is present in bronchial epithelium in patients with SCLC (**Figure 4**). The finding that some specimens of normal or mildly abnormal epithelia accompanying SCLCs have a high incidence of genetic changes (19) suggests that SCLC may arise directly from histologically normal or mildly abnormal epithelium, without passing through a more complex histologic sequence (parallel theory of cancer development).

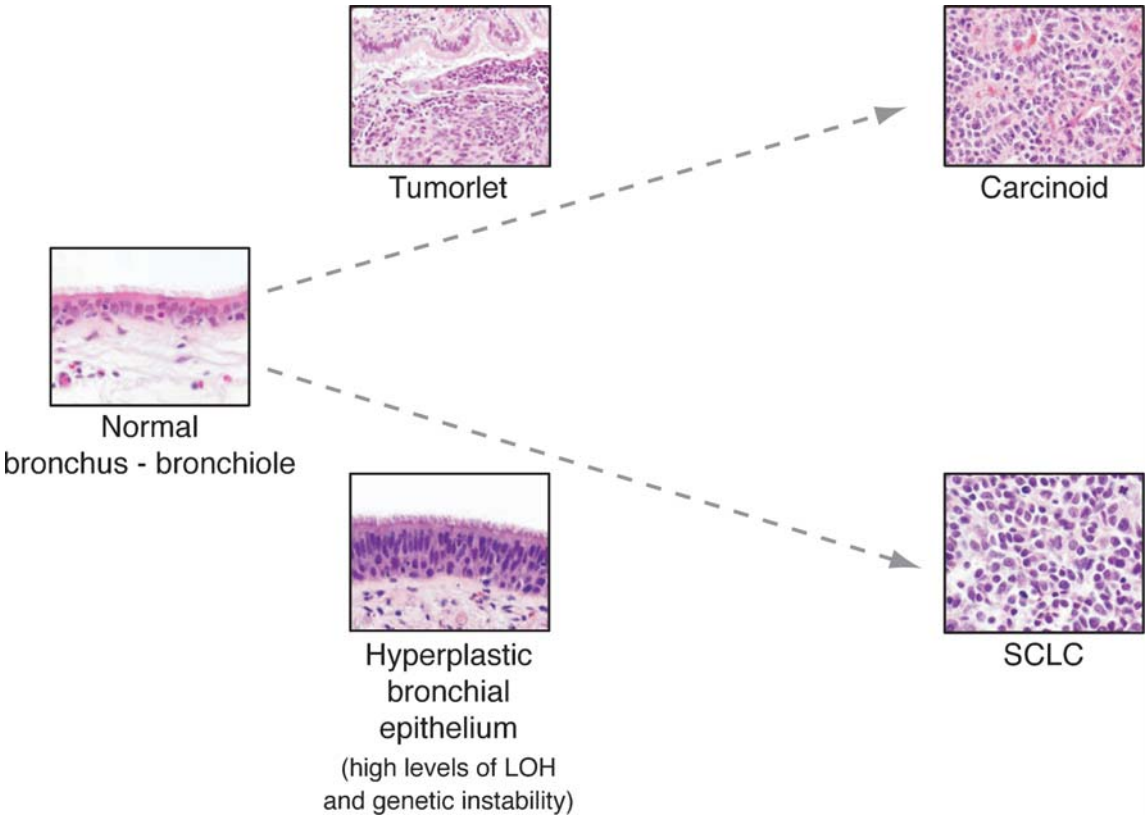

Figure 4

Although the molecular information is limited, available data suggest that tumorlet is the potential precursor for lung carcinoids, and small cell lung carcinoma (SCLC) may arise from molecularly altered, histologically normal, or hyperplastic bronchial epithelium. LOH, loss of heterozygosity.

SMOKING-DAMAGED BRONCHIAL EPITHELIUM

After smoking cessation, the risk of developing lung cancer decreases, but never reaches baseline levels of nonsmokers (91). Advanced lung preneoplastic changes occur more frequently in smokers than nonsmokers, and they increase in frequency with the amount of smoke exposure, adjusted by age (92). Risk factors that identify normal and premalignant bronchial tissue for malignant progression need to be better defined. However, only scant information is available regarding molecular changes in the respiratory epithelium of smokers without cancer. Two independent studies show that the genetic changes (loss of heterozygosity and microsatellite instability) found in invasive cancers and preneoplasia can also be identified in morphologically normal-appearing bronchial epithelium from current or former smokers, and they may persist for many years after smoking cessation (39, 40). In general, such genetic changes are not found in the bronchial epithelium from true nonsmokers. As has been observed in epithelial foci accompanying invasive lung carcinoma (27), allelic losses on chromosomes 3p and 9p are often present. These findings support the hypothesis that identifying genetic abnormalities, such as allelic losses, in biopsies may provide new methods for assessing the risk of smokers developing invasive

lung cancer and monitoring their response to chemoprevention.

We have demonstrated that molecular changes (allelic loss and genomic instability) in the bronchial epithelium may persist long after smoking cessation (39, 40). Of interest, Lee and colleagues (37) reported that smoking appears to elicit a dose-related proliferative response in the bronchial epithelia of active smokers measured by the Ki-67 proliferation index. Although the proliferative response decreased gradually in former smokers, a subset of individuals had detectable proliferation for many years after quitting smoking (37).

Recent results on methylation analysis of several genes, including *RARβ-2*, *H-cadherin*, *APC*, *p16^{INK4a}*, and *RASFF1A*, indicate that abnormal gene methylation is a relatively frequent occurrence in oropharyngeal and bronchial epithelial cells in heavy smokers with evidence of sputum atypia (93). Methylation in one or more of three genes tested (*p16^{INK4a}*, *GSTP1*, and *DAPK*) has been demonstrated in bronchial brush specimens in approximately one third of smoker subjects (94). Aberrant promoter methylation of *p16^{INK4a}* was seen in at least one bronchial epithelial site from 44% of lung cancer patients and cancer-free smokers. No promoter methylation of these genes was detected in bronchial epithelium from nonsmokers. These results indicate that aberrant promoter hypermethylation of the *p16^{INK4a}* gene, and to a lesser extent, *DAPK*, occurs frequently in the bronchial epithelium of lung cancer patients and cancer-free smokers and persists after smoking cessation (95).

SUMMARY POINTS

1. Lung cancer results from the accumulation of multiple genetic and epigenetic changes. Different patterns of molecular alterations have been detected among the major lung cancer histology types.
2. Recent findings indicate that mutation of *KRAS*, *EGFR*, and *Her2/neu* genes occur almost exclusively in lung cancer of adenocarcinoma histology.
3. There are three main morphologic forms of preneoplastic lesions recognized in the lung: squamous dysplasias, atypical adenomatous hyperplasia, and diffuse idiopathic pulmonary neuroendocrine cell hyperplasia. However, these lesions account for the development of only a subset of lung cancers.
4. For squamous cell carcinoma of the lung, the current working model indicates a stepwise sequence of molecular and histopathological changes, with the molecular abnormalities starting in histologically normal and mildly abnormal epithelia.
5. AAH is considered a putative precursor of a subset of lung adenocarcinoma, and they demonstrate similar molecular changes than invasive tumors.
6. Two different molecular pathways have been detected in lung adenocarcinoma pathogenesis: smoking-related pathways associated with *KRAS* mutations and nonsmoking-related pathways associated with *EGFR* mutations; the latter are detected in histologically normal respiratory epithelium.
7. Molecular changes detected in lung tumors and associated preneoplastic lesions have been detected in smoking-damaged epithelium of smokers, including histologically normal bronchial epithelium.

8. Molecular changes in the respiratory epithelium are extensive and multifocal throughout the bronchial tree of smokers and lung cancer patients, indicating a field effect (i.e., field cancerization).

ACKNOWLEDGMENTS

The authors were supported by grant 5U01CA8497102, Specialized Program of Research Excellence (SPORE) in Lung Cancer grant P50CA70907 from the National Cancer Institute, Bethesda, MD (I.I.W. and A.F.G.), and the Department of Defense grant W81XWH-04-1-0142 (I.I.W).

LITERATURE CITED

1. Jemal A, Murray T, Ward E, Samuels A, Tiwari RC, et al. 2005. Cancer statistics, 2005. *CA Cancer J. Clin.* 55:10–30
2. Minna JD, Gazdar A. 2002. Focus on lung cancer. *Cancer Cell* 1:49–52
3. Travis WD, Brambilla E, Muller-Hermelink HK, Harris CC. 2004. Tumours of the lung. In *Pathology and Genetics: Tumours of the Lung, Pleura, Thymus and Heart*, ed. WD Travis, E Brambilla, HK Muller-Hermelink, CC Harris, pp. 9–124. Lyon: IARC
4. Colby TV, Wistuba II, Gazdar A. 1998. Precursors to pulmonary neoplasia. *Adv. Anat. Pathol.* 5:205–15
5. Wistuba II, Mao L, Gazdar AF. 2002. Smoking molecular damage in bronchial epithelium. *Oncogene* 21:7298–306
6. Westra WH. 2000. Early glandular neoplasia of the lung. *Respir. Med.* 1:163–69
7. Kerr KM. 2001. Pulmonary preinvasive neoplasia. *J. Clin. Pathol.* 54:257–71
8. Zochbauer-Muller S, Minna JD. 2000. The biology of lung cancer including potential clinical applications. *Chest Surg. Clin. N. Am.* 10:691–708
9. Viallet J, Sausville EA. 1996. Involvement of signal transduction pathways in lung cancer biology. *J. Cell Biochem. Suppl.* 24:228–36
10. Paez JG, Janne PA, Lee JC, Tracy S, Greulich H, et al. 2004. EGFR mutations in lung cancer: correlation with clinical response to gefitinib therapy. *Science* 304:1497–500
11. Lynch TJ, Bell DW, Sordella R, Gurubhagavatula S, Okimoto RA, et al. 2004. Activating mutations in the epidermal growth factor receptor underlying responsiveness of non-small-cell lung cancer to gefitinib. *N. Engl. J. Med.* 350:2129–39
12. Shigematsu H, Lin L, Takahashi T, Nomura M, Suzuki M, et al. 2005. Clinical and biological features associated with epidermal growth factor receptor gene mutations in lung cancers. *J. Natl. Cancer Inst.* 97:339–46
13. Stephens P, Hunter C, Bignell G, Edkins S, Davies H, et al. 2004. Lung cancer: intragenic ERBB2 kinase mutations in tumours. *Nature* 431:525–26
14. Knudson AG. 1989. Hereditary cancers disclose a class of cancer genes. *Cancer* 63:1888–91
15. Virmani AK, Fong KM, Kodagoda D, McIntire D, Hung J, et al. 1998. Allelotyping demonstrates common and distinct patterns of chromosomal loss in human lung cancer types. *Genes Chromosomes Cancer* 21:308–19
16. Girard L, Zochbauer-Muller S, Virmani AK, Gazdar AF, Minna JD. 2000. Genome-wide allelotyping of lung cancer identifies new regions of allelic loss, differences between small cell lung cancer and non-small cell lung cancer, and loci clustering. *Cancer Res.* 60:4894–906

17. Wistuba II, Behrens C, Virmani AK, Milchgrub S, Syed S, et al. 1999. Allelic losses at chromosome 8p21-23 are early and frequent events in the pathogenesis of lung cancer. *Cancer Res.* 59:1973–79
18. Shivapurkar N, Virmani AK, Wistuba II, Milchgrub S, Mackay B, et al. 1999. Deletions of chromosome 4 at multiple sites are frequent in malignant mesothelioma and small cell lung carcinoma. *Clin. Cancer Res.* 5:17–23
19. Wistuba II, Berry J, Behrens C, Maitra A, Shivapurkar N, et al. 2000. Molecular changes in the bronchial epithelium of patients with small cell lung cancer. *Clin. Cancer Res.* 6:2604–10
20. Wistuba II, Behrens C, Virmani AK, Mele G, Milchgrub S, et al. 2000. High resolution chromosome 3p allelotyping of human lung cancer and preneoplastic/preinvasive bronchial epithelium reveals multiple, discontinuous sites of 3p allele loss and three regions of frequent breakpoints. *Cancer Res.* 60:1949–60
21. Zochbauer-Muller S, Fong KM, Virmani AK, Geradts J, Gazdar AF, Minna JD. 2001. Aberrant promoter methylation of multiple genes in non-small cell lung cancers. *Cancer Res.* 61:249–55
22. Virmani AK, Rahti A, Zöchbauer-Muller S, Sacchi N, Fukuyama Y, et al. 2000. Promoter methylation and silencing of the retinoic acid receptor beta gene in lung carcinomas. *J. Natl. Cancer Inst.* 92:1303–7
23. Burbee DG, Forgacs E, Zochbauer-Muller S, Shivakumar L, Fong K, et al. 2001. Epigenetic inactivation of RASSF1A in lung and breast cancers and malignant phenotype suppression. *J. Natl. Cancer Inst.* 93:691–99
24. Toyooka S, Maruyama R, Toyooka KO, McLerran D, Feng Z, et al. 2003. Smoke exposure, histologic type and geography-related differences in the methylation profiles of non-small cell lung cancer. *Int. J. Cancer* 103:153–60
25. Bhattacharjee A, Richards WG, Staunton J, Li C, Monti S, et al. 2001. Classification of human lung carcinomas by mRNA expression profiling reveals distinct adenocarcinoma subclasses. *Proc. Natl. Acad. Sci. USA* 98:13790–95
26. Beer DG, Kardia SL, Huang CC, Giordano TJ, Levin AM, et al. 2002. Gene-expression profiles predict survival of patients with lung adenocarcinoma. *Nat. Med.* 8:816–24
27. Wistuba II, Behrens C, Milchgrub S, Bryant D, Hung J, et al. 1999. Sequential molecular abnormalities are involved in the multistage development of squamous cell lung carcinoma. *Oncogene* 18:643–50
28. Wistuba II, Behrens C, Virmani AK, Mele G, Milchgrub S, et al. 2000. High resolution chromosome 3p allelotyping of human lung cancer and preneoplastic/preinvasive bronchial epithelium reveals multiple, discontinuous sites of 3p allele loss and three regions of frequent breakpoints. *Cancer Res.* 60:1949–60
29. Shigematsu H, Takahashi T, Nomura M, Majmudar K, Suzuki M, et al. 2005. Somatic mutations of the HER2 kinase domain in lung adenocarcinomas. *Cancer Res.* 65:1642–46
30. Gazdar AF, Shigematsu H, Herz J, Minna JD. 2004. Mutations and addiction to EGFR: the Achilles 'heal' of lung cancers? *Trends Mol. Med.* 10:481–86
31. Keith RL, Miller YE, Gemmill RM, Drabkin HA, Dempsey EC, et al. 2000. Angiogenic squamous dysplasia in bronchi of individuals at high risk for lung cancer. *Clin. Cancer Res.* 6:1616–25
32. Lam S, Kennedy T, Unger M, Miller YE, Gelmont D, et al. 1998. Localization of bronchial intraepithelial neoplastic lesions by fluorescence bronchoscopy. *Chest* 113:696–702
33. Kennedy TC, Lam S, Hirsch FR. 2001. Review of recent advances in fluorescence bronchoscopy in early localization of central airway lung cancer. *Oncologist* 6:257–62

34. Hirsch FR, Prindiville SA, Miller YE, Franklin WA, Dempsey EC, et al. 2001. Fluorescence versus white-light bronchoscopy for detection of preneoplastic lesions: a randomized study. *J. Natl. Cancer Inst.* 93:1385–91
35. Breuer RH, Pasic A, Smit EF, van Vliet E, Vonk Noordegraaf A, et al. 2005. The natural course of preneoplastic lesions in bronchial epithelium. *Clin. Cancer Res.* 11:537–43
36. Hirsch FR, Franklin WA, Gazdar AF, Bunn PA Jr. 2001. Early detection of lung cancer: clinical perspectives of recent advances in biology and radiology. *Clin. Cancer Res.* 7:5–22
37. Lee JJ, Liu D, Lee JS, Kurie JM, Khuri FR, et al. 2001. Long-term impact of smoking on lung epithelial proliferation in current and former smokers. *J. Natl. Cancer Inst.* 93:1081–88
38. Belinsky SA, Nikula KJ, Palmisano WA, Michels R, Saccomanno G, et al. 1998. Aberrant methylation of p16(INK4a) is an early event in lung cancer and a potential biomarker for early diagnosis. *Proc. Natl. Acad. Sci. USA* 95:11891–96
39. Wistuba II, Lam S, Behrens C, Virmani AK, Fong KM, et al. 1997. Molecular damage in the bronchial epithelium of current and former smokers. *J. Natl. Cancer Inst.* 89:1366–73
40. Mao L, Lee JS, Kurie JM, Fan YH, Lippman SM, et al. 1997. Clonal genetic alterations in the lungs of current and former smokers. *J. Natl. Cancer Inst.* 89:857–62
41. Park IW, Wistuba II, Maitra A, Milchgrub S, Virmani AK, et al. 1999. Multiple clonal abnormalities in the bronchial epithelium of patients with lung cancer. *J. Natl. Cancer Inst.* 91:1863–68
42. Hittelman WN. 1999. Molecular cytogenetic evidence for multistep tumorigenesis: implications for risk assessment and early detection. In *Molecular Pathology of Early Cancer*, ed. S Srivastava, AF Gazdar, DE Henson, pp. 385–404. Van Demanstratt, Netherlands: IOS
43. Gartner LP, Hiatt JL. 2001. Respiratory system. In *Color Textbook of Histology*, ed. LP Gartner, JL Hiatt, pp. 343–64. Philadelphia: Saunders
44. Yatabe Y, Mitsudomi T, Takahashi T. 2002. TTF-1 expression in pulmonary adenocarcinomas. *Am. J. Surg. Pathol.* 26:767–73
45. Yatabe Y, Kosaka T, Takahashi T, Mitsudomi T. 2005. EGFR mutation is specific for terminal respiratory unit type adenocarcinoma. *Am. J. Surg. Pathol.* 29:633–39
46. Kitamura H, Kameda Y, Ito T, Hayashi H. 1999. Atypical adenomatous hyperplasia of the lung. Implications for the pathogenesis of peripheral lung adenocarcinoma. *Am. J. Clin. Pathol.* 111:610–22
47. Osanai M, Igarashi T, Yoshida Y. 2001. Unique cellular features in atypical adenomatous hyperplasia of the lung: ultrastructural evidence of its cytodifferentiation. *Ultrastruct. Pathol.* 25:367–73
48. Kim CF, Jackson EL, Woolfenden AE, Lawrence S, Babar I, et al. 2005. Identification of bronchioalveolar stem cells in normal lung and lung cancer. *Cell* 121:823–35
49. Weng SY, Tsuchiya E, Kasuga T, Sugano H. 1992. Incidence of atypical bronchioloalveolar cell hyperplasia of the lung: relation to histological subtypes of lung cancer. *Virchows Arch. A* 420:463–71
50. Nakanishi K. 1990. Alveolar epithelial hyperplasia and adenocarcinoma of the lung. *Arch. Pathol. Lab. Med.* 114:363–68
51. Chapman AD, Kerr KM. 2000. The association between atypical adenomatous hyperplasia and primary lung cancer. *Br. J. Cancer* 83:632–36
52. Koga T, Hashimoto S, Sugio K, Yonemitsu Y, Nakashima Y, et al. 2002. Lung adenocarcinoma with bronchioloalveolar carcinoma component is frequently associated with foci of high-grade atypical adenomatous hyperplasia. *Am. J. Clin. Pathol.* 117:464–70

53. Yokose T, Doi M, Tanno K, Yamazaki K, Ochiai A. 2001. Atypical adenomatous hyperplasia of the lung in autopsy cases. *Lung Cancer* 33:155–61
54. Westra WH, Baas IO, Hruban RH, Askin FB, Wilson K, et al. 1996. K-ras oncogene activation in atypical alveolar hyperplasias of the human lung. *Cancer Res.* 56:2224–28
55. Tominaga M, Sueoka N, Irie K, Iwanaga K, Tokunaga O, et al. 2003. Detection and discrimination of preneoplastic and early stages of lung adenocarcinoma using hmRNP B1, combined with the cell cycle-related markers p16, cyclin D1, and Ki-67. *Lung Cancer* 40:45–53
56. Nakanishi K, Kawai T, Kumaki F, Hiroi S, Mukai M, Ikeda E. 2003. Survivin expression in atypical adenomatous hyperplasia of the lung. *Am. J. Clin. Pathol.* 120:712–19
57. Kitaguchi S, Takeshima Y, Nishisaka T, Inai K. 1998. Proliferative activity, p53 expressin and loss of heterozygosity on 3p, 9 and 17p in atypical adenomatous hyperplasia of the lung. *Hiroshima J. Med. Sci.* 47:17–25
58. Takamochi K, Ogura T, Suzuki K, Kawasaki H, Kurashima Y, et al. 2001. Loss of heterozygosity on chromosome 9q and 16p in atypical adenomatous hyperplasia concomitant with adenocarcinoma of the lung. *Am. J. Pathol.* 159:1941–48
59. Niho S, Yokose T, Suzuki K, Kodama T, Nishiwaki Y, Mukai K. 1999. Monoclonality of atypical adenomatous hyperplasia of the lung. *Am. J. Pathol.* 154:249–54
60. Nakanishi K, Kawai T, Kumaki F, Hirot S, Mukai M, Ikeda E. 2002. Expression of human telomerase RNA component and telomerase reverse transcriptase mRNA in atypical adenomatous hyperplasia of the lung. *Hum. Pathol.* 33:697–702
61. Ghaffar H, Sahin F, Sanchez-Cespedes M, Su GH, Zahurak M, Sidransky D, et al. 2003. LKB1 protein expression in the evolution of glandular neoplasia of the lung. *Clin. Cancer Res.* 9:2998–3003
62. Sugio K, Kishimoto Y, Virmani A, Hung JY, Gazdar AF. 1994. K-*ras* mutations are a relatively late event in the pathogenesis of lung carcinomas. *Cancer Res.* 54:5811–15
63. Brose MS, Volpe P, Feldman M, Kumar M, Rishi I, et al. 2002. BRAF and RAS mutations in human lung cancer and melanoma. *Cancer Res.* 62:6997–7000
64. Pao W, Miller V, Zakowski M, Doherty J, Politi K, et al. 2004. EGF receptor gene mutations are common in lung cancers from "never smokers" and are associated with sensitivity of tumors to gefitinib and erlotinib. *Proc. Natl. Acad. Sci. USA* 101:13306–11
65. Huang SF, Liu HP, Li LH, Ku YC, Fu YN, et al. 2004. High frequency of epidermal growth factor receptor mutations with complex patterns in non-small cell lung cancers related to gefitinib responsiveness in Taiwan. *Clin. Cancer Res.* 10:8195–203
66. Kosaka T, Yatabe Y, Endoh H, Kuwano H, Takahashi T, Mitsudomi T. 2004. Mutations of the epidermal growth factor receptor gene in lung cancer: biological and clinical implications. *Cancer Res.* 64:8919–23
67. Tokumo M, Toyooka S, Kiura K, Shigematsu H, Tomii K, et al. 2005. The relationship between epidermal growth factor receptor mutations and clinicopathologic features in non-small cell lung cancers. *Clin. Cancer Res.* 11:1167–73
68. Amann J, Kalyankrishna S, Massion PP, Ohm JE, Girard L, et al. 2005. Aberrant epidermal growth factor receptor signaling and enhanced sensitivity to EGFR inhibitors in lung cancer. *Cancer Res.* 65:226–35
69. Sonobe M, Manabe T, Wada H, Tanaka F. 2005. Mutations in the epidermal growth factor receptor gene are linked to smoking-independent, lung adenocarcinoma. *Br. J. Cancer* 93:355–63
70. Sasaki H, Shimizu S, Endo K, Takada M, Kawahara M, et al. 2005. EGFR and erbB2 mutation status in Japanese lung cancer patients. *Int. J. Cancer.* In press

71. Mu XL, Li LY, Zhang XT, Wang MZ, Feng RE, et al. 2005. Gefitinib-sensitive mutations of the epidermal growth factor receptor tyrosine kinase domain in Chinese patients with non-small cell lung cancer. *Clin. Cancer Res.* 11:4289–94
72. Soung YH, Lee JW, Kim SY, Seo SH, Park WS, et al. 2005. Mutational analysis of EGFR and K-RAS genes in lung adenocarcinomas. *Virchows Arch.* 446:483–88
73. Yang SH, Mechanic LE, Yang P, Landi MT, Bowman ED, et al. 2005. Mutations in the tyrosine kinase domain of the epidermal growth factor receptor in non-small cell lung cancer. *Clin. Cancer Res.* 11:2106–10
74. Qin L, Tamasi J, Raggatt L, Li X, Feyen JH, et al. 2005. Amphiregulin is a novel growth factor involved in normal bone development and in the cellular response to parathyroid hormone stimulation. *J. Biol. Chem.* 280:3974–81
75. Marchetti A, Martella C, Felicioni L, Barassi F, Salvatore S, et al. 2005. EGFR mutations in non-small-cell lung cancer: analysis of a large series of cases and development of a rapid and sensitive method for diagnostic screening with potential implications on pharmacologic treatment. *J. Clin. Oncol.* 23:857–65
76. Tsao MS, Sakurada A, Cutz JC, Zhu CQ, Kamel-Reid S, et al. 2005. Erlotinib in lung cancer-molecular and clinical predictors of outcome. *N. Engl. J. Med.* 353:133–44
77. Zhang XT, Li LY, Mu XL, Cui QC, Chang XY, et al. 2005. The EGFR mutation and its correlation with response of gefitinib in previously treated Chinese patients with advanced non-small-cell lung cancer. *Ann. Oncol.* 16:1334–42
78. Chou TY, Chiu CH, Li LH, Hsiao CY, Tzen CY, et al. 2005. Mutation in the tyrosine kinase domain of epidermal growth factor receptor is a predictive and prognostic factor for gefitinib treatment in patients with non-small cell lung cancer. *Clin. Cancer Res.* 11:3750–57
79. Cappuzzo F, Hirsch FR, Rossi E, Bartolini S, Ceresoli GL, et al. 2005. Epidermal growth factor receptor gene and protein and gefitinib sensitivity in non-small-cell lung cancer. *J. Natl. Cancer Inst.* 97:643–55
80. Kim KS, Jeong JY, Kim YC, Na KJ, Kim YH, et al. 2005. Predictors of the response to gefitinib in refractory non-small cell lung cancer. *Clin. Cancer Res.* 11:2244–51
81. Mitsudomi T, Kosaka T, Endoh H, Horio Y, Hida T, et al. 2005. Mutations of the epidermal growth factor receptor gene predict prolonged survival after gefitinib treatment in patients with non-small-cell lung cancer with postoperative recurrence. *J. Clin. Oncol.* 23:2513–20
82. Han SW, Kim TY, Hwang PG, Jeong S, Kim J, et al. 2005. Predictive and prognostic impact of epidermal growth factor receptor mutation in non-small-cell lung cancer patients treated with gefitinib. *J. Clin. Oncol.* 23:2493–501
83. Hirsch FR, Varella-Garcia M, McCoy J, West H, Xavier AC, et al. 2005. Increased epidermal growth factor receptor gene copy number detected by fluorescence in situ hybridization associates with increased sensitivity to gefitinib in patients with bronchioloalveolar carcinoma subtypes: A Southwest Oncology Group Study. *J. Clin. Oncol.* 23: 6838–45
84. Kurie JM, Shin HJ, Lee JS, Morice RC, Ro JY, et al. 1996. Increased epidermal growth factor receptor expression in metaplastic bronchial epithelium. *Clin. Cancer Res.* 2:1787–93
85. Tang X, Shigematsu H, Bekele BN, Roth JA, Minna JD, et al. 2005. EGFR tyrosine kinase domain mutations are detected in histologically normal respiratory epithelium in lung cancer patients. *Cancer Res.* 65:7568–72
86. Yoshida Y, Shibata T, Kokubu A, Tsuta K, Matsuno Y, et al. 2005. Mutations of the epidermal growth factor receptor gene in atypical adenomatous hyperplasia and bronchioloalveolar carcinoma of the lung. *Lung Cancer* 50:1–8

87. Wistuba II, Berry J, Behrens C, Maitra A, Shivapurkar N, et al. 2000. Molecular changes in the bronchial epithelium of patients with small cell lung cancer. *Clin. Cancer Res.* 6:2604–10
88. Aguayo SM, Miller YE, Waldron JA Jr, Bogin RM, Sunday ME, et al. 1992. Brief report: idiopathic diffuse hyperplasia of pulmonary neuroendocrine cells and airways disease. *N. Engl. J. Med.* 327:1285–88
89. Armas OA, White DA, Erlanson RA, Rosai J. 1995. Diffuse idiopathic pulmonary neuroendocrine cell proliferation presenting as interstitial lung disease. *Am. J. Surg. Pathol.* 19:963–70
90. Loeb LA. 1991. Mutator phenotype may be required for multistage carcinogenesis. *Cancer Res.* 51:3075–79
91. Peto R, Darby S, Deo H, Silcocks P, Whitley E, Doll R. 2000. Smoking, smoking cessation, and lung cancer in the UK since 1950: combination of national statistics with two case-control studies. *Br. Med. J.* 321:323–29
92. Lam S, leRiche JC, Zheng Y, Coldman A, MacAulay C, et al. 1999. Sex-related differences in bronchial epithelial changes associated with tobacco smoking. *J. Natl. Cancer Inst.* 91:691–96
93. Zochbauer-Muller S, Lam S, Toyooka S, Virmani AK, Toyooka KO, et al. 2003. Aberrant methylation of multiple genes in the upper aerodigestive tract epithelium of heavy smokers. *Int. J. Cancer* 107:612–16
94. Soria JC, Rodriguez M, Liu DD, Lee JJ, Hong WK, Mao L. 2002. Aberrant promoter methylation of multiple genes in bronchial brush samples from former cigarette smokers. *Cancer Res.* 62:351–55
95. Belinsky SA, Palmisano WA, Gilliland FD, Crooks LA, Divine KK, et al. 2002. Aberrant promoter methylation in bronchial epithelium and sputum from current and former smokers. *Cancer Res.* 62:2370–77

Annual Review of Pathology: Mechanisms of Disease

Volume 1, 2006

Contents

DOI:10.1158/1940-6207.CAPR-08-0177

Cancer Prevention Research

Chromosomal Deletions and Progression of Premalignant Lesions: Less Is More

Ignacio I. Wistuba and Matthew Meyerson

Cancer Prev Res 2008;1:404-408. Published online November 5, 2008.

DOI:10.1158/1940-6207.CAPR-08-0177

Perspective

Chromosomal Deletions and Progression of Premalignant Lesions: Less Is More

Ignacio I. Wistuba[1] and Matthew Meyerson[2,3]

Epithelial malignancies arise after a series of progressive pathologic changes including hyperplasia, different grades of dysplasia, and carcinoma *in situ* (1). These premalignant changes can accompany cancer or may occur in the epithelium of individuals at high risk. Sequential premalignant lesions have been defined for many epithelial tumors, including oral squamous cell carcinoma (1) and Barrett's esophageal adenocarcinoma (3). Two of the most exciting areas of current cancer research are (a) novel high-throughput technology for molecular studies of carcinogenesis and (b) the use of this technology in discovering and characterizing genetic abnormalities that underlie the progression of epithelial premalignancy.

Many studies of the last 2 decades have helped to characterize molecular changes of epithelial premalignancy. Encouraged by the development of methodologies (such as laser microdissection) for isolating cells from small histologic lesions, and of techniques to do genomic studies on minute amounts of DNA, several groups have made substantial progress in unveiling the molecular and genetic abnormalities of epithelial premalignant lesions (2, 3–7). These changes involve inactivation of known and putative tumor suppressor genes and several dominant oncogenes. Tumor suppressor genes are believed to be inactivated via a two-step process involving both alleles. Knudson (8) proposed that the first "hit" frequently is a point mutation, whereas the second allele is subsequently inactivated via a chromosomal deletion, translocation, or other event such as methylation of gene promoter regions (9). Dominant oncogenes are frequently activated by mutation, increased copy number, and translocations (9).

The general working model of sequential molecular abnormalities in the pathogenesis of epithelial tumors indicates that genetic changes (*a*) commence in histologically normal epithelium and progress with the increasing severity of epithelial changes, (*b*) follow a sequence from early to late changes, and (*c*) are extensive and multifocal throughout the epithelium, indicating a field effect, also known as "field cancerization" (3). Therefore, in various organ sites, multiple clonal and subclonal patches of molecularly abnormal epithelial cells (with or without cytologic and morphologic abnormalities) can be detected throughout the affected epithelium. New high-throughput genomic and proteomic profiling techniques are now starting to be applied to premalignant or normal-appearing tissue because these techniques are suitable for studying the small amounts of tissue usually available in these precancer settings.

Oral squamous cell carcinoma and Barrett's esophageal adenocarcinoma are on the frontier of innovative discoveries involving molecular events in the progression of premalignant lesions (2, 3). These two diseases are good models of cancer genetic progression because the premalignant epithelium can be safely visualized and biopsied so that genomic changes can be compared in different stages of neoplastic evolution and then studied longitudinally by biopsy surveillance. Several studies have shown that the general working model of progression described above applies to both tumor types.

Oral leukoplakia is the most common head and neck premalignant lesion and has a malignant transformation rate as high as 24% (10). Deletion of one of the two alleles within chromosome arm 3p and chromosome segment 9p21 is the most frequent event in oral lesions with only mild dysplasia and even in some normal-appearing epithelial cells (11). Oral leukoplakias with deletions in the 3p14 (*FHIT*) and 9p21 (*CDKN2A*) regions are reported to carry a higher risk for transformation (2). Barrett's esophagus (BE) is the only known premalignancy of esophageal adenocarcinoma; only a small fraction (0.5-1% annually) of BE patients subsequently develop adenocarcinoma (12). Although less accessible than are oral lesions, BE is a unique model for the study of human neoplastic progression *in vivo*. The standard care of BE requires biopsies according to defined protocols at multiple time points from the same patient, allowing the generation of spatial maps and longitudinal evaluation of genetic alterations that arise during clonal evolution. Several studies of BE indicate that inactivation of *CDKN2A* by loss of heterozygosity (LOH), methylation, and/or mutation is selected as an early event that predisposes to large clonal expansions of the BE tissue (12, 13). Subsequent inactivation of *TP53* by mutation and LOH predisposes to progression to aneuploidy and invasive adenocarcinoma development (13). All these studies have been done using low-throughput methodologies with analysis of abnormalities on few chromosomal foci or specific genes.

In the present issue of the journal, Tsui et al. (14) and Li et al. (15) report their high-throughput analyses of genetic abnormalities in premalignant lesions that provide insights on chromosomal changes in the early pathogenesis of oral squamous cell carcinoma (14) and BE (15). These studies are among the first to use high-throughput DNA copy number analysis by microarrays in the study of the sequential progression of premalignant lesions of any organ site. Comparative genomic

Authors' Affiliations: [1]Departments of Pathology and Thoracic/Head and Neck Medical Oncology, The University of Texas M. D. Anderson Cancer Center, Houston, Texas; [2]Department of Medical Oncology and Center for Cancer Genome Discovery, Dana-Farber Cancer Institute, Boston, Massachusetts; and [3]Broad Institute of Harvard and Massachusetts Institute of Technology, Cambridge, Massachusetts

Received 09/17/2008; accepted 09/29/2008.

Grant support: U.S. Department of Defense, VITAL, grant W81XWH-04-1-0142 (I.I. Wistuba).

Requests for reprints: Ignacio I. Wistuba, Department of Pathology, The University of Texas M. D. Anderson Cancer Center, Unit 85, 1515 Holcombe Boulevard, Houston, TX 77030-4009. Phone: 713-563-9184; Fax: 713-792-0309; E-mail: iiwistuba@mdanderson.org or Matthew Meyerson. E-mail: Matthew_Meyerson@dfci.harvard.edu.

doi:10.1158/1940-6207.CAPR-08-0177

DOI:10.1158/1940-6207.CAPR-08-0177

hybridization (CGH) profiling has been previously applied to oral squamous cell carcinoma (16–18), leading to the identification of novel chromosomal regions (e.g., 5p15.2 and 11q.22.2-22.3) frequently altered in this neoplasm (16). Earlier studies using GCH and single-nucleotide polymorphism (SNP) array have already shown that chromosomal abnormalities increase with the progression of BE lesions, but they analyzed only a few tissue specimens (19, 20). Both of the present studies showed that microarray-based DNA copy number analyses can reveal the progression of chromosomal abnormalities that parallels the clinical and histopathologic progression of premalignancy. The findings of these studies also have some potential to be used to predict the risk of progression of either oral leukoplakia or BE.

Tsui et al. (14) used CGH to evaluate genetic alterations on chromosome 3p in 47 oral premalignant lesions with high-grade dysplastic features (severe dysplasia and carcinoma *in situ*) and compared these alterations with findings in 23 oral squamous cell carcinomas; all samples were formalin-fixed and paraffin-embedded tissues. This study was stimulated by previous laboratory work of this group (21, 22) and others (2, 10, 11), showing that chromosome 3p is frequently altered in the early pathogenesis of oral carcinoma and has been associated with the risk of premalignant lesion progression (2, 10, 11, 21, 22). High-grade dysplastic lesions exhibited six recurrent regions of losses on 3p including 3p25.3-p26.1, 3p25.1-p25.3, 3p24.1, 3p21.31-p22.3, 3p14.2, and 3p14.1, which overlapped losses found in invasive carcinoma. Next, the authors examined these regions in 24 low-grade dysplastic lesions with known outcomes, including 2 hyperplasias and 22 mild and moderate dysplasias, and determined that 3p losses were identified more frequently in low-grade dysplastic lesions with progressive behavior (78%) compared with nonprogressing lesions (20%). This interesting observation obviously will require verification in a larger cohort of patients. In our opinion, one remarkable finding of this report is that the size of 3p segmental losses, or discontinuous LOH (alternating segments showing loss and retention; portrayed in Fig. 1), increased with histologic stage; segmental 3p losses were detected in premalignant lesions, whereas whole-arm loss occurred mainly in invasive tumors.

Li et al. (15) used a medium-density SNP array (containing ~33,000 SNPs) to investigate genome-wide chromosomal copy number changes in whole frozen tissue specimens (obtained by endoscopy or surgical resection) of multiple stages of BE and esophageal adenocarcinoma from 42 patients. This investigation is from the same laboratory that established the working model for BE molecular progression (3) and one of the first laboratories to use SNP arrays for the analysis of human premalignancy (23). The mucosal esophageal tissues used in this cross-sectional study included 24 early-stage BE specimens (with or without aneuploidy and that did not develop cancer during follow-up), 10 late-stage BE specimens (with microscopic invasion), and 8 grossly invasive esophageal adenocarcinoma specimens. Genome-wide copy losses and LOH (the most frequent changes) and copy gains increased in frequency and size between early and late BE, with SNP abnormalities increasing from 2% in early stages to >30% in late stages. A set of statistically significant events was unique to either early or late BE stage, and few chromosomal regions with changes were common in all stages of progression. It is interesting that the total number of genome-wide SNP alterations (gains, losses, and LOH) was highly correlated with DNA content aneuploidy and was sensitive and specific for identifying patients with concurrent esophageal adenocarcinoma. As with chromosome 3p in the study of Tsui et al. (14), Li et al. found that the sizes of chromosome abnormalities were small in early-stage BE compared with late stages, including invasive adenocarcinoma, except in the case of 9p LOH.

How do the articles by Tsui et al. (14) and Li et al. (15) contribute to the general concepts of the parallel progressions of genetic and clinical/histopathologic changes in premalignancy (described above)? First, these investigators have successfully applied high-throughput DNA chromosomal abnormality analysis technologies, array CGH and SNP array analysis, to small specimens of premalignant lesion tissue, formalin-fixed and paraffin-embedded specimens (CGH), and frozen samples (SNP). We hope that these two reports will raise enthusiasm for similar new studies in these and other neoplasm models.

Second, these studies show that chromosomal abnormalities (mostly deletions) at the 3p chromosome (14) and genome-wide (15) levels commence early in oral and BE premalignancies and progress with the increasing severity of epithelial changes and that these chromosomal changes follow a sequence defining early and late molecular changes. Third, these two studies have suggested that the size of chromosomal deletions (at 3p or genome-wide) increases with the severity of histopathologic changes. This interesting finding has been reported previously in the pathogenesis of other epithelial tumors, such as lung tumors, where it has been observed in LOH studies using PCR-based amplification of multiple microsatellites in precisely microdissected histologically normal and premalignant epithelia obtained from lung cancer patients and high-risk individuals (smokers; refs. 24–26). LOH at multiple chromosome 3p (24, 26) and 8p (25) sites was shown to commence at the stage of normal epithelium and to increase with progressive histologic changes in the lung squamous cell carcinoma histology progression model (similar in ways to oral squamous carcinoma). This study used 24 microsatellite markers spanning six continuous chromosome 3p regions in showing that deletions in 3p progressed from dysplasia to invasive squamous carcinoma (Fig. 1). In invasive tumors and carcinoma *in situ*, most of the 3p arm was deleted and the extent of the deletions was greater in all cases than that in corresponding normal and premalignant foci (24). These findings were subsequently expanded in a LOH analysis (using 54 microsatellite markers on 3p) that included samples from a wider spectrum of premalignancy and lung cancer specimens, including samples from smokers and cancers with different histologies (nonsmall and small cell). This detailed allelotyping analysis identified multiple areas of discontinuous LOH and thus multiple breakpoints throughout the 3p arm in many tumor and bronchial epithelial samples (26). Allelic losses present in lung premalignant lesions were not random and followed a sequence, with the earliest and most frequent allelic loss occurring at the 3p21.3 region (24, 26).

Although the two articles in this issue of the journal report that discontinuous LOH marks progression of premalignancy, this LOH also could be an artifact of impurity within the premalignant lesions. In samples with an admixture of DNA from malignant and normal cells, some chromosomal segments

DOI:10.1158/1940-6207.CAPR-08-0177

might seem to be altered and others not altered, although the degree of alteration could be the same across the entire chromosome arm because of nonuniform behavior of copy number probes, which fail to reach a threshold level for detecting an alteration. This failure has been shown for SNP array analysis of mixtures of tumor cell line DNA with matched normal DNA; increasing admixture of normal DNA led to the appearance of discontinuous LOH because of incomplete detection involving regions of uninterrupted chromosome 3p LOH in the pure tumor (27). Further improvements in genomics technologies coupled with careful histologic analysis will be required to address this question.

The mechanism for chromosomal deletions in individual premalignant samples is not well established. LOH is considered to occur through the loss of a whole chromosome because of inappropriate chromosomal segregation at mitosis and also through genetic alterations that change chromosomal structures (28). Whole, terminal, and interstitial chromosome physical deletions have been shown to cause LOH on several chromosomal arms in human tumors (29). On the other hand, mitotic recombination and gene conversion seem to be additional mechanisms causing LOH (30, 31). Unbalanced translocations, which have been confirmed by cytogenetic studies in certain human tumors, have been implicated in LOH development (32). In summary, six chromosomal aberrations (whole chromosome, terminal and interstitial deletions, mitotic recombination, gene conversion, and unbalanced translocation) are considered to be responsible for LOH in human carcinogenesis (Fig. 2). However, the contribution of each chromosome alteration to the occurrence of LOH has been examined only for a few chromosomal regions in few tumor types. It was determined recently that 80% of LOHs are partial chromosome deletions

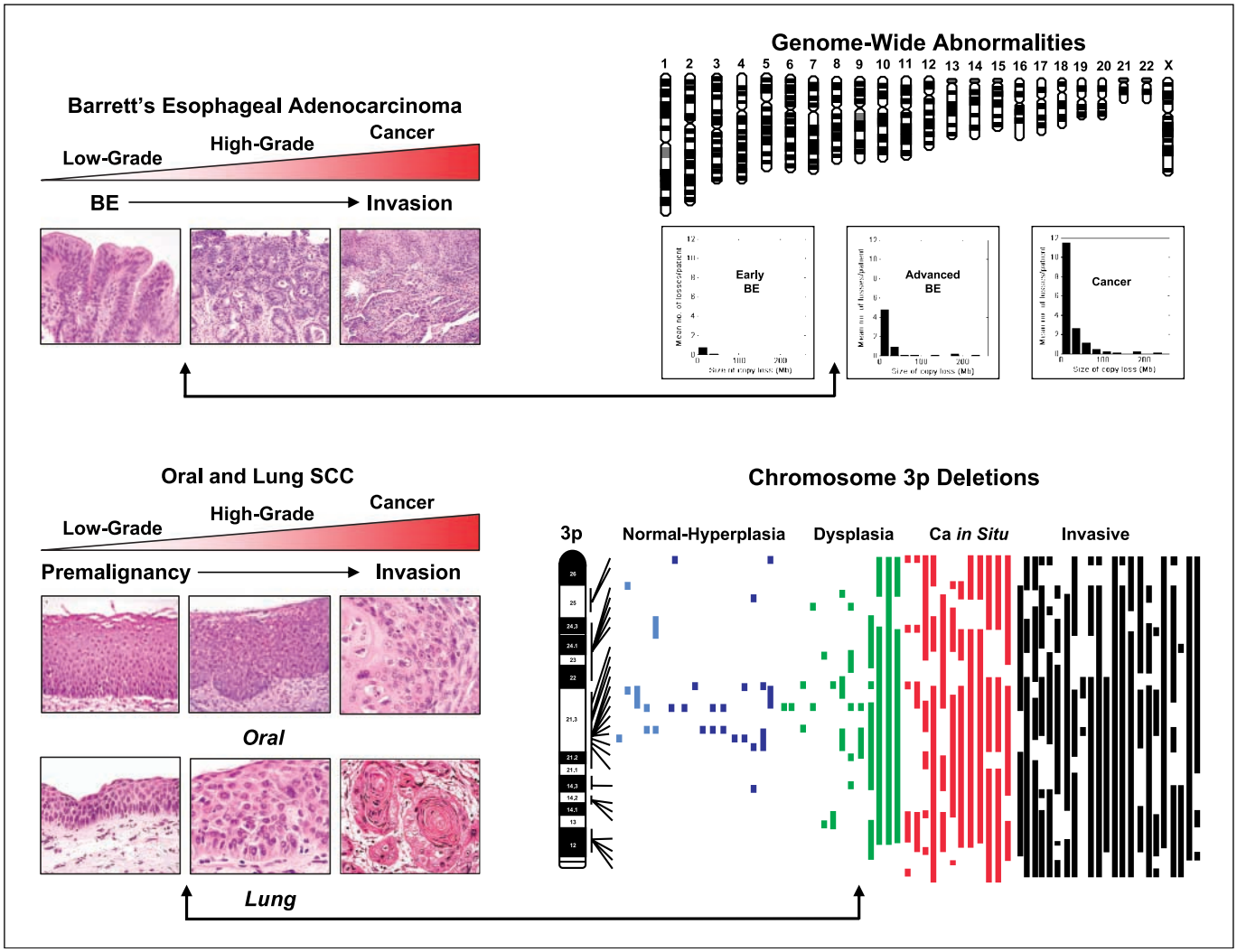

Fig. 1. Progression of premalignancy and molecular changes in Barrett's esophageal adenocarcinoma (*top*) and oral and lung squamous cell carcinomas (*SSC*; *bottom*). Chromosomal deletions at genome-wide and the 3p chromosome levels begin early in esophageal premalignancy (or BE) and, in oral premalignancy, progress and increase in size with increasing histopathologic severity (14, 15). Li et al. (15) showed that the number of larger copy losses (Mb) was significantly higher in advanced BE and esophageal adenocarcinoma compared with early BE lesions (*top*). In oral premalignancy progression, Tsui et al. (14) showed that the size of 3p segmental losses increased with histologic stage, as has been shown previously in progression to lung squamous cell carcinoma (*bottom*; refs. 24–26). In the lung squamous cell carcinoma model, discontinuous segmental losses, or LOH, at 3p are detected in normal epithelium, hyperplasia, and some dysplasias, whereas the whole arm is lost in invasive and *in situ* carcinomas and in a subset of dysplastic lesions; the vertical colored bars (*bottom right*) indicate the size of deletions; the gaps, or retentions, between the bars indicate discontinuous LOH. Histology pictures of BE progression are courtesy of Elizabeth Montgomery, M.D., and of oral leukoplakia progression are courtesy of Adel El-Naggar, M.D., Ph.D.

DOI:10.1158/1940-6207.CAPR-08-0177

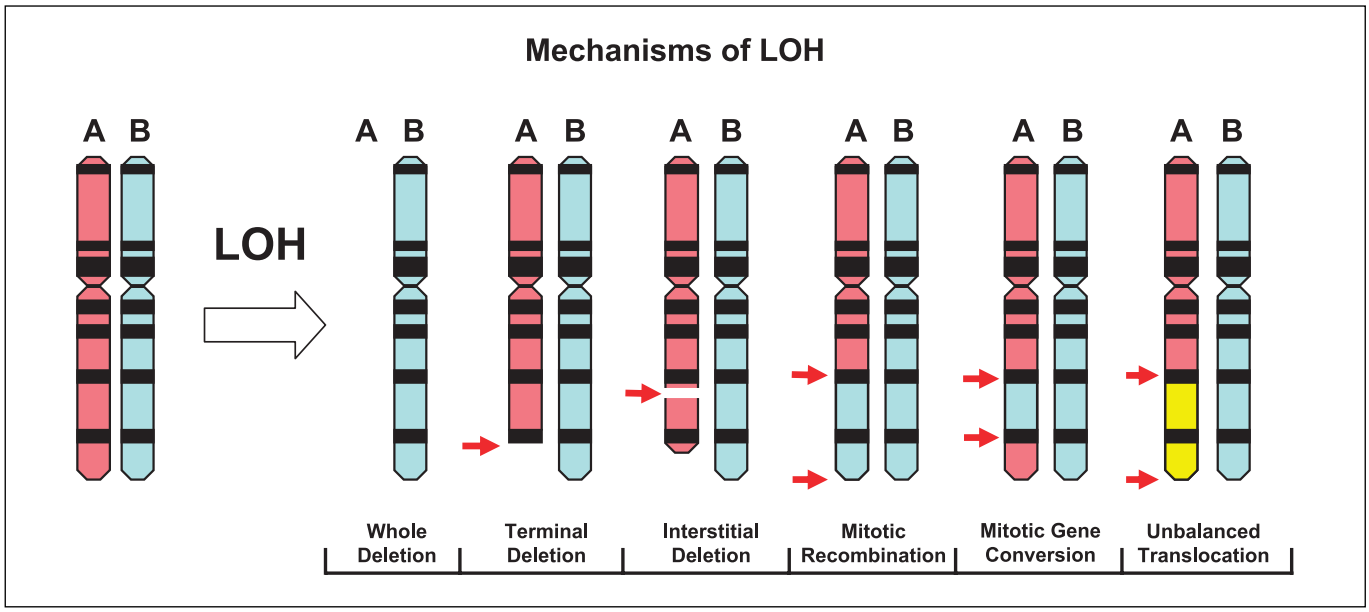

Fig. 2. Chromosomal alterations considered to be responsible for LOH in human carcinogenesis. The whole-chromosome, terminal, and interstitial deletions and unbalanced translocation represent copy number changes. The red arrows indicate sites of chromosomal breaks.

(involving the several chromosomal alterations mentioned above), whereas the remaining 20% were whole-chromosome deletions (33); these results came from integrating information on breakpoints for DNA copy number changes (obtained by a CGH) with numerical and structural chromosomal alterations (obtained by spectral karyotyping in lung cancer cell lines). We know that DNA copy number analyses of tumors have limitations due to the phenomenon that most of these alterations in invasive cancers are large, spanning many genes (tens to hundreds), including many that likely are not involved in oncogenesis. Therefore, studies of premalignant lesions with known outcomes are necessary to better define chromosomal loci and genes responsible for tumor development in humans.

The reports of Tsui et al. (14) and Li et al. (15) on the tumor models oral squamous cell carcinoma and Barrett's esophageal adenocarcinoma give new insights into and hope for understanding the highly complex nature of the progression of premalignancy to cancer. Despite their different pathogenetic features, these two tumors shared some common genetic progression characteristics. The application of high-throughput DNA technology in these models showed the promise of this approach and the merit of extending these methods to other premalignant diseases. It also showed the potential of CGH and SNP arrays to identify new candidate biomarkers and measures of clonal diversity, both of which can be used in patient management and assessment of cancer risk. Is less more? High-throughput approaches generate increasing amounts of data from smaller and smaller tissue samples, and chromosomal deletions appear to increase progression of premalignancy. These examples of "less is more" represent important advances in our understanding of the molecular nature of carcinogenesis.

Disclosure of Potential Conflicts of Interest

No potential conflicts of interest were disclosed.

References

1. Mao L, Hong WK, Papadimitrakopoulou VA. Focus on head and neck cancer. Cancer Cell 2004;5:311–6.
2. Paulson TG, Reid BJ. Focus on Barrett's esophagus and esophageal adenocarcinoma. Cancer Cell 2004;6:11–6.
3. Wistuba I, Gazdar A. Lung cancer preneoplasia. Annu Rev Pathol Mech Dis 2006;1:331–48.
4. Wistuba II, Mao L, Gazdar AF. Smoking molecular damage in bronchial epithelium. Oncogene 2002;21:7298–306.
5. Minna JD, Gazdar A. Focus on lung cancer. Cancer Cell 2002;1:49–52.
6. De Marzo AM, Meeker AK, Zha S, et al. Human prostate cancer precursors and pathobiology. Urology 2003;62:55–62.
7. Dinney CP, McConkey DJ, Millikan RE, et al. Focus on bladder cancer. Cancer Cell 2004;6:111–6.
8. Knudson AG. Hereditary cancers: clues to mechanisms of carcinogenesis. Br J Cancer 1989;59:661–6.
9. Croce CM. Oncogenes and cancer. N Engl J Med 2008;358:502–11.
10. Papadimitrakopoulou VA, Clayman GL, Shin DM, et al. Biochemoprevention for dysplastic lesions of the upper aerodigestive tract. Arch Otolaryngol Head Neck Surg 1999;125:1083–9.
11. Mao L, Lee JS, Fan YH, et al. Frequent microsatellite alterations at chromosomes 9p21 and 3p14 in oral premalignant lesions and their value in cancer risk assessment. Nat Med 1996;2:682–5.
12. Maley CC, Reid BJ. Natural selection in neoplastic progression of Barrett's esophagus. Semin Cancer Biol 2005;15:474–83.
13. Barrett MT, Sanchez CA, Prevo LJ, et al. Evolution of neoplastic cell lineages in Barrett oesophagus. Nat Genet 1999;22:106–9.
14. Tsui IF, Rosin MP, Zhang L, Ng RT, Lam WL. Frequent genetic alterations occurring in oral premalignant lesions: analysis of chromosome 3p. Cancer Prev Res 2008;1:424–9.
15. Li X, Galipeau PC, Sanchez CA, et al. SNP-based genome-wide chromosome copy change, LOH, aneuploidy in Barret's esophagus neoplastic progression. Cancer Prev Res 2008;1:413–23.
16. Baldwin C, Garnis C, Zhang L, Rosin MP, Lam WL. Multiple microalterations detected at high frequency in oral cancer. Cancer Res 2008;1:413–24.
17. Liu CJ, Lin SC, Chen YJ, Chang KM, Chang KW. Array-comparative genomic hybridization to detect genomewide changes in microdissected primary and metastatic oral squamous cell carcinomas. Mol Carcinog 2006;45:721–31.
18. Nakaya K, Yamagata HD, Arita N, et al. Identification of homozygous deletions of tumor suppressor

DOI:10.1158/1940-6207.CAPR-08-0177

gene FAT in oral cancer using CGH-array. Oncogene 2007;26:5300–8.

19. Walch AK, Zitzelsberger HF, Bruch J, et al. Chromosomal imbalances in Barrett's adenocarcinoma and the metaplasia-dysplasia-carcinoma sequence. Am J Pathol 2000;156:555–66.

20. Lai LA, Paulson TG, Li X, et al. Increasing genomic instability during premalignant neoplastic progression revealed through high resolution array-CGH. Genes Chromosomes Cancer 2007; 46:532–42.

21. Ng IO, Xiao L, Lam KY, Yuen PW, Ng M. Microsatellite alterations in squamous cell carcinoma of the head and neck—clustering of loss of heterozygosity in a distinct subset. Oral Oncol 2000;36: 484–90.

22. Rosin MP, Cheng X, Poh C, et al. Use of allelic loss to predict malignant risk for low-grade oral epithelial dysplasia. Clin Cancer Res 2000;6: 357–62.

23. Mei R, Galipeau PC, Prass C, et al. Genome-wide detection of allelic imbalance using human SNPs and high-density DNA arrays. Genome Res 2000; 10:1126–37.

24. Wistuba II, Behrens C, Milchgrub S, et al. Sequential molecular abnormalities are involved in the multistage development of squamous cell lung carcinoma. Oncogene 1999;18:643–50.

25. Wistuba II, Behrens C, Virmani AK, et al. Allelic losses at chromosome 8p21-23 are early and frequent events in the pathogenesis of lung cancer. Cancer Res 1999;59:1973–9.

26. Wistuba II, Behrens C, Virmani AK, et al. High resolution chromosome 3p allelotyping of human lung cancer and preneoplastic/preinvasive bronchial epithelium reveals multiple, discontinuous sites of 3p allele loss and three regions of frequent breakpoints. Cancer Res 2000;60:1949–60.

27. Lindblad-Toh K, Tanenbaum DM, Daly MJ, et al. Loss-of-heterozygosity analysis of small-cell lung carcinomas using single-nucleotide polymorphism arrays. Nat Biotechnol 2000;18:1001–5.

28. Weinberg RA. Tumor suppressor gene. In: Weinberg RA, editor. The biology of cancer. New York: Garland Science, Taylor and Francis Group LLC; 2007. p. 209–54.

29. Lasko D, Cavenee W, Nordenskjold M. Loss of constitutional heterozygosity in human cancer. Annu Rev Genet 1991;25:281–314.

30. Hagstrom SA, Dryja TP. Mitotic recombination map of 13cen-13q14 derived from an investigation of loss of heterozygosity in retinoblastomas. Proc Natl Acad Sci U S A 1999;96:2952–7.

31. Adams J, Williams SV, Aveyard JS, Knowles MA. Loss of heterozygosity analysis and DNA copy number measurement on 8p in bladder cancer reveals two mechanisms of allelic loss. Cancer Res 2005;65:66–75.

32. Roschke AV, Tonon G, Gehlhaus KS, et al. Karyotypic complexity of the NCI-60 drug-screening panel. Cancer Res 2003;63:8634–47.

33. Ogiwara H, Kohno T, Nakanishi H, Nagayama K, Sato M, Yokota J. Unbalanced translocation, a major chromosome alteration causing loss of heterozygosity in human lung cancer. Oncogene 2008;27: 4788–97.

[Cancer Biology & Therapy 6:10, 1614-1620; October 2007]; ©2007 Landes Bioscience

Research Paper

c-FLIP Downregulation Contributes to Apoptosis Induction by the Novel Synthetic Triterpenoid Methyl-2-Cyano-3, 12-Dioxooleana-1, 9-Dien-28-Oate (CDDO-Me) in Human Lung Cancer Cells

Wei Zou[1,†]
Shuzhen Chen[1,†]
Xiangguo Liu[1]
Ping Yue[1]
Michael B. Sporn[2]
Fadlo R. Khuri[1]
Shi-Yong Sun[1,*]

[1]Winship Cancer Institute, Emory University School of Medicine, Atlanta, Georgia USA

[†]These authors contributed equally to this work.

*Correspondence to: Shi-Yong Sun; Winship Cancer Institute; Emory University School of Medicine; 1365-C Clifton Road NE C3088; Atlanta, Georgia 30322 USA; Tel.: 404.778.2170; Fax: 404.778.5520; Email: shi-yong.sun@emory-healthcare.org

Original manuscript submitted: 04/26/07
Revised manuscript submitted: 07/19/07
Manuscript accepted: 07/19/07

Previously published as a *Cancer Biology & Therapy* E-publication: http://www.landesbioscience.com/journals/cbt/article/4763

KEY WORDS

c-FLIP, CDDO-Me, degradation, JNK, apoptosis, lung cancer

ACKNOWLEDGEMENTS

This study is supported by Georgia Cancer Coalition Distinguished Cancer Scholar award (to S-Y S.) and Department of Defense VITAL grant W81XWH-04-1-0142 (to S-Y Sun for Project 4). FR Khuri and S-Y Sun are Georgia Cancer Coalition Distinguished Cancer Scholars. We are thankful to H. A. Elrod in our lab for editing the manuscript.

ABSTRACT

The novel synthetic triterpenoid methyl-2-cyano-3, 12-dioxooleana-1, 9-dien-28-oate (CDDO-Me) induces apoptosis of cancer cells, enhances tumor necrosis factor-related apoptosis-inducing ligand (TRAIL)-induced apoptosis, and exhibits potent anticancer activity in animal models with a favorable pharmacokinetic profile. Thus, CDDO-Me is being tested in Phase I clinical trials. In an effort to understand the mechanism by which CDDO-Me induces apoptosis, particularly in human lung cancer cells, we previously demonstrated that CDDO-Me induces apoptosis involving c-Jun N-terminal kinase (JNK)-dependent upregulation of death receptor 5 (DR5) expression. In the current work, we determined the modulatory effects of CDDO-Me on the levels of c-FLIP, a major inhibitor of death receptor-mediated caspase-8 activation, and its impact on CDDO-Me-induced apoptosis and enhancement of TRAIL-induced apoptosis in human lung cancer cells. CDDO-Me rapidly and potently decreased c-FLIP levels including both long ($FLIP_L$) and short ($FLIP_S$) forms of c-FLIP in multiple human lung cancer cell lines. The presence of the proteasome inhibitor MG132, but not the JNK inhibitor SP600125, prevented CDDO-Me-induced c-FLIP reduction. Moreover, CDDO-Me increased ubiquitination of c-FLIP. Thus, CDDO-Me induces ubiquitin/proteasome-dependent c-FLIP degradation independently of JNK activation. Importantly, overexpression of c-FLIP (e.g., $FLIP_L$) protected cells not only from CDDO-Me-induced apoptosis, but also from induction of apoptosis by the combination of CDDO-Me and TRAIL. Accordingly, silencing of c-FLIP with c-FLIP siRNA sensitized cancer cells to CDDO-Me. Collectively, these results indicate that c-FLIP downregulation contributes to CDDO-Me-initiated apoptosis and also to enhancement of TRAIL-induced apoptosis by CDDO-Me.

INTRODUCTION

The novel synthetic triterpenoid methyl-2-cyano-3, 12-dioxooleana-1, 9-dien-28-oate (CDDO-Me) has been documented to be a potent inducer of apoptosis in several types of human cancer cell lines, including lung cancer cells.[1-5] Thus, CDDO-Me holds promise as a cancer chemopreventive and therapeutic agent. It is well known that there are two major apoptotic pathways: the intrinsic mitochondria-mediated pathway and the extrinsic death receptor-induced pathway, and cross-talk between these pathways is mediated by the truncation of the proapoptotic protein Bid.[6] We and others have demonstrated that CDDO-Me activates both apoptotic pathways.[1,2,7] However, the detailed molecular mechanisms by which CDDO-Me induces apoptosis have not been fully elucidated although it appears to be associated with inhibition of NFκB,[5,8] activation of c-Jun N-terminal kinase (JNK) and p38,[4,7,9,10] generation of reactive oxygen species[4] and induction of death receptor 5 (DR5).[7,9] In addition, CDDO-Me enhances induction of apoptosis by the death receptor ligand tumor necrosis factor (TNF) or TNF-related apoptosis-inducing ligand (TRAIL).[5,7,11]

The cellular FLICE-inhibitory protein (c-FLIP) is a key regulatory protein that inhibits activation of the death receptor-mediated extrinsic apoptotic pathway,[12,13] primarily though binding to Fas-associated death domain (FADD) and caspase-8 at the death-inducing signaling complex, preventing caspase-8 activation.[14] c-FLIP has multiple splice variants, and two main forms have been well characterized: c-FLIP short form ($c\text{-}FLIP_S$), which is 26 kDa in size and contains two death effector domains, and c-FLIP long form ($c\text{-}FLIP_L$), which is 55 kDa in size and contains an inactive caspase-like domain

in addition to the two death effector domains.[12,13] It has been documented that the levels of c-FLIP including both $FLIP_L$ and $FLIP_S$ are regulated by ubiquitin/proteasome-mediated degradation.[15-17] A recent study has shown that JNK activation contributes to ubiquitin/proteasome-mediated degradation of $FLIP_L$ during TNF-induced apoptosis.[17]

It has been documented that elevated c-FLIP expression protects cells from death receptor-mediated apoptosis in various cell types, whereas downregulation of c-FLIP by chemicals or siRNA sensitizes cells to death receptor-mediated apoptosis.[12,13] Moreover, overexpression of c-FLIP also protects cells from apoptosis induced by certain cancer therapeutic agents such as etoposide and cisplatin.[18-20] A previous study has shown that CDDO-Me-induced apoptosis and enhancement of TRAIL-induced apoptosis in human leukemia cells correlates with CDDO-Me's ability to downregulate c-FLIP levels in human leukemia cells.[11] However, direct evidence for participation of c-FLIP in mediating CDDO-Me-induced apoptosis in human cancer cells has not been shown. Here we demonstrate that CDDO-Me facilitates ubiquitin/proteasome-mediated degradation of c-FLIP in a JNK-independent manner, which is associated with induction of apoptosis in human non-small cell lung cancer (NSCLC) cells. The current study complements our previous finding that CDDO-Me induces apoptosis involving DR5 induction in human NSCLC cells.[7,9]

MATERIALS AND METHODS

Reagents. CDDO-Me, which was described previously in reference 21 was dissolved in dimethyl sulfoxide (DMSO) at a concentration of 10 mM, and aliquots were stored at -80°C. Stock solutions were diluted to the desired final concentrations with growth medium just before use. The soluble recombinant human TRAIL was purchased from PeproTech, Inc. (Rocky Hill, NJ). The specific JNK inhibitor SP600125 was purchased from Biomol (Plymouth Meeting, PA). The proteasome inhibitor MG132 was purchased from Sigma Chemical Co. (St. Louis, MO). Rabbit polyclonal anti-DR5 antibody was purchased from ProSci Inc (Poway, CA). Mouse monoclonal anti-FLIP antibody (NF6) was purchased from Alexis Biochemicals (San Diego, CA). Mouse monoclonal anti-caspase-3 was purchased from Imgenex (San Diego, CA). Rabbit polyclonal anti-caspase-8, anti-caspase-9, and anti-PARP antibodies were purchased from Cell Signaling Technology, Inc. (Beverly, MA). Rabbit polyclonal anti-β-actin antibody was purchased from Sigma Chemical Co.

Cell lines and cell culture. The human NSCLC cell lines used in this study were purchased from the American Type Culture Collection (Manassas, VA). The stable transfectants A549-Lac Z-2, A549-Lac Z-9, A549-$FLIP_L$-2 and A549-$FLIP_L$-4 were described previously (ref. 22). The stable transfectants H157-$FLIP_L$-5 and H157-$FLIP_L$-21 that express ectopic $FLIP_L$ and H157-$FLIP_L$-16 transfectant that were infected with lentiviral $FLIP_L$ but did not express $FLIP_L$ were established (as described previously Ref. 23). Both H157-lac Z-5[23] and H157-$FLIP_L$-16 transfectants were used as control cell lines. These cell lines were cultured in RPMI 1640 containing 5% fetal bovine serum at 37°C in a humidified atmosphere of 5% CO_2 and 95% air.

Cell survival assay. Cells were seeded in 96-well cell culture plates and treated next day with the agents indicated. The viable cell number was estimated using the sulforhodamine B (SRB) assay (as previously described in ref. 24).

Detection of apoptosis. Apoptosis was evaluated by Annexin V staining using Annexin V-PE apoptosis detection kit purchased from BD Biosciences (San Jose, CA) following the manufacturer's instructions or by measuring sub-G_1 populations using flow cytometry (as described previously in ref. 25). We also detected caspase activation by Western blotting (as described below) as an additional indicator of apoptosis.

Western blot analysis. Whole-cell protein lysates were prepared and analyzed by Western blotting (as described previously in refs. 26 and 27).

Immunoprecipitation for detection of ubiqutinated c-FLIP. H157-$FLIP_L$-21 cells, which stably express $FLIP_L$, were transfected with HA-ubiquitin plasmid using the FuGENE 6 transfection reagent (Roche Diagnostics Corp., Indianapolis, IN) following the manufactor's instruction. After 24 h, the cells were treated with CDDO-Me or MG132 plus CDDO-Me for 4 h and then were lysed for immunoprecipitation of Flag-$FLIP_L$ using Flag M2 monoclonal antibody (Sigma chemicals) (as previously described in ref. 28) followed by the detection of ubiquitinated $FLIP_L$ with Western blotting using anti-HA antibody (Abgent; San Diego, CA).

Small interfering siRNAs (siRNA)-mediated silencing of c-FLIP. Silencing of c-FLIP was achieved by transfecting non-silencing control or c-FLIP siRNA using RNAifect transfection reagent (Qiagen, Valencia, CA) following the manufacturer's instructions. The control and c-FLIP siRNAs were described previously in references 27 and 29).

RESULTS

CDDO-Me decreases the levels of c-FLIP in human NSCLC cells. To determine whether CDDO-Me modulates the levels of c-FLIP, we detected c-FLIP alterations in two representative NSCLC cell lines, H157 and A549, which undergo CDDO-Me induced apoptosis.[1] After exposure to CDDO-Me for different times, the levels of c-FLIP including both $FLIP_L$ and $FLIP_S$ were decreased in a time-dependent manner starting at 3 h post treatment with CDDO-Me in the both cell lines (Fig. 1A). Reduction of c-FLIP was accompanied with increased levels of cleaved caspase-8 and PARP. We previously have shown that H157 cells were more sensitive than A549 cells to CDDO-Me-induced apoptosis.[1] Accordingly, reduction of c-FLIP levels were more pronounced and rapid in H157 compared to A549 cells, in which cleavage of caspase-8 and PARP were detected at relatively late time points (e.g., 9 h) post treatment (Fig. 1A). These results indicate that c-FLIP downregulation is an early event before the onset of apoptosis. In addition to H157 and A549 cell lines, CDDO-Me also decreased c-FLIP levels in other NSCLC cell lines (i.e., H460, H522 and H1944) in a concentration-dependent manner accompanied with increased cleavage of caspase-8 (Fig. 1B), indicating that CDDO-Me-induced c-FLIP downregulation commonly occurs in NSCLC cells.

CDDO-Me downregulates c-FLIP through enhancement of ubiqitin/proteasome-mediated degradation. To get insight into the mechanism underlying CDDO-Me-induced c-FLIP downregulation, we determined whether CDDO-Me facilitated c-FLIP degradation through a ubiquitin/proteasome-mediated mechanism because c-FLIP proteins are known to be regulated by ubiquitin/proteasome-mediated degradation.[15-17] To this end, we found that CDDO-Me-induced downregulation of c-FLIP was abolished by the

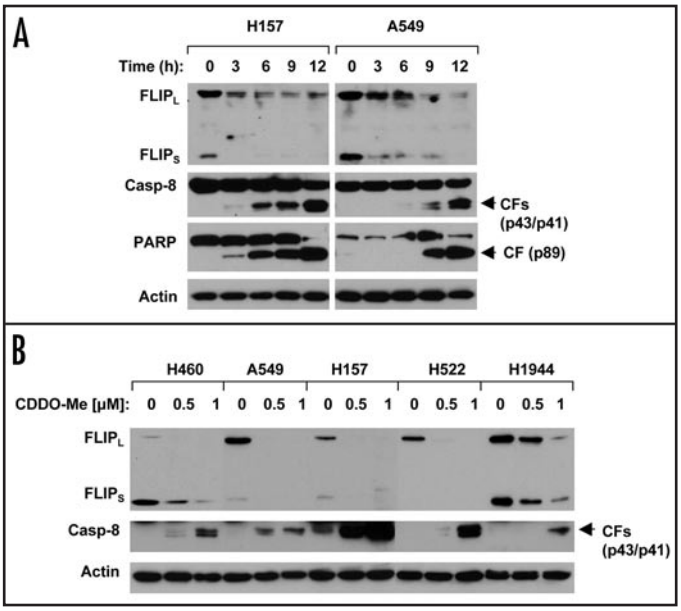

Figure 1. CDDO-Me downregulates c-FLIP levels in time- (A) and dose- (B) dependent manners in human NSCLC cells. The indicated cell lines were treated with 1 μM CDDO-Me for the times as indicated (A) or with the given doses of CDDO-Me for 8 h (B). The cells were then harvested for preparation of whole-cell protein lysates and subsequent Western blot analysis.

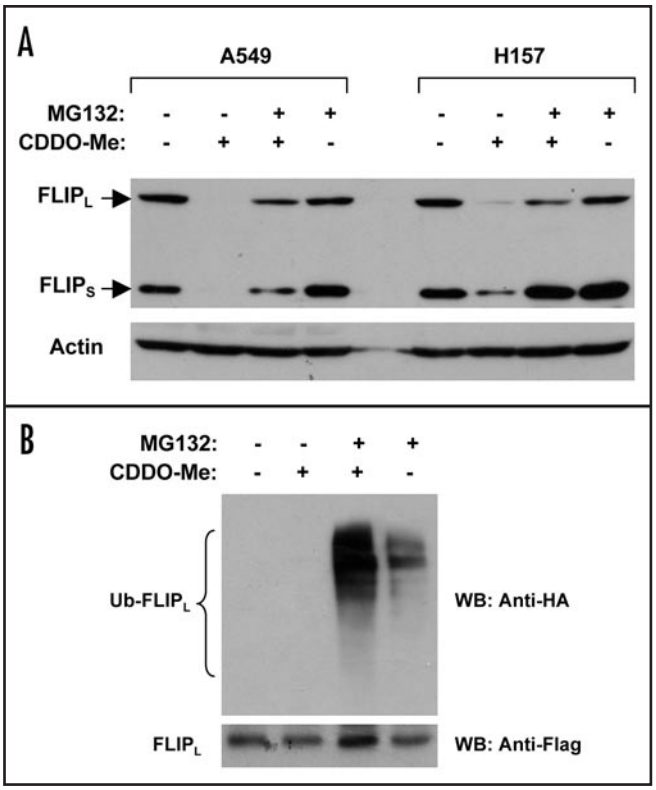

Figure 2. The proteasome inhibitor MG132 prevents CDDO-Me-induced c-FLIP downregulation (A) and detection of CDDO-Me-induced increase of ubiquitinated c-FLIP (B). (A) The given cell lines were pretreated with 20 μM MG132 for 30 minutes and then co-treated with 1 μM CDDO-Me for another 4 h. The cells were then harvested for preparation of whole-cell protein lysates and subsequent Western blot analysis. B, H157-FLIP$_L$-21 cells which stably express ectopic flag-FLIP$_L$ were transfected with HA-ubiquitin plasmid using FuGENE 6 transfection reagent for 24 h. The cells were then pretreated with 20 μM MG132 for 30 minutes and then co-treated with 1 μM CDDO-Me for 4 h. Whole-cell protein lysates were then prepared for immunoprecipitation using anti-Flag antibody followed by Western blotting (WB) using anti-HA antibody for detection of ubiquitinated FLIP$_L$ (Ub-FLIP$_L$) and anti-Flag antibody for detection of ectopic FLIP$_L$.

presence of the proteasome inhibitor MG132 (Fig. 2A), suggesting that CDDO-Me-induced c-FLIP reduction is indeed proteasome-dependent. By immunoprecipitation/Western blotting, we detected the highest levels of ubiqutinated FLIP$_L$ in cells treated with CDDO-Me plus MG132 compared to cells exposed to CDDO-Me alone or MG132 alone (Fig. 2B), indicating that DMC increases c-FLIP ubiquitination. Taken together, we conclude that CDDO-Me facilitates ubiqitin/proteasome-mediated c-FLIP degradation, leading to downregulation of c-FLIP in human NSCLC cells.

CDDO-Me downreglates c-FLIP levels independently of JNK activation. Recently, JNK has been demonstrated to be responsible for tumor necrosis factor-induced, ubiqutin/proteasome-mediated FLIP$_L$ degradation.[17] Our previous study has shows that CDDO-Me activates JNK, which contributes for CDDO-Me-induced DR5 expression and apoptosis in human NSCLC cells.[7] Thus, we next asked whether JNK activation is responsible for c-FLIP down-regulation by CDDO-Me. To this end, we examined the effects of CDDO-Me on c-FLIP reduction in the presence of the JNK-specific inhibitor SP600125[30] in H157 cells. SP600125 at the concentrations of 5-30 μM, as expected, inhibited CDDO-Me-induced increase of p-c-Jun in a dose-dependent fashion. Accordingly, CDDO-induced DR5 upregulation and PARP cleavage were inhibited in the presence of SP600125 (Fig. 3), thus confirming our previous finding that CDDO-Me induces JNK-dependent DR5 expression in human NSCLC cells.[7] However, under such a condition, SP600125 failed to prevent FLIP$_L$ from downregulation by CDDO-Me (Fig. 3), indicating that CDDO-Me induces JNK-independent downregulation of degradation of c-FLIP in human NSCLC cells.

c-FLIP downregulation contributes to CDDO-Me-induced apoptosis. Given that CDDO-Me induces apoptosis of human NSCLC cells involving DR5 upregulation,[7] we speculated that c-FLIP downregulation would further sensitize NSCLC cells to

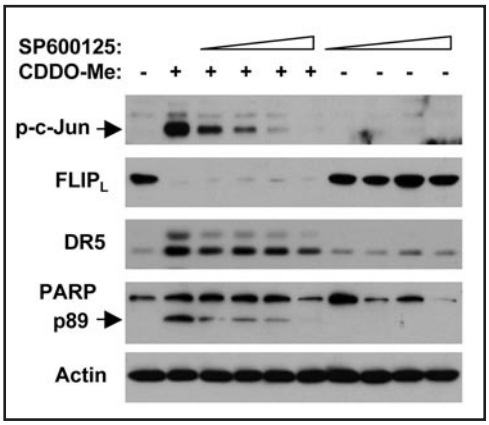

Figure 3. Effects of the JNK inhibitor SP600215 on CDDO-Me-induced c-Jun phosphorylation, c-FLIP downregulation, DR5 induction and PARP cleavage. H157 cells were pretreated with in increased concentrations of SP600125 (5, 10, 20 and 30 μM) for 30 min and then co-treated with 0.5 μM CDDO-Me. After another 8 h, the cells were subjected to preparation of whole-cell protein lysates for detection of the indicated proteins by Western blot analysis.

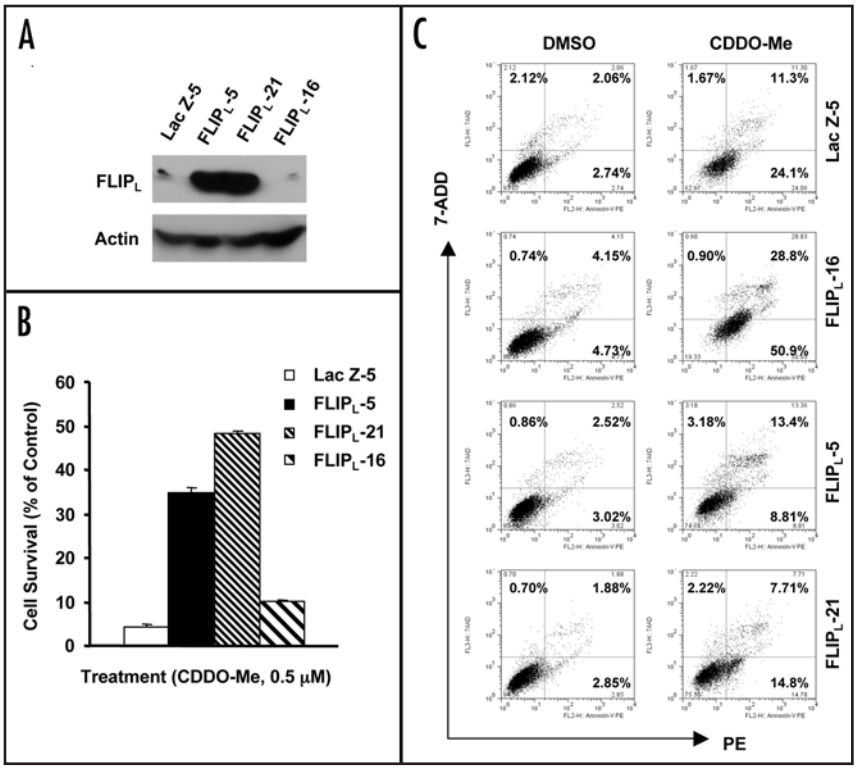

Figure 4. Enforced expression of ectopic FLIP$_L$ (A) confers resistance to CDDO-Me-induced decrease in cell survival (B) and apoptosis (C) in H157 cells. The indicated H157 transfectants that express or do not express ectopic FLIP$_L$ (A) were treated with 0.5 μM CDDO-Me for 24 h. The cell survival was evaluated by the SRB assay (B) and apoptosis was measured by Annexin V staining (C). Data in (B) are means of four replicate determinations. Bars, ± SDs. In the Annexin V assay, the percent positive cells in the upper right and lower right quadrants were added to yield the total of apoptotic cells.

undergo extrinsic death receptor-mediated apoptosis and hence contribute to CDDO-Me-induced apoptosis. To test this hypothesis, we used a lentiviral expression system to enforce c-FLIP overexpression (e.g., FLIP$_L$) in NSCLC cells and then analyzed its impact on CDDO-Me's ability to induce apoptosis. Taking advantage of a lentiviral expression system that achieves stable gene expression, we established H157 cells lines that stably expressed high levels of ectopic FLIP$_L$ (i.e., H157-FLIP$_L$-5 and H157-FLIP$_L$-21) or did not express FLIP$_L$ (i.e., H157-Lac Z-5 and H157-FLIP$_L$-16) (Fig. 4A). We used H157-Lac Z-5 which expressed irrelevant Lac Z protein and H157-FLIP$_L$-16 which did not express FLIP$_L$ albeit being infected with lentiviral FLIP$_L$ as control cell lines. By measuring cell survival, we found that CDDO-Me effectively decreased the survival of H157-Lac Z-5 and H157-FLIP$_L$-16 cells; this effect was strikingly attenuated in H157-FLIP$_L$-5 and H157-FLIP$_L$-21 cells (Fig. 4B), indicating that enforced overexpression of ectopic FLIP$_L$ confers cell resistance to CDDO-Me. By directly measuring apoptosis using Annexin V staining, we detected less apoptotic cells in H157-FLIP$_L$-5 (22%) and H157-FLIP$_L$-21 (23%) cell lines compared to H157-Lac Z-5 (35%) and H157-FLIP$_L$-16 (80%) control cell lines when exposed to CDDO-Me, indicating that enforced overexpression of ectopic FLIP$_L$ attenuates CDDO-Me's ability to induce apoptosis.

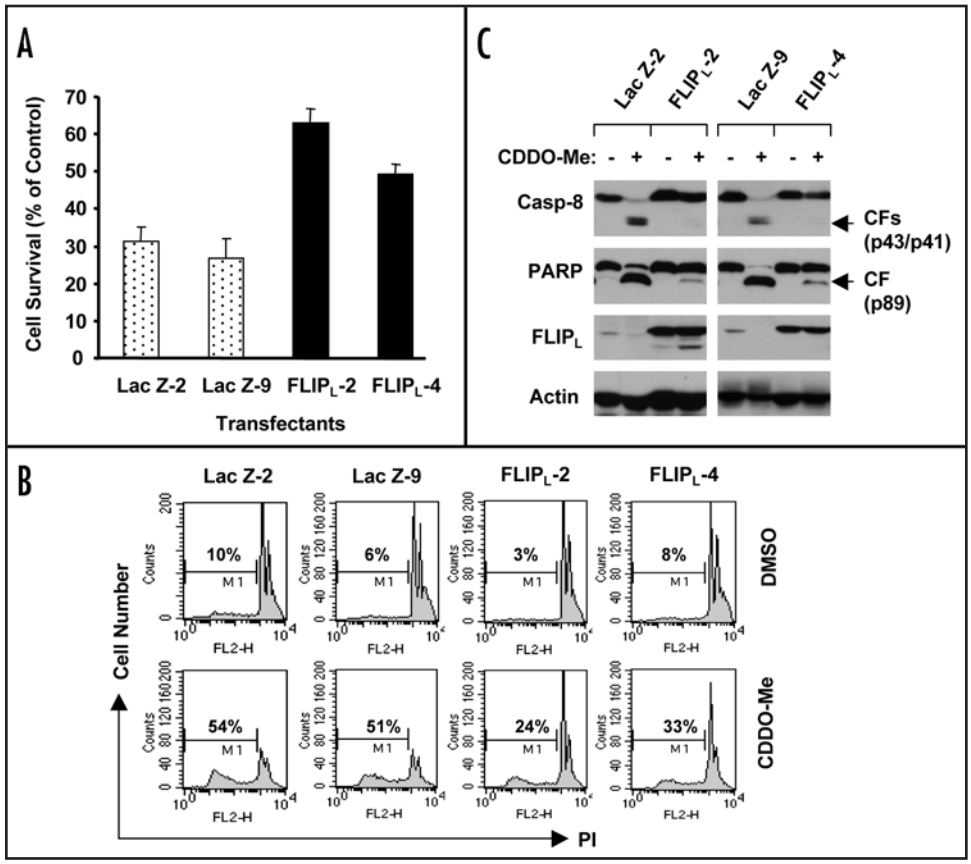

Figure 5. Enforced expression of ectopic FLIP$_L$ confers resistance to CDDO-Me-induced decrease in cell survival (A) and apoptosis (B and C) in A549 cells. The indicated A549 transfectants that express or do not express ectopic FLIP$_L$ (C) were treated with 0.5 μM CDDO-Me for 24 h. Cell survival was evaluated by the SRB assay (A) and apoptosis was measured by flow cytometry for sub-G$_1$ cells (B) and by Western blotting for cleavage of caspase-8 and PARP (C). Data in A are means of four replicate determinations. Bars, ± SDs. CF, cleaved form.

Moreover, we also compared the effects of CDDO-Me on decreasing cell survival and inducing apoptosis in A549 cell lines that stably express ectopic FLIP$_L$ (i.e., A549-FLIP$_L$-2 and A549-FLIP$_L$-4) and control Lac Z (i.e., A549-Lac Z-2 and A549-Lac Z-9), respectively (Fig. 5C). As shown in Figure 5A, CDDO-Me was less effective in decreasing cell survival in A549-FLIP$_L$-2 and A549-FLIP$_L$-4 cell lines (by approximately less than 50% on average) than in A549-Lac Z-2 and A549-Lac Z-9 cell lines (by approximately 70% on average). In agreement, we

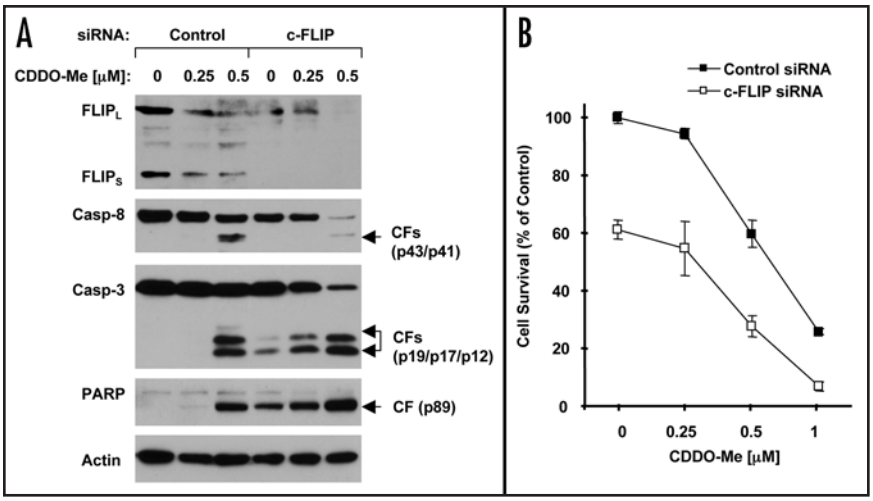

Figure 6. siRNA-mediated reduction of endogenous levels of c-FLIP sensitizes cancer cells to CDDO-Me-induced apoptosis. H1944 cells plated in a 24-well plate (A) or a 96-well (B) plate were transfected with control or c-FLIP siRNA. Twenty-four hour later, the cells were exposed to the indicated concentration of CDDO-Me. After 12 h, the cells were subjected to preparation of whole-cell protein lysates and subsequent detection of the indicated proteins using Western blot analysis (A) or to estimation of cell survival by SRB assay (B). Data in B are means of four replicate determinations. Bars, ± SDs. CF, cleaved form.

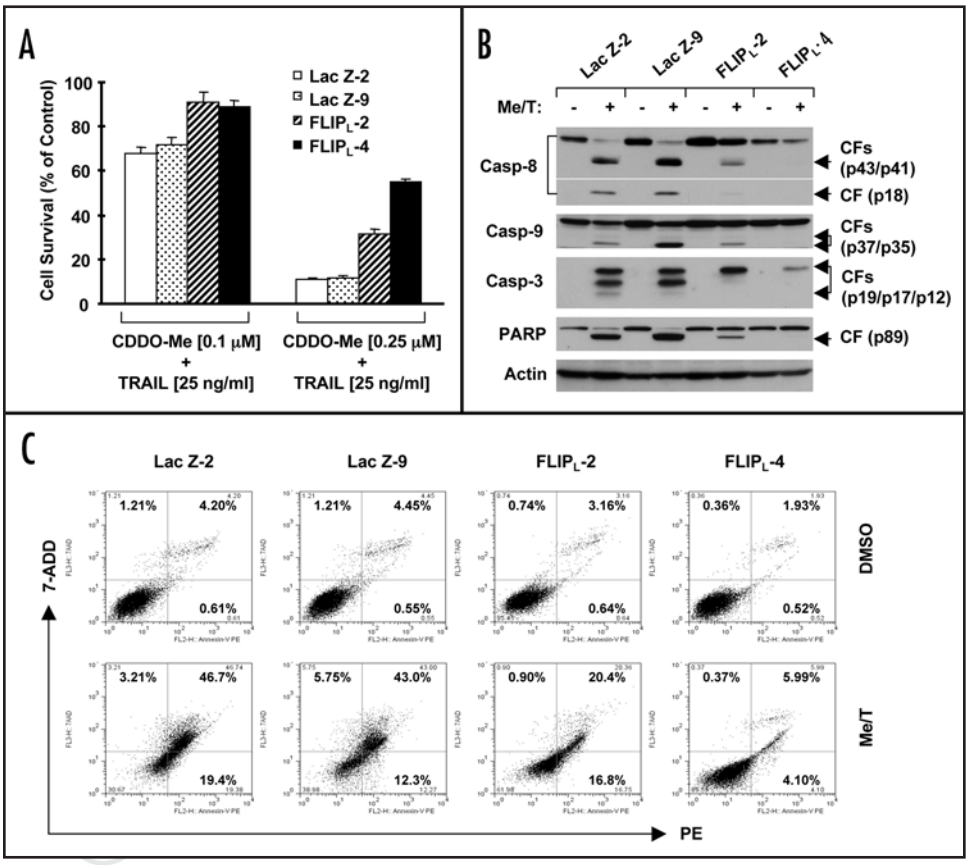

Figure 7. Enforced expression of ectopic FLIP$_L$ decreases cell sensitivity to CDDO-Me/TRAIL combination-induced decrease in cell survival (A) and apoptosis (B and C). The indicated A549 transfectants that express or do not express ectopic FLIP$_L$ were treated with the combinations of the given doses of CDDO-Me and TRAIL (A) or the combination of 0.25 μM CDDO-Me and 25 ng/ml TRAIL) (B and C) for 24 h. Cell survival was evaluated by the SRB assay (A) and apoptosis was measured by Western blotting for cleavage of the given caspases and PARP (B) and by Annexin V staining for Annexin V positive cells (C) and. Data in (A) are means of four replicate determinations. Bars, ± SDs. In the Annexin V assay, the percent positive cells in the upper right and lower right quadrants were added to yield the total of apoptotic cells. CF, cleaved form; Me/T, CDDO-Me plus TRAIL.

detected less apoptotic cells in A549-FLIP$_L$-2 (24%) and A549-FLIP$_L$-4 (33%) cells than in A549-Lac Z-2 (54%) and A549-Lac Z-9 (51%) cells (Fig. 5B). Correspondingly, the cleavage of caspase-8 and PARP was substantially inhibited in A549 cell lines expressing ectopic FLIP$_L$ compared to the Lac Z-transfected control cell lines, evidenced by no reduction of uncleaved forms of caspase-8 and PARP and less amounts of cleaved caspase-8 and PARP (Fig. 5C). Thus these results further show that overexpression of ectopic FLIP$_L$ confers cell resistance to CDDO-Me-induced apoptosis.

To complement our above findings, we further silenced the expression of endogenous c-FLIP and then examined its impact on cell sensitivity to CDDO-Me. Here we chose the H1944 cell line because it has high levels of c-FLIP, which were only weakly reduced by CDDO-Me (Fig. 1B). As presented in Figure 6, transfection of c-FLIP siRNA substantially reduced the levels of both FLIP$_L$ and FLIP$_S$ compared to transfection of control siRNA. Transfection of c-FLIP siRNA alone increased cleavage of caspase-3 and PARP (Fig. 6A) and decreased cell survival (by approximately 40%) (Fig. 6B). CDDO-Me treatment induced more cleavage of caspase-8, caspase-3 and PARP, as evidenced by reduced levels of pro-forms of the proteins and increased levels of cleaved forms (Fig. 6A) and more cell death (Fig. 6B) in c-FLIP siRNA-transfected cells than in control siRNA-transfected cells, indicating that downregulation of endogenous c-FLIP levels sensitizes cancer cells to CDDO-Me-induced apoptotic cell death. Taken together, we conclude that downregulation of c-FLIP plays a critical role in CDDO-Me-induced apoptosis in human NSCLC cells.

Downregulation of c-FLIP contributes to cooperative induction of apoptosis by CDDO-Me and TRAIL combination. Our previous work has demonstrated that CDDO-Me cooperates with TRAIL to augment induction of apoptosis in human NSCLC cells.[7] Given that c-FLIP is a key negative regulator of the TRAIL/death receptor-mediated apoptosis, it was plausible to hypothesize that c-FLIP downregulation might contribute to augmented induction of apoptosis by the combination of CDDO-Me and TRAIL. To test this speculation, we compared induction of apoptosis by the combination of CDDO-Me and TRAIL in A549 trasnfectants aforementioned that express or do not express ectopic FLIP$_L$. The combinations of CDDO-Me and TRAIL at the tested low

doses were more effective in decreasing cell survival in A549-Lac Z-2 and A549-Lac Z-9 cells than in A549-$FLIP_L$-2 and A549-$FLIP_L$-4 (Fig. 7A). This combination potently caused cleavage of caspase-8, caspase-9, caspase-3 and PARP evidenced in both A549-Lac Z-2 and A549-Lac Z-9 cell lines as the pro-forms of the proteins were strikingly decreased and strong cleaved bands were detected by Western blot analysis; these effects were drastically attenuated in A549-$FLIP_L$-2 and A549-$FLIP_L$-4 cells (Fig. 7B). Accordingly, the combination of CDDO-Me and TRAIL induced more apoptotic cells (i.e., annexin V positive cells) in A549-Lac Z-2 (67%) and A549-Lac Z-9 (55%) cells than in A549-$FLIP_L$-2 (37%) and A549-$FLIP_L$-4 (10%) cells (Fig. 7C). Collectively, these results show that enforced expression of ectopic $FLIP_L$ protects cells from CDDO-Me/TRAIL-induced apoptosis, indicating that c-FLIP downregulation is also involved in mediating the cooperative induction of apoptosis by the combination of CDDO-Me and TRAIL.

DISCUSSION

We previously have shown that CDDO-Me induces DR5 upregulation, which contributes to CDDO-Me induced apoptosis and enhancement of TRAIL-induced apoptosis in human NSCLC cells.[7,9] In the present study, we further show that, in addition to DR5 induction, CDDO-Me rapidly and potently downregulates c-FLIP levels in the multiple tested human NSCLC cell lines. Downregulation of c-FLIP appears to participate in CDDO-Me-induced apoptosis and enhancement of TRAIL-induced apoptosis because enforced expression of ectopic c-FLIP (i.e., $FLIP_L$) protected human NSCLC cells from apoptosis induced by either CDDO-Me alone or by the combination of CDDO-Me and TRAIL, whereas reduction of endogenous levels of c-FLIP sensitizes cancer cells to CDDO-Me-induced apoptosis. Given the critical role of c-FLIP in negatively regulating the extrinsic apoptotic pathway, the current results complement our previous findings[7] to further indicate that CDDO-Me induces apoptosis involving activation of the extrinsic apoptotic pathway. It is possible that CDDO-Me induces DR5 expression, resulting in triggering of apoptosis, whereas downregulation of c-FLIP lowers the cell threshold to undergo extrinsic pathway-mediated apoptosis, amplifying CDDO-Me-induced apoptosis. To the best of our knowledge, this is the first direct evidence for the involvement of c-FLIP downregulation in CDDO-Me-induced apoptosis in human cancer cells. We also believe that DR5 induction and c-FLIP downregulation are two key events responsible for CDDO-Me-mediated enhancement of TRAIL-induce apoptosis in human NSCLC cells.

It is known that c-FLIP is subjected to ubquitin/proteasome-dependent degradation.[15-17] In this study, the presence of proteasome inhibitor MG132 prevented c-FLIP (both $FLIP_L$ and $FLIP_S$) from CDDO-Me-induced downregulation. Moreover, increased levels of ubiquitinated c-FLIP (i.e., $FLIP_L$) were detected in cells co-treated with MG132 and CDDO-Me by immunoprecipitation-Western blotting (Fig. 2). Thus, these results collectively indicate that CDDO-Me decreases c-FLIP levels through facilitating ubiquitin/proteasome-dependent degradation of c-FLIP. This is in agreement with the finding that the CDDO-Me's analogue CDDO induces ubiquitin/proteasome-mediated degradation of c-FLIP in other cancer cell lines.[15]

A recent study has shown that JNK activation is involved in regulating ubiquitin/proteasome-dependent degradation of $FLIP_L$.[17] In our study, we found that the JNK inhibitor SP600125 at concentrations (5–30 μM) that inhibited JNK activation (e.g., c-Jun phosphorylation) did not prevent $FLIP_L$ from CDDO-Me-induced downregulation. Under the same condition, CDDO-Me-induced DR5 expression and PARP cleavage were indeed inhibited (Fig. 3), confirming our previous demonstration that CDDO-Me induces apoptosis involving JNK-dependent DR5 upregulation in human NSCLC cells.[7,9] Thus, we conclude that CDDO-Me induces ubiquitin/proteasome-mediated degradation of c-FLIP independently of JNK activation. Since c-FLIP downregulation also contributes to CDDO-Me-induced apoptosis, we believe that CDDO-Me induces apoptosis though both JNK-dependent (e.g., DR5 upregulation) and -independent (e.g., c-FLIP degradation) mechanisms.

In summary, the present study has demonstrated that CDDO-Me downregulates c-FLIP levels in human NSCLC cells though JNK-independent ubiquitin/proteasome-mediated degradation of c-FLIP. Importantly, c-FLIP downregulation contributes to CDDO-Me-induced apoptosis and enhancement of TRAIL-induced apoptosis. Thus, the current finding together with our previous finding on the involvement of JNK-dependent DR5 induction in CDDO-Me-induced apoptosis provide compelling evidence for the involvement of the activation of the extrinsic apoptotic pathway in CDDO-Me-induced apoptosis in human NSCLC cells.

References

1. Kim KB, Lotan R, Yue P, Sporn MB, Suh N, Gribble GW, Honda T, Wu GS, Hong WK, Sun SY. Identification of a novel synthetic triterpenoid, methyl-2-cyano-3,12-dioxooleana-1,9-dien-28-oate, that potently induces caspase-mediated apoptosis in human lung cancer cells. Mol Cancer Ther 2002; 1:177-84.
2. Konopleva M, Tsao T, Ruvolo P, Stiouf I, Estrov Z, Leysath CE, Zhao S, Harris D, Chang S, Jackson CE, Munsell M, Suh N, Gribble G, Honda T, May WS, Sporn MB, Andreeff M. Novel triterpenoid CDDO-Me is a potent inducer of apoptosis and differentiation in acute myelogenous leukemia. Blood 2002; 99:326-35.
3. Chintharlapalli S, Papineni S, Konopleva M, Andreef M, Samudio I, Safe S. 2-Cyano-3,12-dioxoolean-1,9-dien-28-oic acid and related compounds inhibit growth of colon cancer cells through peroxisome proliferator-activated receptor gamma-dependent and -independent pathways. Mol Pharmacol 2005; 68:119-28.
4. Ikeda T, Sporn M, Honda T, Gribble GW, Kufe D. The novel triterpenoid CDDO and its derivatives induce apoptosis by disruption of intracellular redox balance. Cancer Res 2003; 63:5551-8.
5. Shishodia S, Sethi G, Konopleva M, Andreeff M, Aggarwal BB. A synthetic triterpenoid, CDDO-Me, inhibits IkappaBalpha kinase and enhances apoptosis induced by TNF and chemotherapeutic agents through down-regulation of expression of nuclear factor kappaB-regulated gene products in human leukemic cells. Clin Cancer Res 2006; 12:1828-38.
6. Hengartner MO. The biochemistry of apoptosis. Nature 2000; 407:770-6.
7. Zou W, Liu X, Yue P, Zhou Z, Sporn MB, Lotan R, Khuri FR, Sun SY. c-Jun NH2-terminal kinase-mediated up-regulation of death receptor 5 contributes to induction of apoptosis by the novel synthetic triterpenoid methyl-2-cyano-3,12-dioxooleana-1, 9-dien-28-oate in human lung cancer cells. Cancer Res 2004; 64:7570-8.
8. Ahmad R, Raina D, Meyer C, Kharbanda S, Kufe D. Triterpenoid CDDO-Me blocks the NF-kappaB pathway by direct inhibition of IKKbeta on Cys-179. J Biol Chem 2006; 281:35764-9.
9. Yue P, Zhou Z, Khuri FR, Sun SY. Depletion of intracellular glutathione contributes to JNK-mediated death receptor 5 upregulation and apoptosis induction by the novel synthetic triterpenoid methyl-2-cyano-3, 12-dioxooleana-1, 9-dien-28-oate (CDDO-Me). Cancer Biol Ther 2006; 5:492-7.
10. Konopleva M, Contractor R, Kurinna SM, Chen W, Andreeff M, Ruvolo PP. The novel triterpenoid CDDO-Me suppresses MAPK pathways and promotes p38 activation in acute myeloid leukemia cells. Leukemia 2005; 19:1350-4.
11. Suh WS, Kim YS, Schimmer AD, Kitada S, Minden M, Andreeff M, Suh N, Sporn M, Reed JC. Synthetic triterpenoids activate a pathway for apoptosis in AML cells involving downregulation of FLIP and sensitization to TRAIL. Leukemia 2003; 17:2122-9.
12. Wajant H. Targeting the FLICE inhibitory protein (FLIP) in cancer therapy. Mol Interv 2003; 3:124-7.
13. Kataoka T. The caspase-8 modulator c-FLIP. Crit Rev Immunol 2005; 25:31-58.
14. Irmler M, Thome M, Hahne M, Schneider P, Hofmann K, Steiner V, Bodmer JL, Schroter M, Burns K, Mattmann C, Rimoldi D, French LE, Tschopp J. Inhibition of death receptor signals by cellular FLIP. Nature 1997; 388:190-5.
15. Kim Y, Suh N, Sporn M, Reed JC. An inducible pathway for degradation of FLIP protein sensitizes tumor cells to TRAIL-induced apoptosis. J Biol Chem 2002; 277:22320-9.

16. Poukkula M, Kaunisto A, Hietakangas V, Denessiouk K, Katajamaki T, Johnson MS, Sistonen L, Eriksson JE. Rapid turnover of c-FLIPshort is determined by its unique C-terminal tail. J Biol Chem 2005; 280:27345-55.
17. Chang L, Kamata H, Solinas G, Luo JL, Maeda S, Venuprasad K, Liu YC, Karin M. The E3 ubiquitin ligase itch couples JNK activation to TNFalpha-induced cell death by inducing c-FLIP(L) turnover. Cell 2006; 124:601-13.
18. Kamarajan P, Sun NK, Chao CC. Up-regulation of FLIP in cisplatin-selected HeLa cells causes cross-resistance to CD95/Fas death signalling. Biochem J 2003; 376:253-60.
19. Longley DB, Wilson TR, McEwan M, Allen WL, McDermott U, Galligan L, Johnston PG. c-FLIP inhibits chemotherapy-induced colorectal cancer cell death. Oncogene 2006; 25:838-48.
20. Abedini MR, Qiu Q, Yan X, Tsang BK. Possible role of FLICE-like inhibitory protein (FLIP) in chemoresistant ovarian cancer cells in vitro. Oncogene 2004; 23:6997-7004.
21. Honda T, Rounds BV, Bore L, Favaloro Jr FG, Gribble GW, Suh N, Wang Y, Spor MB. Novel synthetic oleanane triterpenoids: A series of highly active inhibitors of nitric oxide production in mouse macrophages. Bioorg Med Chem Lett 1999; 9:3429-34.
22. Zou W, Liu X, Yue P, Khuri FR, Sun SY. PPARgamma ligands enhance TRAIL-induced apoptosis through DR5 upregulation and c-FLIP downregulation in human lung cancer cells. Cancer Biol Ther 2007; 6:99-106.
23. Liu X, Yue P, Schonthal AH, Khuri FR, Sun SY. Cellular FLICE-inhibitory protein down-regulation contributes to celecoxib-induced apoptosis in human lung cancer cells. Cancer Res 2006; 66:11115-9.
24. Sun SY, Yue P, Dawson MI, Shroot B, Michel S, Lamph WW, Heyman RA, Teng M, Chandraratna RA, Shudo K, Hong WK, Lotan R. Differential effects of synthetic nuclear retinoid receptor-selective retinoids on the growth of human non-small cell lung carcinoma cells. Cancer Res 1997; 57:4931-9.
25. Sun SY, Yue P, Shroot B, Hong WK, Lotan R. Induction of apoptosis in human non-small cell lung carcinoma cells by the novel synthetic retinoid CD437. J Cell Physiol 1997; 173:279-84.
26. Sun SY, Yue P, Wu GS, El-Deiry WS, Shroot B, Hong WK, Lotan R. Mechanisms of apoptosis induced by the synthetic retinoid CD437 in human non-small cell lung carcinoma cells. Oncogene 1999; 18:2357-65.
27. Liu X, Yue P, Zhou Z, Khuri FR, Sun SY. Death receptor regulation and celecoxib-induced apoptosis in human lung cancer cells. J Natl Cancer Inst 2004; 96:1769-80.
28. Chen C, Sun X, Ran Q, Wilkinson KD, Murphy TJ, Simons JW, Dong JT. Ubiquitin-proteasome degradation of KLF5 transcription factor in cancer and untransformed epithelial cells. Oncogene 2005; 24:3319-27.
29. Elrod HA, Lin YD, Yue P, Wang X, Lonial S, Khuri FR, Sun SY. The alkylphospholipid perifosine induces apoptosis of human lung cancer cells requiring inhibition of Akt and activation of the extrinsic apoptotic pathway. Mol Cancer Ther 2007; 6:2029-38.
30. Bennett BL, Sasaki DT, Murray BW, O'Leary EC, Sakata ST, Xu W, Leisten JC, Motiwala A, Pierce S, Satoh Y, Bhagwat SS, Manning AM, Anderson DW. SP600125, an anthrapyrazolone inhibitor of Jun N-terminal kinase. Proc Natl Acad Sci USA 2001; 98:13681-6.

[Cancer Biology & Therapy 6:1, 99-106, January 2007]; ©2007 Landes Bioscience

Research Paper

PPARγ Ligands Enhance TRAIL-induced Apoptosis through DR5 Upregulation and c-FLIP Downregulation in Human Lung Cancer Cells

Wei Zou
Xiangguo Liu
Ping Yue
Fadlo R. Khuri
Shi-Yong Sun*

Department of Hematology and Oncology; Winship Cancer Institute; Emory University School of Medicine; Atlanta, Georgia USA

*Correspondence to: Shi-Yong Sun; Winship Cancer Institute, Emory University School of Medicine; 1365-C Clifton Road, C3088; Atlanta, Georgia 30322 USA; Tel.: 404.778.2170; Fax: 404.778.5520; Email: shi-yong.sun@emoryhealthcare.org

Original manuscript submitted: 10/06/06
Manuscript accepted: 10/29/06

Previously published online as a *Cancer Biology & Therapy* E-publication:
http://www.landesbioscience.com/journals/cc/abstract.php?id=3555

KEY WORDS

PPARγ ligands, death receptor 5, c-FLIP, TRAIL, apoptosis, lung cancer cells

ACKNOWLEDGEMENTS

We thank Dr. Jürg Tschopp (University of Lausanne, Switzerland) for c-FLIP cDNAs. S-Y. Sun and F. Khuri are Georgia Cancer Coalition Distinguished Cancer Scholars. This work is supported in part by the Georgia Cancer Coalition Distinguished Cancer Scholar award (to S-Y. Sun) and Department of Defense VITAL grant W81XWH-04-1-0142 (to S-Y. Sun for Project 4).

ABSTRACT

Peroxisome proliferator-activated receptor γ (PPARγ) ligands are potential chemopreventive agents. Many studies have shown that PPARγ ligands induce apoptosis in various types of cancer cells including lung cancer cells. Some PPARγ ligands have been shown to downregulate c-FLIP expression and thus enhance tumor necrosis factor-related apoptosis-inducing ligand (TRAIL)-induced apoptosis in some cancer cell lines. In the current study, we further show that PPARγ ligands induced the expression of death receptor 5 (DR5) and increased DR5 distribution at the cell surface in addition to reducing c-FLIP levels in human lung cancer cells. These agents cooperated with TRAIL to enhance induction of apoptosis in human lung cancer cells. Both overexpression of c-FLIP and knockdown of DR5 abrogated PPARγ ligand's ability to enhance TRAIL-induced apoptosis. Thus, it appears that not only c-FLIP downregulation but also DR5 upregulation contribute to PPARγ ligand-mediated enhancement of TRAIL-induced apoptosis in human lung cancer cells. Both the PPARγ antagonist GW9662 and silencing PPARγ expression failed to diminish PPARγ ligand-induced DR5 upregulation or c-FLIP downregulation, indicating that PPARγ ligands modulate the expression of DR5 and c-FLIP through a PPARγ-independent mechanism. Collectively, we conclude that PPARγ ligands exert PPARγ-independent effects on inducing DR5 expression and downregulating c-FLIP levels, leading to enhancement of TRAIL-induced apoptosis.

INTRODUCTION

Tumor necrosis factor-related apoptosis-inducing (TRAIL) is a soluble protein that induces apoptosis upon binding to death receptor 4 (DR4, also named TRAIL-R1) or death receptor 5 (DR5, also named TRAIL-R2, TRICK2, or Killer/DR5). TRAIL preferentially induces apoptosis in transformed or malignant cells, demonstrating potential as a tumor-selective apoptosis-inducing cytokine for cancer treatment.[1,2] Importantly, many small molecules including traditional chemotherapeutic agents are able to augment TRAIL-induced apoptosis in multiple types of cancer cells including lung cancer cells. Thus, TRAIL shows a strong potential as a cancer therapeutic agent and is being tested in phase I clinical trials.

There are several key components that modulate TRAIL-induced apoptosis. One such component is death receptor 5, which is one of the apoptotic death receptors that compose of a cysteine-rich extracellular domain and cytoplasmic death domain.[3] DR5 locates at the cell surface, becomes activated or oligomerized (trimerized) upon binding to its ligand TRAIL, and then signals apoptosis through caspase-8-mediated rapid activation of caspase cascades.[3,4] Another important protein involved in TRAIL signaling is cellular FLICE-inhibitory protein (c-FLIP; also called Casper/I-FLICE/FLAME-1/CASH/CLARP/MRIT), which is the major negative regulator of TRAIL/death receptor-induced apoptosis.[5,6] c-FLIP binds to Fas-associated death domain (FADD) and caspase-8 at the death-inducing signaling complex (DISC), and thereby inhibits death receptor-mediated apoptosis.[7] c-FLIP has multiple splice variants, and two main forms have been well characterized: c-FLIP short form (c-FLIP$_S$) and c-FLIP long form (c-FLIP$_L$).[5,6] It has been well documented that elevated c-FLIP expression protects cells from death receptor-mediated apoptosis in various cell types, whereas downregulation of c-FLIP by chemicals or siRNA sensitizes cells to death receptor-mediated apoptosis.[5,6] Both DR5 and c-FLIP are subjected to modulation by certain cancer therapeutic agents. Generally speaking, agents that either upregulate DR5 expression and/or downregulates c-FLIP levels often exhibit activity in enhancing TRAIL induced apoptosis.[8]

Peroxisome proliferator-activated receptor γ (PPARγ) ligands are potential cancer chemopreventive and therapeutic agents.[9,10] Many preclinical studies have shown that PPARγ ligands induces growth arrest and apoptosis in various types of cancer cells including lung cancer cells in vitro and inhibit tumor growth and carcinogenesis in animal models.[9,11,12] Moreover, these agents can be combined with other agents to exhibit enhanced anticancer activity.[13,14] Some PPARγ ligands have been shown to downregulate c-FLIP expression and thus enhance TRAIL-induced apoptosis in certain types of cancer cell lines.[15,16] In contrast to c-FLIP, the studies on the modulation of PPARγ ligands on DR5 expression have generated conflicting results. The PPARγ agonists 15-deoxy-$\Delta^{12,14}$-prostaglandin J_2 (15d-PGJ_2) and troglitazone, but not pioglitazone and rosiglitazone, were shown to induce DR5 expression.[16,17] However, 15d-PGJ_2 was not shown to have such an effect in a different study.[15] Moreover, it is not clear whether DR5 upregulation is involved in enhancement of TRAIL-induced apoptosis by PPARγ ligands.

In the current study, we investigated the modulatory effects of synthetic PPARγ ligands on the TRAIL/death receptor-mediated apoptotic pathway in human lung cancer cells. In addition to downregulation of c-FLIP, we, for the first time, demonstrate that PPARγ ligands also induce DR5 expression in various lung cancer cell lines. Like c-FLIP downregulation, DR5 upregulation also contributes to enhancement of TRAIL-induced apoptosis by PPARγ ligands.

MATERIALS AND METHODS

Reagents. Troglitazone, pioglitazone and rosiglitazone were purchased from LKT Laboratories Inc (St. Paul, MN). Cigolitazone and GW1929 were purchased from Tocris (Ellisville, MO). WY14363 was purchased from Biomol (Plymouth Meeting, PA). CDDO was provided by Dr. M. B. Sporn (Dartmouth Medical School, Hanover, NH). These agents were dissolved in dimethyl sulfoxide (DMSO) at a concentration of 10 mM or 100 mM, and aliquots were stored at -80°C. Stock solutions were diluted to the desired final concentrations with growth medium just before use. Soluble recombinant human TRAIL was purchased from PeproTech Inc (Rocky Hill, NJ). Rabbit polyclonal anti-DR5 antibody was purchased from ProSci Inc (Poway, CA). Mouse monoclonal anti-caspase-3 was purchased from Imgenex (San Diego, CA). Rabbit polyclonal anti-caspase-9, anti-caspase-8, and anti-PARP antibodies were purchased from Cell Signaling Technology, Inc. (Beverly, MA). Mouse monoclonal anti-FLIP antibody (NF6) was purchased from Alexis Biochemicals (San Diego, CA). Rabbit polyclonal anti-β-actin antibody was purchased from Sigma Chemical Co. (St. Louis, MO).

Cell lines and cell cultures. All lung cancer cell lines used in this study were purchased from the American Type Culture Collection (Manassas, VA). These cell lines were grown in monolayer culture in RPMI 1640 medium supplemented with glutamine and 5% fetal bovine serum (FBS) at 37°C in a humidified atmosphere consisting of 5% CO_2 and 95% air.

Establishment of stable cell lines that overexpress c-$FLIP_L$ or c-$FLIP_S$. c-$FLIP_L$ and c-$FLIP_S$ coding regions were amplified by PCR using plasmids containing full length cDNAs of $FLIP_L$ and $FLIP_S$, respectively, which were provided by Dr. J. Tschopp (University of Lausanne, Switzerland).[7] The amplified fragments were then ligated into the pT-easy vector (Promega, Madison WI) following the manufacturer's protocol as pT-easy-$FLIP_L$ and pT-easy-$FLIP_S$, respectively, using the primers: c-$FLIP_L$ sense, 5'-GACTAGTGCCGCCACCATGGATTACAAAGACGATGACG-3', and $FLIP_L$ antisense, 5'-CGGGCCCTTATGTGTAGGAGAGGATAAGTTTC-3'. c-$FLIP_S$ sense, 5'-GACTAGTGCCGCCACCATGTCTGCTGAAGTCATCCATCAGG-3' and c-$FLIP_S$ antisense, 5'-CGGGCCCTCACATGGAACAATTTCCAAG -3'. Both pLenti-DcR1 (a lentiviral vector harboring the DcR1 gene, which was constructed using the pLenti6/V5 Directional TOPO Cloning kit purchased from Invitrogen) and pT-easy-$FLIP_L$ or pT-easy-$FLIP_S$ were cut with *Spe*I and *Apa*I restriction enzymes. The released fragment containing c-$FLIP_L$ or c-$FLIP_S$ gene was then cloned into the digested pLenti6/V5 vector and the resultant constructs were named pLenti-Flag-$FLIP_L$ and pLenti-$FLIP_S$, respectively. In this study, we used pLenti-Lac Z as a vector control, which was included in the pLenti6/V5 Directional TOPO Cloning kit. Lentiviral production and titer determination were done following the manufacturer's instruction. To establish stable cell lines, A549 cells were infected with the lentiviruses at ten of multiplicity of infection (MOI) with 10 μg/mL polybrene. After a two-week selection using 50 μg/mL blasticidin post infection, the survival clones were picked up and screened for c-FLIP expression by Western blotting using c-FLIP antibody. The clones with the highest levels of c-FLIP expression were used in the experiment.

Cell survival assay. Cells were seeded in 96-well cell culture plates and treated on the second day with the indicated agents. At the end of treatment, cell number was estimated by the sulforhodamine B (SRB) assay as previously described.[18] The cell survival was presented as percentage of control as calculated by using the equation: *A*t/*A*c x 100, where *A*t and *A*c represent the absorbance in treated and control cultures, respectively.

Western blot analysis. The procedures for preparation of whole-cell protein lysates and Western blot analysis were the same as described previously.[19,20]

Detection of cell surface DR5. In this study, cell surface DR5 expression was analyzed using flow cytometry. The procedure for direct antibody staining and subsequent flow cytometric analysis of cell surface protein was described previously.[21] The mean fluorescence intensity (MFI) that represents antigenic density on a per cell basis was used to represent DR5 expression level. Phycoerythrin (PE)-conjugated mouse anti-human DR5 monoclonal antibody (DJR2-4) and PE mouse IgG1 isotype control (MOPC-21/P3) were purchased from eBioscience (San Diego, CA).

Detection of caspase activation and apoptosis. Caspase activation and their substrate cleavage were detected by Western blot analysis as described above. Apoptosis was detected by estimating sub-G_1 population as described previously.[22] In addition, the amounts of cytoplasmic histone-associated DNA fragments (mononucleosome and oligonucleosomes) formed during apoptosis were also measured using a Cell Death Detection ELISA^{Plus} kit (Roche Molecular Biochemicals, Indianapolis, IN) according to the manufacturer's instructions.

Silencing of DR5 expression using small interfering RNA (siRNA). High purity control (nonsilencing) and DR5 siRNA oligos were described previously[20] and synthesized from Qiagen (Valencia, CA). The transfection of siRNA was conducted in a 24-well plate (1 μg/well) using RNAiFect^{TM} transfect reagent purchased from Qiagen following the manufacturer's instruction. Forty-eight hours after the transfection, cells were treated with a PPARγ ligand alone, TRAIL alone and their combination. Gene silencing effect was evaluated by Western blot analysis and apoptosis was measured as described above.

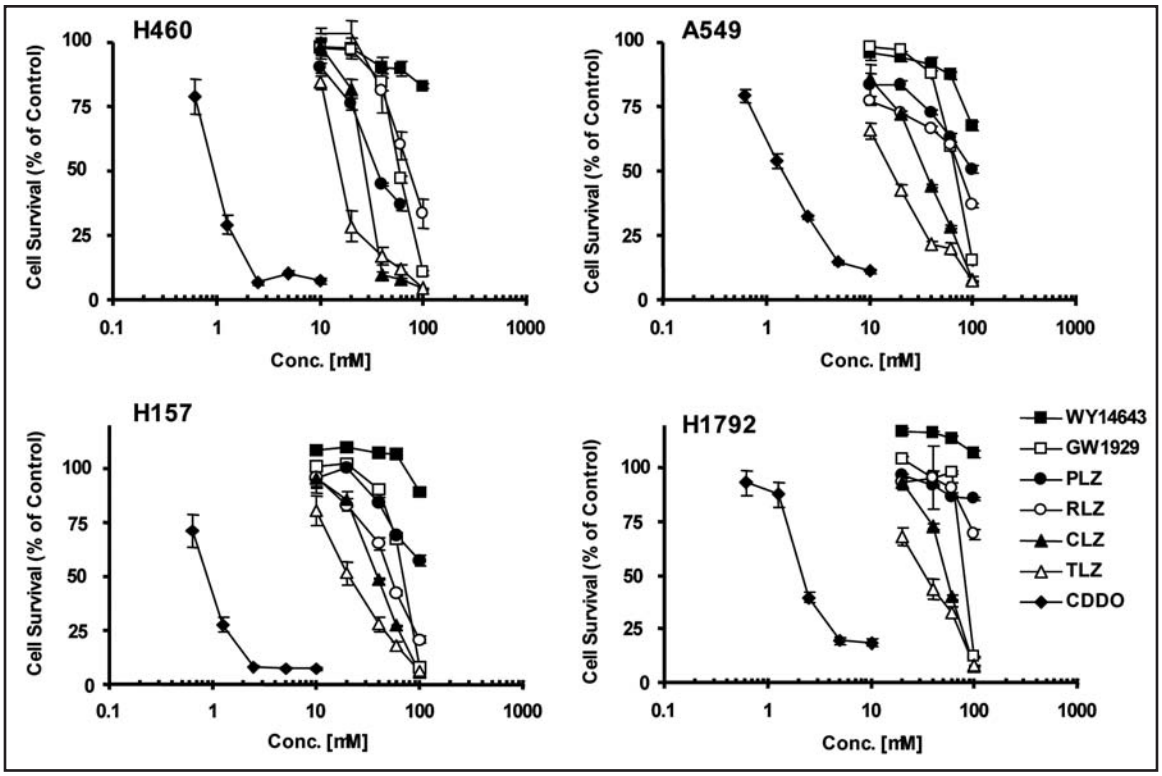

Figure 1. Effects of various PPARγ ligands on the growth of human lung cancer cells. The indicated cell lines were seeded in 96-well cell culture plates. On the second day, the cells were treated with different concentrations ranging from 0.5 to 100 μM of the given PPARγ ligands and WY14643 which is a PPARα ligand. After three days, the cells were fixed and subjected to estimation of cell number using the sulforhodamine B (SRB) assay. Each data value is a mean ± SD of four replicates. PLZ, pioglitazone; RLZ, rosiglitazone; CLZ, ciglitazone; TLZ, troglitazone

RESULTS

PPARγ ligands inhibit the growth of human lung cancer cells. To determine the concentration ranges or potencies of individual PPARγ ligands that effectively inhibit the growth of human lung cancer cells, we treated four lung cancer cell lines with several PPARγ ligands for three days and then evaluated their effects on the growth of the given cell lines. As presented in Figure 1, WY14643, a PPARα ligand, even at a concentration of 100 μM had minimal effects on decreasing the survival of four lung cancer cell lines tested, whereas all PPARγ ligands at the tested concentrations ranges effectively decreased cell survival at least in one of the tested cell lines albeit with various degrees. Among these ligands, CDDO stood out to be the most potent with IC_{50}s of 0.5–2 μM. Pioglitizone and roglitizone showed the weakest activity in decreasing the survival of the lung cancer cell lines with IC_{50}s' ranging from 40 μM to > 100 μM. Cigolitazone, troglitazone and GW1929 were in between with IC50s ranging from 15 μM to 100 μM. Therefore, we chose to use cigolitazone, troglitazone and GW1929 in our following experiments.

PPARγ ligands cooperate with TRAIL to induce apoptosis in human lung cancer cells. To determine whether the combination of a PPARγ ligand with TRAIL exhibits enhanced effects on induction of apoptosis in human lung cancer cells as observed in other types of cancer cell lines, we first examined the effects of PPARγ ligands on the survival of human lung cancer cells in the presence of TRAIL. As presented in Figure 2A, the addition of low doses of TRAIL, which itself minimally decreased cell survival (no more that 20%), greatly enhanced the effects of either of the tested PPARγ ligands (i.e., troglitazone, cigolitizone and GW1929) in the lung cancer cell lines tested. For example, troglitazone alone at 50 μM and TRAIL alone at 20 ng/ml decreased the survival of A549 cells by approximately 20%, whereas their combination decreased cell survival by >75%. Thus, it appears that the combination of a PPARγ ligand with TRAIL exhibits enhanced effects on decreasing the survival of lung cancer cells.

Following the cell survival study, we analyzed apoptosis in cells exposed to the combination of a PPARγ ligand and TRAIL. The single agent of the given PPARγ ligands or TRAIL at the concentrations tested caused minimal apoptosis (<15%). However, the combination of TRAIL with either PPARγ ligand tested induced apoptosis in >40% of cells (Fig. 1B). In agreement, we detected minimal cleaved forms of caspase-8, caspase-9, caspase-3 and PARP from cells treated with TRAIL or the PPARγ ligands tested alone under the tested conditions by Western blot analysis. However, we easily detected the cleaved forms from cells exposed to the respective combinations of TRAIL with PPARγ ligands (Fig. 2C). Collectively, these results clearly show that PPARγ ligands cooperate with TRAIL to enhance induction of apoptosis in human lung cancer cells.

PPARγ ligands induces DR5 expression in addition to downregulation of c-FLIP expression. It has been documented that some PPARγ ligands decrease c-FLIP expression, which contributes to enhancement of TRAIL-induced apoptosis by PPARγ ligands in certain types of cancer cells.[15] Thus, we examined effects of PPARγ ligands on c-FLIP expression in human lung cancer cells. The three PPARγ ligands trgolitizone, cigolitazone and GW1929 decreased the levels of both $FLIP_L$ and $FLIP_S$ in a dose-dependent manner in A549 cells (Fig. 3A). The downregulation of c-FLIP occurred after 6 h treatment with the given ligands (Fig. 3B), indicating that

c-FLIP downregulation is an early event induced by PPARγ ligands. Downregulation of c-FLIP expression by PPARγ ligands occurred not only in A549 cells as described, but also in other lung cancer cells (e.g., H157, H460, and H1792) as presented in (Fig. 3C). Therefore, it appears that downregulation of c-FLIP by PPARγ ligands commonly occurs in human lung cancer cells.

DR5 is also a key protein involved in TRAIL-mediated apoptosis and is susceptible to modulation by certain small molecules. Therefore, we were interested in determining whether PPARγ ligands modulate DR5 expression. To this end, we treated A549 cells with different concentrations of trgolitizone, cigolitazone or GW1929 for 12 h and then detected DR5 expression in these cells by Western blot analysis. Similar to modulation of c-FLIP expression, all three ligands increased DR5 expression in a concentration-dependent maner. These ligands even at 25 μM were able to upregulate DR5 expression (Fig. 3A). Similar to c-FLIP downregulation, DR5 expression was increased after 6 h exposure to the ligands (Fig. 3B), indicating that DR5 upregulation is also an early event induced by PPARγ ligands. These ligands increased DR5 expression in other lung cancer cell lines as well (Fig. 3C), indicating that induction of DR5 by PPARγ ligands is also a common event in lung cancer cells. Because DR5 is a cell surface protein, we further analyzed DR5 distribution on the cell surface in cells treated with different PPARγ ligands. As presented in Figure 3D, these ligands increased the mean fluorescent intensity (MFI) of DR5 staining in both H1792 and A549 cells, indicating that PPARγ ligands increase cell surface DR5 levels in addition to upregulating the total levels of DR5.

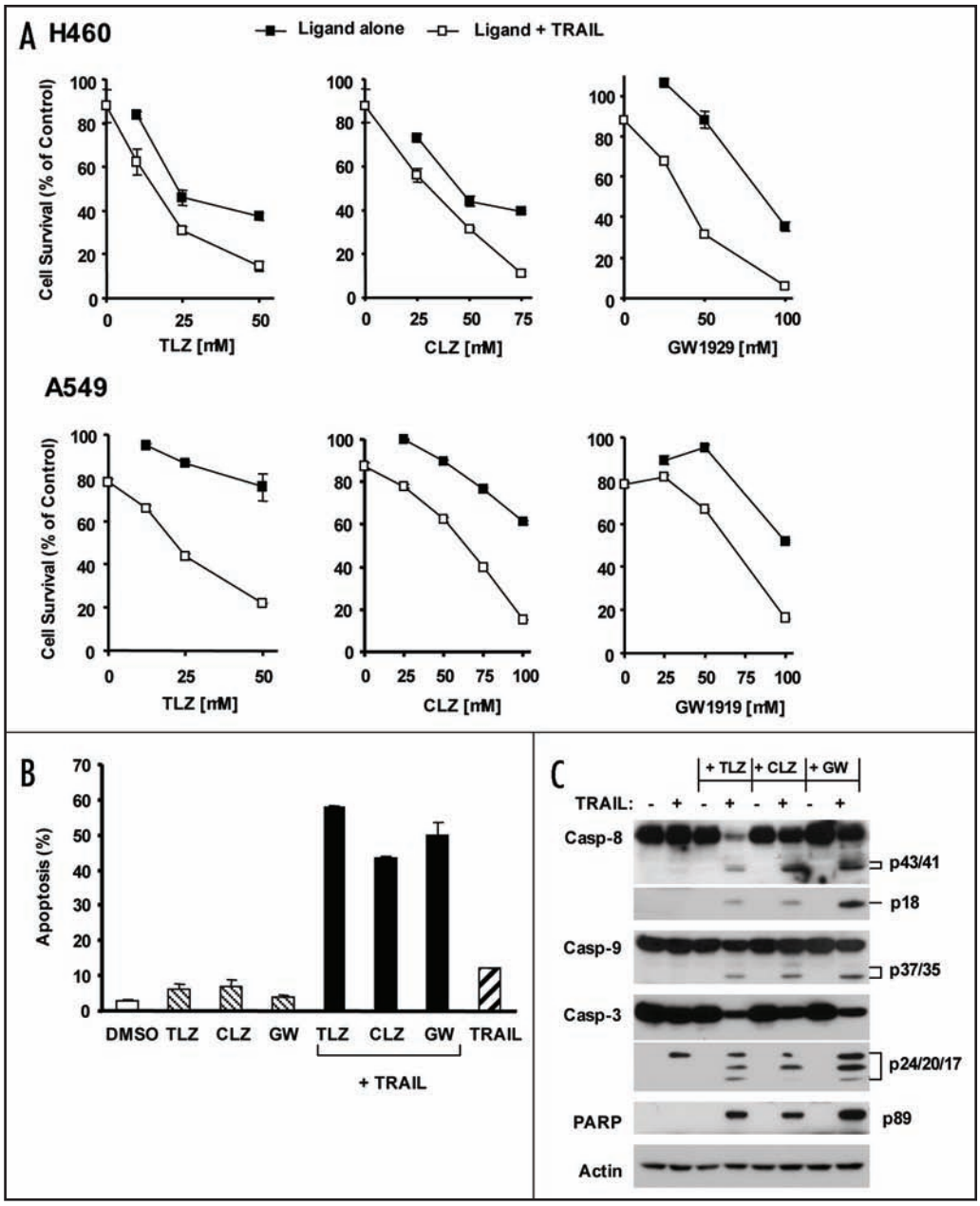

Figure 2. Effects of PPARγ ligands in combination with TRAIL on cell survival (B) and apoptosis (B and C) in human lung cancer cells. (A) H460 and A549 cell lines were seeded in 96-well plates. On the second day, the cells were treated with the indicated concentrations of troglitazone (TLZ), ciglitazone (CLZ), or GW1929 alone, 20 ng/ml TRAIL alone, and the combination of TRAIL with the respective PPARγ ligand. After 24 h, the cells were fixed and subjected to estimation of cell number using the SRB assay. Each data value is a mean ± SD of four replicates. (B and C) A549 cells were treated with 50 μM of the indicated PPARγ ligands alone, 20 ng/ml TRAIL alone and their respective combinations. After 24 h (B) or 12 h (C), the cells were harvested for detection of apoptosis by analyzing sub-G_1 population using flow cytometry (B) or for detection of activation of the indicated caspases using Western blot analysis (C). Each column in (B) is the mean ± SD of duplicate determinations. Casp, caspase.

Small interfering RNA (siRNA)-mediated silencing of DR5 expression confers resistance to induction of apoptosis by the combination of a PPARγ ligand and TRAIL. To determine whether DR5 upregulation contributes to cooperative induction of apoptosis by the combination of a PPARγ ligand and TRAIL, we used DR5 siRNA to silence DR5 expression and then examined its impact on the apoptosis-inducing effect of the combination. The result in Figure 4A demonstrates the successful silencing the expression of DR5. The combination of troglitazone and TRAIL was much more potent than each single agent in decreasing the levels of uncleaved forms of caspase-8 and caspase-3 or increasing the levels of cleaved form of caspase-9 and PARP (Fig. 4B) and in increasing DNA fragment levels (Fig. 4C) in control siRNA-transfected A549 cells. These effects were all diminished in the cells transfected with DR5 siRNA (Fig. 4B and C). Thus, these results demonstrate that DR5 upregulation contributes to enhanced induction of apoptosis by the combination of a PPARγ ligand and TRAIL.

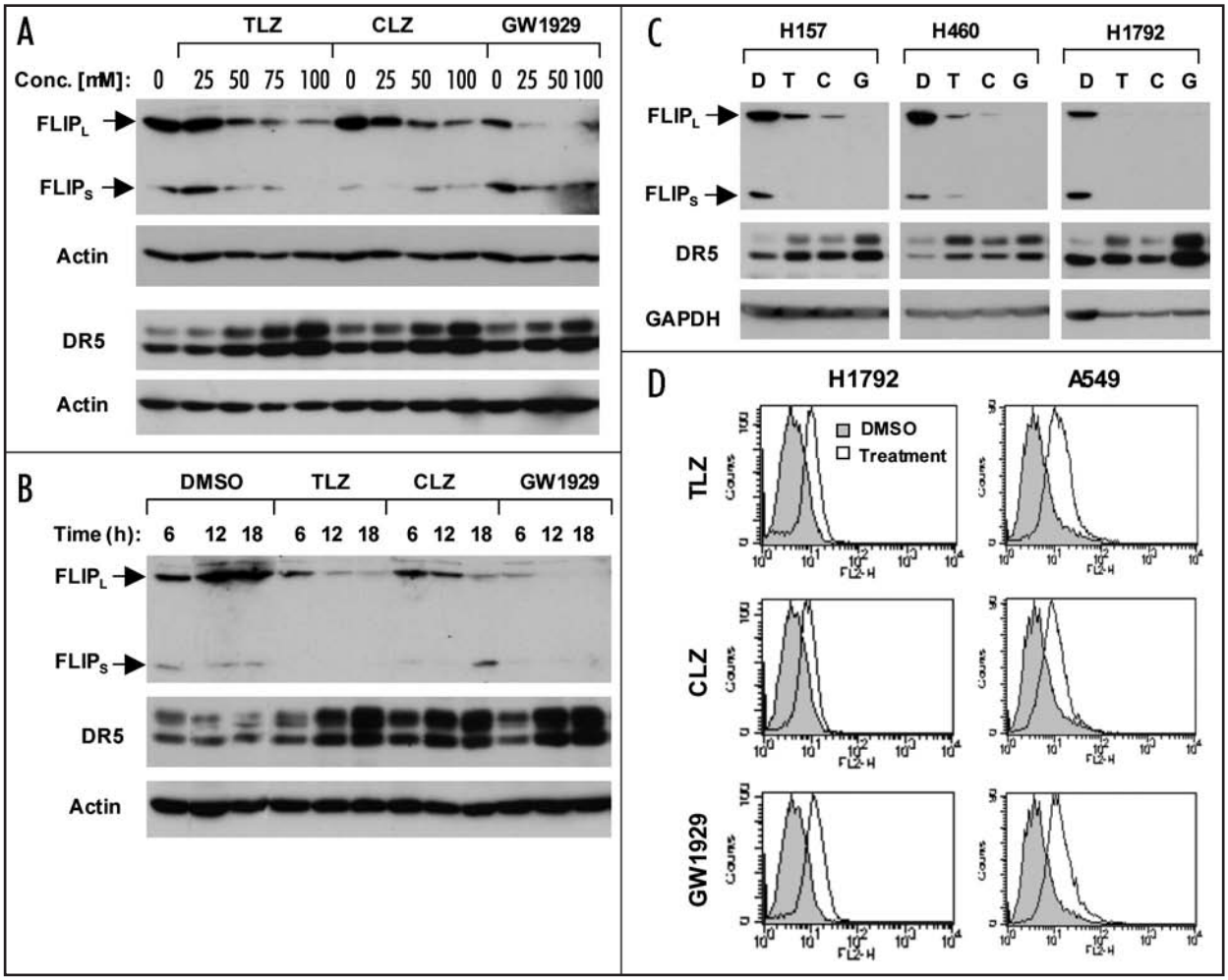

Figure 3. PPARγ ligands increase DR5 expression in addition to downregulation of c-FLIP expression (A–C) and increase cell surface DR5 (D) in human lung cancer cells. (A and B) A549 cells were treated with the indicated concentrations of troglitazone (TLZ), ciglitazone (CLZ) or GW1929 for 12 h (A) or 50 μM of the agents for the indicated times (B). Whole-cell protein lysates were then prepared from aforementioned treatments for detection of DR5, c-FLIP and actin using Western blot analysis. (C) The indicated lung cancer cell lines were treated with DMSO (D), 50 μM of troglitazone (T), ciglitazone (C) or GW1929 (G) for 12 h and then subjected to preparation of whole-cell protein lysates and subsequent Western blot analysis for the indicated proteins. (D) Both H1792 and A549 cell lines were exposed to 50 μM of the indicated PPARγ ligands for 12 h. The cells were then harvested, stained with PE-conjugated DR5 antibody, and analyzed by flow cytometry.

Enforced c-FLIP overexpression protects cells from induction of apoptosis by the combination of a PPARγ ligand and TRAIL. To determine the involvement of c-FLIP downregulation in enhancement of TRAIL-induced apoptosis by PPARγ ligands, we established A549 stable cell lines that overexpress Lac Z (serves as a control), $FLIP_L$ or $FLIP_s$ as presented in Figure 5A. In agreement with aforementioned results, the combination of troglitazone and TRAIL exhibited enhanced induction of apoptosis compared to each single agent in Lac Z-2 and Lac Z-9 cell lines. This effect was inhibited in all cell lines expressing either $FLIP_L$ or $FLIP_S$, particularly in cell lines expressing $FLIP_L$ (Fig. 5A). Consistently, apoptosis induced by TRAIL alone was also inhibited in c-FLIP-overexpressing cell lines (Fig. 5A). Results in (Fig. 5B) shows representative expression levels of $FLIP_L$ (i.e., $FLIP_L$-2) and $FLIP_S$ ($FLIP_S$-8) in the given cell lines. In agreement with induction of apoptosis, the combination of troglitazone and TRAIL strongly induced cleavage of both caspase-8 and PARP in Lac Z-2 cells, but only minimally in $FLIP_S$-8 cells and in $FLIP_L$-2 cells (Fig. 5B). Collectively, these results clearly show that overexpression of c-FLIP protects cells from induction of apoptosis by the combination of TRAIL with a PPARγ ligand. In another words, downregulation of c-FLIP contributes to enhanced induction of apoptosis by the combination of a PPARγ ligand and TRAIL.

PPARγ ligands modulate the expression of DR5 and c-FLIP independently of PPARγ. To determine whether PPARγ plays a role in mediating the modulation of DR5 or c-FLIP expression by PPARγ ligands, we compared the effects of troglitazone on the expression of DR5 and c-FLIP in the absence and presence of the PPARγ antagonist GW9662. As presented in Figure 6A, the presence of GW9662 at 50 μM and the maximal tolerated dose of 75 μM failed to impair the ability of troglitazone to induce DR5 or downregulate c-FLIP expression in both A549 and H1792 cells. Moreover, we silenced the expression of PPARγ and then examined its impact on PPARγ ligand-induced DR5 upregulation and c-FLIP downregulation. As shown in Figure 6B, transfection of PPARγ siRNA into A549 cells substantially decreased the levels of PPARγ. However, both troglitazone and GW1929 induced DR5 expression and decreased c-FLIP levels in both control siRNA- and PPARγ siRNA transfected cells with comparable degrees, indicating that silencing of PPARγ expression does not affect the effects of PPARγ ligands on modulation of DR5 and c-FLIP. Taken together, we conclude that PPARγ

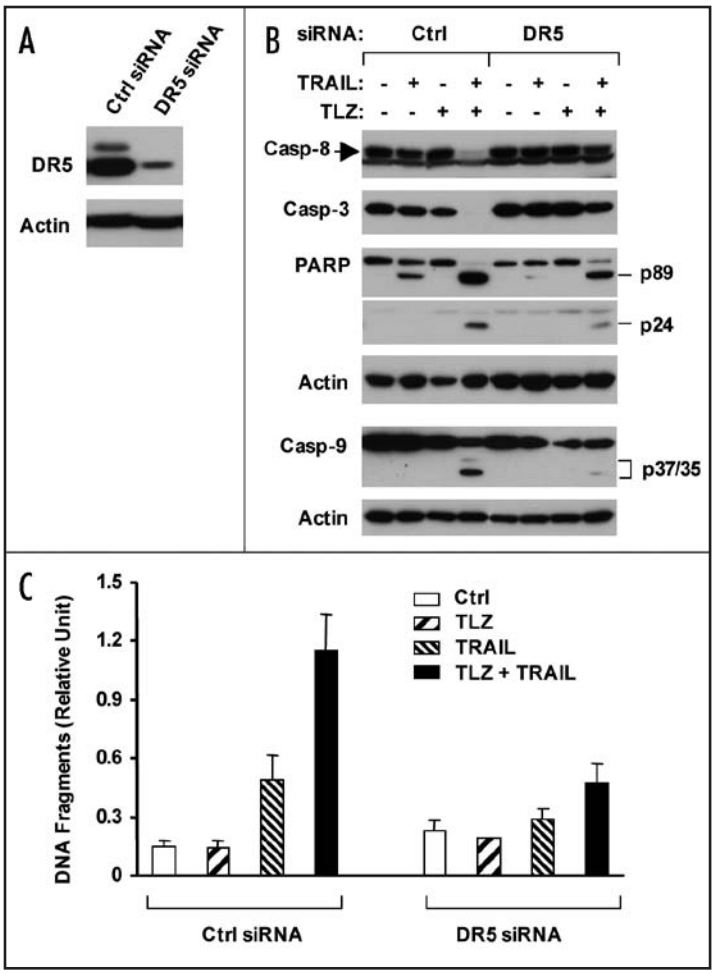

Figure 4. Silencing of DR5 expression by DR5 siRNA (A) attenuates caspase activation (B) and apoptosis (C) induced by the combination of troglitazone (TLZ) and TRAIL. A549 cells were seeded in a 24-well cell culture plate and on the second day transfected with control (Ctrl) or DR5 siRNA. Forty hours later, the cells were treated with 50 μM TLZ, 20 ng/ml TRAIL and their combination. After 12 h (A and B) or 24 h (C), the cells were harvested for preparation of whole-cell protein lysates and subsequent Western blot analysis (A and B) or for detection of DNA fragmentation using an ELISA kit. Each column (C) represents the mean ± SD of triplicate determinations.

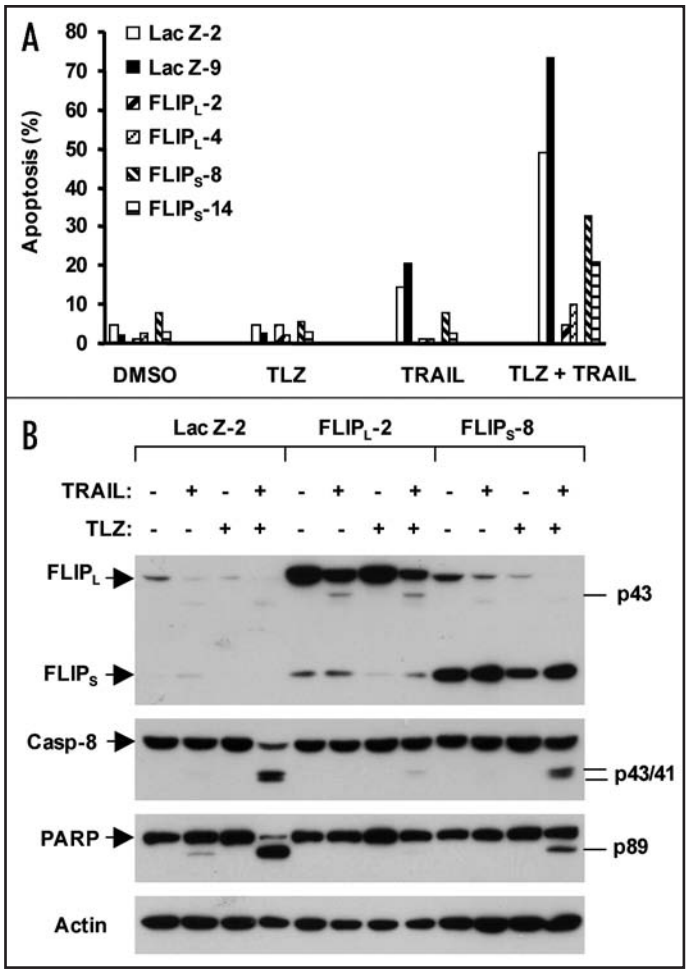

Figure 5. Enforced c-FLIP expression protects cells from induction of apoptosis (A) and caspase activation (B) by the combination of troglitazone (TLZ) and TRAIL. The indicated A549 cell lines expressing lac Z (control), $FLIP_L$ or $FLIP_S$ were treated with DMSO, 50 μM TLZ alone, 10 ng/ml TRAIL alone and the combination of TLZ and TRAIL, respectively. After 24 h (A) or 12 h (B), the cells were harvested and subjected to detection of apoptotic cells by analyzing sub-G_1 population using flow cytometry (A) or detection of caspase activation using Western blot analysis (B).

ligands modulate the expression of DR5 and c-FLIP independently of PPARγ.

DISCUSSION

Enhancement of TRAIL-induced apoptosis by PPARγ ligands has been documented in certain types of cancer cell lines including glioma, neuroblastoma, breast, ovarian, prostate and colon cancer cells in vitro[15,16,23,24] and in breast cancer in vivo.[24] Our current study confirms and extends this finding in human lung cancer cells. PPARγ ligands alone in general have weak apoptosis-inducing activity as demonstrated in our study (Fig. 1). However, the presence of a low dose of TRAIL can result in enhanced or synergistic induction of apoptosis in various types of cancer cells by previous studies[15,16,23,24] and our current finding. Given that some PPARγ ligands are marketed drugs for treatment of type II diabetes, these findings warrant the clinical testing of the combination of a PPARγ ligand with TRAIL as an effective cancer therapeutic regimen.

Downregulation of c-FLIP, survivin and cyclin D3 or induction of $p21^{waf1/cip1}$ has been documented to account for the mechanisms by which PPARγ ligands enhance TRAIL-induced apoptosis.[15,16,23,24] Among these mechanisms, downregulation of c-FLIP by PPARγ ligands and its role in sensitizing cancer cells to TRAIL-induced apoptosis were extensively studied.[15,16] In agreement with these findings, we also found that PPARγ ligands such as troglitazone, cigolitazone and GW1929 decreased the levels of both $FLIP_L$ and $FLIP_S$ in human lung cancer cells (Fig. 3). Moreover, we demonstrate that downregulation of c-FLIP contributes to enhancement of TRAIL-induced apoptosis by PPARγ ligands because enforced expression of exogenous c-FLIP (either $FLIP_L$ or $FLIP_S$) inhibited induction of apoptosis by the combination of TRAIL with troglitazone (Fig. 5). Taken together, it appears that c-FLIP downregulation is an important mechanism accounting for PPARγ ligand-mediated enhancement of TRAIL-induced apoptosis in human cancer cells.

By far, the few reports on the modulation of DR5 expression by PPARγ ligands have conflicting results.[15-17] Moreover, the involvement of DR5 modulation in PPARγ ligand-mediated enhancement of TRAIL-induced apoptosis in cancer cells has not been addressed. In this study, we clearly show that several PPARγ ligands including troglitazone, cigolitazone and GW1929 induced DR5 expression

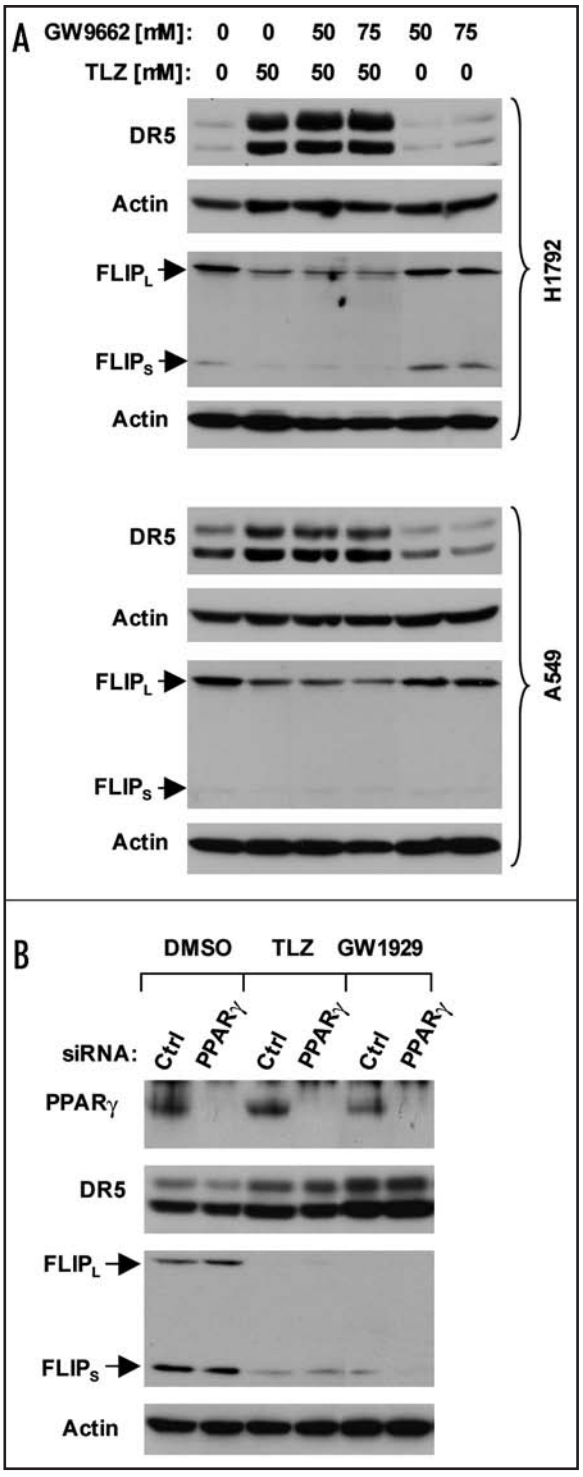

Figure 6. Effects of the PPARγ antagonist GW9662 (A) and the silencing of PPARγ expression (B) on PPARγ ligand-induced modulation of DR5 and c-FLIP expression. A, The indicated cell lines were pretreated with the given doses of GW9662 and then cotreated with 50 μM troglitazone (TLZ). After 12 h, the cells were subjected to preparation of whole-cell protein lysates and subsequent Western blot analysis. B, A549 cells were transfected with control (Ctrl) or PPARγ siRNA. After 48 h, the cells were treated with DMSO control, 50 μM TLZ or GW1929. Twelve hours later, the cells were harvested for preparation of whole-cell protein lysates and subsequent Western blot analysis.

while downregulating c-FLIP levels in multiple human lung cancer cell lines (Fig. 3), indicating that both DR5 upregulation and c-FLIP reduction are concurrent events in cells exposed to PPARγ ligands. By siRNA-mediated silencing of DR5 expression, we found that the enhanced induction of apoptosis including caspase activation and DNA fragmentation by the combination of troglitazone and TRAIL was substantially attenuated. Thus, we conclude that DR5 upregulation also contributes to cooperative induction of apoptosis by the combination of a PPARγ ligand and TRAIL. This should be the first demonstration for the involvement of DR5 upregulation in sensitization of cancer cells to TRAIL-induced apoptosis by PPARγ ligands.

The downregulation of c-FLIP by PPARγ ligands was documented to be independent of PPARγ,[15] as was the induction of DR5 by 15d-PGJ$_2$.[17] In our study, the presence of a PPARγ antagonist or siRNA-mediated silencing of PPARγ expression failed to inhibit the modulation of either DR5 or c-FLIP expression by PPARγ ligands (Fig. 6). Thus, we conclude that PPARγ ligands induce DR5 and downregulate c-FLIP expression independently of PPARγ in human lung cancer cells.

In summary, we demonstrate that PPARγ ligands enhance TRAIL-induced apoptosis in human lung cancer cells. In addition to downregulation of c-FLIP, PPARγ ligands also upregulate DR5 expression, both of which contribute to PPARγ ligand-mediated enhancement of TRAIL-induced apoptosis. Thus, our findings extend our understanding on the mechanisms by which PPARγ ligands sensitize cancer cells to TRAIL-induced apoptosis.

References

1. Almasan A, Ashkenazi A. Apo2L/TRAIL: Apoptosis signaling, biology, and potential for cancer therapy. Cytokine Growth Factor Rev 2003; 14:337-48.
2. Kelley SK, Ashkenazi A. Targeting death receptors in cancer with Apo2L/TRAIL. Curr Opin Pharmacol 2004; 4:333-9.
3. Ashkenazi A, Dixit VM. Death receptors: Signaling and modulation. Science 1998; 281:1305-8.
4. Wajant H, Gerspach J, Pfizenmaier K. Tumor therapeutics by design: Targeting and activation of death receptors. Cytokine Growth Factor Rev 2005; 16:55-76.
5. Wajant H. Targeting the FLICE Inhibitory Protein (FLIP) in cancer therapy. Mol Interv 2003; 3:124-7.
6. Kataoka T. The caspase-8 modulator c-FLIP. Crit Rev Immunol 2005; 25:31-58.
7. Irmler M, Thome M, Hahne M, Schneider P, Hofmann K, Steiner V, Bodmer JL, Schroter M, Burns K, Mattmann C, Rimoldi D, French LE, Tschopp J. Inhibition of death receptor signals by cellular FLIP. Nature 1997; 388:190-5.
8. Sun SY. Chemopreventive agent-induced modulation of death receptors. Apoptosis 2005; 10:1203-10.
9. Sporn MB, Suh N, Mangelsdorf DJ. Prospects for prevention and treatment of cancer with selective PPARgamma modulators (SPARMs). Trends Mol Med 2001; 7:395-400.
10. Rumi MA, Ishihara S, Kazumori H, Kadowaki Y, Kinoshita Y. Can PPAR gamma ligands be used in cancer therapy? Curr Med Chem Anticancer Agents 2004; 4:465-77.
11. Koeffler HP. Peroxisome proliferator-activated receptor gamma and cancers. Clin Cancer Res 2003; 9:1-9.
12. Li MY, Lee TW, Yim AP, Chen GG. Function of PPARgamma and its ligands in lung cancer. Crit Rev Clin Lab Sci 2006; 43:183-202.
13. Chang TH, Szabo E. Enhanced growth inhibition by combination differentiation therapy with ligands of peroxisome proliferator-activated receptor-gamma and inhibitors of histone deacetylase in adenocarcinoma of the lung. Clin Cancer Res 2002; 8:1206-12.
14. Avis I, Martinez A, Tauler J, Zudaire E, Mayburd A, Abu-Ghazaleh R, Ondrey F, Mulshine JL. Inhibitors of the arachidonic acid pathway and peroxisome proliferator-activated receptor ligands have superadditive effects on lung cancer growth inhibition. Cancer Res 2005; 65:4181-90.
15. Kim Y, Suh N, Sporn M, Reed JC. An inducible pathway for degradation of FLIP protein sensitizes tumor cells to TRAIL-induced apoptosis. J Biol Chem 2002; 277:22320-9.
16. Schultze K, Bock B, Eckert A, Oevermann L, Ramacher D, Wiestler O, Roth W. Troglitazone sensitizes tumor cells to TRAIL-induced apoptosis via down-regulation of FLIP and Survivin. Apoptosis 2006.
17. Nakata S, Yoshida T, Shiraishi T, Horinaka M, Kouhara J, Wakada M, Sakai T. 15-Deoxy-Delta12,14-prostaglandin J(2) induces death receptor 5 expression through mRNA stabilization independently of PPARgamma and potentiates TRAIL-induced apoptosis. Mol Cancer Ther 2006; 5:1827-35.

18. Sun SY, Yue P, Dawson MI, Shroot B, Michel S, Lamph WW, Heyman RA, Teng M, Chandraratna RA, Shudo K, Hong WK, Lotan R. Differential effects of synthetic nuclear retinoid receptor-selective retinoids on the growth of human nonsmall cell lung carcinoma cells. Cancer Res 1997; 57:4931-9.
19. Sun SY, Yue P, Wu GS, El-Deiry WS, Shroot B, Hong WK, Lotan R. Mechanisms of apoptosis induced by the synthetic retinoid CD437 in human nonsmall cell lung carcinoma cells. Oncogene 1999; 18:2357-65.
20. Liu X, Yue P, Zhou Z, Khuri FR, Sun SY. Death receptor regulation and celecoxib-induced apoptosis in human lung cancer cells. J Natl Cancer Inst 2004; 96:1769-80.
21. Sun SY, Yue P, Hong WK, Lotan R. Induction of Fas expression and augmentation of Fas/Fas ligand-mediated apoptosis by the synthetic retinoid CD437 in human lung cancer cells. Cancer Res 2000; 60:6537-43.
22. Sun SY, Yue P, Shroot B, Hong WK, Lotan R. Induction of apoptosis in human nonsmall cell lung carcinoma cells by the novel synthetic retinoid CD437. J Cell Physiol 1997; 173:279-84.
23. Goke R, Goke A, Goke B, El-Deiry WS, Chen Y. Pioglitazone inhibits growth of carcinoid cells and promotes TRAIL-induced apoptosis by induction of p21waf1/cip1. Digestion 2001; 64:75-80.
24. Lu M, Kwan T, Yu C, Chen F, Freedman B, Schafer JM, Lee EJ, Jameson JL, Jordan VC, Cryns VL. Peroxisome proliferator-activated receptor gamma agonists promote TRAIL-induced apoptosis by reducing survivin levels via cyclin D3 repression and cell cycle arrest. J Biol Chem 2005; 280:6742-51.

Print this Page

AACR 101st ANNUAL MEETING 2010
April 17-21, 2010 • Walter E. Washington Convention Center • Washington, DC

Presentation Abstract

Abstract Number:	787
Presentation Title:	Differences in protein expression patterns in lung adenocarcinomas arising in never versus ever smokers
Presentation Time:	Sunday, Apr 18, 2010, 2:00 PM - 5:00 PM
Location:	Exhibit Hall A-C, Poster Section 30
Poster Section:	30
Poster Board Number:	6
Author Block:	Carmen Behrens[1], Heather Lin[1], Maria Nunez[1], Ping Yuan[1], Luisa Solis[1], Maria G. Raso[1], Ludmila Prudkin[1], Menghong Sun[1], Xiaoling Li[1], Ximing Tang[1], Jack A. Roth[1], John D. Minna[2], David J. Stewart[1], Waun K. Hong[1], J. Jack Lee[1], Ignacio I. Wistuba[1]. [1]UT M.D. Anderson Cancer Ctr., Houston, TX; [2]UT Southwestern Medical Center, Dallas, TX

Abstract Body:

Background**.** Approximately 25% of lung cancer cases worldwide, mostly adenocarcinomas, are not attributable to tobacco use. Despite that some striking differences have been identified in the epidemiological, clinical and molecular characteristics of lung cancer arising in never smokers versus smokers, our current knowledge of lung adenocarcinoma in never smokers is still limited.

Methods**.** We examined the immunohistohemical (IHC) expression of 101 proteins in surgically resected lung adenocarcinoma tissue microarray specimens obtained from 52 never smokers and compared the findings with 152 tumors obtained from ever smokers. The markers examined included a wide variety of tumor-related proteins, representing all hallmarks of cancer (Hanahan and Weinberg, Cell 2000). The IHC expression was assessed at cytoplasm [c], membrane [m], and nucleus [n] of malignant cells, and in stromal cells. Univariate and multivariate (adjusting by patients' sex, and tumor stage and EGFR mutation status) statistical analyses were performed to assess the statistical differences in the expression of markers according to smoking status. The expression of the markers was correlated with patients' clinical characteristics and tumors' pathological features and *EGFR* mutational status.

Results**.** In the multivariate analysis, tumors from smokers showed a relatively high number of markers (n=32) with significant higher expression compared with tumors from never smokers. Interestingly, in the univariate analysis, nine markers showed significantly higher expression in tumors from never smokers compared with ever smokers, including FGFR-1 [n], FGFR-2 [n], ER-alpha [n], CD44 [c], FOLR1 [m], IGFBP3 [n], IL-1alpha [c], NF-kB [n], survivin [n] and RGS17 [n]. In the multivariate analysis, six markers showed significantly higher expression in tumors from never smokers, including FGFR-2 [n] *(P*=0.018), CD44 [c] *(P*=0.001), c-Met [c] (*P*=0.045) and [m] (*P*=0.017), E-Cadherin [m] (*P*=0.003), IGFBP3 [n] (*P*=0.0009) and p-HER3 [m] (*P*=0.035). Twenty-nine markers showed significant association with *EGFR* mutations in tumors in the multivariate analysis adjusting by patients' sex and smoking status, and tumor stage. Additionally, 47 markers showed significant differences in the level of expression comparing patients' smoking status, including current, former and never smokers.

Conclusion**.** Our findings indicate that there are multiple molecular differences between lung adenocarcinomas arising in never and ever smokers, suggesting that they are different entities. These findings have implications for the selection of molecular targets for developing novel therapy in patients with lung adenocarcinoma based on their smoking history (Supported by grant VITAL W81XWH-04-1-0142 and UT-Lung SPORE P50CA070907).

[Proc Amer Assoc Cancer Res, Volume 46, 2005]

Prevention Research 2: Molecular Markers in Prevention Research
Abstract #765

Immunohistochemical validation of differentially expressed protein markers in the sequential pathogenesis of non-small cell lung cancer using premalignant and malignant lung tissue microarrays

Carmen Behrens, Ignacio I. Wistuba, Lei Feng, J. Jack Lee, Waun Ki Hong and Reuben Lotan

UT M.D. Anderson Cancer Ctr., Houston, TX

Lung cancer is the leading cause of cancer mortality at least in part due to its diagnosis at advanced stages. Therefore, the identification of novel molecular markers for risk assessment and early detection is of paramount importance. Recently, we used a high throughput western immunoblotting technique and an in vitro lung carcinogenesis cell system to identify proteins that are expressed differentially in normal, immortalized, transformed, and tumorigenic human bronchial epithelial cells. In the present study, we selected four of these proteins for validation as potential important molecules in the sequential pathogenesis of non-small cell lung carcinomas in vivo. We performed an immunohistochemical analysis of E-cadherin (membranous), Caspase-8 (cytoplasmic), Stat-5 (cytoplasmic), and p70s6k (nuclear) in paraffin-embedded tissue samples from lung cancers (n=60) and adjacent normal and preneoplastic epithelial tissues (n=223) placed in tissue microarray (TMA). The lung samples examined included: 30 adenocarcinomas (ADCAs), 30 squamous cell carcinomas (SCCs), 30 normal bronchial epithelia, 72 bronchial hyperplasias, 29 squamous metaplasia, 28 squamous dysplasias, and 64 alveolar adenomatous hyperplasias (AAHs). The main findings were as follows: a) E-cadherin expression was reduced ($p<0.001$), and Caspase-8, Stat-5, and p70s6k were increased ($p<0.001$-0.008) in tumors compared to normal epithelium specimens. b) In SCCs, an increasing level of abnormal expression was detected for all four markers with increasing severity of histology, and significant differences ($p<0.001$) between normal

epithelium and high-grade dysplasia were detected for E-cadherin, Stat-5, and p70s6k. c) In ADCAs, an abnormal expression trend was detected between normal bronchial epithelium, AAH and tumors for all markers except for p70s6k, with significant differences ($p<0.001$-0.017) between AAHs and ADCAs in E-cadherin, Caspase-8 and Stat-5. Our studies demonstrate that protein immunohistochemical expression analysis using TMAs of lung tumor and preneoplastic specimens are suitable methodology for the validation of proteomic data and the study of new markers in the pathogenesis of lung cancer. Our findings that E-cadherin, Caspase-8, Stat-5, and p70s6k are expressed differentially in the sequential pathogenesis of SCC and ADCA suggest that they play an important role in NSCLC tumorigenesis. Supported by Early Detection Research Network grant U01 CA86390 from the NCI and by the Department of the Army grant W81XWH-04-1-0142.

Print this Page

Presentation Abstract

Abstract Number:	3196
Presentation Title:	EZH2 expression is an early event in the pathogenesis of non-small cell lung cancer (NSCLC) and correlates with tumor progression
Presentation Time:	Tuesday, Apr 05, 2011, 8:00 AM -12:00 PM
Location:	Exhibit Hall A4-C, Poster Section 14
Poster Section:	14
Poster Board Number:	3
Author Block:	Carmen Behrens[1], Ping Yuan[2], Luisa Solis[1], Pierre Saintigny[1], Humam Kadara[1], Junya Fujimoto[1], Cesar Moran[1], Stephen G. Swisher[1], John V. Heymach[1], Ignacio I. Wistuba[1]. [1]UT M.D. Anderson Cancer Ctr., Houston, TX; [2]Md Anderson, Houston, TX

Abstract Body:

Background. The molecular events associated with NSCLC pathogenesis and tumor progression need to be better elucidated. The enhancer of zeste homolog 2 (EZH2) is a DNA methyl transferase involved in malignant transformation and tumor progression of several human carcinomas, including lung. We investigated EZH2 expression by immunohistochemistry (IHC) in the early pathogenesis of NSCLC and progression in a large series of clinically well-annotated tissue specimens.

Methods. We examined by IHC nuclear EZH2 expression using formalin-fixed and paraffin-embedded tissue specimens obtained from surgically resected tumors in tissue microarrays (TMAs) including: a) stage I-III NSCLC tumors (SCCs, n=272; adenocarcinomas, n=456); b) paired primary tumors and brain metastases (n=70); and, c) bronchial preneoplastic squamous lesions (n=51) and mildly abnormal/normal bronchial epithelia (n=203). In stage I-III tumors, we correlated EZH2 expression with clinico-pathological features, including patients' recurrence-free survival (RFS), and overall survival (OS), in a subset of these tumors, with IHC expression of 80 proteins and *EGFR* and *KRAS* mutation status.

Results. EZH2 expression was significantly (P<0.0001) higher in SCC (mean score=128.6) compared to adenocarcinoma (mean score=56.8). In adenocarcinoma, higher EZH2 expression significantly correlated with ever-smoking status (P<0.0001) and less differentiated histology features (solid histology pattern; P<0.0001). In multivariate analysis, for adenocarcinoma patients, higher EZH2 expression, as a continuous variable, associated with significantly worse RFS (HR 1.006 95%CI 1.0-1.011; P=0.03) and OS (HR 1.004 95%CI 1.0-1.009; P=0.03). In publicly available array datasets of lung adenocarcinoma patients, high *EZH2* mRNA correlated with worse RFS and OS. NSCLC brain metastases showed significantly (P=0.0004) higher EZH2 expression than corresponding primary tumors. In bronchial epithelia, normal and hyperplastic cells demonstrated low levels of EZH2 expression; significantly higher expression was associated with increasing severity of squamous dysplastic changes (P<0.0001). In NSCLC tumors, EZH2 expression positively correlated (P<0.0001) with IHC expression of Ki67, FEN1, and UBE2C. In lung adenocarcinomas, *EGFR*-mutant tumors showed significantly lower EZH2 expression than wild-type tumors.

Conclusions. Our findings indicate that EZH2 is frequently expressed in NSCLC, particularly in poorly differentiated adenocarcinomas. In adenocarcinomas, EZH2 associates with worse patient outcomes. These data suggest that EZH2 expression represents an early event in NSCLC pathogenesis and associates with tumor progression and metastasis, representing a novel target for chemoprevention and therapeutic strategies. Supported by DoD grants W81XWH-04-1-0142 and DoD W81XWH-07-1-0306.

American Association for Cancer Research
615 Chestnut St. 17th Floor
Philadelphia, PA 19106

100th AACR Annual Meeting-- Apr 18-22, 2009; Denver, CO

Death Receptors and IAPs in Apoptosis Regulation -- Oral Presentations - Proffered Abstracts

Abstract #2041: Differential roles of DR4, DR5 and c-FLIP in regulation of geranylgeranyltransferase I inhibitor-induced augmentation of tumor necrosis factor-related apoptosis-inducing ligand-induced apoptosis

Shuzhen Chen, Lei Fu, Shruti M Raja, Ping Yue, Yuri K Peterson, Fadlo R Khuri and Shi-Yong Sun

Winship Cancer Institute, Atlanta, GA; Department of Pharmacology and Cancer Biology,Duke University, Durham, NC

Abstract

Geranylgeranyltransferase I (GGTase I) has emerged as a cancer therapeutic target. Accordingly, small molecules that inhibit GGTase I have been developed and exhibit encouraging anticancer activity both *in vitro* and *in vivo* in preclinical studies. However, the underlying anticancer mechanisms of GGTase I inhibitors remain unclear. Here we have demonstrated a novel mechanism by which GGTase I inhibition modulates apoptosis. Inhibition of GGTase I by GGTI-298 induced apoptosis and augmented tumor necrosis factor-related apoptosis-inducing ligand (TRAIL)-induced apoptosis in human lung cancer cells. GGTI-298 induced the expression of both DR4 and DR5, two cell surface death receptors for TRAIL, and downregulated the expression of c-FLIP, a key inhibitor of death receptor-induced apoptosis. Consistently, another highly selective GGTase I inhibitor, GGTI-DU40, but not its inactive analog SN-DU40, exerted similar effects. Enforced expression of c-FLIP or knockdown of DR5 expression protected cells from induction of apoptosis by the combination of GGTI-298 and TRAIL, indicating that induction of DR5 and downregulation of c-FLIP mediate augmentation of TRAIL-induced apoptosis by GGTase I inhibition. Surprisingly, blockade of DR4 induction by knocking down DR4 expression sensitized cancer cells to GGTI298/TRAIL-induced apoptosis, suggesting that DR4 induction may play an opposite role to DR5 induction in regulating GGTI298/TRAIL-induced apoptosis. The combination of GGTI-298 and

TRAIL was more effective than each single agent in decreasing the levels of IκBα and p-Akt, implying that GGTI298/TRAIL activates NF-κB and inhibits Akt. Interestingly, knockdown of DR5, but not DR4, prevented GGTI298/TRAIL-induced IκBα and p-Akt reduction, suggesting that DR5 mediates reduction of IκBα and p-Akt induced by GGTI298/TRAIL. In contrast, DR4 knockdown further facilitated IκBα and p-Akt reduction by GGTI298/TRAIL, suggesting that DR4 also plays an opposite role to DR5 in regulation of GGTI/TRAIL-induced apoptotic signaling. To our knowledge, this is the first demonstration that DR4 and DR5 may play differential roles in regulation of death receptor-mediated apoptosis. Collectively, we conclude that inhibition of GGTase I with GGTI inhibitors induces DR5 and downregulates c-FLIP, leading to augmentation of TRAIL-induced apoptosis. Thus, inhibition of GGTase I can be a novel strategy for enhancing TRAIL-based cancer therapy. (Supported by the Georgia Cancer Coalition Distinguished Cancer Scholar award, Department of Defense grant W81XWH-04-1-0142-VITAL, and NIH/NCI SPORE P50 grant CA128613-01; SY Sun, and FR Khuri are Georgia Cancer Coalition Distinguished Cancer Scholars)

Citation Information: In: Proc Am Assoc Cancer Res; 2009 Apr 18-22; Denver, CO. Philadelphia (PA): AACR; 2009. Abstract nr 2041.

98th AACR Annual Meeting-- Apr 14-18, 2007; Los Angeles, CA

Apoptosis 1: Poster Presentations
Abstract #3598

Dimethyl-celecoxib, a derivative of the COX-2 inhibitor celecoxib that lacks COX-2 inhibitory activity, sensitizes human lung cancer cells to tumor necrosis factor-related apoptosis-inducing ligand (TRAIL) through induction of DR5 and downregulation of c-FLIP

Shuzhen Chen, Xiangguo Liu, Ping Yue, Axel H. Schonthal, Fadlo R. Khuri and Shi-Yong Sun

Winship Cancer Institute, Emory University, Atlanta, GA, University of Southern California, Los Angeles, CA

The cyclooxygenase-2 (COX-2) inhibitor, celecoxib, exhibits anticancer activity in both preclinical studies and clinical practice. However, celecoxib has relatively weak apoptosis-inducing activity and modest cancer therapeutic efficacy. Therefore, efforts have been made to develop derivatives of celecoxib with superior anticancer activity. Dimethyl-celecoxib (DMC) is just such a derivative which lacks COX-2-inhibitory activity. Several preclinical studies have demonstrated that DMC has better apoptosis-inducing activity than celecoxib albeit with undefined mechanisms and exhibits anticancer activity in animal models. In this study, we examined the effects of DMC on the growth of human lung cancer cells as well as its cooperative effect with tumor necrosis factor-related apoptosis-inducing ligand (TRAIL) on induction of apoptosis and the underlying mechanisms. By comparing the effects of DMC and celecoxib on the growth of a group of human lung cancer cell lines, we found that DMC decreased cell survival with IC_{50}s ranging from 10 μM to 20 μM, whereas celecoxib did so with IC_{50}s ranging between 20 and 30 μM, indicating that DMC is more effective than celecoxib in decreasing the survival of lung cancer cells. When cells were treated with the combination of DMC and TRAIL, enhanced or synergistic effects in reduction of cell survival and induction of apoptosis including activation of caspases were observed in comparison with the effects in cells exposed to each agent alone. To understand the mechanisms underlying this synergy, we also analyzed the effects of DMC on modulation of several apoptosis-related

genes. We found that DMC rapidly increased DR5 levels and reduced c-FLIP (both $FLIP_L$ and $FLIP_S$) levels starting from 2 h post treatment while having limited effects on modulating the levels of other proteins including DR4, Bcl2, Bcl-X_L and Bax. Importantly, enforced expression of $FLIP_L$ or silencing of DR5 expression using DR5 small interfering RNA (siRNA) abrogated the enhanced effects on induction of apoptosis by the combination of DMC and TRAIL, indicating that both DR5 upregulation and c-FLIP reduction contribute to cooperative induction of apoptosis by the combination of DMC and TRAIL. Collectively, we conclude that DMC sensitizes TRAIL-induced apoptosis in human lung cancer cells via induction of DR5 and downregulation of c-FLIP. (Supported by GCC Distinguished Cancer Scholar award and DOD grant W81XWH-04-1-0142-VITAL)

100th AACR Annual Meeting-- Apr 18-22, 2009; Denver, CO

Death Receptors -- Poster Presentations - Proffered Abstracts

Abstract #5132: The eIF4E/eIF4G interaction inhibitor 4EGI-1 augments TRAIL-induced apoptosis through DR5 induction and c-FLIP downregulation independent of inhibition of cap-dependent protein translation

Songqing Fan, Yikun Li, Ping Yue, Fadlo Khuri and Shi-Yong Sun

Winship Cancer Institute, Emory University School of Medicine, Atlanta, GA

Abstract

Cap-dependent protein translation plays an important role in regulation of oncogenesis primarily through regulation of the expression of certain oncogenic proteins (e.g., cyclin D1 and HIF1α,). Thus inhibition of cap-dependent protein translation has emerged as an attractive therapeutic strategy. The small molecule 4EGI-1 was identified as an inhibitor of cap-dependent translation initiation by disrupting eIF4E/eIF4G association through binding to eIF4E and exhibits growth-inhibitory and apoptosis-inducing activity in cancer cells. We were interested in its therapeutic effects in human lung cancer cells. 4EGI-1 as a single agent inhibited the growth and induced apoptosis of human lung cancer cells. When combined with the death ligand tumor necrosis factor-related apoptosis-inducing ligand (TRAIL), enhanced apoptosis-induced activity was observed. In lung cancer cells, 4EGI-1 inhibited eIF4E/eIF4G interaction, reduced the levels of cyclin D1 and HIF1α, both of which are regulated by a cap-dependent translation mechanism. Moreover, 4EGI-1 upregulated DR5 expression and downregulated c-FLIP levels. Small interfering RNA (siRNA)-mediated blockade of DR5 induction or enforced expression of c-FLIP abrogated 4EGI-1's ability to enhance TRAIL-induced apoptosis, indicating that both DR5 induction and c-FLIP downregulation contribute to enhancement of TRAIL-induced apoptosis by 4EGI-1. However, inhibition of eIF4E/eIF4G interaction by eIF4E siRNA-mediated knockdown of eIF4E effectively reduced the levels

of cyclin D1 and HIF1α, but failed to induce DR5 expression, downregulate c-FLIP levels, and augment TRAIL-induced apoptosis. As well, the mTOR inhibitor rapamycin, which inhibits cap-dependent translation initiation, did not enhance TRAIL-induced apoptosis. Collectively, we conclude that 4EGI-1 augments TRAIL-induced apoptosis through induction of DR5 and downregulation of c-FLIP independent of inhibition of cap-dependent protein translation. (S. Fan. and Y. Li share first authorship; this work was supported by the Georgia Cancer Coalition Distinguished Cancer Scholar award, DOD grant W81XWH-04-1-0142-VITAL, NIH RO1 CA118450-01 and NIH SPORE P50 grant CA128613-01; SY Sun, and FR Khuri are Georgia Cancer Coalition Distinguished Cancer Scholars)

Citation Information: In: Proc Am Assoc Cancer Res; 2009 Apr 18-22; Denver, CO. Philadelphia (PA): AACR; 2009. Abstract nr 5132.

Print this Page

Presentation Abstract

Abstract Number:	2203
Presentation Title:	Implication of GPRC5A loss in lung carcinogenesis in patients with and without chronic obstructive pulmonary disease
Presentation Time:	Monday, Apr 04, 2011, 1:00 PM - 5:00 PM
Location:	Exhibit Hall A4-C, Poster Section 10
Poster Section:	10
Poster Board Number:	24
Author Block:	Junya Fujimoto[1], Humam Kadara[1], Carmen Behrens[1], Diane Liu[1], J. Jack Lee[1], Luisa M. Solis[1], Edward Kim[1], Amir Sharafkhaneh[2], Ignacio I. Wistuba[1], Lotan Reuben[1]. [1]UT M.D. Anderson Cancer Ctr., Houston, TX; [2]Baylor College of Medicine, Houston, TX
Abstract Body:	Lung cancer is often associated with inflammation induced by cigarette smoke. In addition, chronic obstructive pulmonary disease (COPD), typically associated with inflammation, is a leading cause of morbidity and mortality in the United States and presents an increased risk of lung cancer development compared to patients without COPD. Mice with knockout of both alleles of the G-protein coupled receptor, family C, group 5, member A (Gprc5a) gene develop spontaneous lung adenomas and adenocarcinomas at a much higher incidence than their wild-type littermates, indicating that this gene is a novel lung-specific tumor suppressor gene. Interestingly, the majority of tumors in the Gprc5a knockout mice are associated with inflammatory cell infiltration, possibly due to increased NF-κB activation in mouse lung epithelial cells and tissues. Furthermore, the human GPRC5A can suppress NF-κB activation in human lung adenocarcinoma cells. Therefore, in the present study we investigated the expression patterns of GPRC5A in clinical specimens, including normal bronchial epithelia (NBE) of COPD patients with and without overt lung cancer as well as in non-small cell lung cancer (NSCLC) tumors by immunohistochemical (IHC) analysis. We performed IHC analysis of a tissue microarray (TMA) comprised of 311 lung adenocarcinomas and 166 squamous cell carcinomas (SCCs), as well as of normal bronchial epithelial specimens from 50 patients with COPD, which included 24 cancer-free cases and 26 cases with NSCLC (12, adenocarcinoma; 12, SCC; 2, bronchioalveolar carcinoma). Kruskal-Wallis test was used to compare GPRC5A levels among histology levels. All statistical tests were two-sided, and p values of 0.05 or less were considered to be statistically significant. Cytoplasmic GPRC5A expression was significantly higher in lung adenocarcinomas compared to SCCs ($p<0.001$). Moreover, GPRC5A expression exhibited a positive correlation with never-smoking status ($p=0.005$). Interestingly, we noted a statistically significant inverse correlation between the expression of GPRC5A and that of NF-κB ($p<0.001$), which we had previously found to be activated and elevated following loss of the GPRC5A tumor suppressor. Furthermore, analysis of two NBE obtained from each of 50 COPD patients demonstrated statistically significant decreased expression of GPRC5A in NBE of COPD patients with NSCLC compared to NBE from NSCLC-free COPD patients ($p<0.001$). Our findings demonstrate that decreased GPRC5A expression may be associated with development of lung malignancies, especially in individuals with chronic lung inflammation, and pinpoints GPRC5A's potential suppressive effects on a lung tumor-promoting microenvironment. Assessment of GPRC5A's potential use as a risk factor for NSCLC development in COPD patients is warranted. Supported by the Samuel Waxman Cancer Research Foundation and by W81XWH-04-1-0142.

Print this Page

American Association for Cancer Research 102nd ANNUAL MEETING
April 2-6, 2011 • Orange County Convention Center, Orlando, Florida

Presentation Abstract

Presentation Number:	PL01-03
Presentation Title:	The landscape of cancer prevention: Personalized approach in lung cancer
Presentation Time:	Sunday, Apr 03, 2011, 10:00 AM -10:30 AM
Location:	West Hall D, Orange County Convention Center
Author Block:	*Waun Ki Hong, Edward S. Kim, J. Jack Lee, Ignacio Wistuba, Scott Lippman.* UT MD Anderson Cancer Ctr., Houston, TX
Webcast:	http://webcast.aacr.org/portal/p/2011annual/518

Abstract Body:

Recent data indicate that lung cancer causes over 1.3 million deaths worldwide each year, over 157,000 deaths in the U.S. alone. Although the overall incidence of cancer in the U.S. has decreased (1.3 % for men; 0.5% for women) largely because of declines in breast, prostate, lung, and colon cancer, lung cancer in women is increasing.

Tobacco causes more than 30% of cancer, not just of the lung but in at least 12 other cancers, including the head and neck, esophagus, pancreas, stomach, and bladder. Smoking cessation is an important approach for decreasing cancer risk but is not sufficient because 50% of new lung cancers arise in former smokers. The molecular mechanisms of lung-cancer pathogenesis in former smokers are under intense investigation.

Cancer screening and early detection have made substantial progress in cervical, colorectal, breast, prostate, and lung cancers. Very recently, the National Lung Screening Trial (NLST) demonstrated that spiral chest CT scanning reduced lung-cancer mortality by 20% in heavy smokers. This finding is extremely important and should be capitalized on by complementary targeted lung-cancer chemoprevention strategies that could further improve public health.

The fundamental concept of cancer chemoprevention, defined by Sporn as the use of pharmacologic agents to impede, arrest, or reverse carcinogenesis at earlier, preinvasive stages, was based on the biological understanding that genetic and epigenetic alterations through multistep carcinogenesis and field effects of carcinogen exposure lead to cancer. These biologic processes comprise the hallmarks of cancer development that were well described by Hanahan and Weinberg - evasion of apoptosis, self sufficiency of growth signals, insensitivity to antigrowth signals, strong replication potential, and sustained angiogenesis.

Cancer prevention trials of single or combined molecular-targeted agents in the breast, prostate, and colorectum and of vaccines in cervical cancer have met with very positive results. Several agents are currently approved by the Food and Drug Administration (FDA) for treating precancerous lesions or reducing the risk of cancer. These agents include bacillus Calmette-Guérin (BCG) in the bladder, hormone-related modulators to prevent breast cancer, nonsteroidal anti-inflammatory drugs to prevent colorectal and skin cancers, and human papillomavirus vaccines to prevent cervical cancer. Other agents, not FDA approved, also are established for reducing cancer risk in definitive phase III prevention trials.

Despite the availability of these agents to reduce some cancer risks, many are not accepted for cancer prevention by the public because of concerns over their toxicity and the need for long-term treatment. These agents can have paradoxical biologic effects; e.g., tamoxifen reduces estrogen-receptor-positive breast cancer but increases endometrial cancer, and finasteride reduces prostate cancer incidence but appeared in initial reports to induce high-grade prostate cancer. Therefore, cancer chemoprevention, in contrast to chemoprevention of cardiovascular disease with statins or antihypertensive agents, is highly controversial even in the setting of high-risk individuals. This controversy should be openly debated in regard to agent risk versus prevented-cancer risk and agent benefit versus agent risk in the primary, secondary, and tertiary prevention settings.

Lung cancer is the most lethal major cancer, with a 16% 5-year survival rate despite aggressive combined-modality treatment. This grim statistic has provided a strong rationale for conducting lung cancer chemoprevention trials over the last two decades and for the extraordinary efforts to prevent smoking and treat smoking addiction. Many chemopreventive agents (e.g., beta-carotene and vitamin A and E) were selected for clinical trials based largely on epidemiologic data; many were tested in large randomized controlled trials that produced quite disappointing results. Major reasons for the negative findings of these trials were a lack of understanding of the molecular underpinnings, heterogeneity of the targeted carcinogenesis and insufficient identification of the drivers of cancer development that could serve as molecular targets.

Lung cancer incidence by smoking status is as follows: former smokers, 50%; current smokers, 40%; and non-smokers, 10 %. Lung cancer in non- or former smokers is related to *EGFR* mutations and EML-ALK fusion as major drivers toward lung carcinogenesis. Therefore, the rationale for using EGFR inhibitors as chemopreventive agents in mutated-*EGFR* lung cancer is strong based on the field effect of mutant *EGFR* in normal epithelium adjacent to the tumor.

Lung cancer presents one of the biggest challenges and one of the greatest opportunities to make an impact on the global burden of cancer in the future. Our increased understanding of the biology of lung cancer has enabled us to develop biologic risk models and identify new targeted agents for the adjuvant or preventive settings that will enable more personalized chemoprevention.

Recent data provide a proof of principle of the potential of pharmacogenetics to personalize cancer prevention. These data come from genotyping studies in, for example, the head and neck (isotretinoin), colorectum (aspirin, celecoxib, statins), prostate (selenium), and bladder (BCG). Similar personalized genotyping approaches are being applied to research in tobacco dependence and cancer therapy.

We have investigated personalized targeted therapy in advanced lung cancer in our Biomarker-integrated Approaches of Targeted

Therapy for Lung Cancer Elimination (BATTLE) trial. Lessons learned from BATTLE are trickling down in a reverse migration to the development of a BATTLE prevention strategy. We are in the process of developing a biologic risk model for recurrence and second primary tumors (SPTs) through our Department of Defense (DoD)-supported lung cancer prevention programs, with parallel efforts to identify molecular drivers of recurrence as drug targets. The BATTLE program could have several roles in the prevention setting: A model of trial design, with its innovative Bayesian statistical design and emphasis on biomarker discovery; a discovery platform for targets, as provided by its analyses of multiple blood and tissue biomarkers; and a source of experience with targeted agents such as sorafenib. Sorafenib is a well-tolerated oral multi-kinase inhibitor with potent antiangiogenic activity. Studies of biomarkers predicting a benefit from sorafenib in the BATTLE study show a trend towards improved disease control in patients with *KDR* and *PDGFR* amplification, and BATTLE evidence also shows that circulating angiogenic factors may predict for efficacy of antiangiogenic agents such as sorafenib. The lessons we have learned from the BATTLE program may help us in studying sorafenib and other agents for cancer chemoprevention.

The first approach toward personalized lung cancer chemoprevention should occur in the tertiary prevention setting of patients with a history of resected lung cancer due to the high risk of these patients and their accessibility for molecular studies in tumor and adjacent tissue. These patients are at high risk for recurrence and SPTs, which can be histologically and molecularly similar or even indistinguishable from one another. Histologically normal tissue near a tumor often has molecular abnormalities due to field "cancerization" and/or clonal spread that may lead to a second cancer. Though predictive and prognostic signatures have been described in patients with, or at a high risk of, lung cancer, none are currently used clinically.

Using all that we have learned from our BATTLE and biological risk-modeling experience, we propose a personalized chemoprevention trial in the tertiary setting of resected lung cancer: Biomarker-integrated Approaches of Targeted Lung-cancer Elimination (BATTLE) Adjuvant and Prevention Trial. Following resection of adenocarcinoma, biomarker analyses would be performed on tumors and adjacent epithelium. Treatment groups would be determined by the molecular drivers of tumorigenesis. Patients whose tumors are driven by *EGFR* mutations could receive an EGFR inhibitor; *KRAS* and *BRAF* mutations, a Ras/Raf inhibitor; EML4-ALK translocation, an ALK inhibitor; VEGFR overexpression, vandetanib or other VEGFR inhibitors. Patients with alterations in the PI3K pathway could receive an Akt inhibitor. Primary endpoints would be recurrence and SPTs. Secondary endpoints would be tolerability, biomarker modulation, and correlation of biomarker modulation with outcome. Issues of dosing and informative biomarkers for patient selection must be optimized before this trial can begin; nevertheless, the basic BATTLE prevention design likely will become more common in the future, as our understanding of the biology of lung cancer tumorigenesis improves.

In this opening plenary session, specific strategic directions of personalized targeted chemoprevention, including study design issues of the use of spiral lung CT screening, targeted agents, and clear endpoints, will be discussed thoroughly.

American Association for Cancer Research
615 Chestnut St. 17th Floor
Philadelphia, PA 19106

Print this Page

Presentation Abstract

Abstract Number:	4817
Presentation Title:	A five-gene signature predictive of survival in lung adenocarcinoma but not in squamous cell carcinoma
Presentation Time:	Tuesday, Apr 20, 2010, 3:10 PM - 3:25 PM
Location:	Room 204, Washington Convention Center
Author Block:	Humam N. Kadara, Waun K. Hong, Ignacio I. Wistuba, Reuben Lotan. UT M.D. Anderson Cancer Ctr., Houston, TX

Abstract Body:

Identification of novel molecular markers for lung carcinogenesis, outcome and response to therapy is expected to improve the clinical management of lung cancer such as non-small cell lung cancer (NSCLC). Previously, we have derived gene expression signatures indicative of differential gene expression among cells constituting an in vitro model of human lung carcinogenesis and relevant to survival in NSCLC. In this study we assess the prognostic efficacy of our previously described six genes by using several prediction algorithms and a leave-one-out-cross-validation (LOOCV) strategy as well as risk-score prediction models. The NCI Director's Challenge datasets (n=443) were used as a training set and gene expression data of adenocarcinomas from the Duke and Harvard cohorts (DH cohort; n=183) were pooled as a validation set. In addition, two independent published datasets comprised of 130 and 58 lung squamous cell carcinomas (SCCs) served as a SCC validation cohort. A Five-gene in vitro lung carcinogenesis model signature (FILM) classifier was derived and found to be superior in prediction as the lowest specificity or sensitivity of the six prediction algorithms was 0.943. Importantly, all six prediction algorithms showed that the overall survival of all-stage or stage-I only human lung adenocarcinoma patients in the DH validation cohort that expressed FILM was significantly poorer than that of patients predicted to lack the signature. Moreover, no differences in overall survival between lung SCCs predicted to express or lack FILM were observed demonstrating the prognostic specificity of this classifier for lung adenocarcinomas. We then developed a risk score-prediction model for lung adenocarcinoma based on the Cox regression coefficients and expression of FILM genes. Lung adenocarcinoma patients identified to be at high risk based on the FILM risk model exhibited significantly worse survival (p=5.4 x 10-7, 100 months follow-up) than patients at low risk. For validation of the FILM risk model, Cox regression coefficients and the dichotomization cut-off threshold generated from the training cohort (n=443) were directly applied to the DH validation cohort (n=183). All stages or stage-I only lung adenocarcinoma patients in the validation cohort and predicted to be at high risk displayed significantly worse survival than patients predicted to be at low risk by the FILM risk model (p=0.0006 and p=0.0005 of the log-rank test, respectively). Our findings highlight a novel five-gene signature which, although derived originally from an in vitro cell model, is highly effective in predicting survival of lung adenocarcinoma patients. Studies to validate the effectiveness of FILM in predicting, in particular, the response of lung adenocarcinoma patients to various therapies are highly warranted. Supported by DOD grant W81XWH-04-1-0142 and NCI lung cancer SPORE (P50 CA70907).

Print this Page

Presentation Abstract

Abstract Number:	3674
Presentation Title:	Gene expression analysis of field of cancerization in early stage NSCLC patients towards development of biomarkers for personalized prevention
Presentation Time:	Tuesday, Apr 05, 2011, 8:00 AM -12:00 PM
Location:	Exhibit Hall A4-C, Poster Section 33
Poster Section:	33
Poster Board Number:	6

Author Block: Humam Kadara[1], Pierre Saintigny[1], Youhong Fan[1], Chi-Wan Chow[1], ZuoMing Chu[1], Wenhua Lang[1], Carmen Behrens[1], Kathryn Gold[1], Diane Liu[1], J. Jack Lee[1], Li Mao[2], Edward S. Kim[1], Waun K. Hong[1], Ignacio I. Wistuba[1]. [1]UT MD Anderson Cancer Center, Houston, TX; [2]University of Maryland, Baltimore, MD

Abstract Body: Background: The identification of early stage non-small cell lung cancer (ES NSCLC) patients (pts) at higher risk for recurrence or second primary tumor (SPT) development is vital to personalizing prevention and therapy. We sought to decipher spatial and temporal patterns of gene expression in the airway field of ever-smoker ES NSCLC pts to better understand lung cancer pathogenesis and predict recurrence or SPT development.
Methods: Pts on the prospective Vanguard study had definitively treated ES (I/II) NSCLC, were current/former smokers, and had bronchoscopies with brushings obtained from the main carina (MC) at baseline, 12, and 24 months following resective surgery and from different anatomical regions at baseline. Expression profiling is ongoing for all eligible pts (41 pts, 326 samples). To query temporal and spatial airway expression profiles, two sets of six pts were selected based on complete processed time point and baseline airway site (3 different sites per pt) arrays (Affymetrix Human Gene 1.0 ST), respectively. Temporally and spatially differentially expressed genes were independently identified based on a $p<0.01$ of a univariate t-test with estimation of the false discovery rate (FDR), studied by hierarchical clustering and principal component analysis (PCA), and functionally analyzed using network analysis.
Results: 871 gene features were differentially expressed among MCs of six NSCLC pts at baseline, 12 and 24 months and were shown to separately group the MCs as evident in both cluster and PC analyses. Moreover, pathways analysis of the temporally modulated genes showed that a gene-network mediated by extracellular regulated kinase (ERK1/2) was most significantly elevated ($p<0.001$) in function between MCs at 24 months versus baseline. 763 and 931 gene features were differentially expressed between MCs and adjacent-to-resected tumors (ADJ) airways and between MC, ADJ and non-adjacent (distant-to-resected tumor) (NON-ADJ) airways, respectively. Moreover, pathways analysis of the spatially modulated genes revealed that gene-networks mediated by nuclear factor-κB (NF-κB) and ERK1/2-mediated were most significantly elevated ($p<0.001$) in function in ADJ airway samples versus MCs. Furthermore, PCA revealed that while ADJ airway samples grouped separately and closely together, one MC and 3 NON-ADJ airway samples resided closely with ADJ samples, which were then found to originate from 3 pts with evidence of recurrence, SPT or suspicion of recurrence.
Conclusions: Our findings highlight expression signatures and pathways (ERK1/2 and NF-κB) in a “cancerization field” that may drive lung cancer pathogenesis and be associated with recurrence or SPT development in ES NSCLC pts and thus useful for derivation of biomarkers to guide personalized prevention strategies. Supported by DoD grants W81XWH-04-1-0142 and W81XWH-10-1-1007.

American Association for Cancer Research
615 Chestnut St. 17th Floor
Philadelphia, PA 19106

[Proc Amer Assoc Cancer Res, Volume 47, 2006]

Chemistry 5: Serum and Plasma Proteomics
Abstract #2864

Detecting low-abundant proteins in human plasma proteome by using multi-lectin affinity chromatography and two-dimensional gel electrophoresis

Hidetoshi Kawaguchi, Hening Ren, Wenhua Lang, Zuoming Chu, You-Hong Fan and Li Mao

University of Texas M.D. Anderson Cancer Center, Houston, TX

Glycosylation is one of the most common post-translational protein modifications and plays a fundamental role in a diverse set of biologic processes. These plasma glycoproteins can be enriched using lectins, which bind to specific sugar structures. To determine the utility of a multi-lectin column, we analyzed two independent sets of plasma samples, each consisting of 400µl mixture of plasma from five healthy controls. Captured proteins in the column were released sequentially using inhibitory carbohydrates and collected stepwise. The total glycoprotein bound to the column was 10.9% of total plasma proteins including 2.3% to jacalin, 3.7% to ConA, and 4.9% to WGA. Therefore, this column provides 20-44 folds enrichment of plasma glycoproteins in each fractionation. We further performed two-dimensional gel electrophoresis (2-DE) and generated reproducible profiles of enriched plasma glycoproteins. Several major plasma proteins, such as albumin, transferrin, immunoglobulin G, and α1-antitrypsin, were largely removed by the enrichment strategy. In the areas of high molecular weight proteins on the 2-DE gels, substantially more protein spots were visible in the sample with enrichment than its un-enriched counterpart (289 spots vs. 117 for WGA fractionation as an example). Our results demonstrate that the multi-lectin affinity-2-DE approach can help visualize lower-abundant plasma proteins and may improve the identification of plasma protein markers. This strategy has potential to be used to identify plasma protein markers associated with diseases, such as cancer. (Supported in part by Department of Defense grants DAMD17-01-1-01689-1 and W81XWH-04-1-0142; National Cancer Institute grants CA91844 and CA106451)

100th AACR Annual Meeting-- Apr 18-22, 2009; Denver, CO

Endocrinology 1 -- Poster Presentations - Proffered Abstracts

Abstract #793: Elevated epithelial insulin-like growth factor expression is a risk factor for lung cancer development

Woo-Young Kim, Quanri Jin, Seung-Hyun Oh, Edward Kim, Youn Yang, Lei Feng, Carmen Behrens, Ludmila Prudkin, York Miller, J. Lee, Scott Lippman, Waun Hong, Ignacio Wistuba and Ho-Young Lee

University of Texas M. D. Anderson Cancer Center, Houston, TX; University of Colorado Denver, Denver, CO

Abstract

Insulin-like growth factor 1 receptor (IGF-1R) signaling has been implicated in several human neoplasms. However, the role of serum levels of insulin-like growth factors (IGFs) in lung cancer risk is controversial. Our study assessed the role of tissue-derived IGFs in lung carcinogenesis. We found that IGF-1 and IGF-2 levels in bronchial tissue specimens containing high-grade dysplasia were significantly higher than in those containing normal epithelium, hyperplasia, and squamous metaplasia. Derivatives of human bronchial epithelial cell lines with activation mutation in *KRAS* (V12) or loss of p53, genetic changes frequently observed during lung carcinogenesis, overexpressed IGF-1 and IGF-2. Tobacco carcinogen (TC) 4-(methylnitrosamino)-1-(3-pyridyl)-1-butanone (NNK) enhanced transformed characteristics of these cells, which were significantly suppressed by the inhibiting the action of IGF-1, IGF-2, or the insulin-like growth factor receptor (IGFR). We further determined the role of IGF expression in lung tumorigenesis using a mouse model with a lung-specific *IGF-1* transgene after exposure to TCs, including urethane or NNK plus benzo[a]pyrene (BaP). Finally, we demonstrated antitumor activities of the selective IGF-1R tyrosine kinase inhibitor *cis*-3-[3-(4-methyl-piperazin-l-yl)-cyclobutyl]-1-(2-phenyl-quinolin-7-yl) -imidazo[1,5-*a*]pyrazin-8-ylamine (PQIP) in IGF-1 transgenic mice carrying NNK/BaP-induced lung tumors. Our results demonstrate that airway epithelial cells produce IGFs in an autocrine manner, and these IGFs act jointly with TCs to stimulate lung

carcinogenesis. Thus, the use of selective IGF-1R inhibitors may be a rational approach to controlling lung cancer.

This work was supported by National Institutes of Health grants R01 CA109520 and CA100816-01A1 (to H.-Y. Lee); and in part: by U.S. Department of Defense grant W81XWH-04-1-0142-01-VITAL (to W.K. Hong); M. D. Anderson Cancer Center Specialized Programs of Research Excellence Grant in head and neck cancer P50 CA58187 (to W.K. Hong); and a Department of Veterans Affairs Merit Review Grant (both to Y.E.M.).

Citation Information: In: Proc Am Assoc Cancer Res; 2009 Apr 18-22; Denver, CO. Philadelphia (PA): AACR; 2009. Abstract nr 793.

Print this Page

AACR 101st ANNUAL MEETING 2010
April 17-21, 2010 • Walter E. Washington Convention Center • Washington, DC

Presentation Abstract

Abstract Number:	4127
Presentation Title:	***EGFR and K-Ras* mutations and resistance of lung cancer to the IGF-1R tyrosine kinase inhibitors**
Presentation Time:	Tuesday, Apr 20, 2010, 2:00 PM - 5:00 PM
Location:	Exhibit Hall A-C, Poster Section 11
Poster Section:	11
Poster Board Number:	1
Author Block:	Woo-Young Kim, Quanri Jin, Ludmilla Prudkin, Jin-Soo Kim, Floriana Morgillo, Lei Feng, Edward S. Kim, Bryan Hennessy, Ju-Seog Lee, Gordon Mills, J. J. Lee, Bonnie Glisson, Scott M. Lippman, Ignacio I. Wistuba, Ho-Young Lee. UT M.D. Anderson Cancer Ctr., Houston, TX
Abstract Body:	**Background: The majority of patients with non-small cell lung cancer (NSCLC) has responded poorly to epidermal growth factor receptor (EGFR) tyrosine kinase inhibitors (TKIs). We investigated (1) the involvement of insulin-like growth factor 1 receptor (IGF-1R) signaling in primary resistance to EGFR TKIs and (2) the molecular determinants of resistance to IGF-1R TKIs. Methods: Phosphorylated IGF-1R/insulin receptor (pIGF-1R/IR) was immunohistochemically evaluated in NSCLC tissue microarrays. The antitumor effects of IGF-1R TKIs (PQIP, OSI906), either alone or in combination with small-molecular inhibitors or siRNA targeting K-Ras or MAPK/extracellular signal-regulated kinase kinase (MEK) were analyzed in vitro and in vivo in 4-(methylnitrosamino)-1-(3-pyridyl)-1-butanone (NNK)-transformed human bronchial epithelial (HBE) cells and in NSCLC cells with variable histologic features and mutations in EGFR or K-Ras. Results: pIGF-1R/IR expression in NSCLC specimens was positively correlated with presence of a history of tobacco smoking, squamous cell carcinoma, mutant (mut) K-Ras, and wild-type (wt) EGFR, all of which have been strongly associated with poor response to EGFR TKIs. IGF-1R TKIs exhibited significant antitumor activity in NNK-transformed HBE cells and in NSCLC cells harboring wt EGFR and wt K-Ras, but not those with mutations in these genes. Introduction of mut K-Ras attenuated the effects of IGF-1R TKIs on wt K-Ras-expressing NSCLC cells. Conversely, inactivation of MEK restored sensitivity to IGFR-TKI in cells carrying mut K-Ras. Conclusions: The mutation status of both EGFR and K-Ras could be a predictive marker for response to IGF-1R TKIs. Also, MEK antagonism can abrogate primary resistance of NSCLC to IGF-1R TKIs. This work was supported by NIH grants R01 CA-109520-01 and CA-100816 (all to H-YL.) and in part by DOD grant W81XWH-04-1-0142 VITAL and W8XWH-06-1-0303 BATTLE (W-K H.)**

(Abstract submitted to the ENAR meeting, March 2005)

A response surface model for drug combinations

Maiying Kong and J. Jack Lee
Department of Biostatistics and Applied Mathematics
University of Texas M.D. Anderson Cancer Center

When drugs having like effect are given in combinations, investigators often want to assess whether the joint effect is additive, synergistic, or antagonistic. Several response surface models (Machado and Robinson 1994; Greco *et al* 1990; Carter *et al.* 1988; Plummer and Short 1990) have been proposed in the literature by using a single parameter to capture synergism or antagonism. Limitation of these models exists when combinations at certain doses are synergistic while at other doses of the exact same drugs are antagonistic.

We propose a response surface model, where a function of doses in a combination Instead of a single parameter will be used to identify and quantify departures from additivity for different combinations. The proposed model can be considered as a generalized form of Plummer and Short's model (1990), and could capture all forms of synergism, antagonism, and additivity at different combinations of the two drugs. Examples will be given to illustrate the advantages of using the proposed method.

98th AACR Annual Meeting-- Apr 14-18, 2007; Los Angeles, CA

Molecular Signatures of Tumor Biology and Patient Outcome: Poster Presentations
Abstract #2956

Identification of biomarkers for human lung carcinogenesis by analysis of transcriptomes of cell lines representing different stages of lung carcinogenesis

Ludovic Lacroix, Eiji Tahara, Carmen Behrens, Humam Kadara, Dafna Lotan, Ignacio Wistuba and Reuben Lotan

UT M.D. Anderson Cancer Ctr., Houston, TX

Detection of tumors at early stages of lung carcinogenesis appears to be an efficient approach to reduce lung cancer morbidity and mortality because patients diagnosed with early stage lung cancer exhibit better prognosis than those diagnosed with advanced cancers. Identification of biomarkers in premalignant lung lesions is challenging due to limited availability of adequate biopsy samples. Therefore, we hypothesized that certain genes that are expressed differentially among cultured cells representing different stages of lung cancer progression can serve as biomarkers for early detection and targets for clinical intervention. As an *in vitro* human lung carcinogenesis model, we used normal (NHBE), immortalized (BEAS-2B and 1799), transformed (1198), and tumorigenic (1170-I) human bronchial epithelial (HBE) cells. The transcriptome of these cells was analyzed using the Affymetrix U133A GeneChip®. Subsequent bioinformatic analysis allowed us to identify 346 up-regulated genes and 466 down-regulated genes that displayed expression level variation from NHBE and normal small airway epithelial cells (SAEC) to the tumorigenic cell line (1170-I). Functional pathway analysis of the gene array data revealed modulation of expression of many genes involved in cell cycle, DNA regulation, cell adhesion, and enzymatic pathways. Several genes, mainly related to cell cycle (e.g., G2/M) or DNA replication, have previously been related to chromosomal instability and to cancer prognosis, and other genes such as PCNA and MCM2 have also been reported to be up-regulated in preneoplastic tissues consistent with our findings. The differential expression of putative biomarkers (UBE2C, MCM2, MCM6, BIRC5, FEN-1, TPX2, SFN, S100A8 and

S100A4) was confirmed at the mRNA and protein levels in the premalignant cell line model as well as in cell lines derived from human lung cancers by quantitative real-time PCR and Western blotting, respectively. We also analyzed the expression levels of those genes, using quantitative real time-PCR, in 41 non-small cell lung carcinomas (NSCLC) and their non-tumoral counterparts. Furthermore, the expression levels of ubiquitin-conjugating enzyme E2C (UBE2C), mini-chromosome maintenance 2 (MCM2), Flap Endonuclease-1 (FEN-1), and S100 calcium binding protein A4 (S100A4) were assessed by immunohistochemistry in several normal, preneoplastic, and neoplastic human lung tissues. Although many of the potential biomarkers have to be validated in a larger collection of human lung cancer and premalignant lesions, our findings demonstrate that this *in vitro* human lung carcinogenesis model is a useful system for discovering potential early and late biomarkers of lung carcinogenesis and putative targets for chemoprevention. Supported in part by Department of Defense grant DAMD W81XWH-04-1-0142.

99th AACR Annual Meeting-- Apr 12-16, 2008; San Diego, CA

Molecular Correlates 1: Poster Presentations - Proffered Abstracts

Abstract #2166

STAT1 protein frequently overexpressed in non-small cell lung carcinoma

Xiaoling Li, Ximing Tang, carmen Behrens, Wenli Dong, Natalie ozburn, Denise Woods, Guosheng Yin, Waun ki Hong, Cesar Moran and Ignacio Wistuba

1 UT MD Anderson 2 Liaoning province Tumor Hospital, 1 Houston 2 Shenyang China, TX, UT MD Anderson, Houston, TX

Despite recent advances, the prognosis of non-small-cell lung cancer (NSCLC) is still dismal. The recurrence rate of early-stage NSCLC is ~40% within five years after a potentially curative treatment. Because of the limited prognostic power of the current pathologic and clinical criteria, providing accurate molecular prediction of the clinical outcome is currently needed. Recently, using cDNA microarray and RT-PCR methods it has been reported that the expression of genes *HER3*, *LCK* (lymphocyte-specific protein tyrosine kinase), *DUSP6* (dual-specificity phosphatase 6), and *STAT1* (signal transducer and activator transduction 1) closely associate with recurrence-free and overall survival among NSCLC patients (Chen et al, New Eng J Med 2007: 356:11-20). As only HER3 protein expression has been previously reported in lung cancer, we investigated the immunohistochemical (IHC) expression of those four genes' proteins in a large set of NSCLC tissue microarray specimens (N=306; 194 adenocarcinomas and 112 squamous cell carcinomas), and correlate their expression with clinico-pathologic features, including prognosis. Protein expression was examined semi-quantitatively using both intensity and extension of staining, and a final score was calculated for each marker. HER3 and DUSP6 proteins were expressed only in the cytoplasm of tumor cells (38% and 78% of the tumors, respectively), STAT-1 expressed in both tumor and stromal cell compartments (55% of tumors in each compartment), and LCK expressed only in inflammatory stromal cells (85% of tumors). None of the markers expression correlated with patients' recurrence-free and overall survival. STAT1 expression was lost in 45% of NSCLCs and was significantly lower in patients with squamous cell carcinoma compared to adenocarcinoma (*P*=0.01),

non-smoking history compared to smokers (P=0.0015), and in more advanced TNM stages (P=0.015). Our findings point out the difficulties of validation gene expression data using protein expression analysis and that tissue-based *in situ* methodologies are important to identify the type of cells expressing specific molecular markers. We have confirmed at protein level that STAT1 is frequently lost in NSCLC tumor tissues and the pattern of immunostaining in tumor cells is compatible with tumor suppressor gene activity and may represent a novel tumor suppressor gene for this neoplasm (Supported by Grant DoD-W81XWH-04-1-0142 and W81XWH-05-2-0027).

100th AACR Annual Meeting-- Apr 18-22, 2009; Denver, CO

Hormones, Signal Transduction, and Cancer -- Poster Presentations - Proffered Abstracts

Abstract #5055: The mechanism of EGF-induced hyperplasia in NHTBE cells

Jangsoon Lee, Seung-Hee Ryu, Wen-Cheng Chung, Shin-Myung Kang and Ja Seok Koo

UT M.D. Anderson Cancer Ctr., Houston, TX

Abstract

Lung cancer has been reported as causing the highest cancer mortality in both sexes worldwide. Early detection and/or development of clinically efficient novel preventive/therapeutic targets for lung cancer are urgently required to reduce the high mortality rate associated with this disease. During the development of squamous cell carcinoma (SCC) in the lung, bronchial epithelial cells exhibit a progressive series of morphologically distinct changes: hyperplasia, squamous metaplasia, dysplasia, carcinoma *in situ*, and finally invasive SCC. Here, we investigated molecular mechanisms involved in hyperplasia of bronchial epithelial cells. We demonstrated that ErbB1 ligands, including epidermal growth factor (EGF), TGF-alpha, and amphiregulin, completely disrupted apical-basal polarity and induces hyperplasia of normal human tracheobronchial epithelial (NHTBE) cells. EGF-induced hyperplasia was completely blocked by an EGFR inhibitor, erlotinib, and MEK1/2 inhibitor, U0126, suggesting involvement of MEK-ERK signaling. Further studies showed that EGF substantially upregulated cyclin D1 and these inhibitors completely blocked the upregulation. Promoter analysis of cyclin D1 revealed that Ap-1 transcription factor regulates the overexpression of cyclin D1. Depletion of AP-1 component c-Jun using siRNA completely abrogated EGF-induced cyclin D1 expression and also inhibited EGF-induced hyperplasia in NHTBE cells. In conclusion, we showed that EGF induced hyperplasia of primary bronchial epithelial cells and AP-1 plays a crucial role in lung carcinogenesis.
Grant Support: Department of Defense VITAL grant (W81XWH-04-1-0142).

Citation Information: In: Proc Am Assoc Cancer Res; 2009 Apr 18-22; Denver, CO. Philadelphia (PA): AACR; 2009. Abstract nr 5055.

98th AACR Annual Meeting-- Apr 14-18, 2007; Los Angeles, CA

TNF and TNF Receptors, DNA Damage, and Chemotherapeutics: Poster Presentations
Abstract #2406

The proteasome inhibitor PS-341 (Bortezomib) upregulates death receptor 5 expression leading to induction of apoptosis and enhancement of TRAIL-induced apoptosis despite increase of c-FLIP and survivin in human lung cancer cells.

Xiangguo Liu, Ping Yue, Shuzhen Chen, Liping Hu, Sagar Lonial, Fadlo Khuri and Shi-yong Sun

Winship Cancer Inst. at Emory Univ., Atlanta, GA

The proteasome inhibitor PS-341 (Bortezomib or Velcade), an approved drug for treatment of patients with multiple myeloma, is currently being tested in clinical trials against various malignancies including lung cancer. Preclinical studies have demonstrated that PS-341 induces apoptosis and enhances tumor necrosis factor-related apoptosis-inducing ligand (TRAIL)-induced apoptosis in human cancer cells with undefined mechanisms. In the present study, we focused on revealing the mechanisms by which PS-341 induces apoptosis and enhances TRAIL-induced apoptosis in human lung cancer cells. PS-341 increased cleavage of caspase-8 and apoptosis. Prevention of caspase-8 activation by silencing caspase-8 expression using caspase-8 small interfering RNA (siRNA) abrogated PS-341-induced apoptosis. These results indicate that PS-341 induces caspase-8-depenent apoptosis. PS-341 induced expression of death receptor 5 (DR5) and cooperated with TRAIL to induce apoptosis in human lung cancer cells. Importantly, DR5 induction by PS-341 correlated with PS-341's ability to induce apoptosis, whereas blockage of PS-341-induced DR5 upregulation using DR5 siRNA rendered cells less sensitive to apoptosis induced by either PS-341 or its combination with TRAIL. These results demonstrate that DR5 upregulation mediates PS-341-induced apoptosis and enhancement of TRAIL-induced apoptosis in human lung cancer cells. We exclude the involvement of c-FLIP and survivin in mediating these events because c-FLIP (i.e., $FLIP_S$)

and survivin protein levels were actually elevated upon exposure to PS-341. Reduction of c-FLIP with c-FLIP siRNA sensitized cells to PS-341-induced apoptosis, suggesting that c-FLIP elevation protects cells from PS-341-induced apoptosis. Thus, the present study highlights the important role of DR5 upregulation in PS-341-induced apoptosis and enhancement of TRAIL-induced apoptosis. (Supported by GCC Distinguished Cancer Scholar award and DOD grant W81XWH-04-1-0142-VITAL)

[Proc Amer Assoc Cancer Res, Volume 47, 2006]

Cellular and Molecular Biology 10: Death Receptors 1
Abstract #752

FLIP downregulation and its impact on celecoxib-induced apoptosis in human lung cancer cells

Xiangguo Liu, Ping Yue, Fadlo R. Khuri and Shi-Yong Sun

Emory University Winship Cancer Institute, Atlanta, GA

The cyclooxygenease-2 (COX-2) inhibitor celecoxib is an approved drug in the clinic for colon cancer chemoprevention and has been tested for its chemopreventive and therapeutic efficacy in various clinical trials. Celecoxib induces apoptosis in a variety of human cancer cells including lung cancer cells. Our previous work has demonstrated that celecoxib upregulates DR5 expression, resulting in induction of apoptosis and enhancement of tumor necrosis factor-related apoptosis-inducing ligand (TRAIL)-induced apoptosis in human lung cancer cells (Liu et al, JNCI, 2004). In the current study, we found for the first time that celecoxib downregulated the expression of FLIPs (i.e., $FLIP_L$ and $FLIP_S$), major negative regulators of the death receptor-mediated extrinsic apoptotic pathway, in human lung cancer cells. Overexpression of FLIPs, particularly $FLIP_L$, inhibited not only celecoxib-induced apoptosis, but also apoptosis induced by the combination of celecoxib and TRAIL. These results thus indicate that FLIP downregulation also contributes to celecoxib-induced apoptosis and enhancement of TRAIL-induced apoptosis, which compliment our previous finding that the DR5-mediated extrinsic apoptotic pathway plays a critical role in celecoxib-induced apoptosis in human lung cancer cells. Collectively, we conclude that celecoxib induces apoptosis in human lung cancer cells through activation of the extrinsic apoptotic pathway, primarily by induction of DR5 and downregulation of FLIP. (Supported in part by WCI faculty start-up research fund, GCC Distinguished Cancer Scholar award and DOD VITAL grant W81XWH-04-1-0142).

[Proc Amer Assoc Cancer Res, Volume 47, 2006]

Epidemiology 1: Genes and Biomarkers in Tobacco-related Cancer
Abstract #462

Existence of clonal and subclonal outgrowths in the bronchial epithelium and stroma of current smokers

Tao Lu, Ignacio I. Wistuba and Walter N. Hittelman

UT MD Anderson Cancer Center, Houston, TX

The identification of individuals at high risk for lung cancer is critical for individualized clinical management and is important for the identification of suitable subjects for chemoprevention trials. Using chromosome in situ hybridization (CISH) technology, we previously demonstrated the presence of chromosomal instability and multifocal clonal/subclonal outgrowths in the bronchial epithelium of current and former smokers. We also verified the presence of these clonal/subclonal outgrowths in normal-appearing bronchial epithelium in lung cancer resections using fluorescence inter-simple sequence repeat PCR (FISSR-PCR) analysis, a DNA fingerprinting methodology. To evaluate and compare FISSR-PCR and CISH technologies for accessing genetic instability and clonal/subclonal outgrowth, we subjected frozen bronchial biopsies obtained prior to entry onto a chemoprevention trial to FISSR-PCR analysis from sixteen (16) current smokers without lung cancer. The group of biopsies from these same individuals have previously been analyzed by CISH and exhibited a wide range of chromosomal changes. Multiple regions (i.e., 1-4 areas each) of bronchial epithelium and stroma were microdissected, and purified genomic DNA was analyzed by FISSR-PCR using three sets of primers ($(CA)_8RG$, $(CA)_8RY$, and $(AGC)_4Y$), providing a maximum of 350 informative DNA bands of varying lengths. Overall, we detected from 0 to 55 total band changes per microdissected epithelial region (median = 1.6 per 100 DNA bands). Different regions within the same bronchial biopsies showed both common and distinct DNA band changes, suggesting subclonal variations even within a single biopsy. We also detected from 0-20 total band changes per microdissected stromal region (median = 1.0 per 100 DNA bands), suggesting the

presence of clonal outgrowths even in the stroma. Interestingly, bronchial biopsies with high clonal frequencies showed increased clonal change in the associated stroma ($p = 0.04$, two-tailed chi square). Importantly, bronchial biopsies from individuals showing high clonal changes by FISSR-PCR also showed evidence of high clonal change by CISH ($R^2 = 0.3$). These results confirm the existence of clonal/subclonal outgrowths in both the bronchial epithelium and stroma of smokers. With future improvements in microdissection, automated genomic DNA extraction, and DNA sequencing, FISSR-PCR has potential to be a sensitive method with high dynamic range to detect clonal/subclonal outgrowths in lung tissue. Such a methodology may be of use in identifying individuals at high risk for developing lung cancer. Supported in part by DAMD17-02-1-0706, NIH/NCI CA-91844, and EDRN NCI CA-86390.

99th AACR Annual Meeting-- Apr 12-16, 2008; San Diego, CA

Molecular Correlates 1: Poster Presentations - Proffered Abstracts

Abstract #2165

Immunohistochemical expression of estrogen and progesterone receptors identifies a subset of non-small cell lung cancers and correlates with *EGFR* Mutations

Maria Raso, Carmen Behrens, Suyu Liu, Ludmila Prudkin, Denisse Woods, Natalie Ozburn, Cesar Moran, J Jack Lee and Ignacio Wistuba

MD ANDERSON CANCER CENTER, Houston, TX

Estrogen (ER) α and β and progesterone (PR) receptors are transcription factors that regulate the expression of multiple genes and have been involved in the pathogenesis of non-small cell lung cancer (NSCLC). There are conflictive results reported on the immunohistochemical (IHC) expression of ER receptors in NSCLC tissue specimens using different commercially available antibodies (Abs). Correlation between ER expression and *EGFR* mutation status has been reported in lung cancer cell lines. Our aims were to compare the IHC expression pattern in tumor tissues of six commercially available ER antibodies (four α and two β) in a large set (N=317) of NSCLCs tissue microarrays containing 201 adenocarcinomas and 116 squamous cell carcinomas, and correlate the expression of ER and PR with patients' clinical-pathologic characteristics, and in adenocarcinomas with *EGFR* mutation status. The Abs used were: a) ERα: clone 6F11(2 abs), clone HC-20 and clone 1D5N; b) ERβ: clone H-150 and 14C8; and, c) PR: polyclonal. ER α and β expression were detected in the cytoplasm (ERα clone HC-20 and clone 1D5N)18%-42%; ERβ 20-98%) and the nucleus (ERα 5%-36%; ERβ 42-56%) of malignant cells, however the frequency of expression in tumors varied between Abs. PR expressed only at nuclear level in 63% of tumors. Higher nuclear expression of most ERα Abs significantly correlated with adenocarcinoma tumor histology, female gender and never smoking history. The Ab raised against the ERα N-terminus protein (clone 1D5N, Lab Vision Co, Fremont, CA) significantly correlated with all those variables when

stained in the nucleus and with worse recurrence free survival (HR 1.77, 95% CI 1.12, 2.82; *P*=0.015) when stained in the cytoplasm. Higher nuclear and cytoplasmic expressions of ERα Abs clones HC-20 and 1D5N, and higher nuclear expression an ERβ Ab clone H150 correlated with the presence of *EGFR* mutation in adenocarcinomas (*P*=0.0029 to <0.00001). We conclude that both ERs and PR express in NSCLC, and we identified Abs against ERs that distinguish a subset on NSCLC having defined clinical-pathologic features, including *EGFR* mutation in lung adenocarcinoma histology. Then, we studied the expression of ER and PR in the early pathogenesis of lung cancer, and for ER we selected one Ab for each type of receptor (α clone 1D5N; β clone H150). We found that cytoplasmic ERβ and nuclear PR were frequently expressed in the normal bronchial and bronchiolar epithelium (n=194) adjacent to lung adenocarcinomas as a field effect phenomenon. Of interest, normal and hyperplastic alveolar cells did not express those receptors, suggesting a cell type-based specific field abnormality. Our findings suggest that hormonal receptor antagonist therapy could be considered in the development of novel therapeutic and chemopreventive strategies in NSCLC (Supported by Grant DoD-W81XWH-04-1-0142 and W81XWH-05-2-0027).

Immunohistochemical Expression of Nuclear Receptors PPARγ, LXR-β and LRH-1 in NSCLC and correlation with clinicopathologic features.

Maria Gabriela Raso[1], Yang Xie[2], Carmen Behrens[1], Denise Woods[1], Yang Jeong[2], Reza Mehran[1], David Mangelsdorf[2], Cesar Moran[1], John Minna[2], Ignacio Wistuba[1].

University of Texas Southwestern, Hamon Center for Therapeutic Oncology Research, Dallas TX[2], University of Texas, MD Anderson Cancer Center, Houston TX[1]

Background. Peroxisome proliferator activated receptor gamma (PPARγ), Liver X Receptor β (LXR-β), and Liver Receptor Homolog-1 (LRH-1), are members of the nuclear receptor (NR) super family of ligand dependent transcription factors that regulate the expression of genes controlling physiological processes. These NRs have been involved in cancer development, but not well characterized in lung cancer. Recently, we developed a prognostic signature based on mRNA expression analysis of NR in NSCLC tumors (Jeong et al, unpublished data). Our goal was to investigate in a large set of NSCLCs the immunohistochemical (IHC) expression of these three NRs and correlate the expression with tumors' characteristics and patients' clinicopathologic data.
Methods. Tumor tissue from 309 NSCLCs in tissue microarrays, including 196 adenocarcinomas (AC) and 113 squamous cell carcinoma (SCC), were analyzed for protein expression by IHC of NRs PPARγ, LXR-β and LRH-1. Protein expression was quantified using a semi quantitative score (range 0-300), combining intensity and extension of the immunostaining.
Results. Protein expression of all three NR was present in the nucleus and cytoplasm of malignant NSCLC cells. Different levels of expression of these receptors were detected by NSCLC histology: adenocarcinomas expressed significantly higher expression of nuclear PPARγ (mean score AC 35.7; SSC 16.7; $P<0.001$), while squamous cell carcinomas showed significantly higher expression of cytoplasmic PPRγ (mean score AC 4.3; SCC 33.3; $P< 0.001$) and nuclear LXR-β (mean score AC 127.2; SCC 147.2; $P=0.0226$). LRH-1 was expressed only in the nucleus of squamous cell carcinomas at very low levels. Correlative analysis of the NRs expression with the clinicopathologic features showed significant differences according to gender and smoking: a) while cytoplasmic expression of PPARγ was significantly higher in males ($P=0.0095$), nuclear expression was higher in females ($P=0.0489$); b) cytoplasmic PPAR γ ($P=0.0005$) and LRH-1 ($P=0.0255$) were significantly higher in ever smokers compared with never smokers. In stages I/II tumors, multivariate analysis showed that higher levels of cytoplasmic (HR 1.005; $P=0.0123$) and nuclear (HR 1.005; $P=0.0061$) LXR-β expression significantly correlated with worse disease free survival, and higher cytoplasmic (HR 1.004; $P=0.0117$) expression correlated with worse overall survival.
Conclusions. Our study confirms that PPARγ , LXR-β and LRH-1 proteins are expressed in NSCLC tissue specimens. The expression of these NRs correlated with NSCLC patients' clinicopathologic features, and LXR-β expression correlates with patients' outcome. Finally, our study may aid in the development of prognostic biomarkers, and identification of new therapeutic targets for prevention and treatment of NSCLCs.
Supported by grants DoD W81XWH-04-1-0142 and UT-Lung SPORE P50CA70907.

[Proc Amer Assoc Cancer Res, Volume 47, 2006]

Chemistry 6: Tumor Proteome Analysis
Abstract #3582

Protein profiles of lung tumorigenesis using immmobilized metal ion adsorption chromatography

Hening Ren, David Hawke, Zuo M Chu and Li Mao

UT MD Anderson Cancer Center, Houston, TX

Understanding the molecular process of lung cancer development is important for development of novel diagnostic, preventive, and therapeutic strategies. Proteomics is a promissing approache to extend such understanding. One of the major limitations of this approache is the inability to reveal and identify lower abundant proteins. Fractionation and enrichment of cancer proteome is a logic step in expanding the application of proteomics in tumor classification and biomarker discovery. Immobilized metal ion adsorption chromatography (IMAC), also know as metal chelate affinity chromatography (MCAC), selectively enrich proteins with exposed surface histidine, cysteine, and tryptophan. To test the utility of IMAC in protein marker identification, we performed IMAC enrichment using proteins extracted from 4 lung cancer cell lines and 4 immortalized human bronchia epithelia (HBE) cell lines, followed by 2-dimensional electrophoresis (2DE) of the enriched proteins. Using this strategy, we observed substantially more proteins differentially presented between the two groups of cell lines. More than 100 such proteins were revealed when a broad range (pH 3-10) isoelectric focusing condition was used. The identities of 33 of the protein spots were further characterized by tandem mass spectrometry. Many of the proteins were low abundant proteins. Among them, stratifin, thioredoxin peroxidase, and guanine monophosphate synthetase, have transcript abundance ranging from 0.3% to 5% of the abundance of the actin transcript in lung tissues. Our results demonstrate a utility of IMAC-2DE approach in proteomics analysis of tumorigenic processes. (Supported by Department of Defense grant W81XWH-04-1-0142)

Print this Page

Presentation Abstract

Abstract Number:	392
Presentation Title:	CXCR2 expression in tumor cells is associated with an adverse outcome in a large set of non-small-cell lung cancer (NSCLC)
Presentation Time:	Sunday, Apr 03, 2011, 1:00 PM - 5:00 PM
Location:	Exhibit Hall A4-C, Poster Section 18
Poster Section:	18
Poster Board Number:	8
Author Block:	Pierre Saintigny, Diane Liu, J. Jack Lee, Yuan Ping, Carmen Behrens, Luisa M. Solis Soto, John V. Heymach, Edward S. Kim, Waun Ki Hong, Jonathan M. Kurie, Ignacio I. Wistuba, Ja Seok Koo. UT M.D. Anderson Cancer Ctr., Houston, TX
Abstract Body:	Background: CXCR2 plays an important role in inflammation, and stimulation of CXCR2-expressing endothelial cells by ELR+ CXC chemokines promotes angiogenesis. Our goal was to study the expression of CXCR2 by tumor cells and its impact on prognosis in NSCLC. Material and Methods: CXCR2 expression was determined using immunohistochemistry and a large set of tissue microarray including 458 NSCLC. The association between cytoplasmic CXCR2 (cCXCR2) expression in tumor cells and clinico-pathological factors as well as survival was analyzed. Distribution of CXCR2 and its ligands (IL8, CXCL1, CXCL2, CXCL3, CXCL5, CXCL6 and CXCL7) gene expression was studied using publicly available gene expression profiles from 52 NSCLC cell lines (GSE4824) and 444 lung adenocarcinomas (adc) (NCI Director's Challenge). To summarize the effect of CXCR2/CXCR2 ligands biological axis, Principal Component Analysis (PCA) and unsupervised hierarchical clustering were performed using CXCR2 and its ligands gene expression in both cell lines and lung adc. The first Principal Component (PC1) was correlated (Pearson) with the whole genome in 52 NSCLC cell lines. All genes were ranked according to their correlation with PC1, and used for Gene Set Enrichment Analysis (GSEA) "pre-ranked" analysis. Results: Using the median of expression to dichotomize the patients in a high versus low expression group, 238 (52.1%) tumors expressed high cCXCR2. No association was observed with gender, race, smoking habits, histology, and stage. High cCXCR2 was associated with overall survival (Hazard ratio (HR) 1.5696; confidence interval (CI)=1.176-2.096, p-value=0.002) and recurrence-free survival (HR 1.321; CI=1.027-1.698, p-value=0.030) in a univariate Cox proportional hazards (CPH) model. High cCXCR2 remained significant for overall in a multicovariate CPH after adjusting for age, gender, histology, stage, neoadjuvant chemotherapy for overall survival (HR 1.465; CI=1.088-1.972, p-value=0.012) and a trend was observed for recurrence-free survival (HR 1.261; CI=0.973-1.633, p-value=0.080). Gene expression distribution of CXCR2 and its ligands were strikingly similar in cell lines and lung adc. In both cases, hierarchical clustering showed a cluster mostly driven by CXCR2, CXCL5, and CXCL7, representing 20% of the samples. PC1 accounted for 48.25 and 46.15% of the variation of the PCA in cell lines and lung adc respectively. KRAS and NFKB oncogenic pathways were the top 2 gene sets associated with PC1. Using the median as a cutoff, PC1 was associated with a worse overall survival in 444 lung adc (Log-rank P=0.006). Conclusion: cCXCR2 expression in NSCLC tumor cells is frequent and associated with an adverse outcome. CXCR2/CXCR2 ligands biological axis may be associated with an activation of KRAS and NFKB pathways, and a poor prognosis in lung adc. Funding Source: Department of Defense-VITAL.

American Association for Cancer Research
615 Chestnut St. 17th Floor
Philadelphia, PA 19106

99th AACR Annual Meeting-- Apr 12-16, 2008; San Diego, CA

Cancer Genomics 5: MicroRNA Profiling II: Poster Presentations - Proffered Abstracts

Abstract #5046

microRNA (miRNA) species differentially expressed between immortalized normal bronchial epithelial cells and non-small cell lung cancer (NSCLC) cells

Pierre Saintigny, Hening Ren, Xiaochuan Zou and Li Mao

University of Texas MDAnderson Cancer Center, Houston, TX, LC Sciences, LLC, Houston, TX

Background: miRNAs are involved in the regulation of gene expression during development and carcinogenesis. Although previous studies have compared miRNA expression profiles between NSCLC tissues and the corresponding normal lungs, the complex cellular structures of the normal lung tissues may complicate data interpretation, which may impact the accuracy of conclusions and direction of future studies. The objective of this study is to identify differentially expressed miRNAs between normal and malignant lung epithelial cells using immortalized normal bronchial epithelial cell lines and NSCLC cell lines and to determine biological roles of the differentially expressed miRNAs in lung tumorigenesis. ***Methods***: Four immortalized Human Bronchial Epithelial Cell (HBEC) lines and four NSCLC cell lines were used. HBEC cells were cultured with Keratinocyte-SFM media system whereas NSCLC cells were cultured with DMEM/F-12 low glucose supplemented and 5% fetal bovine serum. Total RNA was extracted using *mir*Vana™ miRNA Isolation Kit (Ambion, Austin, TX). Microarray fabrication, hybridization, and data acquisition were performed at LC Sciences (Houston, TX USA). The expression profiles of 445 unique mature miRNAs were determined. The expression ratios between the two groups of samples were analyzed and differentially expressed miRNAs with P values < 0.01 were considered significant. ***Results***: Fourteen of the 445 miRNAs were differentially expressed including 5 down-regulated and 9 up-regulated in NSCLC cells compared to HBEC cells. Interestingly, 4 of the 5 down-regulated miRNAs (let-7a, let-7c, miR-126, and miR-30a-5p) have been reported down-regulated in

NSCLC whereas only 1 (miR-17-3p) of the 9 up-regulated miRNAs has been documented to be up-regulated in NSCLC previously. ***Conclusions***: We revealed a panel of differentially expressed miRNAs potentially important in lung cancer initiation and progression. The low concordance of the up-regulated miRNAs identified here compared to those found using tumor/normal tissues suggests a contribution of the non-epithelial components of the normal lung tissues. Further studies are needed to determine expression of the candidate miRNAs in primary bronchial epithelial cells and NSCLC and to determine the biological roles of the candidate miRNAs in lung cancer initiation and progression. (This work is supported by Department of Defense grant: W81XWH-04-1-0142)

[Proc Amer Assoc Cancer Res, Volume 46, 2005]

Carcinogenesis 6: Animal, In Vitro, and Other Models of Carcinogenesis
Abstract #3896

Genetic manipulation of immortalized normal human bronchial epithelial cells

Mitsuo Sato, Luc Girard, Michael Peyton, Ruben D. Ramirez, Noriaki Sunaga, Adi F. Gazdar, Jerry W. Shay and John D. Minna

UT Southwestern Medical Center, Dallas, TX

Purpose: To evaluate the oncogenic impact of p53 knockdown, mutant K-RAS^{V12}, mutant EGFR alone and their combination on tumorigenicity of a newly developed immortalized human bronchial epithelial cell line. Background: Molecular analysis of lung cancer has revealed several genetic and epigenetic alterations in the multistep pathogenesis of lung cancer. However, little is known about the relative importance of each individual alteration on the tumorigenic process. One approach is to use a model system in which the contribution of each genetic alteration to lung tumorigenesis can be assessed individually and combinatorially. We have developed an *in vitro* model system using normal human bronchial epithelial cells that overexpress Cyclin-dependent kinase 4 and human telomerase. Ectopic expression of these two genes enables the cells to bypass the growth inhibitory signals of the p16/Rb pathway and also replicative senescence induced by shortened telomeres. We manipulated this cell line (HBEC3), by stably knocking down p53 using RNA interference, by introducing a mutant form of K-RAS^{V12}, and by introducing a mutant epidermal growth factor receptor (EGFR), alone and in combination. Methods: pSuper.retro vector was used for p53 knockdown and a mutant K-RAS^{V12} and mutant EGFRs (EGFR$^{del746\text{-}750}$ and EGFR^{L858R}) were introduced using viral expression vectors. To test the genetically manipulated lines for changes in their malignant potential, growth in liquid culture, colony formation ability, growth factor dependence, and growth as xenografts in immuno-compromised mice were performed. To determine the effect of tyrosine kinase inhibitors (TKIs) (gefitinib and erlotinib) on manipulated HBEC3 cells and to assess their potential as chemopreventive agents, the cells were

evaluated both in the presence or absence of these drugs for colony forming ability. Results: Stable knockdown of p53 and overexpression of mutant EGFR were confirmed by immunoblotting in manipulated cells. K-RAS^{V12} expression was confirmed by RFLP analysis. p53 knockdown and K-RAS^{V12} alone caused cells to be less sensitive to contact inhibition and to be capable of partial anchorage-independent growth. The combination of p53 knockdown and K-RAS^{V12} further enhanced the tumorigenic phenotype by growth in soft agar but failed to cause cells to form tumors in nude mice. In addition, the ability of both anchorage-dependent and-independent cell growth of HBEC3 cells was highly dependent on epidermal growth factor (EGF) and this ability was completely inhibited with TKIs. Both types of mutant EGFRs enhanced the tumorigenic phenotype by growth in soft agar. Importantly, introduction of mutant EGFR^{L858R} into the HBEC3-p53 knockdown cells abrogated EGF dependence as measured by anchorage-independent colony formation ability. These results demonstrate that this isogenic *in vitro* model system is a powerful approach for studying lung cancer development.

[Proc Amer Assoc Cancer Res, Volume 47, 2006]

Carcinogenesis 6: Animal and Cell Models of Cancer Abstract #2849

Oncogenic manipulation and biologic selection for complete tumorigenic transformation of immortalized normal human bronchial epithelial cells

Mitsuo Sato, Woochang Lee, Luc Girard, Ruben D. Ramirez, David S. Shames, Adi F. Gazdar, Jerry W. Shay and John D. Minna

UT Southwestern Medical Center, Dallas, TX

Purpose: To develop an *in vitro* model system to study the multi-step pathogenesis of lung cancer. Introduction: We established a series of cdk4/hTERT-immortalized human bronchial epithelial cell lines (HBECs) which can be genetically manipulated, are able to differentiate into mature airway cells in organotypic cultures, but do not form colonies in soft agar or tumors in nude mice. Previously, we observed that combinations of p53 knockdown with mutant *EGFR* or with physiological levels of oncogenic $KRAS^{V12}$ progressed HBECs part but not all of the way towards malignancy. These cells form colonies in soft agar, but fail to form tumors in nude mice. In the present study we evaluated various combinations of oncogenic manipulation, higher levels of expression of oncogenic $KRAS^{V12}$, and the biologic behavior of clones selected to grow to large size in soft agar. Methods: HBEC3 immortalized with cdk4 and hTERT was engineered with various vectors systems to have stable: p53 knockdown (with shRNA); PTEN knockdown; express oncogenic $KRAS^{V12}$ at physiologic or 10 fold higher; express mutant EGFR (deletion and missense mutants). These were made alone and in combination. These and selected colonies were then tested for soft agar colony formation and subcutaneous and orthotopic tumor formation in nude mice. Results: Without oncogenic manipulation soft agar colony forming efficiency (CFE) was <~0.1%. With various oncogenic manipulations including higher expression of $KRAS^{V12}$ alone soft agar colony CFEs were ~3%, and the combination of higher $KRAS^{V12}$ and p53 knockdown increased CFE to 8%. None of these were tumorigenic. However, the combination of higher $KRAS^{V12}$

and p53 knockdown but not high KRAS^{V12} alone led to development of a subset of very large soft agar colonies (~0.1-0.2%). These large colonies were isolated and found to have CFE of 10~15% with large colony numbers increased 10 fold. 5 of the large colonies were expanded and tested for tumorgenicity and 2 were capable of forming subcutaneous and orthotopic (bronchus) tumors. Of interest one was an adenocarcinoma and the other was a squamous cell carcinoma. In addition, the adenocarcinoma expressed high levels of KRAS^{V12} and the squamous carcinoma expressed normal levels of KRAS^{V12}. Conclusion: Multiple oncogenic changes found in lung cancer (telomerase expression, p16 bypass, p53 ablation, mutant EGFR, oncogenic KRAS) introduced into HBECs are still not capable of full oncogenic transformation. However, a subset of cells selected for the ability to form large colonies in soft agar are capable of tumor formation and tend to differentiate into two non-small cell lung cancer phenotypes (adenocarcinoma and squamous cell cancer). The expression, genetic, and epigenetic changes as well as the stem cell like characteristics of these subsets of cells are being investigated to delineate the key final steps in lung cancer pathogenesis.

[Proc Amer Assoc Cancer Res, Volume 46, 2005]

Cellular and Molecular Biology 46: Molecular Genetics 5: Brain and Respiratory Cancers
Abstract #3630

Caveolin-1 abnormal expression is a frequent and early event in the pathogenesis of lung cancer

M. Loreto Spencer, Ximing Tang, Natalie Ozburn, Lakshmi Kakarala, B. Nebiyou Bekele, Ara Vaporciyan, Jack A. Roth, John D. Minna and Ignacio I. Wistuba

UT M.D. Anderson Cancer Ctr., Houston, TX and UT-Southwestern Medical Center, Dallas, TX

Caveolin-1 (CAV1), an essential structural constituent of caveolae that plays an important role in cellular process such as transport and signaling, has been implicated in the development of several human cancers, including lung. Recently, *CAV1* gene expression was detected reduced or absent in 95% of small cell lung carcinomas (SCLC) whereas it was retained in 76% of non-small cell lung carcinoma (NSCLC; squamous cell and adenocarcinoma) cell lines, suggesting that *CAV1* acts like a tumor suppressor gene in SCLC, where it appears to be required for survival and growth of NSCLC. To better understand the pathogenesis of Caveolin-1 in the pathogenesis of lung cancers, we investigated its cytoplasmic immunohistochemical expression in 411 surgically resected and paraffin-embedded lung cancers placed in tissue microarrays, including 268 adenocarcinomas, 119 squamous cell carcinomas, and 24 SCLCs. In addition, 183 normal bronchial epithelia (n=33) and squamous preneoplastic lesions (n=150) adjacent to NSCLCs were examined. The major findings were as follows: a) While high level of cytoplasmic immunohistochemical expression of Caveolin-1 was detected in NSCLC specimens, no expression was detected in all SCLCs examined. b) In NSCLCs, the mean level of expression was significantly ($p<0.0001$) higher in squamous cell carcinomas compared to adenocarcinomas. c) In adenocarcinomas, significant correlation between Caveolin-1 expression and smoking history was detected, with never smokers exhibiting significant lower levels compared to current smokers ($p<0.025$). d) No correlation between lung cancer stage and overall survival and Caveolin-1 expression was found. e) Histologically normal epithelium from NSCLC patients

demonstrated a relatively high level of Caveolin-1 expression, and higher levels were detected in high-grade squamous dysplasias compared to low-grade dysplasias and squamous metaplasia. Our findings confirm and extend previous observations in lung cancer cell lines that differential expression in Caveolin-1 is detected between SCLC and NSCLC, and suggest different effect of smoking in Caveolin-1 expression among the different lung normal and neoplastic cells. In addition, caveolin-1 over-expression is a frequent and early event in the pathogenesis of lung squamous cell carcinomas. Supported by grants NIH SPORE P50CA70907 and The VITAL Department of Defense grant W81XWH-04-1-0142.

98th AACR Annual Meeting-- Apr 14-18, 2007; Los Angeles, CA

Candidate Tumor Suppressors 2: Poster Presentations Abstract #3677

Inhibition of lung cancer cell growth by the putative tumor suppressor gene KLF6 through activation of PKC α pathway and inhibition of PI3Kinase pathway

Eiji Tahara, Humam Kadara, Ludovic Lacroix, Dafna Lotan and Reuben Lotan

UT M.D. Anderson Cancer Center, Houston, TX

The Kruppel-like transcription factor 6 (KLF6), a member of the basic zinc finger transcription factors, is associated with the control of cell proliferation and apoptosis, possibly by directly regulating the expression of $p21^{WAF1/CIP1}$. KLF6 is down regulated in many cancers and is considered to be a candidate tumor suppressor gene. In this study, we addressed the mechanisms regulating KLF6 gene expression, which are still unclear. First, we showed that KLF6 expression is reduced at both the mRNA and protein levels in non-small cell lung cancer (NSCLC) cells and is inversely correlated with lung cancer progression in an *in vitro* lung carcinogenesis model. Then, we attempted to increase KLF6 expression using modulators of epigenetic silencing including retinoic acid, histone deacetylase inhibitors, and demethylating agent, however this was not successful. Phorbol 12-myristate 13-acetate (PMA) was reported to induce KLF6 but the mechanism of this effect is not known. We found that PMA induced KLF6 through activation of the Protein Kinase C (PKC) α / mitogen-activated protein kinase (MAPK) pathway in H358 lung cancer cells. Moreover, KLF6 mediated the cell growth arrest induction by PMA or the PKC activator Bryostatin-1 through up-regulation of the cyclin-dependent kinase inhibitors (CDKIs) $p21^{WAF1/CIP1}$, $p27^{KIP1}$, and $p15^{INK4B}$. Interestingly, the combination of PMA or Bryostatin-1 and the phophatidyl-inositol-3 kinase (PI3K) inhibitor LY294002, enhanced KLF6 expression and phosphorylated levels of the p38MAPK, as well as induced cell growth arrest more than either agent alone. Furthermore, inhibition by KLF6 siRNA of induction of KLF6 by PMA partially protected the cells from growth inhibition, our results highlight the key role of KLF6 in PMA-induced cell growth arrest in lung cancer

cells and suggest that the combination of a PKC activator and a PI3K inhibitor might present a potential novel lung cancer therapy module through up-regulation of the candidate tumor suppressor gene, KLF6.
Supported in part by Department of Defense DAMD W81XWH-04-1-0142.

[Proc Amer Assoc Cancer Res, Volume 47, 2006]

Cellular and Molecular Biology 72: Molecular Genetics: Markers and Genes
Abstract #5683

"Field" defect abnormalities in lung adenocarcinoma: *KRAS* vs. *EGFR* mutant tumors.

Ximing Tang, Xiaoquin Bi, Natalie Ozburn, Waun Ki Hong and Ignacio I. Wistuba

MD Anderson Cancer Center, Houston, TX

Lung adenocarcinoma is characterized by diagnosis at advanced stages, and new strategies for early diagnosis are needed. Although little is known about the histological precursors and the molecular events preceding the development of lung adenocarcinoma, at least 2 molecular pathways have been identified: *KRAS* and *EGFR* mutation; the latter associated to non-smoking and East Asian ethnicity. We recently reported that *EGFR* mutations were detected in normal bronchial/bronchiolar epithelium (NBE) in 43% of patients with *EGFR* mutant lung adenocarcinomas (Cancer Res 65: 7568, 2005), indicating that this mutation represents an early "field" event in the pathogenesis of this neoplasm. To further investigate the molecular abnormalities in the lung respiratory epithelium "field" in lung adenocarcinoma, we performed a detailed mapping analysis of *KRAS* and *EGFR* mutations in NBE adjacent to mutant and wild-type tumors. In NBE we correlated *EGFR* mutation status with immunohistochemical (IHC) expression of EGFR and TTF-1 (a marker for lung terminal respiratory cell differentiation) proteins. We selected 191 NBE sites obtained from 50 resected lung adenocarcinomas, including 12 *KRAS* mutant, 24 *EGFR* mutant (12, East Asian ethnicity), and 14 wild-type tumors. *KRAS* (codons 12 and13) and *EGFR* (exons 19 and 21) mutation analysis was performed by PCR-sequencing using DNA extracted from microdissected tissue. Semi-quantitative IHC expression analysis of EGFR, phosphorylated EGFR (p-EGFR) and TTF-1 was performed. Our main findings were: a) No *KRAS* mutation was detected in 61 NBE sites obtained from 12 *KRAS* mutant and 11 wild-type tumors. b) Examining more cases than the previously published, similar frequency of *EGFR* mutation in NBE by patients (12/24, 50%) and by NBE site (22/73, 30%) were

detected in *EGFR* mutant adenocarcinomas. However, now we found *EGFR* mutation in 6 (11%) NBE sites from 3 (12%) patients with *EGFR* wild-type tumors. d) Previously, the same type of *EGFR* mutation was detected comparing NBE and corresponding tumor; however, now we identified 5 NBE sites from 3 East Asian patients demonstrating different mutation pattern than the corresponding tumors. e) No correlation between EGFR and p-EGFR expression and *EGFR* mutation was detected in NBE, and, interestingly, 13/21 (62%) of *EGFR* mutant NBE sites did not expressed TTF-1. Our findings indicate that in lung adenocarcinoma a "field" defect phenomenon is observed in respiratory epithelium for *EGFR* mutation, but not for *KRAS* mutation. We have extended our recently published findings by detecting *EGFR* mutation in NBE of a small subset of East Asian patients with wild-type tumors, and by detecting some cases with different mutation patterns comparing NBE and corresponding tumor. The finding that most *EGFR* mutant NBE lacked TTF-1 expression suggests that terminal respiratory epithelial cells may not be the only cell type affected by *EGFR* mutation. Supported by grant W81XWH0410142.

100th AACR Annual Meeting-- Apr 18-22, 2009; Denver, CO

Biomarkers for Diagnosis, Prognosis, and Therapy Response Assessment -- Oral Presentations - Proffered Abstracts

Abstract #3841: *TITF-1* and *EGFR* gene copy variations are associated with prognosis for the patients with non-small cell lung cancer

Ximing Tang, Diane Liu, Carmen Behrens, Dandan He, Menghong Sun, David Rice, J. Jack Lee, Waun Hong and Ignacio Wistuba

UT M.D. Anderson Cancer Center, Houston, TX

Abstract

Thyroid transcription factor -1 (TITF-1, a lineage-specific transcription factor), and the epidermal growth factor receptor (EGFR, a tyrosine kinase membrane receptor) have shown frequent gene amplification in non-small cell lung carcinomas (NSCLC). We investigated the clinico-pathologic characteristics of NSCLCs having *TITF-1* and or *EGFR* gene copy number abnormalities by examining gene copy number status using quantitative polymerase chain reaction (qPCR) and DNA extracted from microdissected formalin-fixed and paraffin-embedded tissue from 53 adenocarcinomas and 29 squamous cell carcinomas. ß-actin gene was used as reference. In tumors, gene copy ratio referred to *ß-actin* ranged from 0.22 to 74.93 (median=1.52) for *TITF-1*, and 0.05 to 6.28 (median=1.51) for *EGFR*. Ratios 1 to 2 were defined as normal gene copy number (NGC). Ratios <1 and >2 were defined as low gene copy (LGC) and high gene copy (HGC) number, respectively. Both, LGC and HGC categories were defined as abnormal gene copy. Similar frequencies of *TITF-1* and *EGFR* copy number categories were detected comparing adenocarcinoma (*TITF-1*: LGC 15, 28%; NGC 20, 38%; HGC 18, 34%; *EGFR*: LGC 9, 17%; NGC 27, 51%; HGC, 17, 32%) with squamous cell carcinoma (*TITF-1*: LGC 8, 28%; NGC 14, 48%; HGC 7, 24%; *EGFR* : LGC 5, 17%; NGC 18, 62%; HGC 6, 21%). We found a statistically significant correlation between *TITF-1* and *EGFR* copy numbers (Spearman correlation coefficient=0.36, *P*=0.0008). In both tumor histologies, neither *TITF-1* nor *EGFR* gene copy increase (ratio >2) correlated with disease

prognosis**.** However, in adenocarcinomas, Kaplan-Meier and log rank tests revealed that the median time to death was longer in patients with normal copy number compared with those with abnormal copies for *TITF-1* (median 4.76 years, 95% CI 2.95~NA, *P* = 0.04) and *EGFR* (4.76 years, 95% CI 3.13~ NA, *P*=0.04). Moreover, adenocarcinoma patients with combined *TITF-1* and *EGFR* abnormal copy showed worse overall survival (3.56 years, 95% CI 3.13~ NA) compared with patients with normal copy status (median not reached, *P*=0.003). In these patients, multicovariate Cox modeling indicated that combined copy abnormality of both genes is an independent factor for worse overall survival (HR 4.566, *P*=0.0057). Our findings suggest that loss and gain of *TITF1* and *EGFR* are frequent abnormalities in both adenocarcinomas and squamous cell carcinomas of the lung, and in adenocarcinoma patients correlate with disease outcome. (Supported by Grant DoD-W81XWH-04-1-0142 and W81XWH-05-2-0027).

Citation Information: In: Proc Am Assoc Cancer Res; 2009 Apr 18-22; Denver, CO. Philadelphia (PA): AACR; 2009. Abstract nr 3841.

98th AACR Annual Meeting-- Apr 14-18, 2007; Los Angeles, CA

DNA Methylation 2: Poster Presentations
Abstract #2869

Caveolin-1 gene methylation is a field effect phenomenon in lung cancer patients

Ximing Tang, Natalie Ozburn and Ignacio Wistuba

UT M.D. Anderson Cancer Ctr., Houston, TX

Caveolin-1 (Cav-1), an essential structural constituent of caveolae that plays an important role in cellular process such as transport and signaling, has been implicated in the development of several cancers, including lung. Reduction and absence of Cav-1 expression has been reported in almost all small cell lung cancers (SCLC) and a subset of non-small cell lung cancers (NSCLC), mostly due to gene promoter methylation. Although several studies have provided information on the molecular characterization of NSCLC premalignant changes, they have been poorly documented for SCLCs. For lung cancer, molecular changes commence in histologically normal epithelium as field effect phenomenon. To better understand the role of *CAV1* gene in the early pathogenesis of lung cancers we investigated gene methylation and protein immunohistochemical (IHC) expression in the lung respiratory field by examining histologically normal respiratory epithelia adjacent to lung tumors. We studied formalin-fixed surgically resected tumor specimens from 100 lung cancers, including 40 SCLCs and 60 NSCLCs (48 adenocarcinomas, AC; 12 squamous cell carcinomas, SCC). For *CAV1* methylation analysis we extracted DNA from 202 precisely microdissected tissue sites, including 101 tumoral and 101 normal epithelial sites (79 small bronchi and 22 bronchioles). Among normal epithelial sites, 30 were located inside tumors (INE), 60 closed to tumors (<1mm, ONE), and 11 were distant to tumors (DNE). The DNA was undergone methylation specific polymerase chain reaction for assessing *CAV1* methylation and the results were confirmed by sequencing. Cav-1 protein IHC expression was studied in the same tumoral and epithelial sites examined for methylation. A high level of *CAV1* methylation rate was detected in tumors, being more frequent in SCLC (100%) compared to AC (49%) and SCC (50%). NSCLCs, but not SCLCs, demonstrated heterogeneity in *CAV1* methylation in all the 6 cases in which multiple tumor sites were examined. *CAV1* methylation was also frequently detected in histologically normal respiratory epithelia adjacent to lung tumors, without

differences in methylation frequency by lung tumor histology (SCLC 64%, AC 69% and SCC 63%), and type (bronchi 65% and bronchioles 66%) and location (INE 67%, ONE 66% and DNE 64%) of respiratory structures examined. Gene methylation was highly correlated with protein expression in tumor (90%) and normal epithelium (95%) tissue sites. Our findings indicate that *CAV1* methylation is a frequent molecular abnormality in lung tumors, especially SCLC. The finding of high frequency of Cav-1 abnormalities in normal bronchial and bronchiolar epithelia adjacent to lung cancers suggests that *CAV1* may be involved in the early pathogenesis of lung cancer as field effect phenomenon (Supported by grant VITAL W81XWH-04-1-0142).

[Proc Amer Assoc Cancer Res, Volume 46, 2005]

Cellular and Molecular Biology 51: Receptor Tyrosine Kinases in Cancer
Abstract #4308

EGFR tyrosine kinase domain mutations are also found in histologically normal lung epithelium of patients containing lung adenocarinomas with EGFR mutations indicating a field effect

Ximing Tang, Hisayuki Shigematsu, Jack A. Roth, John D. Minna, Waun Ki Hong, Adi F. Gazdar and Ignacio I. Wistuba

UT MD Anderson Cancer Center, Houston, TX and UT-Southwestern Medial Center, Dallas, TX

Somatic mutations in the tyrosine kinase domain (exons 19 to 21) of the EGFR gene have been associated with a response of lung cancer to EGFR kinase inhibitors. Recent data indicate those mutations are predominantly detected in lung adenocarcinomas arising in never or lightly smoking patients. Although *EGFR* gene amplification and protein over-expression have been reported in lung cancer, no correlations with the recent discovered mutations have been established. Also, no one has yet demonstrated whether *EGFR* mutation occur early or late in lung cancer pathogenesis. To understand the role of *EGFR* mutations in the pathogenesis of lung adenocarcinomas, we investigated the presence of *EGFR* gene mutation and amplification in histologically normal appearing bronchial and bronchiolar epithelia (n=65 sites) adjacent to 14 surgically resected lung adenocarcinomas harboring *EGFR* mutations in exons 19 (n=8; 6 15-bp in-frame deletion; 1 18-bp in-frame deletion; 1 point mutation E746V with 21-bp in-frame deletion) and 21 (point mutation L858R; n=6). For *EGFR* mutation analysis, DNA extracted from precisely microdissected paraffin-embedded tumor tissues and adjacent normal appearing epithelia were subjected to PCR and direct DNA sequencing for exons 19 and 21. For amplification, FISH analysis of histology sections using EGFR and chromosome 7 centromeric probes were utilized in a subset of adenocarcinoma cases (n=6). *EGFR* mutations in histologically normal bronchial and bronchiolar

epithelium were detected in 9 out of 14 (64%) mutated lung adenocarcinoma patients. Mutations in normal epithelium were more frequently detected in tumor cases having the exon 21 point mutation (5/6, 80%) compared to the exon 19 in-frame deletion (4/8, 50%). Two or more normal epithelium foci demonstrating *EGFR* mutations were detected in 7 cases. All mutations detected were confirmed using additional microdissected samples and multiple independent sequencing experiments in both sense and antisense directions. *EGFR* amplification was detected in 2 out of 6 (33%) mutated lung tumors examined, and no amplification was detected in the adjacent normal epithelium. Our findings indicate that mutation of the tyrosine kinase domain of *EGFR* is an early event in the pathogenesis of a subset of lung adenocarcinomas, and they represent a field effect. Our preliminary *EGFR* amplification data indicate that this phenomenon represents a less frequent and later event compared to the mutation. Supported by grants NIH SPORE P50CA70907 and Department of Defense W81XWH-04-1-0142.

99th AACR Annual Meeting-- Apr 12-16, 2008; San Diego, CA

Molecular Markers for Cancer Diagnosis and Determination of Patient Outcomes: Oral Presentations - Proffered Abstracts

Abstract #4952

TITF-1 gene amplification and protein expression pattern identify adenocarcinoma of lung with worse prognosis

Ximing Tang, Menghong Sun, Carmen Behrens, Ludmina Prudkin, Natalie Ozburn, Adi Gazdar, Cesar Moran, Marileila Varella-Garcia and Ignacio Wistuba

UT M.D. Anderson Cancer Center, Houston, TX, UT Southwestern Medical Center, Dallas, TX, University of Colorado, Aurora, CO

Thyroid transcription factor -1 (TITF-1), a lineage-specific transcription factor frequently overexpressed in lung adenocarcinoma, has been recently reported to show gene amplification in a subset of these tumors. To better characterize *TITF-1* copy number in non-small cell lung carcinomas (NSCLC) and correlate it with protein expression, we studied both gene copy number and protein expression using fluorescent *in situ* hybridization (FISH) and immunohistochesmistry stain (IHC) assays in a large series (N=324) of surgical resected NSCLCs placed in tissue microarrays, including 205 adenocarcinomas and 119 squamous cell carcinomas. We correlated our findings with patients' clinico-pathologic characteristics, and in a subset of adenocarcinomas with *EGFR* (exons 19-21) and *KRAS* (exons 1 and 2) mutation status. *TITF-1* amplification ($FISH^+$, clustered gene signals) was detected in 19% (51 out of 269) of tumors, without differences by histology (18% of squamous cell carcinoma and 19% of adenocarcinoma). TITF-1 protein high level expression (IHC^+, semiquantitative score ≥200, range 0-300) was detected exclusively in adenocarcinomas (48% of cases), and in this tumor type correlated with gene amplification (P=0.005). No correlation between TITF1 abnormalities and patients' age, gender, smoking status and TNM stages was detected. In adenocarcinomas, IHC^+, but not $FISH^+$, correlated with *EGFR* and *KRAS* mutations: IHC^+ was more frequently found in *EGFR* (16/21, 76% vs. 59/172, 34%, P<0.001)

and *KRAS* (8/11, 72% vs. 26/75, 34%, *P*=0.016) mutant compared with wild-types tumors. Survival analysis showed that for adenocarcinoma *TITF-1* $FISH^+$ correlated with worse recurrence-free survival (*P*=0.001), while IHC^+ correlated with better recurrence-free survival (*P*=0.036). Our findings indicate that *TITF-1* amplification occurs in a subset of NSCLCs, including both major tumor histologies: adenocarcinoma and squamous cell carcinoma. The association of TITF1 expression with *EGFR* and *KRAS* mutation in lung adenocarcinomas may correlate with the peripheral airway origin of these tumors. Both *TITF-1* gene amplification and protein expression correlate with NSCLC patients' prognosis. (Supported by Grant DoD-W81XWH-04-1-0142 and W81XWH-05-2-0027).

[Proc Amer Assoc Cancer Res, Volume 47, 2006]

Cellular and Molecular Biology 3: EGFR Family Signaling Abstract #69

Analysis of *EGFR* abnormalities in the sequential pathogenesis and progression of lung adenocarcinoma

Ximing Tang, Marileila Varella-Garcia, Ana C. Xavier, Xiaoqing Bi, Natalie Ozburn, Waun Ki Hong and Ignacio I. Wistuba

UT M. D. Anderson Cancer Center, Houston, TX and University of Colorado Cancer Center, Aurora, CO

EGFR tyrosine kinase (TK) domain mutations, increased gene copy number and protein overexpression have been associated to lung cancer pathogenesis and correlated with response to EGFR TK inhibitors in lung adenocarcinoma. However, the sequence of these molecularly abnormal events in the pathogenesis and progression of lung adenocarcinoma is unknown. To elucidate this question, we performed a detailed mapping analysis correlating in the same tissue sites *EGFR* mutation, gene copy number and protein immunohistochemistry (IHC) expression in 94 formalin-fixed tissue sites comprising normal bronchial/bronchiolar epithelium (NBE; N=22), primary tumor (PT; N=43) and metastasis (MT; N=29) histologies obtained from 9 surgically resected *EGFR* mutant (exons 19 and 21) lung adenocarcinomas. *EGFR* mutation analysis was performed by PCR and direct sequencing from DNA extracted from precisely microdissected tissues. *EGFR* gene copy number analysis was performed using FISH, and high level of polysomy and gene amplification were considered as increased copy number. Semi-quantitative IHC expression analysis of cytoplasmic and cell membrane EGFR and phosphorylated EGFR (p-EGFR) was performed. *EGFR* mutation was found in 18% (4/22) NBE, 91% (39/43) PT and 86% (25/29) MT sites. Low genomic gain was found in 8 NBE sites (37%), but increased copy number was not detected. Of interest, the 4 *EGFR* mutant NBE sites exhibited normal gene copy number. No difference in the frequency of *EGFR* increased copy number was found comparing PT (39/43, 93%) and MT (25/29, 86%) sites. *EGFR* mutation frequency (89% vs. 41%; $P<0.0000$) and mutant to wild-type ratio mean (1.04 vs. 0.49, $P<0.0001$) in the sequencing chromatograms were significantly higher in tissue sites with increased

copy number than areas with normal or low genomic gain. *EGFR* mutation heterogeneity, with two or more mutant genotypes in the same tumor case, was found in 4 out of 9 (44%) PT cases, and this phenomenon was not observed in corresponding MTs. *EGFR* copy number heterogeneity was more frequent in PT than MT; however, significant copy number progression from PT to MT was not observed. Although no correlation was found between EGFR IHC and *EGFR* mutation or copy number status, significantly higher levels of EGFR and p-EGFR IHC expression were detected in mutant MT compared to PT sites (P= 0.005 to <0.0001). Our findings indicate that *EGFR* mutation precedes genomic gain in the sequential pathogenesis of lung adenocarcinoma. In tumor specimens, there was strong correlation between *EGFR* mutation and increased copy number. The heterogeneity of *EGFR* mutation and gene copy number in primary tumor, but not in metastasis, and the increased expression of total and p-EGFR IHC in metastasis sites are probably associated to tumor progression and could have clinical implications when these abnormalities are searched in small clinical specimens. Supported by grants W81XWH0410142, W81XWH0520027.

TITF-1 Protein Expression Associates with Gene Methylation and Gene Copy Gain in Non-Small Cell Lung Carcinoma

Ximing Tang, Fei Yang, Jianan Huang, Denise Woods, Alejandro Corvalan, Waun K. Hong and Ignacio I. Wistuba

UT MD Anderson Cancer Center, Houston, TX 77030, USA

Background: The thyroid transcription factor-1 (TITF-1, NKX2-1) is a lineage-specific transcription factor normally expressed in peripheral pulmonary epithelial cells. TITF-1 protein is frequently expressed in adenocarcinoma, and absent in squamous cell carcinoma of the lung. *TITF-1* gene copy number gain (CNG) has been reported in a relatively small subset of adenocarcinoma of the lung, and we have also recently detected this abnormality in lung squamous cell carcinomas (Tang et al, unpublished data). To better characterize the mechanisms responsible to the different pattern of expression of TITF-1 protein in these two types of non-small cell lung carcinomas (NSCLC), we investigated the correlation between protein expression with CNG and methylation abnormalities in a large series of NSCLC specimens.

Methods: DNA extracted from NSCLC cell lines (n=21) and tumor tissue (n=173) samples was analyzed for *TITF*-1 gene methylation by bisulfite DNA sequencing, CNG by quantitative-PCR (qPCR), and protein expression by immunohistochemistry (IHC).

Results: 14 out of 21 NSCLC cell lines demonstrated *TITF-1* gene methylation in exons 1 and 2, but not in the promoter region. In the 14 methylated cell lines, the percentage of average methylation of CpG sites in exon 2 (43.9%) was much higher than in exon 1 (6.7%). Methylation was more frequently detected in squamous cell carcinoma (48/72, 72%) compared with adenocarcinoma (46/106, 43%, P=0.002). *TITF-1* CNG was detected in 35% of adenocarcinoma and 25% of squamous cell carcinoma, respectively. In adenocarcinomas, TITF-1 protein overexpression was associated with CNG; while in both tumor histologies reduced expression of the protein was correlated with gene methylation (R=-0.4, P=0.002). Of interest, nearly half of NSCLC tumors with CNG also showed gene methylation. No gene methylation and CNG were detected in non-malignant lung tumor tissues adjacent to lung tumors having those abnormalities.

Conclusion: Our findings indicate that, in NSCLC, TITF-1 increase and lack/reduction of protein expression correlates with gene copy number gain and methylation of the gene, respectively, suggesting that these two mechanisms are important for TITF-1 protein expression modulation in lung tumors.

(Supported by Grant DoD-W81XWH-04-1-0142 and W81XWH-05-2-0027).

Expression of Stem Cell Markers in Non-Small Cell Lung Carcinoma (NSCLC) and Correlation with Clinico-pathologic Features

Ping Yuan[1], Carmen Behrens[1], Jiaoti Huang[2], Monica Spinola[3], Ludmila Prudkin[1], Wenli Dong[1], Guosheng Yin[1], Cesar Moran[1], Edward Kim[1], Bin-Bing Zhou[4], John Minna[3], Ignacio Wistuba[1].

University of Texas, M. D. Anderson Cancer Center, Houston TX[1], University of California Los Angeles[2], University of Texas Southwestern Medical Center Dallas TX[3], and Wyeth Pharmaceuticals, Pearl River, NY[4].

Background. Cancer stem cells (CSCs) or cancer-initiating cells represent a minor population of self-renewing tumor cells which are believed to play an important role in tumor development, metastasis and resistance to therapy. Although some CSC markers have been described in NSCLC, there is no comprehensive characterization of multiple CSC markers in this disease. Our aim was to investigate the patterns of protein expression of a panel of CSC-related markers in a large series of NSCLCs, and correlate those findings with patients' clinico-pathologic characteristics.

Methods. We examined protein expression by immunohistochemistry (IHC) of 287 NSCLCs (178 adenocarcinoma, and 109 squamous cell carcinomas (SCC)) of a panel of nine CSC markers: EZH2, SOX2, CD24, CD44, C-kit, HEY1, Shh, BMI-1 and Oct3/4. The patterns of expression of these markers were correlated with patients and tumors' clinico-pathologic characteristics, including disease outcome. In the adenocarcinoma, CSC markers expression was correlated with the *EGFR* and *KRAS* mutation status of the tumors.

Results. EZH2, SOX2, CD44, CD24 and C-kit were detected in the tumor cells. The pattern of Immunochemistry staining varied in each markers, EZH2 and SOX2 in nuclei, CD44 and CD24 in membrane, and C-kit in cytoplasm. Rare cases had HEY1 and Shh expression. We didn't find BMI-1 and Oct3/4 expression in our cases. The expression for these markers correlated with certain clinico-pathologic characteristics, including tumor histology, pathological stage, and patients' smoking history. EZH2, SOX2 and CD44 expressions were significantly higher in SCC than adenocarcinoma (P<0.001), and CD24 expressions was significantly higher in adenocarcinoma than in SCC (P<0.05). Patients with tobacco history showed significantly higher EZH2, SOX2, and CD24 expression compared with patients without tobacco history (P <0.001, P<0.05). The presence of *EGFR* mutation in lung adenocarcinoma correlated significantly with low EZH2 (P=0.03) and high CD44 (P=0.032) expression. We identified a subset of NSCLCs having membrane CD44+/CD24 low or negative expression. Interestingly, in multivariate analysis using the expression scores as a continuous variable, high nuclear expression of EZH2 correlated significantly with worse recurrence free survival (HR=1.004; P=0.021) and overall survival (HR=1.006; P=0.017) in patients with stage I/II adenocarcinoma who didn't

receive pretreatment. Patients with CD44+/CD24- expression had worse overall survival than other subtype in squamous cell carcinoma in male (HR=2.935, p=0.037)

Conclusions. We provide a characterization of multiple CSC markers in a large series of NSCLCs. Our findings indicate that a different pattern of CSC markers expression is detected in adenocarcinoma and squamous cell carcinomas of the lung, and their expression correlates with patients' clinico-pathologic features, including survival. The understanding of the role of CSCs in NSCLC tumor development and progression may provide opportunities to design novel strategies to prevent and treat this disease.

Supported by grants DoD W81XWH-04-1-0142, W81XWH-07-1-0306, and UT-Lung SPORE P50CA70907.

Print this Page

AACR 101st ANNUAL MEETING 2010
April 17-21, 2010 • Walter E. Washington Convention Center • Washington, DC

Presentation Abstract

Abstract Number:	5166
Presentation Title:	**Sex determining region Y-box 2 (SOX2) is a potential cell-lineage gene highly expressed in the pathogenesis of squamous cell carcinomas of the lung**
Presentation Time:	Wednesday, Apr 21, 2010, 8:00 AM -11:00 AM
Location:	Exhibit Hall A-C, Poster Section 12
Poster Section:	12
Poster Board Number:	25

Author Block: Ping Yuan[1], Humam Kadara[1], Carmen Behrens[1], Ximing Tang[1], Denise Woods[1], Luisa M. Solis[1], Jiaoti Huang[2], Monica Spinola[3], Wenli Dong[1], Guosheng Yin[1], Junya Fujimoto[1], Edward Kim[1], Yang Xie[3], Luc Girard[3], Cesar Moran[1], Waun Ki Hong[1], John D. Minna[3], Ignacio Ivan Wistuba[1]. [1]UT M.D. Anderson Cancer Ctr., Houston, TX; [2]David Geffen School of Medicine, Los Angeles, CA; [3]The University of Texas Southwestern Medical Center, Dallas, TX

Abstract Body: Non-small cell lung cancer (NSCLC) represents the majority (85%) of lung cancers and is comprised mainly of adenocarcinomas and squamous cell carcinomas (SCCs). The sequential pathogenesis of lung adenocarcinomas and SCCs occurs through dissimilar phases as the former tumors typically arise in the lung periphery whereas the latter normally arise near the central airway. We assessed the expression of SOX2, an embryonic stem cell transcriptional factor that also plays important roles in the proliferation of basal tracheal cells and whose expression is restricted to the main and central airways and bronchioles of the developing and adult mouse lung, in NSCLC by various methodologies. Here, we found that *SOX2* mRNA levels, from various published datasets, were significantly elevated in lung SCCs compared to adenocarcinomas (all $p<0.001$). Moreover, a previously characterized *OCT4/SOX2/NANOG* signature effectively separated lung SCCs from adenocarcinomas following integration with two independent publicly available gene expression microarray datasets and which correlated with increased *SOX2* mRNA in SCCs. Immunohistochemical analysis of various histological lung tissue specimens demonstrated marked nuclear SOX2 protein expression in all normal bronchial epithelia, alveolar bronchiolization structures and premalignant lesions in SCC development (hyperplasia, dysplasia and carcinoma *in situ*) and absence of expression in all normal alveoli and atypical adenomatous hyperplasias. Moreover, SOX2 protein expression was greatly higher in lung SCCs compared to adenocarcinomas following analyses in two independent large tissue microarray (TMA) sets (TMA set I, n=287; TMA set II, n=511 both $p<0.001$). Furthermore, amplification of *SOX2* DNA was detected in 20% of lung SCCs tested (n=40) and in none of the adenocarcinomas (n=17). Our findings highlight a cell-lineage gene expression pattern for the stem cell transcriptional factor SOX2 in the pathogenesis of lung SCCs and raise the intriguing possibility of the growth addiction of lung SCCs specifically to SOX2-dependent pathways. Supported in part by grants from the Department of Defense (W81XWH-04-1-0142 and W81XWH-07-1-03060), and the Specialized Program of Research Excellence in Lung Cancer grant P50CA70907.
Running title: SOX2 abnormalities in NSCLC

[Proc Amer Assoc Cancer Res, Volume 47, 2006]

Cellular and Molecular Biology 10: Death Receptors 1
Abstract #759

PPARγ ligands induce death receptor 5 (DR5) expression and redistribution in lipid rafts and enhance TRAIL-induced apoptosis in human lung cancer cells

Wei Zou, Xiangguo Liu, Ping Yue, Fadlo R Khuri and Shi-Yong Sun

winship cancer institute, Atlanta, GA

Peroxisome proliferator-activated receptor γ (PPARγ) ligands are potential chemopreventive agents. A recent epidemiological study has shown that administration of PPARγ ligand drugs significantly reduce lung cancer risk and mortality. Many studies have shown that PPARγ ligands induce apoptosis in various cell types of cancer cells including lung cancer cells. However, the underlying mechanism(s) have not been fully elucidated. Some PPARγ ligands have been shown to downregulate FLIP expression and thus enhance tumor necrosis factor-related apoptosis-inducing ligand (TRAIL)-induced apoptosis in some cancer cell lines. In the current study, we further show that PPARγ ligands induced the expression of death receptor 5 (DR5) in addition to reducing FLIP levels in human lung cancer cells. Moreover, PPARγ ligands induced DR5 redistribution to membrane lipid rafts demonstrated by sucrose gradient ultracentrifugation. These agents cooperated with TRAIL to enhance induction of apoptosis in human lung cancer cells. Both overexpression of FLIP and knockdown of DR5 abrogated PPARγ ligand's ability to enhance TRAIL-induced apoptosis. Thus, it appears that not only FLIP downregulation but also DR5 upregulation and redistribution contribute to PPARγ ligand-mediated enhancement of TRAIL-induced apoptosis. In conclusion, our results suggest another mechanism by which PPARγ ligands exert their apoptosis-inducing activity and enhance TRAIL-induced apoptosis. (Supported in part by WCI faculty start-up research fund, GCC Distinguished Cancer Scholar award and DOD VITAL grant W81XWH-04-1-0142).

VITAL Data Summary

Diane D. Liu
J. Jack Lee

February 22, 2011

Patients: N=46
Female 20, Male 26
Age: 62.5 ± 8.0 (45, 81.5)

N=45 for time to event analysis, 13/45 recurred or died

Markers:

*covariate**	*n*	*Mean ± std, median (min, max)*	*covariate*	*n*	*Mean ± std, median (min, max)*
CXCR2_NORM	15	187.11 ± 72.04, 200 (100, 300)	pAMPK_NORM	14	47.62 ± 59.86, 25 (0, 200)
CXCR2_GCM	7	142.86 ± 73.19, 100 (100, 300)	pAMPK_GCM	9	36.11 ± 48.59, 0 (0, 100)
CXCR2_BHG	35	151.51 ± 72.05, 120 (0, 300)	pAMPK_BHG	33	33.13 ± 40.25, 0 (0, 100)
CXCR2_BCH	44	165.81 ± 63.8, 166.67 (36.67, 300)	pAMPK_BCH	45	42.77 ± 38.97, 40 (0, 133.33)
CXCR2_SQM	16	110.52 ± 53.37, 100 (0, 233.33)	pAMPK_SQM	16	12.66 ± 27.04, 0 (0, 100)
CXCR2_DYS	5	115 ± 121.96, 100 (0, 275)	pAMPK_DYS	3	0 ± 0, 0 (0, 0)
CXCR2_max	46	186.88 ± 66.15, 200 (60, 300)	pAMPK_max	46	59.08 ± 46.03, 63.33 (0, 200)
CXCR2_mean	46	154.28 ± 61.94, 142.22 (48.33, 300)	pAMPK_mean	46	37.05 ± 32.23, 33.33 (0, 106.67)
CXCR2_min	46	120.89 ± 69.83, 100 (0, 300)	pAMPK_min	46	17.1 ± 28.44, 0 (0, 100)
CXCR2_max4	46	184.98 ± 65.13, 200 (60, 300)	pAMPK_max4	46	56.69 ± 46.67, 55 (0, 200)
CXCR2_mean4	46	162.15 ± 63.59, 145 (48.33, 300)	pAMPK_mean4	46	39.1 ± 34.52, 40 (0, 116.67)
CXCR2_min4	46	141.35 ± 66.97, 106 (0, 300)	pAMPK_min4	46	23.95 ± 31.63, 0 (0, 100)
EpCAM_NORM	41	266.52 ± 51.26, 300 (137.5, 300)	pMTOR_NORM	22	175.68 ± 78.36, 170.83 (83.33, 300)
EpCAM_GCM	23	198.48 ± 75.8, 200 (100, 300)	pMTOR_GCM	14	145 ± 90.85, 100 (25, 300)
EpCAM_BHG	18	209.26 ± 88.97, 200 (50, 300)	pMTOR_BHG	32	165.03 ± 79.87, 131.67 (0, 300)
EpCAM_BCH	34	263.04 ± 73.6, 300 (50, 300)	pMTOR_BCH	44	185.76 ± 71.49, 200 (26.67, 300)
EpCAM_SQM	15	74.67 ± 39.07, 100 (0, 100)	pMTOR_SQM	16	152.81 ± 94.41, 130 (0, 300)
EpCAM_DYS	2	65 ± 49.5, 65 (30, 100)	pMTOR_DYS	3	158.33 ± 123.32, 100 (75, 300)
EpCAM_max	46	271.97 ± 50.69, 300 (137.5, 300)	pMTOR_max	46	201.85 ± 77.83, 200 (26.67, 300)
EpCAM_mean	46	229.09 ± 58.73, 237.5 (87.92, 300)	pMTOR_mean	46	168.11 ± 66.92, 166.67 (17.22, 300)
EpCAM_min	46	166.52 ± 93.77, 173.33 (0, 300)	pMTOR_min	46	133.19 ± 68.27, 100 (0, 300)
EpCAM_max4	46	271.97 ± 50.69, 300 (137.5, 300)	pMTOR_max4	46	200.04 ± 77.42, 200 (26.67, 300)

*covariate**	*n*	*Mean ± std, median (min, max)*	*covariate*	*n*	*Mean ± std, median (min, max)*
EpCAM_mean4	46	248.07 ± 59.65, 266.67 (87.92, 300)	pMTOR_mean4	46	171.44 ± 65.66, 164.58 (17.22, 300)
EpCAM_min4	46	218.41 ± 77.77, 218.33 (50, 300)	pMTOR_min4	46	143.12 ± 64.38, 100 (0, 300)

* _max – maximum value of each marker for each patient among the multiple readings from 6 possible histologies
_min -- minimum value of each marker for each patient among the multiple readings from 6 possible histologies
_mean – average value of each marker for each patient among the multiple readings from 6 possible histologies
_max4 – maximum value of each marker for each patient among the multiple readings from 4 histologies (BCH, BHG, GCM, NORM)
_min4 -- minimum value of each marker for each patient among the multiple readings from 4 histologies (BCH, BHG, GCM, NORM)
_mean4 – average value of each marker for each patient among the multiple readings from 4histologies (BCH, BHG, GCM, NORM)

Markers – Dichotomized:

*covariate**	*levels*	*N (%)*	*covariate*	*levels*	*N (%)*
hi_CXCR2_NORM	.	31(.%)	hi_pAMPK_NORM	.	32(.%)
	0	6(40%)		0	7(50%)
	1	9(60%)		1	7(50%)
hi_CXCR2_BHG	.	11(.%)	hi_pAMPK_BHG	.	13(.%)
	0	17(48.6%)		1	33(100%)
	1	18(51.4%)	Pos_pAMPK_BHG	.	13(.%)
hi_CXCR2_BCH	.	2(.%)		0	17(51.5%)
	0	21(47.7%)		1	16(48.5%)
	1	23(52.3%)	hi_pAMPK_BCH	.	1(.%)
hi_CXCR2_SQM	.	30(.%)		0	22(48.9%)
	0	2(12.5%)		1	23(51.1%)
	1	14(87.5%)	hi_pAMPK_SQM	.	30(.%)
hi_CXCR2_max	0	22(47.8%)		1	16(100%)
	1	24(52.2%)	pos_pAMPK_SQM	.	30(.%)
hi_CXCR2_mean	0	23(50%)		0	11(68.8%)
	1	23(50%)		1	5(31.3%)
hi_CXCR2_min	0	10(21.7%)	hi_pAMPK_max	0	23(50%)
	1	36(78.3%)		1	23(50%)
hi_CXCR2_max4	0	22(47.8%)	hi_pAMPK_mean	0	21(45.7%)
	1	24(52.2%)		1	25(54.3%)
hi_CXCR2_mean4	0	23(50%)	hi_pAMPK_min	1	46(100%)
	1	23(50%)	pos_pAMPK_min	0	32(69.6%)
hi_CXCR2_min4	0	23(50%)		1	14(30.4%)
	1	23(50%)	hi_pAMPK_max4	0	23(50%)
hi_EpCAM_NORM	.	5(.%)		1	23(50%)
	0	17(41.5%)	hi_pAMPK_mean4	0	22(47.8%)
	1	24(58.5%)		1	24(52.2%)
hi_EpCAM_GCM	.	23(.%)	hi_pAMPK_min4	1	46(100%)
	0	8(34.8%)	pos_pAMPK_min4	0	27(58.7%)

*covariate**	*levels*	*N (%)*	*covariate*	*levels*	*N (%)*
	1	15(65.2%)		1	19(41.3%)
hi_EpCAM_BHG	.	28(.%)	hi_pMTOR_NORM	.	24(.%)
	0	5(27.8%)		0	11(50%)
	1	13(72.2%)		1	11(50%)
hi_EpCAM_BCH	.	12(.%)	hi_pMTOR_GCM	.	32(.%)
	0	9(26.5%)		0	1(7.1%)
	1	25(73.5%)		1	13(92.9%)
hi_EpCAM_SQM	.	31(.%)	hi_pMTOR_BHG	.	14(.%)
	0	5(33.3%)		0	16(50%)
	1	10(66.7%)		1	16(50%)
hi_EpCAM_max	0	14(30.4%)	hi_pMTOR_BCH	.	2(.%)
	1	32(69.6%)		0	18(40.9%)
hi_EpCAM_mean	0	23(50%)		1	26(59.1%)
	1	23(50%)	hi_pMTOR_SQM	.	30(.%)
hi_EpCAM_min	0	23(50%)		0	8(50%)
	1	23(50%)		1	8(50%)
hi_EpCAM_max4	0	14(30.4%)	hi_pMTOR_max	0	17(37%)
	1	32(69.6%)		1	29(63%)
hi_EpCAM_mean4	0	22(47.8%)	hi_pMTOR_mean	0	23(50%)
	1	24(52.2%)		1	23(50%)
hi_EpCAM_min4	0	23(50%)	hi_pMTOR_min	0	28(60.9%)
	1	23(50%)		1	18(39.1%)
			hi_pMTOR_max4	0	18(39.1%)
				1	28(60.9%)
			hi_pMTOR_mean4	0	23(50%)
				1	23(50%)
			hi_pMTOR_min4	0	24(52.2%)
				1	22(47.8%)

* hi_ -- Marker dichotomized by it median
pos_ -- Positive reading vs 0

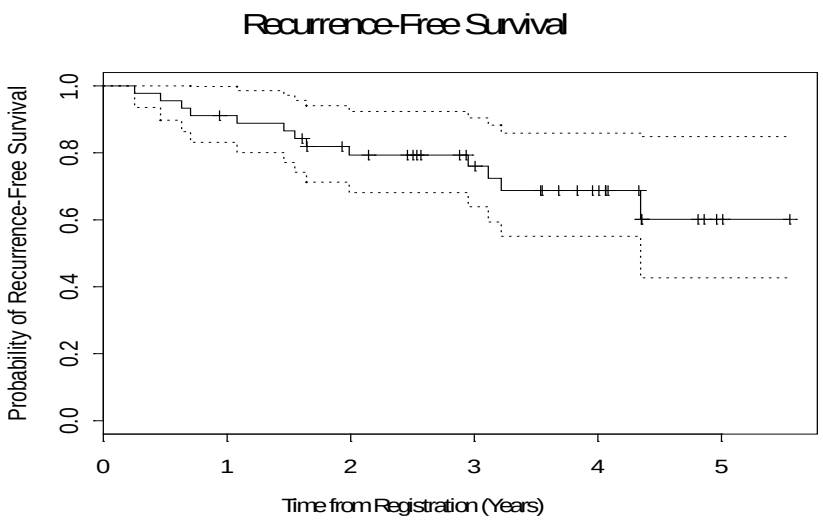

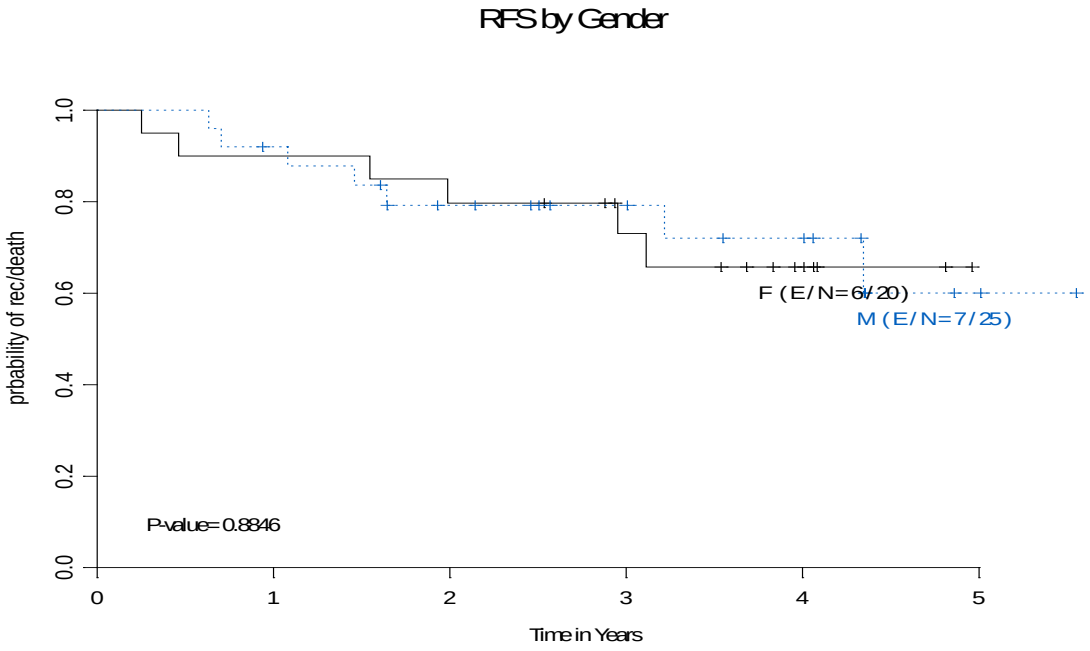

Univariate COX Models:

covariate	*Estimate*	*StdErr*	*HazardRatio*	*HRLowerCL*	*HRUpperCL*	*pValue*	*Total*	*Event*	*Censored*
CXCR2_BCH	-0.0072	0.0046	0.9928	0.9840	1.0017	0.1121	44	13	31
CXCR2_BHG	-0.0026	0.0050	0.9974	0.9878	1.0071	0.6004	34	7	27
CXCR2_NORM	-0.0015	0.0058	0.9985	0.9871	1.0099	0.7919	15	6	9
CXCR2_SQM	-0.0111	0.0104	0.9890	0.9690	1.0094	0.2876	16	4	12
CXCR2_max	-0.0059	0.0041	0.9941	0.9861	1.0022	0.1519	45	13	32
CXCR2_max4	-0.0054	0.0042	0.9946	0.9864	1.0028	0.1956	45	13	32

covariate	*Estimate*	*StdErr*	*HazardRatio*	*HRLowerCL*	*HRUpperCL*	*pValue*	*Total*	*Event*	*Censored*
CXCR2_mean	-0.0064	0.0046	0.9936	0.9847	1.0026	0.1614	45	13	32
CXCR2_mean4	-0.0052	0.0044	0.9948	0.9863	1.0034	0.2366	45	13	32
CXCR2_min	-0.0046	0.0040	0.9954	0.9876	1.0033	0.2578	45	13	32
CXCR2_min4	-0.0044	0.0041	0.9956	0.9876	1.0037	0.2895	45	13	32
EpCAM_BCH	0.0124	0.0142	1.0124	0.9846	1.0411	0.3852	33	7	26
EpCAM_BHG	0.0128	0.0106	1.0129	0.9920	1.0342	0.2273	17	3	14
EpCAM_GCM	0.0088	0.0068	1.0088	0.9954	1.0224	0.1985	22	5	17
EpCAM_NORM	0.0091	0.0067	1.0092	0.9960	1.0226	0.1746	41	13	28
EpCAM_max	0.0066	0.0066	1.0067	0.9937	1.0198	0.3156	45	13	32
EpCAM_max4	0.0066	0.0066	1.0067	0.9937	1.0198	0.3156	45	13	32
EpCAM_mean	0.0107	0.0062	1.0107	0.9984	1.0232	0.0871	45	13	32
EpCAM_mean4	0.0125	0.0072	1.0126	0.9985	1.0269	0.0810	45	13	32
EpCAM_min	0.0066	0.0034	1.0066	1.0000	1.0133	0.0512	45	13	32
EpCAM_min4	0.0116	0.0049	1.0116	1.0019	1.0215	0.0194	45	13	32
Pos_pAMPK_BHG	-0.0471	0.7846	0.9540	0.2050	4.4406	0.9521	32	7	25
hi_CXCR2_BCH	-0.3338	0.5622	0.7162	0.2380	2.1557	0.5527	44	13	31
hi_CXCR2_BHG	0.1850	0.7705	1.2032	0.2658	5.4472	0.8102	34	7	27
hi_CXCR2_NORM	-0.6051	0.8193	0.5460	0.1096	2.7201	0.4602	15	6	9
hi_CXCR2_SQM	-1.0861	1.2273	0.3375	0.0305	3.7410	0.3762	16	4	12
hi_CXCR2_max	-0.8099	0.5753	0.4449	0.1441	1.3739	0.1592	45	13	32
hi_CXCR2_max4	-0.8099	0.5753	0.4449	0.1441	1.3739	0.1592	45	13	32
hi_CXCR2_mean	-0.2476	0.5632	0.7807	0.2589	2.3544	0.6602	45	13	32
hi_CXCR2_mean4	-0.2822	0.5622	0.7541	0.2506	2.2696	0.6156	45	13	32
hi_CXCR2_min	-0.4293	0.6056	0.6510	0.1987	2.1332	0.4784	45	13	32
hi_CXCR2_min4	-0.2967	0.5726	0.7432	0.2419	2.2831	0.6043	45	13	32
hi_EpCAM_BCH	0.5765	1.0807	1.7799	0.2141	14.7994	0.5937	33	7	26
hi_EpCAM_NORM	-0.2082	0.5706	0.8120	0.2654	2.4844	0.7151	41	13	28
hi_EpCAM_max	-0.2299	0.5743	0.7946	0.2578	2.4490	0.6889	45	13	32
hi_EpCAM_max4	-0.2299	0.5743	0.7946	0.2578	2.4490	0.6889	45	13	32
hi_EpCAM_mean	0.5480	0.5708	1.7297	0.5651	5.2947	0.3371	45	13	32
hi_EpCAM_mean4	0.7955	0.5824	2.2156	0.7075	6.9380	0.1720	45	13	32
hi_EpCAM_min	1.2499	0.6605	3.4899	0.9563	12.7356	0.0584	45	13	32
hi_EpCAM_min4	0.7526	0.5742	2.1225	0.6888	6.5406	0.1900	45	13	32
hi_pAMPK_BCH	-0.2785	0.5782	0.7569	0.2437	2.3507	0.6300	45	13	32
hi_pAMPK_NORM	-1.6101	1.1224	0.1999	0.0221	1.8035	0.1514	14	5	9
hi_pAMPK_max	-0.8427	0.6060	0.4305	0.1313	1.4119	0.1643	45	13	32
hi_pAMPK_max4	-0.8278	0.6063	0.4370	0.1332	1.4340	0.1721	45	13	32
hi_pAMPK_mean	-0.2468	0.5630	0.7813	0.2591	2.3553	0.6611	45	13	32
hi_pAMPK_mean4	-0.3583	0.5781	0.6988	0.2251	2.1701	0.5354	45	13	32
hi_pMTOR_BCH	0.0501	0.5706	1.0513	0.3436	3.2166	0.9301	44	13	31

covariate	*Estimate*	*StdErr*	*HazardRatio*	*HRLowerCL*	*HRUpperCL*	*pValue*	*Total*	*Event*	*Censored*
hi_pMTOR_BHG	-0.3227	0.7644	0.7242	0.1619	3.2400	0.6729	31	7	24
hi_pMTOR_GCM	-1.9356	1.4679	0.1443	0.0081	2.5636	0.1873	13	2	11
hi_pMTOR_NORM	-0.3870	0.7659	0.6791	0.1514	3.0468	0.6134	22	7	15
hi_pMTOR_SQM	0.5878	1.2459	1.8000	0.1566	20.6933	0.6371	16	3	13
hi_pMTOR_max	-0.1377	0.5704	0.8713	0.2849	2.6651	0.8092	45	13	32
hi_pMTOR_max4	-0.0717	0.5703	0.9308	0.3044	2.8466	0.9000	45	13	32
hi_pMTOR_mean	0.1570	0.5566	1.1701	0.3930	3.4831	0.7778	45	13	32
hi_pMTOR_mean4	0.1191	0.5578	1.1265	0.3775	3.3615	0.8309	45	13	32
hi_pMTOR_min	0.3052	0.5566	1.3569	0.4558	4.0396	0.5834	45	13	32
hi_pMTOR_min4	-0.0561	0.5568	0.9454	0.3175	2.8154	0.9197	45	13	32
pAMPK_BCH	0.0010	0.0074	1.0010	0.9866	1.0156	0.8972	45	13	32
pAMPK_BHG	0.0012	0.0103	1.0012	0.9812	1.0216	0.9055	32	7	25
pAMPK_NORM	-0.0209	0.0151	0.9793	0.9508	1.0087	0.1656	14	5	9
pAMPK_SQM	0.0169	0.0129	1.0170	0.9917	1.0430	0.1898	16	3	13
pAMPK_max	-0.0037	0.0062	0.9963	0.9843	1.0085	0.5525	45	13	32
pAMPK_max4	-0.0060	0.0064	0.9940	0.9816	1.0065	0.3475	45	13	32
pAMPK_mean	-0.0031	0.0088	0.9969	0.9799	1.0142	0.7240	45	13	32
pAMPK_mean4	-0.0062	0.0087	0.9939	0.9771	1.0109	0.4770	45	13	32
pAMPK_min	-0.0018	0.0099	0.9982	0.9790	1.0178	0.8574	45	13	32
pAMPK_min4	-0.0045	0.0096	0.9955	0.9769	1.0144	0.6360	45	13	32
pMTOR_BCH	-0.0016	0.0036	0.9984	0.9913	1.0055	0.6546	44	13	31
pMTOR_BHG	0.0001	0.0045	1.0001	0.9913	1.0090	0.9867	31	7	24
pMTOR_GCM	0.0057	0.0087	1.0057	0.9887	1.0231	0.5134	13	2	11
pMTOR_NORM	-0.0010	0.0051	0.9990	0.9890	1.0091	0.8413	22	7	15
pMTOR_SQM	0.0028	0.0068	1.0028	0.9896	1.0162	0.6825	16	3	13
pMTOR_max	-0.0017	0.0034	0.9983	0.9916	1.0050	0.6116	45	13	32
pMTOR_max4	-0.0020	0.0034	0.9980	0.9914	1.0047	0.5633	45	13	32
pMTOR_mean	0.0015	0.0042	1.0015	0.9934	1.0098	0.7124	45	13	32
pMTOR_mean4	0.0005	0.0042	1.0005	0.9923	1.0088	0.9017	45	13	32
pMTOR_min	0.0041	0.0040	1.0041	0.9964	1.0119	0.2973	45	13	32
pMTOR_min4	0.0030	0.0042	1.0030	0.9947	1.0114	0.4760	45	13	32
pos_pAMPK_SQM	1.9452	1.2396	6.9951	0.6160	79.4305	0.1166	16	3	13
pos_pAMPK_min	0.1089	0.6030	1.1151	0.3420	3.6352	0.8567	45	13	32
pos_pAMPK_min4	0.0595	0.5761	1.0613	0.3431	3.2828	0.9178	45	13	32

Statistical Report for REVITALIZATION Study

November 22, 2010

Table of Contents

I. Data:

We received biomarker readings from 542 patients. A total of 21 markers have been studied by Drs. HY Lee (IGF1R, IGFBP3, InsulinR, pAKT, pIGF1R, pSRC, pmTOR, pAMPK, pEGFR, pS6), Lotan (FEN1, MCM2, MCM6, SFN, TPX2, UBE2C) and Koo (CASK, CD51, CXCR2, EpCAM, SPP1).

Merging patients' demographic, diagnosis/histology, treatment info and follow-up information with marker data, excluding patients with stage IIIB and IV or wedge resection, a total of 370 patients are included in this analysis.

II. Statistical Methods:

Summary statistics, including frequency tabulation, means, standard deviations, median, and range, were given to describe subject characteristics and biomarkers. Wilcoxon rank sum test or Kruskal-Wallis test was used to test the difference of markers between/among categorical variable levels. The association between gender, histology and smoking status, treatment and stage is test using χ^2 test or Fisher's exact test when appropriate. The continuous markers were dichotomized by either 0 vs positive or median. The Kaplan-Meier method was used to construct overall and progression-free survival curves and log-rank test was used to test the difference in survival by covariates. Univariate and multivariate Cox model were fitted to estimate the effect of prognostic factors, including age, gender, histology, stage, markers (both continuous and dichotomized levels) on time to event endpoints, including overall survival (OS) and recurrence free survival (RFS). All statistical tests were two-sided, and p values of 0.05 or less were considered to be statistically significant.

The predictive accuracy of Cox regression models is quantified by C-index, which provides the area under the receiver operating characteristics curve for censored data [1, 2]. A C-index of 0.5 indicates that outcomes are completely random, whereas a C-index of 1 indicates that the model is a perfect predictor. To protect against overfitting during stepwise regression, we used bootstrap internal-validation, which allows for computation of an unbiased estimate of predictive accuracy, C-index. We also validate the models for calibration accuracy in predicting the probability of surviving 1 year, 3 years or 5 years, or probability of recurrence-free recurrence free at 1 year, 3 years or 5 years. We use 200 bootstrap samples in both bootstrap validation and calibration.

[1] Harrell F. Regression modeling strategies. New York: Springer-Verlag; 2001.

[2] Hanley JA, McNeil BJ. The meaning and use of the area under a receiver operating characteristic (ROC) curve. Radiology 1982;143:29–36.

Notation for marker names:

Original readings:	marker name _*	*=c	cytoplasmic
		=m	membrane
		=n	nucleus
Dichotomized 1:	marker name _*_01	0 = 0	

		1 = positive reading
Dichotomized 2:	marker name _*_01m	0 = < median
		1 = ≥median

III. Main Findings:

1) Patient demographic information, disease characteristics and treatment information are summarized in Table 1 (page 5).
2) Gender and histology are significantly associated with smoking status, more former/current smokers in male than female patients, and more former/current smokers in patients with SCC than with ADENO. Treatment is significantly associated with stage of the disease. Patients with more severe diseases receive more adjuvant or neo-adjuvant treatment.
3) Please find the correlation between markers and comparison of markers by patient characteristics and disease status in the report.
4) With median follow-up time of 5.3 years, 160 deaths have been observed. Median survival=6.4 years. A total of 209 cases with recurrence or deaths have been recorded. In univariate analysis, age, gender, stage of the disease and certain adjuvant or neo-adjuvant treatment are significantly associated with OS (Table 4, page 8). Gender, stage, necrosis, inflammation, and certain adjuvant or neo-adjuvant treatment are found to be significantly associated with RFS (Table 5, page 9).
5) **Dr. HY Lee's data:** Adjusted for age, gender, stage, neoadjuvant (including chemo and radiation or concurrent therapy), both positive cytoplasmic pAMPK (HR=0.68, 95% CI: (0.49, 0.95), p=0.02) and positive cytoplasmic pmTOR (HR=0.62, 95% CI: (0.44, 0.89), p=0.0085) predict longer OS (page 41). When assessing effects of covariates on RFS, adjusted for age, stage and neoadjuvant treatment, cytoplasmic IGF1R (HR=1.003, 95% CI: (0.999, 1.007), p=0.10) and positive membrane insulin (HR=1.49, 95% CI: (1.12, 1.98), p=0.006) are associated with shorter RFS, whereas both positive cytoplasmic pAMPK (HR=0.61, 95% CI: (0.46, 0.82), p=0.001) and positive cytoplasmic pmTOR (HR=0.67, 95% CI: (0.49, 0.93), p=0.015) are significant predictors for longer RFS (page 47).
6) **Dr. Koo's data:** Adjusted for age, gender, stage, neoadjuvant (including chemo and radiation or concurrent therapy), higher cytoplasmic CXCR2 (larger than median) (HR=1.55, 95% CI: (1.12, 2.15), p=0.008) is associated with poor OS and positive cytoplasmic EpCAM (HR=0.61, 95% CI: (0.44, 0.84), p=0.003) predicts longer OS (page 63). When assessing effects of covariates on RFS, adjusted for age, stage and neoadjuvant treatment, higher cytoplasmic CXCR2 (larger than median) (HR=1.35, 95% CI: (1.01, 1.80), p=0.04) is associated with poor RFS, while positive cytoplasmic EpCAM (HR=0.69, 95% CI: (0.52, 0.92), p=0.01) and membrane CASK (HR=0.996, 95% CI: (0.99, 1.00) predict longer RFS (page 66).
7) **Dr. Lotan's data:** Adjusted for age, stage, neoadjuvant (including chemo and radiation or concurrent therapy), both higher nuclear FEN1 (larger than median) (HR=1.27, 95% CI: (0.90, 1.80), p=0.18) and positive nuclear MCM6 (HR=1.62, 95% CI: (0.91, 2.88), p=0.098) are associated, however not significantly, with poor OS (page 81). No significant marker was identified in predicting RFS in multicovariate analysis.

8) **All markers: OS** (page 85) – Adjusted for age and stage, positive cytoplasmic pAMPK, positive cytoplasmic pmTOR and positive cytoplasmic EpCAM are significant predictors in longer OS, whereas higher cytoplasmic CXCR2 (larger than median) and higher nuclear FEN1 (larger than median) are significant predictors in shorter OS. Predictive accuracy of the model from internal validation is 0.66. **RFS** (page 86) -- Adjusted for age and stage, positive membrane insulin and higher cytoplasmic CXCR2 (larger than median) are significant predictors in poor RFS, whereas positive cytoplasmic pAMPK, positive cytoplasmic pmTOR, positive cytoplasmic EpCAM and higher membrane CASK are associated with longer RFS. Predictive accuracy of the model from internal validation is 0.66.

IV. Results:

1. Patient population (N=370):

Table 1. Demographic and pathological information

covariate	*Levels*	*N(%)*	*covariate*	*Levels*	*N(%)*
Gender	F	184(49.7%)	Adj_Chem	No	249(70.7%)
	M	186(50.3%)		Yes	103(29.3%)
Race	Black	21(5.7%)		Unknown	18
	Hispanic	14(3.8%)	Adj_XRT	No	307(87.0%)
	Oriental	5(1.4%)		Yes	46(13.0%)
	White	330(89.2%)		Unknown	17
Tobacco	No	38(10.3%)	Adj_Concurrent	No	346(97.7%)
	Yes	332(89.7%)		Yes	8(2.3%)
Smoker	Current	162(43.8%)		Unknown	16
	Former	170(45.9%)	Adjuvant	No	224(63.6%)
	Never	38(10.3%)		Yes	128(36.4%)
pathT	T1	135(36.5%)		Unknown	18
	T2	214(57.8%)	Neo_Chemo	No	318(86.6%)
	T3	21(5.7%)		Yes	49(13.4%)
pathN	N0	246(67.2%)		Unknown	3
	N1	69(18.9%)	Neo_XRT	No	365(99.5%)
	N2	51(13.9%)		Yes	2(0.5%)
	Unknown	4		Unknown	3
Path stage	IA	103(27.8%)	Neo_Concurrent	No	362(98.6%)
	IB	131(35.4%)		Yes	5(1.4%)
	IIA	22(5.9%)		Unknown	3
	IIB	53(14.3%)	NeoAdjuvant	No	313(85.3%)
	IIIA	61(16.5%)		Yes	54(14.7%)
Histology	ADENO	227(61.4%)		Unknown	3
	Other	17(4.6%)	Adjvant/NeoAdjvant	No	194(54.8%)
	SCC	126(34.1%)		Yes	160(45.2%)
Grade	Poorly	122(34.2%)		Unknown	16
	Moderately	199(55.7%)	Diabetes	No	341(92.9%)

covariate	*Levels*	*N(%)*	*covariate*	*Levels*	*N(%)*
	Well	36(10.1%)		Yes	26(7.1%)
	Unknown	9		Unknown	3
Inflammation	Mild	154(42.7%)	Metformin	No	276(95.5%)
	Moderately	145(40.2%)		Yes	13(4.5%)
	Severe	62(17.2%)		Unknown	81
	Unknown	9			

		Smoking Status			
covariate	*levels*	*Never*	*Former*	*Current*	*p_value*
Gender	F	30(16.3%)	78(42.4%)	76(41.3%)	.0007
	M	8(4.3%)	92(49.5%)	86(46.2%)	
Histology	ADENO	37(16.3%)	103(45.4%)	87(38.3%)	<.0001
	SCC	1(0.8%)	61(48.4%)	64(50.8%)	
	Other	0	6(35.3%)	11(64.7%)	

Table 2. Treatment by Stage

		Stage			
covariate	*levels*	*I*	*II*	*IIIA*	*p_value*
adj_chem	No	182(80.9%)	37(52.1%)	30(53.6%)	<.0001
	Yes	43(19.1%)	34(47.9%)	26(46.4%)	
adj_XRT	No	219(97.3%)	63(88.7%)	25(43.9%)	<.0001
	Yes	6(2.7%)	8(11.3%)	32(56.1%)	
neo_chemo	No	211(90.6%)	66(89.2%)	41(68.3%)	<.0001
	Yes	22(9.4%)	8(10.8%)	19(31.7%)	
Neoadj	No	208(89.3%)	65(87.8%)	40(66.7%)	<.0001
	Yes	25(10.7%)	9(12.2%)	20(33.3%)	
AdjNeoAdj	No	160(70.8%)	25(35.2%)	9(15.8%)	<.0001
	Yes	66(29.2%)	46(64.8%)	48(84.2%)	

Table 3. Continuous variables

covariate	*n*	*mean ± std, median (min, max)*
Age	370	65.71 ± 10.17, 66.31 (32.24, 89.96)
Necrosis	369	11.95 ± 15.67, 5 (0, 90)
Fibrosis	369	21.82 ± 18.85, 20 (0, 95)

Table of RECI by OSI

RECURRENCE	*OS*		
Frequency	*Alive*	*Dead*	*Total*
No	161	56	217
Yes	49	104	153
Total	210	160	370

Table 4. Univariate Cox model assessing effects of common covariates on overall survival (OS), median survival=6.4 years, median follow-up time = 5.3 Years.

covariate	*Estimate*	*StdErr*	*HazardRatio*	*HRLowerCL*	*HRUpperCL*	*pValue*	*Total*	*Event*	*Censored*
Age	0.0154	0.0082	1.0155	0.9994	1.0320	0.0596	370	160	210
Gender (M vs F)	0.3940	0.1598	1.4829	1.0842	2.0282	0.0137	370	160	210
Race (White vs Other)	-0.2604	0.2446	0.7707	0.4772	1.2447	0.2869	370	160	210
Tobacco (Yes vs No)	0.1098	0.2716	1.1160	0.6554	1.9003	0.6861	370	160	210
Smoke							370	160	210
Former vs Never	0.0193	0.2851	1.019	0.583	1.783	0.9461			
Current vs Never	0.2006	0.2830	1.222	0.702	2.128	0.4784			
Histology							370	160	210
ADENO vs SCC	-0.1855	0.1661	0.831	0.600	1.150	0.2639			
Other vs SCC	-0.3688	0.4287	0.692	0.299	1.602	0.3896			
Grade							357	155	202
Poor vs Well	0.3337	0.3101	1.396	0.760	2.564	0.2818			
Moderate vs Well	0.3554	0.2967	1.427	0.798	2.552	0.2310			
pathN (N1-3 vs N0)	0.5782	0.1621	1.7829	1.2976	2.4497	0.0004	366	157	209
Stage							370	160	210
II vs I	0.4009	0.1971	1.493	1.015	2.197	0.0420			

covariate	*Estimate*	*StdErr*	*HazardRatio*	*HRLowerCL*	*HRUpperCL*	*pValue*	*Total*	*Event*	*Censored*
III vs I	0.8296	0.1973	2.292	1.557	3.375	<.0001			
Fibrosis	-0.0067	0.0045	0.9933	0.9845	1.0021	0.1373	369	159	210
Necrosis	0.0076	0.0049	1.0076	0.9980	1.0173	0.1212	369	159	210
Inflammation							361	155	206
Moderate vs Mild	-0.0557	0.1755	0.946	0.671	1.334	0.7509			
Severe vs Mild	-0.2722	0.2368	0.762	0.479	1.212	0.2503			
Neo_Chemo (Yes vs No)	0.4800	0.2085	1.6161	1.0739	2.4321	0.0213	367	158	209
Adj_chem (Yes vs No)	-0.2177	0.1894	0.8044	0.5550	1.1659	0.2504	352	153	199
Adj_XRT (Yes vs No)	0.7453	0.2070	2.1072	1.4043	3.1618	0.0003	353	153	200
Neoadj (Yes vs No)	0.5462	0.2006	1.7266	1.1653	2.5583	0.0065	367	158	209
Adjuvant (Yes vs No)	0.0009	0.1725	1.0009	0.7138	1.4035	0.9957	352	153	199
AdjNeoAdj (Yes vs No)	0.1661	0.1631	1.1807	0.8576	1.6255	0.3085	354	154	200

Table 5. Univariate Cox model assessing effects of common covariates on recurrence free survival (RFS)

covariate	*Estimate*	*StdErr*	*HazardRatio*	*HRLowerCL*	*HRUpperCL*	*pValue*	*Total*	*Event*	*Censored*
Age	0.0081	0.0070	1.0082	0.9944	1.0222	0.2475	370	209	161
Gender (M vs F)	0.3123	0.1395	1.3665	1.0397	1.7962	0.0252	370	209	161
Race (White vs Other)	-0.1981	0.2212	0.8203	0.5317	1.2654	0.3703	370	209	161
Tobacco (Yes vs No)	0.0747	0.2353	1.0775	0.6795	1.7087	0.7510	370	209	161
Smoke							370	209	161
Former vs Never	0.0519	0.2457	1.053	0.651	1.705	0.8328			
Current vs Never	0.0993	0.2469	1.104	0.681	1.792	0.6874			
Histology									
ADENO vs SCC	-0.2131	0.1448	0.808	0.608	1.073	0.1413	370	209	161
Other vs SCC	-0.4543	0.3713	0.635	0.307	1.315	0.2211			
Grade							357	203	154
Poor vs Well	0.2713	0.2713	1.312	0.771	2.232	0.3172			
Moderate vs Well	0.3402	0.2594	1.405	0.845	2.336	0.1897			
pathN (N1-3 vs N0)	0.7049	0.1422	2.0237	1.5313	2.6743	<.0001	366	205	161
Stage							370	209	161
II vs I	0.5203	0.1719	1.683	1.201	2.357	0.0025			

covariate	*Estimate*	*StdErr*	*HazardRatio*	*HRLowerCL*	*HRUpperCL*	*pValue*	*Total*	*Event*	*Censored*
III vs I	0.9498	0.1739	2.585	1.839	3.635	<.0001			
Fibrosis	-0.0055	0.0039	0.9945	0.9870	1.0021	0.1568	369	208	161
Necrosis	0.0090	0.0042	1.0090	1.0008	1.0173	0.0306	369	208	161
Inflammation							361	203	158
Moderate vs Mild	-0.2823	0.1538	0.754	0.558	1.019	0.0665			
Severe vs Mild	-0.4402	0.2094	0.644	0.427	0.971	0.0356			
Neo_Chemo (Yes vs No)	0.4614	0.1879	1.5864	1.0977	2.2926	0.0141	367	207	160
Adj_chem (Yes vs No)	0.0579	0.1564	1.0596	0.7799	1.4396	0.7114	352	199	153
Adj_XRT (Yes vs No)	0.7165	0.1850	2.0472	1.4247	2.9417	0.0001	353	199	154
Neoadj (Yes vs No)	0.5253	0.1799	1.6909	1.1885	2.4058	0.0035	367	207	160
Adjuvant (Yes vs No)	0.2109	0.1469	1.2348	0.9258	1.6469	0.1512	352	199	153
AdjNeoAdj (Yes vs No)	0.3134	0.1422	1.3681	1.0354	1.8077	0.0275	354	200	154

2. Dr. HY Lee

2.1 Markers

Table 6. Descriptive summary of markers

covariate	*n*	*mean ± std, median (min, max)*	*covariate*	*n*	*mean ± std, median (min, max)*
IGF1R_c	367	22.37 ± 36.14, 6.67 (0, 190)	pSRC_c	369	3.05 ± 7.01, 0 (0, 40)
IGF1R_m	367	3.67 ± 14.25, 0 (0, 120)	pSRC_m	370	17.24 ± 35.28, 0 (0, 190)
IGFBP3_c	370	24.61 ± 33.07, 10 (0, 180)	pmTOR_c	369	39.12 ± 51.89, 16.67 (0, 230)
IGFBP3_m	370	11.64 ± 31.5, 0 (0, 240)	pmTOR_m	370	61.52 ± 68.79, 36.67 (0, 240)
Insulin_c	367	44.11 ± 46.47, 30 (0, 186.67)	pAMPK_c	370	40.46 ± 49.02, 16.67 (0, 200)
Insulin_m	366	14.64 ± 28.41, 0 (0, 180)	pAMPK_m	370	2.33 ± 10.36, 0 (0, 110)
pAKT_c	369	3.68 ± 13.16, 0 (0, 86.67)	pEGFR_c	368	18.93 ± 37.45, 0 (0, 190)
pAKT_m	370	0.23 ± 1.96, 0 (0, 30)	pEGFR_m	369	16.57 ± 30.11, 3.33 (0, 160)
pAKT_n	370	1.1 ± 4.33, 0 (0, 40)	pEGFR_n	369	31.24 ± 38.83, 13.33 (0, 160)
pIGF1R_c	368	5.83 ± 13.58, 0 (0, 120)	pS6_c	370	44.55 ± 42.49, 33.33 (0, 200)
pIGF1R_m	368	13.76 ± 39.12, 0 (0, 240)	pS6_m	370	6.05 ± 20.32, 0 (0, 180)

Figure 1. Distribution of markers, Dr. HY Lee (Red line – Mean, Green line – Median)

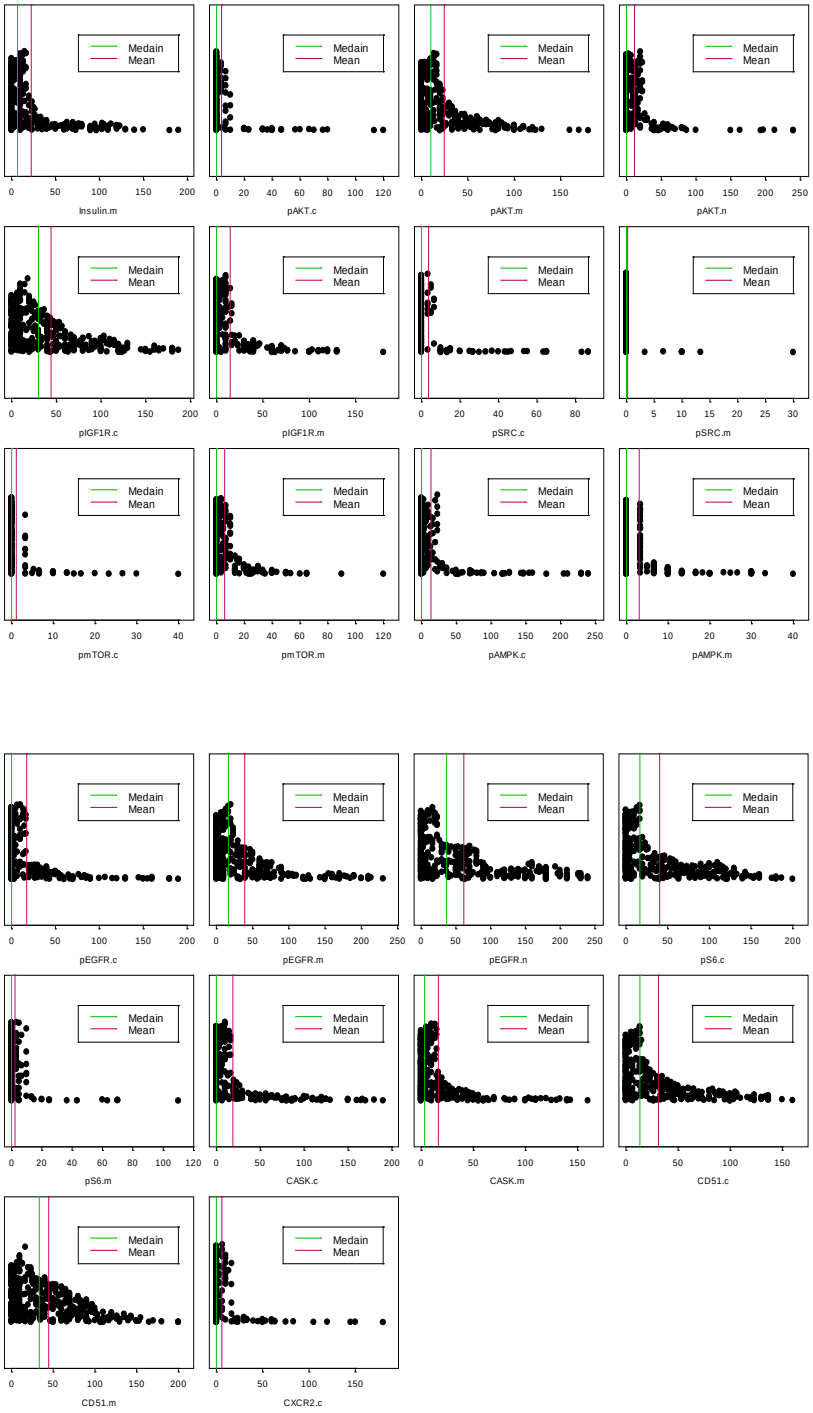

Table 7. Correlation between markers

Spearman Correlation Coefficients
Prob > |r| under H0: Rho=0
Number of Observations

	IGF1R_c	*IGF1R_m*	*IGFBP3_c*	*IGFBP3_m*	*Insulin_c*	*Insulin_m*	*pAKT_c*	*pAKT_m*	*pAKT_n*
IGF1R_c	1	0.54200	0.12708	0.15158	-0.02499	-0.06343	0.22535	0.04874	0.19148
	<.0001	<.0001	0.0148	0.0036	0.6346	0.2280	<.0001	0.3518	0.0002
	367	367	367	367	364	363	366	367	367
IGF1R_m	0.54200	1	0.14013	0.12340	0.02801	-0.01045	0.04542	-0.05391	0.05867
	<.0001	<.0001	0.0072	0.0180	0.5943	0.8427	0.3863	0.3030	0.2622
	367	367	367	367	364	363	366	367	367
IGFBP3_c	0.12708	0.14013	1	0.60804	0.04104	-0.13357	0.07723	0.06800	0.00828
	0.0148	0.0072	<.0001	<.0001	0.4332	0.0105	0.1387	0.1919	0.8738
	367	367	370	370	367	366	369	370	370
IGFBP3_m	0.15158	0.12340	0.60804	1	-0.06140	-0.10337	0.12932	0.04957	0.05407
	0.0036	0.0180	<.0001	<.0001	0.2406	0.0481	0.0129	0.3416	0.2996
	367	367	370	370	367	366	369	370	370
Insulin_c	-0.02499	0.02801	0.04104	-0.06140	1	0.39421	0.03701	-0.03746	-0.06347
	0.6346	0.5943	0.4332	0.2406	<.0001	<.0001	0.4803	0.4744	0.2251
	364	364	367	367	367	366	366	367	367
Insulin_m	-0.06343	-0.01045	-0.13357	-0.10337	0.39421	1	-0.00196	0.05561	0.02261
	0.2280	0.8427	0.0105	0.0481	<.0001	<.0001	0.9703	0.2887	0.6664
	363	363	366	366	366	366	365	366	366
pAKT_c	0.22535	0.04542	0.07723	0.12932	0.03701	-0.00196	1	0.31983	0.55645
	<.0001	0.3863	0.1387	0.0129	0.4803	0.9703	<.0001	<.0001	<.0001
	366	366	369	369	366	365	369	369	369
pAKT_m	0.04874	-0.05391	0.06800	0.04957	-0.03746	0.05561	0.31983	1	0.22558
	0.3518	0.3030	0.1919	0.3416	0.4744	0.2887	<.0001	<.0001	<.0001
	367	367	370	370	367	366	369	370	370
pAKT_n	0.19148	0.05867	0.00828	0.05407	-0.06347	0.02261	0.55645	0.22558	1
	0.0002	0.2622	0.8738	0.2996	0.2251	0.6664	<.0001	<.0001	<.0001
	367	367	370	370	367	366	369	370	370
pIGF1R_c	0.04115	0.07205	0.06407	0.13376	0.10203	0.07733	0.07635	0.05123	0.01247
	0.4332	0.1696	0.2201	0.0102	0.0515	0.1409	0.1443	0.3270	0.8116
	365	365	368	368	365	364	367	368	368
pIGF1R_m	-0.00883	0.03090	0.02782	0.10603	0.06208	0.03266	0.06443	0.05009	0.02256
	0.8665	0.5562	0.5948	0.0421	0.2368	0.5345	0.2182	0.3379	0.6662
	365	365	368	368	365	364	367	368	368
pSRC_c	0.17186	0.13887	0.08455	0.18250	0.01820	0.05065	0.13423	0.10755	0.08164
	0.0010	0.0078	0.1049	0.0004	0.7286	0.3345	0.0099	0.0389	0.1175
	366	366	369	369	366	365	368	369	369

Spearman Correlation Coefficients
Prob > |r| under H0: Rho=0
Number of Observations

	IGF1R_c	*IGF1R_m*	*IGFBP3_c*	*IGFBP3_m*	*Insulin_c*	*Insulin_m*	*pAKT_c*	*pAKT_m*	*pAKT_n*
pSRC_m	0.12782	0.11213	0.07093	0.20326	0.08381	0.09932	0.11583	0.12257	0.06602
	0.0143	0.0318	0.1734	<.0001	0.1089	0.0577	0.0261	0.0183	0.2051
	367	367	370	370	367	366	369	370	370
pmTOR_c	-0.29987	-0.22251	0.02532	-0.09283	0.14796	-0.01566	-0.01393	-0.06009	-0.03707
	<.0001	<.0001	0.6277	0.0749	0.0046	0.7656	0.7900	0.2495	0.4778
	366	366	369	369	366	365	368	369	369
pmTOR_m	-0.31648	-0.22256	-0.06881	-0.14827	0.11020	0.14343	0.00272	-0.03206	0.01129
	<.0001	<.0001	0.1866	0.0043	0.0348	0.0060	0.9584	0.5387	0.8286
	367	367	370	370	367	366	369	370	370

Spearman Correlation Coefficients
Prob > |r| under H0: Rho=0
Number of Observations

	pIGF1R_c	*pIGF1R_m*	*pSRC_c*	*pSRC_m*	*pmTOR_c*	*pmTOR_m*
IGF1R_c	0.04115	-0.00883	0.17186	0.12782	-0.29987	-0.31648
	0.4332	0.8665	0.0010	0.0143	<.0001	<.0001
	365	365	366	367	366	367
IGF1R_m	0.07205	0.03090	0.13887	0.11213	-0.22251	-0.22256
	0.1696	0.5562	0.0078	0.0318	<.0001	<.0001
	365	365	366	367	366	367
IGFBP3_c	0.06407	0.02782	0.08455	0.07093	0.02532	-0.06881
	0.2201	0.5948	0.1049	0.1734	0.6277	0.1866
	368	368	369	370	369	370
IGFBP3_m	0.13376	0.10603	0.18250	0.20326	-0.09283	-0.14827
	0.0102	0.0421	0.0004	<.0001	0.0749	0.0043
	368	368	369	370	369	370
Insulin_c	0.10203	0.06208	0.01820	0.08381	0.14796	0.11020
	0.0515	0.2368	0.7286	0.1089	0.0046	0.0348
	365	365	366	367	366	367
Insulin_m	0.07733	0.03266	0.05065	0.09932	-0.01566	0.14343
	0.1409	0.5345	0.3345	0.0577	0.7656	0.0060
	364	364	365	366	365	366
pAKT_c	0.07635	0.06443	0.13423	0.11583	-0.01393	0.00272
	0.1443	0.2182	0.0099	0.0261	0.7900	0.9584
	367	367	368	369	368	369
pAKT_m	0.05123	0.05009	0.10755	0.12257	-0.06009	-0.03206
	0.3270	0.3379	0.0389	0.0183	0.2495	0.5387
	368	368	369	370	369	370

Spearman Correlation Coefficients
Prob > |r| under H0: Rho=0
Number of Observations

	pIGF1R_c	*pIGF1R_m*	*pSRC_c*	*pSRC_m*	*pmTOR_c*	*pmTOR_m*
pAKT_n	0.01247	0.02256	0.08164	0.06602	-0.03707	0.01129
	0.8116	0.6662	0.1175	0.2051	0.4778	0.8286
	368	368	369	370	369	370
pIGF1R_c	1	0.81730	0.65536	0.66182	0.12378	-0.03251
	<.0001	<.0001	<.0001	<.0001	0.0177	0.5341
	368	368	367	368	367	368
pIGF1R_m	0.81730	1	0.60625	0.59282	0.15051	0.02149
	<.0001	<.0001	<.0001	<.0001	0.0039	0.6812
	368	368	367	368	367	368
pSRC_c	0.65536	0.60625	1	0.82219	0.09120	-0.02066
	<.0001	<.0001	<.0001	<.0001	0.0806	0.6925
	367	367	369	369	368	369
pSRC_m	0.66182	0.59282	0.82219	1	0.04124	-0.06998
	<.0001	<.0001	<.0001	<.0001	0.4296	0.1792
	368	368	369	370	369	370
pmTOR_c	0.12378	0.15051	0.09120	0.04124	1	0.73911
	0.0177	0.0039	0.0806	0.4296	<.0001	<.0001
	367	367	368	369	369	369
pmTOR_m	-0.03251	0.02149	-0.02066	-0.06998	0.73911	1
	0.5341	0.6812	0.6925	0.1792	<.0001	<.0001
	368	368	369	370	369	370

Spearman Correlation Coefficients
Prob > |r| under H0: Rho=0
Number of Observations

	pAMPK_c	*pAMPK_m*	*pEGFR_c*	*pEGFR_m*	*pEGFR_n*	*pS6_c*	*pS6_m*
pAMPK_c	1	0.41941	0.25539	0.14190	-0.03197	-0.05288	-0.11848
	<.0001	<.0001	<.0001	0.0063	0.5404	0.3104	0.0226
	370	370	368	369	369	370	370
pAMPK_m	0.41941	1	0.14041	0.12172	0.07484	-0.08216	0.04847
	<.0001	<.0001	0.0070	0.0193	0.1513	0.1146	0.3525
	370	370	368	369	369	370	370
pEGFR_c	0.25539	0.14041	1	0.67646	0.02341	0.19825	-0.01865
	<.0001	0.0070	<.0001	<.0001	0.6549	0.0001	0.7213
	368	368	368	368	367	368	368
pEGFR_m	0.14190	0.12172	0.67646	1	0.06551	0.18835	0.09597
	0.0063	0.0193	<.0001	<.0001	0.2099	0.0003	0.0656
	369	369	368	369	368	369	369
pEGFR_n	-0.03197	0.07484	0.02341	0.06551	1	0.21804	0.20692
	0.5404	0.1513	0.6549	0.2099	<.0001	<.0001	<.0001
	369	369	367	368	369	369	369
pS6_c	-0.05288	-0.08216	0.19825	0.18835	0.21804	1	0.29661
	0.3104	0.1146	0.0001	0.0003	<.0001	<.0001	<.0001
	370	370	368	369	369	370	370
pS6_m	-0.11848	0.04847	-0.01865	0.09597	0.20692	0.29661	1
	0.0226	0.3525	0.7213	0.0656	<.0001	<.0001	<.0001
	370	370	368	369	369	370	370

Figure 2. Correlation between markers, Dr. HY Lee

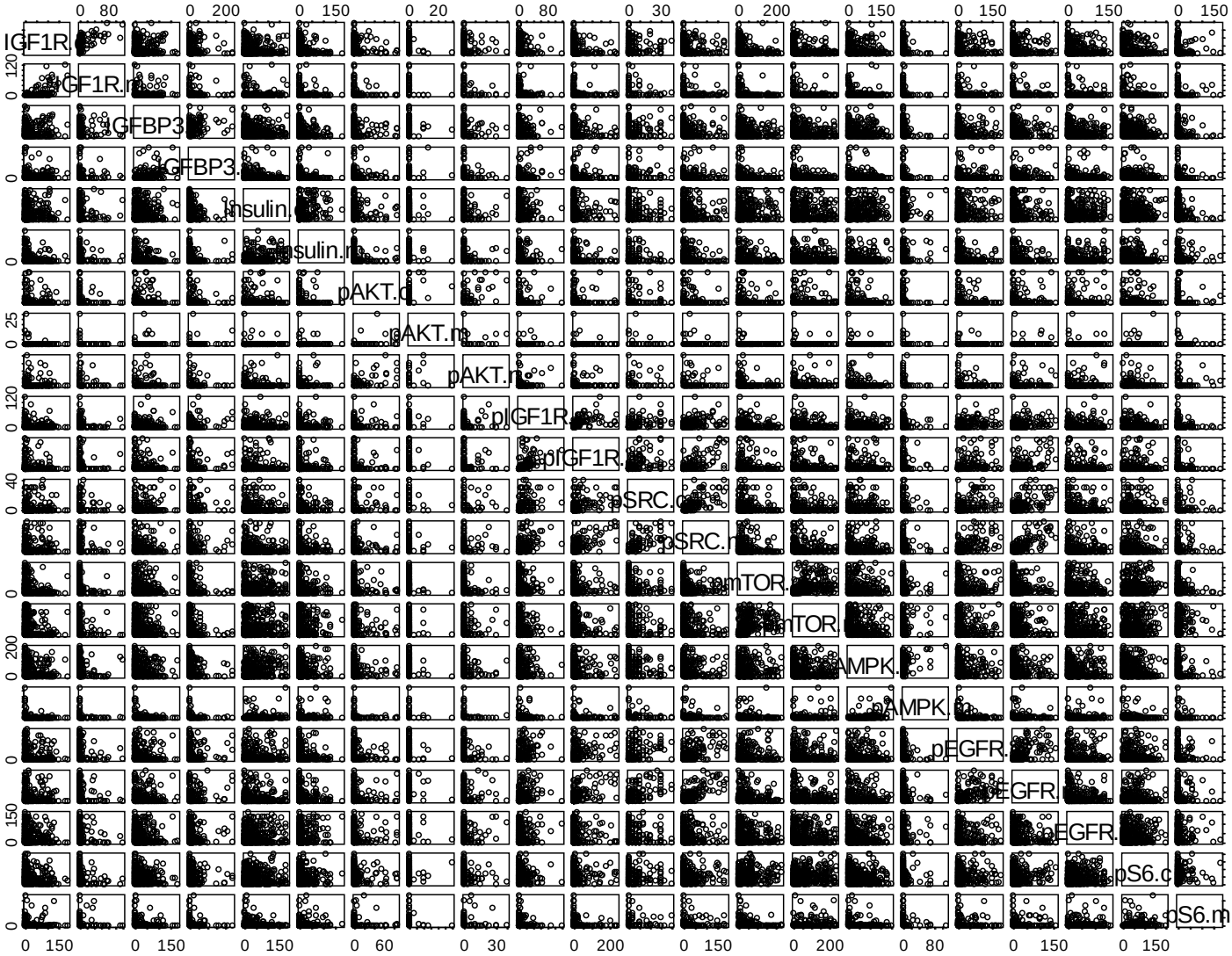

Table 8. Frequency tables for dichotomized markers

covariate	*levels*	*N(%)*	*covariate*	*levels*	*N(%)*
IGF1R_c_01	missing	3	pAMPK_c_01	0	108(29.2%)
	0	157(42.8%)		1	262(70.8%)
	1	210(57.2%)	pAMPK_m_01	0	315(85.1%)
IGF1R_m_01	missing	3		1	55(14.9%)
	0	319(86.9%)	pEGFR_c_01	missing	2

covariate	*levels*	*N(%)*	*covariate*	*levels*	*N(%)*
	1	48(13.1%)		0	209(56.8%)
IGFBP3_c_01	0	118(31.9%)		1	159(43.2%)
	1	252(68.1%)	pEGFR_m_01	missing	1
IGFBP3_m_01	0	245(66.2%)		0	178(48.2%)
	1	125(33.8%)		1	191(51.8%)
Insulin_c_01	missing	3	pEGFR_n_01	missing	1
	0	51(13.9%)		0	107(29%)
	1	316(86.1%)		1	262(71%)
Insulin_m_01	missing	4	pS6_c_01	0	54(14.6%)
	0	212(57.9%)		1	316(85.4%)
	1	154(42.1%)	pS6_m_01	0	297(80.3%)
pAKT_c_01	missing	1		1	73(19.7%)
	0	318(86.2%)	IGF1R_c_01m	Missing	3
	1	51(13.8%)		0	182(49.6%)
pAKT_m_01	0	363(98.1%)		1	185(50.4%)
	1	7(1.9%)	IGFBP3_c_01m	0	172(46.5%)
pAKT_n_01	0	332(89.7%)		1	198(53.5%)
	1	38(10.3%)	Insulin_c_01m	missing	3
pIGF1R_c_01	missing	2		0	179(48.8%)
	0	247(67.1%)		1	188(51.2%)
	1	121(32.9%)	pmTOR_c_01m	missing	1
pIGF1R_m_01	missing	2		0	181(49.1%)
	0	257(69.8%)		1	188(50.9%)
	1	111(30.2%)	pmTOR_m_01m	0	181(48.9%)
pSRC_c_01	missing	1		1	189(51.1%)
	0	268(72.6%)	pEGFR_m_01m	missing	1
	1	101(27.4%)		0	178(48.2%)
pSRC_m_01	0	225(60.8%)		1	191(51.8%)
	1	145(39.2%)	pEGFR_n_01m	missing	1
pmTOR_c_01	missing	1		0	174(47.2%)
	0	91(24.7%)		1	195(52.8%)
	1	278(75.3%)	pS6_c_01m	0	180(48.6%)

covariate	*levels*	*N(%)*	*covariate*	*levels*	*N(%)*
pmTOR_m_01	0	90(24.3%)		1	190(51.4%)
	1	280(75.7%)			

Table 9. Markers by gender

covariate	*Gender*	*n*	*mean ± std, median (min, max)*	*pValue*
IGF1R_c	F	182	17.55 ± 30.6, 3.33 (0, 140)	.0088
	M	185	27.11 ± 40.39, 10 (0, 190)	
IGF1R_m	F	182	2.16 ± 9.41, 0 (0, 66.67)	.0623
	M	185	5.15 ± 17.67, 0 (0, 120)	
IGFBP3_c	F	184	25.79 ± 32.96, 10 (0, 160)	.5033
	M	186	23.44 ± 33.22, 10 (0, 180)	
IGFBP3_m	F	184	13.4 ± 37.42, 0 (0, 240)	.6277
	M	186	9.91 ± 24.24, 0 (0, 196.67)	
Insulin_c	F	182	44.45 ± 47.54, 25.83 (0, 180)	.9066
	M	185	43.78 ± 45.52, 30 (0, 186.67)	
Insulin_m	F	182	13.54 ± 24.19, 0 (0, 115)	.7634
	M	184	15.72 ± 32.07, 0 (0, 180)	
pAKT_c	F	183	4.16 ± 13.46, 0 (0, 83.33)	.3981
	M	186	3.2 ± 12.88, 0 (0, 86.67)	
pAKT_m	F	184	0.34 ± 2.62, 0 (0, 30)	.6791
	M	186	0.11 ± 0.91, 0 (0, 10)	
pAKT_n	F	184	1.16 ± 4.66, 0 (0, 40)	.7469
	M	186	1.05 ± 3.99, 0 (0, 30)	
pAMPK_c	F	184	44.56 ± 51.44, 25.83 (0, 200)	.0997
	M	186	36.42 ± 46.3, 10 (0, 180)	
pAMPK_m	F	184	3.24 ± 13.32, 0 (0, 110)	.5768
	M	186	1.43 ± 6.07, 0 (0, 60)	
pEGFR_c	F	183	22.64 ± 40.73, 0 (0, 190)	.0153
	M	185	15.26 ± 33.6, 0 (0, 166.67)	
pEGFR_m	F	183	18.86 ± 31.8, 3.33 (0, 160)	.0931
	M	186	14.31 ± 28.26, 0 (0, 143.33)	

covariate	*Gender*	*n*	*mean ± std, median (min, max)*	*pValue*
pEGFR_n	F	183	30.73 ± 37.44, 15 (0, 150)	.8814
	M	186	31.74 ± 40.25, 13.33 (0, 160)	
pIGF1R_c	F	183	5.93 ± 13.26, 0 (0, 90)	.4689
	M	185	5.73 ± 13.93, 0 (0, 120)	
pIGF1R_m	F	183	10.18 ± 28.01, 0 (0, 205)	.6528
	M	185	17.31 ± 47.45, 0 (0, 240)	
pS6_c	F	184	47.64 ± 42.23, 40 (0, 180)	.0840
	M	186	41.49 ± 42.64, 30 (0, 200)	
pS6_m	F	184	5.6 ± 15.68, 0 (0, 120)	.3488
	M	186	6.49 ± 24.08, 0 (0, 180)	
pSRC_c	F	184	3.35 ± 7.81, 0 (0, 40)	.8307
	M	185	2.75 ± 6.12, 0 (0, 33.33)	
pSRC_m	F	184	17.57 ± 36.39, 0 (0, 180)	.7911
	M	186	16.91 ± 34.24, 0 (0, 190)	
pmTOR_c	F	183	45.11 ± 54.91, 23.33 (0, 230)	.0014
	M	186	33.22 ± 48.15, 10 (0, 210)	
pmTOR_m	F	184	69.49 ± 69.36, 53.33 (0, 240)	.0019
	M	186	53.63 ± 67.48, 21.67 (0, 240)	

Table 10. Markers by Race

covariate	*Race*	*n*	*mean ± std, median (min, max)*	*pValue*
IGF1R_c	Black	21	30.56 ± 40.83, 10 (0, 120)	.2912
	Hispanic	14	20.48 ± 32.02, 0 (0, 96.67)	
	Oriental	5	18 ± 20.63, 10 (0, 53.33)	
	White	327	21.99 ± 36.24, 6.67 (0, 190)	
IGF1R_m	Black	21	4.6 ± 10.41, 0 (0, 40)	.0941
	Hispanic	14	0 ± 0, 0 (0, 0)	
	Oriental	5	6.67 ± 14.91, 0 (0, 33.33)	
	White	327	3.72 ± 14.75, 0 (0, 120)	
IGFBP3_c	Black	21	15.2 ± 30.61, 2.5 (0, 123.33)	.0670
	Hispanic	14	12.62 ± 16.35, 9.17 (0, 56.67)	

covariate	*Race*	*n*	*mean ± std, median (min, max)*	*pValue*
	Oriental	5	54 ± 47.98, 60 (0, 106.67)	
	White	330	25.27 ± 33.25, 10 (0, 180)	
IGFBP3_m	Black	21	4.13 ± 9.54, 0 (0, 40)	.5420
	Hispanic	14	1.9 ± 3.86, 0 (0, 13.33)	
	Oriental	5	5.33 ± 7.67, 0 (0, 16.67)	
	White	330	12.63 ± 33.12, 0 (0, 240)	
Insulin_c	Black	21	37.7 ± 44.44, 25 (0, 186.67)	.0757
	Hispanic	14	73.93 ± 52.38, 67.5 (10, 165)	
	Oriental	5	28.67 ± 30.97, 10 (0, 70)	
	White	327	43.49 ± 46.23, 30 (0, 180)	
Insulin_m	Black	21	19.76 ± 42.38, 0 (0, 180)	.3724
	Hispanic	14	4.17 ± 9.58, 0 (0, 35)	
	Oriental	5	2 ± 4.47, 0 (0, 10)	
	White	326	14.95 ± 27.98, 0 (0, 130)	
pAKT_c	Black	21	1.19 ± 2.75, 0 (0, 10)	.7927
	Hispanic	14	1.67 ± 4.29, 0 (0, 13.33)	
	Oriental	5	0 ± 0, 0 (0, 0)	
	White	329	3.98 ± 13.87, 0 (0, 86.67)	
pAKT_m	Black	21	0 ± 0, 0 (0, 0)	.8345
	Hispanic	14	0 ± 0, 0 (0, 0)	
	Oriental	5	0 ± 0, 0 (0, 0)	
	White	330	0.25 ± 2.07, 0 (0, 30)	
pAKT_n	Black	21	0.79 ± 2.56, 0 (0, 10)	.5099
	Hispanic	14	0 ± 0, 0 (0, 0)	
	Oriental	5	0 ± 0, 0 (0, 0)	
	White	330	1.19 ± 4.54, 0 (0, 40)	
pAMPK_c	Black	21	43.57 ± 50.51, 20 (0, 160)	.7634
	Hispanic	14	24.88 ± 27.27, 18.33 (0, 80)	
	Oriental	5	43.33 ± 40.69, 53.33 (0, 93.33)	
	White	330	40.88 ± 49.8, 16.67 (0, 200)	
pAMPK_m	Black	21	3.49 ± 15.26, 0 (0, 70)	.7012
	Hispanic	14	0.6 ± 1.55, 0 (0, 5)	

covariate	*Race*	*n*	*mean ± std, median (min, max)*	*pValue*
	Oriental	5	0 ± 0, 0 (0, 0)	
	White	330	2.37 ± 10.28, 0 (0, 110)	
pEGFR_c	Black	20	17.08 ± 36.94, 0 (0, 150)	.3142
	Hispanic	14	14.4 ± 32.37, 0 (0, 120)	
	Oriental	5	0 ± 0, 0 (0, 0)	
	White	329	19.52 ± 37.97, 0 (0, 190)	
pEGFR_m	Black	21	8.33 ± 14.4, 0 (0, 55)	.0718
	Hispanic	14	6.9 ± 12.62, 0 (0, 45)	
	Oriental	5	0 ± 0, 0 (0, 0)	
	White	329	17.76 ± 31.38, 3.33 (0, 160)	
pEGFR_n	Black	21	40.08 ± 43.39, 26.67 (0, 136.67)	.8714
	Hispanic	14	27.2 ± 34.92, 17.08 (0, 116.67)	
	Oriental	5	25.67 ± 24.08, 16.67 (0, 56.67)	
	White	329	30.93 ± 38.93, 13.33 (0, 160)	
pIGF1R_c	Black	21	7.78 ± 14.54, 0 (0, 40)	.8670
	Hispanic	14	2.62 ± 3.5, 0 (0, 10)	
	Oriental	5	1 ± 2.24, 0 (0, 5)	
	White	328	5.91 ± 13.87, 0 (0, 120)	
pIGF1R_m	Black	21	16.03 ± 34.95, 0 (0, 143.33)	.8617
	Hispanic	14	4.29 ± 8.91, 0 (0, 30)	
	Oriental	5	1 ± 2.24, 0 (0, 5)	
	White	328	14.22 ± 40.41, 0 (0, 240)	
pS6_c	Black	21	48.13 ± 43.84, 46.67 (0, 155)	.9868
	Hispanic	14	46.67 ± 49.65, 21.67 (0, 126.67)	
	Oriental	5	56 ± 72.47, 10 (0, 143.33)	
	White	330	44.06 ± 41.75, 33.33 (0, 200)	
pS6_m	Black	21	6.9 ± 26.1, 0 (0, 120)	.3139
	Hispanic	14	0 ± 0, 0 (0, 0)	
	Oriental	5	6.67 ± 14.91, 0 (0, 33.33)	
	White	330	6.24 ± 20.43, 0 (0, 180)	
pSRC_c	Black	21	1.27 ± 3.07, 0 (0, 10)	.0899
	Hispanic	14	0.24 ± 0.89, 0 (0, 3.33)	

covariate	*Race*	*n*	*mean ± std, median (min, max)*	*pValue*
	Oriental	5	0 ± 0, 0 (0, 0)	
	White	329	3.33 ± 7.33, 0 (0, 40)	
pSRC_m	Black	21	12.7 ± 30.78, 0 (0, 115)	.3901
	Hispanic	14	5.6 ± 11.43, 0 (0, 40)	
	Oriental	5	1 ± 2.24, 0 (0, 5)	
	White	330	18.27 ± 36.35, 0 (0, 190)	
pmTOR_c	Black	21	28.33 ± 38.74, 10 (0, 150)	.8374
	Hispanic	14	55.71 ± 65.77, 45 (0, 213.33)	
	Oriental	5	46.67 ± 86.06, 10 (0, 200)	
	White	329	38.98 ± 51.45, 16.67 (0, 230)	
pmTOR_m	Black	21	68.81 ± 74.85, 50 (0, 230)	.4879
	Hispanic	14	33.1 ± 31.52, 37.5 (0, 70)	
	Oriental	5	28.67 ± 30.51, 13.33 (0, 63.33)	
	White	330	62.76 ± 69.72, 36.67 (0, 240)	

Table 10.1. Markers by Smoking Status

covariate	*smoker*	*n*	*mean ± std, median (min, max)*	*pValue*
IGF1R_c	1 Never	38	5.53 ± 8.72, 0 (0, 40)	.0138
	2 Former	168	22.6 ± 35.34, 6.67 (0, 140)	
	3 Current	161	26.1 ± 39.81, 10 (0, 190)	
IGF1R_m	1 Never	38	0.18 ± 1.08, 0 (0, 6.67)	.1261
	2 Former	168	3.13 ± 11.43, 0 (0, 80)	
	3 Current	161	5.05 ± 17.96, 0 (0, 120)	
IGFBP3_c	1 Never	38	19.47 ± 25.54, 8.33 (0, 106.67)	.8088
	2 Former	170	22.73 ± 29.12, 10 (0, 123.33)	
	3 Current	162	27.78 ± 38.03, 10 (0, 180)	
IGFBP3_m	1 Never	38	2.85 ± 7.34, 0 (0, 40)	.0715
	2 Former	170	10.45 ± 30.26, 0 (0, 240)	
	3 Current	162	14.96 ± 35.64, 0 (0, 240)	
Insulin_c	1 Never	38	43.25 ± 47.48, 21.67 (0, 165)	.0876
	2 Former	169	48.13 ± 46.83, 40 (0, 186.67)	

covariate	*smoker*	*n*	*mean ± std, median (min, max)*	*pValue*
	3 Current	160	40.08 ± 45.78, 23.33 (0, 180)	
Insulin_m	1 Never	38	8.64 ± 20.24, 0 (0, 100)	.3680
	2 Former	168	14.98 ± 29.26, 0 (0, 180)	
	3 Current	160	15.71 ± 29.12, 0 (0, 130)	
pAKT_c	1 Never	38	2.11 ± 10.76, 0 (0, 65)	.2861
	2 Former	170	4.01 ± 14.28, 0 (0, 86.67)	
	3 Current	161	3.7 ± 12.47, 0 (0, 86.67)	
pAKT_m	1 Never	38	0 ± 0, 0 (0, 0)	.6018
	2 Former	170	0.31 ± 2.62, 0 (0, 30)	
	3 Current	162	0.19 ± 1.25, 0 (0, 10)	
pAKT_n	1 Never	38	0.83 ± 2.84, 0 (0, 15)	.6878
	2 Former	170	1.03 ± 4.37, 0 (0, 30)	
	3 Current	162	1.25 ± 4.59, 0 (0, 40)	
pAMPK_c	1 Never	38	51.18 ± 52.5, 35.83 (0, 180)	.1287
	2 Former	170	40.08 ± 47.48, 16.67 (0, 200)	
	3 Current	162	38.35 ± 49.77, 10 (0, 186.67)	
pAMPK_m	1 Never	38	3.03 ± 11.87, 0 (0, 70)	.7775
	2 Former	170	2.02 ± 10.55, 0 (0, 110)	
	3 Current	162	2.5 ± 9.81, 0 (0, 70)	
pEGFR_c	1 Never	38	12.81 ± 23.43, 0 (0, 100)	.5448
	2 Former	169	19.81 ± 37.89, 0 (0, 180)	
	3 Current	161	19.45 ± 39.65, 0 (0, 190)	
pEGFR_m	1 Never	38	9.04 ± 21.12, 0 (0, 100)	.0260
	2 Former	170	18.01 ± 30.88, 5 (0, 140)	
	3 Current	161	16.82 ± 30.97, 0 (0, 160)	
pEGFR_n	1 Never	37	25 ± 32.4, 10 (0, 136.67)	.6516
	2 Former	170	30.62 ± 39.48, 13.33 (0, 136.67)	
	3 Current	162	33.31 ± 39.53, 15 (0, 160)	
pIGF1R_c	1 Never	38	2.98 ± 7.93, 0 (0, 40)	.2733
	2 Former	169	5.3 ± 11.19, 0 (0, 65)	
	3 Current	161	7.06 ± 16.53, 0 (0, 120)	
pIGF1R_m	1 Never	38	7.06 ± 25.81, 0 (0, 155)	.5620

covariate	*smoker*	*n*	*mean ± std, median (min, max)*	*pValue*
	2 Former	169	14.41 ± 42.3, 0 (0, 240)	
	3 Current	161	14.67 ± 38.29, 0 (0, 230)	
pS6_c	1 Never	38	48.2 ± 37.85, 43.33 (0, 126.67)	.3319
	2 Former	170	43.61 ± 45.7, 30 (0, 200)	
	3 Current	162	44.69 ± 40.15, 35.83 (0, 200)	
pS6_m	1 Never	38	2.41 ± 7.95, 0 (0, 45)	.3852
	2 Former	170	6.31 ± 22.66, 0 (0, 180)	
	3 Current	162	6.62 ± 19.72, 0 (0, 145)	
pSRC_c	1 Never	38	0.7 ± 3.3, 0 (0, 20)	.0068
	2 Former	169	3.14 ± 6.21, 0 (0, 33.33)	
	3 Current	162	3.51 ± 8.25, 0 (0, 40)	
pSRC_m	1 Never	38	7.06 ± 22.57, 0 (0, 120)	.0356
	2 Former	170	18.19 ± 35.15, 0 (0, 180)	
	3 Current	162	18.63 ± 37.57, 0 (0, 190)	
pmTOR_c	1 Never	38	83.66 ± 71.32, 70 (0, 230)	<.0001
	2 Former	169	32.58 ± 43.49, 13.33 (0, 210)	
	3 Current	162	35.48 ± 49.85, 13.33 (0, 230)	
pmTOR_m	1 Never	38	96.47 ± 69.99, 86.25 (0, 230)	.0003
	2 Former	170	62.72 ± 70.83, 36.67 (0, 240)	
	3 Current	162	52.06 ± 63.82, 23.33 (0, 230)	

Table 11. Markers by Histology

covariate	*histology0*	*n*	*mean ± std, median (min, max)*	*pValue*
IGF1R_c	ADENO	226	8.49 ± 21.54, 0 (0, 190)	<.0001
	Other	17	20.2 ± 31.07, 5 (0, 95)	
	SCC	124	47.96 ± 43.56, 33.33 (0, 180)	
IGF1R_m	ADENO	226	0.84 ± 6.31, 0 (0, 76.67)	<.0001
	Other	17	0.78 ± 1.87, 0 (0, 6.67)	
	SCC	124	9.22 ± 21.99, 0 (0, 120)	
IGFBP3_c	ADENO	227	23.85 ± 30.45, 10 (0, 170)	.0099
	Other	17	6.47 ± 15.34, 0 (0, 63.33)	

covariate	*histology0*	*n*	*mean ± std, median (min, max)*	*pValue*
	SCC	126	28.41 ± 38.22, 10 (0, 180)	
IGFBP3_m	ADENO	227	6.72 ± 18.75, 0 (0, 196.67)	.0001
	Other	17	3.53 ± 14.55, 0 (0, 60)	
	SCC	126	21.61 ± 45.97, 0 (0, 240)	
Insulin_c	ADENO	226	50.83 ± 50.4, 33.33 (0, 186.67)	.0053
	Other	17	40 ± 39.02, 30 (0, 120)	
	SCC	124	32.45 ± 36.88, 20 (0, 170)	
Insulin_m	ADENO	225	16.98 ± 31.06, 0 (0, 180)	.1205
	Other	17	11.96 ± 22.49, 0 (0, 85)	
	SCC	124	10.77 ± 23.37, 0 (0, 130)	
pAKT_c	ADENO	226	3.13 ± 13.09, 0 (0, 86.67)	.0447
	Other	17	2.55 ± 7.02, 0 (0, 26.67)	
	SCC	126	4.81 ± 13.91, 0 (0, 86.67)	
pAKT_m	ADENO	227	0.09 ± 0.94, 0 (0, 10)	.1058
	Other	17	0 ± 0, 0 (0, 0)	
	SCC	126	0.5 ± 3.1, 0 (0, 30)	
pAKT_n	ADENO	227	0.82 ± 4.07, 0 (0, 40)	.1495
	Other	17	2.35 ± 7.52, 0 (0, 30)	
	SCC	126	1.44 ± 4.22, 0 (0, 23.33)	
pAMPK_c	ADENO	227	41.11 ± 51.47, 16.67 (0, 200)	.6716
	Other	17	46.08 ± 46.74, 33.33 (0, 140)	
	SCC	126	38.54 ± 44.9, 15.83 (0, 160)	
pAMPK_m	ADENO	227	3.1 ± 12.75, 0 (0, 110)	.5209
	Other	17	0.29 ± 1.21, 0 (0, 5)	
	SCC	126	1.23 ± 4.43, 0 (0, 43.33)	
pEGFR_c	ADENO	226	13.72 ± 31.78, 0 (0, 170)	.0002
	Other	17	17.16 ± 43.98, 0 (0, 180)	
	SCC	125	28.6 ± 43.86, 6.67 (0, 190)	
pEGFR_m	ADENO	226	12.12 ± 23.58, 0 (0, 140)	.0005
	Other	17	11.18 ± 24.06, 0 (0, 90)	
	SCC	126	25.28 ± 38.45, 6.67 (0, 160)	
pEGFR_n	ADENO	226	31.56 ± 39.55, 13.33 (0, 150)	.6955

covariate	*histology0*	*n*	*mean ± std, median (min, max)*	*pValue*
	Other	17	34.9 ± 34.9, 20 (0, 103.33)	
	SCC	126	30.17 ± 38.28, 14.17 (0, 160)	
pIGF1R_c	ADENO	226	4.56 ± 12.64, 0 (0, 120)	.0007
	Other	17	4.12 ± 10.64, 0 (0, 40)	
	SCC	125	8.35 ± 15.22, 0 (0, 90)	
pIGF1R_m	ADENO	226	9.49 ± 32.56, 0 (0, 240)	.0220
	Other	17	16.86 ± 46.91, 0 (0, 160)	
	SCC	125	21.07 ± 47.27, 0 (0, 240)	
pS6_c	ADENO	227	49.68 ± 42.89, 40 (0, 200)	.0007
	Other	17	43.73 ± 42.62, 35 (0, 143.33)	
	SCC	126	35.42 ± 40.49, 25 (0, 155)	
pS6_m	ADENO	227	6.12 ± 17.82, 0 (0, 150)	.1589
	Other	17	2.06 ± 7.3, 0 (0, 30)	
	SCC	126	6.44 ± 25.2, 0 (0, 180)	
pSRC_c	ADENO	226	1.63 ± 4.51, 0 (0, 30)	<.0001
	Other	17	1.86 ± 3.81, 0 (0, 13.33)	
	SCC	126	5.75 ± 9.74, 0 (0, 40)	
pSRC_m	ADENO	227	9.93 ± 24.41, 0 (0, 160)	<.0001
	Other	17	12.06 ± 25.34, 0 (0, 90)	
	SCC	126	31.11 ± 47.12, 6.67 (0, 190)	
pmTOR_c	ADENO	227	53.53 ± 55.98, 35 (0, 230)	<.0001
	Other	17	48.92 ± 69.33, 13.33 (0, 200)	
	SCC	125	11.61 ± 22.41, 3.33 (0, 110)	
pmTOR_m	ADENO	227	87.12 ± 69.99, 66.67 (0, 240)	<.0001
	Other	17	63.73 ± 74.59, 25 (0, 240)	
	SCC	126	15.09 ± 32.2, 0 (0, 180)	

Table 12. Marker by stage

covariate	*PathStage*	*n*	*mean ± std, median (min, max)*	*pValue*
IGF1R_c	IA	102	22.14 ± 39.2, 3.33 (0, 190)	.5720
	IB	130	20.54 ± 33.45, 6.67 (0, 140)	
	IIA	21	31.19 ± 44.61, 16.67 (0, 180)	
	IIB	53	23.9 ± 34.78, 10 (0, 130)	
	IIIA	61	22.28 ± 35.04, 3.33 (0, 150)	
IGF1R_m	IA	102	3.17 ± 13.61, 0 (0, 80)	.1912
	IB	130	2.13 ± 8.39, 0 (0, 56.67)	
	IIA	21	12.06 ± 34.87, 0 (0, 120)	
	IIB	53	4.21 ± 14.5, 0 (0, 70)	
	IIIA	61	4.43 ± 12.48, 0 (0, 66.67)	
IGFBP3_c	IA	103	20.19 ± 28.61, 6.67 (0, 120)	.1203
	IB	131	27.97 ± 35.66, 10 (0, 160)	
	IIA	22	17.2 ± 17.16, 10 (0, 56.67)	
	IIB	53	24.27 ± 42.09, 3.33 (0, 180)	
	IIIA	61	27.8 ± 29.15, 16.67 (0, 100)	
IGFBP3_m	IA	103	8.22 ± 28.37, 0 (0, 240)	.0463
	IB	131	16.64 ± 40.99, 0 (0, 240)	
	IIA	22	7.12 ± 13.27, 1.67 (0, 60)	
	IIB	53	8.81 ± 26.74, 0 (0, 163.33)	
	IIIA	61	10.79 ± 17.99, 0 (0, 60)	
Insulin_c	IA	100	46.23 ± 48.13, 30 (0, 180)	.2914
	IB	131	45.2 ± 47.1, 30 (0, 186.67)	
	IIA	22	62.05 ± 59.44, 38.33 (0, 180)	
	IIB	53	33.18 ± 36.53, 23.33 (0, 150)	
	IIIA	61	41.34 ± 43.72, 26.67 (0, 180)	
Insulin_m	IA	99	13.28 ± 24.12, 0 (0, 110)	.6856
	IB	131	14.16 ± 27.75, 0 (0, 130)	
	IIA	22	11.44 ± 17.55, 1.67 (0, 60)	
	IIB	53	15.85 ± 36.8, 0 (0, 180)	
	IIIA	61	17.98 ± 31.44, 0 (0, 120)	
pAKT_c	IA	102	3.12 ± 12.3, 0 (0, 83.33)	.0324

covariate	*PathStage*	*n*	*mean ± std, median (min, max)*	*pValue*
	IB	131	5.23 ± 15.6, 0 (0, 86.67)	
	IIA	22	0 ± 0, 0 (0, 0)	
	IIB	53	2.52 ± 13.2, 0 (0, 86.67)	
	IIIA	61	3.61 ± 10.86, 0 (0, 65)	
pAKT_m	IA	103	0.16 ± 1.35, 0 (0, 13.33)	.6326
	IB	131	0.46 ± 3, 0 (0, 30)	
	IIA	22	0 ± 0, 0 (0, 0)	
	IIB	53	0.13 ± 0.92, 0 (0, 6.67)	
	IIIA	61	0 ± 0, 0 (0, 0)	
pAKT_n	IA	103	0.7 ± 2.51, 0 (0, 16.67)	.5173
	IB	131	1.5 ± 5.69, 0 (0, 40)	
	IIA	22	0 ± 0, 0 (0, 0)	
	IIB	53	1.07 ± 3.74, 0 (0, 20)	
	IIIA	61	1.37 ± 4.62, 0 (0, 26.67)	
pAMPK_c	IA	103	46.57 ± 56.15, 16.67 (0, 200)	.5691
	IB	131	41.49 ± 46.37, 30 (0, 186.67)	
	IIA	22	41.59 ± 49.14, 26.67 (0, 160)	
	IIB	53	33.08 ± 42.75, 10 (0, 145)	
	IIIA	61	33.96 ± 46.64, 6.67 (0, 180)	
pAMPK_m	IA	103	3.75 ± 15.91, 0 (0, 110)	.6270
	IB	131	2.19 ± 7.95, 0 (0, 63.33)	
	IIA	22	0.3 ± 0.98, 0 (0, 3.33)	
	IIB	53	1.7 ± 5.18, 0 (0, 25)	
	IIIA	61	1.53 ± 7.93, 0 (0, 60)	
pEGFR_c	IA	103	20.79 ± 41.86, 0 (0, 190)	.9401
	IB	131	20.33 ± 38.81, 0 (0, 180)	
	IIA	22	19.7 ± 39.46, 0 (0, 150)	
	IIB	52	16.51 ± 34.21, 0 (0, 130)	
	IIIA	60	14.5 ± 27.79, 0 (0, 120)	
pEGFR_m	IA	103	16.49 ± 30.59, 3.33 (0, 160)	.4141
	IB	131	18.38 ± 32, 3.33 (0, 140)	
	IIA	22	9.77 ± 24.46, 0 (0, 100)	

covariate	*PathStage*	*n*	*mean ± std, median (min, max)*	*pValue*
	IIB	52	15.1 ± 30.33, 3.33 (0, 143.33)	
	IIIA	61	16.5 ± 27.1, 6.67 (0, 130)	
pEGFR_n	IA	103	28.29 ± 38.02, 10 (0, 150)	.2147
	IB	130	31.79 ± 37.67, 15 (0, 160)	
	IIA	22	20.08 ± 28.53, 3.33 (0, 90)	
	IIB	53	39.97 ± 43.66, 25 (0, 136.67)	
	IIIA	61	31.46 ± 40.92, 15 (0, 136.67)	
pIGF1R_c	IA	101	5.43 ± 12.33, 0 (0, 65)	.8486
	IB	131	7.23 ± 17.01, 0 (0, 120)	
	IIA	22	5.91 ± 9.42, 0 (0, 33.33)	
	IIB	53	4.59 ± 9.99, 0 (0, 43.33)	
	IIIA	61	4.54 ± 11.07, 0 (0, 65)	
pIGF1R_m	IA	101	10.38 ± 35.24, 0 (0, 240)	.4719
	IB	131	14.95 ± 41.21, 0 (0, 230)	
	IIA	22	28.03 ± 56.55, 0 (0, 210)	
	IIB	53	17.83 ± 47, 0 (0, 240)	
	IIIA	61	8.14 ± 20.91, 0 (0, 120)	
pS6_c	IA	103	46.59 ± 47.78, 25 (0, 200)	.4861
	IB	131	44.26 ± 38.7, 36.67 (0, 143.33)	
	IIA	22	29.47 ± 34.05, 18.33 (0, 126.67)	
	IIB	53	48.49 ± 49.01, 35 (0, 200)	
	IIIA	61	43.77 ± 37.22, 40 (0, 153.33)	
pS6_m	IA	103	5.79 ± 22.76, 0 (0, 150)	.4219
	IB	131	5.7 ± 20.27, 0 (0, 180)	
	IIA	22	1.52 ± 5.32, 0 (0, 23.33)	
	IIB	53	5.88 ± 14.06, 0 (0, 60)	
	IIIA	61	8.99 ± 23.87, 0 (0, 120)	
pSRC_c	IA	103	2.72 ± 6.48, 0 (0, 33.33)	.5796
	IB	130	3.63 ± 7.69, 0 (0, 40)	
	IIA	22	3.33 ± 9.32, 0 (0, 40)	
	IIB	53	2.96 ± 6.94, 0 (0, 30)	
	IIIA	61	2.35 ± 5.41, 0 (0, 30)	

covariate	*PathStage*	*n*	*mean ± std, median (min, max)*	*pValue*
pSRC_m	IA	103	15.08 ± 30.14, 0 (0, 145)	.9180
	IB	131	20.8 ± 42.13, 0 (0, 190)	
	IIA	22	18.64 ± 41.45, 0 (0, 180)	
	IIB	53	15.19 ± 31.71, 0 (0, 160)	
	IIIA	61	14.51 ± 27.27, 0 (0, 130)	
pmTOR_c	IA	103	40.73 ± 47.98, 30 (0, 210)	.1905
	IB	131	40.35 ± 53.77, 20 (0, 230)	
	IIA	22	46.29 ± 70.54, 7.5 (0, 230)	
	IIB	52	25.96 ± 37.76, 6.67 (0, 160)	
	IIIA	61	42.38 ± 56.5, 15 (0, 200)	
pmTOR_m	IA	103	68.54 ± 71.87, 55 (0, 240)	.1051
	IB	131	63.57 ± 69.76, 40 (0, 240)	
	IIA	22	54.62 ± 73.73, 5 (0, 226.67)	
	IIB	53	47.11 ± 62.01, 13.33 (0, 230)	
	IIIA	61	60.25 ± 65.16, 35 (0, 230)	

covariate	*stage*	*n*	*mean ± std, median (min, max)*	*pValue*
IGF1R_c	I	232	21.24 ± 36.02, 5 (0, 190)	.3655
	II	74	25.97 ± 37.65, 10 (0, 180)	
	IIIA	61	22.28 ± 35.04, 3.33 (0, 150)	
IGF1R_m	I	232	2.59 ± 10.98, 0 (0, 80)	.1064
	II	74	6.44 ± 22.26, 0 (0, 120)	
	IIIA	61	4.43 ± 12.48, 0 (0, 66.67)	
IGFBP3_c	I	234	24.54 ± 32.91, 10 (0, 160)	.1301
	II	75	22.2 ± 36.59, 6.67 (0, 180)	
	IIIA	61	27.8 ± 29.15, 16.67 (0, 100)	
IGFBP3_m	I	234	12.93 ± 36.16, 0 (0, 240)	.2910
	II	75	8.31 ± 23.52, 0 (0, 163.33)	
	IIIA	61	10.79 ± 17.99, 0 (0, 60)	
Insulin_c	I	231	45.65 ± 47.45, 30 (0, 186.67)	.6956

covariate	*stage*	*n*	*mean ± std, median (min, max)*	*pValue*
	II	75	41.64 ± 45.99, 26.67 (0, 180)	
	IIIA	61	41.34 ± 43.72, 26.67 (0, 180)	
Insulin_m	I	230	13.78 ± 26.2, 0 (0, 130)	.5161
	II	75	14.56 ± 32.3, 0 (0, 180)	
	IIIA	61	17.98 ± 31.44, 0 (0, 120)	
pAKT_c	I	233	4.31 ± 14.26, 0 (0, 86.67)	.0187
	II	75	1.78 ± 11.13, 0 (0, 86.67)	
	IIIA	61	3.61 ± 10.86, 0 (0, 65)	
pAKT_m	I	234	0.33 ± 2.42, 0 (0, 30)	.3904
	II	75	0.09 ± 0.77, 0 (0, 6.67)	
	IIIA	61	0 ± 0, 0 (0, 0)	
pAKT_n	I	234	1.15 ± 4.58, 0 (0, 40)	.5370
	II	75	0.76 ± 3.18, 0 (0, 20)	
	IIIA	61	1.37 ± 4.62, 0 (0, 26.67)	
pAMPK_c	I	234	43.73 ± 50.85, 20 (0, 200)	.2845
	II	75	35.58 ± 44.55, 13.33 (0, 160)	
	IIIA	61	33.96 ± 46.64, 6.67 (0, 180)	
pAMPK_m	I	234	2.88 ± 12.11, 0 (0, 110)	.4512
	II	75	1.29 ± 4.42, 0 (0, 25)	
	IIIA	61	1.53 ± 7.93, 0 (0, 60)	
pEGFR_c	I	234	20.53 ± 40.1, 0 (0, 190)	.6924
	II	74	17.45 ± 35.6, 0 (0, 150)	
	IIIA	60	14.5 ± 27.79, 0 (0, 120)	
pEGFR_m	I	234	17.55 ± 31.34, 3.33 (0, 160)	.4237
	II	74	13.51 ± 28.65, 0 (0, 143.33)	
	IIIA	61	16.5 ± 27.1, 6.67 (0, 130)	
pEGFR_n	I	233	30.25 ± 37.79, 13.33 (0, 160)	.7972
	II	75	34.13 ± 40.67, 15 (0, 136.67)	
	IIIA	61	31.46 ± 40.92, 15 (0, 136.67)	
pIGF1R_c	I	232	6.44 ± 15.15, 0 (0, 120)	.8466
	II	75	4.98 ± 9.78, 0 (0, 43.33)	
	IIIA	61	4.54 ± 11.07, 0 (0, 65)	

covariate	*stage*	*n*	*mean ± std, median (min, max)*	*pValue*
pIGF1R_m	I	232	12.96 ± 38.71, 0 (0, 240)	.7211
	II	75	20.82 ± 49.81, 0 (0, 240)	
	IIIA	61	8.14 ± 20.91, 0 (0, 120)	
pS6_c	I	234	45.28 ± 42.85, 33.33 (0, 200)	.6571
	II	75	42.91 ± 45.74, 30 (0, 200)	
	IIIA	61	43.77 ± 37.22, 40 (0, 153.33)	
pS6_m	I	234	5.74 ± 21.35, 0 (0, 180)	.4846
	II	75	4.6 ± 12.29, 0 (0, 60)	
	IIIA	61	8.99 ± 23.87, 0 (0, 120)	
pSRC_c	I	233	3.23 ± 7.18, 0 (0, 40)	.6189
	II	75	3.07 ± 7.65, 0 (0, 40)	
	IIIA	61	2.35 ± 5.41, 0 (0, 30)	
pSRC_m	I	234	18.28 ± 37.36, 0 (0, 190)	.7722
	II	75	16.2 ± 34.6, 0 (0, 180)	
	IIIA	61	14.51 ± 27.27, 0 (0, 130)	
pmTOR_c	I	234	40.52 ± 51.2, 21.67 (0, 230)	.0625
	II	74	32 ± 50.15, 6.67 (0, 230)	
	IIIA	61	42.38 ± 56.5, 15 (0, 200)	
pmTOR_m	I	234	65.76 ± 70.59, 45 (0, 240)	.0269
	II	75	49.31 ± 65.24, 10 (0, 230)	
	IIIA	61	60.25 ± 65.16, 35 (0, 230)	

Table 13. Marker by Grade

covariate	*grade0*	*n*	*mean ± std, median (min, max)*	*pValue*
IGF1R_c	1 Poorly	122	19.54 ± 33.95, 5.83 (0, 150)	.0002
	2 Moderately	196	26.47 ± 37.61, 10 (0, 180)	
	3 Well	36	9.12 ± 32.83, 0 (0, 190)	
IGF1R_m	1 Poorly	122	2.62 ± 9.26, 0 (0, 60)	.1748
	2 Moderately	196	4.8 ± 17.18, 0 (0, 120)	
	3 Well	36	2.13 ± 12.78, 0 (0, 76.67)	
IGFBP3_c	1 Poorly	122	26.17 ± 34.9, 10 (0, 170)	.8743

covariate	*grade0*	*n*	*mean ± std, median (min, max)*	*pValue*
	2 Moderately	199	25.15 ± 33.2, 10 (0, 180)	
	3 Well	36	22.41 ± 29.26, 6.67 (0, 116.67)	
IGFBP3_m	1 Poorly	122	16.08 ± 43.48, 0 (0, 240)	.3839
	2 Moderately	199	10.44 ± 24.95, 0 (0, 193.33)	
	3 Well	36	5.83 ± 13.41, 0 (0, 60)	
Insulin_c	1 Poorly	121	47.19 ± 47.34, 33.33 (0, 180)	.6229
	2 Moderately	197	43.17 ± 47.77, 25 (0, 186.67)	
	3 Well	36	39.4 ± 37.58, 28.33 (0, 123.33)	
Insulin_m	1 Poorly	121	21.35 ± 32.89, 0 (0, 120)	.0111
	2 Moderately	196	12.67 ± 27.3, 0 (0, 180)	
	3 Well	36	3.43 ± 6.51, 0 (0, 30)	
pAKT_c	1 Poorly	121	3.15 ± 10.32, 0 (0, 65)	.6710
	2 Moderately	199	3.98 ± 14.34, 0 (0, 86.67)	
	3 Well	36	4.26 ± 16.51, 0 (0, 83.33)	
pAKT_m	1 Poorly	122	0.11 ± 1.21, 0 (0, 13.33)	.2640
	2 Moderately	199	0.35 ± 2.49, 0 (0, 30)	
	3 Well	36	0 ± 0, 0 (0, 0)	
pAKT_n	1 Poorly	122	0.75 ± 3.25, 0 (0, 26.67)	.5510
	2 Moderately	199	1.31 ± 4.82, 0 (0, 40)	
	3 Well	36	0.46 ± 1.62, 0 (0, 6.67)	
pAMPK_c	1 Poorly	122	47.61 ± 53.83, 20 (0, 186.67)	.1009
	2 Moderately	199	34.9 ± 45.52, 10 (0, 200)	
	3 Well	36	48.1 ± 50.69, 35 (0, 175)	
pAMPK_m	1 Poorly	122	3.5 ± 12.11, 0 (0, 70)	.1176
	2 Moderately	199	1.95 ± 10.24, 0 (0, 110)	
	3 Well	36	1.34 ± 4.69, 0 (0, 20)	
pEGFR_c	1 Poorly	121	22.62 ± 42.61, 0 (0, 170)	.0983
	2 Moderately	198	18.62 ± 35.6, 0 (0, 190)	
	3 Well	36	7.82 ± 17.72, 0 (0, 70)	
pEGFR_m	1 Poorly	121	16.83 ± 29.5, 3.33 (0, 140)	.0139
	2 Moderately	199	18.24 ± 31.64, 3.33 (0, 160)	
	3 Well	36	7.78 ± 23.16, 0 (0, 120)	

covariate	*grade0*	*n*	*mean ± std, median (min, max)*	*pValue*
pEGFR_n	1 Poorly	122	38.74 ± 41.99, 20 (0, 160)	.0144
	2 Moderately	199	27.37 ± 37.14, 10 (0, 150)	
	3 Well	35	28.69 ± 37.57, 6.67 (0, 123.33)	
pIGF1R_c	1 Poorly	121	6.74 ± 15.96, 0 (0, 120)	.1089
	2 Moderately	198	6.18 ± 13.17, 0 (0, 90)	
	3 Well	36	1.57 ± 4.1, 0 (0, 20)	
pIGF1R_m	1 Poorly	121	14.02 ± 38.38, 0 (0, 240)	.4286
	2 Moderately	198	15.76 ± 43.04, 0 (0, 240)	
	3 Well	36	3.38 ± 7.69, 0 (0, 30)	
pS6_c	1 Poorly	122	44 ± 42.96, 34.17 (0, 200)	.0795
	2 Moderately	199	42.44 ± 41.63, 30 (0, 155)	
	3 Well	36	56.39 ± 43.22, 50 (3.33, 180)	
pS6_m	1 Poorly	122	6.43 ± 18.65, 0 (0, 120)	.3905
	2 Moderately	199	6.62 ± 23.08, 0 (0, 180)	
	3 Well	36	2.5 ± 9.61, 0 (0, 53.33)	
pSRC_c	1 Poorly	122	3.28 ± 7.02, 0 (0, 40)	.0360
	2 Moderately	198	3.28 ± 7.31, 0 (0, 40)	
	3 Well	36	1.57 ± 6.25, 0 (0, 30)	
pSRC_m	1 Poorly	122	20.18 ± 37.08, 0 (0, 180)	.0002
	2 Moderately	199	18.65 ± 37.05, 0 (0, 190)	
	3 Well	36	1.85 ± 8.49, 0 (0, 50)	
pmTOR_c	1 Poorly	121	31.07 ± 39.04, 13.33 (0, 170)	<.0001
	2 Moderately	199	34.62 ± 48.23, 10 (0, 230)	
	3 Well	36	83.89 ± 73.54, 60 (0, 230)	
pmTOR_m	1 Poorly	122	56.5 ± 65.85, 28.33 (0, 240)	.0043
	2 Moderately	199	57.97 ± 68.48, 30 (0, 240)	
	3 Well	36	93.33 ± 70.37, 67.5 (0, 230)	

2.2 Overall survival

Table 14. Univariate Cox model assessing effect of covariates on overall survival

covariate	*Estimate*	*StdErr*	*HazardRatio*	*HRLowerCL*	*HRUpperCL*	*pValue*	*Total*	*Event*	*Censored*
IGF1R_c	0.0026	0.0020	1.0026	0.9987	1.0066	0.1886	367	157	210
IGF1R_c_01	0.3260	0.1663	1.3855	1.0002	1.9192	0.0499	367	157	210
IGF1R_c_01m	0.2856	0.1613	1.3306	0.9699	1.8253	0.0766	367	157	210
IGF1R_m	0.0019	0.0049	1.0019	0.9923	1.0115	0.7007	367	157	210
IGF1R_m_01	0.3614	0.2149	1.4353	0.9419	2.1871	0.0926	367	157	210
IGFBP3_c	0.0003	0.0024	1.0003	0.9955	1.0050	0.9082	370	160	210
IGFBP3_c_01	0.1027	0.1729	1.1081	0.7897	1.5550	0.5525	370	160	210
IGFBP3_c_01m	0.0588	0.1589	1.0605	0.7767	1.4480	0.7115	370	160	210
IGFBP3_m	0.0005	0.0026	1.0005	0.9954	1.0057	0.8347	370	160	210
IGFBP3_m_01	0.1080	0.1648	1.1140	0.8065	1.5388	0.5122	370	160	210
Insulin_c	0.0016	0.0017	1.0016	0.9983	1.0049	0.3366	367	160	207
Insulin_c_01	-0.3352	0.2115	0.7152	0.4725	1.0826	0.1130	367	160	207
Insulin_c_01m	0.1229	0.1586	1.1307	0.8286	1.5430	0.4386	367	160	207
Insulin_m	0.0044	0.0026	1.0044	0.9993	1.0096	0.0915	366	160	206
Insulin_m_01	0.2329	0.1588	1.2622	0.9246	1.7231	0.1426	366	160	206
pAKT_c	-0.0008	0.0059	0.9992	0.9877	1.0108	0.8865	369	159	210
pAKT_c_01	0.2679	0.2101	1.3073	0.8659	1.9735	0.2023	369	159	210
pAKT_m	-0.0164	0.0420	0.9837	0.9059	1.0682	0.6958	370	160	210
pAKT_m_01	-0.8438	0.7144	0.4301	0.1060	1.7444	0.2375	370	160	210
pAKT_n	-0.0070	0.0169	0.9931	0.9607	1.0264	0.6794	370	160	210
pAKT_n_01	0.2613	0.2354	1.2986	0.8187	2.0598	0.2669	370	160	210
pAMPK_c	-0.0032	0.0017	0.9968	0.9934	1.0002	0.0627	370	160	210
pAMPK_c_01	-0.3682	0.1659	0.6920	0.4999	0.9579	0.0265	370	160	210
pAMPK_m	0.0003	0.0077	1.0003	0.9853	1.0155	0.9732	370	160	210
pAMPK_m_01	-0.1535	0.2297	0.8577	0.5468	1.3456	0.5042	370	160	210
pEGFR_c	-0.0003	0.0023	0.9997	0.9953	1.0041	0.8865	368	158	210
pEGFR_c_01	-0.0092	0.1609	0.9908	0.7228	1.3582	0.9543	368	158	210
pEGFR_m	-0.0003	0.0027	0.9997	0.9944	1.0049	0.8967	369	159	210
pEGFR_m_01	-0.0165	0.1589	0.9836	0.7204	1.3430	0.9172	369	159	210

covariate	*Estimate*	*StdErr*	*HazardRatio*	*HRLowerCL*	*HRUpperCL*	*pValue*	*Total*	*Event*	*Censored*
pEGFR_m_01m	-0.0165	0.1589	0.9836	0.7204	1.3430	0.9172	369	159	210
pEGFR_n	0.0002	0.0021	1.0002	0.9961	1.0042	0.9394	369	160	209
pEGFR_n_01	-0.1673	0.1700	0.8460	0.6062	1.1805	0.3252	369	160	209
pEGFR_n_01m	-0.0199	0.1586	0.9803	0.7184	1.3377	0.9001	369	160	209
pIGF1R_c	-0.0027	0.0064	0.9973	0.9848	1.0099	0.6690	368	160	208
pIGF1R_c_01	0.0946	0.1681	1.0993	0.7906	1.5284	0.5735	368	160	208
pIGF1R_m	-0.0020	0.0024	0.9980	0.9933	1.0027	0.4052	368	160	208
pIGF1R_m_01	-0.0056	0.1752	0.9944	0.7055	1.4017	0.9744	368	160	208
pS6_c	-0.0003	0.0018	0.9997	0.9961	1.0033	0.8723	370	160	210
pS6_c_01	0.0114	0.2257	1.0115	0.6499	1.5742	0.9598	370	160	210
pS6_c_01m	-0.0543	0.1583	0.9472	0.6944	1.2918	0.7317	370	160	210
pS6_m	0.0020	0.0034	1.0020	0.9954	1.0086	0.5596	370	160	210
pS6_m_01	0.0711	0.1924	1.0737	0.7364	1.5654	0.7118	370	160	210
pSRC_c	0.0121	0.0102	1.0121	0.9922	1.0325	0.2356	369	160	209
pSRC_c_01	0.2116	0.1717	1.2357	0.8825	1.7301	0.2179	369	160	209
pSRC_m	0.0009	0.0022	1.0009	0.9966	1.0053	0.6719	370	160	210
pSRC_m_01	0.1656	0.1610	1.1801	0.8608	1.6179	0.3035	370	160	210
pmTOR_c	-0.0020	0.0017	0.9980	0.9946	1.0014	0.2392	369	160	209
pmTOR_c_01	-0.4985	0.1708	0.6075	0.4347	0.8489	0.0035	369	160	209
pmTOR_c_01m	-0.3043	0.1589	0.7376	0.5402	1.0071	0.0554	369	160	209
pmTOR_m	-0.0016	0.0012	0.9984	0.9960	1.0007	0.1678	370	160	210
pmTOR_m_01	-0.1991	0.1798	0.8195	0.5761	1.1657	0.2682	370	160	210
pmTOR_m_01m	-0.2709	0.1584	0.7627	0.5591	1.0405	0.0873	370	160	210

Figure 3. Martingale residual from Cox model with age, gender, histology and stage for overall survival against each marker, Dr. HY Lee

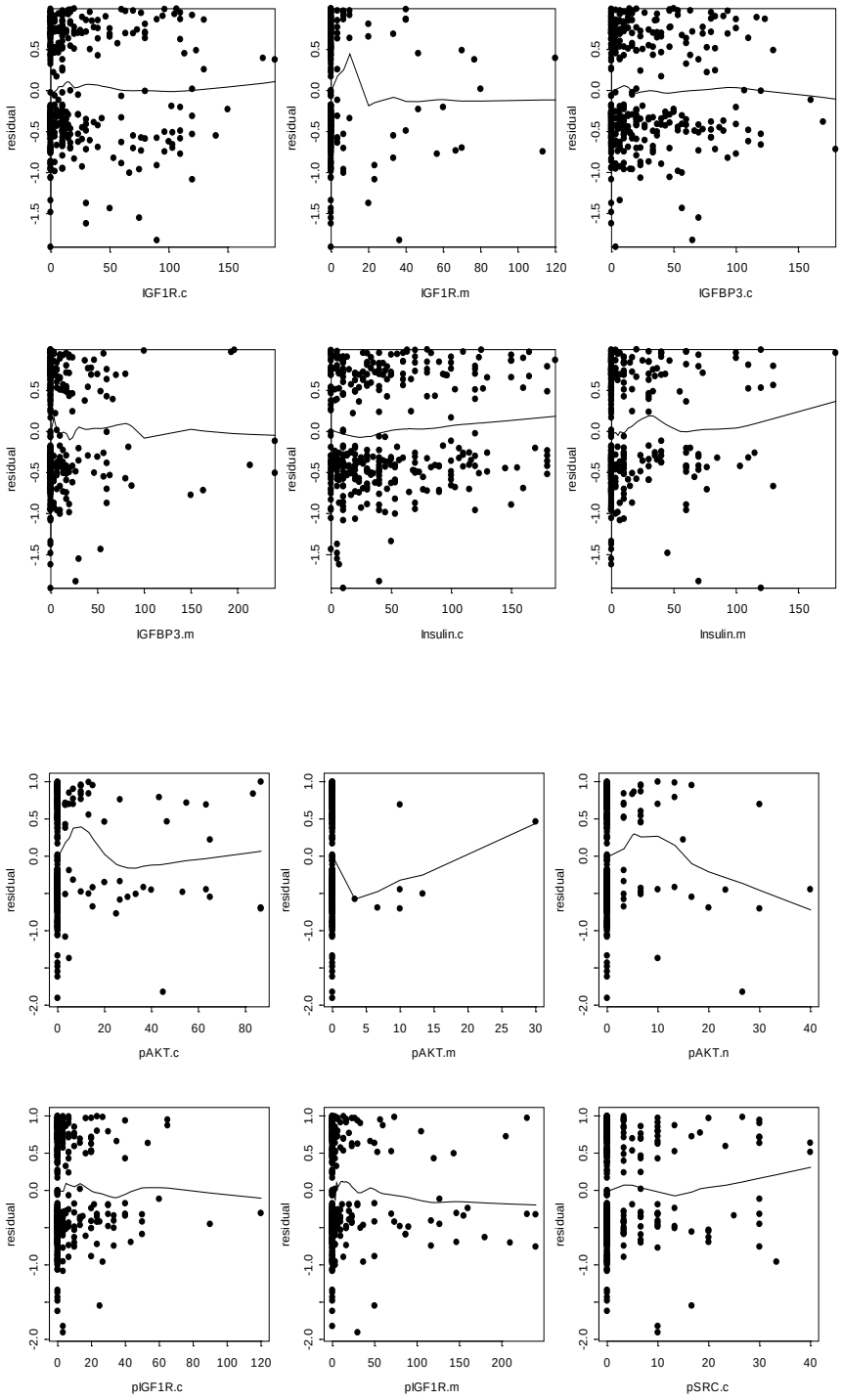

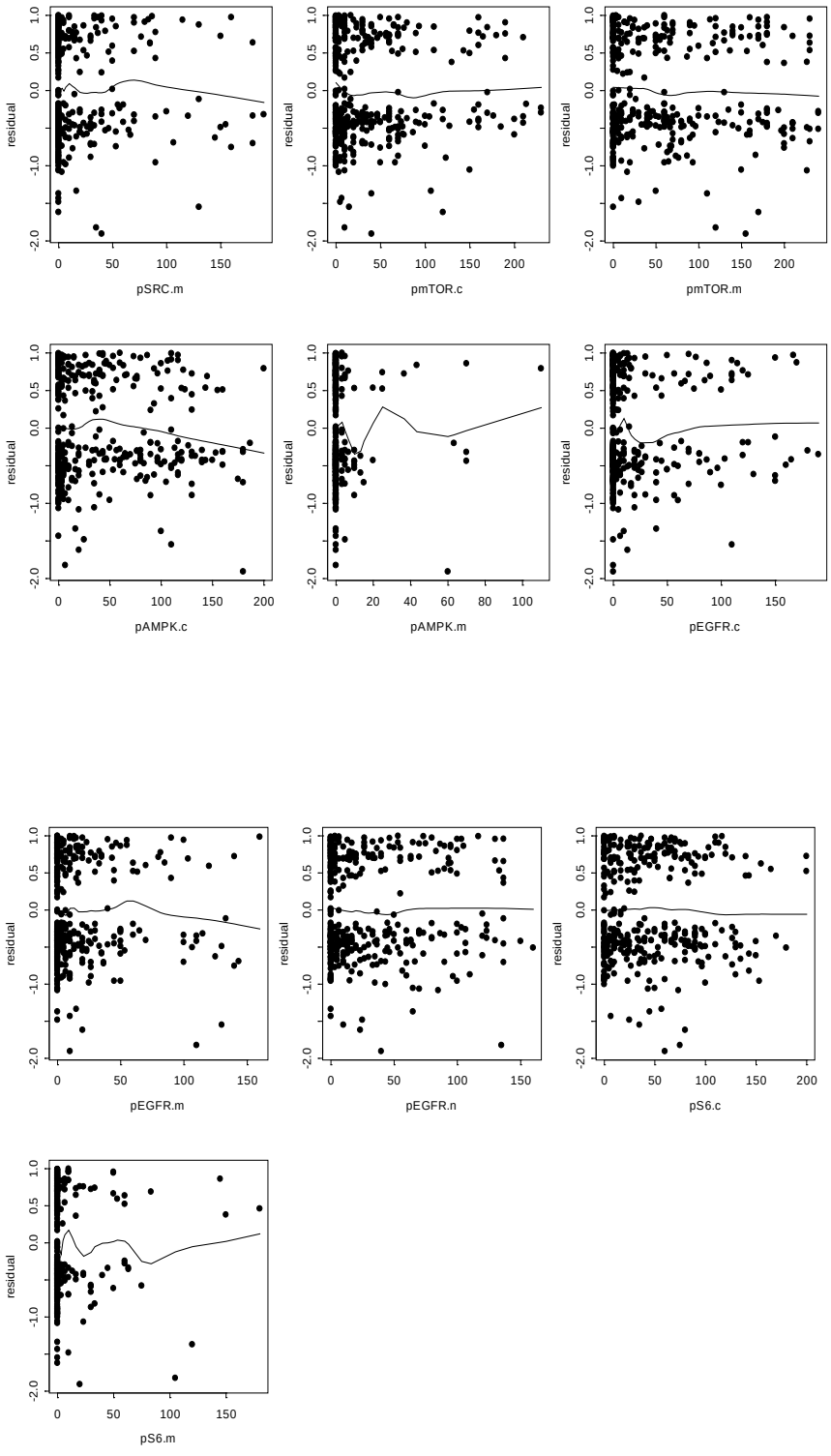
residual
pSRC.m
pmTOR.c
pmTOR.m
pAMPK.c
pAMPK.m
pEGFR.c
pEGFR.m
pEGFR.n
pS6.c
pS6.m

Table 15. Multicovariate Cox model assessing effect of each marker independently on overall survival, adjusting for age, gender, histology, stage and neoadjuvant treatment

covariate	*Estimate*	*StdErr*	*HazardRatio*	*HRLowerCL*	*HRUpperCL*	*pValue*	*Total*	*Event*	*Censored*
IGF1R_c	0.0015	0.0024	1.0015	0.9968	1.0062	0.5275	364	155	209
IGF1R_c_01	0.2619	0.1866	1.2994	0.9014	1.8732	0.1604	364	155	209
IGF1R_c_01m	0.3100	0.1842	1.3635	0.9502	1.9565	0.0924	364	155	209
IGF1R_m	-0.0026	0.0054	0.9974	0.9869	1.0080	0.6295	364	155	209
IGF1R_m_01	0.1450	0.2410	1.1560	0.7208	1.8541	0.5474	364	155	209
IGFBP3_c	-0.0009	0.0025	0.9991	0.9941	1.0041	0.7175	367	158	209
IGFBP3_c_01	0.0452	0.1782	1.0463	0.7378	1.4837	0.7997	367	158	209
IGFBP3_c_01m	-0.0334	0.1652	0.9671	0.6996	1.3370	0.8396	367	158	209
IGFBP3_m	-0.0003	0.0029	0.9997	0.9941	1.0054	0.9296	367	158	209
IGFBP3_m_01	0.0030	0.1730	1.0030	0.7146	1.4078	0.9864	367	158	209
Insulin_c	0.0028	0.0018	1.0028	0.9994	1.0063	0.1083	364	158	206
Insulin_c_01	-0.3243	0.2173	0.7231	0.4723	1.1070	0.1357	364	158	206
Insulin_c_01m	0.1440	0.1638	1.1549	0.8377	1.5921	0.3794	364	158	206
Insulin_m	0.0038	0.0027	1.0038	0.9985	1.0090	0.1579	363	158	205
Insulin_m_01	0.2356	0.1623	1.2657	0.9208	1.7397	0.1466	363	158	205
pAKT_c	-0.0006	0.0060	0.9994	0.9878	1.0111	0.9200	366	157	209
pAKT_c_01	0.3100	0.2203	1.3634	0.8853	2.0996	0.1594	366	157	209
pAKT_m	-0.0037	0.0390	0.9963	0.9230	1.0753	0.9233	367	158	209
pAKT_m_01	-0.6073	0.7190	0.5448	0.1331	2.2299	0.3983	367	158	209
pAKT_n	-0.0135	0.0181	0.9866	0.9522	1.0222	0.4558	367	158	209
pAKT_n_01	0.2472	0.2400	1.2804	0.7999	2.0495	0.3031	367	158	209
pAMPK_c	-0.0028	0.0017	0.9972	0.9938	1.0006	0.1069	367	158	209
pAMPK_c_01	-0.4263	0.1694	0.6529	0.4684	0.9101	0.0119	367	158	209
pAMPK_m	0.0015	0.0077	1.0015	0.9864	1.0168	0.8453	367	158	209
pAMPK_m_01	-0.1301	0.2311	0.8780	0.5582	1.3811	0.5735	367	158	209
pEGFR_c	-0.0002	0.0024	0.9998	0.9952	1.0045	0.9482	365	156	209
pEGFR_c_01	-0.0467	0.1704	0.9544	0.6835	1.3328	0.7841	365	156	209
pEGFR_m	-0.0022	0.0028	0.9978	0.9924	1.0032	0.4280	366	157	209
pEGFR_m_01	-0.1131	0.1625	0.8930	0.6495	1.2279	0.4862	366	157	209
pEGFR_m_01m	-0.1131	0.1625	0.8930	0.6495	1.2279	0.4862	366	157	209

covariate	*Estimate*	*StdErr*	*HazardRatio*	*HRLowerCL*	*HRUpperCL*	*pValue*	*Total*	*Event*	*Censored*
pEGFR_n	-0.0002	0.0021	0.9998	0.9957	1.0040	0.9288	366	158	208
pEGFR_n_01	-0.0957	0.1714	0.9088	0.6495	1.2715	0.5766	366	158	208
pEGFR_n_01m	-0.0261	0.1613	0.9743	0.7102	1.3365	0.8716	366	158	208
pIGF1R_c	-0.0034	0.0068	0.9966	0.9835	1.0100	0.6197	365	158	207
pIGF1R_c_01	0.0132	0.1756	1.0133	0.7183	1.4295	0.9400	365	158	207
pIGF1R_m	-0.0027	0.0026	0.9973	0.9923	1.0023	0.2865	365	158	207
pIGF1R_m_01	-0.0459	0.1810	0.9551	0.6699	1.3618	0.7997	365	158	207
pS6_c	-0.0005	0.0019	0.9995	0.9958	1.0032	0.7888	367	158	209
pS6_c_01	0.0547	0.2376	1.0563	0.6631	1.6826	0.8178	367	158	209
pS6_c_01m	-0.0825	0.1641	0.9208	0.6676	1.2701	0.6151	367	158	209
pS6_m	-0.0007	0.0035	0.9993	0.9925	1.0061	0.8331	367	158	209
pS6_m_01	0.0074	0.2004	1.0075	0.6803	1.4920	0.9704	367	158	209
pSRC_c	0.0099	0.0113	1.0100	0.9879	1.0325	0.3778	366	158	208
pSRC_c_01	0.1417	0.1848	1.1522	0.8021	1.6551	0.4433	366	158	208
pSRC_m	-0.0001	0.0024	0.9999	0.9952	1.0046	0.9526	367	158	209
pSRC_m_01	0.0665	0.1680	1.0688	0.7689	1.4856	0.6921	367	158	209
pmTOR_c	-0.0009	0.0019	0.9991	0.9954	1.0028	0.6315	366	158	208
pmTOR_c_01	-0.5680	0.1997	0.5667	0.3831	0.8381	0.0045	366	158	208
pmTOR_c_01m	-0.1809	0.1783	0.8345	0.5884	1.1837	0.3104	366	158	208
pmTOR_m	-0.0013	0.0014	0.9987	0.9959	1.0015	0.3617	367	158	209
pmTOR_m_01	-0.1737	0.2217	0.8406	0.5443	1.2981	0.4335	367	158	209
pmTOR_m_01m	-0.2320	0.1904	0.7929	0.5460	1.1516	0.2230	367	158	209

Final multicovariate Cox Model assessing the following covariates on overall survival

Analysis of Maximum Likelihood Estimates

Variable		Parameter Estimate	Standard Error	p-value	Hazard Ratio	95% Hazard Ratio Confidence Limits	
Age		0.0317	0.0090	0.0004	1.032	1.014	1.051
Gender	*M vs F*	0.2180	0.1648	0.1859	1.244	0.900	1.718
Stage	*II vs I*	0.3711	0.2074	0.0736	1.449	0.965	2.176
	III vs I	0.9189	0.2146	<.0001	2.507	1.646	3.817
Neoadjuvant (Yes vs No)		0.4398	0.2113	0.0374	1.552	1.026	2.349
pAMPK_c_01 (Pos vs 0)		-0.3884	0.1692	0.0217	0.678	0.487	0.945
pmTOR_c_01 (Pos vs 0)		-0.4720	0.1794	0.0085	0.624	0.439	0.887

2.3 Recurrence free survival

Table 16. Univariate Cox model assessing effect of covariates on recurrence free survival

covariate	*Estimate*	*StdErr*	*HazardRatio*	*HRLowerCL*	*HRUpperCL*	*pValue*	*Total*	*Event*	*Censored*
IGF1R_c	0.0039	0.0018	1.0039	1.0004	1.0075	0.0300	367	206	161
IGF1R_c_01	0.1312	0.1422	1.1402	0.8629	1.5065	0.3562	367	206	161
IGF1R_c_01m	0.1178	0.1401	1.1250	0.8548	1.4805	0.4007	367	206	161
IGF1R_m	0.0011	0.0046	1.0011	0.9921	1.0102	0.8148	367	206	161
IGF1R_m_01	0.3607	0.1925	1.4344	0.9835	2.0919	0.0610	367	206	161
IGFBP3_c	0.0013	0.0020	1.0013	0.9973	1.0053	0.5231	370	209	161
IGFBP3_c_01	0.2362	0.1539	1.2664	0.9366	1.7124	0.1249	370	209	161
IGFBP3_c_01m	0.1895	0.1396	1.2087	0.9193	1.5892	0.1747	370	209	161
IGFBP3_m	-0.0006	0.0024	0.9994	0.9947	1.0041	0.7937	370	209	161
IGFBP3_m_01	0.1059	0.1444	1.1117	0.8377	1.4753	0.4632	370	209	161
Insulin_c	-0.0002	0.0015	0.9998	0.9968	1.0028	0.8965	367	209	158
Insulin_c_01	-0.2956	0.1879	0.7441	0.5148	1.0754	0.1157	367	209	158
Insulin_c_01m	-0.0065	0.1385	0.9935	0.7573	1.3033	0.9623	367	209	158
Insulin_m	0.0036	0.0024	1.0036	0.9990	1.0083	0.1283	366	209	157
Insulin_m_01	0.2649	0.1392	1.3033	0.9922	1.7120	0.0569	366	209	157

covariate	*Estimate*	*StdErr*	*HazardRatio*	*HRLowerCL*	*HRUpperCL*	*pValue*	*Total*	*Event*	*Censored*
pAKT_c	-0.0018	0.0053	0.9982	0.9879	1.0087	0.7368	369	208	161
pAKT_c_01	0.1137	0.1937	1.1205	0.7666	1.6377	0.5570	369	208	161
pAKT_m	-0.0337	0.0411	0.9669	0.8921	1.0479	0.4121	370	209	161
pAKT_m_01	-0.7017	0.5853	0.4958	0.1574	1.5613	0.2306	370	209	161
pAKT_n	-0.0087	0.0151	0.9913	0.9625	1.0210	0.5615	370	209	161
pAKT_n_01	0.1099	0.2174	1.1162	0.7289	1.7093	0.6132	370	209	161
pAMPK_c	-0.0036	0.0015	0.9964	0.9935	0.9993	0.0154	370	209	161
pAMPK_c_01	-0.4203	0.1459	0.6568	0.4935	0.8742	0.0040	370	209	161
pAMPK_m	-0.0023	0.0071	0.9977	0.9840	1.0116	0.7465	370	209	161
pAMPK_m_01	-0.2542	0.2065	0.7755	0.5174	1.1623	0.2182	370	209	161
pEGFR_c	-0.0016	0.0020	0.9984	0.9945	1.0024	0.4375	368	207	161
pEGFR_c_01	-0.1404	0.1414	0.8690	0.6586	1.1466	0.3208	368	207	161
pEGFR_m	-0.0010	0.0024	0.9990	0.9943	1.0037	0.6795	369	208	161
pEGFR_m_01	-0.0561	0.1388	0.9454	0.7202	1.2411	0.6860	369	208	161
pEGFR_m_01m	-0.0561	0.1388	0.9454	0.7202	1.2411	0.6860	369	208	161
pEGFR_n	-0.0006	0.0018	0.9994	0.9959	1.0030	0.7605	369	209	160
pEGFR_n_01	-0.1760	0.1497	0.8386	0.6253	1.1246	0.2397	369	209	160
pEGFR_n_01m	-0.1250	0.1388	0.8825	0.6723	1.1585	0.3679	369	209	160
pIGF1R_c	-0.0083	0.0061	0.9918	0.9800	1.0037	0.1747	368	208	160
pIGF1R_c_01	0.0266	0.1480	1.0270	0.7684	1.3724	0.8574	368	208	160
pIGF1R_m	-0.0022	0.0021	0.9978	0.9938	1.0018	0.2850	368	208	160
pIGF1R_m_01	-0.0806	0.1541	0.9226	0.6820	1.2479	0.6010	368	208	160
pS6_c	-0.0006	0.0016	0.9994	0.9962	1.0025	0.6896	370	209	161
pS6_c_01	0.0294	0.1977	1.0298	0.6990	1.5172	0.8818	370	209	161
pS6_c_01m	0.0127	0.1386	1.0127	0.7718	1.3289	0.9273	370	209	161
pS6_m	0.0044	0.0029	1.0044	0.9986	1.0102	0.1363	370	209	161
pS6_m_01	0.1027	0.1704	1.1081	0.7935	1.5475	0.5467	370	209	161
pSRC_c	0.0071	0.0094	1.0071	0.9888	1.0258	0.4484	369	209	160
pSRC_c_01	0.1245	0.1524	1.1326	0.8401	1.5269	0.4139	369	209	160
pSRC_m	-0.0008	0.0020	0.9992	0.9952	1.0031	0.6761	370	209	161
pSRC_m_01	0.0526	0.1416	1.0540	0.7985	1.3912	0.7104	370	209	161
pmTOR_c	-0.0022	0.0015	0.9978	0.9948	1.0007	0.1383	369	209	160

covariate	*Estimate*	*StdErr*	*HazardRatio*	*HRLowerCL*	*HRUpperCL*	*pValue*	*Total*	*Event*	*Censored*
pmTOR_c_01	-0.4859	0.1502	0.6152	0.4582	0.8258	0.0012	369	209	160
pmTOR_c_01m	-0.4377	0.1394	0.6455	0.4912	0.8485	0.0017	369	209	160
pmTOR_m	-0.0020	0.0011	0.9980	0.9960	1.0001	0.0625	370	209	161
pmTOR_m_01	-0.2257	0.1564	0.7979	0.5873	1.0842	0.1489	370	209	161
pmTOR_m_01m	-0.3023	0.1387	0.7391	0.5631	0.9700	0.0293	370	209	161

Figure 4. Martingale residual from Cox model with age, gender, histology and stage for recurrence free survival against each marker, Dr. HY Lee

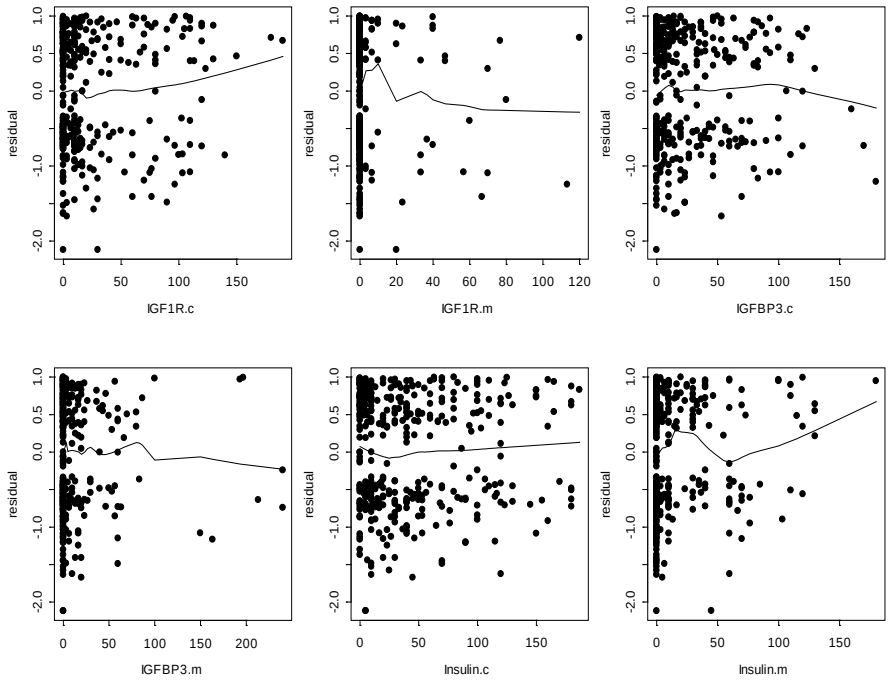

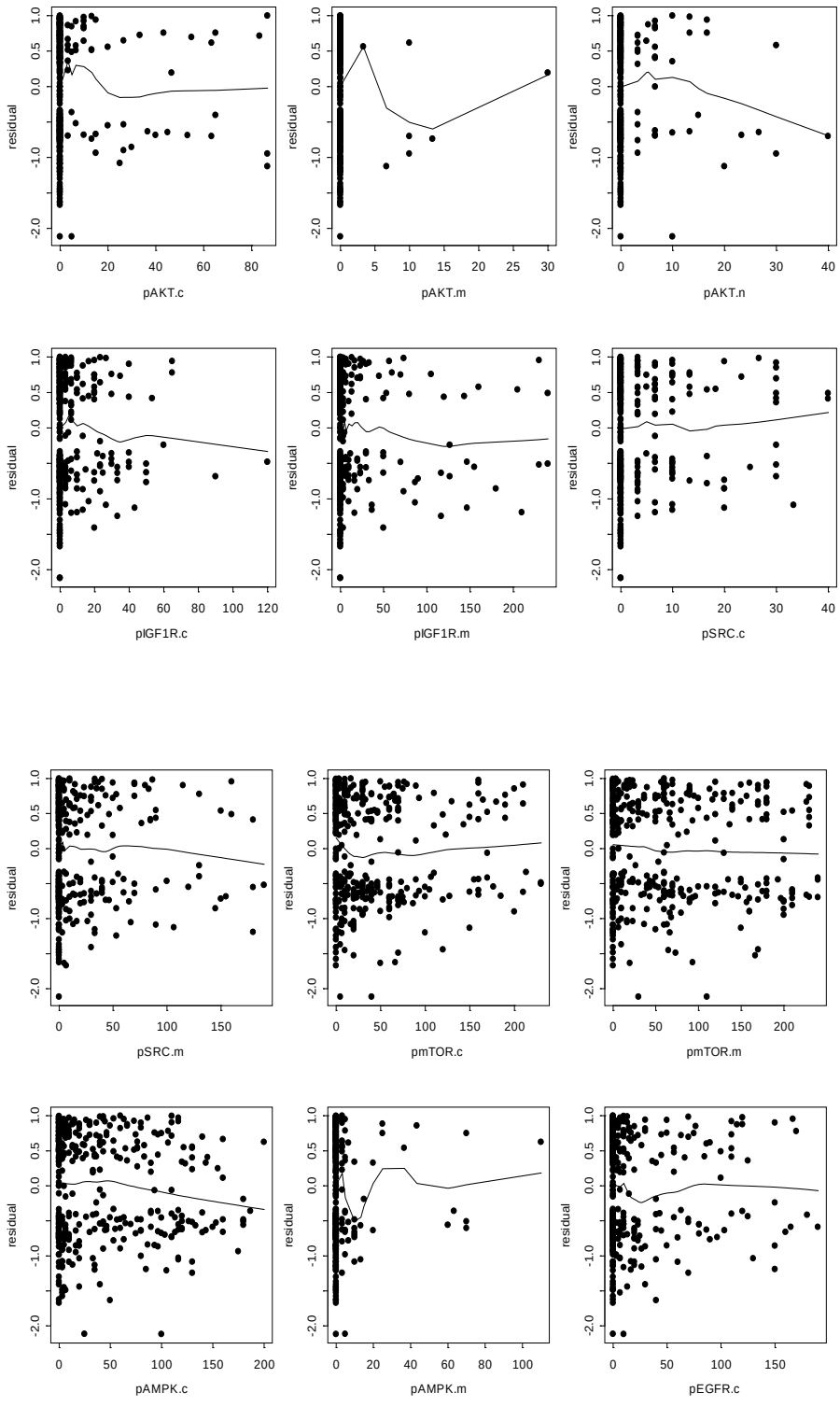
residual
pAKT.c
pAKT.m
pAKT.n
pIGF1R.c
pIGF1R.m
pSRC.c
pSRC.m
pmTOR.c
pmTOR.m
pAMPK.c
pAMPK.m
pEGFR.c

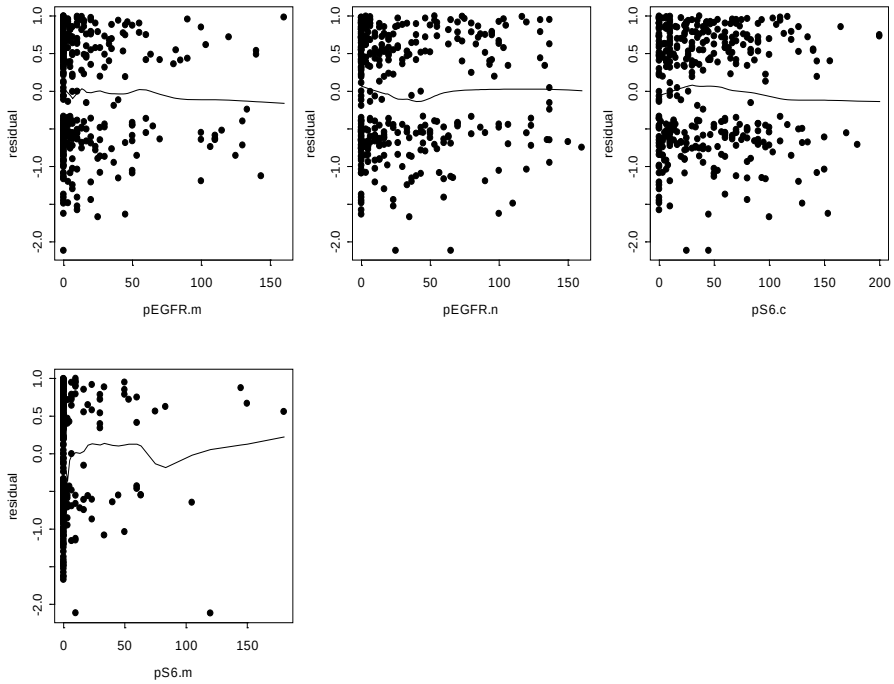

Table 17. Multicovariate Cox model assessing effect of each marker independently on recurrence free survival, adjusting for age, gender, histology, stage and neoadjuvant treatment

covariate	*Estimate*	*StdErr*	*HazardRatio*	*HRLowerCL*	*HRUpperCL*	*pValue*	*Total*	*Event*	*Censored*
IGF1R_c	0.0034	0.0022	1.0034	0.9991	1.0077	0.1257	364	204	160
IGF1R_c_01	0.0189	0.1590	1.0191	0.7462	1.3918	0.9054	364	204	160
IGF1R_c_01m	0.0753	0.1595	1.0782	0.7887	1.4738	0.6370	364	204	160
IGF1R_m	-0.0041	0.0051	0.9959	0.9860	1.0059	0.4174	364	204	160
IGF1R_m_01	0.1278	0.2152	1.1363	0.7453	1.7325	0.5525	364	204	160
IGFBP3_c	-0.0001	0.0021	0.9999	0.9958	1.0041	0.9795	367	207	160
IGFBP3_c_01	0.1661	0.1583	1.1807	0.8657	1.6104	0.2942	367	207	160
IGFBP3_c_01m	0.0760	0.1460	1.0790	0.8104	1.4365	0.6027	367	207	160
IGFBP3_m	-0.0018	0.0027	0.9982	0.9930	1.0034	0.4996	367	207	160
IGFBP3_m_01	-0.0360	0.1522	0.9647	0.7158	1.3001	0.8133	367	207	160
Insulin_c	0.0010	0.0016	1.0010	0.9979	1.0042	0.5218	364	207	157
Insulin_c_01	-0.2639	0.1935	0.7681	0.5256	1.1222	0.1726	364	207	157
Insulin_c_01m	0.0471	0.1427	1.0482	0.7924	1.3866	0.7415	364	207	157
Insulin_m	0.0036	0.0024	1.0036	0.9990	1.0083	0.1267	363	207	156

covariate	*Estimate*	*StdErr*	*HazardRatio*	*HRLowerCL*	*HRUpperCL*	*pValue*	*Total*	*Event*	*Censored*
Insulin_m_01	0.3142	0.1426	1.3692	1.0353	1.8109	0.0276	363	207	156
pAKT_c	-0.0021	0.0053	0.9979	0.9876	1.0083	0.6877	366	206	160
pAKT_c_01	0.1373	0.2007	1.1471	0.7741	1.6999	0.4940	366	206	160
pAKT_m	-0.0222	0.0390	0.9780	0.9060	1.0558	0.5694	367	207	160
pAKT_m_01	-0.5288	0.5902	0.5893	0.1854	1.8737	0.3703	367	207	160
pAKT_n	-0.0150	0.0162	0.9851	0.9544	1.0168	0.3539	367	207	160
pAKT_n_01	0.0474	0.2212	1.0485	0.6797	1.6175	0.8305	367	207	160
pAMPK_c	-0.0030	0.0015	0.9970	0.9940	0.9999	0.0459	367	207	160
pAMPK_c_01	-0.4680	0.1485	0.6263	0.4681	0.8378	0.0016	367	207	160
pAMPK_m	0.0003	0.0070	1.0003	0.9866	1.0141	0.9712	367	207	160
pAMPK_m_01	-0.1904	0.2085	0.8267	0.5493	1.2439	0.3612	367	207	160
pEGFR_c	-0.0014	0.0021	0.9986	0.9945	1.0028	0.5250	365	205	160
pEGFR_c_01	-0.1730	0.1498	0.8411	0.6271	1.1282	0.2482	365	205	160
pEGFR_m	-0.0022	0.0025	0.9978	0.9930	1.0027	0.3767	366	206	160
pEGFR_m_01	-0.1368	0.1421	0.8721	0.6601	1.1523	0.3357	366	206	160
pEGFR_m_01m	-0.1368	0.1421	0.8721	0.6601	1.1523	0.3357	366	206	160
pEGFR_n	-0.0008	0.0018	0.9992	0.9956	1.0028	0.6577	366	207	159
pEGFR_n_01	-0.1134	0.1507	0.8928	0.6644	1.1996	0.4518	366	207	159
pEGFR_n_01m	-0.1426	0.1406	0.8671	0.6582	1.1423	0.3106	366	207	159
pIGF1R_c	-0.0080	0.0063	0.9920	0.9798	1.0044	0.2047	365	206	159
pIGF1R_c_01	0.0032	0.1547	1.0032	0.7408	1.3587	0.9833	365	206	159
pIGF1R_m	-0.0026	0.0022	0.9974	0.9932	1.0017	0.2347	365	206	159
pIGF1R_m_01	-0.0923	0.1587	0.9118	0.6681	1.2445	0.5607	365	206	159
pS6_c	-0.0008	0.0017	0.9992	0.9960	1.0025	0.6503	367	207	160
pS6_c_01	0.1173	0.2101	1.1245	0.7449	1.6976	0.5766	367	207	160
pS6_c_01m	-0.0015	0.1432	0.9985	0.7541	1.3220	0.9914	367	207	160
pS6_m	0.0017	0.0030	1.0017	0.9958	1.0077	0.5715	367	207	160
pS6_m_01	0.0577	0.1754	1.0594	0.7513	1.4940	0.7420	367	207	160
pSRC_c	0.0076	0.0102	1.0076	0.9876	1.0281	0.4582	366	207	159
pSRC_c_01	0.1231	0.1649	1.1310	0.8186	1.5626	0.4554	366	207	159
pSRC_m	-0.0014	0.0022	0.9986	0.9944	1.0029	0.5313	367	207	160
pSRC_m_01	-0.0209	0.1483	0.9793	0.7323	1.3096	0.8879	367	207	160

covariate	Estimate	StdErr	HazardRatio	HRLowerCL	HRUpperCL	pValue	Total	Event	Censored
pmTOR_c	-0.0010	0.0016	0.9990	0.9957	1.0022	0.5308	366	207	159
pmTOR_c_01	-0.4535	0.1710	0.6354	0.4544	0.8885	0.0080	366	207	159
pmTOR_c_01m	-0.3559	0.1561	0.7006	0.5159	0.9513	0.0226	366	207	159
pmTOR_m	-0.0014	0.0012	0.9986	0.9962	1.0010	0.2612	367	207	160
pmTOR_m_01	-0.1325	0.1921	0.8759	0.6010	1.2764	0.4903	367	207	160
pmTOR_m_01m	-0.2206	0.1661	0.8021	0.5792	1.1106	0.1841	367	207	160

Final multicovariate Cox Model assessing the following covariates on recurrence free survival

Analysis of Maximum Likelihood Estimates

Variable		Parameter Estimate	Standard Error	p-value	Hazard Ratio	95% Hazard Ratio Confidence Limits	
Age		0.0255	0.0076	0.0008	1.026	1.011	1.041
Stage	*II vs I*	0.5090	0.1808	0.0049	1.664	1.167	2.371
	III vs I	0.9843	0.1856	<.0001	2.676	1.860	3.850
Neoadjuvant (Yes vs No)		0.2768	0.1884	0.1418	1.319	0.912	1.908
IGF1R_c		0.0032	0.0019	0.1021	1.003	0.999	1.007
Insulin_m_01 (Pos vs 0)		0.3957	0.1455	0.0065	1.485	1.117	1.976
pAMPK_c_01 (Pos vs 0)		-0.4929	0.1504	0.0010	0.611	0.455	0.820
pmTOR_c_01 (Pos vs 0)		-0.3956	0.1627	0.0150	0.673	0.489	0.926

3. Dr. Koo

3.1 Markers

Table 18. Descriptive summary of markers

covariate	*n*	*mean ± std, median (min, max)*
CASK_c	370	23.02 ± 31.18, 10 (0, 150)
CASK_m	370	23.5 ± 41.57, 0 (0, 180)
CD51_c	370	36.11 ± 42.47, 20 (0, 210)
CD51_m	370	29.2 ± 43.02, 10 (0, 240)
CXCR2_c	370	32.41 ± 30.83, 23.33 (0, 150)
CXCR2_n	367	15.29 ± 23.46, 3.33 (0, 120)
EpCAM_c	368	25.04 ± 32.99, 10 (0, 180)
EpCAM_m	370	63.27 ± 64.94, 44.17 (0, 270)
SPP1_c	370	5.3 ± 25.67, 0 (0, 180)
SPP1_n	369	56.53 ± 53.59, 45 (0, 240)

Figure 5. Distribution of markers, Dr. Koo (Red line – Mean, Green line – Median)

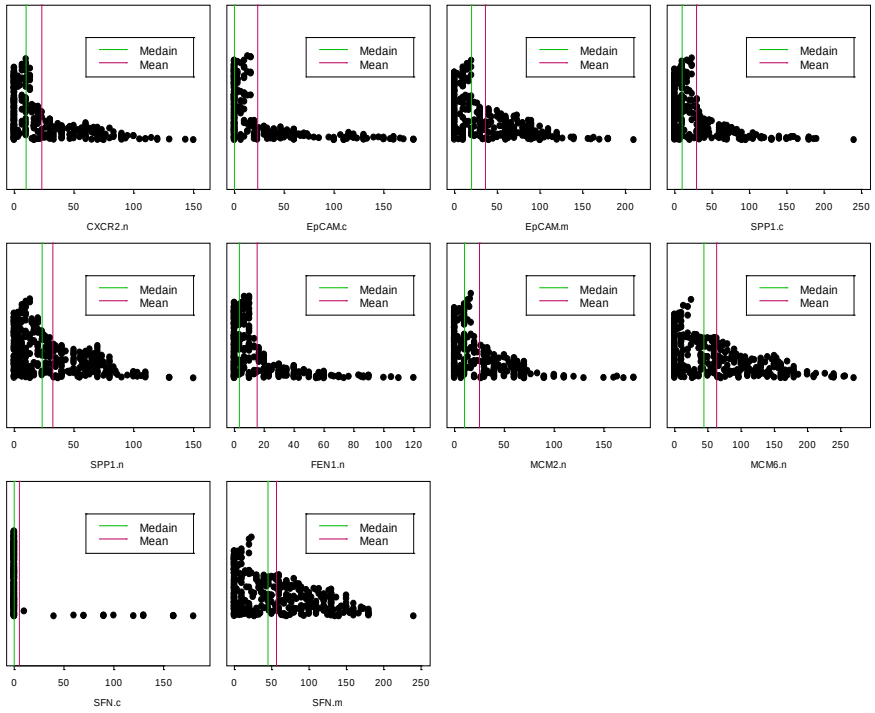

Table 19. Correlation between markers

Spearman Correlation Coefficients
Prob > |r| under H0: Rho=0
Number of Observations

	CASK_c	*CASK_m*	*CD51_c*	*CD51_m*	*CXCR2_c*	*CXCR2_n*	*EpCAM_c*	*EpCAM_m*	*SPP1_c*	*SPP1_n*
CASK_c	1	0.20672	-0.20549	-0.25580	0.15845	-0.07132	0.00706	-0.08818	0.05163	-0.01888
	<.0001	<.0001	<.0001	<.0001	0.0022	0.1727	0.8927	0.0903	0.3220	0.7177
	370	370	370	370	370	367	368	370	370	369
CASK_m	0.20672	1	-0.19539	-0.13551	0.03810	-0.00168	-0.16675	-0.04155	-0.00873	0.13647
	<.0001	<.0001	0.0002	0.0091	0.4650	0.9745	0.0013	0.4255	0.8671	0.0087
	370	370	370	370	370	367	368	370	370	369
CD51_c	-0.20549	-0.19539	1	0.68597	0.19444	0.00772	0.18579	0.11893	0.09961	0.19700
	<.0001	0.0002	<.0001	<.0001	0.0002	0.8828	0.0003	0.0221	0.0556	0.0001
	370	370	370	370	370	367	368	370	370	369
CD51_m	-0.25580	-0.13551	0.68597	1	0.07311	-0.07714	0.04205	0.08436	0.00061	0.23997
	<.0001	0.0091	<.0001	<.0001	0.1605	0.1402	0.4213	0.1052	0.9907	<.0001
	370	370	370	370	370	367	368	370	370	369
CXCR2_c	0.15845	0.03810	0.19444	0.07311	1	-0.00031	0.24559	0.20347	0.21061	0.30982
	0.0022	0.4650	0.0002	0.1605	<.0001	0.9952	<.0001	<.0001	<.0001	<.0001
	370	370	370	370	370	367	368	370	370	369
CXCR2_n	-0.07132	-0.00168	0.00772	-0.07714	-0.00031	1	-0.03994	-0.12380	0.00190	-0.12987
	0.1727	0.9745	0.8828	0.1402	0.9952	<.0001	0.4468	0.0177	0.9711	0.0129
	367	367	367	367	367	367	365	367	367	366
EpCAM_c	0.00706	-0.16675	0.18579	0.04205	0.24559	-0.03994	1	0.47211	0.08455	0.06822
	0.8927	0.0013	0.0003	0.4213	<.0001	0.4468	<.0001	<.0001	0.1054	0.1922
	368	368	368	368	368	365	368	368	368	367
EpCAM_m	-0.08818	-0.04155	0.11893	0.08436	0.20347	-0.12380	0.47211	1	0.08976	0.17398
	0.0903	0.4255	0.0221	0.1052	<.0001	0.0177	<.0001	<.0001	0.0847	0.0008
	370	370	370	370	370	367	368	370	370	369
SPP1_c	0.05163	-0.00873	0.09961	0.00061	0.21061	0.00190	0.08455	0.08976	1	0.01999
	0.3220	0.8671	0.0556	0.9907	<.0001	0.9711	0.1054	0.0847	<.0001	0.7019
	370	370	370	370	370	367	368	370	370	369
SPP1_n	-0.01888	0.13647	0.19700	0.23997	0.30982	-0.12987	0.06822	0.17398	0.01999	1
	0.7177	0.0087	0.0001	<.0001	<.0001	0.0129	0.1922	0.0008	0.7019	<.0001
	369	369	369	369	369	366	367	369	369	369

Figure 6. Correlation between markers, Dr. Koo

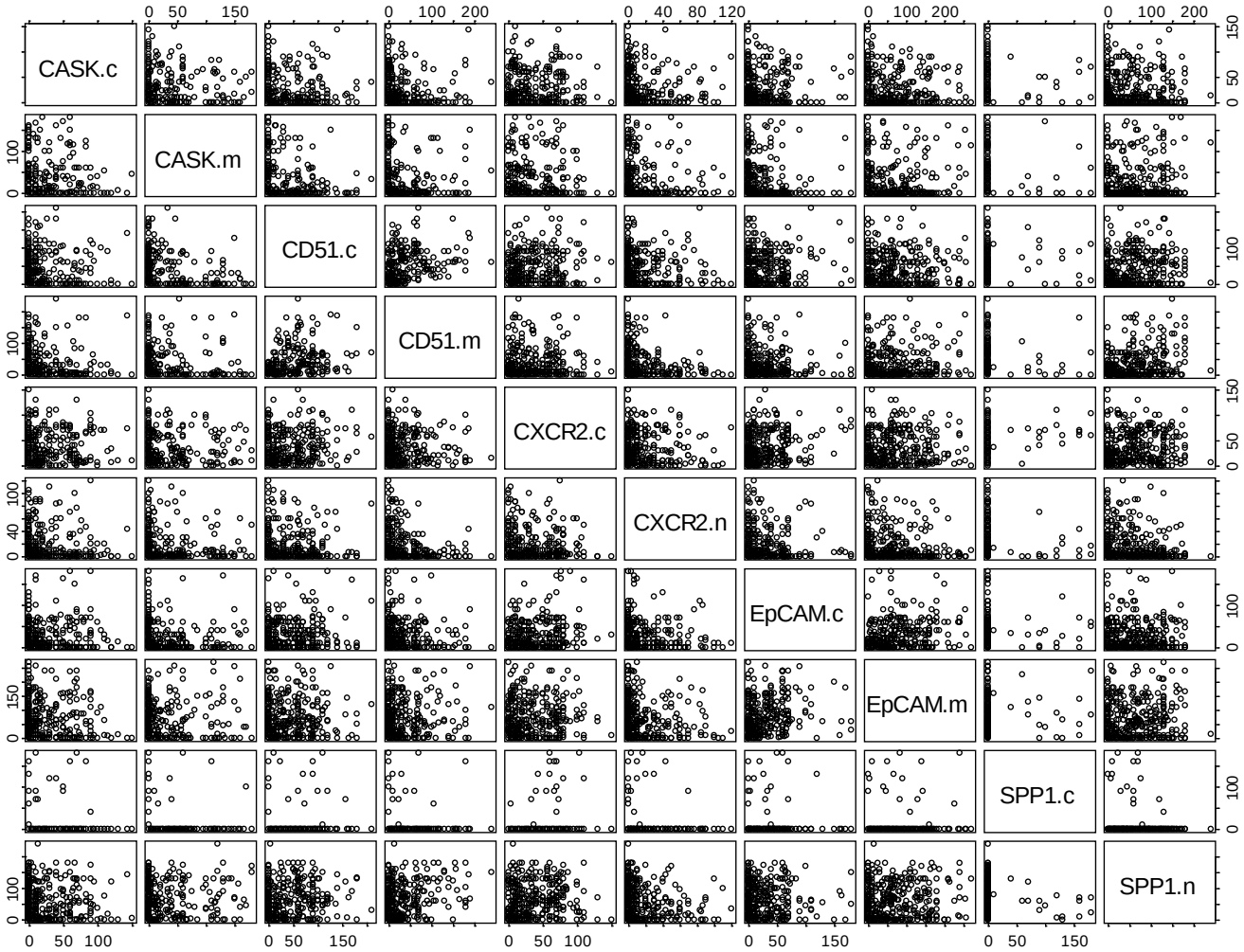

Table 20. Frequency tables for dichotomized markers

covariate	*levels*	*N (%)*	*covariate*	*levels*	*N (%)*
CASK_c_01	0	155(41.9%)	CASK_c_01m	0	178(48.1%)
	1	215(58.1%)		1	192(51.9%)
CASK_m_01	0	212(57.3%)	CD51_c_01m	0	184(49.7%)
	1	158(42.7%)		1	186(50.3%)
CD51_c_01	0	130(35.1%)	CD51_m_01m	0	160(43.2%)
	1	240(64.9%)		1	210(56.8%)
CD51_m_01	0	130(35.1%)	CXCR2_c_01m	0	184(49.7%)
	1	240(64.9%)		1	186(50.3%)

covariate	*levels*	*N (%)*	*covariate*	*levels*	*N (%)*
CXCR2_c_01	0	50(13.5%)	CXCR2_n_01m	missing	3
	1	320(86.5%)		0	158(43.1%)
CXCR2_n_01	missing	3		1	209(56.9%)
	0	156(42.5%)	EpCAM_c_01m	missing	2
	1	211(57.5%)		0	154(41.8%)
EpCAM_c_01	missing	2		1	214(58.2%)
	0	136(37%)	EpCAM_m_01m	0	185(50%)
	1	232(63%)		1	185(50%)
EpCAM_m_01	0	85(23%)	SPP1_n_01m	missing	1
	1	285(77%)		0	181(49.1%)
SPP1_c_01	0	352(95.1%)		1	188(50.9%)
	1	18(4.9%)			
SPP1_n_01	Missing	1			
	0	84(22.8%)			
	1	285(77.2%)			

Table 21. Markers by gender

covariate	*Gender*	*n*	*mean ± std, median (min, max)*	*pValue*
CASK_c	F	184	19.72 ± 30.06, 6.67 (0, 143.33)	.0709
	M	186	26.28 ± 32, 10 (0, 150)	
CASK_m	F	184	24.4 ± 43.94, 0 (0, 180)	.8817
	M	186	22.61 ± 39.18, 0 (0, 180)	
CD51_c	F	184	39.15 ± 42.68, 30 (0, 180)	.0621
	M	186	33.11 ± 42.16, 11.67 (0, 210)	
CD51_m	F	184	31.9 ± 43.14, 10 (0, 190)	.0187
	M	186	26.53 ± 42.85, 10 (0, 240)	
CXCR2_c	F	184	30.33 ± 30.23, 20 (0, 150)	.1397
	M	186	34.47 ± 31.35, 25.83 (0, 130)	
CXCR2_n	F	184	15 ± 22.76, 5 (0, 105)	.4713
	M	183	15.59 ± 24.2, 3.33 (0, 120)	
EpCAM_c	F	184	25.38 ± 34.73, 10 (0, 180)	.7882

covariate	*Gender*	*n*	*mean ± std, median (min, max)*	*pValue*
	M	184	24.7 ± 31.24, 10 (0, 180)	
EpCAM_m	F	184	63.13 ± 67.18, 41.67 (0, 256.67)	.7333
	M	186	63.4 ± 62.84, 46.67 (0, 270)	
SPP1_c	F	184	3.8 ± 20.34, 0 (0, 180)	.6123
	M	186	6.77 ± 30.01, 0 (0, 180)	
SPP1_n	F	184	53.48 ± 50.83, 45.83 (0, 180)	.3588
	M	185	59.56 ± 56.18, 43.33 (0, 240)	

Table 22. Markers by Race

covariate	*Race*	*n*	*mean ± std, median (min, max)*	*pValue*
CASK_c	Black	21	24.29 ± 28.47, 15 (0, 90)	.8357
	Hispanic	14	27.02 ± 40.67, 8.33 (0, 143.33)	
	Oriental	5	29.33 ± 39.54, 3.33 (0, 83.33)	
	White	330	22.67 ± 30.91, 10 (0, 150)	
CASK_m	Black	21	25.32 ± 43.11, 0 (0, 133.33)	.5940
	Hispanic	14	7.38 ± 16.75, 0 (0, 60)	
	Oriental	5	23.33 ± 48.53, 0 (0, 110)	
	White	330	24.07 ± 42.12, 0 (0, 180)	
CD51_c	Black	21	61.43 ± 70.17, 40 (0, 210)	.7053
	Hispanic	14	35.24 ± 45, 20 (0, 140)	
	Oriental	5	36.33 ± 42.63, 10 (0, 90)	
	White	330	34.54 ± 39.73, 20 (0, 180)	
CD51_m	Black	21	37.38 ± 44.2, 23.33 (0, 150)	.7361
	Hispanic	14	25.71 ± 49.5, 7.5 (0, 186.67)	
	Oriental	5	45.33 ± 76.11, 10 (0, 180)	
	White	330	28.59 ± 42.2, 10 (0, 240)	
CXCR2_c	Black	21	36.67 ± 30.72, 33.33 (0, 85)	.7963
	Hispanic	14	39.52 ± 31.56, 60 (0, 76.67)	
	Oriental	5	32.67 ± 35.85, 10 (3.33, 76.67)	
	White	330	31.83 ± 30.82, 20 (0, 150)	
CXCR2_n	Black	21	13.29 ± 19.88, 5 (0, 83.33)	.3951

covariate	*Race*	*n*	*mean ± std, median (min, max)*	*pValue*
	Hispanic	14	24.05 ± 26.99, 13.33 (0, 86.67)	
	Oriental	5	3.33 ± 4.71, 0 (0, 10)	
	White	327	15.23 ± 23.63, 3.33 (0, 120)	
EpCAM_c	Black	21	19.6 ± 29.19, 6.67 (0, 110)	.7884
	Hispanic	14	43.45 ± 59.98, 5 (0, 163.33)	
	Oriental	5	62 ± 80.12, 20 (0, 180)	
	White	328	24.04 ± 30.16, 10 (0, 180)	
EpCAM_m	Black	21	73.89 ± 58.36, 83.33 (0, 166.67)	.3924
	Hispanic	14	43.45 ± 64.52, 20.83 (0, 240)	
	Oriental	5	67.33 ± 68.94, 50 (0, 180)	
	White	330	63.37 ± 65.4, 44.17 (0, 270)	
SPP1_c	Black	21	3.33 ± 15.28, 0 (0, 70)	.1207
	Hispanic	14	20.71 ± 52.98, 0 (0, 160)	
	Oriental	5	32 ± 71.55, 0 (0, 160)	
	White	330	4.36 ± 23.02, 0 (0, 180)	
SPP1_n	Black	21	69.76 ± 60.28, 70 (0, 180)	.7318
	Hispanic	14	42.08 ± 42.62, 31.25 (0, 143.33)	
	Oriental	5	54 ± 61.48, 60 (0, 150)	
	White	329	56.34 ± 53.5, 45 (0, 240)	

Table 23. Markers by Smoking Status

covariate	*smoker*	*n*	*mean ± std, median (min, max)*	*pValue*
CASK_c	1 Never	38	19.25 ± 32.9, 5 (0, 120)	.5451
	2 Former	170	23.76 ± 32.39, 10 (0, 150)	
	3 Current	162	23.12 ± 29.57, 10 (0, 143.33)	
CASK_m	1 Never	38	17.72 ± 33.65, 0 (0, 130)	.9028
	2 Former	170	25.5 ± 45.02, 0 (0, 180)	
	3 Current	162	22.76 ± 39.49, 0 (0, 180)	
CD51_c	1 Never	38	36.45 ± 34.69, 30 (0, 90)	.0634
	2 Former	170	30.72 ± 39.54, 14.17 (0, 210)	
	3 Current	162	41.7 ± 46.41, 25 (0, 180)	

covariate	*smoker*	*n*	*mean ± std, median (min, max)*	*pValue*
CD51_m	1 Never	38	30.92 ± 33.07, 21.67 (0, 130)	.1310
	2 Former	170	25.4 ± 41.44, 10 (0, 240)	
	3 Current	162	32.79 ± 46.46, 10 (0, 186.67)	
CXCR2_c	1 Never	38	24.47 ± 27.99, 13.33 (0, 80)	.0265
	2 Former	170	31.83 ± 33.05, 16.67 (0, 150)	
	3 Current	162	34.88 ± 28.81, 30 (0, 110)	
CXCR2_n	1 Never	38	18.97 ± 25.07, 10 (0, 100)	.0899
	2 Former	170	15.18 ± 22.72, 4.17 (0, 110)	
	3 Current	159	14.54 ± 23.9, 3.33 (0, 120)	
EpCAM_c	1 Never	38	32.79 ± 52.63, 10 (0, 180)	.9193
	2 Former	169	23 ± 26.48, 13.33 (0, 110)	
	3 Current	161	25.36 ± 33.18, 10 (0, 180)	
EpCAM_m	1 Never	38	49.25 ± 53.29, 30 (0, 180)	.6047
	2 Former	170	63.38 ± 63.06, 45 (0, 255)	
	3 Current	162	66.44 ± 69.16, 46.67 (0, 270)	
SPP1_c	1 Never	38	0 ± 0, 0 (0, 0)	.2727
	2 Former	170	4.18 ± 21.88, 0 (0, 180)	
	3 Current	162	7.72 ± 31.53, 0 (0, 180)	
SPP1_n	1 Never	38	45.85 ± 49.49, 34.92 (0, 160)	.3213
	2 Former	169	56.82 ± 55.15, 43.33 (0, 180)	
	3 Current	162	58.73 ± 52.88, 51.67 (0, 240)	

Table 24. Markers by Histology

covariate	*histology0*	*n*	*mean ± std, median (min, max)*	*pValue*
CASK_c	ADENO	227	13.47 ± 23.91, 0 (0, 120)	<.0001
	Other	17	34.22 ± 36.93, 20 (0, 105)	
	SCC	126	38.7 ± 35.08, 30 (0, 150)	
CASK_m	ADENO	227	14.04 ± 31.6, 0 (0, 160)	<.0001
	Other	17	18.04 ± 38.28, 0 (0, 150)	
	SCC	126	41.28 ± 51.21, 16.67 (0, 180)	
CD51_c	ADENO	227	42.37 ± 40.13, 30 (0, 210)	<.0001

covariate	*histology0*	*n*	*mean ± std, median (min, max)*	*pValue*
	Other	17	45.69 ± 54, 10 (0, 156.67)	
	SCC	126	23.54 ± 42.38, 0 (0, 180)	
CD51_m	ADENO	227	33.19 ± 41.5, 16.67 (0, 240)	<.0001
	Other	17	32.75 ± 55.81, 10 (0, 190)	
	SCC	126	21.55 ± 43.14, 0 (0, 186.67)	
CXCR2_c	ADENO	227	31.59 ± 32.04, 20 (0, 150)	.1277
	Other	17	43.92 ± 29.18, 50 (0, 85)	
	SCC	126	32.34 ± 28.64, 23.33 (0, 110)	
CXCR2_n	ADENO	225	16.68 ± 24.38, 5 (0, 105)	.4110
	Other	17	7.57 ± 14.44, 2 (0, 56.67)	
	SCC	125	13.85 ± 22.58, 3.33 (0, 120)	
EpCAM_c	ADENO	226	31.02 ± 34.88, 20 (0, 180)	<.0001
	Other	17	36.86 ± 28.59, 33.33 (0, 90)	
	SCC	125	12.63 ± 25.84, 0 (0, 160)	
EpCAM_m	ADENO	227	77.49 ± 65.39, 60 (0, 270)	<.0001
	Other	17	105.88 ± 74.92, 100 (0, 255)	
	SCC	126	31.9 ± 48.93, 6.67 (0, 200)	
SPP1_c	ADENO	227	2.38 ± 16.12, 0 (0, 130)	.0004
	Other	17	22.35 ± 49.06, 0 (0, 180)	
	SCC	126	8.25 ± 33.23, 0 (0, 180)	
SPP1_n	ADENO	227	52.33 ± 52.04, 40 (0, 180)	.1672
	Other	17	61.67 ± 51.37, 66.67 (0, 166.67)	
	SCC	125	63.45 ± 56.24, 53.33 (0, 240)	

Table 25. Markers by Stage

covariate	*PathStage*	*n*	*mean ± std, median (min, max)*	*pValue*
CASK_c	IA	103	18.07 ± 28.63, 6.67 (0, 150)	.0424
	IB	131	25.66 ± 32.4, 10 (0, 143.33)	
	IIA	22	39.24 ± 36.39, 35 (0, 110)	
	IIB	53	25.75 ± 31.64, 10 (0, 110)	
	IIIA	61	17.46 ± 28.09, 3.33 (0, 130)	

covariate	*PathStage*	*n*	*mean ± std, median (min, max)*	*pValue*
CASK_m	IA	103	21.36 ± 39.14, 0 (0, 156.67)	.2911
	IB	131	23.37 ± 40.52, 0 (0, 170)	
	IIA	22	16.06 ± 39.7, 0 (0, 150)	
	IIB	53	33.18 ± 49.05, 3.33 (0, 180)	
	IIIA	61	21.67 ± 41.4, 0 (0, 180)	
CD51_c	IA	103	31.39 ± 35.77, 20 (0, 160)	.2951
	IB	131	37.53 ± 42.19, 20 (0, 210)	
	IIA	22	21.74 ± 34.24, 10 (0, 120)	
	IIB	53	34.18 ± 44.51, 15 (0, 180)	
	IIIA	61	47.9 ± 51.68, 33.33 (0, 180)	
CD51_m	IA	103	22.02 ± 33.65, 10 (0, 180)	.5473
	IB	131	29.33 ± 41.08, 10 (0, 190)	
	IIA	22	22.27 ± 41.55, 10 (0, 180)	
	IIB	53	33.55 ± 49, 10 (0, 180)	
	IIIA	61	39.78 ± 53.66, 10 (0, 240)	
CXCR2_c	IA	103	25.68 ± 28.83, 16.67 (0, 130)	.0548
	IB	131	35.94 ± 32.28, 30 (0, 130)	
	IIA	22	39.24 ± 28.98, 35 (0, 90)	
	IIB	53	30.75 ± 28.21, 16.67 (0, 100)	
	IIIA	61	35.16 ± 32.52, 26.67 (0, 150)	
CXCR2_n	IA	103	20.57 ± 28.24, 6.67 (0, 110)	.2727
	IB	129	13.29 ± 21.54, 3.33 (0, 90)	
	IIA	22	19.32 ± 30.21, 5 (0, 120)	
	IIB	52	11.83 ± 18.34, 3.33 (0, 73.33)	
	IIIA	61	12.12 ± 17.97, 5 (0, 86.67)	
EpCAM_c	IA	101	21.11 ± 24.1, 10 (0, 110)	.7732
	IB	131	26.32 ± 37.39, 10 (0, 180)	
	IIA	22	31.29 ± 41.92, 10 (0, 180)	
	IIB	53	23.52 ± 31.17, 3.33 (0, 130)	
	IIIA	61	27.88 ± 33.88, 10 (0, 160)	
EpCAM_m	IA	103	51.88 ± 52.17, 40 (0, 186.67)	.7263
	IB	131	69.52 ± 71.97, 50 (0, 256.67)	

covariate	*PathStage*	*n*	*mean ± std, median (min, max)*	*pValue*
	IIA	22	65.83 ± 67.43, 43.33 (0, 240)	
	IIB	53	66.5 ± 70.5, 51 (0, 240)	
	IIIA	61	65.36 ± 62.18, 50 (0, 270)	
SPP1_c	IA	103	1.65 ± 11.21, 0 (0, 90)	.1738
	IB	131	4.05 ± 21.4, 0 (0, 160)	
	IIA	22	0 ± 0, 0 (0, 0)	
	IIB	53	11.13 ± 38.11, 0 (0, 180)	
	IIIA	61	10.98 ± 38.59, 0 (0, 180)	
SPP1_n	IA	103	50.96 ± 55.14, 32.5 (0, 240)	.1666
	IB	130	58.46 ± 51.08, 50 (0, 180)	
	IIA	22	37.95 ± 43.13, 29.17 (0, 180)	
	IIB	53	66.19 ± 56.2, 63.33 (0, 180)	
	IIIA	61	60.14 ± 56.26, 46.67 (0, 180)	

covariate	*stage*	*n*	*mean ± std, median (min, max)*	*pValue*
CASK_c	I	234	22.32 ± 30.96, 10 (0, 150)	.1094
	II	75	29.71 ± 33.43, 15 (0, 110)	
	IIIA	61	17.46 ± 28.09, 3.33 (0, 130)	
CASK_m	I	234	22.49 ± 39.85, 0 (0, 170)	.5254
	II	75	28.16 ± 46.9, 0 (0, 180)	
	IIIA	61	21.67 ± 41.4, 0 (0, 180)	
CD51_c	I	234	34.83 ± 39.53, 20 (0, 210)	.1404
	II	75	30.53 ± 41.92, 10 (0, 180)	
	IIIA	61	47.9 ± 51.68, 33.33 (0, 180)	
CD51_m	I	234	26.11 ± 38.08, 10 (0, 190)	.2465
	II	75	30.24 ± 46.94, 10 (0, 180)	
	IIIA	61	39.78 ± 53.66, 10 (0, 240)	
CXCR2_c	I	234	31.42 ± 31.16, 20 (0, 130)	.3639
	II	75	33.24 ± 28.51, 20 (0, 100)	
	IIIA	61	35.16 ± 32.52, 26.67 (0, 150)	
CXCR2_n	I	232	16.52 ± 24.95, 5 (0, 110)	.6085
	II	74	14.05 ± 22.57, 3.33 (0, 120)	

covariate	*stage*	*n*	*mean ± std, median (min, max)*	*pValue*
	IIIA	61	12.12 ± 17.97, 5 (0, 86.67)	
EpCAM_c	I	232	24.05 ± 32.33, 10 (0, 180)	.6398
	II	75	25.8 ± 34.55, 10 (0, 180)	
	IIIA	61	27.88 ± 33.88, 10 (0, 160)	
EpCAM_m	I	234	61.75 ± 64.49, 41.67 (0, 256.67)	.7502
	II	75	66.3 ± 69.16, 50 (0, 240)	
	IIIA	61	65.36 ± 62.18, 50 (0, 270)	
SPP1_c	I	234	2.99 ± 17.66, 0 (0, 160)	.1985
	II	75	7.87 ± 32.35, 0 (0, 180)	
	IIIA	61	10.98 ± 38.59, 0 (0, 180)	
SPP1_n	I	233	55.14 ± 52.93, 40 (0, 240)	.8341
	II	75	57.91 ± 53.99, 53.33 (0, 180)	
	IIIA	61	60.14 ± 56.26, 46.67 (0, 180)	

Table 26. Markers by Grade

covariate	*grade0*	*n*	*mean ± std, median (min, max)*	*pValue*
CASK_c	1 Poorly	122	23.57 ± 30.42, 10 (0, 115)	.4213
	2 Moderately	199	23.64 ± 32.97, 10 (0, 150)	
	3 Well	36	13.7 ± 20.36, 5 (0, 83.33)	
CASK_m	1 Poorly	122	23.16 ± 43.91, 0 (0, 180)	.4954
	2 Moderately	199	24.45 ± 41.34, 0 (0, 180)	
	3 Well	36	17.73 ± 34.64, 0 (0, 156.67)	
CD51_c	1 Poorly	122	39.56 ± 45.46, 21.67 (0, 180)	.4071
	2 Moderately	199	33.31 ± 41.12, 16.67 (0, 210)	
	3 Well	36	38.24 ± 37.12, 30 (0, 115)	
CD51_m	1 Poorly	122	28.91 ± 44.01, 10 (0, 240)	.3402
	2 Moderately	199	29.43 ± 43.45, 10 (0, 186.67)	
	3 Well	36	26.94 ± 27.15, 18.33 (0, 90)	
CXCR2_c	1 Poorly	122	40.25 ± 30.45, 31.67 (0, 130)	<.0001
	2 Moderately	199	30.25 ± 31, 16.67 (0, 150)	
	3 Well	36	16.39 ± 23.48, 3.33 (0, 80)	

covariate	*grade0*	*n*	*mean ± std, median (min, max)*	*pValue*
CXCR2_n	1 Poorly	120	9.67 ± 17.82, 0 (0, 105)	.0024
	2 Moderately	198	18.43 ± 26.11, 5.83 (0, 120)	
	3 Well	36	18.94 ± 23.56, 10 (0, 100)	
EpCAM_c	1 Poorly	121	29.8 ± 33.2, 20 (0, 160)	.0129
	2 Moderately	198	21.61 ± 32.58, 10 (0, 180)	
	3 Well	36	23.29 ± 34.13, 10 (0, 163.33)	
EpCAM_m	1 Poorly	122	65.98 ± 57.31, 60 (0, 240)	.1450
	2 Moderately	199	60.53 ± 69.12, 33.33 (0, 270)	
	3 Well	36	44.68 ± 44.28, 30.83 (0, 170)	
SPP1_c	1 Poorly	122	9.34 ± 34.52, 0 (0, 180)	.0959
	2 Moderately	199	2.76 ± 16.93, 0 (0, 160)	
	3 Well	36	0 ± 0, 0 (0, 0)	
SPP1_n	1 Poorly	122	68.3 ± 55.12, 66.67 (0, 180)	.0002
	2 Moderately	198	53.06 ± 53.08, 41.67 (0, 240)	
	3 Well	36	32.75 ± 42.41, 10 (0, 150)	

3.2 Overall survival

Table 27. Univariate Cox model assessing effect of covariates on overall survival

covariate	*Estimate*	*StdErr*	*HazardRatio*	*HRLowerCL*	*HRUpperCL*	*pValue*	*Total*	*Event*	*Censored*
CASK_c	0.0002	0.0025	1.0002	0.9953	1.0051	0.9406	370	160	210
CASK_c_01	0.0926	0.1615	1.0970	0.7994	1.5054	0.5663	370	160	210
CASK_c_01m	0.1126	0.1588	1.1192	0.8198	1.5279	0.4783	370	160	210
CASK_m	-0.0019	0.0021	0.9981	0.9941	1.0021	0.3497	370	160	210
CASK_m_01	-0.1135	0.1612	0.8927	0.6509	1.2243	0.4813	370	160	210
CD51_c	0.0014	0.0018	1.0014	0.9978	1.0049	0.4502	370	160	210
CD51_c_01	0.0805	0.1673	1.0838	0.7808	1.5044	0.6304	370	160	210
CD51_c_01m	0.1594	0.1585	1.1728	0.8596	1.5999	0.3146	370	160	210
CD51_m	0.0009	0.0017	1.0009	0.9976	1.0041	0.5970	370	160	210
CD51_m_01	0.1351	0.1684	1.1446	0.8228	1.5922	0.4225	370	160	210
CD51_m_01m	0.2230	0.1620	1.2498	0.9097	1.7169	0.1688	370	160	210

covariate	*Estimate*	*StdErr*	*HazardRatio*	*HRLowerCL*	*HRUpperCL*	*pValue*	*Total*	*Event*	*Censored*
CXCR2_c	0.0031	0.0024	1.0031	0.9985	1.0079	0.1890	370	160	210
CXCR2_c_01	0.4075	0.2566	1.5030	0.9090	2.4853	0.1123	370	160	210
CXCR2_c_01m	0.3306	0.1596	1.3917	1.0180	1.9028	0.0383	370	160	210
CXCR2_n	0.0010	0.0033	1.0010	0.9945	1.0074	0.7723	367	158	209
CXCR2_n_01	-0.0782	0.1602	0.9248	0.6756	1.2659	0.6255	367	158	209
CXCR2_n_01m	-0.0476	0.1602	0.9535	0.6966	1.3052	0.7664	367	158	209
EpCAM_c	-0.0022	0.0026	0.9978	0.9926	1.0029	0.3942	368	159	209
EpCAM_c_01	-0.3790	0.1602	0.6845	0.5001	0.9370	0.0180	368	159	209
EpCAM_c_01m	-0.3786	0.1589	0.6848	0.5016	0.9350	0.0172	368	159	209
EpCAM_m	0.0001	0.0012	1.0001	0.9977	1.0025	0.9551	370	160	210
EpCAM_m_01	0.0339	0.1933	1.0344	0.7082	1.5110	0.8610	370	160	210
EpCAM_m_01m	-0.0802	0.1584	0.9229	0.6766	1.2588	0.6124	370	160	210
SPP1_c	0.0041	0.0027	1.0041	0.9988	1.0094	0.1266	370	160	210
SPP1_c_01	0.4536	0.3273	1.5739	0.8287	2.9892	0.1658	370	160	210
SPP1_n	0.0006	0.0015	1.0006	0.9977	1.0035	0.6815	369	159	210
SPP1_n_01	0.1042	0.1897	1.1098	0.7653	1.6094	0.5828	369	159	210
SPP1_n_01m	0.0779	0.1588	1.0810	0.7918	1.4758	0.6239	369	159	210

Figure 7. Martingale residual from Cox model with age, gender, histology and stage for overall survival against each marker, Dr. Koo

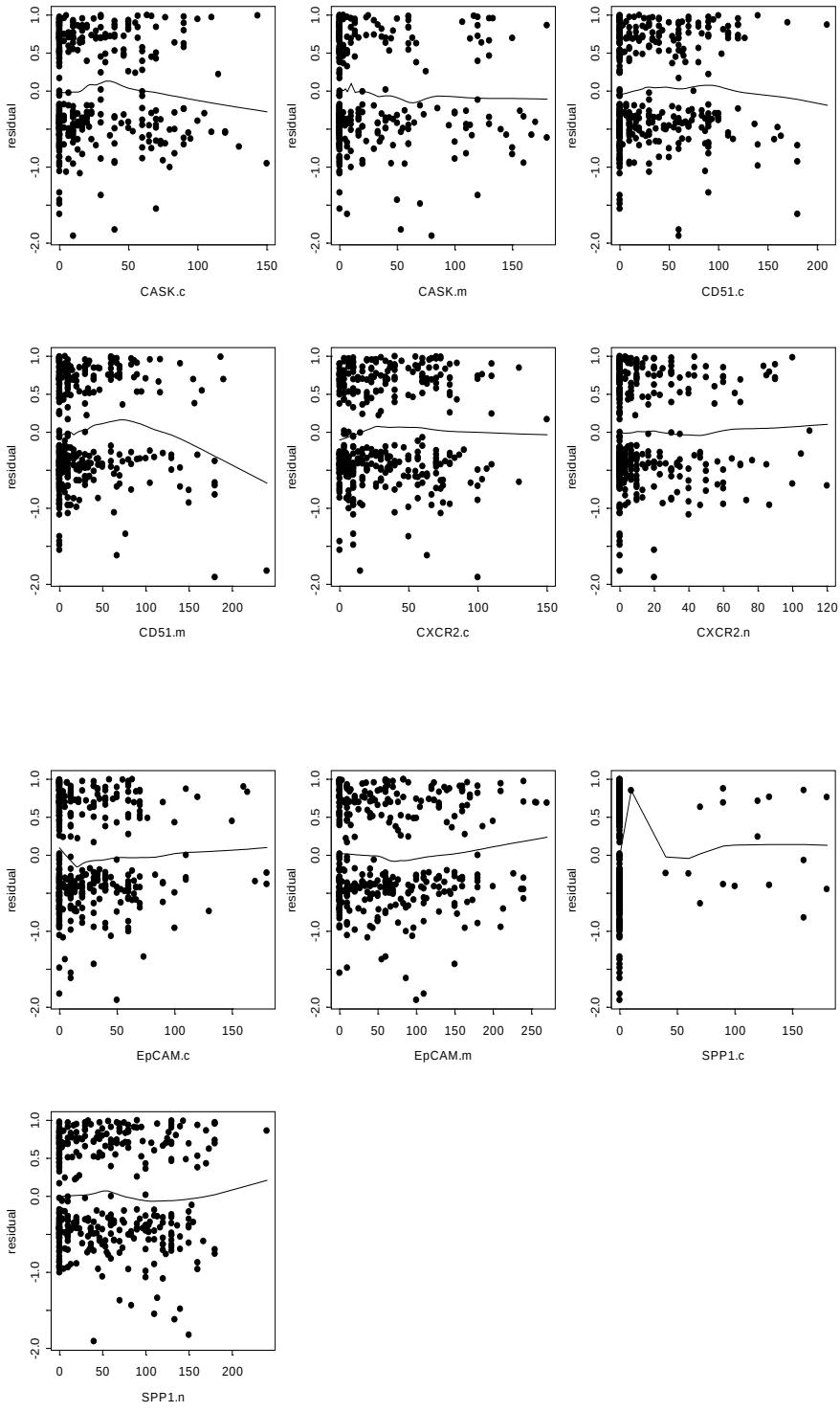

Table 28. Multicovariate Cox model assessing effect of each marker independently on overall survival, adjusting for age, gender, histology, stage and neoadjuvant treatment

covariate	*Estimate*	*StdErr*	*HazardRatio*	*HRLowerCL*	*HRUpperCL*	*pValue*	*Total*	*Event*	*Censored*
CASK_c	-0.0023	0.0029	0.9977	0.9922	1.0034	0.4298	367	158	209
CASK_c_01	0.0482	0.1796	1.0494	0.7379	1.4922	0.7886	367	158	209
CASK_c_01m	0.0458	0.1774	1.0469	0.7394	1.4822	0.7961	367	158	209
CASK_m	-0.0033	0.0022	0.9967	0.9924	1.0011	0.1397	367	158	209
CASK_m_01	-0.2213	0.1696	0.8015	0.5748	1.1177	0.1921	367	158	209
CD51_c	0.0012	0.0018	1.0012	0.9976	1.0048	0.5162	367	158	209
CD51_c_01	0.2402	0.1816	1.2714	0.8907	1.8150	0.1860	367	158	209
CD51_c_01m	0.2333	0.1700	1.2627	0.9050	1.7619	0.1699	367	158	209
CD51_m	-0.0001	0.0016	0.9999	0.9967	1.0031	0.9595	367	158	209
CD51_m_01	0.3009	0.1853	1.3511	0.9397	1.9427	0.1043	367	158	209
CD51_m_01m	0.3323	0.1754	1.3941	0.9885	1.9661	0.0582	367	158	209
CXCR2_c	0.0028	0.0024	1.0028	0.9981	1.0075	0.2396	367	158	209
CXCR2_c_01	0.3365	0.2614	1.4001	0.8389	2.3368	0.1979	367	158	209
CXCR2_c_01m	0.3424	0.1621	1.4083	1.0250	1.9351	0.0347	367	158	209
CXCR2_n	0.0009	0.0033	1.0009	0.9944	1.0073	0.7952	364	156	208
CXCR2_n_01	-0.0189	0.1619	0.9813	0.7145	1.3479	0.9073	364	156	208
CXCR2_n_01m	0.0127	0.1621	1.0127	0.7372	1.3914	0.9377	364	156	208
EpCAM_c	-0.0020	0.0028	0.9980	0.9926	1.0035	0.4805	365	157	208
EpCAM_c_01	-0.4299	0.1710	0.6506	0.4654	0.9096	0.0119	365	157	208
EpCAM_c_01m	-0.4346	0.1720	0.6476	0.4623	0.9071	0.0115	365	157	208
EpCAM_m	0.0004	0.0014	1.0004	0.9977	1.0031	0.7734	367	158	209
EpCAM_m_01	-0.0037	0.2144	0.9963	0.6544	1.5167	0.9862	367	158	209
EpCAM_m_01m	-0.1142	0.1728	0.8921	0.6358	1.2517	0.5088	367	158	209
SPP1_c	0.0024	0.0027	1.0024	0.9971	1.0078	0.3697	367	158	209
SPP1_c_01	0.3789	0.3380	1.4607	0.7532	2.8330	0.2622	367	158	209
SPP1_n	-0.0005	0.0015	0.9995	0.9965	1.0025	0.7297	366	157	209
SPP1_n_01	0.0204	0.1921	1.0206	0.7003	1.4873	0.9154	366	157	209
SPP1_n_01m	-0.0180	0.1639	0.9822	0.7123	1.3543	0.9126	366	157	209

Final multicovariate Cox Model assessing the following covariates on overall survival

Analysis of Maximum Likelihood Estimates

Variable		*Parameter Estimate*	*Standard Error*	*p-value*	*Hazard Ratio*	*95% Hazard Ratio Confidence Limits*	
Age		0.0283	0.0087	0.0012	1.029	1.011	1.046
Gender	*M vs F*	0.2622	0.1628	0.1073	1.300	0.945	1.788
Stage	*II vs I*	0.4139	0.2051	0.0436	1.513	1.012	2.261
	III vs I	0.8970	0.2148	<.0001	2.452	1.610	3.736
Neoadjuvant (Yes vs No)		0.4550	0.2101	0.0303	1.576	1.044	2.379
CXCR2_c_01m (>=23.3 vs < 23.3)		0.4406	0.1651	0.0076	1.554	1.124	2.147
EpCAM_c_01 (Pos vs 0)		-0.4981	0.1673	0.0029	0.608	0.438	0.844

3.3 Recurrence free survival

Table 29. Univariate Cox model assessing effect of covariates on recurrence free survival

covariate	*Estimate*	*StdErr*	*HazardRatio*	*HRLowerCL*	*HRUpperCL*	*pValue*	*Total*	*Event*	*Censored*
CASK_c	0.0016	0.0021	1.0016	0.9975	1.0057	0.4419	370	209	161
CASK_c_01	0.1378	0.1415	1.1477	0.8698	1.5145	0.3301	370	209	161
CASK_c_01m	0.1384	0.1390	1.1485	0.8745	1.5082	0.3194	370	209	161
CASK_m	-0.0018	0.0018	0.9982	0.9948	1.0017	0.3082	370	209	161
CASK_m_01	-0.0642	0.1402	0.9378	0.7124	1.2344	0.6468	370	209	161
CD51_c	-0.0003	0.0016	0.9997	0.9965	1.0028	0.8341	370	209	161
CD51_c_01	0.0360	0.1447	1.0366	0.7807	1.3765	0.8038	370	209	161
CD51_c_01m	0.0986	0.1384	1.1037	0.8414	1.4477	0.4762	370	209	161
CD51_m	0.0022	0.0014	1.0022	0.9994	1.0050	0.1312	370	209	161
CD51_m_01	0.1429	0.1469	1.1536	0.8649	1.5386	0.3308	370	209	161
CD51_m_01m	0.2296	0.1415	1.2581	0.9533	1.6603	0.1048	370	209	161
CXCR2_c	0.0017	0.0022	1.0017	0.9974	1.0061	0.4354	370	209	161
CXCR2_c_01	0.2031	0.2096	1.2252	0.8124	1.8478	0.3327	370	209	161
CXCR2_c_01m	0.1833	0.1390	1.2011	0.9148	1.5771	0.1872	370	209	161
CXCR2_n	0.0004	0.0029	1.0004	0.9947	1.0061	0.8987	367	207	160

covariate	*Estimate*	*StdErr*	*HazardRatio*	*HRLowerCL*	*HRUpperCL*	*pValue*	*Total*	*Event*	*Censored*
CXCR2_n_01	-0.0940	0.1400	0.9103	0.6918	1.1978	0.5020	367	207	160
CXCR2_n_01m	-0.0853	0.1399	0.9183	0.6980	1.2080	0.5422	367	207	160
EpCAM_c	-0.0009	0.0022	0.9991	0.9947	1.0035	0.6857	368	208	160
EpCAM_c_01	-0.2921	0.1409	0.7467	0.5665	0.9842	0.0382	368	208	160
EpCAM_c_01m	-0.2572	0.1393	0.7732	0.5885	1.0160	0.0649	368	208	160
EpCAM_m	-0.0007	0.0011	0.9993	0.9972	1.0014	0.5094	370	209	161
EpCAM_m_01	-0.0447	0.1657	0.9563	0.6911	1.3232	0.7873	370	209	161
EpCAM_m_01m	-0.1261	0.1385	0.8815	0.6719	1.1565	0.3625	370	209	161
SPP1_c	0.0026	0.0025	1.0026	0.9977	1.0075	0.3010	370	209	161
SPP1_c_01	0.2451	0.2978	1.2777	0.7127	2.2906	0.4106	370	209	161
SPP1_n	0.0014	0.0013	1.0014	0.9989	1.0040	0.2680	369	208	161
SPP1_n_01	0.1060	0.1673	1.1119	0.8009	1.5435	0.5263	369	208	161
SPP1_n_01m	0.1294	0.1390	1.1381	0.8667	1.4946	0.3520	369	208	161

Figure 8. Martingale residual from Cox model with age, gender, histology and stage for recurrence free survival against each marker, Dr. Koo

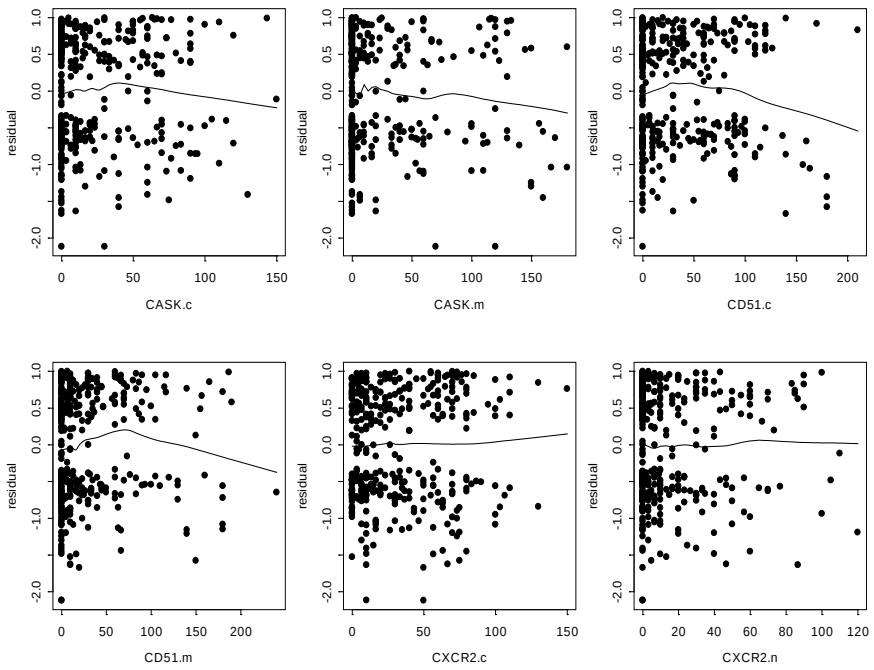

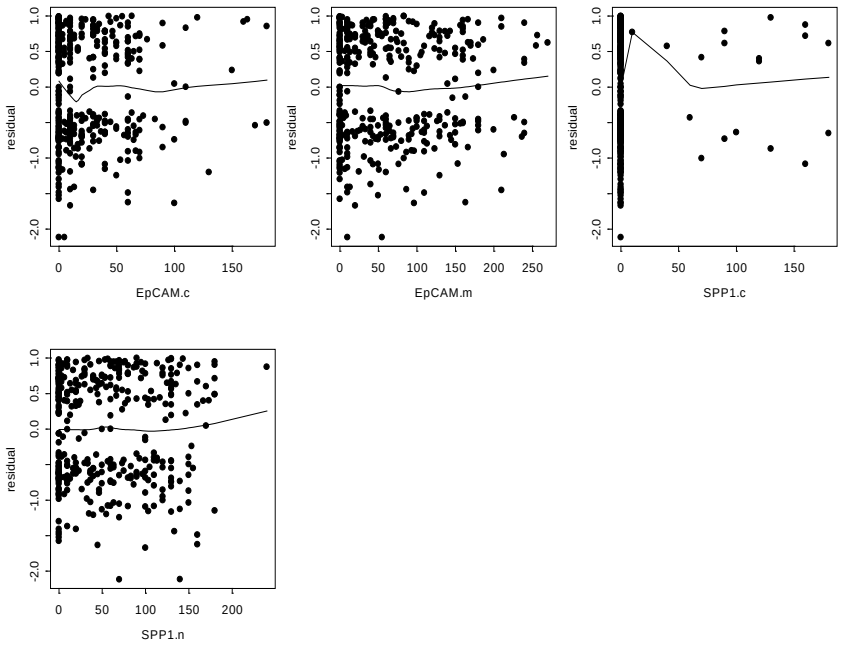

Table 30. Multicovariate Cox model assessing effect of each marker independently on recurrence free survival, adjusting for age, gender, histology, stage and neoadjuvant treatment

covariate	*Estimate*	*StdErr*	*HazardRatio*	*HRLowerCL*	*HRUpperCL*	*pValue*	*Total*	*Event*	*Censored*
CASK_c	-0.0004	0.0024	0.9996	0.9950	1.0042	0.8583	367	207	160
CASK_c_01	0.1208	0.1573	1.1284	0.8291	1.5359	0.4424	367	207	160
CASK_c_01m	0.0717	0.1545	1.0743	0.7936	1.4543	0.6427	367	207	160
CASK_m	-0.0033	0.0019	0.9967	0.9930	1.0005	0.0876	367	207	160
CASK_m_01	-0.1879	0.1479	0.8287	0.6201	1.1075	0.2041	367	207	160
CD51_c	-0.0008	0.0016	0.9992	0.9961	1.0024	0.6355	367	207	160
CD51_c_01	0.1817	0.1564	1.1993	0.8827	1.6294	0.2452	367	207	160
CD51_c_01m	0.1740	0.1479	1.1900	0.8906	1.5901	0.2395	367	207	160
CD51_m	0.0014	0.0014	1.0014	0.9986	1.0041	0.3254	367	207	160
CD51_m_01	0.3010	0.1620	1.3512	0.9835	1.8563	0.0633	367	207	160
CD51_m_01m	0.3275	0.1527	1.3875	1.0285	1.8717	0.0320	367	207	160
CXCR2_c	0.0017	0.0023	1.0017	0.9973	1.0062	0.4442	367	207	160
CXCR2_c_01	0.0934	0.2152	1.0979	0.7200	1.6739	0.6645	367	207	160
CXCR2_c_01m	0.1735	0.1427	1.1894	0.8993	1.5731	0.2240	367	207	160
CXCR2_n	0.0002	0.0029	1.0002	0.9944	1.0060	0.9528	364	205	159

covariate	Estimate	StdErr	HazardRatio	HRLowerCL	HRUpperCL	pValue	Total	Event	Censored
CXCR2_n_01	-0.0670	0.1414	0.9352	0.7089	1.2339	0.6358	364	205	159
CXCR2_n_01m	-0.0622	0.1414	0.9397	0.7123	1.2398	0.6600	364	205	159
EpCAM_c	-0.0003	0.0024	0.9997	0.9951	1.0043	0.8926	365	206	159
EpCAM_c_01	-0.2922	0.1494	0.7466	0.5571	1.0007	0.0505	365	206	159
EpCAM_c_01m	-0.2479	0.1496	0.7804	0.5821	1.0462	0.0974	365	206	159
EpCAM_m	-0.0004	0.0012	0.9996	0.9972	1.0019	0.7085	367	207	160
EpCAM_m_01	-0.0778	0.1836	0.9252	0.6456	1.3258	0.6718	367	207	160
EpCAM_m_01m	-0.1515	0.1504	0.8595	0.6401	1.1541	0.3138	367	207	160
SPP1_c	0.0008	0.0025	1.0008	0.9959	1.0058	0.7373	367	207	160
SPP1_c_01	0.1544	0.3080	1.1670	0.6381	2.1342	0.6161	367	207	160
SPP1_n	0.0004	0.0013	1.0004	0.9978	1.0030	0.7576	366	206	160
SPP1_n_01	0.0637	0.1689	1.0658	0.7653	1.4841	0.7062	366	206	160
SPP1_n_01m	0.0293	0.1431	1.0297	0.7779	1.3631	0.8378	366	206	160

Final multicovariate Cox Model assessing the following covariates on recurrence free surviva1

Analysis of Maximum Likelihood Estimates

Variable		Parameter Estimate	Standard Error	p-value	Hazard Ratio	95% Hazard Ratio Confidence Limits	
Age		0.0227	0.0074	0.0022	1.023	1.008	1.038
Stage	*II vs I*	0.5978	0.1789	0.0008	1.818	1.280	2.581
	III vs I	1.0104	0.1871	<.0001	2.747	1.903	3.964
Neoadjuvant (Yes vs No)		0.3734	0.1865	0.0452	1.453	1.008	2.094
CXCR2_c_01m (>=23.3 vs < 23.3)		0.2999	0.1463	0.0403	1.350	1.013	1.798
EpCAM_c_01 (Pos vs 0)		-0.3722	0.1463	0.0110	0.689	0.517	0.918
CASK_m		-0.0036	0.0018	0.0525	0.996	0.993	1.000

4. Dr. Lotan

4.1 Markers

Table 31. Descriptive summary of markers

covariate	*n*	*mean ± std, median (min, max)*
FEN1_n	366	78.52 ± 61.68, 70 (0, 220)
MCM2_n	369	109.31 ± 84.41, 100 (0, 270)
MCM6_n	370	76.7 ± 75.25, 58.75 (0, 270)
SFN_c	370	32.18 ± 50.29, 6.67 (0, 250)
SFN_m	370	5.03 ± 16.98, 0 (0, 130)
TPX2_c	370	50.66 ± 50.71, 40 (0, 183.33)
TPX2_n	370	6.52 ± 13.73, 0 (0, 106.67)
UBE2C_c	366	26.28 ± 24.71, 20 (0, 130)
UBE2C_n	366	25.15 ± 22.18, 20 (0, 90)

Figure 9. Distribution of markers, Dr. Lotan (Red line – Mean, Green line – Median)

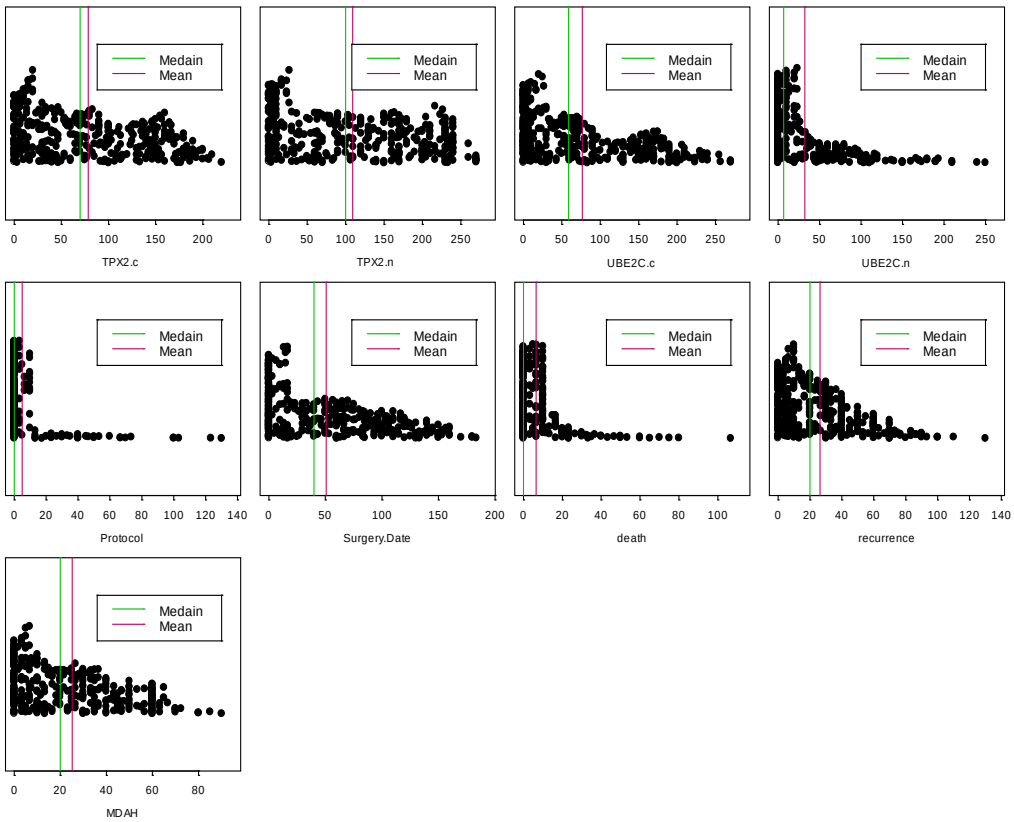

Table 32. Correlation between markers

Spearman Correlation Coefficients
Prob > |r| under H0: Rho=0
Number of Observations

	FEN1_n	*MCM2_n*	*MCM6_n*	*SFN_c*	*SFN_m*	*TPX2_c*	*TPX2_n*	*UBE2C_c*	*UBE2C_n*
FEN1_n	1	0.66287	0.71338	0.30733	0.14547	-0.27785	0.56895	0.64496	0.70561
	<.0001	<.0001	<.0001	<.0001	0.0053	<.0001	<.0001	<.0001	<.0001
	366	365	366	366	366	366	366	362	362
MCM2_n	0.66287	1	0.89878	0.32588	0.25425	-0.41012	0.58737	0.65079	0.65122
	<.0001	<.0001	<.0001	<.0001	<.0001	<.0001	<.0001	<.0001	<.0001
	365	369	369	369	369	369	369	366	366
MCM6_n	0.71338	0.89878	1	0.31998	0.23157	-0.40727	0.59637	0.70428	0.71228
	<.0001	<.0001	<.0001	<.0001	<.0001	<.0001	<.0001	<.0001	<.0001
	366	369	370	370	370	370	370	366	366
SFN_c	0.30733	0.32588	0.31998	1	0.41136	-0.30627	0.36697	0.30834	0.32839
	<.0001	<.0001	<.0001	<.0001	<.0001	<.0001	<.0001	<.0001	<.0001
	366	369	370	370	370	370	370	366	366
SFN_m	0.14547	0.25425	0.23157	0.41136	1	-0.21483	0.20614	0.18474	0.17561
	0.0053	<.0001	<.0001	<.0001	<.0001	<.0001	<.0001	0.0004	0.0007
	366	369	370	370	370	370	370	366	366
TPX2_c	-0.27785	-0.41012	-0.40727	-0.30627	-0.21483	1	-0.56411	-0.24807	-0.27633
	<.0001	<.0001	<.0001	<.0001	<.0001	<.0001	<.0001	<.0001	<.0001
	366	369	370	370	370	370	370	366	366
TPX2_n	0.56895	0.58737	0.59637	0.36697	0.20614	-0.56411	1	0.50280	0.54006
	<.0001	<.0001	<.0001	<.0001	<.0001	<.0001	<.0001	<.0001	<.0001
	366	369	370	370	370	370	370	366	366
UBE2C_c	0.64496	0.65079	0.70428	0.30834	0.18474	-0.24807	0.50280	1	0.88618
	<.0001	<.0001	<.0001	<.0001	0.0004	<.0001	<.0001	<.0001	<.0001
	362	366	366	366	366	366	366	366	366
UBE2C_n	0.70561	0.65122	0.71228	0.32839	0.17561	-0.27633	0.54006	0.88618	1
	<.0001	<.0001	<.0001	<.0001	0.0007	<.0001	<.0001	<.0001	<.0001
	362	366	366	366	366	366	366	366	366

Figure 10. Correlation between markers, Dr. Lotan

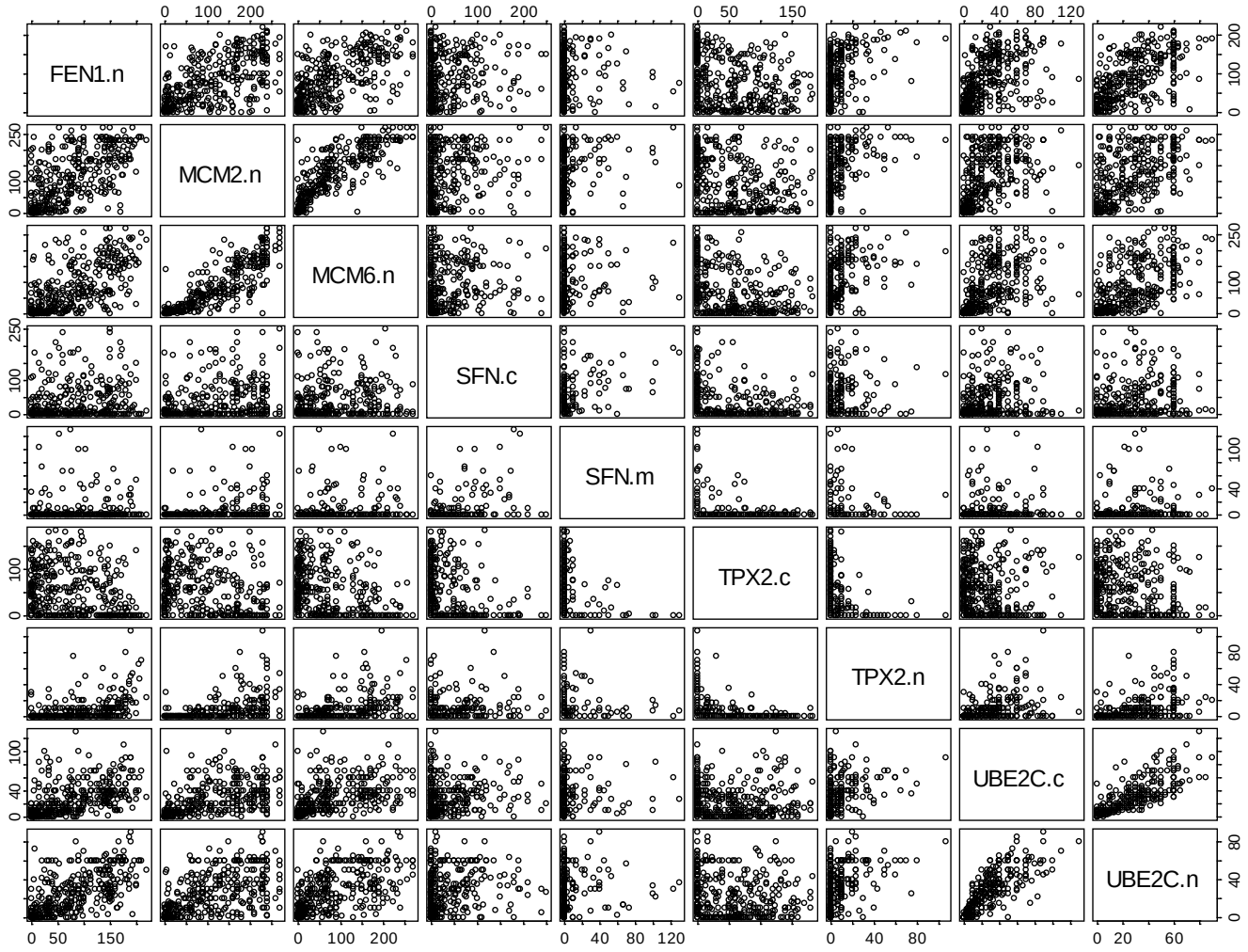

Table 33. Frequency table for dichotomized markers

covariate	*levels*	*N (%)*	*covariate*	*levels*	*N (%)*
FEN1_n_01	missing	4	FEN1_n_01m	missing	4
	0	30(8.2%)		0	178(48.6%)
	1	336(91.8%)		1	188(51.4%)
MCM2_n_01	missing	1	MCM2_n_01m	missing	1
	0	27(7.3%)		0	181(49.1%)
	1	342(92.7%)		1	188(50.9%)
MCM6_n_01	0	60(16.2%)	MCM6_n_01m	0	185(50%)
	1	310(83.8%)		1	185(50%)
SFN_c_01	0	162(43.8%)	SFN_c_01m	0	176(47.6%)
	1	208(56.2%)		1	194(52.4%)
SFN_m_01	0	308(83.2%)	TPX2_c_01m	0	184(49.7%)
	1	62(16.8%)		1	186(50.3%)
TPX2_c_01	0	108(29.2%)	UBE2C_c_01m	missing	4
	1	262(70.8%)		0	169(46.2%)
TPX2_n_01	0	238(64.3%)		1	197(53.8%)
	1	132(35.7%)	UBE2C_n_01m	missing	4
UBE2C_c_01	missing	4		0	172(47%)
	0	59(16.1%)		1	194(53%)
	1	307(83.9%)			
UBE2C_n_01	missing	4			
	0	68(18.6%)			
	1	298(81.4%)			

Table 34. Markers by gender

covariate	*Gender*	*n*	*mean ± std, median (min, max)*	*pValue*
FEN1_n	F	181	72.4 ± 60.86, 60 (0, 206.67)	.0560
	M	185	84.51 ± 62.05, 77.5 (0, 220)	
MCM2_n	F	184	95.99 ± 83.46, 78.33 (0, 270)	.0025
	M	185	122.56 ± 83.47, 120 (0, 270)	
MCM6_n	F	184	68.01 ± 74.01, 35.83 (0, 270)	.0132

covariate	*Gender*	*n*	*mean ± std, median (min, max)*	*pValue*
	M	186	85.3 ± 75.68, 66.67 (0, 270)	
SFN_c	F	184	33.32 ± 55.9, 3.33 (0, 250)	.3176
	M	186	31.05 ± 44.18, 8.75 (0, 193.33)	
SFN_m	F	184	4.35 ± 16.43, 0 (0, 130)	.0677
	M	186	5.7 ± 17.54, 0 (0, 123.33)	
TPX2_c	F	184	52.42 ± 50.83, 40 (0, 183.33)	.4051
	M	186	48.91 ± 50.66, 31.67 (0, 160)	
TPX2_n	F	184	5.99 ± 14.38, 0 (0, 106.67)	.0365
	M	186	7.06 ± 13.07, 0 (0, 75)	
UBE2C_c	F	181	23.18 ± 24, 16.67 (0, 110)	.0051
	M	185	29.32 ± 25.07, 23.33 (0, 130)	
UBE2C_n	F	181	22.51 ± 21.25, 16.67 (0, 80)	.0234
	M	185	27.74 ± 22.82, 25 (0, 90)	

Table 35. Markers by race

covariate	*Race*	*n*	*mean ± std, median (min, max)*	*pValue*
FEN1_n	Black	21	86.23 ± 70.82, 80 (0, 190)	.0336
	Hispanic	14	66.79 ± 56.39, 52.5 (1.67, 170)	
	Oriental	5	7.67 ± 7.23, 10 (0, 15)	
	White	326	79.62 ± 61.22, 72.5 (0, 220)	
MCM2_n	Black	21	141.27 ± 91.86, 170 (0, 260)	.1017
	Hispanic	14	73.33 ± 66.42, 60 (5, 180)	
	Oriental	5	61.33 ± 61.67, 63.33 (0, 160)	
	White	329	109.53 ± 84.27, 100 (0, 270)	
MCM6_n	Black	21	99.56 ± 84.17, 90 (0, 230)	.1870
	Hispanic	14	42.74 ± 60.6, 11.67 (0, 183.33)	
	Oriental	5	33.33 ± 39.3, 16.67 (3.33, 100)	
	White	330	77.34 ± 75.14, 60 (0, 270)	
SFN_c	Black	21	26.87 ± 52.68, 6.67 (0, 180)	.7783
	Hispanic	14	43.69 ± 81.51, 2.5 (0, 240)	
	Oriental	5	30.67 ± 66.72, 0 (0, 150)	

covariate	*Race*	*n*	*mean ± std, median (min, max)*	*pValue*
	White	330	32.05 ± 48.42, 6.67 (0, 250)	
SFN_m	Black	21	3.53 ± 7.92, 0 (0, 26.67)	.7506
	Hispanic	14	0.71 ± 2.67, 0 (0, 10)	
	Oriental	5	20.67 ± 46.21, 0 (0, 103.33)	
	White	330	5.07 ± 17, 0 (0, 130)	
TPX2_c	Black	21	51.11 ± 56.91, 30 (0, 153.33)	.2146
	Hispanic	14	78.57 ± 55.51, 84.17 (0, 160)	
	Oriental	5	35.33 ± 60.17, 3.33 (0, 140)	
	White	330	49.67 ± 49.83, 36.67 (0, 183.33)	
TPX2_n	Black	21	7.62 ± 12.7, 0 (0, 50)	.3958
	Hispanic	14	4.29 ± 13.42, 0 (0, 50)	
	Oriental	5	2.67 ± 5.96, 0 (0, 13.33)	
	White	330	6.61 ± 13.92, 0 (0, 106.67)	
UBE2C_c	Black	21	33.65 ± 30.33, 20 (0, 110)	.2798
	Hispanic	14	16.43 ± 18.36, 10 (0, 70)	
	Oriental	5	22.67 ± 34.19, 10 (0, 83.33)	
	White	326	26.29 ± 24.35, 20 (0, 130)	
UBE2C_n	Black	21	29.05 ± 25.67, 20 (0, 80)	.0917
	Hispanic	14	13.69 ± 19.03, 10 (0, 70)	
	Oriental	5	9.67 ± 7.85, 10 (0, 21.67)	
	White	326	25.63 ± 22.05, 23.33 (0, 90)	

Table 36. Markers by Smoking Status

covariate	*smoker*	*n*	*mean ± std, median (min, max)*	*pValue*
FEN1_n	1 Never	38	34.71 ± 41.77, 15 (0, 165)	<.0001
	2 Former	168	81.88 ± 62.39, 71.67 (0, 220)	
	3 Current	160	85.4 ± 61, 80 (0, 210)	
MCM2_n	1 Never	38	39.04 ± 54.17, 13.33 (0, 240)	<.0001
	2 Former	170	111.72 ± 85.56, 98.33 (0, 270)	
	3 Current	161	123.36 ± 81.22, 126.67 (0, 270)	

covariate	*smoker*	*n*	*mean ± std, median (min, max)*	*pValue*
MCM6_n	1 Never	38	22.5 ± 39.43, 5.83 (0, 190)	<.0001
	2 Former	170	78.58 ± 78.6, 55.83 (0, 270)	
	3 Current	162	87.44 ± 72.96, 73.33 (0, 270)	
SFN_c	1 Never	38	6.54 ± 12.49, 0 (0, 53.33)	.0025
	2 Former	170	33.24 ± 52.15, 6.67 (0, 240)	
	3 Current	162	37.08 ± 52.21, 10 (0, 250)	
SFN_m	1 Never	38	1.32 ± 8.11, 0 (0, 50)	.0264
	2 Former	170	4.72 ± 17.44, 0 (0, 130)	
	3 Current	162	6.23 ± 17.94, 0 (0, 103.33)	
TPX2_c	1 Never	38	68.05 ± 46.74, 60 (0, 180)	.0200
	2 Former	170	50.98 ± 51.38, 38.33 (0, 180)	
	3 Current	162	46.23 ± 50.28, 30 (0, 183.33)	
TPX2_n	1 Never	38	1.23 ± 5.17, 0 (0, 30)	.0005
	2 Former	170	6.09 ± 12.3, 0 (0, 80)	
	3 Current	162	8.23 ± 16.05, 0 (0, 106.67)	
UBE2C_c	1 Never	38	10.5 ± 19.71, 3.33 (0, 100)	<.0001
	2 Former	169	26.5 ± 23.54, 23.33 (0, 110)	
	3 Current	159	29.83 ± 25.64, 20 (0, 130)	
UBE2C_n	1 Never	38	7.52 ± 12.04, 1.67 (0, 60)	<.0001
	2 Former	169	25.89 ± 22.08, 25 (0, 90)	
	3 Current	159	28.59 ± 22.3, 25 (0, 85)	

Table 37. Markers by histology

covariate	*histology0*	*n*	*mean ± std, median (min, max)*	*pValue*
FEN1_n	ADENO	226	57.03 ± 53.67, 40 (0, 206.67)	<.0001
	Other	16	95.1 ± 71.14, 78.33 (0, 210)	
	SCC	124	115.56 ± 55.99, 130 (0, 220)	
MCM2_n	ADENO	226	71.45 ± 73.27, 50 (0, 270)	<.0001
	Other	17	147.84 ± 76.24, 150 (10, 270)	
	SCC	126	172.03 ± 61.7, 170 (0, 270)	

covariate	*histology0*	*n*	*mean ± std, median (min, max)*	*pValue*
MCM6_n	ADENO	227	45.1 ± 59.56, 15 (0, 256.67)	<.0001
	Other	17	107.55 ± 82.29, 90 (0, 270)	
	SCC	126	129.46 ± 68.47, 148.33 (0, 270)	
SFN_c	ADENO	227	10.42 ± 22.83, 0 (0, 173.33)	<.0001
	Other	17	14.51 ± 28.11, 3.33 (0, 106.67)	
	SCC	126	73.76 ± 61.47, 68.33 (0, 250)	
SFN_m	ADENO	227	0.99 ± 6.16, 0 (0, 66.67)	<.0001
	Other	17	1.76 ± 5.67, 0 (0, 23.33)	
	SCC	126	12.74 ± 26.23, 0 (0, 130)	
TPX2_c	ADENO	227	70.28 ± 48.08, 65 (0, 180)	<.0001
	Other	17	68.43 ± 60.74, 65 (0, 150)	
	SCC	126	12.9 ± 27.53, 0 (0, 183.33)	
TPX2_n	ADENO	227	1.66 ± 5.65, 0 (0, 46.67)	<.0001
	Other	17	11.57 ± 23.55, 0 (0, 75)	
	SCC	126	14.61 ± 17.77, 10 (0, 106.67)	
UBE2C_c	ADENO	225	19.49 ± 23.97, 10 (0, 130)	<.0001
	Other	16	39.9 ± 22.33, 40 (6.67, 83.33)	
	SCC	125	36.78 ± 21.9, 33.33 (0, 110)	
UBE2C_n	ADENO	225	17.33 ± 19.78, 10 (0, 90)	<.0001
	Other	16	37.86 ± 19.5, 36.67 (3.33, 63.33)	
	SCC	125	37.61 ± 20.18, 36.67 (0, 85)	

Table 38. Markers by stage

covariate	*PathStage*	*n*	*mean ± std, median (min, max)*	*pValue*
FEN1_n	IA	102	66.34 ± 59.11, 58.33 (0, 200)	.0208
	IB	129	75.5 ± 63.02, 65 (0, 210)	
	IIA	22	86.97 ± 66.3, 85 (0, 186.67)	
	IIB	52	95.14 ± 58.5, 90 (0, 220)	
	IIIA	61	88.09 ± 60.92, 80 (0, 205)	
MCM2_n	IA	103	90.29 ± 82.81, 70 (0, 270)	.0058
	IB	131	104.75 ± 85.62, 90 (0, 270)	

covariate	*PathStage*	*n*	*mean ± std, median (min, max)*	*pValue*
	IIA	21	122.46 ± 89.83, 120 (0, 240)	
	IIB	53	133.9 ± 82.88, 140 (0, 270)	
	IIIA	61	125.34 ± 77.4, 130 (3.33, 260)	
MCM6_n	IA	103	57.38 ± 66, 35 (0, 240)	.0032
	IB	131	75.46 ± 78.54, 43.33 (0, 270)	
	IIA	22	91.89 ± 81.72, 68.33 (0, 240)	
	IIB	53	101.89 ± 82.82, 73.33 (0, 270)	
	IIIA	61	84.6 ± 66.49, 70 (0, 213.33)	
SFN_c	IA	103	33.37 ± 51.43, 10 (0, 250)	.8564
	IB	131	30.44 ± 48.49, 5 (0, 210)	
	IIA	22	26.29 ± 30.98, 16.67 (0, 96.67)	
	IIB	53	42.52 ± 65.63, 6.67 (0, 240)	
	IIIA	61	27.05 ± 41.86, 6.67 (0, 180)	
SFN_m	IA	103	4.56 ± 15.7, 0 (0, 100)	.5230
	IB	131	4.97 ± 15.9, 0 (0, 130)	
	IIA	22	0.76 ± 2.51, 0 (0, 10)	
	IIB	53	7.83 ± 21.96, 0 (0, 123.33)	
	IIIA	61	5.05 ± 19.32, 0 (0, 103.33)	
TPX2_c	IA	103	57.9 ± 52.24, 45 (0, 180)	.1717
	IB	131	51.83 ± 50.67, 40 (0, 180)	
	IIA	22	48.64 ± 54.18, 25 (0, 150)	
	IIB	53	44.53 ± 48.24, 33.33 (0, 160)	
	IIIA	61	41.97 ± 48.59, 16.67 (0, 183.33)	
TPX2_n	IA	103	4.42 ± 10.95, 0 (0, 75)	.0782
	IB	131	6.83 ± 16.39, 0 (0, 106.67)	
	IIA	22	9.09 ± 15.47, 0 (0, 60)	
	IIB	53	8.08 ± 12.21, 0 (0, 50)	
	IIIA	61	7.14 ± 12.2, 0 (0, 65)	
UBE2C_c	IA	102	19.84 ± 20.09, 15 (0, 86.67)	.0026
	IB	129	25.67 ± 25.82, 16.67 (0, 100)	
	IIA	21	25.24 ± 19.65, 20 (0, 60)	
	IIB	53	33.74 ± 28.13, 30 (0, 130)	

covariate	*PathStage*	*n*	*mean ± std, median (min, max)*	*pValue*
	IIIA	61	32.24 ± 25.3, 30 (0, 110)	
UBE2C_n	IA	102	20.85 ± 20.14, 15.83 (0, 72.5)	.0190
	IB	129	23.71 ± 22.46, 15 (0, 80)	
	IIA	21	27.82 ± 24.03, 25 (0, 85)	
	IIB	53	31.76 ± 24.16, 26.67 (0, 90)	
	IIIA	61	28.76 ± 21.12, 25 (0, 70)	

covariate	*stage*	*n*	*mean ± std, median (min, max)*	*pValue*
FEN1_n	I	231	71.45 ± 61.36, 60 (0, 210)	.0076
	II	74	92.71 ± 60.58, 90 (0, 220)	
	IIIA	61	88.09 ± 60.92, 80 (0, 205)	
MCM2_n	I	234	98.38 ± 84.52, 80 (0, 270)	.0024
	II	74	130.65 ± 84.45, 135 (0, 270)	
	IIIA	61	125.34 ± 77.4, 130 (3.33, 260)	
MCM6_n	I	234	67.5 ± 73.69, 38.33 (0, 270)	.0021
	II	75	98.96 ± 82.07, 73.33 (0, 270)	
	IIIA	61	84.6 ± 66.49, 70 (0, 213.33)	
SFN_c	I	234	31.73 ± 49.72, 6.67 (0, 250)	.5994
	II	75	37.76 ± 57.92, 6.67 (0, 240)	
	IIIA	61	27.05 ± 41.86, 6.67 (0, 180)	
SFN_m	I	234	4.79 ± 15.78, 0 (0, 130)	.8210
	II	75	5.76 ± 18.74, 0 (0, 123.33)	
	IIIA	61	5.05 ± 19.32, 0 (0, 103.33)	
TPX2_c	I	234	54.5 ± 51.35, 41.67 (0, 180)	.0680
	II	75	45.73 ± 49.72, 33.33 (0, 160)	
	IIIA	61	41.97 ± 48.59, 16.67 (0, 183.33)	
TPX2_n	I	234	5.77 ± 14.27, 0 (0, 106.67)	.0202
	II	75	8.38 ± 13.15, 0 (0, 60)	
	IIIA	61	7.14 ± 12.2, 0 (0, 65)	
UBE2C_c	I	231	23.1 ± 23.6, 16.67 (0, 100)	.0013
	II	74	31.33 ± 26.16, 25 (0, 130)	

covariate	*stage*	*n*	*mean ± std, median (min, max)*	*pValue*
	IIIA	61	32.24 ± 25.3, 30 (0, 110)	
UBE2C_n	I	231	22.45 ± 21.47, 15 (0, 80)	.0050
	II	74	30.64 ± 24.03, 26.67 (0, 90)	
	IIIA	61	28.76 ± 21.12, 25 (0, 70)	

Table 39. Markers by Grade

covariate	*grade0*	*n*	*mean ± std, median (min, max)*	*pValue*
FEN1_n	1 Poorly	122	101.28 ± 63.58, 100 (0, 220)	<.0001
	2 Moderately	196	74.77 ± 56.97, 66.67 (0, 196.67)	
	3 Well	36	23.19 ± 36.48, 6.67 (0, 155)	
MCM2_n	1 Poorly	122	146.05 ± 77.26, 158.33 (0, 270)	<.0001
	2 Moderately	198	101.06 ± 82.37, 90 (0, 270)	
	3 Well	36	24.12 ± 40.09, 8.33 (0, 160)	
MCM6_n	1 Poorly	122	104.62 ± 74.16, 92.5 (0, 270)	<.0001
	2 Moderately	199	70.86 ± 74.05, 50 (0, 270)	
	3 Well	36	11.48 ± 25.94, 0 (0, 126.67)	
SFN_c	1 Poorly	122	28.19 ± 47.01, 5.83 (0, 250)	<.0001
	2 Moderately	199	40.83 ± 55.23, 10 (0, 240)	
	3 Well	36	7.27 ± 18.96, 0 (0, 96.67)	
SFN_m	1 Poorly	122	4.06 ± 13.38, 0 (0, 100)	.0456
	2 Moderately	199	6.81 ± 20.46, 0 (0, 130)	
	3 Well	36	0.09 ± 0.56, 0 (0, 3.33)	
TPX2_c	1 Poorly	122	48.33 ± 50.81, 34.17 (0, 183.33)	.0517
	2 Moderately	199	47.76 ± 49.6, 30 (0, 180)	
	3 Well	36	66.25 ± 49.88, 60 (0, 180)	
TPX2_n	1 Poorly	122	10.3 ± 17.33, 0 (0, 106.67)	<.0001
	2 Moderately	199	5.13 ± 11.02, 0 (0, 80)	
	3 Well	36	0.83 ± 5, 0 (0, 30)	
UBE2C_c	1 Poorly	122	36.3 ± 27.76, 30.83 (0, 130)	<.0001
	2 Moderately	196	23.34 ± 21.29, 20 (0, 86.67)	

covariate	grade0	n	mean ± std, median (min, max)	pValue
	3 Well	36	4.21 ± 7.85, 0 (0, 36.67)	
UBE2C_n	1 Poorly	122	33.22 ± 22.42, 31.67 (0, 90)	<.0001
	2 Moderately	196	23.51 ± 21.25, 17.5 (0, 85)	
	3 Well	36	4.12 ± 7.35, 0 (0, 26.67)	

4.2 Overall survival

Table 40. Univariate Cox model assessing effect of covariates on overall survival

covariate	Estimate	StdErr	HazardRatio	HRLowerCL	HRUpperCL	pValue	Total	Event	Censored
FEN1_n	0.0028	0.0012	1.0028	1.0003	1.0052	0.0258	366	158	208
FEN1_n_01	0.2005	0.3128	1.2220	0.6620	2.2559	0.5215	366	158	208
FEN1_n_01m	0.5043	0.1624	1.6558	1.2043	2.2766	0.0019	366	158	208
MCM2_n	0.0019	0.0009	1.0019	1.0001	1.0037	0.0425	369	159	210
MCM2_n_01	0.4957	0.3632	1.6416	0.8056	3.3449	0.1723	369	159	210
MCM2_n_01m	0.1819	0.1596	1.1995	0.8773	1.6398	0.2544	369	159	210
MCM6_n	0.0018	0.0010	1.0018	0.9999	1.0038	0.0694	370	160	210
MCM6_n_01	0.6533	0.2637	1.9218	1.1463	3.2222	0.0132	370	160	210
MCM6_n_01m	0.1858	0.1588	1.2042	0.8822	1.6438	0.2418	370	160	210
SFN_c	0.0022	0.0014	1.0022	0.9993	1.0050	0.1360	370	160	210
SFN_c_01	0.0021	0.1590	1.0021	0.7338	1.3685	0.9895	370	160	210
SFN_c_01m	0.0609	0.1584	1.0628	0.7792	1.4497	0.7005	370	160	210
SFN_m	0.0017	0.0041	1.0017	0.9936	1.0099	0.6806	370	160	210
SFN_m_01	-0.0772	0.2150	0.9257	0.6074	1.4108	0.7196	370	160	210
TPX2_c	-0.0012	0.0016	0.9988	0.9956	1.0019	0.4455	370	160	210
TPX2_c_01	-0.1738	0.1710	0.8405	0.6012	1.1750	0.3093	370	160	210
TPX2_c_01m	-0.1873	0.1585	0.8292	0.6077	1.1314	0.2375	370	160	210
TPX2_n	0.0082	0.0050	1.0082	0.9983	1.0182	0.1035	370	160	210
TPX2_n_01	0.2700	0.1620	1.3099	0.9536	1.7993	0.0956	370	160	210
UBE2C_c	0.0069	0.0029	1.0069	1.0012	1.0127	0.0179	366	159	207
UBE2C_c_01	0.5470	0.2569	1.7280	1.0444	2.8592	0.0333	366	159	207
UBE2C_c_01m	0.3326	0.1620	1.3946	1.0152	1.9158	0.0401	366	159	207

covariate	*Estimate*	*StdErr*	*HazardRatio*	*HRLowerCL*	*HRUpperCL*	*pValue*	*Total*	*Event*	*Censored*
UBE2C_n	0.0065	0.0035	1.0065	0.9997	1.0134	0.0621	366	159	207
UBE2C_n_01	0.5520	0.2392	1.7367	1.0866	2.7757	0.0210	366	159	207
UBE2C_n_01m	0.2177	0.1604	1.2432	0.9078	1.7025	0.1747	366	159	207

Figure 11. Martingale residual from Cox model with age, gender, histology and stage for overall survival against each marker, Dr. Lotan

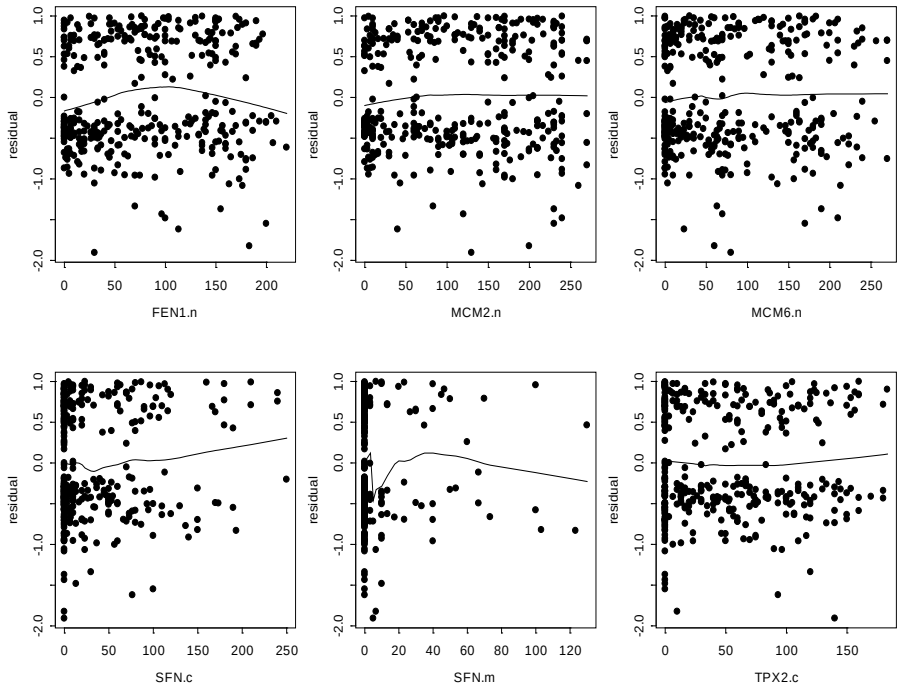

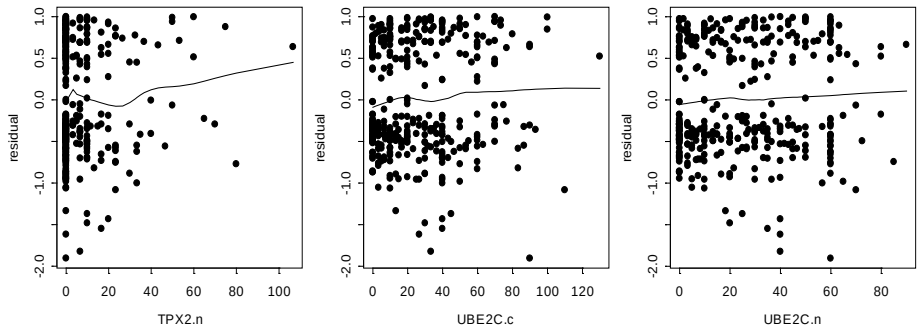

Table 41. Multicovariate Cox model assessing effect of each marker independently on overall survival , adjusting for age, gender, histology, stage and neoadjuvant treatment

covariate	*Estimate*	*StdErr*	*HazardRatio*	*HRLowerCL*	*HRUpperCL*	*pValue*	*Total*	*Event*	*Censored*
FEN1_n	0.0018	0.0014	1.0018	0.9990	1.0046	0.2090	363	156	207
FEN1_n_01	-0.0004	0.3205	0.9996	0.5333	1.8735	0.9990	363	156	207
FEN1_n_01m	0.3721	0.1772	1.4508	1.0251	2.0531	0.0357	363	156	207
MCM2_n	0.0015	0.0012	1.0015	0.9992	1.0038	0.1963	366	157	209
MCM2_n_01	0.3662	0.3747	1.4423	0.6921	3.0058	0.3283	366	157	209
MCM2_n_01m	0.0465	0.2021	1.0476	0.7049	1.5567	0.8182	366	157	209
MCM6_n	0.0017	0.0013	1.0017	0.9992	1.0042	0.1788	367	158	209
MCM6_n_01	0.5623	0.2759	1.7546	1.0218	3.0131	0.0415	367	158	209
MCM6_n_01m	0.0371	0.1913	1.0378	0.7133	1.5099	0.8462	367	158	209
SFN_c	0.0028	0.0018	1.0028	0.9992	1.0064	0.1302	367	158	209
SFN_c_01	0.0090	0.1855	1.0090	0.7015	1.4515	0.9613	367	158	209

covariate	Estimate	StdErr	HazardRatio	HRLowerCL	HRUpperCL	pValue	Total	Event	Censored
SFN_c_01m	0.0720	0.1901	1.0747	0.7404	1.5598	0.7048	367	158	209
SFN_m	-0.0001	0.0044	0.9999	0.9912	1.0086	0.9746	367	158	209
SFN_m_01	-0.2200	0.2284	0.8025	0.5129	1.2558	0.3356	367	158	209
TPX2_c	-0.0005	0.0020	0.9995	0.9956	1.0035	0.8203	367	158	209
TPX2_c_01	-0.1445	0.2249	0.8654	0.5570	1.3447	0.5204	367	158	209
TPX2_c_01m	-0.1643	0.1950	0.8485	0.5790	1.2434	0.3993	367	158	209
TPX2_n	0.0090	0.0059	1.0090	0.9974	1.0208	0.1283	367	158	209
TPX2_n_01	0.1707	0.2001	1.1862	0.8014	1.7557	0.3935	367	158	209
UBE2C_c	0.0053	0.0033	1.0053	0.9989	1.0118	0.1040	363	157	206
UBE2C_c_01	0.4351	0.2715	1.5452	0.9075	2.6310	0.1090	363	157	206
UBE2C_c_01m	0.2086	0.1824	1.2319	0.8615	1.7615	0.2530	363	157	206
UBE2C_n	0.0050	0.0039	1.0050	0.9973	1.0128	0.2024	363	157	206
UBE2C_n_01	0.4580	0.2532	1.5809	0.9625	2.5966	0.0705	363	157	206
UBE2C_n_01m	0.1223	0.1843	1.1301	0.7875	1.6217	0.5069	363	157	206

Final multicovariate Cox Model assessing the following covariates on overall surviva1

Analysis of Maximum Likelihood Estimates

Variable		Parameter Estimate	Standard Error	p-value	Hazard Ratio	95% Hazard Ratio Confidence Limits	
Age		0.0276	0.0088	0.0017	1.028	1.010	1.046
Stage	*II vs I*	0.3833	0.2066	0.0635	1.467	0.979	2.199
	III vs I	0.7788	0.2141	0.0003	2.179	1.432	3.315
Neoadjuvant (Yes vs No)		0.3947	0.2141	0.0652	1.484	0.975	2.258
FEN1_n_01m (>=70 vs <70)		0.2401	0.1775	0.1761	1.271	0.898	1.800
MCM6_n_01 (Pos vs 0)		0.4839	0.2925	0.0981	1.622	0.914	2.878

4.3 Recurrence free survival

Table 42. Univariate Cox model assessing effect of covariates on recurrence free survival

covariate	*Estimate*	*StdErr*	*HazardRatio*	*HRLowerCL*	*HRUpperCL*	*pValue*	*Total*	*Event*	*Censored*
FEN1_n	0.0017	0.0011	1.0017	0.9996	1.0039	0.1127	366	206	160
FEN1_n_01	-0.1908	0.2472	0.8263	0.5090	1.3413	0.4402	366	206	160
FEN1_n_01m	0.3148	0.1405	1.3700	1.0402	1.8043	0.0251	366	206	160
MCM2_n	0.0015	0.0008	1.0015	0.9999	1.0031	0.0643	369	208	161
MCM2_n_01	0.4504	0.2978	1.5690	0.8753	2.8123	0.1304	369	208	161
MCM2_n_01m	0.1715	0.1393	1.1871	0.9034	1.5599	0.2183	369	208	161
MCM6_n	0.0013	0.0009	1.0013	0.9995	1.0030	0.1522	370	209	161
MCM6_n_01	0.4432	0.2097	1.5577	1.0327	2.3497	0.0346	370	209	161
MCM6_n_01m	0.1271	0.1386	1.1355	0.8655	1.4899	0.3590	370	209	161
SFN_c	0.0013	0.0013	1.0013	0.9987	1.0039	0.3183	370	209	161
SFN_c_01	0.0444	0.1394	1.0454	0.7954	1.3739	0.7503	370	209	161
SFN_c_01m	0.0646	0.1386	1.0667	0.8129	1.3997	0.6414	370	209	161
SFN_m	0.0029	0.0035	1.0029	0.9960	1.0099	0.4045	370	209	161
SFN_m_01	0.0384	0.1833	1.0392	0.7256	1.4883	0.8340	370	209	161
TPX2_c	-0.0013	0.0014	0.9987	0.9959	1.0014	0.3503	370	209	161
TPX2_c_01	-0.1557	0.1496	0.8558	0.6384	1.1473	0.2979	370	209	161
TPX2_c_01m	-0.0882	0.1386	0.9155	0.6978	1.2013	0.5243	370	209	161
TPX2_n	0.0060	0.0044	1.0060	0.9973	1.0147	0.1761	370	209	161
TPX2_n_01	0.1739	0.1432	1.1899	0.8988	1.5754	0.2245	370	209	161
UBE2C_c	0.0059	0.0027	1.0059	1.0006	1.0113	0.0301	366	208	158
UBE2C_c_01	0.3728	0.2065	1.4518	0.9686	2.1761	0.0710	366	208	158
UBE2C_c_01m	0.1966	0.1401	1.2172	0.9249	1.6019	0.1606	366	208	158
UBE2C_n	0.0047	0.0031	1.0047	0.9987	1.0108	0.1242	366	208	158
UBE2C_n_01	0.4114	0.1948	1.5089	1.0300	2.2105	0.0347	366	208	158
UBE2C_n_01m	0.1077	0.1396	1.1137	0.8471	1.4643	0.4404	366	208	158

Figure 12. Martingale residual from Cox model with age, gender, histology and stage for recurrence free survival against each marker, Dr. Lotan

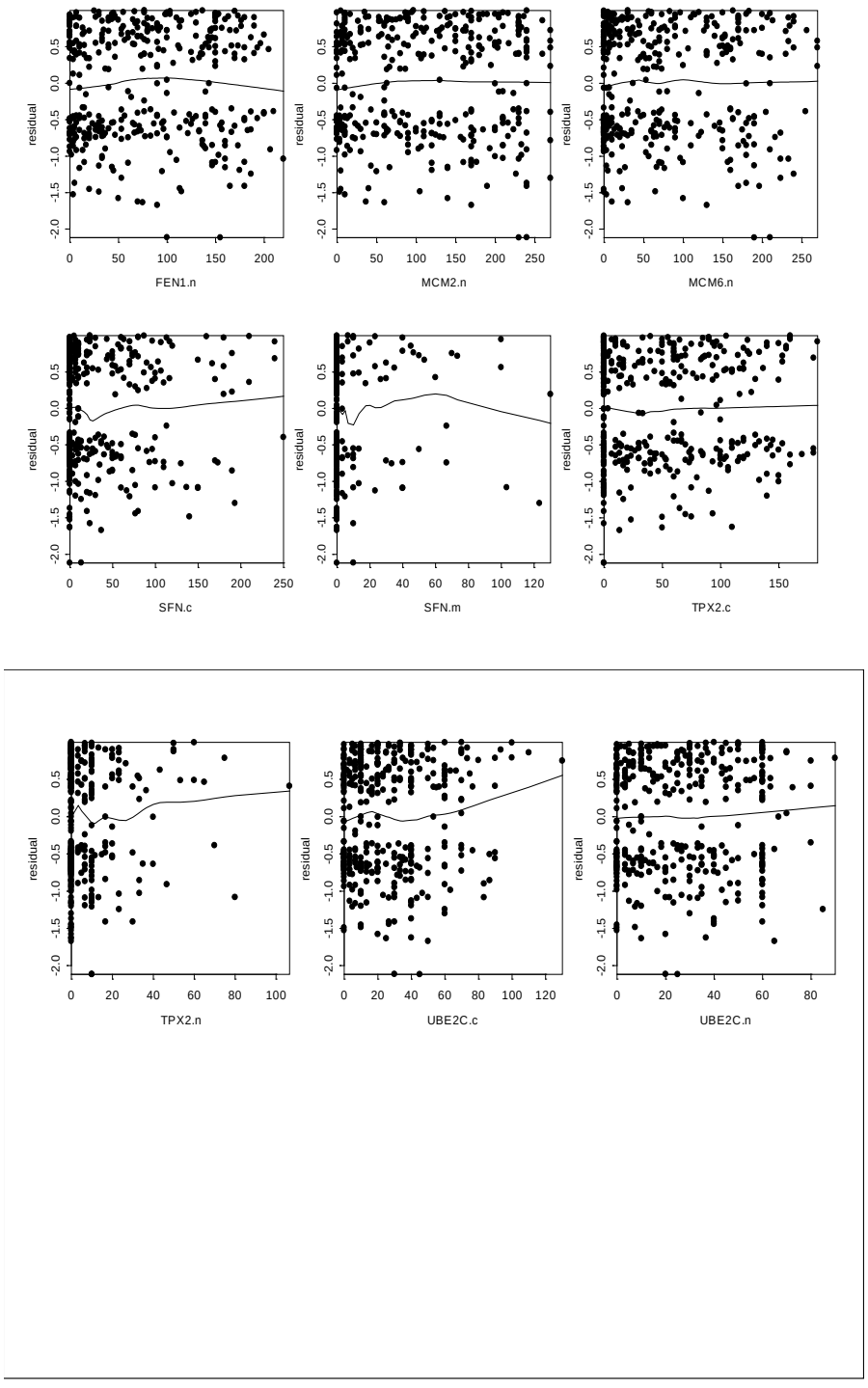

Table 43. Multicovariate Cox model assessing effect of each marker independently on recurrence free survival, adjusting for age, gender, histology, stage and neoadjuvant treatment

covariate	*Estimate*	*StdErr*	*HazardRatio*	*HRLowerCL*	*HRUpperCL*	*pValue*	*Total*	*Event*	*Censored*
FEN1_n	0.0009	0.0013	1.0009	0.9984	1.0034	0.4787	363	204	159
FEN1_n_01	-0.3987	0.2550	0.6712	0.4072	1.1063	0.1179	363	204	159
FEN1_n_01m	0.1649	0.1521	1.1793	0.8753	1.5889	0.2782	363	204	159
MCM2_n	0.0010	0.0010	1.0010	0.9990	1.0030	0.3229	366	206	160
MCM2_n_01	0.3055	0.3087	1.3573	0.7411	2.4858	0.3223	366	206	160
MCM2_n_01m	0.0470	0.1753	1.0482	0.7433	1.4780	0.7885	366	206	160
MCM6_n	0.0008	0.0011	1.0008	0.9986	1.0030	0.4578	367	207	160
MCM6_n_01	0.3322	0.2217	1.3941	0.9027	2.1529	0.1340	367	207	160
MCM6_n_01m	-0.0318	0.1636	0.9687	0.7029	1.3349	0.8458	367	207	160
SFN_c	0.0014	0.0016	1.0014	0.9983	1.0045	0.3689	367	207	160
SFN_c_01	0.0425	0.1609	1.0434	0.7611	1.4303	0.7919	367	207	160
SFN_c_01m	0.0550	0.1637	1.0566	0.7666	1.4563	0.7368	367	207	160
SFN_m	0.0018	0.0037	1.0018	0.9946	1.0090	0.6284	367	207	160
SFN_m_01	-0.0477	0.1966	0.9534	0.6486	1.4015	0.8082	367	207	160
TPX2_c	-0.0008	0.0016	0.9992	0.9960	1.0024	0.6164	367	207	160
TPX2_c_01	-0.0979	0.1901	0.9067	0.6247	1.3161	0.6065	367	207	160
TPX2_c_01m	-0.0733	0.1634	0.9293	0.6746	1.2801	0.6536	367	207	160
TPX2_n	0.0063	0.0051	1.0063	0.9962	1.0165	0.2202	367	207	160
TPX2_n_01	0.0646	0.1728	1.0667	0.7602	1.4968	0.7086	367	207	160
UBE2C_c	0.0041	0.0031	1.0041	0.9981	1.0101	0.1826	363	206	157
UBE2C_c_01	0.2553	0.2202	1.2908	0.8383	1.9875	0.2464	363	206	157
UBE2C_c_01m	0.0329	0.1568	1.0335	0.7601	1.4053	0.8335	363	206	157
UBE2C_n	0.0027	0.0035	1.0027	0.9960	1.0095	0.4296	363	206	157
UBE2C_n_01	0.3079	0.2082	1.3606	0.9048	2.0461	0.1391	363	206	157
UBE2C_n_01m	-0.0249	0.1602	0.9754	0.7126	1.3351	0.8763	363	206	157

5. ALL Markers

Multicovariate Cox Model assessing the following covariates on Overall Surviva1

Analysis of Maximum Likelihood Estimates

Variable		*Parameter Estimate*	*Standard Error*	*p-value*	*HR*	*95% HR CL*	
Age		0.028	0.009	0.0014	1.028	1.011	1.046
Stage	*II vs I*	0.354	0.207	0.0873	1.425	0.950	2.140
	III vs I	0.963	0.210	<.0001	2.620	1.737	3.951
pAMPK_c_01 (Pos vs 0)		-0.401	0.169	0.0176	0.669	0.480	0.932
pmTOR_c_01 (Pos vs 0)		-0.412	0.186	0.0262	0.662	0.460	0.952
CXCR2_c_01m (>=23.3 vs <23.3)		0.450	0.166	0.0069	1.568	1.132	2.173
EpCAM_c_01 (Pos vs 0)		-0.434	0.173	0.0123	0.648	0.461	0.910
FEN1_n_01m (>=70 vs <70)		0.354	0.168	0.0354	1.424	1.024	1.980

Internal validation **C-index = 0.32/2 + 0.5 = 0.66**

Calibration

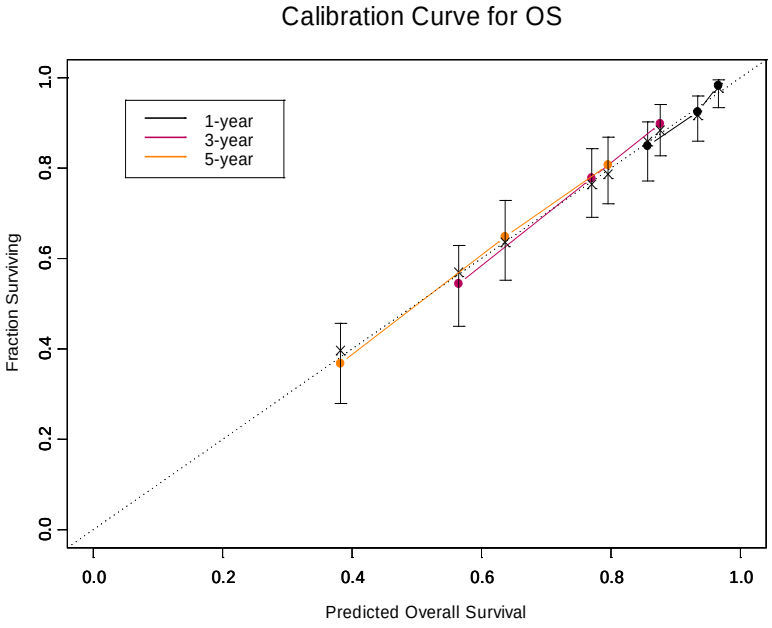

Multicovariate Cox Model assessing the following covariates on Recurrence Free Surviva1

Analysis of Maximum Likelihood Estimates

Variable	*Parameter Estimate*	*Standard Error*	*p-value*	*HR*	*95% HR CL*	
age	0.024	0.007	0.0014	1.024	1.009	1.039
Stage II vs I	0.568	0.181	0.0017	1.765	1.239	2.516
III vs I	0.984	0.182	<.0001	2.676	1.873	3.824
IGF1R_c	0.004	0.002	0.0404	1.004	1.000	1.008
Insulin_m_01 (Pos vs 0)	0.366	0.145	0.0116	1.442	1.085	1.915
pAMPK_c_01 (Pos vs 0)	-0.433	0.150	0.0039	0.648	0.483	0.870
pmTOR_c_01 (Pos vs 0)	-0.363	0.166	0.0286	0.696	0.502	0.963
CXCR2_c_01m (>=23.3 vs <23.3)	0.308	0.149	0.0383	1.360	1.017	1.820
EpCAM_c_01 (Pos vs 0)	-0.345	0.153	0.0242	0.708	0.524	0.956
CASK_m	-0.004	0.002	0.0488	0.996	0.992	1.000

Internal validation **C-index = 0.33/2 + 0.5 = 0.66**

Calibration

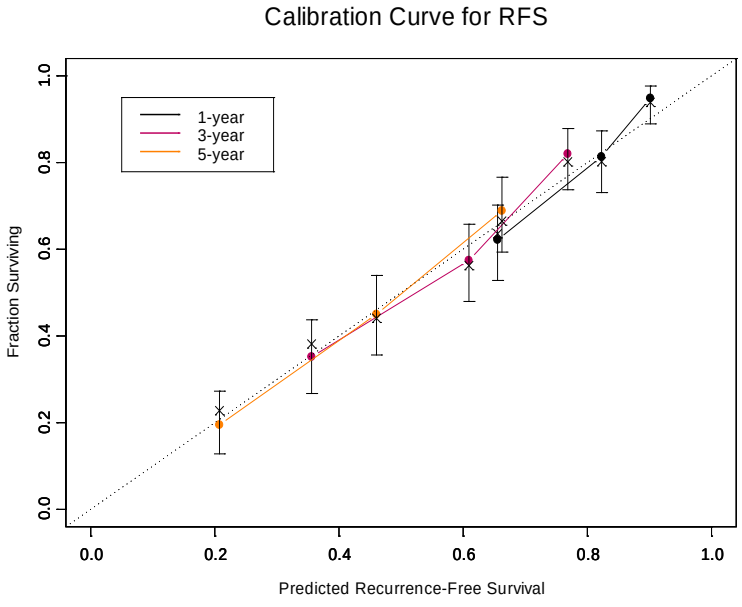

Personnel Report

Project 1

- Sevin Baser
- Mary Carter
- Beverly Casey
- Patricia Cole
- Cecilia Duron
- Ma Rhodora Francisco
- Carolyn Hawkins
- Patricia Hutchinson
- Carlos Jimenez
- Shameka Jones
- Paula Key-Connell
- Jim Klostergaard
- Cashania Langham
- Rodolfo Morice
- Karen Oishi
- Monica Quillian
- Kara Seales
- Ashley White
- Denise Woods

Project 2

- Sevin Baser
- Zuo Chu
- Jiong Deng
- Luc Girard
- Humam Kadara
- Wenhua Lang
- Woochang Lee
- John Minna
- Ashutosh Pathak
- Mitsuo Sato
- Monica Spinola
- Stephen Weber
- Xiaofeng Ye
- Ping Yuan
- Sunny Zachariah
- Jun Zhang

Project 3

- Kyounga Cheon
- Wen-Cheng Chung

- Chun Dai
- Walter Hittelman
- Ji Sung Hwang
- Ja Seok Koo
- Jangsoon Lee
- Yong Liao
- Shangfeng Liu
- Tao Lu
- Hongxia Sun
- Guiying Wang

Project 4

- Sunphil Choi
- Nola Fry
- Quanri Jin
- Woo-Young Kim
- Yoo-Shin Kim
- Ho-Young Lee
- John Kendal Smith
- Zhen Wang
- Guangcheng Zhang
- Huichao Zou

Project 5

- Guofu Fang
- Lei Fu
- Fadlo Khuri
- Shi-Yong Sun

Core A

- Angela Brooks
- Nancy Brown
- Suzanne Davis
- John George
- Carmen Martinez
- Damien Morris
- Mellanie Price
- Beverly Smith
- Wei Sonya Song

Core B

- Danqing Chen
- Kevin Coombes
- J. Jack Lee

- Yan Lin
- Diane Liu
- Suyu Liu
- Waree Rinsurongkawong
- Jing Wang
- Xian Zhou

Core C

- Allen Acomb
- Daniel Berezoski
- Lakshmi Kakarala
- Dimpy Shah
- Milind Suraokar
- Fei Yang
- Xiaoyan Zou
-